ISTITUTO NAZIONALE DI FISICA NUCLEARE
Laboratori Nazionali di Frascati

FRASCATI PHYSICS SERIES

XII INTERNATIONAL CONFERENCE ON HADRON SPECTROSCOPY HADRON 07

Editors:

C. Bloise, L. Benussi, M. Lombardo,
M. Bertani, P. Gianotti, P. Di Nezza,
P. De Simone, R. de Sangro, S. Giovannella,
S. Pacetti, S. Bianco

XII International Conference on Hadron Spectroscopy

FRASCATI PHYSICS SERIES

Series Editor
Stefano Bianco

Technical Editor
Luigina Invidia

Cover by: *Claudio Fedrici*

Volume XLVI

Istituto Nazionale di Fisica Nucleare – Laboratori Nazionali di Frascati
Divisione Ricerca – SIS – Ufficio Pubblicazioni
P.O. Box 13, I–00044 Frascati (Roma) Italy
email: sis.publications@lnf.infn.it

FRASCATI PHYSICS SERIES

XII International Conference on
HADRON SPECTROCOPY

Copyright © 2007, by INFN Laboratori Nazionali di Frascati
SIS – Ufficio Pubblicazioni

All rights reserved. No part of this publication may be reproduced, stored in a retrieval system or transmitted, in any form or by any means, electronic, mechanical, photocopying, recording or otherwise, without the prior permission of the copyright owner.

ISBN—978–88–86409–55–1

Printed in Italy by Poligrafica Laziale
P.le della Stazione 1
00044 Frascati

FRASCATI PHYSICS SERIES

Volume XLVI

XII International Conference on
HADRON SPECTROSCOPY

Editors
L. Benussi, M. Bertani, S. Bianco, C. Bloise, R. de Sangro,
P. de Simone, P. di Nezza, P. Giannotti, S. Giovanella,
M.P. Lombardo, S. Pacetti

Laboratori Nazionali di Frascati, October 7–13, 2007

International Advisory Committee

C. Amsler	*(Zurich University, Switzerland)*
P. Barnes	*(Los Alamos, USA)*
E. Berger	*(Argonne National Lab, USA)*
T. Bressani	*(INFN and Torino University, Italy)*
S. Bianco	*(INFN - Frascati, Italy)*
S. Chung	*(Brookhaven National Lab, USA)*
F. Close	*(Oxford University, UK)*
W. Dunwoodie	*(SLAC, USA)*
A. Dzierba	*(Indiana University, USA)*
F. Gross	*(Jefferson Lab, USA)*
C. Guaraldo	*(INFN - Frascati, Italy)*
E. Klempt	*(Bonn University, Germany)*
H. Koch	*(Bochum University, Germany)*
H. Lipkin	*(Weizmann Institute, Israel)*
U. Lynen	*(GSI, Germany)*
B. Meadows	*(University of Cincinnati, USA)*
V. Metag	*(Giessen University, Germany)*
S. Nagamiya	*(KEK, Japan)*
E. Oset	*(Valencia University, Spain)*
S. Paul	*(Technical University of Munich, Germany)*
E. Predazzi	*(INFN and Torino University, Italy)*
A. Reis	*(CBPF, Brazil)*
K. Seth	*(Northwestern University, USA)*
A. Skrinsky	*(BINP, Novosibirsk, Russia)*
K. Takamatsu	*(KEK, Japan)*
U. Wiedner	*(Uppsala University, Sweden)*
A. Zaitsev	*(IHEP, Protvino, Russia)*
B. Zou	*(IHEP, Beijing, China)*

Local Organizing Committee

L. Benussi	P. De Simone	M. P. Lombardo
M. Bertani	P. Di Nezza	V. Lucherini
S. Bianco	F. L. Fabbri	S. Miscetti
C. Bloise	P. Gianotti	S. Pacetti
C. Curceanu	S. Giovannella	A. Sansoni
R. De Sangro	A. La Monaca	

FOREWORD

More than two-hundred physicists gathered in October 2007 at Laboratori Nazionali di Frascati of the Italian Institute for Nuclear Physics to share results and engage in discussion on hadron physics. The occasion was the 12th edition of the HADRON conference, one of the leading events in the field of heavy and light quark spectroscopy, production dynamics, hadron-matter interactions. The choice of location was significantly connected to the active role of Frascati in hadron physics, with ongoing experimental programs on light-quarks (KLOE), hypernuclei (FINUDA) and kaonic interactions (FINUDA and DEAR), and several groups involved in analysis on heavy quark spectroscopy world-wide. The main focus of the conference was on providing plenary reviews, and to show new results and stimulate discussion in parallel sessions. A round table discussed with vivacity interplay between theory and experiment.

The Conference could not have been a success without the hard work of many, from the IAC members who supported and adviced, expecially those who attended, to the staff of Frascati and its Director who supported unconditionally, to - expecially - all participants and all speakers - to all of you go our thanks.

Stefano Bianco
on behalf of the Local Organizing Committee

CONTENTS

Foreword VII

PLENARY 1

(*Chairs:* K. Seth, A. Reis)

L. Maiani — Opening Address: A new meson Spectroscopy 3

R. Mussa — Heavy Quarkonia: An overview of recent results 17

A. Palano — New Meson States 29

C. Davies — Lattice QCD Status and Prospects 43

C. Salgado — Heavy Ion Collisions Phenomenology Overview 55

Chairs: U. Wiedner, H. Koch

E. Pallante — Light hadrons in chiral perturbation theory 67

A. Reis — Scalar mesons from heavy flavor decays 79

E. Klempt — Exotic mesons, status and future 109

U. Thoma — Recent results from baryon spectroscopy 121

M. Csanád — Milestones of the phenix experiment at RHIC 123

C. Bini — New results on adron physics at ϕ-factories 133

J. Ritman — Hadron physics experiments at the COSY facility 145

R. Beck — Recent results on hadron spectroscopy from ELSA and MAMI 157

(*Chairs:* S. Paul, C. Amsler)

E. De Sanctis — The European Physical Journal (EPJ): Achievements and Perspectives in the context of EPJ A – Hadrons and Nuclei 159

M. Duren — Nucleon spin structure results 165

C. Grab — Hadron Spectroscopy at e-p collisions 177

S. Malvezzi — Heavy flavour decays and light hadrons in the FOCUS experiment: recent results 191

P. Kasper — Review on B_S parameters and rare heavy flavour decays at the Tevatron 203

M. Kreps D and B meson spectroscopy, new states, baryons at the Tevatron 205
E. Robutti Hadronic Physics at BaBar 217
S. Eidelman Hadronic Physics at BELLE 229
S. Jin New results on hadron spectroscopy at BESII and prospects at BESIII 239
M. Shepherd Hadronic Physics with CLEOc 249
J. Harris Exploring the Quark Gluon Plasma at RHIC and LHC – today's perspective 261

(*Chairs:* B. Zou, T. Bressani, C. Guaraldo)
D. S. Carman The strangeness Physics program at CLAS 275
A. Ferrero Selected results and future prospects of the COMPASS experiment 287
J. Russ Spectroscopy in Hyperon Beams 301
S. Piano The search for bound kaonic states in nuclei, experimental status and theoretical predictions 303
K. De Jager Nucleon structure studies in Hall A at JLab 315
Z. Papandreou The GlueX project at Jefferson Lab 327
A. Rotondi Prospects for hadron Physics in PANDA 339
F. Close Three flavours of Hybrid or π exhange: which is more attractive? 351

(*Chairs:* E. Klempt, SU. Chun)
N. Saito Prospects for hadron Physics at JPARC 369
W. Li Status of BESIII experiment 371
F. Forti Plans for a super B-factory 383
R. Covarelli Prospects for hadron spectroscopy at the CMS experiment 385
S. Seidel Properties of heavy flavor hadrons in ATLAS 397
K. Seth Challenges in hadron physics 407

LIGHT MESON SPECTROSCOPY **433**
(*Conveners:* S. Giovannella, S. Miscetti, S. Pacetti)

M. Bettinelli — Electroproduction of omega π^0 with muons 435
I. Yamauchi — Further properties of extra Light vector meson $\omega'(1300)$ and $\rho'(1300)$.....445
T. Maeda — The $q\bar{q}$ S–wave axialvector mesons in the covariant $\tilde{U}(12)$ scheme 455
F. Ambrosino — Study of the $\eta \to 3\pi$ decay Dalitz plot at KLOE 463
B. Di Micco — Measurement of the η' gluonium content and of the η mass at KLOE 465
R. Escribano — Is η' partially made of gluonium? 473
R. Versaci — Observation on the $\eta \to \pi^+\pi^-e^+e^-$ decay at KLOE.....481
E. Czerwinski — Direct measurement of the total width of the η' meson 489
P. Eugenio — Observation of non-exotic hybrid mesons candidates in the $\eta\eta\pi$ decay 497
Q. Zhao — Isospin violations in $\phi \to \omega\pi^0$ 505
A. De Santis — Study of the process $e^+e^- \to \omega\pi^0$ with the KLOE detector 515
C. Hanhart — The effect of isospin violation on scalar meson production.....523
A. Donnachie — Scalar Meson Photoproduction 531
F. Nguyen — Light scalar mesons at KLOE 541
S. Fiore — Search for the $\phi \to K^0\ \bar{K}^0\gamma$ decay with KLOE.....551
D. Black — Study of scalar mesons in chiral Lagrangian frameworks 559
F. Giacosa — Two-photon decay of light scalars: A comparison of tetraquark and quarkonium assignments 567
B.-S. Zou — Study $a_0(980)$–$f_0(a_0(980)$ mixing from $J/\psi \to \phi\ a_0(980) \to \phi\eta\pi$ 577
T. Teshima — Analysis of rare radiative recays of ϕ and mixing between low and high mass scalar mesons 585

A. Nefediev — Radiative decays of hadronic molecules 593
J. Pelaez — Chiral extrapolation of light resonances from unitarized chiral perturbation theory 601
D.V Bugg — $f_0(1370)$ 609
V. Nikolaenko — Search for $f_1(1285) \to \pi^+\pi^-\pi^0$ decay with VES detector 617
E. Fadeeva — Investigation of narrow resonance at 1545 MeV in the system of two K_S-mesons 627
L. Geng — The WA3 data and the two $K_1(1270)$ Resonances 635
K. Yamada — On the existence of ligh-scalar mesons $\kappa(800)$ and $\kappa'(1150)$: the $\tilde{U}(12)$-scheme and BES II data 643
W. Ochs — The glueball among the light scalar mesons 651
W. Guryn — Central production with tagged forward protons and the STAR detector at RHIC 661
Y. Surovtsev — On the assignment of the f_0 and f_2 mesons from analysis of processes with pseudoscalar mesons 669
O. Leitner — The ground scalar nonet in D decays 677
A.-L. Zhang — Exotica possibility of new observations by BES 685
H. Noya — The masses spectrum of the exotic meson 0^{--}, 0^{+-} and 2^{+-} states by the diquark cluster model calculation with $qq\overline{qq}$ system 693
W. Wang — Studies of inclusive and exclusive final states in e^+e^- annihilations at low energies using Initial State Radiation at BaBar 695
S. Serednyakov — Studies of exclusive $e^+e^- \to$ hadrons reactions with baryons or strange particles using Initial State Radiation at BaBar 703
D. Muller — Study of $e^+e^- \to$ quasi–2–body processes at 10.6 GeV at BaBar 713
X. Shen — Recent results on light hadron spectroscopy from BESII 721

A. Sarantsev — The K-matrix analysis of the meson spectra: scalar and tensor states below 2.2 GeV 729
R. Kaminski — $\pi\pi$ and πK final state interactions and CP violation in $B \to \pi\pi K$ decays 737
F. Buccella — Spectrum and decays of multiquarks, including SU(3)F breaking 739

HEAVY IONS **747**
(*Conveners:* P. Di Nezza, M. P. Lombardo)
G. E. Bruno — Heavy flavour in ALICE 749
W. Alberico — Quarkonia in the deconfined phase 757
M. Di Toro — Isospin effects on meson production in relativistic heavy ion collisions 759
C. A. De Sousa — Phase structure, critical points, and susceptibilities in Nambu-Jona-Lasinio type models 767
S. Spataro — Dielectron spectroscopy at 1-2 AGeV with HADES 775
A. Mischke — Recent STAR results on heavy-flavour correlation measurements using leading electrons 783
G. Pancheri — Total cross-section and Rapidity Gap survival Probability at LHC 791
A. Glushkov — Resonance phenomena in heavy nuclei collisions and structurization of the positron spectrum 799

QUARKONIA STATES **801**
(*Convener*: R. De Sangro)
S. D. Glazek — Heavy quarkonia light-front QCD 803
C. Yuan — Recent BES results on charmonium decays 813
A. M. Gabareen — Charmonium spectroscopy at BaBar 821
W-S. Hou — New result on $\Upsilon(5S)$ decay from BELLE – Observation of "$\Upsilon(5S)$" $\to \Upsilon(1S) \to \pi^+\pi^-$, $\Upsilon(2S) \to \pi^+\pi^-$ – 829
D. Gladkov — Charmonium at HERA 837

A.Y. Kalashnikova X(3872) vs X(3875) 839
M. Barabanov Search for the radial excited states of charmonium in experiments using low energy antiproton beams 847
L. Scodellaro Searches for new physics in the top quark samples at the CDF experiment.....857
G. Rong Recent results on D meson and ψ (3770) decays at BES 865
P. Santorelli $\eta_b \to J/\psi\, J/\psi$ decay: the long distance contributions 867

LOW ENERGY QCD **875**
(*Conveners:* S. Giovannella, S. Miscetti, S. Pacetti)
F. Yndurain Experimental status of ππ isoscalar S-wave at low energy 877
M. Lenti ππ scattering lengths from KAON Ke4 and 3π decays by NA48/2 on Ke4 879
Y. Allkofer Search for πK-atoms with DIRAC-II 887
V. Yazkov Measurement of the $\pi^+\pi^-$ atom lifetime at DIRAC 897
M. Martini Recent KLOE results on K_S/K_L decays 905
L. Glozman CHIRAL SYMMETRY AND STRINGS 913
P. Bicudo The large degeneracy of excited hadrons and quark models 915

HEAVY MESON SPECTROSCOPY **923**
(*Conveners:* L. Benussi, F. L. Fabbri)
D. Gamermann Dynamically generated open and hidden charm meson systems 925
J. N Pandya Bottomonium masses, decay rates and scalar charge radii ..927
P.C. Vinodkumar Open flavor charmed mesons 929
V. Lyubovitskij Decays of $D_{s0}^*(2317)$ and $D_{s1}(2460)$ mesons 937
A. Valcarce Charm physics: hints for a mature description of hadrons.... 945
F. Fernandez Excited bottom meson in constituent quark model 953

P. Naik	Dalitz plot analyses at CLEO-c	959
M. Kalanand	Charmed meson dalitz plot analyses at BaBar	967
R. Andreassen	$D^0 - \bar{D}^0$ mixing analyses at BaBar	983
V. Poireau	Charm spectroscopy at BaBar	1003
M. Mazur	Semileptonic decays at BaBar	1011
C. Di Donato	η–η' mixing from electromagnetic transitions to weak decays of charm and beauty hadrons	1019
K. Tackman	Determination of the b-quark mass and other nonperturbative parameters in semileptonic and radiative penguin decays at BaBar	1021
M. Lu	Radiative penguin decays at BaBar	1029
E. Salvati	Leptonic decays at BaBar	1037
G. Mohanty	Charmless hadronic B decays at BaBar	1039
S. Emery-Schrenk	Determination of the angles of the unitarity triangle at BaBar	1047
T. Matsuki	Study of structure of the mass gap between two spin multiplets	1055
C. D. Lu	Study of X(3872) from B_c decays	1063
G. Goldstein	Baryons and mesons with beauty and charm	1065
A. Kraan	Feasibility study of Bc meson at the LHC/CMS	1073
C. Pagliarone	Double flavor violating top quark decays $t \to u_i \tau^{\pm} \mu^{\mp}$ in effective theories	1079

HADRON STRUCTURE **1081**

(*Conveners:* P. Di Nezza, M. P. Lombardo)

S. Anefalos Pereira	Measurement of the $\gamma n(p) \to K^+\Sigma^-$ (p) at Jefferson Lab	1083
J. Salamanca	g8b Experiment at JLab: photoproduction of ϕ meson	1091
C. Djalali	Hadron modification in nuclear matter at CLAS	1093
A. Machavariani	On the experimental determination of the hadron structure in the binary hadron-hadron reactions	1095

G. Salme' Spacelike and timelike nucleon form factors within light-front dynamics 1102
S. Pisano Electromagnetic decays of Vector Mesons in a covariant model 1103
S. Simula Systematic uncertainties of hadron parameters obtained with QCD sum rules 1109
W. Augustyniak New results of exclusive ϕ^0 and ρ^0 vector meson production at HERMES 1117
S. Niccolai Deeply virtual compton scattering and generalized parton distributions 1127
T. Keri Latest HERMES results on hardexclusive processes 1135
R.Czyzykiewicz Study of the low energy interaction of hadrons at COSY–11 1143
D. Melikhov Offlight cone effects in heavytolight form factors 1145
J. Friedrich Pion polarisability measurement at COMPASS 1153
L. Pappalardo Latest HERMES results on transversespin effects in hadron structure and formation 1161
S. Liuti π^0 electroproduction and transversity 1171
P. Rossi Transversity and SIDIS at CLAS 1179
R. Fabbri Recent HERMES results on the helicity substructure of the nucleon 1187
F. Zamani Calculation of nucleon's F_2 structure function using radiative gluons and meson cloud model in the lightcone frame 1191

HADRONS IN MATTER **1197**
(*Conveners:* C. Curceanu, M. Bertani)
M. Iio Precise measurement of kaonic helium atoms X-rays 1199
T. Ishiwatari The SIDDHARTA experiment: kaonic hydrogen and deuterium X-ray spectroscopy 1207

B. Dalena — Study of the (K^+,K^0) reaction on medium light nuclei close to threshold 1215
S. Bufalino — Measurement with high resolution of the proton spectra from the non-mesonic weak decay of $^{5}_{\Lambda}$He, $^{7}_{\Lambda}$Li and $^{12}_{\Lambda}$C 1225
S. Minami — Study of hypernuclei with heavy Ion beams (HypHI) at GSI - Experimental design and performance test of the detector system 1235
C. Sfienti — Particle IDentification at PANDA: recipes and physics application 1243
L. Tolos — Open–charm mesons in hot and dense nuclear matter 1251
T. Nishikawa — Bound kaon approach for the ppK$^-$ system in the Skyrme model 1259
M. Sato — A search for strange tribaryons in ^{4}He (K–stopped, N) reaction 1267
P. Salvini — S= –2 strangeness production in antiproton ^{4}He annihilations at rest 1275
P. Aslanyan — Searches for multibaryon states with lambda hyperon systems in pA collision at 10 GeV/c 1283
O. Vazquez Doce — The AMADEUS experiment: study of the kaonic nuclear clusters at DAΦNE 1293

BARYON SPECTROSCOPY 1299
(*Conveners*: C. Bloise, P. Gianotti)
N. Matagne — Baryon Regge trajectories in the light of the 1/Nc expansion of QCD 1301
T. Melde — Properties of baryon resonances and strong decays 1309
V. Crede — Photoproduction of neutral mesons with CBELSA/TAPS 1317

V. Nikonov — Evidence for new resonances in the combined analysis of recent hyperon photoproduction data 1325
A. Anisovich — Properties of baryon resonances from combined partial wave analysis of the photoand pion induced single and double meson production data 1333
P. Faccioli — Light hadron spectrum in the instanton liquid model 1341
K. Daum — Baryon, heavy stable particle and strange meson production in *ep* collisions 1349
L.–H. Chan — Baryon isospin mass splittings 1357
P. Palazzi — Linear mass rules and hadronic shells: the baryons 1359
J. Vijande — Towards a constituent quark model description of baryon spectroscopy 1367
P. Gonzalez — A plausible explanation of the Δ D35(1930) as a $\omega\Delta$ induced resonance 1375
P.A. Faria Da Veiga — Dynamical eight fold way in strongly coupled lattice QCD 1383
J. A. Oller — Meson-baryon scattering and resonances with strangeness -1 1395
O. Samoylov — Search for an exotic Θ^+ Baryon in ν_μ N in the NOMAD experiment 1403
M. Bashkanov — σ-channel threshold enhancement in double-pionic fusion 1415
T. Skorodko — Excitation of the Roper resonance in single and double-pion production 1423
B. Patel — Masses and magnetic moment of charmed baryons in hyper central model 1431
D. Ebert — Heavy hadrons in the relativistic quark model 1439
E. H. Gajate — Heavy quark spin symmetry in semileptonic decays of doubly heavy baryon 1447

FUTURE FACILITIES **1455**
(*Conveners:* P. Gianotti, P. de Simone)

E. Botta — Future prospects for gamma ray spectroscopy of hypernuclei at Frascati 1457
P. Moskal — The Physics case of KLOE2 1467
D. Domenici — The upgrade of the KLOE detector: KLOE2 1477
T. Stockmanns — Hidden and open charm at Panda 1485
A. Baven — The Physics case of the SuperB facility 1487
E. Paoloni — SuperB: Detector for a very high luminosity electron Positron collider Υ(4s) peak 1495
B. Mele — The Physics case of ILC 1501
A. Calcaterra — Detector design for ILC 1503

POSTER **1511**
(*Convener:* C. Curceanu)

A. Machavariani — Analytical determination of the magnetic moment of the Δ–resonance and screening in the bremstrahlung reactions 1513
T. Matsuki — Construction of Lorentz invariant amplitudes from rest frame wave functions in HQET – Application to isgur-wise function 1515
J. N. Pandya — Bottomonium masses, decay rates and scalar charge radii 1519
O. Leitner — Testing CP and time reversal symmetries in Λ_b decays into polarized resonances 1523
A. Valcarace — Multiquark description of open-charm mesons 1525
M.L.L. Da Silva — Glueball option for X(1835) 1527
O. Khetselius — Spectroscopy of the heavy quarkonia: energy levels splitting and teta-singular potentials 1529
A. Glushkov — Discharge of metastable nuclei during muon capture: energy approach 1531

R. Johnstone — Kaon photoproduction on deuterium using polarised photons with CLAS 1533
Y. Surovtsev — ρρ-like mesons from analysis of the pp scattering 1535
W. Lucha — Stability of the solutions of Salpeter equations with confining interactions 1539
J.-C. Caillon — Relation between the in-medium Ω meson mass and quark condensate un the light of the recent experimental data on the meson properties in nucleai 1543

ROUND TABLE **1547**
C. Davies, R. Faccini, H. Lipkin, L. Maiani (*Chair*), F. J. Yndurain — Methods and Models for nuclear and particle Physics in the 21st century 1549

Participants 1567

PLENARY SESSION

Frascati Physics Series Vol. XLVI (2007), pp. 3–16
HADRON07: XII Int. Conf. on Hadron Spectroscopy – Frascati, October 8-13, 2007
Plenary Session

OPENING ADDRESS: A NEW MESON SPECTROSCOPY

Luciano Maiani
Università di Roma "La Sapienza", Roma, Italy

Abstract

Evidence for mesons beyond the classical $q\bar{q}$ structure is discussed. This includes the sub-GeV scalar mesons, and the X, Y and Z particles recently observed at KEK and SLAC. The tetraquark hypothesis for these particles is illustrated together with other proposals appeared in the recent literature.

1 Introduction

Thirty years after its discovery, we still do not fully control QCD and are unable to predict hadron spectrum and configurations. *Ab initio* calculations based on lattice QCD have still many limitations. Only in few cases, we can produce reliable theoretical predictions and even in these cases we need to rely upon phenomenological input parameters. Scaling violations in Deep Inelastic Scattering are the best example. Inputs are the structure functions at some value

of the momentum scale, Q^2 , but then very precise predictions can be made on the structure function evolution at fixed x, up to the spectacularly high values of Q^2 obtained at HERA [1]. Another case is that of hadrons made of a heavy quark pair. The large quark mass makes it possible to use potential theory. The phenomenological inputs are the parameters of the potential. But then a remarkable accuracy in the mass spectrum and decay rates of $c\bar{c}$ and $b\bar{b}$ states is achieved. A large effort has gone, over the last decades, in this direction [2]. The third case I want to mention, in order of phenomenological reliability, is the constituent quark model [3, 4]. The model envisages non relativistic (valence) quarks endowed with an effective mass and a two body hyperfine, spin-spin, interaction with strength inversely proportional to the masses of the quarks involved. We are unable to justify the model from basic QCD, let alone to compute the values of the parameters, but the model reproduces extremely well the spectrum of the S-vave light hadrons and it has been extended successfully to charmed and beauty hadrons (see [5] for a recent contribution). The last two schemes give us the background against which we can compare new hadrons, to see if they fit in the Hadron Standard Model, namely that baryons are made by three quarks and mesons by $q\bar{q}$ pairs. We shall see that there are reasons to think that there is at least one, so to say, secundary spectroscopic series, a meson sequence made out of tetraquark, $qq\bar{q}\bar{q}$, states. I shall discuss the evidence for non standard light mesons first and then go to the case, much more clear in my opinion, of the X, Y and Z particles recently discovered at the Beauty factories, at KEK ad SLAC.

2 Light Scalar Mesons Resolved

In the complex s-plane, poles of the partial wave S-matrix amplitudes in the second Riemann sheet correspond to zeros in the upper, first sheet. This is because partial wave amplitudes are real analytic functions of s: $S^*(s)=S(s^*)$. From unitarity: $S(s)S^*(s)=1$, one gets at once that $S(s)=1/S(s^*)$. A dispersion relation search of the zeroes of the scattering amplitude in S-wave, based on the Roy equation, has been performed in [6]. Results indicate, beyond doubts, the existence of a low energy zero, corresponding to a broad resonance around 500 MeV, σ, accompanied by a narrow one around 980 MeV, the well established f_0. A similar analysis [7] proves the existence of an S-wave Kπ resonance, the so-called κ. The two results are illustrated in Fig. 1.

Experimental evidence for σ and κ has accumulated recently, in D non leptonic decays [8, 9] and J/ψ decays [10].

With σ(450, I=0), κ(660, I=1/2), f_0(980, I=0) and a_0(980, I=1)) we can fill neatly a nonet, but masses are in reverse order with respect to the standard, $q\bar{q}$, pattern produced by the constituent quark model.

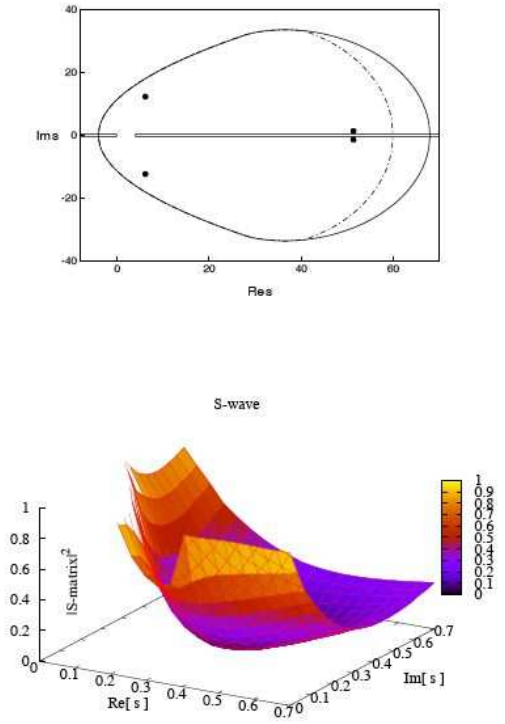

Figure 1: *Upper panel: locations of poles (Im $s < 0$) and zeros (Im $s > 0$) in the complex s-plane of the S wave $\pi\pi$ vamplitude* [6]*; closed curves indicate the region of validity of the Roy equation used in the analysis. Lower panel: absolute value squared of the S wave $K\pi$ amplitude, showing the existence of one shallow zero in the upper complex s-plane* [7].

Lowest scalars are in fact good candidates to be diquark-antidiquark

bound states, following earlier proposals [11, 12] recently reconsidered by our group [13], with diquarks fully antisymmetric in: (i) color (diquark = $\bar{3}_{color}$), (ii) spin (i.e. spin = 0) and (iii) flavor (diquark = $\bar{3}_{flavor}$). The quark structure of the nonet is summarized by:

$$\begin{aligned}
\sigma &= [ud][\bar{u}\bar{d}]; \\
\kappa &= [su][\bar{u}\bar{d}],\ [sd][\bar{u}\bar{d}]\ (+\text{ conjugate doublet}) \\
f_0 &= \frac{[su][\bar{s}\bar{u}] + [sd][\bar{s}\bar{d}]}{\sqrt{2}} \\
a_0 &= [su][\bar{s}\bar{d}];\ \frac{[su][\bar{s}\bar{u}] - [sd][\bar{s}\bar{d}]}{\sqrt{2}};\ [sd][\bar{s}\bar{u}]
\end{aligned} \tag{1}$$

The 4-quark composition of the lightest scalar mesons is indicated by the reversed mass spectrum. The fully antisymmetric diquark explains the absence of truly exotic states, i.e. I=2, $\pi\pi$ resonances, not observed at low energy.

The quark composition in (1) explains also the conspicuous affinity for $K\bar{K}$ decay channels displayed by f_0 decays. The alternative is to describe the f_0 as a $K\bar{K}$ molecule [4, 14]. The existence of σ and κ speaks for tetraquarks. Hadron molecules bound by meson exchange forces would suffer large SU(3)$_{flavor}$ breaking, possibly with only $K\bar{K}$ giving rise to bound states, while tetraquark structure bound by color forces naturally leads to a complete nonet.

There are still open questions in this picture: (i) decays of light scalars are not fully un- derstood, e.g. where does $f_0 \to \pi\pi$ come from? (ii) where is it the $q\bar{q}$, P-wave, scalar nonet? Progress along these lines is reported in [15] and [16].

3 Strings and hadrons

Classical color string configurations for baryons have been studied in [17].

For high excitations, the Y-shaped configuration with a quark at each end of the Y, Fig. 2(a), would collapse in a configuration with a closely packed diquark bound to the other quark. Regge trajectories for mesons and baryons seem to have very similar slopes. This could be understood if excited baryons are described as a diquark bound to a quark.

Replacing the quark in the Y-shaped baryon with another diquark, we obtain an H-shaped tetraquark meson, Fig. 2(b). This configuration allows for

many states, corresponding to radial and orbital excitations.

The situation can be contrasted with meson-meson molecules: color singlet meson exchange provide very short range forces and very few, if at all, excited states.

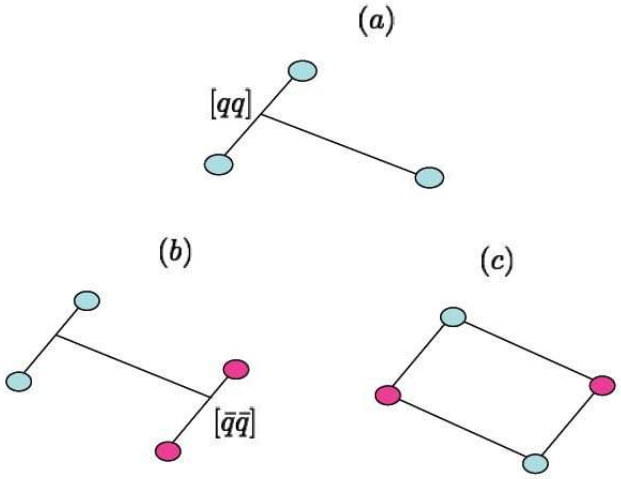

Figure 2: *Color strings configurations: (a) baryons, (b) H-shaped tetraquarks, (c) box-shaped tetraquarks. Gray circles represent quarks, red circles antiquarks. Color strings are oriented, they go from quarks to antiquarks, or converge to (diverge from) a triple point, corresponding to the color composition* $\mathbf{3} \otimes \mathbf{3} \otimes \mathbf{3} \to \mathbf{1}$.

The string topology in Fig. 2(b) is related to the baryon-antibaryon channel: if you stretch the string connecting the diquarks until it breaks with the creation of a $q\bar{q}$ pair, you end up in a baryon-antibaryon pair:

$$[qq][\bar{q}\bar{q}] \to B\bar{B} \tag{2}$$

Below the baryon-antibaryon threshold, the decay mechanism is indicated in Fig. 3, upper panel. It represents a tunneling from colored to uncolored pairs, free to move away from each other, a fully non-perturbative effect. The amplitude may depend strongly on quark masses, as we discuss below, Sect. 6.

One could expect tunneling to be suppressed with respect to the natural process of string breaking. So states below the baryon-antibaryon threshold tend to be narrow. This may be the reason of the narrow X particles observed in B-decays, also discussed below.

Box-shaped tetraquarks have been proposed [18] in connection with 4-quark charmonia, see Fig 2(c). The mechanism for the strong decay of box-mesons is very different from that of H-shaped mesons, Fig. 3. Phenomenological signatures to discriminate between the two possibilities are however not known, at present.

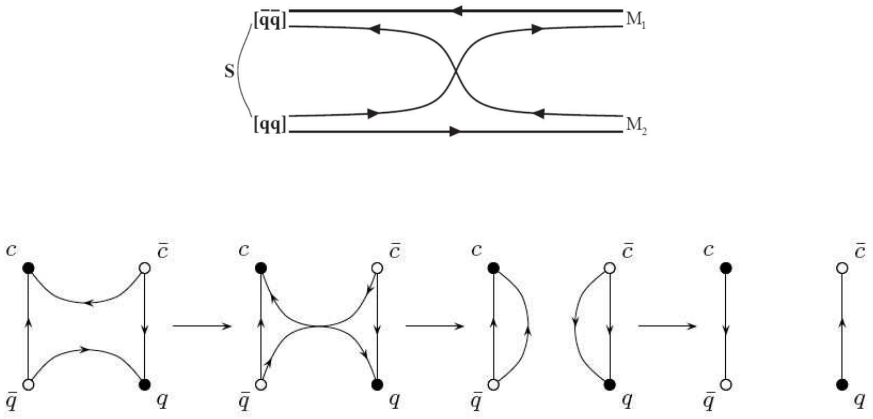

Figure 3: *Upper panel: H-shaped tetraquark decay by quark rearrangement. Lower panel: Box- shaped tetraquark decay.*

Outlook for light tetraquarks. Poor control of QCD in light hadronic systems may make it difficult to identify smoking-gun signals of light tetraquark mesons. Additional signatures, useful to bring about differences with respect to standard $q\bar{q}$ mesons have been identified:

- comparison of the f_0 and η e.m. form factors [19] ($\gamma \to f_0\omega$ vs. $\gamma \to \eta\omega$);
- Nuclear Modification Ratios of f_0 [20] in Relativistic Heavy Ion Collisions at RHIC and LHC.

One can expect to see more clearly tetraquark structures in hadrons containing one or more heavy quarks, for several reasons. Asymptotic freedom makes it more difficult for quark pairs to annhilate, thus making easier to trace the constituent quark composition. In addition, the hyperfine interaction decreases with quark masses and tetraquark should give rise to typical multiplets arising from different spin distributions. This point was made in the DAΦNE 2004 Workshop, see [21].

4 Charmonium states beyond the Standard Model

Hidden-charm mesons are being found by BELLE and BaBar, which seem not to belong to the $c\bar{c}$ family. A first classification, related to the observation channels, goes as follows.

- X-states, seen in non leptonic B decays:

$$B^{\pm} \to K^{\pm} + X^0; \quad B^0 \to K^0 + X^0 \tag{3}$$

$$X^0 \to \psi(nS) + \pi's, \text{ or } D^{(*)}D^{(*)} \tag{4}$$

- Y-states, produced in electron-positron annihilation with an initial state radiation photon (ISR):

$$e^+e^- \to \gamma(\text{initial state}) + Y \tag{5}$$

$$Y \to \psi(nS) + \pi's, \text{ or } D^{(*)}D^{(*)} \tag{6}$$

  Y have $J^{PC} = 1^{--}$, since originate from a virtual photon.

- X states with C=+1 can be searched also in the mass spectra of charmed pair recoiling against a J/ψ in e^+e^- annihilations:

$$e^+e^- \to \psi(1S) + (D^{(*)}D^{(*)})_M \tag{7}$$

The first discovered X and Y states do not fit in the charmonium spectrum, Fig. 4, for either mass and quantum numbers or decay modes.

In more detail. The X(3872), being most likely $J^{PC}=1^{++}$, could be identified with a missing χ_c state. However, its decay into both $\rho\psi$ and $\omega\psi$, with the corresponding large isospin violation, is against a pure $c\bar{c}$ composition and so does the large rate in $\psi\gamma$. The mass of the Y(4260) could well be consistent

with a 1^{--} charmonium, but it lacks the decay in $D\bar{D}$, which is typical of this kind of states.

Given the accuracy reached by predictions about true $c\bar{c}$ states, there are ample reasons to suspect that we are seeing the opening a new spectroscopical series. There are by now several proposal on the nature of X and Y states.

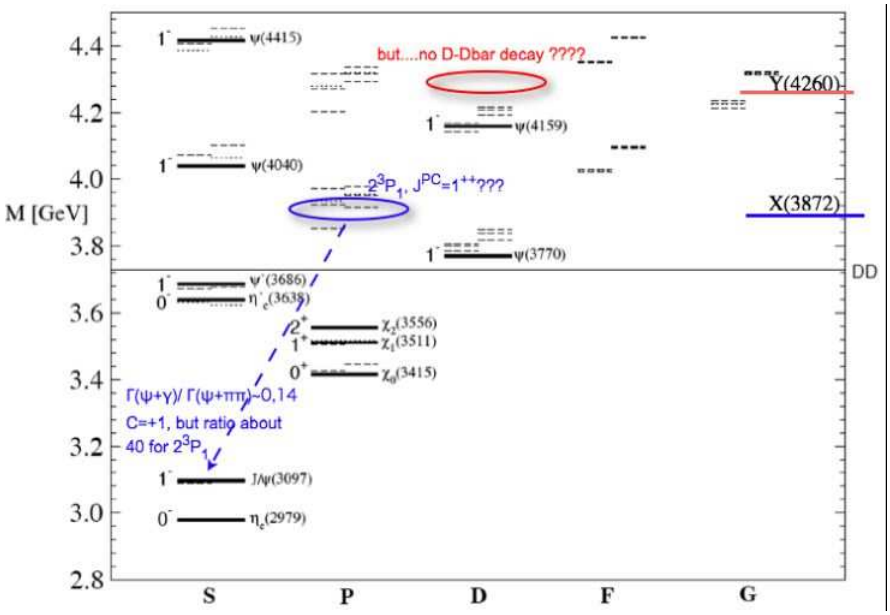

Figure 4: *The predicted spectrum of charmonia from* [22] *and the first two discovered X and Y states.*

X(3872) has been associated with:

- D-D* molecule [23], since: $M(X) - M(D0\bar{D}^{*0}) \simeq +0.6$ MeV;
- diquark-antidiquark [24]: $[(cq)(\bar{c}\bar{q})]_{Swave}, J^{PC} = 1^{++}$; (q = u, d).

Y(4260) has been associated with:

- hybrid state [25]: $(c\bar{c}g)$;
- diquark-antidiquark [26]: $[(cs)(\bar{c}\bar{s})]_{Pwave}$;

- molecular state [27]: $\chi_c + \omega$;
- baryonium [28]: $\Lambda_c + \bar{\Lambda}_c$.

These interpretations have been confronted by the breaking news of last summer, the discovery of $Z^+(4430)$ [29], a structure in the mass distribution of $\psi(2S)+\pi^+$ in:

$$B^{\pm} \to K^0 + Z^{\pm}; \quad B^0 \to K^{\pm} + Z^{\mp} \tag{8}$$

$$Z^+ \to \psi(2S) + \pi^+ \tag{9}$$

see Fig. 5(a). Among particle interpretations, the tetraquark is the simplest. In this case, the resonance would contain four quarks, $cu\bar{c}\bar{d}$, all recognizable from the final state, connected by color strings, either H- [30] or box- [18] shaped. A baryonium interpretation has also been advanced [31].

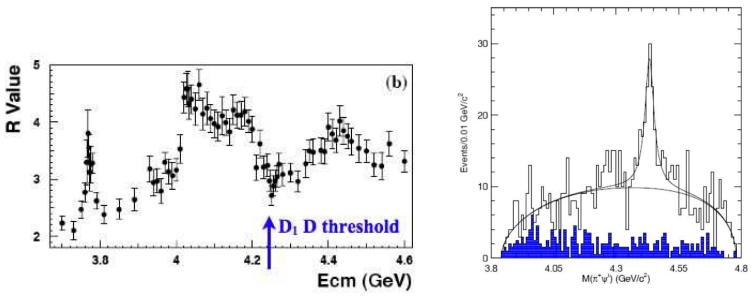

Figure 5: *Left panel: the dip in the e^+e^- cross-section, correlated to the D_1 D threshold. Right panel: Z(4430).*

5 Thresholds, cusps and new states

Dips are observed in various reactions as the effect of the opening of an S-wave threshold in another channel. Ref. [32] quotes several cases like, e.g. the $\gamma p \to p\pi^0$ cross-section in the proximity of the $n\pi^+$ threshold. Most pertinent to our discussion is the e^+e^- cross section. The dip in R between 4.19 and 4.25 GeV, see Fig. 5(b), can be associated [32] with the opening of the D_1 D threshold at 4.285 GeV. In this framework, the charged structure in $\psi(2S)\pi^+$

at 4430 MeV has been interpreted in [33] as a cusp effect related to the opening of the D_1D^* threshold.

6 Two X states?

There is poor agreement among measurements of the X(3872) mass in the two observed decay channels: the X masses in X$\to J/\psi\pi^+\pi^0$ and X$\to D\bar{D}\pi$ differ by about 4σ, Fig. 6, see [34].

The possible solution is that there are indeed two X states, with M= 3872 GeV and M= 3876 GeV, decaying predominatly in disjoint channels, the heavier in DD^* and the lighter in $J/\psi\pi^+\pi^0$ [35]. Two neutral X states is typical of the tetraquark model, the states being $cu\bar{c}\bar{u}$ and $cd\bar{c}\bar{d}$ in appropriate superpositions. The molecule interpretation is instead disfavored by the existence of two states. Can we explain the decay pattern? Yes, if the highest states is predominantly $cu\bar{c}\bar{u}$ and if the $J/\psi\pi^=\pi^0$ mode is suppressed w.r.t. $D\bar{D}\pi$. Both issues are discussed in [35].

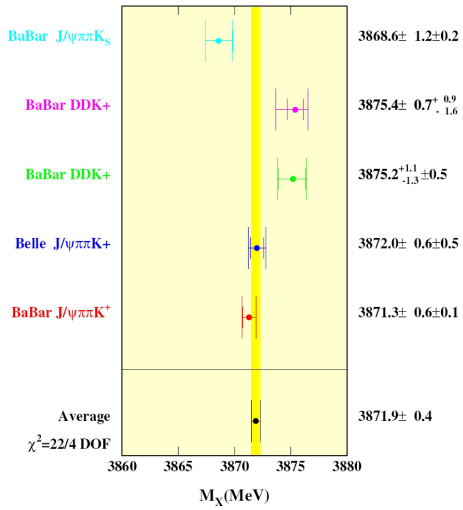

Figure 6: *Accurate mass measurements indicate a systematic discrepancy between X masses in the two decay channels, $\to J/\psi\pi^=\pi^0$ and $D\bar{D}\pi$. The figure is taken from* [34].

7 Outlook

Hadron spectroscopy below 1 GeV seems established: S-wave $q\bar{q}$ and $[qq][\bar{q}\bar{q}]$ mesons.

Scalar meson decays still confront us with the problem of f_0 decay to $\pi\pi$ (is there a new mechanism at work?). In addition, one has to identify firmly the P-wave $q\bar{q}$ scalar nonet, which must be above 1 GeV, but not too much. One possibility is the nonet to which the $a_0(1450)$ belongs, but this identification is not without problems. The $\eta\pi$, $J = 0^{++}$ resonances count scalar nonets, but a systematic study above 1 GeV is still lacking: is there more than the $a_0(1450)$ nonet?

A new spectroscopy is being discovered with the new charmonia. The statement is made possible by the fact that the Standard Charmonium model is so precise: the efforts to compute accurately the $c\bar{c}$ spectroscopy bring now their reward.

The observation of two X states, at 3872 and 3876 MeV, and the discovery of the charged charmonium, $Z^+(4430)$, have added credibility to the tetraquark scheme. In this case, there must exist neutral states close to Z, analogous to the X(3872) and decaying in $\psi(2S)\pi^0$ or $\eta_c(2S)\rho^0$. It is a curious fact that the tetraquark interpretation is consistent only if the observed Z is the second radial excitation, Z(2S). A Z(1S) around 3900 MeV should exist, with $Z(1S) \rightarrow \psi(1S)\pi^+$, to confirm the scheme.

X and Z states should fall in complete nonets, with masses calculable within the constituent quark model that works so well for S-wave hadrons. Investigations in this direction are found in [36].

Finally, it hardly needs to be stressed that, at the moment, there are alternative interpretations of X, Y and Z. More data are badly needed. The spectroscopy of the new hadrons is still in its infancy, theory needs guidance by experiments, as the developments of the last year have amply demonstrated.

8 Acknowledgements

I thank R. Faccini, V. Riquer and A. Polosa for many interesting discussions on the subject and A. Polosa for precious help in preparing this contribution.

References

1. See e.g. C. Gwenlan in *XXIII International Symposium on Lepton and Photon Interactions at High Energy*, Aug 13-18, 2007, Daegu, Korea.
2. See e.g. N. Brambilla *et al.* [Quarkonium Working Group], arXiv:hep-ph/0412158.
3. Y. B. Zeldovich and A. D. Sakharov, Acta Phys. Hung. **22** 153 (1967); H. J. Lipkin, Phys. Rev. Lett. 41 (1978) 1629.
4. A. De Rujula, H. Georgi and S. L. Glashow, Phys. Rev. D **12** (1975) 147.
5. M. Karliner, B. Keren-Zur, H. J. Lipkin and J. L. Rosner, arXiv:0708.4027 [hep-ph].
6. I. Caprini, G. Colangelo and H. Leutwyler, [arXiv:hep-ph/0512364].
7. S. Descotes-Genon and B. Moussallam, Eur. Phys. J. C 48 (2006) 553.
8. E. M. Aitala *et al.* (E791 Collab.) Phys. Rev. Lett. **86** , 770 (2001); ibid. **89**, 121801 (2002).
9. B. Aubert *et al.* [BABAR Collaboration], Phys. Rev. D **72**, 052008 (2005).
10. M. Ablikim *et al.* Phys. Lett. B **598**, 149 (2004); ibid. **633**, 681 (2006).
11. R. L. Jaffe Phys. Rev. D **15** (1977) 28; a more recent discussion is in R. L. Jaffe and F. Wilczek, Phys. Rev. Lett. **91**, 232003 (2003) and references therein.
12. D. Black, A. Fariborz, J. Schechter, Phys. Rev. D **61**, 074001 (2000).
13. L. Maiani, F. Piccinini, A. D. Polosa, V. Riquer, Phys. Rev. Lett. **93**, 212002 (2004).
14. N. A. Tornqvist, Z. Phys. C **61**, 525 (1994).A similar picture for charmonium states is developed in N. A. Tornqvist, arXiv:hep-ph/0308277.
15. G. '. Hooft, G. Isidori, L. Maiani, A. D. Polosa and V. Riquer, arXiv:0801.2288 [hep-ph].
16. A. H. Fariborz, R. Jora and J. Schechter, arXiv:0801.2552 [hep-ph].

17. G. t Hooft, arXiv:hep-th/0408148.

18. Gershtein, A.K. Likhoded and G.P. Pronko, hep-ph 0709.2058.

19. S. Pacetti, 2005, unpublished.

20. L. Maiani, A. D. Polosa, V. Riquer and C. A. Salgado, Phys. Lett. B **645** 138 (2007); same authors arXiv:0707.4578 [hep-ph].

21. L. Maiani in DAΦNE 2004: *Physics at meson factories*, 7-11 June 2004. Laboratori Nazionali di Frascati - Italy.

22. T. Barnes, S. Godfrey and E. S. Swanson, Phys. Rev. D **72** 054026 (2005).

23. F. E. Close and P. R. Page, Phys. Lett. B *578* 119 (2004); N. A. Tornqvist, Phys. Lett. B **590** 209 (2004); E. S. Swanson, Phys. Lett. B **588** 189 (2004).

24. L. Maiani, F. Piccinini, A. D. Polosa and V. Riquer, Phys. Rev. D **71**014028 (2005).

25. F. E. Close and P. R. Page, Phys. Lett. B **628** 215 (2005); E. Kou and O. Pene, Phys. Lett. B **631** 164 (2005).

26. L. Maiani, V. Riquer, F. Piccinini and A. D. Polosa, Phys. Rev. D **72** 031502 (2005).

27. C. Z. Yuan, P. Wang and X. H. Mo, Phys. Lett. B **634** 399 (2006).

28. C. F. Qiao, Phys. Lett. B **639** 263 (2006).

29. K. Abe et al. arXiv:0708.1790v1 [hep-ex].

30. L. Maiani, A. D. Polosa and V. Riquer, arXiv:0708.3997 [hep-ph]; K. m. Cheung, W. Y. Keung and T. C. Yuan, Phys. Rev. D 76 (2007) 117501, propose similar states with b quarks.

31. C. F. Qiao, hep-ph :0709.4066.

32. J. L. Rosner, Phys. Rev. D 74 076006 (2006).

33. J. L. Rosner, Phys. Rev. D 76 114002 (2007); C. Meng and K. T. Chao, arXiv:0708.4222 [hep-ph]; D.V. Bugg, hep-ph :0709.1254.

34. See R. Faccini in *XXIII International Symposium on Lepton and Photon Interactions at High Energy*, Aug 13-18, 2007, Daegu, Korea.

35. L. Maiani, A. D. Polosa and V. Riquer, Phys. Rev. Lett. 99 182003 (2007).

36. Y. Li, C. D. Lu and W. Wang, arXiv:0711.0497 [hep-ph].

Frascati Physics Series Vol. XLVI (2007), pp. 17–28
HADRON07: XII Int. Conf. on Hadron Spectroscopy – Frascati, October 8-13, 2007
Plenary Session

HEAVY QUARKONIA: AN OVERVIEW OF RECENT RESULTS

Roberto Mussa
INFN, Sezione di Torino, Via P. Giuria 1, 10126 Torino, Italy

Abstract

In the last five years, an impressive amount of new and unexpected results has revived the interest on the study of heavy quarkonia. A comprehensive review on the experimental progress on charmonium and bottomonium spectroscopy, production and decays will be given.

1 Introduction

Since the advent of asymmetric B factories, heavy quarkonium spectroscopy is living a second renaissance. The QWG Yellow Report [1)] on these systems, written only three years ago, to summarize the status of theoretical and experimental understanding of these bound states, can be considered obsolete.

Most of the surprises in spectroscopy are related to states above the open flavor thresholds which decay with unexpectedly large transition rates to the

lower narrow states. Production of heavy quarkonia in hadronic interactions is still a challenge for QCD, as recent polarization results from Tevatron [2] are inconsistent with theory predictions. Much progress has been made in NLO calculations to understand the double charmonium production in e^+e^-, but further efforts are needed to sistematically understand the variety of processes which lead to the production of these systems.

2 Charmonium and charmonium-like objects in B decays

The decay of B mesons in charmonium and a kaon has been extensively studied to investigate the CP violation in weak interactions. This has allowed to discover the 'true' $\eta_c(2S)$ state and three (or four?) other resonances, whose nature is still unclear, dubbed with the last letters of the alphabet: X(3872/5), Y(3940), Z(4430).

But the quantitative picture of the hadronization mechanism which leads from the $b \to c\bar{c}s$ current at quark level to the final state products is still incomplete. Table 1 shows the PDG2006 [3] values for the branching ratios of B decays to charmonium known states and the two lowest strange mesons, or anything. By filling the missing slots we may get more clues to the nature of the new states.

Table 1: *B decays to charmonium known states*

$\mathcal{B} \times 10^4$	$K^{\pm}$	K^0	$K^{*\pm}$	K^{*0}	+anything
η_c	9.1 ±1.3	9.1 ±1.9		16 ±7	< 90
J/ψ	10.08±0.35	8.72±0.33	14.1±0.8	13.3±0.6	78± 3
χ_{c0}	1.6±0.5	< 5	< 28.6	< 7.7	
χ_{c1}	5.3±0.7	3.9±0.4	3.6±0.9	3.2±0.6	31.6±2.5
χ_{c2}	< 0.29	< 0.26	< 0.12	< 0.36	16.5±3.1
$\eta_c(2S)$	3.4±1.8				
ψ'	6.48±0.45	6.2±0.6	6.7±1.4	7.2±0.8	30.7±2.1

The table shows that only 25-45% of the inclusive rate to charmonia is explained as a two body decay to charmonium and a pseudoscalar or vector kaon. Feed-down from known transitions (e.g.$\psi' \to \chi_c\gamma$) is already subtracted from the inclusive rates, in the last column. Which other process is responsible for the remaining $J/\psi, \psi'$'s produced in B decays? Multi-body, higher kaon

excitations, or higher charmonia?

2.1 X(3872) and X(3875) : the first tetraquark doublet?

In August 2003, BELLE [4] reported the discovery of X(3872) in:

$$B \to KX(3872) \to J/\psi\pi^+\pi^-$$

One month after, CDF [5] confirmed the existence of the such state, observing it in the same decay channel, but producing it more copiously in prompt $\bar{p}p$ annihilation at $\sqrt{s}$=2 TeV: only 16% of their X(3872) candidate events come from B decays. In the following years, D0 [6] and BABAR [7] confirmed these observations.

The width of X(3872) has not been measured yet: BELLE set the upper limit $\Gamma < 2.7MeV$ at 95% C.L.). The PDG 2007 value for the X(3872) mass (3871.4±0.6) is close to a cluster of thresholds, summarized in table 2; in particular it is just below $M(D^0)+M(\bar{D}^{*0})$. CLEO [8] has recently re-measured the D^0 mass, to reduce the statistical and systematical error on the $D^0\bar{D}^{*0}$ threshold.

Table 2: *Thresholds in the proximity of X(3872)*

Final state	$J/\psi\rho$	$J/\psi\omega$	D^0D^{*0}	$D^{\pm}D^{*\mp}$
Threshold	3872.4±0.3	3879.57±0.12	3871.8±0.4	3879.9±0.4

The evidence (BELLE [9], BABAR [10]) of X(3872) decays to $\gamma J/\psi$ imposes C=+1 for the state. Such results were obtained with samples of 275M (287M) B decays from BELLE (BABAR) and had a significance of 4(3.4) σ's. At present, both experiments have doubled their statistics and should exploit them to reinforce such assessment.

BELLE [9] claims also the observation of a 4σ signal in $B \to KJ/\psi\pi^+\pi^-\pi^0$ with a rate comparable to the $J/\psi\pi\pi$ mode. Even if the ω threshold is 7 MeV above, the three pions are clustering at the high end of their mass spectrum and seem to originate from the decay of a $J/\psi - \omega$ bound state. These evidences indicate that the decay is not conserving isospin, or that the state is not an isospin eigenstate.

Both CDF [11] and BELLE [12] performed an angular analysis on the $J/\psi\pi^+\pi^-$ reaction: the most likely assignments are $J^{PC} = 1^{++}, 2^{-+}$. The

J=2 assignment, though unfavored, cannot be ruled out, as the B coupling is anyway very small: BABAR and BELLE measure:

$$\mathcal{B}(B^+ \to K^+ X(3872)) * \mathcal{B}(X(3872) \to J/\psi \pi^+ \pi^-) = (1.14 \pm 0.20) \times 10^{-5}$$

Can we obtain an absolute value for $\mathcal{B}(B^+ \to K^+ X(3872))$? In principle, it can be obtained from a sample of fully reconstructed B mesons at the Y(4S) peak; by searching for a K in the decay products of the other B meson, and looking for peaks in the inclusive spectrum of what recoils against this kaon, BABAR [13] could set upper limits on $\mathcal{B}$(B $\to$ K X)$< 2.5 * 10^{-4}$.

A large variety of hypotheses have been made in the last years [14] on the nature of X(3872): $D\bar{D}^*$ molecule, cusp, tetraquark. The most appealing implication of the tetraquark model [15] is a set of predictions on possible charged partners which can be verified experimentally, but so far no candidates have been found in the proximity of X(3872). The tetraquark model predicts the hypothesis of the existence of a doublet of neutral states, and BELLE [16] and BABAR [17] reported the evidence of a peak in $D\bar{D}\pi$ approximately 3 MeV above the PDG average for the $J/\psi\pi\pi$ evidence. BELLE measures:

$$\mathcal{B}(B \to KX \to KJ/\psi\pi\pi)/\mathcal{B}(B \to KX \to D\bar{D}\pi) \approx 10\%$$

BABAR also reports an excess in the $D\bar{D}\gamma$ channel, with a branching ratio which is consistent with $\mathcal{B}(D^{0*} \to \gamma D^0)/\mathcal{B}(D^{0*} \to \pi^0 D^0) = 62\%$

Observation of a $D\bar{D}^*$ signal is quite challenging for CDF, but can provide further interesting informations on this state, as the cross check is based on a different production mechanism. Even without detecting the photon or the π^0, feeddown from X(3872) should produce a bump below $\psi(3770)$ in the $D\bar{D}$ mass plot.

2.2 $Z^{\pm}(4430)$: the first charged resonance with hidden charm content

This summer, the BELLE collaboration [18] showed one more structure in the $B \to K\psi'\pi^{\pm}$ Dalitz plot from a sample of 657M $B\bar{B}$ pairs. Outside the known bands corresponding to $K^*(890)$ and $K_2^*(1430)$, a 7 σ bump in the $\psi'\pi^{\pm}$ mass distribution is seen. The state, dubbed $Z^{\pm}(4430)$, has a mass M = 4433$\pm$4$\pm$1 MeV/c^2 and a total width $\Gamma = 44^{+17}_{-13}(stat)^{+30}_{-11}(syst)$ MeV.

Four decay modes of the ψ' are detected: e^+e^-, $\mu^+\mu^-$ and $J/\psi\pi\pi$ with $J/\psi \to \mu^+\mu^-, e^+e^-$. The resonance, is seen both in charged and neutral B

decays, but the significance in $B \to ZK^0_S$ does not exceed 3 σ. The measured product of branching fractions is

$$\mathcal{B}(B \to KZ^+(4430)) \times \mathcal{B}(Z^+(4430) \to \pi^+\psi') = (4.1 \pm 1.0 \pm 1.3) \times 10^{-5}$$

. This evidence opens a Pandora box: can we expect similar structures in the Dalitz plots of B decays to K, π and a lower lying charmonium resonance? How can we exclude possible artefacts from the interference between many broad kaon resonances between 1.2 and 1.9 GeV? BELLE analysis has excluded possible effects from the interference of up to three partial waves, but, with lower lying charmonia, the number of $K\pi$ excitations is going to be larger.

Significantly higher statistics is probably needed to resolve the complex structure of the three-body B decays to charmonium.

2.3 Y(3940): discovery, confirmation, doubts

The Y(3940) is a very broad resonance ($\Gamma = 92 \pm 24$MeV) discovered by BELLE [19] in B decays to $K\omega J/\psi$. The product of branching ratios is

$$\mathcal{B}(B \to Y(3940)K) * \mathcal{B}(Y(3940) \to J/\psi\omega) = (7.1 \pm 1.5 \pm 3.1) * 10^{-5}$$

If we assume to have just one state, and guess that $\mathcal{B}(B \to KY(3940)) < 4 * 10^{-4}$, we anyway get $\mathcal{B}(Y(3940) \to J/\psi\omega)) > 12\%$, and its partial width to $J/\psi\omega$ would be $\Gamma(Y(3940) \to J/\psi\omega) > 7MeV$, by far the largest width for an hadronic transition between charmonia - to be compared with, for instance, $\Gamma(\psi' \to J/\psi\pi\pi) = 0.16$ MeV.

The transition with emission of an ω is unique in the charmonium energy range, but has been observed by CLEO [20] in the bottomonium system: $\chi_{b1,2}(2P) \to \Upsilon(1S)$. Another possible insight on its nature is the proximity of the $D_s\bar{D}_s$ threshold, at 3936 MeV.

Recently, BABAR [21] has confirmed the observation of a peak in $J/\psi\omega$, but narrower and at a lower energy. The analysis is based on a slightly larger sample, 348 fb^{-1}, and gives M=3914.6±3.6±1.9 MeV/c^2 and Γ = 33±10±5 MeV. While it is simple to isolate the ω peak in the 3π system at higher energy, in the region below 4 GeV also the modeling of the phase space may induce some large systematic error. The $J/\psi\omega$ final state is accessible from almost all possible $c\bar{c}$ quantum numbers, and even an angular analysis would give a confusing output, if more states are merging in the same bump. The

Y(3940) signal still needs to be clarified experimentally, before handing it over to theory speculations.

3 Two photon physics

Two photon scattering allows to produce C=+1 states of charmonium with $J = even$. A review of the comprehensive study on the $\gamma\gamma$ production of lower charmonia is given from S.Eidelman [31] at this conference. Above open charm threshold, BELLE has discovered [22] the $\chi_{c2}(2P)$, decaying to $D\bar{D}$. The measured signal (64±18 events, for a 5.3 σ significance) allows to calculate the product $\Gamma \times \mathcal{B}(\gamma\gamma) \times \mathcal{B}(D\bar{D}) = 0.18 \pm 0.05 \pm 0.03$ keV. A confirmation from BABAR and the measurement of its branching ratio to $D\bar{D}^*$ and $D^*\bar{D}^*$ is needed.

4 Modern scanning with radiative return

The high luminosity available to asymmetric B factories allows them to turn the initial state radiation in a powerful tool for scanning the energy region across the open charm threshold, as well as the narrow Y(nS) resonances, with unprecedented statistical power.

4.1 New vector states: the Y(4260,4350,4660)

The ISR scanning is rapidly changing our whole understanding of vector charmonia. Only two years ago, BABAR [23] discovered the Y(4260), in the process $e^+e^- \to J/\psi\pi\pi$. Such discovery was soon confirmed by CLEO [24] and BELLE [25], who found the peak in their ISR data. The most recent values of the Y(4260) mass from these three experiments are summarized in the table 3.

Table 3: *Y(4260): mass and width measurements*

Experiment	M(MeV/c^2)	Γ(MeV)
BABAR	$4258 \pm 8^{+2}_{-6}$	$88 \pm 23^{+6}_{-4}$
BELLE	4263 ± 6	126 ± 18
CLEO	$4283^{+17}_{-16} \pm 4$	$70^{+10}_{-25} \pm 5$

CLEO-c [26] has then taken one data point (12 pb^{-1}) at $\sqrt{s} = 4.26$ finding an excess in $J/\psi\pi^+\pi^-$, $J/\psi\pi^0\pi^0$, and $J/\psi K\bar{K}$. As the real peak position is uncertain, only relative rates can be extracted from these data.

Hybrid charmonium ($c\bar{c}g$) or tetraquark ($cs\bar{s}\bar{c}$) are the most popular theoretical interpretations for this state at the moment.

Searching for the transition $Y(4260) \to \psi'\pi\pi$, BABAR finds evidence [27] of another state, named Y(4350), 90 MeV above the Y(4260) peak. This discovery is confirmed by BELLE soon after: the higher statistics allows to resolve a second peak, dubbed Y(4660) [28]. Both Y(4350) and Y(4660) do not seem to decay to $J/\psi\pi\pi$, a fact that still lacks theoretical explanation. All these states have a large branching ratio to the lower lying charmonia, while the coupling to open charm mesons is suppressed. The unexpected discovery of a new window to access lower charmonia may open new roads to search for the still missing narrow D states.

At this conference, BELLE has shown [29] the first hint of a possible bottomonium counterpart of the Y(4260): the Y(5S) transition rate to Y(1,2S) states is much large than the one of Y(4S). Only a scan [30] around the Y(5S) will allow to confirm the discovery of the first Y_b candidate.

4.2 Complete exclusive decomposition of the R scan from 3.8 to 5 GeV

The study of exclusive channels in ISR not only led to the discovery of new vector states but also allowed to understand better the wide resonances which decay to open charm and were measured from the R scans done by DASP, Mark I, Crystal Ball and BES. Such bumps, known as $\psi(4040), \psi(4160), \psi(4415)$ are listed in the PDG since decades, but without any details on the branching fractions to exclusive channels with charmed mesons.

Recently, CLEO scanned the 3.9-4.2 GeV region to optimize the yields of D and Ds mesons with a twelve point scan, and exclusive results on six two body channels ($D^{(*)}\bar{D}^{(*)}$, $D_s^{(*)}\bar{D}_s{}^{(*)}$) were published last year. The physics reach of such scan goes beyond the above mentioned purpose, as it casts light on the evolution of the R ratio across the resonance region.

Exploiting the large amount of ISR luminosity (22 pb^{-1}/0.1 GeV in the $\sqrt{s} \approx 4GeV$ region) and the excellent performance of its particle ID, BELLE has completed [31] the decomposition of the hadronic cross section into exclusive reactions $D\bar{D}$, $D^*\bar{D}$+c.c., $D^*\bar{D}^*$, and even $D\bar{D}_2^*(2460)$. The most unexpected

result from this analysis is the $D\bar{D}_2^*(2460)$ dominance in the $\psi(4415)$ signal [32], which may indicate a large D wave contribution to this charmonium state.

The sum of the exclusive channels saturates the $e^+e^- \to hadrons$ signal in this range, with the present statistical errors. Contributions from those channels with non strange mesons will allow to compute branching fractions and compare them with the theory predictions, mainly based on the Cornell coupled channel model.

5 Double $c\bar{c}$ in e^+e^- annihilation

Double charmonium production [33] in e^+e^- annihilation, first observed by BELLE in 2002, has been challenging theory predictions based on NRQCD since its discovery. The CM momentum spectrum of inclusive J/ψ's showed an abrupt loss of events much before the kinematical limit, where the color octet term is expected to give a dominant contribution. The mass distribution of objects recoiling against J/ψ and ψ' showed clear peaks belonging to η_c, χ_{c0} and η_c', discovered in B decays few months before. BELLE's signal has been later confirmed by BABAR.

Essentially, the signal from the region with $M_{recoil} < M(\eta_c)$ is consistent with zero, in disagreement with NRQCD predictions. On the other hand, the measured double charmonium cross section is more than five times bigger than the tree level NRQCD prediction. Higher order corrections in α_S and in the quark velocity are quite large.

Table 4 summarizes the updated experimental results vs NRQCD predictions (LO and NLO).

Table 4: $\sigma(e^+e^- \to V_{c\bar{c}}S_{c\bar{c}})$ *(in fb) vs. NRQCD predictions*

$V_{c\bar{c}}; S_{c\bar{c}}$	BELLE	BABAR	LO	NLO
$J/\psi; \eta_c(1S), \mathcal{B}_{>2}$	$25.6\pm2.8\pm3.4$	$17.6\pm2.8^{+1.5}_{-2.1}$	3.78 ± 1.26	$17.6^{+7.8}_{-6.3}$
$J/\psi; \chi_{c0}, \mathcal{B}_{>2}$	$6.4\pm1.7\pm1.0$	$10.3\pm2.5^{+1.4}_{-1.8}$	2.40 ± 1.02	
$J/\psi; \eta_c(2S), \mathcal{B}_{>2}$	$16.5\pm3.0\pm2.4$	$16.4\pm3.7^{+2.4}_{-3.0}$	1.57 ± 1.52	
$\psi'; \eta_c(1S)\mathcal{B}_{>0}$	$16.3\pm4.6\pm3.9$	-		
$\psi'; \chi_{c0}, \mathcal{B}_{>0}$	$12.5\pm3.8\pm3.1$	-		
$\psi'; \eta_c(2S), \mathcal{B}_{>0}$	$16.0\pm5.1\pm3.8$	-		

The comparison with theory calculations at full NLO [34] is possible only for the $J/\psi\eta_c$ channel and shows that an extra 80% is coming from resummation of $O(\alpha_s)$ terms, but an even larger contribution, 145±61% is expected from the higher order terms in v^2. From an experimentalist point of view, below open charm threshold, the challenge is represented by the detection of the $\chi_{c1,2}$ states between the χ_{c0} and $\eta_c(2S)$ peaks, which would allow to quantify the suppression of higher angular momenta in this process.

Given the dominance of NLO terms, theory calculations should be extended to higher orders to test their stability, in order to give a robust pattern of testable predictions on all lower lying C=+1 charmonia (i.e. not just J=0 ones). A good understanding of the double charmonium process below the open charm threshold is necessary, if we want to make statements on the quantum numbers of the other two bumps discovered above 3.8 GeV in the same process, which are described below.

5.1 Spectroscopy advances via the J/ψ recoil method

The J/ψ recoil method led BELLE to the discovery of two new resonances, dubbed X(3940) [35], and the X(4160) [36]. Both states have a significant decay rate to D^* mesons, and the recoil technique has been further refined. By fully reconstructing a large fraction of both charged and neutral D mesons, and exploiting the constraint on M(D), it is possible to single out the D and D^* peaks , and resolve the exclusive processes $e^+e^- \to J/\psi D^{(*)}\bar{D}^{(*)}$.

This allowed to improve the resolution on mass and width of these states, and to measure their branching fractions to open charm mesons: results from a sample of 693 fb^{-1} are summarized in table 5. Also the $e^+e^- \to J/\psi D\bar{D}$ cross section shows structures, that need more statistics to be resolved.

Table 5: *Properties of the new states found in double $c\bar{c}$*

State	signif.	M(MeV/c^2)	Γ(MeV)	decay	$\sigma(J/\psi X) \times \mathcal{B}_{out}$(fb)
X(3940)	6.3σ	$3942^{+7}_{-6} \pm 6$	$37^{+26}_{-15} \pm 8$	$D\bar{D}^*$	$13.9^{+6.4}_{-4.1} \pm 2.2$
X(4160)	5.4σ	$4156^{+25}_{-20} \pm 16$	$139^{+111}_{-61} \pm 22$	$D^*\bar{D}^*$	$24.7^{+12.8}_{-8.3} \pm 5.0$

Conventional charmonium interpretations for these states would point to the $\eta_c(3S)$ and $\chi_{c0}(3P)$ states. A confirmation of these states by BABAR is

needed, as well as further studies to detect them in other processes, e.g. from $\gamma\gamma$ or B decays.

6 The search for parabottomonia

The known bottomonium spectrum is far from complete: all the spin singlet states, i.e. the $\eta_b(1,2,3S)$ and the $h_b(1,2P)$ have not been found yet. Ironically enough, NRQCD is expected to yield reliable predictions especially for the lower lying parabottomonia, e.g. the $\eta_b(1S)$ mass is expected to be 9421 MeV at NLO [37], with a theory error (10 MeV) which is comparable to the one (9 MeV) due to the uncertainty on $\alpha_s(M_Z)$, and the NNLL estimate [38] of its two photon width at NNLL (0.66±0.09 keV), shows a remarkable stability with the renormalization scale.

CLEO-III data samples taken between 2001 and 2002 on the Y(nS) narrow resonances have been thoroughly analized [39], to search inclusively for the signatures of the radiative transitions $Y(2,3S) \to \gamma\eta_b(1,2S)$ and the double transitions $Y(3S) \to h_b(\pi^0,\pi^+\pi^-); h_b \to \eta_b\gamma$, resulting in upper limits which can rule out several theory predictions. Further studies on these samples are still under way, and will hopefully lead to the discovery of the η_b.

The asymmetric B factories have a large unexploited potential on these searches, as their ISR samples are comparable to the data taken by CLEO-III, but the indetermination on the energy of the radiative return prevents from doing inclusive searches. Recently, the BELLE collaboration has taken a record sample of 11M Y(3S) decays in less than a week of running time at the Y(3S) energy, which are currently being analyzed to improve CLEO limits, and hopefully to discover the long awaited parabottomonia. Anyway, an extensive program for the study of the whole parabottomonium spectrum will probably require at least ten times larger samples.

7 Acknowledgments

I'd like to thank S.Bianco, P.Gianotti and all the other organizers of this interesting Conference. I'm grateful to my colleagues in the Quarkonium Working Group, expecially to the experimentalists in BELLE, BABAR and CLEO who greatly contributed to the renewed interest in this field, for the large variety of exciting discussions shared in these last years.

References

1. N. Brambilla *et al.*, Yellow Report CERN-2005-005.
2. A. Abulencia *et al* [CDF II Collab.], *Phys. Rev. Lett.* **99**, 132001 (2007)
   D0 Collaboration, public note 5080-CONF (2007)
3. W. M. Yao *et al.* [Particle Data Group], *J. Phys.* **G33**, 1 (2006)
4. S. K. Choi *et al.* [BELLE Collab.], *Phys. Rev. Lett.* **91**, 262001 (2003)
5. D. Acosta *et al.* [CDF II Collab.], *Phys. Rev. Lett.* **93**, 072001 (2004)
6. V. M. Abazov *et al.* [D0 Collab.], *Phys. Rev. Lett.* **93**, 162002 (2004)
7. B. Aubert *et al.* [BABAR Collab.], *Phys. Rev.* **D71**, 071103 (2005)
8. C. Cawlfield *et al.* [CLEO Collab.], *Phys. Rev. Lett.* **98**, 092002 (2007)
9. K. Abe *et al.* [BELLE Collab.], arXiv:hep-ex/0505037.
10. B. Aubert *et al.* [BABAR Collab.], *Phys. Rev.* **D74**, 071101 (2006)
11. M. Kreps [on behalf of CDF Collab.], arXiv:hep-ex/0611004.
    The CDF Collab., CDF-PUB-7570.
12. K. Abe *et al.* [BELLE Collab.], arXiv:hep-ex/0505038.
13. B. Aubert *et al.* [BABAR Collab.], *Phys. Rev. Lett.* **96**, 052002 (2006)
14. E. S. Swanson, Phys. Rept. **429** (2006) 243
15. L. Maiani *et al.*, *Phys. Rev.* **D72**, 031502 (2005).
16. G. Gokhroo *et al.* [BELLE Collab.], *Phys. Rev. Lett.* **97**, 162002 (2006)
17. B. Aubert *et al.* [BABAR Collab.], arXiv:0708.1565 [hep-ex], (2007)
18. S.K. Choi *et al.* [BELLE Collab.], arXiv:0708.1790 [hep-ex],
19. S.K. Choi *et al.* [BELLE Collab.], *Phys. Rev. Lett.* **94**, 182002 (2005)
20. H. Severini *et al.* [CLEO Collab.], *Phys. Rev. Lett.* **92**, 222002 (2004)

21. A. Mokhtar [for the BABAR Collab.], these Proceedings
B. Aubert *et al.* [BaBar Collab.], arXiv:0711.2047 [hep-ex]

22. S. Uehara *et al.* [BELLE Collab.], *Phys. Rev. Lett.* **96**, 082003 (2006)

23. B. Aubert *et al.* [BABAR Collab.], *Phys. Rev. Lett.* **95**, 142001 (2005)

24. Q.He *et al.* [CLEO Collab.], *Phys. Rev.* **D74**, 091104 (2006)

25. C.Z.Yuan *et al.* [BELLE Collab.], *Phys. Rev. Lett.* **98**, 181804 (2007)

26. T.E.Coan *et al.* [CLEO Collab.], *Phys. Rev. Lett.* **96**, 162003 (2006) [arXiv:hep-ex/0602034].

27. B.Aubert *et al.* [BABAR Collab.], *Phys. Rev. Lett.* **98**, 212001 (2007)

28. X.L.Wang *et al.* [BELLE Collab.], *Phys. Rev. Lett.* **99**, 142002 (2007)

29. W.S.Hou [for the BELLE Collab.], these Proceedings

30. W. S. Hou, *Phys. Rev.* **D74**, 017504 (2006)

31. S. Eidelman [for the BELLE Collab.], these Proceedings

32. G. Packlowa [for the BELLE Collab.], arXiv:0708.3313 [hep-ex]

33. B. D. Yabsley, arXiv:0712.3183 [hep-ex].

34. G. T. Bodwin, J. Lee and C. Yu, arXiv:0710.0995 [hep-ph].

35. K. Abe *et al.* [BELLE Collab.], arXiv:hep-ex/0507019.

36. K. Adachi *et al.* [BELLE Collab.], arXiv:0708.3812 [hep-ex]

37. B. Kniehl *et al.*, *Phys. Rev. Lett.* **92**, 242001 (2004)

38. A. Penin *et al.*, *Nucl.Phys.* **B699**, 183 (2004)

39. M. Artuso *et al.* [CLEO Collaboration], *Phys. Rev. Lett.* **94**, 032001 (2005)

Frascati Physics Series Vol. XLVI (2007), pp. 29–42
HADRON07: XII Int. Conf. on Hadron Spectroscopy – Frascati, October 8-13, 2007
Plenary Session

NEW MESON STATES

Antimo Palano
from the BABAR Collaboration,
INFN and Dipartimento Interateneo di Fisica, Via Orabona 4, 70126 Bari, Italy

Abstract

We report on the most recent progress in charm and charmonium spectroscopy. Many new states have been discovered in the high statistics data sets from B-factories and CLEO-c experiment. Some of these particles are candidates for being exotic non $q\bar{q}$ states. We will concentrate on results obtained at the *BABAR* and Belle B-factories, with some confirmation from CLEO and CDF/D0. The *BABAR* results are based on up to $\approx 370\ fb^{-1}$ of e^+e^- collisions at the $\Upsilon(4S)$ resonance at the PEP-II linear accelerator at SLAC. The Belle results are from up to $\approx 700\ fb^{-1}$ at the KEK-B accelerator at KEK.

1 Charm Mesons

1.1 Introduction

During the last few years many new D, D_s, charmonium, and charmed baryon excited states have been discovered. Some of these states were not expected

theoretically; their masses, widths, quantum numbers, and decay modes did not fit the existing spectroscopic classification, which was based mostly on potential model calculations. The theoretical models had to be improved and new approaches have been developed to explain the data; the possibility of a non-quark-antiquark interpretation of these states has also been widely discussed.

1.2 Non Strange Charm Mesons

The parameters of the broad D_J states have been determined by Belle experiment [1]. They have performed a study of charged $B^- \to D^+\pi^-\pi^-$ and $B^- \to D^{*+}\pi^-\pi^-$ decays.

A study of the dynamics of these three-body decays finds that the $D^+\pi^-\pi^-$ final state is well described by the production of $D_2^*\pi^-$ and $D_0^*\pi^-$ followed by $D^{**} \to D\pi$. From a Dalitz plot analysis they obtain the mass and width of a broad scalar D_0^* meson:

$$M_{D_0^{*0}} = (2308 \pm 17 \pm 15 \pm 28)\,\mathrm{MeV}/c^2, \Gamma_{D_0^{*0}} = (276 \pm 21 \pm 18 \pm 60)\,\mathrm{MeV}.$$

The $D^*\pi\pi$ final state is described by the production of $D_2^*\pi$, $D_1'\pi$ and $D_1\pi$ with $D^{**} \to D^*\pi$. From a coherent amplitude analysis they obtain the mass and width of the broad D_1' resonance:

$$M_{D_1'^0} = (2427 \pm 26 \pm 20 \pm 15)\,\mathrm{MeV}/c^2,\ \Gamma_{D_1'^0} = (384^{+107}_{-75} \pm 24 \pm 70)\,\mathrm{MeV}.$$

1.3 Strange charm mesons

Much of the theoretical work on the $c\bar{s}$ system has been performed in the limit of heavy c quark mass using potential models [2] that treat the $c\bar{s}$ system much like a hydrogen atom. Prior to the discovery of the $D_{sJ}^*(2317)^+$ meson, such models were successful at explaining the masses of all known D and D_s states and even predicting, to good accuracy, the masses of many D mesons (including the $D_{s1}(2536)^+$ and $D_{s2}(2573)^+$) before they were observed. Several of the predicted D_s states were not confirmed experimentally, notably the lowest mass $J^P = 0^+$ state (at around 2.48 GeV/c^2) and the second lowest mass $J^P = 1^+$ state (at around 2.58 GeV/c^2). Since the predicted widths of these two states were large, they would be hard to observe, and thus the lack of experimental evidence was not a concern.

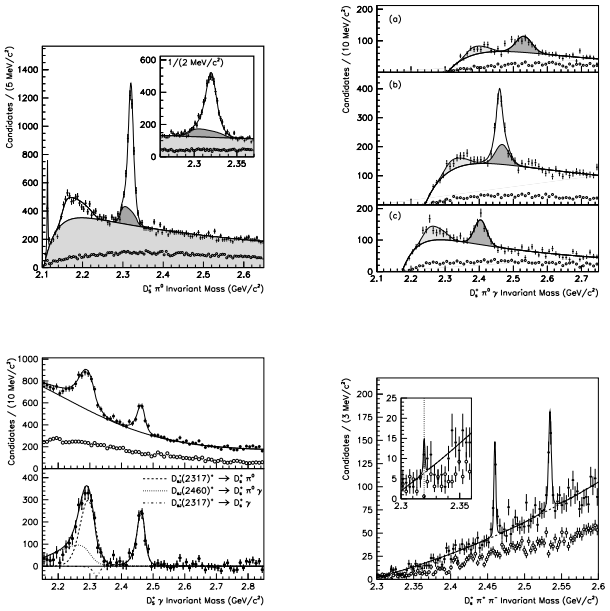

Figure 1: $D_s^+\pi^0$, $D_s^*(2112)^+\pi^0$, $D_s^+\gamma$, $D_s^+\pi^+\pi^-$ mass spectra from *BABAR* analysis.

1.4 $D_{sJ}^*(2317)^+$ and $D_{sJ}(2460)^+$

The $D_{sJ}^*(2317)^+$ meson has been observed in the decay $D_{sJ}^*(2317)^+ \to D_s^+\pi^0$ [3]. The mass is measured to be around 2.32 GeV/c^2, which is below the DK threshold. Thus, this particle is forced to decay either electromagnetically, of which there is no experimental evidence, or through the observed isospin-violating $D_s^+\pi^0$ strong decay. The $D_{sJ}(2460)^+$ meson has been observed decaying to $D_s^+\pi^0\gamma$, $D_s^+\pi^+\pi^-$, and $D_s^+\gamma$ [3].

An updated analysis of the $D_{sJ}^*(2317)^+$ and $D_{sJ}(2460)^+$ mesons using 232 fb^{-1} of $e^+e^- \to c\bar{c}$ data has been performed by *BABAR* experiment [4]. The following final states are investigated: $D_s^+\pi^0$, $D_s^+\gamma$, $D_s^*(2112)^+\pi^0$, $D_{sJ}^*(2317)^+\gamma$, $D_s^+\pi^0\pi^0$, $D_s^*(2112)^+\gamma$, $D_s^+\gamma\gamma$, $D_s^+\pi^\pm$, and $D_s^+\pi^+\pi^-$. The $D_s^+\pi^0$, $D_s^+\pi^0\gamma$ $D_s^+\gamma$ and $D_s^+\pi^+\pi^-$ mass spectra are shown in fig 1. A detailed analysis of in-

variant mass distributions of these final states including consideration of the background introduced by reflections of other $c\bar{s}$ decays produces the following mass values:

$$m(D_{sJ}^*(2317)^+) = (2319.6 \pm 0.2 \pm 1.4)\,\mathrm{MeV}/c^2$$
$$m(D_{sJ}(2460)^+) = (2460.1 \pm 0.2 \pm 0.8)\,\mathrm{MeV}/c^2,$$

where the first error is statistical and the second systematic. Upper 95% CL limits of $\Gamma < 3.8$ MeV and $\Gamma < 3.5$ MeV are calculated for the intrinsic $D_{sJ}^*(2317)^+$ and $D_{sJ}(2460)^+$ widths. The following branching ratios are measured:

$$\frac{\mathcal{B}(D_{sJ}(2460)^+ \to D_s^+\gamma)}{\mathcal{B}(D_{sJ}(2460)^+ \to D_s^+\pi^0\gamma)} = 0.337 \pm 0.036 \pm 0.038$$
$$\frac{\mathcal{B}(D_{sJ}(2460)^+ \to D_s^+\pi^+\pi^-)}{\mathcal{B}(D_{sJ}(2460)^+ \to D_s^+\pi^0\gamma)} = 0.077 \pm 0.013 \pm 0.008,$$

The data are consistent with the decay $D_{sJ}(2460)^+ \to D_s^+\pi^0\gamma$ proceeding entirely through $D_s^*(2112)^+\pi^0$.

The spin-parity of the $D_{sJ}^*(2317)^+$ meson has not been firmly established. The decay mode of the $D_{sJ}^*(2317)^+$ alone implies a spin-parity assignment from the natural J^P series $\{0^+, 1^-, 2^+, \ldots\}$, assuming parity conservation. Because of the low mass, the assignment $J^P = 0^+$ seems most reasonable, although experimental data have not ruled out higher spin.

Experimental evidence for the spin-parity of the $D_{sJ}(2460)^+$ meson is somewhat stronger. The observation of the decay to $D_s^+\gamma$ alone rules out $J = 0$. Decay distribution studies in $B \to D_{sJ}(2460)^+ D_s^{(*)-}$ favor the assignment $J = 1$. This suggests, when combined with the other observations, the assignment $J^P = 1^+$.

If the $D_{sJ}^*(2317)^+$ is the missing 0^+ $c\bar{s}$ meson state and the $D_{sJ}(2460)^+$ is the missing 1^+ $c\bar{s}$ meson state, the narrow width could be explained by the lack of an isospin-conserving strong decay channel. The low mass is more surprising and has led to the speculation that the $D_{sJ}^*(2317)^+$ $D_{sJ}(2460)^+$ and does not belong to the D_s^+ meson family at all but is instead some type of exotic particle, such as a four-quark state [5]. However, no state near the $D_{sJ}^*(2317)^+$ mass is observed decaying to $D_s^+\pi^\pm$.

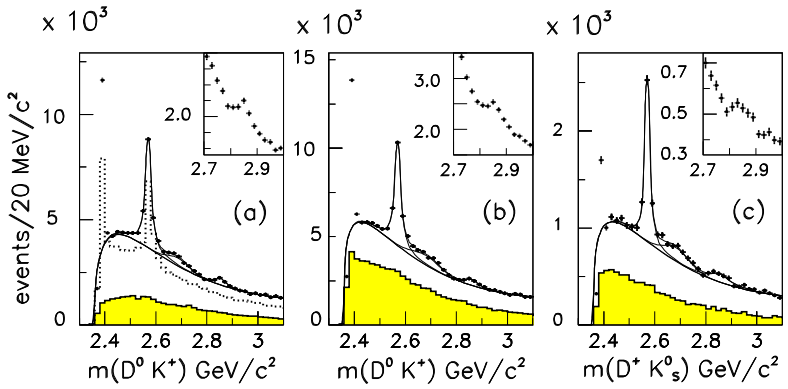

Figure 2: The DK invariant mass distributions for (a) $D^0_{K^-\pi^+}K^+$, (b) $D^0_{K^-\pi^+\pi^0}K^+$ and (c) $D^+_{K^-\pi^+\pi^+}K^0_s$. The shaded histograms are for the D-mass sideband regions. The dotted histogram in (a) is from $e^+e^- \to c\bar{c}$ Monte Carlo simulations.

1.5 New Strange Charmed Mesons

Here, a new $c\overline{s}$ state and a broad structure have been observed in the inclusive decay channels D^0K^+ (with $D^0 \to K^-\pi^+$, $D^0 \to K^-\pi^+\pi^0$) and $D^+K^0_S$ (with $D^+ \to K^-\pi^+\pi^+$), by *BABAR* experiment using 240 fb^{-1} of data. Selecting events in the D signal regions, Fig. 2 shows the D^0K^+ invariant mass distributions for the three channels. The three mass spectra present similar features. The single bin peak at 2.4 GeV/c^2 is due to a reflection from the decays of the $D_{s1}(2536)^+$ to $D^{*0}K^+$ or $D^{*+}K^0_S$ in which the π^0 or γ from the D^* decay is missed. A prominent narrow signal due to the $D_{s2}(2573)^+$ is visible. We also observe a broad structure peaking at a mass of approximately 2.7 GeV/c^2 and an enhancement around 2.86 GeV/c^2.

When the three mass distributions of are fitted simultaneously, the following values are obtained:

$$m(D_{sJ}(2860)^+) = (2856.6 \pm 1.5 \pm 5.0)\ \text{MeV}/c^2$$
$$\Gamma(D_{sJ}(2860)^+) = (47 \pm 7 \pm 10)\ \text{MeV}/c^2.$$

$$m(X(2690)^+) = (2688 \pm 4 \pm 3)\ \text{MeV}/c^2$$

$$\Gamma(X(2690)^+) = (112 \pm 7 \pm 36)\ \text{MeV}/c^2.$$

where the first errors are statistical and the second systematic.

At the same time Belle experiment studied the Dalitz plot of $B^+ \to \bar{D}^0 D^0 K^+$ [6]. They find that the decay proceeds dominantly via quasi-two-body channels: $B^+ \to \bar{D}^0 D_{sJ}^+(2700)$ and $B^+ \to \psi(3770)K^+$, where $D_{sJ}^+(2700) \to D^0 K^+$ with a mass $M = 2715 \pm 11^{+11}_{-14}$ MeV/c^2, width $\Gamma = 115 \pm 20^{+36}_{-32}$ MeV/c^2 and $J^P = 1^-$ (see fig. 3). Based on its observed decay channel, they interpret

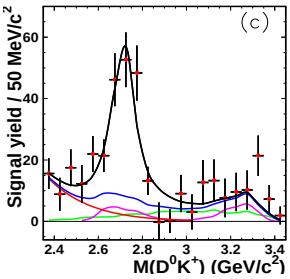

Figure 3: The Belle background-subtracted mass distributions $M(D^0K^+)$ for $M(D^0\bar{D}^0) > 3.85$ GeV/c^2 in $B^+ \to \bar{D}^0 D^0 K^+$.

the $D_{sJ}^+(2700)$ resonance as a $c\bar{s}$ meson.

2 Charmonium.

2.1 Introduction.

The charmonium model is a phenomenological model describing the bound state of the charm and anti-charm quark system [7]. In the case of the well-established states, there is very good agreement between the theory and experiment.

The four different production diagrams for states with charmonium, $c\bar{c}$ are shown in Fig. 4. The Fig. 4(a) is the color suppressed B meson decay where the b quark decays via $b \to c\bar{c}s$. The Fig. 4(b) is the two photon production of the $c\bar{c}$ states via the collision of two virtual photons. The Fig. 4(c) is the production of a pair of $c\bar{c}$ states via a virtual photon from the e^+e^- collision that decays into $c\bar{c}$ quark pairs along with the creation of a $c\bar{c}$ sea quarks. The Fig. 4(d) is the production of $c\bar{c}$ via initial state radiation (ISR) where

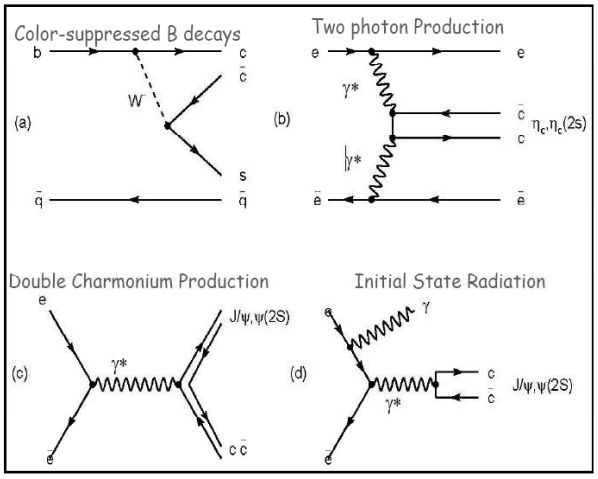

Figure 4: The four different production diagrams for states with charmonium.

either the electron or positron radiates a photon and creates a lower center of mass energy collision between the electron-positron pair that annihilates into a virtual photon that decays into a $c\bar{c}$ state.

The evidence for new charmonium-like [8] states began with the Belle announcement of the discovery of the X(3872) in the decay $X(3872) \to J/\psi\pi^+\pi^-$ in $B \to X(3872)K$. Following confirmations from the CDF, D0, and *BABAR* collaborations, there has been enormous interest in this state as a non-$q\bar{q}$ or exotic meson.

Now more charmonium-like states from the Belle and *BABAR* B-factories have been discovered. All of these new charmonium-like states do not appear to fit into the conventional $q\bar{q}$ meson spectroscopy of u, d, s, c quarks and they are possible candidates for exotic states such as molecules, 4-quark states, hybrids, etc.

2.2 $X(3872) \to J/\psi\pi^+\pi^-$.

A recent remeasurement by Belle of the X(3872) was performed with higher statistics and the resulting $J/\psi\pi^+\pi^-$ invariant masses are shown in Fig. 5 in the modes $B^\pm \to XK^\pm$, and $B^0 \to XK^0$ respectively. The two striking

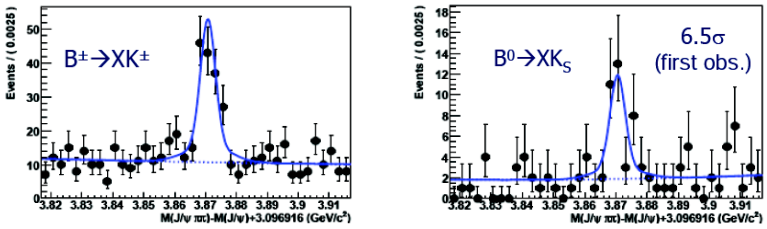

Figure 5: Recent Belle $J/\psi\pi^+\pi^-$ mass plots for X produced from charged and neutral B decays in $B \to XK$.

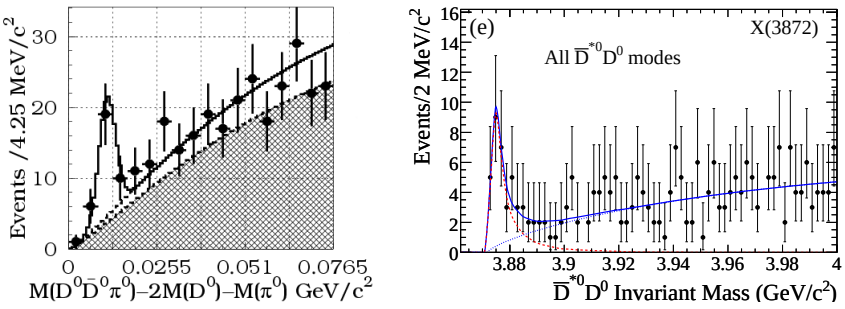

Figure 6: $m(D^0\bar{D}^0\pi^0) - m(D^0\bar{D}^0)$ from Belle and *BABAR* in $B \to D^0\bar{D}^0\pi^0 K$.

properties of the X(3872) are its mass which is observed right at $D^{*0}\bar{D}^0$ mass threshold, and its narrow width. The width is less then the detector resolutions and an upper limit of the width, $\Gamma(X) < 2.3\ MeV/c^2$, has been provided by Belle. The combined evidence favors $J^{PC} = 1^{++}$ for the X. The evidence for $X \to D^0\bar{D}^0\pi^0$ (Belle) and $X \to D^{*0}\bar{D}^0$ (*BABAR*) are shown in Fig. 6. The masses in the $D^{*0}\bar{D}^0$ final state appears to be about 3 MeV/c^2 above of the nominal X mass that is observed in the $J/\psi\pi^+\pi^-$ final state. This apparent mass shift could be explained [9] as a shift of the $D^{*0}\bar{D}^0$ final state mass which is sensitive to its orbital angular momentum due to the closeness of the $D^{*0}\bar{D}^0$ mass threshold.

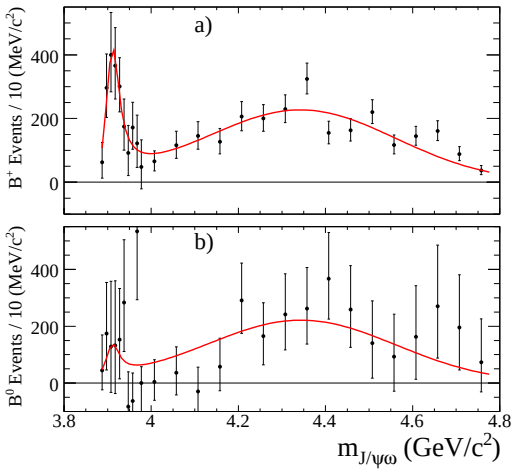

Figure 7: The *BABAR* $m(J/\psi\omega)$ mass distributions from (a) $B^+ \to J/\psi\omega K^+$ and (b)$B^0 \to J/\psi\omega K^0_S$

2.3 X(3940), Y(3930), Z(3940).

Belle has discovered three more charmonium-like states in a similar mass range via distinct production methods and decay modes. All three states have plausible charmonium model interpretations. The X(3940) was discovered by the recoil of the J/ψ in the double-charmonium production of $e^+e^- \to J/\psi X(3940)$ on 350 fb^{-1} of data [10]. It was found to decay to DD^* but not DD. This points towards an assignment as the η_c'' or possibly χ_{c1}'.

The Y(3930) was seen in the decay $B \to KY, Y \to J/\psi\omega$. In Belle's dataset of 278M B decays, they measured a mass and width of $m(Y) = 3943 \pm 11 \pm 13$ MeV/c^2 and $\Gamma(Y) = 87 \pm 22 \pm 26$ MeV [11]. This state was confirmed by *BABAR* [12], but using 385M B decays they measured it to have a mass and width of $m(Y) = 3914.3^{+3.8}_{-3.4} \pm 1.6$ MeV/c^2 and $\Gamma(Y) = 33^{+12}_{-8} \pm 1$ MeV (see fig. 7). An apparent interpretation of the Y(3930) state is the χ_{c1}' charmonium state. Finally, using 395 fb^{-1} of data, Belle has found a new resonance (Z(3930)) in the two-photon process $\gamma\gamma \to Z(3930)$ and decaying to $D\bar{D}$ [13]. The χ_{c2} charmonium assignment is an eminent choice based on its

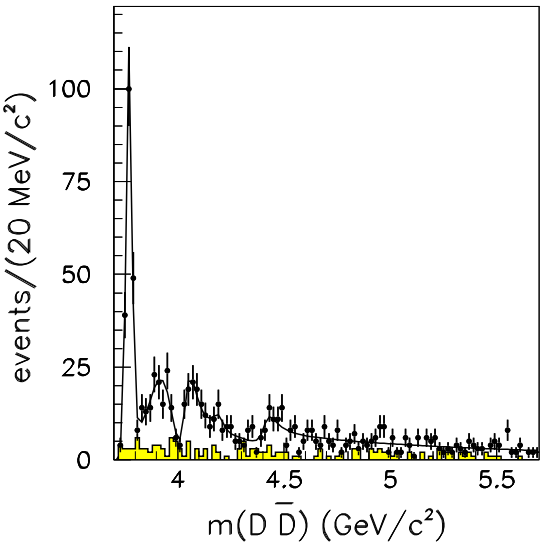

Figure 8: The ISR $D\overline{D}$ mass spectrum from *BABAR* . The shaded mass spectrum is from $D\overline{D}$ mass sidebands.

production, decay, mass, and width.

2.4 States produced in ISR.

Several new states have been discovered via initial-state-radiation production. The first of these was *BABAR*'s discovery [14] of a broad structure in the decay $e^+e^- \to \gamma_{ISR}Y(4260)$, $Y(4260) \to J/\psi\pi^+\pi^-$. Based on 211 fb^{-1} of data, the mass and width of this bump were measured to be $m(Y) = 4259 \pm 8^{+2}_{-6}\, MeV/c^2$ and $\Gamma(Y) = 88 \pm 23^{+6}_{-4}$. Because these states are produced in the annihilation of e^+e^-, they necessarily have $J^{PC} = 1^{--}$. However, all of the 1^{--} charmonium states have already been accounted for, making it difficult to accommodate the $Y(4260)$ as a $c\bar{c}$ state unless one or more of the previous charmonium state assignments is wrong. Following this discovery, CLEO performed a centre-of-mass energy scan and collected data directly at the Y(4260) resonance [15].

Reconstructing 16 decay modes, they confirmed *BABAR*'s discovery. Using 550 fb^{-1} of data, Belle has also confirmed *BABAR*'s discovery [16], measuring a mass of $m(Y) = 4247 \pm 12^{+17}_{-26}\ MeV/c^2$ and a width of $\Gamma(Y) = 108 \pm 19^{+8}_{-10}$. Additionally, Belle claims for a possible second much broader resonance at $m = 4008 \pm 40^{+72}_{-28}\ MeV/c^2$ with a width of $\Gamma = 226 \pm 44^{+87}_{-79} MeV$.

A charmonium state at this mass would be expected to decay predominantly to $D\overline{D}$, $D\overline{D}^*$ or $D^*\overline{D}^*$ [17]. A search for charmonium and other new states is performed by *BABAR* experiment in a study of exclusive initial-state-radiation production of $D\overline{D}$ events [18]. The data sample corresponds to an integrated luminosity of 384 fb^{-1}. The $D\overline{D}$ mass spectrum shows clear evidence of the $\psi(3770)$ plus other structures near 3.9, 4.1, and 4.4 GeV/c^2. No evidence for $Y(4260) \to D\overline{D}$ is observed, leading to an upper limit of

$$\mathcal{B}(Y(4260) \to D\overline{D})/\mathcal{B}(Y(4260) \to J/\psi\pi^+\pi^-) < 1.0$$

at 90% confidence level (see fig. 8).

BABAR's searched also for an accompanying $Y(4260) \to \psi(2S)\pi^+\pi^-$ decay with 298 fb^{-1} of data and turned up a structure at a higher mass that is incompatible with the Y(4260) [19]. This new state was found to have a mass of $m(Y) = 4324 \pm 24\ MeV/c^2$ and a width of $\Gamma(Y) = 172 \pm 33$ MeV. Belle confirmed this discovery on 670 fb^{-1} of data, measuring $m(Y) = 4361 \pm 9 \pm 9\ MeV/c^2$ with a width of $\Gamma(Y) = 74 \pm 15 \pm 10$ MeV, while finding further evidence for a higher resonance with a mass of $m(Y) = 4664 \pm 11 \pm 5\ MeV/c^2$ and width of $\Gamma(Y) = 48 \pm 15 \pm 3$ MeV [20] (see fig. 9). These findings now overpopulate 1^{--} four states, making it impossible to explain these particles within the charmonium model.

2.5 An exotic charmonium state?

The $Z^+(4430)$ particle is the latest discovery announced by Belle [21]. The remarkable aspect of this candidate state is a final state, $\psi(2S)\pi^+$, which is a charged charmonium-like state. The conventional quark model does not permit mesons to strongly decay into a charged state with hidden charm (or strangeness). Hence this candidate is a smoking gun or irrefutable evidence for an exotic meson. This particle is produced in color-suppressed B decays, $B \to \psi(2S)\pi^\pm K^\mp/K^0_S$. The analysis is based on an integrated data sample of 605 fb^{-1}. The Dalitz plot of this three body decay is shown 10. There is

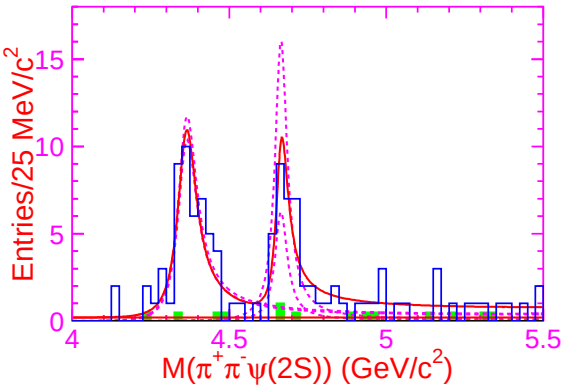

Figure 9: $\psi(2S)\pi^+\pi^-$ mass spectrum in ISR by Belle.

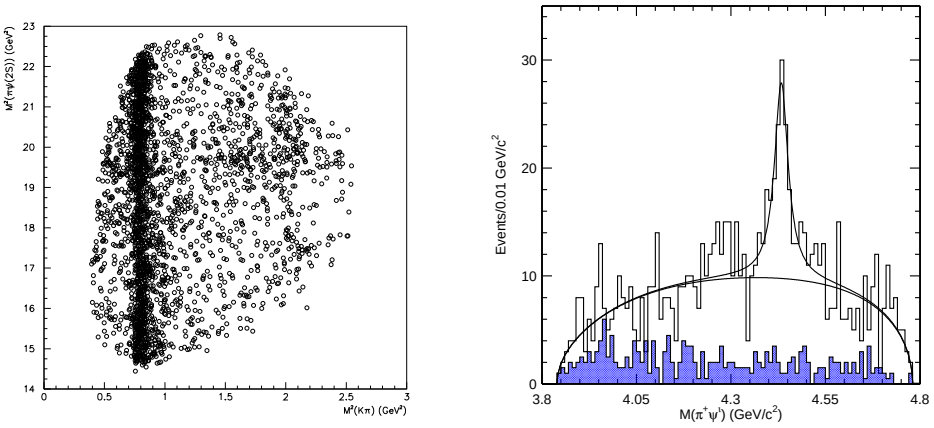

Figure 10: The Belle Dalitz plot of $M^2(\psi(2S)\pi^\pm)$ vs. $M^2(K\pi^\pm)$. The $M(K\pi^\pm)$ mass plot. .

visual evidence for at least three quasi-twobody decays, $B \to \psi(2S)K^*(890)$, $B \to \psi(2S)K_2^*(1430)$ and a possible new state, $B \to Z^+(4430)K$ with $Z^+ \to \psi(2S)\pi^+$. This is evidenced by the horizontal line is near $M(\psi(2S)\pi^+)^2 = 19.6\ (GeV/c^2)^2$. After having removed the $K^*(890)$ and the $K_2^*(1430)$ contribution, the $\psi(2S)\pi^+$ mass plot is always shown in Fig. 10 and a peak is evident at 4.43 GeV/c^2 over a broad background. The fit to the $\psi(2S)\pi^+$ mass distribution gives a mass of $m(Z) = 4433 \pm 4 \pm 1\ MeV/c^2$ and a width $\Gamma(Z) = 44^{+17}_{-13}(stat)^{+30}_{-11}(syst)\ MeV$.

However, one should be vary careful in performing cuts on a Dalitz plot where coherent amplitudes usually produce large interference patterns. A question arises: on very relevant issue like this why not to perform a full Dalitz plot analysis?

3 Conclusion

Although the nature of the newly discovered charm and charmonium resonances is not yet fully understood, the resonances are interpreted as molecular or hybrid states in most theoretical papers. It will be interesting to see if these interpretations are confirmed by future measurements and analyses.

References

1. K. Abe *et al.* (Belle Collaboration), Phys.Rev. **D69** (2004) 112002.
2. S. Godfrey and N.Isgur, Phys. Rev. **D32**, 189 (2005), M. Di Pierro and E. Eichten, Phys. Rev. **D64**, 114004(2001).
3. B. Aubert *et al.* (*BABAR* Collaboration), Phys. Rev. Lett. **90**, 242001(2003); D. Besson *et al* (CLEO Collaboration) Phys. Rev. Lett. **D68** 032002(2003); P. Krokovny *et al.* (Belle Collaboration), Phys. Rev. Lett. **91**, 262002(2003); B. Aubert *et al.* (*BABAR* Collaboration), Phys. Rev. **D69**, 031101(2004); K. Abe *et al.* (Belle Collaboration), Phys. Rev. Lett. **92**, 012002(2004).
4. B. Aubert *et al.* (*BABAR* Collaboration), Phys. Rev. **D69**, 031101(2004).
5. T. Barnes, F. E. Close and H. J. Lipkin, Phys. Rev. **D68**, 054006(2003).
6. J. Brodzicka *et al.* (Belle Collaboration), arXiv:0707.3491 (hep-ex).

7. E. Eichten *et al.* , Phys. Rev. **D17**, 3090 (1978); S. Godfrey and N.Isgur, Phys. Rev. **D32**, 189 (2005).

8. S.-K. Choi *et al.* (Belle Collaboration) Phys. Rev. Lett. **91**, 2620010 (2003).

9. W. Dunwoodie and V. Zielger, arXiv:0710.5191.

10. K. Abe *et al.* (Belle Collaboration) Phys. Rev. Lett. **99**, 082001 (2007).

11. A.-K. Choi *et al.* (Belle Collaboration), Phys. Rev. Lett. **94**, 182002 (2005).

12. B. Aubert *et al.* (*BABAR* Collaboration), arXiv:0711.2047 (hep-ex).

13. S. Uehara *et al.* (Belle Collaboration) Phys. Rev. Lett. **96**, 082003 (2006).

14. B. Aubert *et al.* (*BABAR* Collaboration), Phys. Rev. Lett. **95**, 142001 (2005).

15. T. E. Coan *et al.* (CLEO Collaboration), Phys. Rev. Lett **96**, 162003 (2006).

16. C. Z. Yuan *et al.* (Belle Collaboration), arXiv:0707.2541 (hep-ex).

17. E.J. Eichten, K. Lane, and C. Quigg, Phys. Rev. **D73**, 014014 (2006).

18. B. Aubert *et al.* (*BABAR* Collaboration), arXiv:0710.1371 (hep-ex).

19. B. Aubert *et al.* (*BABAR* Collaboration), Phys. Rev. Lett. **98**, 212001 (2007).

20. X.L. Wang *et al.* (Belle Collaboration), arXiv:0707,3699.

21. S.K. Choi *et al.* (Belle Collaboration), arXiv:0708.1790 (hep-ex).

Frascati Physics Series Vol. XLVI (2007), pp. 43–54
HADRON07: XII Int. Conf. on Hadron Spectroscopy – Frascati, October 8-13, 2007
Plenary Session

LATTICE QCD STATUS AND PROSPECTS

Christine Davies
Dept. of Physics and Astronomy, University of Glasgow, Glasgow, G12 8QQ, UK

Abstract

I review recent progress in lattice QCD calculations, concentrating on those relevant to flavor physics. There have been particularly exciting new results in the charm and strange sectors, providing precision tests against experiment and predictions needed to determine CKM elements. Results from a variety of methods for handling sea quarks are now allowing a comparison for the first time that gives added confidence to lattice QCD calculations.

1 Introduction

QCD is a key component of the Standard Model of particle physics. It gives us a rich spectrum of bound states of quarks and gluons whose properties are predictable from QCD if we can solve the theory. On the other hand, the confinement of quarks complicates the determination of the properties of

quarks from experiment because only hadrons can be studied directly. Lattice QCD enables QCD effects to be calculated 'from first principles' in the hadronic regime where the theory is strongly-coupled and nonlinear. Accurate results can provide stringent tests of QCD when compared to experiment as well as providing key input to our understanding of the Standard Model.

Key advances over the past decade in understanding how to discretise QCD accurately onto a space-time lattice are now allowing us to do this by bringing realistic calculations within the power of current day supercomputers [1]. We can now calculate the masses of 'gold-plated' hadrons (those with small width well below Zweig-allowed decay thresholds) and simple decay matrix elements that include at most one gold-plated hadron in the final state. Lattice QCD can then make an important contribution to flavor physics and the determination of elements of the Cabibbo-Kobayashi-Maskawa matrix. Experiment will achieve errors of a few percent on weak decay rates (and has already done this on mixing rates) for bottom and strange hadrons and needs theoretical input for the Standard Model prediction to extract the appropriate CKM element. I will concentrate on progress and new results in this area. The Proceedings of this year's lattice conference should be consulted for a more general view [2].

2 Lattice calculations

Lattice QCD proceeds by the numerical evaluation of the Feynman path integral [3] in a finite volume of 4-dimensional Euclidean space-time, split into a lattice of points with spacing a. We have to integrate over all possible values of the quark and gluon fields, weighted exponentially by (minus) the action, S (integral of the Lagrangian), of QCD. In the 'data generation' phase of the calculation we generate configurations of possible gluon fields that contribute most to the path integral. The analysis stage consists of 'measuring' various functions of the gluon fields that correspond to a particular observable, such as a correlation function from which a hadron mass can be determined, on each configuration and determining its mean value and statistical error.

The discretisation of the Lagrangian of QCD onto a space-time lattice gives systematic errors from the approximation of derivatives by finite differences. These appear as polynomials in the lattice spacing. Higher-order differencing schemes can be used which correct for the errors and raise the power of

a at which they first appear. This reduces the problem at fixed a or allows the same errors with a cheaper calculation with larger step-size. Since the cost of a calculation grows rapidly as a is reduced this is very important to achieve an affordable accurate calculation.

The gluon piece of the QCD action is relatively straightforward but the quark piece causes a lot of headaches and controversy. Since quark fields anticommute they must be integrated out of the path integral by hand giving an integral over gluon fields *only*, with the effect of quarks being implicit as functions of the gluon field through the Dirac matrix M. For valence quarks we must calculate the 'quark propagator', M^{-1}, and combine quark propagators to make hadron correlation functions. For sea quarks, we need to include $\det(M)$ in the generation of gluon field configurations that include the effect of sea quark-antiquark pairs being produced by energy fluctuations in the vacuum. The inclusion of $\det(M)$ is numerically very costly, especially as the quark mass $m \to 0$. Unfortunately it is the light u, d and s quarks that have a physically important rôle to play in the sea precisely because they can readily be generated by a vacuum energy fluctuation.

Early lattice calculations did not have the computer power to include sea quarks and so they were dropped in the 'Quenched Approximation', which has systematic errors at the 10% level. The numerical cost of including light u and d quarks means that it is important to use a fast and accurate discretisation of the quark Lagrangian so that affordable calculations can be done at moderate values of a (around 0.1fm). Calculations are done at multiple values of the u and d quark masses that are small as possible (values down to $m_s/10$ are now possible) and then extrapolations are made to the physical point. These extrapolations can be guided by chiral perturbation theory [3], which gives an expansion in powers of the u/d quark masses, provided that we are close enough to $m_{u/d} = 0$.

Controversy enters at this point since there are many different formulations for quarks in lattice QCD, depending on the approach taken to the linked problems of maintaining QCD chiral symmetry on the lattice and 'fermion doubling' (where the discretised Dirac Lagrangian describes 16 quarks instead of 1). Figure 1 gives a brief outline of the existing formalisms for which significant numbers of gluon field configurations including the effect of sea quarks have been made. The table briefly describes the good and bad points of each

formalism with respect to speed and chiral symmetry. There are other technical issues associated with each formalism that are discussed in the following reviews: staggered quarks [4]; domain wall quarks [5]; twisted mass [6] and clover [7].

	speed	χal sym.	collab.
Imp. stagg.	fast	OK	MILC/ HPQCD/ FNAL
DW	slow	good	RBC/ UKQCD
clover	fast	poor	PACS-CS QCDSF CERN
tm	fast	OK	ETMC

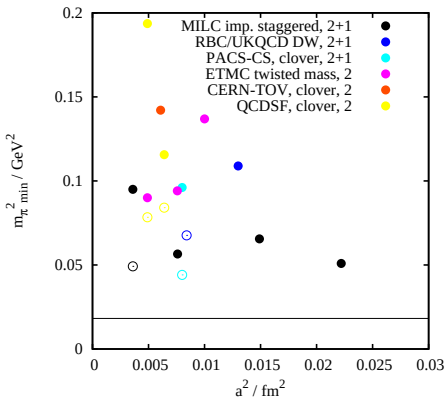

Figure 1: *Formalisms being used by various collaborations to include the effects of u/d sea quarks only ($n_f = 2$) or u, d and s ($n_f = 2 + 1$). The Table gives the names and features of different formalisms and the collaborations associated with them. dw is domain wall and tm twisted mass. The plot shows the parameters of configurations made. The axes are chosen so that is clear how close to the 'real world' (circled at $a = 0$ and $m_\pi = 0$) the configurations are. Systematic errors appear as a^2 and as powers of $m_{u/d}$ which is proportional to m_π^2. Open symbols give parameters for configurations currently being generated.*

Figure 1 shows the recent status of configurations [2]. Improved staggered quarks, having started first and being very fast, have the best coverage of different values of a, but other formalisms are now making good progress.

One basic calculation that a lot of different formalisms have now done is that of the pion decay constant f_π that parameterizes the purely leptonic decay of a charged π to leptons via a W boson. The leptonic decay rate is proportional to the square of f_π multiplied by the square of V_{ud}. Given a very accurate value for V_{ud} from superallowed β decay it is possible to determine f_π from the experimental leptonic decay rate and compare lattice QCD results to

this. The calculation of f_π is relatively simple in lattice QCD for formalisms that have enough chiral symmetry to have a partially conserved axial current (so that no renormalisation is required). Calculations need to be done at several different values of the u/d quark mass, $m_{u/d}$ and a to allow an extrapolation to the physical value of $m_{u/d}$ (that gives the physical value of m_π) and $a = 0$. Using improved staggered quarks or the new Highly Improved Staggered Quarks (HISQ) introduced by the HPQCD collaboration recently [8] agreement with experiment is obtained with 1.5% errors [9]. A similar error has now been obtained in the twisted mass formalism [10] with 2 flavors of sea quarks.

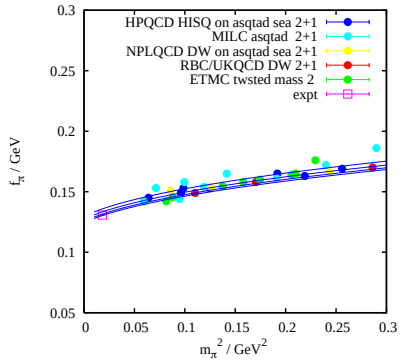

$$\begin{pmatrix} \mathbf{V_{ud}} & \mathbf{V_{us}} & \mathbf{V_{ub}} \\ \pi \to l\nu & K \to l\nu & B \to \pi l\nu \\ & K \to \pi l\nu & \\ \mathbf{V_{cd}} & \mathbf{V_{cs}} & \mathbf{V_{cb}} \\ D \to l\nu & D_s \to l\nu & B \to Dl\nu \\ D \to \pi l\nu & D \to K l\nu & \\ \mathbf{V_{td}} & \mathbf{V_{ts}} & \mathbf{V_{tb}} \\ \langle B_d|\overline{B}_d\rangle & \langle B_s|\overline{B}_s\rangle & \end{pmatrix}$$

Figure 2: On the left: A comparison of results for the pion decay constant obtained from different quark formalisms in lattice QCD including the effect of sea quarks [11, 6, 12, 13, 9]. The results are plotted against m_π^2, proportional to $m_{u/d}$. The lines give the chiral extrapolation for results using the HISQ formalism on the MILC ensembles at each of 3 values of a plus the $a = 0$ line obtained [9]. Some of the other formalisms only have results so far at a single value of a. However, there is encouraging agreement among them. The experimental point uses the π leptonic decay and V_{ud} from super-allowed β decay.
On the right: the CKM matrix with corresponding gold-plated processes that allow the value of each element to be determined by combining experiment with a lattice QCD calculation.

A comparison of different quark formalisms can also be made away from the chiral and continuum limits if discretisation errors are small. Encouraging agreement is seen for formalisms with good chiral symmetry in Figure 2. Results with the clover formalism do not agree as well, perhaps because of renormalisation issues [14]. It is very exciting that we are now able to do such a comparison and more of this will be done in future.

Handling heavy (b and c) quarks on the lattice raises rather different issues from that for light quarks. They appear only as valence quarks. Nonrelativistic formalisms (such as NRQCD [15] or the FNAL clover formalism [16]) have traditionally been used to avoid the problem of large discretisation errors set by powers of $m_Q a$. The new HISQ formalism, however, has such small discretisation errors that it allows c quarks (for which $ma \approx 0.5$) to be handled in the same formalism as u/d and s quarks.

3 Lattice Results 2007

Lattice QCD has an important contribution to make to determining the elements of the CKM matrix. For each CKM element there is a gold-plated electroweak decay or mixing process whose rate, as for π leptonic decay, will be (up to known kinematic factors) the product of that V_{ab}^2 and the square of a lattice QCD amplitude given as a decay constant, form factor or bag parameter that expresses the probability of the quarks confined inside the meson undergoing that process. The CKM matrix is given in Figure 2 with the corresponding processes. Cross-checks against other processes that are similar and well-known experimentally are important, as well as checking a variety of hadron masses. So a complete programme of this kind encompasses the whole range of flavor physics. Figure 3 shows the 2007 update of a range of quantities obtained from lattice QCD calculations with improved staggered sea quarks [1]. The impressive agreement across the board provides strong confirmation that lattice QCD is accurately describing the real world when sea quarks are included.

QCD has very few parameters: a mass for each quark flavor and a coupling constant. For current lattice QCD calculations we ignore the t quark and take the u and d quark masses to be the same. So 5 parameters need to be fixed by setting 5 gold-plated hadron masses or mass differences to their experimental values. The hadron mass being used should be sensitive to the quark mass it is fixing but preferably not sensitive to other quark masses to avoid a complicated

iterative tuning problem. For the improved staggered results shown here the lattice spacing is fixed from the radial excitation energy in the Υ system, i.e. the difference in mass between the Υ' and the Υ, which turns out to be insensitive to all quark masses [17]. The u/d quark mass is then fixed from M_π, the s quark mass from M_K [9, 18], the c quark mass (using HISQ) from M_{η_c} [9] and the b quark mass (using NRQCD) from M_Υ [17]. Other gold-plated quantities can then be calculated with no free parameters as shown in Figure 3. Lattice QCD then provides a very natural and accurate way to determine the parameters of QCD, and results from this have made their way into the particle data tables [19] with further work ongoing.

The decay constant of the K meson can be determined in the same way as that for the π described earlier. Again the experimental leptonic ($Kl2$) decay rate, using a value for V_{us} from elsewhere, can be used to give an experimental f_K to which the lattice result can be compared. This is the result given in Fig. 3. The lattice results in that plot come from HISQ valence u/d and s quarks on the MILC improved staggered ensembles, with lattice errors of 1-2%. The calculation of f_K/f_π in lattice QCD can be done with a smaller error - 0.6% for HISQ on the MILC ensembles - and this can be used, along with the ratio of the experimental leptonic decay rates [20, 19], to determine V_{us}/V_{ud} and therefore V_{us} [21]. In this way the HPQCD collaboration recently obtained $V_{us} = 0.2262(14)$ [9] and the MILC collaboration updated their previous f_K/f_π analysis [18] to give 0.2246(+25-13) [11]. Both are competitive with the result quoted from (semileptonic) $Kl3$ decay in the particle data tables of 0.2257(21). The final result is still completely dominated by theoretical error, however, and to improve it further will require working on larger lattice volumes and reducing the uncertainty in a.

V_{us} can also be determined from K semileptonic decay to $\pi l\nu$. Because this is now a 3-body decay the lattice QCD calculation determines a form factor that depends on q^2, the square of the 4-momentum transfer between the K and the π. The RBC/UKQCD collaboration have new results this year on the $K \to \pi$ form factor using the domain wall quark formalism [12]. The advantage of using K semileptonic decay for V_{us} is that the chiral extrapolation of the form factor is known to be relatively benign. This has been used in the past to estimate the difference of the form factor from 1.0 at $q^2 = 0$ (giving existing V_{us} determinations) but lattice QCD can give a more accu-

rate result. The RBC/UKQCD collaboration find $f_+(0) = 0.9644(49)$ yielding $V_{us} = 0.2249(14)$ [22], with lattice error 0.6% with results available currently at one value of the lattice spacing. Multiple values of a should allow this to be improved.

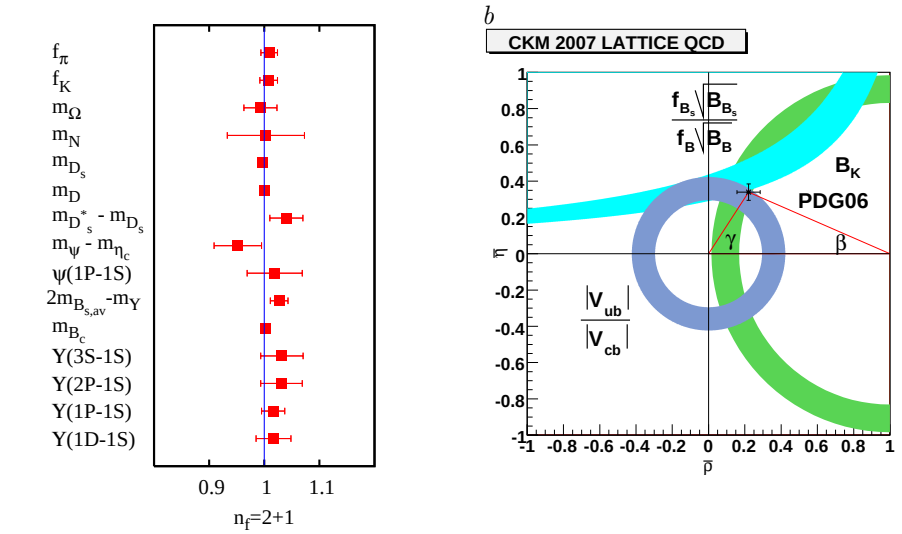

Figure 3: *a) The points show lattice QCD results divided by experiment for a range of quantities from light quark physics to bottomonium physics, compared to the right answer of 1.0. f_π and f_K are the π and K decay constants, described further in the text; m_N is the nucleon mass. $\Upsilon(1P-1S)$ denotes, for example, the difference in mass between the lowest χ_b states (spin-averaged) and the Υ. $\psi(1P-1S)$ is the same quantity for charmonium. The results come from analysis by the FNAL, HPQCD and MILC collaborations on the MILC ensembles that include improved staggered sea u, d and s quarks [9, 8, 23, 17, 24, 25]. b) Constraints on the unitarity triangle from the CKM matrix using current lattice results that include the effect of u, d and s sea quarks. The lattice errors dominate these constraints and they can be halved over the next two years. The cross gives the current constraint on the vertex quoted in the PDG [19].*

This year charm physics results have appeared that are as accurate as those in light quark physics using the new HISQ formalism [8]. One significant test, that has not been available from previous formalisms, is that of the

simultaneous determination of the spectrum of charmonium states and charm-light states with the same charm quark propagators. In QCD there is only one charm quark but most approximations to QCD, such as potential models, cannot handle both sets of states simultaneously since their internal dynamics is very different. On the lattice systematic errors are larger in charmonium so a very accurate discretisation is needed to do this. With HISQ we can fix the value that the charm quark mass needs to take to get the η_c mass correct. The D_d and D_s masses are then non-trivial *predictions* given a u/d mass from m_π and an s quark mass from m_K. Agreement with experiment is found with 7 MeV errors [9] This level of accuracy requires an understanding of corrections to the meson masses in the real world from QED effects and the fact that the u and d masses are not the same, which is very exciting.

The D and D_s decay constants can also be determined for HISQ to an accuracy of 2% using exactly the same method as for f_K and f_π. $f_{D_s} = 241(3)$ MeV [9] to be compared to an updated result from the Fermilab/MILC collaboration using clover quarks of 254(14) MeV. f_{D_s} in the clover formalism does require a renormalisation (and the error associated with this is included in the error estimate) and the mass of the charm quark is fixed from the D_s itself. The two lattice calculations agree well with very different charm quark formalisms, albeit on the same gluon ensembles. Further work is underway from other groups using other formalisms and ensembles. The leptonic decay rates of D and D_s mesons have now been measured by experiment and, given a value for the appropriate CKM element from elsewhere, can be converted into a value for the decay constant that can be compared to lattice results. f_{D_s} values from BaBar, Belle and CLEO-c, using $V_{cs} = V_{ud}$, are clustered around 270 MeV but with sizeable (15 MeV) errors [27]. On this quantity the lattice results are ahead of experiment, although experimental errors are expected to improve by a factor of two over the coming year.

Exclusive B semileptonic decay is an important route to determining the CKM elements V_{cb} and V_{ub}. This year the Fermilab/MILC collaboration have determined the form factor for $B \to D^* l\nu$ [28] at zero recoil, obtaining $h_{A_1}(1) = 0.942(12)(19)$ where the first error is statistical and the second systematic. Using the HFAG experimental average [29], this leads to a value for V_{cb} of $38.7(0.7)(0.9) \times 10^{-3}$ where the first error is from experiment and the second from the lattice. V_{ub} can be extracted from the exclusive $B \to \pi l\nu$ process.

Here lattice results are relatively poor because the important kinematic region is one in which the π mesons are moving fast and this gives a very noisy signal on the lattice. Work is underway to ameliorate this [30]. A recent theoretical determination of V_{ub} using combined lattice results from HPQCD and Fermilab/MILC along with light-cone sum rules gives $V_{ub} = 3.47(29) \times 10^{-3}$ [31]. The issue of compatibility of this result with that from the inclusive $b \to u$ decay is becoming an important one.

4 Conclusions

Lattice calculations including the full effect of u, d and s sea quarks are in excellent shape. Calculations using improved staggered quarks continue to get better and new results are now appearing from other quark formalisms. There have been significant new results this year in strange and charm physics.

In Figure 3 I have collected recent lattice results into a set of constraints on the upper vertex of the standard unitarity triangle plot [32]. The lattice inputs needed are B_K, f_K/f_π, $f_+(K \to \pi l\nu)$, $F(B \to D^* l\nu)$, $f_+(B \to \pi l\nu)$ and $f_{B_s}\sqrt{B_{B_s}}/f_B\sqrt{B_B}$. B_K and B_B are the mixing bag parameters for neutral K and B for which there were also new lattice results this year [5, 33]. It is important to use lattice results from the calculations including the full effect of u, d and s sea quarks. Old results in the quenched approximation are not reliable enough for this and have now been superseded. In the next two years the lattice errors on these CKM constraints should halve. The robustness of our error estimates will be further tested against experiment using other gold-plated results. $\Gamma_{e^+e^-}$ for ψ and Υ are good tests for c and b physics, for example. We have no free parameters when we do this and so it is a very stringent test. The era of precision lattice QCD calculations has really arrived.

5 Acknowledgements

I am grateful to the conference organisers for the opportunity to give this talk and to the following people for assistance in preparing it: Claude Bernard, Peter Boyle, Eduardo Follana, Elvira Gamiz, Andreas Jüttner, Andreas Kronfeld, Jack Laiho, Peter Lepage, Paul Mackenzie, Craig McNeile, Matthew Moulson, Gerrit Schierholz, Enno Scholz, Junko Shigemitsu, Jim Simone, Doug Toussaint, Carsten Urbach, Ruth van de Water and Kit Wong.

References

1. C. T. H. Davies *et al*, Fermilab, HPQCD, MILC, UKQCD collaborations, Phys. Rev. Lett.**92**:022001, 2004.
2. Proceedings of Lattice2007, Regensburg, July 2007, PoS LAT2007.
3. A recent textbook on Lattice QCD is: DeGrand and DeTar, Lattice methods for Quantum Chromodynamics, World Scientific, 2006.
4. A. Kronfeld, PoS LAT2007:016, 2007.
5. P. A. Boyle, PoS LAT2007:005, 2007, arXiv:0710.5880 [hep-lat].
6. C. Urbach, PoS LAT2007:022, 2007.
7. Y. Kuramashi, PoS LAT2007:017, 2007.
8. E. Follana *et al*, HPQCD, UKQCD collaborations, Phys. Rev. D**75**:054502, 2007.
9. E. Follana, C. T. H. Davies, G. P. Lepage and J. Shigemitsu, HPQCD and UKQCD collaborations, arXiv:0706:1726[hep-lat].
10. P. Boucaud *et al*, ETM collaboration, Phys. Lett. B**650**:304, 2007.
11. C. Bernard, *et al*, MILC collaboration, PoS LAT2007:090, 2007.
12. A. Jüttner, PoS LAT2007:014, 2007.
13. S. Beane *et al*, NPLQCD collaboration, Phys. Rev. D**75**:094501, 2007.
14. C. McNeile, PoS LAT2007:019, 2007.
15. P. Lepage *et al*, Phys. Rev. D**46**:4052, 1992.
16. A. X. El-Khadra, A. S. Kronfeld and P. B. Mackenzie, Phys. Rev. D**55**:3933, 1997.
17. A. Gray *et al*, HPQCD and UKQCD collaborations, Phys. Rev. D**72**:094507, 2005.
18. C. Aubin *et al*, MILC collaboration, Phys. Rev. D**70**:114501. 2004.

19. W. M. Yao *et al*, J. Phys. G**33**, 1 (2006).

20. F. Ambrosino *et al*, KLOE collaboration, Phys. Lett. B**632**:76, 2006.

21. W. J. Marciano, Phys. Rev. Lett. **93**:231803, 2004.

22. P. A. Boyle *et al*, RBC and UKQCD collaborations, arXiv:0710.5136[hep-lat].

23. D. Toussaint *et al*, PoS LAT2007:137, 2007.

24. I. Allison *et al*, HPQCD, Fermilab and UKQCD collaborations, Phys. Rev. Lett. **94**:172001, 2005.

25. S. Gottlieb *et al*, Fermilab and MILC collaborations, PoS LAT2005:203, 2006.

26. J. Simone *et al*, Fermilab and MILC collaborations, PoS LAT2007:370, 2007.

27. M. Artuso *et al*, CLEO collaboration, Phys. Rev. Lett.**99**:071802, 2007; T. K. Pedlar *et al*, CLEO collaboration, Phys. Rev. D**76**:072002, 2007; M. Artuso *et al*, CLEO collaboration, Phys. Rev. Lett. **95**:251801, 2005; B. Aubert *et al*, BaBar collaboration, Phys. Rev. Lett. **98**:141801, 2007; L. Widhalm, Belle collaboration, arXiv:0710.0420 [hep-ex].

28. J. Laiho, Fermilab and MILC collaborations, PoS LAT2007:358, 2007.

29. E. Barberio *et al*, HFAG, arXiv:0704.3575[hep-ex].

30. K. Y. Wong *et al*, PoS LAT2007:378, 2007.

31. J. M. Flynn and J. Nieves, Phys. Rev. D**76**:031302, 2007.

32. A. J. Buras, Les Houches 1997, hep-ph/9806471.

33. E. Gamiz *et al*, Fermilab and MILC collaborations, PoS LAT2007:354, 2007, C. T. H. Davies *et al*, HPQCD collaboration, PoS LAT2007:349, 2007.

Frascati Physics Series Vol. XLVI (2007), pp. 55–66
HADRON07: XII Int. Conf. on Hadron Spectroscopy – Frascati, October 8-13, 2007
Plenary Session

HEAVY ION COLLISIONS PHENOMENOLOGY OVERVIEW

Carlos A. Salgado*
Dipartimento di Fisica, Università di Roma "La Sapienza"
and INFN, Roma, Italy
and
Departamento de Física de Partículas and IGFAE,
Universidade de Santiago de Compostela, Spain

Abstract

The reach of collider energies in heavy-ion collisions has profoundly changed our understanding of QCD under extreme conditions. I review some these new developments and comment on the properties of the produced medium as extracted from experimental data, as well as the exciting new opportunities which will be open at the LHC.

QCD is a theory with a very rich dynamical structure but difficult to solve in many situations of phenomenological interest. This structure includes confinement and chiral symmetry breaking as main vacuum properties, a complex phase diagram and hadronic spectrum, asymptotic freedom and others. Among these, only asymptotic freedom has allowed to make extensive experimental tests of the precision of the theory in the short distance regime of the interaction. Lattice calculations allows to test the long distance dynamics giving excellent results for static quantities [1)], but with limitations to study out

of equilibrium situations. Most of the present phenomenological applications require, however, this real-time dynamics. Two examples arise: the recent interpretations about the structure of resonances on different mass regions of the spectrum – extensively discussed at this conference – or the transport properties of the hot medium created in nuclear collisions. The common question of both topics could be phrased as: *what are the relevant building blocks in situations where collective behavior appears and how they organize?*

The experiments of heavy-ion collisions at high energy attempt to answer this question for the hot part of the phase space diagram. The dynamical properties of the created matter, as the equation of state or different transport coefficients, are accessible experimentally and the findings are being interpreted theoretically. Several questions can be addressed which are normally categorized depending on the time scale as i) initial state of the system, ii) thermalization and evolution, iii) probes of the medium. We follow this classification in the following.

1 The initial state and the Color Glass Condensate

The relevant part of the colliding nuclei (or hadrons in general) wave function is dominated at high energies by Lorentz-boosted short-living quantum fluctuations which, with several degrees of sophistication, can be computed perturbatively once some initial condition is provided. This 'small-x gluons' are produced by sequential splitting in a branching process which makes its number to grow exponentially in rapidity $y = -\log x$, the variable playing the role of time for the evolution. When the density number of gluons is very high, the probability of fusion begins to compensate that of branching and a phenomenon of saturation appears [2] – the corresponding scale when this happens is called the saturation scale $Q^2_{\rm sat}$.

A successful implementation of this physics is known under the the generic name of *Color Glass Condensate* [3]. It provides a general framework for the whole collision, based on an effective theory separating the fast modes in the wave function from the *generated* slow modes, associated to small-x gluons, which are treated as classical fields. The quantum evolution equation of this setup is also known and, remarkably, recent attempts exist aiming to provide the link to the subsequent evolution into a thermal system [4].

Interestingly, this formalism provides a way of computing multiparticle

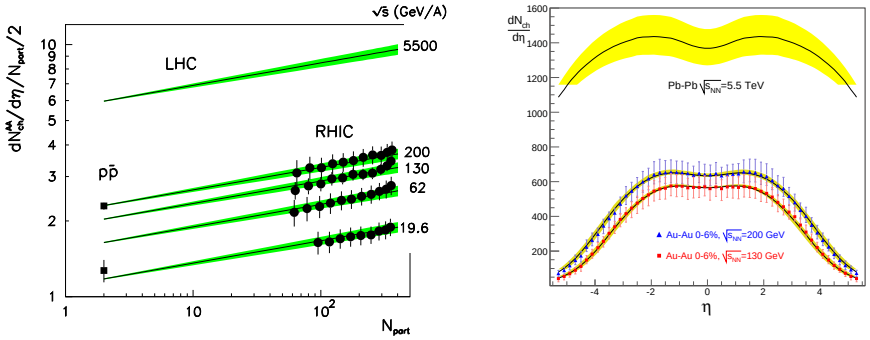

Figure 1: Left: Particle multiplicities in nuclear collisions at different energies using the simple parametrization (1) [6]. Right: Rapidity dependence of the multiplicities in central nucleus-nucleus collisions from Ref. [8].

production. In its simplest implementation, the total multiplicity is proportional to the saturation scale times a geometric factor [5]. A particularly economic description is given by the pocket formula [6]

$$\left.\frac{2}{N_{\rm part}}\frac{dN^{AA}}{d\eta}\right|_{\eta\sim 0} = N_0\sqrt{s}^{\lambda}N_{\rm part}^{\frac{1-\delta}{3\delta}}\,, \qquad (1)$$

where the energy and system size dependences ($\lambda = 0.288$ and $\delta = 0.79$) come from fits to DIS data and only a total normalization factor N_0=0.47 is introduced. Fig. 1 shows the comparison of this simple formula with available data [7]. A step forward in this phenomenology is the description of the experimental multiplicity data by the CGC evolution equations including part of the NLO corrections [8] – also plotted in Fig. 1.

2 The soft bulk and the hydrodynamical evolution

The evolution of the transient system formed in a heavy ion collision should follow a hydrodynamical behavior if thermal equilibrium is reached. In this case, the hydrodynamical equations give the evolution of flow fields, densities and pressures for a given initial configuration provided the equation of state of the system is known. The signals from this behavior are one of the most direct probes of the degree of thermalization in heavy-ion collisions – see e.g. [9] for

a recent summary.

A particularly important measurement is the azimuthal anisotropy with respect to the reaction plane for non-central nuclear collisions[1]: for these collisions, the interaction region is asymmetric with different gradients of density depending on the azimuthal angle. In a hydrodynamical medium, these gradients lead to different accelerations of the particles in the medium, so that the spatial anisotropy translates into momentum anisotropies. This effect is normally parametrized by the first non-trivial coefficient in the Fourier expansion, v_2, which, for the hydrodynamical interpretation, is called *elliptic flow* [10].

The experimentally measured anisotropy is in agreement with a hydrodynamical description with negligible viscosity. This has two important consequences, on the one hand, it indicates that the medium is in a local thermal equilibrium during the evolution and, on the other hand, it characterizes the medium as a liquid rather than a gas – which would present a large viscosity.

3 Hard processes as probes of the medium

Hard processes are those involving large momentum exchanges, for which the factorization theorems of QCD allow for a separation between short- and long-distance contributions to the cross section

$$\sigma^{AB\to h} = f_A(x_1, Q^2) \otimes f_B(x_2, Q^2) \otimes \sigma(x_1, x_2, Q^2) \otimes D_{i\to h}(z, Q^2)\,. \quad (2)$$

Here, the short-distance perturbative cross section, $\sigma(x_1, x_2, Q^2)$ takes place in a very short time, $1/Q$, so that it is unmodified in nuclear collisions. The long-distance terms are non-perturbative quantities involving scales $\mathcal{O}(\Lambda_{\rm QCD})$ which are modified by the interaction with the medium. These modifications allow to characterize the medium properties – see e.g. [11] for a recent review.

A conceptually simple example is the J/Ψ, whose production cross section can be written as

$$\sigma^{hh\to J/\Psi} = f_i(x_1, Q^2) \otimes f_j(x_2, Q^2) \otimes \sigma^{ij\to[c\bar{c}]}(x_1, x_2, Q^2) \langle \mathcal{O}([c\bar{c}] \to J/\Psi) \rangle\,, \quad (3)$$

where now $\langle \mathcal{O}([c\bar{c}] \to J/\Psi) \rangle$ describes the hadronization of a $c\bar{c}$ pair in a given state (for example a color octet) into a final J/Ψ. In the case that the pair is

[1] The extension of the nuclei allow for a definition of the relative distance of the centers at every collision – the impact parameter – so that different system geometries and densities can be studied.

produced inside a hot medium this long-distance part is modified: the potential between the pair is screened and the hadron is dissolved, making $\langle \mathcal{O}([c\bar{c}] \to J/\Psi)\rangle \to 0$. The experimental observation of this effect is a disappearance of the J/Ψ in nuclear collisions [12]. This suppression has been discovered in experiments at the CERN SPS [13] and measured also at RHIC [14].

The J/Ψ-suppression involves the modification of the non-perturbative hadronization probability. From the computational point of view, a theoretically simpler case is the modification of the *evolution* of fragmentation functions of high-p_t particles due to the presence of a dense or finite–temperature medium. Here, highly energetic partons, produced in a hard process, propagate through the produced matter, loosing energy by medium-induced gluon radiation – see Sec. 3.2.

3.1 Nuclear parton distribution functions

A good knowledge of the PDFs is essential in any calculation of hard processes. The usual way of obtaining these distributions is by a global fit of data on different hard processes (mainly DIS) to obtain a set of parameters for the initial, non-perturbative, input $f(x, Q_0^2)$ to be evolved by DGLAP equations. Nuclear analyses (most recent ones in Refs. [15, 16, 17]), using this procedure find a different initial condition, $f_A(x, Q_0^2)$, for the evolution which encodes the nuclear effects. Here, non-linear corrections to the evolution equations are usually neglected. An important consequence of these analysis is that present nuclear DIS and DY data can only constrain the distributions for $x \gtrsim 0.01$ – see Fig. 2. By chance, this region covers most of the RHIC kinematics. For the LHC, where much smaller values of x will be measured, a parallel proton-nucleus program will be essential as a benchmark for genuine hot-medium effects.

3.2 High-p_t studies in heavy ion collisions: Jet quenching

Jet structures are expected to be modified when the branching process initiated after the perturbative production of a high-p_T quark or gluon takes place into a thermal medium. The associated effects are generically known under the name of *jet quenching* and its simplest observational prediction is the suppression of the inclusive yields at high-p_t. This suppression can be traced back to a medium-modification of the fragmentation function $D_{i\to h}(z, Q^2)$ in Eq. (2).

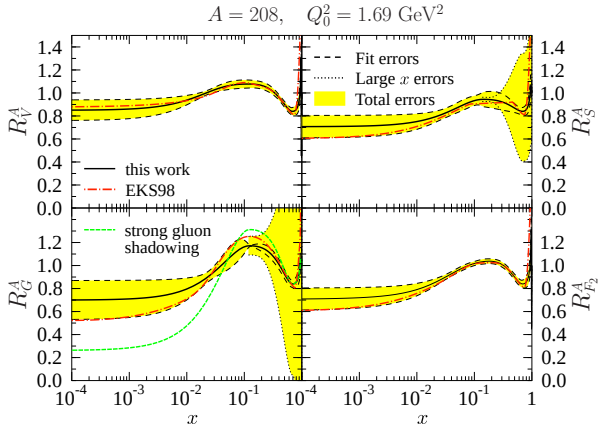

Figure 2: Ratios of nuclear to free proton PDFs for different flavors at the initial scale Q_0^2=1.69 GeV^2 from [16] with error estimates. The green line in the gluon panel is an attempt to check the strongest gluon shadowing supported by present data.

A way of implementing these effects is by a redefinition of the splitting functions

$$P^{\rm tot}(z) = P^{\rm vac}(z) + \Delta P(z,t), \tag{4}$$

in the DGLAP evolution equations. Although this redefinition has not ben proved in general, it has been found to work assuming an independence of the multiple gluon emission when the rescattering with the nuclei is present [18]. This possibility has been exploited in [19] where the additional term in the splitting probability is just taken from the medium-induced gluon radiation [18, 20, 21] by comparing the leading contribution in the vacuum case.

$$\Delta P(z,t) \simeq \frac{2\pi t}{\alpha_s} \frac{dI^{\rm med}}{dzdt}, \tag{5}$$

The fact that the medium-induced gluon radiation is finite in the soft and collinear limits allows for a simplification in which the medium-modified fragmentation functions are given by

$$D_{i\to h}^{\rm med}(z,Q^2) = P_E(\epsilon) \otimes D_{i\to h}(z,Q^2) \tag{6}$$

and where $P_E(\epsilon)$ is given by a Poisson distribution [21]. The medium-induced energy loss probability distribution $P_E(\epsilon)$ – known as *quenching weights*, QW – depends only on the in-medium path-length of the hard parton and the transport coefficient $\hat{q}$. The length is given by geometry and it is not a free parameter of the calculation – although different geometries, including expansion, hydrodynamics, etc. could lead to slightly different results [24]. The transport coefficient encodes all the properties of the medium accessible by this probe and can be related to the average transverse momentum gained by the gluon per mean free path in the medium. Taking it as a free parameter of the calculation and fitting available data, a value of

$$\hat{q} = 5....15\,\mathrm{GeV}^2/\mathrm{fm} \tag{7}$$

is obtained [22, 23]. Once this value is obtained, the formalism predicts the effects for other observables as heavy-quark suppression. In Fig. 3 the description of the data for light mesons (used to fit the value of $\hat{q}$) and non-photonic electrons is shown. For the last, the uncertainty on the relative contribution from charm and beauty decays, shown by a band, is not yet under good theoretical control. The description of the data within the formalism is reasonable but an experimental separation of both contribution will help to understand whether other effects [29] are at work .

3.3 Jets

The most promising signal of the dynamics underlying jet quenching is the study of the modifications of the jet structures [30] in which the characteristic angular dependence of the associated medium-induced radiation should be reflected. Experimentally, the main issue to overcome is the jet energy calibration in a high-multiplicity environment where small-p_t cuts and more or less involved methods of background subtraction will be needed. From a theoretical point of view, identifying signals with small sensitivity to these subtractions is of primary importance [30]. Due to these limitations, jet studies are not possible in AuAu collisions at RHIC but will be abundant at the LHC up to transverse energies of several hundred GeV. In the meantime, jet-like structures are being studied at RHIC by means of two- and three-particle correlations.

An important step forward is the first measurement of two particle azimuthal correlations at large transverse momentum, with negligible combinato-

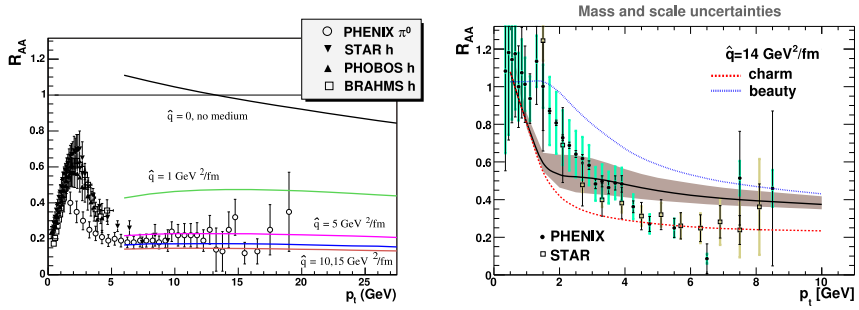

Figure 3: Left: Nuclear modification factor, R_{AA}, for light hadrons in central AuAu collisions [22]. Data from [25]. Right: R_{AA} for non-photonic electrons with the corresponding uncertainty from the perturbative benchmark on the relative b/c contribution [26]. Data from [27, 28]

rial background [32]. These data support the picture of a very opaque medium with large energy losses, but with a broadening of the associated soft radiation hidden underneath the cut-off. Lowering this transverse momentum cut-off the different collaborations find non-trivial angular structures [33] in the form of a double-peak structure, in striking contrast with the typical Gaussian-like shape in proton-proton or peripheral AuAu collisions. Similar structures are found in large angle medium-induced radiation due to the LPM and Sudakov suppression of collinear gluons with energy $\omega \lesssim 2\hat{q}^{1/3} \sim 3$ GeV [31]. In this framework, most of the energy is lost by radiation with negligible deposition in the medium. On the opposite limit, if a large fraction of the jet energy is deposited fast enough into a hydrodynamical medium it will be diffused by sound or dispersive modes. For very energetic particles, traveling faster than the speed of sound in the medium, a shock wave is produced with a characteristic angle which could also be at the origin of the measured structures [34]. Another interpretation of this effect is in terms of Cherenkov radiation [35].

4 Counting the valence quarks of exotic hadrons

Very interesting effects appear in the intermediate region of $2 \lesssim p_\perp \lesssim 6$ GeV/c. The most spectacular of them is the appearance of valence quark number scal-

ing laws for baryons and mesons: (i) R_{CP}, the normalized ratio of high-p_T yields in central to peripheral collisions, seems to depend only on the valence number of the produced particle; (ii) the elliptic flow parameter v_2 is universal when plotted as $v_2(p_\perp/n)/n$, n being the number of valence quarks. A successful model to describe these features is a two component soft+hard model, in which the soft spectrum is assumed to come from the recombination of quarks in a medium in thermal equilibrium [36]. The hard part of the spectrum is given by Eq. (2) with a simplified treatment of the energy loss.

In [37] this model has been extended to the case of a 4-quark meson to study the sensitivity of these observables to make a case for the discovery of exotic states in heavy-ion collisions, in particular for the $f_0(980)$. In Fig. 4, R_{CP} for $\Lambda+\bar{\Lambda}$ baryons is compared with experimental data from RHIC together with the model expectations for the corresponding effects on the $f_0(980)$ as being a normal meson or a 4-quark state – the description for other hadrons could be found in [37].

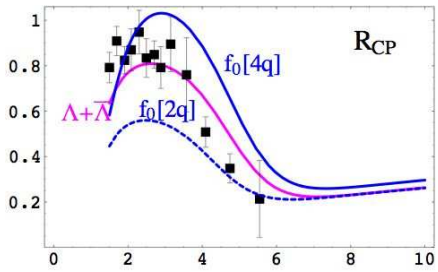

Figure 4: R_{CP} for $\Lambda+\bar{\Lambda}$ and for $f_0(980)$ considered as a $q\bar{q}$ or a 4-quark meson.

Although the analysis presented here is based on a given model implementation, the experimental facts on the quark counting rules indicate that the effect is more general and would survive more sophisticated implementations. These findings show that heavy-ion collisions are ideal tools to study the content of different resonances and to find a definitive answer to the structure of these exotic states. Clearly such a measurements are, at the same time, excellent playgrounds for the study of the relevant degrees of freedom of the produced medium.

5 Final comments

Heavy-ion collisions, together with spectroscopy, have been the two most active areas of discoveries in the strong interaction in the last years. Both deal with the structure of extended objects for which first principle computations in QCD present some limitations. In these conditions a cross talk between theory and experiment is essential to make progress on the understanding of how macroscopic structures organize in QCD and what are their relevant building blocks.

The hot medium created in heavy-ion collisions is found to be extremely dense and with large cross sections. This leads to interesting transport properties, as a very small viscosity or a large $\hat{q}$, which are difficult to reconcile with a perturbative approach. Interestingly, this limitations is leading to a flourishing activity on the relation of these findings with theoretically computable quantities in String Theory by the AdS/CFT correspondence which is opening new ways of facing the challenges on the study of collective properties at the fundamental level.

In the next years, the LHC will provide the largest jump in energy in heavy ion collisions ever. With $\sqrt{s}$ =5.5 TeV/A these collisions will explore *terra incognita* in the phase space diagram of QCD.

Acknowledgements

CAS is supported by the FP6 of the European Community under the contract MEIF-CT-2005-024624.

References

1. C. Davies, these proceedings.
2. L. V. Gribov, E. M. Levin and M. G. Ryskin, Phys. Rept. **100** (1983) 1.
3. For a recent review see e.g. E. Iancu and R. Venugopalan, hep-ph/0303204.
4. T. Lappi and L. McLerran, Nucl. Phys. A **772** (2006) 200; P. Romatschke and R. Venugopalan, Phys. Rev. D **74** (2006) 045011.
5. D. Kharzeev and M. Nardi, Phys. Lett. B **507** (2001) 121.

6. N. Armesto, C. A. Salgado and U. A. Wiedemann, Phys. Rev. Lett. **94** (2005) 022002

7. B. B. Back *et al.*, Nucl. Phys. A **757** (2005) 28.

8. J. L. Albacete, arXiv:0706.1251 [hep-ph].

9. T. Hirano, arXiv:0704.1699 [nucl-th].

10. J. Y. Ollitrault, Phys. Rev. D **46** (1992) 229.

11. C. A. Salgado, arXiv:0706.2264 [hep-ph].

12. T. Matsui and H. Satz, Phys. Lett. B **178** (1986) 416.

13. C. Baglin *et al.* [NA38], Phys. Lett. B **220** (1989) 471; M. C. Abreu *et al.* [NA50], Phys. Lett. B **410** (1997) 337; Phys. Lett. B **477** (2000) 28; R. Arnaldi *et al.* [NA60], Nucl. Phys. A **774** (2006) 711.

14. S. S. Adler *et al.* [PHENIX], Phys. Rev. C **69** (2004) 014901.

15. D. de Florian and R. Sassot, Phys. Rev. D **69** (2004) 074028.

16. K. J. Eskola, V. J. Kolhinen, H. Paukkunen and C. A. Salgado, JHEP **0705** (2007) 002 [arXiv:hep-ph/0703104]; arXiv:0707.0060 [hep-ph]; arXiv:0709.4525 [hep-ph].

17. M. Hirai, S. Kumano and T. H. Nagai, arXiv:0709.3038 [hep-ph].

18. X. N. Wang and X. f. Guo, Nucl. Phys. A **696**, 788 (2001).

19. N. Armesto, L. Cunqueiro, C. A. Salgado and W. C. Xiang, arXiv:0710.3073 [hep-ph].

20. R. Baier, *et al.* Nucl. Phys. B **484** (1997) 265; B. G. Zakharov, JETP Lett. **65** (1997) 615; U. A. Wiedemann, Nucl. Phys. B **588** (2000) 303; M. Gyulassy, P. Levai and I. Vitev, Nucl. Phys. B **594** (2001) 371.

21. C. A. Salgado and U. A. Wiedemann, Phys. Rev. D **68** (2003) 014008; R. Baier, Y. L. Dokshitzer, A. H. Mueller and D. Schiff, JHEP **0109** (2001) 033.

22. K. J. Eskola, H. Honkanen, C. A. Salgado and U. A. Wiedemann, Nucl. Phys. A **747** (2005) 511.

23. A. Dainese, C. Loizides and G. Paic, Eur. Phys. J. C **38** (2005) 461.

24. T. Renk and K. J. Eskola, Phys. Rev. C **75** (2007) 054910.

25. S. S. Adler *et al.* [PHENIX], Phys. Rev. C **69** (2004) 034910; J. Adams *et al.* [STAR], Phys. Rev. Lett. **91** (2003) 172302; B. B. Back *et al.* [PHOBOS], Phys. Lett. B **578** (2004) 297; I. Arsene *et al.* [BRAHMS], Phys. Rev. Lett. **91** (2003) 072305. M. Shimomura [PHENIX], nucl-ex/0510023.

26. N. Armesto, M. Cacciari, A. Dainese, C. A. Salgado and U. A. Wiedemann, Phys. Lett. B**637** (2006) 362; C. A. Salgado Nucl.Phys. A**783** (2007) 225

27. B. I. Abelev *et al.* [STAR], Phys. Rev. Lett. **98** (2007) 192301.

28. A. Adare *et al.* [PHENIX], Phys. Rev. Lett. **97** (2006) 252002.

29. S. Wicks, W. Horowitz, M. Djordjevic and M. Gyulassy, Nucl. Phys. A **784** (2007) 426.

30. C. A. Salgado and U. A. Wiedemann, Phys. Rev. Lett. **93** (2004) 042301.

31. A. D. Polosa and C. A. Salgado, Phys. Rev. C **75** (2007) 041901.

32. J. Adams *et al.* [STAR], Phys. Rev. Lett. **97** (2006) 162301.

33. S. S. Adler *et al.* [PHENIX], Phys. Rev. Lett. **97** (2006) 052301; arXiv:0705.3238 [nucl-ex].

34. H. Stoecker, Nucl. Phys. A **750**, 121 (2005); J. Casalderrey-Solana, E. V. Shuryak and D. Teaney, hep-ph/0411315.

35. V. Koch, A. Majumder and X. N. Wang, Phys. Rev. Lett. **96** (2006) 172302; I. Dremin, Sov. Phys. Usp. **25** (1982) 634 [Usp. Fiz. Nauk **137** (1982) 749].

36. R. J. Fries, *et al.* Phys. Rev. C **68**, 044902 (2003).

37. L. Maiani, A. D. Polosa, V. Riquer and C. A. Salgado, Phys. Lett. B **645** (2007) 138; Updated in arXiv:0707.4578 [hep-ph].

Frascati Physics Series Vol. XLVI (2007), pp. 67–78
HADRON07: XII Int. Conf. on Hadron Spectroscopy – Frascati, October 8-13, 2007
Plenary Session

THE MANY USES OF CHIRAL EFFECTIVE THEORIES

Elisabetta Pallante
*Centre for Theoretical Physics, University of Groningen, The Netherlands**

Abstract

I review basic concepts of chiral effective field theories guided by an historical perspective: from the first ideas to the merging with other effective frameworks, and to the interplay with lattice field theory. The impact of recent theoretical developments on phenomenological predictions is reviewed with attention for rare decays, and charm physics. I conclude with a critical look at future applications.

1 A retrospective

Effective field theories are the protagonists of our modern view of quantum field theory. The idea that any sensible theory is a priori valid only on a limited interval of energies, else distances, became more and more accepted during the last decades. Any such theory carries a dependence on a particular

high energy scale, *the ultraviolet cutoff* which determines its range of validity. It contains the low energy or large distance behaviour of a more fundamental theory. Only the ultimate fundamental theory, if any, must be valid at all energies or distances. This broadened view led us to abandon the concept of renormalizability in a strict sense as the necessary requisite for a theory to be an acceptable theory. Effective field theories are by now one of the main theoretical instruments for exploring a large set of particle physics phenomena, from the very low-energy strong interactions to the candidate models for the physics beyond the electroweak symmetry breaking scale. In this writeup I will care for concepts more than numbers, and make use of what an historical perspective can teach us.

Effective field theories (EFT) started as *phenomenological lagrangians*, aimed at describing the dynamics of strongly interacting matter, mesons and baryons, at low energy. In general, they were aimed at describing any system where the dynamics is governed by a given internal symmetry and its spontaneous breaking. The original works date in the 1960's, mainly by Schwinger, Cronin, Weinberg [1, 2, 3], and the works by Callan, Coleman, Wess, Zumino [4, 5]. The structure of phenomenological lagrangians was purely based on symmetries and much inherited from current algebra; here, the low energy strong interactions could be described by a formulation alternative to Quantum Chromodynamics (QCD)[1], the theory with quarks and gluons degrees of freedom.

Chiral Perturbation theory (ChPT) was formulated more than a decade later by Gasser and Leutwyler in two by now well known papers [7, 8] in 1984 and 1985. ChPT is the descendant of phenomenological lagrangians. It is a particular example of a non-decoupling effective theory. Its fundamental symmetry is the chiral symmetry, with group $SU(2)_L \times SU(2)_R$ or $SU(3)_L \times SU(3)_R$[2], spontaneaously broken down to its diagonal subgroup. The derivation of the ChPT lagrangian and properties by a path integral formulation [7] clarifies its field theoretical connection to QCD. Somewhat more recently Heavy Quark effective theory (HQET) was introduced as a good theoretical approximation

[1] Phenomenological lagrangians evolved together with the concept of *quarks* degrees of freedom [6] and the description of strong interactions with a non abelian gauge theory

[2] I will omit the subscripts L, R in the following.

to describe the dynamics of systems with one heavy quark [9]. It is the merging of these two formulations that gave rise to new types of effective field theories, namely the Heavy Baryon ChPT [10] (HBChPT) for describing the interactions amongst baryons and light mesons, and the Heavy-Light Meson ChPT [11] (HLChPT) for describing the dynamics of bound meson systems such as D, D_s, B, and B_s.

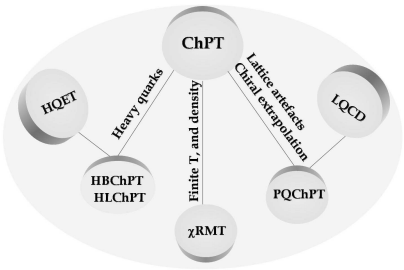

Figure 1: *The merging of ChPT with HQET and lattice QCD gives rise to new effective field theoretical descriptions of physical phenomena like baryon and heavy-light meson physics, field theory at finite volume, on discretized space-time and in the (partially) quenched limit (PQChPT). Another branch in the figure points at the particularly interesting realization of Chiral Random Matrix Theory [14] (χRMT) recently proved to be equivalent to ChPT [15], a powerful tool to explore QCD at finite temperature and nonzero chemical potentials.*

Moving forward in time we encounter a fruitful interplay of this wide class of EFT descriptions with the lattice formulation of field theories and in particular of strong interactions (referred to as Lattice QCD (LQCD)). During the last years it has become clear how the complementary use of both approaches is extremely useful to understand non perturbative aspects of a field theory, possibly gaining insight into the way for an exact solution; one exciting example is the attempt at extending the AdS/CFT conjecture [12] to AdS/QCD [13].

In the following sections I review the basic principles of phenomenological lagrangians, their descendants, and discuss a few topics in the phenomenolgy of hadron interactions, where the role of EFT and LQCD is and will be especially relevant. I conclude with some thoughts on possible future developments and

applications.

2 The Theory

The formalism of phenomenological lagrangians was mainly motivated by the necessity of describing the interactions of phenomenological fields, like the pions, whose appearance is due to the spontaneous breaking of an internal global symmetry. The mathematical problem is equivalent to that of finding all nonlinear realizations of a (compact, connected, semisimple) Lie group which become linear when restricted to a given subgroup [4]. The following problem is the one of constructing nonlinear lagrangian densities which are invariant under the nonlinear field transformations [5].

Consider the chiral group $G = SU(N) \times SU(N)$ which is spontaneously broken down to the diagonal (parity-conserving) subgroup $H = SU(N)_V$. The pattern of symmetry breaking is $SU(N)_L \times SU(N)_R \rightarrow SU(N)_V$ with $N = 2, 3$ flavours. Of the total number of generators of G, there will be $N^2 - 1$ "exact" generators of the subgroup H, and $N^2 - 1$ "broken" generators of the residual subgroup. Fields are associated to the generators of G, and pions, the Goldstone bosons of the spontaneaously broken chiral symmetry, are associated to its broken generators. Current algebra was implying that to correctly describe pion interactions it was necessary to eliminate all non derivative couplings from the lagrangian. The mathematical solution and the construction of the correct lagrangian for pions was reached in two ways: from the old σ-model, by performing [2] a chiral rotation of the four-dimensional field (σ, π) of $SU(2)$, which eliminates the non derivative coupling of σ and π and replaces it with a nonlinear derivative coupling of the chiral rotation vector, identified as the new pion field and transforming as a nonlinear realization of G.[3] The second more elegant way [3, 4, 5] was to directly postulate the nonlinear transformation properties of the pion fields and to construct a G (chiral) invariant lagrangian. The recipe [5] for such a lagrangian amounts to

$$\mathcal{L} = cTr\left[\partial_\mu \left(e^{i\pi\cdot T}\right) \partial^\mu \left(e^{-i\pi\cdot T}\right)\right] , \tag{1}$$

[3]The fact that one can limit the field content to a pion triplet and does not need to add a scalar field is due to the existence of a three-dimensional non linear realization of $SU(2) \times SU(2)$ while there is no three-dimensional linear representation.

where $\pi \cdot T = \sum_{i=1}^{N^2-1} \pi_i T_i$, with T_i the broken generators and π_i the associated pion fields. The coupling constant c is proportional to the scale of the symmetry breaking. This lagrangian describes self-interactions of the phenomenological fields π, and it is nonlinear in the fields: its exponential dependence generates infinitely many interaction terms. Another peculiarity is that it contains only derivative type interactions, which means that at low energies the fields are weakly interacting. In a paper of 1979 [16] entitled "Phenomenological Lagrangians", Weinberg constructed the renormalization group relations amongst the divergent structures appearing in the loop expansion of the theory. These relations clarify in which sense the theory is nonrenormalizable.

The formulation of ChPT appeared in two seminal papers by Gasser and Leutwyler; in the first [7] the $SU(2)$ flavour theory is derived, and in the second [8] the theory is extended to SU(3) to include the heavier strange quark. The lagrangian

$$\mathcal{L}_2 \;=\; \frac{f_\pi^2}{4} Tr\left(D_\mu \Sigma D^\mu \Sigma^\dagger\right) \;+\; \frac{f_\pi^2}{4} Tr\left(\chi^\dagger \Sigma + \chi \Sigma^\dagger\right)$$

is the first order contribution to an expansion in powers of the small energies of the fields $\Sigma = e^{\frac{2i}{f_\pi}\Phi \cdot T}$ and the light quark masses, which are invariantly introduced through the scalar spurion field $\chi = 2B_0\mathcal{M} + \ldots$, with $M = diag(m_u, m_d, m_s)$ and B_0 the parameter proportional to the scalar quark condensate. Covariant derivatives are defined to contain external vector and axial spurion fields $D_\mu \Sigma = \partial_\mu \Sigma - i(v_\mu + a_\mu)\Sigma + i\Sigma(v_\mu - a_\mu)$.

ChPT is the effective description of a strongly coupled theory, which is low energy QCD. Its expansion in powers of small momenta and light quark masses

$$\mathcal{L} \;=\; \mathcal{L}_2 \;+\; \frac{1}{{\Lambda_\chi}^2}\mathcal{L}_4 \;+\; \ldots \qquad\qquad p^2 \sim M_\pi^2 \sim m_q$$

has a predictive power which is dictated by the numerical value of its ultraviolet cutoff, by construction the scale of spontaneous chiral symmetry breaking $\Lambda_\chi \propto f_\pi$, the pion decay constant. The equality $\Lambda_\chi \simeq 4\pi f_\pi \simeq 1\, GeV^4$ guarantees a good predictivity for energies well below 1 GeV.

Flavour physics involving dominant contributions from low energy strong interactions can be explored with ChPT: the SU(2) case completely describes

[4] It is suggested by the numerical behaviour of the loop expansion, and not derived from first principle considerations.

pion physics and the physics of isospin breaking for $m_u \neq m_d$. The SU(3) case describes kaon physics, with $m_u, m_d \ll m_s$ and provided the kaon mass $M_K \ll \Lambda_\chi$. ChPT plays an essential role in the calculation of QCD induced corrections to weak decays of light mesons. Golden channels are certainly the nonleptonic kaon decays, source of the $\Delta I = 1/2$ rule and probe of indirect CP violation through ε'/ε, and rare kaon decays, useful to constrain sources of new physics beyond the standard model. There are special cases where large corrections to $SU(3)$ processes are purely $SU(2)$ effects, as it is for final-state-interactions in $K \to \pi\pi$ decays [17].

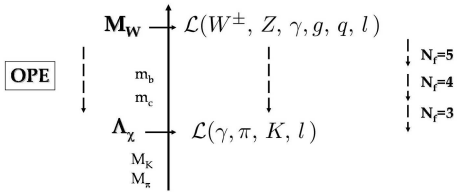

Figure 2: *Flow diagram of the unified EFT description of weak and strong interactions. N_f is the number of active flavours in a given theory. By decreasing energies, the top quark and W boson, the bottom quark, the charm quark are subsequently "integrated out". Λ_χ is the chiral symmetry breaking scale at which the nonperturbative matching of ChPT with QCD is performed.*

The unified description of weak and strong interactions as effective field theories is the perfect example of the two ways in which an EFT can be realized. Weak interactions identify with a weakly coupled theory, where decoupling (of massive modes) takes place and perturbative matching can be performed. In a sequence of decreasing energies (see fig.2), starting at the mass of the W boson, the renormalization group equations and Operator Product expansion (OPE) run the theory to lower energies. Massive modes "decouple" from the theory at each threshold[5] and give rise to a new EFT realization. The matching of two theories above and below the matching scale is genuinely perturbative. Strong

[5]The way decoupling manifests depends on the renormalization scheme used. Smooth decoupling does not arise in the typically used $\overline{MS}$ scheme where the decoupling consists of "integrating out" the corresponding massive particle.

interactions identify with a strongly coupled theory, which does not decouple. Hence, an EFT realization will arise via a nonperturbative matching with the fundamental theory; at the chiral symmetry breaking scale Λ_χ, quarks leave the ground to pions and kaons, through the nonperturbative matching of ChPT with QCD.

3 Its descendants

As symmetries are the foundations of any effective field theory description, we can look for extensions of ChPt through its merging with the realization of additional symmetries and their breaking. A particularly fruitful example is the merging of ChPT with the Heavy Quark Effective Theory (HQET) formulated around 1990 [9]. The additional symmetry is in this case the one recovered in the limit of infinitely heavy fermions: the heavy quark spin symmetry. The descendants of ChPT are nowadays proliferating, especially after it was realized how the interplay of ChPT with lattice QCD can be an invaluable guidance to the theoretical interpretation and improvement of lattice calculations; an EFT description can be formulated for each purpose, describing the dependence upon the volume, the lattice spacing, the fermion masses, mimicking and parameterizing the behaviour of a specific lattice formulation. With the caveat of a limited energy-range of validity, it offers a rigorous theoretical background to interpret physical phenomena on the base of symmetries and group theoretical properties.

3.1 The merging with Heavy Quark Effective Theory

The Dirac theory for spin 1/2 fermions can be reshaped in the limit of an infinitely heavy quark. Additional symmetries are restored in this limit, namely the heavy quark spin symmetry [9]. The merging of HQET with ChPT, gave birth to the effective description of baryon interactions, known as Heavy Baryon ChPT (HBChPT) [10]. When baryon number is conserved and taking into account that $m_B \simeq \Lambda_\chi$, we can factor out the baryon mass from the total momentum and expand in $1/m_B$. The leading order lagrangian describes the interaction of baryons with light meson vector- (V_μ) and axial-currents (A_μ)

$$\mathcal{L} = tr\,\bar{B}_v iv\cdot D B_v + D\,tr\,\bar{B}_v\gamma^\mu\gamma_5\{A_\mu, B_v\} + F\,tr\,\bar{B}_v\gamma^\mu\gamma_5[A_\mu, B_v] + O\left(\frac{1}{m_B}\right) + \mathcal{L}_\pi\,, \tag{2}$$

where

$$B_v(x) = \frac{1+\not{v}}{2}\, B(x)\, e^{i m_B v\cdot x} \qquad\qquad F\,+\,D\;=\;g_A\,, \tag{3}$$

with the field $B_v(x)$ containing the residual momentum dependence, after the large factor $m_B v$ has been factored out. The expansion of HBChPT is therefore a double expansion in $1/m_B$ and in $1/\Lambda_\chi$. The first sets the scale of the breaking of heavy quark spin symmetry, the second sets the scale of the breaking of chiral symmetry. An analogous merging gave rise to the description of hadrons with a heavy quark, the EFT known as Heavy-Light ChPT (HLChPT) [11], which describes the strong interactions of D, D* and B, B* mesons with pions.

3.2 Chiral perturbation theory and lattice QCD

Field theories can be formulated on a euclidean world-grid, where space and time are discretized and the unit distance, the lattice spacing, acts as the ultraviolet regulator of the theory. The euclidean formulation allows for a statistical intepretation of the path integral and its treatment with Monte Carlo methods (see ref. [18] for a review). Typical lattice simulations of QCD are performed on a hypercube with volume $L^3 \times L_t$, with spatial extension $L = Na$, temporal extension $L_t = N_t a$ and lattice spacing a (in some cases a different lattice spacing $a_s \neq a_t$ might be conveniently chosen). For an introduction to lattice field theory and lattice QCD see e.g. [19]. The lattice formulation allows for a *first principle* description of a theory, both in the strong-coupling (non perturbative) and weak-coupling (perturbative) regimes. Ideally $1/L \ll m_\pi \ll \Lambda_\chi \ll 1/a$ guarantees that pions freely move in the lattice box, i.e. their Compton wavelenght is much smaller than L, and they do not feel the discretization of spacetime. The goal is to be as near as possible to the real world limits $L \to \infty$ (the infinite volume limit), $a \to 0$ (the continuum limit), and $m_{u,d} \sim m_{u,d}^{phys}$ (the chiral limit for $m_{u,d}^{phys} \simeq 0$). Typical magnitudes for simulations up to date are $L \sim 2 \div 4\ fm$, $a \leq 0.1\ fm$, and $m_{u,d} \leq m_s/2$. Last years have seen an enormous improvement, with simulations at lattice spacings down to $a \sim 0.05\ fm$ and quark masses as small as $m_{u,d} \sim m_s/8$.

The Symanzik action [20] was the first example of EFT used to guide a lattice calculation, in this case to perform the extrapolation to the continuum limit. The generalization of this approach is an EFT description that guides the extrapolation to all limits, the infinite volume, the continuum and the chiral limit. During many years the quenched approximation of QCD (QQCD),

where the fermionic determinant in the path integral is set to a constant, was a forced choice for lattice calculations[6]. On the way to restore the original content of QCD, one can formulate a partially quenched (PQQCD) version of it and the corresponding (partially) quenched ChPT [21, 22], where sea quarks are distinguished from valence quarks and added at will to the theory content. Valence quarks are quenched, while sea quarks are dynamical. The QCD point is recovered at $N_{sea} = N_{valence}$ and $m_{sea} = m_{valence}$. The symmetry group is the graded extension [21] of the chiral group $SU(N) \times SU(N)$ for N flavours: $SU(N|N) \times SU(N|N)$, with N valence and ghost quarks in the quenched case, and $SU(N+K|N) \times SU(N+K|N)$, for K sea quarks and N valence and ghost quarks, in the partially quenched extension. The construction of (P)QChPT, initiated a stream of results which quickly clarified how the approximation affects observables and their volume dependence, using symmetry arguments, the non-unitarity of the quenched theory, and group theory considerations [23]. Further experience in the EFT approach *à la* Symanzik allowed to guide simulations towards new regimes of masses and volumes, from the usual p-regime to the ε-regime when approaching the chiral limit: the original theoretical formulation [24] was riproposed [25] in a lattice context. From the p-regime, with moderately large volumes and masses, $m_\pi L, m_\pi L_t \gg 1$, $2\pi/L \ll \Lambda_\chi \ll 1/a$ and p/Λ_χ small, one enters the ε-regime while lowering the quark masses, where $m_\pi L, m_\pi L_t \sim \varepsilon \ll 1$. Here the zero modes [26] of the Dirac operator must be resummed: $m_q \langle \bar{q} q \rangle L^3 L_4 \leq O(1)$.

Nowadays, ChPT formulations match every possible lattice strategy, mainly depending on the way fermions are included in the lattice action. The physical prediction is unique, but not the way a specific lattice formulation extrapolates to the chiral and continuum limits.

4 Hot Phenomenology

Hot topics of today phenomenology are those providing a powerful probe of physics beyond the standard model. Restricting to (almost light) hadron phenomenology brings me to mention topics as rare kaon decays, which provide tests of the unitarity of the CKM matrix, and charm physics. The follow-

[6] The fermionic operator is a large sparse matrix of $spins \times colours \times space \times time$, that renders the exact calculation computationally very expensive.

ing short sections are meant to recall a few important aspects, while for an extended analysis I refer the reader to the existing literature.

4.1 Rare decays and CKM unitarity

The semileptonic decay Kl_3 is a gold plated kaon decay. It can provide [27] a precise test of lepton universality, a determination of the amount of SU(2) breaking, through mass ratios, and the amount of SU(3) breaking, through the determination of the CKM matrix element V_{us}. The rare semileptonic processes $K_L \to \pi^0 \nu\bar{\nu}$ and $K^+ \to \pi^+ \nu\bar{\nu}$ are crucial channels to probe new physics contributions. For the latter processes, the accurate knowledge of the charm mass is crucial. All standard model contributions to these processes are being calculated with incresing accuracy and with use of ChPT for long distance contributions. For an updated overview, visit the Kaon 2007 website [28]. Finally, the radiative decays $K \to \pi\gamma\gamma, \pi\pi\gamma$ can further probe the range of validity of ChPT and long distance dynamics.

4.2 Charm physics

The physics of charm is as rich as difficult to decipher. The charm is not heavy enough M_c is not $\gg \Lambda_\chi$ to use the heavy quark expansion with sufficiently high predictive power, and it is not light enough $M_c \simeq \Lambda_\chi$ to use the chiral expansion. However, it is more relativistic than the bottom quark, hence its lattice formulation is affected by smaller discretization errors. We need $m_c \ll 1/a$ on the lattice, and it is now easy to get $m_c a \sim 1/2$ [29]. What is further needed? Two points are worth to be mentioned: i) a more accurate determination of the charm mass (to the percent level), and ii) the prediction of the strong interaction phases of D-meson decays which probe CP violation and are indirect probes of physics beyond the standard model.

5 Conclusive thoughts

During the last two decades we have reshaped our view of quantum field theories. Effective field theories are at the foundation of modern quantum field theory, and the effective field theory of low energy QCD has significantly contributed to this view. Where is the future of EFTs? They will probably remain for long the bread and butter of field theoretical approaches to many phenom-

ena, not only in particle physics, but widely used in condensed matter physics. There are clear places in particle physics where the formulation of an effective field theory description still needs to be fruitfully improved. This is the case for the prediction of the electric dipole moments, tiny observables measured at very high precision low energy experiments [30]. Can one think of a new hybrid EFT formalism to efficiently describe strong interactions in charm decays? or the yet unexplored intermediate regime of baryon densities in neutron stars? One important role of EFT is undeniably the one of uncovering the possible connection of (super)gravity theories to a four-dimensional universe.

References

1. J.A. Cronin, Phys. Rev. **161**, 1483 (1967); J. Schwinger, Phys. Lett. **B24**, 473 (1967).
2. S. Weinberg, Phys. Rev. Lett. **18**, 188 (1967).
3. S. Weinberg, Phys. Rev. **166**, 1568 (1968).
4. S. Coleman, J. Wess, B. Zumino, Phys. Rev. **177**, 2239 (1969).
5. S. Coleman, J. Wess, B. Zumino, Phys. Rev. **177**, 2247 (1969); J. Wess, B. Zumino, Phys. Rev. **163**, 1727 (1967).
6. M. Gell-Mann, Phys. Lett. **8**, 214 (1964); G. Zweig, CERN report no. 8182/TH 401.
7. J. Gasser, H. Leutwyler, Ann. Phys. **158**, 142 (1984).
8. J. Gasser, H. Leutwyler, Nucl. Phys. **B250**, 465 (1985).
9. E.J. Eichten, C.T. Hill, Phys. Lett. **B234**, 511 (1990); H. Georgi, Phys. Lett. **B240**, 447 (1990); N. Isgur, M.B. Wise, Phys. Lett. **B232**, 113 (1989).
10. J. Bijnens,H. Sonoda, M.B. Wise, Nucl. Phys. **B261**, 185 (1985); E. Jenkins, A.V. Manohar, Phys. Lett. **B259**, 353 (1991).
11. G. Burdman, J. Donoghue, Phys. Lett. **B280**, 287 (1992); M.B. Wise, Phys. Rev. **D45**, 2188 (1992).
12. J. Maldacena, Adv. Theor. Math. Phys. **2**,231 (1998).

13. E.V. Shuryak, arXiv:0711.0004 [hep-ph].

14. E.V. Shuryak, J.J.M. Verbaarschot, Nucl. Phys. **A 560**, 306 (1993).

15. F. Basile, G. Akemann, arXiv:0710.0376 [hep-th].

16. S. Weinberg, Physica **96A**, 327 (1979).

17. E. Pallante, A. Pich, Phys. Rev. Lett. **84**, 2568 (2000).

18. M. Creutz, *Quarks, gluons and lattices*, Cambridge Monographs on Mathematical Physics (Cambridge University Press (United Kingdom), 1985).

19. J. Smit, *Introduction to Quantum Fields on a Lattice*, Cambridge Lecture Notes in Physics (Cambridge Un. Press, 2002); H.J. Rothe, *Lattice Gauge Theories*, World Scien. Lecture Notes in Physics - Vol. 74 (World Scien. Publ., 2005).

20. K. Symanzik, Nucl. Phys. **B226**, 187 (1983); **B226**, 205 (1983).

21. C. Bernard, M. Golterman, Phys. Rev. **D46**, 853 (1992); Phys. Rev. **D49**, 486 (1994).

22. G. Colangelo, E. Pallante, Nucl. Phys. **B520**, 433 (1998); E. Pallante, JHEP 9901 (1999) 012.

23. M. Golterman, E. Pallante, Phys. Rev. **D74**, 014509 (2006); arXiv:hep-lat/0610005.

24. J. Gasser, H. Leutwyler, Nucl. Phys. **B307**, 763 (1988).

25. L. Giusti *et al.*, Comput. Phys. Commun. **153**, 31 (2003); L. Giusti *et al.* JHEP 0311:023,2003.

26. H. Leutwyler, A. Smilga, Phys. Rev. **D46**, 5607 (1992).

27. V. Cirigliano, Contribution to KAON 2007.

28. KAON 2007 website: http://www.lnf.infn.it/conference/kaon07/

29. C. Davies, plenary contribution to these proceedings.

30. TRIμP: K. Jungmann, Talk at RECFA Meeting, Amsterdam, 23 September 2005, http://www.nikhef.nl/recfa/Presentations/

Frascati Physics Series Vol. XLVI (2007), pp. 79–108
HADRON07: XII Int. Conf. on Hadron Spectroscopy – Frascati, October 8-13, 2007
Plenary Session

SCALAR MESONS FROM HEAVY FLAVOR DECAYS

Alberto Reis
Centro Brasileiro de Pesquisas Físicas

Abstract

In the past few years the B-factories became unexpected players in the scalar mesons business: in order to access the CP violation effects, it is necessary to handle the dynamics of the strong interaction between the final state hadrons. A number of large statistics studies heavy flavor decays involving a scalar component have been performed recently by Belle and BaBar, who have joined CLEOc, BES, E791 and FOCUS in the effort to understand the physics of the scalar mesons. In this talk, the most recent results from these experiments will be reviewed, with emphasis on the low energy $K\pi$ system and on the f0(1370).

1 Introduction

The identification of the scalar mesons is a long standing problem. There are too many candidates with mass bellow 2 GeV/c^2, although some states, like the κ and the $f_0(1370)$, are still controversial. In addition to the regular $q\bar{q}$ mesons, the observed spectrum may contain other types of states, like glueballs, hybrids, tetraquarks or molecules.

There are difficulties from both experimental and theoretical points of view. Scalars are, in general, broad overlapping states. Since there is no spin,

they decay isotropically. In scattering experiments the production rates for low mass states, like the σ and κ, are suppressed by the Adler zeroes. At higher masses, disentangling the broad, spinless states, like the $f_0(1370)$, from the smooth background is complicated by the interference with other scalars and with the continuum, which distorts the line shapes.

The precise determination of pole positions and couplings to specific modes of all existing scalar particles is an essential step towards the identification of the genuine $q\bar{q}$ states. Such an ambitious task could not be accomplished by one single type of experiment. One has to look at the scalars problem from all possible perspectives, exploring the different constraints imposed by different reactions.

In the past six or seven years there has been lots of new results on scalar mesons from heavy flavor (HF) decays to light quarks (LQ), exploring the unique features of these processes. In this paper we will focus on two crucial problems: the nature of the κ meson and the existence of the $f_0(1370)$. More specifically, we will present the latest results from τ lepton and three-body decays of D and B mesons to light hadrons.

The paper is organized as follows. In Section 1 we discuss why HF decays are a very useful tool for the study of scalar mesons. We will also discuss some aspects of the basic analysis techniques in HF decays. In Section 2 we discuss the situation of the low mass $K\pi$ spectrum. In Section 3 we discuss the issue of the $f_0(1370)$, in the light of hadronic D and B decays. The last Section contains a summary and conclusions.

2 Heavy flavor to light quarks

There are unique features that make decays of D and B mesons to light hadrons very suitable for the study of scalar mesons. These particles are copiously produced in D and B decays, especially when there is a pair of identical particles in the final state. The B-factories already have very large charm samples, with a high degree of purity. Soon there will be also large samples of $B \to h_1 h_2 h_3$ decays ($h_i = \pi, K$) from the LHC experiments. With these high quality data, the $\pi\pi$ and $K\pi$ spectra can be accessed continuously, starting from threshold, and covering the entire elastic range.

Another appealing feature, especially in D decays, is the close connection between the quark content of the initial state and the observed resonances. In

the decay of a D meson the weak decay of the c quark is embedded in a strongly interacting system that leads to the final state hadrons. However, if one goes through the PDG listing, one realizes that, in spite of the complexity of the D decay, nearly the entire hadronic and semileptonic rates can be described by a rather simple scheme, in terms of tree-level valence quark diagrams, and the regular $q\bar{q}$ mesons from the Constituent Quark Model. The dominant amplitudes in D decays are the external (spectator) and internal W radiation. The 'final state valence quarks' result from transition $c \to s(d) + u\bar{d}(\bar{s})$ plus the 'spectator' $\bar{q}$. These quarks define the possible intermediate $q\bar{q}$ states. This simple picture works very well for intermediate states having either a vector, an axial-vector or a tensor resonance. If one excludes the scalar mesons, in D decays there is nothing else than the members of the usual $q\bar{q}$ nonets of the Constituent Quark Model. In other words, D decays can be seen as a '$q\bar{q}$ filter': if a resonance is observed in D decays, then it is very likely to be a $q\bar{q}$ meson. One can expect that this holds also for the scalar resonances, so D decays would also provide clues about the nature of these mesons.

Semileptonic decays of the type $D \to h_1 h_2 l\nu$, and hadronic decays of the τ lepton, $\tau \to h_1 h_2 \nu$, provide a particularly clean environment for the study of the scalar mesons, since there is no strong interaction between the $h_1 h_2$ pair and the leptons. However, the $h_1 h_2$ system is dominantly in P-wave in both cases. The S-wave contribution is typically less than 10%, so very large samples are required. An additional difficulty is the fact that the neutrinos are not reconstructed, so the background level in these decays is relatively large.

Hadronic decays of D mesons, on the other hand, are much easier to be reconstructed. In some final states the S-wave component is largely dominant, like in the $D^+ \to K^-\pi^+\pi^+$ and in the $D^+, D_s^+ \to \pi^-\pi^+\pi^+$ decays. Background levels are typically of the order of a few percent. The problem here is how to disentangle the desired information. The final states are strongly interacting three-body systems, with a complex and unknown production dynamics. The pure $h_1 h_2$ is certainly the main ingredient, but there is no direct route to extract it in a model independent way. Approximations, and, therefore, interpretation of the results, are unavoidable, unfortunately.

Most of the existing data on HF $\to$ LQ come from hadronic three-body D decays. The event distribution in the Dalitz plot is given by,

$$\frac{d\Gamma}{ds_a ds_b} = \frac{1}{32(2\pi M)^3} \mid \mathcal{M}(s_a, s_b) \mid^2, \tag{1}$$

where M is the mass of the decaying particle and s_a, s_b are the two-body invariant masses squared. The phase space density is constant, so any structure in the Dalitz plot reflects directly the dynamics of the decay.

The analysis technique of such decays is by now standard [1]. The decay amplitude is written as a coherent sum of phenomenological amplitudes corresponding to the possible intermediate states,

$$\mathcal{M}(s_a, s_b) = \left| \sum_L \; f_D^L \; \mathcal{S}^L \; \mathcal{A}^L \right|^2 , \tag{2}$$

with

$$\mathcal{A}^L = \sum c_k e^{i\delta_k} A_k^L, A_k^L = f_R^L \times BW_k \tag{3}$$

In the above equations f_D^L and f_R^L are form factors, with L being the orbital angular momentum at the D or at the resonance decay vertex; $\mathcal{S}^L$ is a function accounting for the angular momentum conservation, and BW_k is a relativistic Breit-Wigner function (with an energy dependent width, in general). The complex coefficients $c_k e^{i\delta_k}$ are usually the fit parameters.

Analyzes differ by the way the S-wave, $\mathcal{A}^0$, is modeled. There are three basic approaches.

The most used model is the so called isobar model [2, 3], in which the S-wave is represented by a sum, of Breit-Wigner functions and a nonresonant amplitude, with unknown complex coefficients. The nonresonant amplitude is assumed to be uniform in D decays, but varies across the Dalitz plot in the case of B decays. This model is simple and intuitive, but there are well known conceptual problems with this approach [4]. As we will see, it provides an effective description of the data but, in some cases, the physical interpretation of the results is rather ambiguous.

Another approach is the K-matrix model [5]. This is a very sophisticate tool, but it is based on a very strong assumption: in the D decay, the resonant $h_1 h_2$ system and the bachelor particle recoil against each other without any interaction. This would greatly simplify the problem, although one must acknowledge the lack of experimental evidence supporting this assumption. If

the three-body rescattering is negligible, the evolution of the h_1h_2 system must be the same as in h_1h_2 elastic scattering. In the K-matrix approach the S-wave amplitude is, therefore, fixed by other type of reactions, whereas the production of the h_1h_2 pair is an unknown function to be determined by the fit. This universality of the S-wave is often seen as the most appealing feature of the K-matrix approach. We should not forget that the same constraint should be applied to all partial waves, which, unfortunately, is not the case of the analyzes published so far. In general, good fits are achieved only if an extra energy-dependent phase is added. In the framework of the K-matrix model, the origin of such a phase is attributed to the production of the h_1h_2 pair. This is simply a matter of interpretation, since this phase could also be due to the rescattering of the final state particles. There is no way, with the existing measurements, to distinguish between these two effects.

Finally, there is the PWA approach [6]. Here no assumption is made about the content of the S-wave, which is treated as a generic complex function of the h_1h_2 mass, $\mathcal{A}^0 = a(s)e^{i\phi(s)}$. The h_1h_2 spectrum is divided in bins. At each bin edge the amplitude is defined by two real constants, a_k and ϕ_k, which are fit parameters. The amplitude at any value of the h_1h_2 mass is given by a polynomial interpolation. This method relies on a precise modeling of the P- and D-waves. The problem resides, once more, in the interpretation of the results. The measured S-wave phase $\phi(s)$ includes any rescattering/production effects, which should be disentangled in order to determine the 'bare' h_1h_2 amplitude.

One last remark is in order. A consequence of representing the decay amplitude by a coherent sum of amplitudes is that the decay fractions do not add to 100%. Different amplitudes populate the same region of the phase space, so they are expected to interfere. The amplitudes have phases that vary across the Dalitz plot. The interference can be destructive in some regions of the phase space and constructive in other ones. One should be very careful, though, when the sum of fractions largely exceeds 100%. In almost all cases this large interference occur between the broad amplitudes in the S-wave, involving, in general, the nonresonant amplitude. This is a symptom of a poor modeling of the S-wave. In other words, one may find a mathematical solution to the fit problem, but with a misleading physical interpretation. In the following Sections we will see several instances of this problem.

3 The low energy $K\pi$ spectrum: the κ problem

There are two crucial questions to be answered in the low mass $K\pi$ spectrum. The neutral κ has been observed by different experiments in several types of heavy flavor decays [3, 11, 7], but so far evidence for its charged partner has been scarce and controversial. This casts doubts about the κ being a regular $I = 1/2$ $q\bar{q}$ state. The other issue is the pole position of the κ. There is no data on $K\pi \to K\pi$ elastic scattering bellow 825 GeV/c^2. Determination of the κ pole position [8] must rely on extrapolations of the existing data. New data that fill the existing gap would be highly desirable. This section is devoted to these two issues.

3.1 The $D^0 \to K^+K^-\pi^0$ decay – BaBar

In a recent analysis of the decay $D^0 \to K^+K^-\pi^0$, performed by the BaBar collaboration [9], the issue of the charged κ has been addressed. The data sample has 11K signal events with 98% purity. The Dalitz plot of this decay is shown in Fig. 1. Resonances can be formed in all three axes (the third axis, K^-K^+, is along the diagonal, starting at high $K^\pm\pi^0$ mass) of the Dalitz plot.

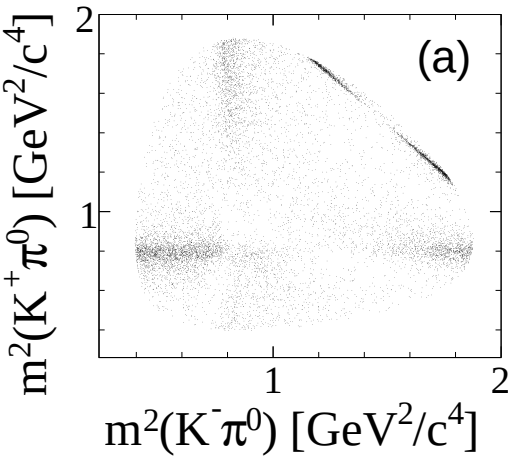

Figure 1: *Dalitz plot of the* $D^0 \to \overline{K}^0\pi^+\pi^+$ *decay* [9]. *The narrow band at the upper edge of the Dalitz plot correspond to the* $\phi\pi^0$ *channel.*

The main diagrams for this decay are shown in Fig. 2. There is a well defined pattern in D decays that proceed via the external W-radiation amplitude (Fig. 2-a): due to the V-A nature of the weak interactions, the W couples much more strongly to a vector or an axial-vector meson than to a pseudoscalar. According to this pattern, one expects a dominant contribution from the $K^*(892)^+K^-$ channel, compared to $K^*(892)^-K^+$. Important contributions from the $K^*(892)^-K^+$ and $\phi\pi^0$ modes are also expected. We can see in Fig. 1 clear structures corresponding to these resonances.

The Dalitz plot of Fig. 1 was fitted using three different models for the $K^\pm\pi^0$ S-wave. In the first fit, the S-wave was represented by the usual isobar model – a constant nonresonant amplitude plus two Breit-Wigner functions for the $\kappa^\pm\pi^0$ and $K_0^*(1430)^\pm\pi^0$ modes – with parameters taken from E791 [3]. The second fit used the E791 PWA S-wave [6] measured from the $D^+ \to K^-\pi^+\pi^+$ decay. Finally, the third fit used the LASS $I = 1/2$ $K^-\pi^+$ S-wave amplitude [10]. The isobar model has the smaller fit probability (χ^2 prob. $< 5\%$). The E791 PWA S-wave provides a good description of the data (χ^2 prob. $=$

23%), but the best fit was obtained using the LASS $I = 1/2$ S-wave. Results of the fits with LASS $I = 1/2$ S-wave are summarized in Table 1. Note that in Model II the exclusion of the $K^*(1410)K$ amplitudes – a 5% contribution in Model I – has a minor impact on the other P-wave components, but causes a dramatic change in the S-wave fraction. Moreover, in Model II the sum of the decay fractions largely exceeds 100%, indicating the existence of large destructive interference effects.

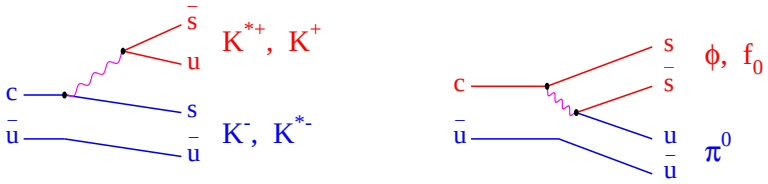

Figure 2: *Valence quark diagrams leading to the $K^+K^-\pi^0$ final state: external (left) and internal (right) W radiation. The resonances that can be formed by the 'final state' quarks are indicated.*

The fit with the LASS amplitude is much better than the one having explicitly the $\kappa^\pm$ amplitude.Note that this result does not rule out the charged κ, since its pole can be found in LASS data [8]. It simply says that the isobar representation of the $K^-\pi^+$ S-wave in the $D^+ \to K^-\pi^+\pi^+$ decay, from E791 [3] and FOCUS [11] analysis, is not a good model for the $K^+\pi^0$ S-wave amplitude in the $D^0 \to K^+K^-\pi^0$ decay. In both E791 and FOCUS analyzes of the $D^+ \to K^-\pi^+\pi^+$ decay, the LASS $I = 1/2$ S-wave amplitude fails to provide a good description of the data, whereas a very good fit was achieved with the isobar model. The origin of this discrepancy is yet to be understood. With a larger $D^0 \to K^+K^-\pi^0$ sample, a model independent measurement of the

Table 1: *Decay fractions (%) of the $D^0 \to K^+K^-\pi^0$ decay. Results are from fits using the $I = 1/2$ LASS S-wave amplitude.*

mode	model I	model II
$K^*(892)^+K^-$	45.2±0.9	44.4±0.9
$K^*(1410)^+K^-$	3.7±1.5	-
$K^+\pi^0(S)$	16.3±0.1	71.1±4.2
$\phi\pi^0$	19.3±0.7	19.4±0.7
$f_0(980)\pi^0$	6.7±1.8	10.5±1.4
$K^*(892)^-K^+$	16.0±0.9	15.9±0.9
$K^*(1410)^-K^+$	2.7±1.5	-
χ^2 prob.	62%	47%

S-wave amplitude could be performed and directly compared to the results of the E791 MIPWA [6].

3.2 The $\tau^- \to \overline{K}^0\pi^-\nu_\tau$ decay – Belle

In hadronic decays of the τ lepton, $\tau \to h_1h_2\nu_\tau$, the h_1h_2 system is not affected by strong interaction with the leptonic current. This would be as close as one could get to the $h_1h_2 \to h_1h_2$ elastic scattering using HF decays. The Belle Collaboration published recently [12] a study of the decay $\tau^- \to \overline{K}^0\pi^-\nu_\tau$. A sample with 53K signal events was selected from the reaction $e^+e^- \to \tau^+\tau^-$. The τ^+ decays to a muon plus two neutrinos, so the signature of the event is one lepton recoiling against three charged prongs in the opposite hemisphere. With a total of three missing neutrinos, it is very difficult to reconstruct the event topology. Immediate consequences are a high background level (∼20% in this analysis) and the lack of an angular analysis.

The angular distribution of the helicity angle was used in FOCUS study [13] of the $D^+ \to K^-\pi^+\mu^+\nu$ decay. The helicity angle is formed by the K^- momentum and the line of flight of the D^+, measured in the $K^-\pi^+$ rest frame. In this decay there is a 5% scalar component. The line shape of the $K^-\pi^+$ spectrum, which is dominated by the $K^*(892)^0$, is not sensitive to the different models for the S-wave component. However, the different possibilities – a complex constant, a Breit-Wigner function, or the LASS $I = 1/2$ S-wave amplitude – lead to different angular distributions, so one can explore this feature in order to understand the nature of the scalar component.

In the case of the $\tau^- \to \overline{K}^0\pi^-\nu_\tau$ decay, the $K^*(892)^-$ alone is not enough to describe the $\overline{K}^0\pi^-$ spectrum, as we can see in Fig. 3-a. There is an excess of events in the lower and in the upper part of the spectrum. The $\overline{K}^0\pi^-$ spectrum was fit with two classes of models : the dominant $K^*(892)^-$ plus the charged κ and one high mass state (either a vector or a scalar resonance); the $K^*(892)^-$ plus the LASS $I = 1/2$ $K^-\pi^+$ S-wave amplitude. The best fit was obtained with the $K^*(892)^-$ plus a pure S-wave, that is, a sum of the κ and the $\overline{K}_0^*(1430)^-$. The confidence level of this fit is 41% (Fig. 3-b). The fit using the LASS amplitude, on the other hand, yielded a C.L. of only 10^{-8}.

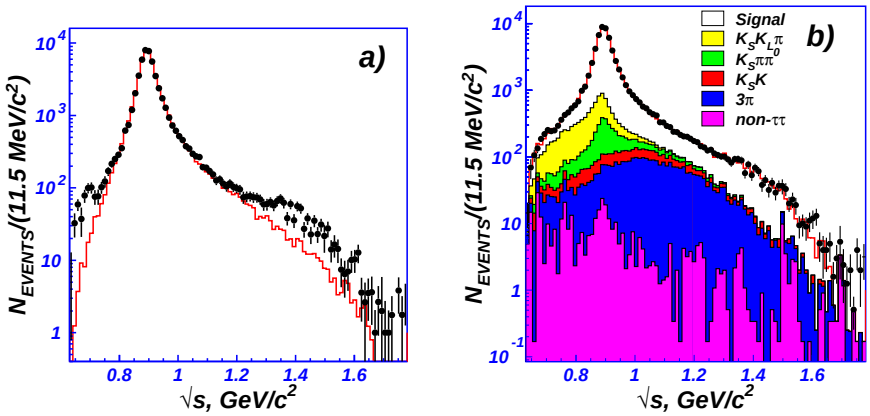

Figure 3: *a) The $\overline{K}^0\pi^-$ mass spectrum [12] (points with error bars). The histogram represents the $K^*(892)^-$ contribution. b) The $\overline{K}^0\pi^-$ mass spectrum with the different background components and the result of the best fit superimposed.*

The result of Belle analysis is in conflict with those of the BaBar study of the $D^0 \to K^+K^-\pi^0$ decay. One could expect that, in the absence of strong interactions, the $\overline{K}^0\pi^-$ S-wave phase would match that of LASS, whereas in the case of $D^0 \to K^+K^-\pi^0$ the rescattering would cause deviations from the elastic phase. This is a rather intriguing result. In both cases the statistics is limited to a few thousands of events, though. The angular analysis on a larger $\tau^- \to \overline{K}^0\pi^-\nu_\tau$ sample may confirm the resonant behavior of the S-wave at low

mass. In this case we would have a compelling evidence of the charged $\kappa(800)$.

3.3 The $D^+ \to K^-\pi^+\pi^+$ decay – FOCUS

The $D^+ \to K^-\pi^+\pi^+$ is a golden mode for the study of scalar mesons. The S-wave accounts for over 60% of the decay rate. In addition, the large branching fraction (9.5%), combined with the long D^+ lifetime and a final state having only charged tracks (the odd charge track being always a kaon), makes the $D^+ \to K^-\pi^+\pi^+$ the easiest charm decay mode to be reconstructed. Using this decay one can measure the $K^-\pi^+$ S-wave amplitude near threshold, filling the existing gap in LASS data.

FOCUS has published recently a study of this decay using the K-matrix approach [11]. A good fit was obtained combining the $I = 1/2$ and $I = 3/2$ LASS S-wave phases with an additional energy dependent phase. This extra phase was interpreted as being originated from the production dynamics of the $K\pi$ system, but it could also be attributed to the rescattering of the final state particles. One important aspect should be stressed. The $I = 3/2$ component is purely nonresonant, whereas all resonances are in the $I = 1/2$ amplitude. The latter has also a nonresonant background. The fractions of each isospin component in the K-matrix fit are (207±28)% and (40± 10)% for the $I = 1/2$ and $I = 3/2$, respectively. The total S-wave fraction amounts to (83±2)%. Here is another instance of large interference between broad components within the S-wave.

The PWA approach for the $K^-\pi^+$ S-wave was used recently by CLEOc [14] and FOCUS [15]. In this new FOCUS study, the $D^+ \to K^-\pi^+\pi^+$ Dalitz plot is fitted using also the isobar model for the $K^-\pi^+$ S-wave. This is a work in progress, based on a sample of 93K signal events and with 98% purity. From here to the end of this Section we will discuss the preliminary results this FOCUS PWA/isobar Dalitz plot analysis.

In the isobar fit, the S-wave model was that of E791 [3]: a sum of an uniform nonresonant amplitude, plus two Breit-Wigner functions for the $\kappa\pi^+$ and $\overline{K}_0^*(1430)\pi^+$ modes. In order to make a direct comparison with E791 and CLEOc, the S-wave Breit-Wigner functions are multiplied by the same Gaussian form factors, $f_D = e^{-p^{*2}r_D^2/12}$. Masses and widths of the scalar resonances are fit parameters.

The fit fractions and resonance parameters are shown in Table 2. Results

Table 2: *Decay fractions (%) of the $D^+ \to K^-\pi^+\pi^+$ decay. Results are from fits using the isobar model for the S-wave amplitude. The masses and widths of scalar resonances are in units of MeV/c^2.*

mode	E791	CLEOc	FOCUS(a)	FOCUS(b)	FOCUS(c)
$\overline{K}^*(892)^0\pi^+$	12.3±1.4	11.2±1.4	11.3±0.3	11.7±0.3	11.2±0.3
$\overline{K}^*(1410)^0\pi^+$	-	-	1.2±0.3	1.1±0.3	1.3±0.3
$\overline{K}^*(1680)^0\pi^+$	2.5±0.8	1.4±0.2	3.3±0.3	2.7±0.3	3.8±0.3
$\overline{K}^*_2(1430)\pi^+$	0.5±0.2	0.4±0.4	0.20±0.05	0.20±0.05	0.20±0.05
$\overline{K}^*_0(1430)\pi^+$	12.5±1.4	10.5±1.3	16.8±0.8	14.3±0.7	18.7±1.2
$\kappa(800)\pi^+$	47.8±13.2	31.2±3.6	43.5±4.5	71.3±5.5	22.3±3.2
nonresonant	10.4±1.4	13.0±7.3	14.3±3.0	7.5±3.1	31.6±4.5
$\kappa(800)$ mass	797±48	805±11	837±12	829±14	867±14
$\kappa(800)$ width	410±97	453±21	443±21	433±18	485±27
$\overline{K}^*_0(1430)$ mass	1461±3	1459±5	1466±4	1468±4	1466±4
$\overline{K}^*_0(1430)$ width	169±5	175±16	193±7	193±7	192±7

from the three experiments are in reasonable agreement, except for the S-wave fraction in CLEOc analysis, which is a bit smaller than E791 and FOCUS. But the most remarkable feature in Table 2 is shown in the last three columns. The isobar fit to FOCUS data was repeated with a little variation of the S-wave parameterization. In FOCUS(b) the value of the scalar form factor parameter, r_D, was set to 6 GeV^{-1} (instead of 5 GeV^{-1} in FOCUS(a)). In FOCUS(c) the value of r_D was set to zero, which is equivalent of having no scalar form factor. All the three FOCUS fits have an equally good confidence level. We observe a dramatic change in the S-wave composition, while the P- and D- waves remain unaltered. The nonresonant fraction varies by a factor of four.

This instability can be readily explained by the interference between the broad κ Breit-Wigner and the uniform nonresonant component. In Fig. 4 the effect of the scalar form factor is illustrated. Fig. 4-a shows the modulus squared of the κ Breit-Wigner. The $K\pi$ mass dependence of the width, in the denominator of the Breit-Wigner, shifts the maximum of the function to a value bellow the $K\pi$ threshold. The introduction of the Gaussian form factor modifies the line shape near threshold (Fig. 4-b). The resulting κ amplitude has a more reasonable behavior. The same effect can be achieved if, instead of multiplying the κ Breit-Wigner by the Gaussian form factor, we add the correct

amount of a constant nonresonant amplitude, with the right phase difference. This is shown in Fig. 4-c.

The case of the $D^+ \to K^-\pi^+\pi^+$ is didactic: the isobar model yields a good fit, but it fails to provide an unambiguous physical picture of the decay dynamics. The model for the S-wave is clearly inadequate. We need to go beyond the isobar model in order to understand the composition of the S-wave.

The $D^+ \to K^-\pi^+\pi^+$ Dalitz plot is also fitted using the PWA method. The $K\pi$ spectrum is divided in forty equally spaced intervals. At the edge of each interval the S-wave amplitude is defined by two fit parameters, $\mathcal{A}_0(s = s_k) = a_k e^{i\phi_k}$. The value of the S-wave amplitude at any point in the $K\pi$ spectrum is given by a spline interpolation of these forty points. The S-wave is determined by an iterative procedure. A first fit is performed fixing the P-wave to that of the isobar analysis. The S-wave is determined (80 fit parameters). A second fit is performed fixing now the S-wave and varying the P-wave. The process is repeated until it converges.

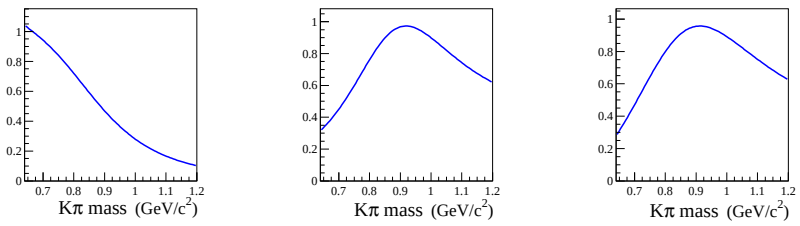

Figure 4: *Left: The modulus squared of the κ Breit-Wigner, without the scalar form factor; center: the modulus squared of the κ Breit-Wigner multiplied by the scalar form factor; right: the modulus squared of the sum of the κ Breit-Wigner, without the scalar form factor, and a complex constant.*

Fig. 5 shows the FOCUS PWA S-wave phase, $\phi(s)$, as a function of the $K\pi$ mass squared. A 80^o overall phase was added to $\phi(s)$ for a better comparison with the $I = 1/2$ and $I = 3/2$ phases from LASS. There is a clear discrepancy between the S-wave phase measured by FOCUS and that of LASS $I = 1/2$ amplitude. The agreement between FOCUS and LASS cannot be

achieved even combining both isospin phases. An extra phase, which depends smoothly on the $K\pi$ mass, is necessary for the matching of the two amplitudes. The origin of such a phase is unclear.

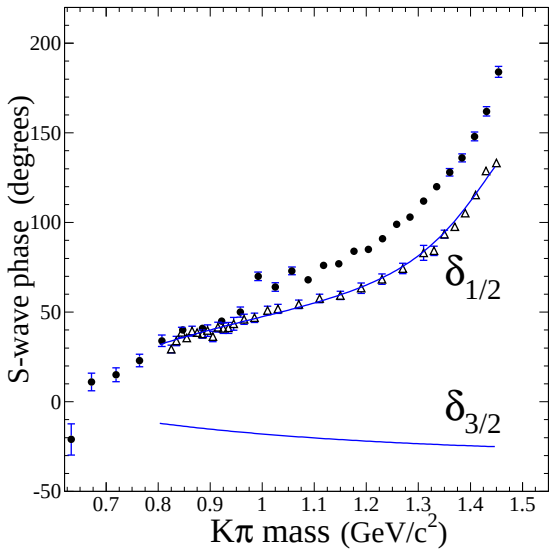

Figure 5: *The phase of the S-wave $K\pi$ amplitude, from the $D^+ \to K^-\pi^+\pi^+$ decay, as a function of the $K\pi$ mass squared. The phase was shifted up by 80 degrees, in order to make a comparison with the LASS $I = 1/2$ S-wave phase, $\delta_{1/2}$. The LASS $I = 3/2$ S-wave phase, $\delta_{3/2}$, is also shown.*

The PWA is as close as one can get to a model independent method, since no hypothesis is assumed for the S-wave. But the method has some technical limitations arising from the large number of free parameters. One limitation is the existence of multiple solutions. With so many parameters, the fit has freedom to cure eventual problems with the P-wave model. A precise representation of the P-wave is mandatory, otherwise some 'leakage' into the S-wave would be unavoidable.

The interpretation of the results is not trivial. The amplitude measured

with the PWA method includes not only the $K\pi$ dynamics, but also any possible contribution from the production of the $K\pi$ pair and rescattering of the final state particles. Some urgent input from theory is required in order to disentangle these effects.

4 Is there an $f_0(1370)$?

In the low energy $\pi\pi$ spectrum the σ pole is now well established, but the situation between 1-2 GeV/c^2 is still controversial. There may be three neighbor scalar states, namely the $f_0(1370)$, the $f_0(1500)$ and the $f_0(1710)$. The $f_0(1500)$ is a narrow, well established state, with mass, width and couplings know to a good degree of accuracy [16], but the uncertainty on the $f_0(1370)$ parameters is very large: $1200 < m_0 < 1500$ GeV/c^2 and $200 < \Gamma_0 < 500$ GeV/c^2. The existence of this state is often questioned.

The $f_0(1370)$ has been observed mostly in central production and $p\bar{p}$ annihilation (see, for instance D. Bugg's recent review on this state [17]). BES has also reported on this state from the decay $J/\psi \to \phi\pi\pi$ [18]. This state is very difficult to be detected because it is broad and very close to the $f_0(1500)$. Its line shape may also be sensitive to the opening of the $\sigma \to 4pi$ channel.

An interesting and related issue: the mass of the lightest scalar glueball is expected to be around 1.5 Gev/c^2. It is widely accepted that the three scalars would mixed states, having both $q\bar{q}$ and gg components in their wave functions.

Heavy flavor decays are particularly useful here, since in these decays the $q\bar{q}$ component of the intermediate resonances are probed.

4.1 The $D_s^+ \to \pi^-\pi^+\pi^+$ decay – FOCUS and E791

The $D_s^+ \to \pi^-\pi^+\pi^+$ decay is particularly suited to the study of scalar mesons. In this decay the S-wave component amounts to over 80% of the decay rate. The dominant diagram is shown in Fig. 6-a, with a small contribution from the annihilation diagram (Fig. 6-b). The $f_0(980)\pi^+$ should be the dominant mode. The $f_0(980)$ has a large coupling to K^+K^- and, therefore, it must have a strong $s\bar{s}$ component in its wave function. An important contribution from the channel $f_2(1270)\pi^+$ is also expected.

FOCUS has collected a sample of 1400 $D_s^+ \to \pi^-\pi^+\pi^+$ signal events. The Dalitz plot, shown in Fig. 7, was fitted with the K-matrix approach [5]. It

was also fitted using the isobar model, but the results of this analysis were not published.

There are two remarkable features in Fig. 7: a very clear structure at 1 $(\mathrm{GeV/c^2})^2$, corresponding to the $f_0(980)$; the concentration of events near the border, at $m^2_{\pi\pi} \sim 2$ $(\mathrm{GeV/c^2})^2$, which is due to the $f_2(1270)$, $\rho(1450)^0$ and to a scalar state, which we refer to as $f_0(X)$. The Dalitz plot was fit [19] using the isobar model for the S-wave, which has three components: the $f_0(980)\pi^+$, the $f_0(X)\pi^+$ and the nonresonant modes. The mass and width of the $f_0(X)$ are fit parameters.

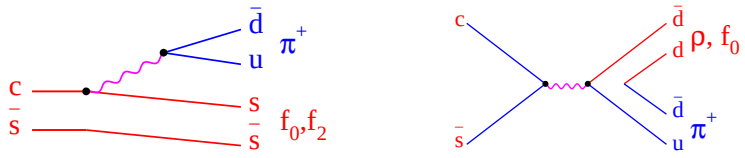

Figure 6: *The dominant diagrams leading to the* $D_s^+ \to \pi^-\pi^+\pi^+$ *decay.*

The fit fractions, as well as the mass and width of the $f_0(X)$, are shown in Table 3 (FOCUS errors are statistical only). FOCUS has about twice as many events as E791. In both analysis the $f_0(980)\pi^+$ is the dominant component, followed by the $f_0(X)\pi^+$. The BES Collaboration [18] measured the mass and width of the $f_0(1370)$ in the $J/\psi \to \phi\pi\pi$ decay, obtaining $m_0 = (1350 \pm 50)$ $\mathrm{GeV/c^2}$ and $\Gamma_0 = (265 \pm 40)$ $\mathrm{GeV/c^2}$. Comparing these values to the ones of the $f_0(X)$, we conclude that the state observed in the $D_s^+ \to \pi^-\pi^+\pi^+$ is not the same as the one observed by BES.

Several variations of the S-wave model were tested. The $\sigma\pi^+$ mode was added to the S-wave, but its contribution is consistent with zero. A fit including the $f_0(1370)\pi^+$ (with BES parameters) was performed, yielding a null contribution of this mode. In both FOCUS and E791, only one $f_0(X)$ is necessary to describe the data, and this state is consistent with being the $f_0(1500)$. The decay fraction of the $f_0(X)$ is very large. Given the diagram of Fig. 6-a, one may conclude that this state has a significant $s\bar{s}$ component in its wave function. In this case we may also expect a large fration of this mode in the $D_s^+ \to \pi^-\pi^+\pi^+$ decay.

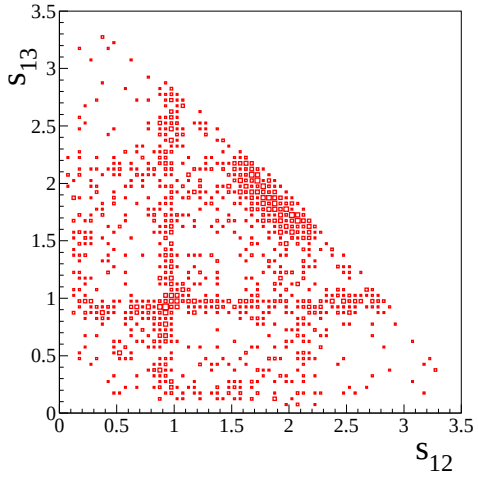

Figure 7: *The Dalitz plot of the $D_s^+ \to \pi^-\pi^+\pi^+$ decay, from FOCUS.*

4.2 The $D_s^+ \to K^-K^+\pi^+$ decay – BaBar

The $D_s^+ \to \pi^-\pi^+\pi^+$ and the $D_s^+ \to K^-K^+\pi^+$ decays share the same dominant diagram (Fig. 6-a). The latter mode can also proceed via the internal W-radiation amplitude (Fig. 8-b). A dominant contribution from the $\phi\pi^+$, $f_0(980)\pi^+$ and $f_0(X)\pi^+$ modes is expected, but there should also be a large $\overline{K}^*(892)^0K^+$ component.

Table 3: *Decay fractions (%) of the* $D_s^+ \to \pi^-\pi^+\pi^+$ *decay. Results are from fits with the isobar model for the* $\pi^-\pi^+$ *S-wave amplitude.*

mode	FOCUS	E791 [20]
$f_0(980)\pi^+$	76.9±4.9	56.5±5.9
$f_0(X)\pi^+$	23.3±0.5	32.4±7.9
nonresonant	13.2±5.7	1±2
$\rho(770)^0\pi^+$	1.2±0.1	5.8±4.4
$\rho(1450)^0\pi^+$	4.0±1.0	4.4±2.1
$f_2(1270)\pi^+$	9.7±1.4	19.7±3.4
$m_0(f_0(X))$ (GeV/c^2)	1.476±5.7	1.434±18
$\Gamma_0(f_0(X))$ (GeV/c^2)	119±18	173±32

BaBar collected a very large (100K signal events) and clean (95% purity) sample [21] of the decay $D_s^+ \to K^-K^+\pi^+$. The Dalitz plot is shown in Fig. 9. BaBar is currently analyzing this data using the PWA method for the S-wave. Here we present preliminary results of the Dalitz plot analysis using the isobar model.

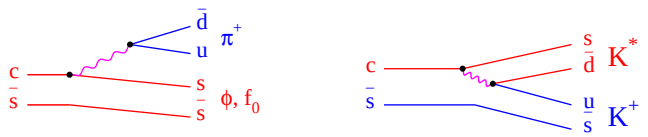

Figure 8: *The dominant diagrams for the decay* $D_s^+ \to K^-K^+\pi^+$.

The fit result is shown in Table 4. In Fig. 9 we have the Dalitz plot projections with the fit result superimposed. In the low K^+K^- mass region there could also be a contribution from $a_0(980)\pi^+$, in addition to the $f_0(980)\pi^+$

Table 4: *Decay fractions (%) of the $D_s^+ \to K^-K^+\pi^+$ decay, from a fit using the isobar model.*

mode	fraction(%)
$f_0(980)\pi^+$	35±14
$f_0(1370)K^+$	6.3±4.8
$f_0(1710)K^+$	2.0±1.0
$\phi(1020)\pi^+$	37.9±1.9
$\overline{K}^*(892)^0K^+$	48.7±1.6

and the $\phi\pi^+$. In practice, is nearly impossible to fit the data with a model having, at the same time, these three amplitudes. The interference between them is very large, the coefficients become highly correlated and the individual fractions become too unstable. A stable fit is obtained with a model having only one of the two scalar amplitudes. The values reported here are from a fit with the $f_0(980)\pi^+$. Note that there is still a large uncertainty in the $f_0(980)\pi^+$ fraction.

The most surprising result is the absence of the $f_0(X)\pi^+$. We can see in Fig. 9-b that there are very few events in the $f_0(X)$ region. There is, on the other hand, a small excess of events next to the $\phi/f_0(980)$ region, which is not well described by an uniform nonresonant amplitude. Instead, a scalar state was introduced. The fitted mass and width of this state are $m_0 = (1.313 \pm 10 \pm 114)$ GeV/c^2 and $\Gamma_0 = (0.395 \pm 8 \pm 133)$ GeV/c^2. The large errors reflect the sensitivity to the details of the S-wave parameterization. One could not really interpret this result as an indication of the $f_0(1370)$, since this is a very complicated region of the K^+K^- spectrum.

The absence of a $f_0(X)$ contribution in $D_s^+ \to K^-K^+\pi^+$ may indicate that the S-wave model used in the study of the $D_s^+ \to \pi^-\pi^+\pi^+$ is not the most correct. BaBar is currently analyzing a sample of the decay $D_s^+ \to \pi^-\pi^+\pi^+$ which is a factor of 10 larger than that of FOCUS. The most important result would be a simultaneous PWA measurement of the S-wave in both final states. The statistics is not a problem for the $D_s^+ \to K^-K^+\pi^+$, but, unfortunately, it is still a bit limited in the case of $D_s^+ \to \pi^-\pi^+\pi^+$, even considering the BaBar sample.

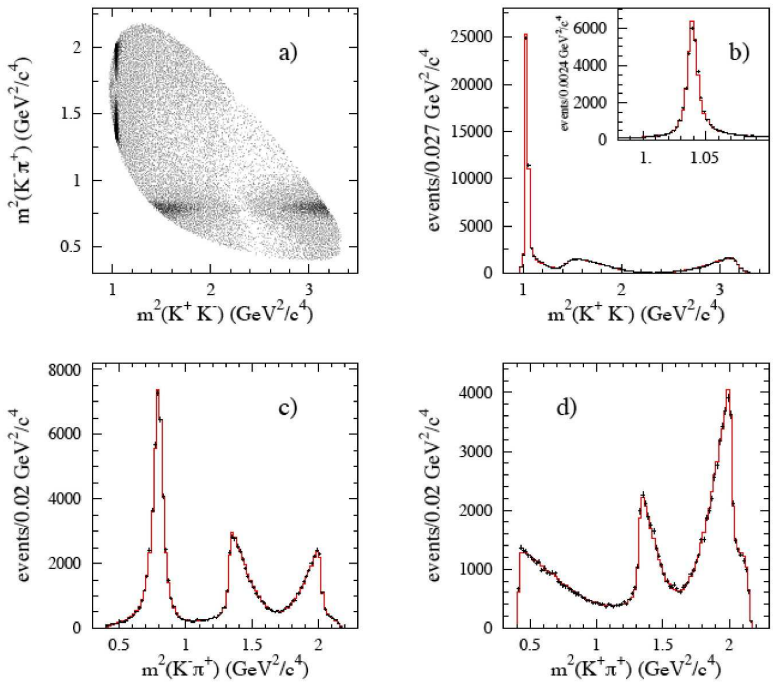

Figure 9: *a) The Dalitz plot of the $D_s^+ \to K^-K^+\pi^+$ decay [21]. Plots b) to d) show the projections of the Dalitz plot into the three axes (points with error bars) with the fit result superimposed (solid histograms).*

4.3 The $D^0 \to \overline{K}^0\pi^+\pi^+$ decay – Belle

Belle and BaBar have collected very large samples of the $D^0 \to \overline{K}^0\pi^+\pi^-$ decay. The Dalitz plot analysis performed by both experiments used the isobar model, and the results are in very good agreement. Here we will discuss the Belle analysis, based on a sample of 534K events [22] with 98% purity.

The diagrams for this decay are shown in Fig. 10. The dominant amplitude should be the $K^*(892)^-\pi^+$ channel, with important contributions from the $\rho(770)\overline{K}^0$ mode and form the $\pi^-\pi^+$ S-wave. The Dalitz plot, shown in Fig.

11, is very complex, since there could be resonances in all three axis. Moreover, there is a small contribution from the doubly Cabibbo suppressed decay $D^0 \to K^0\pi^+\pi^-$. In Fig. 11 the label m^2_- refer to the $\overline{K}^0\pi^-$ mass squared, if the parent is a D^0, or to the the $K^0\pi^+$ combination, in case the parent is a $\overline{D}^0$.

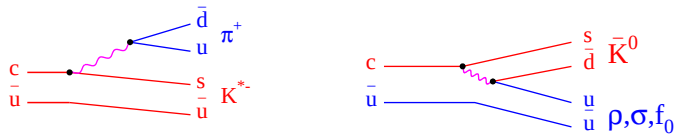

Figure 10: *Diagrams for the* $D^0 \to \overline{K}^0\pi^+\pi^-$ *decay.*

The fit model has 19 amplitudes leading to the $\overline{K}^0\pi^+\pi^-$ final state. The $\pi^+\pi^-$ S-wave contains four amplitudes: $\sigma\overline{K}^0$, the $f_0(980)\overline{K}^0$, $f_0(X)\overline{K}^0$ and an extra scalar state, the $\sigma_2\overline{K}^0$. The $f_0(X)$ parameters were taken from E791 (see Table 3), whereas the σ_2 parameters were determined by the fit. This extra σ_2 amplitude was introduced to account for a structure near $m_{\pi\pi} \sim 1$ GeV/c^2, but it does not correspond to a real state. The parameters obtained by the fit are $m_0 = (1.059 \pm 6)$ GeV/c^2 and $\Gamma_0 = 0.059 \pm 10$ GeV/c^2.

The dominant contribution is, as expected, the $K^*(892)^-\pi^+$ (62%), followed by the $\rho^0\overline{K}^0$ (21%) and the $\pi^+\pi^-$ S-wave ($\sim$15%). The contribution of the $f_0(X)$ is small but significant (1.6%). No errors on the fractions were quoted.

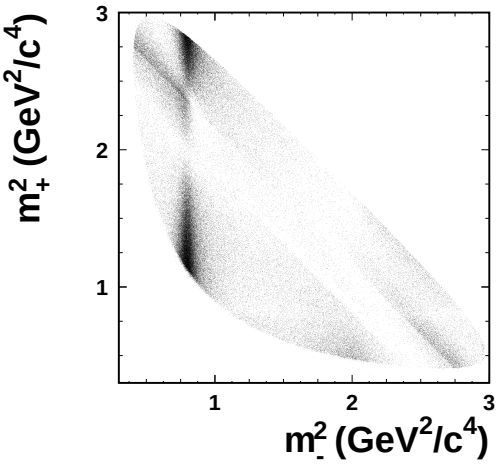

Figure 11: *The Dalitz plot of the decay* $D^0 \to \overline{K}^0\pi^+\pi^-$ [22]. *The label* m^2_- *refer to the* $\overline{K}^0\pi^-$ *mass squared, when the parent is a* D^0*, and to the* $K^0\pi^+$ *mass squared, when the parent is a* $\overline{D}^0$.

In spite of the large number of amplitudes, including the extra 'σ_2', a good fit was not obtained. It is very hard to obtain a good C.L. in fits to very large samples. The goodness-of-fit is accessed by χ^2-like tests, in which the phase space is divided in bins of variable area, so that the number of events is similar in all bins. The isobar approach is, perhaps, too simplistic. With such a large sample, relatively small and localized deviations from the observed Dalitz plot distribution have, in general, large impact in the fit C.L.

The goal of this analysis is to study the mixing phenomenon. The technique is a time dependent Dalitz plot analysis. For this purpose, an effective representation of the data would suffice, according to the authors. Unfortunately the treatment given to the $\pi^+\pi^-$ S-wave do not allow us to draw any conclusion. We cannot interpret the fraction attributed to the $f_0(X)$ as an evidence for this state, since the $\pi\pi$ S-wave is not well understood. No attempt to measure its parameters was reported. A study of the $D^0 \to \overline{K}^0\pi^+\pi^-$ decay

focused at the $\pi\pi$ S-wave and using the PWA method is in order.

4.4 Charmless hadronic three-body decays of B mesons.

Charmless hadronic three-body decays of B mesons are a very promising tool, but there is still a long way to go. The data samples resemble those of D mesons from the late 80's. There are two main problems: statistics is still limited and the background is still high. The nonresonant component is another problem. It is likely to be larger in B than in D decays. A constant nonresonant amplitude is the usual parameterization in the case of D decays, which may be a good approximation given the limited phase space. In B decays, however, the understanding of the nonresonant amplitude is a crucial issue [23], as one can already conclude from the existing data.

There has been intense activity in this area, with many studies from the B-factories. Here we will focus on two analyzes from Belle, the $B^+ \to K^+\pi^+\pi^-$ [24] and $B^0 \to K^0\pi^+\pi^-$ [25] decays, and on two analysis by BaBar, the $B^+ \to K^+K^+K^-$ [26] and $B^0 \to K^0K^+K^-$ [27] decays.

The $B^+ \to K^+\pi^+\pi^-$ signal and the Dalitz plot are shown in Fig. 12. Fig. 12-b illustrates how large is the phase space and how much the action is concentrated near the border.

In these decays the dominant mechanism for the $b \to s$ transition are penguin diagrams, shown in Fig. 13. The diagram of Fig. 13-a leads to final states having three kaons. The $K\pi\pi$ final states proceed via the diagram in Fig. 13-b. We expect dominant contributions from the $K^*(892)\pi^+$, $K_0^*(1430)\pi^+$, $\rho(770)K$ and f_0K modes, in addition to the nonresonant component. We also expect the decay fractions in both $B^0 \to K^0\pi^+\pi^-$ and $B^+ \to K^+\pi^+\pi^-$ to be similar, since the replacement of the d by the u quark in Fig. 13-b turns the B^0 to the B^+ decay.

All studies of charmless hadronic three-body decays of B mesons are performed with the isobar model. The nonresonant is parameterized by empirical formulae, with independent coefficients for each axis. In the two $B \to K\pi\pi$ analyzes by Belle the expression for the nonresonant amplitude is $\mathcal{A}_{NR} = a_1 e^{i\delta_1} f(s_1) + a_2 e^{i\delta_2} f(s_2)$. In both studies the data is better described by a model having one $\pi^+\pi^-$ scalar state at $m_{\pi\pi} \sim 1.5$ GeV/c^2. The results of Dalitz plot fit are in Tables 5 and 6.

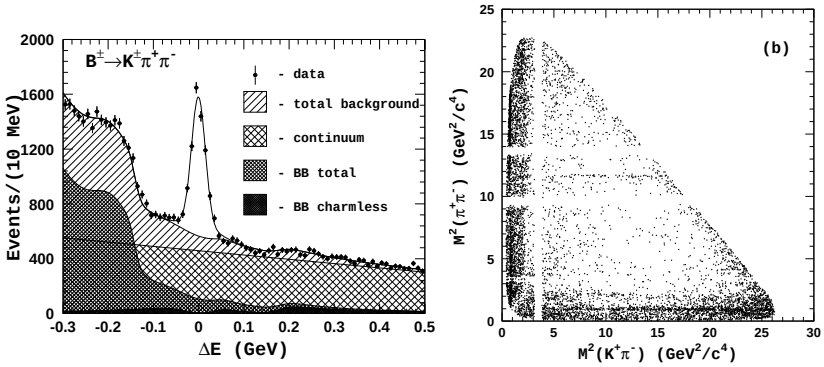

Figure 12: *a) The $B^+ \to K^+\pi^+\pi^-$ signal from Belle [24]. b) The $B^+ \to K^+\pi^+\pi^-$ Dalitz plot.*

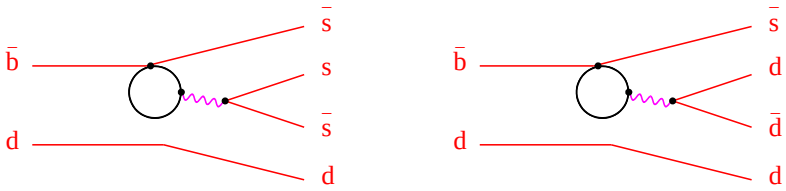

Figure 13: *a) Dominant diagram for $B \to KKK$ decays b) Dominant diagram for $B \to K\pi\pi$ decays.*

The decay fractions are similar in both decays, and correspond to the modes one expect from the diagram of Fig. 13-b. In both B^0 and B^+ decays

Table 5: *Decay fractions (%) of the $B^+ \to K^+\pi^+\pi^-$ decay, from a fit using the isobar model for the S-wave amplitude.*

mode	fraction(%)
$K^*(892)^-\pi^+$	13.0±1.0
$K_0^*(1430)^-\pi^+$	65.5±4.5
$\rho(770)^0 K^+$	7.9±1.0
$f_0(980)K^+$	17.7±3.6
$f_0(X)K^+$	4.1±0.9
nonresonant	34.0±2.7

Table 6: *Decay fractions (%) of the $B^0 \to K^0\pi^+\pi^-$ decay, from a fit using the isobar model for the S-wave amplitude.*

mode	fraction(%)
$K^*(892)^-\pi^+$	11.8±1.7
$K_0^*(1430)^-\pi^+$	64.8±7.8
$\rho(770)^0 K^+$	12.9±2.0
$f_0(980)K^+$	16.0±4.2
$f_0(X)K^+$	3.7±2.4
nonresonant	41.9±5.5

there is a large interference between the $K_0^*(1430)\pi^+$ and the $K\pi$ nonresonant component, which causes the fraction of the $K_0^*(1430)\pi^+$ to be very high. The $K\pi$ S-wave seems to be not well understood. The interference between the $\pi\pi$ S-wave and the corresponding nonresonant amplitude is small, though. The $f_0(X)$ state was represented by a Breit-Wigner function, whose parameters were determined by the data: $m_0 = 1.449 \pm 0.013$ GeV/c^2 and $\Gamma_0 = 0.126 \pm 0.025$ GeV/c^2. These values are in good agreement with the ones obtained from the $D_s^+ \to \pi^-\pi^+\pi^+$ decay by FOCUS and E791.

It is interesting to these results to those from $B \to KKK$. From the diagram in Fig. 13-a one expect significant contributions from the ϕK and $f_0(980)K$. The nonresonant amplitude is parameterized by empirical formulae similar to those used in Belle analysis. In the case of the B^0 the nonresonant amplitude has three independent terms. Like in the $B \to K\pi\pi$ decays, a scalar K^+K^- resonance was introduced, with mass and width determined by the fit.

The K^+K^- projections of the Dalitz plot are shown in Fig. 14. We see a clear bump next to the ϕ peak, at m_{KK} ∼1.5 GeV/c^2. The fit results

are shown in Tables 7 and 8. The contribution of the ϕK decay is similar in both cases. As in the case of the $D_s^+ \to K^+K^-\pi^+$ decay, the fraction of the $f_0(980)K$ mode suffers from large uncertainties. There is a small contribution from the $f_0(1710)K$, but only in the B^+ decay. The most striking features, though, are the very different K^+K^- S-wave composition and the enormous interference between the K^+K^- nonresonant term and what BaBar calls the $X_0(1550)$ state. In the B^+ fit the sum of decay fractions amounts to 300%!.

The Breit-Wigner parameters of the $X_0(1550)$ state were determined in the B^+ analysis. In the B^0 analysis the $X_0(1550)$ parameters were fixed at the values obtained in the B^+ analysis. These are: $m_0 = 1.539 \pm 0.020$ and $\Gamma_0 = 0.257 \pm 0.033$. GeV/c^2. The $X_0(1550)$ parameters are very different from the ones of the $f_0(X)$ state in $B \to K\pi\pi$. However, before drawing any definitive conclusions, the K^+K^- S-wave is understood, as well as the role and form of the nonresonant amplitude.

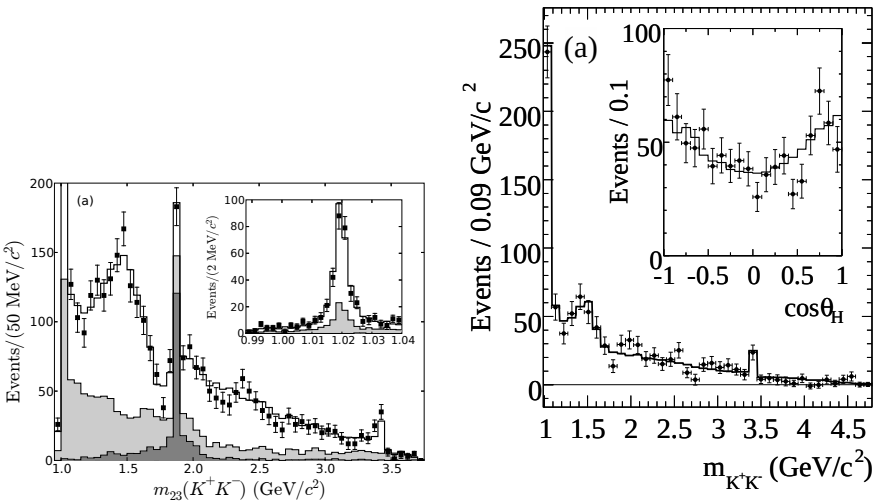

Figure 14: *a) The K^+K^- projections from the $B^+ \to K^-K^+K^-$ (left plot) and $B^0 \to K^0K^+K^-$ (right plot) Dalitz plots.*

Table 7: *Decay fractions (%) of the $B^+ \to K^-K^+K^-$ decay, from a fit using the isobar model for the S-wave amplitude.*

mode	fraction(%)
ϕK^+	11.8±1.2
$f_0(980)K^+$	19±8
$X_0(1550)K^+$	121±20
$f_0(1710)K^+$	4.8±2.9
nonresonant	141±17

Table 8: *Decay fractions (%) of the $B^0 \to K^0K^+K^-$ decay, from a fit using the isobar model for the S-wave amplitude.*

mode	fraction(%)
ϕK^0	12.5±1.3
$f_0(980)K^0$	40.2±9.6
$X_0(1550)K^0$	4.1±1.3
$f_0(1710)K^0$	-
nonresonant	112±15

5 Summary and conclusions

Two of the most challenging problems in the scalar mesons physics have been discussed from the point of view of heavy flavor decays.

In the low energy $K\pi$ spectrum, the neutral κ is now established. An analysis of the elastic scattering data revealed the position of the neutral κ pole, in spite of the lack of data bellow 825 GeV/c^2, and of the suppression of the amplitude due to the Adler zero. The existence of the κ charged partners remain unsettled, though. These issues can be addressed by heavy flavor decays. The $K\pi$ S-wave amplitude was measured in the $D^+ \to K^-\pi^+\pi^+$ decay, including the region bellow 825 GeV/c^2 where LASS data starts. There is, however, one unavoidable task: to extract the $K\pi$ elastic scattering phase from the measured amplitude one has to handle other strong interaction effects.

Evidences for a charged κ are still scarce. The recent results from BaBar ($D^0 \to K^-K^+\pi^0$) and Belle ($\tau^- \to \overline{K}^0\pi^-\nu_\tau$) are rather intriguing. In the τ decay the $K\pi$ system is isolated from any other strong interaction. We would expect that the $K\pi$ phase from this decay to match that of LASS, whereas in the case of the D^0 decay the three-body FSI, or a complex production

amplitude, would cause some deviations from the pure elastic scattering phase. The experimental results, however, show exactly the opposite picture. More data and refined analysis techniques are clearly necessary. In the case of theτ decay, the angular analysis is the crucial and missing piece. If such analysis is performed and confirm the resonant behavior at low $K\pi$ mass, the we will have a compelling evidence for the charged κ.

In the $\pi\pi$ system, the existence of the $f_0(1370)$ has been also addressed in studies of HF decays. The analysis of the $D_s^+ \to \pi^-\pi^+\pi^+$ and $B \to K\pi\pi$ decays show that only one scalar state with mass near 1.5 GeV/c^2 is necessary to describe the data. The measured parameters of this $f_0(X)$ state are consistent with those of the $f_0(1500)$. If we exclude the scalar mesons, in three body D decays the only intermediate states observed are those having a regular $q\bar{q}$ resonance. We could say that it is very likely that the $f_0(1500)$ is a genuine $q\bar{q}$ meson, or has, at least, a strong $q\bar{q}$ component in its wave function. On the other hand, the evidence for the $f_0(1370)$ in HF decays is weak and inconclusive. The puzzling fact, though, is that the fraction of the $f_0(1500)\pi^+$ mode in the $D_s^+ \to \pi^-\pi^+\pi^+$ decay is very large, suggests that the $f_0(1500)$ has a fairly large $s\bar{s}$ component and, therefore, a significant coupling to KK. But this is not true for the $f_0(1500)$, and no indication of this state was found in $D_s^+ \to K^-K^+\pi^+$ decay. One possible interpretation is that the S-wave model used in the $D_s^+ \to \pi^-\pi^+\pi^+$ analysis is incomplete. There are also indications of a scalar state in $B \to KKK$ with mass near 1.5 GeV/c^2, but no conclusions can be drawn before the nonresonant component is understood.

We have seen that hadronic decays of heavy flavor are a very rich environment for the study of the scalar mesons. Thanks to their unique features, the information provided by HF decays are complementary to the traditional hadronic collisions. One must also keep in mind that HF decays have been the only new data available in the past ten years, and this will be so until the commissioning of the new facilities. The B-factories already have very large and clean samples of $D \to h_1h_2h_3$ decays. As for the $B \to h_1h_2h_3$, data with equivalent quality will be available in a few years, from LHCb and the other LHC experiments.

The existence of good data, however, is not enough. The experimentalists need to develop better analysis techniques, going beyond the isobar model. The limitations of the latter appear either when one moves to really high statistics,

or when complex final states are analyzed. Even with a better understanding of the S-wave, it seems that a simple coherent sum of amplitudes may be too simplistic. The improvement of the analysis techniques does not depend only on the experimentalists creativity, but also on a deeper understanding of the decay dynamics, of the role of final state interactions, of the nonresonant amplitude, form factors and line shapes. This requires the urgent intervention of the theoreticians.

In high energy physics most of the attentions are turned to the searches for new physics. There is a widespread belief that we are on the verge of great discoveries, that new particles are right at the corner. One of the most promising fields is the phenomenon of CP violation. The correct measurement of the CP violation effects, however, depends on the accurate understanding of the low energy strong interaction dynamics. That's where the flavor physics and the hadron physics communities meet. Even with somewhat limited analysis tools, there are plenty of good data from the B-factories that should be analyzed in a systematic way, with the focus on the physics of the light quarks and, in particular, of the scalar mesons. This is a very rich and challenging program that needs to be implemented.

References

1. Particle Data Group, D. Asner *et al.*, J.Phys. G: Nucl. Part. Phys. **33**,716 (2006)
2. E.M.Aitala *et al.* (E791 Collaboration), Phys. Rev. Lett. **86**, 770 (2001)
3. E.M.Aitala *et al.* (E791 Collaboration), Phys. Rev. Lett. **89**, 121801 (2002)
4. S.Gardner and U.G.Meissner, Phys. Rev. D **65**, 094004 (2002).
5. J.M.Link *et al.* (FOCUS Collaboration), Phys. Lett **B585**, 200 (2004).
6. E.M.Aitala *et al.* (E791 Collaboration), Phys. Rev.**D73**, 032004 (2006).
7. M.Abiklim *et al.* (BES Collaboration), hep-ex/0506055.
8. S.Descotes-Genon and B.Moussallam, Eur. Phys. J. C**48**, 553 (2006).
9. Babar Collaboration internal note, unpublished.

10. D.Aston *et al.* (LASS Collaboration), Nucl. Phys. B**296**, 493 (1988).

11. J.M.Link *et al.* (FOCUS Collaboration), Phys. Lett **B653**, 1 (2007).

12. D.Epifanov *et al.* (Belle Collaboration), arXiv:0706.2231.

13. J.M.Link *et al.* (FOCUS Collaboration), Phys. Lett **B621**, 72 (2005).

14. G.Bonvicini *et al.* (CLEOc Collaboration), arXiv:0707.3060.

15. FOCUS Collaboration, in preparation.

16. Particle Data Group, W.-M.Yao *et al.*, J.Phys. G: Nucl. Part. Phys. **33**,1 (2006).

17. D.V.Bugg, arXiv:0706.1254.

18. M.Abiklim *et al.* (BES Collaboration), Phys. Lett **B607**, 243 (2005).

19. FOCUS Collaboration internal note, unpublished.

20. E.M.Aitala *et al.* (E791 Collaboration), Phys. Rev. Lett. **86**, 765 (2001).

21. B.Aubert *et al.* (Babar Collaboration), Phys. Rev. **D76**, 011102 (2007).

22. L.M.Zhang *et al.* (Belle Collaboration), arXiv:0704.1000.

23. I.Bediaga *et al.*, arXiv:0709.0075.

24. A. Garmash *et al.* (Belle Collaboration), Phys. Rev. **D71**, 092003 (2005).

25. A. Garmash *et al.* (Belle Collaboration), Phys. Rev. **D75**, 012006 (2007).

26. B.Aubert *et al.* (Babar Collaboration), Phys. Rev. **D74**, 032003 (2006).

27. B.Aubert *et al.* (Babar Collaboration), arXiv:0706.3885.

Frascati Physics Series Vol. XLVI (2007), pp. 109–120
HADRON07: XII Int. Conf. on Hadron Spectroscopy – Frascati, October 8-13, 2007
Plenary Session

EXOTICS MESONS: STATUS AND FUTURE

Eberhard Klempt
Helmholtz-Institut für Strahlen- und Kernphysik Nußallee 14-16 D53115 Bonn

Abstract

The evidence for the existence of mesons with exotic quantum numbers and of hybrid candidates with non-exotic quantum numbers is critically reviewed, including candidates with hidden charm. Aims and methods of future searches for hybrid mesons are briefly discussed.

1 Introduction

The search for exotic mesons is at a turning point. The experiments at BNL, Protvino, and at LEAR which have reported evidence for exotic mesons have terminated data taking; data analysis is completed and the results are published since a few years. On the other hand, new experiments are ahead of us, COMPASS at CERN and BESIII in the immediate future, the Hall-D experiment at the upgraded Jlab facility and PANDA at GSI in the medium-range

future. Hence it seems timely to review the status of exotic mesons to define the platform from which the new experiments are starting. It is custom to start from the assumption that glueballs and hybrids are firmly predicted by Quantum Chromo Dynamics, and experimental results have to concur with this prediction. Here, a different view will is adopted: the question is asked if a convincing argument can be made that the existence of exotic mesons, of hybrids and/or tetraquark mesons, can be deduced unambiguously from past experiments. The search for hybrids is part of the wider quest to understand the role of gluons in spectroscopy [1)].

2 Exotic mesons

2.1 Flavor exotic mesons

Flavor exotic states have a flavor configuration with a minimum of four quarks like doubly charged states ($uu\bar{s}\bar{d}$) or tetraquark states with heavy flavor ($cs\bar{u}\bar{d}$). By definition, such states cannot mix with regular $q\bar{q}$ states. In light-quark meson spectroscopy, there is no accepted flavor exotic candidate (see also [2)]). A $c\bar{c}u\bar{d}$ candidate will be discussed below.

2.2 Spin-parity exotics

Spin-parity exotic mesons have quantum numbers J^{PC} which are not allowed for fermion-antifermion systems, $J^{PC}_{exotics} = 0^{--},\ 0^{+-},\ 1^{-+},\ 2^{+-},\ 3^{-+}\cdots$. The quantum numbers 1^{-+} are part of the series 0^{-+}, 1^{-+}, 2^{-+}, $\cdots$; the isovector states are called π, π_1, π_2, π_3 $\cdots$. In this series, the J-odd states are exotic. A partial wave expansion of the $\pi\eta$ system, e.g., will have components with $L = 0, 1, 2, 3, \cdots$ leading to quantum numbers of the partial waves characterized by a_0, π_1, a_2, π_3, $\cdots$ where the π_1 and π_3 are exotic. Likewise, $\pi\rho$ in P-wave has 1^{-+} quantum numbers, $f_1\pi$ and $b_1\pi$ are $J^{PC} = 1^{-+}$ exotic when they are in S-wave. The corresponding isoscalar states are called η, η_1, η_2, $\cdots$.

Exotic mesons may be hybrid mesons ($q\bar{q}g$), multiquark states ($q\bar{q}q\bar{q}$...), multimeson states (M_1 M_2...) or, possibly, glueballs. Hybrids, tetraquarks (and glueballs) may also have quantum numbers of ordinary ($q\bar{q}$) mesons. In this case, they can mix. In this review, we comment on mesons with exotic mesons, and on hybrids. The lightest hybrid mesons should have a mass in the $1.7 - 2.2$ GeV/c^2 region even though smaller values are not ruled out. Tetraquark states

should have about the same mass.

Most experimental information on spin-parity exotic mesons comes from diffractive or charge exchange scattering of a π^- beam off protons or nuclear targets at fixed beam momenta (in parentheses), from E852 at BNL (18 GeV/c; $\eta\pi^-$, $\eta'\pi^-$, $\rho\pi^-$, $f_1\pi^-$, $b_1\pi^-$, $\eta\pi^0$) and VES at Protvino (28, 37 GeV/c; $\eta\pi^-$, $\eta'\pi^-$, $\rho\pi^-$, $f_1\pi^-$, $b_1\pi^-$, $\eta'\pi^0$). The Crystal Barrel and Obelix collaborations at LEAR, CERN, have reported evidence for exotic mesons from $p\bar{p}$ annihilation at rest ($\eta\pi^\pm$, $\eta\pi^0$, $\rho\pi$, $b_1\pi$). References to earlier experiments can be found in [1].

Resonances, hybrids or tetraquark states, and meson-meson molecular systems can possibly be differentiated. A resonance with $J^{PC} = 1^{-+}$ can decay into $\pi\eta$, $f_1\pi$, $\rho\pi$, and $b_1\pi$. Of course, the fractions are unknown but there is no selection rule expected which may suppress one of these decay modes. If exotic waves originate from diffractive meson-meson scattering, the ρ may be excited to b_1 in $\rho\pi$ scattering but not ρ to the η; in $f_1\pi$ scattering, the f_1 could be de-excited to the η but not excited to the b_1. If diffractive meson-meson scattering were responsible for the exotic-wave amplitudes, we might expect different production characteristics for $\pi\eta$ and πf_1, and for $\rho\pi$ and $b_1\pi$.

2.3 The $\pi_1(1400)$

The data in Fig. 1 exhibit a dominant $a_2(1320)$ in the D_+ and a clear bump at $M \approx 1.4\,\mathrm{GeV/c^2}$ in the (exotic) P_+ partial wave. The E-852 collaboration [3)4)] finds that the data are consistent with a simple ansatz, assuming contributions from two resonances, one in each partial waves. The D_+ wave returns the parameters of $a_2(1320)$, for the P_+ partial wave, mass and width are determined to $M = 1370 \pm 16\ ^{+50}_{-30}$ MeV/c^2; $\Gamma = 385 \pm 40^{+\ 65}_{-105}$ MeV/c^2. A similar fit was used by VES yielding compatible results [5)]. The VES collaboration tried fits without resonance but with a phenomenological background amplitude. The fit gave a significantly worse but not unacceptable χ^2. Both fits are shown in Fig. 1.

The Indiana group [6)] used t channel exchange forces to construct a background amplitude which could mimic $\pi_1(1400)$. The $\pi\eta$ P_+-wave interactions very similar to $\pi\pi$ S-wave interactions were constructed. The latter are characterized by the σ pole; as a consequence, $\pi_1(1400)$ is considered as σ-type phenomenon in $\pi\eta$ P_+-wave interactions. In the words of the authors of [6)],

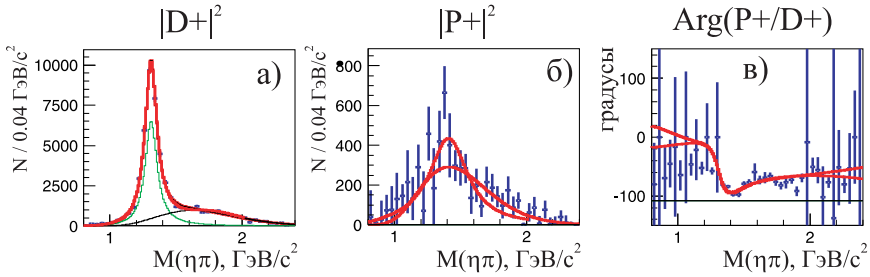

Figure 1: Results of partial-wave analysis of the $\eta\pi^-$ system: a) intensity of D_+ wave, b) intensity of P_+ wave, c) phase difference P_+/D_+ [5].

$\pi_1(1400)$ is 'not a QCD bound state' but rather generated dynamically by meson exchange forces.

Based on $SU(3)$ arguments, a P-wave resonance in the $\eta_8\pi$ channel must belong to a $SU(3)$ decuplet [7]. The decuplet-antidecuplet includes also $K^+\pi^+$ P-wave which shows practically no phase motion at all [8]. Very little phase motion should hence be expected for the $\pi\eta$ P_+-wave.

At BNL, the charge exchange reaction $\pi^-p \to \eta\pi^0 n$, $\eta \to \pi^+\pi^-\pi^0$ at 18 GeV/c was shown to be consistent with a resonant hypothesis for the P_+ wave, and a mass of $1257 \pm 20 \pm 25$ MeV/c^2, and a width of $354 \pm 64 \pm 60$ MeV/c^2 were deduced [9]. The authors left open the question if this object should be identified with $\pi_1(1400)$ or if it is a second state in this partial wave. The VES $\eta\pi^0$ spectrum is dominated by the $a_2^0(1320)$ meson; they did not find evidence for the neutral $\pi_1^0(1600)$.

The Crystal Barrel Collaboration confirmed the existence of the exotic $\pi\eta$ P_+-wave in $\bar{p}n \to \pi^-\pi^0\eta$ [10] and $\bar{p}p \to 2\pi^0\eta$ [11]. The Crystal Barrel [12] and Obelix [13] collaborations found a resonant contribution of the $J^{PC} = 1^{-+}$ wave in $(\rho\pi)$ in $p\bar{p}$ annihilation to four pions. However, the $\pi\eta$ P-wave is produced from spin triplet states of the $N\bar{N}$ system, the exotic $\rho\pi$ wave comes from spin singlet states. Hence these must be different objects, a $\pi_1(1400)$ and a $\tilde{\pi}_1(1400)$, plus a neutral $\pi_1(1260)$ if the latter is another separate resonance. In $p\bar{p}$ annihilation into $\pi\pi\eta$, triangle singularities due to final-state rescattering yield logarithmic divergent amplitudes. The inclusion of rescattering amplitudes was never attempted; it could possibly reduce the need for a true pole. In summary, there is evidence for the existence of a $\pi\eta$ resonance with exotic

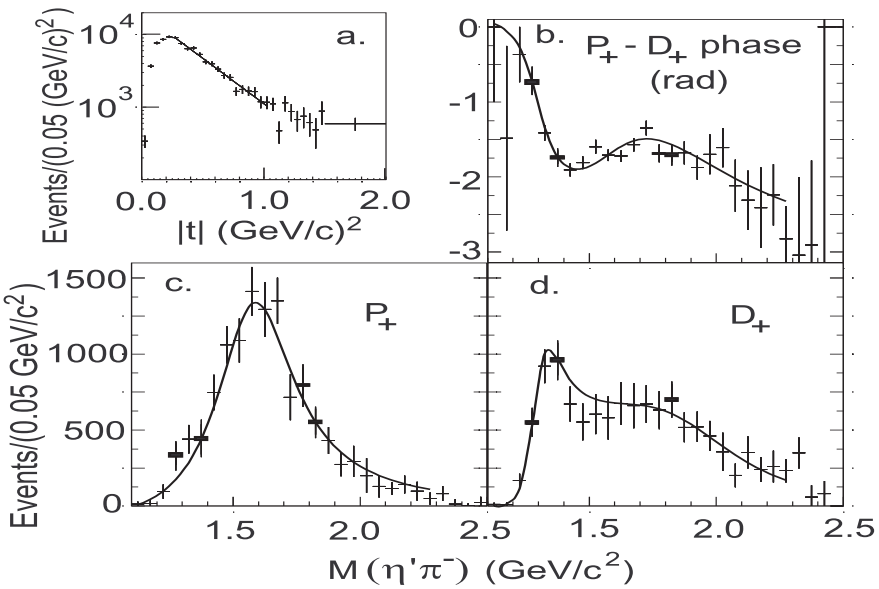

Figure 2: BNL data [4]: (a) The acceptance-corrected $|t|$ distribution fitted with the function $f(t) = ae^{b|t|}$ (solid line). (b), (c), (d) results of a mass-independent PWA and a mass-dependent fit (solid curve) for the P_+ and D_+ partial waves and their phase difference. (b) The $(P_+ - D_+)$ phase difference. (c) Intensity of the P_+ and (d) of the D_+ partial wave.

quantum numbers but there are severe inconsistencies in the overall picture associated with its existence.

2.4 The $\pi_1(1600)$ and $\pi_1(2000)$

Fig. 2 shows the $\eta'\pi^-$ system produced in a diffractive-like reaction at $p_{\pi^-} = 18\,\mathrm{GeV/c}$. The data are from the E-852 collaboration [14]; VES using a beam at $p_{\pi^-} = 37\,\mathrm{GeV/c}$ showed similar distributions [15]. The 1^{-+} wave exceeds in intensity the tensor wave and is readily fitted by a Breit-Wigner resonance at $M \approx 1600$ MeV/c^2 which is listed as $\pi_1(1600)$ in the Review of Particle Properties. The absence of $\pi_1^0(1600)$ can be understood by assuming that

- $\pi_1(1600)$ decouples from $\rho\pi$, or
- $\pi_1(1600)$ originates from meson-meson diffractive scattering

The wave $J^{PC} = 1^{-+}$ in the $\pi^+\pi^-\pi^-$ system was studied in diffractive-like reactions by the VES collaboration [16)17)] and by the E-852 collaboration at $p_\pi = 18$ GeV/c [18)19)] suggesting the existence of an exotic resonance in $\rho\pi$ which we call $\tilde{\pi}_1(1600)$. A new BNL data sample with 10-fold increased statistics was reported in [20)], yielding negative evidence for a resonance in the P_+ wave. The $\tilde{\pi}_1(1600)$ must be different from the $\pi_1(1600)$ seen in $\eta'\pi$; firstly, because of the nearly vanishing coupling of $\pi_1(1600) \to \rho\pi$ and, secondly, for the different production modes: the $\pi_1(1600)$ is produced by natural parity exchange, the $\tilde{\pi}_1(1600)$ by both, natural and unnatural parity exchange in about equal portions.

The dominant wave in $f_1\pi$ is $J^{PC} = 1^{-+}$. It is produced via natural parity exchange; it resembles in production characteristics the $\eta'\pi$ exotic wave [17)]. The E-852 collaboration fitted the PWA intensity distributions and phase differences with a superposition of Breit-Wigner resonances in all channels. In the exotic wave, two resonances are introduced at M=(1709±24±41), Γ=(403±80±115) MeV/c^2 and M=(2001±30±92), Γ=(333±52±49) MeV/c^2 [21)].

Similar observations in $f_1(1285)\pi$ in the $\omega(\pi^+\pi^-\pi^0)\pi^-\pi^0$ channel studied by VES [17)22)] and E-852 [23)]. Three isobars $\omega\rho$, $b_1\pi$ and $\rho_3\pi$ were considered. The BNL collaboration interprets the data by resonances, two of them, called $\tilde{\pi}_1(1600)$ and $\tilde{\pi}_1(2000)$ here, are compatible in mass with the findings from $f_1(1285)\pi$ but are produced via natural and unnatural parity exchange. The VES data find consistency with a resonance interpretation but can describe the data without exotic resonances as well.

2.5 Conclusions on light-quark exotics

Partial waves with exotic spin-parity have been observed in several experiments. The data are consistent with the assumption that the exotic wave originates from diffractive meson-meson scattering. The interpretation of the observation as genuine resonances is controversial.

3 Non-exotic hybrid candidates

3.1 Light-quark hybrid candidates

Figure 3 shows the light quark mesons with known quantum numbers $I^G J^{PC}$ as a function of M^2. The ordering of states follows expectations from potential

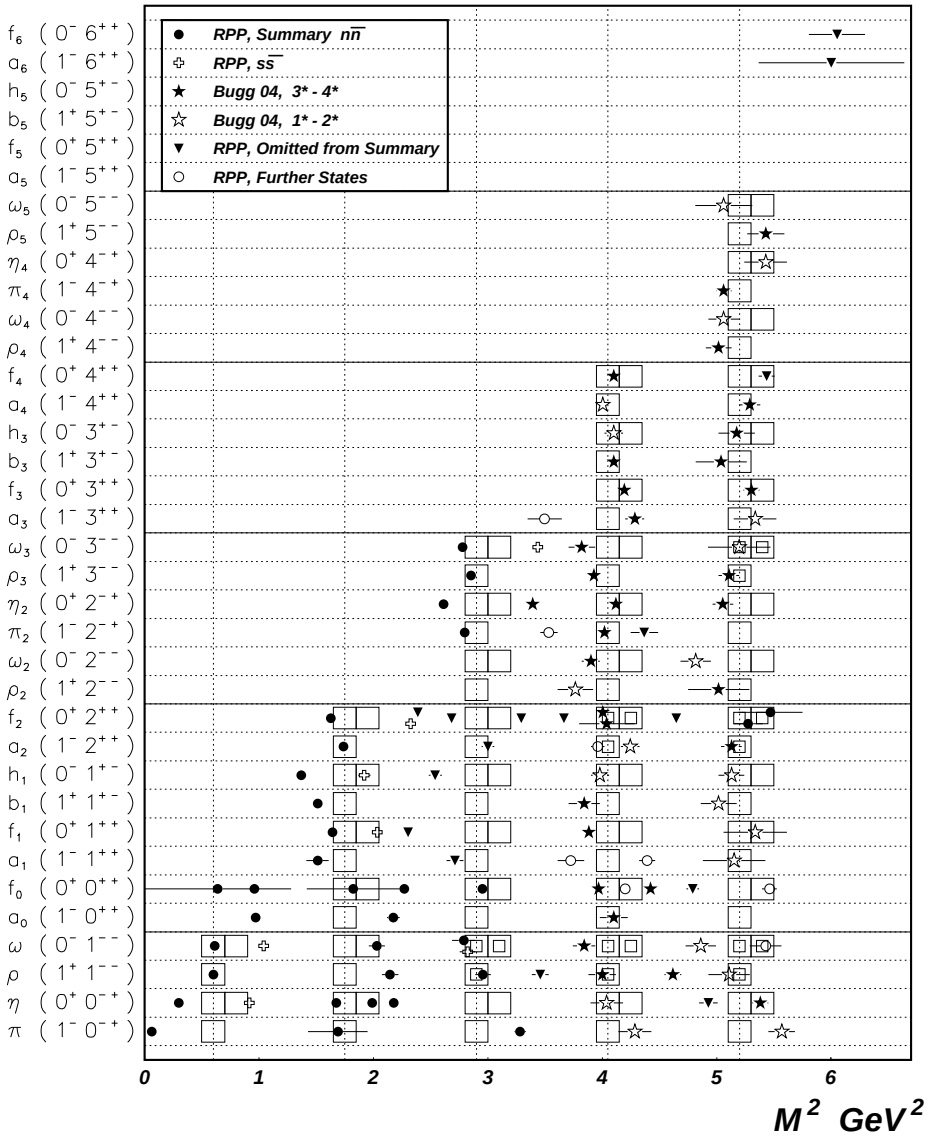

Figure 3: The pattern of light quark meson states.

models for $q\bar{q}$ mesons. The empty boxes indicate the position of states in a simplified model in which masses of mesons are proportional to $l+n$, where l is the orbital and n the radial quantum number. Mesons of zero isospin have two nearby boxes for $n\bar{n}$ and $s\bar{s}$ states or for $SU(3)$ singlet and octet states. Some boxes are doubled because two different states, with $J = l+1, n$ and $J = l-1, n+2$, are expected. Nearly all observed mesons are compatible with a $q\bar{q}$ assignment, with two remarkable exceptions, $\pi_2(1870)$ and $\eta_2(1870)$ [24)–28)]. These two states are meaningful hybrid candidates. When scrutinizing these observation, we notice that comparatively narrow hybrids are predicted for the $J^{PC} = 2^{-+}$ wave which has important S-wave thresholds, $f_2(1270)\pi$ and $a_2(1320)\pi$. Narrow hybrids are also predicted for the $J^{PC} = 1^{++}$ wave. In this wave, there are no important S-wave thresholds, and no hybrid candidates, neither. Certainly, a good understanding of the threshold dynamics is required. High statistics data in several final states are mandatory to resolve this issue.

3.2 Is there restoration of chiral symmetry?

There is a degeneracy of the masses with positive and negative parities which has been interpreted as evidence for restoration of chiral symmetry in highly excited mesons [29)–31)]. A new QCD scale $\Lambda_{CSR} = 2.5\,\mathrm{GeV/c^2}$ is suggested at which chiral symmetry is restored [32)33)].

The l, n degeneracy follows also from a model based on the dual superconductor mechanism of confinement [34)] and from a model guided by the correspondence of the dynamics of quarks in QCD and of strings in a five-dimensional Anti-de-Sitter space [35)]. Both approaches suggest

$$M_n^2(l) = 2\pi\sigma\left(l + n + \frac{1}{2}\right) .$$

which shows that the squared masses are linear in l and n, and degenerate in $n + l$. The string model and the conjectured restoration of chiral symmetry thus both lead to a $n + l$ degeneracy of excited states. The two models make however different predictions for 'stretched' states, for states with $J = l + s$. The string model predicts no parity partners for $a_2(1320)$–$f_2(1270)$, $\rho_3(1690)$–$\omega_3(1670)$, $a_4(2040)$–$f_4(2050)$, $\rho_5(2350)$–ω_5, $a_6(2450)$–$f_6(2510)$ while their existence should be expected if chiral symmetry restoration is at work. Experimentally, there are no chiral partner for any of these 10 states. Hence, at the first glance, data do not support the hypothesis of chiral symmetry restoration.

3.3 J/ψ excitations

With the discovery of the $h_c(1P)$ and $\eta_c(2S)$ resonances, an important milestone was reached: all charmonium states predicted by quark models below the $D\bar{D}$ threshold have been found, and no extra state. Above the $D\bar{D}$ threshold, several surprisingly narrow states were found called $X(3872)$, $X(3940)$, $Y(3940)$, and $Z(3930)$. In spite of some anomalous properties, these states can be assigned to $\chi_1(2P)$, $\eta_c(3S)$, $\chi_0(2P)$, and $\chi_2(2P)$. Reasons for this assignment are discussed in [1]. A particularly demanding state is the $Y(4260)$ which is discussed next.

3.4 The $Y(4260)$

The $Y(4260)$ was discovered by the BaBaR collaboration as an enhancement in the $\pi\pi J/\psi$ subsystem in the initial state radiation (ISR), in $e^+e^- \to \gamma_{\rm ISR} + J/\psi\pi\pi$ [36]. Its mass was determined to $4259 \pm 8 \pm 4$ MeV/c^2, the width to $88 \pm 23 \pm 5$ MeV/c^2, the spin-parity to $J^{PC} = 1^{--}$. The $Y(4260)$ resonance was searched for in the inclusive e^+e^- annihilation cross section [37]. In the $\sqrt{s} = 4.20 - 4.35\,{\rm GeV/c^2}$ region, the cross section exhibits a dip-bump-dip structure which makes it difficult to extract a reliable estimate for a possible $Y(4260)$ contribution. The apparent absence of $Y(4260)$ in this reaction has stimulated the interpretation that it could be a hybrid [38)–40)] or a tetraquark resonance [41]. The upper limit of $Y(4260)$ in the inclusive e^+e^- annihilation cross section depends however on the flexibility of the fit. If constructive and destructive interferences are allowed, the upper limit for $Y(4260)$ is less stringent and a scenario as suggested in Table 1 is not excluded.

At this conference, W.S. Hou reported observation of $e^+e^- \to \Upsilon(1S)\pi^+\pi^-$, $\Upsilon(2S)\pi^+\pi^-$, and $\Upsilon(3S)\pi^+\pi^-$ at $\sqrt{s}$ 10.87 GeV, near the peak of the $\Upsilon(10860)$. If these signals originate from the $\Upsilon(10860)$ resonance, the corresponding partial widths are much larger than expected and would suggest that $\Upsilon(10860)$ – and $Y(4260)$ as well – be a hybrid.

3.5 Is there a $\psi(2S)\pi^+$

A narrow $\psi'\pi^\pm$ resonance was observed by the Belle collaboration in B decays to $K\pi^+\psi'$, with a statistical evidence exceeding 7σ [42]. The resonance, called $Z^+(4430)$, has $4433 \pm 4 \pm 1\,{\rm MeV/c^2}$ mass and a width of $\Gamma = 44^{+17+30}_{-13-11}\,{\rm MeV/c^2}$.

Table 1: Charmonium states with $J^{PC} = 1^{--}$ in our interpretation. The partial widths are given in keV/c^2, the masses in MeV/c^2.

J/ψ	$\psi(3686)$	$\psi(3770)$	$\psi(4040)$	$\psi(4160)$	$Y(4260)$	$\psi(4415)$
	$2S$	$1D$	$3S$	$2D$	$4S$	$5S$
$\Gamma_{e^+e^-}$	2.48 ± 0.06	$0.242^{+0.027}_{-0.024}$	0.86 ± 0.07	0.83 ± 0.07	*0.72*	0.58 ± 0.07
$\Gamma_{J/\psi\pi^+\pi^-}$	107 ± 5	44 ± 8	< 360	< 330	670 ± 240	-
$M_{\psi(nS)} - M_{J/\psi}$	589	674	943	1056	1163	1318
$M_{\Upsilon(nS)} - M_{\Upsilon}$	563		895		1119	

It is the first charged resonance with hidden charm; evidently, it can not belong to the charmonium family. It was interpreted as tetraquark radial excitation [43]. Rosner noticed that the $Z(4430)$ mass is at the $D^*\bar{D}_1(2420)$ threshold and proposed that the state is formed via the weak $b \to c\bar{c}s$ transition, creation of a light-quark pair, and rescattering of the final-state hadrons [44]. Hence at present, there not yet the need for an interpretation beyond the standard quark model using $q\bar{q}$ only.

4 Conclusions and outlook

In the view presented here, there is not yet a convincing answer to the question if hybrid mesons exist. When data are analyzed assuming the existence of hybrids, evidence is observed in several places. If this conjecture is examined with scrutiny, the evidence for hybrids fades away. There are, however, specific predictions for the outcome of future experiments. If exotic partial waves are due to diffractive meson-meson scattering, the π_1 partial wave should not be produced in the charge exchange reaction $\pi^- p \to n\pi_1^0(1400)$. The $\pi_1^0(1400)$ observed in [9] is in conflict with this conjecture, but in conflict with VES data, too. Likewise, there should be no production of $\pi_1^0(1600)$ or $\pi_1^0(2000)$. In central production, a large contribution to the cross section will come from Regge-Pomeron fusion which should be a good place to search for hybrids. With two detected protons, no charged Reggeon is exchanged (with Reggeon exchange = Regge or Pomeron exchange); diffractive meson-meson scattering leads to neutral final states and no hybrids with exotic quantum numbers should

be found. At Jlab, the initial state γp is charged, and partial waves with exotic quantum numbers due to diffractive meson-meson scattering should be observed in their charged state only.

The new BELLE results on $\Upsilon(10860)$ decays reported by W.S. Hou are very suggestive. If the signals are due to an extremely large $\Upsilon(10860) \to \Upsilon(nS)\pi^+\pi^-$ decay mode, hybrids with hidden beauty seem to be a natural consequence. Similarly, the $Y(4260)$ might be of hybrid nature as well. Hence there is room left; Panda at GSI (or, earlier, BELLE) will have to give us the final answer. The existence or not of glueballs – which were not discussed here – is a question which should find its answer from BESIII.

References

1. E. Klempt and A. Zaitsev, "Glueballs, Hybrids, Multiquarks. Experimental facts versus QCD inspired concepts," arXiv:0708.4016 [hep-ph].
2. A. Filippi *et al.*, Nucl. Phys. A **692** (2001) 287.
3. D. R. Thompson *et al.*, Phys. Rev. Lett. **79** (1997) 1630.
4. S. U. Chung *et al.*, Phys. Rev. D **60** (1999) 092001.
5. V. Dorofeev *et al.*, AIP Conf. Proc. **619** (2002) 143.
6. A. P. Szczepaniak, M. Swat, A. R. Dzierba and S. Teige, Phys. Rev. Lett. **91** (2003) 092002.
7. S. U. Chung, E. Klempt and J. G. Korner, Eur. Phys. J. A **15** (2002) 539.
8. P. Estabrooks *et al.*, Nucl. Phys. B **133** (1978) 490.
9. G. S. Adams *et al.*, "Confirmation of a π_1^0 exotic meson in the $\eta\pi^0$ system," arXiv:hep-ex/0612062.
10. A. Abele *et al.*, Phys. Lett. B **423** (1998) 175.
11. A. Abele *et al.*, Phys. Lett. B **446** (1999) 349.
12. W. Dunnweber and F. Meyer-Wildhagen, AIP Conf. Proc. **717** (2004) 388.
13. P. Salvini *et al.*, Eur. Phys. J. C **35** (2004) 21.
14. E. I. Ivanov *et al.*, Phys. Rev. Lett. **86** (2001) 3977.
15. G. M. Beladidze *et al.*, Phys. Lett. B **313** (1993) 276.
16. D. V. Amelin *et al.*, Phys. Lett. B **356**, 595 (1995).

17. D. V. Amelin *et al.*, Phys. Atom. Nucl. **68** (2005) 359.
18. G. S. Adams *et al.*, Phys. Rev. Lett. **81** (1998) 5760.
19. S. U. Chung *et al.*, Phys. Rev. D **65**, 072001 (2002).
20. A. R. Dzierba *et al.*, Phys. Rev. D **73** (2006) 072001.
21. J. Kuhn *et al.*, Phys. Lett. B **595**, 109 (2004).
22. D. V. Amelin *et al.*, Phys. Atom. Nucl. **62** (1999) 445.
23. M. Lu *et al.*, Phys. Rev. Lett. **94**, 032002 (2005).
24. J. Adomeit *et al.*, Z. Phys. C **71** (1996) 227.
25. D. Barberis *et al.*, Phys. Lett. B **471** (2000) 435.
26. D. Barberis *et al.*, Phys. Lett. B **471** (2000) 440.
27. A. V. Anisovich *et al.*, Phys. Lett. B **477** (2000) 19.
28. A. V. Anisovich *et al.*, Phys. Lett. B **500** (2001) 222.
29. L. Y. Glozman, Phys. Lett. B **539** (2002) 257.
30. L. Y. Glozman, Phys. Lett. B **541** (2002) 115.
31. L. Y. Glozman, Int. J. Mod. Phys. A **21** (2006) 475.
32. E. S. Swanson, Phys. Lett. B **582** (2004) 167.
33. S. S. Afonin, Phys. Lett. B **639** (2006) 258.
34. M. Baker and R. Steinke, Phys. Rev. D **65** (2002) 094042.
35. A. Karch *et al.*, Phys. Rev. D **74** (2006) 015005.
36. B. Aubert *et al.*, Phys. Rev. Lett. **95**, 142001 (2005).
37. X. H. Mo *et al.*, Phys. Lett. B **640** (2006) 182.
38. S. L. Zhu, Phys. Lett. B **625** (2005) 212.
39. F. E. Close and P. R. Page, Phys. Lett. B **628** (2005) 215.
40. E. Kou and O. Pene, Phys. Lett. B **631** (2005) 164.
41. L. Maiani *et al.*, Phys. Rev. D **72** (2005) 031502.
42. M. Ablikim *et al.*, Phys. Lett. B **656** (2007) 30.
43. L. Maiani, A. D. Polosa and V. Riquer, "The Charged $Z(4433)$: Towards a New Spectroscopy," arXiv:0708.3997 [hep-ph].
44. J. L. Rosner, "Threshold effect and $\pi^{\pm}\psi(2S)$ peak," arXiv:0708.3496 [hep-ph].

Frascati Physics Series Vol. XLVI (2007), pp. 121
HADRON07: XII Int. Conf. on Hadron Spectroscopy – Frascati, October 8-13, 2007
Plenary Session

RECENT RESULTS FROM BARYON SPECTROSCOPY

U. Thoma
Universitaet Bonn

Written contribution not received

Frascati Physics Series Vol. XLVI (2007), pp. 123–132
HADRON07: XII Int. Conf. on Hadron Spectroscopy – Frascati, October 8-13, 2007
Plenary Session

MILESTONES OF THE PHENIX EXPERIMENT AT RHIC

M. Csanád for the PHENIX Collaboration
Eötvös University, Budapest 1117, Pázmány Péter s. 1/A, Hungary

Abstract

The latest PHENIX results for particle production are presented in this paper. A suppression of the yield of high p_t (transverse momentum) hadrons in central Au+Au collisions is found. In contrast, direct photons are not suppressed in central Au+Au collisions and no suppression of high p_t particles can be seen in d+Au collisions. This leads to the conclusion that the dense medium formed in central Au+Au collisions is responsible for the suppression. It is as well found, that the properties of this medium are similar to the one of a liquid. Further measurements provide information about the chiral dynamics of the system.

1 Introduction

Ultra-relativistic collisions, so called "Little Bangs" of almost fully ionized Au atoms are observed at the four experiments (BRAHMS, PHENIX, PHOBOS

and STAR) of the Relativistic Heavy Ion Collider (RHIC) of the Brookhaven National Laboratory, New York. The aim of these experiments is to create new forms of matter that existed in Nature a few microseconds after the Big Bang, the creation of our Universe.

A consistent picture emerged after the first three years of running the RHIC experiment: quarks indeed become deconfined, but also behave collectively, hence this hot matter acts like a liquid [1)], not like an ideal gas theorists had anticipated when defining the term QGP. The situation is similar to as if prisoners (quarks and gluons confined in hadrons) have broken out of their cells at nearly the same time, but they find themselves on the crowded jail-yard coupled with all the other escapees. This strong coupling is exactly what happens in a liquid [2)].

2 High pt suppression

High transverse momentum particles resulting from hard scatterings between incident partons have become one of the most effective tools for probing the properties of the medium created in ultra-relativistic heavy ion collisions at RHIC. Nuclear modification factor, defined as

$$R_{\rm AA}(p_t) \equiv \frac{\text{Yield in Au+Au events}}{\text{Scaled Yield in p+p events}}, \qquad (1)$$

was measured in central and preripheral Au+Au collisions at the four RHIC experiments [3−10)]. The measurements show a high transverse momentum hadron suppression in central Au+Au collisions compared to (appropriately scaled) p+p collisions, while there is no such suppression in peripheral Au+Au or d+Au collisions [11−13)], as shown in the upper plots of Fig. 1. This shows that the suppression is not due to modification of parton distributions in the colliding nuclei.

The nuclear modification factor has been measured for several hadron species at highest p_t: for π_0, and most recently η mesons [14)], as shown in the lower plots of Fig. 1. This confirms the above evidence for a dense and strongly interacting matter. On the other hand, direct photon measurements, which require tight control of experimental systematics over several orders of magnitude, show that the high p_t photons in Au+Au collisions are not suppressed [15)] and, thus, provide final confirmation that hard scattering processes occur at rates

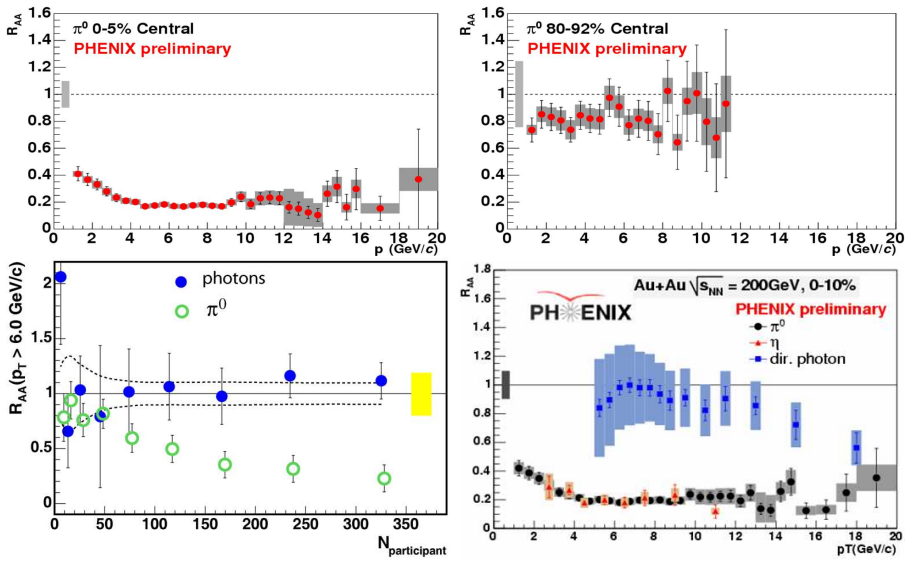

Figure 1: Nuclear modification factor $R_{\rm AA}$ for π_0, η and photon yields in Au+Au collisions as a function of p_t for different centralities (different number of participants). The shaded error band around unity indicate systematic errors.

expected from point-like processes. This observation makes definitive the conclusion that the suppression of high-p_t hadron production in Au+Au collisions is a final-state effect.

3 The perfect fluid of quarks

One of the most important results of RHIC is the relatively strong second harmonic moment of the transverse momentum distribution, referred to as the elliptic flow. The elliptic flow is an experimentally measurable observable and is defined as the azimuthal anisotropy or second Fourier-coefficient of the single-particle momentum distribution $N_1(p)$. The $n^{\rm th}$ Fourier-coefficient is defined as:

$$v_n = \frac{\int_0^{2\pi} N_1(p)\cos(n\varphi)d\varphi}{\int_0^{2\pi} N_1(p)d\varphi}, \qquad (2)$$

φ being the azimuthal (perpendicular to the beam) axis of momentum p with respect to the reaction plane. This formula returns the elliptic flow v_2 for $n = 2$.

Measurements of the elliptic flow by the PHENIX, PHOBOS and STAR collaborations (see refs. [16−21]) reveal rich details in terms of its dependence on particle type, transverse (p_t) and longitudinal momentum (η) variables, and on the centrality and the bombarding energy of the collision. In the soft transverse momentum region ($p_t \lesssim 2$ GeV/c) measurements at mid-rapidity are found to be well described by hydrodynamical models [1, 22−25]. Important is, that in contrast to a uniform distribution of particles expected in a gas-like system, this liquid behavior means that the interaction in the medium of these copiously produced particles is rather strong, as one expects from a fluid. Detailed investigation of these phenomena suggests that this liquid flows with almost no viscosity [26].

Measurement of elliptic flow of pions, kaons, protons, ϕ mesons and deuterons in Au+Au collisions at $\sqrt{s_{NN}} = 200$ GeV, when plotted against scaling variable KE_T (transverse kinetic energy) confirm the prediction of perfect fluid hydrodynamics, that the relatively "complicated" dependence of azimuthal anisotropy on transverse momentum and particle type can be scaled to a single function [26−30]. On the left plot of Fig. 2 we show this scaling. Mesons and baryons gather into two different groups here. If one scales both axes of these plots by the number of constituent quarks of the measured hadrons (as shown on the right plot of Fig. 2), the two curves collapse to one [31]. Thus it appears that quark collectivity dominates the expansion dynamics of these collisions.

4 Heavy flavour

We also have measured electrons from heavy flavor (charm and bottom) decays in Au+Au collisions at $\sqrt{s_{\rm NN}} = 200$ GeV. The nuclear modification factor $R_{\rm AA}$ relative to p+p collisions shows a strong suppression in central Au+Au collisions, indicating substantial energy loss of heavy quarks in the medium produced at RHIC energies. A large elliptic flow, v_2 is also observed indicating substantial heavy flavor elliptic flow. Both $R_{\rm AA}$ and v_2 show a p_t dependence different from those of neutral pions. A comparison to transport models which simultaneously describe $R_{\rm AA}(p_t)$ and $v_2(p_t)$ suggests that the viscosity to entropy density ratio is close to the conjectured quantum lower bound, *i.e.* near

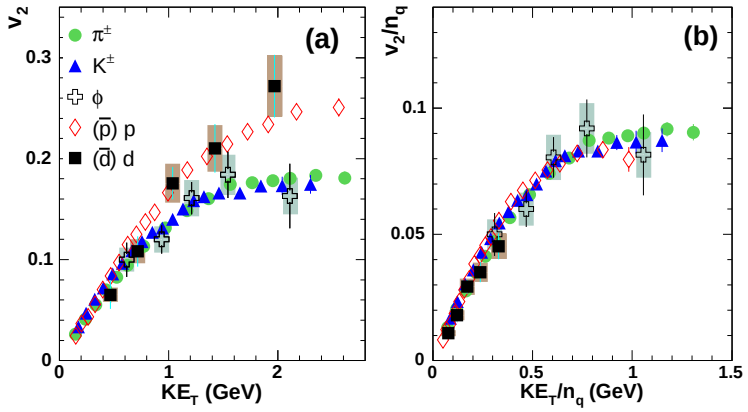

Figure 2: (color online)(a) v_2 vs KE_T for several identified particle species obtained in mid-central (20-60%) Au+Au collisions. (b) v_2/n_q vs KE_T/n_q for the same particle species shown in panel (a). The shaded bands indicate systematic error estimates for $(\overline{d})d$ and ϕ mesons (see text).

a perfect fluid [32–34], as shown on Fig. 3

We see, that even heavy flavour is suppressed beyond extrapolations from cold nuclear matter effects, and even heavy flavour is flowing similarly to hadrons made out of light quarks. This suggests strong coupling of charm and bottom to the medium [11, 35].

5 Chiral dynamics

Correlation functions are important to see the collective properties of particles and the space-time structure of the emitting source, e.g. the observed size of a system can be measured by two-particle Bose-Einstein correlations [37].

The m_t dependence of the strength of the two-pion Bose-Einstein correlation function λ can be used to extract information on the mass-reduction of the η' meson (the ninth, would-be Goldstone-boson), a signal of the $U_A(1)$ symmetry restoration in hot and dense matter: It is known, that if the chiral $U_A(1)$ symmetry is restored, then the mass of the η' boson is tremendously decreasing and its production cross section tremendously increasing. Thus η' bosons are copiously produced, and decaying through η bosons (with a very long lifetime)

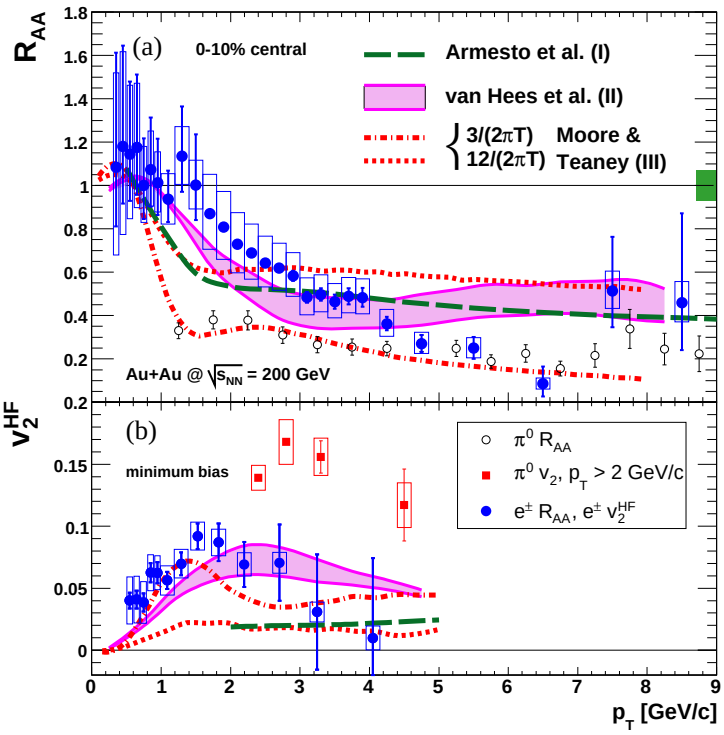

Figure 3: (a) $R_{\rm AA}$ of heavy-flavor electrons in 0-10% central collisions compared with π^0 data [6] and model calculations (curves I [32], II [33], and III [34]). (b) $v_2^{\rm HF}$ of heavy-flavor electrons in minimum bias collisions compared with π^0 data [36] and the same models. Boxes show systematic uncertainty in both plots.

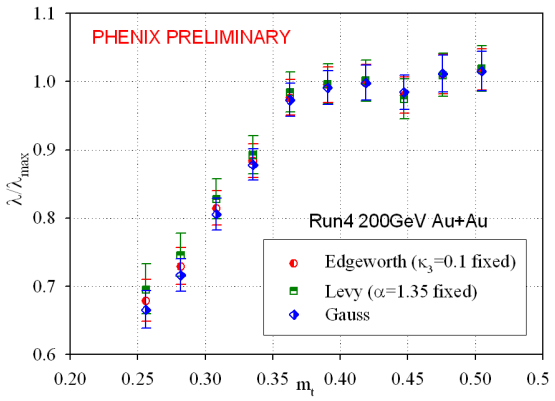

Figure 4: Measured $\lambda(m_t)$ from different methods

into low momentum pions. Hence the strength of the two-particle correlation functions at low relative momenta might change significantly. [38–41].

PHENIX analyzed [42] two-pion Bose-Einstein correlations with fits to two-pion correlation functions using three different shapes, Gauss, Levy and Edgeworth, and determined $\lambda(m_t)$ from it, as described in refs. [42–44]. We re-normed the $\lambda(m_t)$ curves with their maximal value on the investigated m_t interval. This way they all show the same shape, as shown in Fig. 4. This confirms the existence and characteristics of the hole in the $\lambda(m_t)$ distribution.

We conclude that at present, results are critically dependent on our understanding of statistical and systematic errors, and additional analysis is required to make a definitive statement.

The PHENIX experiment has also measured the dielectron continuum in $\sqrt{s_{NN}}$=200 GeV Au+Au collisions [45, 46]. The data below 150 MeV/c^2 are well described by the cocktail of hadronic sources. The vector mesons ω, ϕ and J/ψ are reproduced within the uncertainties. However, in minimum bias collisions, the yield is substantially enhanced above the expected yield in the continuum region from 150 to 750 MeV/c^2. The enhancement in this mass range is a factor of 3.4 $\pm$ 0.2(stat.) $\pm$ 1.3(syst.) $\pm$ 0.7(model), where the first error is the statistical error, the second the systematic uncertainty of the data, and the last error is an estimate of the uncertainty of the expected yield. Above the ϕ meson mass the data seem to be well described by the continuum

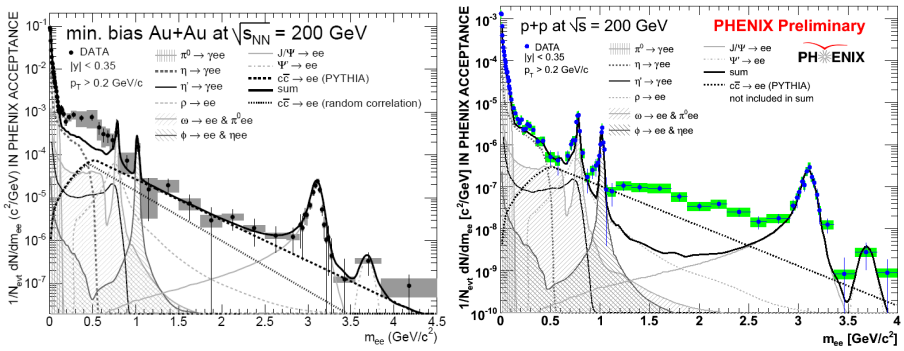

Figure 5: Invariant e^+e^-–pair yield of refs. [45, 46] compared to the yield from the model of hadron decays. The charmed meson decay contribution based on PYTHIA is included in the sum of sources (solid black line). The charm contribution expected if the dynamic correlation of c and $\bar{c}$ is removed is shown separately. Statistical (bars) and systematic (boxes) uncertainties are shown separately; the mass range covered by each data point is given by horizontal bars. The systematic uncertainty on the cocktail is not shown.

calculation based on PYTHIA, as shown in Fig. 5

6 Summary and conclusions

Based on the measurements of suppression of high transverse momentum hadrons and of their elliptic flow, we can make the definitive statement, that in relativistic Au+Au collisions observed at RHIC we see a strongly interacting matter, that has the characteristics of a perfect fluid. We also see signals of chiral dynamics by the enhancement of the dielectron continuum above the expected yield from hadron production and the possible mass modification of the η' meson. Future plan is to explore all properties of the Quark Matter, by analyzing more data and using higher luminosity.

References

1. K. Adcox *et al.*, Nucl. Phys. **A757**, 184 (2005).

2. M. Riordan and W. A. Zajc, Sci. Am. **294N5**, 24 (2006).

3. K. Adcox *et al.*, Phys. Rev. Lett. **88**, 022301 (2002).
4. K. Adcox *et al.*, Phys. Lett. **B561**, 82 (2003).
5. J. Adams *et al.*, Phys. Rev. Lett. **91**, 172302 (2003).
6. S. S. Adler *et al.*, Phys. Rev. Lett. **91**, 072301 (2003).
7. S. S. Adler *et al.*, Phys. Rev. **C69**, 034910 (2004).
8. I. Arsene *et al.*, Phys. Rev. Lett. **91**, 072305 (2003).
9. B. B. Back *et al.*, Phys. Lett. **B578**, 297 (2004).
10. S. S. Adler *et al.*, Phys. Rev. **C76**, 034904 (2007).
11. S. S. Adler *et al.*, Phys. Rev. Lett. **91**, 072303 (2003).
12. J. Adams *et al.*, Phys. Rev. Lett. **91**, 072304 (2003).
13. B. B. Back *et al.*, Phys. Rev. Lett. **91**, 072302 (2003).
14. S. S. Adler *et al.*, Phys. Rev. Lett. **96**, 202301 (2006).
15. S. S. Adler *et al.*, Phys. Rev. Lett. **94**, 232301 (2005).
16. B. B. Back *et al.*, Phys. Rev. Lett. **94**, 122303 (2005).
17. B. B. Back *et al.*, Phys. Rev. **C72**, 051901 (2005).
18. S. S. Adler *et al.*, Phys. Rev. Lett. **91**, 182301 (2003).
19. J. Adams *et al.*, Phys. Rev. **C72**, 014904 (2005).
20. C. Adler *et al.*, Phys. Rev. Lett. **87**, 182301 (2001).
21. P. Sorensen, J. Phys. **G30**, S217 (2004).
22. J. Adams *et al.*, Nucl. Phys. **A757**, 102 (2005).
23. M. Csanád, T. Csörgő, and B. Lörstad, Nucl. Phys. **A742**, 80 (2004).
24. Y. Hama *et al.*, Nucl. Phys. **A774**, 169 (2006).
25. W. Broniowski, A. Baran, and W. Florkowski, AIP Conf. Proc. **660**, 185 (2003).

26. A. Adare *et al.*, Phys. Rev. Lett. **98**, 162301 (2007).

27. M. Csanád *et al.*, nucl-th/0512078.

28. M. Csanád, T. Csörgő, R. A. Lacey, and B. Lörstad, nucl-th/0605044.

29. N. Borghini and J.-Y. Ollitrault, nucl-th/0506045.

30. R. S. Bhalerao, J.-P. Blaizot, N. Borghini, and J.-Y. Ollitrault, Phys. Lett. **B627**, 49 (2005).

31. S. Afanasiev *et al.*, nucl-ex/0703024.

32. N. Armesto *et al.*, Phys. Lett. **B637**, 362 (2006).

33. H. van Hees, V. Greco, and R. Rapp, Phys. Rev. **C73**, 034913 (2006).

34. G. D. Moore and D. Teaney, Phys. Rev. **C71**, 064904 (2005).

35. A. Adare *et al.*, Phys. Rev. Lett. **98**, 232301 (2007).

36. S. S. Adler *et al.*, Phys. Rev. Lett. **96**, 032302 (2006).

37. R. Hanbury Brown and R. Q. Twiss, Nature **178**, 1046 (1956).

38. S. E. Vance, T. Csörgő, and D. Kharzeev, Phys. Rev. Lett. **81**, 2205 (1998).

39. J. I. Kapusta, D. Kharzeev, and L. D. McLerran, Phys. Rev. **D53**, 5028 (1996).

40. Z. Huang and X.-N. Wang, Phys. Rev. **D53**, 5034 (1996).

41. T. Hatsuda and T. Kunihiro, Phys. Rept. **247**, 221 (1994).

42. M. Csanád, Nucl. Phys. **A774**, 611 (2006).

43. T. Csörgő, Heavy Ion Phys. **15**, 1 (2002).

44. T. Csörgő, S. Hegyi, and W. A. Zajc, Eur. Phys. J. **C36**, 67 (2004).

45. S. Afanasiev *et al.*, arXiv:0706.3034 [nucl-ex].

46. A. Toia, Eur. Phys. J. **C49**, 243 (2007).

Frascati Physics Series Vol. XLVI (2007), pp. 133–144
HADRON07: XII Int. Conf. on Hadron Spectroscopy – Frascati, October 8-13, 2007
Plenary Session

KLOE RESULTS ON HADRON PHYSICS

C.Bini
Università "La Sapienza" and INFN Roma

on behalf of the KLOE collaboration:
F. Ambrosino, A. Antonelli, M. Antonelli, F. Archilli, C. Bacci, P. Beltrame, G. Bencivenni, S. Bertolucci, C. Bini, C. Bloise, S. Bocchetta, F. Bossi, P. Branchini, R. Caloi, P. Campana, G. Capon, T. Capussela, F. Ceradini, S. Chi, G. Chiefari, P. Ciambrone, E. De Lucia, A. De Santis, P. De Simone, G. De Zorzi, A. Denig, A. Di Domenico, C. Di Donato, S. Di Falco, B. Di Micco, A. Doria, M. Dreucci, G. Felici, A. Ferrari, M. L. Ferrer, G. Finocchiaro, S. Fiore, C. Forti, P. Franzini, C. Gatti, P. Gauzzi, S. Giovannella, E. Gorini, E. Graziani, M. Incagli, W. Kluge, V. Kulikov, F. Lacava, G. Lanfranchi, J. Lee-Franzini, D. Leone, M. Martini, P. Massarotti, W. Mei, S. Meola, S. Miscetti, M. Moulson, S. Müller, F. Murtas, M. Napolitano, F. Nguyen, M. Palutan, E. Pasqualucci, A. Passeri, V. Patera, F. Perfetto, M. Primavera, P. Santangelo, G. Saracino, B. Sciascia, A. Sciubba, F. Scuri, I. Sfiligoi, T. Spadaro, M. Testa, L. Tortora, P. Valente, G. Venanzoni, R.Versaci, G. Xu

Abstract

The KLOE experiment at the e^+e^- collider DAFNE of the Frascati Laboratories has collected about 8×10^9 decays of the ϕ meson. A review of recent results concerning the properties of the lowest mass mesons is presented.

1 Introduction

The KLOE experiment has been working since 1999 at the e^+e^- collider DAFNE, the ϕ-factory of the Frascati Laboratories. The main mission of the ϕ-factory is the study of kaon physics, 83% of ϕ decays being in kaon pairs. However, as shown in Tab.1, the ϕ-factory is a copious source of the low mass mesons, through the 3 pion decay and the radiative decays in one or more pseudoscalar mesons.

Table 1: *List of the main ϕ decays with their branching ratios taken from the Review of Particle Properties* [1]. *The number of events in the full KLOE data sample is also given.*

decay channel	branching ratio	Events ($\times 10^6$)
K^+K^-	0.49	3700
$K^0\overline{K^0}$	0.33	2500
$\pi^+\pi^-\pi^0$	0.15	1200
$\eta\gamma$	0.013	100
$\pi^0\gamma$	1.2×10^{-3}	9
$\eta'\gamma$	6.2×10^{-5}	0.5
$\pi\pi\gamma$	3×10^{-4}	2.5
$\eta\pi\gamma$	7×10^{-5}	0.6

Along the years KLOE has published several results concerning the properties of low mass mesons. Here a review of the most recent results is given. Detailed descriptions of the single items are contained in other contributions to these proceedings [2, 3, 4, 5, 6, 7, 8, 9].

2 The KLOE experiment

DAFNE has been working at a center of mass energy around 1.02 GeV with a luminosity that reached a peak value of $1.5 \times 10^{32}\mathrm{cm}^{-2}\mathrm{s}^{-1}$, the maximum luminosity ever reached at this energy. KLOE has taken data until year 2006 collecting about 2.7 fb^{-1} total integrated luminosity. Most of these data (2.5 fb^{-1} corresponding to about 8×10^9 ϕ decays) have been taken at the ϕ peak, the others are off-peak data and energy scans around the ϕ.

The KLOE detector consists of a large volume drift chamber for the detection of charged tracks [10] in full stereo geometry filled with a low mass He-IsoButane gas mixture, surrounded by a lead scintillating fibres calorimeter [11] for the measurement of the neutral particles (essentially photons and K_L) and for the identification of the charged particles (pions vs. muons vs. electrons) through time of flight. The calorimeter energy and time resolutions for photons as a function of the photon energy E are respectively: $\sigma(E)/E = 5.4\%/\sqrt{E(GeV)}$ and $\sigma(t) = 55$ ps$/\sqrt{E(GeV)} \oplus 130$ ps. A superconducting coil provides a 0.52 T solenoidal magnetic field allowing a measurement

of the momentum of the charged tracks in the drift chamber with a resolution $\delta p/p$ below 0.4% in the full momentum range (50÷500 MeV/c).

The KLOE physics program goes along three main lines:

1. kaon physics: tests of CP and CPT violation, CKM matrix unitarity and Chiral Perturbation Theory (ChPT);
2. hadron physics: properties of the lowest mass scalar, pseudoscalar and vector mesons and further ChPT tests;
3. measurement of the $e^+e^- \to \pi^+\pi^-$ cross-section [12] below 1 GeV: this is a crucial ingredient for the assessment of the hadronic corrections to the theoretical evaluation of $g_\mu - 2$.

In this review the attention is focused on line number 2.

3 Review of recent results

3.1 Properties of the Pseudoscalar Mesons

The large statistics of ηs and the good statistics of η's (see Tab.1) accumulated by KLOE through the ϕ radiative decays, allow to perform precision measurements of the properties of these particles, some of them being still controversial.

In the last years the precision on the measurement of the η mass has significantly improved. Few experiments, based on completely different experimental methods have pushed the uncertainty well below 100 keV. GEM at Juelich [13] and NA48 at CERN [14] reported two measurements in disagreement. More recently CLEO has reported a further measurement [15] in agreement with NA48 and in disagreement with GEM.

In KLOE the η mass is measured using the decay channel $\phi \to \eta\gamma$ with the subsequent decay $\eta \to \gamma\gamma$, resulting in a fully neutral 3-photon final state [2]. The excellent space and time resolutions of the calorimeter allow, through a kinematic fit constrained, to obtain a background free η sample with a well defined mass peak. The absolute calibration of the mass scale is provided by the measurement of the center of mass energy that, in turn, is normalised to the ϕ mass [16]. The KLOE result is:

$$m(\eta) = 547.873 \pm 0.007 \pm 0.048 \text{ MeV} \quad (1)$$

where the statistical uncertainty is negligible, and the systematic one is mostly due to residual non uniformities in the detector response. The result is compared to the other measurements in Fig. 1.

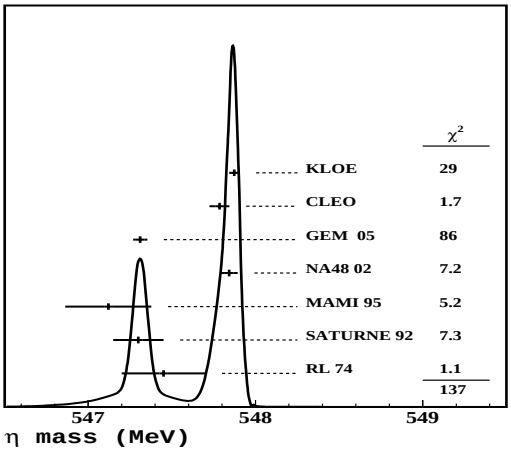

Figure 1: *Review of the η mass measurements. The curve shown and the χ^2 values are obtained according to the prescriptions of PDG* [1)].

A second precision measurement done by KLOE on the pseudoscalar meson sector is the η-η' mixing. Since the ϕ meson is essentially a pure $s\overline{s}$ state, the ratio of branching ratios $R = B.R.(\phi \to \eta'\gamma)/B.R.(\phi \to \eta\gamma)$ is directly related to the pseudoscalar mixing angle ϕ_P in the flavour basis, assuming no gluonium contribution in the η and η' wave-functions [17)]. KLOE has measured the ratio R using 2 different data sets and 2 different final states [18, 19)]. The results are in agreement and the best estimate of the mixing angle is:

$$\phi_P = (41.4 \pm 0.3 \pm 0.9)^o \tag{2}$$

where the systematic uncertainty is dominated by the knowledge of the intermediate η and η' branching ratios entering in the evaluation of R.

If we allow a gluonium contribution in the η' wave function, the ratio R gives a band in the ϕ_P-$Z^2_{\eta'}$ plane, $Z_{\eta'}$ being the fraction of gluonium content. The band is shown in Fig.2. Other bands can be put in the same plot following the analyses of Refs. [20, 21, 22)]. The intersection between the bands define

the allowed region. According to the KLOE analysis [19] the allowed region is about 3 standard deviation away from $Z_{\eta'} = 0$.

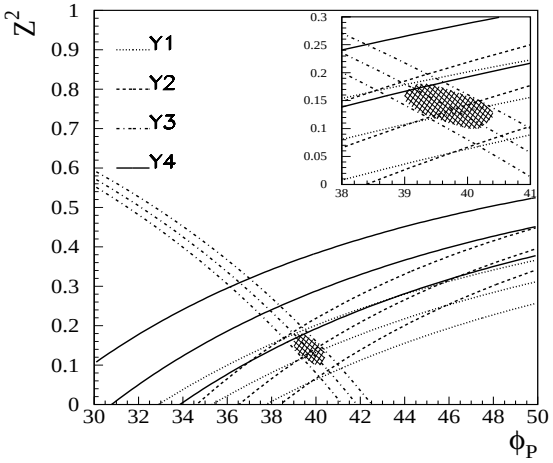

Figure 2: *Analysis of the η' gluonium content. The four bands shown in the $Z^2_{\eta'}$-ϕ_P plane are: (Y1) from $\Gamma(\eta' \to \gamma\gamma)/\Gamma(\pi^0 \to \gamma\gamma)$, (Y2) from $\Gamma(\eta' \to \rho\gamma)/\Gamma(\omega \to \pi^0\gamma)$, (Y3) from the KLOE result (see text) and finally (Y4) from $\Gamma(\eta' \to \omega\gamma)/\Gamma(\omega \to \pi^0\gamma)$.*

The significance of this test can be improved if the experimental uncertainties on $\Gamma(\eta')$, $\Gamma(\eta' \to \gamma\gamma)$ and $\Gamma(\pi^0 \to \gamma\gamma)$ and on some branching ratios of the η' and ω mesons are reduced. KLOE has presented a preliminary measurement of B.R.$(\omega \to \pi^0\gamma)$ [3] based on the $\sqrt{s}$ dependence of the $e^+e^- \to \omega\pi^0$ around the ϕ meson peak (see Fig.3) that reduces the uncertainty on the ω branching ratios.

3.2 Properties of the Lowest Mass Scalar Mesons

The lowest mass scalar nonet is not well established. On one side the two lowest mass states, the I=0 $\sigma(600)$ and the I=1/2 $\kappa(800)$ are both controversial; on the other side the two firmly established highest mass states, the I=0 $f_0(980)$ and the I=1 $a_0(980)$, are interpreted in several different ways. The study of the radiative ϕ decays in $\pi\pi\gamma$, $\eta\pi\gamma$ and $K\overline{K}\gamma$ allows to estimate the couplings of the $f_0(980)$ and the $a_0(980)$ to the ϕ and to the KK, $\pi\pi$ and $\eta\pi$ final states,

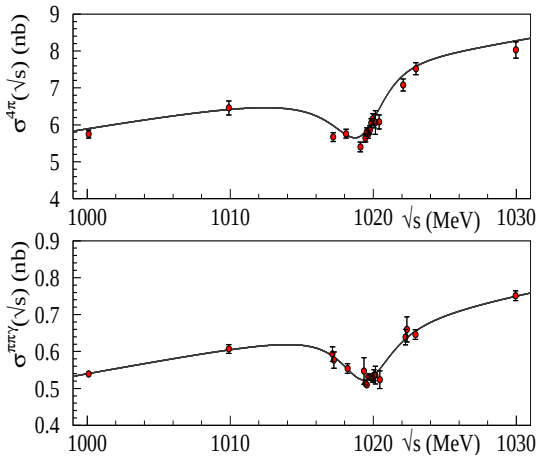

Figure 3: *$\sqrt{s}$ dependence of the $e^+e^- \to \omega\pi^0$ cross section around the ϕ resonance energy: $\omega \to \pi^+\pi^-\pi^0$ (above) and $\omega \to \pi^0\gamma$ (below). From the combined fit the ratio $B.R.(\omega \to \pi^0\gamma)/B.R.(\omega \to \pi^+\pi^-\pi^0)$ is extracted.*

that in turn can be related to the quark structure of the mesons. Moreover the analysis of the $\pi\pi$ low energy mass spectra in $\pi\pi\gamma$ allows to study the $\sigma(600)$.

The final states $\pi^+\pi^-\gamma$ and $\pi^0\pi^0\gamma$ receives contributions from the radiative decays $\phi \to$f$_0(980)\gamma$ and $\phi \to \sigma(600)\gamma$, but also from other processes that give rise to large, unreducible backgrounds. KLOE extracts the scalar part of the amplitude by fitting the mass spectra of $\pi^+\pi^-\gamma$ [23] and $\pi^0\pi^0\gamma$ [24, 25] final states. A good fit is obtained for both spectra [4] by using a scalar amplitude based on the kaon-loop approach including the $\sigma(600)$, the f$_0(980)$ and the interference term between them. The parameters of the σ meson and the phases are fixed according to Ref. [26] while the f$_0$ mass and the couplings to $\pi^+\pi^+$ and KK are left free. The results for these parameters are shown in Tab.2. The fits confirm the fact the $g_{f_0K^+K^-}$ is larger than $g_{f_0\pi^+\pi^-}$ supporting a sizeable strange quark content in the f$_0(980)$. Notice that within the kaon-loop approach, the $\sigma(600)$ is necessary to get an acceptable fit.

The $\eta\pi$ system is a I=1 state, so that the $\eta\pi^0\gamma$ final state is dominated by the radiative decay $\phi \to$ a$_0(980)\gamma$. In this case the possible unreducible backgrounds are much less than in the case of the $\pi\pi$ state.

Table 2: *Results of the fits to the $\pi^+\pi^-\gamma$, $\pi^0\pi^0\gamma$ and $\eta\pi^0\gamma$ kinematic distributions with the kaon-loop scalar amplitudes.*

channel	p(χ^2)	M_{f_0} (MeV)	$g_{f_0K^+K^-}$ (GeV)	$g_{f_0\pi^+\pi^-}$ (GeV)
$\pi^+\pi^-\gamma$	2.5%	983.7	4.7	-2.2
$\pi^0\pi^0\gamma$	6.3%	982.1	4.0	-1.7
		M_{a_0} (MeV)	$g_{a_0K^+K^-}$ (GeV)	$g_{a_0\eta\pi^0}$ (GeV)
$\eta\pi^0\gamma$	11%	983.0	2.2	2.8

KLOE has selected these final states in two ways: looking for $\eta\pi\gamma$ with $\eta \to \gamma\gamma$ (decay 1 in the following) and looking for the same final state but with $\eta \to \pi^+\pi^-\pi^0$ (decay 2). The two decay channels are characterised by different systematic effects and unreducible backgrounds that can affect the measurement. The two independent branching obtained:

$$B.R.(\phi \to \eta\pi\gamma)(1) = (6.92 \pm 0.10_{stat} \pm 0.20_{syst}) \times 10^{-5} \quad (3)$$

$$B.R.(\phi \to \eta\pi\gamma)(2) = (7.19 \pm 0.17_{stat} \pm 0.24_{syst}) \times 10^{-5} \quad (4)$$

are in good agreement. The total uncertainty is improved from 9% of the previous KLOE measurement [27] to 3%.

The two mass spectra are fitted simultaneously with the kaon-Loop model. In this case (see the results shown in Tab.2) $g_{a_0K^+K^-}$ is slightly smaller than $g_{a_0\eta\pi}$. Finally, KLOE has searched for the decay $\phi \to K^0\overline{K^0}\gamma \to K_SK_S\gamma$ with both K_S decaying to the most frequent final state, $\pi^+\pi^-$. The predictions for the branching ratio of this decay depend on the model used to describe the intermediate scalar states: the $f_0(980)$ for the I=0 part of the amplitude and the $a_0(980)$ for the I=1 part. Due to the very small available phase-space, very small branching ratios are predicted, all in the range between 10^{-9} and 10^{-7} as shown in Fig.4. Notice that no experimental measurements are available for this decay.

KLOE finds no signal, only 1 event surviving the selection procedure, compatible with the background estimate. The upper limit on the branching ratio is:

$$B.R.(\phi \to K^0\overline{K^0}\gamma) < 1.8 \times 10^{-8} \ \ (90\%\ C.L.) \quad (5)$$

that allows to exclude several proposed models (see Fig.4).

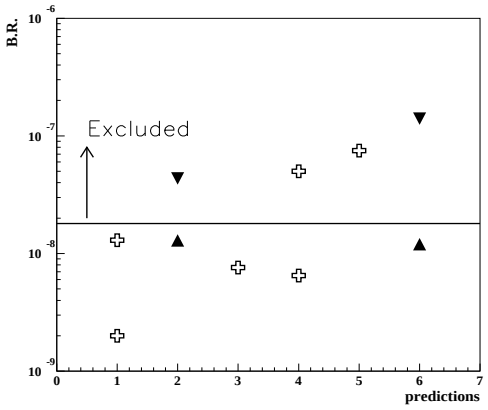

Figure 4: *Published predictions on the branching ratio of the process* $\phi \to K^0\overline{K^0}\gamma$ *(abscissas 1-6 correspond to Refs.* [28, 29, 30, 31, 32, 33]*). The models above the horizontal line are excluded by the data.*

3.3 Tests of Chiral Perturbation Theory

The Chiral Perturbation Theory (ChPT) provides a theoretical scheme to describe the strong interaction processes in the low energy domain and predicts the values of several low energy observables. KLOE has the opportunity to test some of these predictions looking at the decays of η, η' and kaons.

Among these observables we mention first the dynamics of the $\eta \to 3\pi$ decay. The η decay in 3 pions is an isospin-violating process. In fact, a 3-pion system with 0 angular momentum can be only in a I=1 isospin state. Since the η meson cannot decay to 2 pions due to P and CP invariance in strong interactions, the η in 3 pion is the most frequent hadronic η decay with a very small electromagnetic contribution. Models inspired to ChPT allow to evaluate the decay widths and the dynamics [34] of both $\eta \to \pi^+\pi^-\pi^0$ and $\eta \to \pi^0\pi^0\pi^0$. KLOE detects both decays with large statistics and negligible background [6].

The $\eta \to \pi^+\pi^-\pi^0$ Dalitz plot containing 1.34 million of events is fit using an expansion of the amplitude up to third order in the variables $X = \sqrt{3}(T_+ - T_-)/Q_\eta$ and $Y = 3T_0/Q_\eta$, $T_{+,-,0}$ being the kinetic energies of the three pions and $Q_\eta = m_\eta - 2m_{\pi^\pm} - m_{\pi^0}$. The results of the fit indicate that: the odd terms in X are compatible with 0, so that no C violation is observed;

the quadratic term in X is unambiguously different from 0; a cubic term in Y (never observed before) is needed to get an acceptable fit. Moreover the $b = a^2/2$ rule, a and b being the linear and quadratic terms in Y respectively, based on current algebra, is largely violated.

KLOE has also analysed a sample of 0.6×10^6 $\eta \to \pi^0\pi^0\pi^0$. In this case the fit is done assuming a linear expansion for the distribution of $Z = (2/3)\sum_{i=1}^{3}((3E_i - m_\eta)/(m_\eta - 3m_{\pi^0}))^2$. From the fit of the Z spectrum the slope α is extracted:

$$\alpha = -0.027 \pm 0.004 \pm 0.005 \tag{6}$$

in agreement with Crystal Ball result [35]. The comparison of these results with the ChPT predictions is extensively discussed in Ref. [34].

A second test of ChPT is provided by the measurement of the branching ratio of the rare K_S decay $K_S \to \gamma\gamma$ whose amplitude is evaluated at order p^4 in Ref. [36]. A pure K_S sample is obtained in KLOE by identifying a K_L in the calorimeter (tagging method [7]). In this way, due to the properties of the $\phi \to K^0\overline{K^0}$, the K_S is unambiguously tagged and its flight direction and momentum is predicted. The K_S decays to $\gamma\gamma$ are then selected requiring 2 neutral clusters. The main background for this process is given by the decay $K_S \to \pi^0\pi^0$ when 2 out of the 4 photons are lost, that has a branching ratio that is 10^5 times larger than the signal. The result obtained is in agreement with the ChPT predictions at order p^4 but is slightly in disagreement with NA48 result [37].

Finally we mention that KLOE has observed the two rare η decays $\eta \to \pi^+\pi^-e^+e^-$ and $\eta \to \pi^0\gamma\gamma$ that are both important tests of ChPT [8]. In particular the decay $\eta \to \pi^0\gamma\gamma$ is considered the "golden mode" of ChPT since it accesses directly to the p^6 terms in the decay amplitude. The signals of the two decays are shown in Fig.5. Preliminary values of the branching ratios have been presented and we expect to have the final results soon.

4 Summary and outlook

DAFNE is testing in these days a new machine scheme [38] to increase the luminosity for operation at the ϕ center of mass energy. Moreover the possibility to increase the center of mass energy of DAFNE up to 2.5 GeV is considered. An expression of interest has been prepared for a continuation of the KLOE

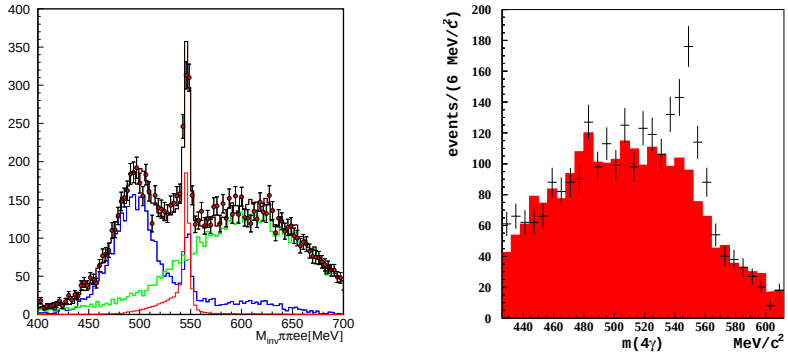

Figure 5: *(left) Invariant mass spectrum of the selected* $\eta \to \pi^+\pi^- e^+ e^-$ *events compared to Montecarlo expectations for signal and background. (right) 4-photons invariant mass spectrum for candidates* $\eta \to \pi^0\gamma\gamma$ *compared to the Montecarlo background expectations (histogram). In both cases the* η *signal is well evident.*

program at "DAFNE-2", upgraded in luminosity and energy [39, 9]. Main topics of the "KLOE-2" physics program are:

- high statistics study of kaon physics including kaon interferometry, CP and CPT tests;
- η and η' decays;
- $\gamma\gamma$ physics using small-angle electron taggers;
- precision measurement of the hadronic cross-section from $\sqrt{s} = 2m_\pi$ up to 2.5 GeV.

Other two proposals have been presented: one concerns the measurement of the time-like form factors of the nucleons and of the lowest mass hyperons [40] and the other aims to study the production and decay of deeply bound kaonic states [41].

Details on several aspects of the "DAFNE-2" physics program can be found in Ref. [42].

References

1. W.M.Yao et al., (Particle Data Group), Journ. of Phys. **G33** (2006) 1.
2. B. Di Micco, these proceedings;
3. A. De Santis, these proceedings;
4. F.Nguyen, these proceedings;
5. S.Fiore, these proceedings;
6. F.Ambrosino, these proceedings;
7. M.Martini, these proceedings;
8. R.Versaci, these proceedings;
9. P.Moskal, these proceedings;
10. M.Adinolfi et al., Nucl. Instr. and Meth. **A488**, (2002) 1.
11. M.Adinolfi et al., Nucl. Instr. and Meth. **A482**, (2002) 364.
12. A.Aloisio et al. (KLOE collaboration), Phys. Lett. **B606**, (2005) 12.
13. M.Abdel-Bary et al. (GEM collaboration), Phys. Lett. **B619** (2005) 281.
14. A.Lai et al. (NA48 collaboration), Phys. Lett. **B533** (2002) 196.
15. D.H.Miller et al. (CLEO collaboration), arXiv:0707.1810, submitted to Phys.Rev.Lett.;
16. A.Akhmetshin et al., (CMD-2 collaboration), Phys. Lett.**B578** (2004) 285.
17. A.Bramon et al., Eur. Phys. J. **C7** (1999) 24.
18. A.Aloisio et al. (KLOE collaboration), Phys. Lett. **B541**, (2002) 45.
19. F.Ambrosino et al. (KLOE collaboration), Phys. Lett. **B648**, (2007) 267.
20. J.L.Rosner, Phys. Rev. **D27** (1983) 1101;
21. A.Bramon et al., Phys. Lett. **B503**, (2001) 271.

22. E.Kou, Phys. Rev. **D63** (2001) 54027;

23. F.Ambrosino et al. (KLOE collaboration), Phys. Lett. **B634**, (2006) 148.

24. A.Aloisio et al., (KLOE collaboration), Phys. Lett. **B537** (2002) 21.

25. F.Ambrosino et al., (KLOE collaboration), Eur. Phys. J. **C49** (2006) 433;

26. N.N.Achasov, A.V.Kiselev, Phys. Rev. **D73** (2006) 054029;

27. A.Aloisio et al. (KLOE collaboration), Phys. Lett. **B536**, (2002) 209.

28. N.N.Achasov and V.N.Ivanchenko, Nucl. Phys. **B315** (1989) 465.

29. N.N.Achasov, V.V.Gubin, Phys.Rev.**D64** (2001) 094016;

30. A.Bramon, A.Grau, G.Pancheri, Phys. Lett. **B289** (1992) 97;

31. J.A.Oller, Phys. Lett. **B426**(1998) 7, Nucl. Phys. **A714** (2003) 161;

32. R.Escribano, Eur. Phys. J. **A31** (2007) 454;

33. A.Gokalp, C.S.Korkmaz, O.Yilmaz hep-ph/0702214.

34. B.Borasoy, R.Nissler, AIP Conf.Proc.796 (2005) 150;

35. W.B.Tippens et al., (Crystal Ball collaboration), Phys. Rev. Lett. 87 (2001) 192001;

36. G.D'Ambrosio, D.Espriu, Phys. Lett. **B175** (1986) 27;

37. A.Lai et al. (NA48 collaboration), Phys. Lett. **B551** (2003) 7;

38. D.Alesini et al., LNF-06/33 (IR);

39. see http://www.lnf.infn.it/lnfadmin/direzione/roadmap/LoIKLOE.pdf;

40. see http://www.lnf.infn.it/conference/nucleon05/FF;

41. see http://www.lnf.infn.it/lnfadmin/direzione/roadmap/LOI MARCH AMADEUS.pdf;

42. F.Ambrosino et al., Eur.Phys.J. **C50** (2007) 729.

Frascati Physics Series Vol. XLVI (2007), pp. 145–156
HADRON07: XII Int. Conf. on Hadron Spectroscopy
Plenary Session

HADRON PHYSICS EXPERIMENTS AT THE COSY FACILITY

James Ritman
Forschungszentrum Juelich and the Ruhr-Univ.-Bochum, Germany

Abstract

The COoler-SYnchrotron (COSY) provides intense beams of polarized and phase space cooled proton and deuteron beams with momenta up to 3.7 GeV/c for a wide range of internal and extracted beam experiments. In this talk a selection of recent major results from the various detectors at this facility will be summarized. These include the following: the non- observation of the exotic Theta+ particle, expressed as upper limits of the production cross section; Production of excited hyperons; Studies of eta-nucleus interactions; vector meson (omega and phi) production in pp and pA reactions; and precise measurements of the eta and eta mass and width, respectively. This discussion will be complemented with an overview of the main detector developments, such as the implementation of double polarization experiments at ANKE, the installation of a large volume straw tube tracker in the TOF experiment, and a first glimpse of data on eta decays from the now fully operational WASA detector at COSY.

1 Intoduction

The Nuclear Physics Institute (IKP) at the Research Center Jülich (FZJ) is vigorously pursuing a coherent program in the field of Physics of Hadrons and Nuclei to investigate the structure and dynamics of hadrons. The goal of this research is to gain a deeper understanding of the strong interaction from low and intermediate energy hadron physics, thus exploring Quantum Chromodynamics (QCD). Although QCD has successfully passed many tests, especially in high energy processes, in the realm of a few GeV and below QCD is characterized by a running coupling constant of the order of unity or larger and thus standard perturbative methods fail. This domain, often called strong QCD, can only be tested and finally understood by a close interplay of precision experiments and accurate calculations, This is achieved by either lattice methods or Effective Field Theories (EFTs) which systematically exploit symmetries of the underlying theory. The major goal of the program is to understand hadron structure and dynamics in a consistent way. This issue makes hadron physics a cornerstone of modern physics and builds a bridge between nuclear, particle and astrophysics.

Since quarks and gluons are never found as free objects, but rather are always confined in hadrons, the only way to make experimental progress is to investigate hadronic systems, i.e. baryons, mesons, with possible admixture of exotic states. Experiments performed at hadron accelerators such as COSY can contribute significantly to deepen our understanding of strong QCD. Physics at energy scales available at COSY is sensitive to the light quarks (u, d, s). In this context experiments utilizing polarization, thus exploring the spin of the interacting hadrons, have proven to be one of the most sensitive tools to analyze this difficult regime.

2 The COSY Facility

The Cooler–Synchrotron COSY has a 184 m circumference and accelerates up to 10^{11} protons or 10^{10} deuterons to momenta of 3.7 GeV/c. The JULIC cyclotron is the injector to COSY and delivers beams of 300 and 550 MeV/c, for p and d, respectively. These beams cam be either polarized or unpolarized. Parallel to the COSY operation the cyclotron beam can be used for irradiation for e.g. radiaoactive trace production. In the lower momentum region the

COSY beam can be phase space cooled by electron cooling, and in the upper momentum region by stochastic cooling. This allows intense, high space density beams to be provided for internal and external experiments.

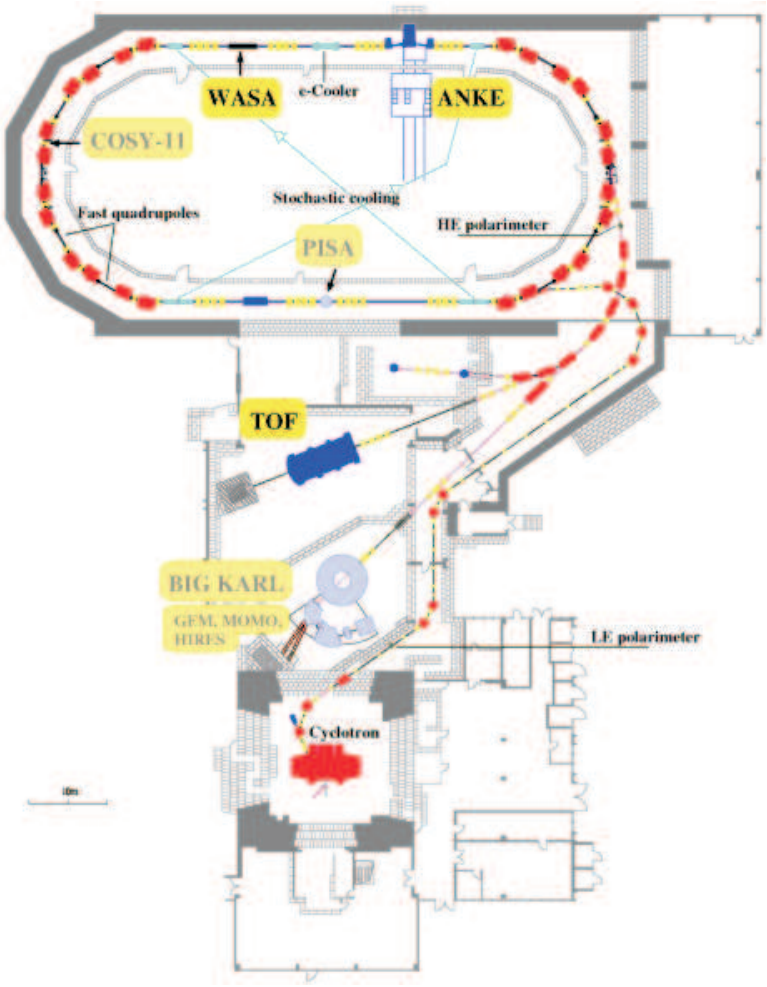

Figure 1: Overview of the COSY facility. The currently active main facilities include the COSY-TOF detector at an extracted beam location, and the internal detectors ANKE and WASA.

An overview of the experimental facilities available at COSY is given in Figure 1. Currently 3 major facilities are in operation. The COSY-TOF detector is located at an extracted beam location. The ANKE and WASA-at-COSY experiments are located inside the COSY ring.

The COSY-TOF detector combines excellent tracking capability with large acceptance and full azimuthal symmetry. The tracking information, in particular close to the interaction point (several mm^3), allows to identify final states with strangeness with almost no background, based on the detection of the displaced decay vertices of Λ hyperons ($\Lambda \rightarrow p\pi^-$) and K_S mesons ($K_S \rightarrow \pi^+\pi^-$) as well as of the kink in the charged particle trajectories at the decay points of Σ^+ hyperons ($\Sigma^+ \rightarrow p\pi^0, n\pi^+$). The large acceptance and the azimuthal symmetry enables TOF to measure complete angular distributions of the produced particles with small systematic uncertainty. Combining these two aspects, TOF is able to measure complete Dalitz plot distributions of 3-body final states with strangeness, almost not affected by background from the much more copiously produced nonstrange events.

ANKE ("Apparatus for Studies of Nucleon and Kaon Ejectiles") is a forward magnetic spectrometer with a wide momentum acceptance. Previously, ANKE has been used to measure meson and hyperon production close to threshold, making use of a cluster-jet target or of various foil targets. A polarized internal target has been installed in 2006, and first double polarization experiments have been performed.

WASA (Wide Angle Shower Apparatus) is a large-acceptance detector for charged and neutral particles, and thus complements the two other large COSY experiments, which are photon blind. It has been operated at the CELSIUS storage ring in Uppsala (Sweden) until June 2005. After the shutdown of CELSIUS the detector setup was relocated to continue its operation at COSY. WASA was installed in summer 2006 and has commenced its program on time in early 2007. The forward part of the detector has been extended by additional hodoscope layers to accommodate the higher particle energies at COSY as compared to CELSIUS. A new data acquisition system with a purely hardware based module readout, buffer and event management has been designed for WASA-at-COSY, including the development of dedicated new digitization modules. The design goal of 3 - 4 read out events per pellet passing the COSY beam corresponding to 20-30μs for a full crate readout was achieved after the

implementation of a novel synchronization and buffering scheme.

3 Meson properties and Interactions

3.1 Investigation of $dp \to \eta^3He$

Differential and total cross sections for the reaction $dp \to \eta^3He$ reaction have been measured at COSY11 [1)] and ANKE [2)] using a continuous beam energy ramp of COSY. This mode allows a slow increase of the beam energy with time in order (∼30 MeV in 2 minutes) to enable precision studies of near threshold effects. The physics motivationof these measurements is to search for a new state of matter in the form of an η^3He quasi-bound state that might be formed by the strong final state interaction between the η-meson and the ^3He nucleus. These two experiments have taken data extremely close to threshold, with unprecedented accuracy in the determination of the beam momentum, and high statistics in the energy range $Q <\sim 10MeV$. These features allow for a very fine binning of the data in the excitation energy Q. Both experiments agree in their results for the total and differential cross sections, which exhibit the following features: The angular distributions indicate that higher partial waves become visible and important already at $Q \sim 4MeV$. The total cross section rises steeply within only 0.5 MeV of threshold and reaches a constant plateau value of about 400 nb. Although COSY-11 finds a scattering length in agreement with previous results, the higher resolution in the ANKE analysis leads to an enormous real part, which effectively masks any effects arising from the imaginary part. The steep rise within 0.5 MeV of threshold implies the presence of an extremely strong η^3He interaction maybe sufficiently strong to produce a quasi-bound state.

3.2 Mass of the η Meson

The COSY-GEM collaboration has published a precision result on the mass of the eta meson [3)] that was consistent with most previous results, except NA48. In the meantime, results from MAMI, KLOE, and CLEO with similar precision agree with the higher value found by NA48, as indicated in Figure 2. This situation is very unusual since the GEM experiment was performed with special kinematics that allow the simultaneous measurement of the $pd \to \eta^3He$ and $pd \to \pi^+ \, ^3H$ in the spectrometers acceptance.

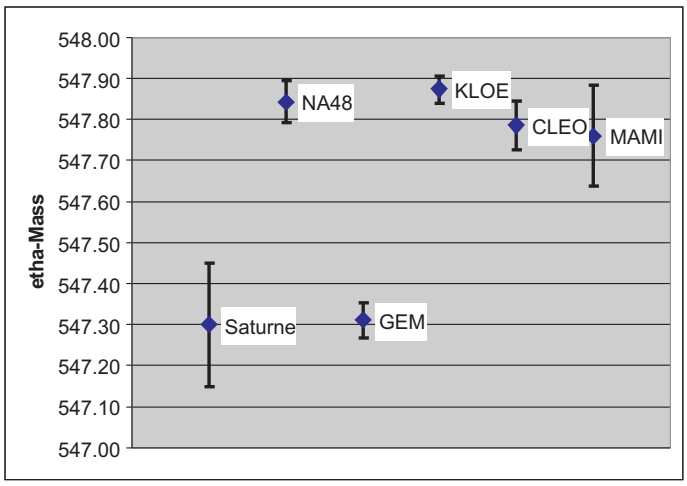

Figure 2: Overview of the existing results on the mass of the eta meson.

In order to resolve this situation the original data are being reanalyzed, and a new measurement with a completely different technique is scheduled. The new measurement uses the step-function like rise of the cross section for the $pd \to \eta^3He$ reaction at threshold, mentioned in the section above. The ANKE spectrometer will measure the momentum of the produced ^3He while the beam momentum is slowly scanned across the resonance. When comparing the *c.m.* momentum of the ^3He as a function of the beam energy a precision of 9 keV for the mass of the η is expected. The absolute value of the beam momentum will be determined by measuring a depolarising resonance induced by a rf-solenoid. The resonance frequency (f_{res}) is related to the revolution freqency of the beam in the synchrotron f_{rev}, the magnetic moment $|G|$ and the Lorentz factor γ of the mean beam velocity

$$f_{res} = f_{rev} \times (1 - \gamma|G|)\,. \tag{1}$$

In test experiments the mean beam momentum has been determined with an accuracy of $\Delta p/p \sim 3 \times 10^{-5}$.

3.3 $\eta \to 3\pi^0$ Dalitz Plot Density

Decays of the η meson provide a perfect testing ground for symmetries and their violation in low-energy QCD. Chiral SU(3) symmetry, its realization in hadron physics at low energies and the role of explicit chiral symmetry breaking due to the light quark masses $m_{u,d,s}$ can be investigated in η decays. The isospin violating decays $\eta(\eta') \to 3\pi$ occur mainly due to the quark mass difference $m_d - m_u$ and offer an excellent opportunity to provide precise constraints on this value. For the decay with neutral pions one expects nearly uniform Dalitz plot with only small deviation due to final $\pi - \pi$ interaction.

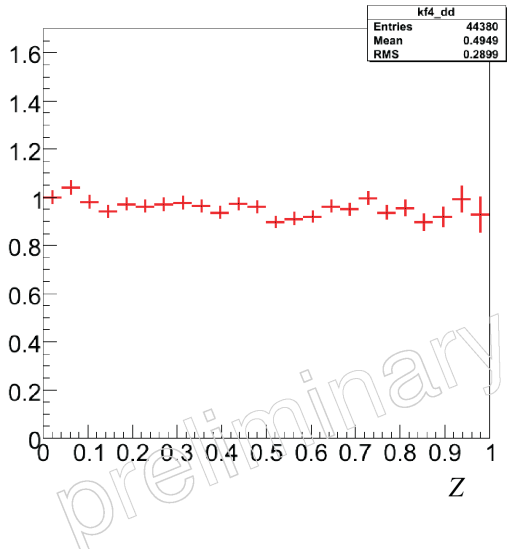

Figure 3: Preliminary distribution of the density within the $\eta \to 3\pi^0$ Dalitz plot for a subset of the existing data.

During the first production run data were taken at a luminosity slightly higher than $10^{31} cm^{-2} s^{-1}$. The η signal can be identified nearly background free in the proton-proton missing mass versus 6γ invariant mass distribution. A data rate of about 1.5 fully reconstructed $\eta \to 3\pi^0 \to 6\gamma$ events per second was achieved. A preliminary version of the the Dalitz plot density distribution

is shown in Figure 3 for a small subset of the data (corresponding to about one day of nominal operation). With the data sample already on tape, it will be possible to determine the asymmetry of the decay Dalitz plot with an accuracy similar to the existing world data.

3.4 Kaon Pair Production

Total and differential cross sections have been measured for Kaon pair production in the $pp \to ppKK$, $pp \to dKK$ and $pn \to dKK$ reactions both below and above the ϕ meson threshold. These results from the COSY-11 and ANKE collaborations are reported in the following reports [4, 5, 6]. The sources of these kaon pairs is dominantly from the decay of non-strange mesons (ϕ and a_0/f_0), as well as the associated production of of excited hyperons ($\Sigma(1385)\Lambda(1405)$). The excitation functions show large deviations from the expectations based on equal population of the available phase space. This can be attributed to final state interactions (FSI) in the outgoing pp system and has a very strong strong effect in the K^-p final state. Only negligible K^+p FSI effects are required to describe the data. These effects can be observed in Figure 4.

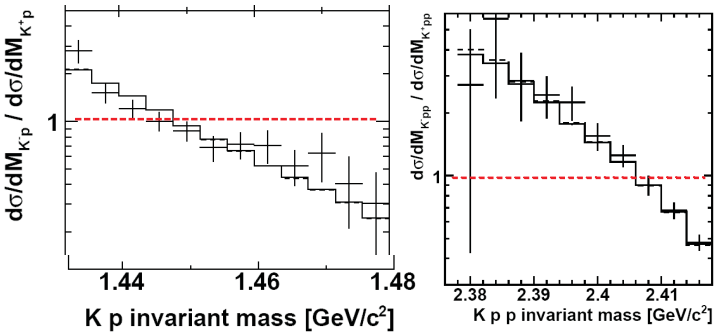

Figure 4: Ratio of the K^-p to the K^+p invariant mass spectra. The solid histogram represents a model estimate including FSI effects in all final state particle pairs.

4 Baryon Interactions and Spectroscopy

4.1 Excited Hyperon Production

Proton-proton collisions with a kaon in the final state are sensitive to the ground state Λ and Σ hyperons as well as the excited resonances $\Sigma^0(1385)$ and $\Lambda(1405)$. Since the $\Lambda(1405)$ is not understood well (3q resonance, K^-p molecule, two-state resonance), it is important to try to obtain additional new information about this state. A difficulty in elucidating the nature of the $\Lambda(1405)$ comes from the fact that it overlaps with the nearby $\Sigma^0(1385)$, and thus it is an experimental task to separate the two states. The cleanest way to do this is through the measurement of the $\Sigma^0\pi^0$ channel, since isospin forbids this for the Σ^0. The strategy to discriminate between them is to (*i*) detect and identify four

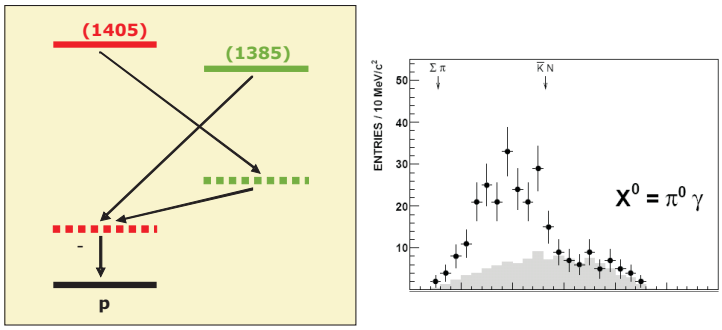

Figure 5: (*left*) Level scheme for the decay of excited Λ and Σ hyperons. (*right*) Invariant mass distribution for decays of the $\Lambda(1405)$. The shaded area corresponds to the calculated background contribution.

charged particles (2 protons, a positive kaon and a negative pion) in coincidence, (*ii*) select those events, for which the mass of a ($p\pi^-$) pair corresponds to that of the Λ, and (*iii*) select the mass of the residue m(X_0) to be that of the π^0 (to tag the $\Sigma^0(1385)$) or to be significantly larger (for a tag on $\Lambda(1405)$). This approach has been used in a recent ANKE-experiment to investigate the line shape of the $\Lambda(1405)$ [7]. The results clearly show the different behavior of the two resonances: while the $\Sigma^0(1385)$ has a Breit-Wigner shape with a width of about 50 MeV/c^2, the $\Lambda(1405)$ shape is influenced by the opening of the $\bar{K}N$ threshold, see Figure 5.

4.2 Pentaquark search at TOF and ANKE

The theory of strong interactionQuantum Chromodynamics (QCD)does not exclude the existence of color singlet objects other than mesons and baryons. A candidate for such states emerged in 2003the narrow exotic S=+1 resonance called Pentaquark $\Theta^+(1530)$. Its anticipated quark sub-structure is $uudd\bar{s}$, leading to decays into either K^0p or K^+n. After early indications for the Θ^+ at TOF [8], they have studied the $pp \to pK^0\Sigma^+ \to p(\pi^+\pi^-)(\pi^+n)$ reaction with substantially improved statistics and extended detection capability at a beam momentum of 3.059 GeV/c. This experiment is unique in its almost

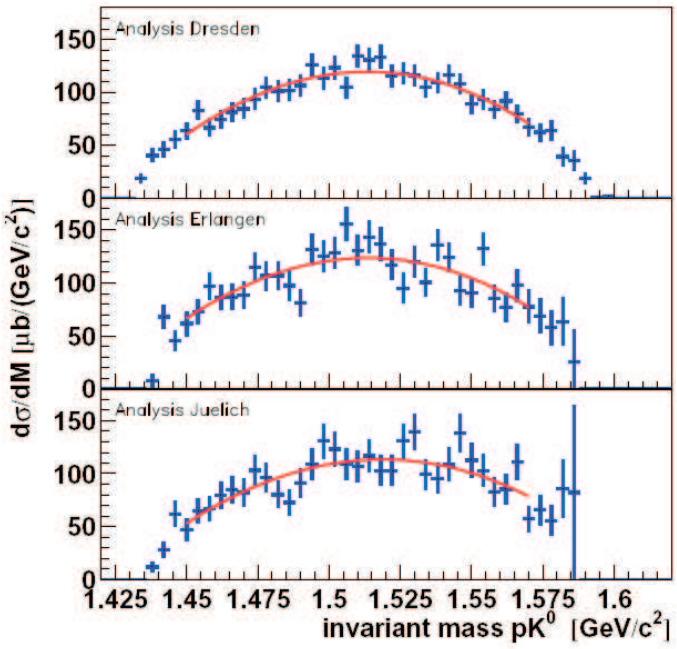

Figure 6: K^0p invariant mass distribution for three differnt analysis approaches. The solid line represents an estimate of the non-resonant $pK\Sigma$ background.

complete coverage of three-body phase space and the exclusive S = +1 final state selection. The extracted K^0p spectra (Figure 6) do not show any evidence for a narrow resonance in the mass region of $1.501.55 GeV/c^2$, thus the earlier

indication for the Θ^+ is not confirmed and an upper limit for the prodution cross section is set to be 150 nb at the 90% confindence level. The figure showsthe results of three independent analysis of the data with very different methods. Furthermore, a blind analysis of the data was performed by using only one half for testing and optimizing the code,and then applying the unchanged code on the second half of the data. A similar conclusion is obtained from the measurement [9] of the reaction $pp \to pK^0\pi^+\Lambda$ at ANKE via the investigation of the $(\pi^+\Lambda)$-missing mass spectrum, see Figure 7.

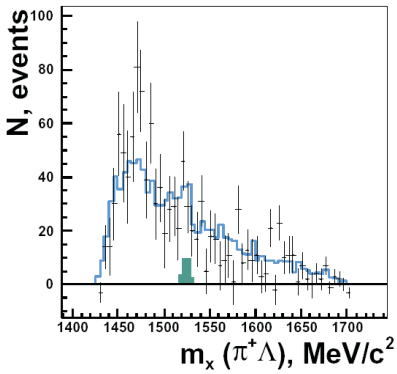

Figure 7: $\pi^+\Lambda$ invariant mass distribution. The solid line represents an estimate of the background contribution, and the filled histogram represents an upper limit for the cross section of the Θ^+ production.

5 Summary

At COSY a wide range of precion experiments in the field of hadronic physics is being carried out. This report has presented a brief overview of some of the recent results. The physics program is well focussed and explores crucial elements for our understanding of strong QCD. In order to persue this program a close relation between theory and experiment is established. The tools developed to persue this work are at the same time an essential basis in the preparation for internal experiments with phase space cooled antiproton beams at the upcoming High Energy Storage Ring at the new FAIR facility.

References

1. J. Smyrski et al., Phys. Lett. B 649 (2007) 258.
2. T. Mersmann et al., Phys. Rev. Lett. 98 (2007) 242301.
3. M. Abdel-Bari *et al.* Phys. Lett. B 619 (2005) 281.
4. P. Winter *et al.*, Phys. Lett. B 635 (2006) 23.
5. Y. Maeda *et al.*, Phys. Rev. Lett. 97 (2006) 142301.
6. M. Hartmann *et al.*, Phys. Rev. Lett. 96 (2006) 242301.
7. I. Zychor et al., arXive:0705.1039v1
8. M. Abdel-Bary et al., Phys. Lett. B 649 (2007) 252.
9. M. Nekipelov et al., J. Phys. G: Nucl. Part. Phys. 34 (2007) 627.

Frascati Physics Series Vol. XLVI (2007), pp. 157
HADRON07: XII Int. Conf. on Hadron Spectroscopy – Frascati, October 8-13, 2007
Plenary Session

RECENT RESULTS ON HADRON SPECTROSCOPY FROM ELSA AND MAMI

R. Beck
HISKP - Bonn Universitaet

Written contribution not received

Frascati Physics Series Vol. XLVI (2007), pp. 159–164
HADRON07: XII Int. Conf. on Hadron Spectroscopy – Frascati, October 8-13, 2007
Plenaryl Session

THE EUROPEAN PHYSICAL JOURNAL (EPJ): ACHIEVEMENTS AND PERSPECTIVES IN THE CONTEXT OF EPJ A - HADRONS AND NUCLEI

Enzo De Sanctis
INFN - Laboratori Nazionali di Frascati, C.P. 13,
00044 Frascati (R.M.), Italy
Christian Caron
Physics Editorial Department, Springer, Tiergartenstraße 17,
69121 Heidelberg, Germany

Abstract

A brief overview is given over the history and recent developments of The European Physical Journal (EPJ). Modern approaches to scientific journal publishing are highlighted in the context of EPJ A - Hadrons and Nuclei.

1 History and development of EPJ

As Europe is celebrating the 50th anniversary of the Treaty of Rome this year, we are left to marvel at the achievements of what is now the economic and political powerhouse the European Union has become. And, to ponder what unification "niches" have been overlooked. Among the few notable examples one could cite, scientific publishing plays a prominent role, as it links economic to scientific and cultural issues and can thus be considered a good testbed for European "self-assurance" in this field.

In the following, we shall restrict our discussion to the physical sciences, though many facets of this issue are more or less readily transferable to other natural sciences fields.

Though it became already evident in the 1960s that the focus of scientific research and related journal publishing in physics had moved from Europe to the US - the rapid growth and development of the *Physical Review* journals and the launch of the currently leading physics journal *Physical Review Letters* in terms of combined size and impact date from those years - it took a long while to realize that the individual journals based in Europe would have to eventually team up, in order to present at least a serious alternative to their efficient US-based counterparts, published by the American Physical Society. Indeed, it is only in 1986 that the first significant merger took place when the *Lettere al Nuovo Cimento* (Italian Physical Society, SIF) combined with *Journal de Lettres Physique* (EDP Sciences/ French Physical Society) to form *Europhysics Letters* (EPL) under the scientific leadership of the European Physical Society.

However, *Europhysics Letters* as a stand-alone letter journal could only be the first step and in the 1990s, negotiations began between the Italian and French Physical Societies and Springer-Verlag to merge a lot if not all of their main physics journals, which represents the most important move in terms of combined size and impact to date. It was in 1998 eventually, that *The European Physical Journal* (EPJ) was launched as a merger of the bulk of *Il Nuovo Cimento*, *Journal de Physique* and *Zeitschrift fr Physik* with, in its combined archives, an unparalleled treasury of 20th century physics publications [1)].

With *EPJ*, the critical mass in European-based physics publishing had been achieved and it triggered a slow but dynamical and ongoing process - this is perfectly visible through the succession of mergers that have taken place in the aftermath of its launch. As of today, EPJ is proud to present itself as merger and continuation of *Acta Physica Hungarica*, *Anales de Fisica*, *Czechoslovak Journal of Physics*, *Il Nuovo Cimento*, *Journal de Physique*, *Portugaliae Physica* and *Zeitschrift fr Physik*. Still, the process is yet remarkably unfinished and the European landscape remains fragmented, an issue that the European Physical Society plans to address in a larger context in the forthcoming years [2)].

For the time being, EPL and EPJ, related to each other through an editorial transfer agreement to allow for a similar transfer of papers as the

one between *Physical Review* and *Physical Review Letters*, represent by far the most serious and advanced effort to implement the ideas of the Treaty of Rome, as far as physics publishing is concerned.

Presently, EPJ is published in seven distinct sections:

- EPJ A - Hadrons and Nuclei
- EPJ B - Condensed Matter and Complex Systems
- EPJ C - Particles and Fields
- EPJ D - Atomic, Molecular, Optical and Plasma Physics
- EPJ E - Soft Matter (since 2000)
- EPJ AP - Applied Physics
- EPJ ST - Special Topics (since 2007)

with further plans for mergers and new launches. The journal also succesfully experiments with new publishing models such open-access publishing and, e.g., EPJ C is shortlisted for talks with the funding consortium SCOAP [3] for negotiations to become an open-access journal altogether [4].

2 Aims and Scope, Editorial Policy and special features of EPJ A - Hadrons and Nuclei

More specifically, the European Physical Journal (EPJA) "Hadrons and Nuclei" is devoted to all aspects of the structure of hadrons and nuclei. The common framework of these systems is that they are few- and many-body systems bound by strong interactions. They comprise the fields of structure and dynamics of hadrons, baryon and meson spectroscopy, hadronic and electroweak interactions of hadrons, non-perturbative approaches to QCD, phenomenological approaches to hadron physics as well as nuclear structure and reactions, few-body and many-body systems, heavy-ion physics, hypernuclei, radioactive beams and nuclear astrophysics.

The hadron and nuclear physics communities are, compared to the other physics disciplines, relatively small and well connected communities, more often than not unified by the experimental research done at a limited number of major labs around the world. Accordingly, since fall 2006 EPJA has developed

into a community journal, becoming a comprehensive platform that addresses all relevant article categories, that is Letters, Regular Articles, Tools for Experiment and Theory/Scientific Notes, and Reviews. Here we give you a short overview of the different categories:

Letters are a fast and concise way to communicate important topical results to a broad audience. They must describe new and original work deserving rapid publication. A letter may be followed by one or more regular articles containing additional details.

In order to promote the latest research results rapidly, the Letter articles accepted for EPJA are, by default, published with immediate Open Access without incurring any fee.

Regular Articles are original works or details in addition to original works previously published in a Letter article. There is no general limitation of the overall size or of the number of figures, nor of the level of details considered to be necessary.

Tools for Experiment and Theory/Scientific Notes is a new session that provides a forum to account for the increasing technical complexity in nuclear and particle physics research and consequently for the growing weight of simulations and data analysis, in particular in the context of larger experiments. It publishes articles presenting original and new developments of particle detectors, readout electronics, computational methods or analysis tools of relevance to current theoretical and experimental investigations. Direct relevance to physics topics within the "Aims and Scopes" of the journal must be demonstrated. An important subgroup are Scientific Notes, typically based on internal notes of experimental collaborations, detailing specific aspects of importance for understanding and assessing the physics results presented in large collaboration papers. Technical details down to the level of construction drawings, electronic circuit diagrams or computer codes should not be included but may be added as electronic-only supplementary material.

One reason for launching such a section is to give (especially young) researchers a chance to profile themselves with the details of the work they did, but which cannot be made that visible in joint collaboration papers. Another

one is that, while we do not want to compete with purely instrumentation journals here, we realize that the complexity of large experiments has gotten such, that the physicists in charge of running the experiments and interpreting the results need to be aware of the intertwining of the physics of the underlying apparatus and the new physics sought after. Thus, we explicitly seek the submission of physics relevant issues on statistics (data interpretation), "discovery" or performance simulations etc of immediate relevance to later pure physics papers.

Reviews is a new session that provides comprehensive and authoritative accounts on specific subjects. Review articles fall into one of the following categories:

1. Traditional reviews comprehensively summarizing a broad field or topic within the Aims and Scopes of the journal. One of their main assets is a definitive and representative bibliography;

2. Reviews on a newly emerging field, providing an up-to-date synthesis and an extended discussion of open questions. The discussion is expected to lead to the recommendations (pro and cons) about the various possible developments of the field with the aim to make a substantial contribution to the decision making progress in planning or running of experimental and observational facilities;

3. Outstanding thesis or working reports, of which the richness and importance of details justifies the exceptional publication of the full length work.

Selected topical issues are preferentially based upon invitation through a guest editor but may, in exceptional cases, be based on meetings. In the latter case, stringent rules apply [5)]. Note expressedly that traditional proceedings are not considered for publication by EPJ A.

EPJA combines these modern approaches with the traditional careful and personalized evaluation of submitted work as well as thorough copy-editing of manuscripts. It is further committed to continue publishing a high-quality paper version, in addition to the electronic edition, as a proven way of ensuring the perennity of archives.

References

1. http://www.epj.org/
2. O Poulsen *Physics in Europe*, Europhys. News 37/2 (2006)
3. http://www.scoap3.org
4. http://www.epj.org/open_access.html
5. http://www.epj.org/special_issues.html

Frascati Physics Series Vol. XLVI (2007), pp. 165–176
HADRON07: XII Int. Conf. on Hadron Spectroscopy – Frascati, October 8-13, 2007
Plenary Session

NUCLEON SPIN STRUCTURE RESULTS

Michael Düren on behalf of the HERMES collaboration
Justus-Liebig-Universität Giessen

Abstract

After finishing a 12 year period of successful running, the HERMES experiment has generated a rich harvest of exciting and novel results on the spin structure of the nucleon, some of which are pioneering, and triggering programs at new facilities. Precision results on the quark spin flavour decomposition of the nucleon spin, and first results on their orbital angular contribution are presented. Basic results on the transverse spin structure and first results on the gluon spin contribution are shown. The recently developed formalism of General Parton Distributions (GPDs) constitutes a unique framework for all these experimental results. After upgrading the spectrometer acceptance by a proton recoil detector, HERMES dedicated the last two years of running to a high luminosity investigation of GPDs in hard exclusive reactions.

1 Introduction

The spin structure of the nucleon became a hot topic in 1988, when EMC discovered the violation of the Ellis-Jaffe sum rule, and hence concluded that the nature of the nucleon contradicts simple relativistic quark models [1)]. The model independent helicity sum rule

$$S_z = \frac{1}{2} = \frac{1}{2}\left(\Delta u + \Delta d + \Delta s\right) + L_q + \Delta G + L_g \tag{1}$$

decomposes the longitudinal projection of the spin into contributions from up-, down-, and strange quark spins (summarized as $\Delta\Sigma$), from gluon spins ΔG and from orbital angular momentum L_q and L_g of quarks and gluons. This apparently simple equation could be formulated only after a detailed theoretical analysis about the scheme dependence of relativistic orbital angular momentum definitions in QCD. In the last 20 years, numerous speculations in context with the spin crisis could be falsified, e.g. the speculation that QCD has to be wrong, that the spin contribution of the quarks is compatible with zero, that the strange sea has a large negative contribution, that the contribution of gluons is large, and that there is no way to measure the orbital angular momentum of relativistic quarks. Today we have many precision results in hand and developed new and deeper questions about the spin structure of the nucleon in terms of quarks and gluons. In many of those fields the HERMES experiment had a leading role.

2 Experimental techniques

The success of HERMES is based on innovative techniques that were distinct from previous experiments in the field [2)]. Large longitudinal or transverse beam polarization was achieved by using spin rotators and new techniques of reducing depolarizing resonances in the high energy electron or positron storage ring of HERA. Relatively large luminosity was achieved by an internal gas target which density was enlarged by an open-ended elliptical storage cell. Highly polarized atomic species (H or D) were produced in a large flux polarized atomic beam source based on Stern-Gerlach separation and radio frequency induced atomic hyper-fine transitions. Precision polarimetry of the beam was achieved by two independent polarimeters based on Compton backscattering of laser light. The degree of dissociation of the target gas in the storage cell was

measured and its polarisation was analysed by a Breit-Rabi polarimeter. In contrast to previous spin experiments, HERMES used an open spectrometer and was able to detect the deep inelastic hadronic final state in coincidence with the scattered lepton. A dual radiator ring image Cherenkov detector allowed for precise particle identification in a large momentum range, especially for a separation of pions and kaons which are used at HERMES to tag and analyse up-, down- and strange-quarks separately. A recently installed proton recoil detector can identify hard exclusive reactions where the scattered nucleon stays intact. With this new detector HERMES can identify in a clean way deeply virtual Compton scattering (DVCS) processes and hard exclusive meson production, both processes that are described by QCD handbag diagrams and GPDs.

3 Polarized structure functions and the spin contribution of quarks

The world data on inclusive polarized deep inelastic scattering as shown in Fig. 1(a) present a consistent picture about the polarization of quarks in nucleons [3]. At small Bjorken x the spin structure function $g_1(x)$ is small, i.e. the sea quarks seem to have no significant spin contribution. At medium x, the polarization is large, for proton targets even larger than for deuteron targets. Using isospin symmetry, it can be directly deduced from this measurement that the polarisation of valence up-quarks is large and positive, whereas the polarization of down-quarks is smaller and negative. The latter means that the spin of down quarks in protons (and also of the up-quarks in neutrons) is oriented anti-parallel to the host nucleon.

The interesting question about the total spin contribution $\Delta\Sigma$ of quarks in the nucleon is answered by integrating the spin contributions over all flavours (up, down, strange) and all values of x. As the inclusive data are lacking a direct access to the strange flavour, one usually applies $SU(3)_f$ symmetry as an addition constraint. Interestingly, because of isospin symmetry, the data on the deuteron target alone are sufficient to extract $\Delta\Sigma$, here given in the $\overline{MS}$ scheme as

$$\Delta\Sigma = \frac{1}{\Delta C_S}\left[\frac{9\Gamma_1^d}{1-\frac{3}{2}\omega_D} - \frac{1}{4}a_8\Delta C_{NS}\right]. \qquad (2)$$

Here ΔC_S and ΔC_{NS} are QCD coefficients, the octet constant a_8 comes from hyperon beta decay data and ω_D is the D-wave contribution in the deuteron

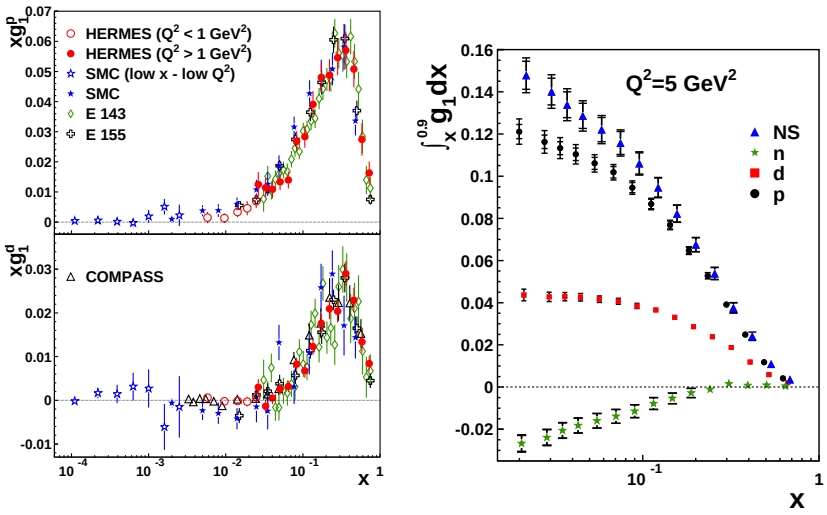

(a) (b)

Figure 1: *(a) The world data on the spin structure functions $g_1^{p,d}(x)$ for proton and deuterium show consistent results. HERMES has the most precise data in the overlap region of sea and valence quarks. (b) The integrated value of the g_1 function approaches a constant value at small x for the deuteron moment.*

wave function. Γ_1^d is the integrated spin structure function of the deuteron. As all experiments have a limited range in x, there is a remaining uncertainty from the contribution of sea quark spins at very small x. Fig. 1(b) shows that the integral $\int_{x_{min}}^{0.9} g_1(x)\,dx$ seems to saturate for the deuteron data when the lower integration limit x_{min} approaches zero. Using the abundant HERMES deuteron sample, the world's most precise value for the spin contribution of quarks in the nucleon is given as

$$\Delta\Sigma = 0.330 \pm 0.011_{theory} \pm 0.025_{experim.} \pm 0.028_{evolution}. \qquad (3)$$

This value is extracted in the $\overline{MS}$ scheme for a Q^2 value of 5 GeV^2 [3]. More details of this analysis are found in this volume by R. Fabbri [5].

4 Flavour spin decomposition and the role of $SU(3)_f$

The Ellis-Jaffe sum rule was derived under the assumption of $SU(3)_f$ symmetry and of a negligible role of strange quark polarisation. The deviation of our measurement from this naive $SU(3)_f$ prediction where $\Delta\Sigma = a_8 = 0.586$, translates in $SU(3)_f$ directly into a sizable negative spin contribution of strange quarks (including strange antiquarks) [3]:

$$\Delta s = \frac{1}{3}(\Delta\Sigma - a_8) = -0.085 \pm 0.013_{theory} \pm 0.008_{experim.} \pm 0.009_{evol}. \quad (4)$$

If this result is real, or if it is just an artefact of a falsely assumed validity of $SU(3)_f$ can be checked by measuring the strange sea polarization directly. The ability of HERMES to measure semi-inclusive reactions and to positively identify charged kaons has been used to extract spin asymmetries for positive and negative kaon production. Event samples with final state kaons have a larger probability to originate from hard strange quark scattering processes than the inclusive event samples. A comparison of the asymmetries from kaon samples compared to inclusive DIS samples can be directly used to extract the strange spin content. A preliminary result is shown in Fig. 2. In contrast to the above result, there is no indication for a negative strange sea polarization. A final analysis will have to show if this apparent discrepancy is due to the limited x-range and statistics of the data, or if it is an indication that the $SU(3)_f$ symmetry is violated in the nucleon spin data. Already some years ago HERMES has done the first direct 5-flavor separation of polarised distribution functions. Also that analysis showed no indication for a non-zero polarization of the quark sea, neither for strange quarks nor for up- or down-antiquarks [4].

5 The role of gluons

During the spin crisis the role of the QCD axial anomaly was investigated and it was tried to attribute the lacking spin contribution by quarks to Q^2 dependent contributions of gluons. Depending on the model, large positive or negative contributions were expected. One way to experimentally access the gluon spin contribution ΔG in the nucleon is based on the Q^2-evolution of the quark and

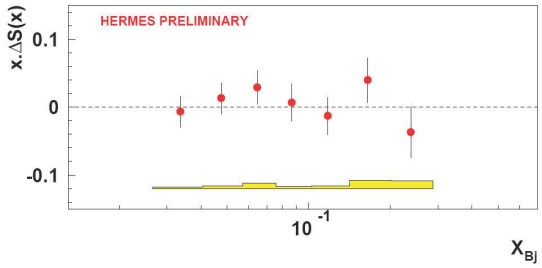

Figure 2: *By identifying kaons in the final state of polarized semi-inclusive DIS on a deuterium target, it was possible to extract the strange quark spin contribution $\Delta s(x)$ in a model independent way. The data are compatible with zero and show – instead of th expected significant negative polarization – a slight positive polarization.*

gluon distribution functions in NLO QCD:

$$g_1^{NLO}(x) = g_1^{LO} + \frac{\alpha_s}{4}\pi \sum_q \left[\Delta q(x,Q^2) \times C_q + \Delta G(x,Q^2) \times C_g\right] \qquad (5)$$

Due to the limited range in Q^2, the QCD fits constrain ΔG only weakly. A more direct measurement of gluon polarization was done the first time in 2000 by HERMES, where hadron pairs with large transverse momentum were used to enhance the fraction of photon gluon fusion processes in a large background of other processes which were not sensitive to the gluon spin. New preliminary results indicate that the gluon polarization is small, however, more precise results are expected by experiments from COMPASS and RHIC in near future. More details are found in this volume by R. Fabbri and A. Ferrero [5, 6].

6 Transverse spin asymmetries and orbital angular momentum

Transversity describes the transverse spin distribution of quarks in a transversely polarized nucleon. Due to the chiral-odd nature of the corresponding operator, transversity effects cancel in inclusive DIS reactions and it has only recently been realized that the transversity function $h_1(x)$ is a leading-twist structure function of equal importance as $F_2(x)$ or $g_1(x)$. In the non-relativistic limit, $h_1(x)$ and $g_1(x)$ are identical, as both functions describe the orientation of the quark spins relative to the nucleon spin, $g_1(x)$ in a helicity frame and $h_1(x)$

in a transverse frame. As boosts and rotations do not commutate, $h_1(x)$ can deviate from $g_1(x)$ and any experimental evidance of such a deviation would be a prove of the relativistic nature of the substructure of the nucleon. The QCD evolution of $h_1(x, Q^2)$ is of special importance, as gluons do not contribute to the DGLAP evolution of h_1 in contrast to the evolution of g_1, where gluons and quarks mix. The chiral-odd transversity function h_1 can be studied in semi-inclusive DIS, where it appears as Collins asymmetry, as the product of the chiral-odd transversity distribution with a chiral-odd Collins fragmentation function. The Collins asymmetry is a single spin azimuthal asymmetry in the angle $\phi + \phi_s$, where ϕ and ϕ_s are certain azimuthal angles which depend on the transverse orientation of the target spin and of the direction of the produced hadron compared to the plane of the scattered lepton. A second new function, the T-odd Sivers function, can be measured in the same semi-inclusive process. The Sivers asymmetry is an azimuthal asymmetry in the angle $\phi - \phi_s$. HERMES was the first experiment that measured non-zero values as well for the Collins as for the Sivers asymmetry and proved the existence of these effects. A two-dimensional fit of the measured azimuthal hadron asymmetries allowed disentangling the contributions in $\phi + \phi_s$ and $\phi - \phi_s$. Figure 3 shows the analysing powers for the Sivers and Collins asymmetries as a function of kinematic variables [7, 8]. In a recent interpretation of the Sivers function it has been found that it is related to the orbital angular momentum of quarks in a nucleon. As sketched in Fig. 4(a), the orbital angular motion of quarks around the spin direction of the nucleon leads to a kind of red or blue shift of the photon-quark interaction, i.e. to different cross sections depending on the impact position of the photon. Due to the attractive final state interaction of the quark while it fragments to a hadron, the hadron is bent to the right or left, depending of the impact position. The correlation of the different cross sections for hadrons bent right or left show up as single spin asymmetries in the experiment. Using this interpretation, the non-zero Sivers asymmetry as measured by HERMES proves the existence of orbital motion of quarks in nucleons.

7 Generalized Parton distributions: partons in phase space

In 1932 Wigner introduced the first phase-space distribution in quantum mechanics. Despite the uncertainty principle and the usual description of quantum

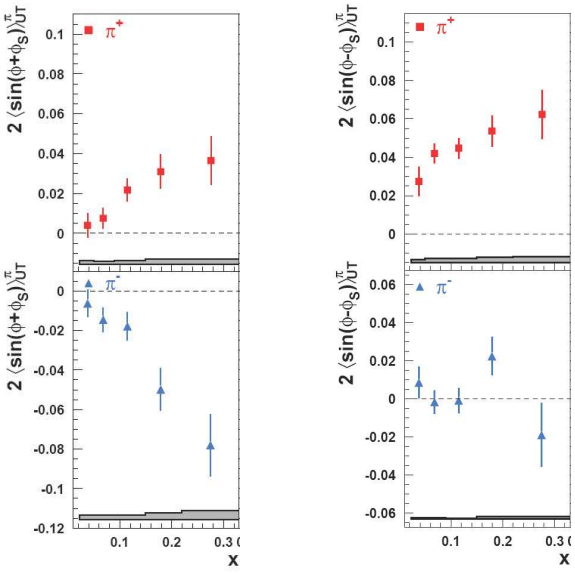

(a) (b)

Figure 3: *The Collins (a) and Sivers (b) moments are shown here as a function of the kinematic variable Bjorken x for positive (upper plots) and negative (lower plots) pion production in semi-inclusive polarized DIS, using a transversely polarized target and an unpolarized beam. Three of the four plots show significant single-spin asymmetries which prove the existance of a non-tivial Sivers, as well as Collins function. (HERMES Preliminary 2002-2005; 8.1% scale uncertainty)*

mechanical systems by complex wave functions, he managed to introduce a real function that contains the complete (one-body) information of a quantum system. Any observable can be calculated from this Wigner function. This concept can be generalized and applied to quarks in nucleons. As the Wigner operator depends on all variables of the relativistic phase space, some of the variables have to be integrated out to limit the number of variables, so that these reduced functions have a chance to be measured in today's experiments. These reduced Wigner distributions are related to the General Parton Distributions (GPDs). As GPDs are related to Wigner functions which describe correlations in phase-space, it is not surprising that GPDs contain information about the

orbital angular momentum of quarks in nucleons, simply in analogy to the classical relation $L = r \times p$. Thus, the interest of the community in GPDs increases constantly since Ji derived the relation between the angular momentum J and the GPDs H_q and E_q:

$$J_q = \frac{1}{2} \int_{-1}^{1} x dx \left[H_q(x, \xi, 0) + E_q(x, \xi, 0) \right] \tag{6}$$

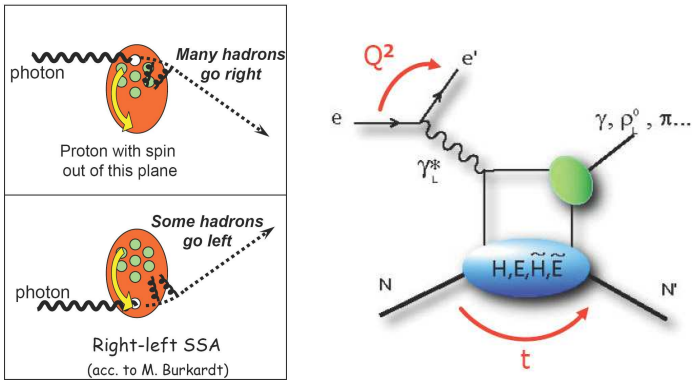

(a) (b)

Figure 4: *(a) The Sivers single spin asymmetry (SSA) is interpreted as an effect of the orbital motion of quarks in a transversely polarized nucleon. Depending on the impact position, quarks appear red- or blue-shifted due to their orbital motion. The attracting final state interaction bends the observed hadrons into a direction opposite of the impact position. (b) The handbag diagram describes processes, where a hard virtual photon γ^* at large Q^2 couples to a quark that consequently emits another high energetic particle, which can be a real photon (in the case of DVCS) or a vector or scalar meson. The remnant quark is reabsorbed by the nucleon. The ability of the nucleon to emit and absorb the quark is described by the GPDs $H, E, \tilde{H}, \tilde{E}$.*

8 Deeply virtual Compton scattering and other hard exclusive processes

The most direct access to GPDs is given by hard exclusive reactions that are described by the QCD handbag diagram as shown in Fig. 4(b): a quark is

emitted by a nucleon, interacts with a virtual photon, emits a photon (in the case of deeply virtual Compton scattering DVCS) or a meson (in the case of hard exclusive meson production) and is re-absorbed by the nucleon without breaking it apart. The virtual photon at large Q^2 defines a hard scale. The diagram factorizes into an upper part of the diagram that can be calculated in pertubative QCD and a lower part of the diagram that sums up all soft contributions and is described by a set of non-pertubative GPDs. In the case of DVCS the diagram interferes with the Bethe-Heitler process which has an identical final state, but there the photon is emitted by the lepton instead of the quark. It turns out that at HERMES energies the Bethe-Heitler diagram dominates the cross section, making a direct measurement of the DVCS contributions impossible. However, as Bethe-Heitler and DVCS processes have indistinguishable final states, the two processes interfere and produce beam spin and beam charge azimuthal asymmetries which would be zero for each of the two processes individually. The possibility to independently flip the beam spin by the HERA spin rotators and the beam charge by injecting positrons instead of electrons at HERA gives HERMES the unique option to measure the beam spin and beam charge asymmetries in the same experiment. Figure 5 shows the beam charge asymmetry [9]. More details of these measurements are found in this volume by T. Keri [10].

Using an unpolarized beam and transversely polarized target gives access a new type of single spin asymmetries, which is sensitive to the GPD function E that is correlated with the total angular momentum of quarks in nucleons. A recent model dependent analysis shows the sensitivity of the results (see Fig. 6) [11]. The combined data on the proton from HERMES and data on the neutron from JLab Hall A give a constraint as well on the angular momentum J_u of up-quarks as J_d of down-quarks. These first (model dependent) results are consistent with results from lattice QCD calculations.

9 Outlook

In the last two years HERMES was running with the new recoil detector which is able to detect the final state proton and can distinguish exclusive hard interactions from semi-inclusive reactions in a clean way. It also allows a precise determination of the kinematics, especially of the squared momentum transfer Mandelstam t. Using an unpolarized gas target with large density, HERMES

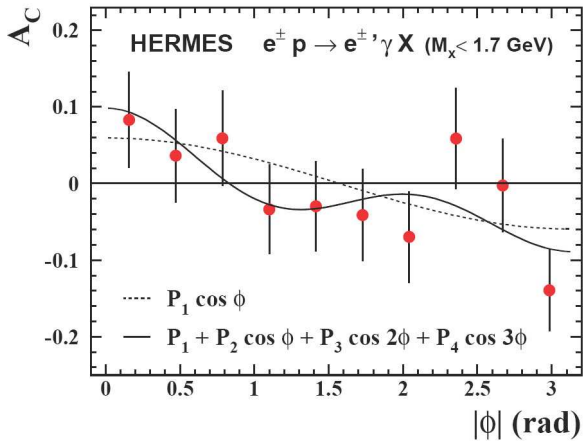

Figure 5: *The beam charge asymmetry is shown as a function of the azimuthal angle ϕ. For symmetry reasons, only the range between 0 and π is relevant. A Fourier decomposition shows a significant* $\cos\phi$ *contribution that can be interpreted by the corresponding GPD, but there are also higher moments present in the data.*

was able to collect about 47,000,000 DIS events. This is a multiple of the luminosity that was previously taken and promises much more precise results on DVCS and other hard exclusive processes, once the data are analysed.

Acknowledgements

We gratefully acknowledge the DESY management for its support, the staff at DESY, and our national funding agency BMBF and the EU for financial support.

References

1. EMC, J. Ashman *et al.*, Phys. Lett. B105 (1988) 364
2. HERMES, K. Ackerstaff, *et al.*, Nucl. Instrum. Meth. **A417**,230 (1998)
3. HERMES, A. Airapetian *et al.*, Phys. Rev. D 75 (2007) 012007

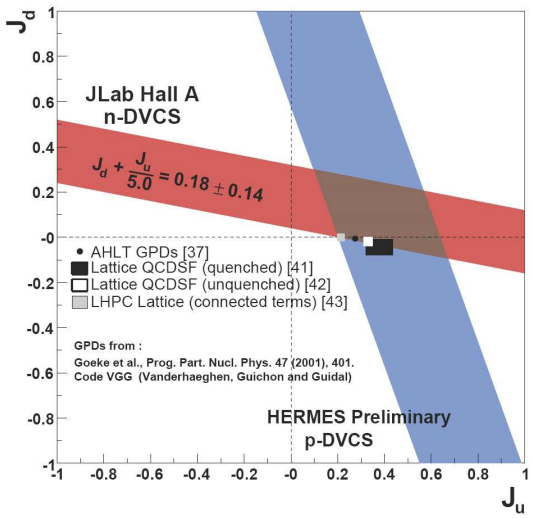

Figure 6: *First data on DVCS processes with unpolarized beam and transversely polarized target have been taken at HERMES and JLab Hall A on proton and on neutron respectively. By using a specific GPD model these data give a first quantitative (but model dependent) value on the angular momentum contribution of up- und down-quarks to the nucleon spin. The data are consistent with lattice calculation.*

4. HERMES, A. Airapetian *et al.*, Phys. Rev D 71 (2005) 012003
5. R. Fabbri, this volume.
6. A. Ferrero, this volume.
7. HERMES, A. Airapetian et al, Phys. Rev. Lett. 94 (2005) 012002
8. L. Pappalardo, this volume.
9. HERMES, A. Airapetian *et al.*, Phys. Rev. D 75 (2007) 011103(R)
10. T. Keri, this volume.
11. HERMES, Zhenyu Ye, arXiv:hep-ex/0606061 (2006)
    JLab Hall A, M. Mazouz *et al.*, arXiv:0709.0450 (2007)

Frascati Physics Series Vol. XLVI (2007), pp. 177–189
HADRON07: XII Int. Conf. on Hadron Spectroscopy – Frascati, October 8-13, 2007
Plenary Session

HADRON SPECTROSCOPY AT e-p COLLISIONS

Christoph Grab
Institute for Particle Physics, ETH Zurich
8093 Zurich, Switzerland
Representing the H1 and ZEUS Collaborations at HERA

Abstract

An overview of the recent results on spectroscopy from the electron-proton collider experiments H1 and ZEUS at HERA is presented. Production of particles with light and strange quarks is discussed. Measurements in the charm sector cover fragmentation sensitive parameters and their comparisons with data from e^+e^- experiments, as well as studies of excited charm states. Finally the status of pentaquark searches at HERA is reviewed.

1 Introduction

The two collider experiments H1 and ZEUS measured collisions of electrons[1] on protons at the HERA collider from 1992 to June 2007.

[1]HERA was operated with both electron and positron beams. A reference to electron hereafter implies a reference to either electron or positron. Most of the results shown were obtained in positron-proton collisions.

The main focus of interest at HERA lies in the study of the structure of the proton, in detailed investigations of the various aspects of perturbative QCD and in searches for new phenomena. Relevant in the context of this conference are the detailed studies of production processes and the differences therein between e.g. mesons, baryons and antiparticles. In addition, details about the non-perturbative aspects of fragmentation are investigated. Search and studies of the production of excited and more "exotic" states in the *ep* environment, such as pentaquarks or glueballs constitute another part of the HERA physics portfolio. Overall, the HERA *ep* results complement the findings of other experiments and help to build phenomenological models with strong predictive power, applicable at other machines.

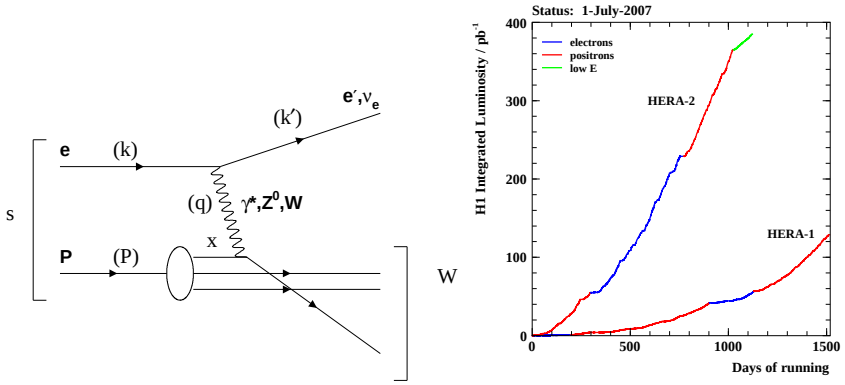

Figure 1: *a) Generic Feynman diagram for ep-scattering. b) The total recorded luminosity in the H1 interaction zone, integrated for the two HERA operation periods HERA-I and HERA-II, running at high proton energies using electrons (blue) and positrons (red) and at low E running (green).*

The kinematics of the *ep* scattering reaction (see the schematic diagram in fig. 1a) are described by the centre-of-mass energy squared $s = (p + k)^2$, by the four-momentum transfer squared Q^2, the Bjorken scaling variable x_{Bjo} or the inelasticity y, defined as

$$Q^2 \equiv -q^2 = -(k - k')^2; \quad x_{Bjo} \equiv \frac{Q^2}{2p \cdot q}; \quad y \equiv \frac{p \cdot q}{p \cdot k}; \quad W^2 = (p + q)^2, \quad (1)$$

where k (k') and p are the four-momenta of the initial (final) state lepton and proton, respectively. When particle masses are neglected the kinematic vari-

ables are related to the lepton-proton centre-of-mass energy $\sqrt{s}$ by $s\,x_{Bjo}\,y = Q^2$. The variable x_{Bjo} is in the leading order approximation identical with the longitudinal momentum fraction x of the proton which is carried by the parton specified by the parton density functions. The $\gamma - p$ centre-of-mass energy squared is given by $W^2_{\gamma p} = W^2 \approx y \cdot s - Q^2$.

It is common at HERA to distinguish two different regimes in Q^2 : *"photoproduction"* denotes low $Q^2 \approx 0$ GeV^2 , also termed γp, where the photon emitted from the electron is quasi-real; and *"deep inelastic scattering (DIS)"* refers to high Q^2 (in practice $Q^2 \geq 2\text{GeV}^2$). In the case of photoproduction, the additional variable x_γ^{obs} describes the momentum fraction of the photon, that participates in the hard interaction. It is used to experimentally distinguish direct photon ($x_\gamma^{obs} \approx 1$) and resolved photon ($x_\gamma^{obs} < 1$) processes.

The overall performance of HERA and the experiments is shown in Fig.1b), where the integrated luminosity taken by H1 is plotted as a function of time. With the ZEUS experiment having collected a similar amount, the total integrated luminosity available for physics at HERA amounts to about 1 fb^{-1}. The results presented below, however, are based on fractions of this.

2 Proton, Deuteron and their Antiparticles Production

Studies of baryon production (protons p, $\bar{p}$, and deuterons d, $\bar{d}$) have been reported by the ZEUS collaboration [1)] in γp and in DIS, based on an integrated luminosity of 120 pb^{-1}. The measurements were performed at a centre-of-mass energy of 300–318 GeV in the central rapidity region η for transverse momentum per unit of mass in the range $0.3 < p_T/M < 0.7$, and the various particle rates were extracted.

The detector-corrected d/p and $\bar{d}/\bar{p}$ ratios are shown in Fig. 2a) as as a function of p_T/M. The antiparticle ratio is in good agreement with the H1 published data [2)] for photoproduction. The production rate of $d(\bar{d})$ is smaller than that for $p(\bar{p})$ by three orders of magnitude, which is in broad agreement with other experiments.

The $\bar{d}/d$ and $\bar{p}/p$ ratios are shown in Fig. 2b) as a function of p_T/M. The $\bar{p}/p$ ratio is consistent with unity in the kinematic range $0.3 < p_T/M < 0.7$, as expected from hadronisation of quark and gluon jets. Due to the significant uncertainties, it is not possible to test models that predict a small baryon-antibaryon asymmetry in the central fragmentation region.

In the same kinematic region, the production rate of d is observed to be higher than that for $\bar{d}$. If this result is confirmed and if this enhancement is produced completely by the primary interaction, then this would mean that the relation between the production ratios $\bar{d}/d \propto (\bar{p}/p)^2$ expected from the coalescence model does not hold in the central fragmentation region of ep DIS collisions, and thus the coalescence model cannot fully describe the $d(\bar{d})$ production in DIS.

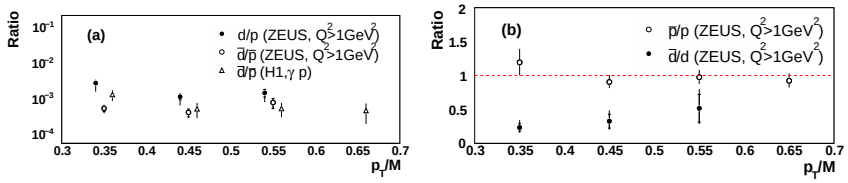

Figure 2: *(a) d/p and $\bar{d}/\bar{p}$ production ratios as a function of p_T/M by ZEUS [1] compared to the H1 photoproduction results [2]. (b) $\bar{p}/p$ and $\bar{d}/d$ production ratios as a function of p_T/M (ZEUS [1]). The points in (a) are slightly shifted horizontally for clarity.*

3 Strange Particle Production

The production of strange quarks can proceed perturbatively by the boson-gluon fusion process ($\gamma g \to s\bar{s}$) and by gluon splitting in parton showers. In addition, the proton parton densities and the non-perturbative string fragmentation can be sources of strange quarks. The strange hadrons are then produced in the hadronization process, or through decays of higher mass states.

A study of K_S and Λ production in three different regions of Q^2 was reported by the ZEUS collaboration [3]: in DIS with $Q^2 > 25\,\mathrm{GeV}^2$, with $5 < Q^2 < 25\,\mathrm{GeV}^2$, and in photoproduction. The various aspects of the production addressed are: single differential cross sections of K_S and Λ, baryon-antibaryon asymmetry, baryon-to-meson ratio, ratio of strange-to-light hadrons, and the Λ and $\bar{\Lambda}$ transverse spin polarization. The spectra include all sources, *i.e.* direct production and all resonance decays. As an example the K^0_S spectra are shown in fig. 3 as function of P_T^{LAB} and η^{LAB} in DIS, and of x_γ^{obs} in γp.

Overall, it was found that the single differential spectra are reasonably well described by the simulations (ARIADNE for high Q^2 and PYTHIA for

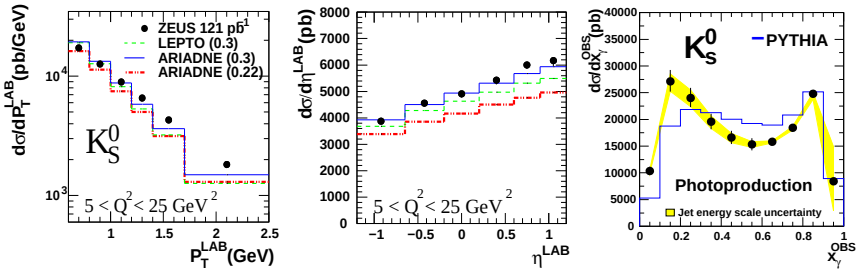

Figure 3: *Distribution of the K^0_S production cross section* [3] *as a function of a) $P_T^{\rm LAB}$, b) $\eta^{\rm LAB}$ for the low Q^2 region, and c) x_γ^{obs} in γp.*

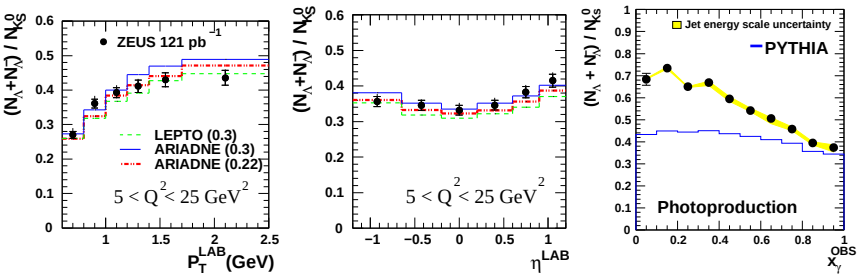

Figure 4: *Distribution of the baryon-to-meson ratio* [3] $[N(\Lambda)+N(\bar\Lambda)]/[N(K^0_S)]$ *as a function of a) $P_T^{\rm LAB}$ and b) $\eta^{\rm LAB}$ in DIS, and c) x_γ^{obs} in photoproduction.*

γp) using a strangeness suppression factor of $\lambda_S = 0.3$. However, a closer look reveals various differences between theory and data. Similar general conclusions can be drawn from the baryon-to-meson ratio distributions (see fig. 4). In both cases, the shape of the x_γ^{obs} distribution in γp including the resolved photon contribution is not properly described by the PYTHIA simulation. For the direct contribution, the baryon-to-meson ratio in γp is similar to the one in DIS and also similar to e^+e^- data. Furthermore, the general features of the strange-to-light hadron ratio (see fig. 5) is pretty well described, however, there a lower λ_S value such as 0.22 is preferred at high Q^2 . There was NO asymmetry observed between Λ and $\bar\Lambda$, which indicates a similar production process for baryons and antibaryons. Studies of angular distributions in the Λ decays did not reveal any non-zero transverse polarization in the Λ or $\bar\Lambda$ production.

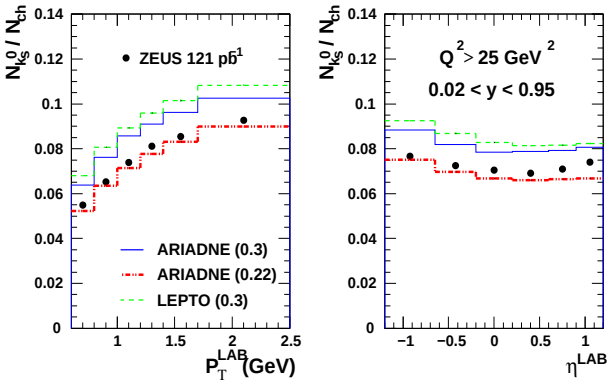

Figure 5: *Distribution of the K^0_S to charged particles ratio $N(K^0_S)/N_{\rm ch}$ as a function of a) $P_T^{\rm LAB}$ and b) $\eta^{\rm LAB}$ for the high Q^2 region (ZEUS [3]).*

4 Charmed Particle Production

The theoretical description of inelastic charm quark production at HERA is based on perturbative QCD (pQCD). In leading order (LO) the direct process of *photon-gluon fusion* is the dominant contribution, *i.e.* $\gamma g \to c\bar{c}$. In photoproduction, resolved photon interactions contribute as well, *i.e.* $gg \to c\bar{c}, q\bar{q} \to c\bar{c}$, and are described with the help of a photon structure function. Beyond LO *only the sum* of direct and resolved processes is a well-defined quantity. The charm quarks from the hard interaction hadronise either in "open states" (e.g. D^2, Λ_c ...) or in "hidden $\bar{c}c$ states", such as J/Ψ. The hadronisation is then described by non-perturbative models, that contain various parameters which need to be determined by experiments.

4.1 Fragmentation Issues

The relative abundance of the various charmed hadrons, given by the primary production rate and the contributions of all possible decay chains leading to that particular hadron, is described experimentally by the fragmentation fractions $f(c \to D)$. The values measured by ZEUS [4] and H1 [5] are shown in fig. 6b), which for comparison also shows the e^+e^- values.

[2]Unless explicitly mentioned, the charge conjugate states are hereafter always implicitly included.

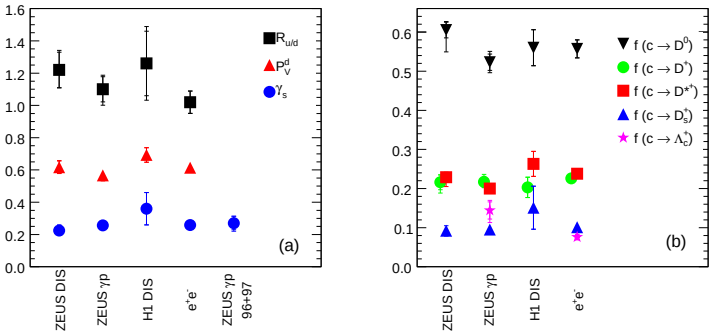

Figure 6: *a) Charm fragmentation sensitive parameters* $R_{u/d}$, P_V^d *and* γ_S, *and b) the fragmentation fractions* $f(c \to D, \Lambda_c)$ *(see* [4] *and* [5]*).*

In addition, ratios of fragmentation fractions are in particular useful to characterise various aspects of fragmentation. Prominent parameters are the relative proportion of light quark flavours u and d (given by $R_{u/d}$), the relative amount of strangeness s created in the fragmentation process (given by γ_S), and the production ratio of different angular momentum states P_V (vector to scalar ratio). Both experiments [4, 5] have determined these parameters $R_{u/d}$, P_V and γ_S and the results are shown in fig. 6a), also in comparison with the numbers observed at e^+e^--colliders.

The actual fragmentation function itself has been determined by a range of experiments (see [6] and refs. therein) and is shown in fig. 7 for the case of D^{*+} decays. Although the detailed definition used for z, the momentum fraction of the charmed quark carried by the charmed hadron, differs in detail, the overall features seen in ep are very similar to the one observed in e^+e^-.

The consistent observations that the fragmentation parameters measured in ep at HERA (DIS and γp) are compatible with the ones in e^+e^-, strongly supports the hypothesis of fragmentation universality, *i.e.* that the fragmentation is independent of the hard subprocess.

4.2 Excited States

The ZEUS collaboration has reported [7] the observation of excited D and D_s mesons in the decay chains $D_1(2420)^0$, $D_2^*(2460)^0 \to D^{*\pm}\pi^\mp, D^\pm\pi^\mp$ and

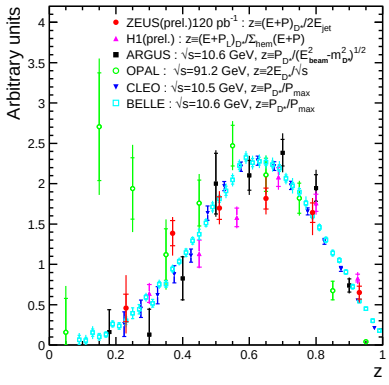

Figure 7: *The fragmentation function* $1/\sigma\ (\mathrm{d}\sigma/\mathrm{d}z)$ *for* D^* *decays, determined in ep (DIS and* γp*) and* e^+e^- *collisions (see* [6] *and refs. therein).*

$f(c \to D_1^0(2420)) =$	$3.5 \pm 0.4^{+0.4}_{-0.6} \pm 0.2\%$
$f(c \to D_2^{*0}(2460)) =$	$3.8 \pm 0.7 \pm 0.6 \pm 0.2\%$
$f(c \to D_{s1}^+(2536)) =$	$1.1 \pm 0.2 \pm 0.1 \pm 0.1\%$
$f(c \to D^{*\prime +}(2640))$	< 0.45 at 95% c.l.

Table 1: Fragmentation fractions f_c of excited D, D_s mesons in %, measured by ZEUS [7].

$D_{s1}^{\pm}(2536) \to D^{*\pm}K_S^0, D^0K^{\mp}$. Based on a sample of ≈ 57000 D^*, ≈ 20400 $D^{\pm}$ and ≈ 22000 D^0 mesons, the resulting observed mass difference spectra are shown in fig. 8. The measured fragmentation fractions for these states f_c in ep are indicated in table 1. They are found to be compatible with the ones observed in e^+e^-, again supporting the universality of fragmentation.

5 Pentaquark Searches

Various theoretical approaches [8] based on Quantum Chromodynamics predict the existence of exotic baryonic states composed of four valence quarks and an anti-quark, commonly known as "pentaquarks". Such states are expected to form a flavour anti-decuplet and are not explicitly forbidden within the

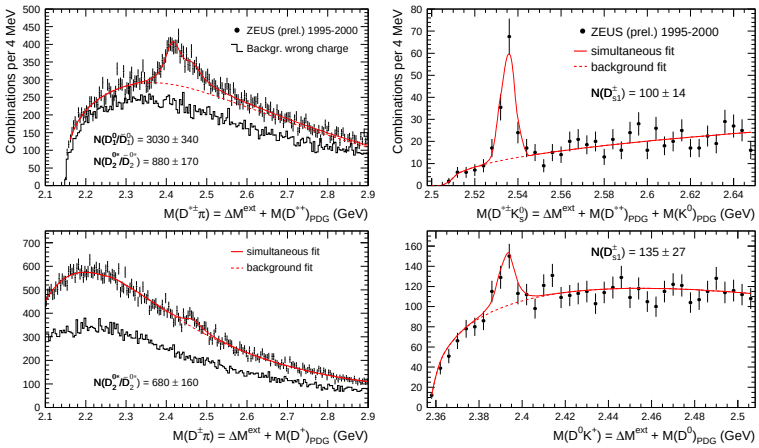

Figure 8: *Mass difference distributions* [7] *for a) charmed excited P-wave meson decays* $D_1(2420)^0$, $D_2^*(2460)^0 \to D^{*\pm}\pi^{\mp}$ *(upper) and* $\to D^{\pm}\pi^{\mp}$ *(lower); and b) the charm-strange particle decays* $D_{s1}^{\pm}(2536) \to D^{*\pm}K_S^0$ *(upper) and* $\to D^0K^{\mp}$ *(lower).*

Standard Model.

Several experiments have reported evidence for a narrow resonance with a mass around 1540 MeV decaying into nK^+ or pK_S^0 final states, whereas others have not observed any signal. Such a state could be interpreted as an exotic strange pentaquark with a minimal quark content of $uudd\bar{s}$, lying in the apex of the spin 1/2 (or 3/2) anti-decuplet, often referred to as the Θ^+. Searches for other members, notably the doubly strange states have also been performed. The large activity in the field during the last years has been discussed e.g. in [9]. The HERA-B collaboration [10] reported limits for Θ^+ and $\Xi^{--/00}$ production in $p + C$ collisions and HERMES [11] on the $\Xi^{--/00}$ production in quasi-real photoproduction. Herein, the actual status of the results on pentaquark searches by the H1 and ZEUS collaborations, notably for the states Θ_s, $\Xi^{++/00}$ and Θ_c is covered.

Strange Pentaquarks: Both experiments have searched for the strange pentaquark candidate Θ_s in the decay $\Theta_s \to pK_S^0$. ZEUS [12] has observed a narrow signal of 221 ± 48 events with (6.1 ± 1.6) MeV width for $Q^2 > 20\,\mathrm{GeV}^2$

at a mass of 1521.5 ± 1.5 MeV. The observed invariant mass distributions of pK^0_S candidates are shown in fig. 9a for $121\,\mathrm{pb}^{-1}$. On the other hand, H1 [13] did not see any significant indication of a signal down to $Q^2 = 5\,\mathrm{GeV}^2$ (see fig. 9b). For the kinematic region where ZEUS quoted a production cross section of $(\sigma \cdot B) = (125 \pm 27^{+36}_{-28})$ pb, H1 has determined an upper limit of $\sigma(ep \to \Theta_s) \cdot B(\Theta_s \to pK^0_S) < 100$ pb at 95% c.l. The ZEUS result is thus not confirmed by H1.

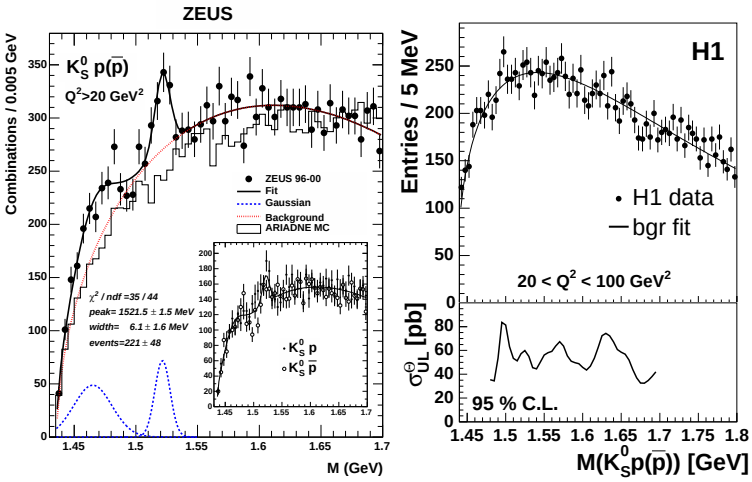

Figure 9: The invariant mass spectrum for $\Theta_s \to pK^0_S$ candidate decays for a) ZEUS [12] and b) H1 [13] data, shown here for comparable kinematic regions of $Q^2 > 20$ GeV^2.

Double Strange Pentaquarks: Furthermore, both experiments have searched for the doubly strange pentaquark candidate states $\Xi^{++/00}$ in both charge combinations (doubly charged or neutral) decaying in $\Xi^{++/00} \to \Xi^+\pi^+$ and $\to \Xi^{\pm}\pi^{\mp}$. Such states could be interpreted as the Ξ^{--}_{5q} ($S = -2$, $I_3 = -3/2$) and the Ξ^0_{5q} ($S = -2$, $I_3 = +1/2$) members of the isospin 3/2 quartet $\Xi_{3/2}$ in the anti-decuplet. The invariant $\Xi\pi$ mass spectra measured by the H1 [14] and ZEUS [15] collaborations do not show any indication of a signal, apart from the well known $\Xi(1530)^0$ baryon resonance, as shown in fig. 10. Therefore the

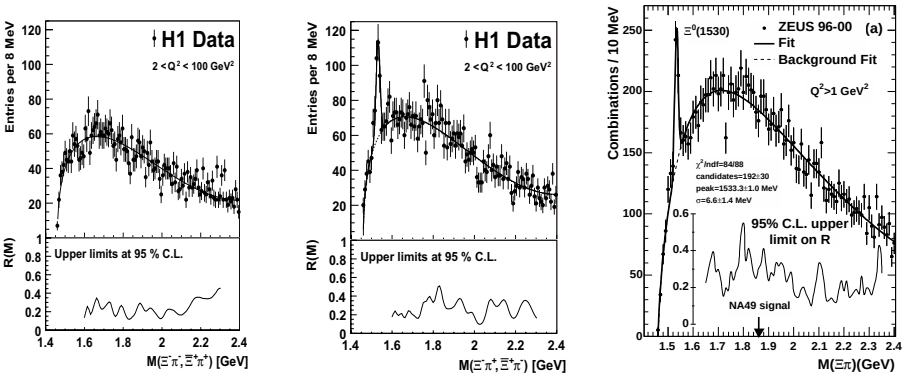

Figure 10: The invariant mass spectrum for a) the H1 [14] doubly charged combinations $\Xi^-\pi^-$ and $\bar{\Xi}^+\pi^+$ (upper part), b) the H1 neutral combinations $\Xi,^-\pi^+$ and $\bar{\Xi}^+\pi^-$ (upper part), and c) the ZEUS [15] sum of all four charge combinations. clearly visible is the well-known $\Xi(1530)^0$ baryon. The lower part shows the 95% C.L. upper limit on the production ratio $R(M)$ relative to the $\Xi(1530)^0$ baryon, as a function of the mass M.

non-observation of any resonance state in the mass range $1600 - 2300$ MeV in neither of the charge combinations limits the production rate of a hypothetical $\Xi^{++/00}$ pentaquark to values of order 20% on average at the 95% C.L. relative to the well known $\Xi(1530)^0$ baryon production rate, depending on the $(\Xi\pi)$-mass.

Charmed Pentaquarks: The H1 experiment had announced [16] a possible signal for yet another pentaquark candidate, for a charmed state Θ_c, observed in the decay $\Theta_c \to D^*p$. A total of (51 ± 11) events of (12 ± 3) MeV width were observed at a mass of (3099 ± 3) MeV. In this case, ZEUS [17] did not see any significant indication of a signal in the same kinematical region. The observed invariant mass distributions of D^*p are shown in fig. 11 for both experiments. A direct comparison between the two experiments can be performed through the ratio of the acceptance corrected Θ_c production yield relative to the D^{*+}production $R(D^*p/D^*)$. H1 obtained a ratio $R = (1.59 \pm 0.33^{+0.33}_{-0.45})$ in the visible range, whereas ZEUS determined an upper limit of $R < 0.51\%$ at 95% c.l., thereby not confirming the H1 findings.

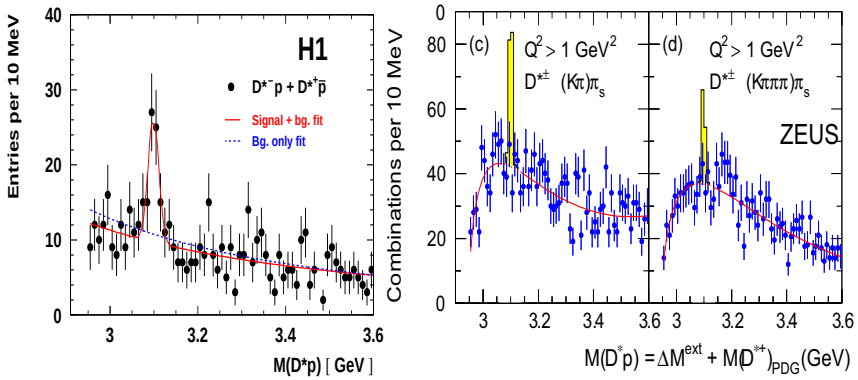

Figure 11: The invariant mass spectrum for D^*p combinations; a) by H1 [16] in the full kinematic region, and b) by ZEUS [17] in $Q^2 > 1\,\mathrm{GeV}^2$. The shaded histogram in b) indicates the extrapolated signal expected according to the H1 signal.

6 Summary

The overall features of the strange particle production are well described by theoretical models. However, there are still many details that need improvements, in particular concerning the treatment of the non-perturbative effects. Measurements in the charm sector have confirmed the hypothesis of fragmentation universality. The status of pentaquark searches at HERA is far from showing a consistent picture between the two experiments. It is hoped, that future results based on the full HERA data set will resolve those open issues.

Acknowledgements

I am grateful to the organiser for the opportunity to attend such a well organised conference. My thanks go to all the colleagues in the H1 and ZEUS collaborations whose efforts lead to these great measurements.

References

1. S. Chekanov *et al.* [ZEUS Collaboration], arXiv:0705.3770 [hep-ex].
2. A. Aktas *et al.* [H1 Collaboration], Eur. Phys. J. C **36** (2004) 413.

3. S. Chekanov *et al.* [ZEUS Collaboration], Eur. Phys. J. C **51** (2007) 1.

4. S. Chekanov *et al.* [ZEUS Collaboration], JHEP **0707** (2007) 074.

5. A. Aktas *et al.* [H1 Collaboration], Eur. Phys. J. C **38** (2005) 447.

6. A. Aktas *et al.* [H1 Collaboration], Contribution to DIS05, AIP Conf.Proc.792:859-862,2005.

7. U. Karshon [ZEUS Collaboration], *Contribution to Int. Conf. on Photon-structure (Photon 2001), Ascona, Switzerland, 2-7 Sep 2001.*

8. For pentaquark phenomenology see R. L. Jaffe, Phys. Rept. **409** (2005) 1.

9. For a review on the experimental search for pentaquark states, see K. H. Hicks, Prog. Part. Nucl. Phys. **55** (2005) 647; and M. Danilov and R. Mizuk, arXiv:0704.3531 [hep-ex].

10. I. Abt *et al.* [HERA-B Collaboration], Phys. Rev. Lett. **93** (2004) 212003.

11. A. Airapetian *et al.* [HERMES Collaboration], Phys. Rev. D **71** (2005) 032004.

12. S. Chekanov *et al.* [ZEUS Collaboration], Phys. Lett. B **591** (2004) 7.

13. A. Aktas *et al.* [H1 Collaboration], Phys. Lett. B **639** (2006) 202.

14. A. Aktas *et al.* [H1 Collaboration], arXiv:0704.3594 [hep-ex].

15. S. Chekanov *et al.* [ZEUS Collaboration], Phys. Lett. B **610** (2005) 212.

16. A. Aktas *et al.* [H1 Collaboration], Phys. Lett. B **588** (2004) 17.

17. S. Chekanov *et al.* [ZEUS Collaboration], Eur. Phys. J. C **38** (2004) 29.

Frascati Physics Series Vol. XLVI (2007), pp. 191–202
HADRON07: XII Int. Conf. on Hadron Spectroscopy – Frascati, October 8-13, 2007
Plenary Session

HEAVY FLAVOR DECAYS AND LIGHT HADRONS IN THE FOCUS EXPERIMENT: RECENT RESULTS

Sandra Malvezzi *
INFN Sezione di Milano Bicocca
P.za della Scienza 3, 20126 Milano Italy

Abstract

Interpretation of D-meson decay-dynamics has revealed itself to be strongly dependent on our understanding of the light-meson sector. The interplay becomes particularly evident in Dalitz plot analyses to study physics within and beyond the Standard Model. Experience and results from FOCUS are presented and discussed. A brief update of the pentaquark search in the experiment is also reported.

1 Introduction

Dalitz analyses are largely applied in modern high-energy experiments to study Heavy Flavor hadronic decays, but also to perform precise measurements of the

* on behalf of the FOCUS Collaboration (http://www-focus.fnal.gov/)

CKM matrix elements and search for new physics. Paradigmatic examples are $B \to \rho\pi$ and $B \to D^{(*)}K^{(*)}$ for the extraction of the α and γ angles of the Unitarity Triangle. The extraction of α in $B \to \rho\pi$ requires filtering the desired intermediate states among all the possible $(\pi\pi)\pi$ combinations, e.g. $\sigma\pi$, $f_0(980)\pi$ etc. The extraction of γ in $B \to D^{(*)}K^{(*)}$ requires, in turn, modeling the D amplitudes. The $\pi\pi$ and $K\pi$ S-wave are characterized by broad, overlapping states: unitarity is not explicitly guaranteed by a simple sum of Breit–Wigner functions. In addition, independently of the nature of the σ, it is not a simple Breit–Wigner. The $f_0(980)$ is a Flatté-like function, and its lineshape parametrization needs precise determination of KK and $\pi\pi$ couplings. Recent analyses of CP violation in the $B \to DK$ channel from the beauty factories *needed* two *ad hoc* resonances to reproduce the excess of events in the $\pi\pi$ spectrum, one at the low-mass threshold, the other at $1.1\,\mathrm{GeV}^2$ [1, 2]. This procedure of "effectively" fitting data invites a word of caution on estimating the systematics of these measurements. A question then naturally arises: in the era of precise measurements, do we know sufficiently well how to deal with strong-dynamics effects in the analyses? We have faced parametrization problems in FOCUS and learnt that many difficulties are already known and studied in different fields, such as nuclear and intermediate-energy physics, where broad, multi-channel, overlapping resonances are treated in the *K-matrix* formalism [3, 4, 5]. The effort we have made consisted mainly in building a bridge of knowledge and language to reach the high-energy community; our pioneering work in the charm sector might inspire future accurate studies in the beauty sector. FOCUS Dalitz plot analyses of the $D+, D_s \to \pi^+\pi^-\pi^+$ and of the $D^+ \to K^-\pi^+\pi^+$ will be discussed.

The collaboration has also taken a complementary non-parametric approach to measuring the $K^-\pi^+$ amplitude in the $D^+ \to K^-K^+\pi^+$ decay using a projective weighting technique. Results will be presented.

2 $D^+, D_s \to \pi^+\pi^-\pi^+$ and $D^+ \to K^-\pi^+\pi^+$ amplitude analyses

The FOCUS collaboration has implemented the *K-matrix* approach in the D_s and $D^+ \to \pi^+\pi^-\pi^+$ analyses. Results and details can be found in [6]. It was the first application of this formalism in the charm sector. In this model [5], the production process, i.e, the D decay, can be viewed as consisting of an initial preparation of states, described by the *P-vector*, which then propagates

according to $(I - iK\rho)^{-1}$ into the final one. The *K-matrix* here is the scattering matrix and is used as fixed input in our analysis. Its form was inferred by the global fit to a rich set of data performed in [7]. It is interesting to note that this formalism, beside restoring the proper dynamical features of the resonances, allows for the inclusion in D decays of the knowledge coming from scattering experiments, i.e, an enormous amount of results and science. No re-tuning of the *K-matrix* parameters was needed. The confidence levels of the final fits are 3.0 % and 7.7 % for the D_s and D^+ respectively. The results were extremely encouraging since the same *K-matrix* description gave a coherent picture of both two-body scattering measurements in light-quark experiments *as well as* charm-meson decay. This result was not obvious beforehand. Furthermore, the same model was able to reproduce features of the $D^+ \to \pi^+\pi^-\pi^+$ Dalitz plot, shown in fig.1, that would otherwise require an *ad hoc* σ resonance. The better treatment of the S-wave contribution provided by the *K-matrix* model was able reproduce the low-mass $\pi^+\pi^-$ structure of the D^+ Dalitz plot. This suggests that any σ-like object in the D decay should be consistent with the same σ-like object measured in $\pi^+\pi^-$ scattering.

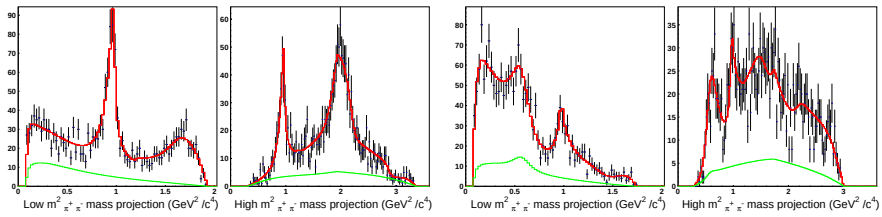

Figure 1: *FOCUS Dalitz-plot projections for D_s and D^+ to three pions with fit results superimposed. The background shape under the signal is also shown.*

Further considerations and conclusions from the FOCUS three-pion analysis were limited by the sample statistics, i.e. 1475 ± 50 and 1527 ± 51 events for D_s and D^+ respectively.

We considered imperative to test the formalism at higher statistics. This was accomplished by the $D^+ \to K^-\pi^+\pi^+$ analysis. The recent FOCUS study of the $D^+ \to K^-\pi^+\pi^+$ channel uses 53653 Dalitz-plot events with a signal fraction of $\sim 97\%$, and represents the highest statistics, most complete Dalitz plot analysis for this channel. Invariant mass and Dalitz plots are shown in

fig.2. Details of the analysis may be found in [8].

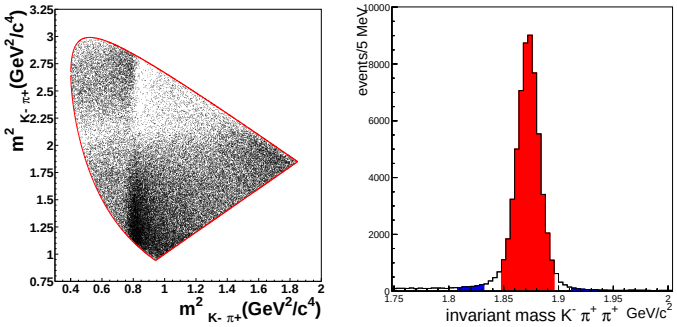

Figure 2: *The $D^+ \to K^-\pi^+\pi^+$ Dalitz plot (left) and mass distribution (right). Signal and sideband regions are indicated: sidebands are at $\pm$(6–8) σ from the peak.*

An additional complication in the $K\pi$ system comes from the presence in the S-wave of the two isospin states, $I = 1/2$ and $I = 3/2$. Although only the $I = 1/2$ is dominated by resonances, both isospin components are involved in the decay of the D^+ meson into $K^-\pi^+\pi^+$. A model for the decay amplitudes of the two isospin states can be constructed from the 2×2 *K-matrix* describing the $I = 1/2$ S-wave scattering in $(K\pi)_1$ and $(K\eta')_2$ (with the subscripts 1 and 2, respectively, labelling these two channels), and the single-channel *K-matrix* describing the $I = 3/2$ $K^-\pi^+ \to K^-\pi^+$ scattering. The *K-matrix* form we use as input describes the S-wave $K^-\pi^+ \to K^-\pi^+$ scattering from the LASS experiment [9] for energy above 825 MeV and $K^-\pi^- \to K^-\pi^-$ scattering from Estabrooks *et al.* [10]. The *K-matrix* form follows the extrapolation down to the $K\pi$ threshold for both $I = 1/2$ and $I = 3/2$ S-wave components by the dispersive analysis by Büttiker *et al.* [11], consistent with Chiral Perturbation Theory [12]. The total D-decay amplitude can be written as

$$\mathcal{M} = (F_{1/2})_1(s) + F_{3/2}(s) + \sum_j a_j \; e^{i\delta_j} \; B(abc|r), \qquad (1)$$

where $s = M^2(K\pi)$, $(F_{1/2})_1$ and $F_{3/2}$ represent the $I = 1/2$ and $I = 3/2$ decay amplitudes in the $K\pi$ channel, j runs over vector and spin-2 tensor resonances and $B(abc|r)$ are Breit–Wigner forms. The $J > 0$ resonances should, in prin-

ciple, be treated in the same *K-matrix* formalism. However, the contribution from the vector wave comes mainly from the $K^*(892)$ state, which is well separated from the higher mass $K^*(1410)$ and $K^*(1680)$, and the contribution from the spin-2 wave comes from $K_2^*(1430)$ alone. Their contributions are limited to small percentages, and, as a first approximation, they can be reasonably described by a simple sum of Breit–Wigners. More precise results would require a better treatment of the overlapping $K^*(1410)$ and $K^*(1680)$ resonances as well. In accordance with SU(3) expectations, the coupling of the $K\pi$ system to $K\eta$ is supposed to be suppressed. Indeed we find little evidence that it is required. Thus the $F_{1/2}$ form for the $K\pi$ channel is

$$(F_{1/2})_1 = (I - iK_{1/2}\rho)^{-1}_{1j}(P_{1/2})_j, \tag{2}$$

where I is the identity matrix, $K_{1/2}$ is the *K-matrix* for the $I = 1/2$ S-wave scattering in $K\pi$ and $K\eta'$, ρ is the corresponding phase-space matrix for the two channels [4] and $(P_{1/2})_j$ is the production vector in the channel j.

The form for $F_{3/2}$ is

$$F_{3/2} = (I - iK_{3/2}\rho)^{-1}P_{3/2}, \tag{3}$$

where $K_{3/2}$ is the single-channel scalar function describing the $I = 3/2$ $K^-\pi^+ \to K^-\pi^+$ scattering, and $P_{3/2}$ is the production function into $K\pi$.

The *P-vectors* are in general complex reflecting the fact that the initial coupling $D^+ \to (K^-\pi^+)\pi^+_{spectator}$ need not be real. Their functional forms are:

$$(P_{1/2})_1 = \frac{\beta g_1 e^{i\theta}}{s_1 - s} + (c_{10} + c_{11}\widehat{s} + c_{12}\widehat{s}^2)e^{i\gamma_1} \tag{4}$$

$$(P_{1/2})_2 = \frac{\beta g_2 e^{i\theta}}{s_1 - s} + (c_{20} + c_{21}\widehat{s} + c_{22}\widehat{s}^2)e^{i\gamma_2} \tag{5}$$

$$P_{3/2} = (c_{30} + c_{31}\widehat{s} + c_{32}\widehat{s}^2)e^{i\gamma_3}. \tag{6}$$

$\beta e^{i\theta}$ is the complex coupling to the pole in the 'initial' production process, g_1 and g_2, s_1 and s_2 are the *K-matrix* couplings and poles. The polynomials are expanded about $\widehat{s} = s - s_c$, with $s_c = 2$ GeV^2 corresponding to the center of the Dalitz plot. The polynomial terms in each channel are chosen to have a common phase γ_i to limit the number of free parameters in the fit and avoid

uncontrolled interference among the physical background terms. Coefficients and phases of the *P-vectors* are the only free parameters of the fit determining the scalar components. $K\pi$ scattering determines the parameters of the *K-matrix* elements and these are fixed inputs to this D-decay analysis. Free parameters for vectors and tensors are amplitudes and phases (a_i and δ_i). Table 1 reports our *K-matrix* fit results. It shows that quadratic terms in $(P_{1/2})_1$ are significant in fitting data, while in both $(P_{1/2})_2$ and $P_{3/2}$ constants are sufficient. The $J > 0$ states required by the fit are listed in table 2.

Table 1: *S-wave parameters from the* K-matrix *fit to the FOCUS* $D^+ \to K^-\pi^+\pi^+$ *data. The first error is statistic, the second error is systematic from the experiment, and the third is systematic induced by model input parameters for higher resonances. Coefficients are for the unnormalized S-wave.*

coefficient	phase (deg)
$\beta = 3.389 \pm 0.152 \pm 0.002 \pm 0.068$	$\theta = 286 \pm 4 \pm 0.3 \pm 3.0$
$c_{10} = 1.655 \pm 0.156 \pm 0.010 \pm 0.101$	$\gamma_1 = 304 \pm 6 \pm 0.4 \pm 5.8$
$c_{11} = 0.780 \pm 0.096 \pm 0.003 \pm 0.090$	
$c_{12} = -0.954 \pm 0.058 \pm 0.0015 \pm 0.025$	
$c_{20} = 17.182 \pm 1.036 \pm 0.023 \pm 0.362$	$\gamma_2 = 126 \pm 3 \pm 0.1 \pm 1.2$
$c_{30} = 0.734 \pm 0.080 \pm 0.005 \pm 0.030$	$\gamma_3 = 211 \pm 10 \pm 0.7 \pm 7.8$
Total S-wave fit fraction $= 83.23 \pm 1.50 \pm 0.04 \pm 0.07$ %	
Isospin 1/2 fraction $= 207.25 \pm 25.45 \pm 1.81 \pm 12.23$ %	
Isospin 3/2 fraction $= 40.50 \pm 9.63 \pm 0.55 \pm 3.15$ %	

The S-wave component accounts for the dominant portion of the decay $(83.23 \pm 1.50)\%$. A significant fraction, $13.61 \pm 0.98\%$, comes, as expected, from $K^*(892)$; smaller contributions come from two vectors $K^*(1410)$ and $K^*(1680)$ and from the tensor $K_2^*(1430)$. It is conventional to quote fit fractions for each component and this is what we do. Care should be taken in interpreting some of these since strong interference can occur. This is particularly apparent between contributions in the same-spin partial wave. While the total S-wave fraction is a sensitive measure of its contribution to the Dalitz plot, the separate fit fractions for $I = 1/2$ and $I = 3/2$ must be treated with care. The broad $I = 1/2$ S-wave component inevitably interferes strongly with the slowly varying $I = 3/2$ S-wave, as seen for instance in [13]. Fit results on the projections are shown in fig. 3.

Table 2: *Fit fractions, phases, and coefficients for the $J > 0$ components from the* K-matrix *fit to the FOCUS $D^+ \to K^-\pi^+\pi^+$ data. The first error is statistic, the second error is systematic from the experiment, and the third error is systematic induced by model input parameters for higher resonances.*

component	fit fraction (%)	phase δ_j (deg)	coefficient
$K^*(892)\pi^+$	13.61 ± 0.98	0 (fixed)	1 (fixed)
	$\pm\ 0.01 \pm 0.30$		
$K^*(1680)\pi^+$	1.90 ± 0.63	1 ± 7	0.373 ± 0.067
	$\pm\ 0.009 \pm 0.43$	$\pm\ 0.1 \pm 6$	$\pm\ 0.009 \pm 0.047$
$K_2^*(1430)\pi^+$	0.39 ± 0.09	296 ± 7	0.169 ± 0.017
	$\pm\ 0.004 \pm 0.05$	$\pm\ 0.3 \pm 1$	$\pm\ 0.010 \pm 0.012$
$K^*(1410)\pi^+$	0.48 ± 0.21	293 ± 17	0.188 ± 0.041
	$\pm\ 0.012 \pm 0.17$	$\pm\ 0.4 \pm 7$	$\pm\ 0.002 \pm 0.030$

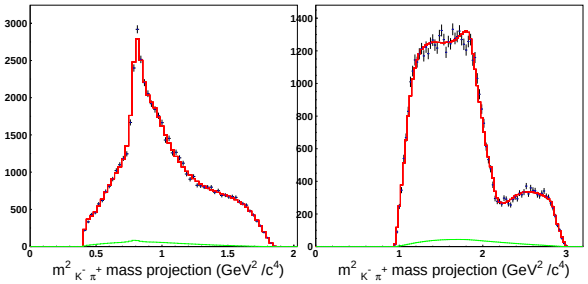

Figure 3: *The Dalitz plot projections with the* K-matrix *fit superimposed. The background shape under the signal is also shown.*

The fit χ^2/d.o.f is 1.27 corresponding to a confidence level of 1.2%. If the $I = 3/2$ component is removed from the fit, the χ^2/d.o.f worsens to 1.54, corresponding to a confidence level of 10^{-5}. These results can be compared with those obtained in the effective isobar model, consisting in a sum of Breit Wigners, which can serve as the standard for fit quality. Two *ad hoc* scalar resonances are required, of mass 856 ± 17 and 1461 ± 4 and width 464 ± 28 and 177 ± 8 MeV/c^2 respectively to reproduce the data and reach a χ^2/d.o.f is 1.17, corresponding to a C.L of 6.8%. A detailed discussion of the results and the systematics can be found in [8]. A feature of the *K-matrix* amplitude analysis is that it allows an indirect phase measurement of the separate isospin

components: it is this phase variation with isospin $I = 1/2$ that should be compared with the same $I = 1/2$ LASS phase, extrapolated from 825 GeV down to threshold according to Chiral Perturbation Theory. This is done in the right plot of fig. 4. In this model [5] the *P-vector* allows for a phase variation accounting for the interaction with the third particle in the process of resonance formation. It so happens that the Dalitz fit gives a nearly constant production phase. The two phases in fig. 4b) have the same behaviour up to $\sim$ 1.1 GeV. However, approaching $K\eta'$ threshold, effects of inelasticity and differing final state interactions start to appear. The difference between the phases in fig. 4a) is due to the $I = 3/2$ component.

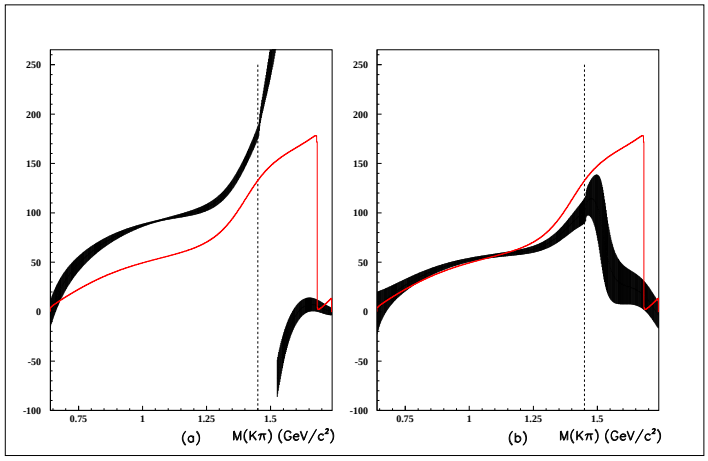

Figure 4: *Comparison between the LASS $I = 1/2$ phase + ChPT (continous line) and the* F-vector *phases (with $\pm 1\,\sigma$ statical error bars); a) total* F-vector *phase; b) $I = 1/2$* F-vector *phase. The vertical dashed line shows the location of the $K\eta'$.*

These results are consistent with $K\pi$ scattering data, and consequently with Watson's theorem predictions for two-body $K\pi$ interactions in the low $K\pi$ mass region, up to $\sim$ 1.1 GeV, where elastic processes dominate. This means that possible three-body interaction effects, not accounted for in the *K-matrix* parametrization, play a marginal role. The *K-matrix* form used in this analysis generates the *S-matrix* pole $E = M - i\Gamma/2 = 1.408 - i0.110$ GeV. Any more distant pole than $K_0^*(1430)$ is not reliably determined as this simple *K-matrix* expression does not have the required analyticity properties. However, our *K-*

matrix representation fits along the real energy axis inputs on scattering data and Chiral Perturbation Theory in close agreement with those used in [14], which locates the κ with a mass of (658 ± 13) MeV and a width of (557 ± 24) MeV by careful continuation. These pole parameters are quite different from those implied by the simple isobar fits. We have thus shown that whatever κ is revealed by our $D^+ \to K^-\pi^+\pi^+$ results, it is the same as that found in scattering data.

3 A non-parametric approach to determine the $K^-\pi^+$ amplitude in $D^+ \to K^-K^+\pi^+$ decay

While making the effort of refining the amplitude formalism, FOCUS identified the $D^+ \to K^-K^+\pi^+$ as an ideal case to apply the projective weighting technique developed in the semi-leptonic sector [15] to the hadronic decays. Details can be found in [16]. The old E687 Dalitz plot analysis [17] concluded that the observed $D^+ \to K^-K^+\pi^+$ Dalitz plot could be adequately described by just three resonant contributions: $\phi\pi^+, K^+\bar{K}^*(892)$ and $K^+\bar{K^*}_0(1430)$. Although $\phi\pi^+$ is an important contribution, the ϕ is a very narrow resonance that can be substantially removed through a cut on $m_{K^+K^-}$, i.e $m_{K^+K^-} > 1050$ MeV/c^2. Since there is no overlap of the ϕ band with the $\bar{K}^*$ and most of the kinematically allowed $\bar{K^*}_0(1430)$ region, there is a relatively small loss of information from the anti-ϕ cut; of course careful systematic evaluation for residual K^+K^- contributions and bias are performed. In the absence of the K^-K^+ resonances, we can write the decay amplitude in terms of $m_{K^-\pi^+} = m$ and the helicity decay angle θ Thus

$$A = \sum_{l}^{s,p.d...} A_l(m) d^l_{00}(\cos\theta), \tag{7}$$

where $d^l_{00}(cos\theta)$ are the Wigner d-matrices describing the amplitude for a $K^-\pi^+$ system of angular momentum l to simultaneously have 0 angular momentum along its helicity axis and the $K^-\pi^+$ decay axis. This technique is an intrinsically one-dimensional analysis. The decay intensity assuming, for simplicity, that only S and P-waves are present, is

$$|A|^2 = |S(m)+P(m)\cos\theta|^2 = |S(m)|^2+2\mathrm{Re}\{S^*(m)P(m)\}\cos\theta+|P(m)|^2\cos^2\theta, \tag{8}$$

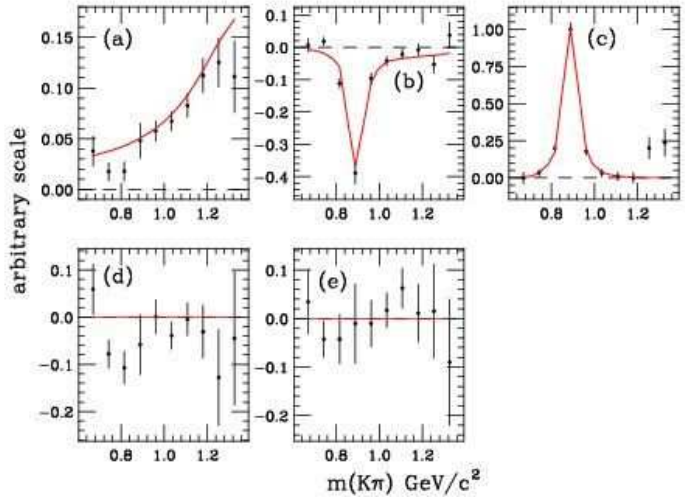

Figure 5: *This figure compares the five projected amplitudes obtained according to their angular dependence (error bars) with the E687 model properly corrected, as explained in the text, to match the data (red curves). The plots are: a) S^2 direct term, b) 2 S×P interference term, c) P^2 direct term, d)2 P×D interference term and e) D^2 direct term.*

The approach is to divide $\cos\theta$ into twenty evenly spaced angular bins. Let

$$\overrightarrow{D} = ({}^{i}n_1, {}^{i}n_2 ... {}^{i}n_{20}) \tag{9}$$

be a vector whose 20 components give the population in data for each of the 20 $\cos\theta$ bins. Here ^{i} specifies the $i^{th} m_{K^-\pi^+}$ bin. Our goal is to represent the $\overrightarrow{D}$ vector in eq. 9 as a sum over the expected populations for each of the three partial waves. For this simplified case there are three such vectors computed for each $m_{K^-\pi^+}$ bin, $\{{}^{i}\overrightarrow{m}_{\alpha}\} = ({}^{i}\overrightarrow{m}_{SS}, {}^{i}\overrightarrow{m}_{SP}, {}^{i}\overrightarrow{m}_{PP})$. Each ${}^{i}\overrightarrow{m}_{\alpha}$ is generated using a phase-space and full detector simulation for $D^+ \to K^-K^+\pi^+$ decay with one amplitude turned on, and all the others turned off. We then use a weighting technique to fit the bin populations in the data to the form ${}^{i}\overrightarrow{D} = F_{SS}(m_i){}^{i}\overrightarrow{m}_{SS} + F_{SP}(m_i){}^{i}\overrightarrow{m}_{SP} + F_{PP}(m_i){}^{i}\overrightarrow{m}_{PP}$. When including the D-wave as well, the results appear just as five weighted histograms in the $m_{K^-\pi^+}$ mass, as in fig. 5, for the five independent amplitude contributions.

The curves in fig. 5 are the model used in E687 but with a $\bar{K}^*{}_0(1430)$

ad hoc arranged to fit the data, i.e represented as a Breit Wigner with a pole at m_0=1412 MeV/c^2 and a width of Γ = 500 MeV/c^2, not consistent with the standard PDG $\bar{K^*}_0(1430)$ parametrization used by E687. This analysis reveals once more, how subtle the inclusion of the broad S-wave resonances in charm Dalitz analysis can be. Although the $D^+ \to K^-K^+\pi^+$ is an ideal case, it might be possible to extend the analysis to the $D_s \to K^-K^+\pi^+$ decay, as well as $D^0 \to K^+K^-\bar{K}^0$ and hadronic four body decays such as $D^0 \to K^-K^+\pi^+\pi^- \to \phi\pi^+\pi^-$.

4 Search for pentaquark candidates

The FOCUS collaboration searched for the charmed $\Theta_c^0(\bar{c}uudd)$ pentaquark candidate in the decay modes $\Theta_c^0 \to D^{*-}p$ and $\Theta_c^0 \to D^-p$ [18]. No evidence for a pentaquark at 3.1 GeV/c^2 or at any mass less than 4 GeV/c^2 was observed. More recently the search was extended to two other candidates: $\Theta^+(\bar{s}uudd) \to pK_s^0$ [19] and $\phi^{--}(1860)(ssddu) \to \Xi^-\pi^-$ [20]. Having found no evidence, limits were calculated. The Θ^+ production cross section was normalized to $\Sigma^*(1385)^\pm$ and $K^*(892)^+$ because the reconstructed decay modes of the particles $\Sigma^*(1385)^\pm \to \Lambda^0\pi^\pm$ and $K^*(892)^+ \to K_S^0\pi^+$ are very similar, in terms of topology and energy release, to the signal. The 95 % C.L upper limits of $\frac{\sigma(\Theta^+)\cdot BR(\Theta^+\to pK_S^0)}{\sigma(K^*(892)^+)} < 0.00012$ (0.00029) and $\frac{\sigma(\Theta^+)\cdot BR(\Theta^+\to pK_S^0)}{\sigma(\Sigma^*(1385)^\pm)} <$ 0.0042 (0.0099) were estimated for a natural width of 0 and 15 MeV/c^2 in the good acceptance region of the detector , i.e. for parent particles with momenta above 25 GeV/c. Analogously the upper limit was calculated for the $\Xi_5^{--}(\phi^{--}(1860))$ candidate with respect to the $\Xi^*(1530)^0 \to \Xi^-\pi^+$ obtaining $\frac{\sigma(\Xi_5^{--})\cdot BR(\Xi_5^{--}\to\Xi^-\pi^-)}{\sigma(\Xi^*(1530)^0} < 0.007$ (0.019) for a natural width of 0 (15) MeV/c^2.

5 Conclusions

Dalitz-plot analysis represents a unique, powerful and promising tool for physics studies within and beyond the Standard Model; however to perform such sophisticate analyses, we need to model the strong interaction effects. FOCUS has performed pilot studies in the charm sector through the *K-matrix* formalism and has started an effort to identify channels where non-parametric approaches can be undertaken. What has been learnt from charm will be beneficial for future accurate beauty measurements.

References

1. B. Aubert *et al.*, Phys. Rev. Lett. **95**, 121802 (2005).
2. A. Poluektov *et al.*, Phys. Rev. **D73**, 112009 (2006) .
3. E. P. Wigner, Phys. Rev. **70**, 15 (1946).
4. S. U. Chung *et al.*, Annalen Phys. **4**, 404 (1995).
5. I. J. R. Aitchison, Nucl. Phys. **A189**, 417 (1972) .
6. J. M. Link *et al.*, Phys. Lett. **B585**, 200 (2004).
7. V. V. Anisovich and A. V. Sarantsev, Eur. Phys. J. A **16**, 229 (2003).
8. J. M. Link *et al.*, Phys. Lett. **B653**, 1 (2007).
9. D. Aston *et al.*, Nucl. Phys. **B296**, 493 (1988).
10. P. Estabrooks *et al.*, Nucl. Phys. **B133**, 490 (1978).
11. P. Büttiker, S. Descotes-Genon and B. Moussallam, Nucl. Phys. Proc. Suppl. **133** (2004) 223; Eur. Phys. J. **C33**, 409 (2004).
12. V. Bernard, N. Kaiser and U. G. Meißner, Phys. Rev. **D43**, 2757 (1991); Nucl. Phys. **B357**, 129 (1991).
13. L. Edera, M. R. Pennington, Phys. Lett. **B623**, 55 (2005).
    Phys. Rev. **D73**, 032004 (2006).
14. S. Descotes-Genon and B. Moussallam, Eur. Phys. J. **C48**, 553 (2006).
15. J. M. Link *et al.*, Phys. Lett. **B633**, 183 (2006).
16. J. M. Link *et al.*, Phys. Lett. **B648**, 156 (2007).
17. P. L. Frabetti*et al.*, Phys. Lett. **B351**, 591 (2007).
18. J. M. Link *et al.*, Phys. Lett. **B622**, 229 (2005).
19. J. M. Link *et al.*, Phys. Lett. **B639**, 604 (2007).
20. J. M. Link *et al.* e-Print: arXiv:0708.1010 [hep-ex]
    Submitted to Phys.Rev.D

Frascati Physics Series Vol. XLVI (2007), pp. 203
HADRON07: XII Int. Conf. on Hadron Spectroscopy – Frascati, October 8-13, 2007
Plenary Session

REVIEW ON Bs PARAMETERS AND RARE HEAVY FLAVOUR DECAYS AT THE TEVATRON

P. Kasper
FERMILAB

Written contribution not received

Frascati Physics Series Vol. XLVI (2007), pp. 205–216
HADRON07: XII Int. Conf. on Hadron Spectroscopy – Frascati, October 8-13, 2007
Plenary Session

D AND B MESON SPECTROSCOPY, NEW STATES, BARYONS AT THE TEVATRON

Michal Kreps on behalf of the CDF and DØ Collaborations
Universität Karlsruhe (TH), Postfach 6980, 76128 Karlsruhe, Germany

Abstract

We review recent results in heavy quark hadron spectroscopy at the Tevatron. With increasing data samples, the Tevatron experiments start to uncover information on the spectroscopy of b-hadrons. Most important are the first observations of the narrow B_s^{**0} as well as $\Sigma_b^{\pm}$, $\Sigma_b^{*\pm}$ and Ξ_b^- baryons. In addition we present updated results on the narrow B^{**0} and B_c mesons.

1 Introduction

Heavy mesons consisting of a light quark and a heavy anti-quark form an interesting laboratory for studying QCD, the theory of strong interaction. They are a close analogue to the hydrogen atom and play a similar role for the study of QCD as hydrogen does for QED. The heavy anti-quark ($\overline{b}$ or $\overline{c}$) takes the role of the source of a static color potential, in which the light quark (u, d or

s) is located. Similarly, the heavy quark baryons with a single heavy quark can in first order be viewed in the same picture, only having a light diquark in the static color field of the heavy quark. If the diquark picture isn't correct, then one would arrive at an object similar to the helium atom with a heavy quark generating the potential in which two light quarks are located. Special case is the B_c meson, which is the only one composed by two distinct heavy quarks. The interplay of the two heavy quarks, which decay through the weak interaction, is important for our understanding of decays of the heavy quark hadrons.

Heavy quark hadrons can be used to test QCD in regions where perturbation calculations cannot be used and many different approximations to solve the QCD have been developed. Just a few examples of them are heavy quark effective theory, non-relativistic and relativistic potential models or lattice QCD. While a large amount of information for c-hadrons exist [1)], the spectroscopy of b-hadrons was almost unknown up to recently. In this paper we review recent measurements in the sector of heavy quark hadrons by the CDF and DØ experiments at the Tevatron collider. It is currently the only place where information about excited b-mesons and b-baryons can be obtained. Charge-conjugate modes are implied throughout this paper unless otherwise stated.

2 Mass measurement of the B_c meson

Up to recently the B_c meson was observed only in its semileptonic decay modes [2, 3)]. While semileptonic decay modes have in general large branching fractions, the precision of the mass measurement is rather limited due to the undetected neutrino. With increasing amount of data at the Tevatron, search in the fully reconstructed decay modes becomes feasible. The decay mode in which the B_c search is done is $B_c \to J/\psi\pi^+$. The CDF collaboration obtained evidence for $B_c \to J/\psi\pi^+$ decay [4)] using 360 pb^{-1} of data.

This measurement [5)] of the $B_c \to J/\psi\pi^+$ decay is based on the data selection developed on the high statistics $B^+ \to J/\psi K^+$ decay. Its main feature is the huge background suppression at a high signal efficiency. After the final selection we observe around 19700 $B^+ \to J/\psi K^+$ signal events on 2.2 fb^{-1} of data. Application of the same selection on $J/\psi\pi^+$ sample yields to the invariant mass distribution shown in Fig. 1. A clear signal at a mass around 6270 MeV/c^2 is visible. To extract the mass and the number of B_c signal

candidates an unbinned maximum likelihood fit is used. The signal is described by a Gaussian and the background by a empirical function. The fit returns 87 ± 13 signal events with a B_c mass of $6274.1 \pm 3.2(\text{stat}) \pm 2.6(\text{sys})$ MeV/c^2. The statistical significance exceeds 8σ. The measurement is compatible with existing predictions (see Ref. [5]), with an experimental uncertainty smaller than theory uncertainties.

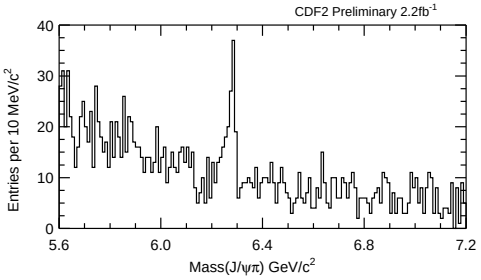

Figure 1: *Invariant mass distribution of the $B_c \to J/\psi\pi^+$ candidates observed by the CDF experiment.*

3 Orbitally excited heavy quark mesons

The bound states of a heavy b anti-quark with a light u or d quark are generically referred to as B mesons. The states with a light s quark are analogous and are referred to as a B_s. The ground states with $J^P = 0^0$ and $J^P = 1^-$ are well established [1], but spectroscopy of the excited states has not been well studied. The first excited state of the B (B_s) meson is predicted to occur when a light quark has an orbital angular momentum of $L = 1$. Those states are collectively known as B^{**0} (B_s^{**0}). Combining the spin of the light quark with its orbital momentum yields two isodoublets with a total spin of light quark $J_l = 1/2$ and $J_l = 3/2$. The doublet $J_l = 1/2$ contains two states, B_0^{*0} with total spin $J = 0$ and B_1^0 with $J = 1$. The members of the doublet with $J_l = 3/2$ are B_1^0 with $J = 1$ and B_2^{*0} with $J = 2$. The $J_l = 1/2$ states decay to $B^{(*)}\pi$ via an S-wave transition. Consequently, these states are expected to be very broad and difficult to observe at the Tevatron. The $J_l = 3/2$ states decay to $B^{(*)+}\pi^-$ via a D-wave transition and are expected to be narrow. The decay

$B_1^0 \to B^+\pi^-$ is forbidden by angular momentum and parity conservation, while both $B_2^{*0} \to B^+\pi^-$ and $B_2^{*0} \to B^{*+}\pi^-$ decays are allowed. The B_s^{**0} system has the same structure, except of the π^- changed to a K^- in the decay. The decay of B_s^{**0} to $B_s\pi^0$ is forbidden by isospin conservation.

Both Tevatron experiments perform studies of the narrow B^{**0} [6] and B_s^{**0} [7] states in the $B^+\pi^-$ and B^+K^- final states. The decays to B^* are included implicitly as B^* decays to $B^+\gamma$ with γ undetected in both experiments. The missing γ will shift the reconstructed mass by the mass difference between B^* and B^+. The B^+ is reconstructed in the $J/\psi K^+$ final state by both experiments. In addition, the $\overline{D}^0\pi^+$ mode is used by CDF in the B_s^{**0} search and the $\overline{D}^0 3\pi$ mode is added to the previous two for B^{**0} studies. The invariant mass difference of $B^+\pi^-$ and B^+K^- combinations obtained by CDF are shown in Fig. 2 and by DØ in Fig. 3. For the first time experiments are able to observe the two B^{**0} states as two separate peaks. The measured masses are listed in Table 1. In addition to the masses, the CDF experiment measures for the first time also the width of the B_2^{*0} state to be $\Gamma(B_2^{*0}) = 22.1^{+3.6}_{-3.1}(\text{stat})^{+3.5}_{-2.6}(\text{sys})$ MeV. Both experiments observe for the first time the B_{s2}^{*0} state with a statistical significance larger than 5σ. The CDF experiment observes in addition the B_{s1}^0 state, which wasn't seen before, with a statistical significance of more than 5σ.

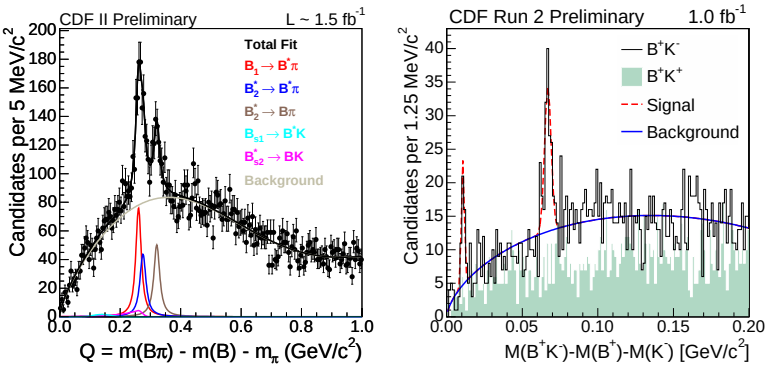

Figure 2: *Invariant mass difference distribution for $B^+\pi^-$ (left) and B^+K^- (right) combinations observed by the CDF experiment.*

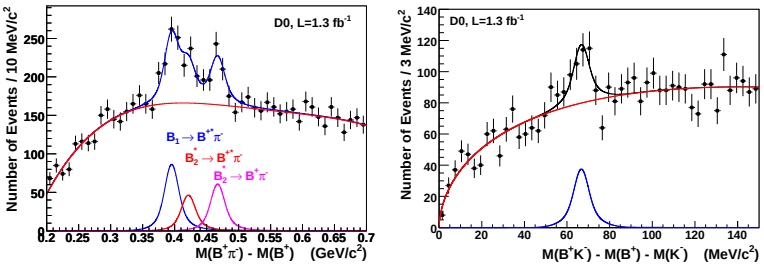

Figure 3: *Invariant mass difference distribution for $B^+\pi^-$ (left) and B^+K^- (right) combinations observed by the DØ experiment.*

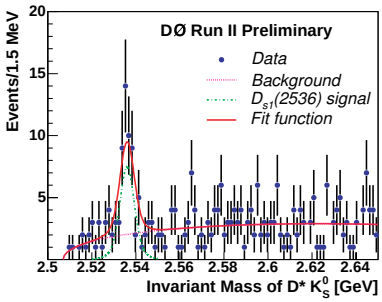

Figure 4: *Invariant mass difference distribution for $D^{*+}K_s^0$ combinations observed by the DØ experiment.*

The DØ experiment performs also a mass measurement of the $D_{s1}^-(2536)$ state [8]. The measurement is done in the context of extraction of the branching fraction of the decay $B_s \to D_{s1}^-(2536)\mu^+\nu X$. In Fig. 4 the invariant mass distribution of the $D^{*+}K_s^0$ combinations coming from semileptonic B_s decays is shown. A very clean signal is obtained, which allows for a precise mass measurement. For completeness, the branching fraction of the decay $B_s \to D_{s1}^-(2536)\mu^+\nu X$ is measured to be $\mathcal{B}(B_s \to D_{s1}^-(2536)\mu^+\nu X) = (0.86 \pm 0.16(\text{stat}) \pm 0.13(\text{sys}) \pm 0.09(\text{ext}))\%$.

Table 1: *Masses of the orbitally excited heavy quark mesons. All values are in* MeV/c^2 *with first uncertainty being statistical and second systematical.*

state	CDF	DØ
B_1^0	$5725.3^{+1.6\ +0.8}_{-2.1\ -1.1}$	$5720.6 \pm 2.4 \pm 1.4$
B_2^{*0}	$5739.9^{+1.7\ +0.5}_{-1.8\ -0.6}$	$5746.8 \pm 2.4 \pm 1.7$
B_{s1}^0	$5829.4 \pm 0.2 \pm 0.6$	-
B_{s2}^{*0}	$5839.0 \pm 0.4 \pm 0.5$	$5839.6 \pm 1.1 \pm 0.7$
$D_{s1}^-(2536)$	-	$2535.7 \pm 0.6 \pm 0.5$

4 Observation of $\Sigma_b^\pm$ and $\Sigma_b^{*\pm}$ baryons

With increasing data samples collected at the Tevatron accelerator, searches for yet unobserved b-baryons begin to be feasible. The first of such searches was performed by the CDF experiment, which searched for the $\Sigma_b^\pm$ baryon and its spin excited partner $\Sigma_b^{*\pm}$ [9]. A general theoretical expectations are the mass difference $M(\Sigma_b) - M(\Lambda_b^0) - M(\pi) = 40-70\,\mathrm{MeV}/c^2$ with $M(\Sigma_b^*) - M(\Sigma_b) = 10-40\,\mathrm{MeV}/c^2$. A small difference on the level of 5 MeV/c^2 is expected between the masses of Σ_b^+ and Σ_b^-. Both the Σ_b and the Σ_b^* are expected to be narrow with a natural width of around 8 and 15 MeV/c^2 with $\Lambda_b^0\pi$ being the dominant decay mode.

The CDF search is based on 1 fb^{-1} of data using fully reconstructed Λ_b^0 baryons. The Λ_b^0 is reconstructed in the $\Lambda_c^+\pi^-$ decay mode with $\Lambda_c^+ \rightarrow pK^-\pi^+$. In total around 3200 Λ_b signal events are reconstructed. In the sample used for the $\Sigma_b^\pm$ search 90 % of events are Λ_b^0 baryons. The search is performed for the charged $\Sigma_b^\pm$'s only, as the neutral one decays by emission of π^0, which is extremely difficult to detect at the CDF experiment.

The selected Λ_b^0 candidates are then combined with charged pions to form $\Sigma_b^\pm$ candidates. After choosing the selection of candidates, the background is estimated while keeping the signal region blinded. The background consists of three basic components, which are combinatorial background, Λ_b^0 hadronization and hadronization of mis-reconstructed B mesons. Relative fractions of these components are taken from the fit of the Λ_b^0 invariant mass distribution. The shape of the combinatorial background is determined using the upper

sideband of the Λ_b^0 invariant mass distribution. For the hadronization of misreconstructed B mesons, the fully reconstructed $B^0 \to D^-\pi^+$ in the data are used. The shape of the largest component, Λ_b^0 hadronization, is determined using a PYTHIA Monte Carlo sample. The observed invariant mass difference distribution is shown in Fig. 5.

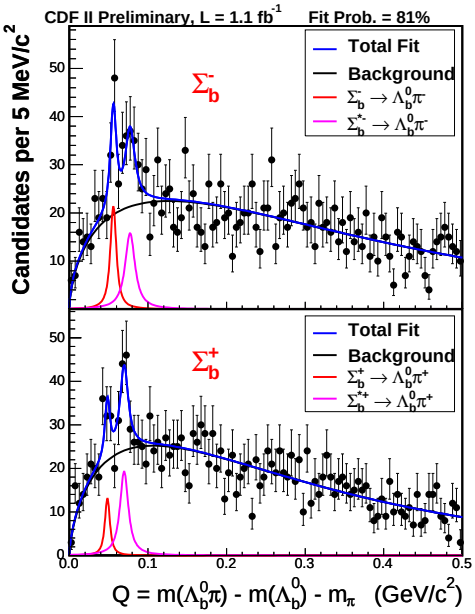

Figure 5: *Projection of the fit result of the $\Sigma_b^{\pm}$ invariant mass difference distribution. The points with error bars represent the data. The blue line corresponds to the result of the fit, the background is shown by the black line while the signals are represented by the red and magenta curves.*

To extract the signal yields and positions of the peaks, an unbinned maximum likelihood fit is performed. The data are described by a previously determined background shape together with Breit-Wigner functions convoluted with a resolution function for each peak. Due to the low statistics, difference $M(\Sigma_b^{*+}) - M(\Sigma_b^+)$ is constrained to be the same as $M(\Sigma_b^{*-}) - M(\Sigma_b^-)$. The values obtained in the fit are summarized in Table 2 and the fit projection is

Table 2: *Result of the fit to the Σ_b invariant mass difference distribution.*

Parameter	Value
$Q(\Sigma_b^+)$ (MeV/c^2)	$48.5^{+2.0\ +0.2}_{-2.2\ -0.3}$
$Q(\Sigma_b^-)$ (MeV/c^2)	$55.9 \pm 1.0 \pm 0.2$
$M(\Sigma_b^*) - M(\Sigma_b)$ (MeV/c^2)	$21.2^{+2.0\ +0.4}_{-1.9\ -0.3}$
Σ_b^+ events	$32^{+13\ +5}_{-12\ -3}$
Σ_b^- events	$59^{+15\ +9}_{-14\ -4}$
Σ_b^{*+} events	$77^{+17\ +10}_{-16\ -6}$
Σ_b^{*-} events	$69^{+18\ +16}_{-17\ -5}$

shown in Fig. 5.

To estimate the significance of the observed signal, the fit is repeated with an alternative hypothesis and the difference in the likelihoods is used. Three different alternative hypotheses were examined, namely the null hypothesis, using only two peaks instead of four and leaving each single peak separately out of the fit. As a result we conclude that the null hypothesis can be excluded by more than five standard deviations. The fit favors four peaks against two and except of the Σ_b^+ peak, each peak has a significance above three standard deviations.

5 Observation of the Ξ_b^- baryon

The latest state observed by the Tevatron experiments is the Ξ_b^- baryon [10], a state with quark content *dsb*. The mass of the Ξ_b^- is expected to be around 5.8 GeV/c^2. The decay is dominated by the weak decay of the b quark. The LEP experiments observed excess in $\Xi^- l^- \nu_l X$ events, which was attributed to the Ξ_b baryon and the lifetime $\tau = 1.39^{+0.34}_{-0.28}$ ps was deduced [1]. Suitable decay modes for the search at the Tevatron are $\Xi_b^- \to J/\psi \Xi^-$, which can be used by both CDF and DØ and the $\Xi_b \to \Xi_c \pi$, $\Xi_b \to D\Lambda$, $\Xi_b \to \Lambda_c K \pi$ decay modes accessible at the CDF experiment. The presented search uses the decay mode $\Xi_b^- \to J/\psi \Xi^-$ which has the advantage of a J/ψ in the final state leading to clean trigger signature. A disadvantage of the used decay mode is that only

the Ξ_b^- is accessible as the Ξ_b^0 contains π^0 in the decay chain.

A complication in the study of the Ξ_b^- state comes from having a Ξ in the final state, which decays through the weak interaction to Λ and π with a subsequent decay of $\Lambda \to p\pi$. As both Ξ and Λ have long lifetime, their decay vertices are significantly displaced from the production point. This requires a special treatment of the track reconstruction comparing to the usual tracks used in b-hadron studies. In addition the Ξ^- is charged and travels several centimeters in the magnetic field which adds to the complexity of the analysis as the bending of the Ξ^- is significant. On the other hand there is a possibility to gain in precision of the secondary vertex resolution by tracking Ξ^- in the silicon detector close to the interaction region. The CDF experiment chosed this approach, leading to improvements in the precision of the Ξ^- impact parameter measurement as well as in determination of the Ξ_b^- secondary vertex position.

Both experiments use the momenta of the Ξ_b^- candidate and its daughters, vertex quality along with the Ξ_b^- decay vertex displacement to select final candidates. The DØ experiment develops the selection based on the signal from simulated events and background from wrong-sign data. The invariant mass distribution of selected candidates is shown in Fig. 6. The CDF collaboration uses a data only approach. As the Ξ^- is tracked in the silicon detector, one can treat it as an ordinary track. In such an approach, the decay $\Xi_b^- \to J/\psi\Xi^-$ is similar to the decay $B^+ \to J/\psi K^+$. This allows to reuse the selection developed on $B^+ \to J/\psi K^+$ decays for the B_c search. The observed invariant mass distribution is shown in Fig. 7. In both experiments a clear signal with a mass slightly below 5.8 GeV/c^2 is visible.

To extract the mass and number of signal events, both experiments perform an unbinned maximum likelihood fit. They obtain the number of signal events $N_s = 14.8 \pm 4.3(\text{stat})^{+1.9}_{-0.4}(\text{sys})$ (DØ) and $N_s = 17.5 \pm 4.3(\text{stat})$ (CDF). The statistical significance of the signal is 5.2σ and 7.7σ for the DØ and CDF experiment respectively. The measured masses are $5774 \pm 11(\text{stat}) \pm 15(\text{sys})$ MeV/c^2 (DØ) and $5792.9 \pm 2.5(\text{stat}) \pm 1.7(\text{sys})$ MeV/c^2 (CDF) are in good agreement between the two experiments.

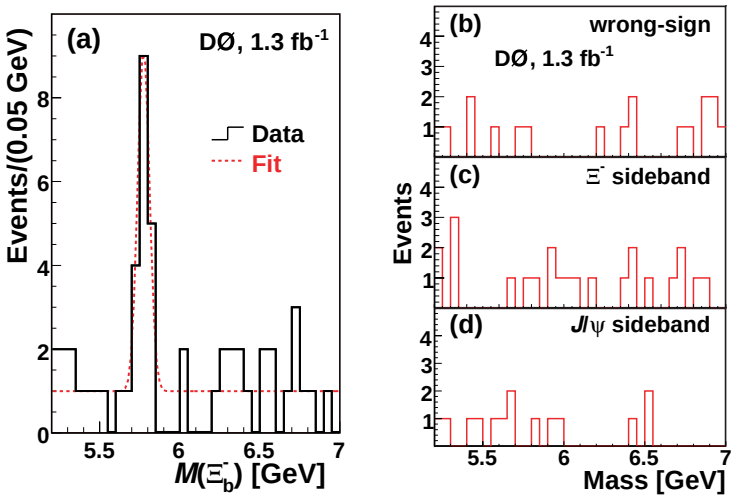

Figure 6: *Invariant mass distribution of the Ξ_b^- candidates observed by the DØ experiment (left) and invariant mass of the various background samples (right).*

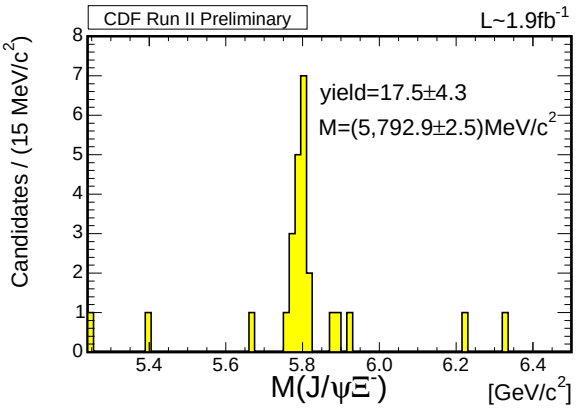

Figure 7: *Invariant mass distribution of the Ξ_b^- candidates observed by the CDF experiment.*

Several cross checks were done by both experiments to strengthen the interpretation of the observed signal as a Ξ_b^- state. The DØ experiment made a detailed examination of the wrong-sign combinations together with the Ξ^- and J/ψ sideband events with no signal observed in any of these (see Fig. 6). In addition the proper decay length distribution from data was compared to the one expected for a typical weakly decaying b-hadron and good consistency was observed. The CDF experiment used its unique opportunity to trigger on events with displaced vertices and searched also for the $\Xi_b^- \to \Xi_c^0\pi^-$ decay mode. Also here evidence for the signal is seen with the mass at same position as in $\Xi_b^- \to J/\psi\Xi^-$. Thus one can conclude that the observed signal is due to the $\Xi_b \to J/\psi\Xi$ decay.

6 Conclusions

Heavy quark states provide an interesting laboratory for testing various approaches to the non-perturbative regime of QCD. The Tevatron experiments have made large effort to improve our knowledge of the b-hadrons. Roughly one and half year ago only few b-mesons were known. The B_c meson was seen only in a semileptonic decay mode with a large uncertainty on the mass measurement. Orbitally excited mesons were not observed (B_s^{**0}) or could not be seen as distinct peaks (B^{**0}). In the b-baryon sector, only Λ_b^0 was directly observed with little information on Ξ_b obtained by the LEP experiments from the excess in $\Xi^- l^- \nu_l X$ events.

Since then the effort of the CDF and DØ collaborations provided new important data. It started with the observation of fully reconstructed $B_c \to J/\psi\pi^+$ decay at CDF, which allowed for a precise mass measurement. Both experiments contributed to studies of the orbitally excited B and B_s mesons. From those studies both $J_l = 3/2$ states of the B_s^{**0} have been observed for the first time. Also the $J_l = 3/2$ states of the B^{**0} have been for the first time seen as two separate peaks. On the side of b-baryons, $\Sigma_b^{\pm}$ and $\Sigma_b^{*\pm}$ as well as Ξ_b^- were observed starting a new era in the study of b-baryons.

To conclude, due to the effort of the Tevatron experiments our knowledge of the b-hadrons was increased considerably, but lot of room to improve our knowledge on the properties of already observed hadrons still exists. On the side of unobserved hadrons, the next focus should be on the η_b search, the last unobserved meson containing a b quark. Also an observation of the Ξ_b^0, which

should be possible at CDF, would strengthen the interpretation of the signal attributed to Ξ_b^-. Last, an observation of the Ω_b would be a nice completion of the Tevatron program on spectroscopy of b-hadrons. With more data coming and the well understood detector we believe that at least some of those searches will be successful.

Acknowledgments

The author would like to thank all his colleagues from the CDF and DØ experiments for performing the studies presented here as well as for their help in the preparation of the talk and this paper.

References

1. W. M. Yao *et al.* [Particle Data Group], J. Phys. G **33**, 1 (2006).
2. F. Abe *et al.* [CDF Collaboration], Phys. Rev. D **58**, 112004 (1998).
3. A. Abulencia *et al.* [CDF Collaboration], Phys. Rev. Lett. **97**, 012002 (2006).
4. A. Abulencia *et al.* [CDF Collaboration], Phys. Rev. Lett. **96**, 082002 (2006).
5. T. Aaltonen *et al.* [CDF Collaboration], CDF Public Note 8004 (2007).
6. V. M. Abazov *et al.* [DØ Collaboration], Phys. Rev. Lett. **99**, 172001 (2007); T. Aaltonen *et al.* [CDF Collaboration], CDF Public Note 8945 (2007).
7. T. Aaltonen *et al.* [CDF Collaboration], arXiv:0710.4199 [hep-ex] (2007); V. M. Abazov *et al.* [D0 Collaboration], arXiv:0711.0319 [hep-ex] (2007).
8. V. M. Abazov *et al.* [DØ Collaboration], DØ Conference Note 5034-CONF (2006).
9. T. Aaltonen *et al.* [CDF Collaboration], accepted by Phys. Rev. Lett., arXiv:0706.3868 (2007).
10. V. M. Abazov *et al.* [D0 Collaboration], Phys. Rev. Lett. **99**, 052001 (2007); T. Aaltonen *et al.* [CDF Collaboration], Phys. Rev. Lett. **99**, 052002 (2007).

Frascati Physics Series Vol. XLVI (2007), pp. 217–228
HADRON07: XII Int. Conf. on Hadron Spectroscopy – Frascati, October 8-13, 2007
Plenary Session

HADRONIC PHYSICS AT BABAR

Enrico Robutti
I.N.F.N. - Sezione di Genova
representing the *BABAR* Collaboration

Abstract

A selection of recent results from the *BABAR* experiment is presented, based on the data sample collected between 1999 and 2007. Results are relevant to the study of hadronic physics, providing tests for various models and the measurement of several parameters involved therein; a variety of different experimental techniques is exploited. In particular, the selection includes the analysis of exclusive hadronic B decays, the study of hadron production processes in e^+e^- annihilations and the measurement of charmed baryon properties.

1 Introduction

The *BABAR* experiment [1], located at the PEP-II asymmetric e^+e^- collider at SLAC, has been taking data at a c.m. energy corresponding to the $\Upsilon(4S)$ mass since 1999. *BABAR* has been conceived for the study of CP violation in

the B meson system, and more in general for the precise determination of the parameters of the Cabibbo-Kobayashi-Maskawa (CKM) mixing matrix, therefore focusing on the electroweak sector of the Standard Model (SM); however, the large variety of processes recorded by the detector and the huge size of the present data sample allow to extend the studies to an extremely rich set of measurements of great relevance for hadronic physics. Among these: meson, baryon and exotics spectroscopy; form factors; study of hadronic matrix elements in hadron production and decay; accurate determination of hadronic contributions in the extraction of CKM matrix elements and other SM parameters.

Results presented in this contribution are based on different subsamples of the data collected by *BABAR* in Run1-6, corresponding to a total integrated luminosity of 477 fb^{-1} (of which 432 fb^{-1} at a c.m. energy of 10.58 GeV and 45 fb^{-1} at 10.54 GeV).

2 Exclusive B decays

B decays provide countless opportunities to test hadronic models, thanks to the very large number of possible decay modes. Factorization allows in principle to separate hadronic contributions from the weak matrix elements; if hadronic penguins or heavy quark pair creation appear in the process, predictions obtained from QCD phenomenological models, including perturbative and non-perturbative contributions, can be tested directly.

2.1 Amplitude analysis of the decay $B^{\pm} \to \phi K^{*\pm}$ [2]

B meson decay to the vector-vector $\phi K(892)^{*\pm}$ state proceeds through the quark-level transition $b \to s\bar{s}s$, which can only occur in the Standard Model in second-order loop diagrams. The relatively large fraction of transverse polarization observed in this mode by *BABAR* [3] and Belle [4] (as well as in other $B \to VV$ modes) disagrees with naive expectations derived from the $(V-A)$ structure of the weak interaction, helicity conservation in the strong interactions and s-quark spin flip suppression in the penguin diagram. Explanations for this disagreement have been proposed both in the framework of the Standard Model and invoking effects of New Physics (see references cited in [2]).

Three helicity amplitudes contribute to the total one, corresponding to the

three possible helicity states of the vector mesons, $\lambda = -1, 0, +1$; the two "transverse" amplitudes, A_{-1} and A_{+1}, can be re-parametrized into a parity-even and a parity-odd one, $A_\parallel$ and $A_\perp$ respectively. The different contributions can be separated by measuring the differential decay rate as a function of the three angles θ_1, θ_2 and Φ shown in Fig. 1(a).
The analysis is performed on a sample of about 384 million $B\overline{B}$ pairs. The $B^\pm \to \phi K^{*\pm} \to (K^+K^-)(K\pi)^\pm$ candidates are reconstructed with $(K\pi)^\pm = K^\pm\pi^0$ or $K^0_S\pi^\pm$. Six observables are extracted from a fit to the data: the branching fraction $\mathcal{B}$, the fractions of longitudinal and perpendicular polarization f_L and $f_\perp$, and the phases of three helicity amplitudes $\phi_\parallel$, $\phi_\perp$ and δ_0: six more observables are added after allowing for CP violation in the decay. In particular, for the polarization fractions the fit yields

$$f_L \equiv |A_0|^2 / \sum_\lambda |A_\lambda|^2 = 0.49 \pm 0.05_{\rm stat} \pm 0.03_{\rm syst},$$
$$f_\perp \equiv |A_\perp|^2 / \sum_\lambda |A_\lambda|^2 = 0.21 \pm 0.05_{\rm stat} \pm 0.02_{\rm syst}.$$

No evidence for CP violation is found. A two-fold ambiguity in the determination of $\phi_\parallel$, $\phi_\perp$ is resolved by studying the dependence on the $K\pi$ invariant mass of the interference between the $J^P(K\pi) = 1^-$ and 0^+ components in the amplitude: the result implies $\phi_\parallel \simeq \phi_\perp$, which is consistent with the approximate hierarchy in the amplitudes:

$$|A_0| \simeq |A_+1| \gg |A_-|.$$

2.2 Study of the decays $B \to \eta_c K^*$, $B \to \eta_c \gamma K^{(*)}$ [5]

Among B decays to the S-wave states of charmonium, those to the triplet states J/ψ, $\psi(2S)$ are best known [6] because of the clear signature offered by the leptonic decay modes $J/\psi \to e^+e^-, \mu^+\mu^-$. Decays to the singlet states η_c, $\eta_c(2S)$ must be reconstructed in specific hadronic final states: only few of these decays modes are known, despite they occur at rates similar to the corresponding ones for the triplet states ($\mathcal{B} \sim 10^{-4} - 10^{-3}$).
For B decays to the P-wave states of charmonium, the color singlet approximation in the factorization scheme, which works reasonably well in the S-wave case, predicts vanishing rates for decays to the $J = 0, 2$ states χ_{c0}, χ_{c2}, h_c. However, exclusive decays to χ_{c0} [7] and inclusive decays to χ_{c2} [8] have been

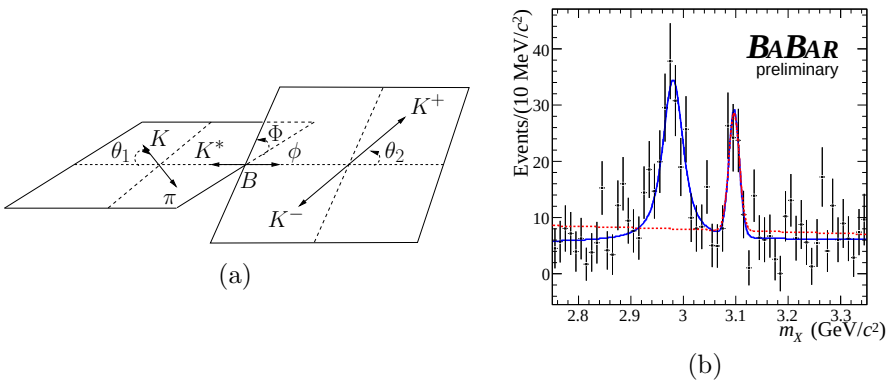

Figure 1: *a) definition of helicity angles for the decay $B \to \phi K^*$ (ϕ and K^* shown in their rest frame); b) background-subtracted invariant mass for the $KK\pi$ system in reconstructed $B \to K^0_S K^\pm \pi^\mp$, $B \to K^+K^-\pi^0$ decays.*

observed with rates comparable to the corresponding ones for χ_{c1}: the inclusion of color-octet terms in non-relativistic QCD calculations gives much better agreement with these results, at least for inclusive rates. No evidence has been found so far for B decays to h_c, and only upper limits to the branching fractions have been set [9].

BABAR has searched for the decays $B^\pm \to h_c K^\pm$, $B^0 \to \eta_c K^{*0}$, $B^0 \to h_c K^{*0}$ on a sample of about 384 million $B\overline{B}$ pairs. K^{*0} mesons are reconstructed as $K^{*0} \to K^+\pi^-$; η_c candidates in the two modes $\eta_c \to K^0_S K^\pm \pi^\mp, K^+K^-\pi^0$; h_c candidates in the radiative decay $h_c \to \eta_c \gamma$, which is expected to be the dominant one ($\mathcal{B} \sim 50\%$). Yields are extracted from fits to the $K\overline{K}\pi(\gamma)$ invariant mass distributions for selected B candidates, after combinatorial background subtraction.

A clear signal is observed for $B^0 \to \eta_c K^{*0}$ (Fig. 1(b)), leading to the measurement of the branching fraction:

$$\mathcal{B}(B^0 \to \eta_c K^{*0}) = (6.1 \pm 0.8_{\rm stat} \pm 1.1_{\rm syst}) \times 10^{-4},$$

representing almost a factor 4 improvement over previous measurements. No signals are found for the h_c modes, leading to the upper limits

$$\mathcal{B}(B^{\pm} \to h_c K^{\pm}) \times \mathcal{B}(h_c \to \eta_c \gamma) < 5.2 \times 10^{-5},$$
$$\mathcal{B}(B^{0} \to h_c K^{*0}) \times \mathcal{B}(h_c \to \eta_c \gamma) < 2.41 \times 10^{-4},$$

at 90% C.L.: the first is consistent with a previous Belle measurement; the second is measured for the first time. All results are preliminary.

3 Hadron production in e^+e^- annihilations

The production cross section for the process $e^+e^- \to b\overline{b}$ at the c.m. energy of the $\Upsilon(4S)$ mass, about 1 nb, is only about 1/3 of the total hadronic cross section. This means that a very rich hadron physics program can be carried out using the *BABAR* "continuum" data sample. Hadron production can be studied both in direct e^+e^- annihilation at the nominal machine energy, or at lower energies via radiative return. In the first case, the reaction mainly proceeds via exchange of a single virtual photon, so that only some quantum numbers and helicity values are possible for the final state. In the second case, a real photon is emitted by the electron (positron) in the initial state, carrying out a fraction of the initial energy: this means that e^+e^- annihilations at virtually all energies from 0 to the $\Upsilon(4S)$ mass can be studied in the same experiment with the same conditions.

3.1 Correlated baryon-antibaryon production

Two different mechanisms have been proposed to describe baryon production in e^+e^- annihilations, leading to the notions of 'local' and 'primary' correlation. In the first case, a quark-antiquark pair is produced in the annihilation, and a baryon-antibaryon pair appears in one of the two resulting jets: these events are generally characterized by a small rapidity separation $|\Delta y|$ between the two baryons. In the second case, a diquark-antidiquark pair emerges instead from the annihilation, giving rise to the production of two leading baryons sharing two out of three flavors: these events are characterized by large $|\Delta y|$ values.
There is currently no compelling evidence for primary production, most experiments obtaining $|\Delta y|$ distributions peaking at low values. However, the CLEO Collaboration has reported a 3.5 ± 0.6-fold excess of events with both a Λ_c^+ and

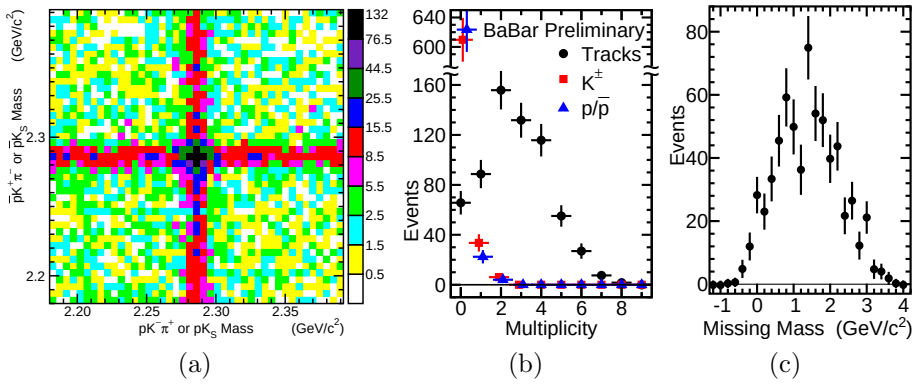

(a) (b) (c)

Figure 2: *a) invariant mass of the $\overline{\Lambda}_c^-$ candidate vs. that of the Λ_c^+ candidate in the same event; b) distribution of the number of additional number of tracks and identified $K^{\pm}$, ($\overline{p}$) in selected $\Lambda_c^+\overline{\Lambda}_c^- X$ events; c) missing mass for the same events (with imaginary masses being given real negative values).*

a $\overline{\Lambda}_c^-$ in e^+e^- annihilations at $\sqrt{s} = 10.6$ GeV with respect to expectations from local production [10].

BABAR has performed a similar study on a sample of data corresponding to an integrated luminosity of 220 fb^{-1}. A Λ_c^+ baryon is reconstructed in the $pK^-\pi^+$ or pK^0_S decay mode and a $\overline{\Lambda}_c^-$ baryon is reconstructed in one of the corresponding charge-conjugate modes. Λ_c^+[1] from $\Upsilon(4S)$ decays are suppressed by requiring the candidate c.m. momentum to exceed 2.3 GeV. Most events with two candidates in a "signal region" close to the Λ_c^+ mass show an opening angle between them larger than 140°: a lower cut at 90° is therefore imposed. The distribution of the invariant mass of the $\overline{\Lambda}_c^-$ cadidate vs. that of the Λ_c^+ candidate for surviving events is shown in Fig. 2(a). Counting the number of events in a region around the Λ_c^+ mass on the two axes and subtracting the estimated background gives a number of signal events $N(\Lambda_c^+\overline{\Lambda}_c^- X) = 649 \pm 31$. This represents a 4.2-fold excess with what would be expected if the production of the two baryons were uncorrelated, consistently with what observed by CLEO. The distribution of the number of additional tracks present in the event is shown in Fig. 2(b), where also the numbers of identified protons and

[1] Charge conjugation is implied here and in the following.

kaons are shown: the multiplicity peaks at low values and there are very few additional protons. A study of the missing mass reveals a low-mass-peaking distribution (Fig. 2(c)), indicating suppressed $n\overline{n}$ production: this leads to an estimate of the numer of 4-baryon events $N_{4-\mathrm{bar}} = 13 \pm 8$. All results are preliminary.

3.2 Study of $e^+e^- \to \pi^+\pi^-\pi^0\pi^0$ with initial state radiation

Precision measurement of the $e^+e^- \to$ hadrons cross section in the low energy ($E \lesssim 2$GeV) region is of particular importance for the calculations of hadronic contributions to the muon anomalous magnetic moment $\alpha_\mu \equiv (g_\mu - 2)/2$ [11] and to the value of the fine structure constant at the Z^0 pole, $\alpha(m_Z^2)$ [12]. In the region between 1 and 2 GeV, which is currently the one giving the largest contribution to the error on α_μ, four-pion final states are dominating.

BABAR has measured the cross section for many exclusive hadronic final states in 'initial state radiation' (ISR) processes $e^+e^- \to \gamma_{\mathrm{ISR}}$ $e^+e^- \to \gamma_{\mathrm{ISR}}$ hadrons. Among these, it has studied the $e^+e^- \to \pi^+\pi^-\pi^0\pi^0$ channel in the energy range $0.95 - 4.5$GeV, on a sample corresponding to an integrated luminosity of 220 fb^{-1}.

The event selection is based on the requirement of observing one photon with energy $E_\gamma > 3$GeV; a kinematic fit is performed in the hypothesis $e^+e^- \to \pi^+\pi^-\pi^0\pi^0\gamma$.

Extraction of the cross section as a function of the 4-pion energy, after background subtraction, results in the shape shown in Fig. 3(a) for the range $0.95 - 2.1$ GeV. Several other experiments have already measured this cross section in this range: their results are shown in the same figure for comparison. *BABAR*'s measurements are in good agreement with most of them, significantly improving the precision (errors are between 7.8% and 10%). For energies $E > 2.4$GeV, the cross section has been measured for the first time: peaks corresponding to the formation of J/ψ and $\psi(2S)$ are clearly seen, allowing in particular the first measurement of the J/ψ branching fraction for this channel: $\mathcal{B}(J/\psi \to \pi^+\pi^-\pi^0\pi^0) = (5.74 \pm 0.74) \times 10^{-3}$. All results are preliminary.

Reviews of recent *BABAR* results on hadron production, including many more exclusive modes, can be found in [13].

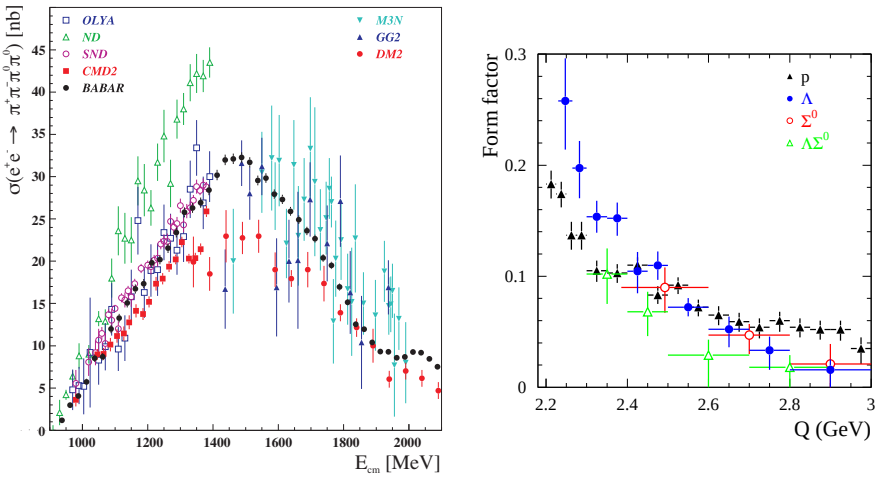

(a) (b)

Figure 3: *a) cross section for $e^+e^- \to \pi^+\pi^-\pi^0\pi^0$ as a function of 4-pion invariant mass: comparison between BABAR results and previous measurements; b) measured time-like baryon form factors as a function of the di-baryon invariant mass.*

3.3 Λ and Σ^0 time-like form factor [14)]

The cross section for baryon-antibaryon production in e^+e^- annihilations, for spin-1/2 baryons, is written in terms of the electric and magnetic form factors as

$$\sigma_{B\overline{B}}(\sqrt{s}) = \frac{4\pi\alpha^2\beta}{3s}\left[\left|G_{\rm M}(\sqrt{s})\right|^2 + \frac{1}{2\tau}\left|G_{\rm E}(\sqrt{s})\right|^2\right],$$

where $\beta = \sqrt{1-4m_B^2/s}$, $\tau = s/4m_B^2$; at threshold, $G_{\rm E} = G_{\rm M}$. An effective form factor $|F(\sqrt{s})|$ is defined by

$$\left|F_{\rm M}(\sqrt{s})\right|^2 = \frac{2\tau\left|G_{\rm M}(\sqrt{s})\right|^2 + \left|G_{\rm E}(\sqrt{s})\right|^2}{2\tau+1}.$$

Experimental information on the reactions $e^+e^- \to \Lambda\overline{\Lambda}$, $\Sigma^0\overline{\Sigma}^0$, $\Lambda\overline{\Sigma}^0$ is very scarce: the cross section for $e^+e^- \to \Lambda\overline{\Lambda}$ has been measured as 100^{+65}_{-35} pb at 2.386 Gev, and only upper limits exists for the other two processes [15)].

BABAR has studied these three modes using initial state radiation on a sample corresponding to an integrated luminosity of 230 fb^{-1}, for dibaryon invariant masses up to 5 GeV. The event selection requires the presence of a photon with energy $E_\gamma > 3$GeV. Λ candidates are reconstructed in the decay mode $\Lambda \to p\pi^-$; Σ^0 candidates are reconstructed in $\Sigma^0 \to \Lambda\gamma$. Kinematic fits are applied.
Cross sections are extracted by counting selected events in a proper signal region and subtracting the estimated background. The corresponding form factors as a function of the dibaryon invariant mass are shown in Fig. 3(b), together with the corresponding results for $e^+e^- \to p\overline{p}$ [16]. All modes display the same behavior; results for the Λ form factor are consistent with the only other existing measurement.
Analysis of the baryons angular distributions would in principle allow the separation of the $G_{\rm E}$ and $G_{\rm M}$ contributions. In this case statistics are too limited to obtain precise results: values for the $|G_{\rm E}/G_{\rm M}|$ ratio for $e^+e^- \to \Lambda\overline{\Lambda}$, extracted in two $\sqrt{s}$ regions, are consistent both with $|G_{\rm E}/G_{\rm M}| = 1$ and with the significant enhancement near threshold observed in $e^+e^- \to p\overline{p}$.

4 Measurement of baryon properties

The large number of baryons produced in e^+e^- interactions at *BABAR* allows the study of their properties, which are in some cases still poorly known. In particular, the analysis of angular distributions can be used to determine their spin, like recently happened for the Ω baryon [17]. Another nice example is reported here.

4.1 Determination of the spin of $\Xi(1530)^0$

The spin and parity of the $\Xi(1530)^0$ baryon are known to be $J^P = 3/2^+$ or $J^P = 5/2^-$ from data analysis of the reaction $K^-p \to \Xi(1530)^{0,-}K^{0,+}$ [18].
BABAR has performed a spin analysis on $\Xi(1530)^0$ baryons produced in the decay chain $\Lambda_c^+ \to \Xi(1530)^0K^+$, $\Xi(1530)^0 \to \Xi^-\pi^+$, on a data sample corresponding to an integrated luminosity of 230 fb^{-1}. Ξ^- baryons are reconstructed through the decay $\Xi^- \to \Lambda\pi^-$, $\Lambda \to p\pi^-$. A kinematic fit is applied and minimum flight lengths are required for the long-lived Ξ^- and Λ baryons.
The helicity angle θ_{Ξ^-} is defined as the angle between the direction of the Ξ^- and the direction opposite to the Λ, in the $(\Xi^-\pi^+)$ system reference frame. Its

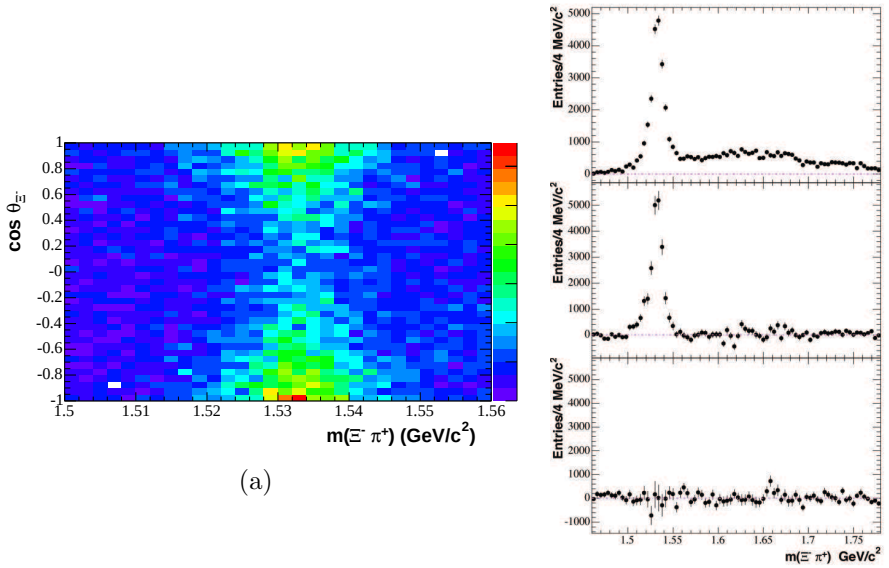

(a) (b)

Figure 4: *a) distribution of the cosine of the* Ξ^- *helicity angle vs. the* $\Xi^-\pi^+$ *invariant mass for selected* Λ_c^+ *candidates; b) efficiency-corrected and background-subtracted Legendre-polynomial moments of the* $\Xi^-\pi^+$ *invariant mass distribution for the same events: from top to bottom:* $\sqrt{2}P_0(\cos\theta_{\Xi^-})$*;* $\sqrt{10}P_2(\cos\theta_{\Xi^-})$*;* $7/\sqrt{2}P_4(\cos\theta_{\Xi^-})$*.*

distribution versus the $(\Xi^-\pi^+)$ invariant mass is shown in Fig. 4 for selected events, where a band corresponding to the $\Xi(1530)^0 \to \Xi^-\pi^+$ dominant channel can be clearly seen.

For a given J value of the resonance spin, the angular distribution for the decay can be written as

$$\frac{\mathrm{d}N}{\mathrm{d}\cos\theta_{\Xi^-}} = N\left[\sum_{l=0}^{l_{\max}}\langle P_l\rangle P_l(\cos\theta_{\Xi^-})\right],$$

where N is a normalization factor, $l_{\max} = 2J-1$ and P_l are the Legendre polynomials. In any invariant mass interval, the number of $\Xi(1530)^0$ events is

well approximated by assigning each event j a weight

$$w_j = \frac{P_{l_{\max}}(\cos\theta^j_{\Xi^-})}{\langle P_{l_{\max}}\rangle}.$$

The non-flat distribution in $\cos\theta^j_{\Xi^-}$ clearly rules out the $J = 1/2$ solution. The weighted invariant-mass distributions (after efficiency correction and background subtraction) for $l_{\max} = 0, 2, 4$ are shown in Fig. 4(b): while essentially all signal is retained with $l_{\max} = 2$, the yield is consistent with zero with $l_{\max} = 4$, thus ruling out the spin-5/2 solution and establishing the $\Xi(1530)^0$ as a $J^P = 3/2^+$ resonance. However, a more detailed analysis of the data indicates that it is necessary to include other $\Xi^-\pi^+$ amplitudes in order to obtain a complete description. Results are preliminary.

5 Conclusions

The large data sample recorded by the *BABAR* detector allows to explore a broad range of processes of great interest to hadronic physics. A small, personal selection of recent results has been presented here, with no claim for completeness: more results can be found in other contributions from *BABAR* to these Proceedings. In particular, many of the recent hot topics in hadron spectroscopy which have not been mentioned here are discussed in [19].

References

1. B. Aubert *et al.* (*BABAR* Collaboration), Nucl. Inst. Meth **A 479**, 1 (2002).
2. B. Aubert *et al.* (*BABAR* Collaboration), Phys Rev. Lett. **99**, 201802 (2007).
3. B. Aubert *et al.* (*BABAR* Collaboration), Phys Rev. Lett. **91**, 171802 (2003); B. Aubert *et al.* (*BABAR* Collaboration), Phys Rev. Lett. **98**, 051801 (2007).
4. K.-F. Chen *et al.* (Belle Collaboration), Phys Rev. Lett. **95**,141801 (2005).
5. B. Aubert *et al.* (*BABAR* Collaboration), arXiv:0707.2843 [hep-ex].
6. W.-M. Yao *et al.* (Particle Data Group), J. Phys. **G 33**, 833 (2006).
7. B. Aubert *et al.* (*BABAR* Collaboration), Phys Rev. **D 69**, 071103 (2004); K. Abe *et al.* (Belle Collaboration), Phys Rev. Lett. **88**, 031802 (2002).

8. B. Aubert *et al.* (*BABAR* Collaboration), Phys Rev. **D 67**, 032002 (2002);
K. Abe *et al.* (Belle Collaboration), Phys Rev. Lett. **89**, 011803 (2002).

9. F. Fang *et al.* (Belle Collaboration), Phys Rev. **D 74**, 012007 (2006).

10. A. Bornheim *et al.* (CLEO Collaboration), Phys Rev **D 63**. 112003 (2001).

11. M. Davier it et al., Eur. Phys. J. **C 31**, 503 (2003).

12. S. Eidelmann, F. Jegerlehner, Z. Phys. **C 67**, 585 (1995).

13. W. Wang, in this Conference's Proceedings;
S. Serednyakov, in this Conference's Proceedings;
D. Muller, in this Conference's Proceedings.

14. B. Aubert *et al.* (*BABAR* Collaboration), Phys. Rev. **D 76**, 092006 (2007).

15. D. Bisello it et al. (DM2 Collaboration), Z. Phys. **C 48**, 23 (1990).

16. B. Aubert *et al.* (*BABAR* Collaboration), Phys. Rev. **D 73**, 012005 (2006).

17. B. Aubert *et al.* (*BABAR* Collaboration), Phys. Rev. Lett. **97**, 112001 (2006).

18. P. Schlein*et al.*, Phys. Rev. Lett. **11**, 167 (1963);
J. Button-Shafer*et al.*, Phys. Rev. **142**, 883 (1966).

19. A. Palano, in this Conference's Proceedings;
A. Gabareen, in this Conference's Proceedings;
V. Poirot, in this Conference's Proceedings.

Frascati Physics Series Vol. XLVI (2007), pp. 229–238
HADRON07: XII Int. Conf. on Hadron Spectroscopy – Frascati, October 8-13, 2007
Plenary Session

HADRONIC PHYSICS AT BELLE

S. Eidelman
(For the Belle Collaboration)
Budker Institute of Nuclear Physics
and Novosibirsk State University
630090 Novosibirsk, Russia

Abstract

Recent results on hadronic physics from the Belle detector are described. Cross sections of $D^*\bar{D}^*$, $D^*\bar{D}$, $D\bar{D}$ production have been measured from threshold to 5 GeV. New charmonium-like structures have been observed in recoil from the J/ψ and in radiative return to the $J/\psi\pi^+\pi^-$ and $\psi(2S)\pi^+\pi^-$. Production of various charmonia in $\gamma\gamma$ collisions is discussed.

1 Introduction

The asymmetric-energy e^+e^- collider KEKB has a world record luminosity of $1.71 \cdot 10^{34}$ cm^{-2} s^{-1}. The Belle detector collected a data sample of about 715 fb^{-1} allowing studies of hadron production in various processes – radiative return, $q\bar{q}$ continuum, B meson and τ lepton decays, $\gamma\gamma$ collisions.

2 Vector States

Four broad ψ-like structures above the open charm threshold are known since 25 years – $\psi(3770)$, $\psi(4040)$, $\psi(4160)$, $\psi(4415)$. However, until recently even their main properties (M, Γ, Γ_{ee}) were known badly based on the measurements of DASP [1] and MARK I [2]. In Ref. [3] an attempt was made to use more precise data from Crystal Ball [4] and BES [5] and it was shown that the above parameters can change strongly. Finally, the BES group performed the analysis of their data [6]. Its problem is to take into account opening thresholds and common decay channels ($D^{(*)}\bar{D}^{(*)}_{(s)}$) of different states. In the model-dependent analysis of BES R is described by a smooth u, d, s background plus a coherent sum of the four ψ states, each an incoherent sum of two-body $D_1 D_2$ states.

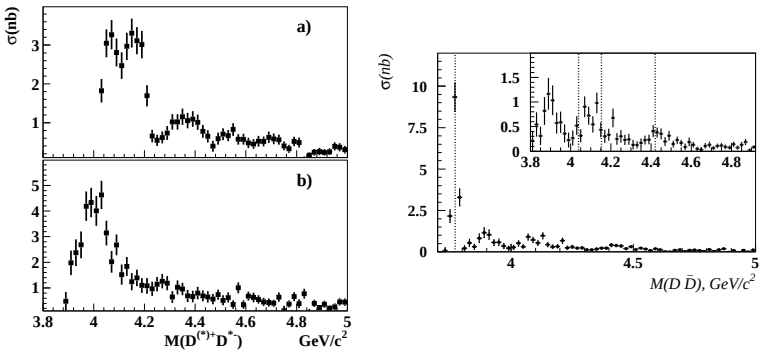

Figure 1: *Cross sections of* $D^*\bar{D}^*$, $D^*\bar{D}$, $D\bar{D}$

Probably most promising would be the R determination from exclusive measurements of different final states with charmed meson pairs. First results of this type were recently obtained in initial-state-radiation analyses at B factories. The cross sections of the reactions $e^+e^- \to D^*\bar{D}^*$, $D^*\bar{D}$, $D\bar{D}$ were measured by Belle. The $D^*\bar{D}^*$ final state (a data sample of 548 fb^{-1}) shows rich structure (Fig. 1) [7]. The $D^*\bar{D}$ final state (also 548 fb^{-1}) is on the contrary featureless, with an excess at $\psi(4040)$ (Fig. 1) [7]. The $D\bar{D}$ final state (673 fb^{-1}) [8] shows some enhancement at 3.9 GeV as in the BES [5] and BaBar [9] and above 4 GeV the shape of its cross section is similar to that of $\sigma(D^{*+}D^{*-})$, see. Fig. 1. Taken together (with some isospin corrections for the

unobserved states), both cross sections reasonably well reproduce the pattern of R observed by BES. Both groups see a minimum in the $Y(4260)$ region, which may be due to $D_s^* D_s^* (DD^{**})$ thresholds or interference effects.

Belle also measured the cross section of the process $e^+e^- \to D^0 D^- \pi^+$ and showed that it is dominated by the production of the $\psi(4415)$ [10]. They determine its parameters and show that most of its decays proceed via the $D\bar{D}_2^*(2460)$ intermediate mechanism.

The BaBar's observation of the new broad state, $Y(4260)$, decaying into $J/\psi\pi^+\pi^-$ [11] and later the $Y(4320)$ with the $\psi(2S)\pi^+\pi^-$ decay [12] added intrigue to the studies of charmonium spectroscopy. Both final states were studies with much larger statistics by Belle using radiative return. Figure 2, left shows the $J/\psi\pi^+\pi^-$ mass spectrum (548 fb^{-1}) [13] whereas its right side illustrates the one for the $\psi(2S)\pi^+\pi^-$ mass (673 fb^{-1}) [14].

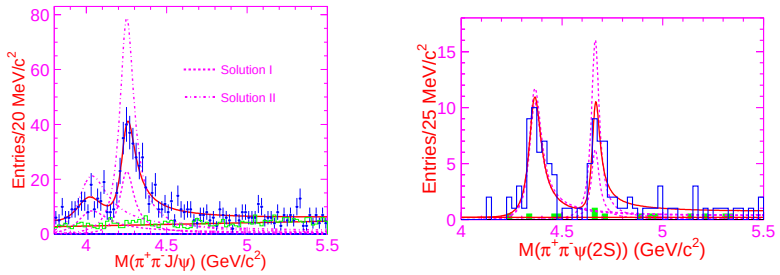

Figure 2: *Mass spectra of* $J/\psi\pi^+\pi^-$ *and* $\psi(2S)\pi^+\pi^-$

The $J/\psi\pi^+\pi^-$ mass spectrum exhibits a clear peak at 4.25 GeV and a cluster of events at 4.05 GeV. A good fit of the spectrum is achieved if two intefering resonances are assumed. Two solutions of equally good quality and with the same mass and width, but different leptonic width are obtained. All parameters of the first solution for the structure at 4.25 GeV are consistent with the $Y(4260)$ parameters of BaBar [11] and CLEO [15] whereas the structure at 4.05 GeV is observed for the first time. The $M_{\pi^+\pi^-}$ spectrum differs from that in the phase space model, Fig. 3.

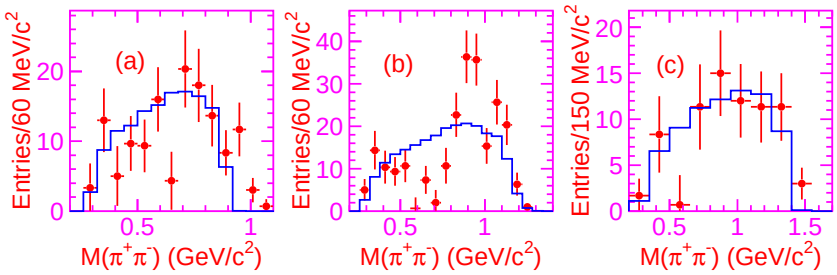

Figure 3: *Dipion mass spectrum of* $J/\psi\pi^+\pi^-$

Although the cross sections for the $\psi(2S)\pi^+\pi^-$ final state are consistent with those of BaBar, their pattern is different. Two distinct peaks, one at 4.36 GeV and one at 4.66 GeV, are seen. Their fit with two resonances has two solutions, however, in both the first structure is much narrower than that of BaBar [12]. The second structure is observed for the first time. These structures differ from those in $J/\psi\pi^+\pi^-$.

Also measured by Belle was the the cross section of the process $e^+e^- \to J/\psi K^+K^-$ (673 fb^{-1}) [16]. A broad structure between 4.5 and 5.5 GeV not described by existing ψ''s can be seen. Two events are found near 4.26 GeV with the cross section consistent with that of CLEO [17]. Belle sets an upper limit $\mathcal{B}(Y(4260) \to J/\psi K^+K^-)\Gamma(Y(4260) \to e^+e^-) < 1.2$ eV at 90% CL. Finally, three $J/\psi K^0_S K^0_S$ events are observed between 4.4 and 5.2 GeV.

Note that coupled-channel and rescattering ($D^{(*)}\bar{D}^{(*)}$) effects may affect the resonance interpretation of these experiments.

3 Other quantum numbers

Belle was the first to suggest an interesting method of studying charmonia with various quantum numbers (but 1^{--}) in ther recoil against the J/ψ and $\psi(2S)$ mesons. Its use resulted in one of the first observation of the $\eta_c(2S)$ [18] and discovery of the new state $X(3940)$ [19]. In its new study based on 693 fb^{-1} Belle looked for the $D^{(*)}\bar{D}^{(*)}$ states produced against the J/ψ [20]. Only one $D^{(*)}_{\rm rec}$ is reconstructed in addition to the J/ψ and the second $D^{(*)}_{\rm ass}$ is then observed as a peak in the spectra of masses recoiling against the reconstructed

$J/\psi D^{(*)}_{\rm rec}$. The distribution of masses recoiling against a) $J/\psi D$ and b) $J/\psi D^*$ is shown in Fig. 4.

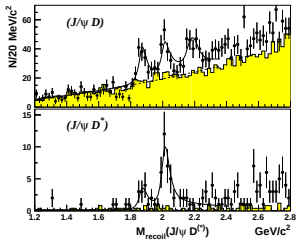

Figure 4: *Recoil mass spectra of a) $J/\psi D$ and b) $J/\psi D^*$*

The signals for the processes $e^+e^- \to J/\psi D\bar{D}$, $D^*\bar{D}$ and $D^*\bar{D}^*$ are clearly seen. After that they study the mass spectra of the $D^{(*)}\bar{D}^{(*)}$ system and observe there for the first time a state $X(4160)$ and confirm $X(3940)$. They also conclude that the inclusive peak in $M_{\rm rec}(J/\psi)$ may consist of several states.

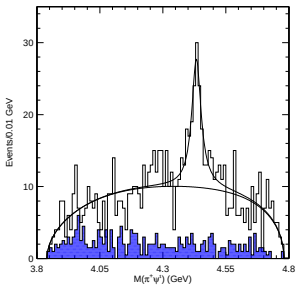

Figure 5: *$\pi^\pm\psi'$ mass spectrum in $B \to K\pi^\pm\psi'$ decays*

One more interesting state, most probably of exotic nature, is observed in $B \to K\pi^\pm\psi'$ decays [21]. Here at a data sample of 605 fb^{-1} they find a new $\pi^\pm\psi'$ structure with a mass of $4433 \pm 4 \pm 2$ MeV and width of $\Gamma =$

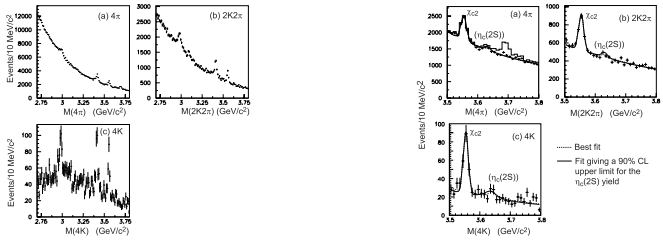

Figure 6: *Search for: left – η_c, right – $\eta_c(2S)$*

$(45^{+18}_{-13}\ ^{+30}_{-13})$ MeV, Fig. 5. It is the first charmonium-like meson with non-zero electric charge and it is very tempting to assume that is has a four-quark nature.

4 Charmonium in $\gamma\gamma$ collisions

Belle has fruitfully exploited $\gamma\gamma$ collisions to study various charmonia. Some of the interesting results are enumerated below. It is worth noting that we always list the quantity, which is directly measured, i.e. the product of the two-photon width and the branching fraction, $\mathcal{G} = \Gamma_{\gamma\gamma}\mathcal{B}$.

The $\chi_{c2}(2P)$ (former $Z(3930)$) meson was discovered in the $D\bar{D}$ final state using 395 fb^{-1} [22]. Its mass is $3929 \pm 5 \pm 2$ MeV and total width is $29 \pm 10 \pm 2$ MeV.

The χ_{c0} and χ_{c2} mesons were studied in the $\pi^+\pi^-$, K^+K^- [23] (87.7 fb^{-1}) and $K^0_S K^0_S$ [24] (397.6 fb^{-1}) final states. The values of $\mathcal{G}$ were determined and various ratios of the branching fractions obtained.

The η_c meson was studied in the following final states with baryons: $p\bar{p}$ [25] (89 fb^{-1}) and $\Lambda\bar{\Lambda}$, $\Sigma^0\bar{\Sigma}^0$ [26] (464 fb^{-1}). Evidence for the new decay mode $\eta_c \to \Sigma^0\bar{\Sigma}^0$ has been obtained, the values of $\mathcal{G}$ were determined.

The properties of the η_c and $\eta_c(2S)$ were studied in the $K^\pm K^0_S \pi^\mp$ final state with a high data sample of 483 fb^{-1} [27]. The values of mass, total width and $\mathcal{G}$ were determined and it was shown that interference effects are very important and may change the two-photon width by an order of magnitude.

Finally, various decay modes of the η_c, χ_{c0} and χ_{c2} were studied in the final states with four tracks: $2\pi^+2\pi^-$, $\pi^+\pi^-K^+K^-$, $2K^+2K^-$ [28] (395 fb^{-1}). For the $\eta_c(1S)$ new values of $\Gamma_{\gamma\gamma}\mathcal{B}$ are a few times smaller than previously. The $\eta_c(2S)$ is not observed in any of these modes, see Fig. 6.

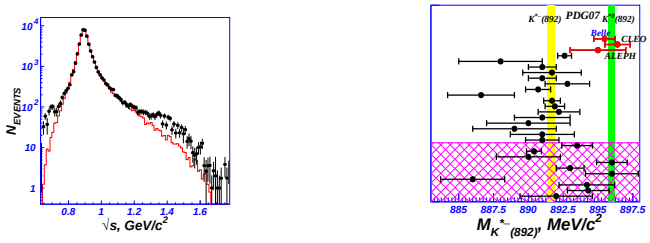

Figure 7: *Belle results on* $\tau^- \to K^0_S\pi^-\nu_\tau$: *left – Mass spectrum of* $K^0_S\pi^-$, *right – Mass of* $K^*(892)^-$

)

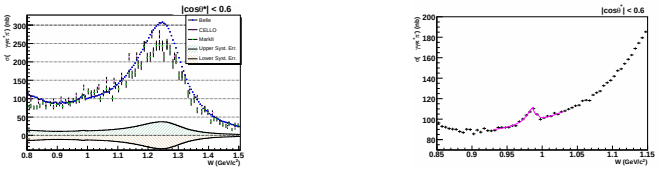

Figure 8: *Belle results on* $\gamma\gamma \to \pi^+\pi^-$: *left – Signal of* $f_2(1270)$, *right – Signal of* $f_0(980)$

5 Studies of light quark states

Belle made a high-statistics analysis of the $\tau^- \to K^0_S\pi^-\nu_\tau$ decay using 53110 events selected from a data sample of 351 fb^{-1} [29]. They studied the $M_{K\pi}$ spectrum and concluded that can well describe it by the following combination of states: $K^*(892)$, $K^*(800)$ (κ) and $K^*_0(1430)$ (or $K^*(1410)$), Fig. 7.

Belle has also measured with high precision the $K^*(892)^-$ mass and width. Quite unexpectedly, the mass value is more than 4 MeV higher than the world average for the charged $K^*(892)$ and is close to the world average for the neutral one [30].

Some new results were obtained in $\gamma\gamma$ collisions. A high-statistics measurement of the cross section of the process $\gamma\gamma \to \pi^+\pi^-$ showed for the first time a clear peak of the $f_0(980)$, Fig. 8, right [31] (85.9 fb^{-1}). Also observed is a prominent signal of the $f_2(1270)$ [32], see Fig. 8, left.

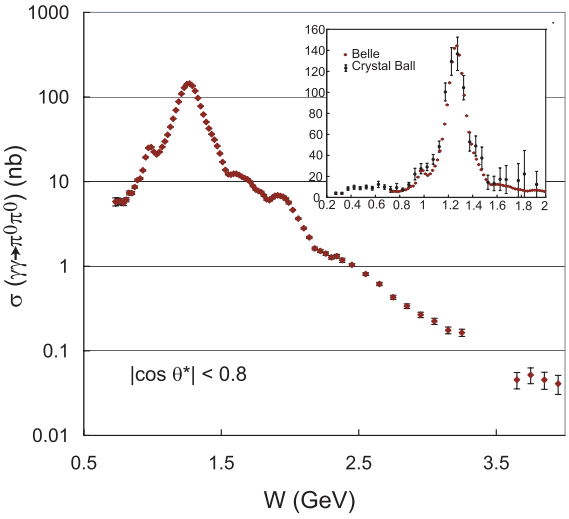

Figure 9: *$\gamma\gamma$ mass spectrum for the process $\gamma\gamma \to \pi^0\pi^0$*

One more final state studied by Belle in $\gamma\gamma$ collisions is $\pi^0\pi^0$ [33]. The $\gamma\gamma$ mass spectrum from a data sample of 95 fb^{-1} shown in Fig. 9 exhibits prominent structures at 0.98, 1.27, 1.65 and 1.95 GeV. The inset to the figure shows that these results are in fair agrrement with the data of the Crystal Ball [34]. A high data sample makes possible analysis of angular distributions which is in progres

6 Acknowledgments

I'd like to thank S. Bianco and other organizers for the excellent Conference. I'm grateful to my colleagues from Belle for useful discussions and help. I acknowledge a travel grant from the Novosibirsk State University.

This work was supported in part by the grants RFFI 06-02-04018, 06-02-16156, 07-02-00816, DFG GZ RUS 113/769/0-2 and INTAS/05-1000008-8328.

References

1. R. Brandelik *et al.*, Phys. Lett. **76B**, 361 (1978).

2. J.L. Siegrist *et al.*, Phys. Rev. Lett. **36**, 700 (1976).
3. K.K. Seth, Phys. Rev. **D72**, 017501 (2005).
4. A. Osterfeld *et al.*, Report SLAC-PUB-4160, 1986.
5. J.Z. Bai *et al.*, Phys. Rev. Lett. **88**, 101802 (2002).
6. M. Ablikim *et al.*, arXiv:0705.4500.
7. G. Pakhlova *et al.*, Phys. Rev. Lett. **98**, 092001 (2007).
8. G. Pakhlova *et al.*, arXiv:0708.0082, accepted by Phys. Rev. D.
9. B. Aubert *et al.*, hep-ex/0607083..
10. G. Pakhlova *et al.*, arXiv:0708.3313, accepted by Phys. Rev. Lett.
11. B. Aubert *et al.*, Phys. Rev. Lett. **95**, 142001 (2005).
12. B. Aubert *et al.*, Phys. Rev. Lett. **98**, 212001 (2007)
13. C.-Z.Yuan *et al.*, Phys. Rev. Lett. **99**, 181804 (2007).
14. X.-L.Wang *et al.*, Phys. Rev. Lett. **99**, 142002 (2007).
15. Q. He *et al.*, Phys. Rev. D **74**, 091104R (2006).
16. C.-Z. Yuan *et al.*, arXiv:0709.2565, accepted by Phys. Rev. D(RC).
17. T.E. Coan *et al.*, Phys. Rev. Lett. **96**, 162003 (2006).
18. K. Abe *et al.*, Phys. Rev. Lett. **89**, 142001 (2002).
19. K. Abe *et al.*, Phys. Rev. Lett. **98**, 082001 (2007).
20. P. Pakhlov *et al.*, arXiv:0708.3812, submitted to Phys. Rev. Lett.
21. S.-K. Choi *et al.*, arXiv:0708.1790, submitted to Phys. Rev. Lett.
22. S. Uehara *et al.*, Phys. Rev. Lett. **96**, 082003 (2006).
23. H. Nakazawa *et al.*, Phys. Lett. B **615**, 39 (2005).
24. W.-T. Chen *et al.*, Phys. Lett. B **651**, 15 (2007).

25. C.-C. Kuo *et al.*, Phys. Lett. B **621**, 41 (2005).

26. C.-C. Kuo *et al.*, hep-ex/0609.048.

27. H. Nakazawa, Talk at the PHOTON-2007 Conference, Paris, 2007.

28. S. Uehara *et al.*, Eur. J. Phys. C, **53**,1 (2008).

29. D. Epifanov *et al.*, Phys. Lett. B **654**, 65 (2007).

30. W.-M. Yao *et al.*, J. Phys. G **33**, 1 (2006) and 2007 partial update for 2008.

31. T. Mori *et al.*, Phys. Rev. D **75**, 051101R (2007).

32. T. Mori *et al.*, J. Phys. Soc. Jpn, **76**, 074102 (2007).

33. K. Abe *et al.*, arXiv:0711.1926.

34. H. Marsiske *et al.*, Phys. Rev. D **41**, 3324 (1990).

Frascati Physics Series Vol. XLVI (2007), pp. 239–248
HADRON07: XII Int. Conf. on Hadron Spectroscopy – Frascati, October 8-13, 2007
Plenary Session

NEW RESULTS ON HADRON SPECTROSCOPY AT BESII AND PROSPECTS AT BESIII

Shan JIN
for BES Collaboration
Institute of High Energy Physics, Beijing 100049, P. R. China

Abstract

I would review a number of new structures at BESII, including the observation of $Y(2175)$ in $\phi f_0(980)$ mass spectrum in $J/\psi \to \eta\phi f_0(980)$ with $f_0(980) \to \pi^+\pi^-$, the observation of a broad 1^{--} resonance of K^+K^- mass in $J/\psi \to K^+K^-\pi^0$ decays. New results on baryonium candidate X(1860) are also presented. Finally I will talk about the prospects of glueball searches at BESIII.

1 Introduction

QCD allows the existence of the multi-quark states, $q\bar{q}$-*gluon* hybrids and glueballs. These states have been searched for more than 20 years by many experiments, however, none of them has been established so far. The 5.8×10^7 J/ψ events, accumulated with BES detector, provide a good laboratory for the search of non-$q\bar{q}$ states and study of light hadron spectroscopy.

2 Observation of $Y(2175)$ in $J/\psi \to \eta\phi f_0(980)$

A new 1^{--} structure, denoted as $Y(2175)$ and with mass $m = 2.175 \pm 0.010 \pm 0.015$ GeV/c^2 and width $\Gamma = 58 \pm 16 \pm 20$ MeV/c^2, was observed by the BABAR experiment in the $e^+e^- \to \gamma_{ISR}\phi f_0(980)$ initial-state radiation(ISR) process [1], [2]. This observation stimulated some theoretical speculation that this state may be an s-quark version of the $Y(4260)$ since both of them are produced in e^+e^- annihilation and decay to similar final states [3]. The $Y(2175)$ has correspondingly been interpreted as a $s\bar{s}g$ [4], a 2^3D_1 $s\bar{s}$ state [5] or a tetraquark $s\bar{s}s\bar{s}$ state [6]. As of now, none of these interpretations have either been established or ruled out by experiment.

With a sample of 5.8×10^7 J/ψ events collected with upgraded Beijing Spectrometer (BESII) detector [7] at Beijing Electron-Positron Collider (BEPC), the decays of $J/\psi \to \eta\phi f_0(980)$, with $\eta \to \gamma\gamma$, $\phi \to K^+K^-$, $f_0(980) \to \pi^+\pi^-$ are analyzed. After the final events selection, an η signal is evident in the $\gamma\gamma$ invariant mass spectrum (Fig. 1(a)); $\eta \to \gamma\gamma$ candidates are defined as γ-pairs with $|M_{\gamma\gamma} - 0.547| < 0.037$ GeV/c^2. A ϕ signal is distinct in the K^+K^- invariant mass spectrum (Fig. 1(b)) and for these candidates we require $|m_{K^+K^-} - 1.02| < 0.019$ GeV/c^2. In the $\pi^+\pi^-$ invariant mass spectrum, candidate $f_0(980)$ mesons are defined by $|m_{\pi^+\pi^-} - 0.980| < 0.060$ GeV/c^2 (Fig. 1(c)). The $\phi f_0(980)$ invariant mass spectrum for the selected events is shown in Fig. 2(a), where a clear enhancement is seen around 2.18 GeV/c^2.

The Dalitz plot of $m^2_{\eta f_0(980)}$ versus $m^2_{\eta\phi}$ for the selected events is shown in Fig. 2(b), where a diagonal band can be seen. This band corresponds to the structure observed around 2.18 GeV/c^2 in the $\phi f_0(980)$ invariant mass spectrum shown in Fig. 2(a).

To clarify the origin of the observed structure, we have made extensive studies of potential background processes using both data and MC. Non-η or non-$f_0(980)$ processes are studied with η-$f_0(980)$ mass sideband events. Non-ϕ processes are studied with ϕ mass sideband events. The total sideband events estimated from all these sidebands (minus double counting) are shown as the shaded histogram in Fig. 2(a). No structure around 2.18 GeV/c^2 is evident.

We fit the $\phi f_0(980)$ invariant mass spectrum and the total sidebands simultaneously. In the fit, the normalization for the background polynomial is constrained to be the same for both the signal and sideband histograms. We use a constant-width Breit-Wigner (BW) convolved with a Gaussian mass res-

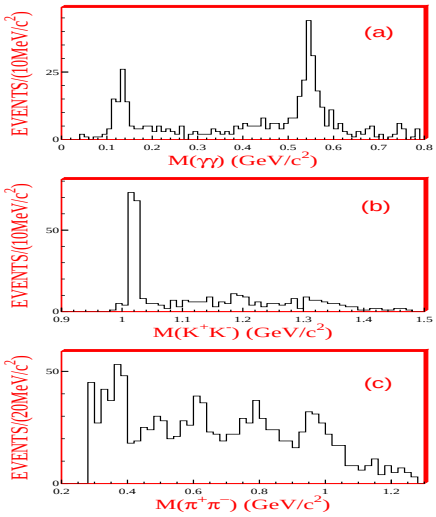

Figure 1: (a) The $\gamma\gamma$ invariant mass spectrum. (b) The K^+K^- invariant mass spectrum. (c) The $\pi^+\pi^-$ invariant mass spectrum.

olution function (with $\sigma = 12\text{MeV}/c^2$) to represent the $Y(2175)$ signal. The statistical significance of the signal is 5.5 σ. The mass and width obtained from the fit (shown as smooth curves in Fig. 3) are $M = 2.186 \pm 0.010(stat) \pm 0.006(syst)$ GeV/c^2 and $\Gamma = 0.065 \pm 0.023(stat) \pm 0.017(syst)$ GeV/c^2, and the product branching ratio is measured to be $Br(J/\psi \to \eta Y(2175)) \cdot Br(Y(2175) \to \phi f_0(980)) \cdot Br(f_0(980) \to \pi^+\pi^-) = (3.23 \pm 0.75(stat) \pm 0.73(syst)) \times 10^{-4}$, using MC-determined selection efficiency of 1.44%. Here, the second errors are systematic errors. The systematic uncertainties on the mass and width are estimated by varying the function form used to represent the background, the fitting range of the invariant mass spectrum, the bin width of the invariant mass spectrum, allowing the sideband and signal background normalizations to differ and possible fitting biases. The latter are estimated from the differences between the input and output mass and width values from MC studies. In addtion to above systematic sources, the systematic error on the branching ratio measurement comes also from the uncertainties of MDC simulation (including systematic uncertainties of the tracking efficiency and the kinematic fits), the photon detection efficiency, the particle identification efficiency, the η

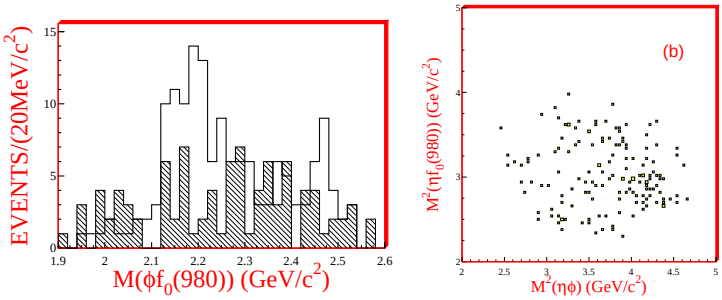

Figure 2: a) The $\phi f_0(980)$ invariant mass spectrum; The open histogram is data and the shaded histogram is sideband-determined background. (b) The Dalitz plot of $m^2_{\eta f_0(980)}$ versus $m^2_{\eta\phi}$.

decay branching ratio to $\gamma\gamma$ and the ϕ decay branching ratio to K^+K^-.

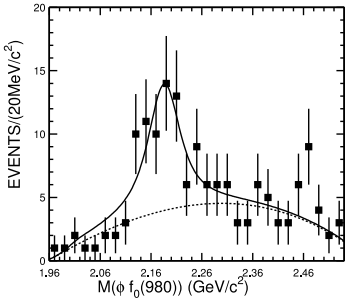

Figure 3: The solid curve is the fit to the data (points with error bars).

3 Observation of a broad 1^{--} resonant structure in the K^+K^- mass spectrum in $J/\psi \to K^+K^-\pi^0$

A broad peak is observed at low K^+K^- invariant mass in $J/\psi \to K^+K^-\pi^0$ decays, detailed analysis is described in Ref. [8].

The Dalitz plot for the selected 10631 events is shown in Fig. 4(b), where a broad K^+K^- band is evident in addition to the $K^*(892)$ and $K^*(1410)$ signals. This band corresponds to the broad peak observed around 1.5 GeV/c^2 in the

K^+K^- invariant mass projection shown in Fig. 4(c).

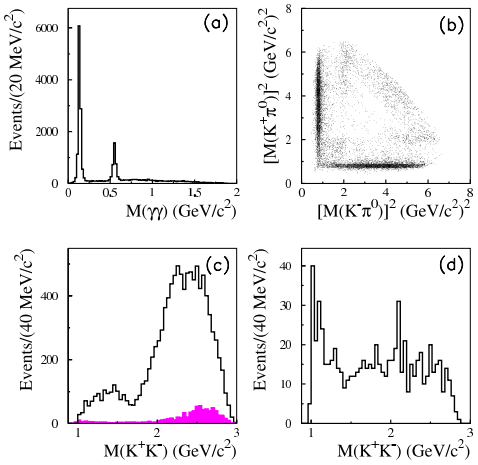

Figure 4: (a) The $\gamma\gamma$ invariant mass distribution. (b) The Dalitz plot for $K^+K^-\pi^0$ candidate events. (c) The K^+K^- invariant mass distribution for $K^+K^-\pi^0$ candidate events; the solid histogram is data and the shaded histogram is the background (normalized to data). (d) The K^+K^- invariant mass distribution for the π^0 mass sideband events (not normalized).

A partial wave analysis shows that the J^{PC} of this structure is 1^{--}. Its pole position is determined to be (1576^{+49+98}_{-55-91}) MeV/c^2 - $i(409^{+11+32}_{-12-67})$ MeV/c^2, and the branching ratio is $B(J/\psi \to X\pi^0)\cdot B(X \to K^+K^-)= (8.5 \pm 0.6^{+2.7}_{-3.6}) \times 10^{-4}$, where the first errors are statistical and the second are systematic. These parameters are not compatible with any known meson resonances.

To understand the nature of the broad 1^{--} peak, it is important to search for a similar structure in $J/\psi \to K_S K^{\pm}\pi^{\mp}$ decays to determine its isospin. It is also intriguing to search for $K^*K, KK\pi$ decay modes. In the mass region of the X, there are several other 1^{--} states, such as the $\rho(1450)$ and $\rho(1700)$, but the width of the X is much broader than the widths of these other mesons. This may be an indication that the X has a different nature than these other mesons. For example, very broad widths are expected for multiquark states.

4 Search for the baryonium candidate X(1860) in $J/\psi \to \omega p\overline{p}$

Decays of the J/ψ meson are regarded as being well suited for searches for new types of hadrons and for systematic studies of light hadron spectroscopy. Recently, a number of new structures have been observed in J/ψ decays. These include strong near-threshold mass enhancements in the $p\overline{p}$ invariant mass spectrum from $J/\psi \to \gamma p\overline{p}$ decays [10], the $p\bar{\Lambda}$ and $K^-\bar{\Lambda}$ threshold enhancements in the $p\bar{\Lambda}$ and $K^-\bar{\Lambda}$ mass spectra in $J/\psi \to pK^-\bar{\Lambda}$ decays [11], the $\omega\phi$ resonance in the $\omega\phi$ mass spectrum in the double-OZI suppressed decay $J/\psi \to \gamma\omega\phi$ [12], and a new resonance, the $X(1835)$, in $J/\psi \to \gamma\pi^+\pi^-\eta'$ decays [13].

The enhancement $X(1860)$ in $J/\psi \to \gamma p\overline{p}$ can be fitted with an S- or P-wave Breit-Wigner (BW) resonance function. In the case of the S-wave fit, the mass is $1859^{+3}_{-10}{}^{+5}_{-25}$ MeV/c^2 and the width is smaller than 30 MeV/c^2 at the 90% confidence level (C.L.). It is of interest to note that a corresponding mass threshold enhancement is not observed in either $p\bar{p}$ cross section measurements or in B-meson decays [14].

This surprising experimental observation has stimulated a number of theoretical interpretations. Some have suggested that it is a $p\bar{p}$ bound state (*baryonium*) [15, 16, 17, 18, 19]. Others suggest that the enhancement is primarily due to final state interactions (FSI) between the proton and antiproton [20, 21].

The CLEO Collaboration published results on the radiative decay of the $\Upsilon(1S)$ to the $p\bar{p}$ system [22], where no $p\bar{p}$ threshold enhancement is observed and the upper limit of the branching fraction is set at $B(\Upsilon(1S) \to \gamma X(1860))B(X(1860) \to p\overline{p}) < 5 \times 10^{-7}$ at 90% C.L.. This enhancement is not observed in BES2 $\psi(2S) \to \gamma p\bar{p}$ data either [23] and the upper limit is set at $B(\psi(2S) \to \gamma X(1860))B(X(1860) \to p\overline{p}) < 5.4 \times 10^{-6}$ at 90% C.L.

The investigation of the near-threshold $p\overline{p}$ invariant mass spectrum in other J/ψ decay modes will be helpful in understanding the nature of the observed new structures and in clarifying the role of $p\overline{p}$ FSI effects. If the enhancement seen in $J/\psi \to \gamma p\overline{p}$ is from FSI, it should also be observed in other decays, such as $J/\psi \to \omega p\overline{p}$, which motivated our study of this channel. In this paper, we present results from an analysis of $J/\psi \to \pi^+\pi^-\pi^0 p\overline{p}$ using a sample of $5.8 \times 10^7 J/\psi$ decays recorded by the BESII detector.

Figure 5 shows the threshold behavior of the $p\bar{p}$ invariant mass distribution where no obvious enhancement is observed. The dotted curve in the figure indicates how the acceptance varies with invariant mass.

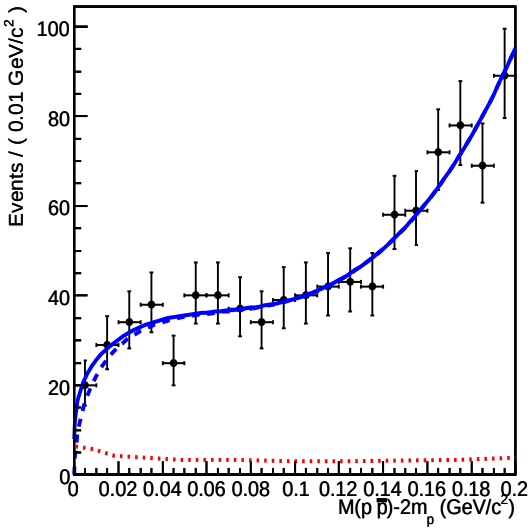

Figure 5: The $M_{p\overline{p}} - 2m_p$ distribution for $J/\psi \to \omega p\overline{p}$ candidate events. The dots with error bars are data. The solid curve is the result of fit described in the text. The dashed curve is the function used to represent the background plus non-resonant $\omega p\overline{p}$ events. The dotted curve indicates how the acceptance varies with $p\overline{p}$ invariant mass.

As shown in Fig. 5, the solid curve is the fit of the $M_{p\overline{p}}$ - $2m_p$ with the BW signal function and $f(\delta)$ function described above. Using the Bayesian method, the 95% C.L. upper limit on the number of observed signal events is 29. Since the J^{PC} of X(1860) is unknown, we use simulated events distributed uniformly in phase space to determine a detection efficiency of $J/\psi \to \omega X(1860)$ ($X(1860) \to p\overline{p}$, $\omega \to \pi^+\pi^-\pi^0$, $\pi^0 \to \gamma\gamma$) of $(4.7 \pm 0.1)\%$. The upper limit of the branching fraction, without considering the systematic errors, is then:

$$B(J/\psi \to \omega X(1860)) \cdot B(X(1860) \to p\overline{p}))$$
$$< \frac{N^{UL}_{obs}}{N_{J/\psi} \cdot \varepsilon \cdot B(\omega \to \pi^+\pi^-\pi^0) \cdot B(\pi^0 \to \gamma\gamma)} = 1.2 \times 10^{-5}.$$

No obvious near-threshold $p\overline{p}$ mass enhancement in $J/\psi \to \omega p\overline{p}$ is observed, and the FSI interpretation of the $p\bar{p}$ enhancement in $J/\psi \to \gamma p\bar{p}$ is disfavored. A conservative estimate of the upper limit is determined by lowering the efficiency by one standard deviation. In this way, a 95% confidence

level upper limit on the branching fraction

$$B(J/\psi \to \omega X(1860)) \cdot B(X(1860) \to p\overline{p})) < 1.5 \times 10^{-5}$$

is determined. The absence of the enhancement $X(1860)$ in $J/\psi \to \omega p\bar{p}$, $\Upsilon(1S) \to \gamma p\bar{p}$ and $\psi(2S) \to \gamma p\bar{p}$ also indicates its similar production property to that of η' [24, 25], *i.e.*, $X(1860)$ is only largely produced in J/ψ radiative decays.

5 Prospects of glueball searches at BESIII

With 10^{10} J/ψ events which is planned to be collected at BESIII, we hope to answer the crucial question in the test of QCD - whether glueballs exists or not. For the scalar glueball, there have been already a few candidate mesons $f_0(1500), f_0(1710), f_0(1790)$, but for the 2^{++} and 0^{-+} glueballs, the situation remains unclear, so I will mainly concentrate on the discussion of 2^{++} and 0^{-+} glueballs

As a tensor gluball candidate in the mass range predicted by the LQCD,, the $\xi(2230)$ was not observed in the mass spectrum of K^+K^-, $\pi^+\pi^-$ or $p\overline{p}$ at BESII. However, in a partial wave analysis (PWA) of $J/\psi \to \gamma KK$ at BESII, the prelimanary results show that it is difficult to exclude the existence of $\xi(2230)$ in this study since it has a significance of 4.5σ and its mass, width and BR are well consistent with what we observed at BESI data [26]. So more careful studies are needed to draw firm conclusions on $\xi(2230$ at BESIII.

In the mass range predicted by the Lattice QCD (LQCD), no other tensor glueball candidates have been observed in the radiative $J\psi$ decays so far. It could be because: 1) The LQCD prediction on the tensor glueball mass is unreliable; 2) The tensor glueball production rate in each exclusive mode is very low; 3) The glueball width is too wide to be observed.

These could also be the similar reasons why no good 0^{-+} glueball candidate was observed so far in $J/\psi \to g\eta'\pi\pi, \gamma\eta\pi\pi, \gamma KK\pi$ in the mass range of 2.3 GeV which is predicted by LQCD. For the above mentioned decay modes, there are experimental difficulties in detecting multi-photon final states at BESII, and significant improvements on these analyses are expected at BESIII with improved detetor especially on the photon detection.

So to sonfirm whether glueball exists in the nature, both experimental and theoretical efforts are needed, especially, the theoretical predictions on the

production rates of glueballs in J/ψ radiative decays and their decay properties (including the full decay width and decay modes) are needed to compare experimental data.

6 Summary

A number of new structures at BESII, including the observation of $Y(2175)$ in $\phi f_0(980)$ mass spectrum in $J/\psi \to \eta\phi f_0(980)$ with $f_0(980) \to \pi^+\pi^-$, the observation of a broad 1^{--} resonance of K^+K^- mass in $J/\psi \to K^+K^-\pi^0$ decays are reviewed New results on baryonium candidate X(1860) are also presented. The non-observation of X(1860) in $J/\psi \to \omega p\overline{p}$ indicates the FSI interpretation of $p\overline{p}$ mass threshold enhancement observed in $J/\psi \to \gamma p\overline{p}$ is obviously disfavored. Finally the prospects of glueball searches at BESIII are discussed.

7 Acknowledgement

The BES collaboration thanks the staff of BEPC and computing center for their hard efforts. This work is supported in part by the National Natural Science Foundation of China under contracts Nos. 10491300, 10225524, 10225525, 10425523, 10625524, 10521003.

References

1. BABAR Collaboration, Phys. Rev. D **74**, 091103(R) (2006).
2. BABAR Collaboration, Phys. ReV. D **76**, 031102 (2007).
3. B. Aubert et al. [BABAR collaboration], Phys. Rev. Lett. **95**, 142001 (2005)
4. Gui-Jun Ding, Mu-lin Yan, Phys. Lett. B **650**, 390-400 (2007).
5. Gui-Jun Ding, Mu-lin Yan, hep-ph/0701047
6. Zhi-Gang Wang, Nucl. Phys. A **791**, 106-116 (2007).
7. BES Collaboration, Nucl. Instr. Meth. A **458**, 627 (2001).
8. BES Collaboration, Phys. Rev. Lett. **97**, 142002 (2006).

9. W.-M. Yao *et al.* (Particle Data Group), J. Phys. G: Nucl. Part. Phys. **33**, 1(2006).

10. J. Z. Bai *et al.* [BES Collaboration], Phys. Rev. Lett. **91**, 022001 (2003).

11. M. Ablikim *et al.* [BES Collaboration], Phys. Rev. Lett. **93**, 112002 (2004); H.X. Yang for the BES Collaboration, Int. J. Mod. Phys. **A20**, 1985 (2005).

12. M. Ablikim *et al.*[BES Collaboration], Phys. Rev. Lett. **96**, 162002 (2006).

13. M. Ablikim *et al.* [BES Collaboration], Phys. Rev. Lett. **95**, 262001 (2005).

14. S. Jin, invited plenery talk at ICHEP04, Beijing, 2004, Int. J. Mod. Phys. A **20**, 5145 (2005).

15. A. Datta and P. J. O'Donnell, Phys. Lett. B **567**, 273 (2003); M. L. Yan, S. Li, B. Wu and B. Q. Ma, Phys. Rev. D **72**, 034027 (2005); B. Loiseau and S. Wycech, Phys. Rev. C **72**, 011001 (2005).

16. J. R. Ellis, Y. Frishman and M. Karliner, Phys. Lett. B **566**, 201 (2003); J. L. Rosner, Phys. Rev. D **68**, 014004 (2003).

17. C. S. Gao and S. L. Zhu, Commun. Theor. Phys. **42**, 844 (2004).

18. G. J. Ding and M. L. Yan, Phys. Rev. C **72**, 015208 (2005).

19. I. S. Shapiro, Phys. Rept. **35**, 129 (1978); C. B. Dover and M. Goldhaber, Phys. Rev. D **15**, 1997 (1977).

20. B. S. Zou and H. C. Chiang, Phys. Rev. D **69**, 034004 (2004).

21. A. Sibirtsev, J. Haidenbauer, S. Krewald, U. G. Meissner and A. W. Thomas, Phys. Rev. D **71**, 054010 (2005).

22. S. B. Athar *et al.* [CLEO Collaboration], Phys. Rev. D **73**, 032001 (2006).

23. M. Ablikim *et al.* [BES Collaboration], Phys. Rev. Lett. **99**, 011802 (2007).

24. S. Jin for the BES Collaboration, talk at ICHEP06, Moscow, 2006

25. E. Klempt and A. Zaitsev, arXiv:0708.4016 [hep-ph].

26. H.B. Liao, PhD thesis, Huazhong Normal Univ. (2005).

Frascati Physics Series Vol. XLVI (2007), pp. 249–260
HADRON07: XII Int. Conf. on Hadron Spectroscopy – Frascati, October 8-13, 2007
Plenary Session

HADRONIC PHYSICS WITH CLEOc

M. R. Shepherd
Indiana University, Bloomington, Indiana 47405

Abstract

The charmonium system provides an opportunity to explore a wide variety of topics in hadronic physics. Studies of the properties of and transitions among $c\bar{c}$ states yield insight into relativistic and non-perturbative QCD effects. At the same time, studies of the decays of charmonium states are a window into gluon dynamics and the role of glueball mixing in the production of light quark states. A collection of preliminary results utilizing the full CLEO-c $\psi(2S)$ data sample is presented including two-body branching fractions of χ_{cJ} decays, a precision measurement of the h_c mass, and results on the hindered M1 transition: $\psi(2S) \to \gamma\eta_c$.

1 The CLEO-c program

The CLEO-c physics program is driven by the wide variety of physics accessible in the charmonium region. Results from large samples of D and D_s decays such

as precision measurements of branching fractions and form factors have direct implication on the global heavy-flavor physics program and searches for new particles or interactions outside of the Standard Model. The CLEO-c program, with the world's largest sample of $\psi(2S)$ decays, is also dedicated to exploring QCD and hadronic physics through studies of the spectrum and decay of $c\bar{c}$ states below open-charm threshold – this physics topic is the focus of what follows.

The CLEO-c detector, from the beam axis outward, consists of a six-layer stereo inner drift chamber, a 47-layer main drift chamber, a ring-imgaging Čerenkov detector (RICH), and a CsI(Tl) crystal calorimeter.[1] The entire detector is immersed in 1-T solenoidal magnetic field. The two drift chambers provide a momentum resolution of $\approx 0.6\%$ for tracks traversing all layers of the chambers. Photon reconstruction with the 7784-crystal calorimeter is achieved with an energy resolution of $\approx 5\%$ at 100 MeV and $\approx 2\%$ at 1 GeV. The detector covers roughly 93% of the full solid angle. The results that follow are derived from a sample of approximately 25 million $\psi(2S)$ decays produced at rest in the lab by symmetric e^+e^- collisions in the Cornell Electron Storage Ring (CESR).

2 Two-body χ_{cJ} decays

The three $\chi_{cJ}(1P)$ states are readily produced in electromagnetic (E1) transitions from the $\psi(2S)$ and provide a venue for the study of a wide variety of QCD phenomena. Each of the analyses below rely on full reconstruction of the entire decay chain: $\psi(2S) \to \gamma\chi_{cJ}$, $\chi_{cJ} \to X$. The initial four-momentum of the $\psi(2S)$ is well known from the beam kinematics; therefore, the experimental resolution can be enhanced by doing a four-contraint kinematic fit of the decay products to the $\psi(2S)$ four-momentum hypothesis.

2.1 $\chi_{c0,2} \to \gamma\gamma$

The two-photon decays of the $\chi_{c0,2}$ states are an ideal place to study relativistic and radiative corrections to QCD in the charmonium system. To first order

[1] Outside of the magnet flux return is a series of muon chambers; however, with a detection threshold of approximately 1.2 GeV/c, the chambers, while ideal for B physics, are only marginally useful for charm physics.

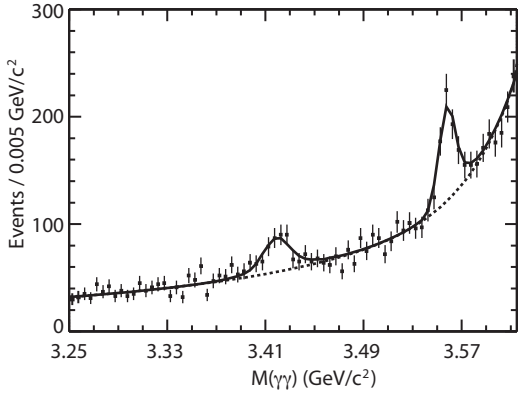

Figure 1: Two-photon invariant mass for χ_c candidates. The χ_{c0} and χ_{c2} peaks are visible. The fit to the spectrum (background contribution) is shown by the solid (dashed) line.

these decays are purely QED. Particular interest is in the ratio $\mathcal{R} \equiv \Gamma(\chi_{c2} \to \gamma\gamma)/\Gamma(\chi_{c0} \to \gamma\gamma)$, which can be calculated simply at first order as $\mathcal{R} = 4/15$ [1]. Deviations from this lowest order calculation result from radiative corrections and relativistic effects; therefore, precise experimental determination of this ratio is important for validating theoretical calculations that consider these effects.

To measure the two-photon widths, events are selected that contain three showers greater than 70 MeV in energy and with $|\cos\theta| < 0.75$. Events with charged particles are vetoed. The signal shapes and efficiencies are derived from a signal Monte Carlo (MC) sample that was generated using the nominal masses and widths of the χ_c states [2]. The angular distributions were modeled as a pure E1 transition from the (beam-axis polarized) $\psi(2S)$ to the χ_c states. The decay of the χ_{c2} state was modeled as a pure helicity-two decay [3].[2] QED-dominated background shapes are obtained from analyzing data off of the $\psi(2S)$ resonance at $\sqrt{s} = 3.671$ GeV and $\sqrt{s} = 3.772$ GeV.

Figure 1 shows the fit to the two-photon invariant mass in data. A total

[2]As a check on the systematic uncertainty due to this assumption up to an 8% helicity-zero component was included, motivated by experimental limits in a_2 decay [4].

Table 1: Various measured parameters for the decays $\chi_{c0,2} \to \gamma\gamma$. The errors are, in order, statististical, systematic, and, where applicable, that due to uncertainty in $\mathcal{B}(\psi(2S) \to \gamma\chi_{c0,2})$ and $\Gamma_{\rm tot}(\chi_{c0,2})$. *All results are preliminary.*

Parameter	This Measurement
$\mathcal{B}(\psi(2S) \to \gamma\chi_{c0}) \times \mathcal{B}(\chi_{c0} \to \gamma\gamma) \times 10^5$	$2.32 \pm 0.33 \pm 0.15$
$\mathcal{B}(\psi(2S) \to \gamma\chi_{c2}) \times \mathcal{B}(\chi_{c2} \to \gamma\gamma) \times 10^5$	$2.82 \pm 0.29 \pm 0.21$
$\mathcal{B}(\chi_{c0} \to \gamma\gamma) \times 10^4$	$2.52 \pm 0.36 \pm 0.16 \pm 0.11$
$\mathcal{B}(\chi_{c2} \to \gamma\gamma) \times 10^4$	$3.20 \pm 0.33 \pm 0.24 \pm 0.18$
$\Gamma(\chi_{c0} \to \gamma\gamma)$ [keV]	$2.65 \pm 0.38 \pm 0.17 \pm 0.25$
$\Gamma(\chi_{c2} \to \gamma\gamma)$ [keV]	$0.62 \pm 0.07 \pm 0.05 \pm 0.06$
$\mathcal{R} \equiv \Gamma(\chi_{c2} \to \gamma\gamma)/\Gamma(\chi_{c0} \to \gamma\gamma)$	$0.235 \pm 0.042 \pm 0.005 \pm 0.030$

of 212 ± 31 and 335 ± 35 events are observed for $\chi_{c0} \to \gamma\gamma$ and $\chi_{c2} \to \gamma\gamma$ respectively. A summary of the preliminary results appears in Table 1. External measurements for $\mathcal{B}(\psi(2S) \to \gamma\chi_{cJ})$ and $\Gamma_{\rm tot}(\chi_{cJ})$ are needed to obtain two-photon branching fractions and partial widths. For these, the PDG average is used [2], and errors due to these external inputs appear as a third, separate systematic error in the table. Dominant experimental systematic errors are due to the fitting method and determination of the signal efficiency.

The obtained preliminary result $\mathcal{R} = 0.24 \pm 0.05$ is the most precise single measurement to date; however, it is not yet precise enough to clearly validate any one particular approach for handling both radiative and relativistic corrections in the charmonium system. When combined with the PDG value of $\mathcal{R} = 0.18 \pm 0.03$ one obtains $\mathcal{R} = 0.20 \pm 0.03$, a value that only marginally disagrees with the zeroth-order prediction of $\mathcal{R} = 4/15 = 0.27$ and motivates more careful experimental and theoretical scrutiny.

2.2 $\chi_{cJ} \to \eta^{(\prime)}\eta^{(\prime)}$

Hadronic decays of χ_c states, like J/ψ, proceed dominantly through annihilation into gluons and provide an ideal environment to try to understand gluon dynamics and glueball production. Hadronic J/ψ decay has received much attention in this regard due to the interesting series of results from BES [5] that study production of scalar f_0 resonances against flavor-tag ω and ϕ states in J/ψ decay. Close and Zhao interpret the results, which appear to be sug-

Table 2: Measured branching fractions and 90% confidence level upper limits for $\chi_{c0,2} \to \eta^{(\prime)}\eta^{(\prime)}$. Where applicable, the errors are statistical, systematic, and due to $\mathcal{B}(\psi(2S) \to \gamma\chi_{cJ})$ respectively. *All results are preliminary.*

X	$\mathcal{B}(\chi_{c0} \to X) \times 10^3$	$\mathcal{B}(\chi_{c2} \to X) \times 10^3$
$\eta\eta$	$3.18 \pm 0.13 \pm 0.18 \pm 0.16$	$0.51 \pm 0.05 \pm 0.03 \pm 0.03$
$\eta\eta'$	< 0.25	< 0.05
$\eta'\eta'$	$2.12 \pm 0.13 \pm 0.11 \pm 0.11$	$0.06 \pm 0.03 \pm 0.004 \pm 0.004$
		(< 0.10)

gestive of large OZI rule violating effects, as a signature for scalar glueball mixing amongst the f_0 states in the 1.5 GeV/c^2 region. Following up on this work, Zhao proposes a factorization scheme in which one can coherently analyze the partial widths of various two-body χ_c decays [7] in terms of singly and doubly OZI suppressed components, where a large doubly OZI suppressed component could also be indicative of strong glueball mixing. A coherent study of $\chi_{cJ} \to \eta^{(\prime)}\eta^{(\prime)}$ provides a testing ground for this production factorization model. In addition Thomas notes [8] that these decays provide a mechanism to explore the gluonic component of the η'.

Like the two-photon decays, analysis of $\chi_{cJ} \to \eta^{(\prime)}\eta^{(\prime)}$ relies on the reconstruction and kinematic fit of the entire event. This analysis is an update of a previous CLEO-c analysis that utilized a subset of the data [9]. The η decay candidates are detected in the modes $\gamma\gamma$, $\pi^+\pi^-\pi^0$, and $\gamma\pi^+\pi^-$, while the η' candidates are reconstructed in $\gamma\pi^+\pi^-$ and $\eta\pi^+\pi^-$ modes. After the kinematic fit, the two body invariant mass distribution is plotted and signals are extracted by fitting the peaks to a Breit-Wigner with widths fixed by the PDG values [2] convoluted with a MC-determined Gaussian resolution. In calculating experimental efficiencies, it is assumed that $\psi(2S) \to \gamma\chi_{c0,2}$ is a pure E1 transition. Branching fractions are summarized in Table 2.

The Zhao model casts the branching fractions as a function of r, a parameter that is equal to the ratio of the strengths of doubly OZI to singly OZI suppressed decays. Figure 2 shows the predicted branching fractions for the $\eta\eta$, $\eta\eta'$, and $\eta'\eta'$ final states as a function of r for both the χ_{c0} and χ_{c2}. One notes that for both the χ_{c0} and χ_{c2} all measured values or limits are consistent with the same value of r lending support for the validity of the model.

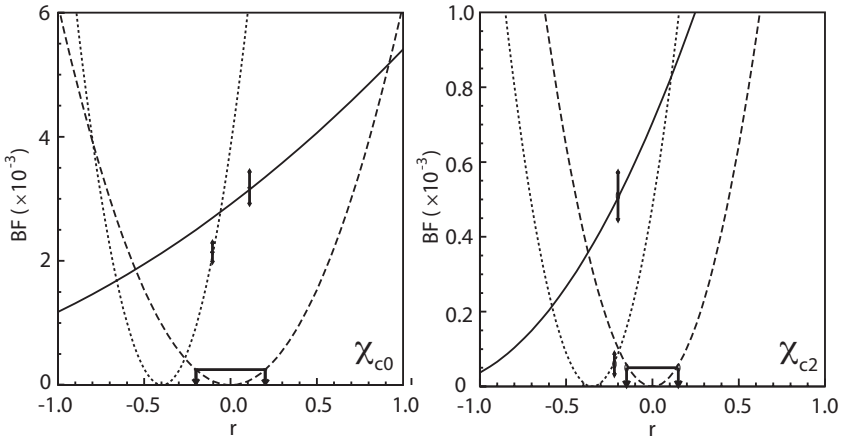

Figure 2: Predictions for the branching fraction of $\chi_{c0,2}$ to $\eta\eta$ (solid), $\eta\eta'$ (dashed), and $\eta'\eta'$ (dotted) as a function the model parameter r, which is the ratio of doubly to singly OZI suppressed decays. Experimental measurements presented in this work are indicated by the arrows.

One also notes that the value of r is close to zero which indicates a relatively small component of doubly OZI suppressed production, consistent with what is commonly accepted as small glueball mixing amongst the isoscalar pseudoscalar mesons. Applications of this technique to the scalar meson sector are underway at CLEO-c and BES.

2.3 Other two-body decays

In addition to probing the role of glueball mixing in production, two-body decays of χ_c states provide an opportunity to explore the role of the color octet mechanism (COM) in P-wave charmonia. The COM was proposed [10] to explain the apparent deficit in theoretically predicated decay rates for nucleon-antineucleon pairs based on the color singlet model, and therefore motivates a new series of precision measurements of two-body P-wave charmonia decay.

The analysis of these decays proceeds in the same fashion as those mentioned above, namely exploiting the power of the full event kinematic fit to improve resolution and reduce background. The final states reconstructed are listed in Tables 3 and 4. The hyperon decays are reconstructed in the following

Table 3: Measured branching fractions for various two-meson χ_{cJ} decays. The errors are statistical, systematic, and due to $\mathcal{B}(\psi(2S) \to \gamma\chi_{cJ})$ respectively. *All results are preliminary.*

X	$\mathcal{B}(\chi_{c0} \to X) \times 10^3$	$\mathcal{B}(\chi_{c2} \to X) \times 10^3$
$\pi^+\pi^-$	$6.37 \pm 0.11 \pm 0.20 \pm 0.32$	$1.59 \pm 0.04 \pm 0.06 \pm 0.10$
$\pi^0\pi^0$	$2.94 \pm 0.07 \pm 0.16 \pm 0.15$	$0.68 \pm 0.03 \pm 0.05 \pm 0.04$
K^+K^-	$6.47 \pm 0.11 \pm 0.29 \pm 0.32$	$1.13 \pm 0.03 \pm 0.05 \pm 0.07$
$K^0_S K^0_S$	$3.49 \pm 0.01 \pm 0.15 \pm 0.17$	$0.53 \pm 0.03 \pm 0.02 \pm 0.03$

Table 4: Measured branching fractions for various two-baryon χ_{cJ} decays. The errors are statistical, systematic, and due to $\mathcal{B}(\psi(2S) \to \gamma\chi_{cJ})$ respectively. *All results are preliminary.*

X	$\mathcal{B}(\chi_{c0} \to X) \times 10^5$	$\mathcal{B}(\chi_{c1} \to X) \times 10^5$	$\mathcal{B}(\chi_{c2} \to X) \times 10^5$
$p\bar{p}$	$25.7 \pm 1.5 \pm 1.5 \pm 1.3$	$9.0 \pm 0.8 \pm 0.4 \pm 0.5$	$7.7 \pm 0.8 \pm 0.4 \pm 0.5$
$\Lambda\bar{\Lambda}$	$33.8 \pm 3.6 \pm 2.3 \pm 1.7$	$11.6 \pm 1.8 \pm 0.7 \pm 0.7$	$17.0 \pm 2.2 \pm 1.1 \pm 1.1$
$\Sigma^0\bar{\Sigma}^0$	$44.1 \pm 5.6 \pm 2.5 \pm 2.2$	$2.1 \pm 1.4 \pm 0.2 \pm 0.1$	$4.1 \pm 1.9 \pm 0.3 \pm 0.3$
$\Sigma^+\bar{\Sigma}^-$	$32.5 \pm 5.7 \pm 4.9 \pm 1.7$	$3.3 \pm 1.8 \pm 0.2 \pm 0.2$	$3.3 \pm 1.9 \pm 0.4 \pm 0.2$
$\Xi^0\bar{\Xi}^0$	$33.4 \pm 7.0 \pm 3.2 \pm 1.7$	$2.5 \pm 2.1 \pm 0.2 \pm 0.2$	$4.0 \pm 2.4 \pm 0.4 \pm 0.3$
$\Xi^-\bar{\Xi}^+$	$51.4 \pm 6.0 \pm 3.8 \pm 2.6$	$8.6 \pm 2.2 \pm 0.6 \pm 0.5$	$14.5 \pm 1.9 \pm 1.0 \pm 0.9$

modes: $\Lambda \to p\pi^-$, $\Sigma^+ \to p\pi^0$, $\Sigma^0 \to \Lambda\gamma$, $\Xi^- \to \Lambda\pi^-$, and $\Xi^0 \to \Lambda\pi^0$. As with the two-photon decays, the kinematically constrained two-body invariant mass distributions are fit to extract the yield for each of the χ_c signal peaks. Experimental efficiency is determined using a MC simulation. For decays of the χ_{c1} and χ_{c2} to two hyperons, the helicity of the final state is unknown and the range of efficiencies for the allowed helicity configurations is used to quantify the systematic error due to this uncertainty.

The results are summarized in Tables 3 and 4 and represent the most precise measurements to date of these two-body branching fractions. While a detailed comparison of the results the COM predictions [10] is not possible here, in general, measured branching fractions tend to be higher than those predicted by the COM-motivated predictions suggesting further theoretical understanding of these decays is needed.

3 The hindered M1 transition: $\psi(2S) \to \gamma\eta_c$

A clear experimental picture of both the hindered ($\psi(2S) \to \gamma\eta_c$) and allowed ($J/\psi \to \gamma\eta_c$) M1 transitions in charmonium is important for understanding a variety of theoretical and experimental issues. For example, there is interest in using radiative transitions in charmonium to explore photon couplings to quarks in lattice QCD [11]. Calculating these two rates has been a challenge for quark models [12]. Both rates are key in normalizing exclusive branching fractions of the η_c; the focus here is on $\mathcal{B}(\psi(2S) \to \gamma\eta_c)$. As will be discussed in detail below, the η_c lineshape in this decay appears to be non-trivial, and this complicates the measurement of the rate.

To examine the lineshape in detail, thirteen signal-rich η_c decay modes (and charge conjugates) are reconstructed: $2(\pi^+\pi^-)$, $\pi^+\pi^-\pi^0\pi^0$, $3(\pi^+\pi^-)$, $2(\pi^+\pi^-\pi^0)$, $2(K^+K^-)$, $K^+K_S\pi^-$, $K^+K^-\pi^0$, $K^+K^-\pi^+\pi^-$, $K^+K_S\pi^+\pi^-\pi^-$, $K^+K^-\pi^+\pi^-\pi^0$, $K^+K^-2(\pi^+\pi^-)$, $\eta\pi^+\pi^-$, and $\eta 2(\pi^+\pi^-)$. Like the χ_{cJ} decays, full event reconstruction and kinematic fitting is employed for these candidates. Figure 3 (left) shows the photon spectrum after it has been sharpened by the kinematic fit. The background is fit to a (MC-motivated) linear function using data in the region $E_\gamma > 900$ MeV and $560 < E_\gamma < 600$ MeV. Peaking backgrounds below 560 MeV are due to $h_c \to \gamma\eta_c$, photon cascades from $\psi(2S)$ to χ_c to J/ψ states, and $\psi' \to \pi^0 J/\psi$, where, for the latter two backgrounds, the two photons merge in the calorimeter. The signal shows a distinct tail on the high energy side of the photon spectrum.

Modification of the line shape for this transition is expected since the natural width is relatively large and the available phase space grows like E_γ^3. In addition the hindered M1 transition has an additional E_γ^2 term in the matrix element [13] that may enhance the line shape distortion. These additional line shape modifications, while theoretically motivated, are not constrained well enough to allow a satisfactory fit to the data and lead one to question whether this transition is suitable for extracting the mass and width of the η_c.

Figure 3 (right) shows the exclusive photon spectrum before kinematic fitting (red line) superimposed on the background-subtracted inclusive photon spectrum (points). The agreement is excellent indicating that the line shape modification is visible also in the raw inclusive photon spectrum. A variety of techniques are used to extract the yield in the inclusive photon spectrum including using an empirical parametrization of the peak and simply counting

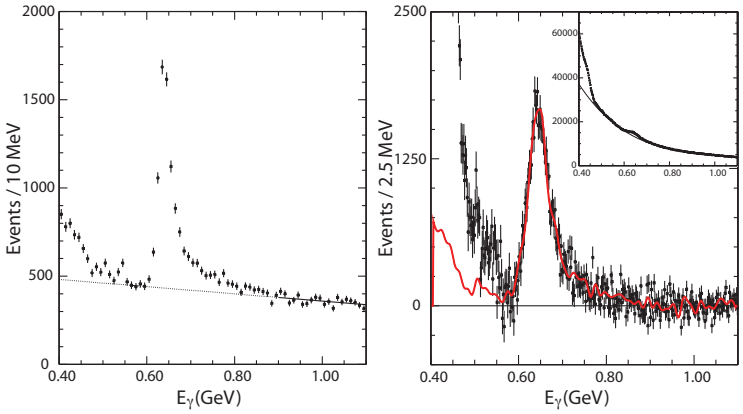

Figure 3: Left: The photon spectrum the process $\psi(2S) \to \gamma\eta_c$ for exclusively reconstructed η_c states and after a full event kinematic fit. The intrinsic lineshape dominates the experimental resolution, which varies from 4-7 MeV depending on η_c decay mode. Right: The background subtracted inclusive photon spectrum (raw shown in inset). The exclusive lineshape before the kinematic fit is superimposed as a solid (red) line.

events above background. The 10% uncertainty in the number of signal events due to uncertainties in background and signal lineshape is the dominant systematic uncertainty in the measurement of $\mathcal{B}(\psi(2S) \to \gamma\eta_c)$. Our preliminary result is $\mathcal{B}(\psi(2S) \to \gamma\eta_c) = (4.02 \pm 0.11 \pm 0.52) \times 10^{-3}$.

4 The mass of the h_c

The singlet $h_c(^1P_1)$ state was the last of the expected charmonium states below $D\bar{D}$ threshold to be identified [14]. There is interest in understanding the hyperfine splittings of the charmonium states as these give insight into the nature of the spin-spin interaction in QCD. In the limit that the confinement term in the QCD potential carries no spin dependence, one expects non-zero hyperfine splitting for only $L = 0$ states, and the mass of the h_c ($L = 1$) should be equal to the spin-averaged χ_{cJ} mass. Therefore precision measurement of this splitting $\Delta M_{\rm hf}(1P) = \langle M(^3P_J)\rangle - M(^1P_1)$ provides experimental input on the spin dependence of the $q\bar{q}$ interaction. The error on $\Delta M_{\rm hf}$ is currently

dominated by error on the mass of the h_c; hence, a more precise measurement is desirable.

The h_c is studied in the isospin-violating process $\psi(2S) \to \pi^0 h_c,\ h_c \to \gamma\eta_c$. Two methods are utilized: one that is inclusive of all η_c decay modes and another that reconstructs the η_c in a collection of exclusive hadronic modes, which mostly overlap with those noted in the previous section. Both require a signal π^0 from the primary transition $\psi(2S) \to \pi^0 h_c$ be identified from two-photon candidates within three standard deviations of the π^0 mass and extract the signal from fits to recoil mass spectrum against this π^0.

The inclusive analysis relies on the identification of a candidate photon for the $h_c \to \gamma\eta_c$ transition with an energy of 503 ± 35 MeV. Removing this criteria overwhelms the signal with background and allows one to determine the background shape. Figure 4 (left) shows the fitted π^0 recoil mass spectrum. The signal shape is Breit-Wigner with width fixed to that of the χ_{c1} convoluted with a Gaussian resolution function of width 2.5 MeV/c^2. The mass obtained is $3525.35 \pm 0.24 \pm 0.21$ MeV/c^2. The angular distribution of the photon in the $h_c \to \gamma\eta_c$ is consistent with that of an $E1$ transition: $dN/d\cos\theta_\gamma \propto 1 + \alpha\cos^2\theta_\gamma$, where $\alpha = 1$. We obtain $\alpha = 1.34 \pm 0.53$ from the data.

The exclusive analysis, like other exclusive analyses mentioned above, relies on full reconstruction and kinematic fit of the entire decay chain. The mass of the η_c candidate was required to be within 30 MeV/c^2 of the nominal η_c mass [2]. The π^0 recoil spectrum from the set of exclusive candidates is shown on the right of Figure 4 and is fit to a linear background plus a Breit-Wigner convoluted with a double-Gaussian resolution function obtained from MC. The mass obtained from the fit is $3525.35 \pm 0.27 \pm 0.20$ MeV/c^2.

Accounting for statistical correlations between the exclusive and inclusive samples, we obtain the preliminary result: $M(h_c) = 3525.35 \pm 0.19 \pm 0.15$ MeV/c^2. This yields a hyperfine splitting $\Delta M_{\rm hf}(1P) = -0.05 \pm 0.19 \pm 0.16$ MeV/c^2, which is remarkably consistent with zero. However, Richard [15] cautions against interpreting this result as a lack of spin-spin interactions in the $1P$ multiplet as $M(h_c)$ should really be compared with the spin-averaged χ_c mass as calculated in the potential model, which is several MeV higher.

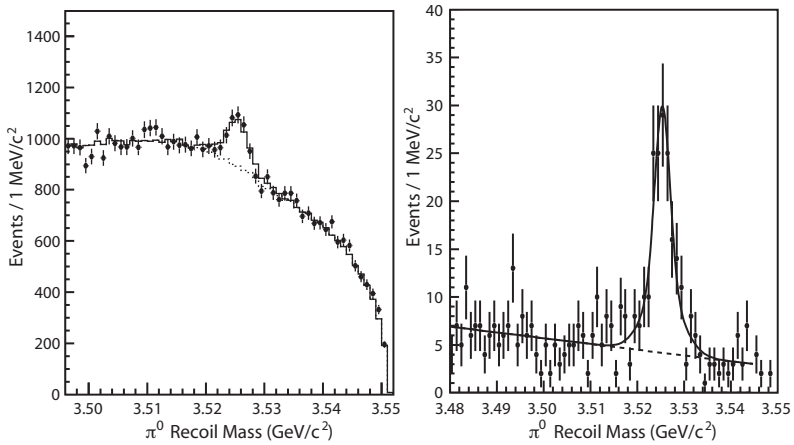

Figure 4: Plots of the recoil mass against the π^0 for inclusive (left) and exclusive (right) η_c selection. The h_c signal is clearly visible in both cases. Fits to the spectra (background contributions) are shown by the solid (dashed) lines.

5 Summary

The charmonium system provides a rich landscape to study QCD. We have presented precision measurements for many two-body decays of the χ_{cJ} states, which have implications in understanding relativistic and radiative corrections in the charmonium system, the role of the color octet mechanism in P-wave decay, and glueball mixing amongst the light scalar mesons. The hindered M1 transition, $\psi(2S) \to \gamma\eta_c$, exhibits a non-trivial lineshape that is necessary to understand theoretically if precision experimental measurements for the partial width for this decay and the mass and width of the η_c are to be obtained. Finally we presented a new precision measurement of the mass of the h_c that is naively consistent with zero hyperfine splitting in the $1P$ multiplet of charmonium.

Analysis of the large sample of $\psi(2S)$ collected with the CLEO-c detector continues, and more exciting hadronic physics results are expected in the coming year. I would like to acknowledge the work of my CLEO colleagues on these analyses. I would also like to thank the HADRON 07 organizers for providing a wonderful venue to present these results.

References

1. R. Barbieri, R. Gatto and R. Kogerler, Phys. Lett. B **60**, 183 (1976).
2. W.-M. Yao *et al.*, Journal of Physics G **33**, 1 (2006) and 2007 partial update for the 2008 edition.
3. Z. P. Li, F. E. Close and T. Barnes, Phys. Rev. D **43**, 2161 (1991).
4. H. J. Behrend *et al.* [CELLO Collaboration], Z. Phys. C **46**, 583 (1990).
5. M. Ablikim *et al.* [BES Collaboration], Phys. Lett. B **607**, 243 (2005); M. Ablikim *et al.* [BES Collaboration], Phys. Lett. B **603**, 138 (2004).
6. F. E. Close and Q. Zhao, Phys. Rev. D **71**, 094022 (2005).
7. Q. Zhao, Phys. Rev. D **72**, 074001 (2005); Q. Zhao, accepted by Phys. Lett. B, arXiv:0705.0101 [hep-ph].
8. C. E. Thomas, JHEP **0710**, 026 (2007).
9. G. S. Adams [CLEO Collaboration], Phys. Rev. D **75**, 071101 (2007) [Erratum-ibid. D **75**, 079901 (2007)].
10. S. M. H. Wong, Eur. Phys. J. C **14**, 643 (2000).
11. J. J. Dudek, R. G. Edwards and D. G. Richards, Phys. Rev. D **73**, 074507 (2006).
12. See, for example: E. Eichten, S. Godfrey, H. Mahlke and J. L. Rosner, arXiv:hep-ph/0701208.
13. N. Brambilla, Y. Jia and A. Vairo, Phys. Rev. D **73**, 054005 (2006).
14. J. L. Rosner *et al.* [CLEO Collaboration], Phys. Rev. Lett. **95**, 102003 (2005); P. Rubin *et al.* [CLEO Collaboration], Phys. Rev. D **72**, 092004 (2005); M. Andreotti *et al.*, Phys. Rev. D **72**, 032001 (2005).
15. J. M. Richard, $15^{\rm th}$ International Workshop on Deep-Inelastic Scattering and Related Subjects (DIS2007), Munich, Germany, 16-20 Apr 2007, arXiv:0706.0158 [hep-ph].

Frascati Physics Series Vol. XLVI (2007), pp. 261–274
HADRON07: XII Int. Conf. on Hadron Spectroscopy – Frascati, October 8-13, 2007
Plenary Session

EXPLORING THE QUARK GLUON PLASMA AT RHIC AND LHC – TODAY'S PERSPECTIVE

John W. Harris
Physics Department, Yale University
P.O. Box 208124, 272 Whitney Avenue, New Haven CT, U.S.A. 06520-8124

Abstract

Ultra-relativistic collisions of heavy ions at the Relativistic Heavy Ion Collider (RHIC) and in the future at the Large Hadron Collider (LHC) form a hot system at energy densities far above where normal hadrons can exist. Results from RHIC indicate temperatures above the quark-hadron phase boundary predicted by Quantum Chromodynamics (QCD) on a lattice. A large amount of collective flow is observed and the final state distributions of hadrons can be described by ideal hydrodynamics with zero viscosity. This suggests that a nearly perfect fluid of quarks and gluons is produced, with viscosities that approach a universal lower bound postulated from string theory. The suppression of both light (u, d, s) and heavy (c, b) hadrons at large transverse momenta and the quenching of di-jets provide evidence for extremely large energy loss of partons as they propagate through a dense, strongly-coupled medium. Future fascinating results are anticipated both at RHIC and the LHC.

1 Introduction

A few micro-seconds after the Big Bang all matter in the Universe existed in the form of a quark-gluon plasma (QGP). As the Universe cooled, a quark-hadron phase transition occurred and the nuclear particles we know today formed from quarks and gluons. Further insight into the behavior and properties of extremely hot matter in Quantum Chromodynamics (QCD) can be gained from investigating the strong force at high temperatures.

The strong coupling constant characterizes the strength of the strong force. Fig.1 depicts the quark-antiquark coupling constant α_{qq} as a function of quark separation for various temperatures as calculated on a lattice in QCD. [1)] As the quark-antiquark separation increases and approaches 1 femtometer (fermi), the strong coupling constant (α_s) becomes increasingly large. So large that quarks become confined within a distance of $\sim$ 1 fermi, which is the size of nuclear particles and they cannot escape - this is called confinement. At the other extreme, that of short distances, the strong coupling constant is weak and quarks interact without much force, almost freely - this is called asymptotic freedom. [2)] The behavior of the strong coupling constant as a function of temperature is important to understanding, among other things, how the hot Universe evolved as it cooled down. As the Universe cooled from a QGP through the quark-hadron phase transition temperature (denoted T_c), the strong coupling constant is seen in Fig.1 to increase in strength making a transition between asymptotically free quarks to quarks confined in hadrons. Calculations of the energy density on the lattice as a function of temperature exhibit a relatively sharp deconfinement transition at a temperature $T_c \sim 175$ MeV. [3)]

The Relativistic Heavy Ion Collider (RHIC) at Brookhaven National Laboratory in the U.S. began colliding nuclei at ultra-relativistic energies in 2000 to investigate the properties of hot, dense QCD. RHIC accelerates and collides a range of nuclei from protons to gold (Au) at center-of-mass energies up to $\sqrt{s}$ = 500 GeV for p + p and $\sqrt{s_{NN}}$ = 200 GeV for Au + Au. RHIC and its four experiments (BRAHMS, PHENIX, PHOBOS, and STAR) are described comprehensively in Ref. [4)]. The Large Hadron Collider (LHC) heavy ion program will explore farther into the high energy density regime of QCD. The LHC will collide nuclei at a top energy of $\sqrt{s_{NN}}$ = 5.4 TeV for Pb + Pb with ALICE, Atlas and CMS expected to participate in heavy ion data-taking.

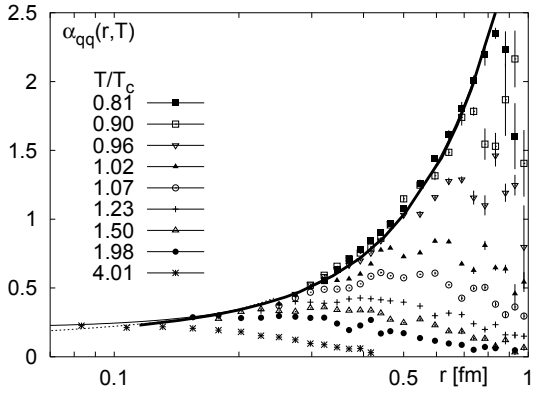

Figure 1: *The quark-antiquark coupling in QCD calculated on a lattice for several temperatures below and above the deconfinement temperature T_c as a function of quark separation.* [1] *Solid curve is the coupling at zero temperature.*

2 Extreme Energy Densities Created at RHIC

An initial objective of RHIC was to determine the energy density in the initial colliding system and to establish whether it surpasses the critical energy density that is necessary for creating the QGP phase transition. Measurements of the transverse energy per unit pseudorapidity $dE_T/d\eta$ and the mean transverse momentum per particle were used to estimate the energy density assuming a Bjorken longitudinal expansion scenario. The energy density can be estimated by $\epsilon_{Bj} = \frac{1}{\tau_o \pi R^2} \times \frac{dE_T}{dy}$, with dE_T/dy the transverse energy per unit rapidity, R the transverse radius of the system, and τ_o the formation time. Assuming a maximum value for the formation time $\tau_o = 1$ fm/c, an estimate of the minimum energy density for the 5% (2%) most central Au + Au collisions at $\sqrt{s_{NN}} = 130$ GeV is 4.3 GeV/fm^3 (4.6 GeV/fm^3) and 4.9 GeV/fm^3 for the 5% most central Au + Au collisions at $\sqrt{s_{NN}} = 200$ GeV. [5] This lower limit on the energy density at RHIC is approximately twenty-five times normal nuclear matter density ($\epsilon_{n.m.} = 0.17$ GeV/fm^3) and seven times the critical energy density ($\epsilon_c = 0.6$ GeV/fm^3) predicted by lattice QCD for formation of the QGP. Energy densities 2 - 4 times larger than observed at RHIC are anticipated with heavy ions at the LHC.

3 Observation of Strong Elliptic Flow at RHIC

Unlike the case for collisions of elementary particles, nuclei colliding with non-zero impact parameter have an inherent spatial asymmetry associated with the asymmetric region of overlap. The larger the impact parameter, the larger the initial matter asymmetry perpendicular to the reaction plane.[1] Hadrons are observed to be emitted preferentially in the reaction plane at RHIC. [6)]

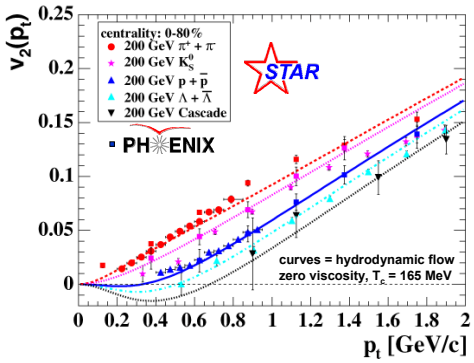

Figure 2: *Elliptic flow* v_2 *for* $\sqrt{s_{NN}}$ *= 200 GeV Au + Au minimum bias collisions as a function of* p_T *for* $\pi^{\pm}$, K^0_s, $p + \overline{p}$, $\Lambda + \overline{\Lambda}$, *and* $\Xi + \overline{\Xi}$. *Curves are predictions of ideal hydrodynamics.*

To study this azimuthal anisotropy in quantitative detail the second Fourier harmonic component of the azimuthal distribution of particles in momentum space is constructed with respect to the reaction plane, $v_2 = \langle \cos(2\phi) \rangle$ where $\phi = \text{atan}\ (p_y/p_x)$. The v_2 is called the elliptic flow. Displayed in Fig.2 is v_2 for $\pi^{\pm}$, K^0_s, $p + \overline{p}$, $\Lambda + \overline{\Lambda}$, and $\Xi + \overline{\Xi}$ as a function of p_T in $\sqrt{s_{NN}} = 200$ GeV Au + Au minimum bias collisions. [7)] This has only been explained by the presence of large pressure gradients that generate the elliptic flow early in the collision process. The elliptic flow is well described at these low transverse momenta by hydrodynamical models (curves in Fig.2) incorporating a softening of the equation of state due to quark and gluon degrees of freedom and

[1]The reaction plane is the plane containing the incident beam and impact parameter vectors.

zero viscosity. [8] Such low viscosities were not expected nor observed before for hadronic or nuclear systems.

The v_2 measured for $\pi^{\pm}$, K^0_s, p + $\overline{p}$, $\Lambda + \overline{\Lambda}$, and $\Xi + \overline{\Xi}$ at higher p_T are displayed in Fig. 3a for $\sqrt{s_{NN}} = 200$ GeV Au + Au minimum bias collisions. [7] The mesons and baryons cross over near $p_T = 2$ GeV/c, above which the baryons exhibit higher values of v_2 than the mesons. This is more easily seen in Fig.3b where the v_2 is plotted as a function of the transverse kinetic energy (KE_T) of the identified hadrons. The data converge to two distinct groups, one for baryons and one for mesons. Larger values of v_2 for baryons than mesons may result from the creation of hadrons in soft processes and boosted to higher p_T by collective flow. Coalescence of quarks to form composite hadrons may also contribute.

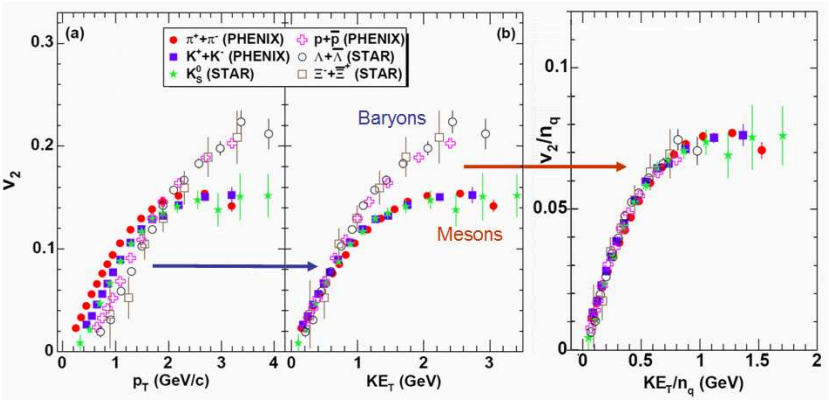

Figure 3: *Elliptic flow v_2 measured for $\pi^{\pm}$, K^0_s, $p + \overline{p}$, $\Lambda + \overline{\Lambda}$, and $\Xi + \overline{\Xi}$ as a function of a) p_T and b) transverse kinetic energy KE_T. c) Elliptic flow per quark (v_2/n_q) as a function of KE_T per quark (KE_T/n_q).*

Displayed in Fig. 3c is v_2 per quark (v_2/n_q) for $\pi^{\pm}$, K^0_s, p + $\overline{p}$, $\Lambda + \overline{\Lambda}$, and $\Xi + \overline{\Xi}$ as a function of KE_T per quark (KE_T/n_q). [7] When v_2 is plotted per quark (v_2/n_q) for baryons and mesons, the values of v_2/n_q scale with KE_T/n_q over the entire range of KE_T. This is consistent with a quark coalescence picture for hadrons and is evidence for early collective flow at the quark level. This observation coupled with the extremely low to non-existent viscosity has led to descriptions of the system in terms of a nearly perfect liquid

(non-viscous) of quarks and gluons. [9]

There has been recent application of string theoretical concepts to describe the observation of the extremely low viscosity at RHIC. This utilizes a conjecture [10] of the equivalence between a string theory in an n-dimensional space and a quantum field theory on the n-1 dimensional conformal boundary of this space. This equivalence between our 4-dimensional (4D) Universe and its 5-dimensional (5D) space-time volume has been termed the Holographic Principle by t'Hooft and Susskind. [11] Also, a black hole singularity in a particular 5D volume was shown to correspond to a hot system of quarks and gluons on the 4D space-time boundary. [12] Therefore, the so-called AdS/CFT (anti-De-Sitter space/conformal field theory) correspondence is a conjectured equivalence between a string theory with gravity in a space-time volume, and a quantum field theory without gravity on the conformal boundary of this volume. This AdS/CFT correspondence can be used to determine the viscosity in a 4D world, assuming a strongly coupled N = 4 super-symmetric Yang-Mills (SUSY YM) conformal field theory, from a completely different approach with a tractable calculation and solution in a 5D space (AdS_5). A universal lower bound is found for the shear viscosity (η) to entropy (s) ratio of $\eta/s = 1/4\pi$. [13] This lower bound is similar in value to the η/s extracted at RHIC and considerably lower than other known fluids. It will be interesting to see the extent to which the properties of the hot system formed with heavy ions at the LHC are similar or dissimilar to those at RHIC.

4 Is the System Thermalized?

If the system can be described in terms of equilibrium thermodynamics, the ratios of the various types of particles must be reproduced with a consistent set of thermodynamic variables. Statistical and thermodynamic models reproduce the measured ratios using as variables the chemical freeze-out temperature (T) and the baryo-chemical potential (μ_B). These models employ hadronic degrees of freedom in a grand canonical ensemble. Displayed in Fig. 4 are the particle ratios measured at RHIC along with results of a statistical-thermal model fit. [14] The particle ratios for $\sqrt{s_{NN}} = 130$ GeV Au + Au can be fit with the parameters T = 176 MeV and $\mu_B = 41$ MeV. For $\sqrt{s_{NN}} = 200$ GeV Au + Au, T = 177 MeV and $\mu_B = 29$ MeV are required. The statistical-thermal model fits reproduce the data extremely well. When the same approach is

applied to lower energy data [15] and the RHIC data, chemical freeze-out follows a curve in the (μ_B, T) plane that approaches the deconfinement phase transition boundary that is predicted by lattice QCD. The μ_B and T parameters fit to the ratios of hadrons observed at the LHC are not expected to differ much from those observed at RHIC, since the these parameters only reflect the chemical freeze-out stage of the collision, which should not change appreciably.

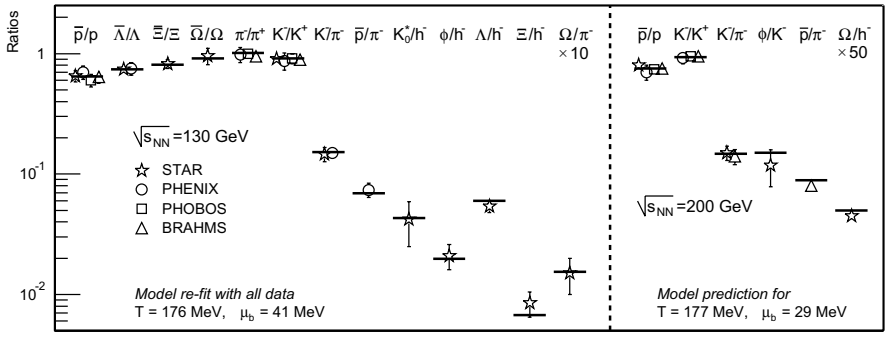

Figure 4: *Particle ratios measured in RHIC experiments denoted by symbols in the legend for central collisions of Au + Au at $\sqrt{s_{NN}}$ = 130 GeV (left panel) and 200 GeV (right panel). Results from a statistical-thermal model fit to the entire set of data are shown as a horizontal line for each ratio. Parameters (μ_B, T) for the best fit at each energy are shown at the bottom of each panel.*

5 Suppression of Large Transverse Momentum Particles

Hard scattering can be used to probe the medium through which the hard-scattered partons propagate. The radiation energy loss of a parton traversing a dense medium is predicted to be significant and is sensitive to the gluon density of the medium. [16] To investigate parton energy loss in the medium, the RHIC experiments have measured hadron spectra and azimuthal correlations of hadrons with large transverse momentum.

In order to compare results from relativistic heavy ion collisions to elementary p + p interactions, a nuclear modification factor R_{AA} is defined as $R_{AA}(p_T) = \frac{dN^2/dp_T dy\ (AA)}{\langle N_{binary}\rangle dN^2/dp_T dy\ (NN)}$. $\langle N_{binary}\rangle$ is the number of binary collisions in a geometrical model in order to scale from elementary nucleon-nucleon

(NN) collisions to nucleus-nucleus (AA) collisions. When $R_{AA} = 1$, AA collisions can be described as an incoherent superposition of NN collisions, as predicted by perturbative QCD (pQCD). This corresponds to scaling with the number of binary collisions (binary scaling).

5.1 Light Hadrons

Suppression of the charged hadron spectra at large transverse momenta has been observed in a reduction of the measured nuclear modification factors by a factor of 4 - 5 for $p_T > 2$ GeV/c in central Au + Au collisions at mid-rapidity at RHIC. [17] In addition, R_{AA} of γ, π^0 and η have been measured as a function of p_T for central Au + Au collisions. [18] $R_{AA}(\gamma) \sim 1$, as expected for the non-strongly-interacting photon, while the $R_{AA}(\pi^0)$ and $R_{AA}(\eta)$ are suppressed by $\sim$ 4 - 5 like that for charged hadrons. Peripheral collision Au + Au data and d + Au data (not shown) exhibit no nuclear modification, i.e. $R_{AA} \sim 1$, within errors. Also shown in Fig. 5 is a calculation of parton energy loss with a gluon density $dn_{gluon}/dy = 1100$ [19] which describes the suppression of light hadrons at RHIC. This is equivalent to an energy loss per unit length that is approximately 15 times that of normal nuclear matter.

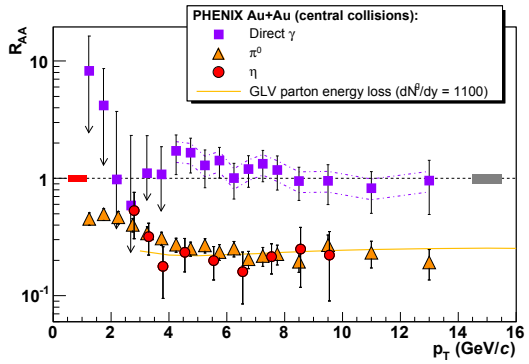

Figure 5: *Nuclear modification factor for $\sqrt{s_{NN}}$ = 200 GeV central Au + Au from PHENIX for γ, π^0 and η as a function of p_T from PHENIX. The curve is a pQCD calculation with parton energy loss. See text for description.*

5.2 Charm and Beauty Hadrons

Heavier charm and beauty quarks are expected to lose less energy than light quarks while propagating through a dense colored medium. The large heavy quark mass reduces the available phase space for gluon radiation. This has been called the "dead cone effect". [20] PHENIX and STAR have measured the spectra of non-photonic electrons in $\sqrt{s_{NN}}$ = 200 GeV p + p and Au + Au collisions over a range of impact parameters. After subtraction of electrons from photon conversions and light hadron decays, the resulting non-photonic electron spectra are predominantly from semi-leptonic decays of heavy quarks (D- and B-meson decays). The R_{AA} for non-photonic electrons from decays of D- and B- mesons measured in central collisions at RHIC [21] are found to be suppressed to approximately the same degree as that of light hadrons.

5.3 Model Descriptions of Suppression

The non-photonic electron results can be compared to predictions of various models. A calculation that utilizes energy loss from induced gluon radiation with a gluon density of $dn_{gluon}/dy = 1000$ describes the observed light quark suppression. [22] Utilizing BDMPS radiative energy loss for charm and beauty from multiple soft collisions with a transport coefficient $\hat{q}$ = 14 GeV^2/fm, is also consistent with light quark suppression. [23] But, neither calculation produces sufficient energy loss and suppression to reproduce the heavy quark (non-photonic electron) suppression. When elastic scattering energy and effects of gluon radiation are included, the resulting suppression is still insufficient to account for the measured heavy quark suppression and energy loss. [24] Overall, the inability of the models to reproduce the heavy quark suppression calls into question our understanding of the propagation of heavy quarks in the medium. Further experimental results at RHIC and the LHC that separate charm and beauty are necessary to resolve this dilemma. The large heavy quark production cross sections make this a lucrative enterprise with heavy ions at the LHC.

Initial calculations of jet quenching have been performed using AdS/CFT correspondence. [25] The results give $\hat{q}$ = 4.5, 10.6, 20.7 GeV^2/fm for a range of temperatures of the medium of T = 300, 400, 500 MeV, respectively. This is remarkably close to what is expected at RHIC.

6 Effects of Jet Quenching on Azimuthal Correlations

Two-particle correlations of high p_T hadrons can be used to extract the hard scattering component from the soft background at RHIC. The fragmentation of partons produces jets, a phase space clustering of particles in a small region of relative azimuth ($\Delta\phi$) and pseudorapidity ($\Delta\eta$). As seen in Fig. 6 an enhancement is observed at $\Delta\phi = 0$ in azimuthal correlations near midrapidity upon correlating charged hadrons having $4 < p_T^{trig} < 6$ GeV/c with all other charged hadrons having 2 GeV/c $< p_T < p_T^{trig}$ in the same event. This has been seen in collisions of Au + Au at $\sqrt{s_{NN}} = 130$ and 200 GeV ranging from minimum bias to central collisions, and in p + p and d + Au at $\sqrt{s} = 200$ GeV. [6, 26] The peak at small relative azimuthal angle is indicative of short range correlations, i.e. jets. Data from p + p, d + Au, Cu + Cu and peripheral Au + Au exhibit a distinct back-to-back correlation, a characteristic of hard-parton scattering, with peaks at $\Delta\phi = 0$ and π, indicating di-jets. This is shown in Fig. 6 for p + p and d + Au reactions. However, for the most central Au + Au collisions the backward ($\Delta\phi = \pi$) correlation disappears. These results provide further evidence that in central Au + Au collisions a strong interaction results in quenching of high p_T partons.

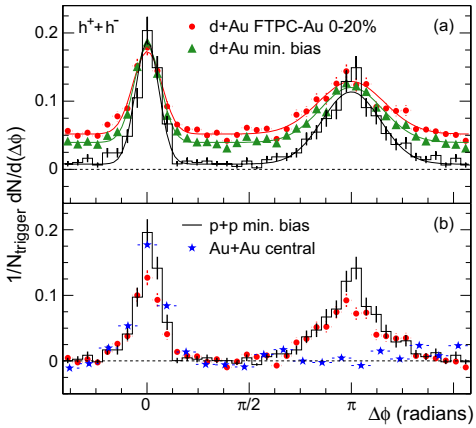

Figure 6: *Charged hadron correlation functions at $\sqrt{s_{NN}}$ = 200 GeV for a) p + p interactions, and minimum bias and central collisions of d + Au, and b) p + p, central d + Au, and central Au + Au collisions.*

When the p_T of the charged particles correlated with the trigger particle is lowered, the away-side peak re-appears, but broadened and possibly split. [27] This has led to descriptions of the broadening of this away-side particle distribution in terms of Mach-shock waves, conical flow, Cherenkov-like gluon radiation and color wakes. [28] Further experimental and theoretical investigation into the behavior of particles on the away-side of a high momentum trigger particle or jet should lead to a better understanding of the medium, its properties and its response to large energy deposition. The larger parton densities anticipated with heavy ions at the LHC should result in larger dissipation in the medium and possibly significant differences from what is observed at RHIC.

7 J/ψ

An early prediction of a deconfinement signature was the suppression of J/ψ production in a deconfined medium. J/ψ suppression has been observed in central nucleus-nucleus collisions at the SPS and initial measurements at RHIC. [29] Alternative models based on interactions with hadronic co-movers have been proposed, but have problems reproducing the suppression as a function of centrality. If the suppression at the SPS is due to deconfinement, then the J/ψ should also be suppressed at RHIC energies. On the other hand, coalescence of $c\overline{c}$ pairs and statistical-thermal models predict significant J/ψ production at RHIC. [30] First measurements of J/ψ by PHENIX at RHIC in $\sqrt{s_{NN}}$ = 200 GeV p + p and Au + Au collisions disfavor significant enhancement due to $c\overline{c}$ coalescence and thermal $c\overline{c}$ production, while still not able to distinguish between models for suppression relative to binary scaling. The high statistics measurements from PHENIX for J/$\psi \rightarrow e^+e^-$ at mid-rapidity and J/$\psi \rightarrow \mu^+\mu^-$ at forward rapidities will provide data to adequately address the J/ψ production and evolution mechanisms.

The higher c.m. energies at the LHC make it possible to measure the yields of various members of the J/ψ and Υ (quarkonium) families. Due to a range of binding energies for quarkonia, a study of quarkonium suppression at the LHC should elucidate the initial temperatures in the collisions and possibly provide information on the mechanism of deconfinement.

8 Summary and Conclusions

In Au + Au collisions at RHIC, the observation of strong elliptic flow, and the scaling of the flow with the number of quarks in the final state hadrons lead to characterization of the medium as a nearly perfect liquid of quarks and gluons. This liquid has a shear viscosity (divided by entropy density) that approaches a quantum lower bound derived using strongly-coupled N = 4 super-symmetric Yang-Mills theory. [13)]

The observed ratios of the many different hadrons produced at RHIC represent equilibrium abundances predicted from thermal models. The final state hadrons are formed and thermally distributed at the universal hadronization temperature (175 MeV) with a collective flow derived from their quark predecessors. The suppression of hadrons at large transverse momentum in Au + Au collisions, absent in d + Au, provides evidence for a high density medium, consistent with the initial determination of large energy densities created at RHIC. The observed quenching of the away-side jet (and its absence in central collisions) in Au + Au collisions requires a strongly-coupled colored medium, rather than the perturbative one expected from the initial lattice calculations.

Much still needs to be understood. The new results on suppression of heavy quark hadrons defy predictions. More detailed experimental investigation of B- and D-meson decays are anticipated at RHIC and the LHC. A complete quarkonium program at the LHC and upgraded RHIC luminosities will be instrumental in determining the initial temperatures and degree of deconfinement. Studies of jet quenching will expand at the LHC to include measurements of complete jets at higher jet energies to determine parton energy loss mechanisms and the response of the medium to large energy deposition.

References

1. O.Kaczmarek et al., hep-lat/0503017.
2. D.J. Gross and F. Wilczek, PRL 30 (1973) 1343; H.D. Politzer, PRL 30 (1973) 1346.
3. F. Karsch, Nuc. Phys. A698 (2002) 199c.
4. "The Relativistic Heavy Ion Collider and its Detectors", eds. M. Harrison, T. Ludlam, and S. Ozaki, Nuc. Inst. Meth. A499 (2003) p. 235-824.

5. K. Adcox et al. (PHENIX) Phys. Rev. Lett. 87 (2001) 052301; J. Adams et al. (STAR), nucl-ex/0407003; C. Adler et al. (STAR), Phys. Rev. Lett. 87 (2001) 112303.

6. C. Adler et al. (STAR) Phys. Rev. Lett. 90 (2003) 032301.

7. C. Adler et al (STAR), Phys. Rev. Lett. 87 (2001) 182301 and Phys. Rev. Lett. 89 (2002) 132301; J. Adams et al (STAR), Phys. Rev. Lett. 95 (2005) 122301; S.S. Adler et al (PHENIX), Phys. Rev. Lett. 91, 182301 (2003); J. Adams et al (STAR), Phys. Rev. C 72 (2005) 014904.

8. P.F. Kolb et al., Phys. Lett. B500 (2001) 232; P.F. Kolb et al., Nucl. Phys. A696 (2001) 197; P. Huovinen et al., Phys. Lett. B 503 (2001) 58; D. A. Teaney, J. Phys. G30 (2004) S1247.

9. T. Hirano and M. Gyulassy, nucl-th/0506049v2.

10. J.M. Maldacena, Adv. Theor. Math. Phys. 2 (1998) 231.

11. G. t'Hooft, gr-qc/9310026; L. Susskind, J. Math. Phys. 36 (1995) 6377.

12. E. Witten, Adv. Theor. Math. Phys. 2 (1998) 253.

13. P.K. Kovtun, D.T. Son, A.O. Starinets, Phys. Rev. Lett. 94 (2005) 111601.

14. P. Braun-Munzinger, K. Redlich, and J. Stachel, preprint nucl-th/0304013; P. Braun-Munzinger, D. Magestro, K. Redlich, and J. Stachel, Phys. Lett. B518 (2001) 41 and D. Magestro (private communication); for another statistical approach see F. Becattini, J. Phys. G28 (2002) 1553.

15. P. Braun-Munzinger, I. Heppe, and J. Stachel, Phys. Lett. B465 (1999) 15; see also F. Becattini et al., Phys. Rev. C64 (2001) 024901; F. Beccatini, M. Gazdzicki, and J. Sollfrank, Eur. J. Phys. C5 (1998) 143.

16. see R. Baier, D. Schiff, and B. G. Zakharov, Annu. Rev. Part. Sci. 50 (2000) 37 and references therein.

17. K. Adcox et al (PHENIX), Phys. Rev. Lett. 88 (2002) 022301; C. Adler et al (STAR), Phys. Rev. Lett. 89 (2002) 202301; B.B. Back et al. (PHOBOS), nucl-exp/0302015v1; K. Adcox et al (PHENIX), Phys. Rev. Lett. 91 (2003) 072303; J. Adams et al (STAR), Phys. Rev. Lett. 91 (2003) 072304.

18. S.S. Adler et al. (PHENIX), Phys. Rev. Lett. 96 (2006) 202301.

19. I. Vitev and M. Gyulassy, Phys. Rev. Lett. 89 (2002) 252301; and I. Vitev, J. Phys. G 30 (2004) S791.

20. Y.L. Dokshitzer and D.E. Kharzeev, Phys. Lett. B519 (2001) 199.

21. S.S. Adler et al. (PHENIX), Phys.Rev.Lett. 96 (2006) 032301); B.I. Abelev et al. (STAR), Phys. Rev. Lett. 98 (2007) 192301.

22. M. Djordjevic et al., Phys. Lett. B632 (2006) 81.

23. N. Armesto et al., Phys. Lett. B 637 (2006) 362.

24. S. Wicks et al., Nucl. Phys. A784 (2007) 426.

25. H. Liu, K. Rajagopal and U. A. Wiedemann, Phys. Rev. Lett. 97 (2006) 182301.

26. C. Adler et al. (STAR) Phys. Rev. Lett. 89 (2002) 202301.

27. N. Grau et al. (PHENIX) nucl-ex/0612019; F. Wang et al. (STAR) nucl-ex/0610011.

28. Mach-shock: H. Stoecker, Nucl. Phys A750 (2005) 121; Conical flow: J. Casalderrey-Solana, E.V. Shuryak and D. Teaney, Nucl. Phys. A774 (2006) 577; Cherenkov cone: V. Koch, A. Majumbder and X.N.Wang, Phys. Rev. Lett 96 (2006) 172302; Color wakes: J. Ruppert and B. Muller, Phys. Lett. B618 (2005) 123.

29. Theory: T. Matsui and H. Satz, Phys. Lett. B 178 (1986) 416; SPS data: M.C. Abreu et al (NA50), Phys. Lett. B 477 (2000) 28, ibid. Phys. Lett. B 521 (2001) 195, L. Ramello et al (NA50), Nucl. Phys. A715 (2003) 243c; RHIC data: S.S. Adler et al (PHENIX), Phys. Rev. C69 (2004) 014901.

30. Coalescence: R.L. Thews, M. Schroedter, and J. Rafelski, Phys. Rev. C 63 (2001) 054905; Thermal: L. Grandchamp and R. Rapp, Nucl. Phys. A709 (2002) 415, A. Andronic et al, nucl-th/0303036.

Frascati Physics Series Vol. XLVI (2007), pp. 275–286
HADRON07: XII Int. Conf. on Hadron Spectroscopy – Frascati, October 8-13, 2007
Plenary Session

THE STRANGENESS PHYSICS PROGRAM AT CLAS

Daniel S. Carman
Jefferson Laboratory, 12000 Jefferson Ave., Newport News, VA, U.S.A.
carman@jlab.org

Abstract

An extensive program of strange particle production off the nucleon is currently underway with the CEBAF Large Acceptance Spectrometer (CLAS) in Hall B at Jefferson Laboratory. This talk will emphasize strangeness electroproduction in the baryon resonance region between W=1.6 and 2.4 GeV, where indications of s-channel structure are suggestive of high-mass baryon resonances coupling to kaons and hyperons in the final state. Precision measurements of cross sections and polarization observables are being carried out with highly polarized electron and real photon beams at energies up to 6 GeV. The near-term and longer-term future of this program will also be discussed.

1 Introduction

An important key to understand the structure of the nucleon is to understand its spectrum of excited states. However, understanding nucleon reso-

nance excitation provides a serious challenge to hadronic physics due to the non-perturbative nature of QCD at these energies. Recent symmetric quark model calculations predict more states than have been seen experimentally [1]. Mapping out the spectrum of these excited states will provide for insight into the underlying degrees of freedom of the nucleon.

Most of our present knowledge of baryon resonances comes from reactions involving pions in the initial and/or final states. A possible explanation for the so-called missing resonance problem could be that pionic coupling to the intermediate N^* or Δ^* states is weak. This suggests a search for these hadronic states in strangeness production reactions. Beyond different coupling constants (e.g. g_{KNY} vs. $g_{\pi NN}$), the study of the exclusive production of $K^+\Lambda$ and $K^+\Sigma^0$ final states has other advantages in the search for missing resonances. The higher masses of the kaon and hyperons, compared to their non-strange counterparts, kinematically favor a two-body decay mode for resonances with masses near 2 GeV, a situation that is experimentally advantageous. In addition, baryon resonances have large widths and are often overlapping. Studies of different final states can provide for important cross checks in quantitatively understanding the contributing amplitudes. Although the two ground-state hyperons have the same valence quark structure (uds), they differ in isospin, such that intermediate N^* resonances can decay strongly to $K^+\Lambda$ final states, while both N^* and Δ^* decays can couple to $K^+\Sigma^0$ final states.

The search for missing resonances requires more than identifying features in the mass spectrum. QCD cannot be directly tested with N^* spectra without a model for the production dynamics [2]. The s-channel contributions are known to be important in the resonance region in order to reproduce the invariant mass (W) spectra, while t-channel meson exchange is also necessary to describe the diffractive part of the production and u-channel diagrams are necessary to describe the back-angle strength. Thus measurements that can constrain the phenomenology for these reactions are just as important as finding one or more of the missing resonances.

Theoretically, there has been considerable effort during the past decade to develop models for the KY photo- and electroproduction processes. However, the present state of understanding is still limited by a sparsity of data. Model fits to the existing cross section data are generally obtained at the expense of many free parameters, which leads to difficulties in constraining theory.

Moreover, cross section data alone are not sufficient to fully understand the reaction mechanism, as they probe only a portion of the full response. In this regard, measurements of spin observables are essential for continued theoretical development in this field, as they allow for improved understanding of the dynamics of this process and provide for strong tests of QCD-inspired models.

In this talk I focus on the strangeness electroproduction program in Hall B at Jefferson Laboratory using the CLAS detector [3]. Presently there is very limited knowledge of $N^*, \Delta^* \rightarrow KY$ couplings. With the existing CLAS program, the present lack of data will be remedied with a wealth of high quality measurements spanning a broad kinematic range.

2 Theoretical Models

With the recently available data from the photo- and electroproduction of KY final states from CLAS and elsewhere, there have been renewed efforts on the development of theoretical models. The majority of these are single-channel models that represent tree-level calculations, where the amplitude is constructed from the lowest-order Feynman diagrams. More recent work has moved beyond the single-channel approach with the development of coupled-channels models [4–7] or by fitting simultaneously to multiple but independent reaction channels [8, 9]. However, as a combined coupled-channels analysis of the photo- and electroproduction reactions is not yet available, a tree-level approach currently represents the best possibility of studying both reactions within the same framework. While most of the recent theoretical analyses have focussed solely on the available photoproduction data, it has been shown that electroproduction observables can yield important complementary insights to improve and constrain the theory.

At JLab energies, perturbative QCD is not yet capable of providing analytical predictions for the observables for kaon electroproduction. In order to understand the underlying physics, effective models must be employed that ultimately represent approximations to QCD. In this work we compare our data against three different model approaches. The first is a traditional hadrodynamic (resonance) model, the second is based on a Reggeon-exchange model, and the third is a hybrid Regge plus resonance approach.

In the hadrodynamic model approach, the strong interaction is modeled by an effective Lagrangian, which is constructed from tree-level Born and ex-

tended Born terms for intermediate states exchanged in the s, t, and u reaction channels. Each resonance has its own strong coupling constants and strong decay widths. A complete description of the physics processes requires taking into account all possible channels that could couple to the initial and final state measured, but the advantages of the tree-level approach include the ability to limit complexity and to identify the dominant trends. In the one-channel, tree-level approach, several dozen parameters must be fixed by fitting to the data, since they are poorly known and not constrained from other sources.

The hadrodynamic models shown in this work were developed by Mart and Bennhold [10] and the Ghent group [11]. In these models, the coupling strengths have been determined mainly by fits to existing $\gamma p \to K^+Y$ data (with some older electroproduction data included), leaving the coupling constants as free parameters (constrained loosely by SU(3) symmetry requirements). The model parameters are not based on fits to any CLAS data. The specific resonances included with these models include the $S_{11}(1650)$, $P_{11}(1710)$, $P_{13}(1720)$, and $D_{13}(1895)$ N^* states in the s-channel, and the $K^*(892)$ and $K_1^*(1270)$ in the t-channel. The Ghent model also includes hyperon exchange in the $K^+\Lambda$ u-channel and couplings of s-channel $S_{31}(1900)$ and $P_{31}(1910)$ Δ^* states for the $K^+\Sigma^0$ final state.

In this work, we also compare our results to the Reggeon-exchange model from Guidal *et al.* [12]. This calculation includes no baryon resonance terms at all. Instead, it is based only on gauge-invariant t-channel K and K^* Regge-trajectory exchange. It therefore provides a complementary basis for studying the underlying dynamics of strangeness production. It is important to note that the Regge approach has far fewer parameters compared to the hadrodynamic models. These include the K and K^* form factors and the coupling constants g_{KYN} and g_{K^*YN} (taken from photoproduction studies).

The final model included in this work was also developed by the Ghent group [13], and is based on a tree-level effective field model for Λ and Σ^0 photoproduction from the proton. It differs from traditional isobar approaches in its description of the non-resonant diagrams, which involve the exchange of t-channel K and K^* Regge trajectories. A selection of s-channel resonances are then added to this background. This "Regge plus resonance" approach has the advantage that the background diagrams contain only a few parameters that are constrained by high-energy data where the t-channel processes dominate. In

addition to the kaonic trajectories, this model includes the s-channel resonances $S_{11}(1650)$, $P_{11}(1710)$, $P_{13}(1720)$, and $P_{13}(1900)$. Apart from these, the model includes either a $D_{13}(1900)$ or $P_{11}(1900)$ state in the $K^+\Lambda$ channel.

3 CLAS *KY* Electroproduction Results

CLAS has measured exclusive $K^+\Lambda$ and $K^+\Sigma^0$ electroproduction on the proton for a range of momentum transfer Q^2 from 0.5 to 5.4 GeV^2 with electron beam energies from 2.6 to 5.7 GeV. For this talk I will focus attention mainly on our 2.6 GeV data set. The final state hyperons were reconstructed from the $(e, e'K^+)$ missing mass, with an average hyperon resolution of $\sim$8 MeV.

The most general form for the virtual photoabsorption cross section of a kaon from an unpolarized proton target is given by:

$$\frac{d\sigma}{d\Omega_K^*} = \sigma_T + \epsilon\sigma_L + \epsilon\sigma_{TT}\cos 2\phi + \sqrt{\epsilon(1+\epsilon)}\sigma_{LT}\cos\phi + h\sqrt{\epsilon(1-\epsilon)}\sigma_{LT'}\sin\phi.$$

In this expression, the cross section is decomposed into five structure functions, σ_T, σ_L, σ_{TT}, σ_{LT}, and the helicity-dependent $\sigma_{LT'}$ term, which are, in general, functions of Q^2, W, and θ_K^* only. ϵ is the virtual photon polarization and Φ is the angle between the electron scattering and hadronic reaction planes. One of the goals of the electroproduction program is to provide a detailed tomography of the structure functions vs. Q^2, W, and $\cos\theta_K^*$. In the first phase of the analysis, we have measured the unseparated structure function ($\sigma_U = \sigma_T + \epsilon\sigma_L$) and, for the first time in the resonance region away from parallel kinematics, the interference structure functions σ_{TT} and σ_{LT}. Exploiting the Φ dependence of the reaction allows us to extract the separate terms. The Q^2 dependence of the data provides sensitivity to the associated form factors. All of the published CLAS data are contained in the official CLAS data base [14].

A small sample of the available results from this analysis is shown in Fig. 1 vs. W for each of our six angle bins for the kaon [15]. The kinematic dependence of the unpolarized structure functions shows that Λ and Σ^0 hyperons are produced very differently. σ_U at forward angles for $K^+\Lambda$ is dominated by a structure at W=1.7 GeV. For larger kaon angles, a second structure emerges at about 1.9 GeV, consistent with a similar signature in photoproduction. σ_{TT} and σ_{LT} are clearly non-zero and reflect the structures in σ_U. The fact that σ_{LT} is non-zero is indicative of longitudinal strength. For the $K^+\Sigma^0$ final state,

σ_U is centrally peaked, with a single broad structure at 1.9 GeV. This is consistent with the photoproduction data. σ_{TT} reflects the features of σ_U, with σ_{LT} consistent with zero everywhere, indicative of σ_L being consistent with zero.

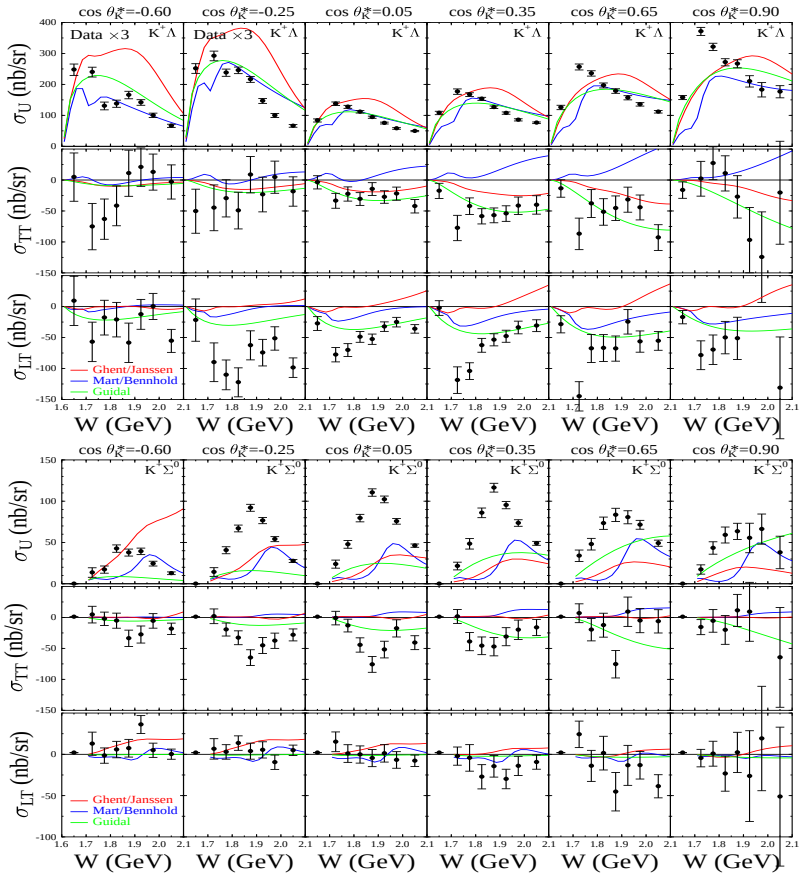

Figure 1: Separated structure functions σ_U, σ_{LT}, and σ_{TT} (nb/sr) vs. W (GeV) for $K^+\Lambda$ (top) and $K^+\Sigma^0$ at 2.6 GeV and Q^2=0.65 GeV^2 [15]. The curves correspond to the indicated model calculations.

Using our data sets at 2.6 and 4.2 GeV, we have performed a Rosenbluth separation to extract σ_L and σ_T for several W bins over the full kaon angular range for a single bin at Q^2=1.0 GeV^2 where the data sets overlap. Our data indicate that σ_L is consistent with zero over all kinematics probed for the $K^+\Sigma^0$ final state. For the $K^+\Lambda$ final state, σ_L is consistent with zero everywhere

except at our highest W bin (1.95 GeV) and only a very forward kaon angles. This analysis is consistent with our earlier results of σ_L/σ_T extracted from our polarization data [16].

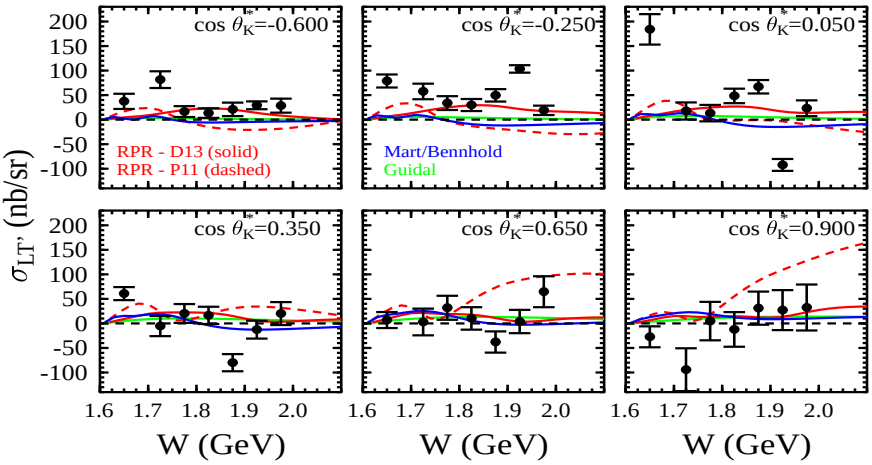

Figure 2: Polarized structure function $\sigma_{LT'}$ (nb/sr) vs. W (GeV) for $K^+\Lambda$ for Q^2=1.0 GeV^2 and $\cos\theta^*_K$ points as indicated. The curves correspond to the indicated model calculations.

The polarized-beam asymmetry provides access to the fifth structure function $\sigma_{LT'}$. This observable probes imaginary parts of the interfering L and T amplitudes (as opposed to the real parts of the interference from σ_{LT}). These imaginary parts vanish identically if the resonant state is determined by a single complex phase, which is the case for an isolated resonance. A representative sample of our data at 2.6 GeV and Q^2=1.0 GeV^2 is shown in Fig. 2 for the $K^+\Lambda$ final state [17]. Note the strong interference effect seen at central angles near 1.9 GeV. The calculations shown are not able to reproduce the features seen in the data.

The first measurements of spin transfer from a longitudinally polarized electron beam to the Λ hyperon produced in the exclusive $p(\vec{e},e'K^+)\vec{\Lambda}$ reaction have also been completed at CLAS [18]. A sample of the results highlighting the angular dependence of P' summed over all Q^2 for three different W bins is shown in Fig. 3 at 2.6 GeV. The polarization along the virtual photon direction $P'_{z'}$ decreases with increasing θ^*_K, while the orthogonal component in the hadronic reaction plane $P'_{x'}$ is constrained to be zero at $\cos\theta^*_K = \pm 1$ due to angular momentum conservation, and reaches a minimum at $\theta^*_K \sim 90°$. The

component normal to the hadronic reaction plane $P'_{y'}$ is statistically consistent with zero as expected. The accuracy of these data, coupled with the spread in the theory predictions, indicates that these data are sensitive to the resonant and non-resonant structure of the intermediate state.

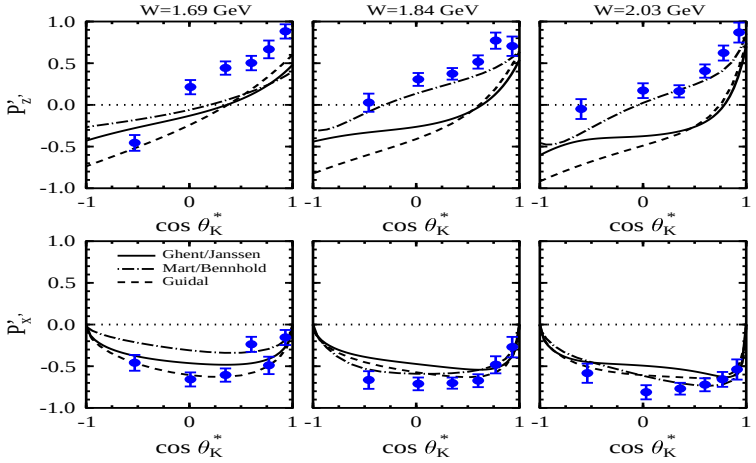

Figure 3: CLAS transferred polarization [18] from $\vec{e}p \to e'K^+\vec{\Lambda}$ vs. $\cos\theta^*_K$ at 2.6 GeV for three different W bins summed over Φ and Q^2. The curves correspond to the indicated model calculations.

4 What Has Been Learned?

According to the listings of the Particle Data Group [19], the current knowledge of the $N^* \to KY$ and $\Delta^* \to K\Sigma$ couplings is quite limited. Table 1 shows what has been determined experimentally. The dominant couplings of $N^* \to K\Lambda$ include the $S_{11}(1650)$, $P_{11}(1710)$, and $P_{13}(1720)$ resonances. There are no known states that have been shown to couple to $K\Sigma$. From the standpoint of $\Delta^* \to K\Sigma$ couplings, only the $P_{33}(1920)$ has a measured strength. In addition, the available photocoupling amplitudes that do exist, have rather large uncertainties. Clearly there is significant room for improvement.

In the last several years, there has been some progress on the development of $K^+\Lambda$ coupled-channels models based on fits to the available photoproduction data. These include several thousand differential cross section and single and double polarization data points from CLAS, SAPHIR, and LEPS. However, the lessons learned from these studies have not served to clarify our

understanding of the $N^* \to K\Lambda$ couplings. A coupled-channels model from Bonn [8] has indicated that the most relevant states include the $P_{13}(1720)$, $P_{11}(1840)$, $D_{13}(1870)$, $D_{13}(2070)$, and $P_{13}(2200)$. A second coupled-channels model from Saghai *et al.* [20] has indicated that the most relevant states include the $S_{11}(1535)$, $P_{13}(1900)$, $D_{13}(1520)$, $F_{13}(1680)$, and $F_{17}(1990)$, along with other required states given by $S_{11}(1650)$, $F_{15}(1680)$, $F_{15}(2000)$, $D_{13}(1954)$, $S_{11}(1806)$, and $P_{13}(1893)$. The models have come to orthogonal conclusions as to the contributing states.

State	PDG	B.R. ($K\Lambda$)	B.R. ($K\Sigma$)
$N^*(1650)\ S_{11}$	****	3-11%	-
$N^*(1675)\ D_{15}$	****	<1%	-
$N^*(1680)\ F_{15}$	****	-	-
$N^*(1700)\ D_{13}$	***	<3%	-
$N^*(1710)\ P_{11}$	***	5-25%	-
$N^*(1720)\ P_{13}$	***	1-15%	-
$N^*(1900)\ P_{13}$	**	-	-
$N^*(1990)\ F_{17}$	**	-	-
$N^*(2000)\ F_{15}$	**	-	-
$\Delta^*(1900)\ S_{31}$	**		-
$\Delta^*(1905)\ F_{35}$	****		-
$\Delta^*(1910)\ P_{31}$	****		-
$\Delta^*(1920)\ P_{33}$	***		2.1%
$\Delta^*(1930)\ D_{35}$	***		-
$\Delta^*(1940)\ D_{33}$	*		-
$\Delta^*(1950)\ F_{37}$	****		-

Table 1: N^* and Δ^* states and their known branching ratios into $K\Lambda$ and $K\Sigma$ final states [19]. The second column gives the PDG star-rating for the states.

Finally, a new multipole model from Mart and Sulaksono [21] has determined that the extracted $N^* \to K\Lambda$ couplings are highly dependent on the data used as input. Based on fits to the SAPHIR and LEPS photoproduction data, they have found that the most relevant states include the $S_{11}(1650)$, $P_{13}(1720)$, $D_{13}(1700)$, $D_{13}(2080)$, $F_{15}(1680)$, and $F_{15}(2000)$. However, using the CLAS and LEPS photoproduction data, they find instead that the dominant states include the $P_{13}(1900)$, $D_{13}(2080)$, $D_{15}(1675)$, $F_{15}(1680)$, and $F_{17}(1990)$. The

difficulties here arise due to important shape differences between the CLAS and SAPHIR angular distributions. CLAS is continuing to examine this issue.

Ultimately, the KY photo- and electroproduction data should be fit simultaneously with a full set of channels (e.g. πN, ηN, ωN, ϕN, $\pi\pi N$). The inclusion of electroproduction data should provide powerful new information to better separate the resonant and non-resonant contributions. At the current time, this approach is too difficult. However, several groups are working in this direction, and we expect that a more complete coupled-channels approach will be possible in the not too distant future.

5 Future Plans

Studies of strangeness final states represent an important part of the overall CLAS physics program. A variety of observables have been published to date for both our photo- and electroproduction data. In the near future, CLAS will provide additional new high quality data in the W range from 1.6 to 2.4 GeV using both circularly and linearly polarized photons. Three measurement programs are currently in progress to study strangeness physics with CLAS.

The first program is called g13. This experiment, which completed a long run with CLAS in the first half of 2007, was designed to study γn interactions on an unpolarized deuterium target. This experiment will study $K^0\Lambda$, $K^0\Sigma^0$, and $K^+\Sigma^-$ final states. The second program is called g9, and will take data in CLAS in the second half of 2007. This experiment will study $K^+\Lambda$ and $K^+\Sigma^0$ final states. The target for this experiment employs a novel frozen spin target that allows studies with both longitudinally and transversely polarized protons. The final program will employ the HD-ice target from Brookhaven National Lab [22] to study $\gamma n \to K^0\Lambda$, $K^0\Sigma^0$, and $K^+\Sigma^-$ reactions. This target is now in the process of being modified for use in CLAS.

The combined FROST and HD-ice programs will provide a complete set of observables with high statistics in both the γp and γn channels for both the $K\Lambda$ and $K\Sigma$ final states. The ability to take data for all combinations of beam, target, and recoil polarization observables with the same detector will allow systematics to be minimized. These high profile programs at JLab will provide important input to disentangle the N^* spectrum.

At the present time, JLab is well underway with its plans to upgrade the accelerator from a maximum energy of 6 GeV to a maximum energy of

12 GeV. Along with the accelerator upgrade, the experimental halls will also be upgraded. The CLAS detector will be modified to a new configuration called CLAS12. The new large acceptance detector will still be based on a toroidal design, but the new magnet will be outfitted with new drift chambers and a new central detector system. The calorimetry, time-of-flight, and Čerenkov detector systems of CLAS will also undergo significant upgrades.

The new CLAS12 experiment is presently slated to begin its physics program in 2014. An important aspect of the program is the continued study of strangeness physics. This program includes both semi-inclusive and exclusive measurements focussing on spectroscopy, quark distribution functions, and deep-inelastic scattering.

6 Summary and Conclusions

In this talk I have reviewed some of the key reasons why the photo- and electroproduction processes of open-strangeness production are important for the investigation of baryonic structure and missing quark model states. I have discussed several aspects of the CLAS strangeness physics program highlighting the breadth and quality of our photo- and electroproduction data sets on the nucleon. These data will provide not only high statistics differential cross sections, but high precision data for all combinations of beam, target, and recoil polarization observables on the proton and neutron. Our analyses indicate that the data are highly sensitive to the ingredients of the models, including the specific baryonic resonances included, along with their associated form factors and coupling constants. New complete amplitude-level analyses are called for to more fully unravel the contributions to the intermediate state.

This work has been supported by the U.S. Department of Energy and the National Science Foundation.

References

1. S. Capstick and W. Roberts, Phys. Rev. D **58**, 74011 (1998).
2. T.-S.H. Lee and T. Sato, Proceedings of the N*2000 Conference, eds. Burkert *et al.*, (World Scientific, Singapore, 2001), p. 215.

3. B.A. Mecking *et al. (CLAS Collaboration)*, Nucl. Inst. and Meth. A **503**, 513 (2003).
4. B. Julia-Diaz *et al.*, Phys. Rev. C **73**, 055204 (2006).
5. W.T. Chiang *et al.*, Phys. Rev. C **69**, 065208 (2004).
6. V. Shklyar, H. Lenske, and U. Mosel, Phys. Rev. C **72**, 015210 (2005).
7. T.-S.H. Lee and L.C. Smith, J. Phys. G **34**, S83 (2007).
8. A.V. Sarantsev *et al.*, Eur. Phys. J A **25**, 441 (2005).
9. A. Anisovich *et al.*, Eur. Phys. J. A **24**, 111 (2005); A. Anisovich *et al.*, Eur. Phys. J. A **25**, 427 (2005).
10. T. Mart and C. Bennhold, Phys. Rev. C **61**, 012201 (2000).
11. S. Janssen *et al.*, Phys. Rev. C 65, 015201 (2002).
12. M. Guidal, J.-M. Laget, and M. Vanderhaghen, Phys. Rev. C **61**, 025204 (2000).
13. T. Corthals *et al.*, Phys. Rev. C **75**, 045204 (2007); T. Corthals *et al.*, preprint arXiv:0704.3691, submitted for publication (2007).
14. CLAS physics database, http://clasweb.jlab.org/physicsdb.
15. P. Ambrozewicz *et al.* (CLAS Collaboration), Phys. Rev. C **75**, 045203 (2007).
16. B.A. Raue and D.S. Carman, Phys. Rev. C **71**, 065209 (2005).
17. R. Nasseripour *et al. (CLAS Collaboration)*, to be submitted to Phys. Rev. C, (2007).
18. D.S. Carman *et al. (CLAS Collaboration)*, Phys. Rev. Lett. **90**, 131804 (2003).
19. W.-M. Yao *et al.*, Journal of Physics G **33**, 1 (2006).
20. B. Saghai *et al.*, Phys. Rev. C **73**, 055204 (2006).
21. T. Mart and Sulaksono, nucl-th/0701007, (2007).
22. X. Wei *et al.*, Nucl. Inst. and Meth. A **526**, 157 (2004).

Frascati Physics Series Vol. XLVI (2007), pp. 287–299
HADRON07: XII Int. Conf. on Hadron Spectroscopy – Frascati, October 8-13, 2007
Plenary Session

SELECTED RESULTS AND FUTURE PROSPECTS OF THE COMPASS EXPERIMENT

Ferrero Andrea
European Organization for Nuclear Research, CERN,
CH-1211 Genéve 23, Switzerland

Abstract

The COMPASS experiment at CERN addresses a wide variety of physics topics related to the structure and spectroscopy of hadrons.
The high energy muon beam is used to investigate how partons contribute to the spin of the nucleon. New measurements of the quark and gluon polarization, and of the transversity distribution functions, are presented, based on the data sets collected during the years 2002-2004.
A pilot measurement with a high energy hadron beam has also been performed in 2004, and the preliminary results of the pion electric and magnetic polarizabilities extracted from these data are discussed. A brief outline of future measurements with hadron beams is also given.

1 Introduction

The COMPASS experiment [1)] at the CERN SPS accelerator facility addresses a wide variety of physics topics related to the structure and spectroscopy of hadrons. Fundamental questions like the contribution of gluons to the nucleon spin, the measurement of the quark transverse spin distribution functions, the existence of non-$q\overline{q}$ mesons, or the magnitude of the pion electric and magnetic polarizabilities are investigated using both high energy muons and hadrons as probes.

The physics with muon beams mainly aims at measuring the contribution of quarks and gluons to the nucleon spin. The EMC spin asymmetry measurements [2, 3)], later confirmed with higher precision by experiments at CERN, DESY and SLAC, led to the conclusion that the contribution of quarks to the nucleons spin $\Delta\Sigma$ is only of about 30%, in disagreement with the quark model expectations. Theory and experiments can still be reconciled via the axial anomaly, if the gluon polarization ΔG is large ($\approx 2.5 - 3$). Therefore, the measurement of ΔG represents a fundamental ingredient to understand the spin dynamics of nucleon. In sec.2 and 3 the COMPASS results for $\Delta\Sigma$ and ΔG are presented. About 20% of the COMPASS data has been collected with a transversely polarized target. In this configuration a number of new distribution functions can be accessed, among which of particular interest are the transversity distribution functions $\Delta_T q(x)$ and the Sivers functions. Results are presented in sec.4.

The physics with hadron beams comprises a large variety of measurements, including light meson spectroscopy, study charmed and doubly-charmed baryons, and the measurement of pion and kaon polarizabilities. Among those, only the last item has been partly addressed so far, during a pilot data taking that took place in the fall of 2004. Preliminary results for the pion electric (α_π) and magnetic (β_π) polarizabilities are presented in sec.5, while a brief overview of future meson spectroscopy measurements is given in sec.6.

2 Inclusive asymmetries

COMPASS has performed a new measurement of the A_d^1 spin asymmetry from inclusive Deep Inelastic Scattering (DIS) $\mu d \to \mu' X$ events in the $Q^2 > 1$ (GeV/c)^2 region, using the data sample collected during the years from 2002

to 2004. The A_d^1 asymmetry is related to the counting rate asymmetry $A^{\mu d}$ by the relation

$$A^{\mu d} = \frac{1}{f P_B P_T} \left(\frac{N^{\uparrow\uparrow} - N^{\uparrow\downarrow}}{N^{\uparrow\uparrow} + N^{\uparrow\downarrow}} \right) = D(A_1^d + \eta A_2^d), \tag{1}$$

where the $N^{\uparrow\uparrow}$ ($N^{\uparrow\downarrow}$) denotes the number of events observed with parallel (anti-parallel) orientations of the spins of the incoming muon and the target deuteron, P_B and P_T are respectively the beam and target polarizations, f is the target dilution factor (i.e. the fraction of polarizable nucleons in the target material), and D is the virtual photon depolarization factor. The A_2^d asymmetry was measured by SLAC experiments as well as by SMC and found to be small; moreover, η is also small in the kinematical range covered by COMPASS. Therefore, the expression for A_1^D can be safely approximated to

$$A_1^d \approx A^{\mu d}/D. \tag{2}$$

The result for A_1^d as function of x is shown in fig.1 (left), where COMPASS points are compared to other experiments. The lower band shows the systematic effect associated to each of the COMPASS points; the systematic uncertainties include the contribution of possible false asymmetries, of radiative corrections, and of the uncertainty on f, P_B and P_T. For the region of $x < 0.03$ the statistical precision of the COMPASS points if a factor 3-4 better then the previously existing measurements; in particular, the trend toward negative values suggested by the SMC points is not confirmed.

The helicity-dependent structure function g_1^d is obtained from the A_1^d asymmetry using the relation

$$g_1^d \approx \frac{F_2^d}{2x(1+R)} A_1^d, \tag{3}$$

where F_2^d is the spin-independent structure function of the deuteron, and R is the ratio of longitudinal to transverse photo-absorption cross-sections. For F_2^d, the SMC parameterization of [4] is used for $x > 0.0009$ and $Q^2 > 0.2$ (GeV/c)^2, and the one of [5] elsewhere. The COMPASS results are shown in fig.1 (right) together with the published SMC data points. A new Next-to-Leading-Order (NLO) QCD fit to the world g_1 data from deuteron, proton and ^3He targets, including the COMPASS results, has been performed; in total 230 data points were used. The fit gives two equally acceptable solutions, one for $\Delta G > 0$ and

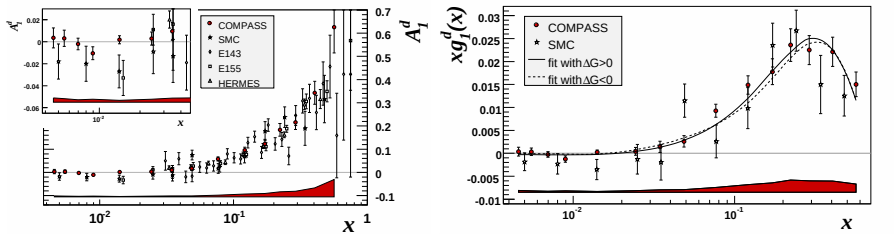

Figure 1: *COMPASS results for the A_1^d asymmetry as a function of x, compared to other experiments (left). COMPASS results for xg_1^d as a function of x, compared to SMC (right). Two equally acceptable solutions of NLO QCD fits to world g_1 data are also shown on the plot.*

one for $\Delta G < 0$, with about the same absolute value of the first moment of the polarized gluon distributions $|\eta_G| \simeq 0.2 - 0.3$. Details of the NLO analysis can be found in [6].

The relevance of the precise COMPASS measurements at low x is better seen when $g_1^N = g_1^d/(1 - 1.5\omega_D)$ (i.e. g_1^d corrected for the deuteron D-wave, where $\omega_D = 0.05 \pm 0.01$) is plotted as a function of x, as shown in fig.2 (left). The COMPASS data points, evolved to $Q^2 = 3$ (GeV/c)^2, are compared with a curve derived from the three parameterizations of BB, GRSV and LSS05, and with the new NLO QCD fits to world g_1 data. The negative trend at low x of standard fits is not supported by COMPASS data. Nevertheless, the statistical accuracy of present low-x points is not sufficient to discriminate between the two possible solutions with opposite sign of ΔG, although a large value of $\Delta G \sim 2.5 - 3$ is disfavored.

From the COMPASS data alone the integral of g_1^N has been calculated:

$$\Gamma_1^N(Q^2 = 3(\mathrm{GeV/c})^2) = 0.05 \pm 0.003(stat) \pm 0.002(evol) \pm 0.005(syst), \quad (4)$$

with a contribution of the unmeasured x regions of $\sim 2\%$. From this value, and assuming $SU(3)_f$ symmetry, one gets the following result for the flavour-singlet axial current matrix element at $Q^2 = 3(\mathrm{GeV/c})^2$:

$$a_0(Q^2 = 3(\mathrm{GeV/c})^2) = 0.35 \pm 0.03(stat) \pm 0.05(syst). \quad (5)$$

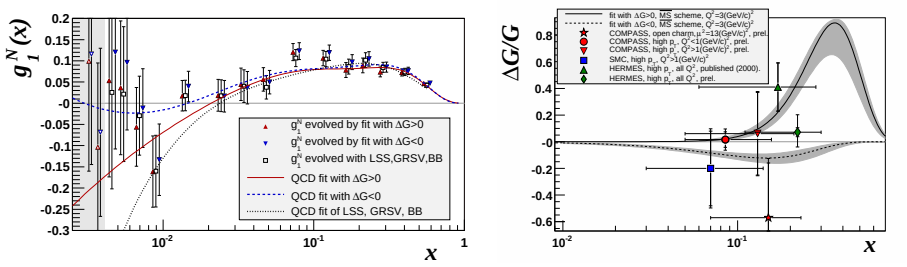

Figure 2: *COMPASS results for g_1^N; all data points have been evolved to $Q^2 = 3$ $(GeV/c)^2$ using three different parameterizations (standard and new QCD fits) (left). COMPASS results for $\Delta G/G$ from high-p_T pairs and open charm production; the curves show the parameterizations at 3 GeV^2 in the $\overline{MS}$ scheme for the $\Delta G > 0$ and $\Delta G < 0$ solutions of the new QCD fits to g_1 data. Published results from SMC and HERMES are also shown (right).*

3 Direct measurements of $\Delta G/G$

The Photon-Gluon Fusion (PGF) process provides a way to directly measure ΔG in lepton-nucleon scattering. Two different approaches are used in COMPASS to select PGF events:

1. the selection of events with hadron pairs emitted at large transverse momenta (high-p_T)
2. the selection of open charm events

In the high-p_T analysis [7] the events are selected by requiring two hadrons in the final state having each $p_T > 0.7$ GeV/c and $\sum p_T^2 > 2.5$ $(\mathrm{GeV/c})^2$. These cuts have been tuned to maximize the fraction of PGF events, R_{PGF}, in the final sample; events from background processes, the most important of which are QCD Compton and the leading order process, cannot be completely rejected by the cuts. The gluon polarization is then obtained from the measured longitudinal double-spin asymmetry A_{LL}:

$$A_{LL} = R_{PGF} a_{LL}^{PGF} \Delta G/G + A_{bgd}, \tag{6}$$

where a_{LL}^{PGF} represents the analyzing power of the PGF sub-process and A_{bgd} is the background asymmetry.

A_{LL} is measured either in the $Q^2 > 1$ (GeV/c)^2 or $Q^2 < 1$ (GeV/c)^2 regions; for the latter, the available statistics is about 10 times larger but an additional background from resolved photons has to be considered. R_{PGF}, a_{LL}^{PGF} and the probed x_g range have to be determined from MonteCarlo (MC) simulations, using either LEPTO ($Q^2 > 1$ (GeV/c)^2) or PYTHIA ($Q^2 < 1$ (GeV/c)^2) for event generation; R_{PGF} is typically of the order of 30%. Bounds are used for the unknown parton distributions in the photon, resulting in an additional contribution to the systematic error.

In the $Q^2 > 1$ (GeV/c)^2 we obtain, from the analysis of the 2002 and 2003 data, a preliminary value of

$$\frac{\Delta G}{G} = 0.06 \pm 0.31(stat) \pm 0.06(syst) \tag{7}$$

at $< x_g >= 0.13 \pm 0.08$ and at a scale $< \mu^2 >= 3$ (GeV/c)^2. For $Q^2 < 1$ (GeV/c)^2 and the full 2002-2004 data we obtain a preliminary value of

$$\frac{\Delta G}{G} = 0.016 \pm 0.058(stat) \pm 0.055(syst) \tag{8}$$

at $< x_g >= 0.085$ and at a scale $< \mu^2 >= 3$ (GeV/c)^2. The systematic errors include the experimental systematics, the uncertainties derived from MC simulations and for $Q^2 < 1$ (GeV/c)^2 the estimated contribution of resolved photons.

Open charm production in DIS can be used to select a sample of PGF events with virtually no backgrounds. Due to the high charm quark mass, PGF is by far the most probable process that produces charm quarks in DIS, while the intrinsic charm content of the nucleon or the production of charm quarks during fragmentation can be neglected. In addition, in the independent fragmentation of a $c\overline{c}$ pair most frequently D mesons are produced. Therefore, DIS events with at least one D meson in the final state allows in principle to select a clean PGF sample.

The D^0 mesons are reconstructed from their $K\pi$ decays ($BR = 3.8\%$). Given the thickness of the COMPASS target, D mesons cannot be identified by their decay vertex and have to be selected on the basis of the reconstructed invariant mass. To do that, pairs of tracks with opposite charge and originating from the primary interaction vertex, one of which is positively identified as a kaon by the Ring Imaging Cherenkov (RICH) detector, are combined. This

sample is characterized by a large combinatorial background, that is significantly suppressed by selecting the decay chain $D^* \rightarrow D^0\pi \rightarrow K\pi\pi$; an additional soft pion in the final state is required in this case.

The gluon polarization is calculated from the longitudinal double-spin asymmetry

$$A_{LL} = P_B P_T f a_{LL} \frac{S}{S+B} \frac{\Delta G}{G}, \tag{9}$$

where P_B and P_T are the beam and target polarizations respectively, and f is the target dilution factor. The analyzing power a_{LL} depends on the PGF kinematical variables, that are not completely determined at COMPASS since only one of the D mesons is observed. A parameterization was used obtained from a neural network trained with Monte Carlo events. From the analysis of 2002-2004 data a preliminary value of $\Delta G/G$ from open charm events is obtained at $< x_g >= 0.15$ and at a scale $< \mu^2 >= 13$ (GeV/c)^2:

$$\frac{\Delta G}{G} = -0.57 \pm 0.41(stat) \pm 0.17(syst). \tag{10}$$

The COMPASS results for $\Delta G/G$ from high-p_T and open charm events are summarized in fig. 2 (right) together with the published results of SMC and HERMES. The curves corresponding to the two solutions of the NLO QCD fits of g_1 data are also shown on the plot. The accuracy of the present data points does not allow to discriminate between the two curves; nevertheless, they indicate that ΔG is small in the region of $x_g = 0.1$.

4 Measurements with transversely polarized deuteron target

The transversity distribution functions $\Delta_T q(x)$ are chiral odd quantities and therefore cannot be measured in inclusive DIS measurements. However they can be measured in semi-inclusive DIS, in combination with a chiral odd fragmentation function. A mechanism giving rise to a modulation in the azimuthal distribution of hadrons produced off a transversely polarized target has been proposed by Collins [8]. The number of hadrons observed at a given azimuthal angle is given by

$$N_h(\Phi_C) = N_h^0(1 + P_T \cdot f \cdot D_{nn} \cdot A_{Col} \sin \Phi_C), \tag{11}$$

where P_T and f are the target polarization and dilution factor, respectively, $D_{nn} = (1-y)/(1-y+y^2/2)$ is the spin transfer coefficient, and Φ_C is the

difference between the azimuthal angle of the hadron and that of the spin of the struck quark after the interaction (assuming that the quark spin was initially aligned with the target polarization vector). The Collins asymmetry A_{Col} is given by the product of the transversity distributions $\Delta_T q(x)$ and the chiral odd Collins fragmentation function $\Delta D_q^0(z, p_T^h)$:

$$A_{Col} = \frac{\sum_q e_q^2 \Delta_T q(x) \Delta D_q^0(z, p_T^h)}{\sum_q e_q^2 q(x) D_q^h(z, p_T^h)}, \tag{12}$$

where z is the fraction of energy carried by the hadron and p_T^h is the hadron transverse momentum.

A different mechanism leading to an azimuthal modulation of hadron production has been proposed by Sivers [9]. In this case the azimuthal modulation is produced by a correlation between the nucleon spin and the intrinsic quark transverse momentum k_T, and is given by

$$N_h(\Phi_S) = N_h^0(1 + P_T \cdot f \cdot A_{Siv} \sin \Phi_S), \tag{13}$$

where Φ_S is the difference between the azimuthal angle of the hadron and that of target polarization vector. The Sivers asymmetry A_{Siv} is given by

$$A_{Siv} = \frac{\sum_q e_q^2 \Delta_0^T q(x) D_q^h(z, p_T^h)}{\sum_q e_q^2 q(x) D_q^h(z, p_T^h)}, \tag{14}$$

where $\Delta_0^T q(x)$ is the so-called "Sivers function".

Figure 3 shows the Collins and Sivers asymmetries measured by COMPASS on the transversely polarized deuteron target, as a function of x, z and p_T^h. Data from leading positive (dots) and negative (open circles) hadrons are plotted in the graphs. All points are compatible with zero within statistical errors, at variance to the significant effect observed by HERMES on a proton target. This could be explained by the opposite sign expected from the u and d quark distribution, causing a cancellation of the asymmetries in the case of an isoscalar target. Details can be found in [10].

5 Measurement of pion polarizabilities via inverse Compton scattering

The electric (α_π) and magnetic (β_π) polarizabilities characterize the way a pion interacts with an external electromagnetic field. Theoretical predictions for

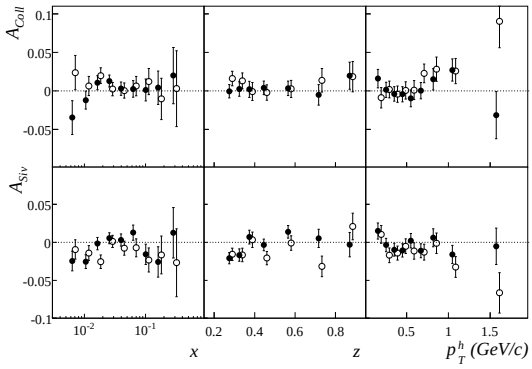

Figure 3: *COMPASS results for the Collins and Sivers asymmetries for leading hadrons, as a function of x, z and the hadron transverse momentum p_T^h. Dots correspond to positive hadrons, open circles to negative hadrons.*

their values are provided by various models: chiral perturbation theory (χPT), dispersion sum rules, lattice calculations, QCD sum rules. The χPT predicts the following values for the pion polarizabilities (two-loop approximation):

$$\alpha_\pi = (2.4 \pm 0.5) \cdot 10^{-4}\ fm^3 \tag{15}$$

$$\beta_\pi = (-2.1 \pm 0.5) \cdot 10^{-4}\ fm^3. \tag{16}$$

A precise experimental determination of α_π and β_π represents a fundamental test of the validity of such models. Experimental measurements have been carried out using three different types of reaction mechanisms:

- inverse Compton scattering (Primakoff reaction):

$$\pi + (A, Z) \ \rightarrow \ \pi + (A, Z) + \gamma, \tag{17}$$

  in which a charged pion interacts with a nuclear target via the exchange of a virtual photon that emerges as a high energy real photon in the final state

- pion photo-production:

$$\gamma + (A, Z) \ \rightarrow \ \gamma + (A, Z) + \pi \tag{18}$$

- $\pi^+\pi^-$ production in e^+e^- collisions:

$$\gamma + \gamma \;\rightarrow\; \pi^+ + \pi^- \tag{19}$$

The presently available experimental values suffer from large statistical and systematic uncertainties, and no conclusion can be derived concerning the validity of theoretical predictions.

At COMPASS we have performed a measurement of the Primakoff scattering using a 190 GeV π^- beam and a 3 mm thick lead target. The cross-section for the reaction can be written as follows:

$$\frac{d\sigma^2_{\gamma\pi}}{dE_{\gamma^*} d\cos\theta} \;=\; Z^2 \left\{ F^{pt}_{\gamma\pi}(\theta) + \frac{m_\pi E_{\gamma^*}}{\alpha} \cdot \frac{\alpha_\pi(1+\cos^2\theta) + 2\beta_\pi \cos\theta}{[1 + E_{\gamma^*}/m_\pi(1-\cos\theta)]^3} \right\}, \tag{20}$$

where E_{γ^*} is the energy of the virtual photon and θ is the photon scattering angle, both computed in the anti-laboratory system, and $F^{pt}_{\gamma\pi}(\theta)$ is the Compton term for a point-like spinless particle.

If the relation $\alpha_\pi = -\beta_\pi$ is assumed, the ratio between the measured and point-like cross-sections can be approximated as follows:

$$R(\omega) \;=\; \frac{d\sigma_{exp}}{d\sigma^{pt}_{MC}} \;\approx\; 1 + \frac{3}{2}\frac{m_\pi^2}{\alpha}\frac{\omega^2}{1-\omega}\beta_\pi, \tag{21}$$

where $\omega = E_\gamma / E_{beam}$ in the laboratory system. Therefore β_π can be determined by fitting the experimental points (after taking into account radiative corrections) with $R(\omega)$. The preliminary COMPASS data points and the result of the fit are shown in fig.4 (left). Details of the data analysis procedure and of the events selection can be found in [11].

One unique peculiarity of the COMPASS experiment is the availability of both pion and muon beams of the same energy and with similar characteristics. Since muons are point-like particles with a mass very close to that of the pion, the kinematics (and hence the experimental acceptance) is very similar in the two cases and the measurement of α_μ and β_μ provides a powerful check of possible systematic effects. The result of this measurement if shown in fig.4 (right) and is found to be compatible with zero as it should.

From the analysis of the 2004 data we have extracted a preliminary value of the pion polarizabilities:

$$\alpha_\pi \;=\; -\beta_\pi \;=\; (2.5 \pm 1.7_{stat} \pm 0.6_{sys}) \cdot 10^{-4}\ \mathrm{fm}^3, \tag{22}$$

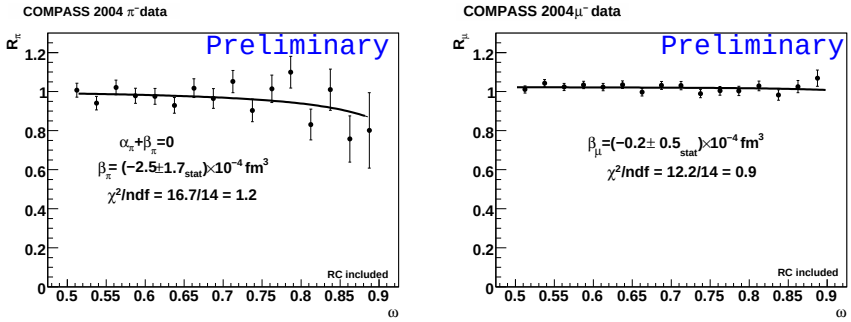

Figure 4: *Ratio between the experimentally measured cross-section and the one for point-like particles from MonteCarlo simulations, in bins of* $\omega = E_\gamma/E_{beam}$. *Left plot refers to incident pions, right one to incident muons.*

where the systematic error includes the result of the muon measurement, the contribution of radiative corrections, the contribution of diffractive and other backgrounds and the contribution of the muon and electron components in the hadron beam.

6 Light meson spectroscopy at COMPASS

The part of the COMPASS physics program requiring hadronic probes has been only marginally addressed during the 2004 data taking, with the measurement of the pion polarizabilities and a pilot diffractive scattering measurement. The program will continue during the next 2 years by addressing the more general topic of light meson spectroscopy, using protons, pions and kaons as projectiles. Among the topics to be addressed, the existence and properties of glueballs and hybrid mesons are of fundamental importance to verify the predictions of models of non-perturbative QCD. For a comprehensive review on the subject the reader is referred to [12].

The production of glueballs and hybrids is expected to be enhanced in central collisions and diffractive meson excitation. The final states produced by the two processes have significantly different kinematical properties (large rapidity gap, with particles emitted at low momenta/large angles in the first case, forward kinematics in the second), which led to the construction of dedicated

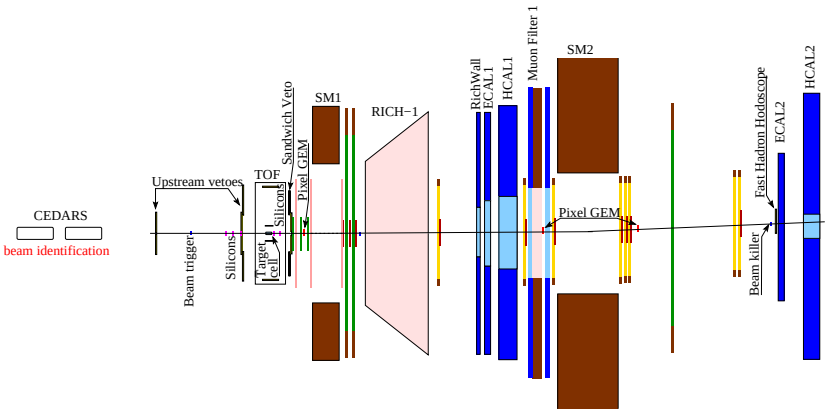

Figure 5: *Schematic view of the COMPASS experimental layout for light meson spectroscopy.*

central production or diffractive scattering experiments in the past. The large acceptance and high momentum resolution of the COMPASS spectrometer, as well as the availability of both proton and pion beams, will on the contrary allow to study the two processes simultaneously.

The experimental setup foreseen for meson spectroscopy measurements is for the major part identical to that of used for the measurements with muon beams [1)]. The main modifications concern the target region, the electromagnetic calorimetry, the beam tracking and the trigger, and are only briefly outlined here. The polarized target installed in the muon setup will be substituted by a liquid Hydrogen target, with a cell of 40 cm length and 3.5 cm diameter. The slow recoil protons produced at large angles in the central and diffractive collisions will be detected by a Time of Flight (TOF) system surrounding the target. The TOF detector was originally designed for the NA12 experiment [13)], and has been modified to match the COMPASS acceptance and target length. Two telescopes of silicon microstrip detectors, located upstream and downstream of the target and providing a typical spatial resolution of 10 μm per plane, precisely measure the direction of the beam and of the secondary particles produced in the target. New GEM detectors, with a pixelized readout in the central region, have been developed to replace a major

fraction of the scintillating fiber detectors for the tracking of particles at very small angles, thus significantly reducing the amount of material in the beam region. The second electromagnetic calorimeter ECAL2 will be equipped with new Shashlik-type modules in the central region, thus improving the radiation hardness and the energy resolution in the most irradiated region. Finally, new trigger hodoscopes will be installed to detect the forward scattered hadrons and the charged particle multiplicities. The foreseen experimental layout is schematically sketched in fig.5.

References

1. P. Abbon *et al*, Nucl. Ins. Meth. **A577**, 455 (2007)
2. EMC, J. Ashman *et al*, Phys. Lett. **B206**, 364 (1988)
3. EMC, J. Ashman *et al*, Phys. Lett. **B328**, 1 (1989)
4. B. Adeva *et al*, Phys. Rev. **D58**, 112001 (1998); Erratum *ibid* **D62**, 079902.
5. B. Badelek and J. Kwiecinski, Phys. Lett. **B295**, 263 (1992).
6. COMPASS, V.Yu. Alexakhin *et al*, Phys. Lett. **B647**, 8 (2007)
7. COMPASS, E.S. Ageev *et al*, Phys. Lett. **B633**, 25 (2006)
8. J.C. Collins, Nucl. Phys **B396**, 161 (1993)
9. D.W. Sivers, Phys. Rev. **D41**, 83 (1990)
10. COMPASS, E.S. Ageev *et al*, Nucl. Phys. **B765**, 31 (2007)
11. J. Friedrich, these proceedings
12. C. Amsler and N.A. Törnqvist, Phys. Rep. **389**, 61 (2004)
13. D. Alde *et al.*, Nucl. Inst. Meth. **A342**, 389 (1994)

Frascati Physics Series Vol. XLVI (2007), pp. 301
HADRON07: XII Int. Conf. on Hadron Spectroscopy – Frascati, October 8-13, 2007
Plenary Session

SPECTROSCOPY IN HYPERON BEAMS

J. Russ
Carnegie Mellon University

Written contribution not received

Frascati Physics Series Vol. XLVI (2007), pp. 303–314
HADRON07: XII Int. Conf. on Hadron Spectroscopy – Frascati, October 8-13, 2007
Plenary Session

THE SEARCH FOR BOUND KAONIC SYSTEMS IN NUCLEI, EXPERIMENTAL STATUS AND THEORETICAL PREDICTIONS

Stefano Piano
INFN Sezione di Trieste, via Valerio 2, Trieste, Italy

Abstract

An overview of both experimental and theoretical results in the search of deeply bound kaonic aggregates with two or three baryons is reported.

1 Introduction

1.1 Theoretical overview

The search for deeply bound kaon-nuclear states (DBKS) is one of the hottest topics in hadron physics today. The existence of such aggregates, formed by nucleons bound rather tightly by an antikaon, might have important repercussions on astrophysical scale, since strange nuclear matter might be a constituent of star cores. Moreover, deeply bound states of mesons formed in a nucleus offer

a way to study the mechanism of spontaneous breaking of chiral symmetry in nuclear matter.

From the theoretical point of view the opinions on the existence of kaon-nucleon aggregates are quite discordant. A general understanding of $\overline{K}N$ and $\overline{K}A$ interactions [1)] does not foresee detectable levels; in fact, their binding energies are predicted to be $10 \div 30$ MeV and their widths $80 \div 100$ MeV, which largely exceed the level separation thus preventing their observation.

Recent theoretical works tend to confirm this scenario, namely, a preference for shallower potentials and large widths. On the other hand, phenomenological approaches have been developed, which call for the existence of strongly-bound and narrow nucleon systems, therefore easily detectable.

A model asserting the existence of such states was developed by Akaishi and Yamazaki [2)], which is based on a phenomenological reproduction of the $\overline{K}N$ interaction through a G-matrix approach. The existence of the $\Lambda(1405)$ resonance, probably a $\overline{K}N$ bound state, suggests that the $\overline{K}N$ interaction in the $I = 0$ configuration is attractive. More composite states are interpreted as molecules formed by the $\Lambda(1405)$ and few nucleons. The force bounding the system is a sort of covalent bond between the K^- and the nucleons, which results to be much stronger than the nuclear force [3)]. In this configuration the presence of the K^- should increase the binding energy of the system against the incompressibility of the core nucleus, and systems of this kind should be very stable and compact, with a central density several times bigger than the density of ordinary nuclear matter. According to [3)], these aggregates should be formed with higher probabilities when kaons interact with light nuclei. The model predicts the existence of kaon-multinucleon aggregates with binding energy of 86 MeV for ^{4}He+K^- and 113 MeV for ^{8}Be+K^-, and widths of 20 MeV for ^{3}He+K^- and 38 MeV for ^{8}Be+K^-. A consequence of the high binding energy is that these aggregates cannot decay into the $\Sigma\pi$ channel, while the $\Lambda\pi$ channel is suppressed due to isospin conservation. This approach, however, has been criticized for the simplified treatment of kaon absorption.

Other models, which predict the existence of kaon-nuclear aggregates, foresee shallower potentials, which do not necessarily entail weak binding energies ($-ReV_{opt} \simeq 50 \div 75$ MeV against $150 \div 200$ MeV), however they predict large widths, which prevent the experimental observation [4)]. Those theories based on a microscopic chiral approach [5)] predict binding energies of about

30-40 MeV and widths around 80-100 MeV. The same resuts is obtained by approaches based on three-body Faddeev calculations [6]. According to a dynamical approach [7], the kaon-nucleus potential is found to depend on density, which predict for nuclei heavier than ^{12}C, narrow states, less than 50 MeV, with binding energy $B_{\overline{K}} \simeq 100 \div 200$ MeV. Furthermore, for lighter nuclei $\overline{K}$-nuclear bound states are broader. A further approach based on the Green chiral function method applied to phenomenological optical potentials [8] suggests that such structures could in principle be formed but with small production rates, therefore their experimental observation is questionable.

In summary, no precise prescriptions for the observation of such states nor for their decay modes are provided by theories, although suggesting a preference for the formation in heavy nuclei; yet, in the latter case, the effects of Final State Interactions would probably dominate, which suggests to start the experimental investigation on light systems.

1.2 Experimental approaches and first observations

Two techniques have been used so far to search for kaon bound states, namely the missing mass method, and the invariant mass spectroscopy. In the first case, the analysis is based on the study of $A(K^-, N)X$ inclusive or semi-inclusive spectra, where the presence of a peak in the momentum spectrum of the X recoiling particle is interpreted as an bound state. In the second case, possible nuclear aggregates are deduced from their invariant mass spectra. The invariant mass approach is more complete and less subject to misinterpretation. Moreover, the reconstruction of the full event allows one to look for correlations between kinematical observables; as for instance, the angular correlation between particles in the final state. This approach was applied not only in the study of kaon induced reactions but also in the search for kaon-nuclear states in antiproton annihilation reactions (CERN-OBELIX) and in heavy ion collisions (GSI-FOPI).

The initial results from experiments regarding the quest of kaon-nuclear bound systems have changed with the time. The KEK-PS-E471 findings [10] concerning two states consistent with the Akaishi-Yamazaki predictions have been withdrawn. These findings, based on the inclusive proton and neutron spectra of the ^{4}He$(K^-_{stop}, p)X$ and ^{4}He$(K^-_{stop}, n)X$ reactions, have been contradicted by recent high-statistic measurements [11]. A candidate of $^{15}_{K^-}$O state

still survives. It has been measured by the AGS-E930 Experiment [12] with a binding energy of about 90 MeV. It has been deduced by means of the missing mass method in inclusive spectra, which may draw to questionable conclusions.

An example of this is given by the analysis of the proton inclusive spectrum of the ^{6}Li$(K^-_{stop}, p)X$ reaction measured by FINUDA [13]. Here, a peak at about 500 MeV/c has been observed in the inclusive proton momentum spectrum (Fig. 1 left), similar to the signal seen by KEK-PS E471, which led to the discovery of $S^0(3115)$. The capability of FINUDA to have complete information for each event showed that the peak is simply due to the $K^-(np) \rightarrow \Sigma^- p$ reaction, thus avoiding exotic explanations.

Fig. 1 (center) shows the momentum distribution of protond in coincidence with negative pions. A signature for $K^-(np) \rightarrow \Sigma^- p$ reaction is given by ∼505 MeV/c protons emitted in opposite direction with respect to pions of momenta exceeding 275 MeV/c. Such constraints have been applied to pions, which give rise to the peak at ∼505 MeV/c (full histogram in Fig. 1). In addition, Fig. 1 (right) shows the opening angle distribution formed by negative pions and protons measured in coincidence, The distribution is peaked at 180^O, which contradicts the expected isotropic decay due to a bound kaonic nuclear state.

2 The kaon-nuclear aggregates with two baryons

According to the Akaishi-Yamazaki model, the simplest kaon-nucleon aggregate beyond $\Lambda(1405)$ is $(K^- pp)$. The presence of the $\overline{K}$ bounds two protons to form a kaon nuclear state with a binding energy of 48 MeV, a mass of 2232 MeV/c^2, and with a width of 61 MeV. A $(K^- pp)$ state can be studied by means of the Λp decay channel. A FINUDA first measurement showed the presence of a signal, which has been identified with a bound kaonic state: a bump in the Λp invariant mass spectrum has been found at about 2.25 GeV/c^2. The events were preferentially back-to-back emitted, and the bump summed up the contributions of light targets, ^{6}Li, ^{7}Li and ^{12}C [14]. The bump, shown in Fig. 2 before and after (inset) the acceptance correction, cannot be explained as due to $K^- pp \rightarrow \Lambda p$ reaction leaving the daughter nucleus in the ground state. Such a reaction would require a peak close to the threshold of the reaction $K^- A \rightarrow A' \Lambda p$, with A' the daughter nucleus in the ground state, (i.e., for ^{12}C ∼2.34 GeV/c^2), while the observed signal has a significantly lower mass (2.25

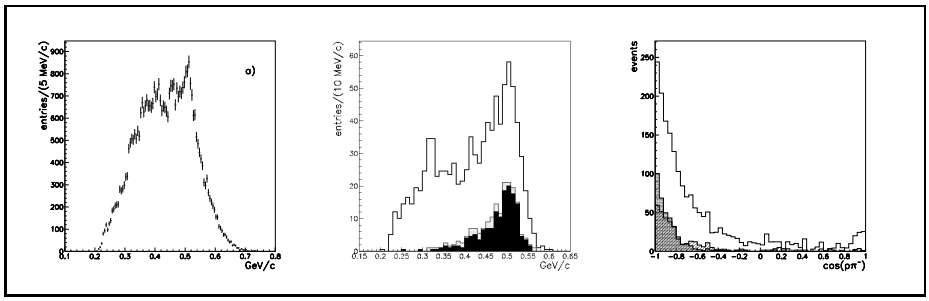

Figure 1: Left: Inclusive momentum spectrum of protons from the K^-_{stop} ^{6}Li $\rightarrow$ p X reaction; Center: open histogram: proton momentum distribution in coincidence with negative pions; grey histogram: events with a π^- with momentum larger than 275 MeV/c; black: same events with an additional back-to-back angular cut ($\cos\Theta_{\pi^- p} < -0.8$); Right: distribution of the angle between a proton and a π^- track: the white histogram is for all events, the shaded one for events with the pion momentum larger than 275 MeV/c, the hatched one for events with the proton momentum in the window (275 $\div$ 350) MeV/c, that can be addressed to the quasi-free absorption reaction $K^- n \rightarrow \Lambda\pi^-$. These angular distributions are acceptance corrected and normalized to the number of selected events in each sample.

GeV/c^2).

The $K^- pp \rightarrow \Sigma^0 p$ reaction along with the $\Sigma^0 \rightarrow \Lambda\gamma$, cannot explain the bump features, since a peak of a lower invariant mass (74 MeV/c^2) and of a narrower width would be expected. In addition, the relative branching fractions of the two channels $\Lambda p/\Sigma^0 p$ favors Λp decay [15]. Therefore, even if the $\Sigma^0 p$ events fall within the relevant mass range, the strength of this channel is too small to have a significant effect in the main peak observed by FINUDA. The measurement establishes a value of 2255$\pm$9 MeV/c^2 for the mass of the peak observed in the Λp system corresponding to a binding energy $B_{\overline{K}} = (115^{+6}_{-5}(stat)^{+3}_{-4}(sys))$ MeV a width $\Gamma = (67^{+14}_{-11}(stat)^{+2}_{-3}(sys))$ MeV, and a formation rate of the order of $0.1\%/K^-_{stop}$.

An interpretation of the 2255 MeV/c^2 was suggested by Magas *et al.* [16], which doesn't need the formation of a deeply-bound kaon-nuclear state. Namely, it is stated that the bump results from the angular cuts applied to a $m_{\Lambda p}$ phase space distribution distorted by Final State Interactions (FSI).

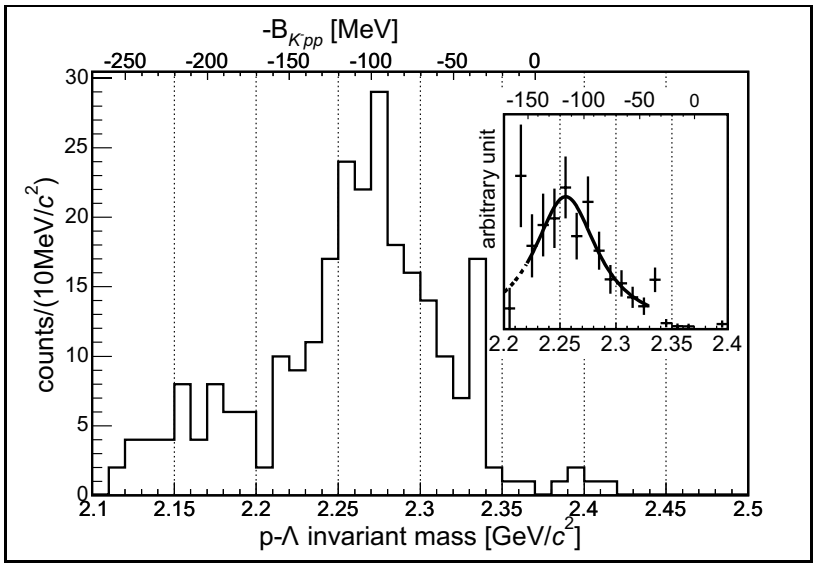

Figure 2: Invariant mass of the Λp system, for K^- interactions in the ^{6}Li, ^{7}Li and ^{12}C targets of FINUDA. The events have been selected with the Λ and proton almost back-to-back. The inset reports the spectrum obtained after acceptance correction. More details are given in the text.

However, the FINUDA data have shown that FSI alone is not able to explain the shape of the $m_{\Lambda p}$ distribution. In fact, the same signature is observed even without applying the above mentioned angular cuts, $cos\Theta_{\Lambda p} < -0.8$. Moreover, a similar signal has been observed in the annihilation of antiprotons on ^{4}He, where the expected FSI effects are not sizeable. The $p\Lambda$ system was studied by the OBELIX collaboration by using the annihilation reaction $\bar{p}^4\mathrm{He} \rightarrow (p\pi^-)pK^0X$ [17], which yielded a signal with a statistical significance of 3.7σ (Fig. 3, left) whereas it is absent in the $pp\pi^+$ invariant mass (Fig. 3, right).

The experiment is not suitable for the detection of particles out of secondary vertices, and the coherent background, due to phase-space, as well as the background from N^* and Δ decays, is rather large. However, the observed signal is narrow (< 24 MeV) and has a binding energy rather large (~ 160 MeV), which exceeds the value quoted by FINUDA. The collected statistics for

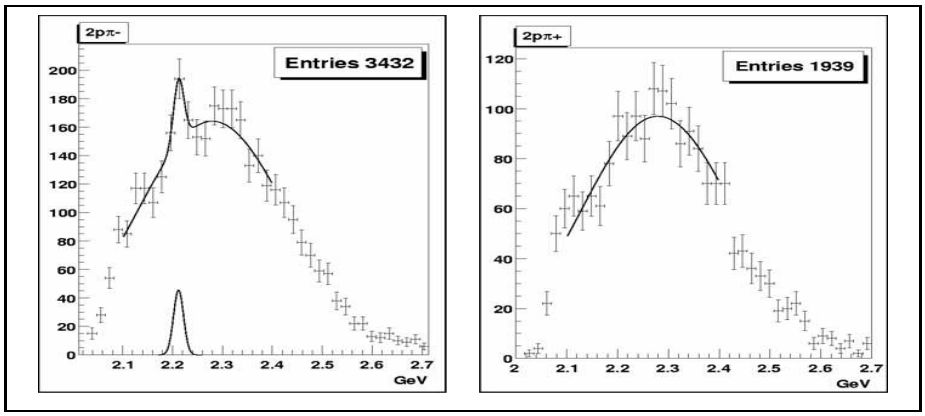

Figure 3: Left: Invariant mass of $2p\pi^-$s. The solid curve is a fit with phase-space line deduced from $2p\pi^+$ invariant mass (Fig. 3 Right) with a Gaussian function to account for the peak; Right: $2p\pi^+$ invariant mass from Ref. [17]. In these events, the $\pi^- p$ invariant mass has been selected in a mass window around the Λ peak.

this reaction is rather limited, which does not allow further conclusion to be drawn.

3 The kaon-nuclear aggregates with three baryons

According to the model by Akaishi and Yamazaki, tri-baryon kaonic states should be observed with masses around 3120 MeV/c^2, binding energies of about 190 MeV and a widths of 13 MeV if their isospin configuration is $T = 1$. For $T = 0$, the expected mass is 3152 MeV/c^2, binding energy is 170 MeV, and width 21 MeV.

Presently, experiment observations rely on low statistics data. However, the FINUDA data (run ended at June 2007) will supply about an order of magnitude of more statistics, which allow a better study of this kind of aggregates to be pursued.

The first observation of $[K^- ppn]$ bound state decaying into the Λd channel has been put forward by FOPI in the study of the Ni+Ni collision at 1.93 AGeV [18]. The observed K-nucleon state has a binding energy of 151 MeV, a width

Γ = 100 MeV and at a mass of about 3160 MeV/c^2. However, these results have never been confirmed. In the same mass range, OBELIX has measured few Λd events in the $\bar{p}^4$He annihilation, quoting a binding energy of 120 MeV and a width less than 60 MeV.

FINUDA cannot inspects, due its acceptance, the mass region below 3200 MeV/c^2. However, above it, FINUDA noticed the presence of a bump in the Λd invariant mass spectrum, which cannot be explained by kaon two-nucleon absorption. For this experiment, Λ-hyperons have been selected in coincidence with deuterons. Protons and negative pions, coming from Λ decay are inquired to have well defined tracks out of a secondary vertex. A total of 25 events have been collected for ^{6}Li. The acceptance corrected invariant mass spectrum of the Λd pairs is reported in Fig. 4; where a bump can be observed at about 3250 MeV/c^2. The same doesn't occur for the ^{12}C, which might be due to Final State Interactions. Conversely, the reaction K$^-$ ^{6}Li ($\equiv \alpha \oplus$ d) $\rightarrow \Lambda$ d 3N, which may involve the α-substructure of ^{6}Li, should slightly be affected by FSI, since the residual nucleus is constituted only by 3 nucleons not necessarily bound. The curves in the picture are arbitrarily normalized to the experimental spectrum and are phase-space simulations for the above reaction channels. The dashed line shows the phase space simulation for the $[\Lambda d]nnp$ channel, the dotted line the simulations for the $[\Lambda d]nd$ channel, and the dot-dashed line the simulations for the $[\Lambda d]t$ channel. The only way to fit the bump is to add a Gaussian curve (convoluted by the experimental resolution $\sigma_{\Lambda d}$ = 6.0 MeV/c^2), to a linear combination of the three mentioned channels. The best fit returns the following parameters for the bump: $m_{\Lambda d} = 3251 \pm 6$ MeV/c^2 and $\Gamma_{\Lambda d} = 36.6 \pm 14.1$ MeV/c^2. The production rate is $Y_{\Lambda d} = (4.4 \pm 1.4) \times 10^{-3}/K^-_{stop}$, while the statistical significance of the bump is found to be $\mathcal{Z} = 3.9\sigma$.

A study of the missing kinetic energy distribution suggests that the most probable reaction is the $K^-\alpha$ absorption, which leaves a spectator deuteron as residual nucleus. The $[K^-\alpha]$ system then decays and FINUDA reconstructs the Λd pairs. The undetected neutrons from the $K^-\alpha \rightarrow \Lambda dn$ have a kinetic energy of 25 $\pm$ 25 MeV, which is determined by the missing kinetic energy of the K^- ^{6}Li absorption.

In the inset of Fig. 4 is shown the angular distribution between Λs and ds for $m_{\Lambda d}$ constrained between 3220 and 3280 MeV/c^2. This distribution shows a marked back-to-back correlation, which suggests that the (Λd) bound system

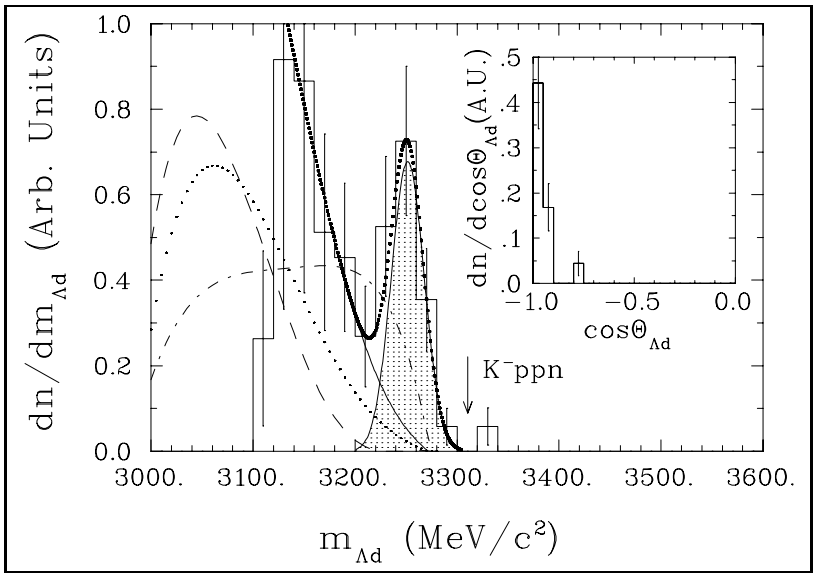

Figure 4: Invariant mass distribution of the (Λd) system for events from the ^{6}Li$(K^-_{stop},\ \Lambda d)3N$ reaction, solid line histogram; superimposed are the results of phase space simulations of several channels: dashed line $[\Lambda d]nnp$, dotted line $[\Lambda d]nnp$, dot-dashed line $[\Lambda d]t$. The bold dotted-line is a fit of the experimental data with a Gaussian function and a linear combination of the above mentioned absorption reactions; the solid line shows the contribution of the simulated background only. The arrow indicates the overall mass of the unbound K^-ppn system. Inset, cos$\Theta_{\Lambda d}$ distribution of the events populating the bump at 3250 MeV/c^2.

decays at rest.

An alternative explanation has recently been arisen by the E549 collaboration at KEK, which has measured the Λd correlation for the ^{4}He(K^-_{stop}, d) reaction [20]. According to it analysis, the peak they have observed at 3282 MeV/c^2 can simply be interpreted as due to the absorption on three nucleons, $K^-ppn(n) \rightarrow \Lambda d(n)$. It must be observed that the detector of KEK experiment is affected by limited acceptance, which allows only back-to-back deuterons and protons to be detected. Therefore, their conclusion needs to be carefully tested.

4 Summary and Conclusions

The experimental observations collected up to now in the search of K^--nuclear bound systemss are far from being conclusive, as they are not in particular agreement with any of the proposed models. Concerning the (K^-pp) aggregate, the experimental values for the binding energy largely exceeds the theoretical expectations, while the quoted widths are in better agreement with theory. Only the OBELIX experiments reports a small Γ. For the (K^-ppn) aggregates only few experimental values are available, which are rather spread out. It is therefore hard to find out an agreement with the expected values yielded by the A-Y model, which is the only model capable of predictions. Therefore, the debate is still very lively and new measurements are eagerly awaited to pove (or disprove) the existing experimental results.

Nowadays just a few experiments are on the floor capable of shedding further light on the problem. One of them is FINUDA, which has recently concluded its data taking. It has collected about 1 fb^{-1} of data being able to deliver soon results concerning the interaction of K^- on several light targets. With the collected statistics, the A-dependence of the production of possible Λp and Λd bound states, will be possible. Other active experiments presently in this field are E459 at KEK, and FOPI at GSI. The latter will study Λp and Λd states via pp collision at 3.5 AGeV, which will help to understand the dynamics of the production processes in a high temperature environment.

Projects dedicated to future studies have been proposed and currently a large community of physicists is engaged in building experimental apparata: at J-PARC the E15 experiment aims to investigate the existence of K^--nuclear aggregates in the ^{3}He(K^-, n) reaction in flight; at LNF, the AMADEUS collaboration will study K^- induced interactions in ^{4}He and ^{3}He targets.

As well theorists show an increasing interest for this topic, which will surely bring about a reliable framework for the experimental data. The search for bound kaon-nuclear systems is therefore a challenging topic for the hadron community.

References

1. S. Hirenzaki *et al.*, *Phys. Rev.* **C61** (2000), 055205
2. Y. Akaishi, T. Yamazaki, *Phys. Rev.* **C65** (2002), 044005

T. Yamazaki, Y. Akaishi, *Nucl. Phys.* **B535** (2002), 70
Y. Akaishi *et al.*, *Phys. Lett.* **B613** (2005), 140
T. Yamazaki, Y. Akaishi, *Nucl. Phys.* **A792** (2007), 229

3. T. Yamazaki, Y. Akaishi, *Proc. Jpn. Acad.* **B83** (2007),144

4. J. Schaffner-Bielich *et al.*, *Nucl. Phys.* **A 669** (2000), 153
A. Cieply *et al.*, *Nucl. Phys.* **A696** (2001), 173
W. Weise, contribution presented at *EXA2005 Conference*, Vienna, February 2005, arXiv:nucl-th/0507058 (2005) and references therein

5. A. Ramos, E. Oset, *Nucl. Phys.* **A671** (2000), 153
E. Oset, contribution presented at the *HYP2006 Conference*, Mainz, October 2006, arXiv: nucl-th/0701023

6. N. Shevchenko *et al.*, *Phys. Rev. Lett.* **98** (2007), 082301

7. J. Mareš *et al.*, *Nucl. Phys.* **A770** (2006), 84

8. J. Yamagata *et al.*, *Phy. Rev.* **C74** (2006), 014604

9. E. Oset, H. Toki, *Phys. Rev.* **C74** (2006), 015207

10. T. Suzuki *et al.*, *Phys. Lett.* **B597** (2004), 263
T. Suzuki *et al.*, *Nucl. Phys.* **A754** (2005), 375c

11. M. Sato *et al.*, arXiv:nucl-ex/0708.2968

12. T. Kishimoto, *et al. Nucl. Phys.* **A754** (2005), 383c

13. M. Agnello *et al.*, *Nucl. Phys.* **A775** (2006), 35

14. M. Agnello *et al.*, *Phys. Rev. Lett.* **94** (2005), 212303

15. C. Vander Velde-Wilcquet *et al.*, *Nuovo Cim.* **A39** (1977), 538
P.A. Katz *et al.*, *Phys. Rev.* **D1** (1970), 1267

16. V. K. Magas, E. Oset. A. Ramos and H. Toki, arXiv:nucl-th/0601013v1 Jan. 2006

17. G. Bendiscioli *al.*, *Nucl. Phys.* **A789** (2007), 222

18. N. Herrmann, presentation at ETC* *Workshop on Exotic hadronic atoms*, Trento, June 2006

19. M. Agnello *et al.*, *Phys. Lett.* **B** (2007), **B654** (2007), 80
M. Agnello *et al.*, *Eur. Phys. J.* **A33** (2007), 283

20. T. Suzuki, *et al.*, arXiv:nucl-ex/0709.0996

Frascati Physics Series Vol. XLVI (2007), pp. 315–326
HADRON07: XII Int. Conf. on Hadron Spectroscopy – Frascati, October 8-13, 2007
Plenary Session

NUCLEON STRUCTURE STUDIES IN HALL A AT JLAB

Kees de Jager
Jefferson Laboratory
12000 Jefferson Avenue, Newport News, VA 23606, USA

Abstract

Three examples are presented from the broad program of nucleon structure research in Hall A at Jefferson Lab (JLab): a measurement of the neutron charge form factor to double the squared momentum-transfer of present data, highly accurate cross-section measurements of Deeply Virtual Compton Scattering and a program of parity-violating asymmetry studies with the 12 GeV upgrade that will provide sensitive probes of the Standard Model and its extensions.

1 Introduction

The nucleon electro-magnetic form factors (EMFF) are of fundamental importance for the understanding of the nucleon's internal structure. The Generalized Parton Distributions (GPD) relate the spatial and momentum distributions of a parton in a nucleon by providing a consistent framework for the EMFF

and the parton distribution functions (PDF). Deeply Virtual Compton scattering (DVCS) is the most accessible reaction to study GPDs. Parity violation in the neutral weak-current interaction is observed in scattering experiments with polarized electron beams. Two classes of such experiments are proposed with the 12 GeV upgrade at JLab. First, precise measurements of the parity-violation asymmetry in deep-inelastic electron-deuteron and electron-proton scattering (PVDIS) will probe the quark substructure of the nucleon. Second, the high quality of the JLab polarized beam will allow a Møller scattering experiment that will determine the running of the weak mixing angle $\sin^2(\theta_W)$ with a precision comparable to that obtained at high-energy colliders.

The base instrumentation in Hall A [1)] has been used for experiments which require high luminosity and high resolution in momentum and/or angle of at least one of the reaction products. The central elements are the two High Resolution Spectrometers (HRS), to which recently a third spectrometer has been added with a large acceptance (BigBite). It is also the largest of the three experimental halls, making it the prime candidate for the installation of special large instrumentation.

2 Neutron Charge Form Factor

In the past decade a series of double-polarization measurements of neutron knock-out from a polarized ^{2}H or ^{3}He target have provided accurate data on G_E^n. The ratio of the beam-target asymmetry with the target polarization perpendicular and parallel to the momentum transfer is directly proportional to the ratio of the electric and magnetic form factors,

$$\frac{G_E^n}{G_M^n} = -\frac{P_x}{P_z}\frac{E_e + E'_e}{2M}\tan(\frac{\theta_e}{2}), \tag{1}$$

where P_x and P_z denote the polarization component perpendicular and parallel to $\vec{q}$. Corrections for the (small) d-state component and for charge-exchange contributions from the protons in ^{3}He can be calculated accurately with the Generalized Eikonal Approximation [3)] at Q^2-values larger than ~ 1.5 GeV^2. A similar result is obtained with an unpolarized deuteron target when one measures the polarization of the knocked-out neutron as a function of the angle over which the neutron spin is precessed with a dipole magnet.
Experiment E02-013 [2)] measured the charge form factor of the neutron G_E^n

by studying the spin asymmetry in the reaction $^3\vec{\mathrm{He}}(\vec{e}, e'n)$ at four values of Q^2 up to 3.5 GeV^2. The scattered electron and the knocked-out neutron were detected in coincidence using the open-geometry electron spectrometer BigBite and the large neutron detector BigHAND, respectively.

The BigBite spectrometer (with a solid-angle acceptance of roughly 76 msr) consisted of a large dipole magnet and a detector package containing three wire chambers and a lead-glass shower counter, separated into a pre-shower and full-absorption region. The front and back wire chambers each had six planes of sensitive wires, the middle chamber three planes. A hit above a high threshold in the shower counter together with a neutron event from BigHAND provided the basic coincidence trigger for the experiment.

The BigHAND neutron detector (with an active detection area of around 8 m^2 and a total weight of ∼80 tons) contained over 200 neutron bars arranged in seven vertical walls sandwiched between iron. It also contained two veto walls with ∼180 veto counters protected from the target by two inches of lead.

The polarized ^{3}He target that sat on the pivot in Hall A was basically designed from the ground up. A magnetic holding field of roughly 2 mT was produced using a large iron box that also provided shielding from the fringe field of BigBite and served as a scattering chamber. The sealed glass target cells in which the ^{3}He was polarized contained a mixture of potassium and rubidium, in contrast with previous target cells in which the only alkali-metal present was rubidium. This hybrid optical pumping technique yielded a substantially higher polarization, quicker pump-up times, and less sensitivity to depolarization from the passage of the electron beam. Light from high-power diode-laser arrays was brought to the target using optical fibers. The optics used for polarizing the light and focusing it onto the target cells were mounted directly on top of the target enclosure. The target held a polarization of about 50% during many weeks of continuous running with an 8 μA electron beam. With the 40 cm long target cells containing ^{3}He at roughly 10 atm, E02-013 operated at a luminosity of $5 \cdot 10^{36}$ /cm^2/s. With such a high luminosity, improved target polarization, and the large acceptance of the BigBite/BigHAND combination, a Figure-of-Merit was achieved that was at least 15 times larger than that of any previous G_E^n experiment.

The analysis of the BigBite optics resulted in a vertex reconstruction of 5 mm and a momentum resolution of ∼1%. The shower detector was calibrated before

the experiment with cosmic rays. A resolution of ∼0.5 ns after corrections was achieved for the time-of-flight (TOF) measurement in BigHAND. The veto efficiency per counter is about 95%, consistent with expectations at the high counting rate. Quasi-elastic events were selected through cuts on the invariant mass W and on the transverse component of the missing momentum P_{per}. The dilution of the measured beam asymmetry due to proton leakage through charge-exchange reactions was extracted from measurements on various targets and found to be in good agreement with simulations. A preliminary analysis of the data at $Q^2 = 1.8$ GeV^2 has yielded a value of G_E^n close to the Belitsky scaling prediction with an accuracy of ∼15%, which is the total error expected for each of the four Q^2-values, as illustrated in the left part of Fig. 1.

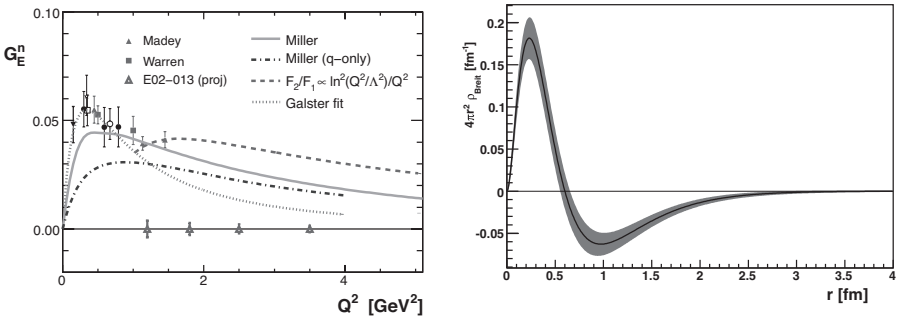

Figure 1: *Left: Selected world data on G_E^n with the values of Q^2 in E02-013 and the expected accuracy, shown relative to the Galster fit. The solid curve is a calculation in the relativistic constituent quark model by G. Miller* [4]. *The dashed curve takes its shape from the pQCD prediction by A. Belitsky et al.* [5], *normalized to the experimental G_E^n value at 1.3 GeV^2. Right: The radial distribution of the charge in the neutron, extracted from an analysis of the world data.*

In the Breit frame the nucleon form factors can be written as Fourier transforms of the charge and magnetization distributions. However, if the wavelength of the probe is larger than the Compton wavelength of the nucleon, i.e. if $|Q| \geq M_N$, the form factors also contain dynamical effects due to relativistic boosts. The negative lobe at ∼1 fm in the radial charge distribution shown in the right part of Fig. 1 supports the model of the neutron in which for part of

the time it consists of a π^- circling a proton, which is consistent with Miller's calculation that shows a large contribution of the pion at low Q^2-values.

3 Deeply Virtual Compton Scattering

The E00-110 experiment [6] ran with 5.75 GeV electrons incident on a 15 cm long liquid H_2 target. The luminosity was typically $10^{37}/\mathrm{cm}^2/\mathrm{s}$ with a 76% beam polarization. The scattered electrons were detected in one High Resolution Spectrometer (HRS), while photons above a 1 GeV energy threshold (and $\gamma\gamma$ coincidences from π^0 decay) were detected in a 11×12 array of $3 \times 3 \times 18.6$ cm^3 PbF_2 crystals, whose front face was located 110 cm from the target center. DVCS events were selected from electron-photon coincidences, after subtraction of the π^0 yield - estimated from two-photon events - and application of a missing-mass cut $M_X^2 < (M + m_\pi)^2$.
To order twist-3 the DVCS helicity-dependent ($d\Sigma$) and helicity-independent ($d\sigma$) cross sections are given by [8]:

$$\begin{aligned}
\frac{d^4\Sigma}{d^4\Phi} &\equiv \frac{1}{2}\left[\frac{d^4\sigma^+}{d^4\Phi} - \frac{d^4\sigma^-}{d^4\Phi}\right] = \qquad (2)\\
&= \sin(\phi_{\gamma\gamma})\Gamma_1^{\Im}\,\Im\mathrm{m}\left[\mathcal{C}^I(\mathcal{F})\right] - \sin(2\phi_{\gamma\gamma})\Gamma_2^{\Im}\,\Im\mathrm{m}\left[\mathcal{C}^I(\mathcal{F}^{\mathrm{eff}})\right],\\
\frac{d^4\sigma}{d^4\Phi} &\equiv \frac{1}{2}\left[\frac{d^4\sigma^+}{d^4\Phi} + \frac{d^4\sigma^-}{d^4\Phi}\right] = \frac{d^4\sigma(|DVCS|^2)}{dQ^2 dx_{\mathrm{Bj}} dt d\phi_{\gamma\gamma}} + \frac{d^4\sigma(|BH|^2)}{dQ^2 dx_{\mathrm{Bj}} dt d\phi_{\gamma\gamma}} \qquad (3)\\
&+ \Gamma_{0,\Delta}^{\Re}\,\Re e\left[\mathcal{C}^I + \Delta\mathcal{C}^I\right](\mathcal{F}) + \Gamma_0^{\Re}\Re e\left[\mathcal{C}^I(\mathcal{F})\right]\\
&- \cos(\phi_{\gamma\gamma})\Gamma_1^{\Re}\Re e\left[\mathcal{C}^I(\mathcal{F})\right] + \cos(2\phi_{\gamma\gamma})\Gamma_2^{\Re}\Re e\left[\mathcal{C}^I(\mathcal{F}^{\mathrm{eff}})\right],
\end{aligned}$$

where $\phi_{\gamma\gamma}$ denotes the azimuthal angle of the detected photon. The $\Gamma_n^{\Re,\Im}$ are kinematic factors with a $\phi_{\gamma\gamma}$ dependence that arises from the electron propagators of the BH amplitude. The $\mathcal{C}^I$ and $\Delta\mathcal{C}^I$ angular harmonics depend on the interference of the BH amplitude with the set $\mathcal{F} = \{\mathcal{H}, \mathcal{E}, \tilde{\mathcal{H}}, \tilde{\mathcal{E}}\}$ of twist-2 Compton form factors (CFFs) or the related set $\mathcal{F}^{\mathrm{eff}}$ of effective twist-3 CFFs:

$$\mathcal{C}^I(\mathcal{F}) = F_1\mathcal{H} + \xi G_M\tilde{\mathcal{H}} - \frac{t}{4M^2}F_2\mathcal{E} \qquad (4)$$

$$\left[\mathcal{C}^I + \Delta\mathcal{C}^I\right](\mathcal{F}) = F_1\mathcal{H} - \frac{t}{4M^2}F_2\mathcal{E} - \xi^2 G_M\left[\mathcal{H} + \mathcal{E}\right], \qquad (5)$$

in which F_1, F_2 and $G_M \equiv F_1 + F_2$ denote the elastic form factors.

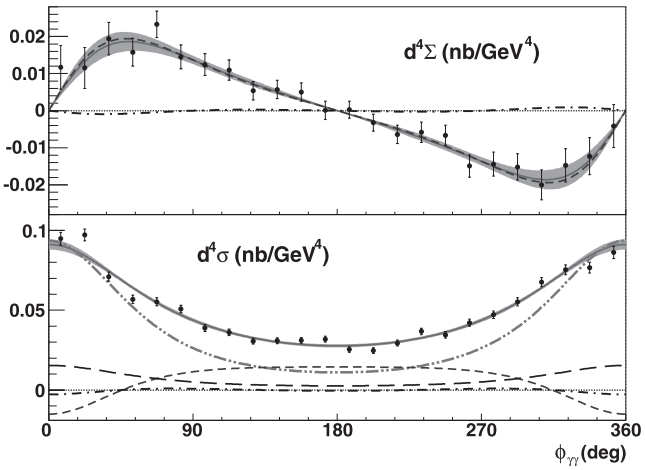

Figure 2: *Data and fit to $d^4\Sigma$, and $d^4\sigma$, as a function of $\phi_{\gamma\gamma}$, in the bin $\langle Q^2, t\rangle = (2.3, -0.28)$ GeV^2 at $\langle x_{\rm Bj}\rangle = 0.36$. The solid lines show total fits with one-σ statistical error bands. The dot-dot-dashed line is the $|{\rm BH}|^2$ contribution to $d^4\sigma$. The short-dashed lines are the contributions from the fitted $\Im m$ and $\Re e$ parts of $\mathcal{C}^{\mathcal{I}}(\mathcal{F})$. The long-dashed line is the fitted $\Re e[\mathcal{C}^{\mathcal{I}} + \Delta\mathcal{C}^{\mathcal{I}}](\mathcal{F})$ term. The dot-dashed curves are the fitted $\Im m$ and $\Re e$ parts of $\mathcal{C}^{\mathcal{I}}(\mathcal{F}^{\rm eff})$.*

$d\Sigma$ measures the imaginary part of the BH-DVCS interference term and provides direct access to GPDs at $x = \xi$, while $d\sigma$ determines the real part of the BH-DVCS interference term and measures the integral of GPDs over its full domain in x.

Figure 2 shows $d\Sigma$ and $d\sigma$ for one $(Q^2, x_{\rm Bj}, t)$ bin. Clearly, the twist-3 terms make only a very small contribution to the cross sections. Note also that $d\sigma$ is much larger than the BH contribution alone, especially from 90° to 270°. This indicates that the Beam Spin Asymmetry (BSA $= d^4\Sigma/d^4\sigma$) can not be simply equated to the imaginary part of the BH-DVCS interference divided by the BH cross section. Figure 3 (Left) shows the Q^2-dependence of the (twist-2) angular harmonic $\Im m[\mathcal{C}^{\mathcal{I}}]$ over the full t domain. The absence of a Q^2 dependence of $\Im m[\mathcal{C}^{\mathcal{I}}(\mathcal{F})]$ within its 3% statistical uncertainty provides crucial support to the dominance of twist-2 in the DVCS amplitude. $\Im m[\mathcal{C}^{\mathcal{I}}(\mathcal{F})]$ is thus a direct measurement of the linear combination of GPDs. Figure 3 (Right) displays the twist-2 $\mathcal{C}$ angular harmonics as a function of t, together with the VGG model

estimates [9]. The VGG model is in qualitative agreement with the $\Im m[\mathcal{C}^{\mathcal{I}}(\mathcal{F})]$ results, but significantly underpredicts the $\Re e$ parts of the angular harmonics.

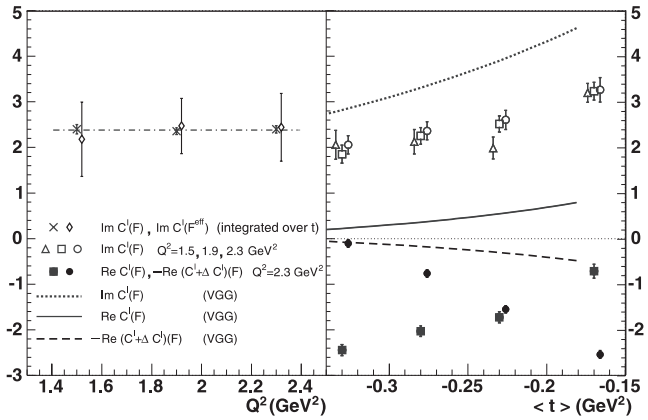

Figure 3: *Left: Q^2-dependence of the $\Im m$ parts of (twist-2) $\mathcal{C}^{\mathcal{I}}(\mathcal{F})$ and (twist-3) $\mathcal{C}^{\mathcal{I}}(\mathcal{F}^{\rm eff})$ angular harmonics, averaged over t. The horizontal line is the fitted average of $\Im m[\mathcal{C}^{\mathcal{I}}(\mathcal{F})]$. Right: Extracted real and imaginary parts of the twist-2 and twist-3 angular harmonics as a function of t.*

Following the E00-110 experiment, the E03-106 experiment [10] explored DVCS off the neutron. Because of the very small magnitude of the Dirac form factor F_1 in the neutron case, this observable is expected to be sensitive to $\mathcal{E}$, the least constrained GPD. Within the Impulse Approximation the main contributions to electroproduction of photons on the deuteron come from coherent (d-DVCS) and incoherent (p-DVCS) and (n-DVCS) scattering. The n-DVCS cross-section difference is obtained by first subtracting the proton contribution measured on a hydrogen target and then separating the neutron and deuteron contributions in each t-bin via a global analysis, that used the dynamical separation $(-t/2)$ between these two channels and the different kinematical factors that dominate their $\sin(\phi)$ moments. The resulting neutron moments turn out to be small and negative (Fig. 4), consistent with theoretical expectations; the sensivity to the GPD $\mathcal{E}$ through the quark angular momentum is also shown on the figure. A correlated constraint on the orbital angular momenta of the valence quarks, J_u and J_d, is then extracted from a fit with the VGG model [9].

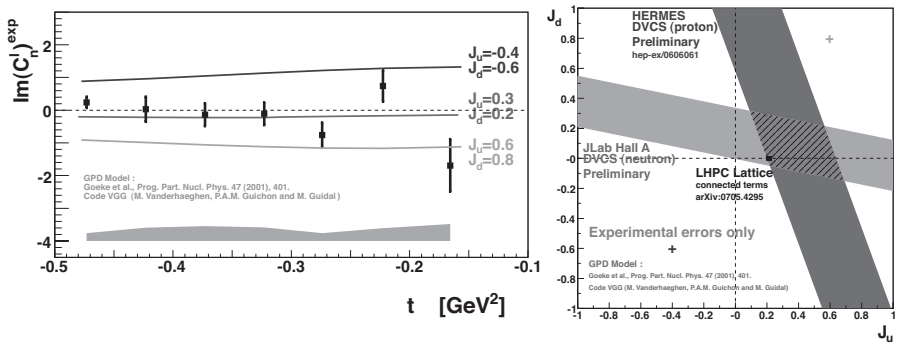

Figure 4: *Left: the t-dependence of the* $\sin(\phi_{\gamma\gamma})$ *moments for incoherent n-DVCS, compared to VGG calculations for different values of the orbital angular momenta of the valence quarks,* J_u *and* J_d*; right: experimental constraint on* J_u *and* J_d *from the present n-DVCS results. A similar constraint from HERMES* [12] *and the result from a LQCD-based calculation* [13] *are also shown.*

4 Low-Energy Tests of the Standard Model

In the past decade there has been impressive progress at JLab in improving the quality of the polarized beam, such that a beam can be delivered routinely with a polarization of 85% and an intensity of up to 200 μA. Equally impressive are the extremely small helicity-correlated properties - better than 2 nm in position and 1 nrad in angle at the target -, resulting in systematic errors in parity-violating asymmetries of a few parts per billion. These technological achievements have opened the possibility for highly accurate tests of the Standard Model, at beam energies much lower than used at high-energy colliders, but with a comparable sensitivity.

The upgrade of JLab to 11 GeV incident energy for the existing halls will allow such precision measurements in deep inelastic scattering, that will also provide access to various aspects of nucleon structure, such as charge symmetry violation (CSV) and valence quark structure. The parity-violating asymmetry in DIS, A_{PV}, can be written as

$$A_{PV} = Q^2 \frac{G_F}{2\sqrt{2}\pi\alpha} \left[a(x) + \frac{1-(1-y)^2}{1+(1-y)^2} b(x) \right], \qquad (6)$$

$$a(x) \equiv \sum_i f_i(x) C_{1i} q_i / \sum_i f_i(x) q_i^2,$$
$$b(x) \equiv \sum_i f_i(x) C_{2i} q_i / \sum_i f_i(x) q_i^2.$$

Here, $f_i(x)$ are the parton distribution functions (PDF) for the ith quark flavor, $C_{1i}(C_{2i})$ the weak vector (axial-vector) charges and q_i the quark electromagnetic charges. For an isoscalar nucleus such as the deuteron, the PDF contributions largely cancel out, especially at x-values where the contributions from the anti-quarks can be neglected. Thus, a 0.5% measurement of the PVDIS asymmetry at $Q^2 \approx 5$ GeV^2 and $x \approx 0.4$ would provide a first accurate value of the parameter $b(x)$, using the existing precise knowledge of $a(x)$. A broad program of further measurements will be required to bring the systematic error due to higher twist and CSV effects under control. Combined with other measurements precise constraints could then be derived for the lesser-known axial-vector quark couplings C_{2i} - see Fig. 5 (left) -, providing a sensitive test of electro-weak theory at the TeV scale.

Under the assumption of charge symmetry the u-quark distribution in the proton is the same as the d-quark distribution for the neutron, and vice-versa for the d-quark distribution in the proton. If one defines CSV parameters as:

$$\delta u(x) = u^p(x) - d^n(x); \delta d(x) = d^p(x) - u^n(x), \tag{7}$$

the dependence on A_{PV} for an isoscalar target becomes:

$$\frac{\delta A_{PV}}{A_{PV}} = 0.28 \frac{\delta u - \delta d}{u + d} \equiv 0.28 R_{CSV}. \tag{8}$$

Thus, an accurate measurement of A_{PV} over a range of x-values will provide sensitive information on R_{CSV}, especially at large x-values where $u + d$ might fall off more rapidly than $\delta u - \delta d$. These results could very well resolve the 3σ discrepancy between the NuTeV result [17] and the accepted running of the weak mixing angle $\sin^2 \theta_W$.

For PVDIS off the proton $a(x)$ is given by:

$$a(x) = \left[\frac{u(x) + 0.91 d(x)}{u(x) + 0.25 d(x)} \right], \tag{9}$$

making it quite sensitive to the ratio $d(x)/u(x)$. At high x-values this ratio constrains very important parts of the nucleon wave function. Different mod-

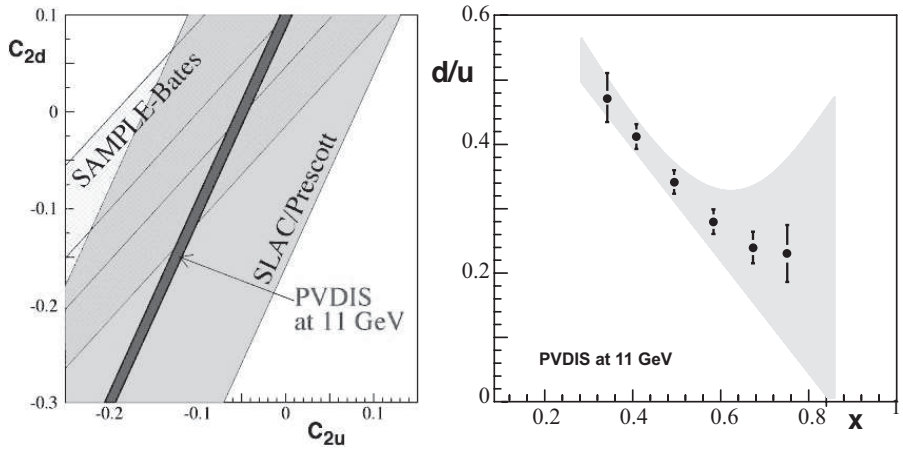

Figure 5: *Projected measurements of PVDIS with the 12 GeV upgrade. On the left the results are shown for the two electron-quark coupling constants C_{2q}, in comparison to those of the SLAC experiment [14] and of the SAMPLE experiment [15]. The right figure shows those for the ratio of the d- and u-quark momentum distributions, $d(x)/u(x)$, at large x. The shaded band represents the uncertainty in existing measurements due to nuclear Fermi motion effects.*

els, from simple SU(6) symmetry through pQCD, predict a range of values of this ration from 0 to 0.5. Its knowledge is also required to constrain PDFs and impacts predictions for QCD processes at high-energy colliders. Current estimates of d/u are extracted from DIS data on the deuteron, that are strongly hampered by uncertainties in the correction for Fermi motion. Figure 5 (right) shows the precision one can reach from A_{PV} measurements with an accuracy of 0.5%. Such measurements do not suffer from any nuclear corrections, since they are made on a single nucleon, the proton.

To cover all aspects of a PVDIS program as presented above, A_{PV} has to be measured with an accuracy of 1% or better over an x-range from 0.3 to 0.7, with a lever arm of at least a factor of 2 in Q^2 to constrain higher-twist effects. The invariant mass W has to be larger than 2 GeV in order to avoid contributions from nucleon resonances. The JLab upgrade to 11 GeV will provide the kinematical coverage, but to achieve sufficient statistics over the full range a detector with a large azimuthal acceptance is required. Preliminary

studies have indicated that a large-volume and high-field solenoidal magnet would provide the required geometry. Such a large-acceptance spectrometer can in addition be used for a broad program of exclusive and semi-inclusive reaction processes.

The SLAC E158 experiment [18] has provided the most accurate low-energy measurement of $\sin^2(\theta_W)$ by measuring A_{PV} in the Møller scattering of 50 GeV longitudinally polarized electrons off electrons in a liquid hydrogen target. The final result showed a statistical (systematic) accuracy of 14 (10) ppb, resulting in a test of the "running" of $\sin^2(\theta_W)$ at the 6σ level. A future measurement of Møller scattering with the JLab 11 GeV upgrade is expected to achieve a factor of 5 improvement over the E158 result, by measuring the 40 ppb asymmetry with an accuracy of 2%. Such a measurement would provide a value of $\sin^2(\theta_W)$ with an uncertainty of 0.00025, directly competitive with the best available results at the Z^0 pole with high-energy colliders, and could resolve the present 3σ discrepancy between the two most accurate available data [19]. Since the figure of merit of a Møller scattering experiment increases linearly with the beam energy, the JLab measurement would be the most accurate until the availability of a future linear collider.

5 Summary

The analysis of experiment E02-013 will extend the existing data on G_E^n to double the Q^2-range. Experiment E00-110 has yielded the first measurements of the DVCS cross section in the valence quark region. The Q^2-dependence of the angular harmonics of the helicity-dependent cross section provided solid evidence of twist-2 dominance in DVCS. The unexpectedly large contribution of the DVCS^2 term observed in the cross section impedes the direct extraction of GPDs from BSA measurements. The 12 GeV upgrade at JLab will allow precise measurements of parity-violating asymmetries in electron scattering that will yield sensitive tests of physics beyond the Standard Model.

6 Acknowledgements

The author gratefully acknowledges detailed discussions with drs. B. Wojtsekhowski, C. Hyde and K. Kumar. This work was supported by DOE contract DE-AC05-06OR23177, under which Jefferson Science Associates, LLC,

operates the Thomas Jefferson National Accelerator Facility.

References

1. J. Alcorn *et al.*, Nucl. Instrum. Methods Phys. Res. A **522**, 294 (2004).
2. G. Cates, N. Liyanage and B. Wojtsekhowski, JLab experiment E02-013.
3. M. M. Sargsian *et al.*, Phys. Rev. C **71**, 044615 (2005).
4. G. A. Miller, Phys. Rev. C **66**, 032201 (2002).
5. A. Belitsky, X. Ji and F. Yuan, Phys. Rev. Lett. **91**, 092003 (2003).
6. P. Bertin, C. Hyde, R. Ransome and F. Sabatié, JLab experiment E00-110.
7. C. Muñoz Camacho *et al.*, Phys. Rev. Lett. **97**, 262002 (2006).
8. A. V. Belitsky, D. Mueller and A. Kirchner, Nucl. Phys. B **629**, 323 (2002).
9. M. Vanderhaeghen, P. A. M. Guichon and M. Guidal, Phys. Rev. D **60**, 094017 (1999).
10. P. Bertin, C. Hyde, F. Sabatié and E. Voutier, JLab experiment E03-106.
11. M. Mazouz *et al.*, arXiv:0709.0450 [nucl-ex], accepted by Phys. Rev. Lett.
12. Z. Ye, arXiv:hep-ex/060606.
13. Ph. Hägler *et al.*, arXiv:0705.4295 [hep-lat].
14. C.Y. Prescott *et al.*, Phys. Lett. B **84**, 524 (1979).
15. T.M. Ito *et al.*, Phys. Rev. Lett. **92**, 102003 (2004).
16. J.T. Londergan, D.P. Murdock and A.W. Thomas, Phys. Rev. D **73**, 076004 (2006).
17. J.T. Londergan and A.W. Thomas, Phys. Rev. D **67**, 111901 (2003).
18. P.L. Anthony *et al.*, Phys. Rev. Lett. **95**, 081601 (2005).
19. S. Schael *et al.*, Phys. Rept. **427**, 257 (2006).

Frascati Physics Series Vol. XLVI (2007), pp. 327–338
HADRON07: XII Int. Conf. on Hadron Spectroscopy – Frascati, October 8-13, 2007
Plenary Session

THE GLUEX PROJECT AT JEFFERSON LAB

Zisis Papandreou
Department of Physics, University of Regina, Regina, SK S4S0A2 Canada

Abstract

One of the main scientific questions that remains unanswered in subatomic physics is the nature and behaviour of the "glue" which holds the quarks together. The puzzling feature of this construction is that quarks are never found free, a phenomenon known as confinement. Since gluons carry colour charge they cause the formation of chromoelectric flux tubes, which may yield unusual objects such as glueballs or hybrids. In certain models the latter can be produced with quantum numbers not allowed in the simple quark model and these are a powerful signature for hybrid meson spectroscopy. An international experiment (GlueX) at Jefferson Lab, Virginia, is being designed to search for such exotic hybrid mesons and thus elucidate the phenomenon of confinement. GlueX is considered a "discovery" experiment; its salient features and the planned methodology of amplitude analysis will be presented.

1 Introduction

The primary goal of the GlueX/Hall-D project is the definitive and detailed mapping of the spectrum of a new family of particles called *hybrid mesons*, starting with those that carry exotic quantum numbers. Linearly polarized photons produced by electrons from an energy-doubled Jefferson Lab will be the probe used to uncover this spectrum. This experimental information is absolutely critical in achieving a quantitative understanding of the confinement mechanism in quantum chromodynamics.

The Hall-D/GlueX Collaboration was formed at a workshop held in July 1997 at Indiana University. The project has successfully passed several internal and external reviews that culminated in the Department of Energy's (DOE) award of Critical Decision Zero (CD-0, 'mission need') in 2004 and, most recently, of CD-2 ('baseline performance') in November 2007. CD-4 ('start of operations') is expected in 2015. Further details on the project can be found in references [1, 2, 3].

2 Theoretical Motivation

2.1 Overview

Strong interactions are described by quantum chromodynamics (QCD), the field theory in which quarks interact through a *color* force carried by gluons. Lattice QCD (LQCD) numerical simulations support the notion that a string-like chromoelectric flux tube forms between distant static color charges, leading to quark confinement and a potential energy between quarks that increases linearly with the distance between them. It qualitatively explains confinement: infinite energy would be needed to separate quarks to infinity. Confinement is the most novel and spectacular feature of QCD.

Figure 1 illustrates the chromodynamic energy density in the vicinity of a quark and antiquark based on a LQCD calculation [4]. This calculation is for heavy quarks in the quenched approximation. The ground state potential between the quarks has a $1/r$ dependence at small distances and is linear for large distances. The energy peaks at the positions of the quarks and in the space between the quarks the energy is confined to a flux tube. Such flux tubes arise because of the self-interaction of the gluons of QCD.

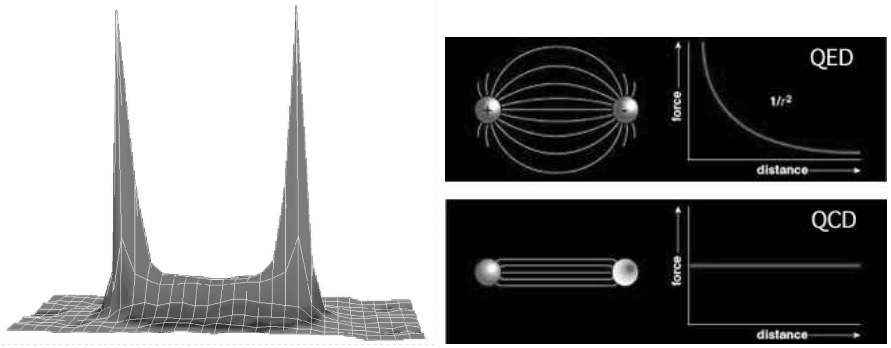

Figure 1: *Left: A LQCD calculation of the energy density in the color field between a quark and an anti-quark in a meson with a separation of 1.2 fm. Right: QED and QDC dipoles; note the difference in the field lines and in the corresponding dependence of force on quark separation.*

Although this picture must be extended to yet lighter quarks, nevertheless, the most important properties of this system are determined by the model-independent features described above. In particular, in a region around 2 GeV/c^2, a new form of hadronic matter must exist in which the gluonic degree of freedom of mesons is excited. The unique characteristic of these new states is that the vibrational quantum numbers of the string, when added to those of the quarks, can produce a total angular momentum J, a total parity P, and a total charge conjugation symmetry C not allowed for ordinary $q\bar{q}$ states. These unusual states are referred to as *exotic hybrid mesons*. The levels of these states and their orderings will provide experimental information on the mechanism which produces the flux tube.

2.2 Quark Model and QCD

QCD incorporates the experimental fact that the quarks and gluons do not exist as free particles by requiring that only color singlet combinations exist as free particles in nature. In addition to the color singlet combinations $q\bar{q}$ and qqq others are possible, such as $q\bar{q}g$ (*hybrid mesons*) and gg or ggg (*glueballs*). These new states, collectively known as *gluonic excitations*, are fascinating since this is the only case of a theory in which the gauge particle is also a

constituent. The analogous states in QED, like atoms of light, cannot exist.

The early version of the quark model described the observed mesons as bound states of a quark and antiquark, where the quarks were assumed to be the u, d and s quarks. Thus mesons were grouped in families with nine members – a nonet – characterized by a given J^{PC} determined by the relative spin of the two quarks and their relative orbital angular momentum. Radial excitations are also allowed.

The rules for allowed values of J^{PC} follow from the requirements of a fermion–antifermion system: the quark spins can be parallel ($S = 1$) or antiparallel ($S = 0$) with relative orbital angular momentum (L), $\vec{J} = \vec{L} + \vec{S}$, $P = (-1)^{L+1}$ and $C = (-1)^{L+S}$. Exotic (e.g. $J^{PC} = 1^{-+}$) combinations are not allowed for $q\bar{q}$ systems. Indeed, the initial absence of such combinations gave credence to the quark model.

2.3 Gluonic Excitations

At short distances – the regime of asymptotic freedom – perturbative techniques are applicable and QCD describes high energy experimental phenomena and data both qualitatively and quantitatively. At large distance scales – the confinement regime – the situation is far different. Here we must rely on first-principles LQCD calculations or QCD-inspired models. Recent advances in algorithms and computing power now make possible LQCD predictions for masses of exotic hybrid mesons [5] and eventually their widths and decay modes.

Within the flux-tube model, conventional mesons result when the flux tube is in its ground state whereas excitations of the flux tube lead to hybrid mesons. The first excited state of the flux tube is a transverse excitation. The flux tube, or string, spins clockwise or counter-clockwise around the $q\bar{q}$ line leading to two degenerate states – degenerate since the energy should not depend on which way the flux tube is spinning. LQCD and flux tube models both indicate that the lowest excited flux tube has $J = 1$ [6, 7, 8]. The linear combinations of the clockwise or counter-clockwise rotations are eigenstates of parity and charge conjugation leading to two possibilities for the excited flux tube: $J^{PC} = 1^{-+}$ or $J^{PC} = 1^{+-}$. Suppose we start with the $q\bar{q}$ in the $S = 0$ and $L = 0$ (or $J^{PC} = 0^{-+}$ – the π or K) configuration. Combining this with $J^{PC} = 1^{-+}$ or $J^{PC} = 1^{+-}$ of the excited flux tube results in hybrid mesons

with $J^{PC} = 1^{++}$ or $J^{PC} = 1^{--}$. These are non-exotic quantum numbers. If, however, we start with $q\bar{q}$ in the $S = 1$ and $L = 0$ (or $J^{PC} = 1^{--}$ – the vector photon) configuration, the resulting hybrid meson can have $J^{PC} = [0, 1, 2]^{+-}$ for the flux tube with $J^{PC} = 1^{-+}$ and $J^{PC} = [0, 1, 2]^{-+}$ for the flux tube with $J^{PC} = 1^{+-}$. We note that of these six possible J^{PC} combinations, three are exotic: $J^{PC} = 0^{+-}$, $J^{PC} = 1^{-+}$ and $J^{PC} = 2^{+-}$. Figure 2 shows our current knowledge of conventional and exotic $q\bar{q}$ states.

After about two decades of experimental searches there have been reports of experimental observations of states with exotic $J^{PC} = 1^{-+}$. The conclusion from these studies is that, whereas there are tantalizing hints of gluonic excitations in both the glueball and hybrid sectors, the results are not conclusive.

3 Photon Beam

As mentioned above, the photon is expected to be particularly effective in producing hybrids with exotic J^{PC}. Figure 3 illustrates the differences between a π and a γ probe. If the scattering results in excitation of the flux tube, one expects exotic hybrid mesons to be suppressed in π-induced interactions and enhanced in photoproduction. Current phenomenology supports the notion that photons should be more effective at producing exotic hybrids [9, 10], and recent flux-tube model calculations [11, 12] suggest that the coupling between a conventional meson, a photon and a hybrid meson are not small and that we may expect copious production of hybrid mesons. The assumptions underlying such models need to be tested in a framework closer to QCD.

There are virtually no data on the photoproduction of mesons below 3 GeV/c^2. Thus, experimenters have not been able to search for exotic hybrids precisely where they are expected to be found. From considerations related to the production yield and boost of the exotic mesons, ability to separate meson from baryon resonances, and degree of linear polarization, the optimum photon beam energy is between 8 and 9 GeV, which translates into an electron beam energy of 12 GeV. Figure 4 shows the accelerator complex at Jefferson Lab with the existing three experimental Halls A, B and C and the planned Hall D. The addition of state-of-the-art accelerating units (*cryomodules*) in the existing space in the linear sections of the accelerator, along with upgrading of magnets in the arcs, will bring the electron energy up from the current maximum of 5.5 MeV to 12 MeV. New accelerator technology will yield a beam with high

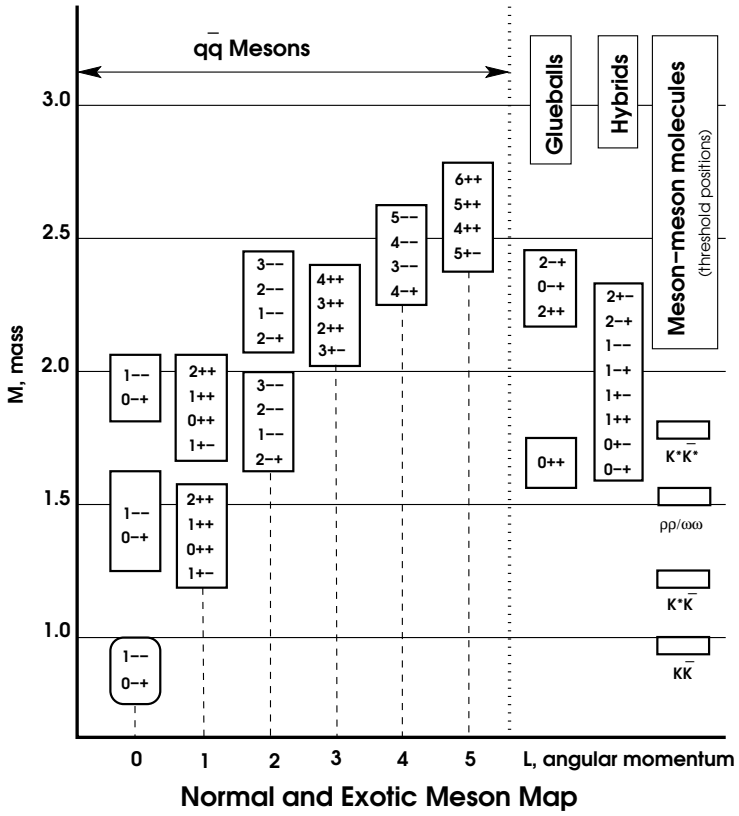

Figure 2: *A level diagram showing conventional nonets and expected masses of glueballs, hybrids, and meson-meson molecular thresholds. The vertical axis is in units of GeV/c^2. L refers to the angular momentum between the quarks and each box with J^{PC} numbers refers to a nonet of mesons. The exact association of an observed meson with a particular $q\bar{q}$ state within a nonet depends on a good understanding of the various decay modes of the meson as well as its mass, width and production characteristics. The range of masses of the known conventional meson nonets and their radial excitations extend from the π mass up to about 2.5 GeV/c^2. The low-lying glueballs mix with conventional $q\bar{q}$ mesons, which complicates their identification. In contrast, hybrid mesons can possess J^{PC} numbers not possible for $q\bar{q}$ and thus have a smoking gun signature. Note also that exotic J^{PC} – 0^{+-}, 1^{-+}, 2^{+-} – occur only among the hybrids for the range of masses shown.*

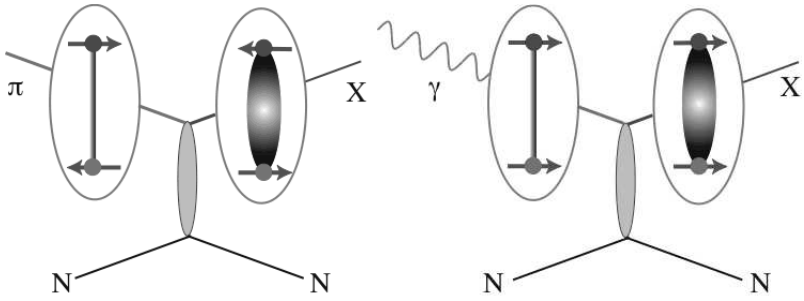

Figure 3: *Left: With a π probe the incoming quarks have $L = 0$ and $S = 0$. The excited flux tube from the scattering results in hybrid mesons with non-exotic quantum numbers. Right: With a photon probe the incoming quarks have $L = 0$ and $S = 1$. When the flux tube is excited, hybrid mesons with exotic quantum numbers are possible.*

flux, large duty factor, low emittance and small spot size.

The photon beam is produced by having the electron beam incident on a thin ($\sim$20 μm) diamond wafer. The technology to produce these wafers is only now being perfected. After passing through the wafer, the electron beam is bent by a dipole magnet (the tagger magnet) into the beam dump. A small fraction, about 0.01% of the electrons, emit a photon via incoherent bremsstrahlung or coherent bremsstrahlung, the latter leading to an enhancement over the incoherent spectrum at a photon energy determined by the angle between the incident electron direction and the wafer. By exploiting the tight energy-angle correlation for the coherent photons, collimation of the photon beam can be used to enhance the fraction of photons of the coherent radiation incident on the GlueX target. This has the effect of increasing the degree of linear polarization and eliminating a large fraction of the low-energy photons that dominate the incoherent component of the spectrum. An active collimator, with a 3.5 mm hole, will be placed just upstream of the GlueX detector and about 75 m downstream of the tagger magnet. The electrons emitting the bremsstrahlung photons will be momentum analyzed using a focal plane spectrometer leading to a photon energy resolution of 0.2%. This technique allows separating the coherent from the incoherent and in the process turns the coherent spectrum with its large incoherent background into a spectrum at the target that is

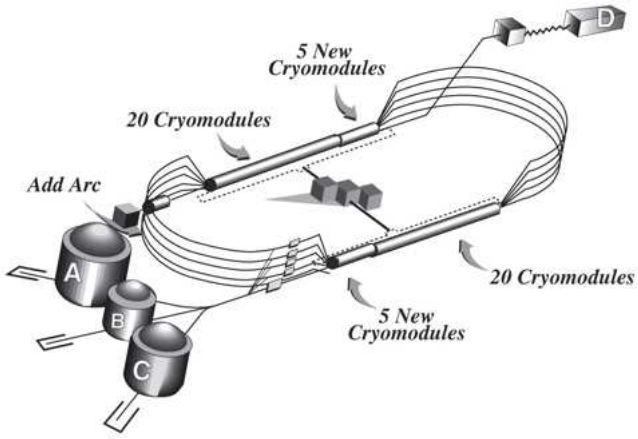

Figure 4: *The current CEBAF multi-pass electron accelerator at JLab, showing the three existing experimental Halls (A, B and C) and the planned Hall D.*

almost (loosely) monochromatic. This reduces the hadronic background from uwanted low energy photons and makes JLab unique. Even with only 10% of the eventual photon flux of 10^8/sec, the experiment will accumulate statistics during the first year of operation that will exceed published data with pions by at least an order of magnitude.

The linear polarization of the photons is important in carrying out the amplitude analysis needed to identify the J^{PC} of produced mesons and is essential in separating the production mechanism by natural parity exchange from unnatural parity exchange. The latter, for example, can be used to reduce backgrounds from dominant processes, such as diffractive production.

4 Amplitude Analysis on a Grid

Discoveries in particle physics, typically made at the frontiers of energy or precision, are facilitated by developments in technology. Likewise, the discovery of exotic hybrid mesons will require the development of a new paradigm for conducting precise analyses of large data sets. The data provide information on mesons decays, that can be theoretically described in terms of quantum mechanical amplitudes. Modern cyber infrastructure offers the opportunity

to build an open access suite of services and data repositories that enable transparent analysis of data. Existing Grid-based tools will be utilized to move data and perform unbinned likelihood fits over multiple processors. The GlueX Collaboration is pursuing the development of such an infrastructure that would expedite collaboration among physicists by providing ready access to data and the fitting and visualization tools needed to conduct precision analyses of it, and it will be applied to existing data.

To identify the J^{PC} quantum numbers of a meson it is necessary to perform an *amplitude analysis*, which determines production amplitudes by fitting decay angular distributions. The fit includes information on the polarization of the beam and target, the spin and parity of the resonance, the spin and parity of any daughter resonances and any relative orbital angular momenta. The analysis seeks to establish the production strengths, production mechanisms and the relative phase motion of various production amplitudes.

There are both empirical and intrinsic difficulties in the implementation of such an analysis. Empirically, instrumentation effects, such as detector acceptance and resolution, can conspire to make one distribution look like another; intrinsic mathematical ambiguities exist for certain final states; and, backgrounds can limit one's ability to measure phase motion.

Another challenge lies in the selection of the amplitudes. For example, the analysis of the $\pi N \to \pi\pi\pi N$ reaction in the Brookhaven E852 experiment assumed the isobar model and processes like the Deck Effect (diffractive dissociation followed by quasi on-shell scattering) were not included. Another assumption admits a factorization within the isobar model that separates the production amplitude (to be fitted) from the (fixed) decay amplitude and much simplifies the numerical fit problem. As an application of the amplitude analysis toolkit, Deck-style production amplitudes will be implemented along with the familiar isobar model production amplitudes and fits will be run to expose the relative weights. The toolkit will be checked versus well established mesons in order to establish trustworthy error estimations.

5 The GlueX Detector

The GlueX detector (see Figure 5) is optimized for 8-9 GeV incident photons. Momentum analysis will be provided by a 2.2 T superconducting solenoid magnet. The use of a solenoidal spectrometer allows for the measurement of

charged particles with excellent efficiency and momentum determination and the solenoidal field acts as a magnetic shield, containing the shower of unwanted electron-positron pairs associated with the photon beam. A 30 cm long liquid hydrogen vessel will be used as the production target.

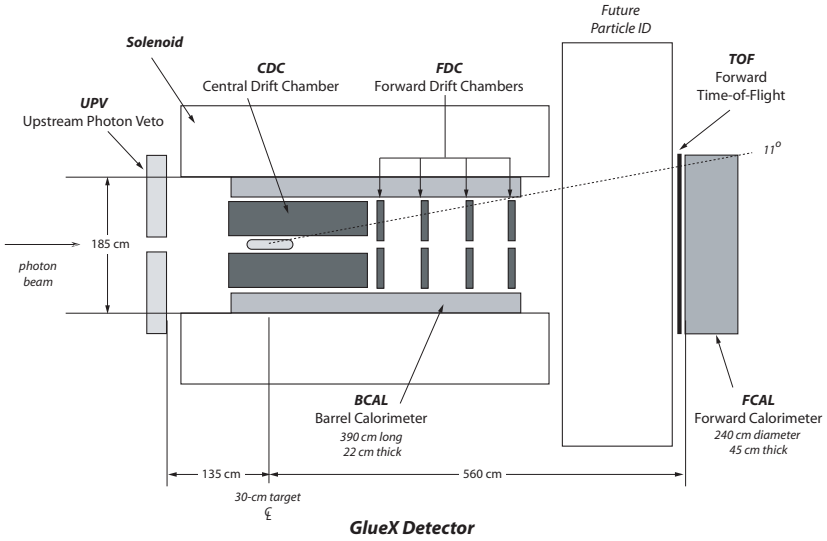

Figure 5: *A side-view schematic of the GlueX detector.*

5.1 Calorimetry

A circular lead glass array will serve as the forward ($\theta < 11^\circ$) electromagnetic calorimeter for the GlueX detector. An existing detector, the LGD used in the Brookhaven E852 experiment, will be reconfigured to this end. The circular stack matches the aperture of the solenoid and mimimizes the number of detector channels ($\sim$2800) while maximizing the target to FCAL distance.

BCAL will cover polar angles of $11^\circ < \theta < 126^\circ$ and will consist of alternating layers of thin (0.5 mm) lead sheets and 1-mm-diameter scintillating fibers. It will be segmented into 48 modules and will have a radiation length of 15.5 X_0. Beam test results from a prototype module exhibit performance characteristics for the energy and timing resolution that meet or exceed the design specifications, based on the KLOE calorimeter. However, the 2.2 T

field places constraints on the readout of the BCAL. The only devices that can solve this problem in a field-resistant and compact manner are state-of-the-art silicon photodiodes, operating in limited Geiger mode. Novel, large-area (1.3 cm^2) units are currently in the R&D phase and show much promise.

5.2 Tracking

The system of tracking chambers in the GlueX detector must cover as close to a 4π solid angle as possible over a wide range of particle momenta and must have sufficient momentum resolution to be able to identify missing particles. Near the target it will provide very accurate vertex information. Finally, it is necessary that near the target the tracking can separate π's and K's up to about 0.5 GeV/c — a regime where dE/dx measurements will work.

The central drift chamber will track particles with polar angles between 20° and 170°, and is designed to minimize the material to traversing particles at forward angles. This straw-tube chamber will contain 3349 straws, each of which is 1.6 cm in diameter. The straws are arranged in 25 layers, eight of which will be stereo, tilted by ±6° from the straight tubes. The tubes are assumed to have an $r-\phi$ resolution of 150 μm, and a resolution along the length of the wire of about 200 μm/sin(6°).

The forward drift chambers, FDC, are disk-shaped drift chambers, of outer radius 60 cm. The basic drift package of six layers of cathodes and anodes with 150 μm spatial resolution between two cathode strip planes. The strips are arranged in a u- and v-geometry with respect to the wires. The devices will provide 200 μm resolution and will have a total of $\sim$ 12000 channels.

5.3 Particle Identification

Particle identification (PID) in GlueX will use input from nearly all of the detector systems in the experiment. Time-of-flight information will be obtained from both BCAL and the forward TOF system. The latter will consist of two walls of scintillator bars oriented perpendicular to each other; the bars will be 2.52 m long and have a 6 cm width and 2.54 cm thickness. A future PID device will provide information on forward going tracks while the CDC will provide dE/dx information. In order to effectively use all of this information, GlueX plans to develop of likelihood-based PID system coupled to kinematic fitting to perform a global PID.

6 Summary

The nature of confinement is an outstanding and fundamental question in QCD. Lattice QCD and phenomenology strongly indicate that the gluonic field between quarks forms flux tubes and that these qualitatively account for confinement. The excitation of the gluonic field leads to an entirely new spectrum of mesons having exotic J^{PC} quantum numbers, with properties predicted by QCD. Data and sophisticated amplitude analysis tools are required to validate these predictions. The definitive experiment for this search will be GlueX at the energy-upgraded Jefferson Lab.

7 Acknowledgements

This work was presented on behalf of the GlueX Collaboration and was supported in part by NSERC (Canada) and Jefferson Lab (USA).

References

1. The GlueX Collaboration, "Presentation to Jefferson Lab PAC30 (2006).
2. A. R. Dzierba *et al.*, American Scientist, **88**, 406 (2000).
3. A. R. Dzierba and N. Isgur, CERN Courier **40** No. 7:23 (2000).
4. G. Bali *et al.*, Phys. Rev. D **62** (2000) 054503.
5. C. Bernard *et al.*, Phys. Rev. D **56**, 7093 (1997).
6. N. Isgur *et al.*, Phys. Rev. D **31**, 2910 (1985).
7. C. Bernard *et al.*, Phys. Rev D **56**, 7039 (1997).
8. P. Lacock *et al.*, Phys. Lett. B **401**, 308 (1997).
9. A. Afanasev and P. R. Page, Phys. Rev. D **57**, 6771 (1998).
10. A. P. Szczepaniak and M. Swat, Phys. Lett. B **516**, 72 (2001).
11. F. E. Close and J. J. Dudek, Phys. Rev. D **69**, 034010 (2004).
12. F. E. Close and J. J. Dudek, Phys. Rev. Lett. **91**, 142001 (2003).

Frascati Physics Series Vol. XLVI (2007), pp. 339–350
HADRON07: XII Int. Conf. on Hadron Spectroscopy – Frascati, October 8-13, 2007
Plenary Session

PROSPECTS FOR HADRON PHYSICS IN PANDA

Alberto Rotondi
for the PANDA Collaboration
Dipartimento di Fisica Nucleare e Teorica and
Istituto Nazionale di Fisica Nucleare, INFN
Via Bassi, 6 27100 Pavia, Italy

Abstract

The FAIR future facility at Darmstadt, the HESR antiproton ring and the PANDA experiment are briefly described. Some issues of the physics program of PANDA for hadron physics with antiprotons are discussed in the light of the present knowledge.

1 The Facility for Antiproton and Ion Research (FAIR)

FAIR will be an international accelerator facility constructed in the site of the existing GSI laboratories at Darmstadt. The map is shown in Fig. 1. The core of the system is a double ring synchrotron SIS100/300 with a circumference of 1100 m, that will deliver 29 GeV/c protons and heavy ions up to 35 GeV/c per nucleon for U^{92+} with unprecedented intensities. The existing GSI accelerators UNILAC and SIS 18 will serve as injectors for the new facility.

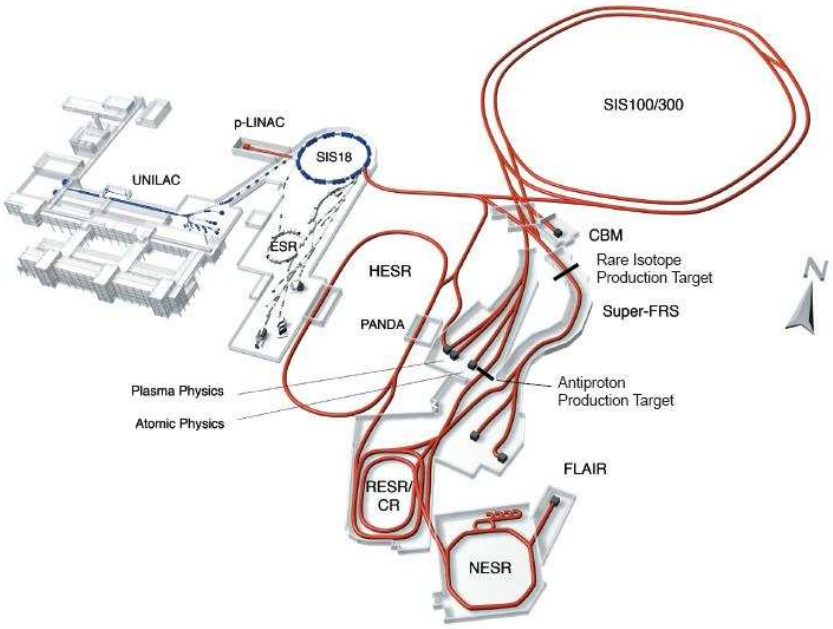

Figure 1: *The existing GSI facility (on the left) and the planned FAIR facility (on the right with the beam lines).*

The intrinsic cycle time of the accelerator and storage cooler rings will allow up to four research programs to run in full parallel mode. The multidisciplinary physics program will cover different fields: test of QCD, nucleus-nucleus collisions, nuclear structure and nuclear astroparticle investigations with nuclei far off stability, high density plasma physics, atomic and material science studies, radio-biological and other applicative researches.

The High Energy Storage Ring (HESR) will allow QCD studies with cooled beams of 1.5-15 GeV/c ($2.3 < \sqrt{s} < 5.5$ GeV) antiprotons with momentum resolution down to $\delta p/p \simeq 10^{-5}$, corresponding to a beam energy spread less than 30 keV, about a factor ten better than the previous machines.

The perspective of this antiproton beam of exceptionally good quality has motivated the formation of the PANDA Collaboration (antiProton ANnihilation at DArmstadt, 15 countries, 47 Institutes, about 370 scientists) with the aim to perform a wide hadron physics program. [1)]

2 The PANDA detector

PANDA can be considered the next generation experiment in hadron physics. It is designed to fulfill many highly demanding requirements: the detector must have 4π angular coverage, high momentum resolution on charged particles (1%), full neutral and charged particle identification, high rate compatibility (10^7 annihilations/s), good vertex resolution (better that 100 μm), high magnetic field, modularity and flexibility. [1)]

The general layout of PANDA is based on two magnetic spectrometers and is shown in Fig. 2.

The target will be either a stream of small pellets of frozen hydrogen (pellet target) or a homogeneous gas stream (cluster jet target). Both options are under test; in any case, the chosen solution must assure a luminosity up to $L = 2 \cdot 10^{32}$ cm^{-2} s^{-1} when in the HESR ring there are 10^{11} circulating particles. [2)]

The interaction region is placed in a superconducting solenoid which provides an axial field of 2T. The interaction point is surrounded by a silicon Micro Vertex Detector (MVD), which has five barrel shaped layers plus five disk-shaped detectors in the forward direction. The three innermost layers are composed of pixel detectors for the optimal detection of secondary vertices (with resolution $\simeq$ 100 μm) and maximum acceptance close to the interaction point. The identification of low momentum particles will be possible via $\mathrm{d}E/\mathrm{d}x$.

The MVD is surrounded by a cylindrical tracker. Two options are currently discussed, a Straw Tube Tracker (STT) consisting up to 28 layers of self supporting straws and a Time Projection Chamber (TPC) with an ungated charge collection based on a Gas Electron Multiplier (GEM) readout. The TPC is technically more complicated, but offers less material and a better particle identification via $\mathrm{d}E/\mathrm{d}x$.

The next detector is a Cherenkov counter based on the DIRC principle, consisting of quartz rods in which the light is internally reflected to an array of photon detectors in backward directions. Various types of readout (photomultipliers, APD) are under study and the details can be found in ref. [1)]

An electromagnetic calorimeter consisting of about 20,000 crystals read by APD is placed outside the DIRC. As detector material $PbWO_4$ is under study, since it is faster than BGO, although with a worse light output. Finally,

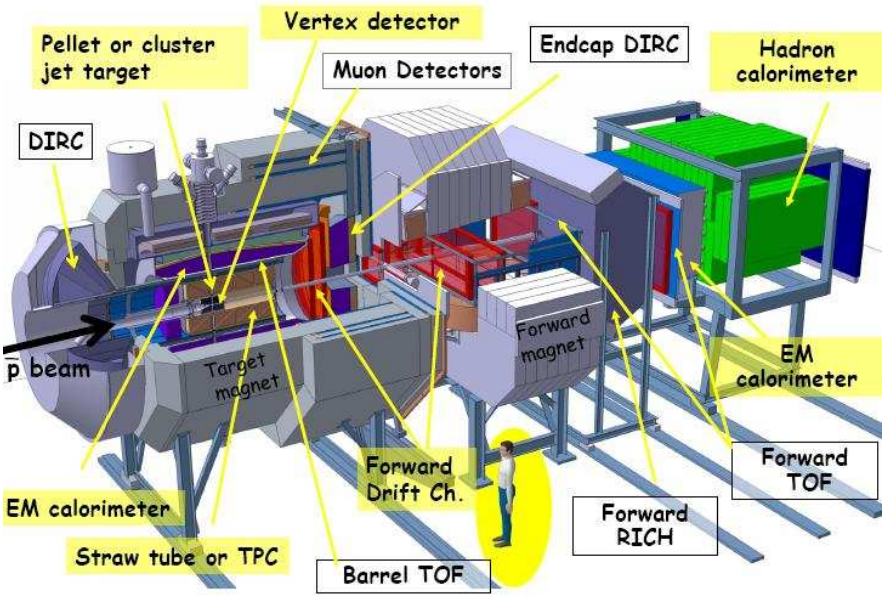

Figure 2: *The PANDA apparatus.*

outside the central magnet and its iron return yoke, drift tubes are placed to detect the muons exiting the spectrometer. A time of flight detector in the central region is also under study, to detect low momentum particles.

In the forward direction a series of mini drift chambers is used to track particles entering in the forward spectrometer, which is based on a dipole with a field integral of 2 Tm. The system accepts particles emitted forward below 5^0 and 10^0 in the horizontal and vertical directions, respectively.

The option of a third Cherenkov detector, based on gas or aerogel is still under investigation. In addition, a time of flight detector is considered for charged particle identification.

A forward electromagnetic calorimeter will also be used, based on lead-scintillator sampling and fiber readout, with a resolution within 3-5%/$\sqrt{E}$ (GeV). A study is under way on the use of the refurbished MIRAC (from WA80) as a hadron calorimeter placed after the electromagnetic calorimeter.

To provide maximum flexibility, a hardware trigger is not foreseen. The readout electronics will perform intelligent data reduction, to transfer only the physically relevant information. All data will be marked by a timestamp by

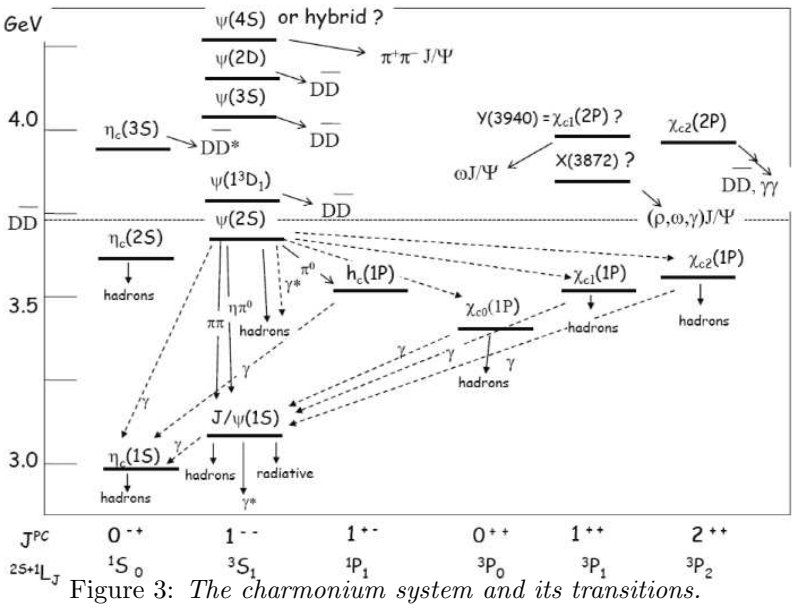

Figure 3: *The charmonium system and its transitions.*

which event building can be performed at a later stage.

3 The PANDA physics program

3.1 Charmonium spectroscopy

Large scale simulations of QCD on discrete Euclidean space-time volumes show that the gluonic flux tube that connects two infinitely heavy color sources at a given distance can be well approximated by a potential. Because of the high value of the c-quark mass ($m_c \simeq 1.5\mathrm{GeV/c^2}$) this quark-antiquark potential is essentially non relativistic ($\beta \simeq 0.2$), with some relativistic corrections [3].

The potential models predict eight states below the $D\overline{D}$ threshold of 3730 MeV (see fig. 3), with masses in agreement with the measurements within less than 1% [4]. The BaBar, BES, BELLE and CLEO-c experiments are producing a lot of high precision results on the masses of these charmonia and new data on their widths and decay modes. However, spin singlets can not be directly produced in e^+e^- annihilation and their population via electromagnetic transitions from the vector states is either suppressed (for η_c, η_c') or C-forbidden (for h_c). In the η_c case, hindered M1 transitions distort the resonance line shape in a non trivial way. [5] Hence, data on singlet masses and widths of accuracy comparable with that of the other mesons are still missing; for example, the

error on the $\eta_c(2S)$ width is 50% (14 ± 7 MeV [6]).

On the other hand, in $p\overline{p}$ annihilation all the hyperfine levels of Fig. 3 can be populated more or less with the same intensity. For example, the cross section of $\sigma(p\overline{p} \to \eta_c) \simeq 500$ nb [1], compared with $\sigma(e^+e^- \to e^+e^-\eta_c)$ which is of the order of pb [7]. With an antiproton beam the masses and widths of all states can be measured very accurately, being determined only by the parameters of the accelerator. In this case the detector has to be optimized for the selection of the final state and for an efficient background rejection. Many high precision results on spin singlets and on χ_c spin triplets in P wave have been obtained in this way by the E835 and E760 Fermilab experiments. [6, 8]

The high luminosity, the beam energy resolution of HESR and the high performances of the PANDA detector will allow to continue and to extend these measurements of resonance formation by performing scans in step less than 1 MeV. Leptonic modes will be detected in parallel to the radiative and hadronic ones.

The mass region above the $D\overline{D}$ threshold is still poorly known. Only 5 states have been identified of the 32 $c\overline{c}$ states predicted by the potential models [4] in the energy range $3 \leq E \leq 4.5$ GeV. In addition, many surprising and unexpected states are emerging from the high statistics samples of CLEO-c [5], BaBar [10] and BELLE [9].

There are several theoretical and experimental investigations of the nature of these states. Their interpretations as glueball, hybrids or multiquark states are numerous (see ref. [11]) and many of them have been presented at this Conference. We quote only the $Z(4430)$ meson [9, 12], that is the first charmonium-like charged state, a property consistent with a $[qu\overline{Qd}]$ multiquark structure.

All the predictions indicate that the lowest energy charmed hybrids ($c\overline{c}g$) states have masses between 3.9 and 4.5 GeV/c^2, including the spin exotic state 1^{-+}. The glueball spectrum extends to 5 GeV/c^2, with the lightest 2^{+-} spin exotic meson (oddball) at 4.3 Gev/c^2. The identification of these states requires high statistics to perform reliable spin-parity analyses. Favorable decay channels would be $\phi\phi$ or $\phi\eta$, which are easily distinguishable in PANDA from others annihilation channels.

In the search of these exotic states PANDA can exploit the filter action of the $p\overline{p}$ system: all the states with non-exotic quantum numbers are accessible in

formation, J^{PC} exotic states X_c as $0^{+-}, 1^{-+}, 2^{+-}$ are accessible in production or in associated production processes as $p\overline{p} \to \pi X_c$. The expected cross sections range from hundreds of pb for the associated production [13] up to some nb, so that in PANDA one expects $10^2 - 10^5$ of such events per day.

3.2 Open-charm physics

The open charm $c\overline{q}$ states, called D mesons, are usually described in terms of different potential models deduced from charmonium studies or from effective lagrangians with chiral and heavy quark symmetries [4].

The announcement [14] of a very narrow $D_s(2317)$ low mass state seen in the $D_s\pi^0$ decay mode and lying approximately 160 MeV below the calculations of the majority of models, has renewed the interest in open charm spectroscopy. Another narrow state is the $D_s(2460)$, [14, 15] which lies below most model predictions. Mass predictions near to the experimental values are obtained from a tetraquark $|c\overline{s}(u\overline{u} + d\overline{d}) >$ model [16].

The HESR running with full luminosity at laboratory momenta larger than 6.4 GeV/c can be considered a factory for tagged open charm. The accelerator will produce about 10^7 D meson pairs per year in the $\psi(3770)$ mass region. The background conditions are expected to be favorable for PANDA, because the charm hadrons will be produced at threshold without phase space for other hadrons in the same process. These conditions will allow the detailed study of the structure of the rich spectrum of the D mesons and of their dominant and rare decays.

3.3 Antibaryon-baryon production in $p\overline{p}$ annihilation

The quark rearrangement and the annihilation and creation of quark-antiquark pairs can be studied in a particularly clean way in the $p\overline{p} \to Y\overline{Y}$ baryon-antibaryon production process. In the absence of polarization, the angular distribution of the final products of the reaction can be written as:

$$I(\theta_i, \theta_j) \propto 1 + \alpha P_Y + \overline{\alpha} P_{\overline{Y}} + \alpha\overline{\alpha} \sum_{i,j} C_{ij} \cos\overline{\theta_i} \cos\theta_j \ ,$$

where $i, j = x, y, z$ and α is the decay asymmetry parameter. The angles refer to the decay directions in the $Y, \overline{Y}$ rest frame. This distribution has been

extensively studied for the $p\overline{p} \to \Lambda\overline{\Lambda} \to p\pi^-\overline{p}\pi^+$ reaction by the PS185 experiment at the LEAR accelerator of CERN. [17] The study of the polarization and of the spin correlation coefficients C_{ij}, showing that the $s\overline{s}$ pairs are predominantly produced with parallel spin, put severe constraints to the quark-gluon and meson exchange models, whereas the depolarization coefficient data from a polarized target do not match at present with any model. [17].

The magnitude of the polarization of the Y and $\overline{Y}$ must be the same if CP invariance holds, with $\alpha_Y = -\alpha_{\overline{Y}}$. Consequently, one can define the parameter $A_{Y\overline{Y}} = (\alpha_{\overline{Y}} + \alpha_Y)/(\alpha_{\overline{Y}} - \alpha_Y)$ that should be zero if CP is conserved. The average value of A in the case of the $p\overline{p} \to \Lambda\overline{\Lambda}$ reaction is $A_{\Lambda\overline{\Lambda}} = 0.006 \pm 0.014$ [17] which is lower than what is quoted in PDG (0.012 ± 0.021) [6]. The discovery of a CP violation in the hyperon decay would be the first observation in a baryonic system. The effect is expected to be smaller than 10^{-4} [17].

These topics can be further studied in PANDA and extended to doubly strange and charmed hyperons. Nothing is known experimentally on the $p\overline{p} \to Y_c\overline{Y}_c$ reactions. For example, it would be very interesting to investigate whether the creation of a $c\overline{c}$ pair in the $p\overline{p} \to \Lambda_c^+\overline{\Lambda_c^+}$ reaction will show the same features as the $s\overline{s}$ creation in the $\Lambda\overline{\Lambda}$ case.

For the channels with only charged particles in the final state, the overall reconstruction efficiency is around 20%. [1] The production cross sections are orders of magnitude greater than those from e^+e^- annihilation and a number of reconstructed events/month from 10^4 to 10^9 is expected for the production of $\Lambda_c\,\overline{\Lambda}_c$ and $\Lambda\,\overline{\Lambda}$ pairs, respectively.

3.4 Drell-Yan processes

In Drell-Yan processes $p\overline{p} \to l^+l^-X$ the angular distribution of dileptons, for the unpolarized case is:

$$\frac{1}{\sigma}\frac{\mathrm{d}\sigma}{\mathrm{d}\Omega} = \frac{3}{4\pi}\frac{1}{\lambda+3}\left(1 + \lambda\cos^2\theta + \mu\sin^2\theta\cos\phi + \frac{\nu}{2}\sin^2\theta\cos 2\phi\right) ,$$

where θ and ϕ are defined in the rest frame of the lepton pair. In the simple parton model, one would get $\lambda = 1$ and $\nu = \mu = 0$. At leading-order (LO) and next-to-leading-order (NLO), perturbative QCD calculations produce $\lambda \simeq 1$ and $\mu \simeq \nu \simeq 0$ (for a discussion see ref. [18]).

On the other hand, a series of experiments on high energy collisions of pions and antiprotons with various unpolarized nuclei reported a largely asym-

metric azimuthal distribution, namely $\lambda \simeq 1$ and $\mu \ll \nu \simeq 30\%$, with $1-\lambda-2\nu$ large and negative. [19]

This can be interpreted as a genuine non-perturbative effect, relating the size of ν to the Boer-Mulders distribution $h_1^\perp$, which describes how in an unpolarized hadron the momentum distribution of a parton is distorted by its transverse polarization. This distribution, belonging to the family of chiral-odd parton densities, is not observable in fully inclusive deep inelastic scattering and for this reason at present it is unknown.

In $p\overline{p}$ collisions, $h_1^\perp$ for valence quarks appears at leading twist level; the generated observable asymmetry allows to study spin-orbit correlations of transversely polarized partons even using unpolarized beams and targets. Monte Carlo simulations for Drell-Yan $p\bar{p} \to \mu^+\mu^- X$ reactions show that in a reasonable running time (one month) some 10^4 events with an azimuthal asymmetry up to 10% can be produced for the unpolarized case. [18]

3.5 Time-like proton form factors

The electric and magnetic proton form factors G_E and G_M can be connected to the lepton angular distribution of the $p\overline{p} \to e^+e^-$ reaction through the one-photon exchange QED formula:

$$\frac{\mathrm{d}\sigma}{\mathrm{d}\Omega} = \frac{\alpha^2}{4\beta_p\, s}\left[|G_M|^2(1+\cos^2\theta) + \frac{4m_p^2}{s}|G_E|^2\sin^2\theta\right] ,$$

where θ is the CM angle between the electron and the proton and β_p is the CM proton velocity. Data at high $Q^2 = s$ are crucial to test the onset of the asymptotic scaling region of perturbative QCD, where the space-like and time-like form factors should become equal. In this region the contribution of the electric term is suppressed. For this reason, due to the limited statistics at high momenta, up to now $|G_E|$ and $|G_M|$ have not been measured separately and have been determined with the assumption $|G_E| = G|_M|$.

One of the goals of PANDA will be to make angular distribution measurements with high statistics and full angular coverage to measure the magnitude of the two form factors separately from threshold up to 20-25 $\mathrm{GeV}^2/\mathrm{c}^4$. Most of these measurements could be performed in parallel with other programs, avoiding resonance peaks in order to reduce systematic uncertainties.

3.6 Further options

A study of charmed mesons in nuclear matter will be performed in PANDA, by replacing the jet target with wires of various materials. These studies will explore the partial restoration of the $q\bar{q}$ chiral symmetry in nuclear matter and can be considered equivalent to the Higgs searches in electroweak theory.

In the case of charmonium, multigluon exchange should generate an attractive potential between a $c\bar{c}$ meson and a nucleon, with a binding energy of the order of 10 MeV [20], giving measurable effects on the charmonium by shifting its mass and increasing its width. Here the difficulty is to select final states, as e^+e^-, carrying the unperturbed information outside the nuclear medium. In PANDA some hundreds of such events per day are expected on a Carbon target. [21]

The magnitude of the J/Ψ nucleon absorptive cross section is essential to interpret the J/Ψ suppression as a signal for the formation of the quark-gluon plasma formation. It can be measured by the accurate scanning of the $\overline{p}A \rightarrow J/\Psi + (A-1)$ reaction between 3.5 and 4.5 GeV/c.

Recent GSI experiments have shown that charged pions and kaons exhibit effective masses in the nuclear medium different from those in vacuum. [22] This effect is due to the quark condensates and is an important input for qq and $q\bar{q}$ potential models. A similar behaviour is predicted also for the open charm mesons D^+ and D^- but it has not yet been observed. PANDA could make this observation for the first time, measuring with high accuracy the shifting of D^-/D^+ masses and of the $D\overline{D}$ production threshold in nuclear matter.

The investigation of hypernuclei requires the modification of the PANDA vertex region. [1] One of the most interesting topics is the study of double-Λ hypernuclei that can be produced using the two step reaction:

$$\overline{p}(2.6\,\mathrm{GeV/c}) + \mathrm{A} \rightarrow \Xi^-_{\mathrm{slow}} + \overline{\Xi^-}_{\mathrm{trigger}}\,; \qquad \Xi_{\mathrm{slow}} + \mathrm{A}' \rightarrow_{\Lambda\Lambda} \mathrm{A}' + \ \gamma'\mathrm{s}\ .$$

As a secondary active target (A') high resolution solid state micro tracking detectors will be used and a position sensitive Ge-γ array will allow high rate spectroscopy. One can estimate a rate of 14 500 stopped Ξ^- in ^{12}C nuclei per day and, taking into account the PANDA acceptance on hypernuclear events [1], a rate of 320 produced $\Lambda\Lambda$ hypernuclei per day is expected.

Finally, the large amount of data collected by PANDA will also allow the study of rare channels with cross sections of the order of pb. Among these,

the most interesting are probably the $p\bar{p} \to \gamma\gamma$ annihilation, which should give complementary information on Generalized Parton Distributions, rare D decays as $D^+ \to \mu^+\nu$ to test LQCD calculations, and the D^+/D^- decay ratios to detect direct CP violation in Cabibbo-suppressed decays.

4 Conclusions

The charmonium and open charm spectroscopy challenge our understanding of QCD. The field is evolving in an interesting and exciting way, and, on the experimental side, this will require many years (perhaps decades) of intense experimentation to find mass, width, decay modes and spin-parity of all the states. In this field, many relevant contributions from antiprotons and PANDA are expected.

The $p\overline{p}$ annihilation tests quark rearrangement and quark-gluon dynamics. The production of baryon-antibaryon pairs is copious and with PANDA it will be possible to extend these studies also to the charm sector.

The production of Drell-Yan lepton pairs in $p\bar{p}$ annihilations is one of the best ways to investigate the internal hadron structure and in particular the quark spin-orbit correlations. The particle identification capabilities and the hermeticity of PANDA will play a crucial role in collecting high statistics clean samples of data.

Many other issues of hadron physics are accessible to PANDA and have been briefly described here. The unique properties of the HESR $\bar{p}$ beam, coupled with the performances of PANDA, will play a leading role for the hadron physics with antiprotons in the near future.

5 Acknowledgements

It is a pleasure to thank the organizers of the Conference for the invitation and Diego Bettoni, Gianluigi Boca, Fulvio Piccinini and Marco Radici for useful discussions.

References

1. M. Kotulla *et al.*, PANDA Collaboation, Technical Progress Report, FAIR, http://www-panda.gsi.de/auto/_home.htm, Darmstadt (2005).

2. A. Lehrach *et al.*, Nucl. Instr. and Meth. A **561**, 289 (2006).

3. G. Bali *et al.*, *Heavy Quarkonium Physics, QWG*, CERN Report 2005-005, (Geneva, 2005).

4. E.S. Swanson, Phys. Rep. **429**, 243 (2006).

5. M. Shepherd, CLEO-c Collaboration, this Conference.

6. Particle Data Group, J. of Phys. G **33**, 1 (2006).

7. G. Branderburg *et al.*, Phys. Rev. Let. **85**, 3095 (2000).

8. M. Andreotti *et al*, E835 Collaboration, Nucl. Phys. B **717**, 34 (2005), T.A. Armstrong *et al.*, E760 Collaboration, Nucl. Phys. B **373**, 35 (1992).

9. S.Eidelman, BELLE Collaboration, this Conference.

10. E. Robutti, BaBar Collaboration, this Conference.

11. E. Eichten *et al.*, hep-ph/0701202 (2007).

12. K. Abe *et al.*, BELLE Collaboration, hep-ex0708.1790 (2007).

13. A. Lundborg, T. Barnes ans U. Wiedner, Phys. Rev.**D73**, 096003 (2006).

14. B. Aubert *et al.*, BaBAr Collaboration, Phys. Rev. Lett. **90**, 242001 (2003).

15. D. Besson *et al.*, BaBAr Collaboration, Phys. Rev. D **68**, 032002 (2003).

16. L. Maiani *et al.*, Phys. Rev. D **71** 014028 (2005).

17. T. Johansson *et al.* Nucl. Phys. B Proc. Suppl. A **56**, 46 (1997), K.D.Paschke *et al.*, Phys. Rev. C **74**, 015206 (2006)

18. A. Bianconi and M. Radici, Phys. Rev. D **71**, 074014 (2005).

19. S. Falciano *et al.*, NA10 Collaboration, Z. Phys. **C31**, 513 (1986), M. Guanziroli *et al.*, NA10 Collaboration, Z. Phys. **C37**, 545 (1988)

20. S.J. Brodsky and G.A. Miller, Phys Lett B **412**, 125 (1997).

21. S.H. Lee andC.M. Ko, Phys. Rev. C **6**, 038202 (2003).

22. R. Barth, Phys. Lett. **78**, 4007 (1997), T. Yamazaki *et al.*, Phys. Lett. B **418**, 246 (1998).

Frascati Physics Series Vol. XLVI (2007), pp. 351–367
HADRON07: XII Int. Conf. on Hadron Spectroscopy – Frascati, October 8-13, 2007
Plenary Session

EXHANGE: WHICH IS MORE ATTRACTIVE π EXHANGE: WHICH IS MORE ATTRACTIVE?

F.E. Close
Rudolf Peierls Centre for Theorerical Physics;
University of Oxford; Oxford OX1 3NP; England

Abstract

This review summarises issues that have arisen since the appearance of "Rumsfeld Hadrons". We show that signals $\phi(2175)$; $Y(4260)$ and $\Upsilon(10890)$ in the $s\bar{s}$, $c\bar{c}$ and $b\bar{b}$ share features that point to the possible role of π exchange forces between flavoured mesons generating effects that can mimic hybrid mesons. The flavour dependence of these phenomena may help to resolve this question.

1 Introduction

The first part of my talk replicated much of what was reported in "Rumsfeld Hadrons" and will not be repeated here. For that see [1]. Here I review some subsequent developments concerning the possible discovery of hybrid charmonium. In summary: there are undoubtedly signals in the 1^{--} wave that have the a priori character of hybrid mesons. The data in the charm sector seem to

rule out a particular tetraquark interpretation and are consistent with a charmonium hybrid. However, there are reasons to consider the role of π exchange, which gives an attraction in this channel. Comparisons of hybrid predictions and attractive forces from π exchange as a function of flavour may resolve this question.

2 Charmonium: the $Y(4260)$

First let's consider the lightest of the novel charmonium states, the $X(3872)$ at $D^0 D^{*0}$ threshold.

This state now appears to have $C = +$ and be consistent with 1^{++} [2]. This J^{PC} was first suggested in Ref. [3] and a dynamical picture of it as a quasi-molecular $D^{*0}\bar{D}^0$ state discussed in Refs. [3, 4]. In $e^+e^- \to \psi + X$ there is no sign of the $X(3872)$: the suppression of this state among prominent $C = +$ charmonium states [5] is consistent with its molecular versus simple $c\bar{c}$ nature.

It is generally agreed that the $X(3872)$ has a tetraquark affinity; whether it is a genuine $D^0 D^{*0}$ molecule or a compact $cu\bar{c}\bar{u}$ is a more subtle issue. If the quark-pairs are tightly clustered into di-quarks, then a $S = 0$ and $S = 1$ are required to make the 1^{++}. Consequently other states, combinations of $0^+ - 0^+$ and $1^+ - 1^+$ would be expected. The absence of such a rich spectrum suggests that the overriding dynamics is that the constituents rearrange into loosely bound colour singlet $c\bar{u}$-$u\bar{c}$, or $D^0 D^{*0}$.

That such a molecular state can be generated by the attractive force of π exchange was suggested in ref [4, 6]. Ref [7] also has discussed the dynamical generation of such states. What is particularly interesting is that it had been predicted long ago that the π exchange that is known to bind the deuteron, may also act between metastable mesons and cause attractions in certain channels [8], which Tornqvist referred to as "deusons". One such example was the $D\bar{D}^*$ channel. A test of this picture is that π exchange can also occur between D and D^* (i.e with no $\bar{D}$ [8]) leading to structures in channels with charm $= \pm 2$. Searching for such states among the debris at KEK, GSI and LHC could be important in isolating evidence for this π exchange dynamics.

Before invoking exotic explanations of the various signals that have recently appeared in charmonium, such as $Y(4260)$ in $\psi\pi\pi$, $X(4350)$ in $\psi'\pi\pi$ and $X(4430)$ in $\psi'\pi$, we should satsify ourselves that there are not more mundane explanations. As each of these states is near an S-wave threshold involving

charmed mesons that are metastable on the timescale of the strong interaction, then the role of π exchange here needs to be assessed.

3 Attractive π exchange

The analysis that Tornqvist applied to $D\bar{D}^*$ can be applied to other combinations of D, D^*, D_0, D_1 and their charge conjugates, and to their bottom analogues. I have been looking at this in collaboration with Qiang Zhao and Christopher Thomas [9]. This is relevant as the three novel states are in the vicinity of the S-wave thresholds D^*D_0 and DD_{1L} ($Y(4260)$); DD_{1H} and D^*D_2 ($X(4350)$); D^*D_1 ($X(4430)$).

The basic idea is that π exchange has both a direct Yukawa term $C(r)$ and also a tensor interaction $T(r)$ that links $S-D$ waves [8]. In the deuteron there is attraction within the ${}^3S_1$; repulsion in ${}^3D_1$ but an attractive coupling between these waves that enables binding. The effective potential in a basis of ${}^3S_1$ and ${}^3D_1$ states may be summarised as

$$V = -\frac{25}{3}V_0\Big[\begin{pmatrix} 1 & 0 \\ 0 & 1 \end{pmatrix} C(r) + \begin{pmatrix} 0 & \sqrt{8} \\ \sqrt{8} & -2 \end{pmatrix} T(r)\Big]. \quad (1)$$

The known binding of the deuteron normalises the strength of the above, which Tornqvist [8] then applied to mesons, for example the $D\bar{D}^* \pm D^*\bar{D}$ case (note the two charge conjugation eigenstates which will have opposite overall signs, leading to attraction in one and repulsion in the other). For the 1^{++} channel this becomes [8]

$$V = -3V_0\Big[\begin{pmatrix} 1 & 0 \\ 0 & 1 \end{pmatrix} C(r) + \begin{pmatrix} 0 & -\sqrt{2} \\ -\sqrt{2} & 1 \end{pmatrix} T(r)\Big]. \quad (2)$$

Notice that relative to the deuteron, in this case the signs in the tensor interaction are inverted relative to the deuteron and binding is enhanced.

The flavour dependence of the binding is interesting in that [8] noted that the net attraction is greater for heavy flavours such as than for light; $B\bar{B}^*$ being bound; $D\bar{D}^*$ being around threshold and $K\bar{K}^*$ being an attractive enhancement above threshold. At first sight this appears a paradox as for heavy-light states, it is only the light flavour that couple to the pion, and the heavy flavour is apparently a passive spectator, so how can its mass affect the result? This is because the larger kinetic energy of the light flavoured

states tends to counterbalance the overall potential leading tobetter binding of bottom than charm, and of charm than strange. Hence Tornqvist gives only tentative suggestions about possible attractions in the strange sector; for the charm sector there begins to be hints of possible states appearing at threshold, which may now have some confirmation in the case of the $1^+(3872)$; for bottom mesons the model appears to imply some bound states should occur.

This pattern will have relevance later when we consider the flavour dependence of hybrid meson masses.

We find that the structure of eq(2) also applies in the cases of DD_1 and D^*D_0 in 1^-. Note that parity conservation requires the π vertex to link $D \leftrightarrow D^*$; and $D_0 \leftrightarrow D_1$. In the heavy quark limit the latter is D_{1L}; in general π-exchange couples the D_0 to the $p_{1/2}$ combination of each of the two axial mesons. These remarks apply also to the charge conjugate states. Consider first the S-wave 1^- channel accessible to $D_1\bar{D}$ and $D_0\bar{D}^*$ (or their charge conjugate analogues, which is understood always). The π exchange gives an off diagonal potential linking $D_1\bar{D} \leftrightarrow D_0\bar{D}^*$.

In the case of $D\bar{D}^* \pm D^*\bar{D}$ Tornqvist found attraction in I=0 1^{++} and repulsion in 1^{+-}. In the off-diagonal case, $D_1\bar{D} \leftrightarrow D_0\bar{D}^*$ (+*c.c.*) we find that the channels for strong attraction are isoscalar for *both* 1^{--} and 1^{-+}. Thus we find attractions in the 1^{--} channel, where the $Y(4260)$ and possibly $Y(4350)$ are seen coupling to e^+e^-, and also in the exotic 1^{-+} channel. It is intriguing that it is in these $1^{-\pm}$ channels and in this mass region where hybrid mesons are also predicted to occur; furthermore they are predicted to have preferred couplings to these very DD_1 and D^*D_0 states. Possible implications of this will be discussed later.

In the case of $Z(4430)$ seen in $\psi'\pi$, Bugg [10] has also noticed the nearness to the D^*D_1 threshold and argued that the existence of this state and the threshold could be linked. In the absence of a model for the attractive force he was unable to predict the J^P, but if we apply the π exchange analysis to this case (which is the last remaining combination of thresholds for S and P wave $c\bar{q}$ states) then we can predict possible quantum numbers. Here we will consider first the $D^*\bar{D}^*$ and the ${}^1S_0$ and ${}^5D_0$ basis for which

$$V = -\frac{\gamma}{2}V_0[\begin{pmatrix} 2 & 0 \\ 0 & -1 \end{pmatrix} C(r) + \begin{pmatrix} 0 & \sqrt{2} \\ \sqrt{2} & 2 \end{pmatrix} T(r)]. \qquad (3)$$

where the overall scale factor γ depends on the J^P and is discussed below. The

same pattern emerges for the $D^* \bar{D}_1$ (and charge conjugate).

The tensor term adds to the attraction if the leading term is already attractive. For other spin combinations the matrix structure is more involved but the tensor terms do not essentially alter the attraction or repulsion systematics of the leading term. Thus in S-wave the couplings are to $(0, 1, 2)^-$ and one finds the following attractive channels, which are listed in the sequence J^P, isospin, relative strength of attraction.

In the heavy quark limit, at $D^* D_{1L}$ we have for the scale factors γ

$$\begin{array}{lll} 0^- & I = 0 & 12 \\ 1^- & I = 0 & 6 \\ 2^- & I = 1 & 2 \end{array} \tag{4}$$

while at $D^* D_{1H}$ we find attraction in the complementary channels

$$\begin{array}{lll} 0^- & I = 1 & 2 \\ 1^- & I = 1 & 1 \\ 2^- & I = 0 & 3 \end{array} \tag{5}$$

If this state with both hidden charm and isospin is confirmed then it definitely goes beyond charmonium and demands tetraquarks. To distinguish π exchange molecules from tight clustered diquark-antidiquark will involve finding other examples and collating their J^P pattern. The pattern from π exchange differs from the richer spectroscopy of tetraquarks. In particular the most likely J^P would be 0^- or 2^-. However, one would expect even larger effects in the $I = 0$ sector in the 0^- and also 1^-. Thus if this signal is driven by attractive π-exchange, then some signal in this same mass region should also occur in $e^+e^- \to \psi\eta/\eta'$ with at least as big strength.

A challenge for dynamics is also to explain why the state is seen in $\pi\psi'$ but not apparently in $\pi\psi$. As conjectured by Bugg [10], it is possible to force a suppression due to nodes in wavefunctions [11] but it is not an overwhelming effect and while such a state should be expected to have some strength in $\psi\pi$, one should also anticipate I=0 partners in $\psi\eta$ among other channels.

A final reminder [8]: π exchange also leads to potential bound states in double charm combinations, not just in the hidden charmonium channel.

In principle this could discriminate these molecular combinations from others, such as hybrid charmonium, though their associated production in order to conserve charm will imply many particle final states and impose severe challenges to analysis.

I will now focus on the best established state, the $Y(4260)$ [12], and review interpretations as hybrid $c\bar{c}$ [13, 14] or $cs\bar{c}\bar{s}$ tetraquark [15]. The data already appear to disfavour the latter. The challenge will be to distinguish the former from the π exchange. One way will be to look for analogues in the $s\bar{s}$ and $b\bar{b}$ sectors.

4 Hybrid Quarkonium: Theory

Mass predictions for the J^{PC} exotic 1^{-+} hybrids were reviewed in ref [16]. Previous results based on lattice QCD, such as flux tube models, had assumed an adiabatic approximation. Ref [16] made numerical studies that relaxed that assumption and found that hybrid signals should arise in the following mass regions

$$\begin{aligned} s\bar{s}: &\quad 2.1 - 2.2\ GeV \\ c\bar{c}: &\quad 4.1 - 4.2\ GeV \\ b\bar{b}: &\ 10.8 - 11.1\ GeV \end{aligned} \tag{6}$$

The adiabatic approximation was found to be good for $b\bar{b}$ and reasonable for the lighter flavours.

In view of the signals that could be candidates for the 1^{--} hybrids, which we shall discuss later, let's first look at these in more detail.

Eight low-lying hybrid charmonium states were predicted in the flux-tube model to occur at $4.1 - 4.2$ GeV [16], and in UKQCD's quenched lattice QCD calculation with infinitely heavy quarks the exotic 1^{-+} was predicted to be 4.04 ± 0.03 GeV (with un-quenching estimated to raise the mass by 0.15 GeV) [17]. Quenched lattice QCD indicates that the $c\bar{c}g$ 1^{--}, $(0,1,2)^{-+}$ are less massive than 1^{++}, $(0,1,2)^{+-}$ [22]. The spin splitting for this lower set of hybrids in quenched lattice NRQCD is $0^{-+} < 1^{-+} < 1^{--} < 2^{-+}$ [21], at least for $b\bar{b}g$. This agrees with the ordering found in the model-dependent calculations for $q\bar{q}g$ [19] in the specific case of $c\bar{c}g$ [18, 20] though there is considerable

uncertainty in the magnitudes [21]. In particular, the cavity QCD calculations have not included the contribution from four-gluon vertex; although higher order in α_s. it is possible such contributions are not negligible [23].

Thus the consensus is that the resulting pattern is, in decreasing mass, $1^{--}; 1^{-+}; 0^{-+}$ with the mass gap between each state being the same and of the order of 10-100 MeV. Thus theory strongly indicates that if $Y(4260)$ is $c\bar{c}g$, and the splittings are not due to mixing or coupled channel effects, then the J^{PC} exotic 1^{-+} and non-exotic 0^{-+} $c\bar{c}g$ are below $D^{**}\bar{D}$ threshold, making them narrow by virtue of the selection rules. The 1^{-+} decay modes [24] and branching ratios [25] have extensively been discussed. Thus on the basis of masses alone, it is consistent to identify possible states as $1^{--}(4.25); 1^{-+}(4.1); 0^{-+}(3.9)$ and to speculate whether there are two states $1^{-+}(4.1); 0^{-+}(3.9)$ in either the $X/Y(3940)$ structures of Belle or $e^+e^- \to \psi + X$. This is clearly a question that statistics from a super-B factory may resolve for the B-decays or $e^+e^- \to \psi + X$.

To the extent that these spin dependent arguments are relevant to the more realistic situation, one expects for hybrid $b\bar{b}$ state that the mass of the 1^{--} state will be similar or at most some tens of MeV more massive than the 1^{-+}, whereas for $s\bar{s}$ the splitting could be $O(100)$ MeV [19]. In practice I suspect that the strong S-wave coupling of such states to flavoured channels that are near to threshold, such as $c\bar{c} \to DD_1; D^*D_0$ in the case of charmonium, may cause significant mass shifts [26] and potentially dominate the spin-dependence of such masses.

Ref [27] identified prominent hadron decays modes for such masses to include $s\bar{s} \to KK_1(1400; 1270)$ in S-wave and KK_2 in D-wave; . The analogous situation for $b\bar{b}$ would be to BB_1 and B^*B_0. Given that the anticipated hybrid masses are already in the vicinity of thresholds to which they are predicted to have strong S-wave couplings, and further the fact that π exchange is predicted to give attractions among these mesons in the overall I=0 $1^{-\pm}$ channels, it would be surprising if signals were not seen in these $1^{-\pm}$ modes at least. Determining whether they are pure molecule or require a short range $Q\bar{Q}$ seed, is one challenge; if such a seed is present, then for the 1^{--} case we would need to determine whether it has S=1 (as for a conventinoal quarkonium) or S=0 (as for a hybrid). To do so will require studies of $c\bar{c}$, $b\bar{b}$ and $s\bar{s}$.

5 Hybrid Quarkonium: Phenomena

Mass arguments alone will not be convincing; we need to understand the dynamics of production and decay and show that these fit best with hybrid states. I now turn to hybrid charmonium and evaluate the prospects that it is being exposed in the enigmatic vector state $Y(4260)$ which is seen in $e^+e^- \to \psi\pi\pi$, with no observed decay into $D\bar{D}$. The mass, large width into $\psi\pi\pi$, small leptonic width ($O(5-80)$eV, contrast O(keV) for known states), affinity for DD_1 threshold and apparent decay into $\psi\sigma$ or $\psi f_0(980)$ are all consistent with predictions made for hybrid vector charmonium [13].

The fact that there is no sign of established 3S/2D(4040/4160) 4S(4400) in the $\psi\pi\pi$ data already marks this state as anomalous, and its characteristics are tantalisingly similar to what has been predicted for hybrid charmonium. However, the fact that it is near the DD_1 threshold might be the reason for the large $\psi\pi\pi$ signal independent of its nature: the DD_1 are produced in S-wave, with small relative momenta and as such there is every likelihood that they can interchange constituents, leading to $c\bar{c} + q\bar{q}$ final states, such as $\psi\pi\pi$, without any $O(\alpha_s)$ suppressions from intermediate perturbative gluons (in contrast to the case for $\psi(3685)$ and $c\bar{c}$ resonances at other masses).

A lattice-inspired flux-tube model showed that the decays of hybrid mesons, at least with exotic J^{PC}, are suppressed to pairs of ground state conventional mesons [28, 29]. This was extended to all J^{PC}, for light or heavy flavours in Ref. [27]. A similar selection rule was found in constituent gluon models [14], and their common quark model origin is now understood [30]. It was further shown that these selection rules for light flavoured hybrids are only approximate, but that they become very strong for $c\bar{c}$ [20, 27]. This implied that decays into $D\bar{D}$, $D_s\bar{D}_s$, $D^*\bar{D}^*$ and $D_s^*\bar{D}_s^*$ are essentially zero while $D^*\bar{D}$ and $D_s^*\bar{D}_s$ are very small, and that $D^{**}\bar{D}$, if above threshold, would dominate. (P-wave charmonia are denoted by D^{**}). As $c\bar{c}g$ is predicted around the vicinity of $D^{**}\bar{D}$ threshold, the opportunity for anomalous branching ratios in these different classes was proposed as a sharp signature [16, 27].

More recently the signatures for hybrid charmonia were expanded to note the critical region around $D^{**}\bar{D}$ threshold as a divide between narrow states with sizable branching ratio into $c\bar{c}$ + light hadrons and those above where the anomalous branching ratios would be the characteristic feature [24, 25]. It was suggested to look in e^+e^- annihilation in the region immediately above charm

threshold for state(s) showing such anomalous branching ratios [25]. The leptonic couplings to e^+e^-, $\mu^+\mu^-$ and $\tau^+\tau^-$ were expected to be suppressed [32] (smaller than radial S-wave $c\bar{c}$ but larger than D-wave $c\bar{c}$, but with some inhibition due to the fact that in hybrid vector mesons spins are coupled to the $S = 0$, whose coupling to the photon is disfavoured [25]).

Thus several of the theoretical expectations for $c\bar{c}g$ are born out by $Y(4260)$: (1) Its mass is tantalizingly close to the prediction for the lightest hybrid charmonia; (2) The expectation that the e^+e^- width should be smaller than for S-wave $c\bar{c}$ is consistent with the data [13]; (3) The predicted affinity of hybrids to $D^{**}\bar{D}$ could be related to the appearance of the state near the $D^{**}\bar{D}$ threshold. The formation of $D^{**}\bar{D}$ at rest may lead to significant rescattering into $\psi\pi^+\pi^-$, which would feed the large signal; (4) The absence of any enhancement in "ground state charm" such as $D\bar{D}, D^*\bar{D}, D^*\bar{D}^*, D_s\bar{D}_s$ etc is also an explicit signature for hybrid charmonium.

It has become increasingly clear recently that there is an affinity for states that couple in S-wave to hadrons, to be attracted to the threshold for such channels [31]. The hybrid candidate 1^{--} appearing at the S-wave $D_1(2420)\bar{D}$ is thus interesting. However, one could argue that *any* $c\bar{c}$ resonance in this region would be attracted likewise, so these phenomena do not necessarily imply a hybrid meson rather than a conventional $c\bar{c}$ as the source. Ways of distinguishing these are discussed later.

The nearness of $Y(4260)$ to the $D_1(2420)\bar{D}$ threshold, and to the $D_1'\bar{D}$ threshold, with the broad D_1' found at a mass of ~ 2427 MeV and width ~ 384 MeV [33], indicate that these states are formed at rest. Also, these are the lowest open charm thresholds that can couple to 1^{--} in S-wave (together with $D_0\bar{D}^*$, where the D_0 mass ~ 2308 MeV and width ~ 276 MeV [33]). Flux-tube model predictions are that the D-wave couplings of 1^{--} $c\bar{c}g$ to the 1^+ and 2^+ D^{**} are small [20, 27, 34]; and there is disagreement between various versions of the model on whether the S-wave couplings to the two 1^+ states are large. If these couplings are in fact substantial, the nearness of $Y(4260)$ to the thresholds may not be coincidental, because coupled channel effects could shift the mass of the states nearer to a threshold that it strongly couples to; and it would experience a corresponding enhancement in its wave function. The broadness of $Y(4260)$ also implies that its decay to $D_1(2420)\bar{D}$, $D_1'\bar{D}$ and $D_0(2308)\bar{D}^*$ which feed down to $D^*\bar{D}\pi$ and $D\bar{D}\pi$ [35] would be allowed by

phase space and should be searched for to ascertain a significant coupling to D^{**}.

Flux-tube model width predictions for other charm modes are $1-8$ MeV for $D^*\bar{D}$ [34], with $D\bar{D}$, $D_s\bar{D}_s$, $D^*\bar{D}^*$ and $D_s^*\bar{D}_s^*$ even more suppressed. Thus a small $D\bar{D}$ and $D_s\bar{D}_s$ mode could single out the hybrid interpretation, which is very different from the $c\bar{s}s\bar{c}$ four-quark interpretation for $Y(4260)$ which decays predominantly in $D_s\bar{D}_s$ [15].

The data [36] on $e^+e^- \to D_s\bar{D}_s$ show a peaking above threshold around 4 GeV but no evidence of affinity for a structure at 4.26 GeV. This is suggestive and if these data are confirmed, then as well as ruling out a $cs\bar{c}\bar{s}$ at this mass, they will also add support to the hybrid interpretation. The same data also show there is no significant coupling of $Y(4260)$ to $D\bar{D}; D^*\bar{D}$ or $D^*\bar{D}^*$, all of which are in accord with predictions for a hybrid state.

Theory $s\bar{s}$, $c\bar{c}$ and $b\bar{b}$

If the large $\psi\pi\pi$ signal is solely due to the presence of S-wave $DD_1; D^*D_0$ thresholds and constituent interchange, there should be analogous phenomena in $\phi\pi\pi$ and $\Upsilon\pi\pi$ associated with the corresponding flavoured thresholds. By seeking evidence for these channels, and comparing any signals, or lack of, it may be possible to identify the dominant dynamics.

For example, if a 1^{--} hybrid meson of $s\bar{s}$, $c\bar{c}$ or $b\bar{b}$ flavours is involved, and the lattice QCD or flux-tube models are reliable guide to the masses, then we anticipate activity in the energy regions

$$\begin{aligned} s\bar{s}: &\quad 2.1 - 2.2\ GeV \\ c\bar{c}: &\quad 4.1 - 4.2\ GeV \\ b\bar{b}: &\ 10.8 - 11.1\ GeV \end{aligned} \tag{7}$$

If the effect is simply due to S-wave threshold, without any direct channel resonant enhancement, then for $b\bar{b}$ we need to look in the vicinity of BB_1 and B^*B_0 thresholds. The mass splitting of B and B^* is 46 MeV; that of the B_2 and B_{1H} is 26 MeV. The threshold for BB_{1H} is 11.00 GeV; we expect that π-exchange effects arise near to the threshold for BB_{1L} and B^*B_0 and so we need to estimate at what energy this is. In the case of $c\bar{d}$ the D_{1L}-D_{1H} mass gap is some 60 MeV in theory but the data could have them nearly degenerate.

The D_s sector is confused by the light D_{s0} and D_{s1}, which may be quasi-molecular. A similar possiblity cannot be ruled out in the B sector. Thus what at first sight appeared to be a straightforward question in the B sector, namely where are the thresholds and will π exchange create attractions, is less clear. We may anticipate that the thresholds for BB_1 and B^*B_0 are certainly below 11.00 GeV, perhaps by as much as 200 MeV, and that the splitting between them will be of the order of tens of MeV. Thus, here again we find the S-wave threshold region and the prediction for vector hybrid to be very similar.

For $s\bar{s}$ we have

$$\begin{aligned} KK_1(1270) &= 1760\ MeV \\ KK_1(1410) &= 1900\ MeV \\ K^*K_0 \quad &= 2320\ MeV. \end{aligned} \tag{8}$$

though the latter pair at least are smeared over some 200 MeV due to widths. The π-exchange attractions are expected to occur above threshold in the $s\bar{s}$ sector (see remartks in section III), and once again, in the vicinity of the predicted mass of the hybrid 1^{--}.

Thus in all flavours, we expect vector hybrids, coupling strongly to 0^-1^+ or to 1^-0^+ in S-wave, to be amplified by the π-exchange and to be manifested around these thresholds. Consequently we should expect signals (perhaps being wise after the event!) and the challenge is to determine if they are resonant, and if so, whether they are hybrid or conventional.

The spread in threshold masses for $s\bar{s}$ and the expected near-degeneracy for $b\bar{b}$ would become exact degeneracy in the heavy quark limit $M_{s,c,b} \to \infty$. This has a consequence for the nature of the $\pi\pi+$ [$s\bar{s}$, $c\bar{c}$, $b\bar{b}$] final state. If there is a direct channel 1^{--} $s\bar{s}$, $c\bar{c}$ or $b\bar{b}$ resonance feeding S-wave flavoured mesons, which rearrange their constituents to give the superficially OZI violating $\pi\pi+$ [$s\bar{s}$, $c\bar{c}$, $b\bar{b}$] final state, then the spin of the heavy flavours is preserved in the $M_Q \to \infty$ limit. In that limit, a hybrid $c\bar{c}$ vector meson (whose $c\bar{c}$ are coupled to zero!) would dominantly feed channels where $c\bar{c}$ has spin zero; hence $h_c\eta$ rather than $\psi\pi\pi$ [37]. Conversely, a conventional ψ^*, $c\bar{c}$ coupled to spin one, would naturally feed the $\psi\pi\pi$. Thus the ratios of branching ratios to $c\bar{c}$ (S=0 or 1) and light hadrons can test the nature of the initial spin state and distinguish hybrid from either conventional resonance or π-exchange.

When the meson loops are calculated, there is a destructive interference between the DD_1 and D^*D_0 channels. This is exact in the degenerate case, which applies in the $M_Q \to \infty$ limit. Conversely, for non-degenerate channels the cancellation fails. Thus in the case of $s\bar{s}$ there is little to be learned, while for $b\bar{b}$ it should be a clean test; for $c\bar{c}$ it is indeterminate until such time as h_c or η_c channels are quantified.

A further strategic test is to measure the polarization of the respective vector mesons in $\pi\pi + \phi; \psi; \Upsilon$. Predicting it is highly model dependent but a similar, or monotonic behaviour with flavour, would hint at a common origin whereas significantly different amounts of polarization could reveal more than one dynamics is important.

Phenomena in $s\bar{s}$, $c\bar{c}$ and $b\bar{b}$

Intriguing phenomena are showing up not just in the $c\bar{c}$, but also in both the $s\bar{s}$ and $b\bar{b}$ sectors.

The cross section for $e^+e^- \to K^+K^-\pi^+\pi^-$ has significant contribution from $e^+e^- \to KK_1$ with rescattering into $\phi\pi\pi$. A resonance with width $\Gamma = 58 \pm 16 \pm 20$MeV with large branching ratio into $\phi\pi\pi$ is seen with mass of 2175MeV [38, 39]. Not only does the mass agree with the predictions of eq7, simple arithmetic shows that the mass gap from this state to $m(\phi)$ is within the errors identical to that between $Y(4260)$ and $m(\psi)$. This coincidence (?) has also been noticed by Jon Rosner [40]. This is perhaps reasonable if the cost of exciting the gluonic flux-tube is not sensitive to the masses of the $q\bar{q}$ involved (as lattice QCD seems to suggest), in which case a hybrid vector production and decay is consistent with data. The KK_1 and K^*K_0 thresholds do not relate so readily to the 2175 state as do the analogous charm states with the 4260, which makes it less likely perhaps that the 4260 and 2175 can be simply dismissed as non-resonant effects associated solely with S-wave channels opening.

During this conference evidence for similar happenings in the $b\bar{b}$ sector [41]. The decays of $\Upsilon(10.88)$ show an enhanced affinity for $\Upsilon\pi\pi$, in marked contrast to the decays of other Υ^* initial states. As in the $s\bar{s}$and $c\bar{c}$ cases, the mass of 10.88 GeV agrees with the hybrid prediction in eq(7).

A problem in sorting this out may be that any resonances that happen by chance to lie near the S-wave thresholds will feed, via rearrangement, the $\pi\pi + \phi; \psi; \Upsilon$ channels. To determine whether the source is hybrid or not will require

measuring, or placing limits on, analogous rearrangement channels to spin-0 onia states and comparison to their spin-1 analogues. Thus for the $b\bar{b}$ case, the appearance of a signal in $\Upsilon\pi\pi$ suggests that a spin-1 $b\bar{b}$ initial state rather than a hybrid resonance may be driving the phenomenon.

If this 4260 state is not hybrid vector charmonium, then where is it?

Suppose that it is. Where else should we look? Clearly the $[0,1]^{-+}$ states predicted to lie below the $Y(4260)$ become interesting. The properties and search pattern for such states are discussed in ref. [25]. In $e^+e^- \to \psi + X$ it is possible that such states could feed the signal at 3940MeV. If the production is via strong flux-tube breaking there is a selection rule [42] that suppresses $\psi + X$ when X has negative parity. However, it is possible that the dominant production for $c\bar{c}\ + c\bar{c}$ is by "preformation" [43], where a perturbative gluon creates the second $c\bar{c}$ pair (the highly virtual photon having created the initial pair). In such a case there is no selection rule forbidding $X \equiv [0,1]^{-+}$ hybrids; however, the amplitude will be proportional to the short distance wavefucntion of the hybrid, which is expected to be small compared to those of e.g. $\eta_c(3S)$ though perhaps comparable to those of χ_J. Thus it would be interesting to measure the J^{PC} of the $X(3940)$ region to see if it contains exotic 1^{-+}. Note that both hybrid mesons and also π-exchange between flavoured mesons lead us to expect signals in the exotic 1^{-+} channel. Model predictions for production rates are required, or practical ways of looking for manifestly flavoured (such as double charm or double strange) states in the latter case, in order to resolve this conundrum.

What should we do next?

There are clearly tantalising signals in each of the $s\bar{s}$, $c\bar{c}$ and $b\bar{b}$ sectors. The latter appears, on heavy flavour arguments, to be more likely associated with a conventional S=1 $b\bar{b}$ resonance than a hybrid. If one could determine the polarization of the outgoing Υ in the $\Upsilon\pi\pi$ final state and compare with the polarization in the $\psi\pi\pi$ and $\phi\pi\pi$, that could have some strategic interest and stimulate model predictions.

The results of ref [43] show how the relative decay amplitudes to $DD_1, D^*D_{0,1,2}$ may be used to determine the structure of $c\bar{c}$ states that are near to the S-wave thresholds. In particular this applies to $Y(4260)$ and

$Y(4325)$. There are characteristic zeroes that may occur for vector meson decays:

$$\Gamma(^3S_1 \to D_{1H}D) = 0 \quad (9)$$

$$\Gamma(^3D_1 \to D_{1L}D) = 0 \quad (10)$$

$$\Gamma(^1\Pi P_1(\text{hybrid})] \to D_1(^1P_1)D) = 0 \quad (11)$$

The first pair of zeroes arise from the affinity of light and heavy D_{1L}, D_{1H} for S and D couplings respectively, and the zero in eq.(9) was noted by ref. [44]. For the hybrid decay the result follows from the conclusion of lattice QCD that decays are driven by $q\bar{q}$ creation in spin-triplet, which implies that a pair of spin-singlets (such as D and $^1P_1$) cannot be produced from a spin-singlet, such as a hybrid vector $c\bar{c}$. In practice these predictions will be affected by mixing, which can be determined from other processes (e.g. see [45]), and by phase space. The relative rates are insensitive to form factor effects at low momenta (see for example refs [45–47]).

Hence, if the axial mixing angles are known from elsewhere, the pattern of charm pair production can identify the nature of the decaying ψ state. Determining whether the $c\bar{c}$ content of these states is $S = 0$ (as for a hybrid) or $S = 1$ then follows from the relative production rates of various combinations of charmed mesons, in particular of their DD_1 branching ratios.

Given that gluonic (hybrid) states are so confidently predicted to occur in the region of ~ 1.5 GeV above the lowest vector meson, I would conclude that such states would naturally be attracted towards these S-wave thresholds, given their affinity for coupling to these very modes [27–29]. The search for hybrids and arguments over interpretation would have analogues with the competing dynamics in the scalar mesons, $f_0/a_0(980)$, which are associated with the S-wave $K\bar{K}$ threshold, and the $D_s(2317)$ and $D_s(2460)$ which appear at the DK and D^*K thresholds. In all of these cases the consensus appears to be that there is a short range QCD "seed" (be it tetraquarks in the case of the scalars or $c\bar{s}$ for the D_s states) which becomes modified by the coupling to S-wave meson pairs [48]. I suspect that the vector meson signals that I have discussed here are analogously caused by the hybrid seed coupling with the S-wave mesons near to threshold. However, if it should turn out that they are not driven by hybrids, then the question of where hybrids are, and how ever they are to be isolated, will demand serious attention.

6 Acknowledgements

I am indebted to the organisers for inviting me to give this talk, and to Chris Thomas and Qiang Zhao for discussions. This work is supported, in part, by grants from the UK Science and Technology Facilities Council (STFC), and the EU-RTN programme contract No. MRTN-CT-2006-035 482: "Flavianet".

References

1. F E Close, arXiv0706.2709 hep-ph; Proceedings of Flavor Physics and CP Violation Conference, Bled, Slovenia; fpcp07-241
2. CDF Collaboration, "Measurement of the dipion mass spectrum in $X(3872) \to J/\psi\pi^+\pi^-$) decays"; http://www-cdf.fnal.gov/physics/new/bottom/050324.blessed.X/.
3. F.E. Close, and P.R. Page, Phys. Lett. B **578**, 119 (2003).
4. E. Swanson, Phys. Lett. B **588**, 189 (2004)
5. Belle Collaboration, K. Abe *et al.*, hep-ex/0507019.
6. F E Close and P R Page, Phys. Letters B **578** (2004) 119
7. D. Gamermann, E. Oset, D. Strottman, M.J. Vicente Vacas, hep-ph 0612179; D. Gamermann, E. Oset, arXiv:0704.2314
8. N Tornqvist hep-ph/0308277; Phys Rev lett **67** (1992) 556; Z Phys **C61** (1994) 526
9. F E Close, C E Thomas and Q.Zhao, (unpublished)
10. D Bugg, arXiv:0709.1254
11. C Thomas, private communication
12. BaBar Collaboration, B. Aubert *et al.*, hep-ex/0506081.
13. F E Close and P R Page, Phys. Lett. B **628** (2005) 215
14. E. Kou, and O. Pene, Phys Lett **B631** (2005) 164 [arXiv:hep-ph/0507119].

15. L. Maiani, F. Piccinini, A.D. Polosa, and V. Riquer, Phys.Rev. **D72** (2005) 031502 [arXiv: hep-ph/0507062].

16. T. Barnes, F.E. Close, and E.S. Swanson, Phys. Rev. D **52**, 5242 (1995).

17. P. Lacock, C. Michael, P. Boyle, and P. Rowland, Phys. Lett. B **401**, 308 (1997).

18. J. Merlin, and J. Paton, Phys. Rev. D **35**, 1668 (1987).

19. T. Barnes and F.E. Close, Phys. Lett. B **116**, 365 (1982); M. Chanowitz and S. Sharpe, Nucl. Phys. B **222**, 211 (1983); T. Barnes, F.E. Close and F. de Viron, Nucl. Phys. B. **224**, 241 (1983).

20. P.R. Page, D.Phil. thesis, Univ. of Oxford, unpublished (1995).

21. I.T. Drummond *et al.*, Phys. Lett. B **478**, 151 (2000); T. Manke *et al.*, Nucl. Phys. Proc. Suppl. **86**, 397 (2000).

22. J.J. Juge, J. Kuti, and C.J. Morningstar, Nucl. Phys. Proc. Suppl. **83**, 304 (2000); T. Manke *et al.*, Phys. Rev. D **57**, 3829 (1998).

23. O. Lakhina and E. Swanson, arXiv:hep-ph/0608011

24. F.E. Close, I. Dunietz, P.R. Page, S. Veseli, and H. Yamamoto, Phys. Rev. D **57**, 5653 (1998).

25. F.E. Close, and S. Godfrey, Phys. Lett. B **574**, 210 (2003).

26. T Barnes and E Swanson, arXiv:0711.2080

27. F.E. Close, and P.R. Page, Nucl. Phys. B **443**, 233 (1995).

28. N. Isgur, R. Kokoski and J. Paton, Phys. Rev. Lett. **54**, 869 (1985).

29. N. Isgur and J. Paton, Phys. Rev. D **31**, 2910 (1985).

30. P.R. Page, Phys. Lett. B **402**, 183 (1997)
T.Burns, D Phil thesis, Oxford University (2007)

31. F.E. Close, Conference summary talk at Hadron03, hep-ph/0311087.

32. S. Ono *et al.*, Z. Phys. C **26**, 307 (1984); Phys. Rev. D **34**, 186 (1986).

33. BELLE Collaboration, K. Abe *et al.*, Phys. Rev. D **69**, 112002 (2004).

34. P.R. Page, E.S. Swanson, and A.P. Szczepaniak, Phys. Rev. D **59**, 034016 (1999).

35. F. E. Close and E. S. Swanson, Phys. Rev. D **72**, 094004 (2005) [arXiv:hep-ph/];

36. M.S. Dubrovin "D Hadronic Analyses at CLEO" arXiv:0705.3476

37. L Maiani, private communication.

38. B Aubert et al,(BaBaR Collaboration) Phys Rev **D71** 052001 (2005)

39. B Aubert et al,(BaBaR Collaboration) Phys Rev **D74** 091103 (2006)[arXiv: hep-ex/0610018]

40. J R Rosner, Moriond QCD 2007: Theory Summary. e-Print: arXiv:0704.2774 [hep-ph]

41. George W.S. Hou, private communication and talk at Hadron07

42. T Burns, hep-ph/0611132

43. T Burns, F E Close and C Thomas, arXiv:0709.1816

44. T Barnes, S Godfrey and E Swanson, arXiv:hep-ph/0505002, Phys. Rev. D72, 054026 (2005)

45. F E Close and E S Swanson, arXiv:hep-ph/0505206; Phys. Rev. **D72** 094004 (2005)

46. A Le Yaouanc, L Oliver, O Pene and J Raynal, Phys. Rev. D8 2223 (1973); G Busetto and L Oliver, Z. Phys. C20 247 (1983); R Kokoski and N Isgur, Phys. Rev. D35 907 (1987); P Geiger and E Swanson, Phys. Rev. D50 6855 (1994); H G Blundell and S Godfrey, Phys. Rev. D53 3700 (1996)

47. T Barnes, F E Close, P R Page and E Swanson, Phys. Rev. D55 4157 (1997)

48. F E Close and N Tornqvist, J Phys G 28 R249 (2001)

Frascati Physics Series Vol. XLVI (2007), pp. 369
HADRON07: XII Int. Conf. on Hadron Spectroscopy – Frascati, October 8-13, 2007
Plenary Session

PROSPECTS FOR HADRON PHYSICS AT JPARC

N. Saito
(KEK)

Written contribution not received

Frascati Physics Series Vol. XLVI (2007), pp. 371–382
HADRON07: XII Int. Conf. on Hadron Spectroscopy – Frascati, October 8-13, 2007
Plenary Session

STATUS OF BESIII EXPERIMENT

Weiguo Li, representing BESIII Collaboration
Institute of High Energy Physics, 19 Yuquan Road, Beijing 100049, China

Abstract

The current status and progress of BESIII is described. The constructions of various detector components are nearly finished with good quality and within the schedule. The status of BEPCII machine is also briefly mentioned. The detector is planned to move into the beam line next April, and the machine should reach a luminosity of $3 \times 10^{32}\ cm^{-2}s^{-1}$ at the end of 2008. Some test runs and physics data taking are foreseen in 2008.

1 Introduction

The BESIII detector [1)] is designed for the e^+e^- collider running at the tau-charm energy region, called BEPCII, which is currently under construction at IHEP, Beijing, P.R. China. The accelerator has two storage rings with a circumference of 224 m, one for electron and one for positron, each with 93

Table 1: *$\tau-$Charm productions at BEPC-II in one year's running($10^7 s$).*

Data Sample	Central-of-Mass energy (MeV)	Luminosity ($10^{33}\mathrm{cm}^{-2}\mathrm{s}^{-1}$)	#Events per year
J/ψ	3097	0.6	10×10^9
$\tau^+\tau^-$	3670	1.0	12×10^6
$\psi(2S)$	3686	1.0	3.0×10^9
$D^0\overline{D}^0$	3770	1.0	18×10^6
D^+D^-	3770	1.0	14×10^6
$D_S^+D_S^-$	4030	0.6	1.0×10^6
$D_S^+D_S^-$	4170	0.6	2.0×10^6

bunches spaced by 8 ns [2]. The total current of each beam is 0.93 A, and the crossing angle of two beams is designed to be 22 mrad. The machine is designed to work with a c.m. energy from 2.0 to 4.2 GeV, and 4.6 GeV should be possible. The peak luminosity is expected to be 10^{33} $\mathrm{cm}^{-2}\mathrm{s}^{-1}$ at the beam energy of 1.89 GeV, the bunch length is estimated to be 1.5 cm and the energy spread will be 5.16×10^{-4}. Right now, the LINAC has been installed and successfully tested, all the design specifications are satisfied. The storage rings have been installed, two synchrotron radiation runs provided beams for the users last year, with a maximum current reach of 200 mA at 2.5 GeV, the beam life time reached 6.5 hours. Collisions were realized with 100 mA by 100 mA beams with normal quadruple magnets. Now the super-conducting quadruple magnets were repaired and magnetic fields were successfully measured with the detector super-conducting magnet. The machine is scheduled to re-commissioning in Oct. of 2007.

The physics program of the BESIII experiment includes light hadron spectroscopy, charmonium physics, electro-weak physics from charm mesons, QCD and hadron physics, tau physics and search for new physics etc. Due to its huge luminosity and small energy spread, the expected event rate per year is huge, as listed in table 1. In order to achieve its physics goal and fully utilize the potential of the accelerator, the BESIII detector [1], as shown in Fig. 1, is designed from inside out to consist of a drift chamber with a small cell structure filled with a helium-based gas; time-of flight counters for particle identification made of plastic scintillators; an electromagnetic calorimeter made of CsI(Tl) crystals; a super-conducting magnet providing a field of 1.0 tesla; and a muon

system made of Resistive Plate Chambers(RPC). In the following, all the sub-detectors will be described together with results of their performance tests, as well as their current status.

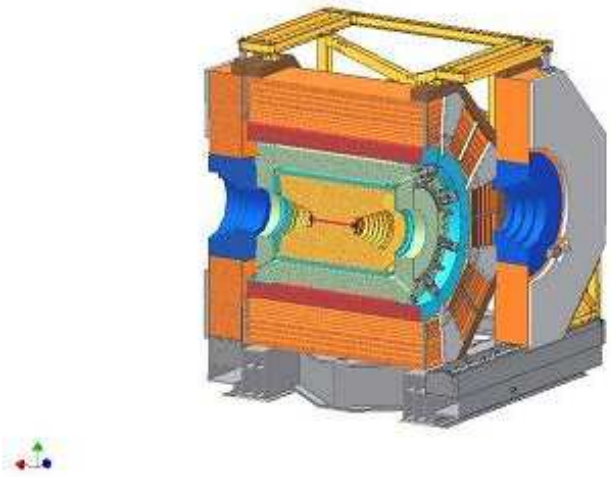

Figure 1: *Schematics of the BESIII detector.*

2 Drift Chamber

The drift chamber has a cylindrical shape with two chambers jointed at the end flange, without a wall between. To make the room for super-conducting quadruples, Cone-shaped endplates are formed by a total of 6 stepped flanges made of 18 mm Al plates. The inner radius of the chamber is 63 mm and the outer radius is 810 mm, the length of the chamber at the outer radius is 2400 mm. Both the inner and outer cylinder of the chamber are made of carbon fiber with a thickness of 1 mm and 10 mm respectively. The geometrical acceptance of the chamber is $cos\theta$ of 0.93. A total of about 7000 gold-plated tungsten wires(3% Rhenium) with a diameter of 25 μm are arranged in 43 layers, together with a total of about 22000 gold-plated Al wires for field shaping. The small drift cell structure of the inner chamber has a dimension of 6×6 mm^2 and the outer chamber of 8×8 mm^2. The working gas is a mixture of 60% helium and 40% propane. The designed single wire spatial resolution and dE/dx resolution

are 130 μm and 6%, respectively.

Figure 2: The mechanical structure during the assembly.

The mechanical structure of the drift chamber, including the ultra-high precision (25 μm) drilling of a total of about 30000 holes, and the high precision (50 μm) assembly of 6 cylinders have been completed successfully. Fig. 2 shows the mechanical structure during the assembly. The mass production of the feed-through are completed and carefully tested one by one. A total of about 30000 wiring are completed with a very high quality, the wire tension and the leakage current are well controlled. The chamber was tested for gas leakage, and the leakage is quite small, about 0.03 liters per minute.

Several prototypes of the chamber have been tested at the beam in KEK and IHEP [3, 4]. Good results have been obtained in all the cases. Using a high momentum pion beam, the chamber showed a space resolution of 114 μm and a dE/dx resolution of 4.9%. A prototype of readout electronics with 512 channels including the data acquisition system has been also tested in the laboratory for its long-term stability. The mass production of all electronics boards is finished, and tested. All the front-end electronics were mounted on the chamber. The chamber was tested with partially powered electronics using cosmic rays, the wire space resolution from position differences in a super-layer is about 120 μm, as shown in Fig. 3. The trigger system was tested together with MDC, some sparking problems were found and solved. The test showed that both MDC and the trigger track finding system work well.

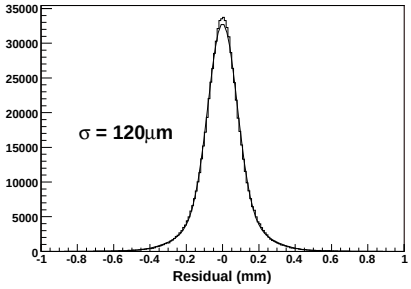

Figure 3: the averaged single wire resolution from cosmic ray data.

3 CsI(Tl) Crystal Calorimeter

The CsI(Tl) crystal electromagnetic calorimeter consists of 6240 crystals, 5280 in the barrel, and 960 in two endcaps. Each crystal is 28 cm long, with a front face of about 5.2×5.2 cm^2, and a rear face of about 6.4×6.4 cm^2. All crystals are tiled by 1.5^o in the azimuthal angle and 1-3 ^{o} in the polar angle, respectively, and point to a position off from the interaction point by a few centimeters as shown in Fig. 4. They are hanged from the back by 4 screws without partition walls between crystals in order to reduce dead materials. The designed energy and position resolution are 2.5% and 6 mm at 1 GeV, respectively. Right now all the barrel crystals have arrived, been tested, and assembled to crystal modules. The light yield of arrived crystals is about 56% with respect to the reference crystal, as shown in left plot of Fig.5, much more than the initial specification of more than 35%. The average uniformity is better than 5%, as shown in the right plot of Fig. 5, while the initial specification is less than 7%. The crystals were tested to be radiation hard, by putting small sample crystal produced at the same time with the real crystals in the radiation hard environment. All the photodiodes (PD) have been delivered, and their performances before and after the accelerated aging, such as dark current, noise, photon-electron conversion efficiency and capacitance etc., have been tested. All delivered crystals have been assembled and tested using cosmic rays. The mechanical structure of the barrel is completed.

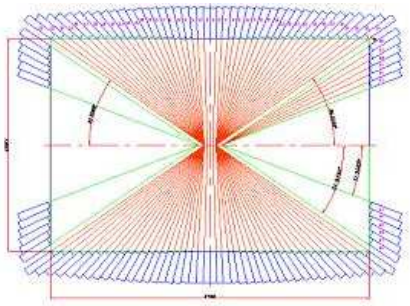

Figure 4: Schematic view of the CsI(Tl) crystal calorimeter.

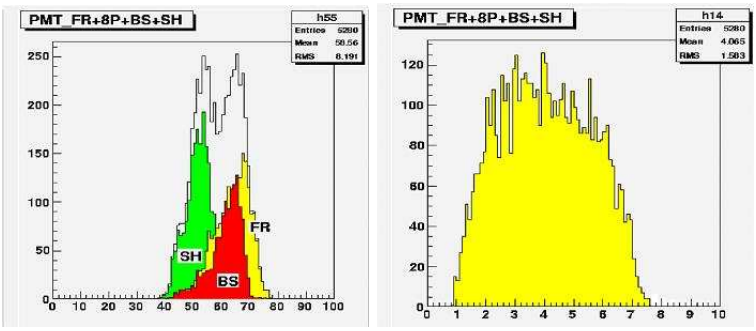

Figure 5: Left plot: The light yield of crystals; Right plot: The uniformity of crystals. This is for all barrel crystals, SH from Shanghai, BS from Beijing, FR from France companies.

The readout electronics of crystals, including the preamplifier, the main amplifier and charge measurement modules are tested at the IHEP E3 beam line together with a crystal array and photodiodes. Results from the beam test show that the energy resolution of the crystal array reached the design goal of 2.5% at 1 GeV and the equivalent noise achieved the level of less than 1000 electrons, corresponding to an energy of 220 keV. A prototype with 384 channels has been tested for long term stability. The mass production of preamplifiers

and other modules are finished and tested. Now the barrel calorimeter is fully assembled, tested and inserted into the detector, as shown in Fig. 6. The barrel calorimeter will be tested again when all the cables are connected. The endcap crystal calorimeters are being assembled.

Figure 6: *Barrel EMC inserted into the detector.*

4 Time-Of-Flight system

The particle identification at BESIII is based on the momentum and dE/dx measurements by the drift chamber, and the Time-of-Flight(TOF) measurement by plastic scintillators. The barrel scintillator bar is 2.4 m long, 5 cm thick and 6 cm wide. A total of 176 such scintillator bars constitute two layers, 88 counters each, to have a good efficiency and time resolution. For each side of the endcap, a total of 48 fan-shaped scintillators form a single layer. A 2 inch fine mesh phototube R5924 from Hamamashu is directly attached to each side of barrel counters and to the inner side of endcap counters to collect the light. The intrinsic time resolution is designed to be better than 90 ps. Such a time resolution, together with contributions from the beam size, electronics and the clock, momentum uncertainty, etc, the total time resolution for barrel (two layers) and endcap TOF should be around 100 ps and 110 ps respectively. This performance can distinguish charged π from K mesons for a momentum up to 0.9 GeV at the 2σ level.

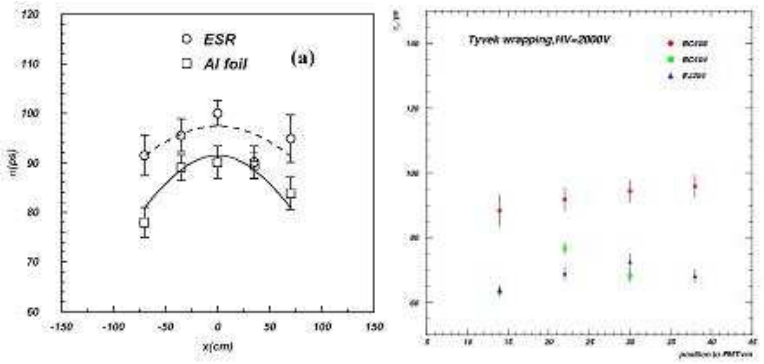

Figure 7: Left plot:Time resolution of the barrel TOF module from a beam test. Right plot: Time resolution of the endcap TOF module from a beam test.

Beam tests of TOF prototypes have been performed at IHEP E3 beam line using pions, electrons and protons [5, 6]. Different scintillator types such as BC404, BC408 and EJ200, with different thickness are tested, together with different wrapping materials. The results, as shown in Fig. 7, show that the time resolution using a prototype of readout electronics including actual cables are better than 90 ps and 75 ps for the barrel and the endcap, respectively. Right now, all the scintillator counters have been delivered, the phototubes are tested inside the magnetic field and attached to the HV distribution circuit. The mass production of preamplifiers and other readout modules are finished and tested. All the barrel counters are assembled and are ready to be mounted on the MDC. The endcap counters are mostly finished. A laser system will be used to monitor the TOF counters.

5 Muon counter

The BESIII muon chamber is made of Resistive Plate Chambers(RPC) interleaved in the magnet yoke. There are a total of 9 layers in the barrel and 8 layers in the endcap, with a total area of about 2000 m^2. The readout strip is 4 cm wide, alternated between layers in x and y directions. The RPC is made of bakelite with a special surface treatment without linseed oil [7]. Such a simple

technique for the RPC production shows a good quality and stability at a low cost. All RPCs have been manufactured, tested, assembled and installed with satisfaction. In the mass production, after one week training, most of chambers has a noise rate of about 0.1 Hz/cm^2, which will be reduced to typically 0.04 Hz/cm^2 after one month training. Fig. 8 shows the measured efficiency of installed RPCs, which is more than 95% in all the region, using cosmic-rays.

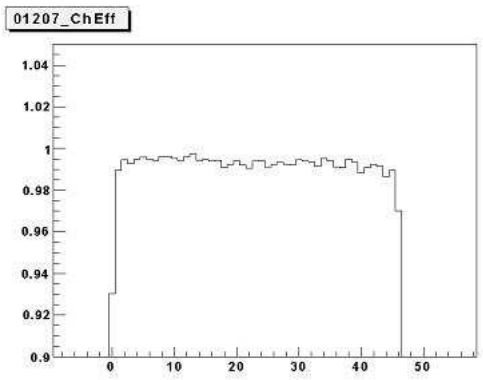

Figure 8: Measured efficiency of a RPC after installation using cosmic rays.

6 Superconducting magnet

The BESIII super-conducting magnet has a radius of 1.48 m and a length of 3.52 m. It uses the Al stabilized NbTi/Cu conductor with a total of 920 turns, making a 1.0 T magnetic field at a current of 3400 A. The total cold mass is 3.6 tons with a material thickness of about 1.92 X_0. In collaboration with WANG NMR of California, the magnet is designed and manufactured at IHEP. The left plot in Fig. 9 shows the coil winding at IHEP by technicians. The magnet was successfully installed into the iron yoke of the BESIII, as shown in the right plot of Fig. 9, together with the valve box. The magnet has been successfully cool down to the super-conducting temperature with a heat load within the specification. A stable magnetic field of 1.0 T at a current of 3368 A was achieved. The dump resistor and dump diode, switches of the quench protection devices are installed and tested successfully. The field

mapping together with super-conducting quadruple magnets has been carried out successfully in Aug. of 2007.

Figure 9: Left plot: Coil winding at IHEP. Right plot: the magnet during the installation.

7 Trigger and DAQ System

The BESIII trigger rate is estimated to be about 4000 Hz and the trigger system is designed largely based on the latest technology such as fiber optics, pipelines and FPGA chips. Information from sub-detector electronics is fed into sub-detector trigger system via fiber optical cables in order to avoid grounding loops. The VME based main trigger and all the sub-trigger boards communicate with each other via copper cables. All trigger logics stored in FPGA chips are programmable and can be downloaded via VME bus. The trigger latency is designed to be 6.4 μs and the pipeline technique is used for all the readout electronics. The radiation hardness of fiber cables and their connectors are tested at BEPC beam test facility. Some of the sub-trigger systems share the same hardware design of the board using different firmware in order to reduce number of board types and save the cost. Latest large FPGA chips with RocketIO technology are adopted in such a board design. All the modules have been designed, prototyped, tested and most have completed the mass production. The trigger system, mainly the tracking hardware was tested with MDC with partially powered electronics, and proved to work as expected. The trigger system will be tested with calorimeter and TOF as they are installed

and the cables connected to the readout electronic modules.

The total data volume at BESIII is about 50 Mbytes/s for a trigger rate of about 4000 Hz. The DAQ system shall read out the event fragments from the front-end electronics distributed over more than 40 VME crates, and build them into a complete event to be transmitted for recording onto the persistent media. The DAQ software, based on the ATLAS TDAQ, includes database configuration, data readout, event building and filtering, run control, monitoring, status reporting and data storage, etc. Every component has been tested successfully at an average event rate of 8000 Hz and 4500 Hz with an event size of 12 kB and 25 kB, respectively. The software has been used for cosmic rays and beam test for a Drift Chamber prototype and an EMC crystal array. Different working modes such as normal data taking, baseline, calibration, debugging of the readout electronics and waveform sampling have been tested. As a distributed system, the entire DAQ system must keep synchronized, so a state machine is implemented in the PowerPC readout subsystem to keep the absolute synchronization with the DAQ software, which guarantees the coherency of the whole system. And lately the data taking system was tested with MDC with partially powered electronics, and the system worked well and the online event display and event analysis software demonstrated to work adequately.

8 Offline computing and software

The BESIII offline computing system is designed to have a PC farm of about 2000 nodes for both data and Monte Carlo production, as well as data analysis. A computing center at IHEP and several local centers at collaborating universities are anticipated. A 1/10 system has been built at IHEP and the full system will be built soon.

The offline software consists of a framework based on Gaudi, a Monte Carlo simulation package based on GEANT4, an event reconstruction package, a calibration and a database package using MySQL. Currently all codes are working as a complete system, and tests against cosmic-ray and beam test data are underway. Analysis tools such as particle identification, secondary vertex finding, kinematic fitting, event generator and partial wave analysis are completed for several package release. The package was tested by another group to see its performance and to 1st degree the offline package works. But a lot of work are still needed for detailed tuning of the code for different conditions

and complicated events topology. Especially when the real data are available, major efforts are required to calibrate the detector, tune the reconstruction code, and to understand the detector performances.

A group of physicists, including the theorists and experimenters, have worked for last two years, to prepare the physics yellow book for guiding the physics analyses when the real data come. Many physics channels are simulated and analyzed. The book is nearly ready to become public.

9 Summary

The BEPCII and BESIII construction went on smoothly. For BESIII, most of the components are constructed, assembled and mounted. The quality and performances tested are matched to the designed specifications. The detector should be moved into the beam line in the April of 2008, and to be commissioned together with the BEPCII. It is expected that some test runs and then physics data will be taken, the detector will be fully debugged and calibrated. It will be exciting to see that the machine and detector work well and some physics results will be produced soon.

Acknowledgments

The author thanks all the BEPCII staff for their excellent work towards the construction of the accelerator, and all the BESIII staff for completing the detector R&D and construction on time and in good quality.

References

1. BESIII design report, http://bes.ihep.ac.cn.
2. BEPCII design report(in Chinese).
3. J. B. Liu, *et al.*, Nucl. Instrum. And Meth. **A 557** 436(2006).
4. Z. H. Qing *et al.*, Nucl. Instrum. And Meth. **A 571** 612(2007).
5. C. Wu, *et al.*, Nucl. Instrum. And Meth. **A 555** 142(2005).
6. S. H. An *et al.*, Meas. Sci. Technol. **17** 2650(2006).
7. J. W. Zhang, *et al.*, Nucl. Instrum. Meth. **A580** 1250(2007).

Frascati Physics Series Vol. XLVI (2007), pp. 383
HADRON07: XII Int. Conf. on Hadron Spectroscopy – Frascati, October 8-13, 2007
Plenary Session

PLANS FOR A SUPER B-FACTORY

F. Forti
INFN Pisa

Written contribution not received

Frascati Physics Series Vol. XLVI (2007), pp. 385–396
HADRON07: XII Int. Conf. on Hadron Spectroscopy – Frascati, October 8-13, 2007
Plenary Session

PROSPECTS FOR HADRON SPECTROSCOPY AT THE CMS EXPERIMENT

Roberto Covarelli
Universitá degli Studi-INFN di Perugia

Abstract

The CMS detector at the LHC will be able to detect hadron production at an unprecedented center-of-mass energy of 14 TeV. We present dedicated simulation studies for the measurement of the B_c^+-meson mass and lifetime using the exclusive decay channel $B_c^+ \to J/\psi\pi^+$. Moreover, quarkonium reconstruction capabilities in CMS are presented in terms of efficiency and expected resolution both in proton-proton collisions (J/ψ reconstructed from the $B_s^0 \to J/\psi\phi$ decay channel) and in heavy ion collisions.

1 The CMS detector

CMS [1)] is a multi-purpose solenoidal detector designed for 7 TeV-7 TeV proton beam collisions at the Large Hadron Collider (LHC).

Its innermost detector is a large silicon tracking device: the inner part consists of 3 (2) layers of silicon pixels in the barrel (endcap) region, while

the outer part is equipped with 10 (12) layers of micro-strip silicon detectors, providing a very good tracking efficiency and transverse momentum resolution up to high values of the pseudo-rapidity.

For a precise determination of electron and photon energies, an electromagnetic calorimeter, consisting of over 80,000 lead-tungstate ($PbWO_4$) crystals, equipped with avalanche photodiodes or vacuum phototriodes, covers both barrel and endcap regions. Energy and direction of jets and of missing transverse energy flow in events are measured by means of hadronic sampling calorimeters with 50-mm-thick copper absorber plates interleaved with 4-mm-thick scintillator sheets.

The calorimeters are surrounded by a superconducting coil that provides a solenoidal magnetic field of 4 T.

The return yoke of the magnet is made of iron and equipped with chambers used to detect muons. Drift Tubes and Resistive Plate Chambers are used in the barrel region, while Cathode Strip Chambers and Resistive Plate Chambers cover the two endcap regions, giving a very good efficiency for muon detection and a solid-angle acceptance close to 4π.

The trigger of the experiment [2] is divided in two levels: the Level 1 (L1) is a hardware-based trigger, using only information from muon chambers and calorimeters. Transverse momentum thresholds are expected to be as low as 6 GeV/c for single muons, while they can reach 3 GeV/c for dimuons in a low-luminosity scenario. The other trigger level, the High Level Trigger (HLT) uses information from the whole event: at this stage partial track reconstruction and vertexing from the tracking systems, as well as invariant mass of simple composite candidates, can be exploited to define a number of highly efficient trigger streams. Most analyses discussed in this paper are based on the opposite-sign dimuon HLT stream.

2 The LHC Data-Taking Plans

The LHC will start delivering beams in 2008 and will be operated in different conditions:

- for most of the data-taking time, proton-proton beams will be circulated and collided at a center-of-mass energy of 14 TeV. After the start-up, two luminosity scenarios can be foreseen according to the machine design:

the low-luminosity scenario, as assumed in CMS analyses, is based on a luminosity value of $\mathcal{L}_{\rm low} = 2 \times 10^{33}$ cm^{-2}s^{-1}, while, after some years of operation, this value is expected to reach $\mathcal{L}_{\rm high} = 10^{34}$ cm^{-2}s^{-1} (high-luminosity scenario).

- for about one twelfth of the running time, heavy ion beams will replace the proton beams. Most of these will be ^{208}Pb-^{208}Pb collisions at a center-of-mass energy of 5.5 TeV. The expected luminosity is $\mathcal{L}_{\rm ions} = 4 \times 10^{26}$ cm^{-2}s^{-1}, posing a significant challenge to CMS, due to the extreme occupancy of the inner detectors in these conditions.

3 Heavy Flavor Physics at CMS

The CMS physics program is mostly devoted to searches related to Higgs and new physics particles [3]. Heavy flavor physics is also a field where many interesting measurements can be carried out, both in terms of hadron production and decays, especially in the low-luminosity scenario. Heavy flavor processes are also interesting because they can constrain indirectly transitions that involve scales much higher then m_b, through loop propagation of new particles.

Dedicated experiments for heavy flavor and heavy ion physics are being designed for LHC. These experiments will take some advantage over CMS, having large acceptance, excellent hadron identification possibilities and lower $p_\perp$ muon triggers. On the other hand, CMS will have a very good muon resolution and acceptance, due to the muon chamber coverage, the high magnetic field and the full-silicon tracker. These characteristics can allow CMS to perform heavy flavor analyses also in a high-luminosity scenario.

4 J/ψ Reconstruction Studies

Charmonium is mainly detected in the $J/\psi \to \mu^+\mu^-$ decay channel [4]. The large production cross section predicted at LHC for both prompt J/ψ and J/ψ from b-hadron decays will allow for an accurate understanding of muon reconstruction performances.

The study has been performed using a large sample of J/ψ ($\sim$200 000) from Monte Carlo simulation of events where the $B_s^0 \to J/\psi\phi$, decay is forced, with the J/ψ decaying into muons. The reconstruction efficiency has been determined both for single muons and for J/ψ candidates and has been studied

as a function of $p_\perp$, $|\eta|$ and $\Delta\Omega_{\mu\mu}$, i.e. the 3-dimensional angular separation of the muon pair. The efficiency has been calculated at different analysis levels: applying geometric acceptance cuts only, after J/ψ candidate reconstruction, after L1 decisions and HLT decisions, as defined in Sec. 1.

From this study we conclude that:

- The offline reconstruction efficiency for $J/\psi \to \mu^+\mu^-$ is about 10.1% averaging on all values of $p_\perp(J/\psi)$, while is in the range 50-70% for $p_\perp(J/\psi) > 20$ GeV/c. The mass resolution is 34 MeV/c^2.

- The efficiency is slightly reduced for small and large angles of $\Delta\Omega_{\mu\mu}$. Small values of $\Delta\Omega_{\mu\mu}$ happen mainly in the endcap region, close to the acceptance cut, and the efficiency loss is mainly caused by track overlap, while large values of $\Delta\Omega_{\mu\mu}$ are correlated with low-$p_\perp$ muons.

- The L1 trigger retains almost all events with large $p_\perp(J/\psi)$. A specific HLT trigger path for the J/ψ decay has been defined, removing the tracker isolation requirement on the muon tracks. Figure 1 shows the L1 and HLT efficiencies vs. $p_\perp(J/\psi)$ with different possible choices for the $p_\perp(\mu)$ threshold in the last trigger stage.

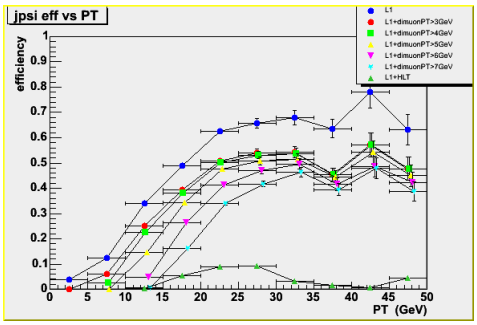

Figure 1: *Total HLT efficiency for J/ψ reconstruction as a function of the J/ψ reconstructed transverse momentum in the lab frame. The blue circles represent the efficiency after L1, the green triangles is after the default HLT requirements (isolation included). Other markers stand for the corrected HLT requirements at different values of the $p_\perp$ threshold.*

5 Study Of The Decay $B_c^+ \to J/\psi\pi^+$

The study of the $B_c^+ \equiv \bar{b}c$ meson[1] is important to test theoretical predictions of potential models, because this is the only known meson composed of two distinct heavy quarks [5]. As such, it decays only weakly, having thus a long lifetime. The theoretical expectations for the B_c^+ mass and lifetime are $m(B_c^+) = (6.24 \pm 0.05)$ GeV/c^2 and $\tau(B_c^+) = (0.54 \pm 0.15)$ ps [6].

These quantities have been measured by the CDF collaboration [7] to be:

$$m(B_c^+) = [6.2741 \pm 0.0032(\text{stat.}) \pm 0.0026(\text{syst.})] \text{ GeV}/c^2 \quad (1)$$

using the $B_c^+ \to J/\psi\pi^+$ channel, and:

$$\tau(B_c^+) = [0.462^{+0.073}_{-0.065}(\text{stat.}) \pm 0.036(\text{syst.})] \text{ ps} \quad (2)$$

using the $B_c^+ \to J/\psi\mu^+\nu_\mu$ channel.

The production rate at LHC is 16 times larger than at the Tevatron, so experiments at LHC could potentially collect many more B_c^+ mesons. In CMS the only decay mode studied so far is $B_c^+ \to J/\psi\pi^+$.

The signal event generation is performed using a dedicated generator for B_c^+ physics (BCVEGPY), while comparison with PYTHIA is used to estimate systematics from the theoretical B_c^+ production model. The backgrounds considered are: J/ψ production from other b-hadron decays (B^0, B^+, B_s^0 and Λ_b), prompt J/ψ production, both in color singlet and octet states, semileptonic decays $b\bar{b}$, $c\bar{c} \to \mu^+\mu^- X$, as well as W, Z plus jets and generic QCD events. Trigger requirements are applied at generator level to achieve an affordable event generation time.

A cut-based selection is then applied:

- A kinematically-constrained vertex fit to the muon pair is required to converge.
- The muon pair invariant mass must lie between 3.0 and 3.2 GeV/c^2.
- The dimuon mass is then constrained to the nominal J/ψ mass and a charged track (π) is added to make the B_c^+ candidate. We require $p_\perp(\pi) > 2.4$ GeV/c, $|\eta(\pi)| < 2.2$ and that it must pass a muon-ID veto.

[1] Charge conjugation is always implied.

- The proper decay length in the transverse plane must be greater than 60 μm, while the corresponding decay length in the CMS frame must have a significance of 2.5 at least.
- Finally, the cosine of the pointing angle, i.e. the angle between the B_c^+ momentum direction and the line connecting the primary and secondary vertices, must be greater than 0.8.

With this selection, we obtain a very good signal-to-background ratio in a mass window of 200 MeV/c^2 around the generated B_c^+ mass (6.4 GeV/c^2). The number of selected signal and background events is respectively 120 ± 11 and 2.6 ± 0.4 in a Monte Carlo equivalent integrated luminosity of 1 fb^{-1}.

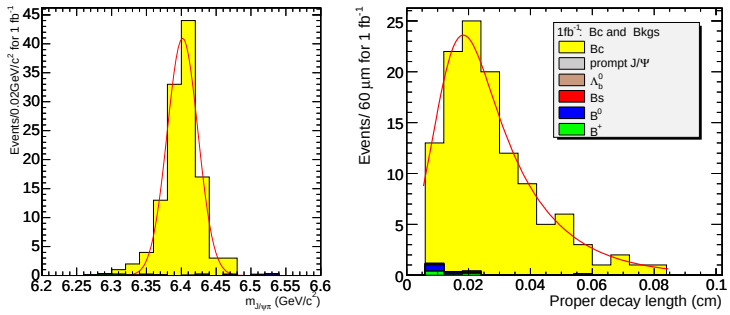

Figure 2: *Left: Gaussian fit to the $J/\psi\pi^+$ invariant mass distributions. Right: Fit to the B_c^+ proper decay time distribution with an exponential convolved to a resolution function. Various background components are superimposed to the total distributions.*

Fits to the mass and lifetime distributions are shown in Figure 2. The results of the fits are:

$$m(B_c^+) = [6.402 \pm 0.002(\text{stat.})]\ \text{GeV}/c^2 \quad \text{generated} = 6.400\ \text{GeV}/c^2 \quad (3)$$

$$c\tau(B_c^+) = [149 \pm 13(\text{stat.})]\ \mu\text{m} \quad \text{generated} = 150\ \mu\text{m}, \quad (4)$$

showing that no biases are induced by the selection procedure.

Preliminary systematic studies have been performed, considering as possible sources of uncertainty: the tracker and muon chamber misalignment,

the limited background Monte Carlo statistics, possible cut variations and the theoretical model assumed in B_c^+ production processes. The final expected uncertainties are:

$$[\pm 0.002(\text{stat.}) \pm 0.015(\text{syst.})] \text{ GeV}/c^2$$

on $m(B_c^+)$, and

$$[\pm 0.044(\text{stat.}) \pm 0.010(\text{syst.})] \text{ ps}$$

on $\tau(B_c^+)$.

The main systematic uncertainty on the mass is coming from a worst-case misalignment scenario. With real data, a a more realistic study of the systematic errors can be obtained. Also, control samples like $B^+ \to J/\psi K^+$ can be used to understand and keep under control misalignment effects.

6 Quarkonium Production In Heavy Ion Collisions

Heavy ion collisions are important because they allow matter to reach temperatures of the order of the critical temperature $T_c \sim 180$ MeV, where QCD predicts quark deconfinement and therefore the possible formation of quark-gluon plasma (QGP). Matsui and Satz [8] have shown that one of the experimental signatures of QGP formation is a suppression of quarkonia yields: QGP can, in fact, screen the color-binding potential, preventing heavy quarks from forming bound states.

Many experiments have been devoted to measuring this effect. NA38 first reported a smooth J/ψ suppression with respect to the Drell-Yan dimuon production, that could also be explained by nuclear absorption of charm quarks. The first evidence of departure from the nuclear absorption scheme was found by NA50 [9] and the measured suppression factor was 0.77 ± 0.04. RHIC experiments are now taking data with Pb-Pb collisions at a canter-of-mass energy of 200 GeV. Recent studies [10] have shown that J/ψ could survive at a temperature as high as $1.5T_c$, that could be out of range for RHIC: in this case, Υ production measurements also become interesting.

In CMS we determine ψ and Υ quarkonia yields in the dimuon decay channel, within the nominal Pb-Pb collision luminosity scenario [11]. Since quarkonia cross-sections are many orders of magnitudes smaller than the total inelastic Pb-Pb cross-section, full simulation of events would require a too large

amount of time and data to be performed. Events are therefore generated using a fast simulation technique, that includes theoretical production models and detector effects.

Signal consists of events containing J/ψ, ψ', Υ, Υ' or Υ'' states decaying to $\mu^+\mu^-$, and $\sigma_{prod} \cdot BR_{\mu^+\mu^-}$ is about 50 mb for the sum of the ψ states and 400 μb for the sum of the Υ states.

The backgrounds considered are:

- muons from decays in flight of soft hadrons (π/K) coming from the nucleus-nucleus collision. Two cases are considered, the first with a high charged particle multiplicity for central collisions ($dN^{\pm}/d\eta|_{\eta=0} = 5000$) and the second with a lower multiplicity ($dN^{\pm}/d\eta|_{\eta=0} = 2500$), based on the extrapolation of RHIC measurements to the LHC energies.

- muons from open c- and b-hadron pair production (estimated with the PYTHIA generator).

The detector effect simulation is done in steps. Trigger efficiencies are considered using muon trigger tables in $p_\perp$ and η bins. Muon and di-muon reconstruction efficiencies are also estimated vs. $p_\perp$ and η for the different background types. Resolutions found in invariant mass distributions (34 MeV/c^2 for J/ψ, 85 MeV/c^2 for Υ) are used as smearing factors in the fast simulation. The resulting quarkonia acceptance (1.3% for J/ψ, 23% for Υ) is taken into account.

The invariant mass distributions from fast simulation samples are shown in Figure 3 top, where the Monte Carlo has been rescaled to an equivalent luminosity of 0.5 nb^{-1} (one month data-taking). Figure 3 bottom shows how a better signal-to-background ratio can be attained by requiring both muons to be in the barrel detectors, but the significance is actually lower, so this cut is not applied. Background subtraction is done using bin-by-bin distributions of same sign dimuon combinations and using the estimate:

$$N_{signal} = N^{+-} - 2\sqrt{N^{++}N^{--}} \tag{5}$$

No evidence is found of a ψ' measurable yield. All other yields are summarized in Tables 1 and 2.

The main systematic uncertainty associated to the Monte Carlo result is from the limited background statistics of the fast-simulated sample that

Table 1: *$c\bar{c}$ quarkonia yields in the two multiplicity scenarios considered.*

	$N(J/\psi)$	S/B
$dN^{\pm}/d\eta\|_{\eta=0} = 2500$	180 000	1.2
$dN^{\pm}/d\eta\|_{\eta=0} = 5000$	150 000	0.6

Table 2: *$b\bar{b}$ quarkonia yields in the two multiplicity scenarios considered.*

	$N(\Upsilon)$	$N(\Upsilon')$	$N(\Upsilon'')$	S/B
$dN^{\pm}/d\eta\|_{\eta=0} = 2500$	25 000	7 300	4 400	0.12
$dN^{\pm}/d\eta\|_{\eta=0} = 5000$	20 000	5 900	3 500	0.07

enters the reweighting technique: this has currently a relative impact on the yield of $\sim 20\%$ for J/ψ and $\sim 25\%$ for Υ. Comparison between fast and full simulation gives results well within these uncertainties, so it does not contribute significantly.

Other systematic uncertainties come from the limitations in detector description, since the results are extremely sensitive to the dependence of the tracker efficiency on the multiplicity of the event. These effects can be determined by comparing reconstructed states using muon chambers only and tracker plus muon chambers, at each tracker occupancy level.

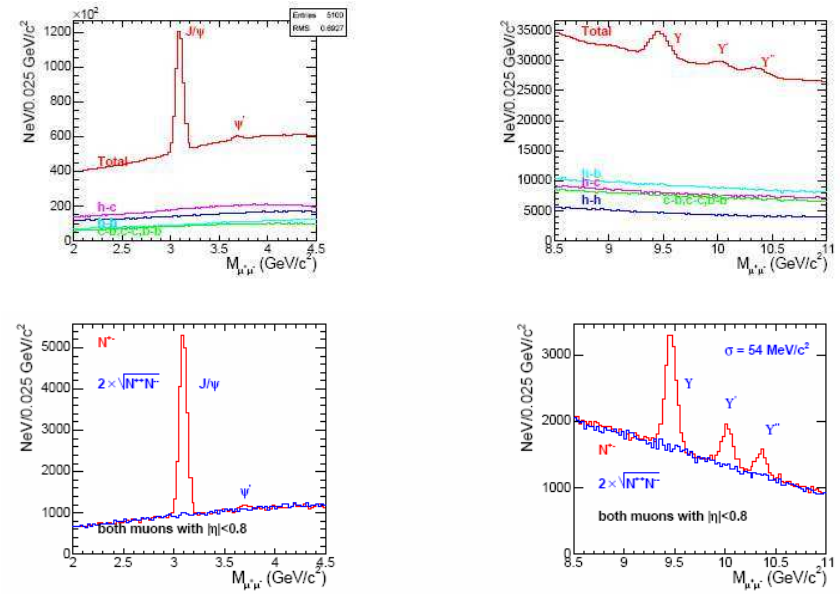

Figure 3: *Top: The invariant mass distributions from quarkonia simulated samples in the ψ (left) and Υ (right) mass regions for the low-multiplicity scenario ($dN^{\pm}/d\eta|_{\eta=0}$ = 2500). All considered backgrounds are added and detailed in the figures (c or b stand for c- or b-hadron decays, h is either a K or a π produced in the collision). Bottom: The same distributions with both muons in the CMS barrel region ($|\eta| < 0.8$, in red). Same-sign dimuon distributions are also superimposed (in blue) to show effectiveness of the background subtraction technique.*

7 Summary

We have shown the potentials of the CMS detector in hadron spectroscopy by focusing on three physics topics.

We first presented the measurement of reconstruction performances of the J/ψ resonance, which is the most abundant state associated to the dimuon

channel triggers. The efficiency of the HLT selection has been found to be up to 40-50% at high transverse momentum values ($p_\perp(J/\psi) > 20$ GeV/c).

An important test of potential models in the SM is provided by the measurement of the mass and lifetime of the B_c^+ meson. In the $B_c^+ \to J/\psi\pi^+$ decay mode and with 1 fb^{-1} integrated luminosity, CMS expects to obtain uncertainties of $[\pm 0.002(\text{stat.}) \pm 0.015(\text{syst.})]$ GeV/c^2 on $m(B_c^+)$ and of $[\pm 0.044(\text{stat.}) \pm 0.010(\text{syst.})]$ ps on $\tau(B_c^+)$. This precision is comparable to that obtained by CDF, provided a more realistic understanding is reached of the systematics from misalignment effects, that can be achieved using control samples from data, like $B^+ \to J/\psi K^+$.

We also presented the capabilities of detecting quarkonia in heavy ion collisions. Up to 180 000 J/ψ and 36 000 Υ mesons can be cleanly reconstructed in the first 0.5 nb^{-1} of data, using a background subtraction technique based on same-sign dimuons. This could allow one to measure suppressions in the quarkonia production that would represent a hint of QGP formation.

References

1. The CMS collaboration, CMS Physics TDR, Volume I, CERN-LHCC-2006-001 (2006).
2. The CMS collaboration, The Trigger System TDR, CERN-LHCC-2000-38 (2000).
3. The CMS collaboration, CMS Physics TDR, Volume II, CERN-LHCC-2006-021 (2006).
4. Z. Yang and S. Qian, CMS-NOTE-2007/017.
5. A. Kraan, Feasibility study for the B_c^+ meson at CMS, in this volume; X.-W. Meng *et al.*, CMS-NOTE-2006/118.
6. W. Kwong and J. Rosner, Phys. Rev. **D**44, 212 (1991); E. Eichten and C. Quigg, Phys. Rev. **D**49, 5845 (1994); I.I. Bigi, Phys. Lett. **B**371, 105 (1996); M. Beneke and G. Buchalla, Phys. Rev. **D**53, 4991 (1996).
7. F. Abe *et al.* (CDF Collaboration) Public Note 07-07-12; F. Abe *et al.* (CDF Collaboration), Phys. Rev. Lett. **97**, 012002 (2005).

8. T. Matsui and H. Satz, Phys. Rev. **B**178, 416 (1991).

9. A. Abreu *et al.* (NA50 Collaboration), Phys. Rev. **B**450, 456 (2002).

10. F. Karsch, D. Kharzeev and H. Satz, Phys. Rev. **B**637, 75 (2005).

11. M. Bedjidian and O. Kodolova, CMS-NOTE-2006/089.

Frascati Physics Series Vol. XLVI (2007), pp. 397–405
HADRON07: XII Int. Conf. on Hadron Spectroscopy – Frascati, October 8-13, 2007
Plenary Session

PROPERTIES OF HEAVY FLAVOR HADRONS IN ATLAS

Sally Seidel
Department of Physics and Astronomy
University of New Mexico, Albuquerque, NM 87131 USA
for the ATLAS Collaboration

Abstract

The LHC will offer an opportunity for study of QCD at unprecedented energy scales. ATLAS, which will cover central proton-proton collisions, plans to study heavy flavor hadrons including quarkonium states. The expected statistics will permit high precision measurements of production polarization of the Λ_b and J/ψ. We also present new studies of production mechanisms, lifetime, and branching ratios for decays in the B_c and Υ systems and a program of studies of χ_b decays to resonant and non-resonant states.

1 Introduction

The Large Hadron Collider (LHC), which will provide 7 TeV-on-7 TeV proton-proton collisions, will offer unprecedented energy scales for QCD studies. ATLAS, one of the four LHC detectors, will cover collisions to pseudorapidity $|\eta| \leq 2.4$ for high precision measurements. The LHC has a 27 km circumference and 40 kHz crossing rate. The total $b\overline{b}$ production cross section there

will be 500μb: one $b\overline{b}$ pair in every 100 collisions. The goal is to take 10 fb^{-1} per year (at luminosity 10^{33}cm^{-2}sec^{-1}) in Years 1–3 and 100 fb^{-1} per year subsequently.

The features of the ATLAS detector have been described elsewhere. [1)] ATLAS is well instrumented for B Physics, having been designed with precision vertexing and tracking, good muon identification, high resolution calorimetry, and a flexible dedicated B trigger. A rich B Physics program is planned, including CP violation studies (especially for the Λ_b and B_s systems, which are not accessible to the B factories), rare decays sensitive to new physics (including $b \to sl^+l^-$ and $b \to dl^+l^-$), and baryons and heavy flavor mesons which are the subject of this paper.

The ATLAS Collaboration's planned high statistics studies of heavy flavor hadrons, including quarkonia, will throw light on the properties of bound states, the spin dependence of quark confinement, the nature of the strong potential, factorization in Heavy Quark Effective Theory, the source of CP Violation, and perhaps the resolution of some puzzles in existing data on hyperon polarization and cross sections.

ATLAS triggers have been described elsewhere. [2)] Muons will provide a reliable flavor tag. The studies described in this paper will make use of three threshold-dependent Level 1 triggers. Those trigger types are referred to as the "Dimuon" (which requires muon transverse momentum $p_T > 6$ GeV/c in the barrel or > 3 GeV/c in the endcaps), the "Muon + EM" (which requires one muon with $p_T > 6$ GeV/c in the barrel and an electromagnetic cluster with transverse energy $E_T > 5$ GeV, and the "Muon + Jet" (which requires one muon with $p_T > 6$ GeV/c in the barrel and an electromagnetic cluster with $E_T > 10$ GeV. Level 1, which uses only the calorimeter and muon trigger chambers, identifies Regions of Interest and outputs at 75 kHz. Level 2 uses the Regions of Interest and dedicated online algorithms, reconfirms the muon and calorimeter information, refits tracks in the Inner Detector, and outputs at 1 kHz. The final stage is the Event Filter, which uses full event buffers and processor subfarms and applies offline algorithms with alignment and calibration. The Event Filter reconstructs decay vertices and selects exclusive final states via mass and decay length requirements. It outputs at 200 Hz.

2 Λ_b Production, Lifetime, and Polarization

Existing data [3] on the polarization of Λ particles produced inclusively in proton-proton and proton-Beryllium collisions shows the unexpected feature that the polarization rises with p_T to large negative values and, beginning at a p_T around 1 GeV/c, reaches a plateau whose amplitude depends upon x and which does not diminish even at the highest p_T values recorded. The shape is unexpected; small polarization is expected for Λ's produced inclusively. Most models predict negligible polarization at high p_T and high energy. These data raise questions about the production mechanisms for different flavors and the relationship between polarization and quark mass. A measurement of the Λ_b polarization may cast light upon this issue.

There is, additionally, a longstanding puzzle in the B-baryon lifetime data. The ratio of lifetimes of the Λ_b and B^0 are not consistent with theoretical predictions made by models which nonetheless succeed in predicting the ratio of lifetimes of B^0 and $B^{\pm}$. Probing this puzzle in a new energy regime, with improved precision and models, may clarify the issue. Thirdly, a measurement of the Λ_b polarization will probe CP violation in a new way, since if CP is not conserved, the asymmetry parameters of the b and $\overline{b}$ quarks should differ. This study takes as its goals the world's first measurement of the asymmetry parameter α_b and polarization P_b for Λ_b, to precision 2%, and a measurement of the Λ_b lifetime, to 0.3%.

The selection process uses the channel $\Lambda_b \to \Lambda \mathrm{J}/\psi$, where $\Lambda \to \pi^- p$ and $\mathrm{J}/\psi \to \mu^+\mu^-$. The number of Λ_b events anticipated in 30 fb^{-1} is predicted to be 18000 by combining the acceptance for Λ_b detection, estimated with the generator PYTHIA [4] at 0.157%; the production cross section for Λ_b, 0.00828113 mb; the branching ratio for $\Lambda_b \to \mathrm{J}/\psi$, 4.7×10^{-4}; the branching ratio for $\Lambda \to \pi^- p$, 0.64, the branching ratio for $\mathrm{J}/\psi \to \mu^+\mu^-$, 0.06, and the combined efficiency for trigger and selection cuts, 0.004. An equal number of $\overline{\Lambda}_b$ is expected as well. The selection strategy begins with the requirement of two muons with p_T values greater than 4 GeV/c and 2.5 GeV/c, respectively; combination of a pion and a proton with p_T values greater than 0.5 GeV/c each; and a restriction of $|\eta| < 2.7$ for all tracks. The expected number of background $pp \to \mathrm{J}/\psi \Lambda X$ events is 3.2×10^6.

The polarization measurement, which has been described elsewhere [5],

assumes a general decay amplitude of the form

$$M = \overline{\Lambda}_b(p_{\Lambda_b})\epsilon^*_\mu(p_{\mathrm{J}/\psi})\left[A_1\gamma^\mu\gamma^5 + A_2\frac{p^\mu_{\Lambda_b}}{m_{\Lambda_b}}\gamma^5 + B_1\gamma^\mu + B_2\frac{p^\mu_{\Lambda_b}}{m_{\Lambda_b}}\right]\Lambda_b(p_{\Lambda_b}), \quad (1)$$

where A_1, A_2, B_1, and B_2 depend on the choice of perturbative QCD model. If one defines

$$a_+ = |a_+|e^{i\alpha_+} \equiv M_{+1/2,0} \quad (2)$$

$$a_- = |a_-|e^{i\alpha_-} \equiv M_{-1/2,0} \quad (3)$$

$$b_+ = |b_+|e^{i\beta_+} \equiv M_{-1/2,-1} \quad (4)$$

$$b_- = |b_-|e^{i\beta_-} \equiv M_{+1/2,+1} \quad (5)$$

where M_{λ_1,λ_2} is the amplitude for decay into Λ with helicity λ_1 and J/ψ with helicity λ_2, then for normalized amplitudes,

$$\alpha_b = |a_+|^2 - |a_-|^2 + |b_+|^2 - |b_-|^2. \quad (6)$$

The angular distribution for $\Lambda_b \to \mathrm{J}/\psi(\mu^+\mu^-)\Lambda(p\pi^-)$ is

$$w(\vec{A},\vec{\alpha},\vec{\theta}) = \sum_{k=0}^{19} f_{1k}(\vec{A})f_{2k}(\vec{\alpha})F_k(\vec{\theta}) \quad (7)$$

where parameters f_{1i}, f_{2i}, and F_i are defined in [5]. The angular distribution depends on nine unknown parameters: P_b and the four amplitudes and four phases of the a_+, a_-, b_+, and b_-. After normalization of the amplitudes and application of the global phase constraint, the number of independent unknowns is seven. These are extracted from the measured decay angles by a fit of the likelihood function,

$$L = -2\sum_{j=1}^{N} log(w_{obs}(\vec{\theta'},\vec{A},P_b)) \quad (8)$$

where N = number of events,

$$w_{obs}(\vec{\theta'},\vec{A},P_b) = \frac{\int w(\vec{\theta},\vec{A},P_b)T(\vec{\theta},\vec{\theta'})d\vec{\theta}}{\int\int w(\vec{\theta},\vec{A},P_b)T(\vec{\theta},\vec{\theta'})d\vec{\theta}d\vec{\theta'}} \quad (9)$$

and

$$T(\vec{\theta},\vec{\theta'}) = \epsilon(\vec{\theta})R(\vec{\theta},\vec{\theta'}) \quad (10)$$

for acceptance $\epsilon =$ and resolution $R =$. The resolutions on the angles measured is anticipated to be about 10 mrad. Detector acceptance corrections come from a Monte Carlo data sample with $P = 0$.

3 Quarkonium Production and Decay

One of the goals of this and the following section is a comparison of ATLAS data to predictions by the quarkonium production models, especially the Color Singlet Model [6] (which assumes that each quarkonium state can be produced only by a $q\overline{q}$ pair in the same color and angular momentum J state as the quarkonium) and non-relativistic (NR) QCD with the Color Octet Mechanism [7] (which treats quarkonium as a non-relativistic system so that $q\overline{q}$ pairs produced with one set of quantum numbers can evolve into a quarkonium state with different quantum numbers by emitting low energy gluons). NR QCD with the Color Octet Mechanism agrees with CDF data [8] on the J/ψ p_T cross section with free normalization up to accessible (Tevatron) energies; however, data at higher p_T, and for quarkonia farther from the QCD scale, are needed. The goal of this ATLAS study is measurements of the distributions in p_T, η, and polarization for the J/ψ, measurements of the ratio of Υ and J/ψ production cross sections, and an assessment of hadronic activity associated with quarkonium production.

The LHC will produce heavy quarkonia with high p_T at a high rate. In 10^6 seconds at luminosity $10^{31}\mathrm{cm}^{-2}\mathrm{s}^{-1}$, for muon pairs selected with the requirement that one have $p_T > 6$ GeV/c and the other, $p_T > 4$ GeV/c, 175000 $J/\psi \to \mu\mu$ and 36000 $\Upsilon \to \mu\mu$ events may be available.

Several strategies are being applied to maximize the ratio of signal to background. One is an examination of the option to lower the dimuon trigger threshold from 6 GeV/c + 4 GeV/c to 4 GeV/c + 4 GeV/c. This captures a subtantially larger fraction of the signal, especially for the Υ. It also is expected to increase the contribution of color singlet production, which dominates for $p_T < 10$ GeV/c. A second strategy is the application of a cut on pseudo-proper time to separate direct from indirect J/ψ's. As expected, the resolution worsens with increasing p_T and η. The third strategy involves measuring the quarkonium spin. For the angle θ between the positive muon in the quarkonium reference frame and the quarkonium direction in the lab frame,

$$\frac{d\Gamma}{d\cos\theta} \propto 1 + \alpha\cos^2\theta, \tag{11}$$

where

$$\alpha \equiv \frac{\sigma_T + 2\sigma_L}{\sigma_T - 2\sigma_L}. \tag{12}$$

The parameter α takes the values 0, +1, and -1 for unpolarized, transversely polarized, and longitudinally polarized mesons, respectively. Octet production predicts transverse polarization at large p_T.

From a study of the reconstructed and "truth" $\cos\theta$ distributions of simulated J/ψ events in the ranges $9 < p_T < 12$ GeV/c and $p_T > 21$ GeV/c, ATLAS observes that the acceptance in $\cos\theta$ is limited by the p_T of the second muon and concludes that a single muon trigger would be useful to this analysis if the rate could be reduced by some other means. Present NR QCD formalisms model Tevatron data well up to $p_T = 20$ GeV/c. High acceptance is predicted for $J/\psi \to \mu_{(6\mathrm{GeV/c})}\mu_{(4\mathrm{GeV/c})}$ and $\Upsilon \to \mu_{(6\mathrm{GeV/c})}\mu_{(4\mathrm{GeV/c})}$ such that this agreement can be tested with precision to $p_T \approx 50$ GeV/c at least. A fourth strategy involves analysis of the level of hadronic activity associated with the quarkonium production. The Color Singlet and Color Octet models may predict different levels. ATLAS is preparing to study this with isolation cones about the quarkonium direction. As a first step, we study the application of the cone to the muon direction. Challenges to this technique include the procedure for subtracting the muon contribution to the energy captured in the quarkonium cone; modelling the energetic photon associated with the χ_c decay which produces 29% of the J/ψ's; and accommodating the fact that the photon and muon are almost collinear for the J/ψ.

4 χ_b Resonant and Non-resonant Decay

A single measurement of the branching ratio for $\chi_{c0} \to \phi\phi$ exists and is substantially larger than its prediction. [9] This motivates the question as to whether the enhancement reflects internal motion of the quarks in the hard part of the amplitude. A study of the analogous channel $\chi_{bJ} \to \psi\psi X$ could provide an answer. A second motivation for the study of χ_b comes from the known inconsistency between Tevatron data and the predictions of the Color Singlet Model for ψ production via $gg \to \psi g$.

Preparations are underway to search for the process $\chi_{b0,2} \to \psi\psi \to \mu^+\mu^-\mu^+\mu^-$. At luminosity $10^{33}\mathrm{cm}^{-2}\mathrm{s}^{-1}$, the production cross section for $pp \to \chi_{bi}X$ is enhanced at the LHC relative to the Tevatron by ratios of $1.5\mu\mathrm{b} : 250\mathrm{nb}$ (for $i = 0$) and $2.0\mu\mathrm{b} : 320\mathrm{nb}$ (for $i = 2$). Combining these LHC cross sections with the branching ratio for $\chi_{bi} \to \psi\psi$, $2.2 \times 10^{-4} (i = 0)$ or $5 \times 10^{-4} (i = 2)$, the branching ratio for $J/\psi \to \mu^+\mu^-$, 5.93%, and selecting

events with muon $p_T^{\rm Level1} > 6$ GeV/c, muon $p_T^{\rm Level2} > 4$ GeV/c, and muon $\eta > 2.5$ for Levels 1 and 2, estimating the detection efficiency at 1.63% predicts 200 (generator-level) χ_{b0} events per year. This signal, though small, is likely to be backgroundless, as the combinatorics of four muons forming two J/ψ masses is vanishingly small.

5 B_c Production and Decay

A precision reconstruction of B_c ground and excited states can be used to constrain models of the strong potential. The combination of the doubly-heavy quark system with the restriction that the decays must go weakly predicts that the states will be narrow and in a regime sensitive to non-perturbative as well as perturbative effects.

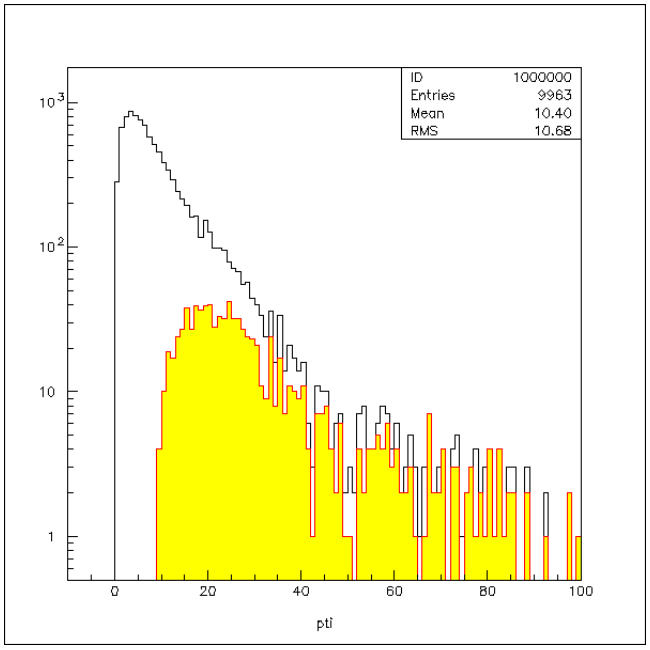

Figure 1: *The transverse momentum of B_c particles (white) and of those whose muons pass the 6 GeV/c + 4 GeV/c p_T requirement (shaded), for events generated with the program BCVEGPY2.1.* [10]

We select hadronic B_c decays connecting states with the largest possible mass difference to maximize efficiency for observing the final state tracks. Several channels, including

$$B_c^*(2^1S_0) \rightarrow B_c(1^1S_0)\pi^+\pi^- \tag{13}$$

and

$$B_c^*(2^1S_1) \rightarrow B_c^*(1^1S_1)\pi^+\pi^- \tag{14}$$

are predicted to have mass differences in the realm of 600 MeV. Efficient tracking at very low p_T will be essential, as will be generation and simulation of realistic decays of the excited states in the PYTHIA framework. Figure 1 predicts the p_T distributions of all B_c's (white histogram) and those whose muons pass the 6 GeV/c and 4 GeV/c requirements (shaded histogram). The predicted number of B_c events in 20 fb^{-1} integrated luminosity at ATLAS is 10000.

6 Conclusions

With 1 fb^{-1} integrated luminosity, Λ_b studies will yield the Λ_b lifetime, known better than the present world average, and first results on Λ_b polarization. The large predicted quarkonia cross sections at the LHC will permit definitive studies of quarkonium spin alignment as a test of the Color Octet Mechanism, for which 100 pb^{-1} of integrated luminosity are needed for a competitive polarization measurement. The large cross sections may also permit a comparison of jet activity associated with quarkonium decay to levels predicted by the Color Singlet and Color Octet mechanisms. With 10 pb^{-1}, ATLAS will measure ratios of quarkonia cross sections to constrain NR QCD octet matrix elements. Subsequent statistical power will fix the matrix elements. The LHC will be the first opportunity for significant statistics on excited states in the B_c family. These measurements can constrain models of the strong potential and cast light on interaction between the electroweak and strong forces. Finally, χ_b decays may point the way to solving longstanding puzzles in the $gg \rightarrow \psi g$ and $e^+e^- \rightarrow \psi\eta_c$ cross sections.

References

1. ATLAS Technical Proposal, CERN-LHCC-1994-043 (1994).
2. ATLAS High Level Trigger Technical Design Report, CERN-LHCC-2003-022 (2003).
3. J. Lach, Proc. Int. Wkshp. on Flavor and Spin in Hadronic and Electromagnetic Interactions, Torino (1992).
4. T. Sjöstrand, S. Mrenna, and P. Skands, JHEP **0605**, 026 (2006).
5. J. Hrivnac et al., J. Phys. **G21**, 629 (1995); M. Biglietti et al., Nucl. Phys. B (Proc. Suppl.) **156**, 151 (2004).
6. E. L. Berger and D. Jones, Phys. Rev. **D23**, 1521 (1981); R. Baier and R.R̃ückl, Phys. Lett. **B102**, 364 (1981).
7. G. T. Bodwin, E. Braaten, and G. P. Lepage, Phys. Rev. **D51**, 1125 (1995); erratum *ibid.* **D55**, 5853 (1997).
8. F. Abe et al., Phys. Rev. Lett. **69**, 3704 (1992).
9. J. Z. Bai et al., Phys. Rev. **D60**, 072001 (1999).
10. C.-H. Chang et al., Comput. Phys. Commun. **174** 241 (2006).

Frascati Physics Series Vol. XLVI (2007), pp. 407–431
HADRON07: XII Int. Conf. on Hadron Spectroscopy – Frascati, October 8-13, 2007
Plenary Session

CHALLENGES IN HADRON PHYSICS

Kamal K. Seth
Northwestern University, Evanston, IL 60208, USA
kseth@northwestern.edu

Abstract

The status of hadron physics at the end of the HADRON07 Conference is reviewed. The latest results presented at the conference, as well as those important developments in the field which were not represented, are included.

For this closing talk, I was encouraged to be different and not attempt to mention over and over again the talks that you have already heard. And there have been a lot of talks, 36 plenaries and 146 parallel presentations. Instead, I will try to present a summary of the challenges we face at the end of 2007 as hadron spectroscopists, what we have achieved and what we must strive to achieve.

This series of two–yearly HADRON conferences began at Maryland in 1983. The first one I attended in 1991 defined our charter as **"hadron spectroscopy and some areas of related hadron structure"**, i.e., strong interaction physics, which in the modern language means QCD. So, let me walk across the landscape of hadron physics and survey the challenges. I will talk

about things which have been presented at this conference, as well as those which have not. And the presentation will be admittedly subjective.

For an overall survey of the recent progress in experimental hadron spectroscopy, I will often turn to the PDG, which provides us with the only Bible we have, imperfect as it might be.

1 BARYONS

Two quarks are easier than three, but I begin with baryons because we live in a Universe built of baryons, to be more specific — nucleons, and not mesons.

1.1 The Nucleons

We have been working on the nucleon for close to 100 years, and all we want to know is what the nucleon looks like. How do its static properties, mass, charge, magnetic moment, spin, and structure arise, and how it reacts when it is tickled by an external probe? Not too much to ask!!

We are told that there is a super-duper new way of tickling the nucleon, **Deeply Virtual Compton Scattering (DVCS)/Deeply Virtual Meson Production (DVMP)**, which leads to the Generalized Parton Distributions (GPD's), and they can give all the information that we used to try to get by measuring form factors and Deep Inelastic Scattering (DIS). Maybe so!

Indeed, nearly all the labs in the business, JLab, H1, Zeus, Hermes, Brookhaven, CERN(COMPASS), now have very active programs for measuring GPD's (see Fig. 1).

Unfortunately, life is not so easy. The observables are all integrals over x(Bjorken) and deconvolution is required to get to the true GPD's, H, $\tilde{H}$, E, $\tilde{E}$, which are functions of x, ξ, and t. And that is neither easy nor unique. So, like the GDP, which is supposed to contain all the information about a country's economy, the whole story is not in the GPD measurements, either. For the present, therefore, we go back to the more directly interpretable form factor and DIS measurements.

1.2 Form Factors

There has been recent progress in form factor measurements, both for spacelike and timelike momentum transfers.

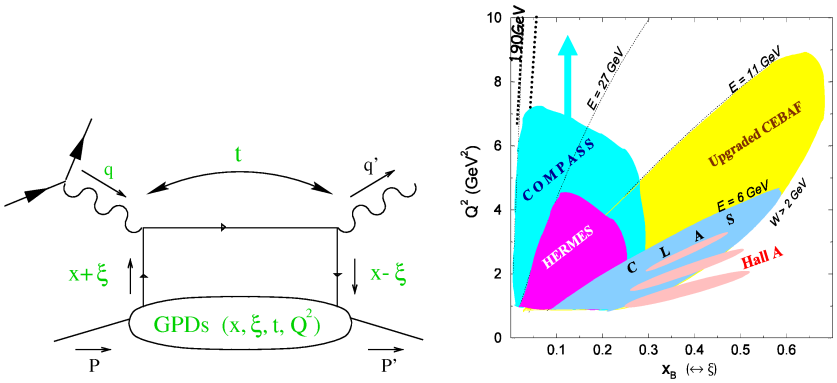

Figure 1: (Left) Schematic representation of the DVCS measurement of GPD's. (Right) Illustrating the $x_B - Q^2$ domain accessible to GPD measurements at different laboratories.

1. The Challenge of G_E(proton) for Spacelike Momentum Transfers

The recent JLab polarization measurements for spacelike momentum transfers up to $Q^2 = 5.5$ GeV^2 show clearly that the $\mu G_E(p)/G_M(p)$ of the proton monotonically falls with increasing Q^2, or equivalently, Q^2F_2/F_1 monotonically rises, as shown in Fig. 2. The naive pQCD expectation was that both $\mu G_E(p)/G_M(p)$ and Q^2F_2/F_1 were constant for large Q^2. What happened? Many **post**dictions have been made. Suffice it to say that there are no clear-cut consensus explanations. JLab proposes to extend these measurements to $Q^2 = 8.6$ GeV^2 by which time $\mu G_E(p)/G_M(p)$ should have arrived at zero, i.e., $G_E = 0$. What does $G_E = 0$, mean? If the trend continues, with the 12 GeV upgrade G_E will be found to be negative. What does **that** mean?

We do not know, but it is clear that the measurements have to be made, and the theorists have to work harder to tell us what they mean.

2. The Challenge of G_E(proton) for Timelike Momentum Transfers

In the perturbative regime of large momentum transfer Q^2, QCD makes two predictions about the relationship between form factors at spacelike and

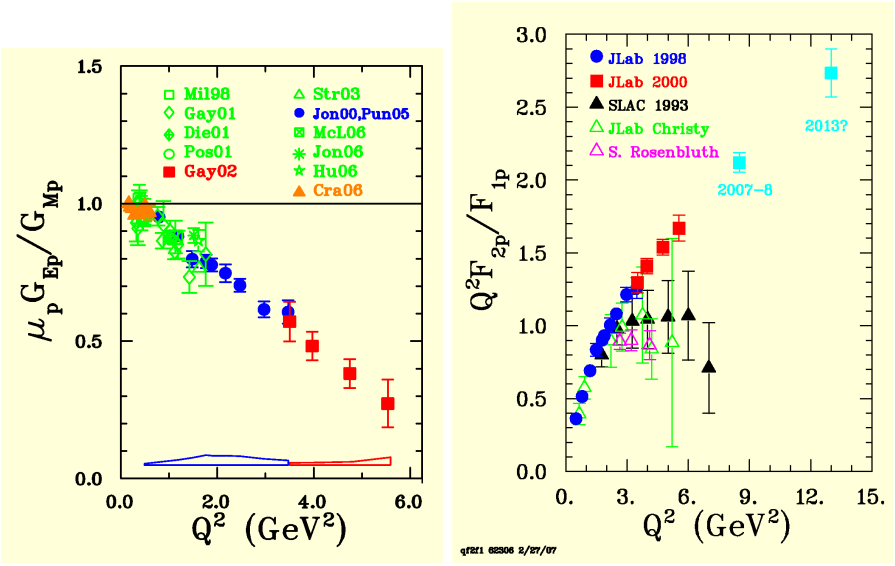

Figure 2: (Left) Results for $\mu G_E^p/G_M^p$ as a function of Q^2 as measured in the polarization experiments at JLab. (Right) The results presented as $Q^2F_2^p/F_1^p$.

timelike momentum transfers. The first, based on quark counting rules, is that for both, $Q^4G_M(p)$ should be constant except for the variation of α_S^2. The second is that in this regime, the two should be equal (actually, this follows from Cauchy's theorem because form factors are analytic functions). The general expectation was that $Q^2 \geq 10$ GeV^2 should be large enough for both these predictions to be true. Fermilab $p\bar{p} \to e^+e^-$ measurements for $Q^2 = 8.8 - 13.1$ GeV^2 showed that while the $1/Q^4$ and α_S^2 variations were essentially confirmed, the timelike form factors were twice as large as the corresponding spacelike form factors (see Fig. 3). Since then, the experimental measurements of Fermilab have been confirmed and extended by the reverse reaction measurements of $e^+e^- \to p\bar{p}$ by BES, CLEO, and BaBar. So, the factor two is more than confirmed, and we have to understand how it arises. Let me add a very important point here. For timelike form factors, lattice is totally impotant. The practitioners admit that they are stuck in Euclidean time and cannot handle timelike form factors because they live in Minkowski time. So, there!

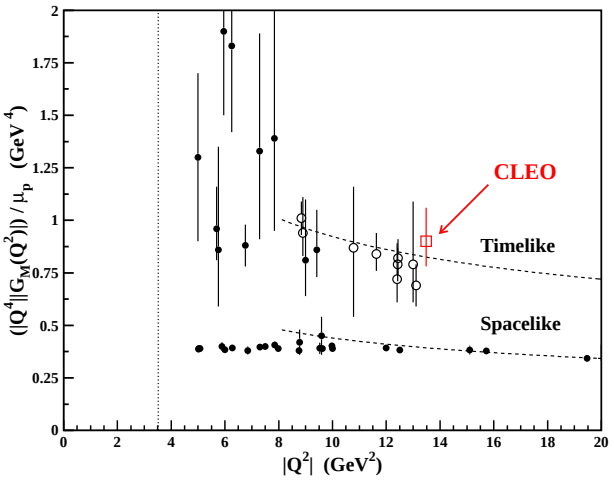

Figure 3: Measurements of timelike magnetic form factors of the proton presented as $Q^4 G_M/\mu_p$ versus $|Q^2|$. Also shown are the spacelike form factors as measured at SLAC. The dotted curves illustrate the α_S^2 variation predicted by pQCD.

This poses a challenge. Why half–agreement and half–disagreement with pQCD? One way out that has been suggested is that the proton does not look like a Mercedes star, with three symmetrically placed quarks, but more like a T, with a diquark-quark configuration, and the diquark model does succeed in explaining the factor two discrepancy. Many people do not buy the diquark model, and so seek refuge in the possibility that $Q^2 \sim 15$ GeV^2 is not large enough for pQCD to be valid. This, of course, throws the challenge to the experimentalists: measure timelike form factors at larger Q^2. Easier said than done!! Recall that $G_M^p(|Q^2|)$ varies as $1/Q^4$, and the cross section varies as $1/Q^{10}$ or $1/s^5$. So, in going from 15 GeV^2 to 25 GeV^2 the cross section would fall a factor 20 from < 1 pb to $\mathbf{< 50\ fb}$. That is a difficult measurement. In principle, BES III and PANDA could tackle it, but it will be very hard.

What about $G_E(p)/G_M(p)$ for timelike momentum transfers? In principle, this could be done because the angular dependence of G_E and G_M is different. In fact, BaBar has tried to do this in their measurement of $p\bar{p}$ pro-

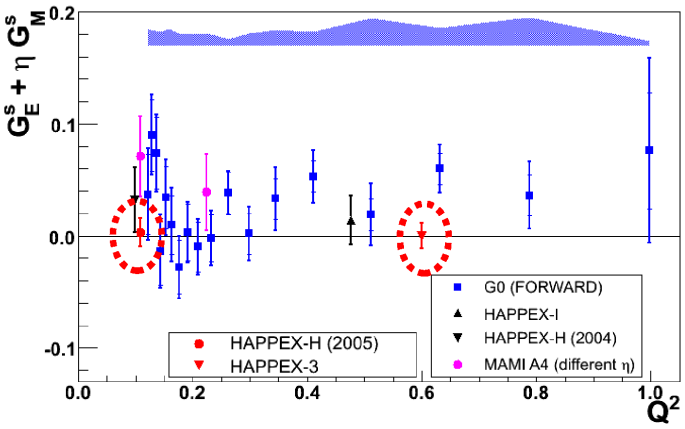

Figure 4: Strange quark form factors ($G_E + \eta G_M$) as measured by parity violating electron scattering.

duction in ISR–mediated annihilation of e^+e^-. The errors are large (and there is the familiar Rosenbluth ansatz), but essentially $\mu_p G_E/G_M$ is found to be constant $\approx 1.3 \pm 0.2$ in the entire region $Q^2 = 3.5 - 9.0$ GeV^2. Recall that by $Q^2 = 5.4$ GeV^2 the spacelike $\mu_p G_E/G_M$ has fallen down to ~ 0.3, and it extrapolates to zero by $Q^2 \approx 9$ GeV^2. If the BaBar results hold up with better statistics, we have a serious problem on our hands. To confirm and reconcile these results is an important challenge to both theorists and experimentalists.

3. The Challenge of Strange Quark Form Factors

For a long time there has been the nagging question about the role of the strange quarks in the nucleon. Several experiments (SAMPLE at Bates(MIT), PVA4 at Mainz, and G^0 and HAPPEX at JLab) have addressed this question by making the very demanding measurements of parity violating electron scattering. So far the data have been limited to $Q^2 \leq 1$ GeV^2.

A global analysis of the world data for $Q^2 \leq 0.48$ GeV^2 leads to the conclusion that for $Q^2 = 0.1$ GeV^2, $G_E^s(p) = -0.008 \pm 0.016$, and $G_M^s(p) = 0.29 \pm 0.21$, i.e., both are consistent with zero. The same analysis reaches

essentially the same conclusion for the sixteen individual Q^2 data points from 0.12–0.48 GeV^2 (see Fig. 4).

The experimental challenge is to see if this conclusion holds for larger Q^2 at which both G^0 and HAPPEX plan to take data in the near future.

Before I leave form factors, let me add that there has been very encouraging progress recently in measuring form factors of the neutron. Excellent JLab measurements of $G_M^{(n)}$ extend up to ~ 4.7 GeV^2 and for $G_E^{(n)}$ up to ~ 1.5 GeV^2, and there are plans to go to larger Q^2.

1.3 The Challenge of the Nucleon Spin

We all know what this is about. The quark spins just don't add up to the spin 1/2 of the proton. So what accounts for the rest?

Proton spin $= 1/2 = \frac{1}{2}\Delta\Sigma + \Delta G + L_z$,
where $\Delta\Sigma = \Delta u + \Delta d + \Delta s$, $\quad \Delta q = (q_+ - q_-) + (\bar{q}_+ - \bar{q}_-)$
The latest results are

$$\Delta\Sigma = 0.35 \pm 0.06 \text{ (COMPASS)}, \; 0.33 \pm 0.04 \text{ (HERMES)}$$

That leaves a large part for $(\Delta G + L_z)$ to account for.

Attempts have been made to measure ΔG via DIS, polarized semi-inclusive DIS, polarized pp collisions, and all results are consistent with $|\Delta G| \leq 0.3$.

The sign of ΔG is so far undetermined. If ΔG is positive, L_z is small. If ΔG is negative, one will need large L_z from quarks and gluons. So the spin crisis remains unresolved after 20 years of experiments.

1.4 The Challenge of N^* and Δ Resonances

Both quark model and lattice calculations predict scores of N^* and Δ resonances, and most of them remain missing (see Fig. 5). The claimed N^* and Δ resonances remain stuck in the PDG with their poor star ratings since before 1996. Thus, for example, of the 20 reported resonances with $M > 2000$ MeV, 15 remain stuck with 1 and 2 stars, i.e., their existence is doubtful. The old data was mostly produced with pion beams, and there are no new pion beams around, To boot, pions can not be polarized!!

The only hope is to search for the resonances in photo– and electro–production, and decays into final states with η, η', ω. However, Capstick and Roberts have warned that these amplitudes tend to be "quite small" and the

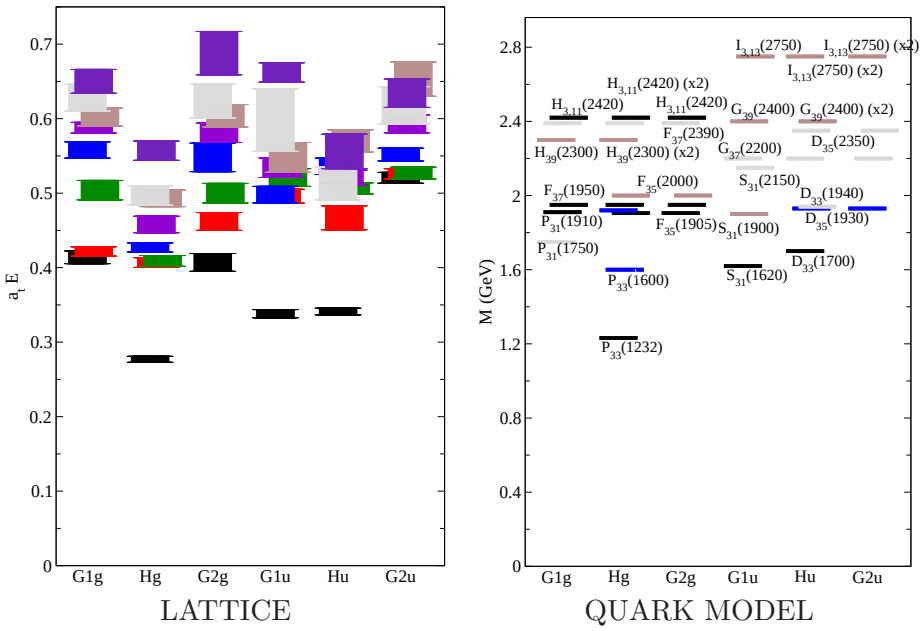

Figure 5: Predictions for N^* and Δ resonances as functions of lattice symmetry variables: (Left) Lattice predictions, (Right) Quark model predictions.

going is going to be tough. Nevertheless, valiant groups at MAMI, ELSA, and JLab are trying. On the analysis side, new and more comprehensive general purpose tools of PWA analysis are being developed. It is time that these efforts had some good luck!

1.5 Λ, Σ, and Ξ Baryon Resonances

The situation here is also quite bleak. PDG07 summarizes it as follows:

> Λ and Σ: "The field remains at a standstill and will only be revived if a kaon factory is built."
> Ξ: "Nothing of significance on Ξ resonances has been added since our 1998 review."

What can we expect in the near future? The only kaon factory on the horizon is JPARC and hopefully they will put high priority on Λ and Σ **formation**

experiments. Other than that, we have only production experiments possible, in pp collisions at COSY, and photoproduction experiments at JLab. In fact, some low–lying Λ and Σ are being currently studied in photoproduction experiments at JLab with polarized photons, and an ambitious program of Ξ spectroscopy has been proposed at JLab. Unfortunately, we do not have any finished results so far.

1.6 Charmed Baryons ($\boldsymbol{C = +1,\ (+2),\ (+3)}$)

Here progress is more encouraging. Adding charm quarks to the SU(3) octet and decuplet of u, d, s quarks gives 18 baryons with one c-quark, 6 baryons with two c-quarks and one baryon Ω_{ccc}^{++} with three c-quarks.

Prior to 2005, most of the charm baryon results came from CLEO and ARGUS from e^+e^- annihilations in the Upsilon($4S$) region, and from FOCUS at Fermilab and NA38 at CERN. Now that the B–factories have weighed in, we have five new charmed baryons just this year. BaBar has reported the discovery of $\Lambda_c(2940)$ and $\Omega_c(2770)$, and Belle has reported $\Sigma_c(2800)$, $\Xi_c(2980)$, and $\Xi_c(3080)$. These are clean-cut states with small widths. For example, $\Gamma(\Xi_c(3080)) = 6.2$ MeV!

Since 2002, we have had SELEX report the doubly charmed $\Xi_{cc}^+(3519)$, but nobody else (Belle, BaBar) seems to find any evidence for it. So, it remains hanging. The holy-grail particle Ω_{ccc}^{++} remains undiscovered so far. Let me only add the hope that PANDA can reach for it.

1.7 Bottom Baryons ($\boldsymbol{B = +1}$)

One expects bottom baryons Λ_b, Ξ_b, Σ_b, and Ω_b just as the charmed baryons. Before 2006, only one bottom baryon Λ_b^0 was known. Now, from CDF and DØ we have $\Sigma_b^{\pm}$, Σ_b^*, and Ξ_b. These are extremely challenging measurements, resolving states at ~ 6 GeV separated by ~ 20 MeV, e.g., $m(\Sigma_b^*) - m(\Sigma_b^{\pm}) = 21.2 \pm 0.2$ MeV.

1.8 Threshold States of Two Baryons

Long ago, in the era of prehistory, there was great excitement about the possible existence of **dibaryons**, which were predicted in bag–models. Many, many people (including me) made many, many measurements, and in the end, nobody found any dibaryons that anybody else would believe. Then there was

the search for **baryonium**, the bound state of a baryon–antibaryon. Again, many measurements were made searching for a $p\bar{p}$ baryonium, and finally it was agreed that there was no evidence for it. Recently, a pseudo-baryonium has resurfaced as an enhancement in $p\bar{p}$ invariant mass at threshold, observed by BES in $J/\psi \to \gamma p\bar{p}$. BES interpreted it as due to a below-threshold resonance with the $p\bar{p}$ bound by about 20 MeV. Belle and BaBar also observed similar enhancements over phase space in various B decays, but did not venture into the bound-state conjecture. The enhancement was not observed in $J/\psi \to \pi^0 p\bar{p}$ or $\psi' \to (\pi^0, \eta)p\bar{p}$, and the resonance interpretation has languished. In the meanwhile, BES has reported similar near-threshold enhancements in $p\Lambda$, $\Lambda\overline{\Lambda}$, and $\omega\phi$ invariant mass. The enhancements appear real, but the resonance interpretations appear more like wishful thinking. It is more likely that these are manifestations of near-threshold final state interactions when the two particle go out with very small relative momenta. Certainly more experimental and theoretical investigations are desirable, and some are in progress at CLEO.

1.9 Baryon Summary

Little progress has been made with light quark baryons. Optimism for future progress has to rest particularly on what JLab and JPARC can do. Heavy quark baryons have shown more life recently due to contributions from the B–factories at KEK and SLAC.

To cap this section, let me mention that the exotic baryons, the $\Theta^+(1540)$ pentaquark, $\Phi(1860)$, $\Theta_c^0(3100)$ appear to have mercifully expired!

2 LIGHT QUARK MESONS

Once again I begin with my semi-serious quotation from the Bible, the PDG. In contrast to the baryons, which did not add a single page (148/148) between 2004/2006, the mesons showed a lot of activity, going from 358 to 430 pages. Most of the new activity (90% of it) came from the heavy quark (charm and bottom) sectors, with charmonium ($c\bar{c}$) showing a 63% increase. This indicates that a lot of the challenges in the light quark (up, down, strange) mesons have remained unanswered. So, let me begin with them.

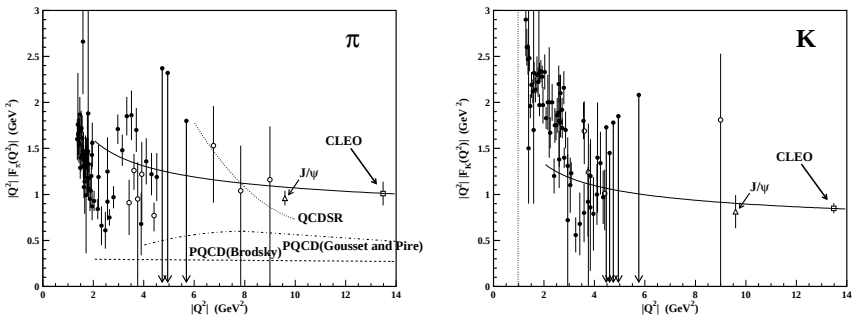

Figure 6: Timelike form factors: (left) for pions, (right) for kaons presented as Q^2F_m versus $|Q^2|$. The solid curve, arbitrarily normalized, shows variation of α_S.

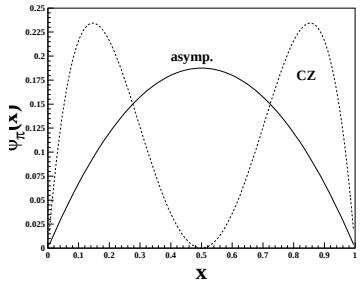

Figure 7: Schematic illustration of the alternative momentum distributions of the quarks in a pion. The solid curve is the asymptotic single hump distribution, and the dotted curve is the QCDSR–based dumbbell-like distribution.

2.1 The Challenge of the Meson Form Factors

Earlier, I posed the question, "Is it too much to ask what the proton looks like?" Now I am ready to ask what ought to be a simpler question because it involves only two quarks, "What does a meson look like?" Unfortunately, the answer to this question is even more elusive. Some of you may recall the animated controversy between two illustrious theoretical groups — Brodsky & colleagues, and Isgur & Llwellyn–Smith, about when in Q^2, 10 GeV^2 or 100's of GeV^2,

pQCD begins to become valid. And the primary experimental data available to either side (with errors less than 50 to 100%) were pion form factors for spacelike momentum transfers $Q^2 < 4.5$ GeV^2 (see Fig. 6). No wonder one could not decide whether the pion distribution amplitudes looked like a dumbbell or a bell (see Fig. 7). Long after the original controversy, lots of theoretical predictions kept on being made, unconstrained by any new experimental data, Well, the situation has changed, because new measurements of **pion** and **kaon** form factors for timelike momentum transfers of $Q^2 = 13.48$ GeV^2 have been made at CLEO with errors of $\pm 13\%$ and $\pm 5\%$, respectively. As Figure 6 (left) for pions shows, none of the theoretical calculations, either pQCD or QCD sum rule based, make any sense at all. This is undoubtably a strong challenge to the theorists. For kaons there are no theoretical predictions. The naive expectation $F(\pi)/F(K) = f^2(\pi)/f^2(K) = 0.67 \pm 0.02$ is also found to be in disagreement with the CLEO result of 1.19 ± 0.15. That adds to the challenge for the theorists. There is also a challenge for the experimentalists, in this case for BES III, to measure these form factors in the $Q^2 = s = 4 - 10$ GeV region to see if $Q^2 F_\pi$ varies as α_S, as predicte by pQCD counting rules, and if the ratio $F(\pi)/F(K)$ changes.

2.2 Light Quark Scalars

This has been **the** hot topic in the light quark sector for a long time, and has become even more so because it intersects wth the question of the lowest mass 0^{++} glueball, and even with the very concept of what constitutes a "resonance". It is such a hot topic that a recent review (arxiv.org/abs/0708.4016[hep-ph]), devotes 60 pages to the topic. It offers several provocative suggestions with many of which I do not agree, but then the authors honestly admit that they offer "a series of clear statements with little reasoning or justification."

The essential problem with the scalars is that in the quark model, with three light quarks you expect three scalars, two isospin–zero f_0 and one isospin–one a_0. But we have an embarressment of riches. We have at least five f_0's: $f_0(600)$ or $\sigma(600)$, $f_0(980)$, $f_0(1370)$, $f_0(1500)$, and $f_0(1710)$. So, we have to somehow disqualify at least three of these as non–$q\bar{q}$ mesons.

2.2.1 *The Challenge of the σ and κ*

Even at HADRON05, the reality of the σ meson which decays almost exclusively into $\pi\pi$ was open to question. Now, all the evidence has converged, and there appears to be little disagreement with the conclusion that σ is a real Breit-Wigner resonance with it proper pole structure, and (give or take 10 MeV or so)

$$M(\sigma) = 480 \text{ MeV}, \quad \Gamma(\sigma) = 570 \text{ MeV}$$

What is still an open question is "what is σ?" The debate is wide open. Is it $q\bar{q}$? Is it a glueball? Is it a 4–quark state? Or, is it (despite its Breit–Wigner character) the result of a final state $\pi\pi$ interaction? The challenge here is to find a way to distinguish between these various possibilities. I cannot think of anything except that a strong production of σ in two photon fusion would perhaps eliminate the glueball hypothesis.

The case of $\kappa(980)$ is more complicated and controversial. The "evidence" comes from $K\pi$ scattering (LASS), $K\pi$ production in decays of D mesons (FOCUS), and radiative decay of J/ψ (BES). The different analyses give very different masses

$$M(\kappa) = 658 - 841 \text{ MeV}$$

albeit with large errors. The spread in widths is even worse

$$\Gamma(\kappa) = 410 - 840 \text{ MeV}$$

In my mind, the existence of κ remains questionable, although I hold in high respect the work based on dispersion relation based analysis of $K\pi$ scattering. Personally, I intend to look at our own essentially background free data for $D \to K\pi\pi$ to see if we can shed some new light on both σ and κ.

2.2.2 *The $f_0(980)$, $a_0(980)$, and 4-quark States*

Unlike the σ and κ, there is no doubt about the existence of $f_0(980)$ and $a_0(980)$. They have been observed in e^+e^- and $p\bar{p}$ annihilation, in pp central collisions, in two photon fusion, and in radiative decays of J/ψ and ϕ (for which we have an excellent contribution from KLOE here). There is no doubt that f_0 and a_0 are relatively narrow ($\Gamma < 100$ MeV) and have strong decays to $K\overline{K}$.

The fact that the masses of f_0 and a_0 are very close, $M(K^+K^-) = 987.5$ MeV and $M(K_SK_L) = 995.3$ MeV, and that they decay strongly into

$K\overline{K}$, has given rise to the long–standing proposition that these are $K\overline{K}$ molecules. On the other hand, a canonical calculation of $q\bar{q}$ masses by Godfrey and Isgur predicts the first f_0 and a_0 to each have masses of 1090 MeV, within shooting distance of 980 MeV. Unfortunately, Godfrey and Isgur also predict much larger ($\times 5$) total widths. Not knowing any better, I am ready to consider the wave functions for these states mixtures of $q\bar{q}$ and four quark ($qq\bar{q}\bar{q}$ or $q\bar{q}q\bar{q}$) configurations. Unless somebody can devise a "smoking gun" measurement which would determine which configuration (if any) is dominant, I am content to live with this ad-hoc compromise.

I must emphasize, however, that even these mixed configuration mesons must be included in the $q\bar{q}$ meson count. Although many more 4-quark states can be configured, it is generally agreed that only those 4-quark configurations survive which can mix with $q\bar{q}$. As long as we are in the land of unproven conjectures, it is my conjecture that the $f_0(q\bar{q})$ and $a_0(q\bar{q})$ predicted by Godfrey & Isgur at 1090 MeV have moved down by mixing with four quark configurations, or something else to, 980 MeV, and $f_0(980)$ and $a_0(980)$ are the legitimate members of the $q\bar{q}$ scalar nonet. This is, of course, in contradiction to what the review authors of the PDG would have me believe. They propose an inverted spin–orbit splitting with f_0 and a_0 nearly 110 MeV **above** f_2 and a_2!!

2.2.3 The $f_0(1370)$, $f_0(1500)$, $f_0(1710)$ and the Glueballs

Sometime ago there were questions about this triad. Does $f_0(1370)$ really exist? Does $f_0(1710)$ really have $J^{PC} = 0^{++}$? There is now widespread belief that $f_0(1370)$ exists, and it is firmly established that $f_0(1710)$ has $J^{PC} = 0^{++}$. The challenge now is: can we draw any conclusions about **the 0^{++} scalar glueball?** Ten years ago, there were almost partisan discussions about which one of these is **THE (pure) GLUEBALL**, and all kinds of "semi-smoking gun" criteria were suggested to make the choice. Among them were: glueballs should be narrow (why? and how narrow?), glueballs should decay flavour-blind, glueballs should be supernumary to quark model expectations. Now everybody agrees that the scalar glueball not only can, but must mix with all of the other f_0's in its neighborhood. So, the "smoking gun" does not have to smoke very much! The mixed glueballs can be broad, and the their decays can have large departures from flavor-blindness. **In fact, the search for the uniquely identifiable glueball does not make much sense!**

At the generic level, we have expectations of four low mass isoscalars, two $q\bar{q}$, one glueball, and throw in a four-quark state. And they all mix, to give us $f_0(980)$, $f_0(1370)$, $f_0(1500)$, and $f_0(1710)$. Problem solved, or is it? Let the games go on! And isn't that challenging!!

The 2^{++} tensor glueball is likely to have the same fate as the scalar. The narrow $\xi(2230)$ has evaporated, Godfrey and Isgur predict **six** $f_2(q\bar{q})$ below 2400 MeV, and at least **twelve** have been claimed by one experiment or another. So the putative tensor glueball will also have plenty of friends to mix with!

As long as we are talking about glueball admixtures in mesons, it is worth noting that a beautiful measurement at KLOE has estimated the gluonium content of $\eta'(958)$ to be $14 \pm 4\%$, assuming that $\eta(548)$ has none. They do it by a long awaited precision measurement of $\mathcal{B}(\phi \to \eta'\gamma)/\mathcal{B}(\phi \to \eta\gamma) = (4.77 \pm 0.21) \times 10^{-3}$.

2.2.4 Light Quark Hybrids

As is well known, three $J^{PC} = 1^{-+}$ states, $\pi_1(1400,\ 1600,$ and $2000)$ have been reported by the Brookhaven and Protvino groups. Since $J^{PC} = 1^{-+}$ is forbidden for $q\bar{q}$ mesons, these states are obviously "exotic". However, their interpretation as $q\bar{q}g$ hybrids is not universally accepted. This status remains unchanged since their discovery. It is claimed that photoproduction of hybrids holds great promise, particularly at JLab, but that is also not without controversy. Unfortunately, experimental resolution of this controversy has to wait for the JLab upgrade, which may come as late as ten years from now.

3 HEAVY QUARK MESONS

Heavy quark (charm, beauty or bottom) mesons have several advantages over their light quark partners. They do not have the multitude of light quark mesons in their neighborhood. So their spectra are generally cleaner. Also, because α_S at heavy quark masses is smaller, and relativistic effects are weaker, perturbative predictions for heavy quark mesons are expected to be more reliable.

3.1 The Challenge of the Open Flavor Mesons

The open flavour mesons make the heavy-light system $(Q\bar{q},\ \overline{Q}q)$. Life is supposed to become simpler because the heavy quark Q (c or b), with spin S_Q, provides a more-or-less static core around which the light quark (u, d, s) with $j_q = l + S_q$ orbits. This gives rise to the heavy-quark effective theory, or HQET, for the heavy-light system with $J = j_q + S_Q$, which has been very successful.

3.1.1 The Open Charm or D Mesons (=$c\bar{n},\ c\bar{s}$)

In 2003, BaBar and CLEO discovered $D_s^*(c\bar{s})$, $J = 0^+$ and 1^+ mesons which were expected to lie above the thresholds for DK (2367 MeV) and DK^* (2508 MeV) and therefore to be wide. Instead, they turned out to have masses 2318 MeV and 2456 MeV, i.e., each 50 MeV below their respective thresholds, and both were < 5 MeV wide. As always, when the unexpected happens, there is no dearth of possible explanations for the observed mesons, $c\bar{s}$ displaced by mixing, DK molecules, tetraquark, etc., but there is no consensus. In the meanwhile, there are more challenges.

The analogues of $D_s^*(0^+, 1^+)$, the $D^*(\sim 2218, 0^+)$ and $D^*(\sim 2360, 1^+)$ which are expected to be broad have not yet been identified. Further, BaBar has announced a new relatively narrow D_s with $M/\Gamma = 2857/48$ MeV, and a broad D_s with $M/\Gamma = 2688/112$ MeV. Belle can not find $D_s(2857)$ and reports a $J^P = 1^-$ $D_s(2708)$, which is presumably the same as BaBar's, $D(2688)$. Are these radially excited D_s states? Time will tell, as more radially excited states are discovered.

3.1.2 The Open Beauty or B Mesons (=$b\bar{n},\ b\bar{s},\ b\bar{c}$)

This is the domain of CDF and DØ contributions, and they have made many precision measurements of B-mesons, $(B_1^0,\ B_{s1}^0)$, $(B_2^0,\ B_{s2}^0)$. The latest triumph is a precision measurement of the B_c meson, $M(B_c) = 6274.1 \pm 4.1$ MeV.

A remarkable, at least to me, conclusion is that the B_s mesons are always 100 ± 5 MeV heavier than the B mesons. This is exactly what was observed for the D-mesons. It looks like that the s-quark marble is just 100 MeV heavier than the u, d quark marbles. Life should always be so simple!

Of course, the main thrust in the study of the open flavor mesons is weak interactions, decay constants, form factors, and CKM matrix elements, and the

Standard Model. CLEO and CDF, DØ, Belle, and BaBar have been working hard on these measurements, and comparison with lattice predictions, but I will continue to confine myself to strong interactions.

Let me now turn to Quarkonia, $c\bar{c}$ charmonium, $b\bar{b}$ bottomonium, and the newly discovered surprising states.

3.2 Quarkonia: The Hidden–Flavour Mesons

The $SU(3)$ light quarks have such similar masses (within 100 MeV) that it is difficult, and even meaningless, to look for pure $u\bar{u}$, $d\bar{d}$, $s\bar{s}$ mesons. They invariably mix (despite the near purity of ϕ as a $s\bar{s}$). However, the charm quark and the bottom quark have much different masses and essentially do not mix with other flavors. So we have pure $c\bar{c}$ charmonium and $b\bar{b}$ bottomonium. By far the greatest activity in strong interaction physics has been in the charmonium region, which I define as $\sim 3-5$ GeV. So let me begin with charmonium and what has come to be known as charmonium-like mesons.

3.2.1 Challenges in Charmonium Spectroscopy

We are all familiar with the story of the discovery of J/ψ and the beginning of the QCD era with it. Over the years tremendous activity followed at SLAC, Frascati, DESY, ORSAY, and more recently at Fermilab, CLEO, and BES in laying down the QCD–based foundation of quarkonium spectroscopy. BES and CLEO have in recent years made many high precision measurements of decays of bound charmonium states, but here I want to talk about several recent discoveries.

(a) The Spin–Singlet States

A close examination of the spectroscopy of charmonium states will reveal that most of what was discovered and studied until recently was about **spin–triplet states**, the $\psi(^3S_1)$, $\chi_{cJ}(^3P_J)$ states of charmonium and $\Upsilon(^3S_1)$, $\chi_{bJ}(^3P_1)$ states of bottomonium. The **spin–singlet states** were too difficult to access, and remained unidentified (with the exception of $\eta_c(1^1S_0)$). This meant that we had very little knowledge of the hyperfine interaction which splits the spin–singlet and spin–triplet states.

To emphasize the importance of the spin–spin, or hyperfine interaction, let me remind you (as Prof. Miani also did) of the textbook discussion of the

ground state meson masses in the elementary quark model, i.e.,

$$M(q_1\bar{q}_2) = m(q_1) + m(q_2) + \frac{8\pi\alpha_S}{9m_1m_2}|\psi(0)|^2\vec{\sigma}_1\cdot\vec{\sigma}_2$$

In other words, the only ingredient required other than the quark masses is the spin–spin, $\vec{\sigma}_1\cdot\vec{\sigma}_2$ interaction. It is, of course, the same interaction which gives rise to the hyperfine, or spin–singlet/triplet splitting in quarkonium spectra.

Yet, until very recently, all that we knew was the singlet–triplet splitting for $\eta_c(1^1S_0)$ and $J/\psi(1^3S_1)$, with $\Delta M_{hf}(1S) = 117\pm 2$ MeV. We knew nothing about whether the hyperfine interaction varies with the radial quantum number or quark mass, or what all of it means with respect to the spin dependence of the long range $q\bar{q}$ interaction which is dominated by its confinement part.

The $\eta_c(2^1S_0)$ State

The breakthrough came in 2003 with the identification of $\eta_c'(2^1S_0)$ by Belle, CLEO, and BaBar. The result, $\Delta M_{hf}(2S) = 48 \pm 2$ MeV, nearly 1/3 of $\Delta M_{hf}(1S)$ came as a surprise. Although one or another potential model calculator will tell you that this was no surprise, the fact is that they were fully at peace with the old (wrong by $\sim$ factor two) Crystal Ball value, $\Delta M_{hf}(2S) = 92 \pm 5$ MeV. The most common explanation offered for the present result is that it is due to mixing with the continuum states, but in my mind a still-open possibility is the existence of a long–range spin–spin interaction in the confinement region.

The $h_c(1^1P_1)$ State

The second breakthrough in the understanding of the hyperfine interaction comes from the even more recent identification of the P–wave singlet state $h_c(1^1P_1)$, which had eluded numerous earlier attempts. Two years ago, CLEO announced the discovery of h_c in both inclusive and exclusive analysis of the isospin–forbidden reaction

$$\psi(2S) \to \pi^0 h_c,\ h_c \to \gamma\eta_c,\ \pi^0 \to 2\gamma$$

The data, based on $\sim$ 3 million $\psi(2S)$, had limited statistical precision, as did a recent E835 attempt. Now CLEO has analyzed their latest data for 24 million $\psi(2S)$. More than a thousand h_c have been identified, illustrating the adage that yesterday's "enhancement" can become today's full–blown

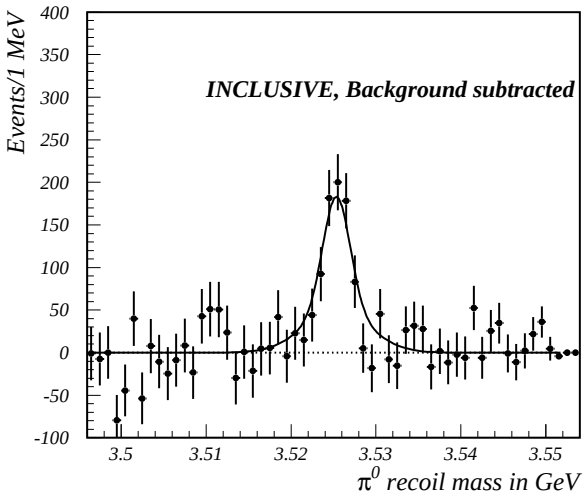

Figure 8: Background subtracted CLEO spectrum for h_c for the inclusive analysis of 24 million $\psi(2S)$.

resonance (see Fig. 8). The precision result obtained by CLEO is

$$M(h_c) = 3525.34 \pm 0.19 \pm 0.14 \text{ MeV},$$

which leads to

$$\Delta M_{hf}(1P) \equiv M(\langle {}^3P_J \rangle) - M({}^1P_1) = -0.04 \pm 0.19 \pm 0.15 \text{ MeV}.$$

This would appear to be just what one expected, because the one-gluon exchange hyperfine interaction is supposed to be a contact interaction and therefore non-existent in $L \neq 0$ states, i.e., $\Delta M_{hf}(1P) = 0$. Actually, the above experimental result is based on determining

$$M({}^3P_J) = M|\langle {}^3P_J \rangle| = (5M({}^3P_2) + 3M({}^3P_1) + M({}^3P_0))/9.$$

J. M. Richard and A. Martin have repeatedly pointed out that this is the wrong way to determine $M({}^3P_J)$, because the $L \cdot S$ splitting of ${}^3P_J$ states is not

perturbatively small, being 141 MeV. The correct way to determine $M(^3P_J)$ and $\Delta M_{hf}(1P)$ is to turn the $L\cdot S$ and T interactions off and directly determine $M(^3P_J)$ and $M(^1P_1)$. In fact, when this is done in a typical potential model calculation with no explicit long-range hyperfine interaction, $\Delta M_{hf} = 9$ MeV is obtained. So how can we explain the $\Delta M_{hf}(1P) = 0$ experimental result? Apparently, there are subtle problems connected with the regularization of the spin–dependent interactions, and nobody really knows how to handle these subtleties.

In any case, with η_c' and h_c identified, the spectrum of the bound states of charmonium is now complete, and we can move on to the unbound states above the $D\overline{D}$ threshold at 3739 MeV.

(b) Charmonium-like States, or The Bounty of Unexpected States Above $D\overline{D}$

The vector states $\psi(3770, 4040, 4160, 4415)$ above the $D\overline{D}$ threshold at 3.74 GeV have been known for a long time. However, little more than their total and leptonic widths was known. Now we know a lot more. CLEO and BES, and more recently Belle, have contributed much new information about their decays into $D\overline{D}$, $D\overline{D}_s$, $D_s\overline{D}_s$. The CLEO work is primarily motivated by trying to find the optimum energies to run in order to produce maximum yields of D and D_s for weak interaction studies.

The real excitement in this domain of spectroscopy has come about by the discovery of seveeral unexpected states by the B-factories of Belle and BaBar. It began with X(3872). Then came the states X, Y, Z with nearly degenerate masses of 3940 MeV. This was followed by Y(4260). And now we have reports of Y(4360), Y(4660), X(4160), and $\mathrm{Z}^{\pm}$(4433).

All these states decay into final states containing a c quark and a $\bar{c}$ quark, hence the designation "charmonium-like". Another point worth noticing is that while X(3872) and Y(4260) have been observed by several laboratories, and X(4360) perhaps by both Belle and BaBar, the X, Y, Z(3940), X(4160), and X(4660) have been only reported by Belle, with an ominous silence by BaBar. And finally, even a charged state $Z^{\pm}(4433)$ has just been claimed by Belle!

The Challenge of X(3872)

Of all the unexpected new states, only X(3872) is firmly established as a single narrow resonance with

$$M(\mathrm{X}(3872)) = 3871.4 \pm 0.6 \text{ MeV}, \quad \Gamma(\mathrm{X}) < 2.3 \text{ MeV}$$

From the beautiful angular correlation studies done by CDF, its spin is limited to $J^{PC} = 1^{++}$ or 2^{-+}. The discovery mode of its decay was X(3872)$\rightarrow$ $\pi^+\pi^- J/\psi$, but many other modes have been studied since. There were originally many theoretical suggestions for the nature of X(3872), but the limited choice of spin now only allows 1^{++} $\chi'_{c1}(2^3P_1)$ or $2^{-+}(1^1D_2)$ in the charmonium option, and 1^{++} in the popular $D\overline{D}^*$ molecule or tetraquark options, which were among the first and almost obvious suggestions made because of the very close proximity of $M(\mathrm{X}(3872))$ to the sum of D^0 and D^{*0} masses. A recent precision measurement of the D^0 mass makes the binding energy of the molecule very small, 0.6 ± 0.6 MeV, which has a strong bearing on the D^0 and $\overline{D}^{*0}(\rightarrow \overline{D}^0\pi^0)$ falling apart. The challenge for the experimentalists is obviously to measure both $M(\mathrm{X}(3872))$ and $M(D^0)$ with even greater precision, so that even stricter limits on the $D^0\overline{D}^{0*}$ binding energy can be put. Also, Belle needs to measure the decay $\mathrm{X} \rightarrow D^0\overline{D}^0\pi^0$ with greater precision, because their present measurement is at strong odds with the prediction of the molecule model. Recently, the branching factor for X(3872) decaying to $\overline{D}^{*0}D^0$ has been reported. In order to explain its nearly factor 200 larger value than can be accomodated in the molecular model, it has been claimed that there is another resonance just a few MeV away. However, the experimental evidence for this is very shaky.

So what is X(3872)? I consider the question still open.

The Challenge of Y(4260)

The Y(4260) has been observed by BaBar, CLEO, and Belle in ISR production and decay into $\pi\pi J/\psi$. The production in ISR ensures that its spin is 1^{--}. The fact that its mass is precisely where $R \equiv \sigma(e^+e^- \rightarrow \text{hadrons})/\sigma(e^+e^- \rightarrow \mu^+\mu^-)$ has a deep minimum indicates that it is a very unusual vector. Also, all the charmonium vectors up to 4.4 GeV are spoken for. These problems with a charmonium interpretation have led to the suggestion that Y(4260) is a hybrid 1^{--}, and you have already heard impassioned advocacy of it. So I will stay

away from it, except to point out that if this is true, we should expect to see 1^{-+} and 0^{-+} hybrids at nearby lower masses.

On the experimental side, new problems have emerged. Belle has revived the question of whether Y(4260) is a single resonance or two, Y(4008) and Y$'$(4247). Not only that, Belle also reports that the peak positions of Y are different in its decays to $\pi^+\pi^- J/\psi$ and $\pi^+\pi^-\psi(2S)$ by ~ 120 MeV. So, what looked like a simple state, perhaps hybrid, now appears to be rather complicated, and the rush to judgement about its nature might be premature.

The Challenge of X, Y, Z(3940)

In quick succession Belle reported three different states produced in different initial channels, and decaying into different final states, but all having nearly identical masses. I will not go into the details which you have heard in several plenary and parallel talks, but will summarize the results in Table I.

My personal summary of the situation is that X and Z exist and their charmonium interpretation requires confirmation. I have serious doubts about Y. In fact, BaBar's recent attempt to confirm it leads to quite different parameters.

Ever More States

And now we have four more states. We are running out of alphabets now. These are states at 4160, 4360, and 4664 MeV decaying into $\psi(2S)\pi^+\pi^-$, and at 4433 MeV decaying into $\psi(2S)\pi^\pm$, as listed in Table II. BaBar does not confirm any of these.

I have to admit that the proliferation of these states is getting to be so much that one cannot help becoming incredulous. Will all these bumps survive? Unfortunately, yes! For no reason other than the fact that no other measurements appear to be possible in the near future to check them.

3.2.2 Challenges in Bottomonium Spectroscopy

In principle, the bottomonium system can lead to clearer insight into the onium spectroscopy, both because α_S is smaller ($\alpha_S \approx 0.2$) than for charmonium ($\alpha_S \approx 0.35$), and also because relativistic effects are smaller. However, $b\bar{b}$ cross sections are smaller, the states are denser, and no $p\bar{p}$ production has so far

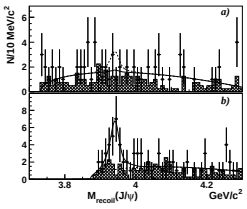	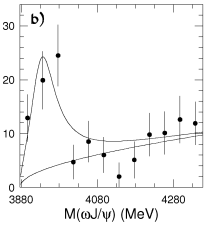	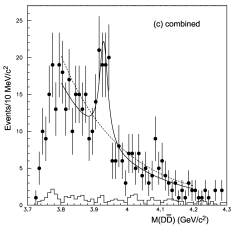
X(3943)	**Y(3943)**	**Z(3929)**
$N(\mathrm{X}) = 24.5\pm$	$N(\mathrm{Y}) = 58 \pm 11$	$N(\mathrm{X}) = 64 \pm 18$
$M(\mathrm{X}) = 3943 \pm 10$ MeV	$M(\mathrm{Y}) = 3943 \pm 17$ MeV	$M(\mathrm{Z}) = 3929 \pm 5$ MeV
$\Gamma(\mathrm{X}) = 15.4 \pm 10.1$ MeV	$\Gamma(\mathrm{Y}) = 87 \pm 26$ MeV	$\Gamma(\mathrm{Z}) = 20 \pm 8$ MeV
	Production	
Double Charmonium ($J = 0$?)	$B \to KY$	$\gamma\gamma$ fusion $J = 2$
	Decay	
$X \to D^*\overline{D} > 45\%$	$Y \to \omega J/\psi$	$Z \to D\overline{D}$
$X \nrightarrow D\overline{D} < 41\%$, $X \nrightarrow \omega J/\psi < 26\%$	$Y \nrightarrow D\overline{D}$	
	Best Guess	
$\eta_c''(3^1S_0)$	hybrid??	$\chi_{c2}'(2^3P_2)$
	Search for	
production in $\gamma\gamma$	decay in $D\overline{D}$, $D^*\overline{D}$	decay in $D^*\overline{D}$

Table 1: Spectra for X, Y, Z as observed by Belle. Details are listed below.

	Source	Mass (MeV)	Width (MeV)	Events	Reaction
X′	Belle	4160(30)	$139(^{113}_{65})$	$24(^{12}_{8})$	$e^+e^- \to J/\psi + D^*D^*$
X″	Belle	4360(13)	74(18)	~ 50	$e^+e^- \to \psi(2S)\pi^+\pi^-$
X‴	Belle	4664(12)	48(15)	~ 36	$e^+e^- \to \psi(2S)\pi^+\pi^-$
$\mathrm{Z}^\pm$	Belle	4433(4)	$45(^{35}_{18})$	121(30)	$B \to (K)\psi(2S)\pi^\pm$

Table 2: The new states announced by Belle.

been available. For the Upsilon (1^{--}) states, all we known is their masses, total widths, and branching fractions for leptonic, radiative, and $\Upsilon(nS) \to \pi^+\pi^-\Upsilon(n'S)$ decays. A scarce $\Upsilon(3S) \to \omega\chi_b(2S)$ transition has been observed, but huge gaps remain. By far the greatest gap is once again about the lack of any knowledge of singlet states. Even the ground state of bottomonium ($\eta_b(1^1S_0)$) has never been identified, and neither has $h_b(1^1P_1)$. Since nobody is presently planning e^+e^- or $p\bar{p}$ annihilations in new searches for η_b, the only possible source is CLEO, which has the largest samples of $\Upsilon(1S, 2S, 3S)$ data

from its earlier runs. Indeed, serious efforts are being presently made at CLEO to identify η_b in the radiative decay of $\Upsilon(1S)$.

This then is a great challenge — find η_b and h_b.

Of course, I have long had a dream of doing $b\bar{b}$ spectroscopy in $p\bar{p}$ annihilation. Unfortunately, neither a fixed target $p\bar{p}$ facility (needs about 50 GeV $\bar{p}$ beams), nor a $p\bar{p}$ collider (with ~ 6 GeV beams) appears to be on the horizon. So, this dream is not likely to be fulfilled anytime soon.

In the meantime, one long-cherished dream may come to fruition soon if CLEO is successful in identifying η_b.

4 Mesons in the Nuclear Medium

It has been conjectured for a long time that meson properties, notably their masses, widths, and elementary cross sections, should be modified in the nuclear medium. It has been predicted that the masses may change by tens of MeV, and widths may be broadened by large amounts. Also, cross sections for meson+A collisions should be quite different than meson+p collisions (color transparency). We are now beginning to get some answers, and as is always true, more questions.

It is claimed that color transparency has been experimentally observed at high energies, with some unexplained observations at lower energies. The interesting problem of J/ψ attenuation in heavy ion collisions, so important for the QGP question, remains provocatively open, because $\sigma(J/\psi - \text{nucleon})$ in nuclear medium remains unmeasured.

About mesons masses there are experimental controversies, for example, there are reports of a large shift in vector meson masses by KEK, and there are reports of almost no shift by JLab. The situation at the moment is fluid, and it calls for more measurements with high precision and high mass resolution.

To summarize my own talk, let me say that many, many extremely interesting questions in hadron spectroscopy remain unanswered at present. However, there is every hope that the upcoming facilities, PANDA at GSI, JPARC at KEK, and the 12 GeV upgrade at JLab, will rise to meet the challenges posed by these questions and the theorists will find them deserving of serious attention even in this era of the Higgs and Beyond the Standard Model!!

Epilogue

Since this is the last talk of the Conference, let me take the opportunity, on behalf of all of us, to thank the organizers for their warm welcome, a very pleasant and successful conference, and also for the beautiful Frascati weather!

LIGHT MESON SPECTROSCOPY

Frascati Physics Series Vol. XLVI (2007), pp. 435–443
HADRON07: XII Int. Conf. on Hadron Spectroscopy – Frascati, October 8-13, 2007
Light Meson Spectroscopy

EXCLUSIVE $\omega\pi^0$ PRODUCTION WITH MUONS

M. Bettinelli and W. Dünnweber
Universität München, D-85748 Garching, Germany

On behalf of the COMPASS Collaboration

Abstract

Using 160 GeV muon scattering data collected with the COMPASS Experiment at CERN, the exclusive production of $\omega\pi^0$ via virtual photons was studied. Selective population of a peak around 1250 MeV is observed. Possible contributions from spin-parity 1^- are searched for, inspecting decay angular correlations. In particular, the orientation of the ω decay plane may allow a distinction from the 1^+ $b_1(1235)$ state. Our observation is compared with indications of a $\rho'(1250)$ in annihilation and in γp.

1 Motivation

Identification of the radially excited ρ meson is debated since a long time [1) 2)]. An early photoproduction experiment [3)], using photons with energy between 20 and 70 GeV, observed an enhancement in the $\omega\pi^0$ channel with mass around 1250 MeV and width of about 200 MeV. For spin-parity analysis it was assumed that the produced meson retains the helicity of the incoming photon (s-channel helicity conservation, SCHC). A dominant 1^- contribution was deduced.

However, subsequent investigations at the CERN SPS [4] and at SLAC [5] employing linearly polarized photons, revealed a dominance of the well known $J^{PC} = 1^{+-}$ state $b_1(1235)$, leaving only about 20% for a $\rho'(1^{--})$ contribution at the same mass. Angular distributions were found inconsistent with SCHC in these experiments where the mean photon energy was 20–30 GeV.

Supportive evidence for a ρ' state at this mass came from a Crystal Barrel study [6] of the annihilation reaction $\bar{p}n \to \omega\pi^-\pi^0$, suggesting ρ excitations at 1200, 1400 and 1700 MeV. The lowest lying state stands out by dominant $\omega\pi$ decay, in contrast to other non-ω related 4π decays.

The experimental situation has been reviewed by Donnachie and Kalashnikova [2], including results from e^+e^- annihilation and τ decay. In their interpretation, two 1^{--} states with mixed configurations are present between the ground state $\rho(770)$ and the first orbital excitation (1^3D_1) $\rho'(1700)$: the one at 1250 MeV with dominant $q\bar{q}$ configuration 2^3S_1 (the radial ρ' excitation), decaying preferably via $\omega\pi$, and the heavier one at ∼1450 MeV, with dominant hybrid or quartet configuration, preferring alternative decay channels like e.g. $a_1\pi$.

Concerning b_1 and ρ' competition in photoproduction, it was suggested [7] that helicity-flip Regge exchange, resulting in b_1, prevails at the mean photon energies of Ref. [4] [5], while helicity conserving Pomeron exchange, resulting in ρ', wins at higher energy.

We report on the first study of $\omega\pi^0$ production with virtual, quasi-real photons in inelastic muon scattering. According to the suggested systematics [7], b_1 and ρ' production should be of comparable size at the available γ^*p c.m. energy W≈13 GeV.

2 Experimental setup

COMPASS [8] is a two stage magnetic spectrometer installed at the end of the M2 beam extraction line at the CERN SPS machine. The extracted μ^+ beam of an intensity of about $2{\cdot}10^8$ per spill, with 5 s spill length and 16 s repetition, had an energy of 160 GeV and a polarisation of about 80%. It was directed on a two-cells polarized ^{6}LiD target, where the (longitudinal) polarisation was + and − 56%.

Charged particle tracking involves silicon strip detectors, scintillation fibers, micromegas and GEMs at small angles and straw drift tubes and mul-

tiwire proportional chambers at large angles. In addition, muon-hadron separation is obtained with μ-filters.

For neutral particle detection in 2004 a lead glass detector, covering angles up to ± 35 mrad as viewed from the target, served as electromagnetic calorimeter (ECAL2).

3 Event selection

A data sample collected in 8 weeks of the 2004 COMPASS run was analyzed. To select the exclusive process

$$\mu + N \rightarrow \mu' + \omega(\pi^+\pi^-\pi^0)\pi^0 + N, \tag{1}$$

with $\pi^0 \rightarrow \gamma\gamma$, the following criteria were applied:

— a primary reaction vertex with an identified incoming and scattered μ and (only) two additional particles of opposite charge is fully reconstructed;
— 4 and only 4 clusters not associated with a reconstructed charged track are found in ECAL2. To reduce background, only clusters with energy above 1 GeV are accepted.
— π^0's are selected cutting on the 2 photon invariant mass, 120 MeV $< m(\gamma\gamma) <$ 150 MeV, and on the decay opening angle, $\theta_{\gamma\gamma} < 0.025$ rad;
— a ω candidate is selected imposing the cut 750 MeV $< m(\pi^+\pi^-\pi^0) <$ 815 MeV;
— exclusivity is defined by means of the missing energy

$$E_{miss} = \frac{M^2_{miss} - M^2_P}{2M_P}, \tag{2}$$

where M_P is the proton mass and M_{miss} is the missing mass. The exclusive $\omega\pi^0$ final sample is selected with the cut $-6 < E_{miss} < 4$ GeV.

Figure 1, left, shows the missing energy versus the 4π invariant mass for events with a uniquely identified $\omega\pi^0$ without the exclusivity cut: evident is the presence of an exclusive sample around $E_{miss} = 0$. The E_{miss} window used for selection was adapted to the exclusivity peak visible in the projection (right).

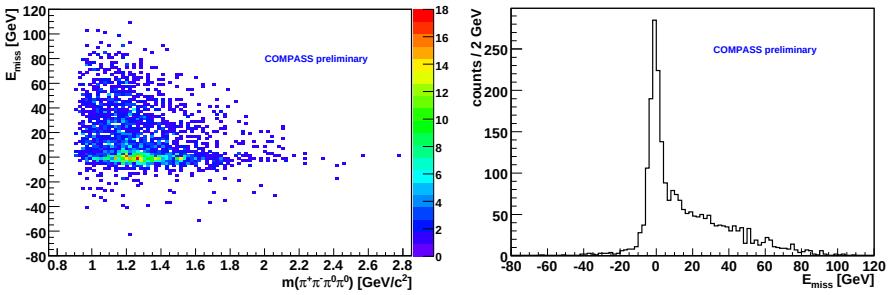

Figure 1: *Missing energy E_{miss} vs. $\pi^+\pi^-\pi^0\pi^0$ invariant mass for events with a single reconstructed $\omega(\pi^+\pi^-\pi^0)\pi^0$ (left) and projection on the E_{miss} axis (right).*

4 Results

Figure 2 shows the $\omega\pi^0$ invariant mass spectrum. A peak with a mean value of about 1250 MeV and a width of about 300 MeV is observed. Its shape and the selectivity for this peak is not strongly affected by the experimental acceptance (not corrected for), which decreases almost linearly from threshold (915 MeV) to 2800 MeV by a factor of 3. The peak features are consistent with the results of the quoted photoproduction experiments.

To access non-ω background, the $\pi^+\pi^-\pi^0$ invariant mass cut was somewhat relaxed. Figure 3 (left) shows the 3π versus the 4π invariant mass: events in the ω mass region correspond to the 4π invariant mass interval around 1250 MeV. The projection on the 3π mass axis (right), puts in evidence the ω contribution; the width is due to the experimental resolution.

For a quantitative determination of the non-ω background, we have considered the λ distribution, defined by

$$\lambda = \frac{|\vec{p_1} \times \vec{p_2}|^2}{|\vec{p_1} \times \vec{p_2}|^2_{max}}, \tag{3}$$

where $\vec{p_1}$ and $\vec{p_2}$ are the momenta of any two of the three pions. In this analysis, the two charged ones were chosen. The observed linear increase of the intensity with λ is a unique signature of $J^P = 1^-$, already applied in the original J^P assignment for the ω [9]. In contrast, the λ distribution for events outside the exclusivity window is flat. From the linear fit in figure 4, we deduce a

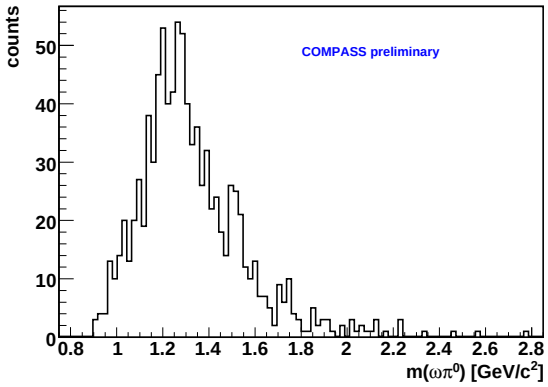

Figure 2: *Invariant mass spectrum of exclusively produced* $\omega\pi^0$*. The acceptance (not corrected for) decreases by 50% from 1 to 2* GeV/c^2*.*

background contribution of 12% in the final sample.

Figure 5 shows some important kinematic distributions for the final sample: the virtual photon mass squared $Q^2 = -q^2$, the Bjorken scale variable x_B, the $\gamma^* p$ center of mass energy W, and the $\omega\pi^0$ momentum in the laboratory system. The mean value of the latter corresponds to $E(\gamma^*) \approx 90$ GeV. The 4-momentum transfer squared $t = (q - v)^2$ (not shown) is characterized by an exponential shape, as is typical of diffractive processes.

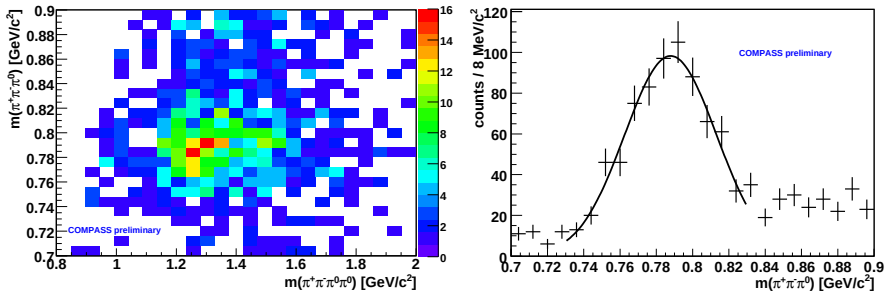

Figure 3: 3π *vs.* 4π *invariant mass for events in the exclusivity region (left) and corresponding* 3π *mass projection (right).*

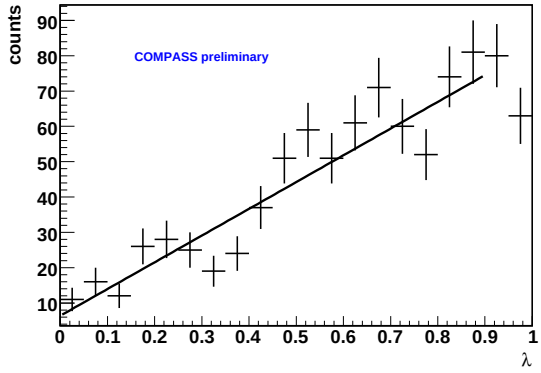

Figure 4: λ *distribution, eq. (3).*

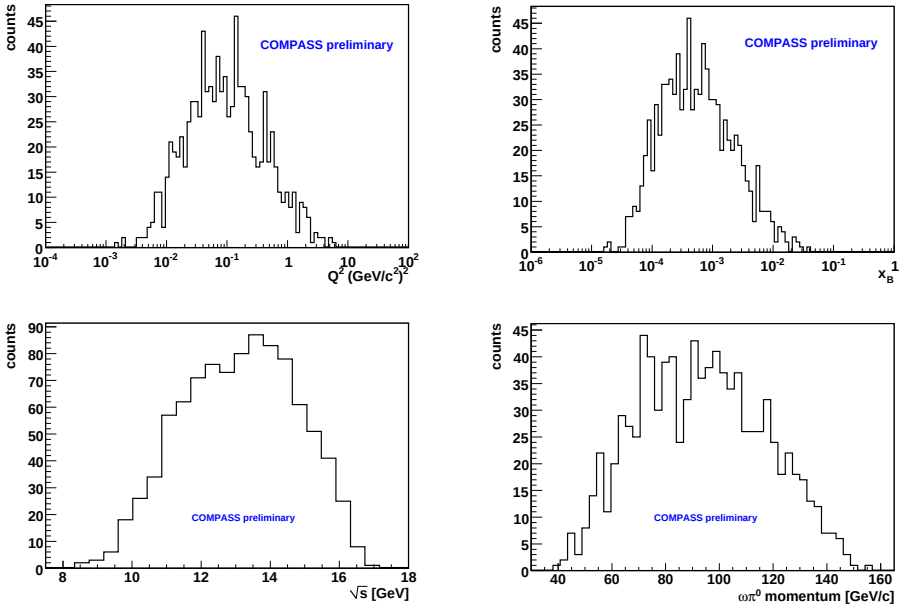

Figure 5: *Kinematic distributions for the exclusive* $\omega\pi^0$ *final sample (not acceptance corrected). Top-left: Virtual photon mass squared* Q^2*; Top-right: Bjorken scale variable; Bottom-left:* $\gamma^* p$ *c.m. energy W; Bottom-right:* $\omega\pi^0$ *momentum in laboratory frame.*

5 Angular distributions

Three types of angular correlations are suited for spin-parity studies. The first two characterize the decay of the $\omega\pi^0$ resonance:

(i) the angle ψ of the ω momentum $\vec{p}_\omega$ relative to the $\omega\pi^0$ direction (reference axis z) in the overall $\gamma^* p$ c.m. system;
(ii) the angle θ between the vector $\vec{n}_\omega$ perpendicular to the ω decay plane (in the ω rest frame) and the z axis.

For electroproduction via quasi-real photons, one can assume linear polarization of the γ^* in the primary scattering plane and adopt the corresponding angular correlation formalism [10]. Following Ballam *et al.* [11], we define appropriate "spin analyzers" $\vec{a} = \vec{n}_\omega \times \vec{p}_\omega$ and $\vec{a} = \vec{n}_\omega$ for $J^P = 1^-$ and 1^+ states, respectively. Their direction with respect to the γ^* polarization is described by:

(iii) the azimuthal angle Ψ between μ scattering plane and $\vec{a}$.

Assuming SCHC, the two sets of angular distributions in table 1 are predicted [3] for the two different J^P assignments to $\omega\pi^0$. The quantity $x \approx 0.07$ is the known D/S-wave amplitude ratio squared of b_1.

Monte Carlo simulations for pure 1^+ and 1^- states reveal a strong acceptance dependance of the distribution (i), whereas (ii) is only weakly affected. As shown in figure 6, the characteristic shapes of $I(cos\theta)$ are roughly maintained after taking into account detector and selection acceptance. Our preliminary experimental results (not shown) are in favour of the 1^- case. However the dependence on the SCHC assumption should be kept in mind. This holds as well for the distribution (iii), which shows an indication of a $cos2\Psi$ contribution, characteristic of $J^P = 1^-$. Interference between S- and P-wave, corresponding to 1^+ and 1^- decay in $\omega\pi^0$, would give rise to a forward-backward anisotropy in

Table 1: *Decay angular distributions for $J^P = 1^\pm$ assignments to $\omega\pi^0$.*

J^P	$I(cos\psi)$	$I(cos\theta)$
1^+ $(b_1(1235))$	$\sim 1 + xcos^2\psi$	$\sim sin^2\theta$
1^- (ρ')	$\sim 1 + cos^2\psi$	$\sim 1 + cos^2\theta$

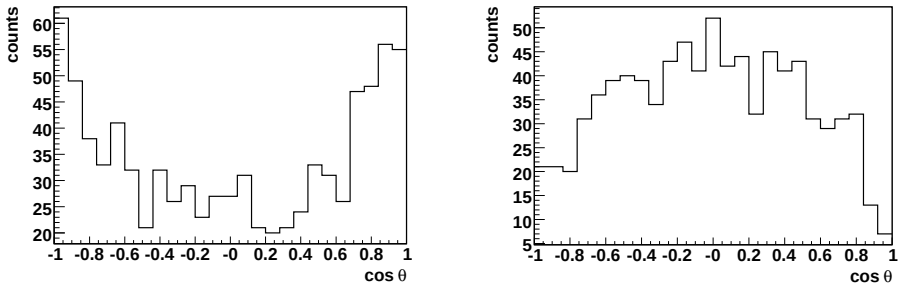

Figure 6: *Estimate of the cosθ distributions, based on Monte Carlo simulations of the detector and selection acceptance, for* $J^P(\omega\pi^0) = 1^-$ *(left) and* 1^+ *(right).*

the distribution (i), irrespective of the SCHC assumption. Detailed acceptance studies are required for partial-wave decomposition of this distribution.

6 Conclusion

We have observed the exclusive production of $\omega\pi^0$ in muon scattering via virtual photons in the energy range around 90 GeV lab. energy. The mass spectrum is dominated by a peak at 1250 MeV and width 300 MeV, which is consistent with previous photoproduction experiments. Preliminary results on angular correlations are consistent with the presence of a 1^- contribution, if SCHC holds. An appreciable increase in statistics is expected with the 2006 and 2007 COMPASS data.

7 Acknowledgements

We would like to thank Drs. A. Donnachie, D. Ryabchikov and Č. Zupančič for helpful discussions. This research was supported by the DFG cluster of excellence Origin and Structure of the Universe (www.universe-cluster.de) and by the BMBF.

References

1. A. Donnachie, Y. S. Kalashnikova, Phys. Rev. **D60**, 114011 (1999).

2. A. Donnachie, Y. S. Kalashnikova, Proc. HADRON 01, AIP Conf. Proc. 619, p. 5 (2002).

3. D. Aston *et al.*, Phys. Lett., **92B**, 211 (1980).

4. M. Atkinson *et al.*, Nucl. Phys., **B243**, 1 (1984).

5. J. E. Brau *et al.*, Phys. Rev. **D37**, 2379 (1988).

6. Crystal Barrel Collaboration, C. Amsler *et al.*, Nucl. Phys., **A 740**, 130 (2004).

7. A. Donnachie, Phys. Lett. **B611**, 255 (2005).

8. COMPASS Collaboration, P. Abbon *et al.*, Nucl. Instr. Meth. **A 577**, 455 (2007).

9. M. L. Stevenson *et al.*, Phys. Rev., **125**, 687 (1962).

10. K. Schilling, G. Wolf, Nucl. Phys. **B61**, 381 (1973).

11. J. Ballam *et al.*, Nucl. Phys. **B76**, 375 (1974).

Frascati Physics Series Vol. XLVI (2007), pp. 445–454
HADRON07: XII Int. Conf. on Hadron Spectroscopy – Frascati, October 8-13, 2007
Light Meson Spectroscopy

FURTHER PROPERTIES OF EXTRA LIGHT VECTOR MESON $\omega'(1300)$ AND $\rho'(1300)$

Ichiro Yamauchi
Tokyo Metropolitan Collage of Industrial Technology Tokyo, 140-0011, Japan
Toshiko Komada
Nihon University, Chiba 274-8501, Japan

Abstract

Previously we have presented some indication of existence of low-mass extra vector mesons $\omega'(1300)$ and $\rho'(1300)$ by analyzing the relevant data on mass spectra of $\pi^+\pi^-\pi^0$ and $\omega\pi^0$ system, respectively, in e^+e^- annihilation.

In this work we reanalyze the data, focusing on the relative phases of photon-vector couplings among all low-mass vectors, $\omega(782)$, $\rho(770)$ and the extra vector mesons, and show that the results are in favor of the prediction of the covariant classification scheme $\widetilde{U}(12)_{SF}$.

1 Introduction

Existence of low mass extra vector mesons $\omega'(1300)$ and $\rho'(1300)$, other than conventional $\rho(770)$ nonet, have been controversial for long time[1)]. In a previous work at HADRON '05, we presented some indication of existence of

these extra vector mesons, and gave preliminary values of their resonance parameters[2]. The ρ-like mesons ($\rho(1250)$, $\rho(1450)$, $\rho(1600)$) in $\pi\pi$ scattering are reported at this HADRON '07 by Yu.S. Surovtsev and P. Bydžovský.[3] And there is some enhancement around 1250 MeV, $J^{PC} = 1^{--}$ in $\omega\pi^0$mass distribution of photoproduction experiment at COMPASS Collaboration, which are reported by M. Bettinelli also at this HADRON '07.[4]

In order to get the more reliable values for mass, width and production coupling of the relevant resonances, we are going to reanalyze in this work carefully the mass spectra of $\pi^+\pi^-\pi^0$ and $\omega\pi^0$ systems in the e^+e^- annihilation obtained by the several experiments; SND[5] and BABAR[6] for the former and CMD-2[7], SND[8] and DM2[9] for the latter, respectively.

We give a special attention on the relative phases between ω and ω', and between ρ and ρ', and on the magnitude of these amplitudes.

Recently the $\widetilde{U}(12)$ level-classification scheme of hadrons has been proposed[10], which is a covariant generalization of non-relativistic scheme based on $SU(6)_{SF}$. In this scheme, the extra vector meson nonet is predicted to exist in the ground S-wave state of $(q\bar{q})$ system, and to have opposite sign[11] of production amplitude.

The results of these phenomenological analyses seem to be favorable to identify the extra-vector mesons as the relativistic S-wave states, out of conventional framework.

2 Analysis of the $e^+e^- \to \pi^+\pi^-\pi^0$ and indication of extra vector meson $\omega'(1300)$

In this work we are going to reanalyze the combined mass spectrum of the $\pi^+\pi^-\pi^0$ data in the e^+e^- annihilation obtained by SND[5] and by BABAR[6]. The former presents high statistics data at the lower mass region and the latter covers the whole mass region interested.

The relevant process $e^+e^- \to \pi^+\pi^-\pi^0$ is, applying the vector meson dominance model (VMD), considered to occur dominantly through intermediate production of vector meson "VM" as that $e^+e^- \to \gamma \to$"VM"$\to \rho\pi \to 3\pi$. The analysis results obtained by SND and by BABAR show vectors, $\omega(782)$, $\phi(1020)$ (hereafter we denote ω and ϕ shortly), $\omega(1420)$ and $\omega(1650)$, but no $\omega(1250)$. The width parameter for $\omega(1420)$ is obtained to be rather wider in each analysis, as shown in Table 1. It is recognized, however, a huge event

Table 1: Masses and widths of $\omega(1420)$ in $e^+e^- \to \pi^+\pi^-\pi^0$.

$\omega(1420)$	M (MeV)	Γ (MeV)
BABAR[6]	$1350 \pm 20 \pm 20$	$450 \pm 70 \pm 70$
SND[5]	$1400 \pm 50 \pm 130$	$870^{+500}_{-300} \pm 450$
PDG	1400 – 1450	180 – 250

accumulation exists around 1.3 GeV/c^2 in the 3π mass spectrum. It may be naturally interpreted to correspond to the $\omega(1200)$, which was pointed out in ref. 12, rather than $\omega(1420)$.

In order to make clear the situation on the existence of $\omega(1200)$, a possible contribution of a low mass state $\omega'(1300)$ instead of $\omega(1200)$ is considered explicitly in this work in addition to the higher vector mesons $\omega(1420)$ and $\omega(1650)$.

2.1 Method of analysis

The cross section formula for relevant process shown in Fig. 1, is given as

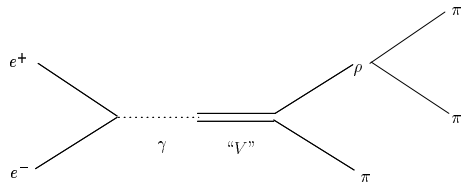

Figure 1: Diagram of $e^+e^- \to \pi^+\pi^-\pi^0$

$$\sigma(s) = \frac{4\pi\alpha^2}{s^{\frac{3}{2}}}(\frac{g_{\omega\rho\pi}}{3f_\omega})^2 \left| A_\omega \frac{m_\omega^2\sqrt{F_\omega(s)}}{m_\omega^2 - s - im_\omega\Gamma_\omega} + A_\phi \frac{e^{i\theta_{\omega\phi}} m_\phi^2\sqrt{F_\phi(s)}}{m_\phi^2 - s - im_\phi\Gamma_\phi} + \sum_{i=1}^{3} A_i \frac{m_{\omega_i}^2\sqrt{F_{\omega_i}(s)}}{m_{\omega_i}^2 - s - im_{\omega_i}\Gamma_{\omega_i}} \right|^2 4\pi\Gamma_\rho, \quad (2.1)$$

where ω_1, ω_2 and ω_3 denote vector states above 1 GeV/c^2. In Eq. (2.1) we have introduced form factor F for respective resonances

$$F_R(s) = \frac{2m_R^2}{m_R^2 + s}\ , \quad (2.2)$$

and the photon-vector coupling parameters A_i for ω_i (i=1,2,3), defined by

$$A_\phi = \frac{(\frac{-\sqrt{2}g_{\phi\rho\pi}}{3f_\phi})}{(\frac{g_{\omega\rho\pi}}{3f_\omega})} = -\sqrt{2}\frac{f_\omega}{f_\phi}\frac{g_{\phi\rho\pi}}{g_{\omega\rho\pi}}, \quad A_i = \frac{(\frac{g_{\omega_i\rho\pi}}{3f_{\omega_i}})}{(\frac{g_{\omega\rho\pi}}{3f_\omega})} = \frac{f_\omega}{f_{\omega_i}}\frac{g_{\omega_i\rho\pi}}{g_{\omega\rho\pi}}, i = 1, 2, 3. \tag{2.3}$$

In Eq. (2.1) the argument s is invariant mass square of 3π system, and the common factor Γ_ρ, 2π decay width of $\rho(770)$ is irrelevant to our analysis. In Eq. (2.3) A_i's are treated as fitting parameters, while the values of A_ω, $A\phi$ and $\theta\omega\phi$ have been estimated from the relevant low mass data.

There are contrastive structures in the relevant data below and above 1 GeV. Below 1 GeV region the data has two clear and huge peaks coming from ω and ϕ, while above 1 GeV region it shows some complex structures[5)6)].

Before the 3π mass spectrum of $e^+e^- \to \pi^+\pi^-\pi^0$ in the relevant energy region from 1.06 to 2.0 GeV by BABAR and by SND is analyzed, the constant parameters $A\omega$, $A\phi$ and $\theta\omega\phi$ of the relative phase between ω and ϕ in Eq. (2.1) are necessary to be fixed by analysis of the spectrum below 1 GeV.

2.2 Results of analysis

In the $\theta\omega\phi$ scan, the resonance parameters of ω, ϕ are restricted to be consistent with PDG tables[13)] . Then $\theta\omega\phi$ is fixed at 202.5 deg.. The value of other parameters are used as initial values, as described in the following two cases of analysis, respectively.

In the first case, the values of mass and width of ω_3, corresponding to $\omega(1650)$, are restricted to be consistent with PDG tables[13)], while the parameters of $\omega_1$are not restricted. In this case, the experimental data are well reproduced. Obtained values of mass and width of ω_1 is lower and wider, respectively compared with PDG values of $\omega(1420)$.

In the second case, the values of mass and width of ω_2 and ω_3, corresponding $\omega(1420)$ and $\omega(1650)$, are restricted to be consistent with PDG tables[13)], while the parameters of ω_1, supposed to be corresponding to the extra $\omega'(1300)$, are not restricted. In this case, the experimental data are also well reproduced, where contributions of ω_1 and ω_3 are large, while ω_2 is very small.

The results of two cases are shown in Fig. 2(a) and Fig. 2(b). The obtained values of parameters and $\chi^2/N_{d.o.f.}$ in the two cases are listed in Table 2. The almost same values of $\chi^2/N_{d.o.f.}$ are obtained in the two cases. This reflects that the contribution of $\omega(1420)$ in the second case is very small. The result of fitting of the second case indicates the existence of $\omega'(1300)$ in addition to the higher state $\omega(1650)$. The relative phase between ω, $\omega'(1300)$, $\omega(1420)$ and $\omega(1650)$ are $+$, $-$, $-$, $-$ in the second case. In first case the relative phase between ω, $\omega'(1300)$ and $\omega(1650)$ are $+$, $-$ and $-$, respectively.

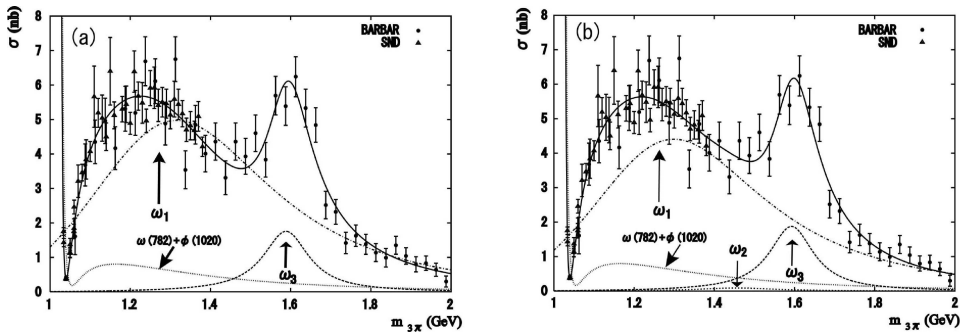

Figure 2: Results of analysis on 3π mass specturm of $e^+e^- \to \pi^+\pi^-\pi^0$ from SND and BABAR. Solid line is fitted curve and dotted lines present the contribution of each amplitude. (a) fit with $\omega_1$and ω_3 (b) fit with ω_1, ω_2 and ω_3.

Table 2: The obtained value of parameters and $\chi^2/N_{d.o.f.}$ in the analysis of the first and second cases.

	First case (with $\omega(1300)$ and $\omega(1650)$)			Second case (with $\omega(1300)$, $\omega(1420)$ and $\omega(1650)$)		
	$\omega(1300)$	$\omega(1420)$	$\omega(1650)$	$\omega(1300)$	$\omega(1420)$	$\omega(1650)$
χ^2	170			168		
$N_D - N_P$	$155 - 14 = 141$			$155 - 17 = 138$		
$\widetilde{\chi^2}$	1.21			1.22		
M(MeV)	1243±2	—	1588±5	1229±14	1450	1592±6
Γ(MeV)	672±5	—	139±5	635±55	250	135±19
A	−0.530 ±0.003	—	−0.039 ±0.001	−0.486 ±0.076	−0.019 ±0.012	−0.039 ±0.007

3 Analysis of the $e^+e^- \to \omega\pi^0$ and indication of extra vector meson $\rho'(1300)$

In this work we are also going to reanalyze the combined mass spectrum of the $\omega\pi^0$ data in e^+e^- annihilation obtained by CMD-2[7], by SND[8]and by DM2[9]. The process is also, applying the VMD, considered to occur dominantly through intermediate production of vector mesons "V" as that $e^+e^- \to \gamma \to$"VM"$\to$

$\rho\pi \rightarrow \omega\pi^0$. The analysis results obtained by CMD-2 show vectors, $\rho(770)$, $\rho(1450)$ and $\rho(1700)$, while mass and width value of $\rho(1450)$ are scattered in each study[13]. There is recognized a huge event accumulation around 1.3 GeV in the $\omega\pi^0$ mass spectrum. It may be naturally interpreted to correspond to the $\rho'(1300)$ with mass around 1.3 GeV which has a lower mass than $\rho(1450)$. Actually the existence of $\rho'(1300)$ was pointed out by several experimental groups[14)15)] and in review articles.[16)13)]

In order to make clear the situation on the existence of extra light-vector mesons, a possible contribution of $\rho'(1300)$ is also considered explicitly in the present work in addition to the higher vector mesons $\rho(1450)$ and $\rho(1700)$.

3.1 Method of analysis

The relevant processes is shown in Fig. 3.

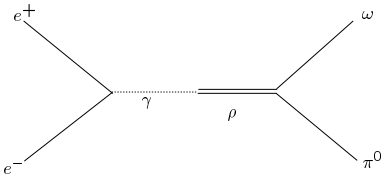

Figure 3: Diagram of $e^+e^- \rightarrow \omega\pi^0$

The formula of cross section for the relevant process is given as

$$\sigma_0(s) = \frac{4\pi\alpha^2}{s^{\frac{3}{2}}} \left(\frac{g_{\rho\omega\pi}}{f_\rho}\right)^2 \left| \frac{m_\rho^2\sqrt{F_\rho(s)}}{D_\rho(s)} + \sum_{i=1}^{3} A_i \frac{m_{\rho_i}^2\sqrt{F_{\rho_i}(s)}}{m_{\rho_i}^2 - s - i m_{\rho_i}\Gamma_{\rho_i}} \right|^2 P_f(s), \quad (3.1)$$

where

$$F_R(s) = \frac{2m_R^2}{m_R^2+s} \quad , \quad P_f(s) = \frac{1}{3}|\mathbf{p}_\omega(s)|^3 \cdot B_{\omega\rightarrow\pi^0\gamma} \quad . \quad (3.2)$$

Here $\mathbf{p}_\omega(s)$ is three momentum of ω in ρ at rest and $B_{\omega\rightarrow\pi^0\gamma}$ is branching ratio of $\omega \rightarrow \pi^0\gamma$ to be 0.085±0.005. The coupling constants are estimated by VMD using experimental values to be f_ρ= 5.04 and $g_{\rho\omega\pi} = 12.47$. A_i's are the fitting parameters.

3.2 Results of analysis

The $\omega\pi$ mass spectrum of $e^+e^- \rightarrow \omega\pi^0$ below 2.2 GeV is used in the analysis. We analyze the spectrum in the following two cases, similarly as ω's analysis in section 2. In the first case, two resonances are considered above 1 GeV region,

where the values of mass and width of ρ_3, corresponding to $\rho(1700)$, are restricted to be consistent with PDG tables[13], while the parameters of ρ_1 are not restricted. In this case, the experimental data are well reproduced, although obtained values of mass and width of ρ_1 are lower and wider, respectively. In the second case three resonances are considered above 1 GeV region, the values of mass and width of ρ_2 and ρ_3, corresponding to $\rho(1450)$ and $\rho(1700)$, respectively, are restricted to be consistent with PDG tables[13], while the parameters of ρ_1 are not restricted. The results are obtained similarly as ω's case that experimental data are well reproduced, where the contribution of ρ_1 is large, while those of ρ_2 and ρ_3 are very small comparing to that of ρ_1.

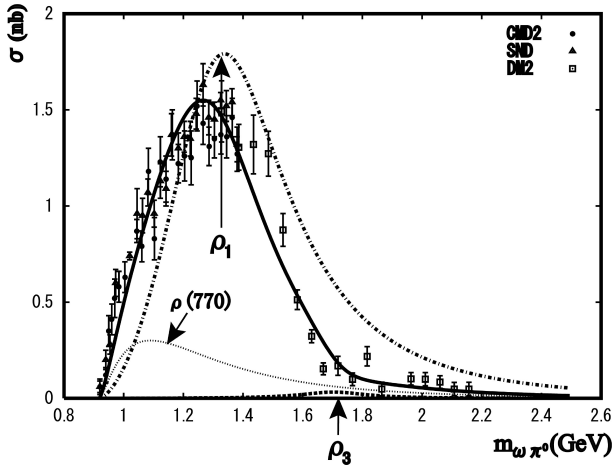

Figure 4: Results of analysis (fit with ρ_1 and ρ_3) on $\omega\pi^0$ mass spectrum of $e^+e^- \to \omega\pi^0$ data CMD-2, SND and DM2. Solid line is fitted curve and dotted lines represent the contribution of each amplitude.

Table 3: The obtained value of parameters and $\chi^2/N_{d.o.f.}$ with (ρ_1 and ρ_3)

	$\rho(1300)$	$\rho(1450)$	$\rho(1700)$
	$\frac{\chi^2}{N_D - N_P} = \frac{214}{65-7} = 3.69$		
$m[MeV]$	1264 ± 2	—	1700
$\Gamma[MeV]$	560 ± 4	—	267
A	-0.524 ± 0.003	—	0.017 ± 0.003

The almost same values of $\chi^2/N_{d.o.f.}$ are obtained in the two cases. It shows that the analysis results of the first case are acceptable. The results of the first and second cases indicate strongly the existence of the low mass extra vector meson $\rho'(1300)$, while $\rho(1450)$ and $\rho(1700)$ signals are very weak in this process. The results of fitting in comparison with experiments in the first case are shown in Fig. 4. The obtained values of resonance parameters and $\chi^2/N_{d.o.f.}$ in this case are listed in Table 3.

It may be noted that CMD-2 data and SND data cover below 1.4 GeV of $\omega\pi$ mass spectrum, while the DM2 data cover above 1.4 GeV. The combined data of two regions below and above 1.4 GeV are used[1] in the present analysis.

4 Concluding Remarks

4.1 Summarizing the results of analysis

In the analysis results of $\omega'(1300)$, as are shown in Table 4, the photon-meson coupling of ω_2 is very small relative to ω_1, and their signs of relative phases of (ω, ω_1 and ω_3) are to be are $(+\ ,-\ ,-)$ respectively.

In the analysis results of $\rho'(1300)$ in the mass spectra of $\omega\pi^0$, we take into account ρ, $\rho(1300)$, $\rho(1450)$ and $\rho(1700)$ in Eq.(3.1). As is shown in Table 4, the contribution of ρ is large and that of ρ_3 is small relative to ρ_1 (E.q.(3.1)), and that of ρ_2 is very small relative to ρ_1. Signs of the amplitudes (ρ, ρ_1 and ρ_3) are $(+\ ,\ -,\ +)$ respectively, while we can't determine the sign of ρ_2, since the contribution is very small.

The obtained values of masses and widths are

$m_{\omega'(1300)} = 1243 \pm 2\ (Mev/c^2)$, $\Gamma_{\omega'(1300)} = \quad 672 \pm 5\ (Mev/c^2)$,
$m_{\rho'(1300)} = 1264 \pm 2\ (Mev/c^2)$, $\Gamma_{\rho'(1300)} = \quad 560 \pm 4\ (Mev/c^2)$.

4.2 Remarks

The used data are combined one coming from different experiments performed in different mass regions. However, we expect that the main feature on mass spectra may be maintained, independently of a bias factor.

The present results seem to be consistent with the expectation[10)] of the $\widetilde{U}(12)$-scheme. In this scheme $\omega'(1300)$ and $\rho'(1300)$ are assigned as the S-wave chiral states, while $\omega(1420)$ and $\rho(1450)$ are assigned as P-wave states. Accordingly the contributions of $\omega(1420)$ and $\rho(1450)$ are expected to be very small compared with those of $\omega(1300)$ and $\rho(1300)$, respectively, reflecting the strength at the origin of their wave functions, $|\psi_P(0)| \sim 0$, $|\psi_S(0)| \sim 1$.

[1] A bias factor 1.18 is applied on DM2 data by CMD-2.

Table 4: Interpretations of the analysis results $\omega'(1300)$ and $\rho'(1300)$

$\omega'(1300)$ analysis	Analysis results A_i	Non relativistic Q. M. (PDG)	$\widetilde{U}(12)$ -scheme
$\omega(782)$	$Large$	1^3S_1	1^3S_1
$\omega'(1300)$	-0.53	—	1^3S_1
$\omega(1420)$	—	2^3S_1	1^1P_1
$\omega(1650)$	-0.039	1^3D_1	2^3S_1
$\rho'(1300)$ analysis	Analysis results A_i	Non relativistic Q. M. (PDG)	$\widetilde{U}(12)$ -scheme
$\rho(770)$	$Large$	1^3S_1	1^3S_1
$\rho'(1300)$	-0.52	—	1^3S_1
$\rho(1450)$	—	2^3S_1	1^1P_1
$\rho(1700)$	0.017	1^3D_1	2^3S_1

References

1. K. Takamatsu, KEK Proc. 2003-7, 109.
2. T. Komada, AIP Conf. Proc. **814** (2006) 458.
3. Yu.S. Surovtsev and P. Bydžovský, Rho-like mesons from analysis of the pion-pion scattering, Poster Sessions at Int. Conf. on Hadron Spectroscopy Hadron07 (8-13 October 2007, Frascati, Italy), to be published in Frascati Physica Serie, Volume XLVI(2007); see also arXiv:0711.4748v1.
4. M. Bettinelli, Electroproduction of omega π^0 with Muons, Talk at Int. Conf. on Hadron Spectroscopy Hadron07 (8-13 October 2007, Frascati, Italy), to be published in Frascati Physica Serie, Volume XLVI(2007).
5. M. N. Achasov et al. (SND Collaboration), Phys. Rev. **D68** (2003) 052006.
6. B. Aubert et al. (BABAR Collaboration), Phys. Rev. **D70** (2004) 072004.
7. R. R. Akhmetshin et al. (CMD-2 Collaboration), Phys. Lett. **B562** (2003) 173.
8. M. N. Achasov et al. (SND Collaboration), Phys. Lett. **B486** (2000) 29.
9. Nuclear Physics B (Proc. Suppi.) **21** (1991) 111-117.
10. S. Ishida, M. Ishida and T. Maeda, Prog. Theor. Phys. **104** (200) 785; S. Ishida and M.Y. Ishida, Phys. Lett. **B539** (2002) 249-256.

11. S. Ishida, T. Maeda and K. Yamada, to be published.

12. M.N. Achasov et al. (SND Collaboration), Phys. Lett. **B462** (1999) 365-370.

13. Particle Data Group, W. M. Yao et al., J. Phys. G. **33** (2006) 1.

14. D. Aston et al. (LASS Collaboration), SLAC-PUB-5606 (1994).

15. A. Bertin et al. (OBELIX Collaboration), Phys. Lett. **B414** (1997) 220.

16. A. Donnachie and Yu.S. Karashnikowa, Proc. 9th Hadron Conf. 2001, AIP Conf. Proc. **619** (2002) 5; A. Donnachie, Phys. Rept. **403-404** (2004) 281-301.

Frascati Physics Series Vol. XLVI (2007), pp. 455–462
HADRON07: XII Int. Conf. on Hadron Spectroscopy – Frascati, October 8-13, 2007
Light Meson Spectroscopy

THE $q\bar{q}$ S-WAVE AXIAL-VECTOR MESONS IN THE COVARIANT $\widetilde{U}(12)$-SCHEME

Tomohito Maeda, Kenji Yamada,
Department of Engineering Science, Junior College Funabashi Campus,
Nihon University, Funabashi 274-8501, Japan
Masuho Oda,
School of Science and Technology,
Kokushikan University, Tokyo 154-8515, Japan
Shin Ishida,
Research Institute of Science and Technology,
College of Science and Technology,
Nihon University, Tokyo 101-8308, Japan

Abstract

We study the properties of axial vector mesons a_1 and b_1 as relativistic S-wave states which are predicted in the $\widetilde{U}(12)$-scheme, through the analyses of their radiative and pionic decays. Specifically, partial widths of the strong $a_1(b_1) \to \rho(\omega)\pi$ processes, their D/S-wave amplitude ratios, and radiative transition widths of $a_1(b_1) \to \pi\gamma$ processes are calculated by using a simple decay interaction model, and made a comparison with the respective experimental values.

1 Introduction

In recent years we have proposed the $\widetilde{U}(12)$-scheme [1, 2], a relativistically covariant level-classification scheme of hadrons. In this scheme, the ground state (GS) of light $q\bar{q}$ meson system is assigned as $\mathbf{12} \times \mathbf{12}^* = \mathbf{144}$- representation

of the $U(12)_{SF}$-group at their rest frame. The $U(12)_{SF}$-group includes, in addition to the conventional non-relativistic $SU(6)_{SF}$-group, the new symmetry $SU(2)_\rho$ [1], which corresponds to the degree of freedom associated with negative energy Dirac spinor solutions of confined quarks inside hadrons. By inclusion of this extra $SU(2)$ spin freedom, it leads to the possible existence of some extra multiples, called *chiral states*, which do not exist in the ordinary non-relativistic quark model (NRQM). As an example, the light scalar $f_0(600)/\sigma$ meson, a controversial particle for long time, is identified as S-wave chiral state as well as π meson, and they play mutually the role of chiral partners in the $\widetilde{U}(12)$-scheme. As it is well known, in conventional level classification scheme based on NRQM, lowest scalar meson is obliged to be assigned as orbital P-wave excited state. As an another example, the a_1 meson is possibly to be identified as the $q\bar{q}$ S-wave axial-vector mesons in the $\widetilde{U}(12)$-scheme. They form a linear representation of chiral symmetry with the S-wave ρ meson. Here it is notable that these σ and a_1 mesons are expected to have the light mass compared with the conventional case of the P-wave states. Furthermore, **144**-representation includes another axial-vector meson state with $J^{PC} = 1^{+-}$, to be identified with the b_1 meson.

In this work, we try to elucidate the properties of our new-type S-wave axial-vector mesons, a_1 and b_1, whose existence are predicted in the $\widetilde{U}(12)$-scheme, through the analyses of their radiative and pionic decay. In the actual analyses, we identify our chiral S-wave a_1 and b_1 mesons as the experimentally well-known states, $a_1(1260)$ and $b_1(1235)$, respectively. Then, by using a simple decay interaction, their partial widths of the strong a_1 $(b_1) \to \rho$ $(\omega)\pi$ decays (with D/S-wave amplitude ratios) and radiative transition widths of a_1 (b_1) $\to \pi\gamma$ processes are calculated in comparison with the respective experimental values.

2 Wave functions of the a_1 and b_1 mesons as S-wave chiral states

In this section we collect the concrete expressions of meson wave function (WF) in our scheme necessary for the relevant applications [2].

[1] The new degree of freedom corresponding to the $SU(2)_\rho$-symmetry is called the ρ-spin, after the well-known $\rho \otimes \sigma$-decomposition of Dirac matrices.

[2] In more detail, see Ref. [1, 2, 4]

The basic framework of our level-classification scheme is what is called the boosted LS-coupling (bLS) scheme. In this scheme, the WF of $q\bar{q}$ GS mesons are given by the following (bi-local Klein Gordon) field with one each upper and lower indices [3],

$$\Phi(X,x)^{(+)B}_{A} = Ne^{+iP\cdot X}\ W(v)^{(+)\beta,b}_{\alpha,a}\ f_G(v,x). \tag{1}$$

Where $A=(\alpha,a)$ ($B=(\beta,b)$) denotes Dirac spinor and flavor indices respectively, X_μ (x_μ) represents the center of mass (CM) (relative) coordinate of the composite meson. The P_μ ($v_\mu = P_\mu/M$, M being the mass of meson; $v_\mu^2=-1$, $v_0=+1$) denotes 4-momentum (4-velocity) of the relevant mesons. In the bLS scheme, respective spin ($W(v)_A{}^B$) and space-time [4] ($f_G(v,x)$) parts of WF are, separately, made covariant by boosting from the corresponding parts of NR ones.

Important feature of $\widetilde{U}(12)$-scheme is that the spin WF contains extra $SU(2)$ spin degree of freedom, called ρ-spin. As expansion bases of spinor WF, we use the Dirac spinor with hadron on-shell 4-velocity,

$$\{u_+(v), u_-(v)\}. \quad (\rho_3\ u_\pm = \pm u_\pm) \tag{2}$$

Here, u_+ corresponds to conventional constituent quark degree of freedom, while u_- is indispensable for covariant description of confined quarks [5] . Accordingly, expansion basis of $q\bar{q}$ meson WF is given by direct product of the respective spinor WF corresponding to the relevant constituent quark. They consist of totally 16 members in $\tilde{U}(4)_S$-space as,

$$W(v)_\alpha{}^\beta = u_r(v)_\alpha \bar{v}_{r'}(v)^\beta. \quad (r,r^{'}) = (\rho_3, \bar{\rho}_3) \tag{3}$$

We show the specific form of spin WF for the respective members of $q\bar{q}$ S-wave mesons, appeared in the relevant applications, in Table 1. Here it should be noted that, in the actual application, being based on its success [6] with $SU(6)_{SF}$-description for $\rho(770)$-nonet, it seems that its WF should be taken as the form containing only positive ρ_3-states. This is made by taking the equal-weight superposition of two spin WF which belongs to the different chiral representation, respectively.

---

[3] For simplicity, only the positive frequency part of WF is shown here.

[4] We have been adopted a definite metric type 4-dimensional oscillator function as $f_G(v,x)$ [7].

[5] They form the chiral partner in basic representation of the chiral group.

Table 1: *Spin wave functions of S-wave mesons applying for in this work, at their rest frame. Note that the physical ρ meson WF is given by as a sum of the following two vector WF, the one only with $(\rho_3, \bar{\rho}_3) = (+,+)$.* (i=1,2,3)

Mesons	J^{PC}	$W(v=0)^{(+)}$	$SU(2)_L \otimes SU(2)_R$	$(\rho_3, \bar{\rho}_3)$
$a_1(1260)$	1^{++}	$\frac{\gamma_5\gamma_i}{2}$	$(1_L, 0_R) \oplus (0_L, 1_R)$	$\frac{(-,+)+(+,-)}{\sqrt{2}}$
$b_1(1235)$	1^{+-}	$\frac{i\gamma_5\sigma_{i4}}{2}$	$(\frac{1}{2}_L, \frac{1}{2}_R)$	$\frac{i((-,+)+(+,-))}{\sqrt{2}}$
$\rho(770)$	1^{--}	$\frac{i\gamma_i}{2}$	$(1_L, 0_R) \oplus (0_L, 1_R)$	$\frac{(+,+)+(-,-)}{\sqrt{2}}$
$\rho(1250)$ [9]	1^{--}	$\frac{\sigma_{i4}}{2}$	$(\frac{1}{2}_L, \frac{1}{2}_R)$	$\frac{(+,+)-(-,-)}{\sqrt{2}}$
$\pi(140)$	0^{-+}	$\frac{i\gamma_5}{2}$	$(\frac{1}{2}_L, \frac{1}{2}_R)$	$\frac{(+,+)+(-,-)}{\sqrt{2}}$

3 Radiative decays of the a_1 and b_1 mesons

At first, we will consider the radiative decays of a_1 and b_1 mesons. In this work, we focus on the radiative transitions among the GS mesons. Therefore we are able to adopt simply the effective spin-type interaction,

$$H = \bar{q}\, \sigma_{\mu\nu} F_{\mu\nu}((iv\gamma)g + g')\, q\ . \tag{4}$$

Here we introduced two independent coupling parameters g and $g^{'}$. The g term contributes only to quark chirality conserving transitions, while the $g^{'}$ term to chirality non-conserving ones. By applying the quark-photon interaction (4), the effective meson current is given by the following formulas,

$$J_\mu(P,P^{'}) = J_{1,\mu}(P,P^{'}) + J_{2,\mu}(P,P^{'}). \tag{5}$$

Here, subscript 1 (2) represents the coupling of the emitted single photon with the relevant meson system through constituent quark (anti-quark). The specific form of the current is represented by

$$J_{1,\mu}(P,P^{'}) = e_q I_G^{(\gamma)}\ \langle \bar{W}^{(-)}(v^{'})[2gi\sigma_{\mu\nu}q_\nu] iv\gamma W^{(+)}(v) iv\gamma\rangle\ , \tag{6}$$

$$J_{2,\mu}(P,P^{'}) = e_{\bar{q}} I_G^{(\gamma)}\ \langle iv\gamma W^{(+)}(v) iv\gamma[-2g(-i\sigma_{\mu\nu}q_\nu)]\bar{W}^{(-)}(v^{'})\rangle \tag{7}$$

for the case of the chirality conserving transition; and similarly

$$J^{'}_{1,\mu}(P,P^{'}) = e_q I_G^{(\gamma)}\ \langle \bar{W}^{(-)}(v^{'})[2g^{'} i\sigma_{\mu\nu}q_\nu] W^{(+)}(v) iv\gamma\rangle\ , \tag{8}$$

$$J^{'}_{2,\mu}(P,P^{'}) = e_{\bar{q}} I_G^{(\gamma)}\ \langle iv\gamma W^{(+)}(v)[-2g^{'}(-i\sigma_{\mu\nu}q_\nu)]\bar{W}^{(-)}(v^{'})\rangle\ , \tag{9}$$

for the case of the chirality non-conserving transition. Here $q_\mu = P_\mu - P_\mu^{'}$ denotes the 4-momentum of emitted photon, $I_G^{(\gamma)}$ is overlapping integral (OI) of space-time oscillator function, which gives a Lorentz invariant transition form factor as

$$I_G^{(\gamma)} = \int d^4x f_G^*(v^{'},x) f_G(v,x) e^{-i\frac{1}{2}q_\mu x_\mu} \tag{10}$$

$$= (\frac{2MM^{'}}{M^2+M^{'2}})\exp[-\frac{1}{2\Omega}\frac{(M^2-M^{'2})^2}{M^2+M^{'2}}], \tag{11}$$

where we introduce the parameter Ω corresponding to the Regge slope inverse. In our scheme the relativistic covariance of the spin current, due to the inclusion of Dirac spinor with negative ρ_3-value, plays an important role in some radiative transition processes. To clarify this point, we rewrite the spin current vertex operator as

$$\sigma_{\mu\nu} i q_\nu A_\mu = \sigma_{\mu\nu} F_{\mu\nu} = \boldsymbol{\sigma}\cdot\mathbf{B} - i\rho_1 \boldsymbol{\sigma}\cdot\mathbf{E} \quad . \tag{12}$$

In the cases of transition between both positive (negative) ρ_3 Dirac spinors, as it is well known, the main contribution comes from the magnetic interaction. On the other hand, in the case of transitions between Dirac spinors with positive and negative ρ_3-values, the electric interaction, coming from the $\sigma_{i4} i q_i A_4$-term, becomes a dominant contribution. As a results, this *intrinsic electric dipole* [5] transition gives an important role for the transition accompanied with their parity change, such as $a_1(b_1) \to \pi\gamma$ processes.
In this work, we take the following values of parameters in our scheme.

- $(g,\, g^{'})$=(2.59, 1.40) from $\Gamma_{\rm EXP}(b_1^+ \to \pi^+\gamma)$ and $\Gamma_{\rm EXP}(\rho^+ \to \pi^+\gamma)$
- $\Omega_{n\bar{n}} = 1.13$ GeV^2 from $\Omega = M(^3P_2)^2 - M(^3S_1)^2 = M(a_2(1320))^2 - M(\rho(770))^2$

The masses of the respective mesons are taken from PDG [3], except for the one of the pion in the form factor with $M_\pi = 0.78$ GeV. The estimated widths are in comparison with experiment in Table 2. Results for this calculation are consistent with experiments.

Table 2: *Radiative decay widths (keV) in comparison with experiment. Experimental data are taken from PDG* [3].

Process	Our results	Experimental values
$\rho(770) \to \pi\gamma$	68 (input)	68±7
$b_1(1235) \to \pi\gamma$	230 (input)	230±60
$a_1(1260) \to \pi\gamma$	604	640±246

4 Pion emissions of a_1 and b_1 mesons

Next we consider the strong decays with one pion emission. We adopt simply the following two types of effective quark-pion interactions;

$$L_{ps} = g_{ps}\ \bar{q}(-i\gamma_5)q\ \pi, \tag{13}$$

$$L_{pv} = g_{pv}\ \bar{q}(-i\gamma_5\gamma_\mu)q\ \partial_\mu\pi. \tag{14}$$

Note that here, π (and σ) meson is treated as an external local-field. Resultant matrix elements are given as a sum of two terms;

$$T = T_{ps} + T_{pv}\ , \tag{15}$$

$$T_{ps} = g_{ps} I_G^{(\pi)}\ \langle W(v^{'})(-i\gamma_5\pi)W(v)iv\gamma\rangle + c.c.\ \ , \tag{16}$$

$$T_{pv} = g_{pv} I_G^{(\pi)}\ \langle W(v^{'})(-\gamma_5\gamma_\mu q_\mu\pi)W(v)iv\gamma\rangle + c.c.\ \ . \tag{17}$$

In the above case, the OI of the space-time WF is given by

$$I_G^{(\pi)} = \int d^4x f_G^*(v^{'},x) f_G(v,x) e^{-i\frac{1}{2}q_\mu x_\mu} \tag{18}$$

$$= (\frac{2MM^{'}}{M^2+M^{'2}-m_\pi^2})\exp[-\frac{(M^2-M^{'2})^2 - m_\pi^2(M^2+M^{'2})}{2\Omega\,(M^2+M^{'2}-m_\pi^2)}], \tag{19}$$

where $q^2 = -m_\pi^2$, $q_\mu = P_\mu - P_\mu^{'}$ being the 4-momentum of emitted pion. The relevant decay amplitude is

$$T = f_1\ \epsilon_\mu(v')\epsilon_\mu(v)\ +\ f_2\ (q_\mu\epsilon_\mu(v'))(q_\nu\epsilon_\nu(v)). \tag{20}$$

The explicit forms of f_1 and f_2 are shown in Table 3. It may be worthwhile to note that at least two coupling types (expressed f_1 and f_2 in the above) are required to reproduce the experimental data on D/S-wave amplitude ratios.

Our decay interaction contains two independent coupling parameters, g_{ps} and g_{pv}, which will be commonly applied to all quark-pion vertices [6]. These are determined from the experimental data of D/S-wave amplitude ratio and total width of b_1 meson as,

- $\frac{g_{ps}}{g_{pv}} = 0.149$ GeV from $T_D/T_S|_{\rm EXP}(b_1^+ \to \omega\pi^+) = +0.277$
- $g_{pv} = 14.0$ from $\Gamma_{\rm EXP}(b_1^+ \to \omega\pi^+) \approx \Gamma_{\rm EXP}(b_{1\,\rm total}^+) = 142$ MeV.

The masses of the relevant mesons are taken from PDG [3]. The numerical results are shown in Table 4.

Table 3: *Coefficients of decay amplitude (20) for* $a_1 \to \rho\pi$ *and* $b_1 \to \omega\pi$ *process.*

	$b_1 \to \omega\pi$	$a_1 \to \rho\pi$
f_1	$I_G \times (-g_{ps} + (\omega M - M^{'})g_{pv})$	$I_G \times (-g_{ps}\omega + (M - \omega M^{'})g_{pv})$
f_2	$I_G \times (-g_{pv}\frac{1}{M'})$	$I_G \times (g_{ps}\frac{1}{MM'} + g_{pv}\frac{1}{M})$

Table 4: *Numerical results for pion emissions of* a_1 *and* b_1 *mesons. Experimental data are taken from PDG* [3].

	T_D/T_S		Width (MeV)	
process	Our results	Experimental values	$\Gamma^{\rm theor.}_{\rm partial}$	$\Gamma^{\rm Exp.}_{\rm total}$
$b_1 \to \omega\pi$	0.277(input)	0.277± 0.027	142(input)	142±9
$a_1 \to \rho\pi$	-0.344	-0.108± 0.016	191	$250 \sim 600$

5 Concluding remarks

In this work, we investigate the decay properties of $q\bar{q}$ S-wave a_1 and b_1 mesons in the $\tilde{U}(12)$-scheme, by assigning them with $a_1(1260)$ and $b_1(1235)$ mesons, respectively.

At first, it is shown that the radiative decay widths of $(a_1, b_1, \rho) \to \pi\gamma$ processes are consistently reprocuced by using the simple spin-type quark-photon effective interaction in the framework of the $\widetilde{U}(12)$-scheme.

[6] As an example, it is applied to the study of 'extra'- κ meson [8].

Secondly, for the strong one-pion emission decays, assuming the ps- and pv-type quark-pion effective interactions, the D/S-wave amplitude ratios and partial widths of $a_1(b_1) \to \rho(\omega)\pi$ decays are evaluated. As a results, by inputting the data for the b_1 meson, the sign of D/S-wave amplitude ratio for the $a_1 \to \rho\pi$ decay agrees with the experiments, but its absolute value is about three time larger than experiment. Partial width of $a_1 \to \rho\pi$ is predicted with $\Gamma(a_1 \to \rho\pi) \sim 200$ MeV.
The interaction adopted in this work for the radiative/strong decays should be tested by applying it to other various decay processes.

References

1. S. Ishida *et al.*, Prog. Theor. Phys. **104**, 785 (2000).
2. S. Ishida and M. Ishida , Phys. Lett. **B 539**, 249 (2002).
3. W.-M. Yao *et al.*, Journal of Physics **G 33**, 1 (2006) .
4. S. Ishida *et al.*, hep-ph/0408136 v3.
5. S Ishida *et al.*, AIP Conf. Proc. **717**, 716 (2004).
   Also in e-Print Archive: hep-ph/0310061.
6. M. Oda, M. Ishida, and S. Ishida, Prog. Theor. Phys. **101**,1285 (1999).
7. S. Ishida and K. Yamada, Phys. Rev. **D 35**, 265 (1987).
8. K. Yamada, these proceedings.
9. I. Yamauchi, these proceedings.

Frascati Physics Series Vol. XLVI (2007), pp. 463
HADRON07: XII Int. Conf. on Hadron Spectroscopy – Frascati, October 8-13, 2007
Light Meson Spectroscopy

STUDY OF THE $\eta \to 3\pi$ DECAY DALITZ PLOT AT KLOE

F. Ambrosino
Naples University and INFN)

Written contribution not received

Frascati Physics Series Vol. XLVI (2007), pp. 465–472
HADRON07: XII Int. Conf. on Hadron Spectroscopy – Frascati, October 8-13, 2007
Light Meson Spectroscopy

MEASUREMENT OF THE η' GLUONIUM CONTENT AND OF THE MASS AT KLOE

The KLOE collaboration[1]
presented by B. Di Micco
Università degli Studi di Roma Tre
I.N.F.N. sezione di Roma Tre

Abstract

Here we update the measurement of the η' gluonium content and present the final result of the η mass measurement. The η' gluonium content is estimated by fitting the ratio $R_\phi = \mathrm{BR}(\phi \to \eta'\gamma)/\mathrm{BR}(\phi \to \eta\gamma)$ together with other decay branching ratios. The analyses have been performed on 450 pb^{-1} of data collected in the years 2001 and 2002.

[1]F. Ambrosino, A. Antonelli, M. Antonelli, F. Archilli, P. Beltrame, G. Bencivenni, S. Bertolucci, C. Bini, C. Bloise, S. Bocchetta, F. Bossi, P. Branchini, P. Campana, G. Capon, T. Capussela, F. Ceradini, S. Chi, P. Ciambrone, E. De Lucia, A. De Santis, P. De Simone, G. De Zorzi, A. Denig, A. Di Domenico, C. Di Donato, S. Di Falco, B. Di Micco, A. Doria, M. Dreucci, G. Felici, M. L. Ferrer, S. Fiore, C. Forti, P. Franzini, C. Gatti, P. Gauzzi, S. Giovannella, E. Graziani, W. Kluge, G. Lanfranchi, J. Lee-Franzini, D. Leone, M. Martini, P. Massarotti, S. Meola, S. Miscetti, M. Moulson, S. Müller, F. Murtas, M. Napolitano, F. Nguyen, M. Palutan, E. Pasqualucci, A. Passeri, V. Patera, F. Perfetto, P. Santangelo, B. Sciascia, A. Sciubba, A. Sibidanov, T. Spadaro, M. Testa, L. Tortora, P. Valente, G. Venanzoni, R. Versaci, G. Xu.

1 Determination of the η' gluonium content

The η' meson, being a pure SU(3) singlet, has been considered for years the meson where gluon condensate contributions can show up. The η and η' wave functions can be decomposed in three terms: the u, d quark wave function $|q\bar{q}\rangle = \frac{1}{\sqrt{2}}(|u\bar{u}\rangle + |d\bar{d}\rangle)$, the strange component $|s\bar{s}\rangle$ and the $|glue\rangle$. The wave functions get written in the following way:

$$\begin{aligned} |\eta' > &= \cos\varphi_G \, \sin\varphi_P \, |q\bar{q} > + \cos\varphi_G \, \cos\varphi_P \, |s\bar{s} > + \sin\varphi_G \, |glue > \\ |\eta > &= \cos\varphi_P \, |q\bar{q} > - \sin\varphi_P \, |s\bar{s} > \end{aligned}$$

where φ_P is the η, η' mixing angle and $\cos\phi_G$ the gluon contribution. The ratio of the two branching ratios: $R_\phi = \mathrm{BR}(\phi \to \eta'\gamma)/\mathrm{BR}(\phi \to \eta\gamma)$ is related to this decomposition with the formula:

$$R_\phi = \cot^2\varphi_P \, \cos^2\varphi_G \left(1 - \frac{m_s}{\bar{m}} \frac{Z_{NS}}{Z_S} \frac{\tan\varphi_V}{\sin\, 2\varphi_P}\right)^2 \left(\frac{p_{\eta'}}{p_\eta}\right)^3 . \qquad (1)$$

Theoretical parameters such as the effective quark mass ratio $m_s/\bar{m}$, the overlapping parameters Z_{NS}, Z_S and the vector meson mixing angle ϕ_V are taken from [1] where the $\mathrm{BR}(\phi \to \eta'\gamma)$ and $\mathrm{BR}(\phi \to \eta\gamma)$ are fitted together with other $V \to P\gamma$ decays. Here V indicates the vector mesons ρ, ω, ϕ and P the pseudoscalars π^0, η, η'.
We fit the ratio R_ϕ from the KLOE measurement [2]

$$R_\phi = \frac{\mathrm{Br}(\phi \to \eta'\gamma)}{\mathrm{Br}(\phi \to \eta\gamma)} = 4.77 \pm 0.09_{\mathrm{stat.}} \pm 0.19_{\mathrm{syst.}}$$

together with the available data [3] on $\Gamma(\eta' \to \gamma\gamma)/\Gamma(\pi^0 \to \gamma\gamma)$, $\Gamma(\eta' \to \rho\gamma)/\Gamma(\omega \to \pi^0\gamma)$ and $\Gamma(\eta' \to \omega\gamma)/\Gamma(\omega \to \pi^0\gamma)$. The dependence of these ratios from the mixing angle φ_P and the gluonium content $\cos\phi_G$ is shown here:

$$\begin{aligned} \tfrac{\Gamma(\eta'\to\gamma\gamma)}{\Gamma(\pi^0\to\gamma\gamma)} &= \tfrac{1}{9}\left(\tfrac{m_{\eta'}}{m_{\pi^0}}\right)^3 \left(5\cos\phi_G \sin\varphi_P + \sqrt{2}\tfrac{f_q}{f_s}\cos\phi_G\cos\varphi_P\right)^2 \\ \tfrac{\Gamma(\eta'\to\rho\gamma)}{\Gamma(\omega\to\pi^0\gamma)} &= 3\tfrac{Z_{NS}}{\cos\phi_V}\left(\tfrac{m_{\eta'}^2 - m_\rho^2}{m_\omega^2 - m_\pi^2}\cdot\tfrac{m_\omega}{m_{\eta'}}\right) X_{\eta'}^2 \qquad (2) \\ \tfrac{\Gamma(\eta'\to\omega\gamma)}{\Gamma(\omega\to\pi^0\gamma)} &= \tfrac{1}{3}\left(\tfrac{m_{\eta'}^2 - m_\omega^2}{m_\omega^2 - m_\pi^2}\cdot\tfrac{m_\omega}{m_{\eta'}}\right)^3 \left[Z_{NS}X_{\eta'} + 2\tfrac{m_s}{\bar{m}}Z_S\cdot\tan\phi_V Y_{\eta'}\right]^2 . \end{aligned}$$

Using the value of Z_{NS} and Z_S from [1], we obtain $\varphi_P = (39.7 \pm 0.7)^\circ$ and $Z_G^2 = \sin^2 \varphi_G = 0.14 \pm 0.04$, $P(\chi^2) = 49\%$. Imposing $\varphi_G = 0$ the χ^2 probability of the fit decreases to 1 % and the φ_P value becomes $(39.7 \pm 0.7)^\circ$. The ratio of the Γ's are obtained using the branching fractions of the decay and the total decay widths Γ_ω, Γ_{π^0} from [3]. All the correlations among the measurements of the several branching ratios are taken into account. This correlation is due to the choice to normalise all decay widths to the $\Gamma(\omega \to \pi^0\gamma)$ and to the use of constrained fit technique in order to obtain more accurate estimates in [3].

The parameters $m_s/\bar{m}$ is mainly determined by $K^{*+} \to K^+\gamma$ while ϕ_V is given by $V \to \pi^0\gamma$ transitions, giving negligible correlations with the φ_P and Z_G^2 parameters. On the other side the parameters Z_S, Z_{NS} are strongly correlated to the mixing angle parameter, φ_P, in the equation (1). The constraint $\Gamma(\eta' \to \gamma\gamma)/\Gamma(\pi^0 \to \gamma\gamma)$ is instead independent from the parameters Z_{NS} and Z_S.

In ref. [4] a similar procedure to the one of [1] was followed taking into account also the possibility to have a non null gluonium content, ϕ_G. They find $Z_G^2 = 0.04 \pm 0.09$ that deviates of 1 σ from our result but with a larger error.

In [4] and [5] this difference was attributed to the use of overlapping parameters obtained by a fit which assumes no gluonium content. In order to check this possibility, we have performed several tests on the fit procedure. We first perform a new fit using the overlapping parameter Z_S and Z_{NS} extracted by the fit in ref. [4], where the gluonium content was left free, together with all the other parameters: $Z_{NS} = 0.86 \pm 0.03$, $Z_S = 0.79 \pm 0.05$, $\phi_V = (3.2 \pm 0.1)^\circ$, $\frac{m_s}{\bar{m}} = 1.24 \pm 0.07$. We obtain a result in perfect agreement with the previous determination: the errors remain unchanged while the central values move to $\varphi_P = 40.1$, $Z_G^2 = 0.12$. The value of the fit has been also repeated for different values of Z_{NS} and Z_S in a range $0.5 - 1.3$, and the resulting Z_G^2 varied between 0.07 and 0.18, showing small sensitivity to the used parameter Z_{NS} and Z_S that cannot be the reason for the different result obtained by [4]. Excluding the $P \to \gamma\gamma$ constraint from the fit we obtain $\varphi_P = (40.4 \pm 0.9)^\circ$ and $Z_G^2 = 0.12 \pm 0.05$, showing that this constraint improves the sensitivity for the gluonium content. A global fit to all $V \to P\gamma$ ratio of branching fraction is in progress. This will allow to leave free the overlapping parameters as in the approach of ref. [4], that is quite different than ours for both fit procedure and

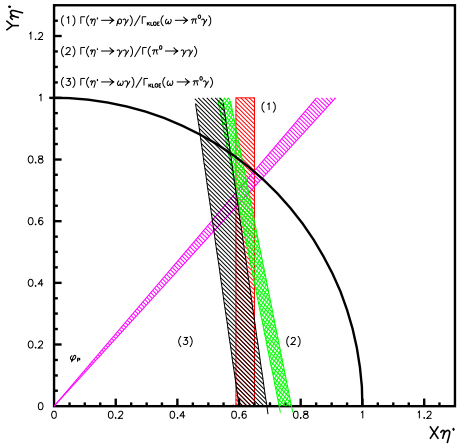

Figure 1: 68% C.L. region in the plane $[X_{\eta'} = \cos\varphi_G \sin\varphi_P, Y_{\eta'} = \cos\varphi_G \cos\varphi_P]$ for different decay width ratios.

input values.

1.1 New value using KLOE $\Gamma(\omega \to \pi^0\gamma)$ measurement

We have recently published [6] a new preliminary measurement of the $B\mathrm{R}(\omega \to \pi^0\gamma) = (8.40 \pm 0.19)\%$. Using this value we obtain $Z_G^2 = 0.13 \pm 0.04$ and $\varphi_P = (40.0 \pm 0.7)^\circ$. The allowed regions in the plane $[X_{\eta'} = \cos(\varphi_G)\sin(\varphi_P), Y_{\eta'} = \cos(\varphi_G)\cos(\varphi_P)]$, corresponding to the constraints in equations (2), are shown in Fig. 1. Theoretical parameters are taken from [1]. It is evident that all the allowed regions overlap far from the no-gluonium line $X_{\eta'}^2 + Y_{\eta'}^2 = 1$.

2 The measurement of the η mass

The value of the η-meson mass was poorly determined for many years and the picture is still not fully clarified today. The first measurements were done about 40 years ago studying η decays in bubble chamber experiments [7] with a mass resolution of $\sim$1 MeV; these resulted in mass values clustered around 548.5 MeV. A lower value with better precision was obtained in 1974 measuring the missing mass spectrum of $\pi^- p \to Xn$ close to threshold, $m_\eta = (547.45 \pm 0.25)$ MeV [8]. This result was confirmed by other experiments studying the

production of η at threshold in pd [9] and γp [10] reactions. More recently, the mass was precisely measured by the GEM experiment using the reaction $dp \to \eta\,{}^3\mathrm{He}$ at threshold: $m_\eta = (547.311 \pm 0.028 \pm 0.032)$ MeV [11]. Thus all the experiments at threshold give consistent results.

However, this value of η mass is highly inconsistent with that one measured by the NA48 experiment studying the decay $\eta \to \pi^0\pi^0\pi^0$: $m_\eta = (547.843 \pm 0.030_{stat.} \pm 0.041_{syst.})$ MeV [12], the difference being about eight standard deviations. This discrepancy between threshold and decay experiments has been confirmed by the preliminary η mass measurement carried out by the KLOE experiment [13] $m_\eta = (547.822 \pm 0.005_{\mathrm{stat.}} \pm 0.069_{\mathrm{syst.}})$. A recent result from the CLEO-c collaboration gives $m_\eta = (547.785 \pm 0.017 \pm 0.057)$ MeV [14] using $\psi(2S) \to \eta J/\psi$ decays and combining different η decay modes. In this paper, we report the best measurement of the η mass to date using the $\phi \to \eta\gamma$ decay. This decay chain, assuming the ϕ meson at rest, is a source of monochromatic η-mesons of 362.792 MeV/c, recoiling against a photon of the same momentum. Detection of such a photon signals the presence of an η-meson. Photons from $\eta \to \gamma\gamma$ cover a continuum flat spectrum between $147 < E_\gamma < 510$ MeV in the laboratory reference frame. The photon energies are measured in KLOE but for 3 γ events the main accuracy is ultimately due to the accurate measurement of the photon emission angles. Together with the stability of the continuously calibrated detector and the very large sample of η-mesons collected we have been able to obtain a very accurate measurement of the η-mass [15].

Events are selected requiring at least three energy clusters in the barrel calorimeter with polar angle $50^\circ < \theta_\gamma < 130^\circ$. A kinematic fit imposing energy-momentum conservation is performed. The kinematic fit uses the value of the total energy, the ϕ transverse momentum and the average value of the beam-beam interaction point; these values are determined with good precision run by run by analyzing $e^+e^- \to e^+e^-$ elastic scattering events. The energy resolution gets largely improved due to the good calorimeter angular resolution.

Fig. 2 shows the $m^2_{\gamma_2\gamma_3}$,$m^2_{\gamma_1\gamma_2}$ Dalitz plot population, with the energies ordered as $E_{\gamma_1} < E_{\gamma_2} < E_{\gamma_3}$. The $m^2_{\gamma_1\gamma_2} \simeq m^2_{\pi^0}$, $m^2_{\gamma_1\gamma_2} \simeq m^2_\eta$ and $m^2_{\gamma_1\gamma_3} = m^2_\eta$ bands are clearly visible. We apply a cut $m^2_{\gamma_1\gamma_2} + m^2_{\gamma_2\gamma_3} \leq 0.73$ GeV^2, "background-rejection cut" in the following, shown by the line in Fig. 2. Events below the line are retained for the analysis. The resulting $m_{\gamma_1\gamma_2}$ distribution, for a data subsample, is shown in Fig. 2, right-top. The $m(\gamma_1\gamma_2)$ distribution

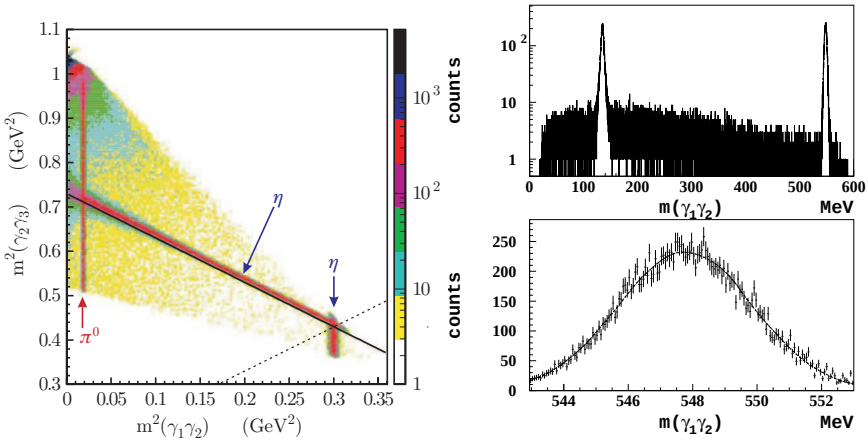

Figure 2: Left: Population in the invariant mass squared $m^2_{\gamma_2\gamma_3}$, $m^2_{\gamma_1\gamma_2}$ plane. The photon energies are ordered as $E_{\gamma_1} < E\gamma_2 < E_{\gamma_3}$. The η and π^0 signal are quite evident; Right-top: distribution of the invariant mass $m_{\gamma_1\gamma_2}$ for a subsample of the events selected by the cut. Right-bottom: same distribution of the invariant mass $m_{\gamma_1\gamma_2}$ around the value of the η mass and the Gaussian fit. The result of the fit is $m_\eta = (547.777 \pm 0.016)$ MeV with $\chi^2/\text{n.d.f} = 168/161$.

in the 542.5 to 552.5 interval is fitted well with a single Gaussian with $\sigma = 2.0$ MeV as shown in Fig. 2, right-bottom.

To estimate systematic uncertainties we have studied the effects of the detector response and alignment, event selection cuts, kinematic fit and beam energy calibration that can influence our measurement. The values of the systematic errors are summarized in Table 1.

2.1 Results

The same procedure has been applied to events $\phi \to \pi^0\gamma, \pi^0 \to \gamma\gamma$ in order to evaluate the π^0 mass and the ratio $R = m_\eta/m_{\pi^0}$. The values obtained are:

$$m_{\pi^0} = (134.906 \pm 0.012_{\text{stat}} \pm 0.049_{\text{syst}}) \quad \text{MeV} \tag{3}$$

$$m_\eta = (547.874 \pm 0.007_{\text{stat}} \pm 0.029_{\text{syst}}) \quad \text{MeV} \tag{4}$$

$$\frac{m_\eta}{m_{\pi^0}} = 4.0610 \pm 0.0004_{\text{stat}} \pm 0.0014_{\text{syst}} \tag{5}$$

Table 1: Systematic errors evaluated for m_η, m_{π^0} and the ratio $R = m_\eta/m_{\pi^0}$.

Systematic effect	m_η (keV)	m_{π^0} (keV)	R ($\times 10^{-5}$)
Vertex position	4	6	19
Calorimeter energy scale	4	1	6
Calorimeter non-linearity	4	11	31
θ angular uniformity	10	44	120
ϕ angular uniformity	15	12	37
χ^2 cut	<1	4	13
Background-rejection cut	12	4	18
ISR emission	8	9	28
$\sqrt{s}$ calibration	16	3.4	-
Total	29	49	136

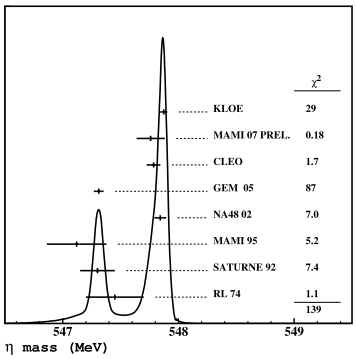

Figure 3: Comparison among the measurements of the η mass. The continuous line and the χ^2 contributions are obtained according the procedure described in [3].

Our η mass measurement is the most precise result to date and is in good agreement with the recent measurements based on η decays shown in fig. 3. Averaging these measurements we obtain $m_\eta = 547.851 \pm 0.025$ MeV which differs of $\sim 10\ \sigma$ from the average of the measurements done studying the production of the η meson at threshold in nuclear reactions.

References

1. A. Bramon, R. Escribano and M.D. Scadron, Phys. Lett. B **503** (2001) 271.
2. F. Ambrosino *et al.* Phys. Lett. **B648** (2007) 267.
3. W.-M. Yao et al., Journal of Physics G33 (2006) 1.
4. R. Escribano and J.Nadal (Barcelona, IFAE) JHEP **05** (2007) 6. e-Print: hep-ph/0703187
5. C.E. Thomas JHEP **10**(2007) 26.
6. F. Ambrosino *et al.* arXiv:0707.4130
7. P. Bastien et al., Phys. Rev. Lett. 8 (1962) 114; C. Alff et al. Phys. Rev. Lett. 9 (1962) 322; H. Foelsche and H. Kraybill, Phys. Rev. 134 (1964) B1138; M. Foster et al., Phys. Rev. 138 (1965) B652.
8. A. Duane et al., Phys. Rev. Lett. 32 (1974) 425
9. F. Plouin et al., Phys. Lett. B276 (1992) 526
10. B. Krusche et al., Zeit.Phys. A351 (1995) 237
11. M. Abdel-Bary et al., Phys. Lett. B619 (2005) 281
12. A. Lai et al., Phys. Lett. B533 (2002) 196
13. B. Di Micco et al., Acta Phys. Slov. (2006) 403
14. D. H. Miller et al., Phys. Rev. Lett. 99 (2007) 122002
15. B. Di Micco, "Precise measurement of the η mass", KLOE note 217 (2007)[1]

[1]KLOE notes are public at `http://www.lnf.infn.it/kloe/`

Frascati Physics Series Vol. XLVI (2007), pp. 473–480
HADRON07: XII Int. Conf. on Hadron Spectroscopy – Frascati, October 8-13, 2007
Light Meson Spectroscopy

IS η' PARTIALLY MADE OF GLUONIUM?

Rafel Escribano
Grup de Física Teòrica and IFAE, Universitat Autònoma de Barcelona, E-08193 Bellaterra (Barcelona), Spain

Abstract

A phenomenological analysis of radiative $V \to P\gamma$ and $P \to V\gamma$ decays is performed in order to determine the gluonic content of the η' wave function. Our result shows that there is no evidence for such a gluonium contribution, $Z_{\eta'}^2 = 0.04 \pm 0.09$. In terms of a mixing angle description this corresponds to $\phi_P = (41.4 \pm 1.3)^\circ$ and $|\phi_{\eta' G}| = (12 \pm 13)^\circ$.

1 Introduction

Is η' partially made of gluonium? To answer this question we perform a phenomenological analysis of radiative $V \to P\gamma$ and $P \to V\gamma$ decays, with $V = \rho, K^*, \omega, \phi$ and $P = \pi, K, \eta, \eta'$, in order to determine the gluonic content of the η' wave function. Similar analyses were driven in the seminal work by Rosner [1], where the allowed gluonic admixture in the η' could not be

established due to the lack of data on $\phi \to \eta'\gamma$, and, later on, by Kou who pointed out that the η' gluonic component might be as large as 26% [2]. More recently, the study by C. E. Thomas over a large number of different processes concludes that while the data hint at a small gluonic component in the η', the results depend sensitively on unknown form factors associated with exclusive dynamics [3].

From the experimental side, the KLOE Collaboration, combining the new measurement of $R_\phi \equiv B(\phi \to \eta'\gamma)/B(\phi \to \eta\gamma)$ with other constraints, has estimated the gluonium content of the η' meson as $Z^2_{\eta'} = 0.14 \pm 0.04$ [4]. This new result contrasts with the former value $Z^2_{\eta'} = 0.06^{+0.09}_{-0.06}$, which was compatible with zero and consistent with a gluonium fraction below 15% [5]. The sole difference between the two analyses is the inclusion in the amplitudes of Ref. [4] of two extra parameters to deal with the overlap of the vector and pseudoscalar meson wave functions produced in the transitions $V \to P\gamma$ or $P \to V\gamma$, a feature first introduced in Ref. [6]. However, the new analysis of Ref. [4] uses the most recent experimental data taken from Ref. [7] in association with the values for the parameters related to the overlap which were obtained in Ref. [6] from a fit to available experimental data at that time. Therefore, a reanalysis of this uncomfortable situation is needed before drawing definite conclusions on the gluon content of the η' meson. This is the main motivation of the present work. A more extensive version including a detailed analysis also for the case of the η, the effects of considering the newest (not reported in the PDG) data, a comparison with other approaches, and a discussion of the $P \to \gamma\gamma$ decays within this context can be found in Ref. [8].

2 Notation

We will work in a basis consisting of the states $|\eta_q\rangle \equiv \frac{1}{\sqrt{2}}|u\bar{u} + d\bar{d}\rangle$, $|\eta_s\rangle = |s\bar{s}\rangle$ and $|G\rangle \equiv |\text{gluonium}\rangle$. The physical states η and η' are assumed to be linear combinations of these:

$$\begin{aligned} |\eta\rangle &= X_\eta|\eta_q\rangle + Y_\eta|\eta_s\rangle + Z_\eta|G\rangle \ , \\ |\eta'\rangle &= X_{\eta'}|\eta_q\rangle + Y_{\eta'}|\eta_s\rangle + Z_{\eta'}|G\rangle \ , \end{aligned} \tag{1}$$

with $X^2_{\eta(\eta')} + Y^2_{\eta(\eta')} + Z^2_{\eta(\eta')} = 1$ and thus $X^2_{\eta(\eta')} + Y^2_{\eta(\eta')} \leq 1$. A significant gluonic admixture in a state is possible only if $Z^2_{\eta(\eta')} = 1 - X^2_{\eta(\eta')} - Y^2_{\eta(\eta')} > 0$ [1]. This mixing scheme assumes isospin symmetry, *i.e.* no mixing with π^0, and

neglects other possible admixtures from $c\bar{c}$ states and/or radial excitations. An interesting situation occurs when the gluonium content of the η meson is assumed to vanish, $Z_\eta \equiv 0$. In this particular case, the rotation between the physical states (η, η' and ι) and the orthonormal mathematical states (η_q, η_s and G) can be written in terms of two mixing angles, ϕ_P and $\phi_{\eta' G}$, which would correspond to

$$\begin{array}{lll} X_\eta = \cos\phi_P \ , & Y_\eta = -\sin\phi_P \ , & Z_\eta = 0 \ , \\ X_{\eta'} = \sin\phi_P \cos\phi_{\eta' G} \ , & Y_{\eta'} = \cos\phi_P \cos\phi_{\eta' G} \ , & Z_{\eta'} = -\sin\phi_{\eta' G} \ , \end{array} \tag{2}$$

where ϕ_P is the η-η' mixing angle (in the quark-flavour basis) in absence of gluonium, *i.e.* $\phi_{\eta G} = \phi_{\eta' G} = 0$. It is related to its octet-singlet basis analog through $\theta_P = \phi_P - \arctan\sqrt{2} \simeq \phi_P - 54.7^\circ$.

3 A model for $VP\gamma$ $M1$ transitions

We will work in a conventional quark model where pseudoscalar and vector mesons are simple quark-antiquark S-wave bound states with characteristic spatial extensions fixed by their respective quark-antiquark P or V wave functions. We take the good $SU(2)$ limit with $m_u = m_d \equiv \bar{m}$ and with identical spatial extension of wave functions within each P and each V isomultiplet. $SU(3)$ will be broken in the usual manner taking constituent quark masses with $m_s > \bar{m}$ but also, and this is a specific feature of our approach, allowing for different spatial extensions for each P and V isomultiplet. Finally, we will consider that $VP\gamma$ transitions fully respect the usual OZI-rule.

In our specific case of $VP\gamma$ $M1$ transitions, these generic statements translate into three characteristic ingredients of the model: *i)* A $VP\gamma$ magnetic dipole transition proceeds via quark or antiquark spin-flip amplitudes proportional to $\mu_q = e_q/2m_q$. This effective magnetic moment breaks $SU(3)$ in a well defined way and distinguishes photon emission from strange or non-strange quarks via $m_s > \bar{m}$; *ii)* The spin-flip $V \leftrightarrow P$ conversion amplitude has then to be corrected by the relative overlap between the P and V wave functions; *iii)* Indeed, the OZI-rule reduces considerably the possible transitions and their respective VP wave-function overlaps: C_s, C_q and C_π characterize the $\langle\eta_s|\phi_s\rangle$, $\langle\eta_q|\omega_q\rangle = \langle\eta_q|\rho\rangle$ and $\langle\pi|\omega_q\rangle = \langle\pi|\rho\rangle$ spatial overlaps, respectively. Notice that distinction is made between the $|\pi\rangle$ and $|\eta_q\rangle$ spatial extension due to the gluon or $U(1)_A$ anomaly.

The relevant $VP\gamma$ couplings are written in terms of a $g \equiv g_{\omega_q \pi\gamma}$ as

$$\begin{aligned} g_{\rho\eta^{(\prime)}\gamma} &= g\, z_q\, X_\eta^{(\prime)} \ , \\ g_{\omega\eta^{(\prime)}\gamma} &= \tfrac{1}{3} g \left(z_q\, X_\eta^{(\prime)} \cos\phi_V + 2\tfrac{\bar{m}}{m_s} z_s\, Y_\eta^{(\prime)} \sin\phi_V \right) \ , \\ g_{\phi\eta^{(\prime)}\gamma} &= \tfrac{1}{3} g \left(z_q\, X_\eta^{(\prime)} \sin\phi_V - 2\tfrac{\bar{m}}{m_s} z_s\, Y_\eta^{(\prime)} \cos\phi_V \right) \ , \end{aligned} \tag{3}$$

where we have redefined $z_q \equiv C_q/C_\pi$ and $z_s \equiv C_s/C_\pi$.

4 Data fitting

We proceed to fit our theoretical expressions for the amplitudes comparing the available experimental information on $\Gamma(V \to P\gamma)$ and $\Gamma(P \to V\gamma)$ taken exclusively from Ref. [7]. In the following, we leave the z's free and allow for gluonium in the η' wave function only. This will permit us to fix the gluonic content of the η' in a way identical to the experimental measurement by KLOE, that is, under the hypothesis of no gluonium in the η wave function. Unfortunately, a simultaneous fit of the z's and the gluonic admixture in the η *and* η' is not possible. However, as a matter of comparison, we first consider the absence of gluonium in both mesons, *i.e.* $\phi_{\eta G} = \phi_{\eta' G} = 0$. The result of the fit gives χ^2/d.o.f.=4.4/5 with

$$\begin{gathered} g = 0.72 \pm 0.01 \ \text{GeV}^{-1} \ , \quad \phi_P = (41.5 \pm 1.2)^\circ \ , \quad \phi_V = (3.2 \pm 0.1)^\circ \ , \\ \tfrac{m_s}{\bar{m}} = 1.24 \pm 0.07 \ , \quad z_q = 0.86 \pm 0.03 \ , \quad z_s = 0.78 \pm 0.05 \ . \end{gathered} \tag{4}$$

If we fix the z's to unity, the fit gets much worse (χ^2/d.o.f.=45.9/8). This shows that allowing for different overlaps of quark-antiquark wave functions and, in particular, for those coming from the gluon anomaly affecting only the η and η' singlet component, is indeed relevant.

In Table 1, we present a comparison between experimental data for the relevant $VP\gamma$ transitions with $P = \eta, \eta'$ and the corresponding theoretical predictions (in absolute value) calculated from the fitted values in Eq. (4). The agreement is very good and all the predictions coincide with the experimental values within 1σ.

Now that we have performed a fit under the hypothesis of no gluonium we assume $\phi_{\eta G} = 0$, *i.e.* $Z_\eta = 0$, and then proceed to fit the gluonic content of

Transition	$g^{\rm exp}_{VP\gamma}$(PDG)	$g^{\rm th}_{VP\gamma}$(Fit 1)	$g^{\rm th}_{VP\gamma}$(Fit 2)
$\rho^0 \to \eta\gamma$	0.475 ± 0.024	0.461 ± 0.019	0.464 ± 0.030
$\eta' \to \rho^0\gamma$	0.41 ± 0.03	0.41 ± 0.02	0.40 ± 0.04
$\omega \to \eta\gamma$	0.140 ± 0.007	0.142 ± 0.007	0.143 ± 0.010
$\eta' \to \omega\gamma$	0.139 ± 0.015	0.149 ± 0.006	0.146 ± 0.014
$\phi \to \eta\gamma$	0.209 ± 0.002	0.209 ± 0.018	0.209 ± 0.013
$\phi \to \eta'\gamma$	0.22 ± 0.01	0.22 ± 0.02	0.22 ± 0.02

Table 1: *Comparison between the experimental values $g^{\rm exp}_{VP\gamma}$ (in GeV^{-1}) for the transitions involving η or η' taken from the PDG [7] and the corresponding predictions for $g^{\rm th}_{VP\gamma}$ from Eqs. (4) —Fit 1— and (5) —Fit 2—.*

the η' wave function under this assumption. The results of the new fit are[1]

$$g = 0.72 \pm 0.01 \text{ GeV}^{-1} , \quad \tfrac{m_s}{\bar{m}} = 1.24 \pm 0.07 , \quad \phi_V = (3.2 \pm 0.1)^\circ ,$$
$$\phi_P = (41.4 \pm 1.3)^\circ , \quad |\phi_{\eta' G}| = (12 \pm 13)^\circ , \qquad (5)$$
$$z_q = 0.86 \pm 0.03 , \quad z_s = 0.79 \pm 0.05 ,$$

with χ^2/d.o.f.=4.2/4. The quality of the fit is similar to the one obtained assuming a vanishing gluonic admixture for both mesons (χ^2/d.o.f.=4.4/5). The result obtained for $\phi_{\eta' G}$ suggests a very small amount of gluonium in the η' wave function, $|\phi_{\eta' G}| = (12\pm13)^\circ$ or $Z^2_{\eta'} = 0.04\pm0.09$. This is the main result of our analysis. Our values contrast with those reported by KLOE recently, $\phi_P = (39.7 \pm 0.7)^\circ$ and $|\phi_{\eta' G}| = (22 \pm 3)^\circ$ —or $Z^2_{\eta'} = 0.14 \pm 0.04$— [4]. In Table 1, we also include the theoretical predictions for the various transitions involving η or η' calculated from the fitted values in Eq. (5). As expected, there is no significant difference between the values obtained allowing for gluonium (Fit 2) or not (Fit 1) in the η' wave function.

Our main results can also be displayed graphically following Refs. [1, 2, 4]. In Fig. 1, we plot the regions for the $X_{\eta'}$ and $Y_{\eta'}$ parameters which are allowed by the experimental couplings of the $\eta' \to \rho\gamma$, $\eta' \to \omega\gamma$ and $\phi \to \eta'\gamma$ transi-

[1] There is a sign ambiguity in $\phi_{\eta' G}$ that cannot be decided since this angle enters into $X_{\eta'}$ and $Y_{\eta'}$ through a cosine.

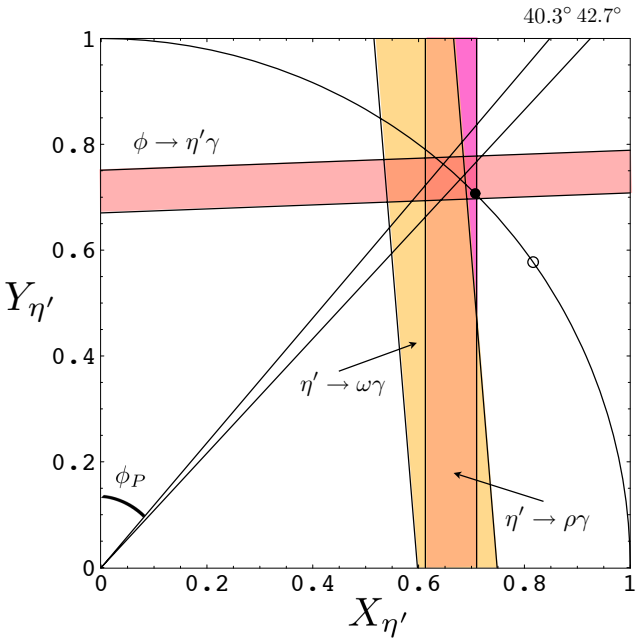

Figure 1: Constraints on non-strange ($X_{\eta'}$) and strange ($Y_{\eta'}$) quarkonium mixing coefficients in the η'. The mixing solutions corresponding to the η' being a pure singlet ($X_{\eta'} = \sqrt{2}Y_{\eta'} = \frac{1}{\sqrt{3}}$) —open circle— and ($X_{\eta'} = Y_{\eta'} = \frac{1}{\sqrt{2}}$) —closed circle— are shown. The vertical and inclined bands are the regions for $X_{\eta'}$ and $Y_{\eta'}$ allowed by the experimental couplings of the $\eta' \to (\rho, \omega)\gamma$ and $\phi \to \eta'\gamma$ transitions.

tions (see Table 1). The limits of the bands are given at 68% CL or 1σ. The remaining parameters are taken from Eq. (5). In addition to the bands, we have also plotted the circular boundary denoting the constraint $X^2_{\eta'} + Y^2_{\eta'} \leq 1$ as well as the favoured region for the η-η' mixing angle assuming the *absence of gluonium*, $40.3^\circ \leq \phi_P \leq 42.7^\circ$, obtained at 1σ from the corresponding fitted value in Eq. (4). There exists an intersection region of the three bands inside and on the circumference. As most of this region is interior but close to the circular boundary it may well indicate a small but non necessarily zero gluonic content of the η'. Indeed, we have found $Z^2_{\eta'} = 0.04 \pm 0.09$ (or $|Z_{\eta'}| = 0.2 \pm 0.2$) or using the angular description $|\phi_{\eta' G}| = (12 \pm 13)^\circ$. The size of the error is precisely what prevent us from drawing a definite conclusion concerning the

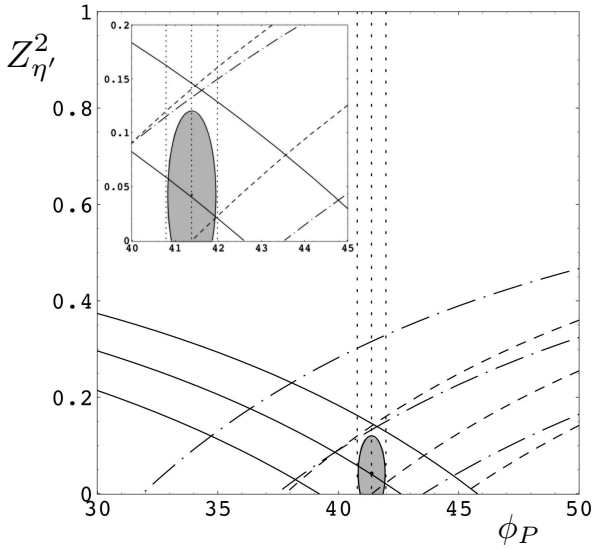

Figure 2: The gray ellipse in the $(\phi_P, Z^2_{\eta'})$ plane corresponds to the allowed region at 68% CL of the solution in Eq. (5) assuming the presence of gluonium. The different bands are the regions for ϕ_P and $Z^2_{\eta'}$ allowed by the experimental couplings of the $\eta' \to \rho\gamma$ (dashed line), $\eta' \to \omega\gamma$ (dot-dashed line), $\phi \to \eta\gamma$ (dotted line), and $\phi \to \eta'\gamma$ (solid line) transitions in Table 1.

amount of gluonium in the η' wave function. More refined experimental data, particularly for the $\phi \to \eta'\gamma$ channel, will contribute decisively to clarify this issue (see below). Clearly, the inclusion of this process is of major importance for the determination of the gluonic admixture in the η', as observed for the first time in Ref. [1]. In the present analysis, the "democratic" mixing solution is excluded at the 1σ level whereas the singlet solution is clearly excluded.

To make our bounds more graphical, we follow Ref. [4] and plot in Fig. 2 the constraints from $\eta' \to (\rho, \omega)\gamma$ and $\phi \to (\eta, \eta')\gamma$ in the $(\phi_P, Z^2_{\eta'})$ plane together with the 68% CL allowed region for gluonium as obtained from Eq. (5). The point corresponding to the preferred solution, $(\phi_P, Z^2_{\eta'}) = (41.4°, 0.04)$, is also shown. The allowed region is very constrained in the ϕ_P axis by the experimental value of the $g_{\phi\eta\gamma}$ coupling, whose vertical band denotes its non dependence on $Z^2_{\eta'}$. The other three bands, all dependent on ϕ_P and $Z^2_{\eta'}$, constrain the amount of gluonium down to a value compatible with zero at 1σ.

5 Summary and conclusions

In this work we have performed a phenomenological analysis of radiative $V \to P\gamma$ and $P \to V\gamma$ decays with the purpose of determining the gluon content of the η' meson. The present approach is based on a conventional $SU(3)$ quark model supplemented with two sources of $SU(3)$ breaking, the use of constituent quark masses with $m_s > \bar{m}$ and the different spatial extensions for each P or V isomultiplet which induce different overlaps between the P and V wave functions. The use of these different overlapping parameters —a specific feature of our analysis— is shown to be of primary importance in order to reach a good agreement.

Our conclusions are the following. First, accepting the absence of gluonium for the η meson, the current experimental data on $VP\gamma$ transitions indicate within our model a negligible gluonic content for the η' meson, $Z^2_{\eta'} = 0.04 \pm 0.09$. Second, this gluonic content of the η' wave function amounts to $|\phi_{\eta' G}| = (12 \pm 13)^\circ$ and the η-η' mixing angle is found to be $\phi_P = (41.4 \pm 1.3)^\circ$. Third, imposing the absence of gluonium for both mesons one finds $\phi_P = (41.5 \pm 1.2)^\circ$, in agreement with the former result. Finally, we would like to stress that more refined experimental data, particularly for the $\phi \to \eta'\gamma$ channel, will contribute decisively to clarify this issue.

References

1. J. L. Rosner, Phys. Rev. D **27** (1983) 1101.
2. E. Kou, Phys. Rev. D **63** (2001) 054027 [arXiv:hep-ph/9908214].
3. C. E. Thomas, JHEP **0710** (2007) 026 [arXiv:0705.1500 [hep-ph]].
4. F. Ambrosino *et al.* [KLOE Collaboration], arXiv:hep-ex/0612029.
5. A. Aloisio *et al.* [KLOE Collaboration], Phys. Lett. B **541** (2002) 45 [arXiv:hep-ex/0206010].
6. A. Bramon, R. Escribano and M. D. Scadron, Phys. Lett. B **503** (2001) 271 [arXiv:hep-ph/0012049].
7. W. M. Yao *et al.* [Particle Data Group], J. Phys. G **33** (2006) 1.
8. R. Escribano and J. Nadal, JHEP **0705** (2007) 006 [arXiv:hep-ph/0703187].

Frascati Physics Series Vol. XLVI (2007), pp. 481–488
HADRON07: XII Int. Conf. on Hadron Spectroscopy – Frascati, October 8-13, 2007
Light Meson Spectroscopy

OBSERVATION ON THE $\eta \to \pi^+ \pi^- e^+ e^-$ DECAY AT KLOE

KLOE collaboration*
presented by Roberto Versaci,
Laboratori Nazionali di Frascati dell'INFN, Frascati, Italy

Abstract

For this study 622 pb^{-1} of $\mathrm{e}^+\mathrm{e}^-$ events collected by the KLOE detector at the ϕ-factory DAΦNE have been used. The analysis is based on the reconstruction of the invariant mass of charged particles recoiling against a monocromatic photon in $\phi \to \eta\gamma$ events. The backgrounds are well reduced by kinematic cuts. About 700 signal event after background subtraction have been observed, while previous experiments collected less than 20 events. A preliminary estimate of the branching ratio is $(24 \pm 2 \pm 4) \times 10^{-5}$. Montecarlo studies show that the measurement of the angular asymmetry between pions and electrons decay planes, which could reveal possible CP violation beyond the Standar Model, is feasible.

* F. Ambrosino, A. Antonelli, M. Antonelli, F. Archilli, P. Beltrame, G. Bencivenni, S. Bertolucci, C. Bini, C. Bloise, S. Bocchetta, F. Bossi, P. Branchini, P. Campana, G. Capon, T. Capussela, F. Ceradini, S. Chi, P. Ciambrone, E. De Lucia, A. De Santis, P. De Simone, G. De Zorzi, A. Denig, A. Di Domenico, C. Di Donato, B. Di Micco, M. Dreucci, G. Felici, M. L. Ferrer, S. Fiore, C. Forti, P. Franzini, C. Gatti, P. Gauzzi, S. Giovannella, E. Graziani, W. Kluge, G. Lanfranchi, J. Lee-Franzini, D. Leone, M. Martini, P. Massarotti, S. Meola, S. Miscetti, M. Moulson, S. Müller, F. Murtas, M. Napolitano, F. Nguyen, M. Palutan, E. Pasqualucci, A. Passeri, V. Patera, F. Perfetto, P. Santangelo, B. Sciascia, A. Sciubba, A. Sibidanov, T. Spadaro, M. Testa, L. Tortora, P. Valente, G. Venanzoni, R.Versaci, G. Xu

1 Motivations

There are several theoretical reasons to study the $\eta \rightarrow \pi^+ \pi^- e^+ e^-$ decay. First, by using the virtual photon it is possible to probe the structure of the η meson in the time-like region of four momentum transfer square, q^2, which is equal to the invariant mass squared of the lepton pair. [1] One may also compare the predictions of the branching ratio value based on two different model, Vector Meson Dominance and Chiral Perturbation Theory. [2, 3, 4, 5] Moreover, it would be possible to study CP violation beyond the prediction of the Standard Model. [6] CPV can be introduced by a flavor-conserving, CP violating, four quark operators involving two strange quarks together with combinations of other light quarks. It can be experimentally tested by measuring the angular asymmetry between pions and electrons decay planes.

2 DAΦNE and KLOE

The DAΦNE e^+e^- collider operates at a total center of mass energy $\sqrt{s} = 1020$ MeV, the mass of the $\phi(1020)$ meson.

The KLOE detector consists of a large cylindrical drift chamber surrounded by a lead/scintillating-fiber electromagnetic calorimeter. The drift chamber [7] is 4 m in diameter and 3.3 m long. The momentum resolution is $\sigma(p_T)/p_T \sim 0.4\%$. Two track vertexes are reconstructed with a spatial resolution of ~ 3 mm. The calorimeter, [8] composed of a barrel and two end-caps, covers 98% of the solid angle. Energy and time resolution are $\sigma(E)/E = 5.7\%/\sqrt{E[\mathrm{GeV}]}$ and $\sigma(t) = 57$ ps$/\sqrt{E[\mathrm{GeV}]} \oplus 100$ ps. A superconducting coil around the detector provides a 0.52 T magnetic field.

The KLOE trigger [9] uses calorimeter and drift chamber information. For the present analysis only the calorimeter triggers have been used. Two energy deposits above threshold, $E > 50$ MeV for the barrel and $E > 150$ MeV for the end-caps, have been required.

3 Data sample

Since 2001, KLOE has collected an integrated luminosity of about 2.5 fb^{-1}. The samples used in this analysis are: 622 pb^{-1} from 2004-2005 data taking;

Montecarlo signal and background equivalent to 46×10^3 pb^{-1} and 1723 pb^{-1} respectively.

4 Event selection

The algorithm for the selection of the η meson decay in four charged particles requires: 1) four tracks coming from the interaction point, IP; the fiducial volume around the IP is a cylinder having radius $R = 4$ cm and height $h = 20$ cm; 2) at least one neutral cluster having energy $E_{cl} \geq 250$ MeV; 3) zero neutral clusters having energy in the range $50 \leq E_{cl} \leq 250$ MeV. A neutral cluster is defined as an energy deposit in the calorimeter without any associated tracks, having a polar angle in the range $(23°, 157°)$ and a time compatible with photons (i.e.: $|t_{cl} - r_{cl}/c| < min(5\ \sigma_t,\ 2\ ns)$).

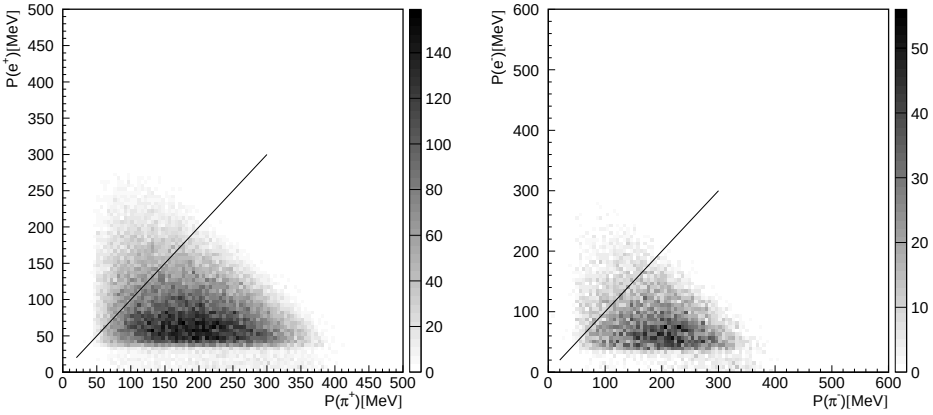

Figure 1: Momenta distribution for signal Montecarlo. Left: $P(e^+)$ vs $P(\pi^+)$. Right: $P(e^-)$ vs $P(\pi^-)$ for events having $|\vec{p}(e^+)| > |\vec{p}(\pi^+)|$.

It can happen that the track of a particle is poorly reconstructed and splits in two. A dedicated algorithm has been developed to recover broken tracks: for each pair of tracks, the four possible inward-outward combinations (i.e.: FirstHit-FH, FH-LastHit LH-FH, LH-LH) are considered. If any combination satisfies both the checks on the differences of the momenta: $\Delta p_T < 4.5$ MeV and $\Delta p_z < 3.0$ MeV the two tracks are considered as coming from the same

particle. The track having the largest distance to the IP is flagged as broken and discarded. The candidate tracks are ordered according to their momentum (separately per charge). The first is classified as pion and the second as electron. This simple criterion provides a correct particle identification in the 84% of the cases (see figure 1). Four candidate tracks are required, two positive and two negatives.

5 Background rejection

The main backgrounds after event selection are listed in table 1. The first ($\phi \to \pi^+\pi^-\pi^0$) simulates the signal when the π^0 undergoes a Dalitz decay or a photon converts in an e^+e^- pair. It is also useful to notice that in $\eta \to \pi^+\pi^-\gamma$ events, with photon conversion, the invariant mass of the four tracks reproduces the η mass peak.

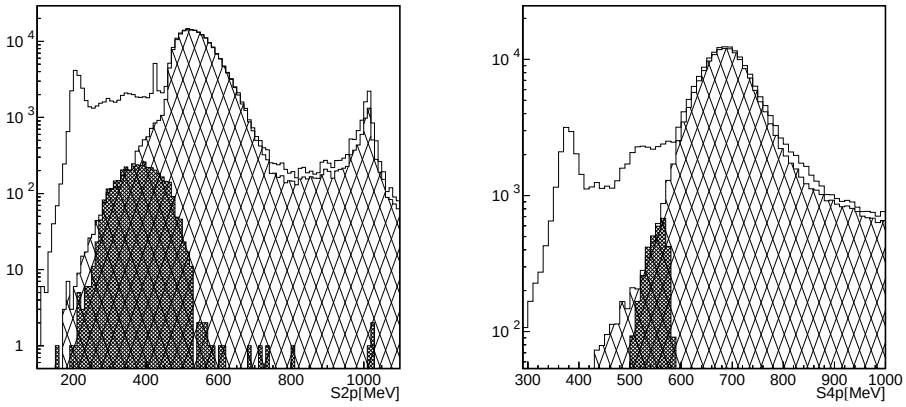

Figure 2: $S2p$ (left) and $S4p$ (right) spectra. Continuum line is signal plus all backgrounds; light hatching corresponds to $\phi \to \pi^+\pi^-\pi^0$ background; dense hatching corresponds to MC signal.

Background are reduced cutting on the sum of the momenta of the two particles classified as pions ($S2p = |\vec{p}(\mathrm{p}_1^+)| + |\vec{p}(\mathrm{p}_1^-)|$) and on the sum of the momenta of the four selected tracks ($S4p = \sum_1^4 |\vec{p}_i|$). It is required that: $270 < S2p < 470\ MeV$ and $450 < S4p < 600\ MeV$. Distribution are shown

Table 1: *Background over signal ratio for the main sources of background.*

B/S	$\phi \to \pi^+\pi^-\pi^0$	$\phi \to \eta\gamma$	$\phi \to K^+K^-$	Other
Event selection	90(1)	4.57(8)	15.9(2)	7.8(1)
Background rejection	1.58(5)	2.62(7)	1.84(6)	0.68(3)

in figure 2. The background over signal ratios (B/S) before and after the background rejection are listed in table 1.

6 Four tracks invariant mass

For the selected events it is possible to reconstruct the invariant mass of the four tracks according to the mass hypothesis previously defined.

To improve the resolution on the track momenta and on the energy of the neutral cluster, a kinematic fit is performed imposing the four-momentum conservation and the timing of the cluster.

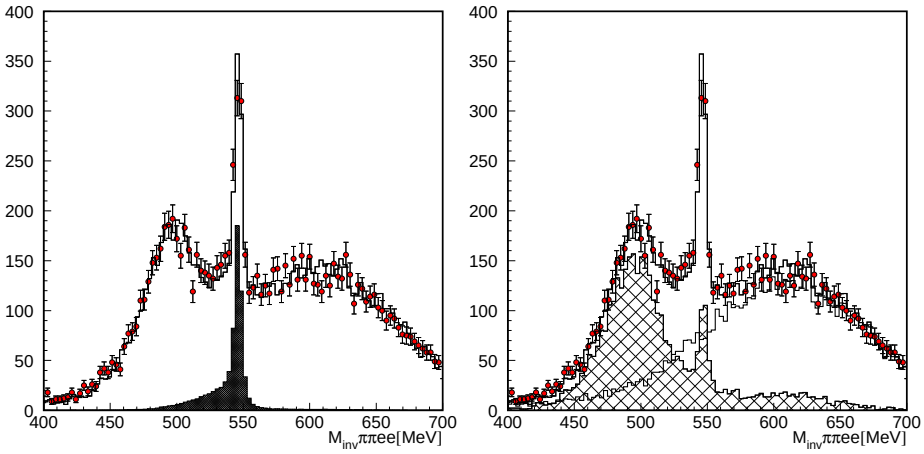

Figure 3: Fit to the invariant mass of the four selected tracks after background rejection. Dots: data. Solid line: total MC. On the left panel, MC signal is displayed as filled histogram. On the right panel the hatched histogram corresponds to $\phi \to \eta\gamma$ background while the continuous line is for all other sources of background.

To evaluate the number of signal events we use the MC shapes to fit the data spectrum taking into account both data and MC statistics for the calculation of the uncertainty. We have fit the spectrum in the range [400:700] MeV with 3 MeV per bin and using three MC shapes to fit the data: signal, other η decays and non-η backgrounds. We have chosen this background shape parametrization on order to minimize correlations among the shapes. Anyway we have performed the fit changing the parametrization and the result remained stable. It is stable also with respect to change of the fit range and of the size of the bins.

The fit to the distribution of the reconstructed invariant mass of the four tracks, constrained after the kinematic fit, is shown in figure 3. It is evident the peak of the signal corresponding to the η mass. The smaller background contribution peaked on the η mass is due to $\eta \to \pi^+\pi^-\gamma$ events with photon conversion into an electron-positron pair. A dedicated study to reject this background is ongoing.[1]

We have found $N_{events} = 733 \pm 62$ events, with $\chi^2/dof = 92/97$, corresponding to a χ^2 probability $P(\chi^2) = 0.61$.

7 Preliminary results

The preliminary value of the branching ratio has been obtained using the formula:

$$BR = \frac{N_{events}}{\sigma_\phi \cdot BR(\phi \to \eta\gamma) \cdot \mathcal{L} \cdot \epsilon} \tag{1}$$

where σ_ϕ is the cross section of the process $e^+e^- \to \phi$ and $\mathcal{L}$ is the luminosity of the data sample used for the measurement. The selection efficiency of our signal, ϵ, is evaluated by MC: $\epsilon = 0.1175(5)$. A correction to the efficiency, accounting for Data/MC discrepancies, is under evaluation. Based on previous studies done on 2001-2002 data, it is expected to of the order of 5-10%.

[1]The branching ratio of the $\eta \to \pi^+\pi^-\gamma$ decay used in this analysis is the one reported by the PDG 2006. [10] Recently the CLEO collaboration has published a new measurement [11] which is 15% lower: $BR(\eta \to \pi^+\pi^-\gamma) = (3.96 \pm 0.14 \pm 0.14) \times 10^{-2}$. This value would lead to an increase of our estimate of the BR($\eta \to \pi^+ \pi^- e^+ e^-$).

Table 2: *Comparison between the theoretical predictions of the branching ratio and the experimental results available in literature. Note that the prediction made by Jarlskog and Pilkuhn is proportional to the BR of the* $\eta \to \pi^+\pi^-\gamma$ *decay:* $BR(\eta \to \pi^+ \pi^- e^+ e^-) = 0.0065 \times BR(\eta \to \pi^+\pi^-\gamma)$. *Therefore the prediction changes if it is taken the PDG 2006 fit result* [10] *or the recent CLEO* [11] *measurement.*

Theory / Experiment	BR $\times 10^{-5}$
Jarlskog, Pilkuhn 1967 PDG's BR($\eta \to \pi^+\pi^-\gamma$)	30.5 ± 0.7
Jarlskog, Pilkuhn 1967 CLEO's BR($\eta \to \pi^+\pi^-\gamma$)	25.7 ± 1.3
Picciotto, Richardson 1993	32 ± 3
Faessler *et al.* 2000	36
Borasoy, Nissler 2007	29.9^{+6}_{-9}
CMD-2	$37\ ^{+25}_{-18}\ _{Stat.} \pm 3\ _{Syst.}$
Celsius-Wasa	$43 \pm 13\ _{Stat.} \pm 4\ _{Syst.}$

The preliminary value for the branching ratio is:

$$BR(\eta \to \pi^+ \pi^- e^+ e^-) = (24 \pm 2_{Fit} \pm 4_{Syst.}) \times 10^{-5} \qquad (2)$$

where the systematic error accounts for the uncertainty on the efficiency and on the background rejection. Comparison with theoretical predictions and other experiments is shown in table 2. A preliminary MC study on the asymmetry in the decay plane distribution shows that the cuts used in the analysis do not introduce any relevant distortion on the asymmetry shape.

References

1. L. G. Landsberg, Phys. Rept. **128** (1985) 301.
2. Jarlskog, C., & Pilkuhn, H., Nucl. Phys. B **1** (1967) 264.
3. A. Faessler, C. Fuchs and M. I. Krivoruchenko, Phys. Rev. C **61** (2000) 035206.
4. C. Picciotto and S. Richardson, Phys. Rev. D **48** (1993) 3395.
5. B. Borasoy and R. Nissler, arXiv:0705.0954 [hep-ph].
6. D. N. Gao, Mod. Phys. Lett. A **17** (2002) 1583.
7. M. Adinolfi *et al.*, [KLOE Collaboration], *Nucl. Instrum. Meth* **A 488** 2002 51.
8. M. Adinolfi *et al.*, [KLOE Collaboration], *Nucl. Instrum. Meth* **A 482** 2002 364.
9. M. Adinolfi *et al.*, [KLOE Collaboration], *Nucl. Instrum. Meth* **A 492** 2002 134.
10. W.-M. Yao et al., J. Phys. G**33**, 1 (2006).
11. A. Lopez *et al.* [CLEO Collaboration], arXiv:0707.1601 [hep-ex].

Frascati Physics Series Vol. XLVI (2007), pp. 489–496
HADRON07: XII Int. Conf. on Hadron Spectroscopy – Frascati, October 8-13, 2007
Light Meson Spectroscopy

DIRECT MEASUREMENT OF THE TOTAL WIDTH OF THE η' MESON

E. Czerwiński[†*], P. Moskal[†*], D. Grzonka[*], A. Budzanowski[⋆],
R. Czyżykiewicz[†], D. Gil[†], M. Janusz[†*], L. Jarczyk[†], B. Kamys[†],
A. Khoukaz[‡], P. Klaja[†*], W. Oelert[*], C. Piskor-Ignatowicz[†], J. Przerwa[†*],
B. Rejdych[†], J. Ritman[*], T. Sefzick[*], M. Siemaszko[§], M. Silarski[†],
J. Smyrski[†], A. Täschner[‡], M. Wolke[*], P. Wüstner[*], M. Zieliński[†], W. Zipper[§]
[†] *Institute of Physics, Jagiellonian University, Cracow, Poland*
[*] *IKP & ZEL, Forschungszentrum Jülich, Germany*
[‡] *IKP, Westfälische Wilhelms-Universität, Münster, Germany*
[§] *Institute of Physics, University of Silesia, Katowice, Poland*
[⋆] *Institute of Nuclear Physics, 31-342 Cracow, Poland*

Abstract

Using stochastically cooled proton beam of the cooler synchrotron COSY and the COSY-11 apparatus we have measured the mass distribution of the η' meson producing it via the $pp \to pp\eta'$ reaction. The preliminary analysis shows that the achieved experimental mass resolution amounts to about 0.3 MeV (FWHM). Such precision with about 2300 events gathered at five excess energies should permit for the extraction of the width of the η' meson with an accuracy of about 10 keV. In this article we describe the method of the measurement and present preliminary results.

1 Introduction

Studies of the η' meson decays [1)] and production [2)] are of interest on its own and provide inputs to the phenomenology of the Quantum Chromo-Dynamics in the non-perturbative regime [3)]. Specifically, precise determinations of the

partial widths for the η' decay channels should be helpful for the development of the Chiral Perturbation Theory. However, the experimental precision of the partial width for various decay channels – where only the branching ratio is known or will be measured – is governed by the precision of the knowledge of the total width. In the case of the η' meson the branching ratios are typically known with accuracy better than 1.5%, while the total width is established about 10 times less accurate [4]. Therefore, we expect that the precise determination of the natural width of the η' meson will have an impact on the physics results which will be derived from measurements at such facilities like e.g. COSY, DAϕNE-2 or MAMI-C carried out by collaborations: WASA-at-COSY [5], KLOE-2 [7, 8] and CBall-at-MAMI [6] respectively.

In the last issue of the Review of Particle Physics only two direct measurements of the natural width of the η' meson are reported [4]. In the first experiment the width was established from the missing mass spectrum of the $\pi^- p \to nX$ reaction measured close to the threshold for the production of the η' meson [9]. The achieved experimental mass resolution was equal to 0.75 MeV/c^2 (FWHM) and the extracted value of $\Gamma_{\eta'}$ amounts to (0.28 $\pm$ 0.10) MeV/c^2. In the second experiment the value of $\Gamma_{\eta'} = (0.40 \pm 0.22)$ MeV/c^2 was derived from the threshold excitation function of the $pd \to {}^3He\,X$ reaction [10]. The mean value from the two direct measurements [9, 10] amounts to (0.30$\pm$0.09) MeV/c^2 [4] and differs strongly from the value of (0.202$\pm$0.16) MeV/c^2 determined indirectly from the combinations of partial widths obtained from integrated cross sections and branching ratios [4].

During the many years of studies of the η' meson [11, 12, 13] by means of the stochastically cooled proton beam of COSY [14, 15] and the COSY-11 apparatus (Fig. 1) we have achieved the accuracy of the mass determination comparable to the value of the natural width of the η' meson. This encouraged us to conduct the investigations of the $\Gamma_{\eta'}$ directly from the missing mass distribution of the $pp \to pp\eta'$ reaction measured near the kinematical threshold. The advantage of a study close to the threshold is that the uncertainties of the missing mass determination are considerably reduced since at threshold $\partial(mm)/\partial p$ tends to zero (mm = missing mass, p = momentum of the outgoing protons).

2 Experiment

The measurement of the $pp \to pp\eta'$ reaction was conducted for five discrete beam momenta: 3211, 3213, 3214, 3218, and 3224 MeV/c, where the threshold momentum is at 3208.3 MeV/c. It was carried out at the cooler synchrotron

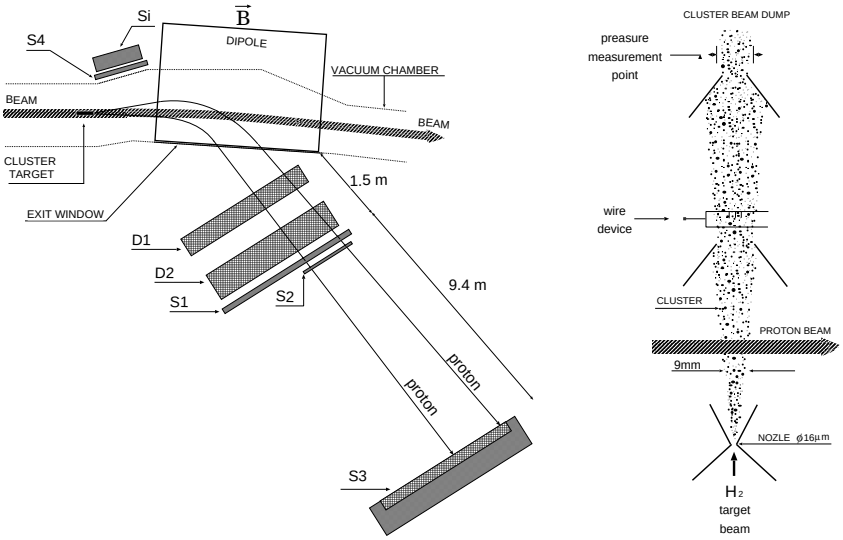

Figure 1: (left) COSY–11 detection setup with drift chambers (D1, D2) used for reconstruction of trajectories of positively charged ejectiles and scintillator hodoscopes (S1, S2, S3) for the time of flight determination. The silicon pad (Si) and scintillator (S4) detectors register the elastically scattered protons used for the monitoring purposes. (right) Schematic view of the target and beam crossing.

COSY [14, 15] using the COSY-11 facility [16, 17, 18]. At the intersection point of the cluster beam with the COSY proton beam the collisions of protons may result in the production of the η' meson. The ejected protons of the $pp \to pp\eta'$ reaction, having smaller momenta then the beam protons, are separated from the circulating beam by magnetic field, leave the vacuum chamber through a thin exit foil, and are registered by the detection system consisting of drift chambers and scintillation counters as depicted in Fig. 1 (left).

The measurement of the track direction by means of the drift chambers, and the knowledge of the dipole magnetic field and the target position allow to reconstruct the momentum vector for each registered particle. The time of flight measured between the S1 and the S3 scintillators gives the particle velocity. Independent determination of the momentum and velocity provides the particle identification. The knowledge of the momenta of both protons before and after the reaction allows to calculate the mass of a not observed particle or system of particles in the outgoing channel, which in case of the $pp \to pp\eta'$ reaction should be equal to the mass of the η' meson.

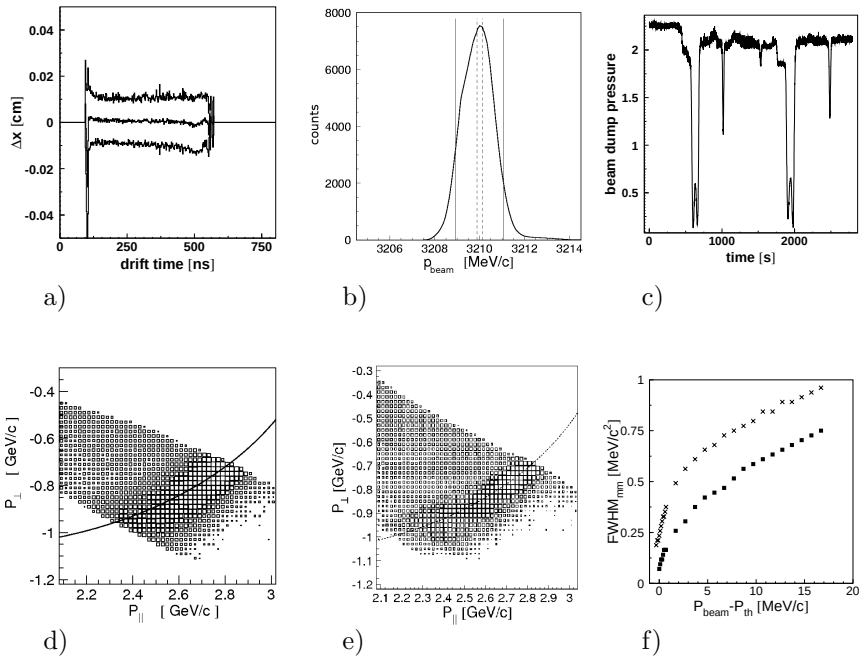

Figure 2: a) Average deviation (ΔX) between the measured and the fitted distances of tracks from the sense wire as a function of the drift time. The line around 0 corresponds to the average value of the ΔX distribution and the upper and lower lines denotes the spatial resolution ($\pm 1\sigma$) of the drift chamber. b) Beam momentum distribution obtained from the Schottky frequency spectrum measured during one of the previous COSY-11 runs. The range "seen" by 9 mm and 1 mm target is marked by the solid and dashed lines respectively. c) Distribution of the pressure measured during the wire device rotation. d,e) Momentum distribution of the forward scattered particles (in a logarithmic scale) with the superimposed kinematical ellipses (solid lines) expected for the elastically scattered protons. d) Data obtained with the target width of 9 mm and p_{beam} =2010 MeV/c [21]. e) On-line data from the reported here experiment conducted with the target width of circa 1 mm and p_{beam} =3211 MeV/c. f) FWHM of the missing mass signal as a function of beam momentum above the threshold for the η' meson creation in proton-proton collision simulated for 9 mm (crosses) and 1 mm (squares) target width [22].

In comparison to the previous measurement of the η' meson production, in order to improve the experimental resolution of the four-momentum determina-

tion and in order to decrease the spread of the momentum of the beam protons reacting with the target two major changes have been applied to the COSY-11 setup (Fig. 1). Namely, the spatial resolution of the drift chambers was improved by increasing the supply voltage up to the maximum allowed value and also the size of the target in the direction perpendicular to the COSY beam was decreased from 9 to circa 1 mm [19, 20].

2.1 Drift chambers

A charged particle passing through the drift cell ionizes gas molecules and the electrons drift towards the sense wire with a drift time related to the distance between the sense wire and the particle trajectory. The drift time to distance relation was calibrated for each 20 - 24 hours of the data taking period in order to minimize fluctuations of the drift velocity caused by variations of the atmospheric pressure, air humidity and gas mixture changes. Figure 2a illustrates that the obtained spatial resolution equals to about 100 μm.

2.2 Target

Due to the dispersion at the position of the COSY-11 target, the decrease in the target width results in a significant reduction of the momentum spread contributing to the measured events as shown in Fig. 2b. As can be clearly implied from the figure, the information about target size is crucial for determination of the beam momentum spread. It is also of great importance for the estimation of an error of momentum reconstruction of outgoing protons. Therefore, the spatial size of the target perpendicular to the COSY beam was controlled applying two independent methods. The first one is based on the movement of a wire through the cluster target beam which produces a pressure increase when a part of the cluster beam hits the wire. Several wires of different thicknesses on a rotating frame were used. The wire device was rotated several times through the cluster beam. The resulting pressure distribution as a function of rotation time is shown in Fig. 2c. Based on a preliminary analysis we expect to achieve an accuracy for the determination of the target size of about 0.2 mm.

The second technique used for monitoring the target beam size rest on the measurement of the momentum distribution of the elastically scattered protons (Fig. 2d,e). The momentum reconstruction of registered protons is performed by tracing back the trajectories from the drift chambers through the dipole magnetic field to the target centre. In reality, however, the reactions take place in a region of finite dimensions where beam and target overlap. Consequently, assuming in the analysis a point-like target implies a smearing of the momentum vectors. According to two–body kinematics, the momentum

components parallel and perpendicular to the beam axis form an ellipse. An example is shown in Fig. 2d,e. The spread around the expected kinematical ellipse can be used as a measure of the size of the interaction region [17]. For the appraisal of the effect in Fig. 2d,e we present results obtained with target widths of 9 and 1 millimetres.

2.3 Systematic uncertainty

The measurement of the missing mass distributions at five different beam energies will allow for monitoring the systematic uncertainties in the determination of the experimental mass resolution. This is mainly because the smearing of the missing mass due to the natural width of the η' remains unaltered when the beam momentum changes, whereas the smearing caused by the experimental uncertainties will narrow with decreasing beam momentum and at threshold it will reach a constant value directly proportional to the spread of the beam momentum. The effect is shown in Fig. 2f, which also illustrates that the reduction of the target thickness by 8 mm results in a change of the mass resolution by about 0.3 MeV. Since we expect to control the target thickness with an accuracy better then 0.2 mm, the systematical error due to the determination of the target size would be smaller than 0.01 MeV even if the measurement was conducted at only one excess energy.

Moreover, we can also distinguish the influence on the mass resolution caused by different experimental sources. For example angular distributions of the missing mass spectrum will permit to estimate contributions to the mass resolution due to the spread of the beam momentum and due to the proton momentum reconstruction [22]. This is because the resolution of the missing mass due to the spread of the beam momentum is almost independent of the polar emission angle of the η' meson, whereas the smearing of the missing mass due to the uncertainty of the proton momentum reconstruction does depend on this angle significantly [22].

3 Preliminary results

An on-line analysis has revealed a signal originating from the production of the η' meson at each of the investigated beam momenta (Fig. 3). As expected the width of the signal from the η' meson decreases with decreasing beam momentum, and closest to the threshold it equals to approximately 0.4 MeV (FWHM). Taking into account that the width of the η' is around 0.2 MeV we may estimate the achieved experimental resolution to be about 0.3 MeV, just at the same order as the searched signal. The presented spectra were obtained with a very preliminary calibration of the detection system. Hence,

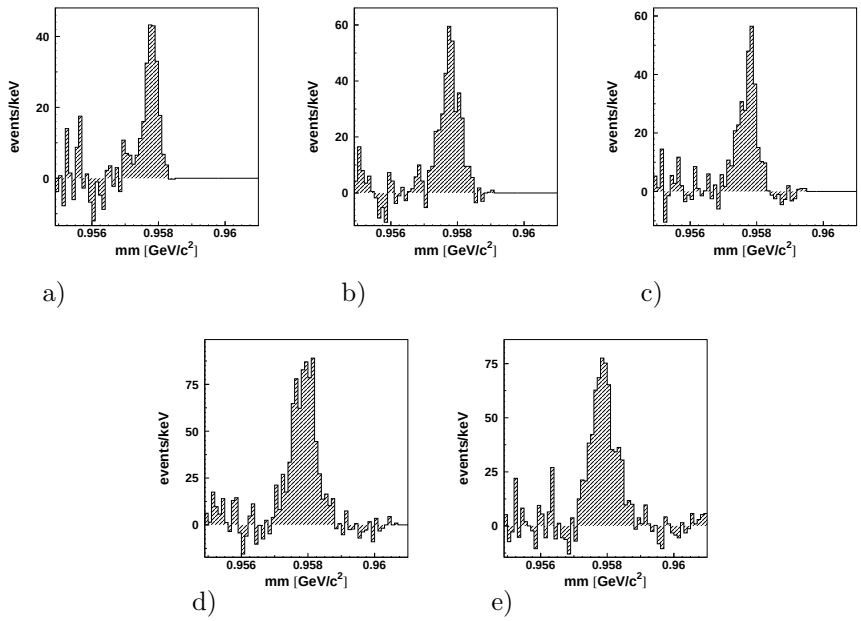

Figure 3: Preliminary background-corrected missing mass spectra for the $pp \to pp\eta'$ reaction measured using the COSY–11 detection setup at the nominal beam momenta: a) 3211, b) 3213, c) 3214, d) 3218, e) 3224 MeV/c.

there is still a room for the improvement of the experimental resolution in the ongoing off-line analysis. In addition, independently of the improvement of the calibrations we will correct also for the effect of the possible broadening due to the changes of the beam optics which could cause variations of the beam momentum in the order of 10^{-5}. In order to enable such corrections we have monitored various parameters which could influence the beam conditions like current intensity in the COSY dipoles, the temperature of the cooling water of the magnets, air temperature, humidity, and barometric pressure inside the COSY tunnel. Independently, it will be possible to correct the variation of the beam momentum based on the distribution of the elastically scattered protons measured simultaneously with the $pp \to pp\eta'$ reaction.

4 Acknowledgements

We acknowledge the support of the European Community-Research Infrastructure Activity under the FP6 programme (Hadron Physics, N4:EtaMeson-

Net, RII3-CT-2004-506078), the support of the German Research Foundation (DFG) and the support of the Polish Ministry of Science and Higher Education under the grants No. 3240/H03/2006/31 and 1202/DFG/2007/03.

References

1. A. Kupść, AIP Conf. Proc. **950**, 165 (2007).
2. P. Moskal, e-Print: hep-ph/0408162 (2004).
3. B. Borasoy and R. Nißler, AIP Conf. Proc. **950**, 180 (2007).
4. W.-M. Yao *et al.* (Particle Data Group), J. Phys. G **33**, 1 (2006).
5. H.-H. Adam *et al.*, e-Print Archive: nucl-ex/0411038 (2004).
6. A. Thomas, AIP Conf. Proc. **950**, 198 (2007).
7. F. Ambrosino *et al.*, Eur. Phys. J. **C50**, 729 (2007).
8. C. Bloise, AIP Conf. Proc. **950**, 192 (2007).
9. D. M. Binnie *et al.*, Phys. Lett. B **83**, 141 (1979).
10. R. Wurzinger *et al.*, Phys. Lett. B **374**, 283 (1996).
11. P. Moskal et al., Phys. Rev. Lett. **80**, 3202 (1998);
12. P. Moskal et al., Phys. Lett. **B 474**, 416 (2000);
13. A. Khoukaz et al., Eur. Phys. J **A 20**, 345 (2004);
14. D. Prasuhn *et al.*, Nucl. Instr. & Meth. A **441** 167 (2000).
15. H. Stockhorst *et al.*, AIP Conf. Proc. **950**, 239 (2007).
16. S. Brauksiepe *et al.*, Nucl. Instr. & Meth. A **376**, 397 (1996).
17. P. Moskal *et al.*, Nucl. Instr. & Meth. A **466**, 448 (2001).
18. J. Smyrski *et al.*, Nucl. Instr. & Meth. A **541**, 574 (2005).
19. H. Dombrowski *et al.*, Nucl. Instrum. Meth. A **386**, 228 (1997).
20. A. Täschner *et al.*, AIP Conf. Proc. **950**, 85 (2007).
21. R. Czyżykiewicz, e-Print: nucl-ex/0702010; PhD thesis, Jagiellonian University (2007).
22. E. Czerwiński, Diploma thesis, Jagiellonian University (2006).

Frascati Physics Series Vol. XLVI (2007), pp. 497–504
HADRON07: XII Int. Conf. on Hadron Spectroscopy – Frascati, October 8-13, 2007
Light Meson Spectroscopy

OBSERVATION OF NON-EXOTIC HYBRID MESONS CANDIDATES IN THE $\eta\eta\pi$ DECAY

Paul Eugenio and Alexander Ostrovidov
Florida State University, Tallahassee, FL USA

on behalf of the BNL-E852 Collaboration

Abstract

A study of the reaction $\pi^- p \to p\eta\eta\pi^-$ at 18 GeV/c has been performed on a data sample of 4,000 events obtained by Brookhaven experiment E852. A partial-wave analysis was performed. The J(PC) = 0(+) $\pi(1800)$ state is observed in the $a_0(980)\eta$ and $f_0(1500)\pi$ decay modes. The J(PC) = 2(+) $\pi_2(1880)$ meson is observed decaying through $a_2(1320)\eta$. Both states are potential candidates for non-exotic hybrid mesons.

1 Introduction

We present the results of a partial-wave analysis of the reaction $\pi^- p \to \eta\eta\pi^- p$ at 18 GeV/c pion beam momentum. The data were obtained by experiment E852 at Brookhaven National Laboratory. The primary goal of E852 was to search for candidates of non-$q\bar{q}$ mesons which are predicted to exist in QCD. In addition to multiquark states ($q\bar{q}q\bar{q}$, etc.) and quark-less glueballs (ggg), hybrid mesons with excited gluonic degrees of freedom ($q\bar{q}g$) should also exist.

Some of the non-$q\bar{q}$ resonances are expected to have exotic quantum numbers $J^{PC} = 0^{--}, 0^{+-}, 1^{-+}, 2^{+-}, ...$ which are forbidden for ordinary mesons. Other non-$q\bar{q}$ states may have non-exotic J^{PC} and those will mix with normal $q\bar{q}$ mesons. In this case identification of the hybrid nature of a non-exotic state becomes difficult and requires, at a minimum, the study of its branching ratios into various decay channels.

In the framework of the flux-tube model a $J^{PC} = 0^{-+}$ hybrid meson is expected to have a mass of 1.9-2.0 GeV/c^2 [1]. However the same model also predicts that the second radial excitation of a pion should have approximately the same mass. Moreover, their total widths are expected to be similar, on the order of 230-240 MeV/c^2. Only the branching ratios are predicted to be different [1]. While no particular decay mode is expected to dominate the decay of the radial excitation (with the $\rho\omega$ partial width being the largest), the hybrid state is predicted to decay predominantly through the $f_0(1300)\pi$ channel.

The $\pi(1800)$ state was discovered in the 3π decay mode by the SERPUKHOV-080 group in 1981 [2] and confirmed by the VES and E852 experiments. VES has seen the $\pi(1800)$ in the $\pi^+\pi^-\pi^-$, $K^+K^-\pi^-$, $\eta'\eta\pi^-$, and $\eta\eta\pi^-$ final states [3, 4, 5]. E852 has observed this state in the $\pi^+\pi^-\pi^-$ channel [6]. It is interesting to note that the previous measurements of the $\pi(1800)$ mass can be separated into two groups: one group with the mass around 1780 MeV/c^2 ($f_0(980)\pi$, $f_0(1300)\pi$, $K_0^*(1430)K$), and another group at 1860 MeV/c^2 ($\sigma\pi$, $\eta'\eta\pi^-$, $\eta\eta\pi^-$). Ref. [1] suggested that two different states may have been observed.

The $\pi_2(1880)$ resonance was first observed in 2001 by Anisovich *et al.* [7] through its $a_2(1320)\eta$ decay, together with a higher mass $\pi_2(2000)$ state in $a_0(980)\eta$ decay [8]. These states were soon confirmed by E852 in the $f_1\pi$ [9] and $\omega\rho$ [10] decay modes. The mass of $\pi_2(2000)$ matches well with the value expected for a radial $^1D_2$ quark-model state [8]. This leaves the $\pi_2(1880)$ resonance as a strong hybrid-meson candidate [7]. A hint of the $\pi_2(1880)$ presence was seen earlier by VES in their $\eta\eta\pi$ analysis [3], which is the most relevant to our case due to similarities in the production mechanisms.

2 Data sample.

A description of the experimental apparatus can be found in Ref. [11]. More details about the analysis can be found on our website [12]. A Cerenkov tagged π^- beam of momentum 18.3 GeV/c and a 30 cm liquid hydrogen target were used. The online trigger required three forward-going charged tracks and one charged recoil track. A total of 265 million events of this type were recorded during the second run of the experiment. After event reconstruction, candidate events having one positive pion, two negative pions, and four photons were selected. To reduce background additional cuts were applied on the vertex position, missing mass, and the direction of the missing momentum. Soft pions from recoil baryon decays were also rejected.

A 3-C kinematic fit was made to select the $\eta\pi^+\pi^-\pi^0\pi^-p$ event sample. One pair of photons was required to come from a π^0 decay and the other pair from an η decay, and the missing mass was required to be consistent with a proton. Events with a confidence level greater than 5% were selected.

Similar fits were made to other hypotheses. The most important competing hypothesis is $\pi^0\pi^+\pi^-\pi^0\pi^-p$ because the probability of 4 photons coming from the decay of 2 neutral pions is much greater than that for the $\pi^0\eta$ case. Any event which had a confidence level greater than 10% for a competing hypothesis was rejected. Approximately 180 000 $\eta\pi^+\pi^-\pi^0\pi^-p$ events were selected at this stage.

Only events with at least one $\pi^+\pi^-\pi^0$ combination below 650 MeV/c^2 were used in the final kinematic fit to the reaction $\pi^-p \to \eta\eta\pi^-p$, with a 5% confidence level cut. This resulted in about 4 400 $\eta\eta\pi^-$ events. The final data sample consisted of about 4 000 events in the mass and momentum transfer ranges selected for partial wave analysis (PWA).

3 Partial Wave analysis.

A detailed description of the partial wave formalism used in this analysis can be found in Ref. [13]. The analysis was performed within the framework of an isobar model, with a sequential decay of a 3-body state into an isobar and a final particle followed by a 2-body decay of the isobar into 2 other final particles. Each partial wave is characterized by: the total spin, parity and C-parity J^{PC}, the projection M of the total spin, the reflectivity ϵ of the system,

the type of isobar, and the orbital angular momentum L between the isobar and the bachelor particle. The notation M^ϵ is omitted below because PWA studies indicated that only $M^\epsilon = 0^+$ waves are present in this sample. Positive reflectivity indicates that production is dominated by natural-parity exchange such as ρ or Pomeron exchange.

All waves with $J \leq 3$ and $L \leq 3$ were tried in the fits. Odd-spin waves 1^{++} and 3^{++} were found to be insignificant, in contrast to even-spin waves 0^{-+} and 2^{-+}.

Among isobars, the $a_0(980)\eta$, $a_2(1320)\eta$, $f_0(1300)\pi$, $f_2(1270)\pi$, and $f_0(1500)\pi$ combinations were considered. Simple Breit-Wigner parameterizations were used to describe the isobars. There was no significant contribution from the $f_0(1300)\pi$ and $f_2(1270)\pi$ modes.

Resonance parameters from the PDG [14] were used for the $a_0(980)$ and $a_2(1320)$ isobars. To determine the best $f_0(1500)$ parameters from our data, we made a scan of the $f_0(1500)$ mass and width in 10 MeV steps performing a new PWA fit at each step. The best overall likelihood was achieved with $M = 1480 \pm 25$ MeV and $\Gamma = 120^{+50}_{-30}$ MeV, which is in reasonably good agreement with values given in PDG. According to the likelihood ratio test, the presence of the $f_0(1500)\pi$ partial wave is required at the confidence level of more than 99.9% because a logarithm of the likelihood changes by 12-14 points for 4 extra parameters in the mass bins near 1.8 GeV in the PWA fits with and without this partial wave.

The final fit required only four partial waves: $0^{-+}a_0(980)\eta\ S$, $0^{-+}f_0(1500)\pi\ S$, $2^{-+}a_2(1320)\eta\ S$, and $2^{-+}a_0(980)\eta\ D$. In addition, an isotropic non-interfering background wave was introduced in the fit to absorb the non-$\eta\eta\pi$ background. The fitted background intensity was 5% to 15% of the total intensity over the mass range of the fit.

The final PWA fit was done in the mass range from 1.5 to 2.5 GeV/c^2 in 50 MeV/c^2 steps and for the momentum transfer $-t$ less than 1.2 (GeV/c)^2. Figure 1 shows the intensities of the partial waves and Figure 2 shows some of the phase differences between them. Both 0^{-+} waves (Fig.1a,b) peak at 1.8 GeV/c^2, indicating the presence of the $\pi(1800)$ meson. A peak corresponding to the $\pi_2(1880)$ is observed in the $2^{-+}a_2(1320)\eta$ S-wave (Fig.1c). The $2^{-+}a_0(980)\eta$ D-wave (Fig.1d) is structureless but it accounts for the majority of events above 2 GeV/c^2.

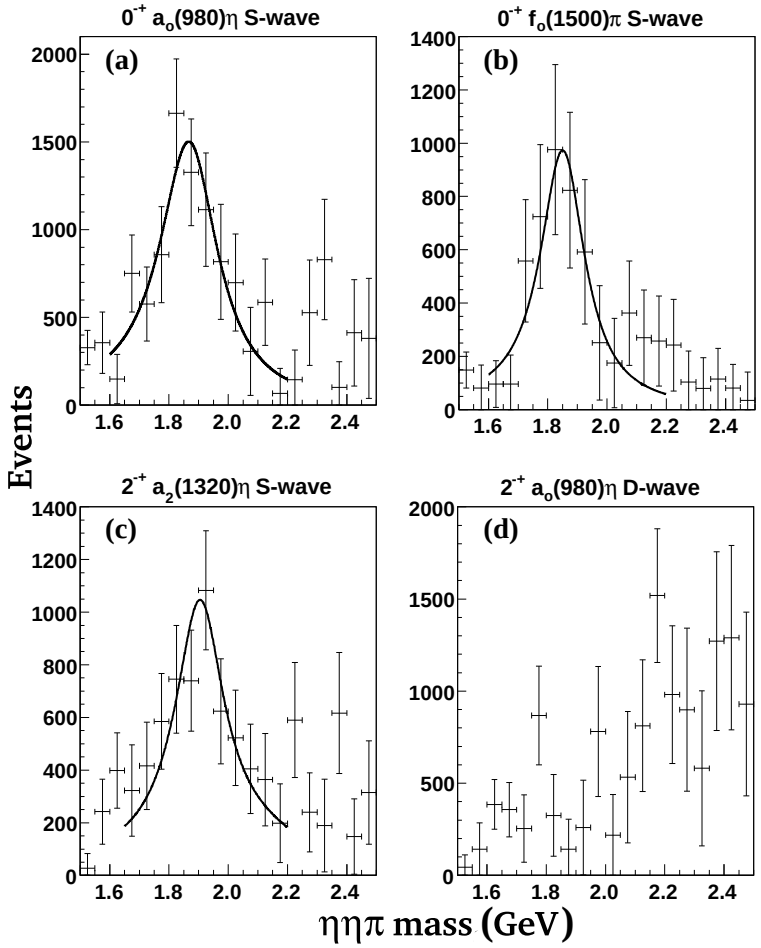

Figure 1: Intensities for the following partial waves: a) $0^{-+}a_0(980)\eta$ $S-$wave; b) $0^{-+}f_0(1500)\pi$ $S-$wave; c) $2^{-+}a_2(1320)\eta$ $S-$wave; d) $2^{-+}a_0(980)\eta$ $D-$wave. Smooth lines show results of the resonant Breit-Wigner fits.

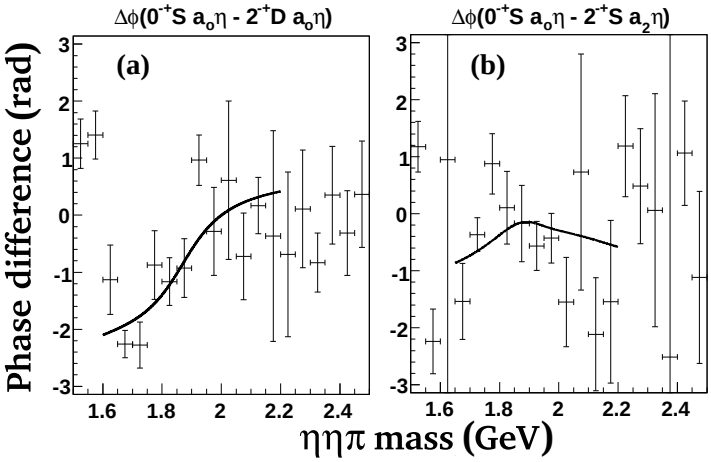

Figure 2: Phase difference between the following partial waves: a) $0^{-+}a_0(980)\eta$ $S-$wave and $0^{-+}a_0(980)\eta$ $D-$wave. b) $0^{-+}a_0(980)\eta$ $S-$wave and $2^{-+}a_2(1320)\eta$ $S-$wave. Smooth lines show results of the resonant Breit-Wigner fits.

The phase of the $0^{-+}a_0(980)\eta$ S-wave is rising in relation to the presumably non-resonant phase of the $2^{-+}a_0(980)\eta$ D-wave (Fig.2a) due to the presence of the $\pi(1800)$ resonance. The phase difference of the same wave relative to the $2^{-+}a_2(1320)\eta$ S-wave (Fig.2b) can be explained then by the presence of an additional resonance at somewhat higher mass in the 2^{-+} wave.

To confirm this conclusion, mass-dependent χ^2 fits were performed. Each of the resonant waves was parameterized with a single-pole relativistic Breit-Wigner form including Blatt-Weiskopf barrier factors. To accomodate the subthreshold behavior of the $a_2\eta$ and $f_0\pi$ waves at low $\eta\eta\pi$ mass, integration over the available width of decay isobars (a_2, a_0, and f_0) was used in the parameterization.

First the intensities of the two 0^{-+} waves were fitted to find the parameters of the $\pi(1800)$ state. When the poles in the $a_0\eta$ and $f_0\pi$ waves were treated independently the fit resulted in a mass of $M = 1882 \pm 19$ MeV/c^2 and a width of $\Gamma = 236 \pm 42$ MeV/c^2 for $a_0\eta$, and $M = 1865 \pm 25$ MeV/c^2 and $\Gamma = 191 \pm 55$ MeV/c^2 for $f_0\pi$. This fit has $\chi^2/\mathrm{dof} = 14.97/18$. The results are shown as solid curves in Figs.1a,b. As an illustration, the phase of the $0^{-+}a_0\eta$ S-wave is plotted against the presumably constant phase of the non-resonant

$2^{-+}a_0\eta$ D-wave in Fig.2a to confirm the resonant nature of the former.

Unfortunately, the phase of the $0^{-+}f_0(1500)\pi$ wave cannot be measured reliably. The interference region of the $0^{-+}f_0(1500)\pi$ and $2^{-+}a_2(1320)\eta$ waves is outside of the $\eta\eta\pi$ Dalitz plot. The other important interference term of the $f_0\pi$ wave (with the $0^{-+}a_0(980)\eta$ wave) is isotropic in all angles, which makes it highly ambiguous with the isotropic background term over the limited Dalitz plot. Without a reliable and stable phase measurement, the present identification of the $f_0(1500)\pi$ decay mode for $\pi(1800)$ is based solely on the Breit-Wigner shape of the wave intensity.

Assuming the same resonance in both 0^{-+} waves, a single-pole fit of their intensities was performed. It has $\chi^2/\text{dof} = 23.91/20$ with the following parameters for the $\pi(1800)$ state:

$$M = 1876 \pm 18 \pm 16 \text{ MeV}/c^2, \Gamma = 221 \pm 26 \pm 38 \text{ MeV}/c^2.$$

The systematic errors were found by varying the mass range of the fit and by adding different background parameterizations.

With these parameters fixed, the intensity of the $2^{-+}a_2\eta$ wave and its phase difference with the $0^{-+}a_0\eta$ wave were fitted. This fit has $\chi^2/\text{dof} = 19.86/18$ and is shown in Fig.1c and Fig.2b. The $\pi_2(1880)$ state has the following parameters:

$$M = 1929 \pm 24 \pm 18 \text{ MeV}/c^2, \Gamma = 323 \pm 87 \pm 43 \text{ MeV}/c^2.$$

Previous measurements [7] yield a $\pi_2(1880)$ mass and width of 1880 ± 20 MeV/c^2 and 255 ± 45 MeV/c^2, respectively, which agrees with the present result.

The fitted Breit-Wigner shapes for the same-pole fit were integrated to determine the predicted number of events for each state. The following ratio of branching ratios was obtained:

$$\frac{BR[\pi^-(1800) \to f_0(1500)\pi^-, f_0 \to \eta\eta]}{BR[\pi^-(1800) \to a_0^-(980)\eta, a_0^- \to \eta\pi^-]} = 0.48 \pm 0.17$$

A similar value of 0.40 ± 0.15 was obtained in a different maximum-likelihood PWA fit in which the branching ratio itself was one of the fitted parameters. In both cases our value is higher than the value of 0.08 ± 0.03 determined by VES [3] or the value of 0.030 ± 0.014 from Anisovich [7] but not inconsistent due to large statistical error.

In summary, a partial-wave analysis of the reaction $\pi^- p \to \eta\eta\pi^- p$ at 18 GeV/c^2 was carried out on a sample of 4 000 events. We observe the $0^{-+}\pi(1800)$ meson decaying through $a_0(980)\eta$ and $f_0(1500)\pi$. We also observe the $2^{-+}\pi_2(1880)$ meson in its $a_2(1320)\eta$ decay.

This research was supported in part by the U.S. Department of Energy, the U.S. National Science Foundation, and the Russian Ministry of Science and Education.

References

1. T. Barnes, F. E. Close, P. R. Page, and E. S. Swanson, Phys. Rev. D **55**, 4157 (1997).
2. SERPUKHOV-080 Collaboration, G. Bellini et al.. Phys. Rev. Lett. **48**, 1697 (1981).
3. VES Collaboration. D. V. Amelin *et al.*, Phys. At. Nucl. **59**, 976 (1996).
4. VES Collaboration. D. V. Amelin *et al.*, Phys. Lett. B **356**, 595 (1995).
5. VES Collaboration. D. V. Amelin *et al.*, Phys. Lett. B **337**, 219 (1994).
6. E852 Collaboration. S. U. Chung *et al.*, Phys. Rev. D **65**, 072001 (2002).
7. A. V. Anisovich *et al.*, Phys. Lett. B **500**, 222 (2001).
8. A. V. Anisovich *et al.*, Phys. Lett. B **517**, 273 (2001).
9. E852 Collaboration. J. Kuhn *et al.*, Phys. Lett. B **595**, 109 (2004).
10. E852 Collaboration. M. Lu *et al.*, Phys. Rev. Lett. **94**, 032002 (2005).
11. E852 Collaboration. S. U. Chung *et al.*, Phys. Rev. D **60**, 092001 (1999), and references therein.
12. http://hadron.physics.fsu.edu/etaetapi/.
13. S. U. Chung, "Formulas for Partial-Wave Analysis", Report BNL-QGS-93-05, Brookhaven National Laboratory (1993), (unpublished); J. P. Cummings and D. P. Weygand, "The New BNL Partial Wave Analysis Programs", Report BNL-64637, Brookhaven National Laboratory (1997), (unpublished).
14. W.-M. Yao *et al.*, Journal of Physics G **33**, 1 (2006).

Frascati Physics Series Vol. XLVI (2007), pp. 505–514
HADRON07: XII Int. Conf. on Hadron Spectroscopy – Frascati, October 8-13, 2007
Light Meson Spectroscopy

ISOSPIN VIOLATIONS IN $\phi \to \omega\pi^0$

Gang Li[1,3], Qiang Zhao[1,2,3], and Bing-Song Zou[1,3]
1) Institute of High Energy Physics, CAS, Beijing 100049, China
2) Department of Physics, Univ. of Surrey, Guildford, GU2 7XH, U.K.
3) Theoretical Physics Center for Science Facilities
CAS, Beijing 100049, China

Abstract

In this proceeding we report a recent progress on the study of isospin violation mechanisms in $\phi \to \omega\pi^0$, where the electromagnetic (EM) transitions and intermediate meson loops are identified as two major sources of contributions and quantified in an effective Lagrangian approach.

1 Motivation

During the past years, the phi-factory has collected a large number of ϕ events which allows precise tests of low-energy QCD dynamics. One interesting mechanism studied at the phi-factory is the isospin breaking in $\phi \to \omega\pi^0$, where a small branching ratio $BR(\phi \to \omega\pi^0) = (5.2^{+1.3}_{-1.1}) \times 10^{-5}$ has been measured [1, 2]. This is also a channel where the OZI-rule violation is present.

These two mechanisms, which generally account for different aspects of the underlying dynamics, are hence correlated in this channel.

In this proceeding, we try to clarify the role played by the electromagnetic (EM) transitions and strong isospin violations using an effective field theory approach. The EM contributions are described by the vector meson dominance (VMD) model, which possesses some advantages. Since the ϕ and ω meson masses are very close to the ρ mass, the EM form factors can be constrained by the precise data for the ρ^0 meson mass and width [2]. Meanwhile, contributions from other heavier vectors are expected to be small since they are much off-shell in this kinematic region.

The other source of isospin violation originates from the mass differences between the u and d quark due to chiral symmetry spontaneous breaking [3]. It can contribute to $\phi \to \omega\pi^0$ via OZI-rule-evading intermediate meson loops at low energies [4, 5, 6, 7, 8, 9]. Such a mechanism can be described as follows: In $\phi \to \omega\pi^0$, the intermediate charged and neutral kaon loop transitions are supposed to cancel out if the isospin symmetry is conserved. However, due to small mass differences between the u and d quarks, the charged and neutral kaons will also have small differences in mass, i.e. $m_{K^0} - m_{K^\pm} = 3.972 \pm 0.027$ MeV [2], and they are coupled to the ϕ meson with slightly different strength. The hadronic loops will then have "imperfect" cancellations and lead to measurable isospin violating branching ratios. This drives us to investigate the contributions from the intermediate meson exchanges to $\phi \to \omega\pi^0$, which are not only an OZI-rule violating mechanism, but also a source of isospin violations.

As follows, we first outline the major ingredients of the model, and then present the numerical results with discussions. The details of this approach can be found in Ref. [10].

2 EM transition contributions

In the VMD model, we consider that the pion is emitted at either ω creation or ϕ meson annihilation vertex with the corresponding amplitudes M_{fi}^{EM-I} and M_{fi}^{EM-II} respectively to be

$$M_{fi}^{EM-I} = \sum_V \frac{e}{f_V} \frac{M_V^2}{M_\phi^2 - M_V^2 + iM_V\Gamma_V} \frac{e}{f_\phi} \frac{g_{\omega V\pi}}{M_\omega} \varepsilon_{\alpha\beta\mu\nu} p_\omega^\alpha \varepsilon_\omega^\beta p_\phi^\mu \varepsilon_\phi^\nu \ , \quad (1)$$

and

$$M_{fi}^{EM-II} = \sum_V \frac{e}{f_V} \frac{M_V^2}{M_\omega^2 - M_V^2 + iM_V\Gamma_V} \frac{e}{f_\omega} \frac{g_{\phi V\pi}}{M_\phi} \varepsilon_{\alpha\beta\mu\nu} p_\omega^\alpha \varepsilon_\omega^\beta p_\phi^\mu \varepsilon_\phi^\nu \ , \qquad (2)$$

where $g_{\omega V\pi}$ is the VVP strong coupling constant, and Γ_V is the total width of the intermediate vector meson. This allows a compact expression for the EM amplitude:

$$M_{fi}^{EM} \quad = \quad M_{fi}^{EM-I} + M_{fi}^{EM-II} \equiv \frac{\tilde{g}_{EM}}{M_\phi} \varepsilon_{\alpha\beta\mu\nu} p_\omega^\alpha \varepsilon_\omega^\beta p_\phi^\mu \varepsilon_\phi^\nu \ , \qquad (3)$$

where $\tilde{g}_{EM}$ is the EM coupling. Since we adopt experimental data for $\phi \to \rho^0\pi^0$ in EM-II to determine the $g_{\phi\rho^0\pi^0}$ coupling, contributions from higher order intermediate vector mesons have been included and of which the effects should be small.

The vector-meson-photon couplings, e/f_V, can be determined by data for $V \to e^+e^-$ [2], while $g^2_{\omega\rho^0\pi^0} \simeq 85$, can be well determined by either $\omega \to \gamma\pi^0$ or $\omega \to \pi^0 e^+e^-$ [2] in the same framework [10]. For $g_{\phi\rho^0\pi^0}$, the KLOE measurement suggests that $\phi \to \rho\pi \to \pi^+\pi^-\pi^0$ has a weight of 0.937 in $\phi \to \pi^+\pi^-\pi^0$ [11]. This allows us to determine $g_{\phi\rho^0\pi^0}$ using the $\phi \to \pi^+\pi^-\pi^0$, and we find it is in a good agreement with that determined in $\phi \to \gamma\pi^0$ by assuming that the ρ^0 is the dominant contribution to the form factor. With the width of the ρ meson included, we obtain $BR^{EM} = 1.68 \times 10^{-5}$, with $M_\rho = 775.9$ MeV and $\Gamma_\rho = 143.9$ MeV [11]. This explicitly shows not only an important role played by the ρ meson, but also the necessity of contributions from strong isospin violations.

3 Intermediate meson loop contributions

In principle, all the possible intermediate meson exchange loops should be included in the calculation. In reality, the break-down of the local quark-hadron duality allows us to pick up the leading contributions as a reasonable approximation [4, 5]. In the ϕ meson decay, the leading branching ratio is via $\phi \to K\bar{K}$, which makes the intermediate $K\bar{K}$ rescattering via K^* exchange a dominant contribution. Apart from this, $\phi K^*\bar{K}$ coupling is sizeable in the SU(3) flavor symmetry which also makes the intermediate $K\bar{K}^* + c.c.$ rescattering via kaon and/or K^* exchange important contributions in $\phi \to \omega\pi^0$.

Contributions from higher mass states turn to be suppressed at the ϕ mass region. We take this as a reasonable approximation, and formulate the contributions from i) intermediate $K\bar{K}(K^*)$ loop; ii) intermediate $K\bar{K^*}(K)$ loop; and iii) intermediate $K\bar{K^*}(K^*)$ loop.

A general expression for the transition amplitude via an intermediate meson loop can be expressed as follows:

$$M_{fi} = \int \frac{d^4p_2}{(2\pi)^4} \sum_{K^* pol} \frac{T_1 T_2 T_3}{a_1 a_2 a_3} \mathcal{F}(p_2^2) \ . \tag{4}$$

For $K\bar{K}(K^*)$, the vertex functions are

$$\left\{ \begin{array}{lcl} T_1 & \equiv & ig_1(p_1 - p_3) \cdot \varepsilon_\phi \\ T_2 & \equiv & \frac{ig_2}{M_\omega} \varepsilon_{\alpha\beta\mu\nu} p_\omega^\alpha \varepsilon_\omega^\beta p_2^\mu \varepsilon_2^\nu \\ T_3 & \equiv & ig_3(p_\pi + p_3) \cdot \varepsilon_2 \end{array} \right. \tag{5}$$

where $g_{1,2,3}$ are the coupling constants at the meson interaction vertices. The four vectors, p_ϕ, p_ω, and p_{π^0} are the momenta for the initial ϕ and final state ω and π meson; the four-vector momentum, p_1, p_2, and p_3 are for the intermediate mesons, respectively, while $a_1 = p_1^2 - m_1^2$, $a_2 = p_2^2 - m_2^2$, and $a_3 = p_3^2 - m_3^2$ are the denominators of the propagators of intermediate mesons.

The vertex functions for the $K\bar{K^*}(K) + c.c.$ loop are

$$\left\{ \begin{array}{lcl} T_1 & \equiv & \frac{if_1}{M_\phi} \varepsilon_{\alpha\beta\mu\nu} p_\phi^\alpha \varepsilon_\phi^\beta p_3^\mu \varepsilon_3^\nu \ , \\ T_2 & \equiv & if_2(p_1 - p_2) \cdot \varepsilon_\omega \ , \\ T_3 & \equiv & if_3(p_\pi - p_2) \cdot \varepsilon_3 \ , \end{array} \right. \tag{6}$$

and for the $K\bar{K^*}(K^*) + c.c.$ loop,

$$\left\{ \begin{array}{lcl} T_1 & \equiv & \frac{ih_1}{M_\phi} \varepsilon_{\alpha\beta\mu\nu} P_\phi^\alpha \varepsilon_\phi^\beta p_3^\mu \varepsilon_3^\nu \ , \\ T_2 & \equiv & \frac{ih_2}{m_2} \varepsilon_{\alpha'\beta'\mu'\nu'} p_2^{\alpha'} \varepsilon_2^{\beta'} P_\omega^{\mu'} \varepsilon_\omega^{\nu'} \ , \\ T_3 & \equiv & \frac{ih_3}{m_3} \varepsilon_{\alpha''\beta''\mu''\nu''} p_2^{\alpha''} \varepsilon_2^{\beta''} p_3^{\mu''} \varepsilon_3^{\nu''} \end{array} \right. \tag{7}$$

where $f_{1,2,3}$ and $h_{1,2,3}$ are the coupling constants and $\mathcal{F}(p_2^2)$ is the form factor.

The couplings for the charged and neutral meson interactions may be different as one evidence is the different branching ratios for $\phi \to K^+K^-$ and $\phi \to K_S K_L$ even after the kinematic corrections. In the loop calculations due to the mass differences between the charged and neutral intermediate mesons, these two loops cannot cancel out exactly. The residue part is what we are interested in as follow.

To proceed, we consider two different approaches for the intermediate meson loops. One is to take an on-shell approximation. The other is to carry out a Feynman loop integration.

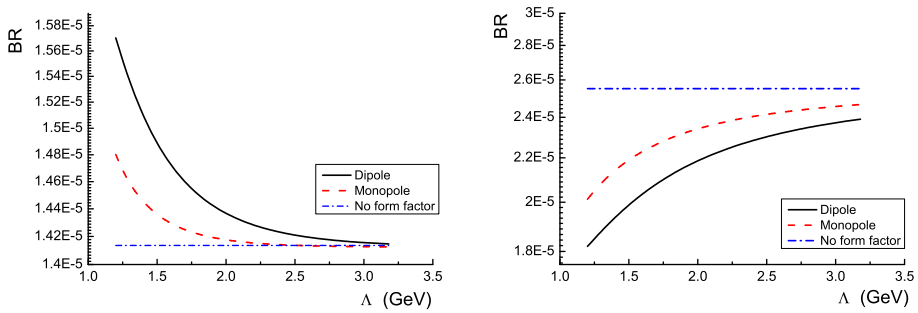

Figure 1: *The Λ-dependence of the sum of the EM and $K\bar{K}(K^*)$ loop amplitudes in the on-shell approximation. The left panel indicates results for a destructive addition and the right panel for a constructive addition. The solid, dashed and dot-dashed curves denote different considerations for the form factors, i.e. dipole, monopole and no form factor, respectively.*

In the on-shell approximation, the intermediate mesons are required to be on their mass shell. As a result, only the imaginary part of a loop transition amplitude contributes. Nevertheless, for those intermediate mesons, whose open threshold is above the initial meson mass, their contributions (only via the real part) will thus vanish. In $\phi \to \omega\pi^0$, this leads to exclusive contributions from the $K\bar{K}(K^*)$ loop while the other loop contributions are zero.

Meanwhile, we consider three cases for the form factor effects: i) with no form factor, i.e., $\mathcal{F}(p_2^2) = 1$; ii) with a monopole form factor, i.e., $\mathcal{F}(p_2^2) = (\Lambda^2 - m_2^2)/(\Lambda^2 - p_2^2)$; and iii) with a dipole form factor, $\mathcal{F}(p_2^2) = [(\Lambda^2 - m_2^2)/(\Lambda^2 - p_2^2)]^2$.

For the loop integrations, a form factor is necessary to kill the ultraviolet divergency. Both monopole and dipole form factors are examined. The redundant formulaes are given in Ref. [10]. In the numerical calculations the cut-off energy Λ is the only unknown parameter to be determined by the experimental data.

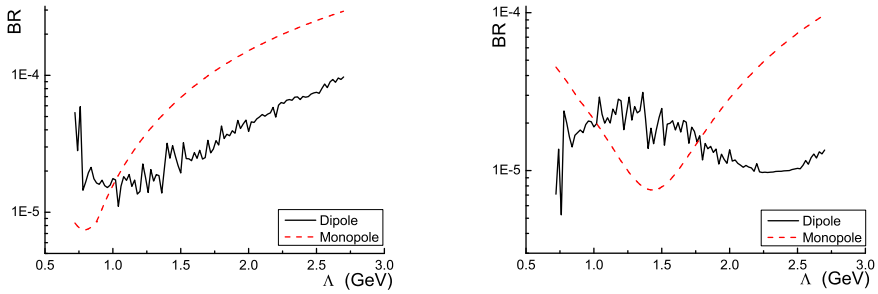

Figure 2: *The Λ-dependence of the constructive (left panel) and destructive additions (right panel) between the EM and hadronic loops. The dashed curves denote the results for adopting a monopole form factor for the hadronic loops, while the solid curves for adopting a dipole form factor.*

4 Numerical results

Combining the EM amplitude, we first examine the Λ-dependence of the branching ratios for those three treatments of the form factors in the on-shell approximation. Since there might exist a relative phase between the EM and hadronic loop amplitudes, results for the EM and hadronic loops *in phase* and *out of phase* are both shown (see Fig. 1).

On the left panel, where the EM amplitude is out of phase to the hadronic loop (destructive addition), the horizontal line indicates the largest cancellation between these two amplitudes with no form factor suppressions. At small Λ region, the cancellations are small for both monopole and dipole calculations since the hadronic loop amplitudes are small in both cases. These three curves smoothly approach the same value at high Λ where the hadronic loop contributions become negligibly small.

On the right panel the EM amplitude is in phase to the hadronic loop (constructive addition). Without form factor in the hadronic loop, the constructive addition of the these two amplitudes gives $BR = 2.55 \times 10^{-5}$. For the monopole and dipole form factor, the constructive effects increase with param-

eter Λ since the exclusive hadronic loop contributions are small in the small Λ region. It shows by the dashed and solid curve that the inclusive branching ratios converge to the dot-dashed curve at large Λ. In this constructive addition, the maximum branching ratio is still smaller than the experimental data, which is a sign for the underestimate of the hadronic loop contributions in the on-shell approximation, and implies the need for contributions from the dispersive part, i.e. from intermediate mesons above the ϕ mass.

In Fig. 2, results combining the EM amplitude and hadronic loops from Feynman integrations are presented.

Adding the hadronic loops to the EM amplitude coherently, we examine two phases in Fig. 2 in terms of the Λ, i.e. constructive (left panel) and destructive additions (right panel). It shows that with $\Lambda = 1.8 \sim 2.3$ GeV, the constructive addition with the dipole form factor for the hadronic loops gives the branching ratio in a good agreement with the experimental data, while with the monopole form factor, Λ requires a range of $1.2 \sim 1.5$ GeV. These cut-off energy ranges are consistent with the commonly accepted values. For a destructive addition between the EM and hadronic loop amplitudes as shown on the right panel, we find that the dipole form factor cannot reproduce the data within $\Lambda = 1 \sim 2.6$ GeV due to the significant cancellations between the EM and hadronic loop transitions. In contrast, with a monopole form factor for the hadronic loops the destructive addition can still reproduce the data around $\Lambda = 2.3$ GeV. However, this value of Λ turns to be out of the commonly accepted range for a monopole cut-off energy. In this sense, it shows that the data favor a constructive phase between the EM and hadronic loop amplitudes.

The dipole form factor might be even more preferable. Since the P-wave decay will generally favor a dipole form factor, we hence argue that the constructive addition between the EM and hadronic loop amplitudes with a dipole form factor is a favorable mechanism accounting for the experimental observation of $BR(\phi \to \omega\pi^0) = (5.2^{+1.3}_{-1.1}) \times 10^{-5}$ [2]. In Tab. 1, branching ratios of the exclusive and coherent (constructively) additions of the EM and hadronic loops with the dipole and monopole form factors are listed with the data.

In comparison with the results given by the on-shell approximation, it shows that the dispersive part of the loop transitions plays an important role in reproducing the data.

	Λ (GeV)	EM	(I)	(II)	(III)	Total	Exp.
Di.	2.14	1.66	0.23	0.33	~ 0.0	5.2 ± 0.2	$(5.2^{+1.3}_{-1.1})$
Mono.	1.38	1.66	0.14	0.56	~ 0.0	5.3 ± 0.5	$(5.2^{+1.3}_{-1.1})$

Table 1: Exclusive and coherent (constructive) contributions of the EM and hadronic loops to the $\phi \to \omega\pi^0$ branching ratios (in 10^{-5}) with a dipole and monopole form factor. (I), (II), and (III) correspond to loop $K\bar{K}(K^*)$, $K\bar{K}^*(K)$, and $K\bar{K}^*(K^*)$, respectively. The data are a world average from PDG2006 [2].

5 Summary

The isospin-violating mechanisms due to the EM and strong transitions in $\phi \to \omega\pi^0$ are quantified by the VMD model and the hadronic loop contributions, respectively. At hadronic level, the OZI-rule violations are recognized through the nonvanishing cancellations between the charged and neutral intermediate meson exchange loops, which also lead to the observation of the strong isospin violations. By extracting the vertex coupling information from independent processes, we can constrain the model parameters and make a quantitative assessment of the strong isospin violations via leading $K\bar{K}(K^*)$, $K\bar{K}^*(K)$ and $K\bar{K}^*(K^*)$ loops. Contributions from the different couplings of the intermediate mesons to the initial and final state mesons are also quantified. It shows that the dispersive part of the hadronic loop amplitudes have important contributions to the isospin violation and they produce crucial interferences with the EM transitions though their exclusive contributions are relatively smaller than the EM ones in $\phi \to \omega\pi^0$ decay.

Our approach is different from those in the literature, where the isospin violation in $\phi \to \omega\pi^0$ was studied by isoscalar and isovector mixing, e.g. ϕ-ω-ρ^0 and η'-η-π^0 mixings [12, 13, 14, 15, 16]. As such a scenario contains both EM and strong transitions in an s-channel, and allow the $\phi \to \omega\pi^0$ decay without violating the OZI-rule [17, 18], the EM and strong decays cannot be separated out. Our approach separates the EM and strong processes by explicitly introducing the EM amplitude as an s-channel process, while the hadronic loop contributions as t-channel processes. This provides an alternative view of the isospin violation mechanisms, and from which some novel insights

into the underlying dynamics can be gained.

It should be noted that intermediate meson loop contributions might be a general feature in a lot of transitions. Such a mechanism may be useful for understanding of some of those long-standing questions such as a_0-f_0 mixing [9, 19], and M1 transition puzzle in $J/\psi(\psi') \to \gamma\eta_c$ [20].

Supports from the U.K. EPSRC (Grant No. GR/S99433/01), National Natural Science Foundation of China (Grant No.10675131 and 10521003), and Chinese Academy of Sciences (KJCX3-SYW-N2), are acknowledged.

References

1. M. N. Achasov *et al.*, Phys. Lett. B **449**, 122 (1999).
2. W. M. Yao *et. al.* [Particle Data Group], J. Phys. G **33**, 1 (2006).
3. G. A. Miller, B. M. K. Nefkens and I. Slaus, Phys. Rept. **194**, 1 (1990).
4. H. J. Lipkin, Nucl. Phys. B **291**, 720 (1987).
5. H. J. Lipkin, Phys. Lett. B **179**, 278 (1986).
6. P. Geiger and N. Isgur, Phys. Rev. D **47**, 5050 (1993).
7. N. Isgur and H.B. Thacker, Phys. Rev. D **64**, 094507 (2001).
8. H.J. Lipkin and B.S. Zou, Phys. Rev. D **53**, 6693 (1996).
9. J. J. Wu, Q. Zhao and B. S. Zou, Phys. Rev. D **75**, 114012 (2007).
10. G. Li, Q. Zhao and B.S. Zou, arXiv:0706.0384[hep-ph].
11. A. Aloisio *et al.* [KLOE Collaboration], Phys. Lett. B **561**, 55 (2003) [Erratum-ibid. B **609**, 449 (2005)].
12. A. Bramon, Phys. Rev. D **24**, 1994 (1981).
13. J.F. Donoghue, B.R. Holstein, and D. Wyler, Phys. Rev. Lett. **69**, 3444 (1992).
14. L. Ametller, C. Ayala and A. Bramon, Phys. Rev. D **30**, 674 (1984).
15. S.A. Coon, B.H.J. McKellar, and M.D. Scadron, Phys. Rev. D **34**, 2784 (1986); S. A. Coon and R. C. Barrett, Phys. Rev. C **36** (1987) 2189.

16. H. Genz and S. Tatur, Phys. Rev. D **50**, 3263 (1994).

17. V. A. Karnakov, Yad. Fiz. **42** (1985) 1001.

18. N. N. Achasov and A. A. Kozhevnikov, Int. J. Mod. Phys. A **7**, 4825 (1992).

19. C. Hanhart, B. Kubis and J. R. Pelaez, Phys. Rev. D **76**, 074028 (2007).

20. G. Li and Q. Zhao, arXiv:0709.4639 [hep-ph].

Frascati Physics Series Vol. XLVI (2007), pp. 515–522
HADRON07: XII Int. Conf. on Hadron Spectroscopy – Frascati, October 8-13, 2007
Light Meson Spectroscopy

STUDY OF THE PROCESS $e^+e^- \to \omega\pi^0$ WITH THE KLOE DETECTOR

KLOE Collaboration*
presented by Antonio De Santis
Università "La Sapienza" e Sezione INFN, ROMA, Italy.

Abstract

Using ~ 600 pb^{-1} collected with the KLOE detector at DAΦNE, we have studied the production cross section of $\pi^+\pi^-\pi^0\pi^0$ and $\pi^0\pi^0\gamma$ final states in e^+e^- collisions at center of mass energies between 1000 and 1030 MeV. By fitting the observed interference pattern around M_ϕ for both final states, we extract a measurement (preliminary) for the ratio $\Gamma(\omega \to \pi^0\gamma)/\Gamma(\omega \to \pi^+\pi^-\pi^0) = 0.0934 \pm 0.0022$. Since these two final states represent the 98% of the ω decay channels, we use the existing measurements on the remaining rarer decays to derive BR$(\omega \to \pi^+\pi^-\pi^0) = (89.94 \pm 0.23)\%$ and BR$(\omega \to \pi^0\gamma) = (8.40 \pm 0.19)\%$. Moreover, the parameters describing the $e^+e^- \to \pi^+\pi^-\pi^0\pi^0$ reaction around M_ϕ are used to extract the branching fraction for the OZI and G-parity violating $\phi \to \omega\pi^0$decay: BR$(\phi \to \omega\pi^0) = (5.63 \pm 0.70) \times 10^{-5}$.

*F. Ambrosino, A. Antonelli, M. Antonelli, F. Archilli, C. Bacci, P. Beltrame, G. Bencivenni, S. Bertolucci, C. Bini, C. Bloise, S. Bocchetta, F. Bossi, P. Branchini, R. Caloi, P. Campana, G. Capon, T. Capussela, F. Ceradini, S. Chi, G. Chiefari, P. Ciambrone, E. De Lucia, A. De Santis, P. De Simone, G. De Zorzi, A. Denig, A. Di Domenico, C. Di Donato, B. Di Micco, A. Doria, M. Dreucci, G. Felici, A. Ferrari, M. L. Ferrer, S. Fiore, C. Forti, P. Franzini, C. Gatti, P. Gauzzi, S. Giovannella, E. Gorini, E. Graziani, W. Kluge, V. Kulikov F. Lacava, G. Lanfranchi, J. Lee-Franzini, D. Leone, M. Martini, P. Massarotti, W. Mei, S. Meola, S. Miscetti, M. Moulson, S. Müller, F. Murtas, M. Napolitano, F. Nguyen, M. Palutan, E. Pasqualucci, A. Passeri, V. Patera, F. Perfetto, M. Primavera, P. Santangelo, G. Saracino, B. Sciascia, A. Sciubba, A. Sibidanov, T. Spadaro, M. Testa, L. Tortora, P. Valente, G. Venanzoni, R. Versaci, G. Xu

1 Introduction

In the energy region of few tens of MeV around M_ϕ, the $\omega\pi^0$ production cross section is largely dominated by the non-resonant processes $e^+e^- \to \rho/\rho'$. However, in a region closer to M_ϕ, a contribution from the OZI and G-parity violating decay $\phi \to \omega\pi^0$ is expected. This strongly suppressed decay can be observed only through the interference pattern with the previous reaction, which shows up as a dip in the production cross section as a function of the center of mass energy ($\sqrt{s}$). The interference scheme depends on the different final states used in this analysis ($\pi^+\pi^-\pi^0\pi^0$ and $\pi^0\pi^0\gamma$).

2 The KLOE detector

The KLOE [1)] experiment operates at DAΦNE, [2)] the Frascati ϕ-factory. DAΦNE is an e^+e^- collider running at a center of mass energy of $\sim$ 1020 MeV, the mass of the ϕ-meson. Equal-energy positron and electron beams collide at an angle of π-25 mrad, producing ϕ-mesons nearly at rest.

The KLOE detector consists of a large cylindrical drift chamber, DC, surrounded by a lead-scintillating fiber electromagnetic calorimeter, EMC. A superconducting coil around the EMC provides a 0.52 T field. The drift chamber, [3)] 4 m in diameter and 3.3 m long, has 12,582 all-stereo tungsten sense wires and 37,746 aluminium field wires. The chamber shell is made of carbon fiber-epoxy composite and the gas used is a 90% helium, 10% isobutane mixture. These features maximize transparency to photons and reduce $K_L \to K_S$ regeneration and multiple scattering. The position resolutions are $\sigma_{xy}\sim$150 μm and $\sigma_z\sim$ 2 mm. The momentum resolution is $\sigma(p_\perp)/p_\perp \approx 0.4\%$. Track vertices are reconstructed with a spatial resolution of $\sim$3 mm. The calorimeter [4)] is divided into a barrel and two endcaps, for a total of 88 modules, and covers 98% of the solid angle. The modules are read out at both ends by photo-multipliers, both in amplitude and time. The readout granularity is $\sim (4.4\times4.4)$ cm^2, for a total of 2440 cells. The energy deposits are obtained from the signals amplitude while the arrival times of particles and the positions in three dimensions are obtained from the time differences. Cells close in time and space are grouped into a calorimeter cluster. The cluster energy E is the sum of the cell energies. The cluster time T and position $\vec{R}$ are energy weighed averages. Energy and time resolutions are $\sigma_E/E = 5.7\%/\sqrt{E\ (\mathrm{GeV})}$ and $\sigma_t = 57\ \mathrm{ps}/\sqrt{E\ (\mathrm{GeV})} \oplus 100$ ps, respectively. The KLOE trigger [5)] uses both calorimeter and chamber infor-

mation. A cosmic veto reject events where at least two outermost EMC layers are fired.

3 The $\sqrt{s}$ dependence of $e^+e^- \to \pi^+\pi^-\pi^0\pi^0/\pi^0\pi^0\gamma$ cross sections

As mentioned before, in the energy region below 1.4 GeV the $\pi^+\pi^-\pi^0\pi^0/\pi^0\pi^0\gamma$ production cross sections are dominated by the non-resonant process $e^+e^- \to \rho/\rho' \to \omega\pi^0$. At $\sqrt{s} \sim M_\phi$, the decay $\phi \to \omega\pi^0$ also contributes and interferes with the other processes. In the neutral channel there are also contributions from $\phi \to S\gamma$ and $\phi \to \rho\pi^0$. The dependence of the cross section on the center of mass energy can be parametrized in the form: [6)]

$$\sigma(\sqrt{s}) = \sigma_{NR}(\sqrt{s}) \cdot \left|1 - Z\frac{M_\phi\Gamma_\phi}{D_\phi}\right|^2 \tag{1}$$

where $\sigma_{NR}(\sqrt{s})$ is the bare cross section for the non-resonant process, Z is the complex interference parameter (i.e. the ratio between the ϕ decay amplitude and the other processes), while M_ϕ, Γ_ϕ and D_ϕ are the mass, the width and the inverse propagator of the ϕ meson respectively. Since in the considered center of mass energy range the non-resonant cross section increases almost linearly, we assume a simple linear dependence:

$$\sigma_{NR}(\sqrt{s}) = \sigma_0 + \sigma'(\sqrt{s} - M_\phi) \tag{2}$$

4 Data analysis

All the available statistics collected at the ϕ peak in 2001–2002 data-taking periods, corresponding to 450 pb^{-1}, has been analyzed. Moreover four scan points ($\sqrt{s}$= 1010 MeV, 1018 MeV, 1023 MeV and 1030 MeV) of $\sim$ 10 pb^{-1} each and the off-peak data ($\sqrt{s}$= 1000 MeV) acquired in 2005-2006 have been included in this analysis. All runs are grouped in center of mass energy bins of 100 keV.

4.1 $e^+e^- \to \omega\pi^0 \to \pi^+\pi^-\pi^0\pi^0$

In the $\pi^+\pi^-\pi^0\pi^0$ analysis, data are filtered by selecting events with the expected final state signature: two tracks connected to a vertex inside a small cylindrical fiducial volume around the Interaction Point (IP) and four neutral

clusters with minimum energy (10 MeV) in the prompt Time Window (TW), defined as $|T_\gamma - R_\gamma/c| < MIN(3.5 \cdot \sigma_T, 2 \text{ ns})$.

A kinematic fit requiring total four-momentum conservation and time of flight (TOF) for photons ($T_\gamma = R_\gamma/c$) improves the energy resolution. The resulting χ^2 ($\chi^2_{\rm Kfit}$) is used to select a signal enriched ($\chi^2_{\rm Kfit} < 50$), $\rm S_{evts}$, and a background dominated ($\chi^2_{\rm Kfit} > 50$), $\rm B_{evts}$, samples. The signal selection efficiency in the $\rm S_{evts}$ sample has been evaluated by Montecarlo (MC). The resulting value $\varepsilon \sim 40\%$ is dominated by the acceptance requirements and has a small dependence as a function of $\sqrt{s}$.

The main background contributions come from $\phi \to K_S K_L \to \pi^+\pi^-\pi^0\pi^0$ and $\phi \to K^+K^-$ with $K^\pm \to \pi^\pm\pi^0$, which have the same final state. The other two background components ($\phi \to \eta\gamma$ with $\eta \to \pi^+\pi^-\pi^0$, and $\phi \to \pi^+\pi^-\pi^0$) mimic the final state signature because of additional accidental clusters and/or shower fragments (splitting). In the signal enriched region, the expected contamination at $\sqrt{s} \sim M_\phi$ is $\sim 12\%$. The signal counting on data is performed for each $\sqrt{s}$ bin by fitting the reconstructed π^0 recoil mass ($M_{\rm rec}$) distribution for both $\rm S_{evts}$ and $\rm B_{evts}$ samples with MC signal and background shapes. The fit procedure takes into account both data and MC statistics. In Fig. 1, data-MC comparison of few relevant distributions for the most populated energy bin is shown. In the last distributions ($M_\pm = M_{\pi^+\pi^-}$, $M_{\rm mix} = M_{\pi^\pm\pi^0}$), the peaks due to $K^0 \to \pi^+\pi^-$ and $K^\pm \to \pi^\pm\pi^0$ backgrounds are clearly visible.

4.2 $e^+e^- \to \omega\pi^0 \to \pi^0\pi^0\gamma$

The acceptance selection for $\pi^0\pi^0\gamma$ events requires five neutral clusters with energy $E_\gamma \geq 7$ MeV and a polar angle $|\cos\theta_\gamma| < 0.92$ in the prompt Time Window. After applying a first kinematic fit (Fit1) imposing total four-momentum conservation, photons are paired to π^0's by minimizing a χ^2 built using the invariant mass of the two $\gamma\gamma$ pairs ($M_{\gamma\gamma}$). A second kinematic fit (Fit2) imposes also constraints on the π^0 masses.

The background with final state different from $\pi^0\pi^0\gamma$ is rejected by requiring $\chi^2_{\rm Fit2}/\text{Ndf} \leq 5$ and $\Delta M_{\gamma\gamma} = |M_{\gamma\gamma} - M_\pi| \leq 5\,\sigma_{\gamma\gamma}$, where $M_{\gamma\gamma}$ and $\sigma_{\gamma\gamma}$ are evaluated using the photon momenta from Fit1. After these cuts the remaining sample is dominated by $e^+e^- \to \omega\pi^0 \to \pi^0\pi^0\gamma$ and $\phi \to S\gamma \to \pi^0\pi^0\gamma$ events. Signal is then selected neglecting the interference between the two processes and cutting on the intermediate state mass: only events satisfying $|M_{\pi\gamma} - M_\omega| < 3\,\sigma_{M_\omega}$ are retained, where $M_{\pi\gamma}$ is the closest mass to M_ω of

the two $\pi^0\gamma$ combinations. The residual 10% background contamination comes predominantly from $\phi \to \eta\gamma \to \pi^0\pi^0\pi^0\gamma$ events where two photons are lost or merged. The overall selection efficiency for the identification of the signal is evaluated by applying the whole analysis chain to signal MC events: $\varepsilon_{\pi\pi\gamma} \sim 40\%$, almost flat in $\sqrt{s}$. In Fig. 2 data-MC comparison for events in the most populated $\sqrt{s}$ bin is shown. The ψ variable is the minimum angle between the photon and the π^0's in the di-pion rest frame. A good agreement is observed both after acceptance selection and after applying analysis cuts.

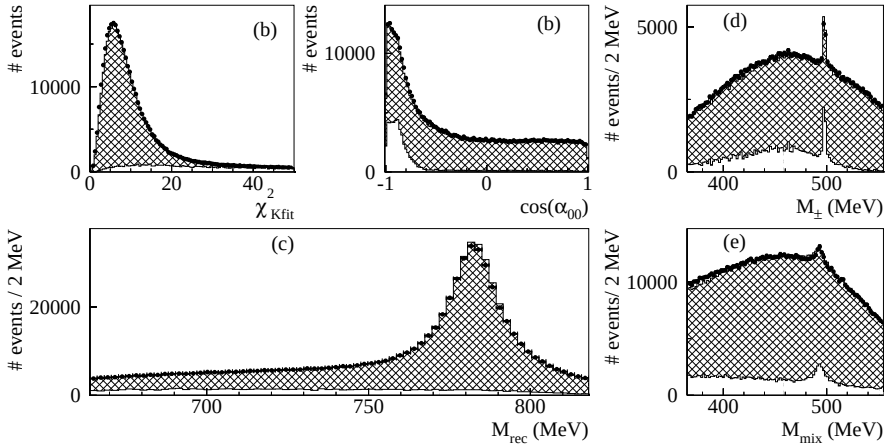

Figure 1: *Data-MC comparison for $\pi^+\pi^-\pi^0\pi^0$ signal enriched distribution using events taken at 1019.75 MeV : (a) $\chi^2_{\rm Kfit}$ (Ndf=8); (b) cosine of the angle between the two reconstructed π^0's; (c) π^0 recoil mass; invariant mass of the charged (d) and mixed (e) pion pairs. Black dots are data, while hatched and white histograms are MC signal and background shapes respectively, weighted by our fit results.*

5 Fit results and ω branching ratios extraction

The measured values of visible cross section are fitted with the parametrization (1), convoluted with a radiator function. [7)] The free parameters are: σ_0^i, $\Re(Z_i)$, $\Im(Z_i)$ and σ_i', where i is the 4π or $\pi\pi\gamma$ final state. In Fig. 3 data points with the superimposed fit function are shown for both channels. The preliminary values for the extracted parameters are reported in Tab. 1. The resulting

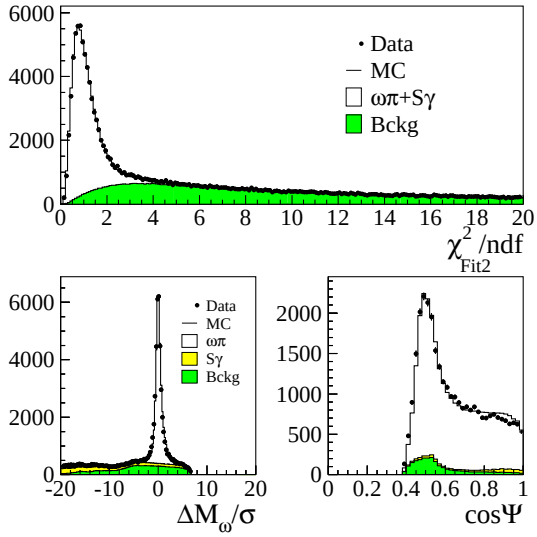

Figure 2: *Data-MC comparison for $\pi^0\pi^0\gamma$ events taken at 1019.75 MeV. Top: normalized χ^2 of the second kinematic fit after acceptance cuts. Bottom: $\pi^0\gamma$ invariant mass (left), and $\cos\psi$ distribution after cutting on $M_{\pi\gamma}$ (right). In the upper panel all the background is grouped together, while in the lower ones the small $\phi \to S\gamma$ contribution is shown alone.*

χ^2/N_{df} are 12.8/15 ($P(\chi^2) = 62\%$) for the fully neutral channel and 13.4/13 ($P(\chi^2) = 42\%$) for the other one.

From the two previous measurements, taking into account the phase space difference between the two decays, [6] we obtain:

$$\frac{\Gamma(\omega \to \pi^0\gamma)}{\Gamma(\omega \to \pi^+\pi^-\pi^0)} = 0.0934 \pm 0.0021 \tag{3}$$

Since these two final states correspond to $\sim 98\%$ of the ω decay channels, this ratio and the sum of the existing BR measurements on the remaining rarer decays [8] are used to extract the main ω branching fractions imposing the unitarity:

$$BR(\omega \to \pi^+\pi^-\pi^0) = (89.94 \pm 0.23)\% \tag{4}$$

$$BR(\omega \to \pi^0\gamma) = (8.40 \pm 0.19)\% \tag{5}$$

with a correlation of 82%. Comparison between our evaluation and the values reported by PDG [8] is shown in Fig. 3.

Table 1: *Fit results for the* $e^+e^- \to \pi^+\pi^-\pi^0\pi^0$ *and* $e^+e^- \to \pi^0\pi^0\gamma$ *cross sections.*

Parameter	4π channel	$\pi\pi\gamma$ channel
σ_0 (nb)	8.12 ± 0.14	0.776 ± 0.012
$\Re(Z)$	0.097 ± 0.012	0.013 ± 0.013
$\Im(Z)$	-0.133 ± 0.009	-0.155 ± 0.007
σ' (nb/MeV)	0.072 ± 0.008	0.0079 ± 0.0006

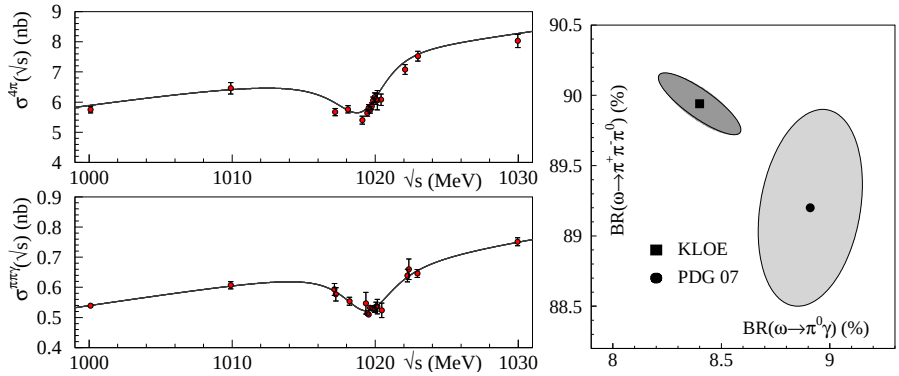

Figure 3: *Cross section fit results for the* $e^+e^- \to \pi^+\pi^-\pi^0\pi^0$ *(top-left) and* $e^+e^- \to \pi^0\pi^0\gamma$ *(bottom-left) channels. Black dots are data, solid line is the resulting fit function. Branching fraction for the two main* ω *decay channels (right). The square is the KLOE fit result, while the dot is the PDG constrained fit result. The shaded regions are the 68% C.L.*

6 BR($\phi \to \omega\pi^0$) evaluation

The measured $\sigma_0^{4\pi}$ and $Z_{4\pi}$ parameters of the $\pi^+\pi^-\pi^0\pi^0$ final state are related to the BR($\phi \to \omega\pi^0$) through the relation:

$$BR(\phi \to \omega\pi^0) = \frac{\sigma_0(m_\phi)|Z_{4\pi}|^2}{\sigma_\phi}, \tag{6}$$

where $\sigma_0(m_\phi)$ is the total cross section of the $e^+e^- \to \omega\pi^0$ process and σ_ϕ is the peak value of the production cross section for the ϕ resonance.

Using the parameters obtained from the $\pi^+\pi^-\pi^0\pi^0$ analysis, the Γ_{ee} measurement from KLOE [9] for the evaluation of σ_ϕ, and our value for $BR(\omega \to \pi^+\pi^-\pi^0)$ we extract

$$BR(\phi \to \omega\pi^0) = (5.63 \pm 0.70) \times 10^{-5}, \tag{7}$$

in agreement and with better accuracy with respect to what obtained by the SND experiment ($5.2^{+1.3}_{-1.1} \times 10^{-5}$). [6]

7 Conclusions

From the measurement of $e^+e^- \to \pi^+\pi^-\pi^0\pi^0$ and $e^+e^- \to \pi^0\pi^0\gamma$ production cross section at center of mass energy around M_ϕ, we obtain the most precise measurement of $BR(\phi \to \omega\pi^0)$ and the measurement of the main ω's branching fractions, with a better statistical accuracy with respect to what reported by PDG. [8]

It is important to note that the value of $BR(\omega \to \pi^0\gamma)$ is one of the ingredients for the controversial measurement of the gluonium content in η'. [10] Our measurement is lower than the one used in the cited analysis by 6%. This could lead to a shift in the gluonium content of η'.

References

1. KLOE Collaboration, LNF **92/019** IR (1992) LNF **93/002** IR (1993).
2. S. Guiducci *et al.*, Proc. of the 2001 PAC (Chicago, Illinois, USA), P. Lucas S. Webber Eds., (2001), 353.
3. M. Adinolfi *et al.* [KLOE Collaboration], NIM **A488** (2002) 51.
4. M. Adinolfi *et al.* [KLOE Collaboration], NIM **A482** (2002) 363.
5. M. Adinolfi *et al.* [KLOE Collaboration], NIM **A492** (2002) 134.
6. V.M. Aulchenko *et al.*, JETP **90** (2000) 927.
7. M. Greco *et al.*, PL **B318** (1993) 635.
8. W. M. Yao *et al.*, JP **G 33** (2006) and 2007 partial update for 2008 edition [*http://pdg.web.cern.ch/pdg*]
9. F. Ambrosino *et al.* [KLOE Collaboration], PL **B608** (2005) 199.
10. F. Ambrosino *et al.* [KLOE Collaboration], PL **B648** (2007) 267.

Frascati Physics Series Vol. XLVI (2007), pp. 523–530
HADRON07: XII Int. Conf. on Hadron Spectroscopy – Frascati, October 8-13, 2007
Light Meson Spectroscopy

THE EFFECT OF ISOSPIN VIOLATION ON SCALAR MESON PRODUCTION

C. Hanhart[1], B. Kubis[2], and J. R. Peláez[3]
[1]*Institüt für Kernphysik (Theorie), Forschungzentrum Jülich, D-52425 Jülich, Germany*
[2]*HISKP (Theorie), Universität Bonn, Nussallee 14-16, D-53115 Bonn, Germany.*
[3]*Departamento de Física Teórica II, Universidad Complutense, E-28040 Madrid. Spain*

Abstract

We investigate the isospin-violating mixing of the light scalar mesons $a_0(980)$ and $f_0(980)$ within the unitarized chiral approach. Isospin-violating effects are considered to leading order in the quark mass differences and electromagnetism. In this approach both mesons are generated through meson-meson dynamics. Our results provide a description of the mixing phenomenon within a framework consistent with chiral symmetry and unitarity, where these resonances are not predominantly $q\bar{q}$ states. We discuss in detail the reactions $J/\Psi \to \phi S$, where S denotes a suitable pair of pseudo–scalar mesons in the scalar channel, namely $\pi^0\eta$, K^+K^-, and $K^0\bar{K}^0$. In this work predictions for the cross section in the kaon channels are given for the first time with isospin violating effects included.

1 Introduction

Although the light scalar mesons $a_0(980)$ and $f_0(980)$ have been established as resonances long ago, there is still a heated debate going on in the literature regarding the very nature of these states. Naively one might assign them a conventional $q\bar{q}$ structure, however, at present no quark model is capable of describing both states simultaneously as $q\bar{q}$ states — see, e.g., Ref. [1]. On the other hand, as early as 1977 it was stressed that especially in the scalar channel the interaction of four-quark systems (two quarks, two antiquarks) is attractive [2]. Some authors have found indications for the existence of compact four-quark states [3–5]. However, the same short-ranged interaction can also be the kernel to the scattering of pseudoscalars, giving rise to extended four-quark states that one might call hadronic molecules or extraordinary hadrons [6–9]. Independently, a similar conclusion was found in different approaches [10–13].

In Refs. [14, 15] it is stressed that the effective coupling constants of the scalar mesons to the $K\bar{K}$ channel contain the essential structure information. Especially, the larger the molecular component, the larger the residue at the resonance pole, which acquires its maximum value in case of a pure molecule. It should be stressed, however, that this connection can be made rigorous only for stable bound states and if the bound state pole is on the first sheet very close to the elastic threshold [14]. However, if the state of interest is narrow and the inelastic threshold is sufficiently far away, the argument should still hold [15]. Note that both conditions apply for $a_0(980)$ and $f_0(980)$. Therefore one should aim at observables that are very sensitive to the effective coupling constants. The resonance signal, as seen in production experiments for both states, is not very useful to determine those couplings, for it turned out to be mainly sensitive to ratios of couplings [16]. It is therefore important to investigate other observables.

When this formalism was applied to the scalar mesons $a_0(980)$ and $f_0(980)$ it was found from an analysis of a series of reactions [17] that the latter is indeed predominantly a $K\bar{K}$ molecule, in line with the results of Refs. [7, 10, 11, 13], while the results for the former did not lead to an unambiguous interpretation. This might either point at a prominent non–molecular contribution to the a_0 structure, or the a_0 is not a bound state, but a virtual state. To decide on this issue it is important to collect more information especially on the a_0. In Ref. [18] it was stressed that the amplitude for the isospin violating $a_0 - f_0$

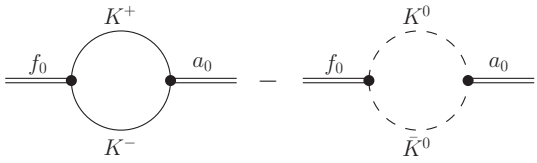

Figure 1: *Graphical illustration of the leading contribution to the $a_0 - f_0$ mixing matrix element, driven by the kaon mass differences.*

transition should be very sensitive to the product of the effective coupling to the two–kaon channels of the f_0 and the a_0. If we assume that the f_0 is a molecule, its coupling to the $K\bar{K}$ channel is fixed, as discussed above. Then the value for the $a_0 - f_0$ mixing amplitude should be very sensitive to the structure of the a_0.

The reason why the mixing amplitude of a_0 and f_0 is sensitive to the effective couplings is that it gets a prominent contribution from the kaon–loops (see Fig. 1). Their isospin violating part is driven by the kaon mass differences giving rise to an effect that can be shown to scale as $\sqrt{(m_d - m_u)/m_s}$. In contrast to this, normal isospin violating effects should be of order $(m_d - m_u)/m_s$ — those could be parameterized, e.g., by isospin–violating coupling constants (see Fig. 2). In Ref. [19] the latter effects were calculated for the first time as well to provide a better quantitative estimate of the mixing amplitude. For this a particular model needs to be used. We chose the chiral unitary approach which is a special unitarization procedure for amplitudes calculated using chiral perturbation theory. The latter provides a systematic inclusion of quark mass effects while the former allows for an extension of the formalism into the resonance region — see Ref. [20] for a recent review. In addition we also include the isospin breaking effect of the soft–photon exchange.

In this work we investigate different final states for the reactions $J/\Psi \to \phi S$ [1], where S denotes a suitable pair of pseudo–scalar mesons in the scalar channel, namely $\pi^0\eta$, K^+K^-, and $K^0\bar{K}^0$ — predictions for the cross section in the kaon channels are given for the first time with isospin violation included. The latter two channels are expected to constrain the charge dependence of the coupling of the f_0 to kaons and should therefore provide an independent cross

[1] This decay was identified as very useful to study isospin violation for scalar mesons in Refs. [21, 22].

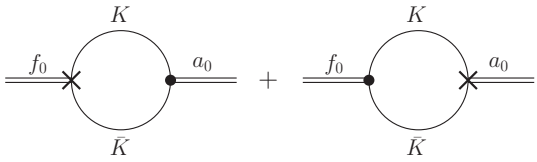

Figure 2: *Graphical illustration of the subleading contribution to the $a_0 - f_0$ mixing matrix element, driven by isospin-violating vertices, denoted by the crosses.*

check for the size of corrections of order $(m_d - m_u)/m_s$. In the next section the formalism is briefly reviewed and the results are given. We close with a short summary.

2 Formalism and Results

Details on the formalism are given in Ref. [19]. Thus, here we will only repeat the essential physics that went into the calculations. In the Standard Model there are two sources of isospin violation present, namely the up–down quark mass difference as well as electromagnetism. Both appear in a well defined form in the corresponding Lagrange density formulated in terms of the fundamental degrees of freedom, here photons, gluons, and quarks. Chiral perturbation theory [23, 24] allows for a consistent representation of those terms for a theory describing the interaction of the (pseudo) Goldstone bosons with each other. At leading order in the chiral Lagrangian the only parameter that appears, in addition to the various particle masses, is the pion decay constant. Thus, also the leading effect of isospin violation is predicted. It should be stressed that already at leading order both isospin violating mass differences as well as isospin violating interactions are present.

Already in isospin symmetric calculations of meson–meson scattering amplitudes, when unitarizing the leading chiral Lagrangian, an a priori unknown constant needs to be adjusted to the data. In addition, a few more parameters need to be fitted to the production data — in our case they were fixed from a fit to the data on $J/\Psi \to \phi\pi^+\pi^-, K^+K^-$ as well as $J/\Psi \to \omega\pi^+\pi^-$ [25]. Once this is done, the isospin violating signals emerge as predictions. Our results for the various channels are shown in Fig. 3. The predicted signal in the $\pi^0\eta$ channel was already published in Ref. [19]. Note that in an isospin symmetric

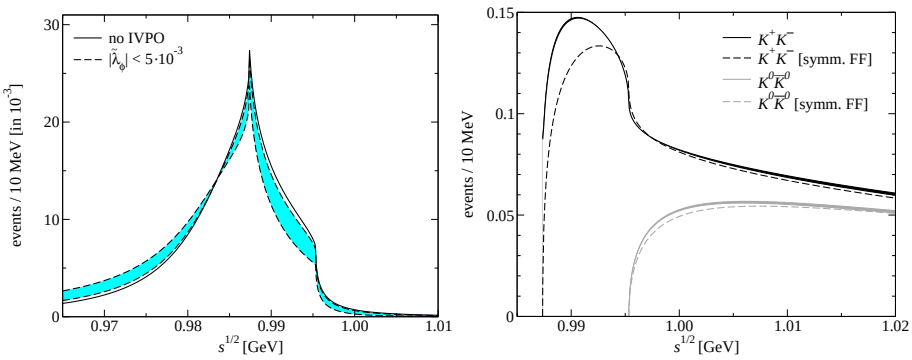

Figure 3: *Left: predicted signal for $J/\Psi \to \phi\pi^0\eta$. The solid line shows the result without isospin violation in the production operator (IVPO), while the band shows the effect of its inclusion. Right: predicted signal for $J/\Psi \to \phi K\bar{K}$. For both kaon channels the solid band, which includes the uncertainties, is the full result, while for the dashed line the same decay amplitude was used in both channels (see text).*

world this reaction would not be allowed, thus any signal is directly proportional to the square of an isospin violating amplitude. Based on very general scale arguments one can show that in addition this amplitude is dominated by the isospin violation that emerges from $a_0 - f_0$ mixing [26]. This was confirmed on the grounds of the current model: the filled band in the left panel of Fig. 3 shows the effect of possible isospin violation in the production operator. The right panel of the same figure shows the J/Ψ decay with a pair of kaons in the final state. Please note that for these two channels there would be a decay rate also in an isospin symmetric world, however, then both signals would agree. The solid lines show our results for the two channels including the effects of isospin violation as described in Ref. [19]. In addition, the presence of charged particles in the final state called for an additional treatment of soft photons. Here we followed Ref. [27]. The decay spectrum for $J/\Psi \to \phi K^+K^-$, based on an isospin symmetric calculation, is shown in Ref. [25].

To see how much of the difference in the two kaon channels originates from the different phase space thresholds alone ($2m_{K^+} - 2m_{K^0} = 8$ MeV), in the figure we also show the signals that emerge when the same decay amplitude is used for both channels (dashed lines). For this calculation we took the

average of the charged and the neutral kaon amplitudes, corresponding to a formal isospin 0 combination. Obviously the by far most important difference between the channels is driven by the displacement of the thresholds, the effect of which is further enhanced by the strongly varying amplitudes precisely in this threshold region. The original idea was to extract information on the charge dependence of the couplings of the f_0 to kaons from a comparison of $J/\Psi \to \phi K^+K^-$ and $J/\Psi \to \phi K^0\bar{K}^0$. However, as can be seen from the figure, the differences between the solid and the dashed lines are too small to be accessible experimentally. Therefore we do not expect data for the kaon channels to be sufficiently sensitive to extract isospin violating effects in the decay amplitudes.

3 Summary

In this work we calculated the reactions $J/\Psi \to \phi S$, where S denotes a suitable pair of pseudo–scalar mesons in the scalar channel, namely $\pi^0\eta$, K^+K^-, and $K^0\bar{K}^0$. The goal of this study was to gain a better quantitative understanding of the phenomenon of $a_0 - f_0$ mixing, which should eventually reveal important information on the structure of the $a_0(980)$. In addition to the $\pi^0\eta$ channel, the kaon channels including isospin violation were discussed here for the first time. We found that, at least within the current model, the impact of the charge dependence of the coupling of the f_0 to kaons is too small to be deduced from a comparison of the rates for K^+K^-, and $K^0\bar{K}^0$. On the other hand the $\pi^0\eta$ decay channel appears to be not only very sensitive to the effective coupling constants that encode the structure information but also theoretically under control [19]. For a discussion of additional background effects see Ref. [22]. The corresponding measurements can be performed, once BES III is in operation.

4 Acknowledgments

The authors acknowledge partial financial support by the EU integrated infrastructure initiative HADRONPHYSICS PROJECT, under contract RII3-CT-2004-506078. B.K. is supported by the DFG (SFB/TR 16). The research of J.R.P. is partially funded by Banco Santander/Complutense contract PR27/05-13955-BSCH and Spanish CICYT contracts FPA2007-29115-E, FPA2005-02327, BFM2003-00856.

References

1. C. R. Münz, J. Resag, B. C. Metsch and H. R. Petry, Nucl. Phys. A **578**, 418 (1994) [arXiv:nucl-th/9307027].
2. R. L. Jaffe, Phys. Rev. D **15**, 267 (1977).
3. N. N. Achasov, Phys. Atom. Nucl. **67**, 1529 (2004) [Yad. Fiz. **67**, 1552 (2004)] [arXiv:hep-ph/0309118].
4. F. Giacosa, Phys. Rev. D **74**, 014028 (2006) [arXiv:hep-ph/0605191].
5. J. Vijande, F. Fernández, A. Valcarce and B. Silvestre-Brac, arXiv:hep-ph/0206263.
6. R. L. Jaffe and F. E. Low, Phys. Rev. D **19**, 2105 (1979).
7. J. R. Peláez, Phys. Rev. Lett. **92**, 102001 (2004) [arXiv:hep-ph/0309292].
8. J. R. Peláez and G. Ríos, Phys. Rev. Lett. **97**, 242002 (2006). [arXiv:hep-ph/0610397].
9. R. L. Jaffe, arXiv:hep-ph/0701038.
10. J. D. Weinstein and N. Isgur, Phys. Rev. Lett. **48**, 659 (1982); Phys. Rev. D **27**, 588 (1983); Phys. Rev. D **41**, 2236 (1990).
11. G. Janssen, B. C. Pearce, K. Holinde and J. Speth, Phys. Rev. D **52**, 2690 (1995) [arXiv:nucl-th/9411021].
12. E. van Beveren and G. Rupp, Eur. Phys. J. C **22**, 493 (2001) [arXiv:hep-ex/0106077].
13. J. A. Oller and E. Oset, Nucl. Phys. A **620**, 438 (1997) [Erratum-ibid. A **652**, 407 (1999)] [arXiv:hep-ph/9702314].
14. S. Weinberg, Phys. Rev. **130**, 776 (1963); Phys. Rev. **131**, 440 (1963); Phys. Rev. **137**, B672 (1965).
15. V. Baru, J. Haidenbauer, C. Hanhart, Y. Kalashnikova and A. Kudryavtsev, Phys. Lett. B **586**, 53 (2004) [arXiv:hep-ph/0308129].

16. V. Baru, J. Haidenbauer, C. Hanhart, A. E. Kudryavtsev and U.-G. Meißner, Eur. Phys. J. A **23**, 523 (2005) [arXiv:nucl-th/0410099].

17. C. Hanhart, Yu. S. Kalashnikova, A. E. Kudryavtsev and A. V. Nefediev, Phys. Rev. D **75**, 074015 (2007) [arXiv:hep-ph/0701214]; Yu. Kalashnikova, A. E. Kudryavtsev, A. V. Nefediev, J. Haidenbauer and C. Hanhart, Phys. Rev. C **73**, 045203 (2006) [arXiv:nucl-th/0512028]; Yu. S. Kalashnikova, A. E. Kudryavtsev, A. V. Nefediev, C. Hanhart and J. Haidenbauer, Eur. Phys. J. A **24**, 437 (2005) [arXiv:hep-ph/0412340].

18. N. N. Achasov, S. A. Devyanin and G. N. Shestakov, Phys. Lett. B **88**, 367 (1979).

19. C. Hanhart, B. Kubis and J. R. Peláez, Phys. Rev. D **76**, 074028 (2007) [arXiv:0707.0262 [hep-ph]].

20. J. R. Peláez, Mod. Phys. Lett. A **19**, 2879 (2004) [arXiv:hep-ph/0411107].

21. F. E. Close and A. Kirk, Phys. Lett. B **489**, 24 (2000) [arXiv:hep-ph/0008066].

22. J. J. Wu, Q. Zhao and B. S. Zou, Phys. Rev. D **75**, 114012 (2007) [arXiv:0704.3652 [hep-ph]].

23. S. Weinberg, Physica A **96**, 327 (1979); J. Gasser and H. Leutwyler, Annals Phys. **158**, 142 (1984); Nucl. Phys. B **250**, 465 (1985).

24. R. Urech, Nucl. Phys. B **433**, 234 (1995) [arXiv:hep-ph/9405341].

25. T. A. Lähde and U.-G. Meißner, Phys. Rev. D **74**, 034021 (2006) [arXiv:hep-ph/0606133].

26. C. Hanhart, AIP Conf. Proc. **688**, 61 (2004) [arXiv:nucl-th/0306073]; C. Hanhart, Phys. Rept. **397**, 155 (2004) [arXiv:hep-ph/0311341].

27. G. Isidori, arXiv:0709.2439 [hep-ph].

Frascati Physics Series Vol. XLVI (2007), pp. 531–539
HADRON07: XII Int. Conf. on Hadron Spectroscopy – Frascati, October 8-13, 2007
Light Meson Spectroscopy

SCALAR MESON PHOTOPRODUCTION

A. Donnachie
School of Physics and Astronomy, University of Manchester, Manchester M13 9PL, England
Yu S. Kalashnikova
ITEP, 117259 Moscow, Russia

Abstract

The scalar mesons $f_0(1370)$, $f_0(1500)$ and $f_0(1710)$ are of interest as there is as yet no consensus of their status, or indeed of the existence of the $f_0(1370)$. Radiative decays to ρ and ω have been shown to provide effective probes of their structure and to discriminate among models. Scalar-meson photoproduction is proposed as an alternative and it is shown that it represents a feasible approach.

1 Introduction

The fundamental structure of the light scalar mesons is still a subject of debate. The $a_0(1450)$ and the $K_0^*(1430)$ are generally regarded as the $u\bar{d}$ and $u\bar{s}$ members of the same SU(3) flavour nonet, to which the $f_0(1370)$ can be attached as the $(u\bar{u}+d\bar{d})$ member [1)]. There then remain two possibilities for the ninth member of the nonet, the $f_0(1500)$ and the $f_0(1710)$. In this picture, it is usually assumed that the surplus of isoscalar scalars in the 1300 to 1700 MeV mass region can be attributed to the presence of a scalar glueball. This

assumption has been supported in the past by calculations in quenched LQCD, which predict a scalar glueball in this mass range [2]. The three physical states are then viewed as mixed $q\bar{q}$ and gluonium states, although there is not agreement in detail about the mixing [3, 4]. However calculations in unquenched LQCD [5] suggest that there is a sizeable contribution from glueball interpolating operators to the states around or below 1 GeV, casting some doubt on the mixing models. Further, it has been argued that the $f_0(1370)$ may not exist [6, 7]. This is strongly contested by Bugg [8]. If the $f_0(1370)$ does not exist the lowest scalar nonet can be taken to comprise the $a_0(980)$, the $f_0(980)$, the $f_0(1500)$ and the $K_0^*(1430)$, the $f_0(980)$ and the $f_0(1500)$ being mixed such that the former is close to a singlet and the latter close to an octet. The lightest scalar glueball is then considered to be a broad object extending from 400 MeV to about 1700 MeV. So a variety of interpretations is possible.

Radiative transitions offer a particularly powerful means of probing the structure of hadrons as the coupling to the charges and spins of the constituents reveals detailed information about wave functions and can discriminate among models. In the case of the $f_0(1370)$, $f_0(1500)$ and $f_0(1710)$ being considered as mixed $n\bar{n}$, $s\bar{s}$ and glueball states their radiative decays to a vector meson, $S \to V\gamma$, are strongly affected by the degree of mixing between the basis $q\bar{q}$ states and the glueball [9]. Three different mixing scenarios have been proposed: the bare glueball is lighter than the bare $n\bar{n}$ state [4]; its mass lies between the bare $n\bar{n}$ state and the bare $s\bar{s}$ state [4]; or it is heavier than the bare $s\bar{s}$ state [3]. We label these three possibilities L, M, H respectively. Assuming that the $q\bar{q}$ basis of the $f_0(1370)$, $f_0(1500)$ and $f_0(1710)$ is in the 1^3P_0 nonet, the discrimination among the different mixing scenarios is strong [9]. Preliminary results on the implications of this particular scenario for photoproduction are presented here.

Photoproduction of the scalar mesons at medium energy provides an alternative to direct observation of the radiative decays. It is this possibility that we explore here and show that it is viable. The dominant mechanism is Reggeised ρ and ω exchange, both of which are well understood in pion photoproduction [10]. The energy must be sufficiently high for the Regge approach to be applicable but not too high as the cross section decreases approximately as s^{-1}. In practice this means approximately 5 to 10 GeV photon energy. In addition to photoproduction on protons we consider coherent photoproduc-

tion on ^{4}He, encouraged in this by a recently-approved experiment at Jefferson Laboratory [11].

2 The Model

The differential cross section is given by

$$\frac{d\sigma}{dt} = \frac{|M(s,t)|^2}{64\pi|\mathbf{p}|^2 s}. \tag{1}$$

For the exchange of a single vector meson

$$\begin{aligned} |M(s,t)|^2 &= \tfrac{1}{2}A^2(s,t)(s(t-t_1)(t-t_2) + \tfrac{1}{2}st(t-m_S^2)^2) \\ &\quad + A(s,t)B(s,t)m_p s(t-t_1)(t-t_2) \\ &\quad + \tfrac{1}{8}B(s,t)^2 s(4m_p^2 - t)(t-t_1)(t-t_2). \end{aligned} \tag{2}$$

where t_1 and t_2 are the kinematical boundaries

$$\begin{aligned} t_{1,2} &= \frac{1}{2s}\Big(-(m_p^2 - s)^2 + m_S^2(m_p^2 + s) \\ &\quad \pm (m_p^2 - s)\sqrt{((m_p^2 - s)^2 - 2m_s^2(m_p^2 + s) + m_S^4)}\Big), \end{aligned} \tag{3}$$

and

$$A(s,t) = \frac{g_S(g_V - 2m_p g_T)}{m_V^2 - t}, \qquad B(s,t) = -\frac{2g_S g_T}{m_V^2 - t}. \tag{4}$$

In (4), g_V and g_T are the VNN vector and tensor couplings, g_S is the γVN coupling. The ωNN couplings are rather well defined [12], with $13.8 < g_V^\omega < 15.8$ and $g_T^\omega \approx 0$. We have used $g_V^\omega = 15$ and $g_T^\omega = 0$ as this gives a good description of π^0 photoproduction [10]. The ρNN couplings are not so well defined, with two extremes: strong coupling [12] or weak coupling [13]. We are again guided by pion photoproduction [10] and choose the strong coupling solution with $g_V^\rho = 3.4$, $g_T^\rho = 11$ GeV^{-1}. The $SV\gamma$ coupling, g_S, can be obtained from the radiative decay width through [14]

$$\Gamma(S \to \gamma V) = g_S^2 \frac{m_S^3}{32\pi}\left(1 - \frac{m_V^2}{m_S^2}\right)^3. \tag{5}$$

Obviously in practice the amplitudes for ρ and ω exchange are added coherently.

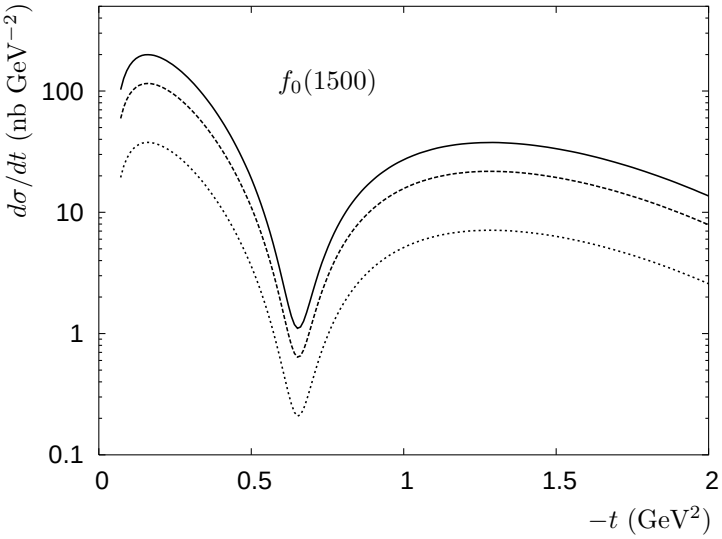

Figure 1: *Differential photoproduction cross section on hydrogen for* $f_0(1500)$ *at* $E_\gamma = 5$ GeV. *The glueball masses are L (solid), M (dashed) and H (dotted).*

The standard prescription for Reggeising the Feynman propagators in (2), assuming a linear Regge trajectory $\alpha_V(t) = \alpha_{V0} + \alpha'_V t$, is to make the replacement

$$\frac{1}{t - m_V^2} \to \Big(\frac{s}{s_0}\Big)^{\alpha_V(t)-1} \frac{\pi\alpha'_V}{\sin(\pi\alpha_V(t))} \frac{-1 + e^{-i\pi\alpha_V(t)}}{2} \frac{1}{\Gamma(\alpha_V(t))}. \qquad (6)$$

This simple prescription automatically includes the zero observed at $t \approx -0.6$ GeV^2 in both ρ and ω exchange and provides a satisfactory description of the ρ and ω exchange contributions to pion photoproduction [10].

For photoproduction on ^{4}He we assume that the cross section is given by

$$\frac{d\sigma(\gamma N \to f_0 \mathrm{He})}{dt} = \frac{d\sigma(\gamma N \to f_0 N)}{dt} \Big(4F_{\mathrm{He}}(t)\Big)^2, \qquad (7)$$

where $F_{\mathrm{He}}(t)$ is the helium form factor [15], $F_{\mathrm{He}}(t) \approx e^{9t}$. The justification for the assumption (7) is the low level of nuclear shadowing observed on ^{4}He at the energies with which we are concerned, for both pion and photon total cross sections [16].

Table 1: *Integrated photoproduction cross sections in nanobarns on protons and* ^{4}*He at* $E_\gamma = 5$ GeV *for the three different mixing scenarios: light glueball (L), medium-weight glueball (M) and heavy glueball (H).*

	proton			^{4}He		
Scalar	L	M	H	L	M	H
$f_0(1370)$	27.1	68.6	94.2	0.64	1.63	2.23
$f_0(1500)$	89.9	52.1	17.0	1.55	0.90	0.29
$f_0(1710)$	0.7	1.6	11.8	0.001	0.002	0.016

We assume non-degenerate ρ and ω trajectories

$$\alpha_\rho = 0.55 + 0.8t, \qquad \alpha_\omega = 0.44 + 0.9t. \tag{8}$$

3 Cross Sections

The differential cross sections have the structure expected, that is vanishing in the forward direction due to the helicity flip at the photon-scalar vertex and having a deep dip at $-t \approx 0.6$ GeV^2 due to the zeroes in the exchange amplitudes in (6). It does not go to zero in the dip because of the non-degenerate trajectories (8). This is illustrated for $f_0(1500)$ photoproduction at $E_\gamma = 5$ GeV in figure 1. The integrated cross sections for photoproduction of the scalars on protons and ^{4}He at $E_\gamma = 5$ GeV are given in table 1 for light (L), medium (M) and heavy (H) glueball masses. In the case of ^{4}He the integration over $d\sigma/dt$ is for $|t| > 0.1$ GeV^2 due to the experimental requirement that $|t| \gtrsim 0.1$ GeV^2 for the recoiling helium to be detected. The cross sections for photoproduction on protons at higher energies are similar in shape, but the magnitude decreases with energy at the rate expected from (6). For example the cross sections at $E_\gamma = 10$ GeV are about half those in table 1. However the cross sections for photoproduction on ^{4}He do not decrease, and for the $f_0(1500)$ and $f_0(1710)$ actually increase. This is due the combined effect of the ^{4}He form factor enhancing the contribution from small t and the maximum of the differential cross section on protons moving to smaller $|t|$ with increasing energy.

The reasons for the cross sections for scalar photoproduction on ^{4}He being very much smaller than those for scalar photoproduction on protons are (i)

Table 2: *Branching fractions in percent for the $f_0(1500)$ from the PDG [1], the WA102 experiment [17] from the analysis of Close and Kirk [4] (CK) and the Crystal Barrel experiment [18] (CB).*

Channel	PDG	WA102/CK	CB
$\pi\pi$	34.9 ± 2.3	33.7 ± 3.4	33.9 ± 3.7
$\eta\eta$	5.1 ± 0.9	6.1 ± 0.1	2.6 ± 0.3
$\eta\eta'$	1.9 ± 0.8	3.2 ± 0.7	2.2 ± 0.1
$K\bar{K}$	8.6 ± 0.1	10.7 ± 2.4	6.2 ± 0.5
4π	49.5 ± 3.3	46.3 ± 8.5	55.1 ± 16.9

switching off ρ exchange for photoproduction on protons reduces the cross section by a factor of about 16, cancelling the factor 16 from coherent production (ii) the helium form factor suppresses the cross section except at very small t (iii) there is the experimental requirement that $|t| \gtrsim 0.1$ GeV^2 for the recoiling helium to be detected.

The cross sections in table 1 reflect directly the radiative decay widths and, if it were practical, ratios of cross sections $f_0(1370) : f_0(1500) : f_0(1710)$ would give an immediate result and "weigh" the glueball. In practice there are several problems in realising this ideal scenario. It is unlikely that the decay modes of the scalars with charged particles can be considered because of the very much larger cross sections in $\pi^+\pi^-$, K^+K^-, $2\pi^+2\pi^-$ and $\pi^+\pi^-2\pi^0$ from vector-meson production. The contribution from vector mesons can be eliminated by considering only the all-neutral channels, that is the $\pi^0\pi^0$, $\eta^0\eta^0$ and $4\pi^0$ decays of the $f_0(1370)$, $f_0(1500)$ and $f_0(1710)$. A further difficulty is the uncertainty in the branching fractions of the $f_0(1370)$ and $f_0(1710)$, particularly the former [1, 6], and the small cross section for the $f_0(1710)$.

In contrast the cross sections for photoproduction of the $f_0(1500)$ on protons are reasonable and the branching fractions are well defined. This is demonstrated in table 2 in which the branching fractions, in percent, are given from the PDG [1], the WA102 experiment [17] as obtained in the analysis of Close and Kirk [4] and the Crystal Barrel experiment [18]. Thus photoproduction of the $f_0(1500)$ on protons is the benchmark experiment and the obvious all-neutral channel is $\pi^0\pi^0$, although it should be recalled that the $\pi\pi$ branch-

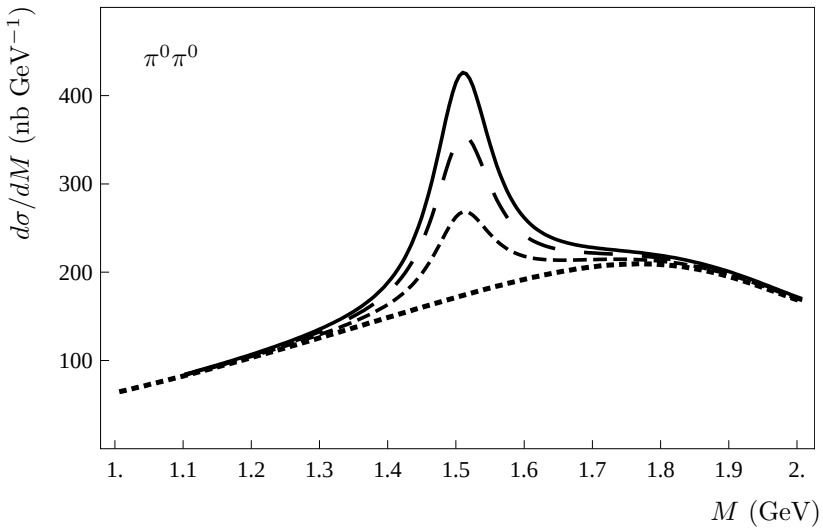

Figure 2: *Continuum $\pi^0\pi^0$ background (dotted) and combined with $f_0(1500)$ at $E_\gamma = 5$ GeV (solid (L), large dashed (M), small dashed (H)) for constructive interference.*

ing fraction shown in table 2 has to be divided by a factor of three. From table 1 we see that the ratio L : M = 1.7 : 1 and the ratio L : H = 5.3 : 1. The latter is certainly appreciably larger than the uncertainties in the model.

Photoproduction of the $f_0(1370)$ can help resolve the ambiguities discussed in the Introduction. Quite apart from the possibility that it does not exist [6, 7], there is considerable variance in the branching fractions. In the analysis of Close and Kirk [4] 4π is the dominant decay mode, with a branching fraction of about 95%, and the $\pi\pi$ branching fraction is very small, (2.7 ± 1.2)%. This pattern is replicated by Crystal Barrel [18], with a 4π branching fraction of about 85% and a $\pi\pi$ branching fraction of (7.9 ± 2.9)%. In direct contrast, $\pi\pi$ is the dominant decay mode in the analysis of Bugg [8] and 4π is small. At resonance the ratio $2\pi : 4\pi$ is given as $6 : 1$. However for the $f_0(1500)$ the $2\pi : 4\pi$ ratio is $0.9 : 1$ so is not incompatible with table 2.

Of course the scalars are not produced in isolation. For example in the $\pi^0\pi^0$ channel there is a continuum background arising from the process $\gamma \to \pi^0\omega(\rho)$ with subsequent rescattering of the $\omega(\rho)$ on the proton by $\rho(\omega)$ exchange to give the second π^0. The new ingredients here are the $\gamma\pi^0\omega(\rho)$ and $\omega\pi^0\rho$

couplings, which can be estimated from [19]. The $\rho(\omega)$ exchange is Reggeised as before. Figure 2 shows the result of this calculation together with the result of constructive interference with the $f_0(1500)$ signal.

References

1. Particle Data Group, J. Phys. G **33**, 1 (2006).
2. C.J. Morningstar and M. Peardon, Phys. Rev. D **60**, 034509 (1999); H.B. Meyer and M.J. Teper, Phys. Lett. B **605**, 344 (2005); Y. Chen *et al*, Phys. Rev. D **73**, 014516 (2006).
3. W. Lee and D. Weingarten, Phys. Rev. D **61**, 014015 (2000).
4. F.E. Close and A. Kirk, Eur. Phys. J. C **21**, 531 (2001).
5. C. McNeile, hep-lat/0710.0985.
6. E. Klempt and A. Zaitsev, hep-ph/0708.4016.
7. W. Ochs, hep-ph/0609207.
8. D.V. Bugg, hep-ex/1706.1341.
9. F.E. Close, A. Donnachie and Yu.S. Kalashnikova, Phys.Rev. D **67**, 074031 (2003).
10. M. Guidal, J.-M. Laget and M. Vanderhaeghen, Nucl. Phys. A **627**, 645 (1997).
11. G. Asryan *et al*, JLab experiment E-07-009.
12. R. Machleidt, K. Holinde and Ch. Elster, Phys. Rep. **149**, 1 (1987).
13. M.G. Olsson and E.T. Osypowski, Phys. Rev. D **17**, 174 (1978; S. Nozawa, B. Blankenbecler and T.-S.H. Lee, Nucl. Phys. A **513**, 459 (1990); H. Garcilazo and E. Moya de Guerra, Nucl. Phys. A **562**, 521 (1994).
14. Yu.S. Kalashnikova, A. Kudryavtsev, A.V. Nefediev, J. Haidenbauer and C. Hanhart, Phys. Rev. C **73**, 045203 (2006).

15. H. Morita and T. Suzuki, Prog. Theor. Phys. **86**, 671 (1991).

16. G. Grammar, Jr and J.D. Sullivan, in Electromagnetic Interactions of Hadrons, vol.2. (eds A. Donnachie and G. Shaw) (Plenum Press, New York, 1978).

17. D. Barberis *et al*, WA102 Collaboration, Phys. Lett. B **479**, 59 (2000).

18. A. Abele *et al*, Crystal Barrel Collaboration, Eur. Phys. J. C **19**, 667 (2001).

19. A. Bramon *et al*, Phys. Lett. B **283**, 416 (1992).

Frascati Physics Series Vol. XLVI (2007), pp. 541–549
HADRON07: XII Int. Conf. on Hadron Spectroscopy – Frascati, October 8-13, 2007
Light Meson Spectroscopy

LIGHT SCALAR MESONS AT KLOE

KLOE Collaboration* – presented by Federico Nguyen
Università degli Studi and Sezione INFN Roma TRE

Abstract

Properties of the $a_0(980)$ and $f_0(980)$ scalar mesons, extracted from several analyses of an integrated luminosity of $\sim 400\,\mathrm{pb}^{-1}$ of KLOE data are presented.

1 Introduction

The main interest in the scalar mesons $a_0(980)$, $f_0(980)$ and $f_0(600)$ – better known as $\sigma(600)$ [1] – lies in the possibility that they are not conventional $q\bar{q}$ mesons, but exotic structures such as $qq\bar{q}\bar{q}$ states [2] or $K\bar{K}$ molecules [3].

* F. Ambrosino, A. Antonelli, M. Antonelli, F. Archilli, P. Beltrame, G. Bencivenni, S. Bertolucci, C. Bini, C. Bloise, S. Bocchetta, F. Bossi, P. Branchini, P. Campana, G. Capon, T. Capussela, F. Ceradini, S. Chi, P. Ciambrone, E. De Lucia, A. De Santis, P. De Simone, G. De Zorzi, A. Denig, A. Di Domenico, C. Di Donato, B. Di Micco, M. Dreucci, G. Felici, M. L. Ferrer, S. Fiore, C. Forti, P. Franzini, C. Gatti, P. Gauzzi, S. Giovannella, E. Graziani, W. Kluge, G. Lanfranchi, J. Lee-Franzini, D. Leone, M. Martini, P. Massarotti, S. Meola, S. Miscetti, M. Moulson, S. Müller, F. Murtas, M. Napolitano, F. Nguyen, M. Palutan, E. Pasqualucci, A. Passeri, V. Patera, F. Perfetto, P. Santangelo, B. Sciascia, A. Sciubba, A. Sibidanov, T. Spadaro, M. Testa, L. Tortora, P. Valente, G. Venanzoni, R.Versaci, G. Xu

The KLOE experiment, working at the e^+e^- Frascati ϕ-factory DAΦNE [4], is perfectly suited for studying the properties of light scalar mesons:

$f_0(980)$ produced in the $\phi \to f_0(980)\gamma \to \pi\pi\gamma$ decay chain, measured both in the $\pi^+\pi^-$ and in the $2\pi^0$ final states;

$a_0(980)$ produced in the $\phi \to a_0(980)\gamma \to \eta\pi^0\gamma$ decay chain, analyzed with both $\eta \to \pi^+\pi^-\pi^0$ and $\eta \to 2\gamma$ channels.

Furthermore, from the analysis of the $\pi\pi$ mass spectra it is possible to extract information on the controversial scalar meson $\sigma(600)$, produced through the decay $\phi \to \sigma(600)\gamma \to \pi\pi\gamma$. In general, the branching fraction BR($\phi \to S\gamma$) [5], the couplings [6] to the $q\bar{q}$ pseudoscalar mesons and the $\phi S\gamma$ coupling [7] yield information upon the internal structure of the light scalar meson S. These quantities are extracted from the measurements discussed in the following.

1.1 DAΦNE and KLOE

DAΦNE operates at the center of mass energy $\sqrt{s} = M_\phi \sim 1.02$ GeV. The beams collide with a crossing angle of $(\pi - 0.025)$ rad. The KLOE detector consists of a cylindrical drift chamber [8] (3.3 m length and 2 m radius), surrounded by a calorimeter [9] made of lead and scintillating fibers. The detector is inserted in a coil producing a solenoidal field $B = 0.52$ T. Large angle tracks from the origin ($\theta > 45°$) are reconstructed with relative momentum resolution $\sigma_p/p = 0.4\%$. Photon energies and times are measured by the calorimeter with resolutions of $\sigma_E/E = 5.7\%/\sqrt{E(\text{GeV})}$ and $\sigma_t = 57$ ps$/\sqrt{E(\text{GeV})} \oplus 100$ ps.

1.2 Parametrizations of the scalar meson production in ϕ decays

The Kaon Loop model (KL) assumes [6] that the ϕ radiative decay proceeds through a virtual K^+K^- pair emitting the photon and subsequently annihilating into a scalar meson. This loop function damps the E_γ^3 behaviour of the rate, typical of a radiative dipole transition, E_γ being the photon energy. The transition amplitude depends on the mass and the couplings to $\pi\pi$ and to KK of the scalar meson. The propagator includes the finite width corrections, relevant close to the $K\bar{K}$ threshold.

In the No Structure model (NS), the dynamics [7] of the scalar meson production is absorbed in the $g_{\phi S\gamma}$ coupling constant. The amplitude is described by a Breit–Wigner propagator with a mass dependent width, properly

accounting for the analytical continuation under the $\pi\pi$ and KK thresholds, plus a complex polynomial describing a continuum background.

2 The $\phi \to f_0(980)\gamma \to \pi^+\pi^-\gamma$ analysis

This decay is searched for in $e^+e^- \to \pi^+\pi^-\gamma$ events [10], where competing processes with either an initial state (ISR) or a final state (FSR) radiation photon are more abundant. In particular, ISR is the dominant contribution

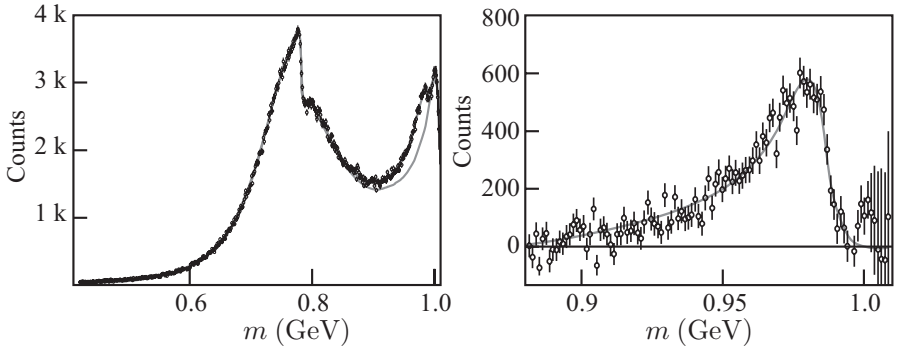

Figure 1: *Left: observed m spectrum compared with the fitting function with and without the* $f_0(980)$. *Right: the fitting function compared to the data spectrum in the* $f_0(980)$ *region, once ISR, FSR and* $\rho\pi$ *are subtracted.*

for small photon polar angle, allowing the extraction of the $e^+e^- \to \pi^+\pi^-$ cross section [11] at lower $\sqrt{s}$ values. The selection consists on the requirement of two tracks of opposite charge from the interaction region and a photon emitted at polar angles $45^\circ < \theta < 135^\circ$. This selection is applied to a total integrated luminosity $\mathcal{L} = 350\ \mathrm{pb}^{-1}$ of data taken in 2001 and 2002, giving 6.7×10^5 events. Figure 1 shows the $\pi^+\pi^-$ invariant mass, m, spectrum before and after the background subtraction. The m spectrum is fitted in the region $m \in [0.42, 1.01]$ GeV including the $\phi \to \rho^\pm\pi^\mp \to \pi^+\pi^-\gamma$ decay chain, defined as $\rho\pi$ term:

$$\frac{d\sigma}{dm} = \frac{d\sigma_{\mathrm{ISR}}}{dm} + \frac{d\sigma_{\mathrm{FSR}}}{dm} + \frac{d\sigma_{\rho\pi}}{dm} + \frac{d\sigma_{S\gamma}}{dm} \pm \frac{d\sigma_{\mathrm{int}}}{dm} \ .$$

Both the KL and the NS models are satisfactory in describing the $f_0(980)$ structure, which appears to interfere destructively with FSR. The $f_0(980)$ re-

sults strongly coupled to kaons and to the ϕ, in both models. Fits show no sensitivity to the $\sigma(600)$ contribution. Estimates of the parameters are shown in tab. 1 and will be discussed together with results of the $\phi \to \pi^0\pi^0\gamma$ analysis.

The $\pi^+\pi^-$ pair has a different charge conjugation eigenvalue depending on whether it is produced from FSR and $f_0(980)$ ($C = +1$) or ISR ($C = -1$). An interference term between two amplitudes of opposite charge conjugation gives rise to C-odd terms that change sign by the interchange of the two pions and results in a forward-backward asymmetry:

$$A_{\rm fb} = \frac{N(\theta_{\pi^+} > 90^\circ) - N(\theta_{\pi^+} < 90^\circ)}{N(\theta_{\pi^+} > 90^\circ) + N(\theta_{\pi^+} < 90^\circ)} \ .$$

Figure 2 shows the comparison of the asymmetry data with the expectations based on the KL parametrization of the $f_0(980)$ [12, 13]. The $A_{\rm fb}$ data distribution is reproduced only by calculations including the $f_0(980)$.

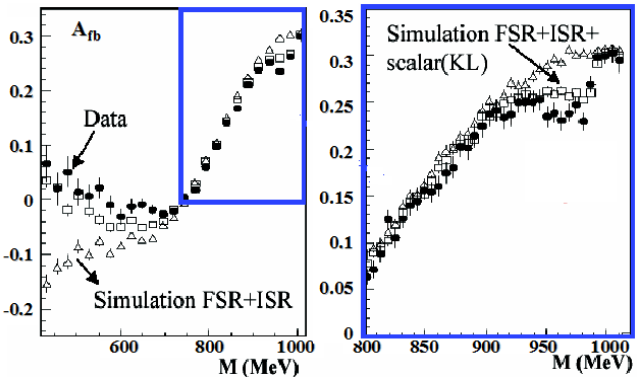

Figure 2: *Left: asymmetry data (full circles) distribution compared with the expectations with and without the scalar meson contribution (FSR + ISR only). Right: zoom of the region of interest for the* $f_0(980)$.

3 The $\phi \to f_0(980)\gamma \to \pi^0\pi^0\gamma$ analysis

An analysis of this process with $\mathcal{L} = 16$ pb^{-1} of 2000 data is already published [14]. In the present contribution the analysis carried on $\mathcal{L} = 450$ pb^{-1} of data taken in 2001 and 2002 is described [15]. Main steps of the selection

are the requirement of five photons from the interaction point and a kinematic fit imposing four-momentum conservation and π^0 masses, after a procedure of

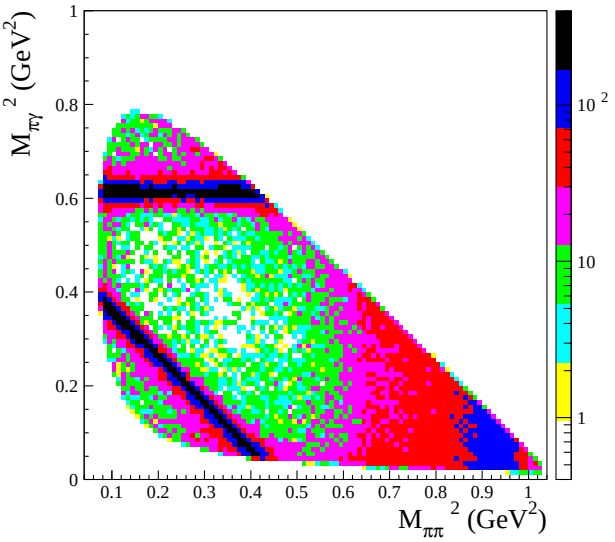

Figure 3: *Dalitz plot in the $\pi^0\pi^0\gamma$ analysis after background subtraction: the two bands at $M^2_{\pi\pi} < 0.5$ GeV^2 are due to $e^+e^- \to \omega\pi^0$ events.*

photon pairing to neutral pions. The efficiency of the selection on signal events is $\sim 50\%$, as evaluated from Monte Carlo, and the residual background contamination is $\sim 20\%$, mostly due to $\phi \to \eta\gamma \to 3\pi^0\gamma$ events with lost or merged photons. Figure 3 shows the Dalitz plot made up of the invariant masses of $\pi^0\pi^0$, $M^2_{\pi\pi}$, and of the two possible $\pi^0\gamma$ combinations, $M^2_{\pi\gamma}$. This is fitted with the coherent sum of the scalar term and the Vector Meson Dominance amplitudes, after folding with reconstruction efficiencies and with the probability for an event to migrate from a bin to another one, due to resolution or wrong photon pairing. The KL model used in this analysis consists of ten sets [16] of parameters, extracted from a combined fit of the 2000 KLOE measurement [14] and of the available $\pi\pi$, KK scattering data. The fit without the $\sigma(600)$ contribution does not yield an acceptable χ^2 value.

Table 1: *Comparison of the best estimates for the parameters of both models.*

model	parameter	$\pi^+\pi^-\gamma$	$\pi^0\pi^0\gamma$	$\pi^0\pi^0\gamma$ updates
KL	m_{f_0} (MeV)	$980 \div 987$	$976.8 \pm 0.3_{\rm fit}\, ^{+0.9}_{-0.6}\,_{\rm sys} + 10.1_{\rm th}$	$984.7 \pm 1.9_{\rm th}$
	$g_{f_0K^+K^-}$ (GeV)	$5.0 \div 6.3$	$3.76 \pm 0.04_{\rm fit}\, ^{+0.15}_{-0.08}\,_{\rm sys}\, ^{+1.16}_{-0.48}\,_{\rm th}$	$3.97 \pm 0.43_{\rm th}$
	$g_{f_0\pi^+\pi^-}$ (GeV)	$3.0 \div 4.2$	$-1.43 \pm 0.01_{\rm fit}\, ^{+0.01}_{-0.06}\,_{\rm sys}\, ^{+0.03}_{-0.60}\,_{\rm th}$	$-1.82 \pm 0.19_{\rm th}$
	$\frac{g^2_{f_0K^+K^-}}{g^2_{f_0\pi^+\pi^-}}$	$2.2 \div 2.8$	$6.9 \pm 0.1_{\rm fit}\, ^{+0.2}_{-0.1}\,_{\rm sys}\, ^{+0.3}_{-3.9}\,_{\rm th}$	
NS	m_{f_0} (MeV)	$973 \div 981$	$984.7 \pm 0.4_{\rm fit}\, ^{+2.4}_{-3.7}\,_{\rm sys}$	
	$g_{f_0K^+K^-}$ (GeV)	$1.6 \div 2.3$	$0.40 \pm 0.04_{\rm fit}\, ^{+0.62}_{-0.29}\,_{\rm sys}$	
	$g_{f_0\pi^+\pi^-}$ (GeV)	$0.9 \div 1.1$	$1.31 \pm 0.01_{\rm fit}\, ^{+0.09}_{-0.03}\,_{\rm sys}$	
	$\frac{g^2_{f_0K^+K^-}}{g^2_{f_0\pi^+\pi^-}}$	$2.6 \div 4.4$	$0.09 \pm 0.02_{\rm fit}\, ^{+0.44}_{-0.08}\,_{\rm sys}$	
	$g_{\phi f_0\gamma}$ (GeV^{-1})	$1.2 \div 2.0$	$2.61 \pm 0.02_{\rm fit}\, ^{+0.31}_{-0.08}\,_{\rm sys}$	

4 Comparison of results

For $\pi^+\pi^-\gamma$ and $\pi^0\pi^0\gamma$, and for both models, the range of values for the estimated parameters, according to theoretical model variants (KL) and systematic uncertainties are shown in tab. 1. Results for the two models are summarized:

[**KL**] in both channels the $f_0(980)$ is strongly coupled to kaons;

[**KL**] the $\sigma(600)$ is required in the $\pi^0\pi^0\gamma$, the $\pi^+\pi^-\gamma$ data have not enough sensitivity;

[**NS**] both $\pi^+\pi^-\gamma$ and $\pi^0\pi^0\gamma$ are well described without the $\sigma(600)$;

[**NS**] the $\pi^0\pi^0\gamma$ fit exhibits a coupling to kaons weaker than $\pi^+\pi^-\gamma$.

Recent updates [16] for the KL model, related to the f_0-σ mixing and the $\sigma\pi\pi$ coupling, let us reduce the spread of parameters in the $\pi^0\pi^0\gamma$ analysis due to model dependence, preliminary values are shown in tab. 1 (last column).

5 The $\phi \to a_0(980)\gamma \to \eta\pi^0\gamma$ analyses: $\eta \to 2\gamma$ and $\eta \to \pi^+\pi^-\pi^0$

Results from these decays are already published [17] using $\mathcal{L} = 16$ pb^{-1} of 2000 data. In this contribution, results are obtained from $\mathcal{L} = 414$ pb^{-1} of

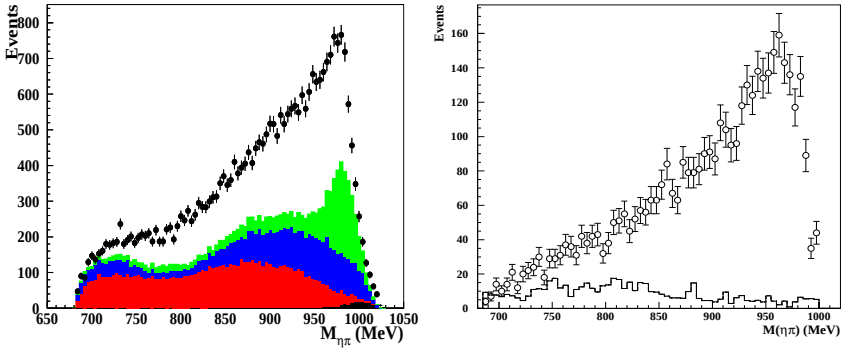

Figure 4: *Left: $M_{\eta\pi}$ spectrum from $\eta \to 2\gamma$ analysis. In decreasing order of contamination yield: $e^+e^- \to \omega\pi^0$, $\phi \to f_0\gamma$, $\phi \to 3\pi^0\gamma$, $\phi \to 3\gamma$. Right: $M_{\eta\pi}$ spectrum from $\eta \to \pi^+\pi^-\pi^0$ analysis. Background distribution is also shown.*

data taken in 2001 and 2002 [18]. Both analyses share the requirement of five

Table 2: *Features of the two η decay channels.*

	signal efficiency	background fraction	BR($\phi \to \eta\pi^0\gamma$) $\times 10^5$
$\eta \to 2\gamma$	40%	55%	$6.92(10)_{stat}(20)_{sys}$
$\eta \to \pi^+\pi^-\pi^0$	20%	15%	$7.19(17)_{stat}(24)_{sys}$

photons from the interaction point. The selection of also two tracks of opposite charge is less efficient, for $\eta \to \pi^+\pi^-\pi^0$ events, but leads to a selected sample with smaller background than in $\eta \to 2\gamma$ events. The absence of a major source of interfering background allows to obtain the branching fraction directly from event counting. Table 2 shows the selection features and the branching fraction values for the two analyses.

Figure 4 shows data spectra in the $\eta\pi$ invariant mass, $M_{\eta\pi}$, for the two η final states, with background shapes from Monte Carlo. The $a_0(980)$ param-

Table 3: *Best estimates of the parameters from the $\eta\pi^0\gamma$ combined fit.*

parameter	Kaon Loop	No Structure
m_{a_0} (MeV)	983 ± 1	983 (fixed)
$g_{a_0K^+K^-}$ (GeV)	2.16 ± 0.04	1.57 ± 0.13
$g_{a_0\eta\pi}$ (GeV)	2.8 ± 0.1	2.2 ± 0.1
$g_{\phi a_0\gamma}$ (GeV^{-1})	–	1.61 ± 0.05

eters are extracted from a simultaneous fit of both $M_{\eta\pi}$ spectra and shown in tab. 3.

6 Conclusions

The 2001-02 KLOE data set allowed for an extensive study of $a_0(980)$ and $f_0(980)$ properties:

- first clear evidence of $f_0(980) \to \pi^+\pi^-$ both in the mass spectrum and in the forward–backward asymmetry;
- accurate Dalitz plot analysis in the $\pi^0\pi^0\gamma$ final state yields the evidence of the $\sigma(600)$ meson;
- good agreement between $\eta\pi^0\gamma$ analyses with different systematics, the combined fit points to a sizeable strange quark content in the $a_0(980)$.

References

1. W. M. Yao *et al.* [Particle Data Group], J. Phys. G **33**, 1 (2006).
2. R. L. Jaffe, Phys. Rev. D **15**, 267 (1977).
3. J. D. Weinstein and N. Isgur, Phys. Rev. Lett. **48**, 659 (1982).
4. S. Guiducci *et al.*, Proc. of the 2001 Particle Accelerator Conference (Chicago, USA), P. Lucas and S. Webber Eds., 353 (2001).
5. F. E. Close, N. Isgur and S. Kumano, Nucl. Phys. B **389**, 513 (1993).
6. N. N. Achasov and V. V. Gubin, Phys. Rev. D **56**, 4084 (1997).

7. G. Isidori, L. Maiani, M. Nicolaci and S. Pacetti, JHEP **0605**, 049 (2006).

8. M. Adinolfi *et al.* [KLOE Collab.], Nucl. Instrum. Meth. A **488**, 51 (2002).

9. M. Adinolfi *et al.* [KLOE Collab.], Nucl. Instrum. Meth. A **482**, 364 (2002).

10. F. Ambrosino *et al.* [KLOE Collab.], Phys. Lett. B **634**, 148 (2006).

11. A. Aloisio *et al.* [KLOE Collab.], Phys. Lett. B **606**, 12 (2005).

12. H. Czyż, A. Grzelińska and J. H. Kühn, Phys. Lett. B **611**, 116 (2005).

13. G. Pancheri, O. Shekhovtsova and G. Venanzoni, Phys. Lett. B **642**, 342 (2006).

14. A. Aloisio *et al.* [KLOE Collab.], Phys. Lett. B **537**, 21 (2002).

15. F. Ambrosino *et al.* [KLOE Collab.], Eur. Phys. J. C **49**, 473 (2007).

16. N. N. Achasov and A. V. Kiselev, Phys. Rev. D **73**, 054029 (2006) [Erratum-ibid. D **74**, 059902 (2006) and private communication].

17. A. Aloisio *et al.* [KLOE Collab.], Phys. Lett. B **536**, 209 (2002).

18. F. Ambrosino *et al.* [KLOE Collab.], arXiv:0707.4609 [hep-ex].

Frascati Physics Series Vol. XLVI (2007), pp. 551–558
HADRON07: XII Int. Conf. on Hadron Spectroscopy – Frascati, October 8-13, 2007
Light Meson Spectroscopy

SEARCH FOR $\phi \to K^0\overline{K^0}\gamma$ DECAY WITH KLOE

Salvatore Fiore
Sapienza Università di Roma and INFN Roma

on behalf of the KLOE collaboration*

Abstract

The KLOE collaboration has searched for the $\phi \to K^0\overline{K^0}\gamma$ decay using a sample of 1.4 fb^{-1} of e^+ e^- collisions at $\sqrt{s} \sim M_\phi$ collected with the KLOE experiment at the Frascati e^+e^- collider DAΦNE. No previous search exists for this decay, while many theoretical models predict a BR of $\sim 10^{-8}$ for this channel. We set a preliminary value of the upper limit on this BR to $1.8 \cdot 10^{-8}$ at 90% C.L.. This limit rules out most of the existing theoretical predictions.

* F. Ambrosino, A. Antonelli, M. Antonelli, F. Archilli, P. Beltrame, G. Bencivenni, S. Bertolucci, C. Bini, C. Bloise, S. Bocchetta, F. Bossi, P. Branchini, P. Campana, G. Capon, T. Capussela, F. Ceradini, S. Chi, P. Ciambrone, E. De Lucia, A. De Santis, P. De Simone, G. De Zorzi, A. Denig, A. Di Domenico, C. Di Donato, B. Di Micco, M. Dreucci, G. Felici, M. L. Ferrer, S. Fiore, C. Forti, P. Franzini, C. Gatti, P. Gauzzi, S. Giovannella, E. Graziani, W. Kluge, G. Lanfranchi, J. Lee-Franzini, D. Leone, M. Martini, P. Massarotti, S. Meola, S. Miscetti, M. Moulson, S. Müller, F. Murtas, M. Napolitano, F. Nguyen, M. Palutan, E. Pasqualucci, A. Passeri, V. Patera, F. Perfetto, P. Santangelo, B. Sciascia, A. Sciubba, A. Sibidanov, T. Spadaro, M. Testa, L. Tortora, P. Valente, G. Venanzoni, R.Versaci, G. Xu

1 Introduction

We present the results of a search for the decay $\phi \to K^0\overline{K^0}\gamma$ using 1.4 fb^{-1} of the KLOE data sample. This decay has never been searched before. The ϕ resonance is produced through e^+e^- collisions at center of mass energy $\sqrt{s}$ ∼1020 MeV. In this decay the $K^0\overline{K^0}$ pair is produced with positive charge conjugation, so that the state of the two kaons can be described as

$$|K^0\overline{K^0}>=\frac{|K_SK_S>-|K_LK_L>}{\sqrt{2}}. \quad (1)$$

The signature of this decay is provided by the presence of either 2 K_S or 2 K_L and a low energy photon. This process has a limited phase space due to the small difference between the ϕ mass (1019.5 MeV) and the production threshold of two neutral kaons (995 MeV). This results in a very narrow photon energy spectrum, ranging from 0 up to a maximum energy obtained when the two kaons are collinear and the KK invariant mass is equal to twice the kaon mass, that is (neglecting the small ϕ momentum due to the e^+e^- crossing angle):

$$E_{\gamma,max}=\frac{M_\phi^2-(2M_K)^2}{2M_\phi}=23.8 \text{ MeV}. \quad (2)$$

Among the possible final states, we searched for that one where a K_SK_S pair has both K_S decaying to $\pi^+\pi^-$. This corresponds to reduce the rate of the searched events of a fraction

$$\frac{1}{2}\times BR(K_S\to\pi^+\pi^-)^2=23.9\% \quad (3)$$

This decay chain is characterized by a clean signature: two vertices close to the interaction region, with both vertices having two tracks with opposite sign, an invariant mass equal to the kaon mass, and an invariant mass of the two kaons significantly lower than the ϕ mass. Moreover, a low energy photon should be present in the event.

In the paper, we first discuss the motivations of this search, we then describe the analysis method including the Monte Carlo (MC) study, and we conclude by extracting the upper limit on the branching ratio and compare it with the theoretical expectations.

2 Motivations

The $\phi \to K^0\overline{K^0}\gamma$ process was considered in the KLOE proposal as a possible background source for the CP violation measurement. The conclusion was that only for branching ratios in excess of $\sim 10^{-6}$ such a background could be critical for the measurement if no selection on the photon and on the kinematics was applied.

On the other hand the value of the branching ratio gives relevant information on the scalar mesons structure. The $K^0\overline{K^0}$ state can have scalar quantum numbers in both triplet and singlet isospin state, so that the reaction is expected to proceed mainly through the chain $\phi \to [f_0(980) + a_0(980)]\gamma \to K^0\overline{K^0}\gamma$. The prediction on the branching ratio depends on the way the scalar dynamics is introduced and on the size of the couplings of the scalars to the kaons. Interference effects between f_0 and a_0 amplitudes can also be present.

Theory predictions on the $BR(\phi \to K^0\overline{K^0}\gamma)$ found in literature spread over several orders of magnitude. The latest evaluations essentially concentrate in the region of 10^{-8}. All of them are well below the critical limit of 10^{-6} so that no significant effect is expected for the CP violation studies at a ϕ-factory.

Some of the reported predictions do not include explicitely the scalar mesons, but consider them as dynamically generated in the theory [1–3]; most of the theory instead includes explicitely the scalars mesons [4–10] in the calculation of the BR, in such a way that the predicted value depends on this modeling. For instance, the two predictions of Ref. [6] are evaluated assuming a 2-quark or a 4-quark struture for the scalar mesons. in such a way that the predicted value depends on the way they are treated. The two predictions differ by one order of magnitude.

In the other cases the width of the allowed band is due to the uncertainty on the coupling constants used in the parametrization of the amplitude which is extracted by experimental analysis of $\phi \to \pi\pi\gamma$ and $\phi \to \eta\pi\gamma$. The latter approach is particularly interesting, since it allows to make a global analysis of KLOE data including $\pi\pi\gamma$ and $\eta\pi\gamma$ [11–14] to test consistency of the overall picture.

Other predictions [15, 16] do not include the scalars so that have to be considered as "backgrounds" in the search for effects due to scalars.

3 Experimental setup

The KLOE experiment is performed at the Frascati ϕ factory DAΦNE, an e^+e^- collider running at $\sqrt{s} \sim 1020$ MeV (ϕ mass). Beams collide with a crossing angle of $(\pi - 0.025)$ rad. From 2001 to 2005, the KLOE experiment has collected an integrated luminosity of 2.5 fb^{-1}.

The KLOE detector consists of a large-volume cylindrical drift chamber [17] (3.3 m length and 4 m diameter), surrounded by a sampling calorimeter [18] made of lead and scintillating fibres. The detector is inserted in a superconducting coil producing a solenoidal field B=0.52 T. Large-angle tracks from the origin ($\theta > 45^\circ$) are reconstructed with momentum resolution $\sigma_p/p = 0.4\%$. Photon energies and times are measured by the calorimeter with resolutions $\sigma_E/E = 5.7\%/\sqrt{E(\text{GeV})}$ and $\sigma_t = 54$ ps$/\sqrt{E(\text{GeV})} \oplus 50$ ps.

4 Analysis strategy

The event selection performed by this analysis is based on kinematic cuts on the charged pion tracks detected by the drift chamber, and on the photon cluster identification in the calorimeter.

We analysed 1.4 fb^{-1} of data collected at the ϕ peak; we also used our MC to generate an equivalent statistics of background, which is mainly due to $\phi \to K_S K_L \to \pi^+\pi^-\pi^+\pi^-$ with the K_L decaying close to the interaction point and an additional photon radiated from the intial or final state. Our simulation is generated on a run-by-run basis, using as input the real data taking conditions for both detector and collider.

We have also generated a MC signal sample of 10k events to study the analysis selection efficiency. The main ingredient of this simulation is the scalar meson's invariant mass shape, which slightly depends on the scalar meson structure. We did not use any of the models quoted above, but instead relied on general assumptions of BR dependence on the radiated photon's energy and on phase space. In Fig. 1 the generated invariant mass spectrum is shown.

We look for two K_S decaying into charged pions, by requiring the presence of two vertices close to the interaction point, inside a fiducial volume defined as a cylinder of 3 cm radius in the transverse plane, and ± 8 cm along the beam line. Each vertex should have two charged tracks attached to.

For each vertex, the two-track reconstructed mass, $M_{2\pi}$, is built in the

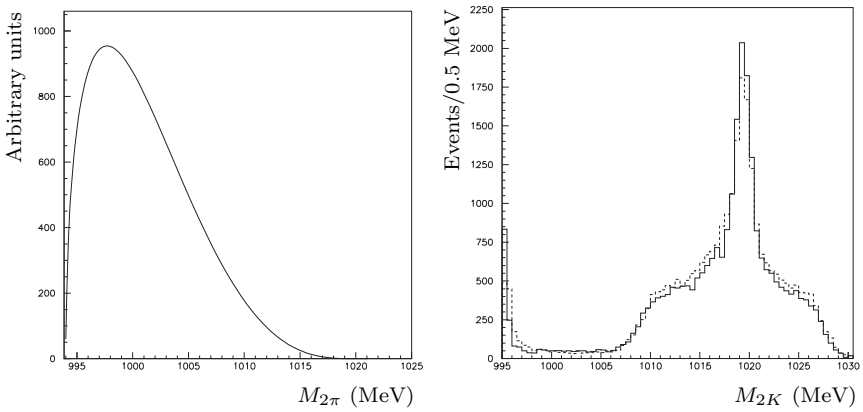

Figure 1: *Left: Expected scalar meson's invariant mass spectrum according to phase-space and radiative decay dinamics. Right: Invariant mass of the kaon pair M_{2K} for Monte Carlo (solid) and Data (dashed).*

pion hypothesys. For the signal, the event density in the $M_{2\pi}(1)$, $M_{2\pi}(2)$ plane is well contained inside a circle of few MeV radius around the K_S mass. We require the events to satisfy a 4 MeV cut on this radius. With the reconstructed masses and momenta of the two K_S candidates we calculate the invariant mass of the kaon pair. As expected by the signal simulated mass spectrum shown in Fig.1, the M_{2K} distribution peaks at 1000 MeV, while the background is peaked at M_ϕ as shown in Fig. 1. A large background reduction is obtained by rejecting events with $M_{2K} > 1010$ MeV. Moreover, the 4-momentum conservation in the $\phi \to K_S K_S \gamma$ decay allows to build a missing 4-momentum quantity $\widetilde{P_\gamma} = \widetilde{P_\phi} - \widetilde{P_{K_1}} - \widetilde{P_{K_2}}$ based only on charged-track reconstructed variables. A selection variable $M^2_\gamma = E^2_{miss} - P^2_{miss}$ is then built, which is expected to be ~ 0 for the signal. We retain events with $|M^2_\gamma| \leq 300$ MeV^2.

Events that survive all these cuts are searched for the presence of one photon matching missing momentum. We require the presence of one cluster in the calorimeter not associated with any charged track. Cluster's timing must be compatible with a photon coming from the interaction point, and cluster's position and energy must agree within resolution with the missing momentum.

5 Results

All the above mentioned cuts have been decided upon an upper limit maximization based on MC samples. We estimate an efficiency of 20.6% for the signal, while we find no event surviving in the background MC. When looking at data we observe one event. Data-MC comparison is still under way, so we do not use background evaluation for this preliminary result. However we can set an upper limit on the $BR(\phi \to K^0\bar{K}^0\gamma)$ using Poisson statistics without background subtraction; in our case with one observed event, the upper limit on the number of events at 90% C.L. is $S_{90\mathrm{CL}}$=3.9 events.

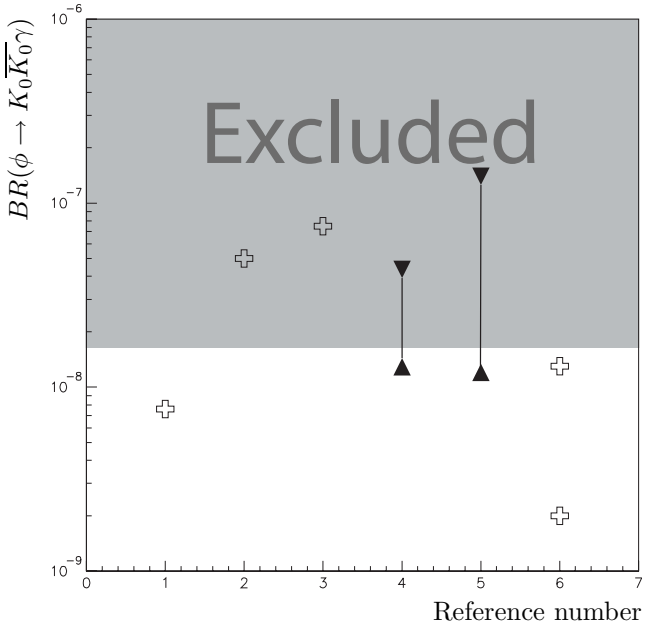

Figure 2: *Comparison between theoretical predictions and our measurement. In abscissa is directly reported the reference number (according to the reference list). For Ref.* [6] *two predictions are reported: the upper one is for 4-quark hypothesys, the lower one for 2-quark hypothesys. For Refs.* [4, 5] *the prediction is represented as a band.*

We evaluate our BR-upper limit in the following way:

$$BR(\phi \to K_0\overline{K_0}\gamma) = \frac{S_{90\mathrm{CL}}}{\int \mathcal{L}dt \cdot \sigma(e^+e^- \to \phi) \cdot \frac{1}{2} \cdot (BR(K_S \to \pi^+\pi^-))^2 \cdot \epsilon} \quad (4)$$

in which $\int \mathcal{L}dt$ is 1.4 fb^{-1}, the factor 1/2 accounts for the fact that we are selecting only the K_SK_S combination for $K_0\overline{K_0}$, ϵ is our signal efficiency. The following limit on the branching ratio is obtained:

$$BR(\phi \to K_0\overline{K_0}\gamma) < 1.8 \cdot 10^{-8} \quad (5)$$

at 90%C.L.. In Fig. 2 our limit is compared to theoretical predictions. Most of them are excluded by our result.

References

1. A. Bramon, A. Grau, G. Pancheri, Phys. Lett. B **289**, 97 (1992).
2. J.A. Oller, Phys. Lett. B **426**, 7 (1998).
3. R. Escribano, Eur. Phys. J. A **31**, 454 (2007).
4. N.N. Achasov, V.V. Gubin, Phys. Rev. D **64**, 094016 (2001).
5. A. Gokalp, C. S. Korkmaz, O. Yilmaz, hep-ph/0702214.
6. N.N. Achasov, V.N. Ivanchenko, Nucl. Phys. B **315**, 465 (1989).
7. S. Nussinov, T.N. Truong, Phys. Rev. Lett. **63**, 1349 (1989), Erratum 2003.
8. J. Lucio, J. Pestieau, Phys. Rev. D **42**, 3253 (1990).
9. F. E. Close, N. Isgur, S. Kumano, Nucl. Phys. B **389**, 513 (1993).
10. S. Pacetti, private comunication.
11. A. Aloisio *et al.* [KLOE Coll.], Phys. Lett. B **536**, 209 (2002).
12. A. Aloisio *et al.* [KLOE Coll.], Phys. Lett. B **537**, 21 (2002).
13. F. Ambrosino *et al.* [KLOE Coll.], Phys. Lett. B **634**, 148 (2006).
14. F. Ambrosino *et al.* [KLOE Coll.], Eur. Phys. J. C **49**, 473 (2007).

15. S. Fajfer, R. J. Oakes, Phys. Rev. D **42**, 2392 (1990).

16. A. Bramon, A. Grau, G. Pancheri, Phys. Lett. B **283**, 416 (1992).

17. M. Adinolfi *et al.* [KLOE Coll.], Nucl. Instr. Meth. A **488**, 51 (2002).

18. M. Adinolfi *et al.* [KLOE Coll.], Nucl. Instr. Meth. A **482**, 364 (2002).

Frascati Physics Series Vol. XLVI (2007), pp. 559–566
HADRON07: XII Int. Conf. on Hadron Spectroscopy – Frascati, October 8-13, 2007
Light Meson Spectroscopy

STUDY OF SCALAR MESONS IN CHIRAL LAGRANGIAN FRAMEWORKS

Deirdre Black and Jonathan Gaunt
Department of Physics, Cavendish Laboratory, Cambridge CB3 OHE, UK

Abstract

We review two previous approaches to studying pseudoscalar meson-meson scattering amplitudes to beyond 1 GeV using non-linear and linear chiral Lagrangians. In these approaches we use two different unitarisation techniques - a generalised Breit-Wigner prescription and K-matrix unitarisation respectively. We also report some preliminary findings on K-matrix unitarisation of the $I = J = 0$ $\pi\pi$ scattering in a non-linear chiral Lagrangian approach and make some remarks about the light scalar mesons.

1 Introduction

Pseudoscalar meson-meson scattering up to the 1-2 GeV energy range is of interest for several related reasons. On the one hand this region is beyond that where chiral perturbation theory has traditionally been applied and below that

where we can use perturbative QCD, so it is a challenge to develop a framework to calculate these amplitudes from first principles. At the same time there are many resonances in this region, some of which are controversial from the point of view of establishing their properties experimentally and their quark substructure. In particular, the scalar mesons are a long-standing puzzle in meson spectroscopy because, for example, there are too many states to fit into a single SU(3) nonet and the masses and decay patterns of some of the scalar resonances are not what one would expect for quark-antiquark scalar states. This talk is based on approaches developed by the Syracuse group. Many other interesting approaches are given in the proceedings of this conference and also cited in the references given in the bibliography.

2 Non-linear chiral Lagrangian approach to meson-meson scattering

We begin [1, 2] with the conventional chiral Lagrangian, including only pseudoscalars:

$$\mathcal{L}_1 = -\frac{F_\pi^2}{8}\mathrm{Tr}\left(\partial_\mu U \partial_\mu U^\dagger\right) + \mathrm{Tr}\left[\mathcal{B}\left(U + U^\dagger\right)\right], \tag{1}$$

in which $U = e^{2i\frac{\phi}{F_\pi}}$, with ϕ the 3×3 matrix of pseudoscalar fields and $F_\pi = 132$ MeV the pion decay constant. $\mathcal{B}$ is a diagonal matrix (B_1, B_1, B_3) with $B_1 = m_\pi^2 F_\pi^2/8 = B_2$ and $B_3 = F_\pi^2(m_K^2 - m_\pi^2/2)/4$.

We add a nonet of scalar mesons, which transform like external fields under chiral transformations. It turns out [3] that the trilinear scalar-pseudoscalar-pseudoscalar interaction that follows from the general chiral invariant extension of $\mathcal{L}_1$ to include a scalar meson nonet is given by

$$\begin{aligned}\mathcal{L}_{N\phi\phi} &= A\epsilon^{abc}\epsilon_{def}N_a^d\partial_\mu\phi_b^e\partial_\mu\phi_c^f + B\mathrm{Tr}\left(N\right)\mathrm{Tr}\left(\partial_\mu\phi\partial_\mu\phi\right)\\ &+ C\mathrm{Tr}\left(N\partial_\mu\phi\right)\mathrm{Tr}\left(\partial_\mu\phi\right) + D\mathrm{Tr}\left(N\right)\mathrm{Tr}\left(\partial_\mu\phi\right)\mathrm{Tr}\left(\partial_\mu\phi\right).\end{aligned} \tag{2}$$

The first term of (2) may be eliminated in favor of the more standard form $\mathrm{Tr}\left(N\partial_\mu\phi\partial_\mu\phi\right)$, but is interesting because it is the OZI rule conserving term for a dual diquark-antidiquark type nonet mentioned below.

The scalar particles with non-trivial quantum numbers are given by:

$$N = \begin{bmatrix} N_1^1 & a_0^+ & \kappa^+ \\ a_0^- & N_2^2 & \kappa^0 \\ \kappa^- & \bar{\kappa}^0 & N_3^3 \end{bmatrix} \tag{3}$$

with $a_0^0 = (N_1^1 - N_2^2)/\sqrt{2}$. There are two iso-singlet states: the combination $(N_1^1 + N_2^2 + N_3^3)/\sqrt{3}$ is an $SU(3)$ singlet while $(N_1^1 + N_2^2 - 2N_3^3)/\sqrt{6}$ belongs to an $SU(3)$ octet. These will in general mix with each other when $SU(3)$ is broken. We can write the general mass term [3)]

$$\mathcal{L}_{mass} = -a\mathrm{Tr}(NN) - b\mathrm{Tr}(NN\mathcal{M}) - c\mathrm{Tr}(N)Tr(N) - d\mathrm{Tr}(N)\mathrm{Tr}(N\mathcal{M}), \quad (4)$$

where a, b, c and d are real constants. $\mathcal{M}$ is the "spurion matrix" $\mathcal{M} = \mathrm{diag}(1, 1, x)$, x being the ratio of strange to non-strange quark masses in the usual interpretation.

We take a convention where the physical particles, σ and f_0, which diagonalize the mass matrix obtained from (4) are related to the basis states N_3^3 and $(N_1^1 + N_2^2)/\sqrt{2}$ by

$$\begin{pmatrix} \sigma \\ f_0 \end{pmatrix} = \begin{pmatrix} \cos\theta_s & -\sin\theta_s \\ \sin\theta_s & \cos\theta_s \end{pmatrix} \begin{pmatrix} N_3^3 \\ \frac{N_1^1+N_2^2}{\sqrt{2}} \end{pmatrix}. \quad (5)$$

For a given set of inputs for the masses of the four scalar mesons σ, $f_0(980)$, $a_0(980)$ and κ the constants a, b, c and d are fixed and there are two possible solutions for the mixing angle θ_s.

We note that there are different possibilities, in addition to quark-antiquark configurations, for the underlying quark substructure of N which all give rise to the same $SU(3)$ transformation properties. For example, forming diquark objects

$$T_a = \epsilon_{abc}\bar{q}^b\bar{q}^c, \qquad \bar{T}^a = \epsilon^{abc}q_b q_c, \quad (6)$$

where the antisymmeterisation of the quark fields is implicit, we can form a pure tetraquark scalar nonet as follows:

$$N_a^b \sim T_a\bar{T}^b \sim \begin{bmatrix} \bar{s}\bar{d}ds & \bar{s}\bar{d}us & \bar{s}\bar{d}ud \\ \bar{s}\bar{u}ds & \bar{s}\bar{u}us & \bar{s}\bar{u}ud \\ \bar{u}\bar{d}ds & \bar{u}\bar{d}us & \bar{u}\bar{d}ud \end{bmatrix} \quad (7)$$

or construct linear combinations of $q\bar{q}$ and $qq\bar{q}\bar{q}$ nonets. We studied s-wave pseudoscalar meson scattering in a framework beginning with Eqs. (1) and (2). If we begin with the tree-level scattering amplitudes, which due to chiral symmetry give good agreement with experiment close to the scattering threshold, we find that they soon deviate from the experimental data. They also violate unitarity. The approach that we took was to add an imaginary piece by hand

to the tree-level propagator of the s-channel resonance. For πK scattering we called the lightest strange scalar resonance κ and made the substitution:

$$m_\kappa^2 - s \longrightarrow m_\kappa^2 - s - i m_\kappa G'_\kappa \tag{8}$$

in the denominator of the s-channel s-wave amplitude. In order to fit to experiment the quantity G'_κ was left as a free parameter, not necessarily equal to the perturbative width, G_κ say. Our fit [2)], shown in Fig. 1 gave $\frac{G_\kappa}{G'_\kappa} = 0.13$ showing a substantial deviation from a Breit-Wigner resonance for which this ratio would be exactly equal to 1. Good agreement with experiment was also found [1)] with this generalised Breit-Wigner prescription for the case of $\pi\pi$ scattering. The other fitting parameters are the scalar-pseudoscalar-pseudoscalar coupling constants, which can all be written in terms of the four coefficients in the interaction terms in Eq. (2), the scalar meson masses and mixing angle.

We note also that, in addition to neatly explaining the mass ordering and general pattern of decays of the scalar states below 1 GeV, a multiquark interpretation for these states is also suggested by the value of the scalar meson octet-singlet mixing angle θ_s defined in Eq. (5), which was a parameter fixed by our fits. Our best fit was about -20^o which, in our mixing convention, would be close to ideal mixing for a "dual" diquark-antidiquark nonet.

3 Pseudoscalar meson-meson scattering in Linear Sigma Models

In the three flavor linear sigma model the pseudoscalar and scalar mesons appear together since the model is constructed from the 3×3 matrix field

$$M = S + i\phi, \tag{9}$$

where $S = S^\dagger$ represents a scalar nonet and $\phi = \phi^\dagger$ a pseudoscalar nonet. Under a chiral transformation $q_L \to U_L q_L$, $q_R \to U_R q_R$ of the fundamental left and right handed light quark fields, M is defined to transform as

$$M \longrightarrow U_L M U_R^\dagger. \tag{10}$$

We considered a general non-renormalizable Lagrangian[1] of the form

$$\mathcal{L} = -\frac{1}{2}\mathrm{Tr}\left(\partial_\mu \phi \partial_\mu \phi\right) - \frac{1}{2}\mathrm{Tr}\left(\partial_\mu S \partial_\mu S\right) - V_0 - V_{SB}, \tag{11}$$

[1]See [4)] and references therein for more detail.

where V_0 is an arbitrary function of the independent $SU(3)_L \times SU(3)_R \times U(1)_V$ invariants $\mathrm{Tr}\left(MM^\dagger\right)$, $\mathrm{Tr}\left(MM^\dagger MM^\dagger\right)$, $\mathrm{Tr}\left((MM^\dagger)^3\right)$ $6\left(\mathrm{det}M + \mathrm{det}M^\dagger\right)$. Of these, only I_4 is not invariant under $U(1)_A$. The symmetry breaker V_{SB} has the minimal form

$$V_{SB} = -2\left(A_1 S_1^1 + A_2 S_2^2 + A_3 S_3^3\right), \tag{12}$$

where the A_a are real numbers which turn out to be proportional to the three light ("current" type) quark masses. In this model there are many constraints among the parameters. For example, many of the trilinear scalar-pseudoscalar-pseudoscalar coupling constants are predicted in terms of the pseudoscalar and scalar meson masses. Another difference is that [compare with Eq. (2)] this trilinear interaction does not involve derivatives. Both models give the "current algebra" results in the limit where the scalar mesons are integrated out.

If we calculate the tree level s-wave amplitudes they deviate from experiment and also violate unitarity as we go beyond the threshold region. We used [4] the well-known K-matrix procedure to unitarise the linear sigma model amplitudes and then checked if the resulting unitary amplitudes can give a good fit to data. In the standard parameterization [6] of a given partial wave S-matrix:

$$S = \frac{1+iK}{1-iK} \equiv 1 + 2iT, \tag{13}$$

we identify

$$K = T_{\mathrm{tree}}. \tag{14}$$

T_{tree} is the given partial wave T-matrix computed at tree level in the Linear Sigma Model and is purely real. This scheme gives exact unitarity for T but violates the crossing symmetry which T_{tree} itself obeys. In Fig. 2 we show our best fit to the $I = J = 0$ $\pi\pi$ scattering data. The parameters in this fit are the "bare" masses of the two $I = 0$ scalar mesons in M and their mixing angle. Using these parameters we can solve for the poles in the unitarised amplitude in the complex s plane. Labelling these poles z_σ and $z_{\sigma'}$ we can identify the physical masses and widths as usual from the Real and Imaginary parts, for example $z_\sigma = m_\sigma^2 - i m_\sigma \Gamma_\sigma$.

4 Summary and comparison between models

We have found good agreement with scattering data in the approaches based on the non-linear chiral Lagrangians outlined in Sections 2 and 3. We are

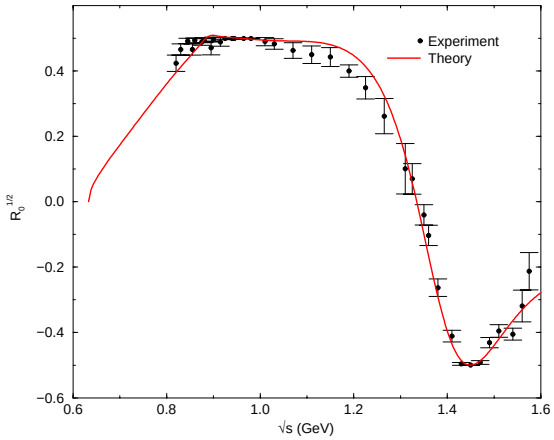

Figure 1: *Best fit to the experimental data* [5] *for the Real part of the* $I=\frac{1}{2}$, $J=0$, πK *scattering amplitude in our non-linear chiral Lagrangian model* [2] *with generalised Breit-Wigner prescription.*

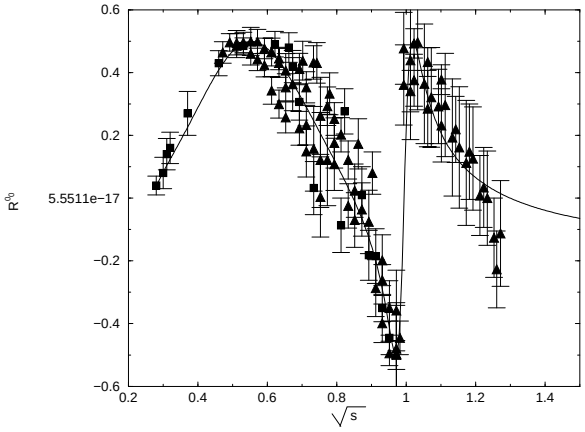

Figure 2: *Best fit to the experimental data* [7] *for the Real part of the* $I=J=0$ $\pi\pi$ *scattering amplitude in a linear sigma model with K-matrix unitarisation* [4].

Table 1: *Results for physical I=0 scalar meson parameters from fits to $\pi\pi$ scattering. Comparison between linear and non-linear chiral Lagrangian models using K-matrix and Generalised Breit-Wigner approaches to unitarisation.*

Scalar parameters (MeV)	Non-linear chiral approach K-matrix (preliminary)	SU(3) Linear Sigma Model [4] K-matrix	Non-linear chiral approach [1] Generalised B-W without/with ρ meson
m_σ	444	457	378/559
Γ_σ	604	632	836/370
m_f	986	993	987
Γ_f	52	51	65

currently studying scattering using the non-linear chiral Lagrangian approach outlined of Section 2, but employing the K-matrix unitarisation as described in Section 3. This may make it easier to compare the linear and non-linear chiral Lagrangian models more directly and to understand the effects of the unitarisation prescriptions in themselves. This was partly motivated by our work on extending the non-linear chiral Lagrangian approach to include vector mesons [8]. This enabled us to study the interesting rare radiative decay processes $\phi \to \pi\pi\gamma$ and $\phi \to \pi\eta\gamma$. We found that the shape of the partial branching fraction depends quite sensitively on whether we use derivative or non-derivative scalar-pseudoscalar-pseudoscalar coupling as in Section 2 or 3 respectively.

A summary of our results is shown in Table 1 for the case of $\pi\pi$ scattering. In the third and fourth columns we show the results of the analyses described in Sections 3 and 2 respectively. In the fourth column we give the results with and without the inclusion of the ρ vector meson. In column 2 we show the results of our current analysis, which are preliminary. However we can see some trends, namely that the $f_0(980)$ parameters are quite stable, whereas the σ parameters seem to depend more on the model and, even more, on the unitarisation procedure. These results are preliminary because we have only done a fit of $\pi\pi$ scattering data over a limited energy range. Also we have not included the inelastic channel and so the important $K\bar{K}$ threshold region. These and a similar study of related scattering channels are interesting directions for future work.

5 Acknowledgements

DB would like to thank the conference organisers for a friendly and stimulating meeting. The work in much of this presentation is part of an ongoing collaboration with Abdou Abdel-Rehim, Amir Fariborz, Masayasu Harada and Joseph Schechter. DB is supported by the Royal Society and JG was supported by a Summer Research Studentship from Trinity College, Cambridge.

References

1. M. Harada, F. Sannino and J. Schechter, Phys. Rev. D. **52** 1991 (1996); Phys. Rev. Lett. **78**, 1603 (1997).
2. D. Black, A.H. Fariborz, F. Sannino and J. Schechter, Phys. Rev. D **58** 054012 (1998).
3. D. Black, A.H. Fariborz, F. Sannino and J. Schechter, Phys. Rev. D **59**, 074026 (1999).
4. D. Black *et al.*, Phys. Rev. D **64** 014031 (2001).
5. D. Aston *et al.*, Nucl. Phys. B **296**, 493 (1988).
6. S.U. Chung *et al.*, Ann. Phys. **4** 404 (1995).
7. E.A. Alekseeva *et al.*, Sov. Phys. JETP **55**, 591 (1982), G. Grayer et al, Nucl. Phys. B **75**, 189 (1974).
8. D. Black, M. Harada and J. Schechter, Phys. Rev. Lett. **88** 181603 (2002); Phys. Rev. D **73** 054017 (2006).

Frascati Physics Series Vol. XLVI (2007), pp. 567-575
HADRON07: XII Int. Conf. on Hadron Spectroscopy – Frascati, October 8-13, 2007
Light Meson Spectroscopy

TWO-PHOTON DECAY OF LIGHT SCALARS: A COMPARISON OF TETRAQUARK AND QUARKONIUM ASSIGNMENTS

Francesco Giacosa
Institut für Theoretische Physik Universität Frankfurt Johann Wolfgang Goethe - Universität Max von Laue–Str. 1 60438 Frankfurt, Germany

Abstract

Two-photon decays of light scalar mesons are discussed within the quarkonium and tetraquark asignements: in both cases the decay rate of the sigma resonances turns out to be smaller than 1 keV.

1 Introduction

The two-photon decay of light mesons represents an important source of information [1]. In particular, the $\gamma\gamma$ decay of light scalar mesons has been considered as a possible tool to deduce their nature. According to the interpretation of light scalars (quarkonia, tetraquarks or molecules) different $\gamma\gamma$-rates are expected [2, 3]. In this proceeding we first study (Section 2) the quarkonium assignments for the light scalar states by studying $SU(3)$-relations for the two-photon decays. While the quarkonium assignment is disfavored when looking

at mass pattern [4], strong decays [3, 5] and large-N_c studies [6] (see the discussion in the recent proceeding [7]), here we adopt a neutral point of view. After a test-study with the well-known pseudoscalar and tensor mesons [8] we turn to the $\gamma\gamma$ decay of light scalars as quarkonia, finding that $f_0(600)$ has a decay rate well below 1 keV. This is in agreement with the microscopic evaluation in the recent work [9], where the two-photon decay of a low-lying quarkonium state with $\overline{n}n = \sqrt{1/2}(\overline{u}u + \overline{d}d)$: contrary to usual results quoted in the literature it is shown that the corresponding two-photon decay rate is well below 1 keV for a mass $M_{\overline{n}n} < 0.8$ GeV. In Section 3 we turn to the two-photon transition within the tetraquark assignment and in Section 4 we briefly summarize our results.

2 Quarkonia into $\gamma\gamma$

2.1 Quarkonia into $\gamma\gamma$: symmetry relations

We first consider the two-photon decay of scalar quarkonia states. However, the formula we introduce are also valid, with simple changes, for the pseudoscalar, tensor and axial vector nonets as we will discuss later on. The charge neutral scalar quarkonia states N, S and a_0^0 are introduced as $N \equiv \overline{n}n = \sqrt{1/2}(\overline{u}u + \overline{d}d)$, $S \equiv \overline{s}s$ and $a_0^0 \equiv \sqrt{1/2}(\overline{u}u - \overline{d}d)$. The 3×3 diagonal matrix $\mathcal{S}^{[\overline{q}q]} \equiv diag\{\overline{u}u, \overline{d}d, \overline{s}s\} = diag\{N/\sqrt{2} + a_0^0/\sqrt{2}, N/\sqrt{2} - a_0^0/\sqrt{2}, S\}$ plays a central role. In flavor (and large-N_c) limit the two-photon decay of these states is described by the effective interaction Lagrangian

$$\mathcal{L}_{S\gamma\gamma} = c_{S\gamma\gamma} Tr\left[Q^2 \mathcal{S}^{[\overline{q}q]}\right] F_{\mu\nu}^2 \tag{1}$$

where $Q = diag\{2/3, -1/3, -1/3\}$ is the quark charge matrix, $F_{\mu\nu} = \partial_\mu A_\nu - \partial_\nu A_\mu$ the field tensor of the electromagnetic field A_μ and $c_{S\gamma\gamma}$ a coupling constant. As a result the decay rates of N, S, and a_0^0 are given by

$$\Gamma_{N\gamma\gamma} = \frac{c_{S\gamma\gamma}^2}{4\pi} M_N^3 \left[\frac{5}{9}\right]^2, \Gamma_{S\gamma\gamma} = \frac{c_{S\gamma\gamma}^2}{4\pi} M_S^3 \left[\frac{1}{9}\right]^2, \Gamma_{a_0^0\gamma\gamma} = \frac{c_{S\gamma\gamma}^2}{4\pi} M_{a_0^0}^3 \left[\frac{3}{9}\right]^2. \tag{2}$$

The physical states, denoted as $f_0(600)$ and $f_0(980)$ in the low-scalar case, are in general a mixing of N and S: $f_0(600) = \cos\theta_S N + \sin\theta_S S$ and orthogonal combination for $f_0(980)$. The two-photon decay rates of $f_0(600)$ and $f_0(980)$

are given by:

$$\begin{aligned}\Gamma_{f_0(600)\gamma\gamma} &= \frac{c^2_{S\gamma\gamma}}{4\pi} M^3_{f_0(600)} \left[\frac{5}{9}\cos\theta_S + \frac{1}{9}\sin\theta_S\right]^2 , \\ \Gamma_{f_0(980)\gamma\gamma} &= \frac{c^2_{S\gamma\gamma}}{4\pi} M^3_{f_0(980)} \left[-\frac{5}{9}\sin\theta_S + \frac{1}{9}\cos\theta_S\right]^2 .\end{aligned}$$

Before studying the scalar case we test these simple expressions on other nonets. In particular, we will be interested to the ratios $\frac{\Gamma_{f_0(600)\gamma\gamma}}{\Gamma_{a_0^0\gamma\gamma}}$ and $\frac{\Gamma_{f_0(980)\gamma\gamma}}{\Gamma_{a_0^0\gamma\gamma}}$ for which the dependence on the unknown parameter $c_{S\gamma\gamma}$ cancels out under the hypothesis that an eventual momentum dependence is weak, see the following discussions.

Pseudoscalar nonet- Here we have $\pi^0 = \sqrt{1/2}(\overline{u}u - \overline{d}d)$ and the isoscalar states η and η', expressed in terms of bare states as

$$\left(\begin{array}{c}\eta\\ \eta'\end{array}\right) = \left(\begin{array}{cc}\cos\varphi_P & \sin\varphi_P\\ -\sin\varphi_P & \cos\varphi_P\end{array}\right)\left(\begin{array}{c}N\\ S\end{array}\right) = \left(\begin{array}{cc}\cos\theta_P & -\sin\theta_P\\ \sin\theta_P & \cos\theta_P\end{array}\right)\left(\begin{array}{c}P^8\\ P^0\end{array}\right) \tag{3}$$

where $P^8 = \sqrt{1/6}(\overline{u}u + \overline{d}d - 2\overline{s}s)$ and $P^0 = \sqrt{1/3}(\overline{u}u + \overline{d}d + \overline{s}s)$. In the literature the angle θ_P is in general discussed. The corresponding Lagrangian is similar to (1): $\mathcal{L}_{P\gamma\gamma} = c_{P\gamma\gamma} Tr\left[Q^2 \mathcal{P}^{[\overline{q}q]}\right] F_{\mu\nu}\widetilde{F}^{\mu\nu}$, where $\widetilde{F}^{\mu\nu} = \varepsilon^{\mu\nu\rho\sigma}F_{\rho\sigma}$: eq. (2) retain the same form. Out of (3) one finds the relation $\theta_P = \arcsin[\sqrt{2/3}] - \varphi_P = 54.736^\circ - \varphi_P$. In [10] the values $\Gamma_{\pi^0\gamma\gamma} = 7.74 \pm 0.55$ eV, $\Gamma_{\eta\gamma\gamma} = 0.510 \pm 0.026$ keV and $\Gamma_{\eta'\gamma\gamma} = 4.30 \pm 0.15$ keV. The corresponding experimental ratios read $\frac{\Gamma_{\eta\gamma\gamma}}{\Gamma_{\pi^0\gamma\gamma}} = 65.9 \pm 8.1$, $\frac{\Gamma_{\eta'\gamma\gamma}}{\Gamma_{\pi^0\gamma\gamma}} = 556 \pm 59$. A fit of φ_P to the latter ratios implies $\varphi_P = 67.6^\circ$, and thus $\theta_P = -12.8^0$. The corresponding ratios evaluated at this mixing angle read $\frac{\Gamma_{\eta\gamma\gamma}}{\Gamma_{\pi^0\gamma\gamma}} = 76.6$ and $\frac{\Gamma_{\eta'\gamma\gamma}}{\Gamma_{\pi^0\gamma\gamma}} = 661.9$ with $\chi^2/2 = 2.48$. Taking into account that we are considering the easiest possible scenario, thus neglecting many possible corrections, these results are very good. In fact, the experimental results range within 3 order of magnitudes: the theoretical dependence on the third power of the mass is well verified. An eventual mass dependence of the effective coupling $c_{P\gamma\gamma}$ has to be small form M_π up to 1 GeV, a remarkable fact. The mixing angle $\theta_P = -12.8^0$ is in the phenomenological range between -10° and -20°, as found also by more refined studies. This simple exercise shows that SU(3) flavor relations, together with the OZI rule allowing to include the flavor singlet in the game, is well upheld and a good starting point to test the quarkonium assignment in a given nonet.

Tensor nonet- As a further test let's consider the tensor nonet (see [8] and refs. therein). The resonances under study are the isovector $a_2(1320)$ with $M_{a_2} = 1318.3$ MeV and the isoscalars $f_2(1270)$ and $f_2'(1525)$ with $M_{f_2} = 1275.1$ and $M_{f_2} = 1525$ (we omit tiny errors, see [10]). As before, the mixing angle φ_T is introduced as $f_2(1270) = \cos\varphi_T N + \cos\varphi_T S$ and orthogonal combination for $f_2'(1525)$. The interaction Lagrangian is $\mathcal{L}_{T\gamma\gamma} = c_{T\gamma\gamma} Tr\left[Q^2 \mathcal{T}_{\mu\nu}^{[\overline{q}q]}\right] \Theta^{\mu\nu}$ where $\Theta^{\mu\nu}$ is the energy-momentum tensor of the electromagnetic fields. The experimental values $\Gamma_{a_2\gamma\gamma} = 1.00 \pm 0.06$ keV, $\Gamma_{f_2\gamma\gamma} = 2.60 \pm 0.24$ keV and $\Gamma_{f_2'\gamma\gamma} = (8.1 \pm 0.9)10^{-2}$ keV lead to the ratios $\frac{\Gamma_{f_2\gamma\gamma}}{\Gamma_{a_2\gamma\gamma}} = 2.6 \pm 0.4$ and $\frac{\Gamma_{f_2'\gamma\gamma}}{\Gamma_{a_2\gamma\gamma}} = (8.1 \pm 1.4)\,10^{-2}$. A fit of the angle φ_T to these values leads to $\varphi_T = 8.19^\circ$ and a very small $\chi^2/2 = 0.015$, thus the experimental values are reproduced almost exactly. The value of $\varphi_T = 8.19^\circ$ is in good agreement with the study of strong decays [8]. Again, the $\gamma\gamma$-ratios can be well described by simple symmetry relations. Indeed, the agreement is even better than in the pseudoscalar case: this is expected because the masses vary in a smaller energy region. In the end, we remind that a quarkonium interpretation works well for vector mesons: here the dominant e.m. transition is into one single photon (i.e. mixing) which is at the basis of the successful phenomenology of the vector meson dominance hypothesis.

Scalar nonet below 1 GeV- Let us now turn back to the scalar states below 1 GeV within a quarkonium assignment. We identify the neutral isovector a_0^0 with $a_0^0(980)$ and, as described above, the isoscalars with $f_0(600)$ and $f_0(980)$. The experimental results for the decay width of a_0 and $f_0(980)$ are given by [10]: $\Gamma_{f_0(980)\gamma\gamma} = 0.39^{+0.10}_{-0.13}$ KeV, $\Gamma_{a_0^0\gamma\gamma} = 0.30 \pm 0.10$ KeV. Thus, the experimental ratio reads then $\frac{\Gamma_{f_0(980)\gamma\gamma}}{\Gamma_{a_0^0\gamma\gamma}} = 1.3 \pm 0.8$ where an average error of 0.115 KeV for $\Gamma_{f_0\gamma\gamma}$ has been used. As noticeable, the error for this ratio is large. Unfortunately, the experimental situation concerning $f_0(600) \to 2\gamma$ is even worse; no average or fit is presented in [10], however two experiments listed in [10] find large $\gamma\gamma$ decay widths: 3.8 ± 1.5 keV and 5.4 ± 2.3 keV, respectively. In a footnote it is then state that these values could be assigned to $f_0(1370)$ (actually, in a older version of PDG [11] these values were assigned to the resonance $f_0(1370)$). It is not clear if the $\gamma\gamma$ signal comes from the high mass tail of the broad σ state or from $f_0(1370)$ (or even from both). We determine the mixing angle θ_S by using the experimental result $\frac{\Gamma_{f_0(980)\gamma\gamma}}{\Gamma_{a_0^0\gamma\gamma}} = 1.3 \pm 0.8$.

Due to the large error we report the possible ranges for θ_S compatible with it: $-41.4^\circ \leq \theta_S \leq -7.78^\circ$, $39.4^\circ \leq \theta_S \leq 73.0^\circ$. Indeed, as we saw previously the angle φ_P in the pseudoscalar sector is positive: the components of N and S are out of phase for η' and in phase for η ($\varphi_P = 67.6^\circ$). Within the NJL model the mixing strength is generated by the 't Hooft term, and turns out to have opposite sign with respect to the pseudoscalar sector: this would favour a negative value of θ_S. Furthermore, studies without the strange meson can reproduce the $f_0(600)$ resonance: this favors small mixing angles. The corresponding two-photon decay rate turns out to be very small: $0.06 \lesssim \Gamma_{f_0(600)\gamma\gamma} \lesssim 0.114$ keV, a factor 15 smaller than the above mentioned (but not established) experimental result. Surely, when including finite width effects the decay rate $\Gamma_{f_0(600)\gamma\gamma}$ increases: in fact, the kinematical factor $M^3_{f_0(600)}$ make the right-tail of the broad distribution of $f_0(600)$ important [3, 12]. However, the rate of increase is not dramatic: it can at most double the above quoted results but not reach values of about 2-5 keV. This result is contrary to the usual belief that a quarkonium decay rate should be well above 1 keV [2, 13]: indeed, as we discuss in the next subsection a careful microscopic calculation of the two-photon decay rate shows that results below 1 keV are expected [9].

For the discussion of scalar states above 1 GeV we refer to [14], where the inclusion of a glueball state mixing with quarkonia also influences the $\gamma\gamma$ decay rate: in fact, a glueball is expected to have a small $\gamma\gamma$-transition amplitude, thus if a resonance will have a consistent glueball component the $\gamma\gamma$ decay rate is small. No $\gamma\gamma$-signal is found for $f_0(1500)$ pointing to a large gluonic amount in its wave function.

2.2 Quarkonium into $\gamma\gamma$: a microscopic evaluation

In this subsection we refer to [9], where the $\gamma\gamma$-decay rate has been carried out within a local and nonlocal microscopic model. Here we discuss only the latter. The relevant nonlocal interaction Lagrangian, involving the mesonic quarkonium field $\sigma(x)$ and the quark fields $q^t = (u, d)$, reads [9, 15]

$$\mathcal{L}_{\rm int}(x) \, = \, \frac{g_\sigma}{\sqrt{2}} \sigma(x) \int d^4y \, \Phi(y^2) \, \bar{q}(x + y/2) q(x - y/2) \, , \qquad (4)$$

where the delocalization takes account of the extended nature of the quarkonium state by the covariant vertex function $\Phi(y^2)$. The (Euclidean) Fourier

transform of this vertex function is taken as $\widetilde{\Phi}(k_E^2) = \exp(-k_E^2/\Lambda^2)$, also assuring UV-convergence of the model. The cutoff parameter Λ is vaired between 1 and 2 GeV, corresponding to an extension of the σ of about $l \sim 1/\Lambda \sim 0.5$ fm. The coupling g_σ is determined by the so-called compositeness condition [9, 15]. In the calculation the quark mass varies between 0.3 and 0.45 GeV.

The two-photon decay occurs via a triangle-diagram of quarks. Notice that due to the presence of the vertex function $\Phi(y^2)$ inclusion of the electromagnetic interaction is achieved by gauging the nonlocal interaction Lagrangian (4): in addition to the usual photon-quark coupling obtained by minimal substitution new vertices arise, where the photon couples directly to the $\sigma\gamma\gamma$ interaction vertex, see [15] for details. Their contribution, important on a conceptual level to assure gauge invariance, is numerically suppressed. In Table 1 we summarize our results for $M_\sigma = 0.6$ GeV varying m_q both for $\Lambda = 1$ GeV and, in parenthesis, for $\Lambda = 2$ GeV.

Table 1: $\Gamma_{\sigma\gamma\gamma}$ *for* $m_q = 0.31 - 0.45$ *GeV,* $\Lambda = 1(2)$ *GeV at* $M_\sigma = 0.6$ *GeV.*

m_q *(GeV)*	*0.31*	*0.35*	*0.40*	*0.45*
$\Gamma_{\sigma\gamma\gamma}$ *(keV) at* $M_\sigma = 0.6$ *GeV*	*0.529 (0.512)*	*0.458 (0.415)*	*0.361 (0.327)*	*0.294 (0.267)*

The decay widths decrease slowly for increasing quark mass while the dependence on the cutoff Λ is very weak. The numerical analysis shows that $\Gamma_{\sigma\gamma\gamma} < 1$ keV for $M_\sigma < 0.7$-0.8 GeV. This result is indeed in agreement with that of the previous subsection: a light quarkonium state has a $\gamma\gamma$ decay rate smaller than 1 keV. However, this doesn't prove that the resonance $f_0(600)$ is a quark-antiquark state. It rather tells us that, being the $\gamma\gamma$ decay width of a quarkonium smaller than what usually believed, care is needed when using $\gamma\gamma$-rates to discuss the nature of light scalars. We also refer to [16] for the evaluation of these diagrams for quarkonia states above 1 GeV.

3 Tetraquarks into $\gamma\gamma$

We consider now the $\gamma\gamma$-transition of tetraquark states [3], whose effective Lagrangian reads

$$\mathcal{L}_{em} = c_1^{\gamma\gamma} \mathcal{S}_{ij}^{[4q]} \left\langle A^i Q A^j Q \right\rangle F_{\mu\nu}^2 - c_2^{\gamma\gamma} \mathcal{S}_{ij}^{[4q]} \left\langle A^i A^j Q^2 \right\rangle F_{\mu\nu}^2, \qquad (5)$$

where $\left(A^i\right)_{jk} = \varepsilon_{ijk}$ and $\mathcal{S}^{[4q]} = diag\{\sqrt{\frac{1}{2}}(f_B^{[4q]} - a_0^{0[4q]}), \sqrt{\frac{1}{2}}(f_B^{[4q]} + a_0^{0[4q]}), \sigma_B^{[4q]}\}$. Within the tetraquark assignment the isoscalars are $f_B^{[4q]} = \frac{\left([u,s][\overline{u},\overline{s}] + [d,s]\left[\overline{d},\overline{s}\right]\right)}{2\sqrt{2}}$, $a_0^{0[4q]} = \frac{\left([u,s][\overline{u},\overline{s}] - [d,s]\left[\overline{d},\overline{s}\right]\right)}{2\sqrt{2}}$ and $\sigma_B^{[4q]} = \frac{1}{2}\left[u,d\right]\left[\overline{u},\overline{d}\right]$. In eq. (5) two terms are present: the one proportional to $c_1^{\gamma\gamma}$ represents the dominant contribution in the large-N_c expansion (switch of a quark with an antiquark), while the second term, proportional to $c_2^{\gamma\gamma}$ (annihilation of a quark-antiquark pair), represents the next-to-leading order correction. As discussed in detail in [3, 7, 17] the latter mechanism can be relevant because it occurs with only one gluon as intermediate state. The decay width into two photons reads $\Gamma_{i\gamma\gamma} = \frac{M_i^3}{4\pi} g_{i\gamma\gamma}^2$ where $i = a_0^{0[4q]}, \sigma_B^{[4q]}, f_B^{[4q]}$. The coupling constants for a_0^0 and for the bare states σ_B and f_B are deduced from (5) and read:

$$g_{a_0^{0[4q]}\gamma\gamma} = \frac{2c_1^{\gamma\gamma} + c_2^{\gamma\gamma}}{3\sqrt{2}},\ g_{\sigma_B^{[4q]}\gamma\gamma} = \frac{4c_1^{\gamma\gamma} + 5c_2^{\gamma\gamma}}{9},\ g_{f_B^{[4q]}\gamma\gamma} = \frac{2c_1^{\gamma\gamma} + 7c_2^{\gamma\gamma}}{9\sqrt{2}} \qquad (6)$$

The mixed physical states $f_0(600)$ and $f_0(980)$ are expressed in the tetraquark framework as $f_0(600) = \cos\theta_S \sigma_B^{[4q]} + \sin\theta_S f_B^{[4q]}$ and orthogonal combination for $f_0(980)$. Let us first consider $c_2^{\gamma\gamma} = 0$. When determining the mixing angle θ_S by using the experimental ratio $\frac{\Gamma_{f_0(980)\gamma\gamma}}{\Gamma_{a_0^0\gamma\gamma}} = 1.3 \pm 0.8$ one obtains very large values: $|\theta_S| \gtrsim 70^\circ$ (indeed $\Gamma_{f_0(980)\gamma\gamma}/\Gamma_{a_0^0\gamma\gamma} \leq 1$ for each θ_S). One of the main advantages of the tetraquark assignment is the explanation of the mass degeneracy of $a_0(980)$ and $f_0(980)$ in the limit $\theta_S = 0$. However, a large mixing angle would completely spoil the mass degeneracy. We thus consider this possibility disfavored, see disucssion in [3]. When $c_2^{\gamma\gamma} \neq 0$ a determination of the parameters form the $\gamma\gamma$-data is no longer possible. However, the mixing angle θ_S can be fixed from strong decays [3]: $\theta_S = -12.8^\circ$. Then we find $0.15 \leq c_2^{\gamma\gamma}/c_1^{\gamma\gamma} \leq 1.39$. Notice that even a small but non vanishing $c_2^{\gamma\gamma}$ can improve a lot the phenomenology: in fact, $c_2^{\gamma\gamma}$ strongly enhances the amplitude $g_{f_B^{[4q]}\gamma\gamma}$, see eq. (6). For $0.15 \leq c_2^{\gamma\gamma}/c_1^{\gamma\gamma} \leq 1.39$ one has $\frac{\Gamma_{f_0(600)\gamma\gamma}}{\Gamma_{a_0^0\gamma\gamma}} \leq 0.35$, again pointing to a small $\gamma\gamma$-rate of $f_0(600)$ as in the quarkonium case. More work is needed but one result is stable: the $\Gamma_{f_0(600)\gamma\gamma}$ is well below 1 keV also in the tetraquark assignment and is indeed of the same order of magnitude of the quarkonium interpretation. One could indeed go further by including mixing of tetraquark below 1 GeV and quarkonia above 1 GeV: however, as found in [17] the latter turns out to be small, thus not changing much the present results.

4 Conclusions

In this work we discussed the two-photon transition of light scalar mesons within the quarkonium and the tetraquark assignment. In both cases the decay rate $\Gamma_{f_0(600)\gamma\gamma}$ is smaller than 1 keV, as confirmed by a microscopic calculation [9] in the quarkonium assignment. These results make a possible identification of the nature of tetraquark states using two-photon experiments more difficult, because no big differences are expected. An open question is the possible role of pion loops, which could change the present results.

References

1. C. Amsler and N.A. Tornqvist, Phys. Rept. **389**, 61 (2004).
2. M.R. Pennington, Phys. Rev. Lett. **97** (2006) 011601; M.R. Pennington, Mod. Phys. Lett. A **22**, 1439 (2007).
3. F. Giacosa, Phys. Rev. D **74** (2006) 014028.
4. R.L. Jaffe, Phys. Rev. D **15** (1977) 267.
5. L. Maiani, F. Piccinini, A.D. Polosa and V. Riquer, Phys. Rev. Lett. **93** (2004) 212002.
6. J.R. Pelaez, Phys. Rev. Lett. **92** (2004) 102001.
7. F. Giacosa, arXiv:0711.3126 [hep-ph].
8. F. Giacosa, T. Gutsche, V.E. Lyubovitskij and A. Faessler, Phys. Rev. D **72** (2005) 114021.
9. F. Giacosa, T. Gutsche and V.E. Lyubovitskij, arXiv:0710.3403 [hep-ph].
10. W.M. Yao *et al.* [Particle Data Group], J. Phys. G **33** (2006) 1.
11. D. E. Groom *et al.* [Particle Data Group Collaboration], Eur. Phys. J. C **15**, 1 (2000).
12. F. Giacosa and G. Pagliara, to appear in Phys. Rev. C, arXiv:0710.3403 [hep-ph].

13. E. van Beveren, F. Kleefeld, G. Rupp and M. D. Scadron, Mod. Phys. Lett. A **17** (2002) 1673; R. Delbourgo, D.S. Liu and M.D. Scadron, Phys. Lett. B **446** (1999) 332.

14. C. Amsler and F.E. Close, Phys. Rev. D **53**, 295 (1996). F.E. Close and A. Kirk, Eur. Phys. J. C **21**, 531 (2001). F. Giacosa, T. Gutsche, V.E. Lyubovitskij and A. Faessler, Phys. Rev. D **72**, 094006 (2005). F. Giacosa, T. Gutsche, V.E. Lyubovitskij and A. Faessler, Phys. Lett. B **622**, 277 (2005).

15. A. Faessler, T. Gutsche, M.A. Ivanov, V.E. Lyubovitskij and P. Wang, Phys. Rev. D **68**, 014011 (2003).

16. F. Giacosa, T. Gutsche and A. Faessler, Phys. Rev. C **71** (2005) 025202.

17. F. Giacosa, Phys. Rev. D **75** (2007) 054007.

Frascati Physics Series Vol. XLVI (2007), pp. 577–584
HADRON07: XII Int. Conf. on Hadron Spectroscopy – Frascati, October 8-13, 2007
Light Meson Spectroscopy

STUDY OF $a_0(980)$-$f_0(980)$ MIXING FROM $J/\psi \to \phi a_0(980) \to \phi\eta\pi^0$

Jia-Jun Wu, Qiang Zhao, Bing-Song Zou
Institute of High Energy Physics, CAS, P.O.Box 918 (4), Beijing 100049
Theoretical Physics Center for Science Facilities, CAS, Beijing 100049, China

Abstract

The possibility of measuring the $a_0^0(980)$-$f_0(980)$ mixing from $J/\psi \to \phi f_0(980) \to \phi a_0^0(980) \to \phi\eta\pi^0$ reaction at upgraded Beijing Electron Positron Collider with BESIII detector is examined. While the branching ratio of this process through the $a_0^0(980)$-$f_0(980)$ mixing is expected to be about $O(10^{-6})$ similar to the estimated total amount from two background reactions $J/\psi \to \gamma^* \to \phi a_0^0(980)$ and $J/\psi \to K^*\bar{K} + c.c. \to \phi a_0^0(980)$, the peak width from the $a_0^0(980)$-$f_0(980)$ mixing is about 8 MeV, much smaller than that from other mechanisms. With 10^9 J/ψ events at BESIII, the $a_0^0(980)$-$f_0(980)$ mixing intensity is expected to be unambiguously and precisely measured.

1 Motivation for studying $a_0(980)$ and $f_0(980)$

In the classical quark model, each meson is composed of a quark and an anti-quark. It gives a natural explanation on the mass pattern of the lowest $q\bar{q}$

S-wave vector meson SU(3) nonet, where $s\bar{s}$-$\phi(1020)$, $d\bar{s}$-$K^{*0}(896)$, $\frac{1}{\sqrt{2}}(u\bar{u}+d\bar{d})$-$\omega(782)$ and $\frac{1}{\sqrt{2}}(u\bar{u}-d\bar{d})$-$\rho(770)$ have their mass difference mainly due to the number of strange quarks involved. However, the expected pattern does not work for the lowest scalar meson SU(3) nonet which is supposed to be $L=1$ excitation of $q\bar{q}$ system in the simple quark model. The most puzzling thing is that the $\frac{1}{\sqrt{2}}(u\bar{u}-d\bar{d})$ candidate $a_0^0(980)$ has a nearly degenerate mass with the $s\bar{s}$ candidate $f_0(980)$, which is much heavier than the $\frac{1}{\sqrt{2}}(u\bar{u}+d\bar{d})$ candidate $f_0/\sigma(600)$ and the $d\bar{s}$ candidate $\kappa^0(800)$. Instead, the mass pattern of the scalar nonet fits well the expectation of tetra-quark picture [1, 2], where $f_0/\sigma(600) = [ud][\bar{u}\bar{d}]$, $\kappa^0(800) = [su][\bar{u}\bar{d}]$, and $f_0(980)/a_0^0(980) = \frac{1}{\sqrt{2}}([us][\bar{u}\bar{s}] \pm [ud][\bar{d}\bar{s}])$.

Because the $f_0(980)$ and $a_0(980)$ have mass just below the $K\bar{K}$ threshold, they were also proposed to be $K\bar{K}$ molecules [3]. Krewald et al. [4] studied the kaon-antikaon system by using the strong interactions generated from vector-meson-exchange in the frame work of the SU(3) invariant effective Lagrangian. They have shown that one-meson exchange potentials derived from this Lagrangian in the non-relativistic limit are sufficient to bind $K\bar{K}$ into a kaonic molecule with a mass and decay width that closely match the experimental values of the $f_0(980)$ meson. However, in their study the momentum dependent terms of potentials are neglected and a quite large cut-off parameter of the form factor is used. If the momentum dependent terms of potentials are kept, the strong interaction cannot make the $K\bar{K}$ molecule [5]. It is also proposed to be a bound state of $K\bar{K}$ and $q\bar{q}$ mixture [6] or dynamical effects of coupled channel meson interactions [7].

To understand the nature of $f_0(980)$ and $a_0(980)$ is crucial for understanding the whole hadron spectroscopy. In the late 1970s, the mixing between the $a_0^0(980)$ and $f_0(980)$ resonances was first suggested theoretically in Ref. [8]. Its mixing intensity is expected to shed important light on the nature of these two resonances, and has hence been studied extensively on its different aspects and possible manifestations in various reactions. In this work we examine the possibility of extracting the $a_0^0(980)$-$f_0(980)$ mixing from $J/\psi \to \phi a_0^0(980) \to \phi\eta\pi^0$ reaction.

2 Mechanism and its prediction for $a_0^0(980)$-$f_0(980)$ mixing

The dominant mechanism for the $a_0^0(980)$-$f_0(980)$ mixing was already pointed out by Achasov and collaborators [8]. For the nearly degenerate $a_0(980)$ (isospin

1) and $f_0(980)$ (isospin 0), both can decay into $K\bar{K}$. Due to isospin breaking effect, the charged and neutral kaon thresholds are different by about 8 MeV. Between the charged and neutral kaon thresholds the leading term to the $a_0^0(980)$-$f_0(980)$ mixing amplitude is dominated by the unitary cuts of the intermediate two-kaon system and proportional to the difference of phase spaces for the charged and neutral kaon systems. The mixing intensity is obtained as [9]

$$|\xi|^2 = \frac{|g_{a_0^0(980)K^+K^-} g_{f_0(980)K^+K^-}|^2 [\rho_{K^+K^-}(s) - \rho_{K^0\bar{K}^0}(s)]^2}{256\pi^2 |D_a|^2} \tag{1}$$

where

$$\begin{aligned} D_a &= m_a^2 - s - i\sqrt{s}[\Gamma^a_{\eta\pi}(s) + \Gamma^a_{K\bar{K}}(s)], & (2)\\ \Gamma^a_{bc}(s) &= \frac{g^2_{abc}}{16\pi\sqrt{s}}\rho_{bc}(s), & (3)\\ \rho_{bc}(s) &= \sqrt{[1-(m_b-m_c)^2/s][1-(m_b+m_c)^2/s]}. & (4) \end{aligned}$$

With the isospin breaking effect, the $a_0^0(980)$ and $f_0(980)$ meson wave function can be expressed as :

$$\begin{aligned} |f_0\rangle &= \cos\theta |I=0\rangle + \sin\theta |I=1\rangle, & (5)\\ |a_0^0\rangle &= \cos\theta |I=1\rangle - \sin\theta |I=0\rangle & (6) \end{aligned}$$

with the mixing angle θ related to the mixing intensity as $|\xi|^2 \approx \sin^2\theta$.

From equations given above, one can see that the mixing intensity $|\xi|^2$ depends on $g_{a_0^0(980)K^+K^-}$, $g_{f_0(980)K^+K^-}$ and $g_{a_0^0(980)\pi^0\eta}$. Various models for the structures of $a_0^0(980)$ and $f_0(980)$ give different predictions for these coupling constants as listed in Table 1 by No. A-D. There have also been some experimental measurements on these coupling constants as listed by No. E-H. The corresponding predictions for the $a_0^0(980)$-$f_0(980)$ mixing intensity $|\xi|^2$ from these various theoretical and experimental values of the coupling constants are calculated and plotted in Fig. 1. In the calculation, the masses for K^+, K^0, π^0 and η are taken from PDG2006 [21] as $m_{K^+} = 493.7$ MeV, $m_{K^0} = 497.7$ MeV, $m_\pi = 135.0$ MeV and $m_\eta = 547.5$ MeV, respectively.

The predictions for $|\xi|^2$ vs M_2 peak in the region between the two thresholds for the charged and neutral kaon systems. The peak value is in the range of 0.01 to 0.20. It is mainly determined by the ratio $g_{a_0K\bar{K}} g_{f_0K\bar{K}}/g^2_{a_0\pi\eta}$. The

No.	model or experiment	a_0 mass	$g_{a_0\pi\eta}$	$g_{a_0K^+K^-}$	$g_{f_0K^+K^-}$
A	$q\bar{q}$ model [10]	0.983	2.03	1.27	1.80
B	$q^2\bar{q}^2$ model [10]	0.983	4.57	5.37	5.37
C	$K\bar{K}$ model [3, 11]	0.980	1.74	2.74	2.74
D	$q\bar{q}g$ model [12]	0.980	2.52	1.97	1.70
E	SND [13, 14]	0.995	3.11	4.20	5.57
F	KLOE [15, 16]	0.985	3.02	2.24	5.92
G	BNL [17]	1.001	2.47	1.67	3.26 [18]
H	CB [19]	0.999	3.33	2.54	4.18 [20]

Table 1: $a_0(980)$ *mass and coupling constants* $g_{a_0\pi\eta}$, $g_{a_0K^+K^-}$, $g_{f_0K^+K^-}$ *with unit GeV from several models (A-D) and experimental measurements (E-H).*

different predictions by various models (No. A-D) indicate that the $f_0 - a_0$ mixing depends on the nature of the scalars with the $K\bar{K}$ molecule giving the largest mixing and the four quark state the second. However, one should keep in mind that the absolute value for the mixing from each model is quite model-dependent and suffers rather big uncertainty, which may make it difficult to discriminate between various pictures as in the case for the radiative decays $\phi \to \gamma a_0/f_0$ [22]. Nevertheless, a reliable measurement of the mixing will be very useful to constrain model parameters and ultimately understand the nature of these scalars. Present available experimental measurements on the coupling constants of $g_{a_0^0(980)K^+K^-}$, $g_{f_0(980)K^+K^-}$ and $g_{a_0^0(980)\pi^0\eta}$ cannot give reliable determination of the $a_0^0(980)$-$f_0(980)$ mixing and hence cannot give much constraint on theoretical models. Direct precise measurement of the $|\xi|^2$ is needed to provide a useful check on these model predictions and previous measurements. Possible experiments to measure the a_0-f_0 mixing were proposed, such as $pp \to p_s(\eta\pi^0)p_f$ [23], $\pi^- p \to \eta\pi^0 n$ with polarized target [24], J/ψ decays [23], and $dd \to \alpha\eta\pi^0$ reactions [25].

3 Possibility of measuring a_0-f_0 mixing from $J/\psi \to \phi\eta\pi^0$ at BESIII

Close and Kirk [23] suggested studying J/ψ decays to the 'forbidden' final states $\omega a_0^0(980)$ and $\phi a_0^0(980)$ where they predicted branching ratios of $O(10^{-5})$. The corresponding J/ψ to $\phi f_0(980)$ and $\omega f_0(980)$ processes have already been stud-

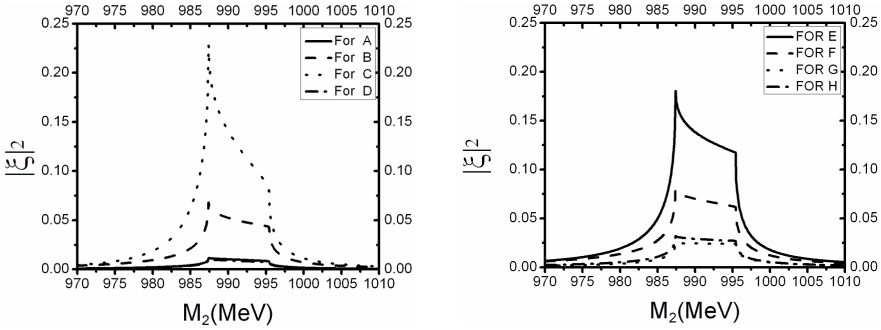

Figure 1: *Predictions for the f_0-a_0 intensity $|\xi|^2$ vs two-meson invariant mass M_2 from various models A-D (left) and various experimental measured coupling constants E-H (right).*

ied by BESII experiments [20, 26]. Although the two channels are found to have similar branching ratios, the $f_0(980)$ peak is very clear in the $\pi\pi$ invariant mass spectrum for the $J/\psi \to \phi\pi^+\pi^-$ process [20] while it is much buried by other components in the $J/\psi \to \omega\pi^+\pi^-$ process [26]. Therefore the $J/\psi \to \phi f_0(980) \to \phi a_0^0(980) \to \phi\eta\pi^0$ is expected to be the best place for studying $a_0^0(980)$-$f_0(980)$ mixing from J/ψ decays. Due to limited statistics and relatively poor detection of multi-photon final states, there is no information available on this channel from BESII experiment. With the increase of statistics by two orders of magnitude and much improved photon detection expected at BESIII, we examined in detail the possibility of measuring the $a_0^0(980)$-$f_0(980)$ mixing from $J/\psi \to \phi\eta\pi^0$ process [27].

The observed $f_0(980)$ contribution to the $J/\psi \to \phi\pi\pi$ [20] is plotted in Fig.2 (left panel) with integration over $m_{\pi\pi}$ equal to the measured branching ratio $(5.4 \pm 0.9) \times 10^{-4}$ for this channel. Then from Eq. (1) and parameter set No. H listed in Table 1, we get the corresponding contribution from $a_0^0(980)$-$f_0(980)$ mixing to the $\eta\pi^0$ invariant mass spectrum for the $J/\psi \to \phi\eta\pi^0$ decay as shown in Fig. 2 (right: line A). A narrow outstanding peak with a width about 8 MeV is predicted. A remarkable fact is that the peak is much narrower than the usual width ($50 \sim 100$ MeV) of $a_0^0(980)$ and should be easily observed even if there are other background contributions for the $a_0^0(980)$ production. Integrated over $m_{\eta\pi}$ for line A, we get the branching ratio about 2.7×10^{-6}.

While parameter set No. G gives a similar branching ratio, parameter sets No. E and No. F give larger branching ratio by a factor 5 and 2, respectively.

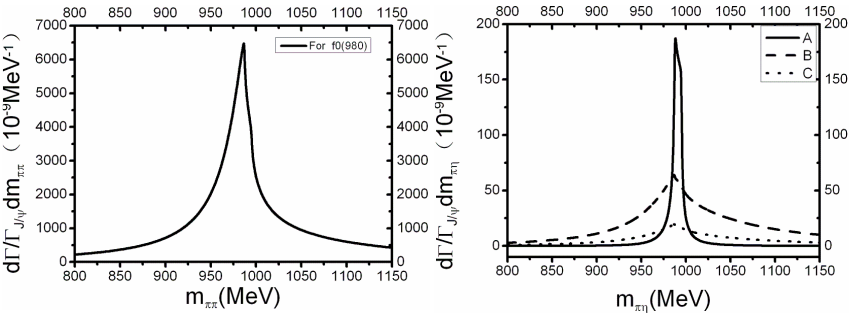

Figure 2: *$\pi\pi$ invariant mass spectrum for $J/\psi \to \phi f_0(980) \to \phi\pi\pi$ [20] (left) and corresponding prediction of the $\pi\eta$ invariant mass spectrum for $J/\psi \to \phi\eta\pi$ through a_0^0-f_0 mixing (right: line A) together with estimation of contribution from $K^*\bar{K}$ rescattering (line B for without form factor; C for monopole form factor with cut-off parameter $\Lambda_K = 1.5$ GeV).*

With 10^9 J/ψ events and a detection efficiency about 30% for the $\phi\eta\pi^0$ channel expected at BESIII, more than 800 events should be observed for this channel with most events in the narrow gap of $\eta\pi^0$ invariant mass between 987.4 MeV and 995.4 MeV.

Besides the contribution from the $a_0^0(980)$-$f_0(980)$ mixing mechanism, those from two background reactions $J/\psi \to \gamma^* \to \phi a_0^0(980)$ and $J/\psi \to K^*\bar{K} + c.c. \to \phi a_0^0(980)$ are also investigated [27]. The branching ratio for $J/\psi \to \gamma^* \to \phi a_0^0(980)$ is obtained as 2.59×10^{-7}. This is much smaller than the contribution from $a_0^0(980)$-$f_0(980)$ mixing and is distributed in much large range of $\eta\pi^0$ invariant mass spectrum. So its influence to the narrow $a_0^0(980)$-$f_0(980)$ mixing peak is negligibly small. The contribution from $J/\psi \to K^*\bar{K} + c.c. \to \phi a_0^0(980)$ is estimated with a similar approach as in Ref. [28]. It gives a branching ratio of $O(10^{-6})$, comparable with that from the $a_0^0(980)$-$f_0(980)$ mixing for the $J/\psi \to \phi a_0^0(980)$. However as shown by line B and line C in Fig. 2, the contribution from K^*K loops gives a much broader distribution in the $\pi\eta$ invariant mass spectrum than that from the $a_0^0(980)$-$f_0(980)$ mixing. Although the integration of line B is about 3.5 times of line A, the peak of

line A is still more than a factor of 2 over the peak of line B. Therefore by separate the narrow peak from the broader peak, we can still get very precise measurement for the $a_0^0(980)$-$f_0(980)$ mixing.

4 Conclusion

The $a_0^0(980)$-$f_0(980)$ mixing gives a branching ratio of $O(10^{-6})$ to the $J/\psi \to \phi a_0^0(980)$ and a narrow peak about 8 MeV at about 990 MeV in the $\eta\pi^0$ invariant mass spectrum. The contribution from $J/\psi \to \gamma^* \to \phi a_0^0(980)$ is negligibly small. The contribution from $J/\psi \to K^*\bar{K} + c.c. \to \phi a_0^0(980)$ also gives a branching ratio of $O(10^{-6})$, but with a much broader width about $50 \sim 100$ MeV which should be easily separated from the narrow structure caused by the $a_0^0(980)$-$f_0(980)$ mixing. With 10^9 J/ψ events and a detection efficiency about 30% for the $\phi\eta\pi^0$ channel expected at BESIII, for $|\xi|^2$ in the range of $0.01 \sim 0.2$, in should be easily measured with a precision $\Delta|\xi|^2/|\xi|^2 < 10\%$.

The width of $a_0^0(980)$ peak in the $\eta\pi^0$ invariant mass spectrum for the $pp \to p_s(\eta\pi^0)p_f$ reaction is found to be 72 ± 16 MeV similar to the width of $a_0^-(980)$ peak in the $\eta\pi^-$ invariant mass spectrum as 61 ± 19 MeV in the WA102 experiment [29]. The $a_0^0(980)$ peak from WA102 experiment is unlikely mainly coming from the $a_0^0(980)$-$f_0(980)$ mixing mechanism.

5 Acknowledgements

This work is partly supported by the National Natural Science Foundation of China (NSFC) under grants Nos. 10435080, 10521003, 10675131 and by the Chinese Academy of Sciences under project No. KJCX3-SYW-N2.

References

1. R. Jaffe, Phys. Rev. D **15**, 281 (1977).
2. L. Maiani *et al.*, Phys. Rev. Lett. **93**, 212002 (2004).
3. J. Weinstein and N. Isgur, Phys. Rev. Lett. **48**, 659 (1982).
4. S. Krewald, R.H. Lemmer and F.P. Sassen, Phys. Rev. D **69**, 016003 (2004).
5. Y.J. Zhang *et al.*, Phys. Rev. D **74**, 014013 (2006).

6. E. van Beveren *et al.*, Phys. Lett. B **641**, 265 (2006).
7. C. Hanhart, B. Kubis and J.R. Pelaez, Phys. Rev. D **76**, 074028 (2007).
8. N.N. Achasov *et al.*, Phys. Lett. B **88**, 367 (1979).
9. A.E. Kudryavtsev and V.E. Tarasov, JETP Lett. **72**, 410 (2000).
10. N.N. Achasov and V.N. Ivanchenko, Nucl. Phys. B **315**, 465 (1989).
11. N.N. Achasov and V.V. Gubin, Phys. Rev. D **56**, 4084 (1997).
12. S. Ishida *et al.*, In *Manchester 1995, Proceedings, Hadron'95*, p.454.
13. M.N. Achasov *et al.*, Phys.Lett. B **485**, 349 (2000).
14. M.N. Achasov *et al.*, Phys. Lett. B **479**, 53 (2000).
15. KLOE Collaboration, Phys. Lett. B **536**, 209 (2002).
16. KLOE Collaboration, Phys. Lett. B **B537**, 21 (2002).
17. S. Teige *et al.* (E852 collaboaration), Phys. Rev. D **59**, 012001 (1998).
18. B.S. Zou and D.V. Bugg, Phys. Rev. D **48**, R3948 (1993).
19. D.V. Bugg *et al.*, Phys. Rev. D **50**, 4412 (1994).
20. BES Collaboration, Phys. Lett. B **607**, 243 (2005).
21. Particle Data Group, J. Phys. G **33**, 1 (2006).
22. Yu.S. Kalashnikova *et al.*, Euro. Phys. J. A **24**, 437 (2005).
23. F.E. Close and A. Kirk, Phys. Lett. B **489**, 24 (2000).
24. N.N. Achasov and G.N. Shestakov, Phys. Rev. Lett **92**, 182001 (2004).
25. WASA-at-COSY Collaboration, nucl-ex/0411038.
26. BES Collaboration, Phys. Lett. B **598**, 149 (2004).
27. J.J. Wu, Q. Zhao and B.S. Zou, Phys. Rev. D **75**, 114012 (2007).
28. Q. Zhao, B.S. Zou and Z.B. Ma, Phys. Lett. B **631**, 22 (2005); M.P. Locher, Y. Lu and B.S. Zou, Z. Phys. A **347**, 281 (1994).
29. WA102 Collaboration, Phys. Lett. B **488**, 225 (2000).

Frascati Physics Series Vol. XLVI (2007), pp. 585–592
HADRON07: XII Int. Conf. on Hadron Spectroscopy – Frascati, October 8-13, 2007
Light Meson Spectroscopy

ANALYSIS OF RARE RADIATIVE DECAYS OF ϕ AND MIXING BETWEEN LOW AND HIGH MASS SCALAR MESONS

T. Teshima, I. Kitamura and N. Morisita
Department of Natural Sciences, Chubu University, Kasugai 487-8501, Japan

Abstract

We studied the decays $\phi \to \eta\pi^0\gamma$ and $\phi \to \pi^0\pi^0\gamma$, assuming that these are caused through the $a_0(980)\gamma$ and $f_0(980)\gamma$ states. Fitting the data of the $\eta\pi^0$ and $\pi^0\pi^0$ invariant mass spectrum, we showed that the processes $\phi \to a_0\gamma$ and $\phi \to f_0\gamma$ are dominated by the K^+K^- loop interaction both for the non-derivative and derivative SPP coupling. The data of $\Gamma[\phi \to f_0\gamma]/\Gamma[\phi \to a_0\gamma]$ predicts $g_{f_0K\bar{K}}/g_{a_0K\bar{K}} \sim 2$. We also studied the decays $a_0 \to \pi\eta$, $a_0 \to K\overline{K}$, $K_0^* \to K\pi$, $f_0 \to \pi\pi$, $f_0 \to K\overline{K}$ and analyzed the SPP coupling strengths of $g_{f_0K\bar{K}}$ and $g_{a_0K\bar{K}}$ considering the mixing between low mass scalar nonet $qq\bar{q}\bar{q}$ states and high mass scalar nonet $q\bar{q}$ states and glueball. Comparing the resultant strengths of $g_{f_0K\bar{K}}$ and $g_{a_0K\bar{K}}$ and the ratio $g_{f_0K\bar{K}}/g_{a_0K\bar{K}} \sim 2$ and the result obtained in the analysis of $\phi \to a_0\gamma$ and $\phi \to f_0\gamma$, we predict that the mixing are rather large and non-derivative SPP coupling is favored.

1 Analysis of the $\phi \to \pi^0\eta\gamma$ and $\phi \to \pi^0\pi^0\gamma$ decays

The invariant mass distribution of the branching ratio for $\phi \to a_0(980)\gamma \to \pi^0\eta\gamma$ decay is expressed as

$$\frac{d\,BR(\phi \to a_0\gamma \to \pi^0\eta\gamma)}{dm} = \frac{2m^2}{\pi}\frac{1}{\Gamma_\phi}\frac{\Gamma(\phi \to a_0\gamma : m)\Gamma(a_0 \to \pi^0\eta : m)}{|D_{a_0}(m^2)|^2}. \quad (1)$$

$\Gamma(a_0 \to \pi^0\eta : m)$ is the decay width on the virtual mass of intermediate a_0 state,

$$\begin{aligned}\Gamma(a_0 \to \pi^0\eta : m) &= \frac{g^2_{a_0\pi\eta}}{8\pi m^2}\frac{\sqrt{(m^2-(m_\pi+m_\eta)^2)(m^2-(m_\pi-m_\eta)^2)}}{2m} \\ &\times \left[\left\{(m^2-m_\pi^2-m_\eta^2)/2\right\}^2\right] \quad (2)\end{aligned}$$

and coupling constant $g_{a_0\pi\eta}$ is defined as

$$M(a_0(q) \to \pi^0(q_1)+\eta(q_2)) = g_{a_0\pi\eta} \times [q_1 \cdot q_2], \quad (3)$$

where, $[\cdots]$ term is replaced to 1 for the non-derivative couping of SPP coupling. $\Gamma(\phi \to a_0\gamma : m)$ is the decay width on the virtual mass of intermediate state a_0,

$$\Gamma(\phi \to a_0\gamma : m) = \frac{\alpha}{3}g^2_{\phi a_0\gamma}(m)\left(\frac{m_\phi^2-m^2}{2m_\phi}\right)^3, \quad (4)$$

where coupling constant $g_{\phi a_0\gamma}(m)$ is defined as

$$M(\phi(p,\epsilon_\phi) \to a_0(q)+\gamma(k,\epsilon_\gamma)) = e g_{\phi a_0\gamma}(m)(p\cdot k\epsilon_\phi\cdot\epsilon_\gamma - p\cdot\epsilon_\gamma k\cdot\epsilon_\phi). \quad (5)$$

For the $\phi a_0\gamma$ coupling , we consider the pointlike interaction and K^+K^- loop interaction as shown in Fig. 1, then $g_{\phi a_0\gamma}(m)$ is expressed as

$$g_{\phi a_0\gamma}(m) = g^{\rm pointlike}_{\phi a_0\gamma} + g^{K\bar{K}\,{\rm loop}}_{\phi a_0\gamma}(m), \quad (6)$$

$$g^{K\bar{K}\,{\rm loop}}_{\phi a_0\gamma}(m) = \frac{g_{\phi K\bar{K}}g_{a_0K\bar{K}}}{2\pi^2 i m_K^2}\left[\frac{2m_K^2-m^2}{2}\right]I(a,b). \quad (7)$$

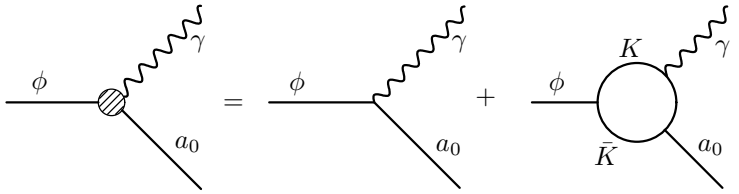

Figure 1: *Diagrams for the pointlike and K^+K^- loop coupling for $g_{\phi a_0\gamma}(m)$*

where, $[\cdots]$ term is replaced to 1 for the non-derivative couping. The loop integral $I(a,b)$ is

$$I(a,b) = \frac{1}{2(a-b)} - \frac{2}{(a-b)^2}\left\{f\left(\frac{1}{b}\right) - f\left(\frac{1}{a}\right)\right\} + \frac{a}{(a-b)^2}\left\{g\left(\frac{1}{b}\right) - g\left(\frac{1}{a}\right)\right\}, \quad (8)$$
$$a = m_\phi^2/m_K^2, \quad b = m^2/m_K^2,$$

where $f(x)$ and $g(x)$ are defined as (upper expressions correspond to $x > \frac{1}{4}$ and lower ones correspond to $x < \frac{1}{4}$)

$$f(x) = \begin{cases} -\left(\sin^{-1}\left(\frac{1}{2\sqrt{x}}\right)\right)^2, \\ \frac{1}{4}\left(\log\frac{\eta_+}{\eta_-} - i\pi\right)^2, \end{cases} \quad , \quad g(x) = \begin{cases} \sqrt{4x-1}\sin^{-1}\left(\frac{1}{2\sqrt{x}}\right), \\ \frac{1}{2}\sqrt{1-4x}\left(\log\frac{\eta_+}{\eta_-} - i\pi\right), \end{cases}$$
$$\eta_\pm = \frac{1}{2x}\left(1 \pm \sqrt{1-4x}\right). \quad (9)$$

These loop calculations have been analysed by many authors [1]. Invariant mass distributions are parameterized by only two parameters G_1 and G_2

$$\frac{d\,BR(\phi \to a_0\gamma \to \pi^0\eta\gamma)}{dm} = G_1 \frac{|G_2 + \frac{1}{i}\left[\frac{2m_K^2 - m^2}{2}\right] I(a,b)|^2}{|G_2 + \frac{1}{i}\left[\frac{2m_K^2 - m_a^2}{2}\right] I(a,b_0)|^2} \left(\frac{m_\phi^2 - m^2}{m_\phi^2 - m_a^2}\right)^3$$
$$\times \frac{m_a}{m} \frac{m_a^2\Gamma_a^2}{(m^2 - m_a^2)^2 + m_a^2\Gamma_a^2} \sqrt{\frac{(m^2 - (m_\eta + m_\pi)^2)(m^2 - (m_\eta - m_\pi)^2)}{(m_a^2 - (m_\eta + m_\pi)^2)(m_a^2 - (m_\eta - m_\pi)^2)}}, \quad (10)$$

where G_1, G_2, b_0 are defined as

$$G_1 = \frac{2}{\pi\Gamma_\phi\Gamma_a^2}\Gamma(\phi \to a_0\gamma : m_a)\Gamma(a_0 \to \eta\pi^0 : m_a),$$
$$G_2 = g_{\phi\gamma a}^{\rm pointlike} \Big/ \left(\frac{g_{\phi K\bar{K}} g_{a_0 K\bar{K}}}{2\pi^2 m_K^2}\right), \quad (11)$$
$$b_0 = \frac{m_a^2}{m_K^2},$$

and $[\cdots]$ term is replaced to 1 for the non-derivative couping. For $\phi \to f_0(980)\gamma \to \pi^0\pi^0\gamma$ decay, almost same discussion can be made.

We fit the data from SND and KLOE collaborations [2] using the Eq. (10), and show the best-fitted curves in Fig. 2.

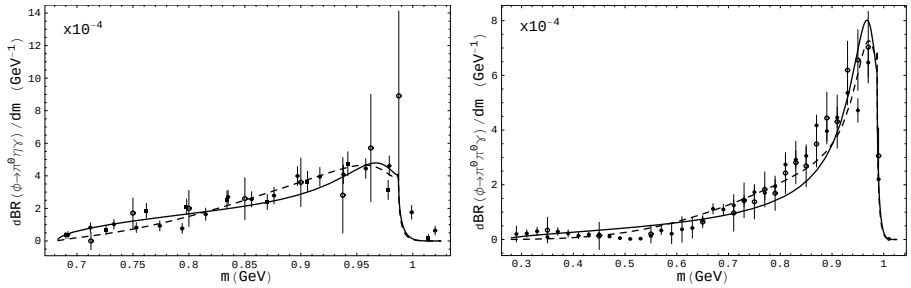

Figure 2: *Best-fitted curves for* $dBR(\phi \to \pi^0\eta\gamma)/dm$ *and* $dBR(\phi \to \pi^0\pi^0\gamma)/dm$. *Solid and dashed line show the best fitted curves for the non-derivative and derivative coupling interaction, respectively. Experimental data indicated by circles, filled circles and filled squares are from the SND collaboration and KLOE collaboration, respectively.*

Best-fit values of G_1 and G_2 are obtained as $G_1 = 4.1 \times 10^{-4}\text{GeV}^{-1}$ and $G_2 = -0.16$ for non-derivative coupling and $G_1 = 3.9 \times 10^{-4}\text{GeV}^{-1}$ and $G_2 = 0.08\text{GeV}^2$ for derivative coupling in $dBR(\phi \to \pi^0\eta\gamma)/dm$ analysis, and $G_1 = 7.1 \times 10^{-4}\text{GeV}^{-1}$, $G_2 = 0.001$ for non-derivative coupling and $G_1 = 6.9 \times 10^{-4}\text{GeV}^{-1}$, $G_2 = 0.055\text{GeV}^2$ for derivative coupling in $dBR(\phi \to \pi^0\pi^0\gamma)/dm$ analysis. These results predict that the K^+K^- loop contributions are dominant in the $\phi \to \pi^0\eta\gamma$ and $\phi \to \pi^0\pi^0\gamma$ processes.

Supposing that the decay $\phi \to a_0\gamma$ and $\phi \to f_0\gamma$ are caused through only the K^+K^- loop interaction, we obtain the following results (upper values are non-derivative coupling ones and lower values are derivative coupling ones) using the experimental data [3]

$$g_{a_0K\bar{K}} = \begin{cases} 2.18 \pm 0.12 \ \text{GeV}, \\ 9.04 \pm 0.50 \ \text{GeV}^{-1}, \end{cases} \quad g_{a_0\pi\eta} = \begin{cases} 1.89 \pm 0.75 \ \text{GeV}, \\ 5.79 \pm 2.32 \ \text{GeV}^{-1}, \end{cases}$$
$$g_{f_0K\bar{K}} = \begin{cases} 4.72 \pm 0.82 \ \text{GeV}, \\ 20.0 \pm 3.48 \ \text{GeV}^{-1}, \end{cases} \quad g_{f_0\pi\pi} = \begin{cases} 1.12 \pm 0.69 \ \text{GeV}, \\ 2.43 \pm 1.50 \ \text{GeV}^{-1}. \end{cases} \tag{12}$$

2 Mixing between Low and High Mass Scalar Mesons

We assume that the low-mass scalar mesons are $qq\bar{q}\bar{q}$ states and high-mass scalar mesons are $q\bar{q}$ and glueball, and these are mixed each other. The low-

mass scalar nonet S_b^a is $\epsilon^{acd}q_cq_d\epsilon_{bef}\bar{q}^e\bar{q}^f$ and have the following flavor configuration:

$$\begin{array}{ccc} \bar{d}\bar{s}su,\ \frac{1}{\sqrt{2}}(\bar{d}\bar{s}ds-\bar{s}\bar{u}su),\ \bar{s}\bar{u}ds & \Longleftrightarrow & a_0^+,\ a_0^0,\ a_0^- \\ \bar{d}\bar{s}ud,\ \bar{s}\bar{u}ud,\ \bar{u}\bar{d}su,\ \bar{u}\bar{d}ds & \Longleftrightarrow & \kappa^+,\ \kappa^0,\ \overline{\kappa^0},\ \kappa^- \\ \frac{1}{\sqrt{2}}(\bar{d}\bar{s}ds+\bar{s}\bar{u}su) & \Longleftrightarrow & f_{NS}\sim f_0(980) \\ \bar{u}\bar{d}ud & \Longleftrightarrow & f_{NN}\sim f_0(600) \end{array}$$

and the high-mass scalar mesons are the ordinary $SU(3)$ nonet $S_b'^a$ plus glueball $G\sim gg$

$$S_b'^a+G\sim\bar{q}^aq_b+gg.$$

The mixing between $qq\bar{q}\bar{q}$ and $q\bar{q}$ states may be large, because the transition between $qq\bar{q}\bar{q}$ and $q\bar{q}$ states is caused by the OZI rule allowed diagram shown in fig. 3, and expressed as,

$$\begin{aligned} L_{\rm int} &= \lambda_{01}[a_0^+a_0'^-+a_0^-a_0'^+ + a_0^0a_0'^0+K_0^{*+}K_0'^{*-}+K_0^{*-}K_0'^{*+}+K_0^{*0}K_0'^{*0} \\ &\quad +\bar{K}_0^{*0}\bar{K}_0'^{*0}+\sqrt{2}f_{NN}f_N'+f_{NS}f_N'+\sqrt{2}f_{NS}f_S'].\end{aligned} \tag{13}$$

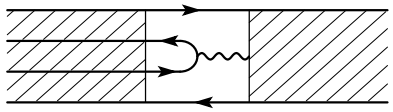

Figure. 3 *OZI rule allowed graph for $qq\bar{q}\bar{q}$ and $q\bar{q}$ states transition.*

When we represent the $I=1$ pure $qq\bar{q}\bar{q}$ and $q\bar{q}$ states by $\overline{a_0(980)}$ and $\overline{a_0(1450)}$, and masses for these states by $m^2_{\overline{a_0(980)}}$ and $m^2_{\overline{a_0(1450)}}$, the mass matrix is represented as

$$\left(\begin{array}{cc} m^2_{\overline{a_0(980)}} & \lambda_{01} \\ \lambda_{01} & m^2_{\overline{a_0(1450)}} \end{array}\right). \tag{14}$$

Diagonalising this mass matrix, we can get the masses for the physical states $a_0(980)$ and $a_0(1450)$ represented as mixing states of $\overline{a_0(980)}$ and $\overline{a_0(1450)}$;

$$\begin{aligned} a_0(980) &= \cos\theta_a\overline{a_0(980)}-\sin\theta_a\overline{a_0(1450)}, \\ a_0(1450) &= \sin\theta_a\overline{a_0(980)}+\cos\theta_a\overline{a_0(1450)}. \end{aligned} \tag{15}$$

Similar expressions for $I=1/2$ states mixing are obtained. The mixing among $I=0$ low-mass and high-mass scalar mesons and glueball is expressed by the

mixing mass matrix as

$$\begin{pmatrix} m^2_{NN}+\lambda_0 & \sqrt{2}\lambda_0 & \sqrt{2}\lambda_{01} & 0 & 0 \\ \sqrt{2}\lambda_0 & m^2_{NS}+2\lambda_0 & \lambda_{01} & \sqrt{2}\lambda_{01} & 0 \\ \sqrt{2}\lambda_{01} & \lambda_{01} & m^2_{N'}+2\lambda_1 & \sqrt{2}\lambda_1 & \sqrt{2}\lambda_G \\ 0 & \sqrt{2}\lambda_{01} & \sqrt{2}\lambda_1 & m^2_{S'}+\lambda_1 & \lambda_G \\ 0 & 0 & \sqrt{2}\lambda_G & \lambda_G & \lambda_{GG} \end{pmatrix}, \qquad (16)$$

where λ_0, λ_1 and λ_G represent the transition strength between $I=0$ $qq\bar{q}\bar{q}$ mesons, the transition strength between $I=0$ $q\bar{q}$ mesons and the transition strength between $I=0$ $q\bar{q}$ mesons and glueball gg, respectively. λ_{GG} is the pure glueball mass square, and $m^2_{NN}=2m^2_{K^*_0(800)}-m^2_{a_0(980)}$, $m^2_{NS}=m^2_{a_0(980)}$, $m^2_{N'}=m^2_{a_0(1450)}$, $m^2_{S'}=2m^2_{K^*_0(1430)}-m^2_{a_0(1450)}$. Diagonalising this mass matrix, we obtain the eigenvalues of low-mass and high-mass scalar mesons $I=0$ states $f_0(600)$, $f_0(980)$, $f_0(1370)$, $f_0(1500)$ and $f_0(1710)$. The eigenstates of these scalar mesons are represented as follows;

$$\begin{pmatrix} f_0(600) \\ f_0(980) \\ f_0(1370) \\ f_0(1500) \\ f_0(1710) \end{pmatrix} = [R_{f_0(M)I}] \begin{pmatrix} f_{NN} \\ f_{NS} \\ f_{N'} \\ f_{S'} \\ f_G \end{pmatrix}, \qquad [R_{f_0(M)I}] =$$

$$\begin{pmatrix} R_{f_0(600)NN} & R_{f_0(600)NS} & R_{f_0(600)N'} & R_{f_0(600)S'} & R_{f_0(600)G} \\ R_{f_0(980)NN} & R_{f_0(980)NS} & R_{f_0(980)N'} & R_{f_0(980)S'} & R_{f_0(980)G} \\ R_{f_0(1370)NN} & R_{f_0(1370)NS} & R_{f_0(1370)N'} & R_{f_0(1370)S'} & R_{f_0(1370)G} \\ R_{f_0(1500)NN} & R_{f_0(1500)NS} & R_{f_0(1500)N'} & R_{f_0(1500)S'} & R_{f_0(1500)G} \\ R_{f_0(1710)NN} & R_{f_0(1710)NS} & R_{f_0(1710)N'} & R_{f_0(1710)S'} & R_{f_0(1710)G} \end{pmatrix} \qquad (17)$$

Using the mass values, $m_{a_0(980)}=(0.9848\pm0.0012)$GeV, $m_{a_0(1450)}=(1.474\pm0.019)$GeV, $m_{K^*_0(800)}=(0.841\pm0.030)$GeV and $m_{K^*_0(1430)}=(1.414\pm0.006)$GeV, and varying the mixing strength λ_{01}, we obtain the mixing angles θ_a, θ_K and parameters λ_0, λ_1, λ_G and λ_{GG}, and mixing parameters $[R_{f_0(M)I}]$ as the functions of λ_{01}.

3 Coupling constant g_{SPP} and mixing between $qq\bar{q}\bar{q}$ and $q\bar{q}$ scalar mesons

We express the g_{SPP}'s by the mixing angle θ_a, θ_K and mixing parameters R_{f_0NS} etc. and obtain the values of the g_{SPP} using the various $S\to PP$ decay

Table 1: *The values of mixing angles θ_a, θ_K, and the mixing parameters $R_{f_0(980)NN}$, $R_{f_0(980)NS}$, $R_{f_0(980)N'}$, $R_{f_0(980)S'}$, $R_{f_0(980)G}$ for the various values of λ_{01}.*

λ_{01}	$\theta_a(^\circ)$	$\theta_K(^\circ)$	$R_{f_0(980)NN}$	$R_{f_0(980)NS}$
(GeV^2)	$R_{f_0(980)N'}$	$R_{f_0(980)S'}$	$R_{f_0(980)G}$	
0.20	9.7 ± 0.5	9.0 ± 0.5	-0.023 ± 0.014	-0.972 ± 0.002
	0.065 ± 0.006	0.226 ± 0.004	-0.010 ± 0.010	
0.25	12.3 ± 0.6	11.4 ± 0.6	-0.027 ± 0.026	-0.954 ± 0.003
	0.086 ± 0.008	0.284 ± 0.005	-0.016 ± 0.016	
0.30	15.0 ± 0.8	13.8 ± 0.8	-0.046 ± 0.024	-0.932 ± 0.004
	0.110 ± 0.009	0.341 ± 0.006	-0.016 ± 0.016	
0.35	17.8 ± 1.0	16.4 ± 1.0	-0.065 ± 0025	-0.902 ± 0.007
	0.140 ± 0.012	0.401 ± 0.007	-0.024 ± 0.024	
0.40	20.8 ± 1.2	19.1 ± 1.2	-0.094 ± 0.021	-0.864 ± 0.010
	0.178 ± 0.014	0.461 ± 0.007	-0.028 ± 0.028	
0.45	24.2 ± 1.6	22.1 ± 1.5	-0.116 ± 0.021	-0.813 ± 0.011
	0.226 ± 0.015	0.523 ± 0.006	-0.014 ± 0.014	

widths and compare these values with the ones obtained from ϕ decays. We use the following expressions for $S(qq\bar{q}\bar{q}$ scalar meson$)PP$, $S'(q\bar{q}$ scalar meson$)PP$ and G(pure glueball$)PP$,

$$\begin{aligned} L_I &= A\varepsilon^{abc}\varepsilon_{def}S_a^d[\partial^\mu]P_b^e[\partial_\mu]P_c^f + A'S_a'^b\{[\partial^\mu]P_b^c,\ [\partial_\mu]P_c^a\} \\ &\quad + A''G\{[\partial^\mu]P_a^b,\ [\partial_\mu]P_b^a\}, \end{aligned} \tag{18}$$

where $[\partial^\mu]$ is replaced to 1 for non-derivative coupling. We define the coupling constants $g_{SPP'}$ in the following expression;

$$\begin{aligned} L_I &= g_{a_0K\overline{K}}[\partial^\mu]\overline{K}\boldsymbol{\tau}\cdot\boldsymbol{a_0}[\partial_\mu]K + g_{a_0\pi\eta}\boldsymbol{a_0}\cdot[\partial^\mu]\boldsymbol{\pi}[\partial_\mu]\eta \\ &\quad + g_{f_0(M)\pi\pi}\frac{1}{2}f_0(M)[\partial^\mu]\boldsymbol{\pi}\cdot[\partial_\mu]\boldsymbol{\pi} + g_{f_0(M)K\overline{K}}f_0(M)[\partial^\mu]K[\partial_\mu]\overline{K} \\ &\quad + \cdots\cdots. \end{aligned} \tag{19}$$

Then the coupling constants g_{SPP}'s are expressed as

$$\begin{aligned} &g_{a_0(980)K\bar{K}} = \sqrt{2}(A\cos\theta_a - A'\sin\theta_a), \\ &g_{a_0(980)\pi\eta} = 2(A\cos\theta_a\sin\theta_P - \sqrt{2}A'\sin\theta_a\cos\theta_P), \\ &g_{f_0(M)\pi\pi} = 2(-AR_{f_0(M)NN} + \sqrt{2}A'R_{f_0(M)N'} + 2A''R_{f_0(M)G}), \end{aligned} \tag{20}$$

$$g_{f_0(M)K\bar{K}} = \sqrt{2}(-AR_{f_0(M)NS} + A'R_{f_0(M)N'} + \sqrt{2}A'R_{f_0(M)S'} + 2\sqrt{2}A''R_{f_0(M)G}).$$

For the best fitting of our model parameters, A, A', A'', θ_P, and then $g_{a_0(980)K\bar{K}}$, $g_{a_0(980)\pi\eta}$, $g_{f_0(M)\pi\pi}$, $g_{f_0(M)K\bar{K}}$, we use the experimental data of the scalar meson decays cited in Ref. [3] : $\Gamma(a_0(980) \to \pi\eta + K\bar{K}) = 75 \pm 25$ MeV, $\Gamma(a_0(1450) \to \pi\eta + \pi\eta' + K\bar{K}) = 265 \pm 13$ MeV, $\Gamma(K_0^*(1430) \to \pi K) = 270 \pm 43$ MeV, $\Gamma(f_0(980) \to \pi\pi + K\bar{K}) = 70 \pm 30$ MeV, $\Gamma(f_0(1370) \to \pi\pi + K\bar{K} + \eta\eta) = 214 \pm 120$ MeV, $\Gamma(f_0(1500) \to \pi\pi + K\bar{K} + \eta\eta + \eta\eta') = 55 \pm 9$ MeV, $\Gamma(f_0(1710) \to \pi\pi + K\bar{K} + \eta\eta) = 137 \pm 8$ MeV. The values for $g_{a_0(980)K\bar{K}}$, $g_{a_0(980)\pi\eta}$, $g_{f_0(M)\pi\pi}$, $g_{f_0(M)K\bar{K}}$ obtained when $\lambda_{01} = 0.30 - 0.35$ GeV^2 are nearest to the values obtained in the analyses of $\phi \to a_0\gamma/\pi^0\eta\gamma$ and $\phi \to f_0\gamma/\pi^0\pi^0\gamma$. The result of the non-derivative coupling is more reasonable than the result of the derivative coupling. Mixing angles and parameters for the mixing strength $\lambda_{01} = 0.30 - 0.35$ GeV^2 are $\theta_a = (15.0 - 17.8)^\circ$, $\theta_K = (13.8 - 16.4)^\circ$,

	$\lvert f_{NN}\rvert$	$\lvert f_{NS}\rvert$	$\lvert f_{N'}\rvert$	$\lvert f_{S'}\rvert$	$\lvert f_G\rvert$
$f_0(600)$	$0.98 \leftrightarrow 0.97$	$0.05 \leftrightarrow 0.07$	$0.20 \leftrightarrow 0.23$	$0.06 \leftrightarrow 0.08$	$0.00 \leftrightarrow 0.01$
$f_0(980)$	$0.05 \leftrightarrow 0.07$	$0.93 \leftrightarrow 0.90$	$0.11 \leftrightarrow 0.14$	$0.34 \leftrightarrow 0.40$	~ 0.02
$f_0(1370)$	$0.13 \leftrightarrow 0.16$	$0.25 \leftrightarrow 0.29$	$0.48 \leftrightarrow 0.49$	$0.83 \leftrightarrow 0.80$	~ 0.02
$f_0(1500)$	$0.02 \leftrightarrow 0.03$	$0.03 \leftrightarrow 0.05$	$0.09 \leftrightarrow 0.10$	$0.02 \leftrightarrow 0.03$	~ 0.99
$f_0(1710)$	$0.16 \leftrightarrow 0.19$	$0.25 \leftrightarrow 0.30$	$0.85 \leftrightarrow 0.82$	$0.44 \leftrightarrow 0.43$	$0.10 \leftrightarrow 0.12$

In the present analysis, $f_0(1500)$ meson is the most reasonable scalar glueball candidate.

References

1. N.N. Achasov and V.N. Ivanchenko, Nucl. Phys. B **315**, 465 (1989); F.E. Close and N. Isgur, and S. Kumano, Nucl. Phys. B **389**, 513 (1993); N.N. Achasov and V.V. Gubin, Phys. Rev. D **56**, 4084(1997).

2. M.N. Achasov *et al.* [SND Collaboration], Phys. Lett. B **479**, 53 (2000); D. Black, M. Harada, and J. Schechter, Phys. Rev. D **73**, 054017 (2006); R.R.R. Akhmetshin *et al.* [CMD-2 Collaboration], Phys. Lett. B **462**, 371, i-bid. 380(1999); A. Aloisio *et al.* [KLEO Collaboration], Phys. Lett. B **536**, 209 (2002); Phys. Lett. B **537**, 21 (2002).

3. W.-M. Yao *et al.* (Particle Data Group), J. Phys. G **33**, 1 (2006).

Frascati Physics Series Vol. XLVI (2007), pp. 593–600
HADRON07: XII Int. Conf. on Hadron Spectroscopy – Frascati, October 8-13, 2007
Light Meson Spectroscopy

RADIATIVE DECAYS OF HADRONIC MOLECULES

A. V. Nefediev
Institute of Theoretical and Experimental Physics,
117218, B. Cheremushkinskaya 25, Moscow, Russia

Abstract

It is argued that radiative decays of scalars $a_0/f_0(980)$ can serve as a decisive tool in establishing the nature of the latter. In particular, predictions for the widths of the radiative decays $S \to \gamma V$ ($S = a_0/f_0(980)$, $V = \omega/\rho/\gamma$) are given in the framework of the molecule model of the scalars. Finite–range corrections are discussed in detail for the two-gamma decays of hadronic molecules, with a special attention payed to the interplay of various scales involved in the problem and to the gauge invariance of the amplitude. The results are applied to the two-photon decay of the $f_0(980)$, and the existing experimental data on this decay are argued to support the molecule assignment for the scalar $f_0(980)$.

The problem of the structure of light scalar mesons is of a fundamental importance for understanding the properties of the entire scalar sector, that is, the sector of states with the quantum numbers of the vacuum, including purely gluonic excitations. In particular, the identification of the $a_0(980)$ and $f_0(980)$

mesons, together with the experimental studies of the lightest scalars (σ and κ), will allow one to establish the structure of multiplets of scalars and to find the signature of the scalar glueball in the spectrum of physical states. There are several models for the $a_0(980)$ and $f_0(980)$. The latter can be considered as $^3P_0$ quark–antiquark states [1] strongly coupled to the mesonic continuum and thus strongly distorted with the unitarisation process. However, due to the proximity of the $K\bar{K}$ threshold, it is natural to assume a considerable admixture of the four–quark component in the wave functions of these mesons, either as a compact four–quark with hidden strangeness [2, 3], or as a $K\bar{K}$ molecule. These might be t-channel exchanges to be responsible for the formation of such a molecule [4, 5, 6, 7]. It is therefore important to establish a test which would allow one to distinguish between these models and thus to reveal the actual nature of these scalars (in particular, efficient methods to discriminate between the molecule and compact states are strongly needed — for the recent progress see [8]). Since years, radiative decays of the $\phi(1020)$, $\phi \to \gamma S$, have been considered as such an experimental tool [9]. Indeed, these decays point to a large $K\bar{K}$ component in the scalars wave function [10, 11, 12]. Still a number of shortcomings of this approach should be mentioned. First of all, the radiative decays of the ϕ do not allow one to probe the nonstrange component of the scalars, and the contribution of the quark loops is strongly suppressed as compared to the contribution of the meson loops. Finally, the phasespace available in the final state of these decays is limited to a large extend. In the meantime, another class of radiative decays involving scalars is known — the radiative decays of the scalars themselves: $S \to \gamma V$, where the vector in the final state is either massive (ρ or ω) or massless, that is one deals with a two–photon decay in the latter case. Whatever model of scalars is used, gauge invariance imposes strong constraints on the decay amplitude:

$$iW^{\mu\nu} = M(a,b)[P_V^\mu P_\gamma^\nu - g^{\mu\nu}(P_V P_\gamma)], \quad a = \frac{m_V^2}{m^2}, \quad b = \frac{m_S^2}{m^2}, \qquad (1)$$

where m is the kaon mass and $P_{V,\gamma}$ are the four–momenta of the vector particles. Below we shall evaluate the widths of the radiative decays involving the scalars $a_0/f_0(980)$ in the molecule assignment for the latter.

First of all, it is important to notice that there are three scales in the problem under consideration, which are (i) the binding force scale $\beta \simeq m_\rho \approx$ 800 MeV, (ii) the kaon mass m, and (iii) the binding energy ε, and the hierarchy

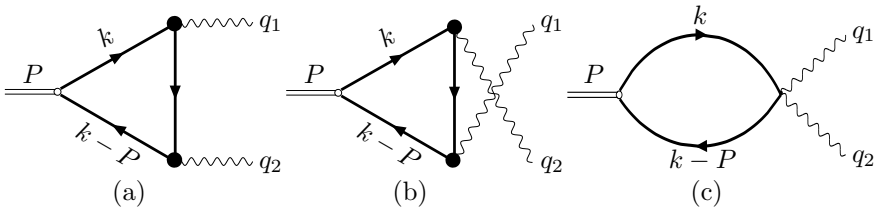

Figure 1: *Diagrams contributing to the scalar decay amplitude.*

of these scales is $\varepsilon \ll m \lesssim \beta$. The last inequality suggests that it is natural to start from the point-like limit of $\beta \to \infty$ and to include finite–range corrections (in the form a $1/\beta$ expansion) afterwards. Thus we stick to the point-like limit. The first ingredient one needs to know is the coupling of the loosely bound molecule state to the $K\bar{K}$ pair, which reads [13]:

$$\frac{g_S^2}{4\pi} = 32m\sqrt{m\varepsilon} \approx 1.12 \text{ GeV}^2, \tag{2}$$

where $m = 495$ MeV and the molecule binding energy is taken to be $\varepsilon = 10$ MeV. In addition, the $\phi K\bar{K}$ and the $VK\bar{K}$ coupling constants can be evaluated using the total width of the ϕ and the $\rho\pi\pi$ constant under the assumption of the SU(3) invariance. One arrives then at $g_\phi = 4.72, \quad g_V = 2.13$. It is straightforward then to arrive at the predictions of the point-like model for the radiative decays involving scalars. We give these predictions in tab. 1. For illustrative purposes and for future references, let us quote the formula for the two-photon decay width of a point-like scalar (see fig. 1 for the diagrams contributing to this decay):

$$\Gamma(S \to \gamma\gamma) = \frac{1}{2}\left(\frac{\alpha}{\pi}\right)^2 \sqrt{m\varepsilon}\left(\frac{2m}{m_S}\right)\left[\left(\frac{2m}{m_S}\right)^2 \arcsin^2\left(\frac{m_S}{2m}\right) - 1\right]^2, \tag{3}$$

where $m_S = 2m - \varepsilon$.

Notice that another approach to two–photon decays of molecules is known in the literature, namely the approach based on the formula $\Gamma(S \to \gamma\gamma) = \frac{\pi\alpha^2}{m^2}|\Psi(0)|^2$ which is written in analogy with that for the positronium two–photon decay. Although this approach appears quite successful in QED, it has to fail in hadronic physics. First of all, the wave function of the kaon molecule is simply not known, so one has to rely on models. Moreover, since $\Psi(0)$ is

Table 1: *The widths (in keV) of the radiative decays involving scalars; θ is the (small) $\phi - \omega$ mixing angle.*

	Quark–antiquark	Molecule	Data (PDG)
$\phi \to \gamma a_0$	$0.37 \sin^2\theta$	0.6	0.32 ± 0.02
$\phi \to \gamma f_0(\bar{n}n)/f_0(\bar{s}s)$	$0.04 \sin^2\theta/0.18$	0.6	0.47 ± 0.03
$a_0 \to \gamma\gamma$	~ 1	0.22	0.30 ± 0.10
$f_0 \to \gamma\gamma$	~ 1	0.22	$0.29^{+0.07}_{-0.09}$
$a_0 \to \gamma\omega/\rho$	125/14	3.4	pending
$f_0(\bar{n}n) \to \gamma\rho/\omega$	125/14	3.4	
$f_0(\bar{s}s) \to \gamma\rho/\omega$	$0/31 \sin^2\theta$	3.4	

very sensitive to the details of the bound–state formation, the predictions of this approach may vary drastically (the predictions found in the literature vary by an order of magnitude, from 0.6 keV in [14] to 6 keV in [15]). Furthermore, any attempt to evaluate corrections to this leading term results in either gauge invariance or energy conservation law breaking. Indeed, the decay amplitude in this approach is usually given as a overlap integral between the molecule wave function and the amplitude of the process $K^+K^- \to \gamma\gamma$:

$$W \propto \int \frac{d^3k}{(2\pi)^3} \psi(\vec{k}) \left[W(K^+(\vec{k})K^-(-\vec{k}) \to \gamma\gamma) \right]. \qquad (4)$$

If the amplitude $W(K^+K^- \to \gamma\gamma)$ is taken off-shell, then it obviously fails to be gauge–invariant. On the contrary, for the on–shell gauge–invariant amplitude W, kaons carry the energy $\sqrt{k^2 + m^2}$, rather than $m_S/2$, so that energy conservation law is violated.

The last, but not the least, argument against using the $\Psi(0)$-based approach to hadronic processes is that the hierarchy of scales has to be different, namely $\varepsilon \ll \beta \ll m$, in order to validate the given formula with $\Psi(0)$.

Finally, we estimate the finite–range corrections to the point-like predictions quoted in tab. 1 — we are interested in the potentially large corrections of order m^2/β^2. If the vector in the final state is massive, then the photon in the final state is soft ($\omega \ll \beta$), and the kinematics of the loop becomes nonrelativistic [7, 19, 13]. Inclusion of the finite-range effects amounts to the substitution $g_S \to \Gamma(\vec{k})$, with a suitable form of the vertex $\Gamma(\vec{k})$. Gauge invariance requires then that the extra momentum dependence coming from the vertex argument

should be gauged, that is

$$\Gamma(\vec{k}) \to \Gamma(\vec{k} + e\vec{A}) \approx \Gamma(\vec{k}) + e\vec{A}\frac{\partial\Gamma(\vec{k})}{\partial\vec{k}} + \mathcal{O}\left(\frac{\omega^2}{\beta^2}\right), \tag{5}$$

and the derivative term gives rise to an extra contact diagram with the photon emission from the scalar vertex. Gauge invariance is therefore preserved to order $\mathcal{O}(\omega/\beta)$. Notice however that one should be extremely careful when treating the loop integrals entering the decay amplitude. Indeed, although the full amplitude is finite, every individual integral is divergent. If a cut-off is introduced then to make them finite, gauge invariance may be badly broken and, as a result, wrong conclusions may be deduced (see, for example, [16] and explanations in [17]). Finally one arrives at the conclusion that no corrections of order m^2/β^2 appear for the point-like predictions [7, 19, 13]. The same conclusion holds for the two–photon decays of scalars, though it is not straightforward to arrive at this conclusion and one needs to develop a self-consistent gauge-invariant approach to this decay. It was suggested in [18] to use an effective kaon interaction Lagrangian (for the neutral-particle exchange, generalisation to the charged-particle exchange being trivial) written to order $1/\beta^2$:

$$L_{\rm int} = \frac{1}{2}\lambda_1(\varphi^\dagger\varphi)^2 + \frac{\lambda_2}{2\beta^2}\left[\partial_\mu(\varphi^\dagger\varphi)\right]^2, \tag{6}$$

with the coupling constants $\lambda_{1,2}$ being of the same order of magnitude. This Lagrangian is subject to renormalisation to order $1/\beta^2$ — see [18] for the details. In the renormalised theory, the kaon propagator and the photon–emission vertex, which are the dressed quantities, built as solutions of the corresponding field theoretical equations, read:

$$S(p) = \frac{Z}{p^2 - m^2}, \quad v_\mu(p,q) = Z^{-1}(2p-q)_\mu + \ldots, \tag{7}$$

where the ellipsis denotes terms which do not contribute to the decays under consideration. The renormalisation constants for the kaon propagator and for the photon emission vertex coincide due to gauge invariance. The kaon mass m is the renormalised physical mass. Finally, the most important ingredient — the scalar vertex beyond the point-like limit — comes as a solution of the homogeneous Bethe–Salpeter equation [18]:

$$\Gamma(p,P) = Z^{-1}g_S\left(1 + \frac{\lambda_2}{\lambda_1}\frac{p(p-P)}{\beta^2}\right). \tag{8}$$

This vertex is to be normalised [20], which gives for the scalar coupling the formula

$$\frac{g_S^2}{4\pi} = 32m\sqrt{m\varepsilon}\left(1 + 2\frac{\lambda_2}{\lambda_1}\frac{m^2}{\beta^2}\right), \tag{9}$$

which coincides with the point-like result (2) as $\beta \to \infty$. With the scalar vertex, the dressed kaon propagator, and the dressed photon emission vertex in hand we are in a position to evaluate the width of the scalar two-photon decay up to the order $1/\beta^2$. The amplitude of the process is given by the set of diagrams formally coinciding with those for the point-like vertex, depicted in fig. 1. Notice, however, an important difference: all ingredients are dressed now, and this is a necessary condition to preserve gauge invariance beyond the point-like limit. The only quantity which should not be dressed is the $KK\gamma\gamma$ vertex in the third diagram. Indeed, the scalar vertex Γ obeys the Bethe–Salpeter equation and thus absorbs all dressing diagrams.

In view of the fact that we deal with an explicitly gauge–invariant amplitude, we use the trick suggested in [21] and, in order to extract the amplitude, we read-off the coefficient at the structure $q_1^\nu q_2^\mu$ in the transition matrix element

$$iW = M(P^2)[q_1^\nu q_2^\mu - g^{\mu\nu}(q_1 q_2)]\epsilon^*_{1\mu}\epsilon^*_{2\nu}, \quad P = q_1 + q_2, \tag{10}$$

which is a particular case of (1) adapted for the two–photon case. Then

$$M(m_S^2) = M^{(0)}(m_S^2) + \frac{\lambda_2}{\lambda_1}\frac{m^2}{\beta^2}M^{(1)}(m_S^2), \tag{11}$$

and, by an explicit calculation, one can find that $M^{(1)}(m_S^2) = 0$. Therefore, no large corrections of order m^2/β^2 appear for the point-like result (3).

We conclude therefore, that finite–range effects give only moderate corrections to the point-like predictions (of order $10 \div 20\%$ in the amplitude), provided they are included in a self-consistent and gauge-invariant way [7, 13, 18]. We refer to the point-like results presented in tab. 1 as to the molecule model predictions for the radiative decays involving scalars. For the sake of comparison, we quote in tab. 1 the results of calculations in the quark–antiquark assignment for the scalars, which can be obtained with the help of the results of [22, 23]. From tab. 1 one can conclude that experimental data are well described in the molecule assignment for the scalars (a recent result by Belle [24] $\Gamma(f_0(980) \to \gamma\gamma) = 0.205^{+0.095}_{-0.083}(\text{stat})^{+0.147}_{-0.117}(\text{syst})$ keV gives an even better coincidence with the point-like prediction). Furthermore, predictions for

the radiative decays of scalars with massive vectors in the final state demonstrate a clear hierarchy, depending on the assignment prescribed to the scalar mesons. This makes these decays an extremely promising tool in establishing the nature of the $a_0/f_0(980)$.

1 Acknowledgements

This work was supported by the Federal Agency for Atomic Energy of Russian Federation and by grants NSh-843.2006.2, DFG-436 RUS 113/820/0-1(R), RFFI-05-02-04012-NNIOa, and PTDC/FIS/70843/2006-Fisica.

References

1. S. Godfrey and N. Isgur, Phys. Rev. **D32**, 189 (1985); M. Kroll, R. Ricken, D. Merten, B. Metsch, and H. Petry, Eur. Phys. J. **A9**, 73 (2000); A.M. Badalyan and B. L. G. Bakker, Phys. Rev. **D66**, 034025 (2002); A.M. Badalian, Phys. Atom. Nucl. **66**, 1342 (2003).

2. R.L. Jaffe, Phys. Rev. **D15**, 267, 281 (1977).

3. N.N. Achasov, S.A. Devyanin, and G.N. Shestakov, Phys. Lett. **B96**, 168 (1980); D. Black, A.H. Fariborz, F. Sannino, and J. Schechter, Phys. Rev. **D59**, 074026 (1999); M. Alford and R.L. Jaffe, Nucl. Phys. **B578**, 367 (2000); L. Maiani, F. Piccinini, A.D. Polosa, and V. Riquer, Phys. Rev. Lett. **93**, 212002 (2004).

4. J. Weinstein and N. Isgur, Phys. Rev. D **27**, 588 (1979).

5. D. Lohse, J.W. Durso, K. Holinde, and J.Speth, Phys. Lett. **B234**, 235 (1990); G. Janssen, B.C. Pearce, K. Holinde, and J. Speth, Phys. Rev **D52**, 2690 (1995).

6. J.A. Oller and E. Oset, Nucl. Phys. A **620**, 438 (1997); (E) Nucl. Phys. A **652**, 407 (1999).

7. V.E. Markushin, Eur. Phys. J. **A8**, 389 (2000).

8. C. Hanhart, presentation at this conference.

9. N.N. Achasov and V.N. Ivanchenko, Nucl. Phys. **B315**, 465 (1989).

10. M.N. Achasov *et al.*, Phys. Lett. **B440**, 442 (1998); M.N. Achasov *et al.*, Phys. Lett. **B485**, 349 (2000).

11. R.R. Akhmetshin *et al.* [CMD-2 Collab.], Phys. Lett. **B462**, 380 (1999).

12. A. Aloisio *et al.* [KLOE Collab.], Phys. Lett. **B536**, 209 (2002); A. Aloisio *et al.*, Phys. Lett. **B537**, 21 (2002).

13. J. Haidenbauer, C. Hanhart, Yu.S. Kalashnikova, A.E. Kudryavtsev, and A.V. Nefediev, Eur. Phys. J. **A24**, 437 (2005).

14. T. Barnes, Phys. Lett. B **165**, 434 (1985).

15. S. Krewald, R.H. Lemmer, and F. Sassen, Phys. Rev. **D69**, 016003 (2004).

16. N.N. Achasov, A.V. Kiselev, Phys. Rev. **D76** 077501, (2007), arXiv:hep-ph/0606268.

17. J. Haidenbauer, C. Hanhart, Yu.S. Kalashnikova, A.E. Kudryavtsev, and A.V. Nefediev, arXiv:hep-ph/0608191.

18. C. Hanhart, Yu.S. Kalashnikova, A.E. Kudryavtsev, and A.V. Nefediev, Phys. Rev. **D75**, 074015 (2007).

19. J. Haidenbauer, C. Hanhart, Yu.S. Kalashnikova, A.E. Kudryavtsev, and A.V. Nefediev, Phys. Rev. **C73**, 045203 (2006).

20. C.H. Llewellyn–Smith, Ann. Phys. (N.Y.) **53**, 521 (1969).

21. F. Close, N. Isgur, and S. Kumano, Nucl. Phys. B **389**, 513 (1993).

22. W. Kwong and J.L. Rosner, Phys. Rev. **D38**, 279 (1988).

23. R. Barbieri, R. Gatto, and R. Kogerler, Phys. Lett. **B60**, 183 (1976).

24. T. Mori *et al.* [Belle Collab.], Phys. Rev. **D75**, 051101 (2007).

Frascati Physics Series Vol. XLVI (2007), pp. 601–608
HADRON07: XII Int. Conf. on Hadron Spectroscopy – Frascati, October 8-13, 2007
Light Meson Spectroscopy

CHIRAL EXTRAPOLATION OF LIGHT RESONANCES FROM UNITARIZED CHIRAL PERTURBATION THEORY

J. R. Peláez[1], C. Hanhart[2] and G. Ríos[1]
[1] *Departamento de Física Teórica II. Universidad Complutense 28040 Madrid. Spain.*
[2] *Institüt für Kernphysik (Theorie), Forschungzentrum Jülich, D-52425 Jülich, Germany*

Abstract

Both scalar and vector light resonances can be generated from the unitarization of one-loop chiral perturbation theory. This amounts to using in a dispersion relation the chiral expansion, which incorporates the correct QCD quark mass dependence. We can thus predict the quark mass dependence of the poles associated to those light resonances. Our results compare well with some recent lattice results for the $\rho(770)$ mass and can be used as a benchmark for future lattice results on the $\rho(770)$ or the $f_0(600)$ also known as the σ.

1 Introduction

Light hadron spectroscopy at low energies lies beyond the realm of perturbative QCD, although lattice QCD provides, in principle, a rigorous way to extract non–perturbative quantities from QCD. However, current lattice results are

typically still done for relatively high quark masses. Thus, in order to make contact with experiment, appropriate extrapolation formulas need to be derived. This is typically done by using Chiral Perturbation Theory (ChPT) [1], which provides a model independent description of the dynamics of the lightest mesons, namely, the pions, kaons and etas, which are identified with the Goldstone Bosons (GB) associated to the QCD spontaneous Chiral Symmetry. Hence, ChPT is built out of only those fields, as a low energy expansion of a Lagrangian whose terms respect all QCD symmetries, and in particular its symmetry breaking pattern. Actually, this chiral expansion becomes a series in momenta and meson masses, generically $O(p^2/\Lambda^2)$, when taking into account systematically the small quark masses of the three lightest flavors that can be treated perturbatively. The chiral expansion scale is $\Lambda \equiv 4\pi f_\pi$, where f_π denotes the pion decay constant. ChPT is renormalized order by order by absorbing loop divergences in the renormalization of parameters of higher order counterterms, known as low energy constants (LEC). Their values depend on the specific QCD dynamics, and have to be determined either from experiment or from lattice QCD — they cannot be calculated from perturbative QCD.

The relevant remark for us is that, thanks to the fact that ChPT has the same symmetries than QCD and that it couples to different kind of currents in the same way, the orthodox ChPT expansion provides a *systematic and model independent* description of how the observables depend on some QCD parameters. This is the case for the leading dependence on the number of colors N_c and, more important for our purposes here, the dependence on the quark masses, which can be implemented systematically up to the desired order in the orthodox ChPT expansion.

In this work we focus on the two lightest resonances of QCD, the $\rho(770)$ and the $f_0(600)$. It is therefore enough to work with the two lightest quark flavors u, d in the isospin limit of an equal mass that we take as $\hat{m} = (m_u + m_d)/2$. The pion mass is given by an expansion $m_\pi^2 \sim \hat{m} + ...$ (see [1] for details). Therefore, studying the quark mass dependence is equivalent to study the pion mass dependence. In $\pi\pi$ scattering at NLO within SU(2) ChPT only four LECs $l_1, \cdots, l_4$ appear. Of course, when changing pion masses we have to take into account that amplitudes are customarily written [1] in terms of the μ independent LECs $\bar{l}$ [1] and the physical pion decay constant $f_\pi = f_0 \left(1 + \frac{m_\pi^2}{16\pi^2 f_0^2} \bar{l}_4 + \cdots\right)$ that depend explicitly on the pion mass, m_π.

2 Unitarization and dispersion theory

S matrix unitarity implies, for physical values of s, that elastic $\pi\pi$ scattering partial waves $t(s)$ of definite isospin I and angular momenta J should satisfy

$$\mathrm{Im}\, t(s) = \sigma |t(s)|^2 \Rightarrow \mathrm{Im}\, \frac{1}{t(s)} = -\sigma(s), \qquad \text{with} \quad \sigma(s) = 2p/\sqrt{s} \tag{1}$$

and p is the CM momenta. Thus $|t^{IJ}| \leq 1/\sigma$, and interactions are said to become strong precisely when this unitarity bound is saturated.

However, the ChPT low energy expansion $t \simeq t_2 + t_4 + ...$, where $t_{2k} \equiv O(p/(4\pi f_\pi))^{2k}$, can only satisfy unitarity perturbatively, i.e:

$$\mathrm{Im}\, t_2 = 0, \qquad \mathrm{Im}\, t_4 = \sigma t_2^2, \qquad \text{etc...} \tag{2}$$

The one-channel Inverse Amplitude Method (IAM) [2, 3] is a unitarization technique that can be derived within a "naive", intuitive, approach by noting that eq.(1), *fixes the imaginary part of the inverse amplitude exactly.* If we then use ChPT to write $\mathrm{Re}\, t^{-1} \simeq t_2^{-2}(t_2 + \mathrm{Re}\, t_4 + ...)$, we find

$$t \simeq= \frac{1}{\mathrm{Re}\, t^{-1} - i\sigma} = \frac{t_2}{1 - t_4/t_2}. \tag{3}$$

However, the above derivation is just formal, since the ChPT series can only be used at low energies. The correct derivation uses dispersion theory, and the fact that the ChPT series of t and $1/t$ beyond leading order have an analytic structure with a "physical cut" from threshold to ∞ and a "left cut" from $-\infty$ to $s = 0$. This leads to the following dispersion relation [3] for t_4

$$t_4 = b_0 + b_1 s + b_2 s^2 + \frac{s^3}{\pi} \int_{s_{th}}^{\infty} \frac{\mathrm{Im\, t_4(s')ds'}}{s'^3(s' - s - i\epsilon)} + LC(t_4), \tag{4}$$

where "LC" stands for a similar integral over the left cut and we have three subtractions to ensure convergence. A similar dispersion relation can be written for the function $G \equiv t_2^2/t$, by simply replacing t_4 by G and changing the name of the subtraction constants. Since t_2 is real, the functions G and t_4/t_2^2 have *exactly* opposite integrals over the physical cut. Their subtractions constants are the value of these functions at $s = 0$ where the ChPT expansion is safe. And finally, they also have opposite left cut contributions up to NNLO ChPT. Such an approximation on the left cut is, of course, only justified for small $|s|$,

but due to the three subtractions this is precisely the region that dominates the left cut integrals. Therefore, the IAM derivation is exact for the integrals over the elastic region and uses ChPT only where it is well justified. The IAM is even more justified if used sufficiently far from the left cut, as it is usually done, due to the additional $1/(s-s')$ suppression.

In the scalar channels there are also contributions to the dispersion relation coming from poles in $1/t$ due to the so-called Adler zeros located well below threshold. Such contributions lead, formally, to $O(p^6)$ corrections in the IAM, and are customarily neglected, leading to the standard IAM we have justified above. However, if not taken into account, the Adler zeros do not appear in the correct place and also unphysical poles occur in the IAM. Still, the influence of these unphysical poles is very localized around those Adler zeros and the standard IAM can be used safely for energies sufficiently far from the Adler zeros.

Nevertheless, in the next section we will show that resonance poles move into the subthreshold region for sufficiently large pion masses and it is thus relevant to include the pole contributions and use a slightly modified IAM, whose results agree with those of the standard IAM, except in the subthreshold region, where the modified version is more reliable. Such modified IAM has already been built and used in [4], by adding an *ad hoc* $O(p^6)$ piece to the $\mathrm{Re}\, t^{-1}$ expansion, within the "naive derivation" explained just before Eq.(3). A rigorous dispersive derivation is in preparation [5].

In summary, there are no model dependences in the approach, but just approximations to a given order in ChPT. Remarkably, the simple formula of the elastic IAM, Eq.(3), (or the slightly modified one to work in the subthreshold region), while reproducing the ChPT expansion at low energies, is also able to generate both the $\rho(770)$ and $f_0(600)$ resonances with values of the LECS compatible with standard ChPT [6, 7]. In other words, the IAM generates the poles [3, 6] associated to these resonances in the second Riemann sheet. The fact that resonances are *not introduced by hand* but generated from first principles and data, is relevant because the existence and nature of scalar resonances is the subject of a long-lasting intense debate.

To be precise, the IAM, when reexpanded, reproduces the orthodox ChPT series up to the order to which the input amplitude was evaluated and, in particular the quark mass dependence agrees with that of ChPT up to that order.

A few of the higher order terms are produced correctly by the unitarization but not the complete series— for a discussion of this issue for the scalar pion formfactor see Ref. [8]. However, the formalism just described still provides us with a fair estimate of the quark mass dependence of the resonance properties. In this case, we can study, without any a priory assumption, the dependence of the resonances positions on QCD parameters like the number of colors N_c [9] or their dependence on the quark masses up to a given order in ChPT.

3 Results

As commented above, since, for the moment, we are only interested in resonances appearing in elastic $\pi\pi$ scattering, we can unitarize $SU(2)$ ChPT at one-loop. For the LECS we take $l_3^r = 0.8 \pm 3.8$, $l_4^r = 6.2 \pm 5.7$, directly from [1], (since the partial waves where the σ and ρ appear are not very sensitive to these two constants), whereas we use $l_1^r = -3.7 \pm 0.2$, $l_2^r = 5.0 \pm 0.4$ obtained from an IAM fit to data up to the resonance region. All LECS are evaluated at $\mu = 770\,\mathrm{MeV}$, and are in fairly good agreement with standard values.

The highest value of m_π we can use is limited since we do not want to spoil the chiral expansion and we want to have some elastic $\pi\pi$ regime below the $K\bar{K}$ threshold. A mass of $m_\pi \leq 500\,\mathrm{MeV}$ satisfies both criteria since we know SU(3) ChPT still works fairly well with a kaon mass that high, and also because if we increase the pion mass to 500 MeV, the kaon mass becomes $\simeq$ 600 MeV, and $\pi\pi$ scattering is still elastic for 200 MeV, before reaching the two-kaon threshold. To reach higher masses we would need a coupled-channel IAM, which is feasible, but lies beyond our present scope.

Thus, in Fig.1 we show the ρ and $f_0(600)$ poles movement in the second Riemman sheet as m_π increases. Note that in order to follow easily the pole movement relative to the two-pion threshold, which is also increasing, we express all quantities in units of M_π, so that the two-pion threshold is shown fixed at $\sqrt{s} = 2$. In this way we clearly see that both poles move closer to the two-pion threshold. Let us recall that for narrow resonances, their mass M and width Γ are related to the pole position as $\sqrt{s_{pole}} \simeq M - i\Gamma/2$ and customarily this notation is also kept for broader resonances. Hence, both the σ and ρ widths decrease for increasing m_π, partly due to phase space reduction. In particular, the ρ pole moves toward the real axis and just when the threshold is reached it jumps into the real axis on the first sheet, thus becoming

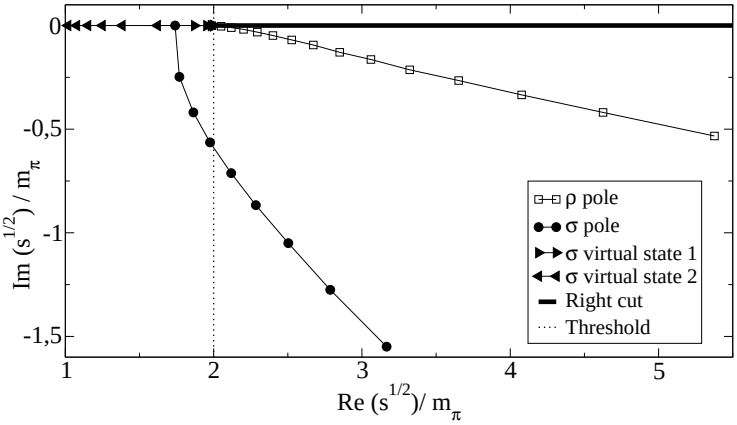

Figure 1: ρ and σ complex plane pole movement with increasing pion mass. To ease the comparison of the pole position relative to the two-pion threshold we normalize by the pion mass that is changing. Note how the sigma pole moves toward the real axis below threshold where it splits in two virtual states, whereas the ρ pole just moves toward threshold.

a traditional bound state, while its conjugate partner remains on the second sheet practically at the very same position as the one in the first. In contrast, when the σ mass reaches the two-pion threshold, its poles remain on the second sheet with a non-zero imaginary part before they meet on the real axis and become virtual states. As m_π increases further, one of those virtual states moves towards the threshold and jumps onto the first sheet, whereas the other one remains in the second sheet. Although, of course, this happens for very large values of m_π, such an analytic structure, with two very asymmetric poles in different sheets of an angular momentum zero partial wave, is a signal for a prominent molecular component [10]. A different P-wave and S-wave pole movement was also found within quark models [11], the latter showing also two second sheet poles on on the real axis below threshold.

In Fig.2 (left) we show in detail, the growth of the σ and ρ masses, starting from the chiral limit up to $\sim$ 500 MeV. We find that both the ρ and σ mass increase, but that of the σ grows faster, until it splits in two virtual states. Then one mass keeps growing, whereas the other one decreases.

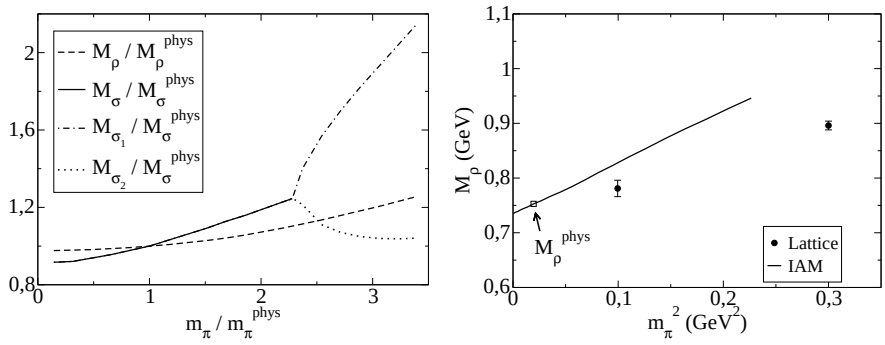

Figure 2: left:ρ and σ mass dependence on m_π. Note that the sigma pole splits in two virtual poles, denoted σ_1 and σ_2 for sufficiently high m_π. Right: IAM ρ mass dependence on m_π versus some recent lattice results (see text).

Finally in Fig.2 (right) we show our central value result for the ρ mass dependence on m_π compared with some recent lattice results [12]. Despite our results refer to the ρ "pole-mass" definition and that those results on the lattice have a zero width for the ρ, we see a reasonable qualitative agreement between both results, although our dependence seems to be somewhat steeper. We have some preliminary indications that if we decrease the ρ width in our approach (by taking the large N_c limit of ChPT), we reproduce even better those lattice results.

A publication with further details is in preparation [13] including results of the $f_0(600)$ and $\rho(770)$ mass and width evolution with the pion mass as well as a comparison with other works and lattice results. Estimates of uncertainties and possibly an extension to the SU(3) coupled channel case are in progress.

4 Acknowledgements

We thank U. G-. Meißner and E. Van Beveren for their suggestions. J.R.P. and G.R. research partially funded by Banco Santander/Complutense contract PR27/05-13955-BSCH and Spanish CICYT contracts FPA2007-29115-E, FPA2005-02327, BFM2003-00856. J.R.P. and C. Hanhart research is part of the EU integrated infrastructure initiative HADRONPHYSICS PROJECT, under contract RII3-CT-2004-506078.

References

1. S. Weinberg, Physica **A96** (1979) 327. J. Gasser and H. Leutwyler, Annals Phys. **158** (1984) 142; Nucl. Phys. B **250** (1985) 465.
2. T. N. Truong, Phys. Rev. Lett. **61** (1988) 2526. Phys. Rev. Lett. **67**, (1991) 2260; A. Dobado, M.J.Herrero and T.N. Truong, Phys. Lett. **B235** (1990) 134.
3. A. Dobado and J. R. Peláez, Phys. Rev. D **47** (1993) 4883. Phys. Rev. D **56** (1997) 3057.
4. D. Fernandez-Fraile, A. Gomez Nicola and E. T. Herruzo, Phys. Rev. D **76**, 085020 (2007)
5. A. G. Nicola, J. R. Pelaez and G. Rios, arXiv:0712.2763 [hep-ph].
6. J. R. Peláez, Mod. Phys. Lett. A **19**, 2879 (2004)
7. F. Guerrero and J. A. Oller, Nucl. Phys. B **537** (1999) 459 [Erratum-ibid. B **602** (2001) 641]. A. Gómez Nicola and J. R. Peláez, Phys. Rev. D **65** (2002) 054009 and AIP Conf. Proc. **660** (2003) 102 [hep-ph/0301049].
8. J. Gasser and U.-G. Meißner, Nucl. Phys. B **357** (1991) 90.
9. J. R. Peláez and G. Rios, Phys. Rev. Lett. **97** (2006) 242002. J. R. Peláez, Phys. Rev. Lett. **92** (2004) 102001
10. S. Weinberg, Phys. Rev. **130** (1963) 776. D. Morgan, Nucl. Phys. A **543** (1992) 632; D. Morgan and M. R. Pennington, Phys. Rev. D **48** (1993) 1185. V. Baru, J. Haidenbauer, C. Hanhart, Yu. Kalashnikova and A. E. Kudryavtsev, Phys. Lett. B **586** (2004) 53
11. E. van Beveren, G. Rupp, N. Petropoulos and F. Kleefeld, AIP Conf. Proc. **660**, 353 (2003) [arXiv:hep-ph/0211411]. E. van Beveren and G. Rupp, Mod. Phys. Lett. A **19**, 1949 (2004) E. van Beveren, J. E. G. Costa, F. Kleefeld and G. Rupp, Phys. Rev. D **74**, 037501 (2006)
12. S. Aoki *et al.* [CP-PACS Collaboration], Phys. Rev. D **60**, 114508 (1999)
13. C. Hanhart, J.R. Peláez and G. Ríos, *in preparation*

Frascati Physics Series Vol. XLVI (2007), pp. 609–616
HADRON07: XII Int. Conf. on Hadron Spectroscopy – Frascati, October 8-13, 2007
Light Meson Spectroscopy

$f_0(1370)$

D.V.Bugg
Queen Mary, University of London, UK

Abstract

A summary is given of the main sets of data requiring the existence of $f_0(1370)$. Crystal Barrel data on $\bar{p}p \to \eta\eta\pi^0$ contain a visible $f_0(1370)$ peak and require at least a 19σ contribution. This alone is sufficient to demonstrate its existence. Extensive data on $\bar{p}p \to 3\pi^0$ at rest contain delicate interferences which determine the mass and width independently in $^1S_0$ and $^3P_1$ annihilation and agree within 5 MeV for both mass and width. The peak in 2π is at 1282 ± 5 MeV, but the rapid increase in 4π phase space with mass displaces the 4π peak to 1360 MeV. BES II data for $J/\Psi \to \phi\pi^+\pi^-$ contain a visible $f_0(1370) \to 2\pi$ signal $> 8\sigma$. In all cases, a resonant phase variation is required.

The $f_0(1370)$ plays a vital role in the spectroscopy of light $J^P = 0^+$ mesons. Some people have questioned its existence, though these criticisms are based on fits to very limited sets of data. To answer those questions, the best available data have been refitted critically. Full details of the analysis are given in Ref. [1)]. Here essential points are summarised.

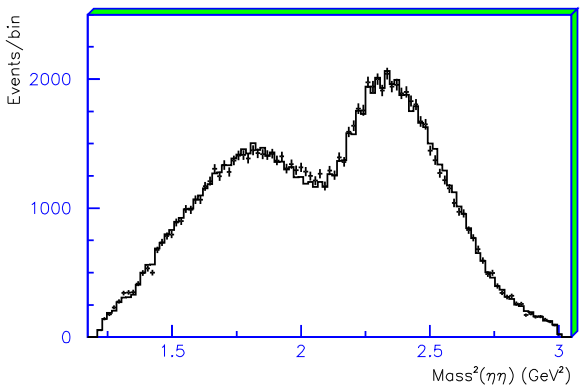

Figure 1: *The $\eta\eta$ mass projection for $\bar{p}p \to \eta\eta\pi^0$ at rest in liquid hydrogen*

Crystal Barrel data on $\bar{p}p \to (\eta\eta)\pi^0$ at rest in liquid and gaseous hydrogen show two clear peaks in $\eta\eta$ at ~ 1330 and 1500 MeV [2], Fig. 1. The low mass peak cannot be due to $f_2(1270)$, whose branching ratio to $\eta\eta$ is 4×10^{-3}. A fit without $f_0(1370)$ is worse by 19 standard deviations, because the peak at 1330 and the dip at 1430 MeV cannot be fitted by $\sigma \to 4\pi$ and $a_0(980)$ alone.

The data which determine resonance parameters best are Crystal Barrel data on $\bar{p}p \to 3\pi^0$ at rest in liquid and gaseous hydrogen [3]. There is a conspicuous signal at low mass due to the σ pole and high mass peaks due to $f_2(1270)$ and $f_0(1500)$. The $f_0(1370)$ hides beneath the $f_2(1270)$, but is clearly separated by angular analysis. Interferences between the three $\pi\pi$ combinations determine the mass and width of $f_0(1370)$ in a very delicate way. The two sets of data allow a clean separation of annihilation from $^1S_0$ and $^3P_1$ initial states. The $f_0(1370)$ is at least a 32 standard deviation signal in $^3S_1$ and 33 standard deviations in $^3P_1$.

The opening of the 4π channel is important. The phase space for $\rho\rho$ and $\sigma\sigma$ are shown in Fig. 2. Relative contributions are poorly known, so the fit to data finds the best compromise: a Fermi function going to 1 at high mass. Half-height is at ~ 1.8 GeV, and 4π inelasticity is small at 1.3 GeV, ultimately the best mass.

The full form of the Breit-Wigner resonance formula,

$$f = 1/[M^2 - s - m(s) - iM\Gamma_{total}(s)] \qquad (1)$$

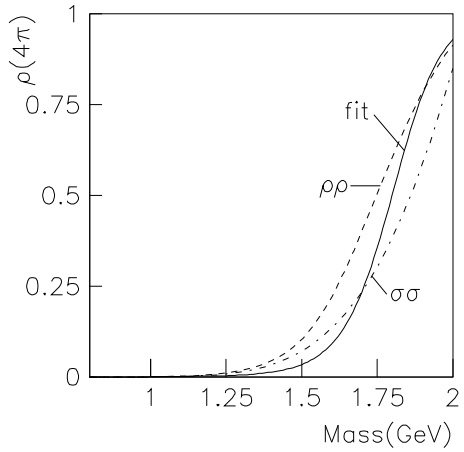

Figure 2: 4π *phase space for* $\rho\rho$ *(dashed),* $\sigma\sigma$ *(chain curve) and the fit adopted (full curve)*

contains a real dispersive term $m(s)$ [4], which for the 4π channel reads

$$m(s) = \frac{s - M^2}{\pi} \int \frac{ds' M \Gamma_{4\pi}(s')}{(s' - s)(s' - M^2)}. \qquad (2)$$

The slope of $m(s)$ near resonance is larger than $(M^2 - s)$. However a good solution emerges naturally. Loop diagrams for production of 4π behave like vacuum polarisation and lead to strong renormalisation effects. Consequently only the ratio of 2π and 4π widths is well determined: absolute values can be varied through a wide range, leaving the line-shape almost unchanged.

Fig. 3 shows the essential points. The $\pi\pi$ peak is at 1282 ± 5 MeV and is cut off towards higher masses by the opening of the 4π channel. The Breit-Wigner denominator is the same for 4π data, but 4π phase space displaces the 4π peak upwards by 78 ± 10 MeV. One must distinguish between experiments fitting (a) two-body channels and (b) 4π data. The centre of the 4π peak at half-height is at 1390 MeV, in close agreement with extensive Crystal Barrel fits [5]. The three dashed curves above 1500 MeV illustrate uncertainty in $\Gamma(4\pi)$.

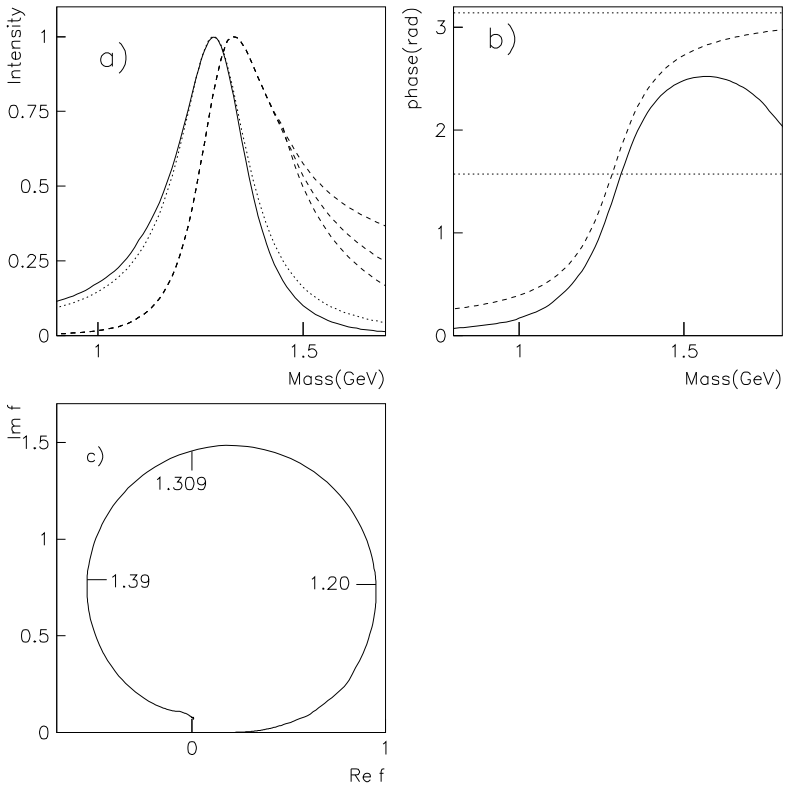

Figure 3: *(a) line-shapes of $f_0(1370)$ for 2π (full curve), a Breit-Wigner amplitude with constant width (dotted), and for 4π (dashed); (b) the phase angle measured from the bottom of the Argand plot (full curve) and for a Breit-Wigner amplitude of constant width (dashed); horizontal lines mark phase shifts of $\pi/2$ and π, (c) Argand plot; masses are shown in GeV.*

A remarkable feature of the new analysis is shown in Fig. 3(c). Despite the strong dispersive effect of the 4π channel, the amplitude follows a circle very closely. The left-hand side of the loop is suppressed by coupling to 4π. The phase shift goes through 90° at 1309 ± 5 MeV, but the circle can be reproduced

well with an effective mass of 1282 MeV and a constant width of 207 ± 15 MeV.

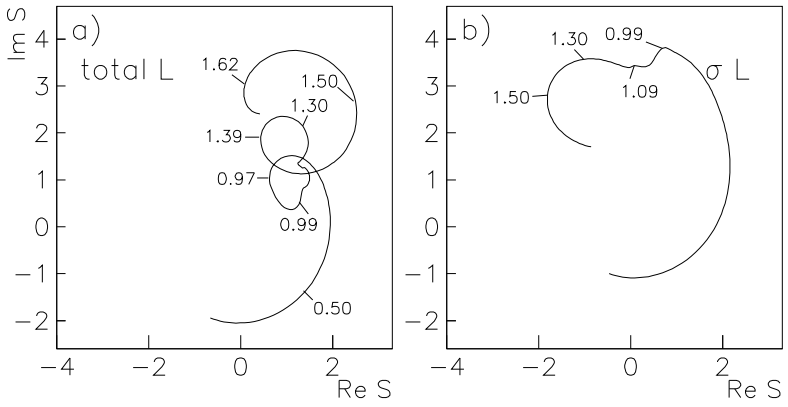

Figure 4: *Argand diagrams for the total $\pi\pi$ S-wave in liquid hydrogen and σ alone; masses are marked in GeV*

Fig. 4 displays the Argand diagram for the $\pi\pi$ S-wave in ${}^1S_0$ $\bar{p}p \to 3\pi^0$. There are successive loops due to the σ pole, $f_0(980)$, $f_0(1370)$ and $f_0(1500)$. The third loop is the crucial one identifying $f_0(1370)$, or $f_0(1300)$ to give it a new and improved mass. An important test is to fit 40 MeV bins from 1100 to 1460 MeV freely in magnitude and phase. Real and imaginary parts of the amplitude move from the fitted curve only by $\sim 15\%$ of the radius of the loop, consistent with experimental errors. This shows that the loop is definitely required.

A vital point in the new analysis is the inclusion of $\sigma \to 4\pi$. This cannot account for the $f_0(1370)$ loop, as illustated on Fig. 4(b). There is a loop near 1500 MeV due to this process, but it is higher and much wider than $f_0(1370)$. A weakness of all current fits to 4π data is the omission of the $\sigma \to 4\pi$ amplitude.

The $f_0(1370)$ and $f_0(1500)$ combine to produce a visible peak in BES data for $J/\Psi \to \phi\pi^+\pi^-$ [6]. That publication fitted the mass and width freely. These data have now been refitted using parameters fitted to the $3\pi^0$ and $\eta\eta\pi^0$ data. The fit of Fig. 5(a) is acceptable. If the $f_0(1370)$ is removed, Fig. 5(b) shows the fit is visibly poor. Incidentally, the $f_0(1370)$ is well separated by angular analysis from $f_2(1270)$ in these data; the latter optimises with mass

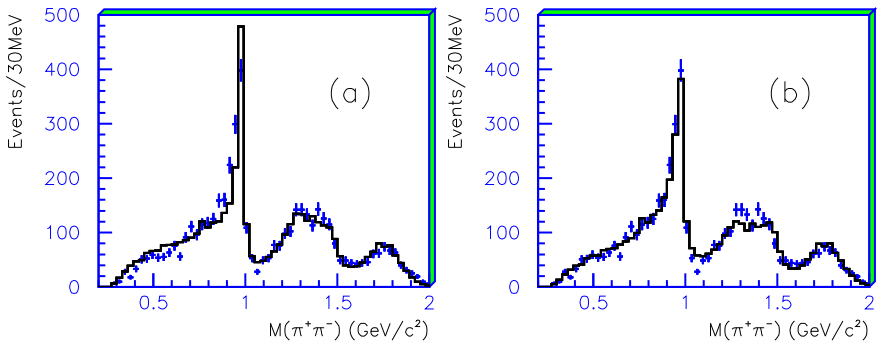

Figure 5: *Fits to BES II data on* $J/\Psi \to \phi\pi^+\pi^-$. *(a) optimum fit; (b) without* $f_0(1370)$.

and width consistent within 10 MeV with PDG values.

All the three sets of data discussed so far require a resonant phase variation for $f_0(1370)$. If the resonance is replaced with a peak of the same line-shape but no phase variation (despite the fact that this is non-analytic), χ^2 is significantly worse in every case.

The $f_0(1370)$ also appears in GAMS data for $\pi^+\pi^- \to \pi^0\pi^0$ at large $|t|$ [7] and in central production of $\pi\pi$ with parameters close to those found here [8]. Historically, it was first identified as $\epsilon(1300)$ in data from the Argonne and Brookhaven labs on $\pi\pi \to KK$ [9]. That identification was not clear-cut because parameters of $f_0(980)$ and $\sigma \to KK$ were not known accurately at that time. Using modern values for those parameters, these early data are entirely consistent with those fitted here [10].

The new fit includes the BES data for $J/\Psi \to \omega\pi\pi$ [11] as an important constraint on the line-shape of the σ up to 1050 MeV; it is clearly visible by eye in the $\pi\pi$ mass projection in those data. The $\pi\pi$ phase shifts predicted by Caprini et al. [12] using the Roy equations are also included. The moments for Cern-Munich data on $\pi\pi \to \pi\pi$ [13] are also refitted. Up to the KK threshold, these data determine $\pi\pi$ phases with errors of $\sim 3.5^\circ$. However, above the KK threshold, real and imaginary parts of the amplitude become very strongly correlated because differential cross sections alone do not separate magnitude and phase. The fit requires inclusion of some mixing between σ, $f_0(1370)$ and

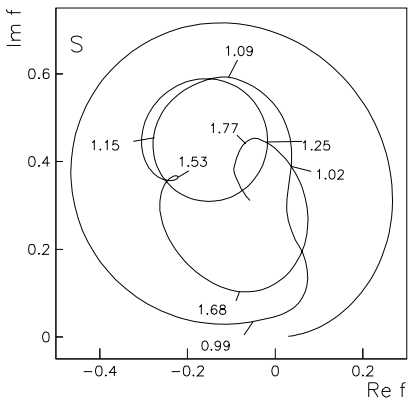

Figure 6: *Argand diagram for $\pi\pi$ $I = 0$ S-wave in elastic scattering*

$f_0(1500)$. The Argand diagram for the $\pi\pi$ $I = 0$ S-wave is shown in Fig. 6. The fit to Cern-Munich data gives $\Gamma_{2\pi}[f_0(1500)] = 61 \pm 5$ MeV. The following branching ratios are also determined: $\Gamma(f_0(1370) \to \eta\eta)/\Gamma(f_0(1370) \to \pi\pi) = 0.19 \pm 0.07$, $\Gamma(f_0(1500) \to \eta\eta)/\Gamma(f_0(1500) \to \pi\pi) = 0.135 \pm 0.05$, $\Gamma(\sigma \to \eta\eta)/\Gamma(\sigma \to \pi\pi) = 0.19 \pm 0.07$.

In summary, the $f_0(1370)$ is definitely required and can be approximated for most purposes with a Breit-Wigner denominator with $M = 1282 \pm 5$ MeV, $\Gamma = 207 \pm 15$ MeV, and appropriate phase space in the numerator for each channel. Together with $a_0(1450)$, $K_0(1430)$, $f_0(1710)$ and $f_0(1500)$, one can complete a nonet together with the 0^+ glueball which mixes with the $q\bar{q}$ states. The $f_0(1790)$ observed in BES data for $J/\Psi \to \phi\pi\pi$ (and several other sets of data) makes the first member of the next nonet. The exotic $\phi\omega$ peak observed by BES in $J/\Psi \to \gamma\phi\omega$ [14] is consistent with the upper half of $f_0(1790)$, suggesting it is locked to this threshold at 1801 MeV, similar to the way $f_2(1565)$ is locked to the $\omega\omega$ threshold.

References

1. D.V. Bugg, Eur. Phys. J C**52** 55 (2007); arXiv: hep-ex/0706.1341
2. C. Amsler *et al*, Phys. Lett. B **291** 347 (1992)

3. A. Abele *et al*, Nucl. Phys. A **609** 562 (1996)

4. A.V. Anisovich *et al*, Nucl. Phys. A **690** 567 (2001)

5. A. Abele *et al*, Eur. Phys. J. C**19** 667 (2001) and **21** 261 (2001)

6. M. Ablikim *et al*, Phys. Lett. B **607** 243 (2005)

7. D. Alde *et al*, Eur. Phys. J. A**3** 361 (1998)

8. D. Barberis *et al*, Phys. Lett. B **474** 423 (2000)

9. V.A. Polychronakos *et al*, Phys. Rev. D **19** 1317 (1979); D. Cohen *et al*, Phys. Rev. D **22** 2595 (1980); A.D. Martin and E.N. Ozmutlu, Nucl. Phys. B **158** 520 (1979) A. Etkin *et al*, Phys. Rev. D **25** 1786 (1982)

10. D.V. Bugg, Euro. Phys. J C **47** 45 (2006)

11. M. Ablikim *et al*, Phys. Lett. B **598** 149 (2004)

12. I. Caprini, I. Colangelo and H. Leutwyler, Phys. Rev. Lett. **96** 032001 (2006)

13. W. Ochs, University of Munich Ph.D. thesis (1974)

14. M. Ablikim *et al*, Phys. Rev. Lett. 96 162002 (2006)

Frascati Physics Series Vol. XLVI (2007), pp. 617–626
HADRON07: XII Int. Conf. on Hadron Spectroscopy – Frascati, October 8-13, 2007
Light Meson Spectroscopy

SEARCH FOR $f_1(1285) \to \pi^+\pi^-\pi^0$ DECAY WITH VES DETECTOR

V. Dorofeev, R. Dzheliadin, A. Ekimov, Yu. Gavrilov,
Yu. Gouz, A. Ivashin, V. Kabachenko, I. Kachaev,
A. Karyukhin, Yu. Khokhlov, V. Konstantinov, M. Makouski,
V. Matveev, A. Myagkov, V. Nikolaenko, A. Ostankov, B. Polyakov,
D. Ryabchikov, N. Shalanda, M. Soldatov, A.A. Solodkov, A.V. Solodkov,
O. Solovianov, A. Zaitsev
IHEP, 142281, Protvino, Moscow region, Russia

presented by V.Nikolaenko

Abstract

The isospin violating decay $f_1(1285) \to \pi^+\pi^-\pi^0$ has been studied at VES facility. This study is based at the statistics acquired in $\pi^- Be$ interactions at 27, 36.6 and 41 GeV/c in diffractive reaction $\pi^- N \to (f_1\pi^-)N$. The $f_1(1285) \to \pi^+\pi^-\pi^0$ decay is observed. The ratio of decay probabilities $BR(f_1(1285) \to \pi^+\pi^-\pi^0)$ to $BR(f_1(1285) \to \eta\pi^+\pi^-) \cdot BR(\eta \to \gamma\gamma)$ is $\sim$ 1.4%.

1 Introduction

The decay $f_1(1285) \to \pi^+\pi^-\pi^0$ violates the isospin symmetry. It can proceed by means of $f_1(1285) \to a_1(1260)$ mixing and by a direct decay $f_1(1285) \to (\pi^+\pi^-\pi^0)$. The $f_1(1285) \to a_1(1260)$ mixing is driven mainly by the difference of light quark mass $\Delta m = m_d - m_u$ [1, 2]. Namely this Δm is responsible for known decays $\omega \to \pi^+\pi^-$, $\phi(1020) \to \pi^+\pi^-$, $\eta \to 3\pi$ and $\eta' \to 3\pi$. In the case of $f_1 \leftrightarrow a_1$ mixing it leads to a_1-like final states: $(\rho\pi), (f_0(600)\pi)$.

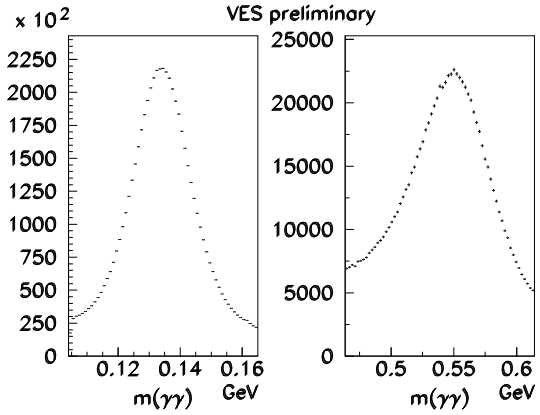

Figure 1: Effective mass of $\gamma\gamma$ pairs a) reaction $\pi^- N \to \pi^+\pi^-\pi^-\pi^0 N$; b) reaction $\pi^- N \to \eta\pi^+\pi^-\pi^- N$.

Another effect can contribute to the decay $f_1(1285) \to \pi^+\pi^-\pi^0$, namely the $a_0(980) \leftrightarrow f_0(980)$ mixing predicted in 1979 [3]. Qualitatively speaking, loops with virtual K^+K^- and $K^0\bar{K}^0$ pairs cancel one another, but this cancellation is not perfect due to the difference in mass of charged and neutral kaons. The isospin symmetry violation reaches the maximum at the region between thresholds for pairs of charged and neutral kaons. The amplitude of the isospin violating transition depends on the couplings of scalar mesons with $K\bar{K}$ pairs, in other words, it can shed light on the structure of scalars. This phenomenon was discussed in details and several possibilities for its experimental observation were proposed, including a special polarization experiment [4], $f_1(1285)$ decays [5] and J/ψ decays [6]. Theoretical aspects of the expected $a_0(980) \leftrightarrow f_0(980)$ mixing are discussed in details in recent paper [7].

Diffractive reaction $\pi^- N \to (f_1\pi^-)N \to (\eta\pi^+\pi^-)\pi^- N$ represents a reach source of the $f_1(1285)$ mesons at low background. The branching ratio of $f_1 \to a_0\pi$ decay is large, $BR = 0.36 \pm 0.07$ [8]. The process chain

$$f_1(1285) \to a_0(980)\pi^0 \to f_0(980)\pi^0 \to (\pi^+\pi^-)\pi^0; \qquad (1)$$

is well suitable for a search of expected isospin violation.

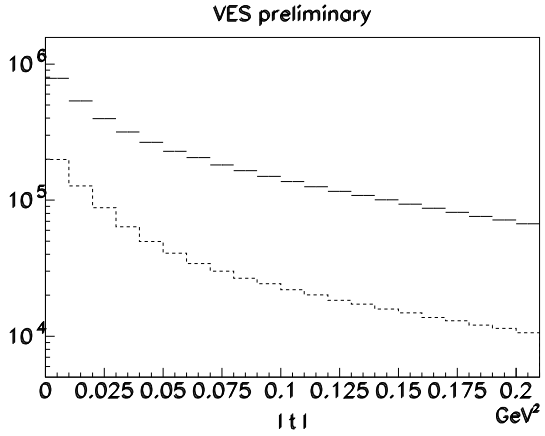

Figure 2: $|t'|$-distributions for reactions $\pi^- N \to \pi^+\pi^-\pi^-\pi^0 N$ (upper distribution) and $\pi^- N \to \eta\pi^+\pi^-\pi^- N$.

2 Experimental procedure

This study is based on the statistics acquired by the VES experiment [9] in interactions of a π^- beam at the momentum of 27, 36.6 and 41 GeV/c on a Be target, in reaction

$$\pi^- N \to \pi^+\pi^-\pi^-\pi^0 N. \tag{2}$$

VES is a wide-aperture magnetic spectrometer equipped with a lead-glass electromagnetic calorimeter and Cherenkov detectors for charged particle identification. Events from reaction

$$\pi^- N \to \pi^+\pi^-\pi^-\eta N \tag{3}$$

were selected also and used for normalization. The π^0 and η mesons were detected in the $\gamma\gamma$ mode. Selection criteria which have been applied for the selection of the $(\pi^+\pi^-\pi^-\eta)$ events are described in [10]. Similar selection procedure was used for the $(\pi^+\pi^-\pi^-\pi^0)$ events; here the effective mass of two photons was requested in the range $(0.105, 0.165)\, GeV/c^2$ (see Fig.1). A kinematical fit to the η or π^0 mass has been performed, respectively. The t-distributions for the reactions (2) and (3) are shown in Fig. 2. The low $|t|$

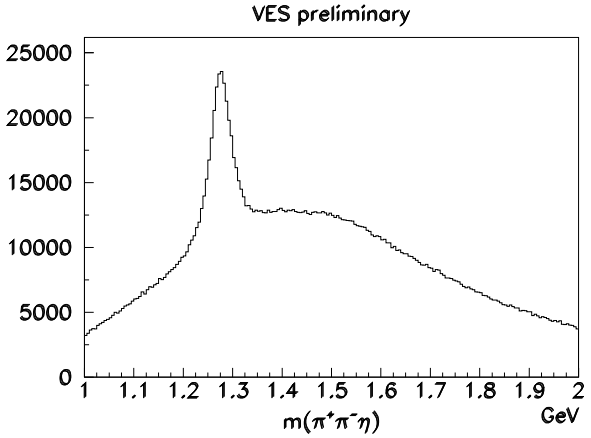

Figure 3: Effective mass of $(\eta\pi^+\pi^-)$ system produced in the reaction $\pi^- N \to (\eta\pi^+\pi^-\pi^-)N$ at low t', $|t'| < 0.04\ GeV^2$. There are two entries per event.

region is relatively higher for the reaction (3), which is a consequence of the diffractive production.

Fig.3 demonstrates the $f_1(1285)$ signal which is observed in the dominant decay channel, $f_1 \to \eta\pi^+\pi^- \to \gamma\gamma\pi^+\pi^-$ at low momentum transfer region, $|t'| < 0.04$. The estimated number of events in the f_1 peak is $N_\eta = 117600 \pm 1300$, assuming the Breit-Wigner shape of the signal. Concerning the f_1 production process, the results of the partial wave analysis of $\eta\pi^+\pi^-\pi^-$ system [11] show that the $(f_1\pi^-)$ system is produced in diffractive reaction. The dominant wave is $J^{PC}M\eta = 1^{++}0+$, here M is the spin projection and the η denotes the exchange naturality. Then the intermediate system with spin-parity 1^+ decays into $f_1(1285)$ and extra π^-, this is a P-wave decay. Then the $f_1(1285)$ decays into $\eta\pi^+\pi^-$, this decay also includes a P-wave. The dominant angular term in the effective amplitude (which describes the chain of processes) is

$$A \sim \sin(\theta_1) \cdot \sin(\theta_2) \cdot \sin(\phi_0 - \phi_2) \tag{4}$$

here θ_1 is the Gottfried-Jackson angle of the extra π^-; θ_2 is polar angle of π^0 at the f_1 rest frame with Z-axis going along the direction of the extra π^- (so called "canonic system"); ϕ_0 and ϕ_2 are the azimuthal angles of the beam particle and the π^0 at the same system. The validity of this formula is demonstrated in

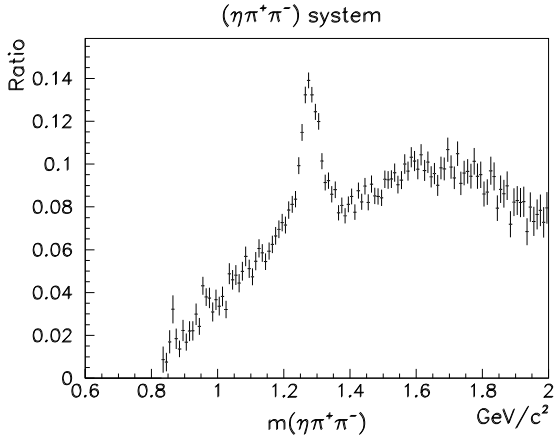

Figure 4: Ratio of two $m(\eta\pi^+\pi^-)$ spectra. The distribution for events at $W > 0.8$ is divided by the spectrum for events at $W < 0.2$ (see text).

Fig.4. Apart from the mass spectrum presented in Fig.3, similar distributions were accumulated in several intervals on the angular weight $W = |A|^2$. The ratio of two mass spectra, one of them for events at high W and another one at low W, is shown. One can see that the angular weight W strengthens the f_1 signal. This weight was used for the identification of the $f_1 \to \pi^+\pi^-\pi^0$ decay.

Now we consider the general characteristics of the reaction (2). Fig.5 demonstrates the mass spectra for the selected $(\pi^+\pi^-\pi^-\pi^0)$ sample. The $b_1(1235)$ signal and a wide peak centered near 1700 MeV are seen at the total mass spectrum (Fig.5a). For the $(\pi^+\pi^-\pi^0)$ system one can see a strong peak from the $\omega \to \pi^+\pi^-\pi^0$ decay and also the $\eta \to \pi^+\pi^-\pi^0$ peak in Fig.5b, as well as an accumulation of events at the mass close to 1300 MeV is seen which is close to the $f_1(1285)$ mass. Detailed analisis of this structure is given below. Concerning the $(\pi^+\pi^-)$ mass spectrum (Fig.5d),a sharp peak from $K^0 \to \pi^+\pi^-$ decay is seen as well as a sharp peak near 780 MeV, the later one is consistent with the ω mass and should be attributed to the suppressed $\omega \to \pi^+\pi^-$ decay. Wide background under the ω signal originates from the $\rho \to \pi^+\pi^-$ decay.

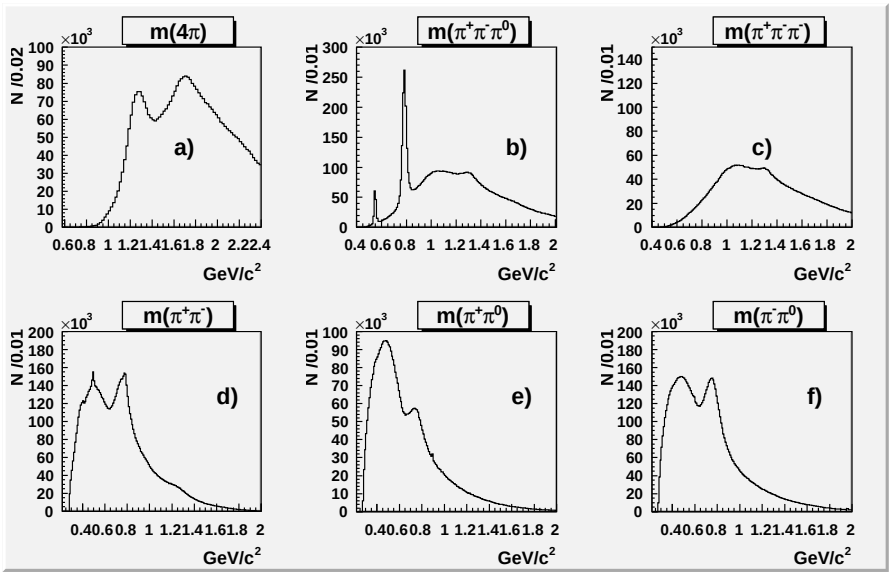

Figure 5: Effective masses for $(\pi^+\pi^-\pi^-\pi^0)$ system. a) total mass; b) $m(\pi^+\pi^-\pi^0)$; c) $m(\pi^+\pi^-\pi^-)$; d) $m(\pi^+\pi^-)$, a zoom of the mass region from 680 to 880 MeV is shown ; e) $m(\pi^+\pi^0)$; f) $m(\pi^-\pi^0)$.

It worth mentioning that the $f_1 \to a_0\pi^0$ sample originates from the diffractive production. The subsequent processes, $a_0 \leftrightarrow f_0$ mixing and $f_0 \to \pi^+\pi^-$ decay, lead to four-pion final state. The background processes, $\pi^- N \to (\pi^+\pi^-\pi^-\pi^0)N$, i. e. production of four pions is not a diffractive process and it is suppressed. This suppression should facilitate the observation.

To improve the signal to background ratio, the following selection criteria have been applied: a) events at the low momentum transfer, $|t'| < 0.04$ were selected; b) events with a signal detected in the target guard system were rejected; c) events with $m(\pi^+\pi^-\pi^0) < 0.800\, GeV/c^2$ at any combination were rejected. First two cuts tend to select diffractive reaction, the third one rejects events with $\omega(780)$ or $\eta(550)$.

Apart from those general cuts, the event selection in different mass intervals for the $(\pi^+\pi^-\pi^0)$ and $(\pi^+\pi^-)$ were tested. The $m(\pi^+\pi^-\pi^0)$ distribution, which was obtained with requirements on the two-pion mass $0.970 < m(\pi^+\pi^-) < 1.000\, GeV$, is presented in Fig.6a. Clear peak is observed, and

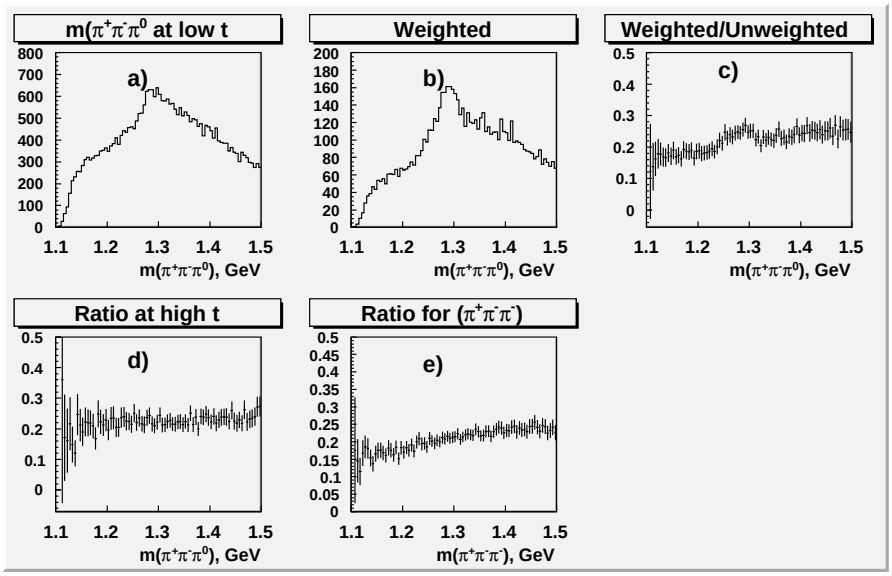

Figure 6: The three-pion mass spectra for $0.970 < m(\pi^+\pi^-) < 1.000$: a) $m(\pi^+\pi^-\pi^0)$ spectrum at low $|t'|$; b) like the previous one but weighted; c) ratio of two previous distributions, weighted/unweighted; d) ratio of weighted to unweighted mass spectra for $(\pi^+\pi^-\pi^0)$ system at high $|t'|$; e) ratio of weighted to unweighted mass spectra for $(\pi^+\pi^-\pi^-)$ system at low $|t'|$.

its mass is close to the $f_1(1285)$ mass. The effect, which arises from the application of the angular weight W to the same event sample, is demonstrated in Fig.6b and 6c. A peak at the same mass region is observed in the ratio of weighted distribution to the unweighted one. A similar procedure was applied for two another samples, namely to the event sample which was selected at large $|t|$ and to the $(\pi^+\pi^-\pi^-)$ system at low $|t|$. The ratios of the weighted to unweighted distributions are shown in Fig.6d and 6e, respectively. No signal is observed.

It is also possible to subdivide the event sample at low $|t|$ into bins on the three-pion mass and look for the mass spectrum of the two-pion system in individual bins. The mass bin width of $10 MeV$ was chosen and the $m(\pi^+\pi^-\pi^0)$ interval from 1200 to 1350 MeV was subdivided to 15 bins. The resulting spectrum for the mass bin $(1280, 1290)\, MeV$ is shown in Fig.7. The $\omega \to \pi^+\pi^-$

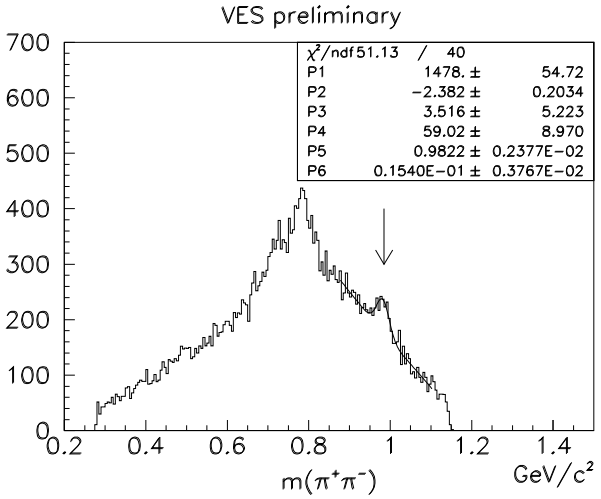

Figure 7: $m(\pi^+\pi^-)$, selected combinations with $m(\pi^+\pi^-\pi^0)$ in the mass interval (1.280,1.290) GeV/c^2.

decay is seen, and another peak with mass close to 985 MeV. A fit by a sum of the Gaussian function for signal and a background term was performed in the mass interval from 880 to 1100 MeV. The product of three-particle phase space by a quadratic function with free coefficients was chosen as the background term. The fit at this bin yields the gaussian mean of $m = 983 \pm 3\ MeV$ and the gaussian $\sigma = 18 \pm 4\ MeV$. The fit $\chi^2/ND = 39.8/40$ and the statistical significance of the gaussial signal is $6.4\,\sigma$.

Similar fitting procedure was applied to all mass bins mentioned above with parameters as determined from the central bin. The result for the number of signal events in all mass bins is presented in Fig.8. The total number of events from decay $f_1 \to \pi^+\pi^-\pi^0$ in all bins is 1572 ± 227. This number of events, taken together with the number of events in $f_1 \to \eta\pi^+\pi^-$ channel, gives the relative branching ratio. The ratio of the detection efficiencies, $R = \varepsilon(\pi^+\pi^-\pi^0)/\varepsilon(\eta\pi^+\pi^-)$ was estimated from a Monte-Carlo simulation and taken into account, $R = 0.95 \pm 0.05$.

The measured dependence of the observed signal on the $m(\pi^+\pi^-\pi^0)$ can be fitted by a Breight-Wigner function, and the result of this fit is shown in

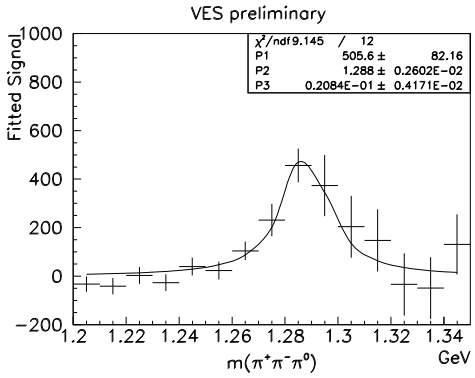

Figure 8: $m(\pi^+\pi^-\pi^0)$; fitted number of signal events as a function of $m(\pi^+\pi^-\pi^0)$.

Fig.8. The fitted peak has $m = 1288.3 \pm 2.6 MeV$ and the width $\Gamma = 21 \pm 4 MeV$, which are in good agreement with the table values.

We tested a presence of a similar signal in charge mode by means of a similar procedure, i.e. by subdivision of the event sample into bins on the $m(\pi^+\pi^-\pi^-)$ and looking for the $m(\pi^+\pi^-)$ spectrum in individual bins. No signal is observed in the vicinity of the $f_1(1285)$.

3 Discussion and conclusions

One can see that the signal at $m(\pi^+\pi^-) \sim 985\, MeV/c^2$ is associated with the peak at $m(\pi^+\pi^-\pi^0) = m(f_1(1285))$ having $J^{PC} = 1^{++}$.

All elements of the obseved pattern fit well with predictions based on the mechanism suggested by Achasov and collaborators in 1979 [3].

The relative branching ratio is determined from the observed number of events in the $\eta\pi^+\pi^-$ and $\pi^+\pi^-\pi^0$ channels. The experimental efficiencies for both reactions are very similar. We estimate

$$\frac{BR(f_1 \to \pi^+\pi^-\pi^0 (0.96 < m(\pi^+\pi^-) < 1.01))}{BR(f_1 \to \eta\pi^+\pi^-) \cdot BR(\eta \to \gamma\gamma)} = (1.41 \pm 0.21 \pm 0.42)\%;$$

here statistical and systematic errors are indicated. This relative branching ratio is consistent with estimation made by Achasov et al. [5].

With PDG values for $BR(f_1 \to \eta\pi\pi) = 0.52 \pm 0.16$ and $BR(\eta \to \gamma\gamma) = 0.3939 \pm 0.0024$ [8, 12] it leads to
$BR(f_1 \to \pi^+\pi^-\pi^0(0.96 < m(\pi^+\pi^-) < 1.01)) = (0.19 \pm 0.09)\%$.

4 Acknowledgements

This work is supported in part by the Russian Foundation of Basic Research grants RFBR 07-02-00631 and by Presidential grant NSh 5911.2006.2.

References

1. S. Coleman and S. L. Glashow, Phys. Rev. Lett.6 (1961) 423; Phys. Rev.134 (1964) B671;
2. S. Weinberg, Phys. Rev. D 11 (1975) 3583;
3. N.N.Achasov, S.A.Devyanin, G.N.Shestakov, Phys. Lett. B88 (1979) 367;
4. N.N.Achasov, G.N.Shestakov, Phys.Rev.D70 (2004) 074015, hep-ph/0312214 ;
5. N.N.Achasov, S.A.Devyanin, G.N.Shestakov, Yad. Fiz. 33 (1981) 1337; Sov.J.Nucl. Phys. 33 (1981) 715;
6. Jia-Jun Wu, Qiang Zhao and B.S.Zou, hep-ph 0704.3652 ;
7. C.Hanhart, B.Kubis, J.R.Pelaez, hep-ph 0707.0262;
8. Particle Data Group, S.Eidelman, et.al., Phys.Lett. B592 (2004) 540;
9. S.I.Bityukov et al., Phys.Lett. B268 (1991) 137;
10. V.Dorofeev et al., Phys.Lett. B651 (2007) 22; D.Amelin et al., Phys.At.Nucl. 68 (2005) 372;
11. Yu.Gouz, et.al., VES collaboration, AIP Conf.Proceedings 272 (1993) 572;
12. Particle Data Group, W.-M.Yao et al., J.Phys.G33 (2006) 542 and 2007 partial update for edition 2008;

Frascati Physics Series Vol. XLVI (2007), pp. 627–633
HADRON07: XII Int. Conf. on Hadron Spectroscopy – Frascati, October 8-13, 2007
Light Meson Spectroscopy

INVESTIGATION OF NARROW RESONANCE AT 1545 MeV IN THE SYSTEM OF TWO K_S- MESONS

E.A. Fadeeva
I.A. Erofeev, O.N. Erofeeva, V.K. Grigor'ev, Yu.V. Katinov,
V.I. Lisin, V.N. Luzin, V.N. Nozdrachev, Yu.P. Shkurenko,
V.V. Sokolovsky and V.V. Vladimirsky
Institute for Theoretical and Experimental Physics, Moscow, Russia

Abstract

Results are presented that were obtained by studying narrow resonance of mass about 1545 MeV. The system of two K_S-mesons has been analyzed in the mass interval 1400–1700 MeV. The experimental data subjected to the analysis come from 6-m spectrometer created at the Institute of Theoretical and Experimental Physics (ITEP, Moscow) and irradiated with a 40-GeV beam of negatively charged pions from U-70 accelerator at the Institute for High Energy Physics (IHEP, Serpukhov). The use of a neutral trigger in the experiment being reported made it possible to suppress both charged particles and photons. The statistical confidence of the observer maximum is better than 6 standard deviation. The mass and width of the resonance feature are M=1545.1±3.1 MeV and Γ=10±3 MeV, respectively. Seeing its very narrow width this resonance is likely to be cryptoexotics (see [1)], [2)] for details)

1 Experimental setup

The experimental data employed in the present analysis were obtained by using the ITEP 6-m spectrometer. A detailed description of the spectrometer was given elsewhere [3]. The spectrometer records, with a high efficiency, K_S-mesons travelling in the forward direction and decaying to two charged pions. A large volume covered by a magnetic field and filled with detectors makes it possible to identify K_S-mesons reliably and to measure the effective mass of the K_SK_S-system to a high precision. The data analyzed in the present study come from exposures where we employed liquid-hydrogen target. The K_SK_S-system recorded under experimental conditions of the 6-m spectrometer is produced in the following two reactions on a hydrogen target:

$$\pi^- p \to K_S K_S n, \tag{1}$$

$$\pi^- p \to K_S K_S + (n + m\pi^0, p + \pi^-, ...). \tag{2}$$

Reaction (eq.1) is selected with the aid of trigger device based on veto counters surrounding the liquid-hydrogen target. The counters formed a double protective layer around the target. In order to suppress not only charged particles but also photons lead converters of thickness about two radiation length are arranged between the counters. Because of nonideal operation of trigger , some fraction of events of the reaction (eq.2) is recorded in the facility used. The majority of such events can easily be omitted by analyzing the missing mass of the system of two K_S-mesons. However, in this study the events from both reaction (eq.1) and (eq.2) were taken into account, due to resonance structure to be discussed is produced in both process. About 40,000 events of these two reactions were accumulated.

We identify K_S-mesons by their decays to a $\pi^+\pi^-$ pair. The detecting efficiency is about 45% for the system of the two K_S-mesons in the mass region around 1545 MeV. It depends on the K_S-meson momenta. The precision of the measurement of the effective mass of the K_SK_S-system is better than 3 MeV in mass region around 1545 MeV.

2 Kinematical variables

The effective mass M_{KK} of a pair of two K_S-mesons, the missing mass squared MM^2, the 4-momentum transfer $-t$ from the beam to the system being studied,

the cosine $cos\theta_{GJ}$ of the Gottfried-Jackson angle, and the Treiman-Yang angle ϕ_{TY} are kinematical variables used in analyzing the K_SK_S system. The angles are calculated in the rest frame of the K_S-meson pair, and the beam-axis direction in this reference frame is taken for the polar axis. The plane from which the Treiman-Yang angle is reckoned is spanned by the momenta of a beam particle and a target proton.

3 Resonance $X(1545)$

The Figure 1 shows the mass spectrum of the K_SK_S-system from 1460 to 1640 MeV with the bin width being 6 MeV. The resonance feature manifests itself as a minimum (fig.1a) and as a maximum (fig.1b) in the vicinity of 1545 MeV.

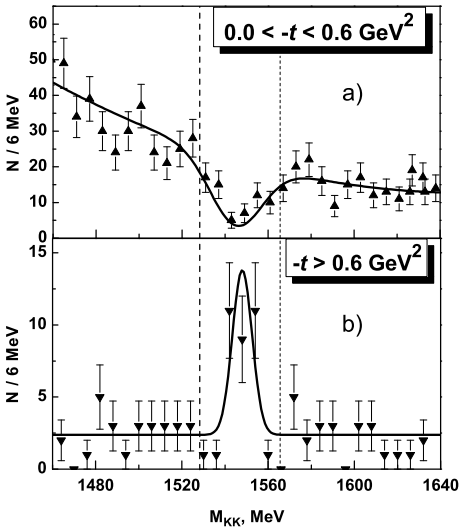

Figure 1: *Effective-mass spectrum of two K_S-mesons with following experimental cuts on transferred momentum: a) 0.0 < -t < 0.6 GeV^2, b) -t > 0.6 GeV^2. The curves are the results of a fit by the maximum-likelihood method.*

In comparison with our previous paper [4] now we observe resonance phenomena $X(1545)$ as a minimum in the range $0.0 < -t < 0.6$ GeV^2 of transferred momentum using special experimental cuts. Special experimental cuts were applied on: the distance between trajectories of two K_S-mesons at the point of their closest approach, number of points on each π-meson track, the effective mass of particles forming a vee etc.

3.1 Angular distributions

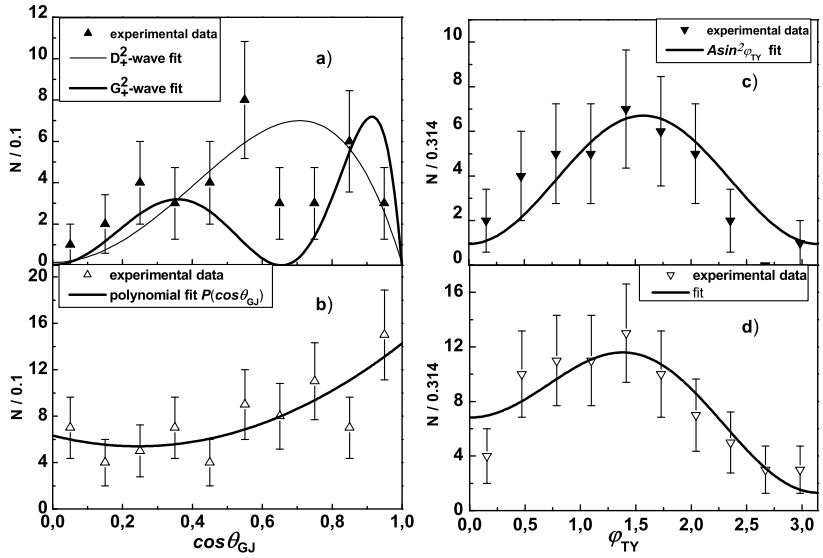

Figure 2: *Cosine of Gottried-Jackson angle: a) for resonance region, 1535 < M_{KK} < 1555 MeV. The thin curve is the result of fitting by D^2_+-wave, the solid curve represents the result of fitting by G^2_+-wave; b) for background region, 1440 < M_{KK} < 1535 and 1555 < M_{KK} < 1640 MeV; and Treiman-Yang angle: c) for resonance region, 1535 < M_{KK} < 1555 MeV; d) for background region, 1440 < M_{KK} < 1535 and 1555 < M_{KK} < 1640 MeV.*

The Figure 2 shows the cosine of Gottried-Jackson angle (fig.2a, fig.2b)

and Treiman-Yang angle (fig.2c, fig.2d) for resonance region ($1535 < M_{KK} < 1555$ MeV) and background region ($1440 < M_{KK} < 1535$, $1555 < M_{KK} < 1640$ MeV) respectively.

3.2 Maximum-likelihood method

In order to determine the parameters of the observed resonance feature and its statistical significance, the experimental data were fitted by the Maximum-likelihood method in the K_SK_S-mass interval 1400-1700 MeV. There are 189 events in this interval. Describing the experimental data, we used the probability-density function $F(P;\Omega)$, where P is the set of the parameters (the amplitude, the mass M, the width Γ appearing in the relativistic Breit-Wigner function and the coefficients of the squared amplitudes of the angular distributions). Elements of the phase space Ω are effective mass of two K_S-mesons, the cosine of the Gottfried-Jackson angle $cos\theta_{GJ}$, the Treiman-Yang angle ϕ_{TY}. The mass dependencies for background and resonance are specified by a second-degree polynomial and a relativistic Breit-Wigner function respectively. In order to obtain the most probable values of the parameters we minimized the functional:

$$L = \int\limits_{\Omega} \epsilon(\Omega) F(P;\Omega) d\Omega - \sum_{i=1}^{N} \ln F(P;\Omega_i). \tag{3}$$

where $\epsilon(\Omega)$ is the event-detection recording, N being the number of events and $L = \prod_{i=1}^{N} F(P;\Omega_i)$ N being the number of events. To compare the probabilities of experimental-data description with different parameter set, we calculated χ^2 by the formula:

$$\chi^2 = -2 \ln L + const. \tag{4}$$

The constant was chosen in such a way that χ^2 value obtained without inclusion of the Breit-Wigner function was equal to 100. The angular dependencies of the background are describing using only the S, D_0 and D_+-waves. The contributions from the other waves are negligibly small. The minimization showed that only D_+ and G_+-waves contributed to the χ^2 value by at least 20 units less than did any other waves. The results of five variants of minimization are presented in the table, where the following data are given: the number of events from each wave of the background and resonance, the central values of mass and width. In the last column the χ^2 values with regard to the number of degrees of freedom N_{df} are given.

Table 1: *Different results of minimization for X(1545).*

	Background waves, N_{events}			Resonance waves, N_{events}				Resonance parameters, MeV		χ^2-
	S	D_0	D_+	S	D_0	D_+	G_+	$M \pm \Delta M$	$\Gamma \pm \Delta\Gamma$	N_{df}
1	62	49	82	–	–	–	–	–	–	100
2	51	38	70	12	8	14	–	1544.6±3.5	10.4 ±3.3	77
3	60	47	51	–	–	37	–	1544.7±3.0	10.3 ±3.0	56
4	66	37	58	–	–	–	32	1545.8±3.0	10.0 ±3.0	60
5	68	39	47	–	–	23	16	1545.1±3.1	11.0 ±3.0	52

It follows from the table that statistical significance of observation of the $X(1545)$ resonance phenomena with the indicated parameters is better than six standard deviation.

The χ^2 values obtained on data fitting by the D_+-wave (third variant of minimization) and G_+-wave (forth variant) are so close to each other so we cannot give preference to either the D_+- or the G_+-wave

4 Conclusion

Let us summarize results. Strong evidence of the existence of a narrow resonance in the K_SK_S-system has been obtained. The statistical significance is better than six standard deviations. The distinguishing features of this resonance are the following— it has a very narrow width and unusual mechanism of formation.

The parameters of the X (1545) resonance are: mass M= 1545.1 ±3.1 ± 3.0 MeV and width Γ= 10.0 ± 3.0 MeV. Number of events in the resonance region is 44 ± 5. The spin-parity of this resonance is $J^{PC} = 2^{++}$ or 4^{++}. The product of the cross section for $X(1450)$ formation and the relevant branching ratio $\sigma Br(K_SK_S)$ is estimated at about 6 ± 4(stat.) ± 4(syst.) nb.

In addition to previous paper [4)] we observe $X(1545)$ in following range of transferred momentum 0.0 < -t < 0.6 GeV^2 as a minimum in the vicinity of 1545 MeV.

References

1. L.G. Landsberg, *Yad. Phys.* **57**, 47 (1994); *Phys. Atom. Nucl.* **57**, 42 (1994).

2. L.G. Landsberg, *Usp. Phys. Nauk* **164**, 1129 (1994); *Phys. Uspekhi* **37**, 1043 (1994).

3. V.N. Nozdrachev *et al*, The resonance structures of $K_S K_S$ and $\Lambda\bar{\Lambda}$ spectrum at MIS ITEP, in: *Hadron Spectroscopy: Ninth International Conference* (edited by D. Amelin and A.M. Zaitsev, Protvino, Russia, 2001), **CP619**, 155 (Melville, New York: AIP Conf. Proceedings, 2002).

4. V. V. Vladimirsky *et al*, Pis'ma Zh. E ksp. Teor. Fiz. **72**, 698 (2000); JETP Lett. **72**, 486 (2000).

Frascati Physics Series Vol. XLVI (2007), pp. 635–642
HADRON07: XII Int. Conf. on Hadron Spectroscopy – Frascati, October 8-13, 2007
Light Meson Spectroscopy

THE WA3 DATA AND THE TWO $K_1(1270)$ RESONANCES

L. S. Geng and E. Oset
Departamento de Fisica Teorica e IFIC,
Centro Mixto Universidad de Valencia, E-46071 Valencia, Spain
L. Roca and J. A. Oller
Departamento de Fisica. Universidad de Murcia. E-30071 Murcia. Spain.

Abstract

Recent studies based on unitary chiral perturbation theory (UχPT) found that the low-lying axial vector mesons can be dynamically generated due to the interaction of the pseudoscalar octet of the pion and the vector nonet of the rho. In particular, two poles in the second Riemann sheet have been associated to the nominal $K_1(1270)$ resonance. In this talk, we present a recent analysis of the WA3 data on $K^-p \to K^-\pi^+\pi^-p$ at 63 GeV using the UχPT amplitudes, and show that it is in favor of the existence of two $K_1(1270)$'s [Phys. Rev. D 75, 014017 (2007)].

1 Introduction

The unitary extension of chiral perturbation theory, UχPT, has been successfully applied to study many meson-baryon and meson-meson interactions. More

recently, it has been used to study the lowest axial vector mesons $b_1(1235)$, $h_1(1170)$, $h_1(1380)$, $a_1(1260)$, $f_1(1285)$, $K_1(1270)$ and $K_1(1400)$ [2, 3]. Both works generate most of the low-lying axial vector mesons dynamically. However, there is a surprising discovery in Ref. [3], i.e., two poles are found in the second Riemann sheet in the $S = 1$ and $I = 1/2$ channel and both are attributed to the $K_1(1270)$.

Although the $K_1(1270)$ has been observed in various reactions, the most conclusive and high-statistics data of the $K_1(1270)$ come from the WA3 experiment at CERN that accumulated data on the reaction $K^- p \to K^- \pi^+ \pi^- p$ at 63 GeV. These data were analyzed by the ACCMOR Collaboration [4]. As will be shown in this paper, the two-peak structure, with a peak at lower energy depending drastically on the reaction channel investigated, can be easily explained in our model with two poles for the $K_1(1270)$ plus the $K_1(1400)$. With only one pole, as has been noted long time ago [4, 5], there is always a discrepancy for the peak positions observed in the $K^*\pi$ and ρK invariant mass distributions.

2 Chiral unitary model and the two $K_1(1270)$'s

In the following, we briefly describe the chiral unitary approach, while detailed formalism can be found in Refs. [1, 3]. In the Bethe-Salpeter formulation of the unitary chiral perturbation theory [6], one has the following unitarized amplitude:

$$T = [1 + V\hat{G}]^{-1}(-V)\,\vec{\epsilon}\cdot\vec{\epsilon}', \tag{1}$$

where $\hat{G} = (1 + \frac{1}{3}\frac{q_l^2}{M_l^2})G$ is a diagonal matrix with the $l-$th element, G_l, being the two meson loop function containing a vector and a pseudoscalar meson:

$$G_l(\sqrt{s}) = i \int \frac{d^4q}{(2\pi)^4} \frac{1}{(P-q)^2 - M_l^2 + i\epsilon} \frac{1}{q^2 - m_l^2 + i\epsilon}, \tag{2}$$

with P the total incident momentum, which in the center of mass frame is $(\sqrt{s}, 0, 0, 0)$. The loop function G_l can be regularized either by a cutoff or by dimensional regularization. In the former case, one has cutoff values, whereas in the latter, one has subtraction constants as free parameters, which have to be fitted to the data.

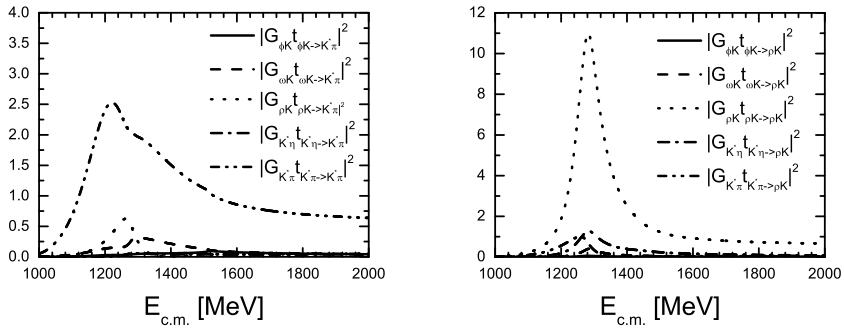

Figure 1: The modulus squared of the coupled channel amplitudes multiplied by the corresponding loop functions in the $S = 1$ and $I = \frac{1}{2}$ channel.

The tree level amplitudes are calculated using the following interaction Lagrangian [7]:

$$\mathcal{L}_I = -\frac{1}{4}\mathrm{Tr}\left\{\left(\nabla_\mu V_\nu - \nabla_\nu V_\mu\right)\left(\nabla^\mu V^\nu - \nabla^\nu V^\mu\right)\right\}, \tag{3}$$

where Tr means SU(3) trace and ∇_μ is the covariant derivative defined as

$$\nabla_\mu V_\nu = \partial_\mu V_\nu + [\Gamma_\mu, V_\nu], \tag{4}$$

where $[,]$ stands for commutator and Γ_μ is the vector current $\Gamma_\mu = \frac{1}{2}(u^\dagger \partial_\mu u + u\partial_\mu u^\dagger)$ with $u^2 = U = e^{i\frac{\sqrt{2}}{f}P}$. In the above equations f is the pion decay constant in the chiral limit and P and V are the SU(3) matrices containing the pseudoscalar octet of the pion and the vector nonet of the rho.

Fig. 1 shows the modulus squared of the $S = 1$, $I = \frac{1}{2}$ amplitudes multiplied by the corresponding loop functions obtained with $f = 115$ MeV, $a(\mu) = -1.85$ and $\mu = 900$ MeV. The pole positions and corresponding widths obtained with this set of parameters are shown in Table 1. From Fig. 1, the two poles are clearly seen: the higher pole manifests itself as one relatively narrower resonance around 1.28 GeV and the lower pole as a broader resonance at ~ 1.20 GeV.

The effective couplings for the coupled channels ϕK, ωK, ρK, $K^*\eta$ and $K^*\pi$, calculated from the residues of the amplitudes at the complex pole po-

Table 1: Effective couplings of the two poles of the $K_1(1270)$ to the five channels: ϕK, ωK, ρK, $K^*\eta$ and $K^*\pi$. All the units are in MeV.

$\sqrt{s_p}$	$1195 - i123$		$1284 - i73$	
	g_i	$\|g_i\|$	g_i	$\|g_i\|$
ϕK	$2096 - i1208$	2420	$1166 - i774$	1399
ωK	$-2046 + i821$	2205	$-1051 + i620$	1220
ρK	$-1671 + i1599$	2313	$4804 + i395$	4821
$K^*\eta$	$72 + i197$	210	$3486 - i536$	3526
$K^*\pi$	$4747 - i2874$	5550	$769 - i1171$	1401

sitions, are tabulated in Table 1 for both the lower pole and the higher pole, respectively. It is clearly seen that the lower pole couples dominantly to the $K^*\pi$ channel while the higher pole couples more strongly to the ρK channel. If different reaction mechanisms favor one or the other channel, they will see different shapes for the resonance. More importantly, it is to be noted that not only the two poles couple to different channels with different strengths, but also they manifest themselves in different final states. In other words, in the ρK final states, one favors a narrower resonance around 1.28 GeV, while in the $K^*\pi$ final states, one would favor a broader resonance at a smaller invariant mass.

3 Studying the WA3 data with the UχPT amplitudes

The reaction $K^-p \to K^-\pi^+\pi^-p$ can be analyzed by the isobar model as $K^-p \to (\bar{K}^{*0}\pi^- \text{ or } \rho^0K^-)p \to K^-\pi^+\pi^-p$. Therefore, one can construct the following amplitudes to simulate this process. Assuming $I = \frac{1}{2}$ dominance for $\bar{K}^{*0}\pi^-$ and ρ^0K^- as suggested by the experiment one has

$$\begin{aligned} T_{K^*\pi} \equiv T_{\bar{K}^{*0}\pi^-} &= \sqrt{\frac{2}{3}}a + \sqrt{\frac{2}{3}}aG_{K^*\pi}t_{K^*\pi\to K^*\pi} + \sqrt{\frac{2}{3}}bG_{\rho K}t_{\rho K\to K^*\pi}, \\ T_{\rho K} \equiv T_{\rho^0K^-} &= -\sqrt{\frac{1}{3}}b - \sqrt{\frac{1}{3}}aG_{K^*\pi}t_{K^*\pi\to\rho K} - \sqrt{\frac{1}{3}}bG_{\rho K}t_{\rho K\to\rho K}, \end{aligned} \quad (5)$$

where t_{ij} are the coupled channel amplitudes obtained in Section 2 and the Clebsch-Gordan coefficient $\sqrt{\frac{2}{3}}(-\sqrt{\frac{1}{3}})$ accounts for projecting the $I = \frac{1}{2}$ $K^*\pi$ (ρK) state into $\bar{K}^{*0}\pi^-(\rho^0 K^-)$. The coefficients a and b are complex couplings.

To contrast our model with data, it is necessary to take into account the existence of the $K_1(1400)$, which is not dynamically generated in our approach. Therefore, we add to the amplitudes in Eq. (5) an explicit contribution of the $K_1(1400)$

$$\begin{aligned} T_{K^*\pi} &\rightarrow T_{K^*\pi} + \frac{g_{K^*\pi}}{s - M^2 + iM\Gamma(s)}, \\ T_{\rho K} &\rightarrow T_{\rho K} + \frac{g_{\rho K}}{s - M^2 + iM\Gamma(s)}, \end{aligned} \tag{6}$$

where $g_{K*\pi}$ and $g_{\rho K}$ are complex couplings, and M and $\Gamma(s)$ are the mass and width of the $K_1(1400)$ with the s-wave width given by

$$\Gamma(s) = \Gamma_0 \frac{q(s)}{q_{\rm on}} \Theta(\sqrt{s} - M_{K^*} - M_\pi). \tag{7}$$

$q(s)$ and $q_{\rm on}$ are calculated by

$$q(s) = \frac{\lambda^{1/2}(s, M_\pi^2, M_{K^*}^2)}{2\sqrt{s}} \quad \text{and} \quad q_{\rm on} = \frac{\lambda^{1/2}(M^2, M_\pi^2, M_{K^*}^2)}{2M}. \tag{8}$$

In our model, Eq. (6), we have the following adjustable parameters: a, b, $g_{K^*\pi}$, $g_{\rho K}$, M and Γ_0. In principle, f and $a(\mu)$ can also be taken as free parameters. One can then fix these parameters by fitting the WA3 data (see Ref. [1)] for details). According to Ref. [8)], for an s-wave resonance, the theoretical differential cross section can be calculated by

$$\frac{d\sigma}{dM} = c|T|^2 q \tag{9}$$

where M is the invariant mass of the $K^*\pi$ or ρK systems, c is a normalization constant, T is the amplitude specified above for the $K^*\pi$ or ρK channels and q is the center of mass three-momentum of $K^*\pi$ or ρK. We have taken c to be 1, or in other words, it has been absorbed into the coupling constants a, b, $g_{K^*\pi}$ and $g_{\rho K}$. The theoretical invariant mass distributions calculated with Eq. (9) are shown in Fig. 2 in comparison with the WA3 data [4)].

From Fig. 2, it is clearly seen that our model can fit the data around the peaks very well. In Fig. 2, the dashed and dotted lines are the separate

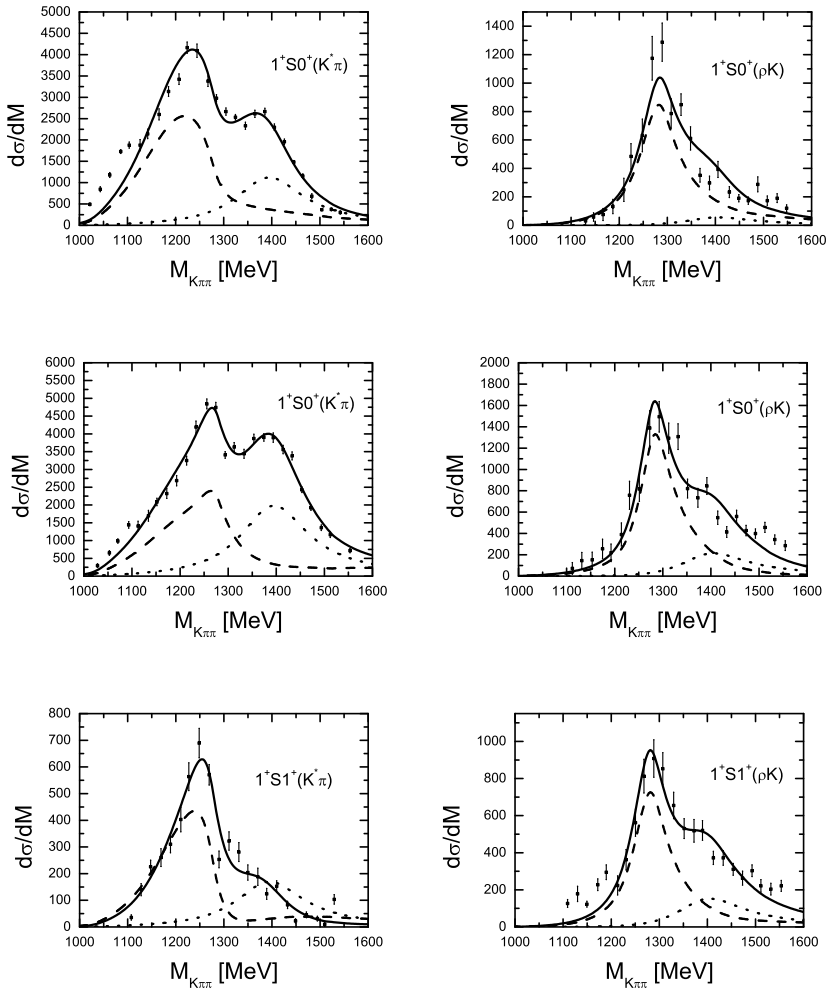

Figure 2: $K^*\pi$ and ρK invariant mass distributions. The data are from the WA3 reaction $K^-p \to K^-\pi^+\pi^-p$ at 63 GeV [4]. Data in the upper panels are for $0 \leq |t'| \leq 0.05$ GeV^2 and those in the middle and bottom panels for $0.05 \leq |t'| \leq 0.7$ GeV^2, where t' is the four momentum transfer squared to the recoiling proton. The data are further grouped by $J^P LM^\eta$ followed by the isobar and odd particle. J is the total angular momentum, P the parity, L the orbital angular momentum of the odd particle. M^η denotes the magnetic substate of the $K\pi\pi$ system and the naturality of the exchange.

contributions of the $K_1(1270)$ and the $K_1(1400)$. One can easily see that the $K_1(1400)$ decays dominantly to $K^*\pi$, which is consistent with our present understanding of this resonance.

It should be mentioned that in our model the lower peak observed in the invariant mass distribution of the $K^*\pi$ channel is due to the contribution of the two poles of the $K_1(1270)$. This is very different from the traditional interpretation. For example, the lower peak observed in the $K^*\pi$ invariant mass distributions of $K^\pm p \to K^\pm\pi^+\pi^- p$ at 13 GeV was interpreted as a pure Gaussian background by Carnegie et al. [9], which has a shape similar to the contribution of the $K_1(1270)$ as shown in Fig. 2. On the other hand, the K-Matrix approach was adopted to analyze the WA3 data [4] and the SLAC data [10] . In this latter approach, the lower peak mostly comes from the so-called Deck background, which after unitarization, also has a shape of resonance. As we mentioned in the introduction, even in the original WA3 paper [4], it was noted that their model failed to describe the $1^+S1^+(K^*\pi)$ data, in the notation $J^P LM^\eta$ with η the naturality of the exchange [4]. The predicted peak is 20 MeV higher than the data. If the fit were done only to the $K^*\pi$ data, the agreement was much better but then the predicted $K_1(1270)$ would be lower by 35 MeV than that obtained when other channels were also considered in the fit.

It is worth stressing that the $K_1(1270)$ peak seen in the upper-left panel of Fig. 2 is significantly broader than that in the upper-right panel. Furthermore the peak positions are also different in the two cases (1240 MeV and 1280 MeV respectively). Both features have a straightforward interpretation in our theoretical description since the first one is dominated by the low-energy (broader) $K_1(1270)$ state, while the second one is dominated by the higher-energy (narrower) $K_1(1270)$ state.

4 Summary and conclusion

Studies based on unitary chiral perturbation theory obtain two poles in the $I = 1/2$, $S = 1$, vector-pseudoscalar scattering amplitudes which can be assigned to two $K_1(1270)$ resonances. One pole is at ~ 1200 MeV with a width of ~ 250 MeV and the other is at ~ 1280 MeV with a width of ~ 150 MeV. The lower pole couples more to the $K^*\pi$ channel whereas the higher pole couples dominantly to the ρK channel. Different reaction mechanisms may prefer dif-

ferent channels and thus this explains the different invariant mass distributions seen in various experiments.

We have analyzed the WA3 data on the $K^- p \to K^- \pi^+ \pi^- p$ reaction since it is the most conclusive and high-statistics experiment quoted in the PDG on the $K_1(1270)$ resonance. Our model obtains a good description of the WA3 data both for the $K^*\pi$ and ρK final state channels. In our model, the peak in the $K\pi\pi$ mass distribution around the 1270 MeV region is a superposition of the two poles, but in the $K^*\pi$ channel the lower pole dominates and in the ρK channel the higher pole gives the biggest contribution.

5 Acknowledgments

This work is partly supported by DGICYT Contract No. BFM2003-00856, FPA2004-03470, the Generalitat Valenciana, and the E.U. FLAVIAnet network Contract No. HPRN-CT-2002-00311. This research is part of the EU Integrated Infrastructure Initiative Hadron Physics Project under Contract No. RII3-CT-2004-506078.

References

1. L. S. Geng, E. Oset, L. Roca and J. A. Oller, Phys. Rev. D **75**, 014017 (2007).
2. M. F. M. Lutz and E. E. Kolomeitsev, Nucl. Phys. A **730**, 392 (2004).
3. L. Roca, E. Oset and J. Singh, Phys. Rev. D **72**, 014002 (2005).
4. C. Daum *et al.* [ACCMOR Collaboration], Nucl. Phys. B **187**, 1 (1981).
5. M. G. Bowler, J. Phys. G **3**, 775 (1977).
6. J. A. Oller and E. Oset, Nucl. Phys. A **620**, 438 (1997) [Erratum-ibid. A **652**, 407 (1999)].
7. M. C. Birse, Z. Phys. A **355**, 231 (1996).
8. S. M. Flatte, Phys. Lett. B **63**, 224 (1976).
9. R. K. Carnegie *et al.*, Nucl. Phys. B **127**, 509 (1977).
10. G. W. Brandenburg *et al.*, Phys. Rev. Lett. **36**, 703 (1976).

Frascati Physics Series Vol. XLVI (2007), pp. 643–650
HADRON07: XII Int. Conf. on Hadron Spectroscopy – Frascati, October 8-13, 2007
Light Meson Spectroscopy

ON THE EXISTENCE OF LIGHT-SCALAR MESONS $\kappa(800)$ and $\kappa'(1150)$: THE $\widetilde{U}(12)$ SCHEME AND BES II DATA

Kenji Yamada and Tomohito Maeda
Department of Engineering Science, Junior College Funabashi Campus, Nihon University, Funabashi 274-8501, Japan

Abstract

We present that there should exist a light strange-scalar meson κ', in addition to the $\kappa(800)$, which has a mass around 1.1-1.2 GeV, a rather narrow width, and couples strongly to $\kappa(800)\sigma(600)$ ($K\pi\pi\pi$) but weakly to $K\pi$, based upon the $\widetilde{U}(12)$-classification scheme of hadrons and BES II data on $J/\psi \to \bar{K}^*(892)^0 K^+\pi^-$ decay.

1 Introduction

Recently, the existence of the light-scalar mesons, $\sigma(600)$ and $\kappa(800)$, has been confirmed by showing the presence of respective poles in the $\pi\pi$ [1, 2] and $K\pi$ [2, 3] scattering amplitudes, in addition to results of Breit-Wigner fits to D- and J/ψ-decay data, respectively, from the E791 [4] and BES [5, 6] collaborations. However, the nature of these resonances, together with the

$f_0(980)$ and $a_0(980)$, has been a long-standing problem in controversy, where it is not obvious how these light-scalar mesons are understood in terms of quarks and gluons in QCD.

Here we focus on the strange scalar mesons and discuss the existence of an extra κ' meson, in addition to the normal $\kappa(800)$, and their strong decay properties.

2 Existence of the extra κ' meson

2.1 The $\widetilde{U}(12)$-classification scheme of hadrons

The $\widetilde{U}(12)$-classification scheme of hadrons, [7, 8] which has a manifestly covariant framework of $\widetilde{U}(12)_{SF} \times O(3,1)_L$, generalized covariantly from nonrelativistic $SU(6)_{SF} \times O(3)_L$ by boosts, separating the spin and space degrees of freedom, gives covariant quark representations for composite hadrons with definite Lorentz and chiral transformation properties. The $\widetilde{U}(12)$-classification scheme has a "static" unitary $U(12)_{SF}$ spin-flavor symmetry in the rest frame of hadrons, embedded in the covariant $\widetilde{U}(12)$-representation space, where $\widetilde{U}(12)$ has as its subgroups the pseudounitary homogeneous Lorentz group for Dirac spinors and unitary symmetry group for light-quark flavors,

$$\widetilde{U}(12)_{SF} \supset \widetilde{U}(4)_D \times U(3)_F. \tag{1}$$

Since

$$U(12)_{SF} \supset U(4)_D \times U(3)_F, \tag{2a}$$

$$U(4)_D \supset SU(2)_\rho \times SU(2)_\sigma, \tag{2b}$$

the static $U(12)_{SF}$ symmetry includes both the nonrelativistic spin-flavor $SU(6)_{SF}$ and chiral $U(3)_L \times U(3)_R$ symmetry[1] as

$$U(12)_{SF} \supset SU(6)_{SF} \times SU(2)_\rho, \tag{3a}$$

$$U(12)_{SF} \supset U(3)_L \times U(3)_R \times SU(2)_\sigma, \tag{3b}$$

[1]Hadron states are classified, aside from flavors, by the quantum numbers ρ, S, L, J, P, where ρ is the net quark ρ-spin concerning $SU(2)_\rho$, S the ordinary net quark σ-spin, L the total quark orbital angular momentum, and J and P the total spin and parity of hadrons.

where $SU(2)_\rho$ and $SU(2)_\sigma$ are the Pauli-spin groups concerning the boosting and intrinsic spin rotation, respectively, of constituent quarks, being connected with decomposition of Dirac γ-matrices, $\gamma = \rho \times \sigma$. This implies that the $\widetilde{U}(12)$-classification scheme is able to incorporate effectively, according to dynamical consequences of QCD, the effects of chiral symmetry and its spontaneous breaking, essential for understanding of properties of the low-lying hadrons, into what is called a constituent quark model.

In the $\widetilde{U}(12)$-classification scheme there are two light-scalar meson multiplets, normal $S^{(N)}$ and extra $S^{(E)}$ with $J^{PC} = 0^{++}$ and 0^{+-}, respectively, in the ground level ($L = 0$). These N- and E-scalar multiplets are the chiral partners, respectively, of the N- and E-pseudoscalar multiplets and they form linear representations of the $U(3)_L \times U(3)_R$ chiral symmetry. Concerning the strange scalar mesons, now we have two κ mesons, $\kappa^{(N)}(0^{++})$ and $\kappa^{(E)}(0^{+-})$. Note that the observed $\kappa(800)$ and missing κ' are generally mixtures of them. [9)]

2.2 The BES II data

The $K^+\pi^-$ mass spectrum in $J/\psi \to \bar{K}^*(892)^0 K^+\pi^-$ decay observed by the BES II experiment [6)] is shown in fig.1 where there seems to be a visible bump structure at 1.1-1.2 GeV. If this structure is attributed to the existence of a new $K\pi$ resonance, its spin-parity will likely be 0^+ or 1^-, since higher spins are unfavorable for such a low-mass state, and also its width is supposed to be narrow, judging from the data structure.

We hereafter refer to the strange scalar meson mentioned above as the $\kappa'(1150)$.[2]

3 Strong decays of the $\kappa(800)$ and $\kappa'(1150)$ mesons

We examine strong two-body decays of the $\kappa(800)$ and $\kappa'(1150)$ as mixtures of the $\kappa^{(N)}$ and $\kappa^{(E)}$ in the $\widetilde{U}(12)$-classification scheme as follows:

$$\kappa(800) \to K + \pi \tag{4}$$

[2]A recent lattice-QCD study on light-scalar mesons by the UKQCD collaboration [10)] suggests that the $a_0(980)$ is predominantly a conventional $\bar{q}q$ state, while the $\kappa(800)$ is too light to be assigned to the $\bar{q}q$ state, which is expected to have a mass about 100-130 MeV heavier than the $a_0(980)$.

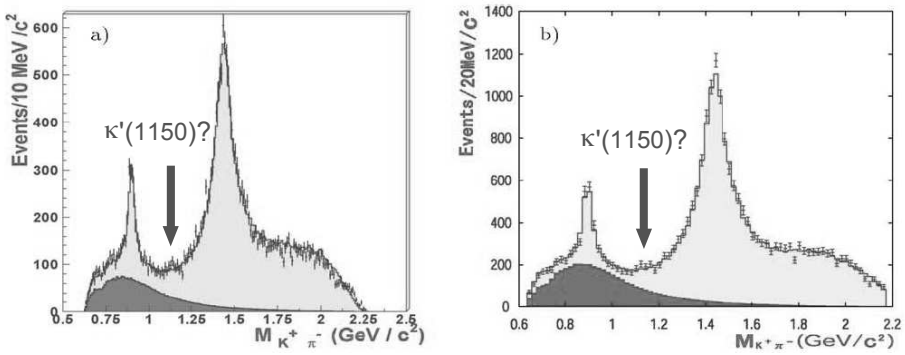

Figure 1: *The $K^+\pi^-$ invariant mass spectrum in $J/\psi \to \bar{K}^*(892)^0 K^+\pi^-$ decay from BES II.* [6] *The dark shaded histograms show contribution from the $\kappa(800)$.*

and

$$\kappa'(1150) \to K + \pi, \tag{5a}$$
$$\to K + \eta, \tag{5b}$$
$$\to \kappa(800) + \sigma(600) \quad [\to K\pi\pi\pi]. \tag{5c}$$

In the actual calculations of decay matrix elements we treat the strange mesons K, κ and κ' as quark-composite $n\bar{s}$ states, while π, η and σ as external local fields.

3.1 Quark-pseudoscalar and quark-scalar couplings

For the effective quark-pseudoscalar coupling inside hadrons we assume the two independent interactions of the forms

$$g_{ps}\bar{q}(-i\gamma_5)q\phi_p \qquad \text{for pseudoscalar type,} \tag{6a}$$
$$g_{pv}\bar{q}(-i\gamma_5\gamma_\mu)q\partial_\mu\phi_p \qquad \text{for pseudovector type.} \tag{6b}$$

The effective quark-scalar coupling is simply related to the quark-pseudoscalar coupling, assuming the σ meson is a chiral partner of the π meson in the linear

representation of chiral symmetry,[3] and given as

$$g_{ps}\bar{q}q\phi_\sigma, \tag{7a}$$

$$g_{pv}\bar{q}\gamma_\mu q\partial_\mu\phi_\sigma. \tag{7b}$$

Then the matrix elements for the pseudoscalar(π,η)-emitted processes are generally given by

$$T^{(P)} = T^{(P)}_{ps} + T^{(P)}_{pv} \tag{8a}$$

with

$$T^{(P)}_{ps} = g_{ps}\langle\overline{W}(v')(-i\gamma_5\phi_p)W(v)iv\cdot\gamma\rangle I^{(P)}_G(q^2) + \text{c.c.}, \tag{8b}$$

$$T^{(P)}_{pv} = g_{pv}\langle\overline{W}(v')(-\gamma_5\gamma_\mu q_\mu\phi_p)W(v)iv\cdot\gamma\rangle I^{(P)}_G(q^2) + \text{c.c.}, \tag{8c}$$

where $W(v)$ and $\overline{W}(v')$ are the spin wave functions of initial- and final-state mesons, [7] $I^{(P)}_G(q^2)$ a space-time part of the Lorentz-invariant transition form factor,[4] v and v' the 4-velocities, q_μ the momentum of emitted pseudoscalar mesons, and $\langle\cdots\rangle$ means the trace taken over the spinor and flavor indices.

The matrix elements for the σ-emitted processes are given likewise by

$$T^{(\sigma)} = T^{(\sigma)}_{ps} + T^{(\sigma)}_{pv} \tag{9a}$$

with

$$T^{(\sigma)}_{ps} = g_{ps}\langle\overline{W}(v')(\phi_\sigma)W(v)iv\cdot\gamma\rangle I^{(\sigma)}_G(q^2) + \text{c.c.}, \tag{9b}$$

$$T^{(\sigma)}_{pv} = g_{pv}\langle\overline{W}(v')(-i\gamma_\mu q_\mu\phi_\sigma)W(v)iv\cdot\gamma\rangle I^{(\sigma)}_G(q^2) + \text{c.c.}. \tag{9c}$$

3.2 Evaluation of the coupling constants

The coupling constants g_{ps} and g_{pv} were evaluated by Maeda et al.. [11] They calculated the D-wave/S-wave amplitude ratio and width of $b_1(1235) \to \omega(782)+\pi$ decay and obtained the values $g_{ps} = 2.07$ GeV and $g_{pv} = 14.0$, using their experimental values $D/S = 0.277$ (± 0.027) and $\Gamma[\omega\pi] \approx \Gamma^{\text{tot}} = 142$ (± 9) MeV [12] as input.

[3]Here we take chiral $SU(2)_L \times SU(2)_R$ as imposed symmetry.

[4]This is obtained from overlap integral of space-time wave functions for initial and final mesons. In the present analysis we simply take $I^{(P)}_G = I^{(\sigma)}_G = 1$, since initial and final mesons both belong to the ground-state ($L = 0$) multiplet in the $\widetilde{U}(12)_{SF} \times O(3,1)_L$-classification scheme.

We now calculate the decay width of $K^*(892) \to K + \pi$ to see the validity of the present decay model and obtain a reasonable value of $\Gamma[K\pi] = 58$ MeV, compared with the experimental value $\Gamma[K\pi] \approx \Gamma^{\rm tot} = 50.8 \pm 0.9$ MeV. [12)]

3.3 Strong decay widths of the $\kappa(800)$ and $\kappa'(1150)$

Since the $\kappa(800)$ and $\kappa'(1150)$ are generally mixtures of $\kappa^{(N)}$ and $\kappa^{(E)}$, we introduce the mixing angle θ, which is the only free parameter in the present analysis, by

$$|\kappa(800)\rangle = \quad \cos\theta\ |\kappa^{(E)}\rangle + \sin\theta\ |\kappa^{(N)}\rangle, \tag{10a}$$

$$|\kappa'(1150)\rangle = -\sin\theta\ |\kappa^{(E)}\rangle + \cos\theta\ |\kappa^{(N)}\rangle. \tag{10b}$$

Here we take the mixing angle θ to be around -65° so that the $\kappa(800)$ has a width of several hundred MeV and the $\kappa'(1150)$ a rather narrow width, in conformity with their observed properties, $\Gamma[\kappa(800)] = 550 \pm 34$ MeV [12)] and the BES II data mentioned above for the $\kappa'(1150)$.

Using the mixing angle $\theta = -65^\circ$, we evaluate the partial decay widths of the $\kappa(800)$ and $\kappa'(1150)$ for respective channels in the following.

3.3.1 Decay of the $\kappa(800)$

If we take a mass of the $\kappa(800)$ to be 800 MeV, we obtain $\Gamma[K\pi] = 354$ MeV for $\kappa(800) \to K + \pi$. This is consistent, though somewhat small, with the experimental value $\Gamma^{\rm tot} \approx \Gamma[K\pi] = 550 \pm 34$ MeV.

3.3.2 Decays of the $\kappa'(1150)$

We take tentatively 1150 MeV for a mass of the missing state $\kappa'(1150)$ and then obtain

$$\Gamma[K\pi] = 18 \text{ MeV} \quad \text{for} \quad \kappa'(1150) \to K + \pi, \tag{11a}$$

$$\Gamma[K\eta] = \ \ 2 \text{ MeV} \quad \text{for} \quad \kappa'(1150) \to K + \eta, \tag{11b}$$

$$\Gamma[\kappa\sigma] \ = 30 \text{ MeV} \quad \text{for} \quad \kappa'(1150) \to \kappa(800) + \sigma(600), \tag{11c}$$

where mass values of the $\kappa(800)$ and $\sigma(600)$ are taken tentatively to be 600 MeV and 350 MeV, respectively, and the singlet-octet mixing angle for the

pseudoscalar mesons η and η' to be $\theta_P = -11.5^\circ$. From these partial decay widths we could estimate the total width to be

$$\Gamma^{\rm tot} \approx \Gamma[K\pi] + \Gamma[K\eta] + \Gamma[\kappa\sigma] = 50 \text{ MeV}. \tag{12}$$

It may be worthwhile to mention that the dominant decay mode of the $\kappa'(1150)$ is not $K\pi$ but $\kappa(800)\sigma(600)$ ($K\pi\pi\pi$), the $K\pi$ branching ratio is $\Gamma[K\pi]/\Gamma^{\rm tot} \approx 0.36$, and therefore the $\kappa'(1150)$ is supposed not to be seen in the $K\pi$ scattering processes.[5]

Here it goes without saying that the present treatment of the $\kappa(800)$ and $\sigma(600)$ as narrow resonances is quite a rough approximation and the evaluated decay width to $\kappa(800)\sigma(600)$ does not really make sense. In practice we should perform a dynamical calculation of the decay chain $\kappa'(1150) \to \kappa(800)\sigma(600) \to K\pi\pi\pi$, taking into account the effects of the broad κ and σ widths.

4 Concluding Remarks

We presented that there should exist an extra κ' meson which has a mass around 1.1-1.2 GeV, a rather narrow width, and couples strongly to $\kappa(800)\sigma(600)$ ($K\pi\pi\pi$) but weakly to $K\pi$, based upon the $\widetilde{U}(12)$-classification scheme and BES II data.

The strong coupling to $\kappa(800)\sigma(600)$ suggests that to observe the κ' meson experimentally it might be favorable to study the $K\pi\pi\pi$ system, for example, in $J/\psi \to K^*(892)(K\pi\pi\pi)$ decay and $e^+e^- \to K^*(892)(K\pi\pi\pi)$ processes. However, if the main component of κ' is $\kappa^{(E)}(0^{+-})$, as is in the present analysis (taking $\theta = -65^\circ$ in eq.10b), the κ' production in these processes[6] would be suppressed by charge-conjugation (C) invariance in the limit of $SU(3)_f$ symmetry. [14] Rather, the $\chi_{c0,1,2} \to K^*(892)(K\pi\pi\pi)$ decay processes would be more promising, since they are C-parity allowed decays in the $SU(3)_f$ limit.

---

[5]This is consistent with experimental data [13] on the S-wave phase of the $K\pi$ scattering amplitude displaying no typical resonance-like behavior around the energy region 1.1-1.2 GeV.

[6]The J/ψ and virtual photon from e^+e^- annihilation have negative C parity. The $\kappa'(1150)$ production in the $J/\psi \to \bar{K}^*(892)^0 K^+\pi^-$ decay process is doubly suppressed by C invariance in the $SU(3)_f$ limit and its small $K\pi$ branching ratio. This suppression coincides with the experimental data of quite small production of the $\kappa'(1150)$ compared to the $\kappa(800)$, as is seen in fig.1.

In a future study it is necessary to calculate dynamically the decay $\kappa' \to \kappa(800)\sigma(600) \to K\pi\pi\pi$ in order to obtain a more realistic decay width and also to make the present decay model more effective by examining various strong decay processes.

References

1. I. Caprini *et al.*, Phys. Rev. Lett. **96**, 132001 (2006); Z.Y. Zhou *et al.*, JHEP **02**, 043 (2005); A. Dobado *et al.*, Phys. Rev. D **56**, 3057 (1997).
2. J.R. Peláez, Mod. Phys. Lett. A **19**, 2879 (2004).
3. S. Descotes-Genon *et al.*, Eur. Phys. J. C **48**, 553 (2006); Z.Y. Zhou *et al.*, Nucl. Phys. A **775**, 212 (2006); H.Q. Zheng *et al.*, Nucl. Phys. A **733**, 235 (2004).
4. E.M. Aitala *et al.* [E791 Collaboration], Phys. Rev. Lett. **86**, 770 (2001); E.M. Aitala *et al.* [E791 Collaboration], Phys. Rev. Lett. **89**, 121801 (2002).
5. M. Ablikim *et al.* [BES Collaboration], Phys. Lett. B **598**, 149 (2004).
6. M. Ablikim *et al.* [BES Collaboration], Phys. Lett. B **633**, 681 (2006).
7. S. Ishida *et al.*, Prog. Theor. Phys. **104**, 785 (2000).
8. S. Ishida *et al.*, Phys. Lett. B **539**, 249 (2002).
9. K. Yamada, in: Proceedings of the Seminar on Perspectives for Studies of Chiral Particles at BES, (eds. W.G. Li *et al.*, IHEP, Beijing, February 2006), 23 (KEK Proceedings 2006-8, November 2006).
10. C. McNeile *et al.* [UKQCD Collaboration], Phys. Rev. D **74**, 014508 (2006).
11. T. Maeda *et al.*, these proceedings.
12. W.-M. Yao *et al.* [Particle Data Group], J. Phys. G **33**, 1 (2006) and 2007 partial update for edition 2008 (URL: http//pdg.lbl.gov).
13. D. Aston *et al.*, Nucl. Phys. **B296**, 493 (1988).
14. H.E. Haber *et al.*, Phys. Rev. D **32**, 2961 (1985).

Frascati Physics Series Vol. XLVI (2007), pp. 651–659
HADRON07: XII Int. Conf. on Hadron Spectroscopy – Frascati, October 8-13, 2007
Light Meson Spectroscopy

THE GLUEBALL AMONG THE LIGHT SCALAR MESONS

Wolfgang Ochs
Max-Planck-Institutfür Physik, Föhringer Ring 6, D-80805 München, Germany

Abstract

The lightest gluonic meson is expected with $J^{PC} = 0^{++}$, calculations in full QCD point towards a mass of around 1 GeV. The interpretation of the scalar meson spectrum is hindered as some states are rather broad. In a largely model-independent analysis of $\pi^+\pi^- \to \pi^+\pi^-$, $\pi^0\pi^0$ scattering in the region 600-1800 MeV a unique solution for the isoscalar S-wave is obtained. The resonances $f_0(980)$, $f_0(1500)$ and the broad $f_0(600)$ or "σ" are clearly identified whereas $f_0(1370)$ is not seen at the level $B(f_0(1370) \to \pi\pi) \gtrsim 10\%$. Arguments for the broad state to be a glueball are recalled. We see no contradiction with the reported large $B(\sigma \to \gamma\gamma)$ and propose some further experimental tests.

1 QCD predictions for the lightest glueball

The existence of gluonic mesons belongs to the early predictions of QCD and first scenarios have been developed back in 1975 [1)]. Today, quantitative results are available from

1. Lattice QCD: In full QCD both glue and $q\bar{q}$ states couple to the flavour singlet 0^{++} states and first "unquenched" results for the lightest gluonic state point towards a mass of around 1 GeV [2]. This is a considerably lower mass value than what is obtained in the pure Yang Mills theory for gluons (quenched approximation) where the lightest glueball is found at masses around 1700 MeV (recent review [3]). Further studies concerning the dependence on lattice spacing and the quark mass appear important.
2. QCD sum rules: Results on the scalar glueball and various decays are obtained in [4]. The lightest gluonic state is found in the mass range (750-1000) MeV with a decay width of (300-1000) MeV into $\pi\pi$ and the width into $\gamma\gamma$ of (0.2-0.3) keV. Other analyses find similar or slightly higher masses (1250 ± 200) MeV for the lightest glueball [5].

2 The scalar meson spectrum and its interpretation

In the search for glueballs one attempts to group the scalar mesons into flavour multiplets (either $q\bar{q}$ or tetraquarks) and to identify supernumerous states. The existence of such states could be a hint for glueballs either pure or mixed with $q\bar{q}$ isoscalars. In other experimental activities one looks for states which are enhanced in "gluon rich" processes and are suppressed in $\gamma\gamma$ processes.

The lightest isoscalar states listed in the particle data group [6] are

$$f_0(600)(\text{or } \sigma),\ f_0(980),\ f_0(1370)(?),\ f_0(1500),\ f_0(1710),\ f_0(2080), \qquad (1)$$

where the question mark behind $f_0(1370)$ will be explained below. There are different routes to group these states into multiplets together with a_0 and K_0^* states.

In a popular approach the two lightest isoscalars in (1) are combined with $\kappa(800)$ and $a_0(980)$ to form the lightest nonet, either of $q\bar{q}$ or of $qq - \bar{q}\bar{q}$ type. Then the next higher multiplet from $q\bar{q}$ would include $a_0(1450)$, $K_0^*(1430)$; near these masses three isoscalars are found in the list (1) at 1370, 1500 and 1710 MeV and this suggests to consider these three mesons as mixtures of the two members of the $q\bar{q}$ nonet and one glueball (for an early reference, see [7]).

A potential problem in this scheme for the glueball is the very existence of $f_0(1370)$, otherwise there is no supernumerous state in this mass range. Some problems with this state will be discussed below, see also the review [8]. The low mass multiplet depends on the existence of κ which we consider as not

beyond any doubt: its observed phase motion is rather weak and it is markedly different from the one of "σ", see below.

There are other approaches for the classification of the scalar mesons where $f_0(980)$ is the lightest $q\bar{q}$ scalar. In the scheme we prefer [9] the lightest $q\bar{q}$ nonet contains $f_0(980)$, $f_0(1500)$ together with $a_0(1450)$, $K_0^*(1430)$. The supernumerous state $f_0(600)$, called previously $f_0(400-1200)$, corresponds to a very broad object which extends from $\pi\pi$ threshold up to about 2 GeV and is interpreted as largely gluonic. No separate $f_0(1370)$ is introduced, nor $\kappa(800)$. Our classification is consistent with various findings on production and decay processes including D, D_s, B and J/ψ decays [9, 10, 11].

Related schemes are the Bonn model [12] with a similar mixing scheme for the isoscalars and the K-matrix model [13] which finds a similar classification (but with $f_0(1370)$ included) and a broad glueball, centered at the higher masses around 1500 MeV.

3 Study of $\pi\pi$ scattering from 600 to 1800 MeV

3.1 Selection of the physical solution for $m_{\pi\pi} > 1000$ MeV

We are interested here in particular in the problem of $f_0(1370)$ and also in the behaviour of the broad "background" which is related to $f_0(600)$ or "σ", alias $f_0(400-1200)$ and describe the results from an ongoing analysis (see also [14]).

Information on $\pi\pi$ scattering can be obtained from production experiments like $\pi p \to \pi\pi n$ by isolating the contribution of the one-pion-exchange process. In an unpolarised target experiment these amplitudes can be extracted by using dynamical assumptions, such as "spin and phase coherence", which have been tested by experiments with polarised target. At the level of the process $\pi\pi \to \pi\pi$ in different charge states one measures the distribution in scattering angle, $z = \cos\theta^*$, or their moments $\langle Y_M^L \rangle$, in a sequence of mass intervals. The $\pi\pi$ partial wave amplitudes $S, P, D, F, \ldots$ can be obtained in each bin from the measured moments up to the overall phase and a discrete ambiguity (characterised by the "Barrelet Zeros"). The overall phase can be fixed by fitting a Breit Wigner amplitude for the leading resonances ρ, $f_2(1270)$ and $\rho_3(1690)$ to the experimental moments $\langle Y_0^2 \rangle$, $\langle Y_0^4 \rangle$ and $\langle Y_0^6 \rangle$ respectively.

Phase shift analyses of this type for $\pi^+\pi^-$ scattering have been performed by the CERN-Munich group: an analysis guided by a global resonance fit (CM-I

15)) and a fully energy-independent analysis by CM-II [17] and by Estabrooks and Martin [16]; the latter two analyses found 4 different solutions above 1 GeV in mass. Up to 1400 MeV a unique solution has been found [20] using results from polarised target and unitarity. Two solutions remain above 1400 MeV, classified according to Barrelet zeros in [17] as $(---)$ and $(-+-)$. corresponding to sols. A,C in [16].

A new result has been added recently [14] by the construction of the isoscalar S wave S_0 from the $\pi^+\pi^- \to \pi^0\pi^0$ data (GAMS collaboration [19]) and the $I = 2$ scattering data. This S_0 wave shows a qualitatively similar behaviour to S_0 obtained from $\pi^+\pi^- \to \pi^+\pi^-$ scattering above, namely a resonance circle in the complex plane (Argand diagram) related to $f_0(1500)$ above a slowly moving circular background amplitude. This has lead us to select the solution $(-+-)$ as unique solution. We relate the differences in the two results to systematic errors introduced through the overall phase and the S_2 wave, but these are only slowly varying effects as function of mass.

3.2 Resonance fit to the isoscalar S wave

The resulting amplitude $S_0(-+-) = (\eta_0^0 \exp(2i\delta_0^0) - 1)/2i$ is shown in Fig. 1 using the CM-II data after correction for the more recent $I = 2$ amplitudes. The curves refer to a fit of the data (CM-II for $M_{\pi\pi} > 1$ GeV, CM-I for $M_{\pi\pi} < 1$ GeV) to an S-matrix in the space of 3 reaction channels $(\pi\pi, K\bar{K}, 4\pi)$ as product of individual S-matrices for resonances $S_R = 1 + 2iT_R$

$$S = S_{f_0(980)} S_{f_0(1500)} S_{\rm broad} \tag{2}$$

$$T_R = [M_0^2 - M_{\pi\pi}^2 - i(\rho_1 g_1^2 + \rho_2 g_2^2 + \rho_3 g_3^2)]^{-1} \times \rho^{\frac{1}{2}T}(g_i g_j)\rho^{\frac{1}{2}} \tag{3}$$

where $\rho_i = 2k_i/\sqrt{s}$. As can be seen in Fig. 1 the fit including 3 resonances gives a reasonable description of the data. For $f_0(1500)$ the fit parameters $M_0 =$ 1510 MeV, $\Gamma_{tot} = 88$ MeV, $B(f_0 \to \pi\pi) = 38\%$ are obtained in remarkable agreement to the PDG numbers, despite the different approaches involved.

3.3 Note on $f_0(600)$, $\kappa(800)$ and $f_0(1370)$

The broad object is also described by a resonance form with mass parameter $M_0 \sim 1100$ MeV and width $\Gamma \sim 1450$ MeV. The elastic width is about 85%

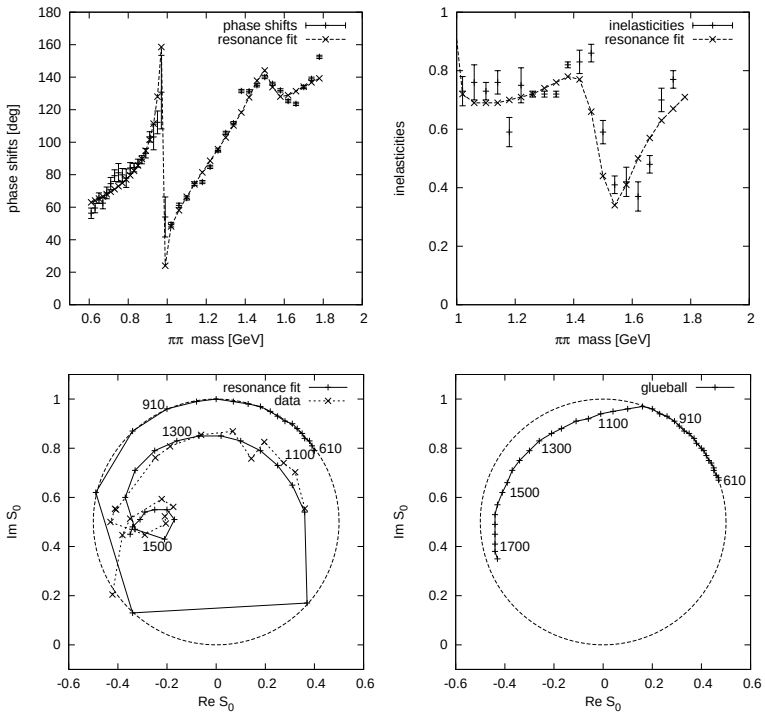

Figure 1: Resonance fit Eq. (2) in comparison with data on the corrected $I = 0$ $\pi\pi$ S-wave ampliotude S_0 (CM-I; CM-II, sol. $-+-$): phase shifts δ_0^0 (top-left) and inelasticities η_0^0 (top-right); Argand diagram for the amplitude S_0 (bottom-left); broad component $f_0(600)/\sigma$ from the fit (bottom-right).

whereas the GAMS data suggest rather a smaller value around 70%. More details will be given elsewhere. This parametrisation is also shown at the bottom-right panel of Fig. 1. It describes about 3/4 of the full resonance circle. The Breit Wigner mass parameter M_0 denotes the mass where the amplitude is purely imaginary. It is different from the pole mass which is referred to as resonance mass. This mass value appears to be considerably lower and requires a more careful study of the line shape in the denominator of (3).

In any case, the data in Fig. 1 suggest there is evidence for a broad state in $\pi\pi$, centered around 1000 MeV along the physical region and what is called $f_0(600)$ or σ refers to the same state, there cannot be two states.

We also note here that the $\pi\pi$ scattering looks considerably different from elastic $K\pi$ scattering in that the phase of the "background" found in the analysis of the LASS data [21] moves more slowly staying below 90° always. The existence of κ would become evident if the phase passed through 90° in forming a circle as in case of σ.

We note that the data presented in Fig. 1 do not give any indication of the existence of $f_0(1370)$ which would show up as a second circle in the Argand diagram with respective signals in η_0^0 and δ_0^0. In fact, none of the energy-independent bin by bin analyses of the CM or CKM data [15, 16, 17, 18] nor of the GAMS data [19, 14] gave such an indication. From our analysis we exclude an additional state with branching ratio $B(f_0(1370) \to \pi\pi) \gtrsim 0.1$ near 1370 MeV (this would correspond to a circle of diameter 0.1).

These results from the bin-by-bin analysis are in apparent conflict with two other analyses presented at this conference [22, 23]. In both studies CM-I moments as well as various other data sets from 3 body final states, have been fitted by model amplitudes with resonances in all relevant partial waves. The amplitude S_0 by Bugg [22] shows $f_0(1370)$ as an extra circle of diameter 0.25 whereas Sarantsev's Argand diagram [23] shows no extra circle but an effect in the phase movement. Obviously, these discrepancies need to be understood.

4 Glueball interpretation of the broad object $f_0(600)$

The following arguments are in favour of this state to be a glueball [9, 10, 11].
1. This state is produced in almost all "gluon rich" processes, including central production $pp \to p(\pi\pi)p$, $p\bar{p} \to 3\pi$, $J/\psi \to \gamma\pi\pi(?)$, $\gamma K\bar{K}, \gamma 4\pi$, $\psi' \to \psi\pi\pi$, $\Upsilon'', \Upsilon' \to \Upsilon\pi\pi$ and finally $B \to K\pi\pi, B \to K\bar{K}K$ related to $b \to sg$. The high mass tail above 1 GeV is seen as "background" in $J/\psi \to \gamma K\bar{K}$ and in B decay channels where it leads to striking interference phenomena with $f_0(1500)$ [11].
2. Within our classification scheme [9] without κ and $f_0(1370)$ the state $f_0(600)$ is supernumerous.
3. The mass and large width is in agreement with the QCD sum rule results and also with the first results from unquenched lattice QCD.
4. Suppression in $\gamma\gamma$ production.
Recently, the radiative width $\Gamma(f_0(600) \to \gamma\gamma) = (4.1 \pm 0.3)$ keV has been determined by Pennington [24] from the process $\gamma\gamma \to \pi\pi$. As this number is larger than expected for glueballs (see Sect.1), he concluded this state "unlikely

to be gluonic". Similar results on this width are obtained by [25, 26]. A resolution of this conflict has been suggested in a recent paper [25].

It is argued that the phenomenology of $\gamma\gamma \to \pi\pi$ at low energies is different from the one at high energies. At low energies, few 100 MeV above threshold, the photons couple to the charged pions and the Born term with one pion exchange dominates in $\gamma\gamma \to \pi^+\pi^-$, in addition there is a contribution from $\pi^+\pi^-$ rescattering. Explicit models with $\pi\pi$ scattering as input and with $f_0(600)$ pole, can explain the low energy processes [27, 28], also calculations in χPT with non-resonant $\pi\pi$ scattering at low energies [29]. In this case of the rescattering contribution, a resonance decaying into $\pi\pi$ would also decay into $\gamma\gamma$ irrespective of the constituent nature of the state.

At high energies, the photons do resolve the constituents of the produced resonances: for example, the radiative widths of tensor mesons f_2, f_2', a_2 in the region 1200-1500 MeV follow the expectations from a $q\bar{q}$ state.

In the model by Mennessier [27] the low energy rescattering and the high energy "direct" component relating to the constituents are added; the unitarization keeps the validity of Watson's theorem. A fit of the data at the lower energies $M_{\pi\pi} < 550$ MeV provides an estimate of the direct contribution from its deviation from the rescattering term. This yields $\Gamma(f_0(600) \to \gamma\gamma)|_{direct} \approx 0.3$ keV ($\pm 50\%$), alternatively, one can express this result as upper limit $\Gamma(f_0(600) \to \gamma\gamma)|_{direct} < 0.5$ keV (90%CL). This result implies that there is no contradiction with a gluonic interpretation of $f_0(600)$.

Finally, we express some expectations for experiment which follow from this interpretation.

1. Because of its large width the state $f_0(600)$ overlaps with both physical regions. Whereas the low energy region is governed by hadronic rescattering there is the transition to high energies with a resolution of the constituents. Therefore we expect that for increasing mass $M_{\pi\pi} \gtrsim 1$ GeV the decay fraction $f_0(600) \to \gamma\gamma$ decreases strongly relative to $f_0(600) \to \pi\pi$ in consequence of the weak intrinsic coupling of the glueball to $\gamma\gamma$ by an order of magnitude.

2. In processes with virtual photons the $\pi\pi$ rescattering contribution should be suppressed with respect to the direct $q\bar{q}$ coupling contribution because of the pion formfactor. This could result in a relative suppression of $f_0(600)$ production at low $\pi\pi$ mass with respect to $f_0(980)$ if the latter state is dominantly $q\bar{q}$; this should hold for both space like ($\gamma_V\gamma \to \pi\pi$) and time like photons

$(\gamma_V \to \pi\pi\gamma)$.

In this way the study of the $\pi\pi$ S wave cross section in two-photon processes (or its upper limit obtained using the positivity of the density matrix [30]) could provide new clues on the interpretation of the broad state $f_0(600)$.

5 Acknowledgements

I would like to thank Gerard Mennessier, Stephan Narison and Peter Minkowski for discussions and the collaboration on subjects of this talk.

References

1. H. Fritzsch and P. Minkowski, Nuovo Cim. **30A**, 393 (1975).
2. A. Hart, C. McNeile, C. Michael and J. Pickavance, Phys. Rev. **D 74**, 114504 (2006).
3. C. McNeile, arXiv:0710.0985 [hep-lat].
4. S. Narison and G. Veneziano, Int. J. Mod. Phys. **A4**, 2751 (1989); S. Narison, Nucl. Phys. **B509**, 312 (1998); Nucl. Phys. **A675** (2000) 54c; Phys. Rev. **D73** 114024 (2006).
5. H. Forkel, Phys. Rev. **D71**, 054008 (2005); **D64**, 034015 (2001); E. Bagan and T.G. Steele, Phys. Lett. **B243**, 413 (1990).
6. W.M. Yao *et al*, J. Phys. **G33**, 1 (2006).
7. C. Amsler and F.E. Close, Phys. Lett. **B353**, 385 (1995).
8. E. Klempt and A. Zaitsev, arXiv:0708.4016 [hep-ph].
9. P. Minkowski and W. Ochs, Eur. Phys. J. **C9**, 283 (1999).
10. P. Minkowski and W. Ochs, Nucl. Phys. B (Proc. Suppl.) **121**, 119 (2003), arXiv:hep-ph/0209223; ibid. p.123, arXiv:hep-ph/0209225.
11. P. Minkowski and W. Ochs, Eur. Phys. J. **C39**, 71 (2005); AIP Conf. Proc. **814**, 52 (2006), arXiv:hep-ph/0511126.
12. E. Klempt, B.C. Metsch, C.R. Münz and H.R. Petry, Phys. Lett. **B361**, 160 (1995).

13. V.V. Anisovich *et al*, Phys. Lett. **B389**, 388 (1996); V.V. Anisovich and A.V. Sarantsev, Eur. Phys. J. **A16**, 229 (2003).

14. W. Ochs, Nucl. Phys. B (Proc. suppl.) **174**, 146 (2007), arXiv: hep-ph/0609207.

15. B. Hyams et al., Nucl. Phys. **B64** (1973) 4; W. Ochs, University Munich, thesis 1973.

16. P. Estabrooks and A.D. Martin, Nucl. Phys. **B95**, 322 (1975).

17. B. Hyams et al., Nucl. Phys. **B100**, 205 (1975); W. Männer, AIP Conf. Proc. **21**, 22 (1974).

18. R. Kamiński, R. Lesniak and K. Rybicki, Z. Phys. **C74**, 79 (1997); Eur. Phys. J. direct **C4**, 4 (2002).

19. D. Alde et al., Eur. Phys. J. **A3**, 361 (1998).

20. R. Kamiński, J.R. Peláez and F.J. Ynduráin, arXiv:hep-ph/0603170.

21. D. Aston et al., Nucl. Phys. **B296**, 493 (1988).

22. D. Bugg, this conference and arXiv:0706.1341 [hep-ex].

23. A.V. Sarantsev, this conference.

24. M.R. Pennington, Phys. Rev. Lett. **97**, 011601 (2006).

25. G. Mennessier, P. Minkowski, S. Narison and W. Ochs, arXiv:0707.4511 [hep-ph].

26. J.A. Oller, L. Roca and C. Schat, arXiv:0708.1659 [hep-ph].

27. G. Mennessier, Z. Phys. **C16**, 241 (1983).

28. R.L. Goble, R. Rosenfeld and J.L. Rosner, Phys. Rev. **D39**, 3264 (1989).

29. J.F. Donoghue, B.R. Holstein and Y.C. Lin, Phys. Rev. **D37**, 2423 (1988); S. Bellucci, J. Gasser and M.E. Saino, Nucl. Phys. **B423**, 80 (1994), Err. ibid **B431**, 413 (1994).

30. W. Ochs, Nuov. Cim. **12A**, 724 (1972); G. Grayer *et al*, Nucl. Phys. **B50**, 29 (1972); S.U. Chung and T.L. Trueman, Phys. Rev. **D11**, 633 (1975).

Frascati Physics Series Vol. XLVI (2007), pp. 661–668
HADRON07: XII Int. Conf. on Hadron Spectroscopy – Frascati, October 8-13, 2007
Light Meson Spectroscopy

CENTRAL PRODUCTION WITH TAGGED FORWARD PROTONS AND THE STAR DETECTOR AT RHIC

Włodek Guryn for the STAR Collaboration
Brookhaven National Laboratory

Abstract

We describe a setup which will allow extend the physics reach of the STAR detector at RHIC to include the measurement of very forward protons. Tagging on very forward protons, detected by the Roman Pots at RHIC energies, selects processes, in which the proton stays intact and the exchange is dominated by one with the quantum numbers of the vacuum, thus enhancing the probability of measuring reactions where colorless gluonic matter dominates the exchange. The processes include both elastic and inelastic diffraction. The capabilities of the STAR detector to detect Gleuballs and Exotics in central production mechanism are described.

1 Introduction

Installing Roman Pots of the pp2pp experiment [1, 2, 3] at STAR [4] detector at RHIC will allow tagging events with very forward protons, thus extending

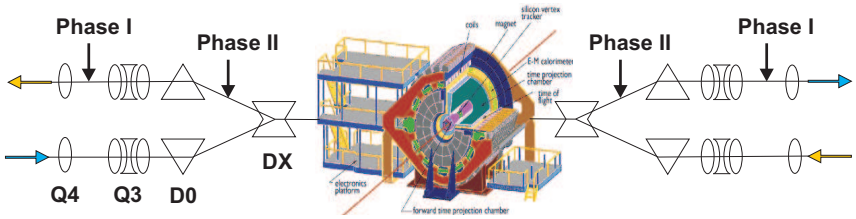

Figure 1: *The Roman pots of the pp2pp experiment in the STAR interaction region, with the arrows indicating proposed locations for Phase I and Phase II.*

physics reach of the experiment to select processes, in which the proton stays intact and the exchange has mainly the quantum numbers of vacuum. Consequently, enhancing the probability of measuring reactions where colorless gluonic matter dominates the exchange. The processes include both elastic and inelastic diffraction.

These processes are related to the photon diffraction that has already been studied by STAR in Ultra Peripheral Collisions (UPC) of gold-gold (AuAu), and deuteron-gold (dAu) ions, where two pion, $\rho \rightarrow \pi^+\pi^-$ [5)] and four pion $\pi^+\pi^-\pi^+\pi^-$ photoproduction has been used to probe Pomeron-heavy nucleus couplings.

In order to characterize those diffractive processes well, the measurement of the momentum of the forward proton is important. Because of the layout of STAR and its solenoidal magnetic field, RHIC accelerator magnets must be used for momentum analysis resulting in forward proton taggers installed downstream from the STAR detector, on either side. There are two possible locations: 1) warm section between the DX-D0 magnets; or 2) in the warm straight section between Q3 and Q4 magnets, see fig. 1. Also, to extend the t and ξ ranges to the lowest values, where t is four-momentum transfer between the incoming and outgoing protons, $\xi = \Delta p/p$ is the momentum fraction carried off by the Pomeron, a moveable detector system, approaching the beam as closely as possible, is needed. Hence the use of pp2pp Roman Pots (RPs) is advantageous not only because it is a working system but because it will also allow maximizing the t and ξ ranges. We describe a scenario of executing the

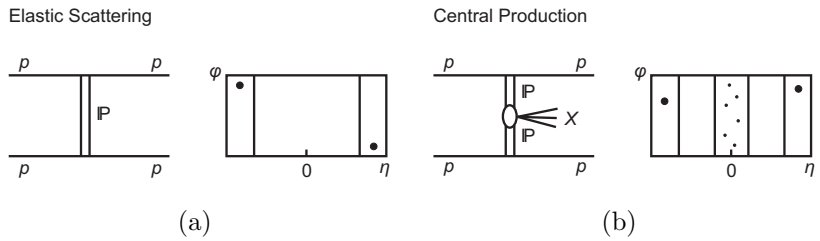

Figure 2: *a) Elastic scattering process b) Diffractive - Central Production Process.*

physics program in two phases, which optimizes the use of available resources and maximizes physics output. Phase I has been implemented and is ready to take data in 2008. In the future the physics reach will be extended to higher values of t and larger data samples will be taken. This would be achieved in Phase II, for which design work is needed.

2 Physics Program

In this section we shall briefly describe physics topics in proton-proton collisions, which can be addressed by using the Roman Pots of the pp2pp experiment and the STAR detector. A more detailed description of the physics can be found in [6, 7]. At RHIC the processes of interest in polarized proton-proton and proton nucleus collisions are [8]: elastic scattering, central production and single diffraction processes. Here we shall focus on the first two, fig. 2.

The common feature of those reactions is that the proton undergoes quasi-elastic or elastic scattering and that they occur via the exchange of colorless objects with the quantum numbers of the vacuum, historically called Pomeron exchange. In terms of QCD, Pomeron exchange consists of the exchange of a color singlet combination of gluons. Hence, triggering on forward protons at high (RHIC) energies dominantly selects exchanges mediated by gluonic matter. In addition, the use of polarized proton beams, unique at RHIC, will allow exploring unknown spin dependence of diffraction.

Tagging and measuring forward protons also removes the ambiguity of a (complementary) rapidity gap tag, which has a background due to the low

multiplicity of diffractive events, and allows the full characterization of the event in terms of t, ξ and M_X.

2.1 Elastic scattering

In studies of the elastic scattering process we will use unique capabilities of RHIC colliding polarized proton beams to measure both spin dependent and spin averaged observables.

Almost the entire energy range of this proposal has been inaccessible to proton-proton scattering in the past. A measurement of the total cross section, σ_{tot} at the highest possible energy will probe the prevalent assumption that the cross sections for pp and $p\bar{p}$ scattering are asymptotically identical.

The measurement of the differential pp cross section $d\sigma/dt$ over the extended t-range will include the region at the lower $|t|$ that is particularly sensitive to the ρ-parameter. This will allow extracting the ρ-parameter and the nuclear slope parameter b in a combined fit to the differential cross section possible and might also lead to an extraction of σ_{tot}.

An asymptotic difference between the differential and total cross sections for pp and $p\bar{p}$ could be explained by a contribution of the Odderon to the scattering amplitude. The absence of an Odderon contribution would lead to identical cross sections, approaching each other roughly as $s^{1/2}$.

By measuring spin related asymmetries one will be able to determine elastic scattering at the amplitude level [11, 12, 13]. The availability of longitudinal polarization at STAR in this first phase would allow measuring A_{LL} in addition to A_{NN}, A_{SS}, and A_N resulting in a significant improvement of our physics capabilities. Full azimuthal coverage for elastic events has been implemented in this phase.

One of the physics motivations to measure the A_N is to study of the $\sqrt{s}$ dependence of the spin-flip to spin-nonflip amplitudes ratio [14]. In other words it may occur that small contribution from hadronic spin-flip to the spin single-spin asymmetry, measured with a polarized jet target at 100 GeV/c, could increase at $\sqrt{s} = 200GeV$. This will help to reveal long standing problem of the energy dependence of the spin flip amplitude, which is best answered experimentally.

2.2 Central Production of glueballs

In the double Pomeron exchange process each proton "emits" a Pomeron and the two Pomerons interact producing a massive system M_X. The massive system could form resonances or jet pairs. Because of the constraints provided by the double Pomeron interaction, glueballs, and other states coupling preferentially to gluons, could be produced with much reduced backgrounds compared to standard hadronic production processes.

In the kinematical region, which we are proposing to cover, those processes allow exploration of the non-perturbative regime of QCD. The strength of the STAR detector: excellent charged particle identification in the central rapidity region and p_T resolution, coupled with ability to tag diffractive events with the forward protons with Roman pots. Central Production using Roman Pots and rapidity gap techniques has been studied at all the hadron colliders: ISR [15], S$p\bar{p}$S [16] and the Tevatron [17] and is planned to be studied at the LHC [18].

The idea that the production of glueballs is enhanced in the central region in the process $pp \to pM_X$p was first proposed by [9] and was demonstrated experimentally [10]. The crucial argument here is that the pattern of resonances produced in central region, where both forward protons are tagged, depends on the vector difference of the transverse momentum of the final state protons $\vec{k}_{T1}$ and $\vec{k}_{T2}$, with $dP_T = |\vec{k}_{T1} - \vec{k}_{T2}|$. The so-called dP_T filter argument is that when dP_T is large (Λ_{QCD}) $q\bar{q}$ states are prominent and when dP_T is small the surviving resonances include glueball candidates [9, 10].

In what we are proposing large data samples of diffractive states can be obtained and analyzed as function of diffractive mass M_X and t ($d^2\sigma/dM_X^2 dt$) for central production.

3 Implementation Plan

We will execute the above physics program in two phases. In both phases Roman Pots and STAR detector shall be used, fig. 1.

3.1 Phase I

The existing pp2pp experimental set-up, already installed at STAR, will measure spin dependence of both elastic scattering in an unexplored t and ξ range,

with respect to what has been done already, and of Central Production described above, for which our studies found that there is good acceptance.

3.1.1 Measurement of elastic scattering

Using the capacity of existing power supplies one can run with optics of $\beta^* = 20m$ and at $\sqrt{s} = 200GeV$. This optics could extend the t coverage to $0.003 < |t| < 0.03(GeV/c)^2$. Reaching such a small $|t|$-value allows measuring the single spin analyzing power A_N close to its maximum at $|t| \approx 0.0024(GeV/c)^2$, where $A_{max} = 0.04(GeV/c)^2$, at $\sqrt{s} = 200GeV$. The A_N and its t-dependence in the covered range is sensitive to a possible contribution of the single spin-flip amplitude, ϕ_5 [14], from the interference between the hadronic spin-flip amplitude with the electromagnetic non-flip amplitude. An additional contribution of the hypothetical Odderon to the pp scattering amplitude can be probed by measuring the double spin-flip asymmetry, A_{NN} [14].

Given polarization 50% and 2.3 mb cross section within our acceptance we shall get 6.7×10^6 events. In the four t subintervals we shall have 1.66×10^6 events in each. The corresponding errors are $\Delta A_N = 0.0017, \Delta A_{NN} = \Delta A_{SS} = 0.0053$. To estimate the error on A_{NN} the ϕ intervals $-45^\circ < \phi < 45^\circ$ and $135^\circ < \phi < 225^\circ$ were used, and complementary intervals for A_{SS}.

For the amount of data we expect to collect in 2008, an estimated error on the slope parameter is $\Delta b = 0.31(GeV/c)^{-2}$ and on the ratio of real to imaginary part $\Delta\rho = 0.01$, which is comparable to the existing measurements from the pp and $p\bar{p}$ data.

3.1.2 Measurement of Central Production

We studied the geometrical acceptance of our setup for both SDD and DPE processes. We have generated protons with t and ξ uniformly distributed in the regions $0.003 \leq |t| \leq 0.04(GeV/c)^2$ and $0.005 \leq \xi \leq 0.05$ respectively. We assumed that the Roman Pots are 10mm from the beam center, which is at least 12σ of the beam size at the detection point.

Our studies indicate that there is good acceptance to measure inelastic diffraction processes DPE with $\beta^* = 20m$ optics for Phase I. With the expected luminosity we can collect about 5×10^6, triggered DPE events. Number of events for which the proton momentum is reconstructed, where it is required that two RPs on each side are used allowing reconstruction of the outgoing

proton momentum, is about factor of ten lower. One assumes a 10 μbarn cross section within our acceptance for the DPE process.

Also, as noted earlier the events seen in the STAR Time Projection Chamber (TPC) in pp Central Production are very similar to those in heavy-ion UPC collisions. The algorithms and reconstruction code that has been developed to deal with those events can also be used in our program. In particular experience gained in dealing with the backgrounds is very valuable.

3.2 Phase II

To maximize the acceptance and the range in t, ξ and M_X in this phase the Roman Pot system needs to be installed between DX-D0 magnets and will be used in conjunction with the STAR TPC to reconstruct and fully constrain events with resonance in central production process. A study needs to be done that range. The search for exotics is one of the topics of interest here, but not the only one.

4 Summary

In summary the physics program with tagged forward protons at STAR will: 1) Study elastic scattering and its spin dependence in unexplored t, ξ and $\sqrt{s}$ range; 2)Study the structure of color singlet exchange in the non-perturbative regime of QCD; 3) Search for diffractive production of light and massive systems in double Pomeron exchange process; 4) Search for new physics, including glueballs and Odderon.

Finally we stress that the studies we are proposing will add to our understanding of QCD in the non-perturbative regime where calculations are not easy and one has to be guided by measurements.

5 Acknowledgements

The research reported here has been performed in part under the US DOE contract DE-AC02-98CH10886.

References

1. S. Bültmann *et al.*, Phys. Lett. **B 579**, (2004) 245-250.

2. S. Bültmann *et al.*, Nucl. Instr Meth. **A535**, (2004) 415-420.

3. W. Guryn *et al.*, RHIC Proposal R7 (1994) (unpublished).

4. K.H. Ackermann *et al.*, Nucl. Instrum. Meth. **A499** (2003) 624.

5. Adler, *et al.*, Phys. Rev. Lett., **89**, No. 27, (2002), 272302.

6. V. Barone, E. Predazzi, High-Energy Particle Diffraction, Texts and Monographs in Physics, Springer-Verlag (2002) ISBN: 3540421076.

7. S. Donnachie, G. Dosch, P. Landshoff, Pomeron Physics and QCD, Cambridge University Press (1998) ISBN: B0006Z3XLM.

8. A. Bravar, W. Guryn, S.R. Klein, D. Milstead, B. Surrow, J.Phys. **G28** (2002) 2885.

9. F. Close, Reports on Progress in Physics 51 (1988) 833 and F. Close, A. Kirk and G. Schuler, Phys. Lett. **B477** (2000) 13.

10. D. Barberis et al., WA102 Collaboration, Phys. Lett. **B479** (2000) 59.

11. B.Z. Kopeliovich, Phys. Rev.**C68** (2003) 044906.

12. 11. N. H. Buttimore, B. Z. Kopeliovich, E. Leader, J. Soffer, T. L. Trueman, Phys. Rev. **D59**, (1999) 114010.

13. 12. N.H. Buttimore, E. Leader, T.L. Trueman, Phys. Rev. **D64** (2001) 094021.

14. Trueman, T. L, arXiv:0711.4593 [hep-ph].

15. T. Åkesson, M. G. Albrow, *et al.*, Nuclear Physics **B264** (1986) 154.

16. A. Brandt *et al.* [UA8 Collaboration], Eur. Phys. J. **C 25**, (2002) 361.

17. CDF Collaboration, T. Aaltonen *et al.*, arXiv:0712.0604v2

18. Albrow, M., *et al.* CERN-LHCC-2006-039.

Frascati Physics Series Vol. XLVI (2007), pp. 669–676
HADRON07: XII Int. Conf. on Hadron Spectroscopy – Frascati, October 8-13, 2007
Light Meson Spectroscopy

ON THE ASSIGNMENT OF THE f_0- AND f_2-MESONS FROM ANALYSIS OF PROCESSES WITH PSEUDOSCALAR MESONS

Yu.S. Surovtsev
Joint Institute for Nuclear Research, 141980 Dubna, Russia
R. Kamiński
Institute of Nuclear Physics, Polish Academy of Sciences, 31342 Cracow, Poland

Abstract

The experimental data on $\pi\pi \to \pi\pi, K\overline{K}, \eta\eta, \eta\eta'$ are analyzed jointly in approach, based on analyticity and unitarity, for studying the f_0- and f_2-mesons. Assignment of scalar and tensor mesons to lower nonets is proposed. The $f_0(1500)$ and $f_2(2000)$ are interpreted as glueballs.

1 Introduction

The lightest glueball, predicted by QCD, must be the scalar one. Maybe, it is the $f_0(1500)$ (see, e.g., [1, 2]). Generally, scalar mesons are the very intriguing objects constituting the Higgs sector of the strong interactions and being the most direct bearers of information on the QCD vacuum. However, the scalar sector is problematic up to now especially as to an assignment of the discovered mesonic states to quark-model configurations (see, e.g., [2] and references there).

In the tensor sector, from thirteen discussed resonances, the nine ones ($f_2(1430)$, $f_2(1565)$, $f_2(1640)$, $f_2(1810)$, $f_2(1910)$, $f_2(2000)$, $f_2(2020)$, $f_2(2150)$, $f_2(2220)$) must be confirmed in various experiments and analyses [1]. Recently in the analysis of $p\overline{p} \to \pi\pi, \eta\eta, \eta\eta'$, five resonances – $f_2(1920)$, $f_2(2000)$, $f_2(2020)$, $f_2(2240)$ and $f_2(2300)$ – have been obtained, one of which ($f_2(2000)$) is a candidate for the glueball [3].

We have used a model-independent approach [4] in the analysis of data. It permits us to omit theoretical prejudice in the extraction of the parameters of the resonances. Considering the obtained disposition of resonance poles on the Riemann surface, coupling constants with channels and resonance masses, we draw definite conclusions about nature of the investigated states.

2 Analysis of isoscalar-scalar sector

First we consider the S-waves of $\pi\pi \to \pi\pi, K\overline{K}, \eta\eta, \eta\eta'$. However, the uniformizing variable method [4] which we will use is applicable only in the 2- and 3-channel cases. Therefore, we have carried out two variants of the 3-channel analysis: (I) the one of $\pi\pi \to \pi\pi, K\overline{K}, \eta\eta$, and (II) of $\pi\pi \to \pi\pi, K\overline{K}, \eta\eta'$.

The 3-channel S-matrix is determined on the 8-sheeted Riemann surface. The elements $S_{\alpha\beta}$, where $\alpha, \beta = 1(\pi\pi), 2(K\overline{K}), 3(\eta\eta$ or $\eta\eta')$, have the right cuts, starting with $4m_\pi^2$, $4m_K^2$, and $4m_\eta^2$ (or $(m_\eta + m_{\eta'})^2$), and the left cuts neglected here in the Riemann surface structure. The surface sheets are numbered according to the signs of analytic continuations of the channel momenta $k_1 = (s/4 - m_\pi^2)^{1/2}$, $k_2 = (s/4 - m_K^2)^{1/2}$, $k_3 = (s/4 - m_\eta^2)^{1/2}$ (or $k_3' = 1/2(s - (m_\eta + m_{\eta'})^2)^{1/2}$) as follows: signs $(\mathrm{Im}k_1, \mathrm{Im}k_2, \mathrm{Im}k_3) = +++, -++, --+, +-+, +--, ---, -+-, +--$ correspond to sheets I, II,$\cdots$, VIII, respectively. (All, related to variant II, is denoted by prime.)

The 3-channel resonances are described by 7 types of pole clusters (of poles and zeros on the Riemann surface) [4] according to 7 possible cases when there are resonance zeros on sheet I only in (**a**) S_{11}; (**b**) S_{22}; (**c**) S_{33}; (**d**) S_{11} and S_{22}; (**e**) S_{22} and S_{33}; (**f**) S_{11} and S_{33}; and (**g**) S_{11}, S_{22}, and S_{33}. The cluster kind is related to the nature of state.

Parameterizing the S-matrix, we use the Le Couteur–Newton relations [5] which express the S-matrix elements of all coupled processes in terms of the Jost matrix determinant $d(k_1, \cdots, k_n)$ that is a real analytic function with the only branch-points at $k_i = 0$. The branch points are taken into account in a

uniformizing variable. When neglecting the $\pi\pi$ threshold, it is [4]

$$w = \frac{k_2 + k_3}{\sqrt{m_\eta^2 - m_K^2}} \text{ for variant I, and } w' = \frac{k_2' + k_3'}{\sqrt{\frac{1}{4}(m_\eta + m_{\eta'})^2 - m_K^2}} \text{ for II.} \quad (1)$$

On the w-plane, the Le Couteur–Newton relations are

$$S_{11} = \frac{d^*(-w^*)}{d(w)}, \quad S_{22} = \frac{d(-w^{-1})}{d(w)}, \quad S_{33} = \frac{d(w^{-1})}{d(w)}, \quad (2)$$

$$S_{11}S_{22} - S_{12}^2 = \frac{d^*(w^{*-1})}{d(w)}, \quad S_{11}S_{33} - S_{13}^2 = \frac{d^*(-w^{*-1})}{d(w)}. \quad (3)$$

The d-function in variant I is $d(w) = d_B d_{res}$ where the resonance part is $d_{res} = w^{-\frac{M}{2}} \prod_{r=1}^{M}(w + w_r^*)$ with M the number of resonance zeros; d_B, describing the background, is $d_B = \exp[-i\sum_{n=1}^{3}(k_n/m_n)(\alpha_n + i\beta_n)]$ where

$\alpha_n = a_{n1} + a_{n\sigma}\ (s - s_\sigma)/s_\sigma\ \theta(s - s_\sigma) + a_{nv}\ (s - s_v)/s_v\ \theta(s - s_v)$,

$\beta_n = b_{n1} + b_{n\sigma}\ (s - s_\sigma)/s_\sigma\ \theta(s - s_\sigma) + b_{nv}\ (s - s_v)/s_v\ \theta(s - s_v)$.

The second terms in α_n and β_n take into account possible channels below roughly 1400 MeV; the third terms, the $\eta\eta'$-, $\rho\rho$-, $\omega\omega$- channels.

In variant II, we should add to α_n' and β_n' the terms $(s-4m_\eta^2)/4m_\eta^2\ a_{n\eta}'\ \theta(s-4m_\eta^2)$ and $(s-4m_\eta^2)/4m_\eta^2\ b_{n\eta}'\ \theta(s-4m_\eta^2)$, allowing for influence of the $\eta\eta$-channel.

References to sources of used data in the I variant can be found in ref. [4]. In variant II, the data on $\pi\pi \to \eta\eta'$ are taken from ref. [6]. We obtain a satisfactory description for both variants. In variant I, the analysis prefers the case when the $f_0(600)$ is described by the (**a**) cluster with poles on the complex energy plane $\sqrt{s}$ (in MeV) $683.5 - i589$ on sheet II, $673.3 - i589$ on sheet III, $593.5 - i589$ on sheet VI, $603.7 - i589$ on sheet VII; $f_0(1370)$ – (**c**) with poles $1398.3 - i287.5$ on sheet V, $1398.3 - i270.5$ on sheet VI, $1398.3 - i154.9$ on sheet VII, $1398.3 - i171.9$ on sheet VIII; $f_0(1500)$ – (**g**) with poles $1502.6 - i357.1$ on sheet II, $1479.1 - i140.2$ on sheet III, $1502.6 - i238.7$ on sheet IV, $1497 - i139.8$ on sheet V, $1497.5 - i191.8$ on sheet VI, $1496.7 - i87.35$ on sheet VII, $1502.6 - i356.5$ on sheet VIII; $f_0(1710)$ – (**b**) with poles $1708.3 - i142.3$ on sheet III, $1708.3 - i160.3$ on sheet IV, $1708.3 - i323.1$ on sheet V, $1708.3 - i305.1$ on sheet VI; the $f_0(980)$ is represented only by poles $1013.4 - i32.8$ on sheet II and $984.1 - i57.5$ on sheet III. The poles on sheets IV, VI, VIII and V, related to the $f_0(1500)$, are of the 2nd and 3rd order, respectively. The total χ^2/NDF

for all three processes is 1.36. The background parameters are: $a_{11} = 0.2006$, $a_{1\sigma} = 0.0141$, $a_{1v} = 0$, $b_{11} = 0$, $b_{1\sigma} = -0.01025$, $b_{1v} = 0.04898$, $a_{21} = -0.7039$, $a_{2\sigma} = -1.4213$, $a_{2v} = -5.951$, $b_{21} = 0.0447$, $b_{2\sigma} = 0$, $b_{2v} = 6.787$, $b_{31} = 0.6456$, $b_{3\sigma} = 0.3348$, $b_{2v} = 0$; $s_\sigma = 1.638$ GeV^2, $s_v = 2.084$ GeV^2.

In variant II, the $f_0(600)$ is described by the $(\mathbf{a}')$ cluster with poles $640.6 - i606$ on sheet II, $646 - i606$ on sheet III, $581.4 - i606$ on sheet VI, $576 - i606$ on sheet VII; $f_0(1370)$ – $(\mathbf{b}')$ with poles $1392.8 - i250.5$ on sheet III, $1392.8 - i269.7$ on sheet IV, $1413.2 - i269.7$ on sheet V, $1413.2 - i250.5$ on sheet VI; $f_0(1500)$ – $(\mathbf{d}')$ with poles $1498.2 - i198.8$ on sheet II, $1500.4 - i239$ on sheet III, $1498.2 - i192.8$ on sheet IV, $1498.2 - i198.8$ on sheet V, $1493.7 - i194.1$ on sheet VI, $1498.2 - i192.8$ on sheet VII; $f_0(1710)$ – $(\mathbf{c}')$ with poles $1726 - i140$ on sheet V, $1726 - i111.2$ on sheet VI, $1726 - i84.2$ on sheet VII, $1726 - i113$ on sheet VIII; the $f_0(980)$ is represented by poles $1009.2 - i32$ on sheet II and $985.9 - i58$ on sheet III. The poles on sheets IV and V, related to the $f_0(1500)$, are of the 2nd order. The total χ^2/NDF is 1.12. The background parameters are: $a'_{11} = 0.0197$, $a'_{1\eta} = -0.0652$, $a'_{1\sigma} = 0$, $a'_{1v} = 0.105$, $b'_{11} = b'_{1\eta} = b'_{1\sigma} = 0$, $b'_{1v} = 0.0439$, $a'_{21} = -3.438$, $a'_{2\eta} = -0.5053$, $a'_{2\sigma} = 1.7616$, $a'_{2v} = -5.064$, $b'_{21} = 0$, $b'_{2\eta} = -0.7349$, $b'_{2\sigma} = 2.7527$, $b'_{2v} = 1.878$, $b'_{31} = 0.5622$, $s_\sigma = 1.638$ GeV^2, $s_v = 2.126$ GeV^2.

These types of resonance pole-clusters and coupling constants from our 2-channel analysis [4] suggest that $f_0(1370)$ and $f_0(1710)$ have a dominant $s\bar{s}$ component; $f_0(1500)$, the dominant glueball one. The $f_0(980)$ is described by a pole on sheet II and shifted pole on sheet III below the $\eta\eta$ threshold without the corresponding poles on sheets VI and VII, as it was expected for standard clusters. This corresponds to the description of the $\eta\eta$ bound state [4].

Masses and widths, calculated from the pole positions with using the resonance part of amplitude in the form $T^{res} = \sqrt{s}\Gamma_{el}/(m^2_{res} - s - i\sqrt{s}\Gamma_{tot})$, are respectively (in the MeV units): 868 and 1212 for $f_0(665)$, 1015.5 and 64 for $f_0(980)$, 1407.5 and 344 for $f_0(1370)$, 1546 and 716 for $f_0(1500)$, and 1709.6 and 276 for $f_0(1710)$.

3 Analysis of isoscalar-tensor sector

Analyzing data [7] on the isoscalar D-waves of processes $\pi\pi \to \pi\pi, K\overline{K}, \eta\eta$ with an explicit allowance also for channel $(2\pi)(2\pi)$ $(i = 4)$, we used the Breit–Wigner forms to generate the resonance poles in the Le Couteur–Newton rela-

tions. The $d(k_1,k_2,k_3,k_4)$ function is $d = d_B d_{res}$ where

$$d_{res}(s) = \prod_r [M_r^2 - s - i\sum_{j=1}^{4} \rho_{rj}^5 R_{rj} f_{rj}^2] \qquad (4)$$

with $\rho_{rj} = 2k_i/(M_r^2 - 4m_j^2)^{1/2}$ and f_{rj}^2/M_r the partial width. $R_{rj}(s, M_r, s_j, r_{rj})$ is a Blatt–Weisskopf barrier factor [8] (s_j is the channel threshold, r_{rj} is a radius of the j-channel decay). From analysis, radii is of 0.955 fm for all resonances in all channels, except for $f_2(1270)$, $f_2'(1525)$ and $f_2(1950)$ for which they are: for $f_2(1270)$, 1.496, 0.704 and 0.604 fm respectively in channels $\pi\pi$, $K\overline{K}$ and $\eta\eta$, for $f_2'(1525)$, 0.576 and 0.584 fm in channels $K\overline{K}$ and $\eta\eta$, and for $f_2(1950)$, 0.178 fm in channel $K\overline{K}$.

The background part is $d_B = \exp[-i\sum_{n=1}^{3}(2k_n/\sqrt{s})^5(a_n + ib_n)]$ where

$a_1 = \alpha_{11} + \alpha_{12}\ (s - 4m_K^2)/s\ \theta(s - 4m_K^2) + \alpha_{10}\ (s - s_v)/s\ \theta(s - s_v))$,

$b_n = \beta_n + \gamma_n\ (s - s_v)/s\ \theta(s - s_v) \quad (n = 1, 2, 3)$

with $s_v \approx 2.274$ GeV^2 the combined threshold of channels $\eta\eta'$, $\rho\rho$, $\omega\omega$.

We obtain a satisfactory description; the total χ^2/NDF ≈ 1.59 already with ten resonance (without $f_2(2020)$). But the analysis of $p\overline{p} \to \pi\pi, \eta\eta, \eta\eta'$ [3] requires one more resonance ($f_2(2020)$), therefore, we have performed also the analysis considering also this state. Parameters of resonances, obtained in both cases, are shown in tab.1. Description in the 2nd case is practically the same one as in the 1st case: the total χ^2/NDF ≈ 1.64.

In the first case the background parameters are: $\alpha_{11} = -0.0785$, $\alpha_{12} = 0.0345$, $\alpha_{10} = -0.2342$, $\beta_1 = -0.06835$, $\gamma_1 = -0.04165$, $\beta_2 = -0.981$, $\gamma_2 = 0.736$, $\beta_3 = -0.5309$, $\gamma_3 = 0.8223$; in the second case: $\alpha_{11} = -0.0785$, $\alpha_{12} = 0.0345$, $\alpha_{10} = -0.2342$, $\beta_1 = -0.06835$, $\gamma_1 = -0.04165$, $\beta_2 = -0.981$, $\gamma_2 = 0.736$, $\beta_3 = -0.5309$, $\gamma_3 = 0.8223$.

4 Discussion and conclusions

1. In the model-independent analysis of data on $\pi\pi \to \pi\pi, K\overline{K}, \eta\eta, \eta\eta'$ in the channel with $I^G J^{PC} = 0^+0^{++}$, an confirmation of the σ-meson with mass 868 MeV is obtained. This mass rather accords with prediction ($m_\sigma \approx m_\rho$) by S. Weinberg [9].

2. Indication for $f_0(980)$ to be the $\eta\eta$ bound state is obtained.

3. The $f_0(1370)$ and $f_0(1710)$ have the dominant $s\bar{s}$ component. Conclusion about the $f_0(1370)$ quite well agrees with the one of work [10] where the

Table 1: *The f_2-resonance parameters (in the MeV units).*

Ten resonances without the $f_2(2020)$						
State	M	f_{r1}	f_{r2}	f_{r3}	f_{r4}	Γ_{tot}
$f_2(1270)$	1275.1±1.8	470.9±5.4	201.5±11.4	89.5±4.76	22.6±4.6	≈212
$f_2(1430)$	1450.8±18.7	128.3±45.9	562.3±142	32.7±18.4	8.2±65	>230
$f_2'(1525)$	1535±8.6	28.6±8.3	253.8±78	92.7±11.5	41.4±160	>76
$f_2(1565)$	1601.4±27.5	75.5±19.4	315±48.6	388.9±27.7	127±199	>170
$f_2(1730)$	1724.4±5.7	78.8±43	289.5±62.4	460.3±54.6	107.6±76.7	>181
$f_2(1810)$	1766.5±15.3	129.5±14.4	259±30.7	469.7±22.5	90.3±90	>177
$f_2(1950)$	1962.8±29.3	132.6±22.4	333±61.3	319±42.6	65.4±94	>119
$f_2(2000)$	2017±21.6	143.5±23.3	614±92.6	58.8±24	450.4±221	>299
$f_2(2240)$	2207±44.8	136.4±32.2	551±149	375±114	166.8±104	>222
$f_2(2410)$	2429±31.6	177±47.2	411±196.9	4.5±70.8	460.8±209	>169
Eleven resonances with the $f_2(2020)$						
State	M	f_{r1}	f_{r2}	f_{r3}	f_{r4}	Γ_{tot}
$f_2(1270)$	1275.3±1.8	469.±5.5	201.4±11.6	89.8±4.79	7.2±4.6	≈211
$f_2(1430)$	1450.4±18.8	128.3±45.9	562.3±144	32.7±18.6	8.2±63	>230
$f_2'(1525)$	1534.8±8.6	28.6±8.5	253.8±79	92.6±12.5	41.4±155	>49
$f_2(1565)$	1601.5±27.9	75.5±19.6	315±50.6	388.9±28.6	127±190	>170
$f_2(1730)$	1720.8±6.2	78.8±43	289.5±62.6	460.3±545.	108.6±76.	>182
$f_2(1810)$	1765±17.6	129.5±14.8	259±32.	469.7±25.2	90.3±89.5	>177
$f_2(1950)$	1962.2±29.8	132.6±23.3	331±61.5	319±42.8	65.4±91.3	>119
$f_2(2000)$	2006±22.7	155.7±24.4	169.5±95.3	60.4±26.7	574.8±211	>193
$f_2(2020)$	2027±25.6	50.4±24.8	441±196.7	58±50.8	128.±190	>107
$f_2(2240)$	2202±45.4	133.4±32.6	545±150.4	381.2±116	168.8±103	>222
$f_2(2410)$	2387±33.3	175±48.3	395±197.7	24.5±68.5	462.8±211	>168

$f_0(1370)$ is identified as $\eta\eta$ resonance. Conclusion about the $f_0(1710)$ is consistent with the experimental facts that this state is observed in $\gamma\gamma \to K_S K_S$ and not observed in $\gamma\gamma \to \pi^+\pi^-$ [11].

4. The $f_0(1500)$ is supposed to be practically the eighth component of octet mixed with a glueball being dominant in this state. Its biggest width among enclosing states tells also in behalf of its glueball nature [2].

5. We propose a following assignment of scalar mesons to lower nonets, excluding the $f_0(980)$ as the $\eta\eta$ bound state. The lowest nonet: the isovector $a_0(980)$, the isodoublet $K_0^*(900)$, and $f_0(600)$ and $f_0(1370)$ as mixtures of the 8th component of octet and the SU(3) singlet. The Gell-Mann–Okubo (GM-O) formula $3m_{f_8}^2 = 4m_{K_0^*}^2 - m_{a_0}^2$ gives $m_{f_8} = 880$ MeV. In relation for masses of nonet $m_\sigma + m_{f_0(1370)} = 2m_{K_0^*}$, the left side is about 26 % bigger than the right one.

For the next nonet (of radial excitations) we find: $a_0(1450)$, $K_0^*(1450)$, and $f_0(1500)$ and $f_0(1710)$ as mixture of the eighth component of octet and

the SU(3) singlet, the $f_0(1500)$ being mixed with a glueball. From the GM-O formula, $m_{f_8} \approx 1450$ MeV. In formula $m_{f_0(1500)} + m_{f_0(1710)} = 2m_{K_0^*(1450)}$, the left side is about 12 % bigger than the right one.

This assignment moves a number of questions, stood earlier, and does not put the new ones. Now an adequate mixing scheme should be found.

6. In the isoscalar-tensor sector, we carried out two analysis – without and with the $f_2(2020)$. We do not obtain $f_2(1640)$, $f_2(1910)$, $f_2(2150)$ and $f_2(2010)$, however, we see $f_2(1450)$ and $f_2(1730)$ related to the statistically-valued experimental points.

7. The $f_2(1270)$ and $f_2'(1525)$ belong to the ground tensor nonet. To the second nonet, one could assign $f_2(1601)$ and $f_2(1767)$ though the isodoublet member yet is not discovered. If one takes the isovector $a_2(1730)$ and if the $f_2(1601)$ is almost the eighth component of octet, then, from the GM-O formula, we would expect this isodoublet mass at about 1635 MeV. Then the relation for masses of nonet would be well fulfilled. There is an experiment [12] in which, in the mode $K_s^0\pi^+\pi^-$, one had observed the strange isodoublet with yet indefinite remaining quantum numbers and with mass 1629 ± 7 MeV. This state might be the tensor isodoublet of the second nonet.

8. The $f_2(1963)$ and $f_2(2207)$ together with the $K_2^*(1980)$ could be put into the third nonet. Then in the relation $M_{f_2(1963)} + M_{f_2(2207)} = 2M_{K_2^*(1980)}$, the left side is only 5.3 % bigger than the right one. If $f_2(1963)$ is the eighth component of octet, then the GM-O formula $M_{a_2} = 4M_{K_2^*(1980)} - 3M_{f_2(1963)}$ gives $M_{a_2} = 2031$ MeV. This value coincides with the one (2030 MeV) for a_2-meson obtained in the analysis [13].

9. As to $f_2(2000)$, the presence of the $f_2(2020)$ in the analysis with eleven resonances helps to interpret it as the glueball. In the case of ten resonances, the ratio of the $\pi\pi$ and $\eta\eta$ widths is in the limits obtained in ref. [3] for the tensor glueball. However, the $K\overline{K}$ width is too large for the glueball. At practically the same description of processes with the consideration of eleven resonances as in the case of ten, their parameters have varied not much, except for the ones for $f_2(2000)$ and $f_2(2410)$. Mass of the latter has decreased by about 40 MeV. As to $f_2(2000)$, its $K\overline{K}$ width has changed significantly. Now all the obtained ratios of the partial widths are in the limits corresponding to the glueball. However, there is not demonstrated clearly the glueball property of accumulating the widths of the enclosing states [2]. The question of interpre-

tation of the $f_2(2020)$ and $f_2(2410)$ is open.
10. Finally we have $f_2(1450)$ and $f_2(1730)$ which are neither $q\bar{q}$ states and nor glueballs. Since one predicts that masses of the lightest $q\bar{q}g$ hybrids are bigger than the ones of lightest glueballs, maybe, these states are the 4-quark ones. Of course, this assumption presupposes an existence of the scalar 4-quark states at lower energies, which are not seen in the analysis. One can think that these states are a part of the background in view of their very large widths.

Yu.S. and R.K. acknowledge support provided by the Bogoliubov–Infeld Program.

References

1. S. Eidelman *et al.* (PDG), Phys. Lett. **B592**, 1 (2004).
2. V.V. Anisovich, Int. J. Mod. Phys. **A21**, 3615 (2006).
3. V.V. Anisovich *et al.*, Int. J. Mod. Phys. **A20**, 6327 (2005).
4. D. Krupa *et al.*, Nuovo Cim. **A109**, 281 (1996); Yu.S. Surovtsev *et al.*, Eur. Phys. J. **A15**, 409 (2002); Int. J. Mod. Phys. **A20**, 561 (2005).
5. K.J. Le Couteur, Proc. Roy. Soc. **A256**, 115 (1960); R.G. Newton, J. Math. Phys. **2**, 188 (1961).
6. F. Binon *et al.*, Nuovo Cim. **A80**, 363 (1984).
7. B. Hyams *et al.*, Nucl. Phys. **B64**, 134 (1973); S.J. Lindenbaum and R.S. Longacre, Phys. Lett. **B274**, 492 (1992).
8. J. Blatt and V. Weisskopf, *Theoretical nuclear physics*, Wiley, N.Y., 1952.
9. S. Weinberg, Phys. Rev. Lett. **65**, 1177 (1990).
10. C. Amsler *et al.*, Phys. Lett. **B355**, 425 (1995).
11. S. Braccini, in: Proc. Workshop on Hadron Spectroscopy, Frascati Physics Series **XV**, 53 (1999); R. Barate *et al.*, Phys. Lett. **B472**, 189 (2000).
12. V.M. Karnaukhov *et al.*, Yad. Fiz. **63**, 652 (2000).
13. A.V. Anisovich *et al.*, Phys. Lett. **B517**, 261 (2001).

Frascati Physics Series Vol. XLVI (2007), pp. 677–684
HADRON07: XII Int. Conf. on Hadron Spectroscopy – Frascati, October 8-13, 2007
Light Meson Spectroscopy

THE GROUND SCALAR NONET AND D DECAYS

Olivier Leitner
Laboratori Nazionali di Frascati, Frascati
and Istituto Nazionale di Fisica Nucleare

Benoît Loiseau
Laboratoire de Physique Nucléaire et des Hautes Énergies, Paris
groupe théorie, IN2P3-CNRS, Universités Paris VI-VII

Jean-Pierre Dedonder
IMNC/Université Paris VII, Denis-Diderot, Paris

Bruno El-Bennich
Argonne National Laboratory, High Energy Physics Division, Argonne

Abstract

A short review on light scalar mesons is performed both in experiment and theory. A naive model, constrained by D branching ratios, is derived in order to make predictions on the wave functions of the $f_0(600)$ and $a_0(980)$ mesons. This leads us to compute transition form factors between the pseudoscalar B and scalar mesons.

1 What is a light scalar meson?

Up to now, there is no global agreement on the interpretation of light mesons with vacuum quantum numbers: the scalar mesons [1)]. At least, one can list two isovectors $a_0(980)$ and $a_0(1450)$, five isoscalars $f_0(600)/\sigma, f_0(980), f_0(1370)$, $f_0(1500)$ and $f_0(1710)$, and finally three isodoublets $K_0^*(800)/\kappa, K_0^*(1430)$ and $K^*(1950)$. One possible way to understand the light scalar spectrum may be to

classify scalars according to their masses, i.e. below and beyond one GeV. Following this proposal, a first group with masses below one GeV (first nonet) contains $f_0(600)$, $K_0^*(800)$, $f_0(980)$ and $a_0(980)$. A second group with a mass beyond one GeV (second nonet) includes $f_0(1370), K_0^*(1430), a_0(1450), f_0(1500)$, $f_0(1710)$ and $K^*(1950)$. Moreover, scalar mesons within their own group are built up according to the hypercharge, Y, and the isospin projection along the z-axis, I_z. The latter group being beyond the scope of this note, let us focus on the former group of light scalars so-called the first $SU(3)$ nonet.

1.1 The first $SU(3)$ nonet

Following the spirit of the quark model, the $f_0(600)$ meson with quantum numbers $I^G(J^{PC}) = 0^+(0^{++})$, the $K_0^*(800)$ meson with quantum numbers $I^G(J^P) = \frac{1}{2}^+(0^+)$, the $f_0(980)$ meson with quantum numbers $I^G(J^{PC}) = 0^+(0^{++})$ and the $a_0(980)$ meson with quantum numbers $I^G(J^{PC}) = 1^-(0^{++})$ constitute altogether the first scalar meson nonet given in fig. 1.

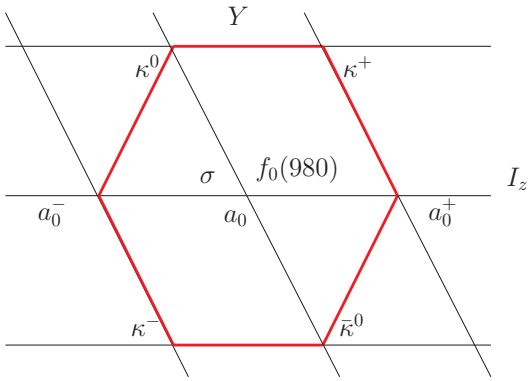

Figure 1: *The $SU(3)$ nonet.*

Regarding masses and widths, from the PDG [2], one has $M_{f_0(600)} = 400 - 1200\,\text{MeV}$, $\Gamma_{f_0(600)} = 600 - 1000\,\text{MeV}$, $M_{K_0^*(800)} = 672 \pm 40\,\text{MeV}$, $\Gamma_{K_0^*(800)} = 550 \pm 34\,\text{MeV}$, $M_{f_0(980)} = 980 \pm 10\,\text{MeV}$, $\Gamma_{f_0(980)} = 70 \pm 30\,\text{MeV}$, and $M_{a_0(980)} = 985.1 \pm 2.7\,\text{MeV}$, $\Gamma_{a_0(980)} = 75 \pm 25$ MeV, respectively. Various theoretical approaches in the study of different processes yield the following values for the pole of the $f_0(600)$ [3]:

$$(489 \pm 26) - i(173 \pm 26)\ , \quad D^+ \to (\pi^+\pi^-)\pi^+\ ,$$
$$(541 \pm 39) - i(252 \pm 42)\ , \quad J/\Psi \to \omega(\pi^+\pi^-)\ ,$$
$$(470 \pm 30) - i(295 \pm 20)\ , \quad \pi\pi \to \pi\pi\ ,$$

for the pole of the $K_0^*(800)$ [3]:

$$(721 \pm 61) - i(292 \pm 131)\ , \quad D^+ \to (K^-\pi^+)\pi^+\ ,$$
$$(841 \pm 82) - i(309 \pm 87)\ , \quad J/\Psi \to K^+\pi^-K^-\pi^+\ ,$$
$$(722 \pm 60) - i(386 \pm 50)\ , \quad K\pi \to K\pi\ ,$$

for the pole of the $f_0(980)$ [3]:

$$(998 \pm 4) - i(17 \pm 4)\ , \quad J/\Psi \to \phi\pi^+\pi^-\ ,$$
$$994 - i14\ , \quad \pi\pi \to \pi\pi \text{ and } KK\ ,$$

and for the pole of the $a_0(980)$ [3]:

$$(1036 \pm 5) - i(84 \pm 9)\ , \quad \bar{p}p \to \eta\pi\pi \text{ and } \omega\eta\pi^0\ .$$

This non-exhaustive list of experimental and theoretical values underlines very well the difficulties we have in understanding the structure and properties of the scalar mesons.

1.2 Experimental evidences of scalar mesons

Unlike the difficulties to describe scalar mesons within a consistent theoretical framework, there are clear and unambiguous experimental evidences [4] of light scalar mesons. Some of these indications also give crucial information on their internal quark structure.

1.2.1 Observations

Let us start with a few experimental signals provided by several collaborations. Regarding the $f_0(600)$ meson [5], which mainly decays into $\pi\pi$, it has been observed in various processes. The phase shift of elastic $\pi\pi$ scattering, when applying the Watson theorem and Roy equations, indicates the existence of $f_0(600)$. The E791 and FOCUS collaborations using isobar model (sum of Breit Wigner resonances) have also reported the $f_0(600)$ meson in $D^+ \to \pi^+\pi^-\pi^+$ decay. Another way of observing $f_0(600)$ is related to the $pp \to p(\pi\pi)p$ central

production (GAMS collaboration) where a double pomeron ($\rightarrow \pi\pi$) governs the process at small momentum transfers between the protons. The BES and DM2 experiments have also noticed the $f_0(600)$ meson when the $\pi\pi$ angular distribution in $J/\psi \rightarrow f_0(600)\omega \rightarrow \pi\pi\omega$ was analyzed. For the $K_0^\star(800)$ meson [6], which mainly decays into $K\pi$, two different analysis have drawn positive conclusions on its existence: firstly, the phase shift of elastic $K\pi$ scattering which was obtained from pion production by the LASS collaboration or from $D^+ \rightarrow K^-\pi^+\pi^+$ by the FOCUS collaboration. Secondly, the E791 collaboration has also used an isobar model applied to $D^+ \rightarrow K^-\pi^+\pi^+$ decay requires the $K_0^\star(800)$ for having a good fit of angular distributions. As regards the $f_0(980)$ meson [7], which mainly decays into $\pi\pi$ and KK, two major observations have been made. The BES II collaboration in $J/\Psi \rightarrow \phi\pi^+\pi^-$ and $J/\Psi \rightarrow \phi K^+K^-$ decays has found prominent signals when data were fitted with a Flatté formula. Another signal has also been observed in $D_s^+ \rightarrow \pi^-\pi^+\pi^-$ decay by the E791 collaboration. The Dalitz plot analysis leads to suggest that a significant contribution is assumed to come from the $f_0(980)\pi^+$ channel and hence gives an experimental evidence of the scalar $f_0(980)$. Concerning the $a_0(980)$ meson [8], which mainly decays into $\eta\pi$, one of the first signal was provided by the E852 collaboration using the $\pi^- p \rightarrow \eta\pi^+\pi^- n$ reaction at 18.3GeV/c^2. The mass and width of the $a_0(980)$ meson were independently determined so that it gave a first clear signal of this scalar state.

1.2.2 Quark structure

The internal quark structure of light scalar is still controversial and only experimental observations can be used to test theoretical hypothesis [4]. For example, let us consider here the case of $f_0(980)$ where several collaborations have confirmed the $s\bar{s}$ component of $f_0(980)$: the branching ratios (provided by the collaboration DM2 as well as by the PDG) of $\mathcal{B}r(J/\psi \rightarrow f_0(980)\phi) = (3.2 \pm 0.9)\times 10^{-4}$ and of $\mathcal{B}r(J/\psi \rightarrow f_0(980)\omega) = (1.4\pm 0.5)\times 10^{-4}$ being different leads to a quark mixing in terms of $u\bar{u}$ and $s\bar{s}$ in $f_0(980)$. Finally, let us have a look at the $a_0(980)$ scalar for which the collaboration KLOE [9] has given the branching ratios for radiative ϕ decays: $\mathcal{B}r(\phi \rightarrow \gamma f_0(980)) = (2.4 \pm 0.1) \times 10^{-4}$ and $\mathcal{B}r(\phi \rightarrow \gamma a_0(980)) = (0.60 \pm 0.05) \times 10^{-4}$. The radiative decay $\phi \rightarrow \gamma a_0(980)$ which cannot proceed if $a_0(980)$ is a $\bar{q}q$ state can be however nicely described in the kaon loop mechanism. This suggests a admixture of the $K\bar{K}$ component

(4-quark state) which is in contradiction with assuming $a_0(980)$ as a 2-quark state. Altogether, observing that $a_0(980)$ and $f_0(980)$ are almost degenerate, one should have a $s\bar{s}$ component in $a_0(980)$ that cannot be since it is an $I = 1$ state.

1.3 Various theoretical models

The fundamental structure of scalar mesons remaining unclear, together with the difficulties related to experimental observation of the effects of light scalars in different processes, have generated a large variety of theoretical models on the market, each of them claiming to explain the structure of light scalars below and beyond one GeV. At least, five open-roads can be followed: the simplest one is the well-known $q\bar{q}$ state for describing light scalars, then the $q\bar{q}$ state plus glueball, then the four quark states $(qq)(\bar{q}\bar{q})$, and finally the mesonic molecules. Let us give a brief overview of their main characteristics [10]. a) The $q\bar{q}$ state model where the $q\bar{q}$ L=0 nonet ($f_0(600), K_0^*(800)$, $a_0(980)$ and $f_0(980)$) is basically built up similarly to the $q\bar{q}$ L=1 nonet (π, ρ...). This model however cannot explain why $a_0(980)$ and $f_0(980)$ are not degenerate, why the $a_0(980)$ and $f_0(600)$ have the same number of non strange quarks but are not degenerate, etc... b) The $q\bar{q}$ state plus glueball model where, according QCD expectations, the lightest glueball should be a scalar particle with quantum numbers $(J^{PC}) = (0^{++})$. In such scenario, the glueball is considered as a very broad object with a width of the order of its mass. It works rather well for scalar particles with masses beyond one GeV. c) The four quark states $(qq)(\bar{q}\bar{q})$ model which allows one to have two configurations in color space: $\bar{3}3$ and $6\bar{6}$. They can therefore rearrange to form a $(q\bar{q})(q\bar{q})$ scalar state. d) Finally, the mesonic molecule model which is similar to the $(qq)(\bar{q}\bar{q})$ case but considering only mesonic degree of freedom (color singlet) such as ρ exchange for example.

2 A toy model applied to the L=0 SU(3) nonet

In our toy model, decay amplitudes for $D(D_s)$ to scalar and pseudoscalar mesons are evaluated by making use of the weak effective Hamiltonian at low energy together with QCD factorization. The associated branching ratios are compared to the experimental ones. It leads to make predictions on transition form factors between pseudoscalar (B and D) and scalar ($f_0(600)$ $K_0^*(800), f_0(980)$ and $a_0(980)$) mesons. We take advantage of these D decays

to efficiently constrain, first the scalar meson wave functions and, then the transition form factors derived within a covariant relativistic formalism.

In Covariant Light Front Dynamics [11] (CLFD), the state vector, which describes the physical bound state is defined on the light-front plane given by the equation $\omega \cdot r = \sigma$. Here, ω denotes an unspecified light-like four-vector ($\omega^2 = 0$) which determines the position of the light-front plane and r is a four-vector position of the system. Any four vector describing a phenomenon can be transformed from one system of reference to another one by using a unique standard matrix which depends only on kinematic parameters and on ω. The particle is described by a wave function expressed in terms of Fock components of the state vector which respects the properties required under any transformation.

2.1 Scalar wave functions

For a scalar particle composed of an antiquark and a quark of same constituent mass, m, the general structure of the two-body bound state has the form:

$$\phi(\mathbf{k}^2) = \frac{1}{\sqrt{2}} \bar{u}(k_2) A(\mathbf{k}^2) v(k_1) \ , \tag{1}$$

where $A(\mathbf{k}^2) = N_S \exp\left[-4\nu \mathbf{k}^2/m^2\right]$ is the scalar component of the wave function. N_S and ν are parameters to be determined from experimental D branching ratios ($D \to \mathit{scalar}\,\pi$ or $D \to \mathit{scalar}\,K$) and theoretical assumptions.

2.2 Transition form factors between pseudoscalar and scalar

In CLFD, the approximate transition amplitude between a pseudoscalar, P, and a scalar, S, explicitly depends on the light front orientation:

$$\langle S(P_2)|J^\mu|P(P_1)\rangle^{CLFD} = (P_1+P_2)^\mu f_+(q^2) + (P_1-P_2)^\mu f_-(q^2) + B(q^2)\omega^\mu \ , \tag{2}$$

where $B(q^2)$ is a non-physical form factor which has to be zero in any exact calculation. Simple algebraic calculations allow us to extract the physical transition form factors $f_\pm(q^2)$, by means of the amplitude $\langle S(P_2)|J^\mu|P(P_1)\rangle^{CLFD}$:

$$\langle S(P_2)|J^\mu|P(P_1)\rangle^{CLFD} = \int_{(x,\tilde{\theta},\mathbf{R}_\perp)} D(x,\tilde{\theta},\mathbf{R}_\perp) \mathrm{Tr}\left[-\bar{\vartheta}_S(m_1 + \not{k}_1)\gamma^\mu\gamma^5(m_2 + \not{k}_2)\vartheta_P(m_3 - \not{k}_3)\right] \frac{1}{1-x'} \ , \tag{3}$$

which is derived from the usual triangular diagram describing transitions between mesons. $D(x, \tilde{\theta}, \mathbf{R}_\perp)$ is the invariant phase space element and ϑ_P and ϑ_S denote respectively the initial pseudoscalar and final scalar wave functions. For more information on the CLFD approach, we refer the reader to the paper [11].

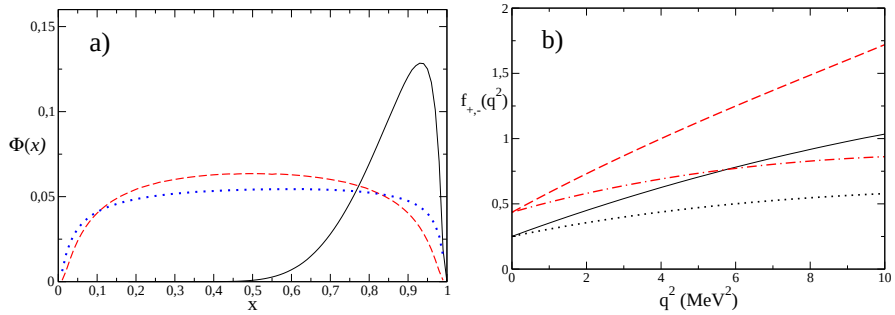

Figure 2: *a) x-distributions for the B meson (full line) as well as for $K^*(800)$ (dashed line) and $a_0(980)$ (dotted line). b) transition form factors, $f_+(q^2), f_-(q^2)$, plotted in case of $B \to f_0(600)$ (full and dotted lines) and $B \to a_0(980)$ (dashed and dotted-dash lines), respectively.*

3 Conclusion

Using normalization and D experimental branching ratios one can model the wave function of scalar mesons for which some x distributions are given in fig. 2a). One can also make predictions on transition form factors between pseudoscalar and scalar mesons as shown (similar results for $D \to$ *scalar* transitions) in fig. 2b). All the results given here are only qualitative due to some uncertainties among them the experimental D branching ratios, the 2-quark description assumption and the meson and quark mass effects. It is therefore crucial to improve our understanding of scalar mesons as they play a major role when analyzing for example the CP violation asymmetry in $B \to \pi\pi\pi(K)$. Better one knows the unitarity triangle, better one can looks for new physics effects, however tiny they may be.

References

1. M. R. Pennington, arXiv:0711.1435 [hep-ph].
2. W. M. Yao *et al*, J. Phys. G **33**, 1 (2006) and references therein.
3. D. V. Bugg, hep-ex/0510014 and references therein.
4. M. R. Pennington, hep-ph/0703256 and references therein.
5. I. Bediaga *et al.*, E791 collaboration, Braz. J. Phys. **34**, 1398 (2004); S. Malvezzi *et al*, FOCUS collaboration, AIP Conf. Proc. **717**, 77 (2004); D. Alde *et al*, GAMS collaboration, Phys. Lett. B **397**, 350 (1997); M. Ablikim *et al.*, BES collaboration, Phys. Lett. B **598**, 149 (2004); J. E. Augustin *et al*, DM2 collaboration, Nucl. Phys. B **320**, 1 (1989).
6. D. Aston *et al*, LASS collaboration, Nucl. Phys. B **296**, 493 (1988); J.M. Link *et al*, FOCUS collaboration, Phys. Lett. B **653**, 1 (2007); C. Gobel *et al*, E791 collaboration, AIP Conf. Proc. **688**, 266 (2004).
7. L. Y. Dong *et al*, BES collaboration, hep-ex/0410040; C. Gobel *et al*, E791 collaboration, Frascati Phys. Ser. **20**, 373 (2001).
8. S. Teige *et al*, E852 collaboration, Phys. Rev. **D59**, 012001 (1999).
9. A. Aloisio *et al*, KLOE collaboration, hep-ex/0107024.
10. a) B. El-Bennich *et al*, Nucl. Phys. A **790**, 510 (2007); b) F. Giacosa *et al*, Phys. Rev. D **72**, 094006 (2005); c) R. L. Jaffe, Phys. Rev. D **15**, 267 (1977); d) N. N. Achasov *et al*, Sov. J. Nucl. Phys. **32**, 566 (1980).
11. J. Carbonell *et al*, Phys. Rept. **300**, 215 (1998).

Frascati Physics Series Vol. XLVI (2007), pp. 685–692
HADRON07: XII Int. Conf. on Hadron Spectroscopy – Frascati, October 8-13, 2007
Light Meson Spectroscopy

EXOTICA POSSIBILITY OF NEW OBSERVATIONS BY BES

Ailin Zhang
Department of Physics, Shanghai University, Shanghai, 200444, China

Abstract

The employment of interpolating currents of existing studies of four-quark state and glueball with QCD sum rule approach is analyzed. In terms of suitable currents, the masses of the lowest lying scalar and pseudo-scalar glueball were determined. The masses of some tetraquark states and their first orbital excitations were obtained through a combination of the sum rule with the constituent quark model. Exotica possibility of the new observations by BES is discussed.

1 QCD sum rules and exotica

QCD is believed the right theory describing strong interactions, quark model is proved successful in describing normal hadrons. However, the low energy behavior of QCD and the mechanism of quark confinement of hadron are not clear. The study of hadron properties with QCD is a great challenge. In history,

many models based on QCD were developed to study hadrons. QCD (SVZ) sum rule [1] is such an effective nonperturbative method of relating fundamental parameters of QCD Lagrangian and vacuum to parameters of hadrons.

In sum rule methods, to detect the properties of hadrons, some correlators are constructed from suitable interpolating currents (local operators). In one hand, the correlator is expanded in perturbative coefficients and condensates. In the other hand, the imaginary part of the correlator (spectral density) is expressed with the parameters of resonances. Through a dispersion relation, the parameters of QCD and vacuum are connected with the parameters of hadrons. To get reasonable conclusions on the properties of hadrons, it is very important to employ suitable currents.

In normal hadron physics ($q\overline{q}$ mesons and qqq baryons), the structure of mesons and baryons is not so complex and the sum rules work well. Exotic hadrons such as glueballs, hybrids and multi-quark states have complex intrinsic structure, there are often different ways to employ interpolating currents. Furthermore, no exotic hadron has been confirmed such that the properties of exotic hadrons are not clear. Whether QCD sum rules work or not has not been proved. Hence, one should be careful to use reasonable currents and to draw corresponding conclusions on exotic hadrons.

2 0^{++} and 0^{-+} glueballs

The existence of glueballs was firstly mentioned by Fritzsch and Gell-Mann [2]. Glueballs were studied in many models. In the sum rule approaches, the interpolating currents consist of gluon fields.

For the 0^{++} glueball, the current was firstly employed by Novikov and coworkers [3],

$$j_s = \alpha_s G^a_{\mu\nu} G^a_{\mu\nu}, \tag{1}$$

where $m_\sigma = 700$ MeV was taken as that of the σ without computation.

Subsequently, the 0^{++} scalar glueball was studied with the same current in many studies. In Narison's [4] work, $m = 1.5 \pm 0.2$ GeV was predicted. In the work of Huang's [5], $m = 1.7 \pm 0.2$ GeV was predicted with a reasonable moment. In the work of Harnett [6], two glueballs were predicted: a heavier $m = 1.4$ GeV and a lighter $m \approx 1.0 - 1.25$ GeV, where the contribution of instantons was taken into account. In a most recent work by Forkel [7], with

a comprehensive inclusion of the contribution of operator product expansion (OPE), $m = 1.25 \pm 0.2$ GeV was predicted.

For the 0^{-+} glueball, the interpolating current was also firstly employed by Novikov and collaborators [8],

$$j_{ps} = \alpha_s G^a_{\mu\nu} \tilde{G}^a_{\mu\nu}. \tag{2}$$

In their computation, $m = 2 - 2.5$ GeV. This interpolating current was also employed to study pseudoscalar glueballs in many other studies. In Narison's [4] work, $m = 2.05 \pm 0.19$ GeV was predicted. With the higher-loop perturbative contributions and instantons taken into account, $m = 2.65 \pm 0.33$ GeV was predicted in the work of Zhang [9]. In Forkel's work, the instanton and the topological charge screening effects were taken into account, and $m = 2.2 \pm 0.2$ GeV. It is widely believed that the mass of the 0^{-+} glueball is larger than that of the 0^{++} glueball.

In the constituent parton model, there are glueballs with two gluons and glueballs with three gluons. In the sum rule method, in addition to the interpolating currents consisting of two gluons field, interpolating currents consisting of three gluons field have been employed. There is a large mass difference between the 0^{-+} and the 0^{++} glueball prediction. The difference may result from the rough calculations or the special features of the 0^{-+} and 0^{++} glueball. For the difficulty in the calculation of the OPE, present results on glueball masses are not definite and may be largely improved with more accurate computations.

The current consisting of three gluon fields was firstly employed by Latorre [10] to compute the mass of the 0^{++} three gluon glueball

$$j_{s3g} = g^3 f_{abc} G^a_{\mu\nu} G^b_{\nu\rho} G^c_{\rho\mu}, \tag{3}$$

with $m_{s3g} = 3.1$ GeV.

The current consisting of three gluon fields was recently employed by Hao [11] to compute the mass of the 0^{-+} pseudoscalar three gluon glueball

$$j_{ps3g} = g^3 f_{abc} \tilde{G}^a_{\mu\nu} \tilde{G}^b_{\nu\rho} \tilde{G}^c_{\rho\mu}, \tag{4}$$

with $m_{ps3g} = 1.9 - 2.7$ GeV.

As well known, two gluon glueballs may mix with three gluon glueballs, and two gluon currents may mix with three gluon currents. Furthermore, these two kinds of currents couple to both kinds of glueballs. How to deal with these

mixing effects is a great challenge in the sum rule approach. Final conclusions on glueballs are expected to depend heavily on these mixing effects.

3 0^{++} and 1^{--} tetraquark states

Four-quark states have been studied in MIT bag model [12], color junction model [13], potential model [14], effective Lagrangian method [15], relativistic quark model [16], QCD sum rules [17–22], and many other methods [23]. More references could be found in [24] and references therein.

Four-quark states consist of two quarks and two anti-quarks. Their intrinsic quarks/anti-quarks may make different clusters (correlations) such as color, flavor, spin, etc. [12, 22, 24]. According to the spatial extension of clusters, there are two different types of four-quark states: $(qq)(\bar{q}\bar{q})$ and $(q\bar{q})(q\bar{q})$. The bound state $(qq)(\bar{q}\bar{q})$ is often called tetraquark state or baryonium, it consists of diquark qq and anti-diquark $\bar{q}\bar{q}$, while $(q\bar{q})(q\bar{q})$ includes the molecule state.

The states $(qq)(\bar{q}\bar{q})$ and $(q\bar{q})(q\bar{q})$ may mix with each other and with normal $q\bar{q}$ meson (the ones mixed with $q\bar{q}$ are usually called crypto-exotic four-quark states). Therefore, a meson observed by an experiment is

$$|\text{meson}>=|q\bar{q}>+|(qq)(\bar{q}\bar{q})>+|(q\bar{q})(q\bar{q})>+\cdots. \tag{5}$$

The quark dynamics of four-quark states is still not clear, so intrinsic color and flavor configurations could not be distinguished unless some special observable is established. Unfortunately, no such an observable has been definitely set up.

To study four-quark states with sum rules, two kinds of interpolating currents, for example: $(q\bar{q})(q\bar{q})$ [17], $(q\bar{q})^2$, $(qq)(\bar{q}\bar{q})$ [18], $(cq)(\bar{q}\bar{q})$ [19], $(cu)(\bar{s}\bar{u})$ [20], $(ud)(\bar{s}\bar{s})$ [21], have been employed. All the calculations are at leading order.

Many conclusions on four-quark states have been drawn using these two kinds of currents. However, in view of the sum rule approach, there is no definite difference between this two kinds currents. The reason is that $(qq)(\bar{q}\bar{q})$ and $(q\bar{q})(q\bar{q})$ can be turned into each other after Fierz transformation [18, 22], and they will mix with each other under renormalization. Therefore, it is useful to remember that conclusions on the structure of four-quark state in constituent quark picture can not be drawn directly from the structure in the current (operator) picture. Similarly, diquark concepts are not meaningful in

Table 1: *Masses of some tetraquark states.*

	0^{++}	1^{-+}
$[qq][\bar{q}\bar{q}]$	~ 490 MeV	$\sim 490 + B'_q$ MeV
$[sq][\bar{q}\bar{q}]$	~ 610 MeV	$\sim 610 + B'_q$ MeV
$sq][\bar{s}\bar{q}]$	~ 730 MeV	$\sim 730 + B'_s$ MeV

current picture [22]. In principle, there is no direct way to turn the current (operator) picture into the constituent quark picture.

To get a reasonable result on four-quark state, suitable mixed interpolating currents and mixture of hadrons should be taken into account, which is also a great challenge in sum rule method.

Following the diquark picture applied to weak hadron decays with sum rules [25], the diquark current with flavor (sq)

$$j_i(x) = \epsilon_{ijk} s_j^T(x) C O q_k(x) \tag{6}$$

was employed and an updated analysis was performed in a recent attempt [22]. The most "suitable" masses for diquark m_{qq} and m_{sq} were obtained as: $m_{qq} \sim 400$ MeV and $m_{sq} \sim 460$ MeV with $s_0 = 1.2$ GeV^2. The diquark mass scale is the same as that of the constituent quarks. The results obtained here are consistent with the fit of Maiani [23].

Once the masses determined by sum rule are taken as the constituent diquark masses, masses of the $L = 0$ and $L = 1$ excited tetraquark state are obtained as the method of Maiani [23]

$$M \approx 2m_{[qq]} - 3(\kappa_{qq})_{\bar{3}}, \quad M \approx 2m_{[qq]} - 3(\kappa_{qq})_{\bar{3}} + B'_q \frac{L(L+1)}{2}.$$

The obtained masses of some four-quark states are listed in tab. 1. Tetraquark states consisting of bad diquark have the same mass scale [23]. It is easy to find the explicit flavor dependence of masses.

4 Exotica possibility of the new observations by BES

Some new observations were reported by BES through its sample of 58 million events of J/Ψ decays.

A $p\bar{p}$ enhancement was observed by BES [26] in the radiative decay $J/\Psi \to \gamma p\bar{p}$. If interpreted as a single $0^{\pm+}$ resonance they find $M = 1859^{+3}_{-10}(stat)^{+5}_{-25}(sys)$

(below $2m_p$) and $\Gamma < 30$ MeV. It was observed also by Belle [31] and BaBar [32] collaborations in other channels. The J^{PC} quantum number assignment is consistent with either 0^{-+} or 0^{++}. This enhancement has been interpreted as a final state interaction effect, baryonium or a threshold cusp.

The state $X(1835)$ has been observed by BES [27] in the decay $J/\Psi \to \gamma\pi^+\pi^-\eta'$ with $M = 1833.7 \pm 6.1(stat) \pm 2.7(syst)$ MeV and $\Gamma = 67.7 \pm 20.3 \pm 7.7$ MeV. It is consistent with expectations for the state that produces the strong $p\bar{p}$-mass threshold enhancement. It has been interpreted as a 0^{-+} glueball or baryonium.

The state $X(1812)$ has been observed by BES [28] in the doubly OZI-suppressed decay $J/\Psi \to \gamma\omega\phi$ with $M = 1812^{+19}_{-26}(stat) \pm 18(syst)$ MeV, $\Gamma = 105 \pm 20 \pm 28$ MeV. It favors $J^P = 0^+$. It has been interpreted as a rescattering effect, a four-quark state, a glueball or a hybrid.

The state $X(1576)$ has been observed by BES [29] in the decay $J/\Psi \to K^+K^-\pi^0$ with the pole position $1576^{+49}_{-55}(stat)^{+98}_{-91}(syst)$ MeV-$i(409^{+11}_{-12}(stat)^{+32}_{-67})$ MeV. This broad peak is believed to have $J^{PC} = 1^{--}$. It has been interpreted as a final state interaction effect or a tetraquark state.

Exotica was often invoked to explain the special features of newly observed states. Based on previous analyses, the glueball and tetraquark possibility for these observations is examined.

In QCD sum rule approach, the two glueball candidates with lower mass are 0^{++} and 0^{-+} glueballs. Therefore, $X(1835)$ and $X(1812)$ may be 0^{++} glueballs, while they are unlike to be the pure 0^{-+} glueballs.

The 0^{++} and 0^{-+} tetraquark states have the same mass scale, and they have lower masses compared with the new observations by BES. It is hard to explain these observations as 0^{++} or 0^{-+} tetraquark states. If $X(1576)$ is confirmed to be 1^{--}, it may be the first orbital excited 1^{--} tetraquark state (orbital excitation of $a_0(980)$ or $f_0(980)$) with a very large excitation energy ~ 596 MeV.

5 Conclusions and discussions

Different interpolating currents have been employed to study exotic states, but the structure of these currents has no direct correspondence to the constituent structure of hadrons. The study of exotica with sum rules requires more exploration.

The masses of 0^{++}, 0^{-+} glueballs and some tetraquark states were determined. According to these studies, the new observations by BES are unlike to be pure 0^{-+} pseudo-scalar glueballs, they are unlikely to be the light tetraquark states, while $X(1576)$ should be the first orbital excitation of the exotic $(sq)(\bar{s}\bar{q})$ tetraquark state.

6 Acknowledgements

This work is supported in part by NSFC under the grant: 10775093. The author warmly thanks the organizing committee for partial financial support.

References

1. M.A. Shifman, A.I. Vainshtein and V.I. Zakharov, Nucl. Phys. B **147**, 385 (1979).
2. H. Fritzsch and M. Gell-Mann, 16th Int.Conf. High-Energy Phys., Chicago, Vol. 2, 135 (1972).
3. V.A. Novikov, *et al.*, Nucl. Phys. B **165**, 67 (1980).
4. S. Narison, Nucl. Phys. B **509**, 312 (1998).
5. T. Huang, *et al.*, Phys. Rev. D **59**, 034026 (1999).
6. D. Harnett and Tom Steele, Nucl. Phys. A **695**, 205 (2001).
7. H. Forkel, Phys. Rev. D **71**, 054008 (2005).
8. V.A. Novikov, *et al.*, Nucl. Phys. B **191**, 301 (1981).
9. Ailin Zhang and Tom Steele, Nucl. Phys. A **728**, 165 (2003).
10. J.I. Latorre, S. Narison and S. Paban, Phys. Lett. B **191**, 437 (1987).
11. G. Hao, C.-F. Qiao and A. Zhang, Phys. Lett. B **642**, 53 (2006).
12. R.L. Jaffe, Phys. Rev. D **15**, 267 (1977); D **15**, 281 (1977).
13. H.-M. Chan and H. Högaasen, Phys. Lett. B **72**, 121 (1977).
14. J. Weinstein and N. Isgur, Phys. Rev. Lett, **48**, 659; Phys. Rev. D **27**, 588 (1983); Phys. Rev. D **41**, 2236 (1990);
N.A. Törnqvist, Phys. Rev. Lett, **67**, 556 (1991);
L.Y. Glozman and D. O. Riska, Phys. Rept, **268**, 263 (1996).

15. D. Black, A.H. Fariborz, J. Schechter, Phys. Rev. D **59**, 074026 (1999).

16. D. Ebert, R.N. Faustov, V.O. Galkin, Phys. Lett. B **634**, 214 (2006).

17. A. Zhang, Phys. Rev. D **61**, 114021 (2000).

18. T. Schafer, Phys. Rev. D **68**, 114017 (2003).

19. M.E. Bracco, A. Lozea, R.D. Matheus, *et al.*, Phys. Lett. B **624**, 217 (2005).

20. H. Kim and Y. Oh, Phys. Rev. D **72**, 074012 (2005).

21. H.-X. Chen, *et al.*, Phys. Rev. D **74**, 054001 (2006).

22. A. Zhang, T. Huang and T. Steele, Phys. Rev. D**76**, 036004 (2007).

23. N.N. Achasov, *et al.*, Phys. Lett. B **108**, 134 (1982);
N.N. Achasov and V.N. Ivanchenko, Nucl. Phys. B **315**, 465 (1989);
J.R. Pelaez, Phys. Rev. Lett. **92**, 102001 (2004);
L. Maiani, F. Piccinini, A.D. Polosa and V. Riquer, Phys. Rev. Lett. **19**, 212002 (2004); Phys. Rev. D **71**, 014028 (2005);
I.V. Anikin, B. Pire and O.V. Teryaev, Phys. Lett. B **626**, 86 (2005);
D.Melikhov and B. Stech, Phys. Rev. D **74**, 034022.

24. S. Godfrey and J. Napolitano, Rev. Mod. Phys. **71**, 1411 (1999);
C. Amsler and N.A. Törnqvist, Phys. Rept. **389**, 61 (2004);
D.V. Bugg, Phys. Rept. **397**, 257 (2004);
R.L. Jaffe, Phys. Rept. **409**, 1 (2005);
E. Klempt, A. Zaitsev, arXiv:0708.4016 [hep-ph].

25. H.G. Dosch, M. Jamin and B. Stech, Z. Phys. C **42**, 167 (1989);
M. Jamin and M. Neubert, Phys. Lett. B **238**, 387 (1990).

26. J.Z. Bai, *et al.* (BES Collaboration), Phys. Rev. Lett. **91**, 022001 (2003)).

27. M. Ablikim, *et al.* (BES Collaboration), Phys. Rev. Lett. **95**, 262001 (2005).

28. M. Ablikim, *et al.* (BES Collaboration), Phys. Rev. Lett. **95**, 262001 (2005).

29. M. Ablikim, *et al.* (BES Collaboration), Phys. Rev. Lett. **96**, 162002 (2006).

30. M. Ablikim, *et al.* (BES Collaboration), Phys. Rev. Lett. **97**, 142002 (2006).

31. M.-Z. Wang *et al.* (Belle Collaboration), Phys. Lett. **B617**: 141 (2005).

32. B. Aubert *et al.* (BaBar Collaboration), Phys. Rev. D **74**: 051101 (2006).

Frascati Physics Series Vol. XLVI (2007), pp. 693
HADRON07: XII Int. Conf. on Hadron Spectroscopy – Frascati, October 8-13, 2007
Ligh Meson Spectroscopy

THE MASSES SPECTRUM OF THE EXOTIC MESON 0^{--}, 0^{+-} AND 2^{+-} STATES BY THE DIQUARK CLUSTER MODEL CALCULATION WITH $qq\overline{qq}$ SYSTEM

H. Noya
Institute of Physics, Faculty of Economics,Hosei University at Tama

Written contribution not received

Frascati Physics Series Vol. XLVI (2007), pp. 695–702
HADRON07: XII Int. Conf. on Hadron Spectroscopy – Frascati, October 8-13, 2007
Light Meson Spectroscopy

STUDIES OF $\sigma(e^+e^- \to$ HADRONS) USING INITIAL STATE RADIATION

W. F. Wang (for the *BABAR* collaboration)
Laboratoire de l'Accélérateur Linéaire,Orsay

Abstract

We present a review of recent *BABAR* results on $e^+e^- \to$ hadrons using the initial state radiation technique. Cross sections over the $\sqrt{s}$ range from threshold to $4-5$ GeV, with very small point-to-point systematic errors, are presented for the $2(\pi^+\pi^-)\pi^0$, $2(\pi^+\pi^-)\eta$ and (preliminary) $\pi^+\pi^-\pi^0\pi^0$ final results. We also study the internal structure of these events and present cross sections for several resonant modes.

1 Introduction

The cross section for $e^+e^- \to$ hadrons at low energy is dominated by single resonances and few-body processes, which provide the main source of information on the properties of the light vector mesons (ρ, ω, ϕ) and their excited states. Besides that, the precise measurements of $R = \frac{\sigma(e^+e^- \to \text{hadrons})}{\sigma(e^+e^- \to \mu^+\mu^-)}$ are

crucial input for calculating the hadronic contribution to i) the muon anomalous magnetic moment [1)] and ii) the running of the electromagnetic coupling α_{QED} [2)]. The interest in this kind of study has been increasing because of discrepancy between the measured muon $g-2$ value [3)] and the one predicted by the Standard Model, where the hadronic contribution to the prediction is calculated from e^+e^- experiments at low energies. Benefiting from the high luminosity and the excellent *BABAR* detector performance [4)], the *BABAR* collaboration has an intensive program for a study of the low energy cross sections and hadron spectroscopy via the Initial State Radiation technique (ISR), and several multi-hadron cross sections have already been measured [5−8)].

2 The ISR method

The ISR cross section for a particular final state f depends on the e^+e^- cross section $\sigma_f(s)$ and is obtained from:

$$\frac{d\sigma(s,x)}{dx} = W(s,x)\cdot\sigma_f(s(1-x)), \tag{1}$$

where $x = \frac{2E_\gamma}{\sqrt{s}}$; E_γ is the energy of the ISR photon in the c.m. frame, and $\sqrt{s}$ is the nominal c.m. energy. The function $W(s,x)$ describes the energy spectrum of the virtual photons and can be calculated with better than 1% accuracy [9−11)]. The *BABAR* acceptance for such photons is around 10 %. ISR photons are produced predominantly along the beam directions, but the *BABAR* acceptance of $\sim 10\%$ allows high-statistics studies of full reconstructed event. An advantage deriving from the use of ISR is that the entire range of effective collision energy is scanned in one experiment. This avoids the relative normalization uncertainties which can arise when data from different experiments are combined. A disadvantage is that the invariant mass resolution of about 8 MeV limits the width of the narrowest structure which can be measured via ISR production. Nevertheless it's sufficient to observe the J/ψ production and measure the product $\Gamma\cdot B_{ee}\cdot B_f$ where Γ and B_{ee}, B_f are the total width, branching fractions of J/ψ to e^+e^- and the final state f.

3 *BABAR* ISR measurements

The *BABAR* ISR program focus on the study of all significant hadronic process $e^+e^- \to$ hadrons from threshold to about 4.5 GeV center of mass (c.m.) energy.

Meanwhile, the spectroscopy of $J^{PC} = 1^{--}$ states and their decays are studied. Here we discuss the latest results on $\pi^+\pi^-\pi^0\pi^0$, $2(\pi^+\pi^-)\pi^0$, $2(\pi^+\pi^-)\eta$ channels and the progress on inclusive measurements. The nucleon form factor and channels with $K\bar{K}$ are covered in the talk [12].

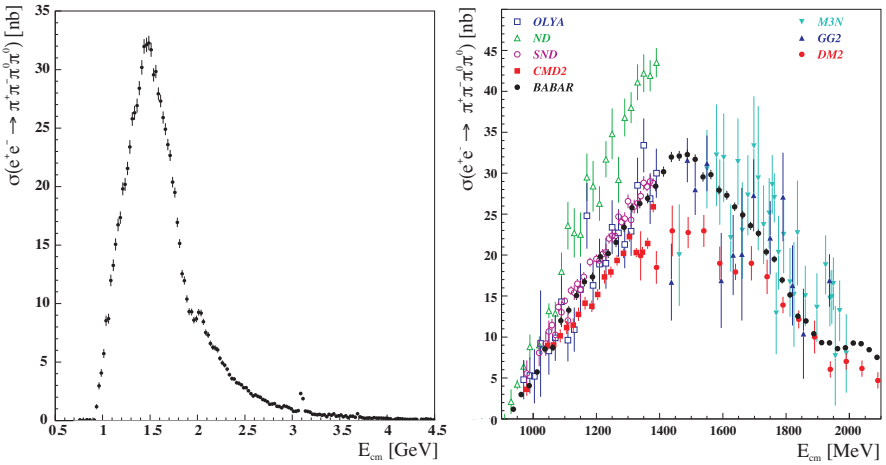

Figure 1: *The $e^+e^- \to \pi^+\pi^-\pi^0\pi^0$ cross section measured by BABAR (left), and the comparison the BABAR data on $\pi^+\pi^-\pi^0\pi^0$ cross section with the other experiments (right).*

3.1 $e^+e^- \to \pi^+\pi^-\pi^0\pi^0$

According the recent progress in the evaluation of the hadronic contribution to a_μ and α_{QED}, the cross section data in the 1-2 GeV range becomes more important. In this energy range, the largest relative error comes from the poorly known channel $\pi^+\pi^-\pi^0\pi^0$. Figure 1 shows *BABAR* preliminary results on $e^+e^- \to \pi^+\pi^-\pi^0\pi^0$. The current systematic error of the measurement varies from 8% in the cross section peak to 14% at 4.5 GeV. The right plot in Fig. 1 shows the comparison with existing data. The *BABAR* results are in agreement with SND data [13] and CMD2 data [14] in the energy range below 1.4 GeV, and show a huge improvement for higher energies (> 1.4 GeV). Only *BABAR* data exists in the range above 2.5 GeV. The substructure study find the dominant intermediate states for $e^+e^- \to \pi^+\pi^-\pi^0\pi^0$ are $\omega\pi^0$, $a_1\pi$ and $\rho^+\rho^-$, shown in Fig. 2. The contribution of $\rho^0 f_0(980)$ is also seen. The surprising large contribution from $e^+e^- \to \rho^+\rho^-$ is seen for the first time.

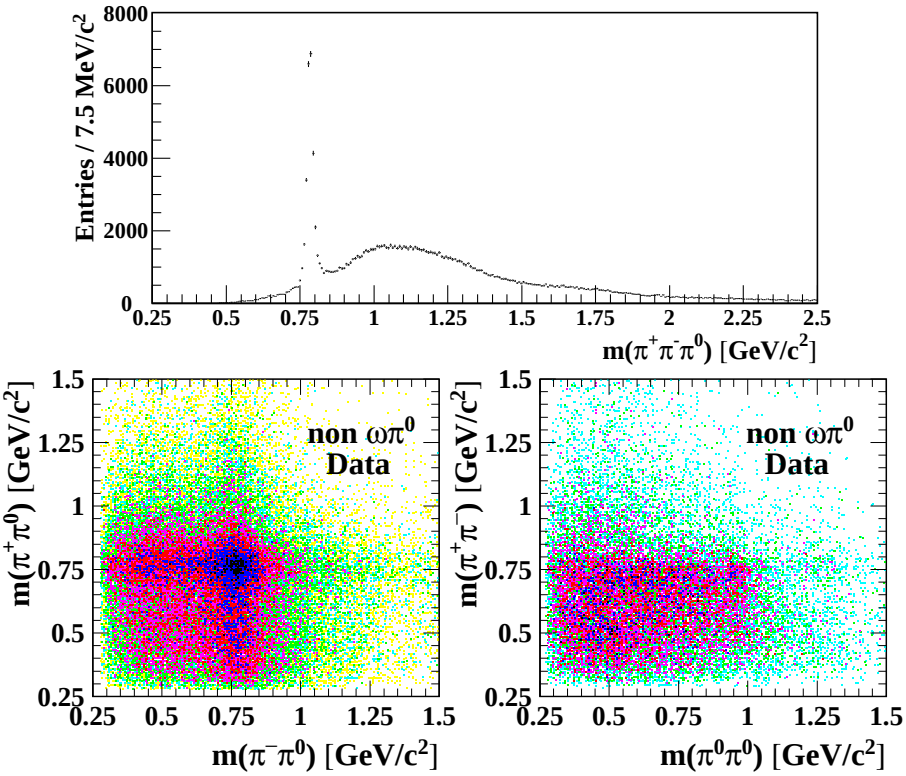

Figure 2: *The $\pi^+\pi^-\pi^0$ invariant mass and the scatter plots $m_{\pi^+\pi^0}$ versus $m_{\pi^-\pi^0}$ and $m_{\pi^+\pi^-}$ versus $m_{\pi^0\pi^0}$ for $2\pi 2\pi^0$ events.*

3.2 $e^+e^- \to 2(\pi^+\pi^-)\pi^0$

Figure 3 shows the $2(\pi^+\pi^-)\pi^0$ invariant mass distribution and the measured cross section from threshold up to 4.5 GeV. The two narrow peaks are apparent at the J/ψ and $\psi(2S)$ masses. The systematic error of the measurement is about 7% at the cross section peak. In the $\pi^+\pi^-\pi^0$ mass distribution, we see the ω and η peaks which corresponds $\omega\pi\pi$ and $\eta\pi^+\pi^-$ intermediate states. The rest of events have $\rho 3\pi$ structure. The cross sections for all above three selected components are measured and shown in Fig. 4.

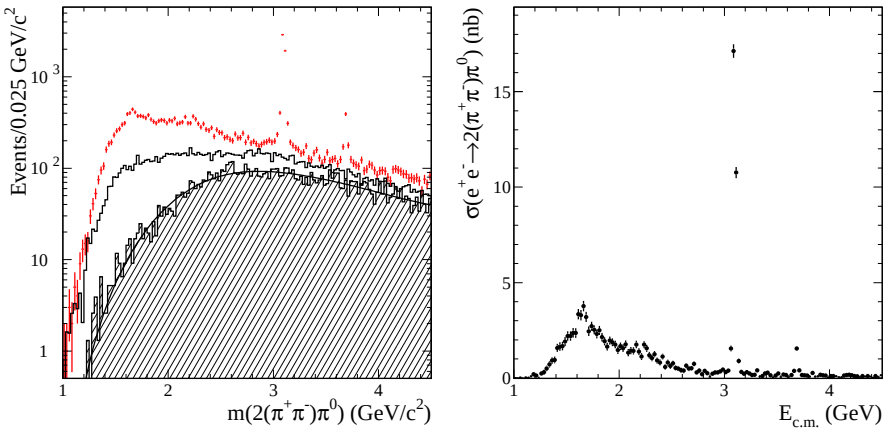

Figure 3: *The $e^+e^- \to 2(\pi^+\pi^-)\pi^0$ invariant mass (right) and measured cross section (left).*

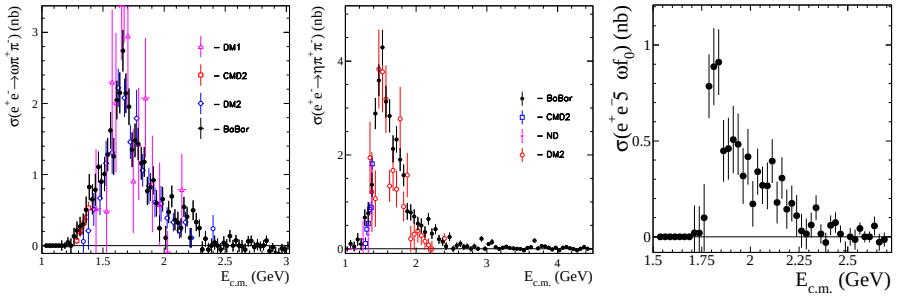

Figure 4: *The cross sections for $e^+e^- \to \omega\pi^+\pi^-$ (left), and the $e^+e^- \to \eta\pi^+\pi^-$ (middle), and $e^+e^- \to \omega f_0$ (right).*

3.3 $e^+e^- \to 2(\pi^+\pi^-)\eta$

We also present the first measurement of the $e^+e^- \to 2(\pi^+\pi^-)\eta$ cross section, as seen in Fig. 5. It shows a peak value of about 1.2 nb at about 2.2 GeV, followed by monotonic decrease toward higher energies, broken only by a peak at the J/ψ mass. Three intermediate states are observed: $\eta\rho(1450) \to \eta 4\pi$,

$\eta'\rho(770)$, and $f_1(1285)\rho(770)$. The two latter cross sections, shown in Fig. 6, are consistent with the shape of $\rho(2150)$ [15].

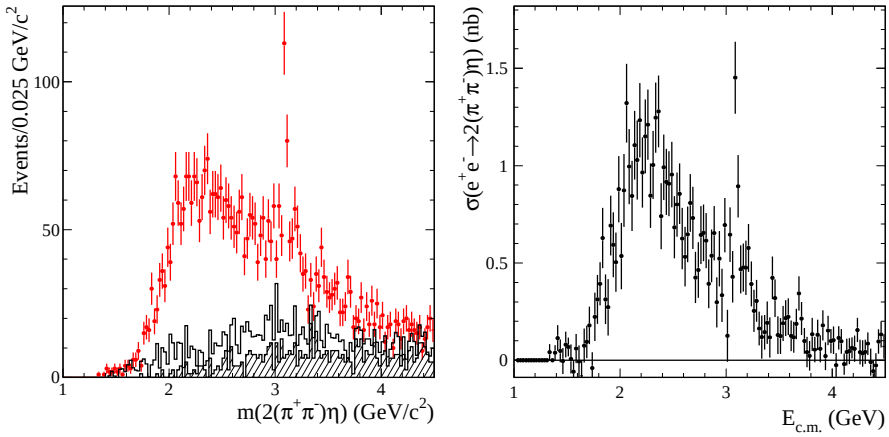

Figure 5: *The invariant mass of* $2(\pi^+\pi^-)\eta$ *(left), and the* $e^+e^- \to 2(\pi^+\pi^-)\eta$ *cross section measured by BABAR(right).*

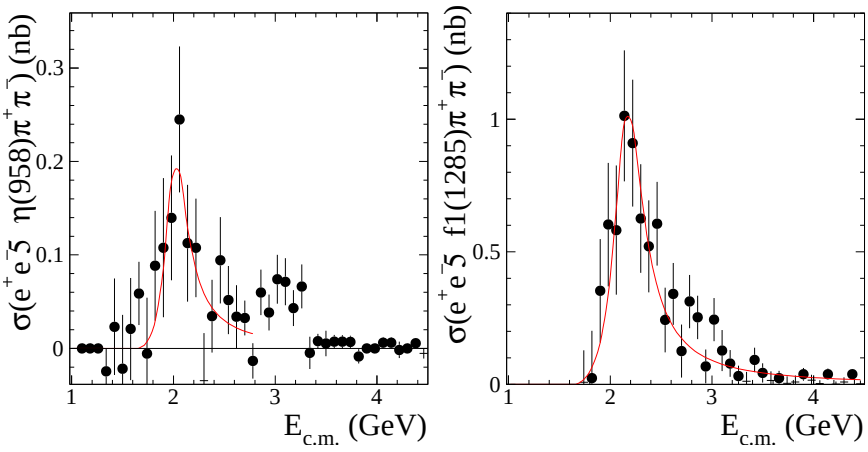

Figure 6: *The cross sections for* $e^+e^- \to \eta'\rho$ *(left) and* $e^+e^- \to f_1(1285)\pi^+\pi^-$ *(right).*

3.4 Progress on an inclusive R measurements

σ_{had} can be also measured inclusively tagging one hard photon, recoiling against a hadronic system. The primary background is QED events with an energetic photon, such as $e^+e^- \to \gamma\gamma$, $e^+e^- \to \gamma e^+e^-$. Events with identified $e^\pm$ are rejected, while the well-understood radiative $\mu\mu$ and $\tau\tau$ backgrounds are subtracted using MC. Background levels after selections are shown in Fig 7. Our photon energy resolution ($\sim 2\%$) smears any narrow structure, fortunately, we can measure the integral:

$$\delta\alpha_{had}(M_Z^2, S_{Max}) = \frac{\alpha M_Z^2}{3\pi}\int_{4m_\pi^2}^{S_{Max}} \frac{d\sigma(e^+e^- \to \gamma\text{hadrons})}{s(M_Z^2 - s)\sigma^0_{ISR}(s)},$$

where $\sigma^0_{ISR}(s) = \frac{4\pi\alpha^2}{3s}W(S,s)$ is the ISR cross section to produce a pair of muons and $W(S,s)$ is the radiator function that expresses the probability to radiate from S down to s. To calculate the hadronic contribution to $g_\mu - 2$ or $\alpha(M_Z)$, we must convolve the observed spectrum with the appropriate kernel. True and reconstructed convolutions for $\alpha(M_Z)$ converge for $\sqrt{s} > 4$ GeV, seen Fig. 7. We expect a $\sim 4\%$ measurement of the contribution from $\sqrt{s} < 6.5$ GeV, improving the overall uncertainty on $\alpha(M_Z)$.

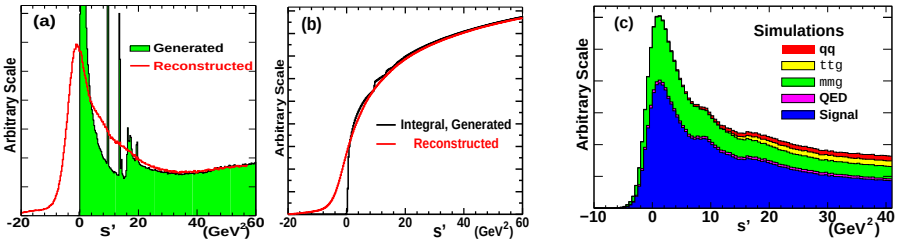

Figure 7: *Cross section generated and reconstructed from simulated ISR photons (a); integral with the $\alpha(M_Z)$ (b); and simulated signal and background events (c).*

4 Summary

A number of $e^+e^- \to$ hadrons processes has been studied at low c.m. energy at *BABAR* via ISR, which gives low bias and small point-to-point systematic

errors over a wide range of energies, from threshold to 4–5 GeV. We extract new information on hadron spectroscopy and the cross sections help to improve our knowledge of g-2 and $\alpha(M_Z)$. The new results on the $\pi^+\pi^-\pi^0\pi^0$ mode and our inclusive studies presented here are especially helpful. We expect improved results with our full data sample, and are studying several other processes: $e^+e^- \to \pi^+\pi^-$, K^+K^-, which give important contributions to vacuum polarization.

References

1. M. Davier *et al.*, Eur. Phys. J. C **27**, 497 (2003).
2. H. Burkhardt and B. Pietrzyk, Phys. Lett. B **513** 46 (2001).
3. G.W. Bennett *et al.*, Phys. Rev. D **73** 072003 (2006).
4. B. Aubert *et al.*, Nucl. Instr. and Meth. A **479**, 1 (2002).
5. B. Aubert *et al.*, Phys. Rev. D **70**, 072004 (2004).
6. B. Aubert *et al.*, Phys. Rev. D **71**, 052001 (2005).
7. B. Aubert *et al.*, Phys. Rev. D **73**, 052003 (2006).
8. B. Aubert *et al.*, Phys. Rev. D **73**, 012005 (2006).
9. A.B. Arbuzov *et al.*, JHEP **9812**, 009 (1998).
10. S. Binner, J.H. Kuehn and K. Melnikov, Phys. Lett. B **459**, 279 (1999).
11. M. Benayoun *et al.*, Mod. Phys. Lett. A **14**, 2605 (1999).
12. S.I. Serednyakov, this proceedings.
13. M.N. Achasov *et al.*, [SND collaboration], INP-2001-34 (2001).
14. R.R. Akhmetshin *et al.*, [CMD-2 collaboration], Phys. Lett. B **466**, 392 (1991).
15. W.-M. Yao *et al*, [Particle Data Group], J. Phys. G **33**, 1 (2006).

Frascati Physics Series Vol. XLVI (2007), pp. 703–712
HADRON07: XII Int. Conf. on Hadron Spectroscopy – Frascati, October 8-13, 2007
Light Meson Spectroscopy

STUDIES OF EXCLUSIVE $e^+e^- \to$ HADRONS REACTIONS WITH BARYONS AND STRANGE PARTICLES USING INITIAL STATE RADIATION AT BABAR

S.I.Serednyakov, for Babar Collaboration
Budker Institute of Nuclear Physics,
Novosibirsk State University,
630090, Novosibirsk, Russia

Abstract

New *BABAR* results on exclusive $e^+e^- \to$ hadrons reactions at low center of mass energy with a baryon-antibaryon or $K\bar{K}$ pair in the final state are presented. Cross sections are measured using the initial state radiation technique from the threshold up to 4–5 GeV. From the measured $e^+e^- \to p\overline{p},\ \Lambda\overline{\Lambda},\ \Sigma^0\overline{\Sigma}^0,\ \Lambda\overline{\Sigma}^0(\Sigma^0\overline{\Lambda})$ cross sections we derive effective baryon form factors and compare with predictions. We measure the $K\bar{K}\pi(\eta),\ K^+K^-\pi\pi,\ K^+K^-3\pi,\ K^+K^-4\pi,\ K^+K^-K^+K^-$ final states and also study their internal structure. A new state is observed, $Y(2175)$, in $e^+e^- \to K^+K^-f_0(980)$, with $f_0 \to \pi\pi$. The total measured e^+e^- annihilation cross section into final states including strange baryons or strange mesons is estimated to be 10% of the full hadronic cross section.

1 Introduction

The $e^+e^- \to$ hadrons reactions with a pair of baryons or strange mesons in the final state has been the subject of the experimental study for many years because of several reasons. At first, they give the considerable contribution into the total e^+e^- hadronic cross section. At second, from the two body cross section one can derive electromagnetic timelike form factors. And last but not least, new states can reveal themselves in the study of these reactions.

In this work a sample of *BABAR* [1] data corresponding to 230 fb^{-1} is analyzed. We search for initial state radiation (ISR) processes $e^+e^- \to f + \gamma$, where γ is the high energy photon $E_\gamma > 3$ GeV and f is a hadronic system with the mass m. (A description of ISR approach is given in Introduction chapter of [2]). Through ISR the wide mass range (from $2m_\pi$ to ~ 10 GeV/c^2) is studied in a single experiment with full efficiency and full angular acceptance beginning from the very threshold. For example, in the reaction $e^+e^- \to p\overline{p}\gamma$, the protons produced at the threshold already have the laboratory momenta ≥ 1 GeV/c.

The ISR approach, applied to B-factories data, is quite competitive with direct e^+e^- experiments, because the effective ISR luminosity is comparable with already stored e^+e^- luminosity. The following final states are studied in this work: $p\overline{p}$, $\Lambda\overline{\Lambda}$, $\Sigma^0\overline{\Sigma}^0$, $\Lambda\overline{\Sigma}^0(\Sigma^0\overline{\Lambda})$ with baryons and $K\bar{K}\pi(\eta)$, $K^+K^-\pi\pi$, $K^+K^-3\pi$, $K^+K^-4\pi$, $K^+K^-K^+K^-$ and other with kaons. Other ISR results are covered in the talk [3].

2 Baryon pair production results

The cross section for the $e^+e^- \to B\overline{B}$ process, where B is a spin-1/2 baryon, has the form:

$$\sigma_{B\overline{B}}(m) = \frac{4\pi\alpha^2\beta}{3m^2}\left[|G_M(m)|^2 + \frac{1}{2\tau}|G_E(m)|^2\right], \qquad (1)$$

where $\beta = \sqrt{1-4m_B^2/m^2}$, $\tau = m^2/4m_B^2$, G_E and G_M are the electric and magnetic form factors. From the total cross section (1) the values of the G_E and G_M can not be extracted separately. Therefore the effective form factor $|F(m)|$ is introduced as $|F(m)|^2 = (2\tau|G_M(m)|^2 + |G_E(m)|^2/(2\tau+1)$. The modulus $|G_E/G_M|$ is determined from the $\cos\theta_B$ distribution, where θ_B is the

polar angle of the baryon with respect to the e^- beam in the e^+e^- center of mass (c.m.) frame. The $\sin^2\theta_B$ term in this distribution is proportional to $|G_E|^2$ and the $1+\cos^2\theta_B$ term to $|G_M|^2$. The fit of the $\cos\theta_B$ distribution then gives the $|G_E/G_M|$ ratio.

The $e^+e^- \to p\bar{p}$ results [2] are shown in Figs. 1, 2, 3. The measured cross section (Fig. 1) is flat at the threshold while the form factor sharply rises in this region (Fig. 2). It has two step-like structures: at 2.15 and 2.9 GeV. The ratio $|G_E/G_M|$ (Fig. 3) is found to be $\geq$ 1 in contradiction with previous works. The measured $e^+e^- \to \Lambda\overline{\Lambda}$ cross section (Fig. 6) [5] agrees with the only previous measurement [4]. The 200 found $\Lambda\overline{\Lambda}$ events are selected by using $\Lambda \to p\pi$ decay. The measured Λ effective form factor is shown in Fig. 7. The ratio G_E/G_M for the Λ baryon is consistent with unity. Using the $\Lambda \to p\pi$ decay allows to measure the relative phase ϕ between the complex G_E and G_M form factors. The transverse polarization ζ of outgoing baryons is proportional to $\sin\phi$. The measurement of ζ is obtained from the angular spectrum of protons in the $\Lambda \to p\pi$ decay. The simulated distribution over ζ_{max} is shown in Fig. 4. The measured $\cos\theta$ distribution, where θ is the angle between the Λ polarization and the proton momentum from the $\Lambda \to p\pi$ decay in the Λ rest frame, is shown in Fig. 5. No $\cos\theta$ asymmetry is observed. The following limits on the Λ polarization $-0.22 < \zeta < 0.28$ and the phase $-0.76 < \sin\phi < 0.98$ are obtained. The limit on $\sin\phi$ is too weak to make any certain conclusion on the phase ϕ between the G_E and G_M for the Λ hyperon.

In the similar way the $e^+e^- \to \Sigma^0\overline{\Sigma}^0$ and $e^+e^- \to \Sigma^0\overline{\Lambda}(\Lambda\overline{\Sigma}^0)$ cross sections have been measured. For the detection of the Σ^0, the decay chain $\Sigma^0 \to \Lambda\gamma \to p\pi\gamma$ is used. About 20 candidate events have been selected for each reaction. The effective Σ^0 and $\Sigma^0\Lambda$ form factors are shown in Fig. 7. We note that Λ, Σ^0 and $\Sigma^0\Lambda$ form factors are of the same order.

3 SU(3) and QCD tests for baryon form factors

New *BABAR* data on baryon form factors give the possibility to check predictions from some form factor models. The fit with the asymptotic power law function, predicted by the perturbative QCD [6],

$$F \sim \alpha_S^2(m^2)/m^4 \sim C/m^4 ln^2(m^2/\Lambda^2), \qquad (2)$$

applied to the proton form factor data, is shown in Fig. 8. Here $\Lambda = 0.3$ GeV, and C is a free parameter. If we neglect the steps at 2.15 and 2.9 GeV, the function (2) (Fig. 8) describes the data fairly well, indicating that the asymptotic behaviour starts already at $2 \div 3$ GeV.

The same power law (2) for the Λ form factor is not so good (see the curve labeled with $n = 4$ in the Fig. 9). A better agreement with the data is obtained by taking a power m^8 in the denominator of Eq. 2 (Fig. 9, curve $n = 8$). A similar behaviour is obtained in fitting the Σ^0 and $\Sigma^0\Lambda$ form factors. We conclude that Λ, Σ^0 and $\Sigma^0\Lambda$ form factors are considerably steeper than the proton form factor.

In SU(3) symmetry model the baryon octet form factors are related to each other. The asymptotic predictions [7] are: $F_n = 1.94\,F_\Lambda$, $F_p = 2.13\,F_n$, $F_{\Sigma^0} = -1.18\,F_\Lambda$, $F_p = 4.1\,F_\Lambda$. A test of these predictions in Fig. 10, for the doubled *BABAR* Λ [5] and Fenice neutron [8] form factors, shows, at 2.4 GeV, good agreement with $F_n = 1.94\,F_\Lambda$. This result is important for the planned neutron form factor measurement [9]. The comparison of the proton and Λ form factors in Fig. 11, shows that the data at $E_{c.m.} < 3$ GeV are far from the asymptotic QCD prediction $F_p = 4\,F_\Lambda$. But the behaviour of both the form factors with energy indicates that, above 4 GeV, the agreement with the QCD predictions should be obtained.

4 Final states including kaon pairs.

The ISR approach is also applied to study e^+e^- annihilation cross sections with a pair of kaons in the final state. Figure 12 shows the $e^+e^- \to K_S K^\pm \pi^\mp$ cross section [10] with a peak at ~ 1.7 GeV mainly from the $\phi'(1680)$ state. The Dalitz plot in Fig. 13 shows that $KK^\star(892)$ and $KK_2^\star(1430)$ intermediate states dominate the $K\bar{K}\pi$ production. The $e^+e^- \to K\bar{K}\pi$ cross sections have been fit with a sum of expected resonant contributions: ϕ, ϕ', ϕ'', ρ^0, ρ', ρ''. The parameters of the ϕ' and other excited vector meson states, obtained from the fit, are compatible with their PDG values.

In the cross section of the $e^+e^- \to \phi\eta$ ($\eta \to \gamma\gamma$) process (Fig. 14) the peak near threshold from the $\phi'(1680)$ is seen. Another small peak is observed with $M = 2139 \pm 35$ MeV, $\Gamma = 76 \pm 62$ MeV and 2σ significance. In general the $e^+e^- \to \phi\eta$ channel is very suitable for the search of ϕ's states, because it is entirely isoscalar and contributions of ω's states are OZI suppressed.

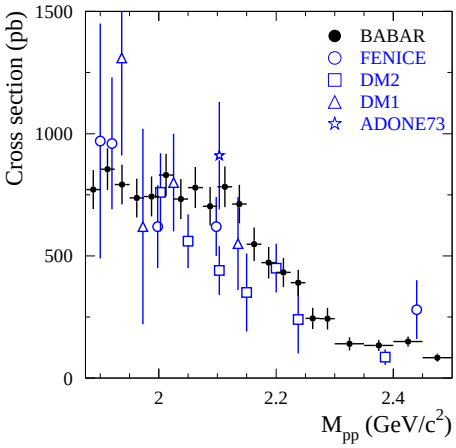

Figure 1: The $e^+e^- \to p\bar{p}$ cross section near threshold.

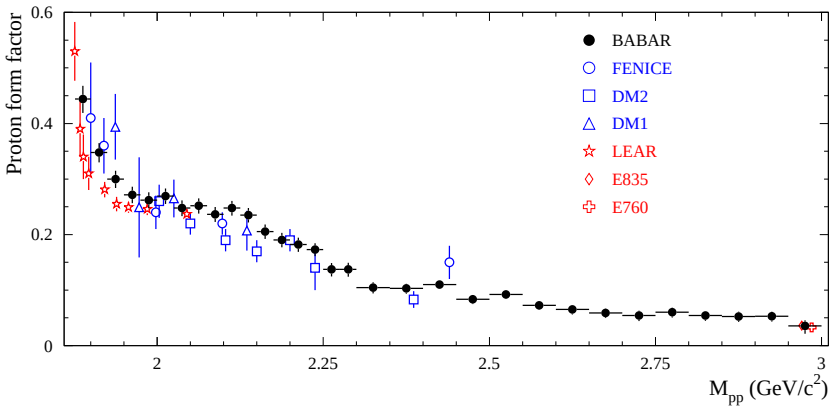

Figure 2: The proton timelike form factor data.

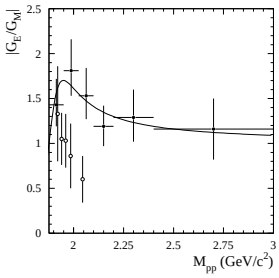

Figure 3: The G_E/G_M ratio for proton.

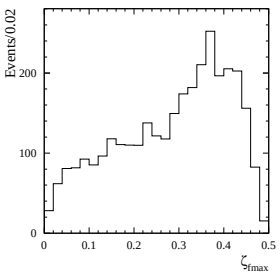

Figure 4: The simulated Λ polarization.

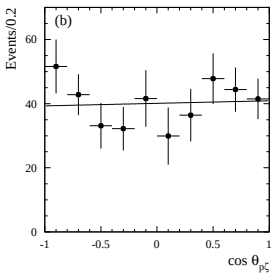

Figure 5: The measured $\cos\theta_{p\zeta}$ distribution.

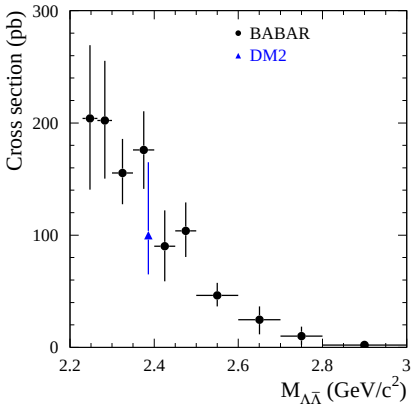

Figure 6: The $e^+e^- \to \Lambda\bar{\Lambda}$ cross section.

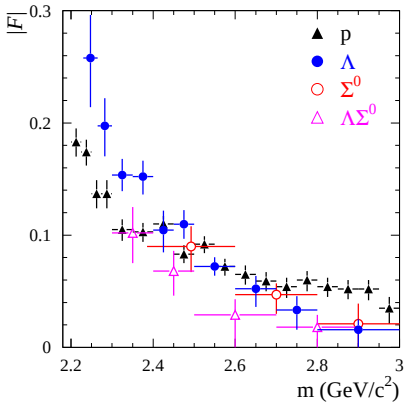

Figure 7: The measured proton, Λ, Σ^0 and $\Lambda\Sigma^0$ form factors.

The other channel $e^+e^- \to \phi\pi^0$ is potentially suitable for the search of exotic states, because the ordinary vector mesons decays into $\phi\pi^0$ are strongly OZI suppressed. The $e^+e^- \to \phi\pi^0$ cross section has been measured for the first time [10] and found to be very small ≤ 0.1 *nb*.

The measured $e^+e^- \to K^+K^-\pi^+\pi^-$ and $e^+e^- \to K^+K^-\pi^0\pi^0$ cross sections [11] are of the order of several nanobarn with an enhancement at 1.7 GeV. In the final state mode $\phi f_0(980)$, $f_0(980) \to \pi^+\pi^-, \pi^0\pi^0$ a peak is observed with $M = 2175 \pm 18$ MeV, $\Gamma = 58 \pm 2$ MeV and $\Gamma_{ee} \simeq 2.5$ eV. The new state is named $Y(2175)$. It is even more distinctly seen in the final state $K^+K^-f_0$ (Fig. 15). The nature of $Y(2175)$ is not yet clear. It might be the ϕ'' state, a four-quark or molecular $(ss\bar{s}\bar{s})$ state or a light analogue of the known $Y(4260)$, because they both are relatively narrow and have close electron widths $[\Gamma_{ee}(Y(4260)) \simeq 5.5$ eV]. If the peak at 2139 MeV in the $\phi\eta$ channel mentioned above is another decay channel of $Y(2175)$, then its electron width should be larger than the quoted 2.5 eV value.

Several new channels with a pair of kaons are studied at *BABAR* [11–13]: $e^+e^- \to K^+K^-K^+K^-$, $K^+K^-\pi^+\pi^-\pi^0$, $K^+K^-\pi^+\pi^-\pi^+\pi^-$, $K^+K^-\pi^+\pi^-\eta$. In the process $e^+e^- \to 4K$ the ϕK^+K^- intermediate state is dominant. In the $e^+e^- \to K^+K^-3\pi$ cross section the $\omega(783)$ and $\eta(550)$ are clearly seen in the 3π mass spectrum. As an example, the $e^+e^- \to K^+K^-4\pi$ cross section is shown in Fig. 16. In general, the substructures in all final states with kaons

deserve more careful study.

5 Estimation of strangeness contribution into the total hadronic cross section

The total hadronic cross section $R = \frac{\sigma(e^+e^- \to \text{hadrons})}{\sigma(e^+e^- \to \mu^+\mu^-)}$ in the low energy region consists of the contributions of u, d, s quarks. For the strange quark the relative contribution is $1/6$. To calculate R, the direct cross section measurements are preferable, because the QCD calculations in the non asymptotic region can be not sufficiently precise. Based on the *BABAR* data reported here the total strangeness cross section is summarized at two points 2.5 and 3 GeV, and found to be equal to 3.3 and 2.1 nb, respectively. This would be compared with the expected 5 and 3.5 nb of the strangeness cross section and 28 and 19 nb of the total hadronic cross section. So the measured cross sections constitute about $2/3$ of the strangeness cross section and 10% of the total hadronic cross section. The rest $1/3$ channels, such as $K_S K_L \pi$, $K^\pm K_S \pi\pi$, $K_S K_S \pi\pi$, etc. can be also measured using the initial state radiation.

6 ISR perspectives

In several years the total integrated luminosity at B-factories is expected to reach ~ 2 ab^{-1}, that is about 10 times larger than that used in the present analysis. This gives a hope for more accurate measurements of the reactions considered here and extending the measurements to larger masses.

7 Conclusions

Using the ISR technique at *BABAR* the cross sections $e^+e^- \to p\overline{p}$, $\Lambda\overline{\Lambda}$, $\Sigma^0\overline{\Sigma}^0$, $\Lambda\overline{\Sigma}^0(\Sigma^0\overline{\Lambda})$ have been measured. The baryon timelike form factors are compared with model predictions. The cross sections with a pair of kaons $e^+e^- \to K\bar{K}\pi(\eta)$, $K^+K^-\pi\pi$, $K^+K^-3\pi$, $K^+K^-4\pi$, $K^+K^-K^+K^-$ are also measured. In the $K^+K^-f_0(980)$ final state, a new state $Y(2175)$ with $M = 2175 \pm 18$ MeV, $\Gamma = 58 \pm 2$ MeV is observed. The total measured strangeness cross section constitutes about $2/3$ of the full strangeness cross section and $\sim 10\%$ of the total hadronic cross section.

Acknowledgment

The author is grateful for fruitful discussions to Vladimir Druzhinin and Victor Chernyak.

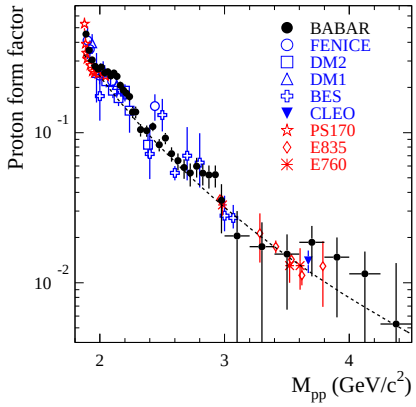

Figure 8: The summary of the proton form factor data and QCD fit.

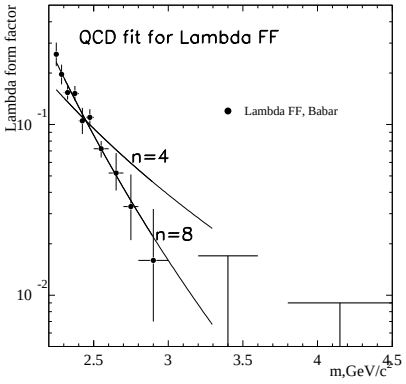

Figure 9: The fitting of Λ form factor data.

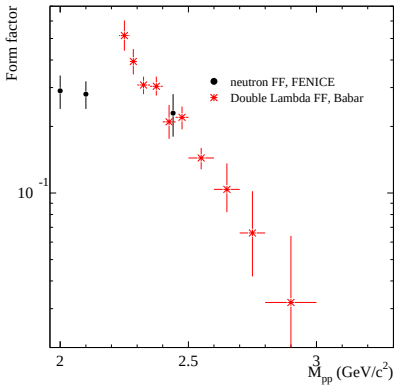

Figure 10: A comparison between doubled Λ and Fenice neutron [8] form factors.

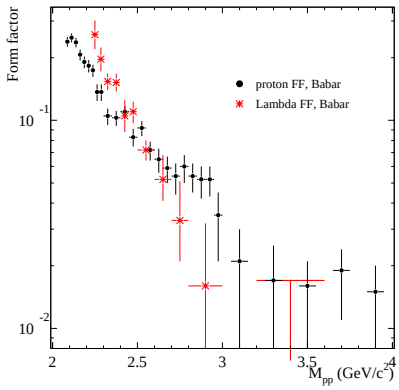

Figure 11: A comparison between proton and Λ form factors.

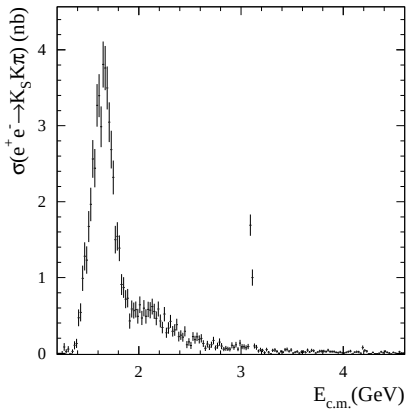

Figure 12: The $e^+e^- \to K_S K^\pm \pi^\mp$ cross section.

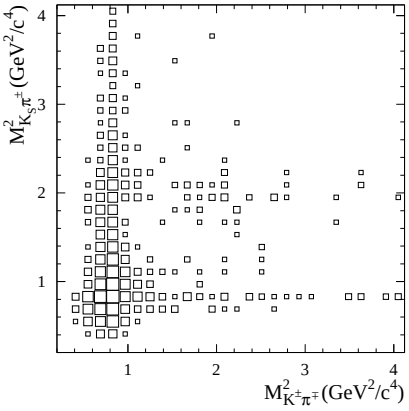

Figure 13: The Dalitz plot for the $K_S K^\pm \pi^\mp$ state.

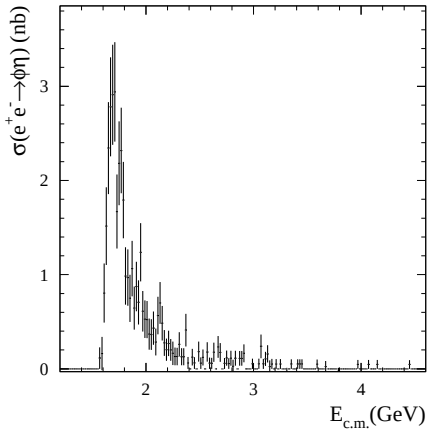

Figure 14: The $e^+e^- \to \phi\eta$ cross section.

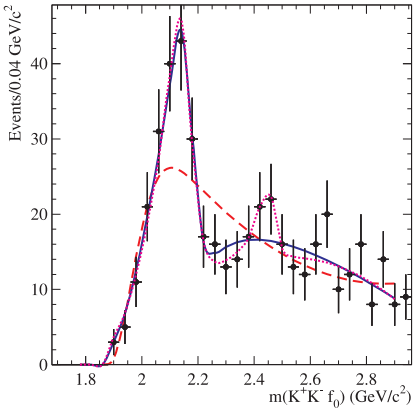

Figure 15: The manifestation of the $X(2175)$ state.

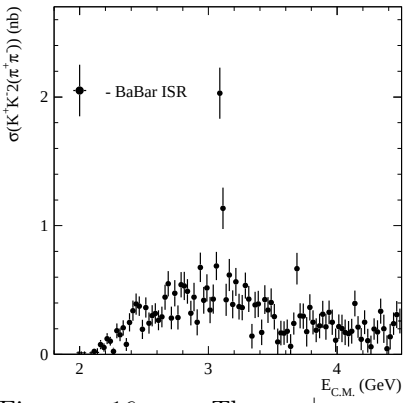

Figure 16: The $e^+e^- \to K^+K^-\pi^+\pi^-\pi^+\pi^-$ cross section.

References

1. B. Aubert *et al.* [*BABAR Collaboration*], Nucl. Instr. and Meth. A **479**, 1 (2002).
2. B. Aubert *et al.* [*BABAR Collaboration*], Phys. Rev. D **73**, 012005 (2006), hep-ex/0512023.
3. W.F. Wang, Talk given at this Conference.
4. D. Bisello *et al.* [*DM2 Collaboration*], Z. Phys. C **48**, 23 (1990).
5. B. Aubert *et al.* [*BABAR Collaboration*], ArXiv:0709.1988 v1 [hep-ex].
6. V.L. Chernyak, A.R. Zhitnitsky, JETP Lett. **25**, 510, (1977); G. Lepage, S. Brodsky, Phys. Rev. Lett. **43**, 545 (1977).
7. V.L. Chernyak *et al.* Z. Phys. C-Particles and fields **42** 569-582.
8. A. Antonelli *et al.* Phys. Lett. B **313**, 283 (1993); Nucl. Phys. B **517**, 3, (1998).
9. A.A. Botov *et al.* Nucl. Phys. B (Proc.Suppl.) **162**, 41 (2006).
10. B. Aubert *et al.* [*BABAR Collaboration*], arXiv:0710.4451 [hep-ex].
11. B. Aubert *et al.* [*BABAR Collaboration*], Phys. Rev. D **76**, 012008 (2007), arXiv:0704.0630 [hep-ex]; Phys. Rev. D **74**, 091103 (2006), hep-ex/0610018.
12. B. Aubert *et al.* [*BABAR Collaboration*], arXiv:0708.2461 [hep-ex].
13. B. Aubert *et al.* [*BABAR Collaboration*], Phys. Rev. D **73**, 052003 (2006), hep-ex/0602006v1.

Frascati Physics Series Vol. XLVI (2007), pp. 713–720
HADRON07: XII Int. Conf. on Hadron Spectroscopy – Frascati, October 8-13, 2007
Light Meson Spectroscopy

STUDIES OF $e^+e^- \to$ QUASI-2-BODY PROCESSES AT 10.6 GeV AT BABAR

David Muller
Stanford Linear Accelerator Center, Stanford, California 94309, USA
Representing the *BABAR* Collaboration

Abstract

We present the first results from a program of studies of e^+e^- annihilations into specific, low-multiplicity final states at a center-of-mass energy $\sqrt{s}=10.6$ GeV. Focussing on the contributions from some dominant quasi-two-body channels, we obtain a number of unique physics results. In the reactions $e^+e^-\to\gamma\eta$ and $\gamma\eta'$, we measure the η and η' transition form factors at the highest q^2 value to date, 112 GeV^2, testing QCD predictions in the asymptotic regime. The $\rho^0\rho^0$ and $\rho^0\phi$ final states constitute the first observation of e^+e^- annihilations into hadrons via two virtual photons. We find the helicity structure in the $\rho^+\rho^-$ final state to be inconsistent with dominance of the helicity component expected by QCD. Comparing the cross section for the reaction $e^+e^-\to\eta\phi$ with data from lower energies, we find an asymptotic energy dependence consistent with $1/s^4$ but not $1/s^3$.

1 Introduction

The very high luminosity at the B-factories allows the study of e^+e^- annihilations into exclusive, low-multiplicity final states at the relatively high center-of-mass (c.m.) energy of $\sqrt{s}=10.6$ GeV. Such processes dominate at low $\sqrt{s}$, but their cross sections generally fall much faster than $1/s$ and are 5–7 orders of magnitude lower than that for the dominant $e^+e^-\to q\overline{q}$ process at 10.6 GeV. However, these are some of the simplest processes involving hadrons, and so their cross sections and internal structures at various $\sqrt{s}$ provide a rich testing ground for QCD. Predictions can be tested for well known hadrons, characteristics can be determined for others, and new states might be found.

We have begun a program at *BABAR* of studying fully reconstructed, low-multiplicity final states, in order to understand both the production processes and the hadrons themselves. The *BABAR* detector covers roughly 85% of the solid angle in the e^+e^- c.m. frame, and features excellent invariant mass resolution on few-body final states and almost complete charged hadron identification. Our current data sample of 475 fb^{-1} corresponds to 1.6 billion $e^+e^-\to q\overline{q}$ events; 224–379 fb^{-1} are used in the results presented here.

2 The $e^+e^-\to\gamma\eta$ and $e^+e^-\to\gamma\eta'$ Reactions

To study the $\gamma\eta$ final state [1)], we select events containing a photon with c.m. energy above 3 GeV recoiling against a pair of oppositely charged tracks and a pair of photons consistent with a π^0 decay. Applying a kinematic fit that imposes 4-momentum conservation and the π^0 mass, we select events with an acceptable χ^2. The distribution of fitted $\pi^+\pi^-\pi^0$ invariant masses in fig. 1a shows a clear peak at the η mass. The background is due mainly to initial state radiation (ISR). It is well understood and very low under the η peak, rising with increasing mass, so we perform a simple fit to extract the $\gamma\eta$ yield.

To study the $\gamma\eta'$ final state, we select events similarly, either with the photon pair consistent with the η mass or having two additional charged tracks in the event that when combined with the π^0 candidate have an invariant mass consistent with the η mass. The $\pi^+\pi^-\eta$ invariant mass distributions from similar kinematic fits are shown for $\eta\to\gamma\gamma$ and $\eta\to\pi^+\pi^-\pi^0$ in figs. 1b and 1c, respectively. Both show clean η' peaks, which we fit to obtain yields.

We correct for detection efficiency to obtain cross sections of about 5 fb for

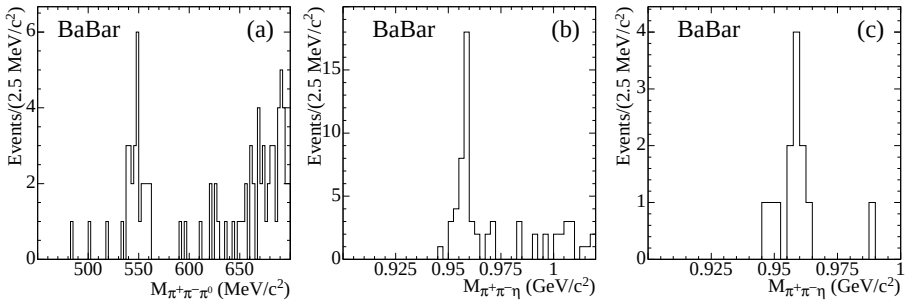

Figure 1: *Invariant mass distributions for a) $\pi^+\pi^-\pi^0$ and $\pi^+\pi^-\eta$ combinations, with b) $\eta\to\gamma\gamma$ and c) $\eta\to\pi^+\pi^-\pi^0$, recoiling against a high-energy photon after the kinematic fit described in the text.*

Table 1: *Cross sections for the reactions $e^+e^-\to\gamma\eta^{(\prime)}$ at $\sqrt{s}=10.6$ GeV, the corresponding transition form factors at $q^2=112$ GeV^2, and theoretical predictions for the latter. The first errors are statistical and the second systematic.*

	Cross Section (fb)	$q^2\|F(q^2)\|$ (GeV)	Predictions
η	$4.5\pm1.2\pm0.3$	$0.229\pm0.030\pm0.008$	0.15–0.22
η'	$5.4\pm0.8\pm0.3$	$0.251\pm0.019\pm0.008$	0.25–0.34
Ratio		1.10 ± 0.17	1.6–2.3

these two reactions, see table 1. We convert these into transition form factors and compare with theoretical predictions, both also shown in table 1. The predictions cover a wide range, due mostly to uncertainty in the η-η' mixing, which is consistent with the data. However our value for η (η') is at the upper (lower) end of this range, and the ratio of 1.10±0.17 is 3σ below the range.

3 The $e^+e^-\to\rho^0\rho^0$ and $e^+e^-\to\rho^0\phi$ Reactions

We select candidate $e^+e^-\to\pi^+\pi^-\pi^+\pi^-$ and $e^+e^-\to K^+K^-\pi^+\pi^-$ events [2)] containing exactly four well reconstructed charged tracks with total charge zero. Two oppositely charged tracks must be identified as pions and the other two as either pions or kaons. The 4π and $2K2\pi$ invariant mass distributions in figs. 2a and 2b, respectively, show strong signal peaks at our c.m. energy. The backgrounds are under study, and here we consider the internal structure

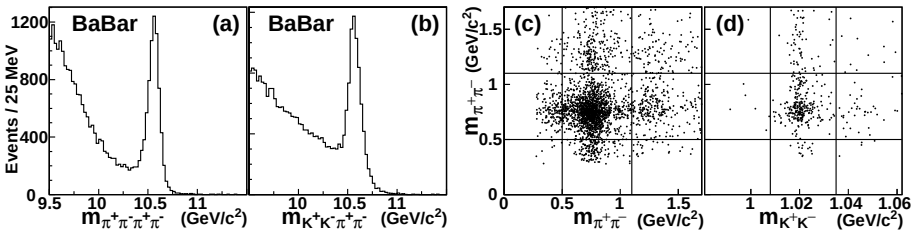

Figure 2: *Invariant mass distributions for candidate a)* $e^+e^- \to \pi^+\pi^-\pi^+\pi^-$ *and b)* $e^+e^- \to K^+K^-\pi^+\pi^-$ *events. The* $\pi^+\pi^-$ *mass vs. c) the other* $\pi^+\pi^-$ *mass or d) the* K^+K^- *mass in events within 170* MeV *of the nominal* $\sqrt{s}$*.*

of those events within 170 MeV of their nominal $\sqrt{s}$.

We show scatter plots of the $\pi^+\pi^-$ invariant mass vs. that of the other $\pi^+\pi^-$ or the K^-K^+ in these events for the low-mass regions in figs. 2c and 2d, respectively. Horizontal ρ^0 and vertical ϕ bands are visible in fig. 2d, and there is a substantial enhancement where they overlap. There is also a concentration of events in the $\rho^0\rho^0$ region, delineated by the lines on fig. 2c, along with a $\rho^0 f_2(1270)$ signal and a background from $e^+e^- \to \rho^0\mu^+\mu^-$ events, in which the $\mu^+\mu^-$ masses cluster at low values. A feature of the high $\sqrt{s}$ is that very small fractions of events from phase space or other resonant channels, such as $a_1\pi$ or $K^*\overline{K}^*$, are in the low-mass ranges. Furthermore, the wrong $\pi^+\pi^-$ pairings from $\rho^0\rho^0$ events are well outside the range, so each channel can be identified cleanly. Fits including the components noted and small nonresonant/background terms show that these regions are dominated by the $\rho^0\rho^0$ and $\rho^0\phi$ channels.

The $\rho^0\rho^0$ and $\rho^0\phi$ final states have positive C-parity, so are forbidden in e^+e^- annihilations via a single virtual photon. However, they are expected in two-virtual-photon-annihilation (TVPA) at about this level, so we study the angular distributions in these events. TVPA predicts that the production angle θ^* of the ρ^0 or ϕ with respect to the e^- beam is distributed approximately as $(1+\cos^2\theta^*)/(1-\cos^2\theta^*)$, i.e. very strongly peaked along the beam directions. The measured angles are consistent with this, and inconsistent with a $1+\cos^2\theta^*$ distribution, the most peaked of other potential processes. The helicity angle distributions are consistent with those expected for transversely polarized ρ^0 and ϕ. The TVPA cross section is proportional to $1/s$, so in contrast to most other exclusive reactions, these would not be visible in our ISR studies, and

indeed we do not observe them [3]. We therefore conclude that we have made the first observation of e^+e^- annihilations into hadrons via two virtual photons.

We quote cross sections in the fiducial range where our acceptance is high, $|\cos\theta^*| < 0.8$, so they are independent of the production mechanism. We also define the ρ^0 and ϕ by the $\pi^+\pi^-$ and K^+K^- mass ranges 500–1100 MeV/c^2 and 1008-1035 MeV/c^2, respectively, so that the results are insensitive to the exact lineshapes and backgrounds near threshold. The results are 20.7±0.7±2.7 fb for $e^+e^- \to \rho^0\rho^0$ and 5.7±0.5±0.8 fb for $e^+e^- \to \rho^0\phi$. Theoretical predictions can be integrated over the above regions and compared with these results. A calculation [4] based on vector dominance is consistent with the data.

4 The $e^+e^- \to \rho^+\rho^-$ Reaction

In contrast to $\rho^0\rho^0$, the $\rho^+\rho^-$ final state is allowed in single-γ^* annihilation, although one particular helicity configurations is expected to dominate [5]. A contribution from TVPA is also possible via a final-state interaction, which might lead to an observable asymmetry in the dihedral angle. We select events containing exactly two well reconstructed, oppositely charged tracks and two $\pi^0 \to \gamma\gamma$ candidates. Requiring the magnitude of the total momentum of the $\pi^+\pi^-\pi^0\pi^0$ system to be less than 200 MeV/c, and a pairing with both the $\pi^+\pi^0$ and $\pi^-\pi^0$ masses below 1.6 GeV/c^2, we obtain the invariant mass distribution shown in fig. 3a, which shows a clean peak at the c.m. energy.

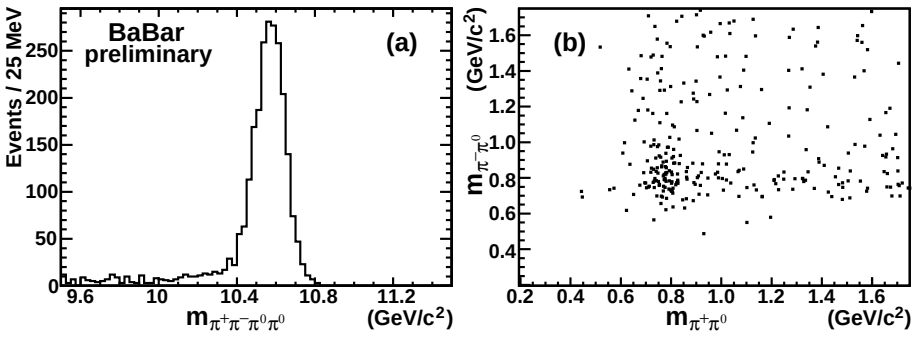

Figure 3: *a) Invariant mass distribution for candidate $e^+e^- \to \pi^+\pi^-\pi^0\pi^0$ events. b) Invariant mass of the $\pi^-\pi^0$ pair vs. that of the $\pi^+\pi^0$ pair in events within 280* MeV *of the nominal $\sqrt{s}$.*

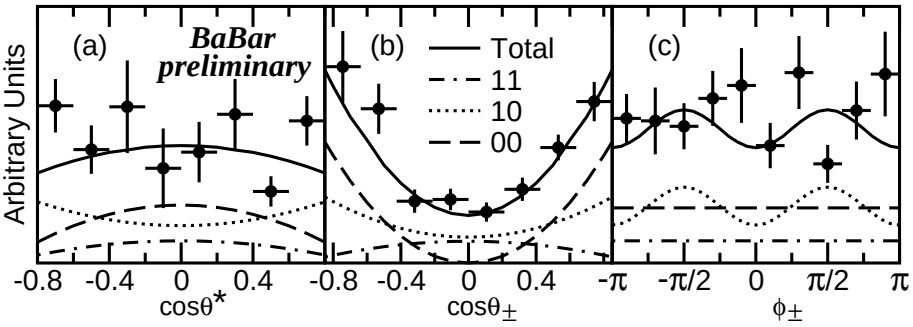

Figure 4: *Distributions of a) production, b) helicity, and c) decay azimuthal angles in $e^+e^- \to \rho^+\rho^-$ events, along with results of the fit described in the text.*

Selecting events within 280 MeV of the nominal $\sqrt{s}$, we obtain the scatter plot of the invariant mass of the $\pi^-\pi^0$ pair vs. that of the $\pi^+\pi^0$ shown in fig. 3b. Horizontal and vertical bands corresponding the to ρ^- and ρ^+, respectively, are visible, and there is a substantial enhancement where they overlap. We perform a 2D fit to extract the event yield, from which we calculate a cross section, in the same fiducial range as above, of $8.5\pm0.7\pm1.5$ fb. This is rather similar to the 20.7 fb measured above for $\rho^0\rho^0$, but TVPA cannot be the sole source, since we observe this mode at lower energies in our ISR data [6].

We study the distributions of: the production angle θ^* between the ρ^+ and the e^- beam directions; the helicity angles $\theta_\pm$ between the $\pi^\pm$ and $\rho^\mp$ momenta in the $\rho^\pm$ rest frame; and the azimuthal angles $\phi_\pm$ of the $\pi^\pm$ momenta about the $\rho^\pm$ momenta with respect to the plane formed by the $\rho^\pm$ and the e^- beam. Subtracting background and correcting for efficiency in each bin of these angles, we obtain the experimental distributions shown in fig. 4. Assuming a single-γ^* production process, there are three independent allowed helicity configurations, labelled 00, 10, and 11, that have different angular distributions. We fit the measured distributions simultaneously, and show the results in fig. 4. The 10 and 11 contributions are strongly anticorrelated, but their sum contributes $48\pm14\%$ of the total rate, inconsistent with the prediction that the 00 contribution should dominate at 10.6 GeV. The 00 (10, 11) components are expected to vary with c.m. energy as $1/s^2$ ($1/s^3$), and an analysis of our ISR data is under way.

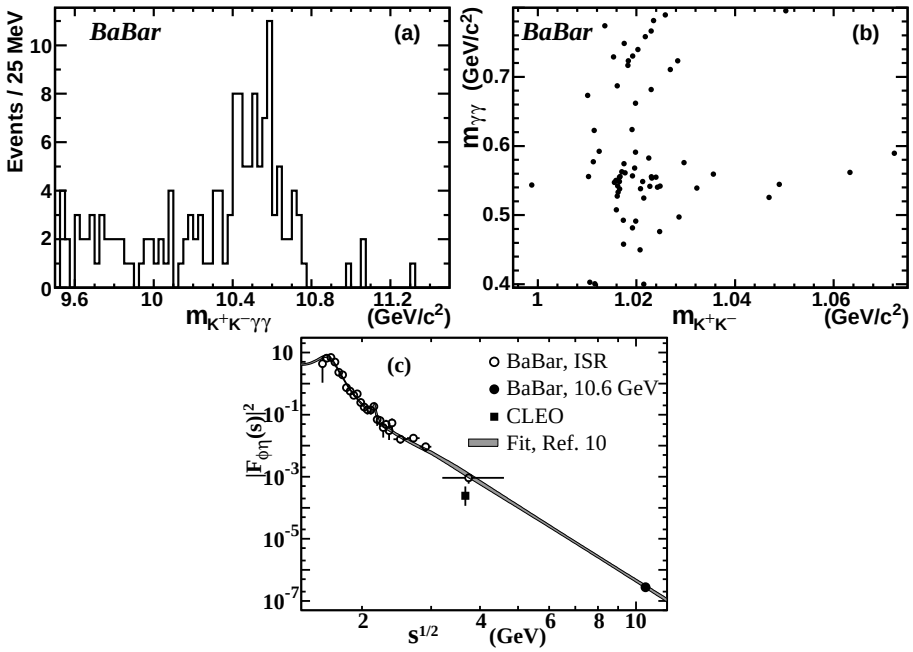

Figure 5: *a) Invariant mass distribution for candidate $e^+e^-\to K^+K^-\gamma\gamma$ events. b) $\gamma\gamma$ mass vs. K^+K^- mass for events in the signal region. c) Transition form factor vs. $\sqrt{s}$, along with the result of the fit described in the text.*

5 The $e^+e^-\to\eta\phi$ Reaction

The $\eta\phi$ final state is analogous to $\eta_c J/\psi$, so its measurement should help understand the high rate of double charmonium events seen by Belle and BaBar. We select events with exactly two well reconstructed, oppositely charged, identified kaons, and two good photons with energy above 500 MeV. For K^+K^- masses below 1100 MeV/c^2 and $\gamma\gamma$ masses in the range 400–800 MeV/c^2, we obtain an invariant mass distribution, fig. 5a, showing a peak at the c.m. energy.

For events within 230 MeV of the nominal $\sqrt{s}$, we obtain the $\gamma\gamma$ vs. K^+K^- mass scatter plot shown in fig. 5b. Horizontal and vertical bands corresponding the to η and ϕ, respectively, are visible, and there is an enhancement where they overlap. We perform a two-dimensional fit to extract the event yield, from which we calculate a fiducial cross section of 2.9±0.5±0.1 fb.

We have measured the cross section for this channel at lower $\sqrt{s}$ in our ISR data [6, 7] and there is a measurement from CLEO [8] at 3.7 GeV. Theory predicts either a $1/s^3$ [9] or $1/s^4$ [5] dependence of the cross section at high s. Figure 5c shows the measurements, converted to transition form factors, as a function of $\sqrt{s}$. The data above ∼2.5 GeV show a strong preference for $1/s^4$ over $1/s^3$. Dispersion relation phenomenology has been developed to describe such form factors [10], and the result of a fit is shown as the gray band on fig. 5c. It is able to describe the data using two resonances and a $1/s^4$ asymptotic form.

6 Summary

The very high luminosity at the B-factories has allowed the study of exclusive, low-multiplicity e^+e^- annihilation reactions at $\sqrt{s} = 10.6$ GeV. First results include measurements of the η and η' transition form factors at high q^2, the first observation of $e^+e^- \to$ hadrons via two virtual photons, a study of the helicity structure of the $\rho^+\rho^-$ final state, and a measurement of the $e^+e^- \to \eta\phi$ cross section that, compared with lower-$\sqrt{s}$ data, favors a $1/s^4$ over $1/s^3$ asymptotic energy dependence. We expect improved results with our full data sample, and measurements of many more channels in the future.

References

1. B. Aubert, *et al.*, Phys. Rev. D **74**, 012002 (2006).
2. B. Aubert, *et al.*, Phys. Rev. Lett. **97**, 112002 (2006).
3. B. Aubert, *et al.*, Phys. Rev. D **71**, 052001 (2005).
4. M. Davier, M.E. Peskin and A. Snyder, hep-ph/0606155 (2006).
5. S.J. Brodsky and G.P. Lepage, Phys. Rev. D **24**, 2848 (1981).
6. W.F. Wang, these proceedings; S.I. Serednyakov, these proceedings.
7. B. Aubert, *et al.*, arXiv:0710.4451, submitted to Phys. Rev. D.
8. G.S. Adams, *et al.*, Phys. Rev. D **73**, 012002 (2006).
9. J.M. Gerard and G. Lopez Castro, Phys. Lett. B **425**, 365 (1998).
10. S. Pacetti, Eur. Phys. J. A **31**, 665 (2007).

Frascati Physics Series Vol. XLVI (2007), pp. 721–728
HADRON07: XII Int. Conf. on Hadron Spectroscopy – Frascati, October 8-13, 2007
Light Meson Spectroscopy

RECENT RESULTS ON LIGHT HADRON SPECTROSCOPY FROM BESII

Xiaoyan Shen
for BES Collaboration
Institute of High Energy Physics, Beijing 100049, P. R. China

Abstract

We reported the observation of $Y(2175)$ in $\phi f_0(980)$ mass spectrum in $J/\psi \to \eta\phi f_0(980)$ with $f_0(980) \to \pi^+\pi^-$. The observation of a broad 1^{--} resonance of K^+K^- mass in $J/\psi \to K^+K^-\pi^0$ and the results from the partial wave analysis of $J/\psi \to \gamma\pi^+\pi^-$ and $\gamma\pi^0\pi^0$ are also presented.

1 Introduction

QCD predicts the existence of the multi-quark states, $q\bar{q}$-*gluon* hybrids and glueballs. These states have been searched for many years by some experiments. However, none of them is well established after all the efforts. The 5.8×10^7 J/ψ events, accumulated with BES detector, provide a good laboratory for the search of non-$q\bar{q}$ states and study of light hadron spectroscopy.

2 Observation of $Y(2175)$ in $J/\psi \to \eta\phi f_0(980)$

A new 1^{--} structure, denoted as $Y(2175)$ and with mass $m = 2.175 \pm 0.010 \pm 0.015$ GeV/c^2 and width $\Gamma = 58 \pm 16 \pm 20$ MeV/c^2, was observed by the BABAR experiment in the $e^+e^- \to \gamma_{ISR}\phi f_0(980)$ initial-state radiation (ISR) process [1, 2]. This observation stimulated some theoretical speculation that this state may be an s-quark version of the $Y(4260)$ since both of them are produced in e^+e^- annihilation and decay to similar final states [3]. The $Y(2175)$ has correspondingly been interpreted as a $s\bar{s}g$ [4], a 2^3D_1 $s\bar{s}$ state [5] or a tetraquark $s\bar{s}s\bar{s}$ state [6]. As of now, none of these interpretations have either been established or ruled out by experiment.

With a sample of 5.8×10^7 J/ψ events collected with upgraded Beijing Spectrometer (BESII) detector [7] at Beijing Electron-Positron Collider (BEPC), the decays of $J/\psi \to \eta\phi f_0(980)$, with $\eta \to \gamma\gamma$, $\phi \to K^+K^-$, $f_0(980) \to \pi^+\pi^-$ are analyzed. After the final events selection, an η signal is evident in the $\gamma\gamma$ invariant mass spectrum (Fig. 1(a)); $\eta \to \gamma\gamma$ candidates are defined as γ-pairs with $|M_{\gamma\gamma} - 0.547| < 0.037$ GeV/c^2. A ϕ signal is distinct in the K^+K^- invariant mass spectrum (Fig. 1(b)) and for these candidates we require $|m_{K^+K^-} - 1.02| < 0.019$ GeV/c^2. In the $\pi^+\pi^-$ invariant mass spectrum, candidate $f_0(980)$ mesons are defined by $|m_{\pi^+\pi^-} - 0.980| < 0.060$ GeV/c^2 (Fig. 1(c)). The $\phi f_0(980)$ invariant mass spectrum for the selected events is shown in Fig. 2(a), where a clear enhancement is seen around 2.18 GeV/c^2.

The Dalitz plot of $m^2_{\eta f_0(980)}$ versus $m^2_{\eta\phi}$ for the selected events is shown in Fig. 2(b), where a diagonal band can be seen. This band corresponds to the structure observed around 2.18 GeV/c^2 in the $\phi f_0(980)$ invariant mass spectrum shown in Fig. 2(a).

To clarify the origin of the observed structure, we have made extensive studies of potential background processes using both data and Monte Carlo (MC). Non-η or non-$f_0(980)$ processes are studied with η-$f_0(980)$ mass sideband events. Non-ϕ processes are studied with ϕ mass sideband events. The total sideband events estimated from all these sidebands (minus double counting) are shown as the shaded histogram in Fig. 2(a). No structure around 2.18 GeV/c^2 is evident.

We fit the $\phi f_0(980)$ invariant mass spectrum and the total sidebands simultaneously. In the fit, the normalization for the background polynomial is constrained to be the same for both the signal and sideband histograms. We

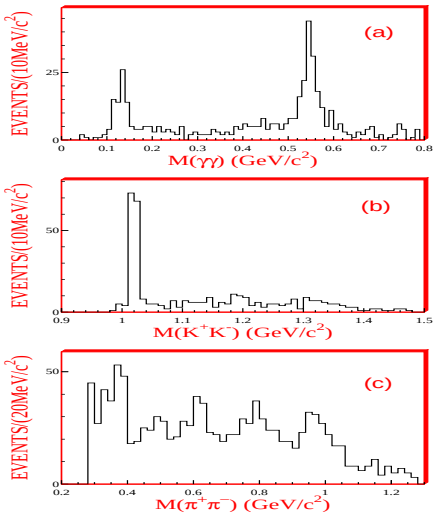

Figure 1: *(a) The $\gamma\gamma$ invariant mass spectrum. (b) The K^+K^- invariant mass spectrum. (c) The $\pi^+\pi^-$ invariant mass spectrum.*

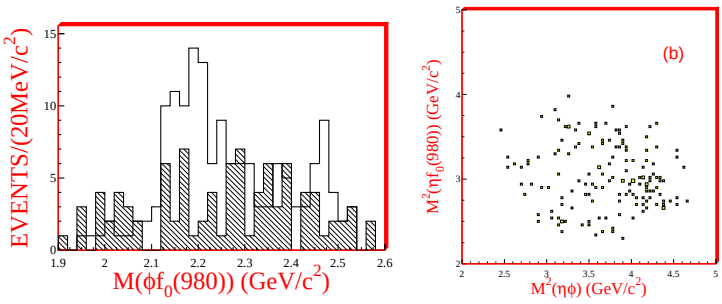

Figure 2: *(a) The $\phi f_0(980)$ invariant mass spectrum; The open histogram is data and the shaded histogram is sideband-determined background. (b) The Dalitz plot of $m^2_{\eta f_0(980)}$ versus $m^2_{\eta\phi}$.*

use a constant-width Breit-Wigner (BW) convolved with a Gaussian mass resolution function (with $\sigma = 12\mathrm{MeV}/c^2$) to represent the $Y(2175)$ signal. The statistical significance of the signal is 5.5 σ. The mass and width obtained from the fit (shown as smooth curves in Fig. 3) are $M = 2.186 \pm 0.010(stat) \pm 0.006(syst)$ GeV/c^2 and $\Gamma = 0.065 \pm 0.023(stat) \pm 0.017(syst)$ GeV/c^2, and the product branching ratio is measured to be $Br(J/\psi \to \eta Y(2175)) \cdot Br(Y(2175) \to \phi f_0(980)) \cdot Br(f_0(980) \to \pi^+\pi^-) = (3.23 \pm 0.75(stat) \pm 0.73(syst)) \times 10^{-4}$, using MC-determined selection efficiency of 1.44%. The systematic uncertainties on the mass and width are estimated by varying the function form used to represent the background, the fitting range of the invariant mass spectrum, the bin width of the invariant mass spectrum, allowing the sideband and signal background normalizations to differ and possible fitting biases. The latter are estimated from the differences between the input and output mass and width values from MC studies. In addition to above systematic sources, the systematic error on the branching ratio measurement comes also from the uncertainties of MC simulation (including systematic uncertainties of the tracking efficiency and the kinematic fits), the photon detection efficiency, the particle identification efficiency, the η decay branching ratio to $\gamma\gamma$ and the ϕ decay branching ratio to K^+K^-.

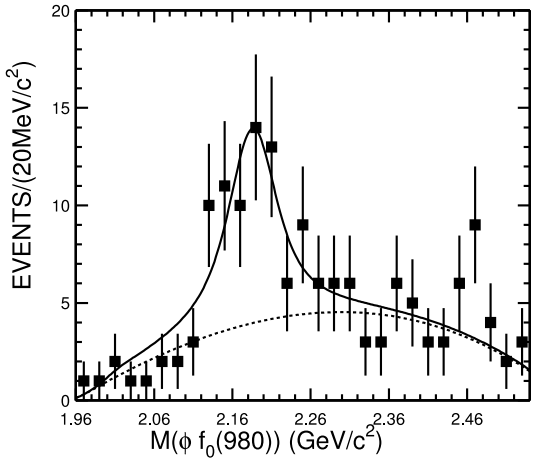

Figure 3: *The solid curve is the fit to the data (points with error bars).*

3 Observation of a broad 1^{--} resonant structure in the K^+K^- mass spectrum in $J/\psi \to K^+K^-\pi^0$

A broad peak is observed at low K^+K^- invariant mass in $J/\psi \to K^+K^-\pi^0$ decays, detailed analysis is described in Ref. [8].

The Dalitz plot for the selected 10631 events is shown in Fig. 4(b), where a broad K^+K^- band is evident in addition to the $K^*(892)$ and $K^*(1410)$ signals. This band corresponds to the broad peak observed around 1.5 GeV/c^2 in the K^+K^- invariant mass projection shown in Fig. 4(c).

A partial wave analysis shows that the J^{PC} of this structure is 1^{--}. Its pole position is determined to be (1576^{+49+98}_{-55-91}) MeV/c^2 - $i(409^{+11+32}_{-12-67})$ MeV/c^2, and the branching ratio is $B(J/\psi \to X\pi^0)\cdot B(X \to K^+K^-)= (8.5 \pm 0.6^{+2.7}_{-3.6}) \times 10^{-4}$, where the first errors are statistical and the second are systematic. These parameters are not compatible with any known meson resonances.

To understand the nature of the broad 1^{--} peak, it is important to search for a similar structure in $J/\psi \to K_S K^{\pm}\pi^{\mp}$ decays to determine its isospin. It is also intriguing to search for $K^*K, KK\pi$ decay modes. In the mass region of the X, there are several other 1^{--} states, such as the $\rho(1450)$ and $\rho(1700)$, but the width of the X is much broader than the widths of these other mesons. This may be an indication that the X has a different nature than these other mesons. For example, very broad widths are expected for multiquark states.

4 Partial wave analysis (PWA) of $J/\psi \to \gamma\pi^+\pi^-$ and $\gamma\pi^0\pi^0$

BES reported the results on J/ψ radiative decays to $\pi^+\pi^-$ and $\pi^0\pi^0$ based on a sample of 58M J/ψ events taken with the BES II detector [9]. Figure 5 shows the $\pi^+\pi^-$ mass spectrum for the selected events, together with the corresponding background distributions and the Dalitz plot. There is a strong $\rho^0(770)$ peak mainly due to background from $J/\psi \to \rho^0\pi^0$. A strong $f_2(1270)$ signal, a shoulder on the high mass side of the $f_2(1270)$, an enhancement at $\sim$ 1.7 GeV/c^2, and a peak at $\sim$ 2.1 GeV/c^2 are clearly visible. The lightly shaded histogram in Fig. 5 corresponds to the dominant background $J/\psi \to \pi^+\pi^-\pi^0$. The other backgrounds are shown as the dark shaded histogram in Fig. 5. Figure 6 shows the $\pi^0\pi^0$ mass spectrum and the Dalitz plot. The shaded histogram corresponds to the sum of estimated backgrounds determined using PDG branching ratios [10]. In general, the $\pi^+\pi^-$ and $\pi^0\pi^0$ mass spectra exhibit

similar structures above 1.0 GeV/c^2.

Partial wave analyses (PWA) are carried out using the relativistic covariant tensor amplitude method in the 1.0 to 2.3 GeV/c^2 $\pi\pi$ mass range. There are conspicuous peaks due to the $f_2(1270)$ and two 0^{++} states in the 1.45 and 1.75 GeV/c^2 mass regions. The first 0^{++} state has a mass of $1466 \pm 6 \pm 20$ MeV/c^2, a width of $108^{+14}_{-11} \pm 25$ MeV/c^2, and a branching fraction $\mathcal{B}(J/\psi \to \gamma f_0(1500) \to \gamma\pi^+\pi^-) = (0.67 \pm 0.02 \pm 0.30) \times 10^{-4}$, which is considered as $f_0(1500)$. Spin 0 is strongly preferred over spin 2.

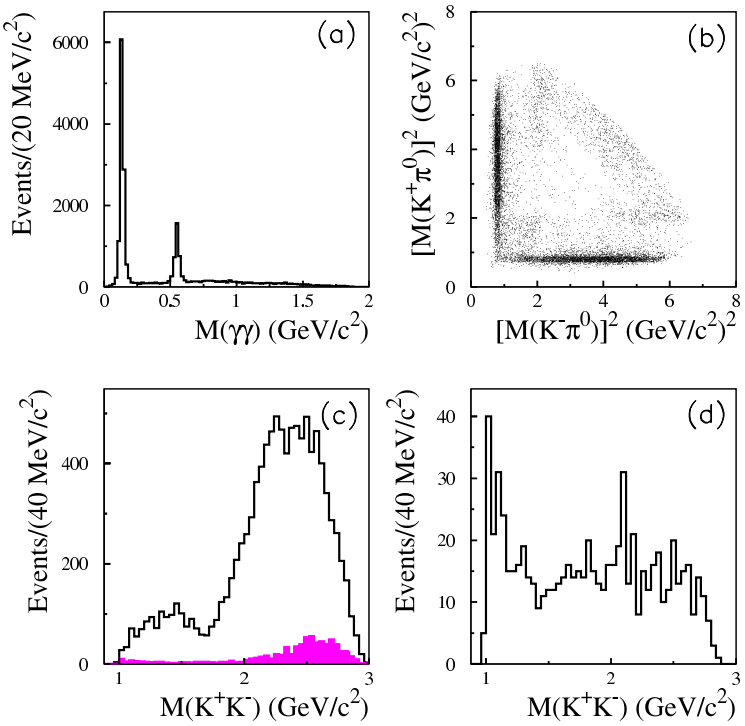

Figure 4: *(a) The $\gamma\gamma$ invariant mass distribution. (b) The Dalitz plot for $K^+K^-\pi^0$ candidate events. (c) The K^+K^- invariant mass distribution for $K^+K^-\pi^0$ candidate events; the solid histogram is data and the shaded histogram is the background (normalized to data). (d) The K^+K^- invariant mass distribution for the π^0 mass sideband events (not normalized).*

5 Summary

With BESII $5.8 \times 10^7 J/\psi$ data, the $Y(2175)$ is observed in $\phi f_0(980)$ mass spectrum in $J/\psi \to \eta\phi f_0(980)$, with the statistical significance of around 5 σ. The measured mass and width are consistent with those of from BABAR. A broad 1^{--} resonance of K^+K^- mass in $J/\psi \to K^+K^-\pi^0$ and the results from the partial wave analysis of $J/\psi \to \gamma\pi^+\pi^-$ and $\gamma\pi^0\pi^0$ are also presented.

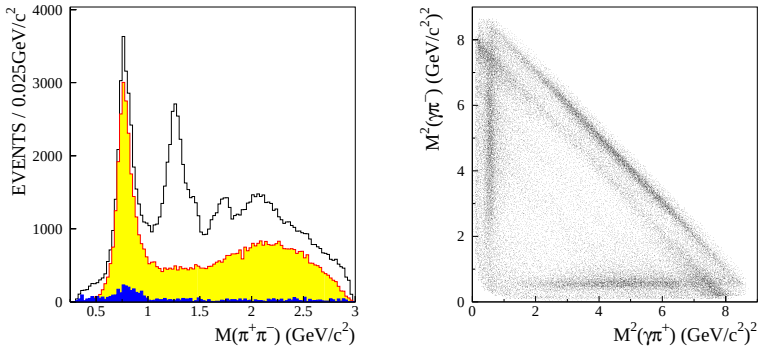

Figure 5: *Invariant mass spectrum of $\pi^+\pi^-$ and the Dalitz plot for $J/\psi \to \gamma\pi^+\pi^-$, where the lightly and dark shaded histograms in the upper panel correspond to $J/\psi \to \pi^+\pi^-\pi^0$ and other estimated backgrounds, respectively.*

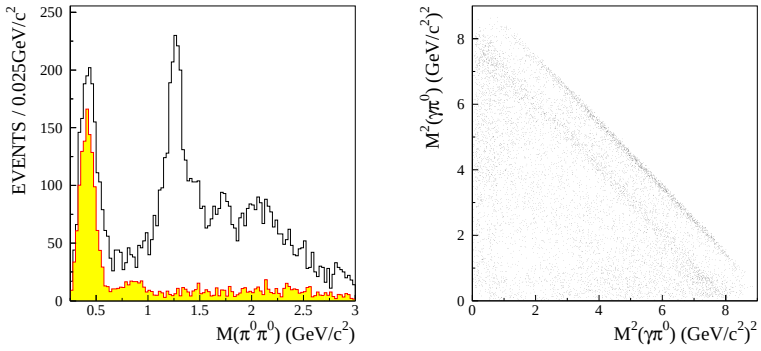

Figure 6: *Invariant mass spectrum of $\pi^0\pi^0$ and the Dalitz plot for $J/\psi \to \gamma\pi^0\pi^0$, where the shaded histogram in the upper panel corresponds to the estimated backgrounds.*

6 Acknowledgement

The BES collaboration thanks the staff of BEPC and computing center for their hard efforts. This work is supported in part by the National Natural Science Foundation of China under contracts Nos. 10491300, 10225524, 10225525, 10425523, 10625524, 10521003.

References

1. B. Aubert *et al.* [BABAR collaboration], Phys. Rev. D **74**, 091103(R) (2006).
2. B. Aubert *et al.* [BABAR collaboration], Phys. ReV. D **76**, 031102 (2007).
3. B. Aubert *et al.* [BABAR collaboration], Phys. Rev. Lett. **95**, 142001 (2005).
4. Gui-Jun Ding, Mu-lin Yan, Phys. Lett. B **650**, 390-400 (2007).
5. Gui-Jun Ding, Mu-lin Yan, hep-ph/0701047.
6. Zhi-Gang Wang, Nucl. Phys. A **791**, 106-116 (2007).
7. BES Collaboration, Nucl. Instr. Meth. A **458**, 627 (2001).
8. BES Collaboration, Phys. Rev. Lett. **97**, 142002 (2006).
9. BES Collaboration, Phys. Lett. B **642**, 441 (2006).
10. W.-M. Yao *et al.* (Particle Data Group), J. Phys. G: Nucl. Part. Phys. **33**, 1(2006).

Frascati Physics Series Vol. XLVI (2007), pp. 729–736
HADRON07: XII Int. Conf. on Hadron Spectroscopy – Frascati, October 8-13, 2007
Light Meson Spectroscopy

THE *K*-MATRIX ANALYSIS OF THE MESON SPECTRUM: SCALAR AND TENSOR STATES BELOW 1.9 GeV

A. Sarantsev
PNPI (Gatchina,Russia) and HISKP (Bonn, Germany)

Abstract

A method for the analysis of the $\pi N \to (\text{mesons})N$ reactions at large momenta of initial pion, based on the reggion exchanges is developed. The method is applied to the analysis of E852 data on $\pi^- p \to \pi^0\pi^0 n$ reaction selected at small and large transferred energies. The contribution of the $f_0(1370)$ state to the S-wave extracted at large $|t|$ is discussed.

1 Cross section for the reaction $\pi N \to (\text{mesons})N$

The information about the meson-meson scattering amplitude can be extracted from πN collision reactions at large energies of the initial pion when the system of final mesons propagates with large momentum in the beam direction. Such reactions are dominantly defined by the t-channel exchanges and the differential cross section for the two meson production can be expanded as a sum of real

parts of spherical functions defined in the Godfrey-Jackson system (GJS):

$$\frac{d^4\sigma}{dtd\Omega dM} = \frac{M|A|^2\rho(s)}{(2\pi)^3 32|\vec{p}_2|^2\, s_{\pi N}} = N(M,t)\sum_{l,m}\langle Y_l^m\rangle ReY_l^m(\Omega)\delta_{lm}. \qquad (1)$$

Here p_1 and p_2 are momenta of the initial pion and nucleon, $s_{\pi N} = (p_1+p_2)^2$, k_1 and k_2 are momenta of the final mesons ($P = (k_1+k_2)$, $s = P^2 = M^2$), $\rho(s)$ is the two meson phase volume and k_3 is momentum of the final nucleon. The q is 4-momentum transferred ($t = q^2$), $\Omega = (\cos\theta, \phi)$ is solid angle of one of the final mesons, $\delta_{l0} = 1$ and $\delta_{lm} = 2$ for $m \geq 1$. The moments $\langle Y_l^m\rangle$ are functions on the total energy of the two meson system only.

1.1 CERN-Munich approach

The CERN-Munich approach was developed for the analysis of the $\pi^- p \to \pi^+\pi^- n$ data taken at small $|t|$ [1)]. It is based partly on the absorbtion model but mostly on the phenomenological observation of the GJS moments behavior. The amplitude is defined by natural and unnatural exchange amplitudes which do not interfere if nucleon polarizations are not detected. The helicity 0 amplitudes are assumed to be defined by unnatural exchanges only and dominantly by the pion exchange. An additional assumption was made that helicity 1 amplitudes are equal for natural ($A_J^{(+)}$) and unnatural ($A_J^{(-)}$) exchanges and the ratio of the helicity 1 and helicity 0 amplitudes is defined by the polynomial which does not depend on the spin of the two meson system J:

$$A_J^{(+)} = A_J^{(-)} = \frac{A_J^0}{C_J \sum\limits_{n=0}^{3} b_n M^n}. \qquad (2)$$

Here C_J ($C_0 = 1$) are normalization parameters and b_n are polynomial coefficients.

The amplitude squared can be rewritten via density matrices

$$\rho_{00}^{nm} = A_n^0 A_m^{0*} \qquad \rho_{01}^{nm} = A_n^0 A_m^{(-)*}, \qquad \rho_{11}^{nm} = 2A_n^{(-)} A_m^{(-)}, \qquad (3)$$

$$|A|^2 = \sum_{J,n,m} Y_J^0 \left(d_{n,m,J}^{0,0,0}\rho_{00}^{nm} + d_{n,m,J}^{1,1,0}\rho_{11}^{nm}\right) + ReY_J^1 \left(d_{n,m,J}^{1,0,1}\rho_{10}^{nm} + d_{n,m,J}^{0,1,1}\rho_{01}^{mn}\right)$$

$$d_{n,m,J}^{i,k,l} = \frac{\int d\Omega\, ReY_n^i(\Theta,\varphi)\, ReY_m^k(\Theta,\varphi)\, ReY_J^l(\Theta,\varphi)}{\int d\Omega\, ReY_J^l(\Theta,\varphi)\, ReY_J^l(\Theta,\varphi)}. \qquad (4)$$

Substituting this expression in eq. (1) one can directly fit the moments $< Y_J^m >$.

1.2 The generalization of CERN-Munich approach

In most partial wave analyses the amplitude is fitted as a sum of amplitudes defined by natural and unnatural exchanges without imposing the condition (2). In the analysis [2, 3] the amplitude is expanded as:

$$|A^2| = |\sum_{J=0} A_J^0 Y_J^0 + \sum_{J=1} A_J^- \sqrt{2}\, Re\, Y_J^1|^2 + |\sum_{J=1} A_J^+ \sqrt{2}\, Im\, Y_J^1|^2, \qquad (5)$$

where the A_J^0 functions are called S_0, P_0, D_0, F_0, ..., the A_J^- functions defined as P_-, D_-, F_-, ... and the A_J^+ functions as P_+, D_+, F_+, ... In the analysis of the $\pi^- p \to \pi^0\pi^0 n$ data selected at large energy transferred two solutions had been found (see Fig. 1). In both these solutions there is a very prominent peak which was associated in [2] with the $f_0(1370)$ state.

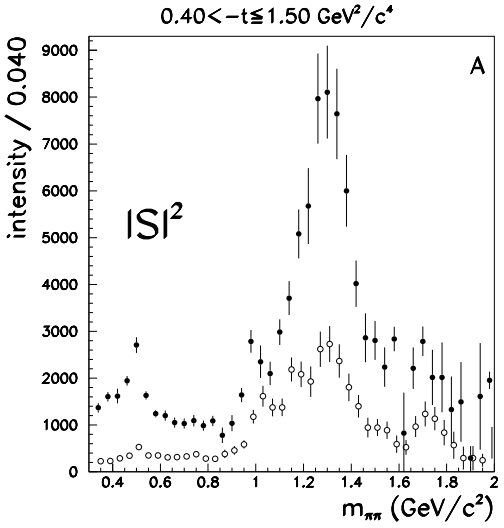

Figure 1: *The S-wave at large energy transferred obtained in the analysis* [2]. *The two solutions are shown as full and open circles.*

2 The analysis based on the reggion trajectory exchanges

The described above approaches are not free from a set of assumptions like relations between amplitudes or a dominance of the one pion-exchange. In reality the interference of the amplitudes defined by exchanges of different particles leads to a more complicated picture than that given by eqs. (4,5). Wolfgang Ochs discussed at HADRON 2005 conference that the peak observed in the S-wave spectrum by E852 collaboration can be a reflection of the $f_2(1270)$ state. Indeed a misidentification of the quantum numbers for the extracted contributions can have place in the approach used in the analysis of E852 group. Therefore the analysis which is based on the particle exchanges and takes into account correctly the interferences between different amplitudes is an important issue in understanding of the πN data.

2.1 The pion and a_1 trajectory exchanges

Amplitudes for the π and a_1 trajectory exchanges can be written as follows:

$$\begin{aligned} A^{(\pi-traj)}_{\pi p\to\pi\pi n} &= \sum_i A(\pi\pi_i\to\pi\pi) R_{\pi_j}(s_{\pi N},q^2)\left(\varphi_n^+(\vec{\sigma}\vec{p}_\perp)\varphi_p\right) g^{(\pi_i)}_{pn}\,. \\ A^{(a_1-\mathrm{traj})}_{\pi p\to\pi\pi n} &= \sum_i A(\pi a_1^{(i)}\to\pi\pi) R_{a_1^{(i)}}(s_{\pi N},q^2)\left(\varphi_n^+(\vec{\sigma}\vec{n}_z)\varphi_p\right) g^{(a_{1i})}_{pn}\,, \end{aligned} \quad (6)$$

where $A(\pi\pi_i\to\pi\pi)$ and $A(\pi a_1^{(i)}\to\pi\pi)$ are the pion-reggeon to two-meson (e.g. two-pion) transition amplitudes, $g^{(\pi_i)}_{pn}$ and $g^{(a_{1i})}_{pn}$ are reggeon-NN vertex couplings and $R(s_{\pi N},q^2)$ is the reggeon propagator:

$$\begin{aligned} R_{\pi_i}(s_{\pi N},q^2) &= \exp\left(-i\frac{\pi}{2}\alpha^{(i)}_\pi(q^2)\right)\frac{\left(s_{\pi N}/s_{\pi N0}\right)^{\alpha^{(i)}_\pi(q^2)}}{\sin\left(\frac{\pi}{2}\alpha^{(i)}_\pi(q^2)\right)\Gamma\left(\frac{1}{2}\alpha^{(i)}_\pi(q^2)+1\right)}\,, \\ R_{a_1^{(i)}}(s_{\pi N},q^2) &= i\exp\left(-i\frac{\pi}{2}\alpha^{(i)}_{a_1}(q^2)\right)\frac{\left(s_{\pi N}/s_{\pi N0}\right)^{\alpha^{(i)}_{a_1}(q^2)}}{\cos\left(\frac{\pi}{2}\alpha^{(i)}_{a_1}(q^2)\right)\Gamma\left(\frac{1}{2}\alpha^{(i)}_{a_1}(q^2)+\frac{1}{2}\right)}\,. \end{aligned} \quad (7)$$

The parameterization of the $\alpha^{(i)}_\pi$ and $\alpha^{(i)}_{a_1}$ (here the (i) index counts leading and daughter trajectories) can be found, for example in [4, 5]. The normalization parameter $s_{\pi N0}$ is of the order of 2–20 GeV^2.

The transition amplitude can be rewritten as:

$$A(\pi\pi_i\to\pi\pi) = \sum_J A^J_{\pi\pi_i\to\pi\pi}(s)(2J+1)N^0_J Y^0_J(\Theta,\varphi)(|\vec{p}||\vec{k}|)^J \quad (8)$$

$$A(\pi a_1^{(i)} \to \pi\pi) = \sum_J (2J+1)|\vec{p}|^{J-1}|\vec{k}|^J \left(W_{0i}^{(J)} Y_J^0(\Theta,\varphi) + W_{1i}^{(J)} Re Y_J^1(\Theta,\varphi) \right)$$

where $\vec{p}$ and $\vec{k}$ are vectors of the initial pion and final pion in the center mass of the two final meson system.

$$\begin{aligned} W_{0i}^{(J)} &= -N_{J0} \left(k_{3z} - \frac{|\vec{p}|}{2} \right) \left(|\vec{p}|^2 A^{(J+)}_{\pi a_1^{(i)} \to \pi\pi} - A^{(J-)}_{\pi a_1^{(i)} \to \pi\pi} \right) \\ W_{1i}^{(J)} &= -\frac{N_{J1}}{J(J+1)} k_{3x} \left(|\vec{p}|^2 J\, A^{(J+)}_{\pi a_1^{(i)} \to \pi\pi} + (J+1) A^{(J-)}_{\pi a_1^{(i)} \to \pi\pi} \right). \end{aligned} \quad (9)$$

Here $A^{(J+)}_{\pi a_1^{(i)} \to \pi\pi}$ is the amplitude produced in πa_1 system with orbital momentum $L = J+1$ and $A^{(J-)}_{\pi a_1^{(i)} \to \pi\pi}$ is the amplitude produced with $L = J-1$.

$$Y_J^m(z,\varphi) = \frac{1}{N_J^m} P_J^m(z) e^{im\varphi} \qquad N_J^m = \sqrt{\frac{4\pi}{2J+1} \frac{(J+m)!}{(J-m)!}}. \quad (10)$$

The leading contribution from π-exchange trajectory can contribute only to the moments with $m = 0$, while a_1-exchange can contribute to the moments up to $m = 2$. The nice feature of a_1 exchange is that moments with $m = 2$ are suppressed compared to moments with $m = 1$ by the ratio k_{3x}/k_{3z} which is small for the two final meson system propagating with a large momentum in the beam direction.

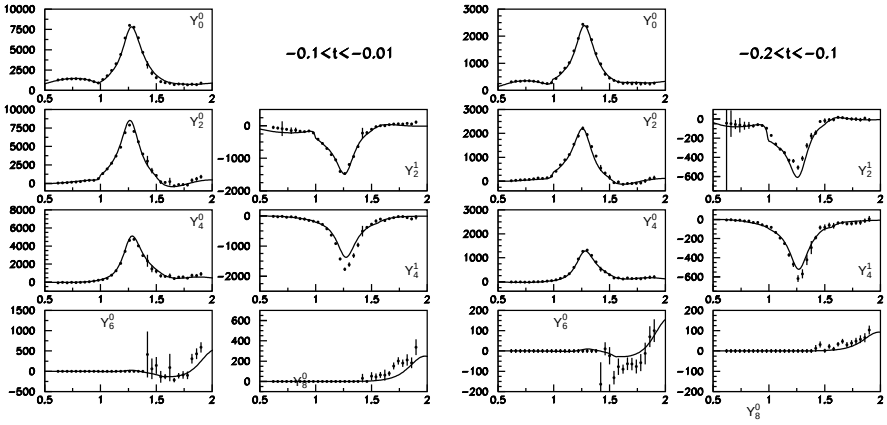

Figure 2: *The description of the moments extracted at energy transferred* $-0.1 < t < -0.01$ GeV^2 *(left) and* $-0.2 < t < -0.1$ GeV^2 *(right).*

The amplitudes defined by the π and a_1 exchanges are orthogonal if the nucleon polarization is not measured. This is due to the fact that the pion trajectory states are defined by the singlet combination of the nucleon spins while a_1 trajectory states are defined by the triplet combination. This phenomenon is not taken into account for the S-wave contribution in eq. (5) which can lead to misidentification of this wave at large energies transferred.

The π_2 particle is situated on the pion trajectory and therefore should be described by the π reggeized exchange. However the π_2 exchange has next-to-leading order contributions defined by the spherical functions with $m \geq 1$. The interference of such amplitudes with the pion exchange can be important (especially at small t) and was taken into account in the present analysis.

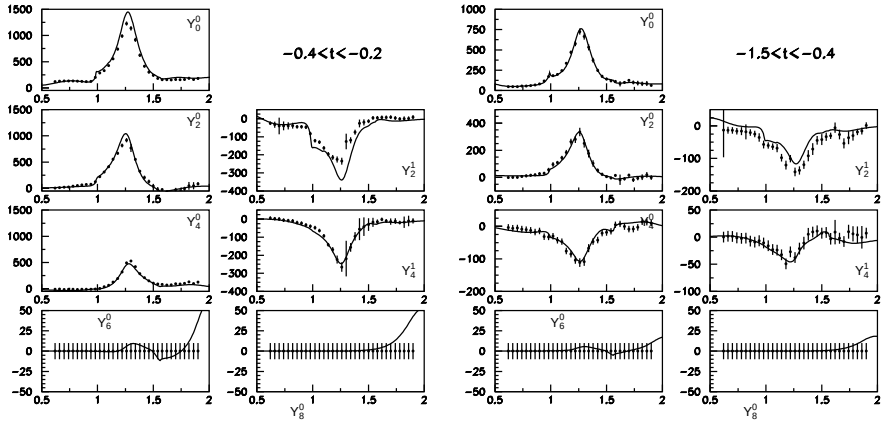

Figure 3: *The description of the moments extracted at energy transferred* $-0.4<t<-0.2$ GeV^2 *(left) and* $-1.5<t<-0.4$ GeV^2 *(right).*

3 Fit of the data

The preliminary analysis of the data on the $\pi^- N \to \pi^0\pi^0$ was performed together with Crystal Barrel data on proton-antiproton annihilation at rest into $3\pi^0$, $\eta\pi^0\pi^0$ and $\eta\eta\pi^0$ channels. Unfortunately the cross section decomposed to the moments is not directly available from the E852 collaboration. Instead the collaboration provided two solutions which can be taken from the Indiana university [6]. To reconstruct the total cross section we used the eq. (5) and decomposed the cross section over moments. The two solutions produced very

close results and we included small differences between them as a systematical error.

The $\pi^- p \to \pi^0\pi^0 n$ data can be described successfully with only π, a_1 and π_2 leading trajectories taken into account. The S-wave was fitted as five-pole five-channel K-matrix with parameterization fixed from [7]. The D-wave was fitted as four-pole four-channel ($\pi\pi$, $\eta\eta$, $\omega\omega$ and 4π) K-matrix. The position of the first two D-wave poles was found to be $(1275 - i\,98)$ and $(1525 - i\,67)$ MeV which corresponds well to the known resonances $f_2(1270)$ and $f_2(1525)$. The third pole has a Flatte structure around $\omega\omega$ threshold. Its position was found to be $(1530 - i\,262)$ MeV on the sheet closest to the physical region above the $\omega\omega$ threshold and $(1699 - i\,216)$ MeV on the sheet closest to the physical region below the $\omega\omega$ threshold. For both poles the closest physical region is the beginning of the $\omega\omega$ threshold where they a relatively narrow (220-250 MeV) structure which corresponds to $f_2(1560)$ state is formed. The forth pole is situated in the region 2 GeV and can not be fixed well in the present analysis.

The description of the moments at small $|t|$ is shown in Fig. 2 and at large $|t|$ in Fig. 3. It is seen that reggion trajectory exchanges can describe the moments at all t-intervals rather well already under simple assumption about the same t-dependence form factor for all partial waves.

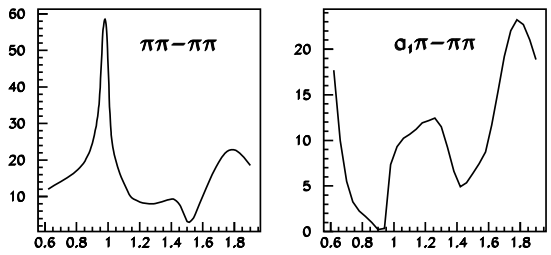

Figure 4: *The S-wave amplitude squared at* $-1.5 < t < -0.4$ GeV^2 *defined by the pion exchange (left) and* a_1*-exchange (right).*

The S-wave contributions defined by the π and α_1 exchanges are shown in Fig. 4. Our analysis did not find a relatively narrow peak in the region 1300 MeV in the S-wave which indicates that the result obtained by E852

collaboration is likely to be a reflection from the $f_2(1270)$ state.

In the amplitude defined by the π-trajectory exchange there is no a significant contribution from $f_0(1370)$. This probably is not a surprise: this resonance rather weakly couples to the $\pi\pi$ channel. In the S-wave amplitude defined by the a_1 exchange the $f_0(1370)$ resonance contributes notably which means that large 4π width of this state can be defined by the decay into the $a_1\pi$ system.

4 Conclusion

We developed the method for the analysis of the meson resonance production off the nucleon based on the reggezied exchanges. The method is applied to the analysis of the $\pi^- p \to \pi^0\pi^0 n$ data selected at small and large energy transferred. Although we did not reproduce a relatively narrow peak in the S-wave in the region 1300 MeV the $f_0(1370)$ state contributed notably to the S-wave part defined by the a_1 trajectory exchange. However the final conclusion can be done only after full systematical study of the obtained solution.

References

1. G. Grayer *et al.*, Nucl. Phys. B **75**, 189 (1974);
   W. Ochs, PhD Thesis, Münich University, (1974).
2. J. Gunter *et al.* (E582 Collaboration), Phys. Rev. D **64**, 07003 (2001).
3. S.U. Chung, Phys. Rev. D **56**, 7299 (1997).
4. A.V. Anisovich, V.V. Anisovich, and A.V. Sarantsev, Phys. Rev. D **62**: 051502(R) (2000).
5. V.V. Anisovich, M.N. Kobrinsky, J. Nyiri, and Yu.M. Shabelski, *"Quark model and high energy collisions"*, 2nd edition, World Scientific, 2004.
6. http://dustbunny.physics.indiana.edu/pi0pi0pwa
7. V.V. Anisovich and A.V. Sarantsev, Eur. Phys. J. A **16**, 229 (2003).

Frascati Physics Series Vol. XLVI (2007), pp. 737
HADRON07: XII Int. Conf. on Hadron Spectroscopy – Frascati, October 8-13, 2007
Ligh Meson Spectroscopy

$\pi\pi$ AND πK FINAL STATE INTERACTIONS AND CP VIOLATION IN B$\to \pi\pi$K DECAYS

R. Kaminski
Institute of Nuclear Physics PAN, Krakow

Written contribution not received

Frascati Physics Series Vol. XLVI (2007), pp. 739–746
HADRON07: XII Int. Conf. on Hadron Spectroscopy – Frascati, October 8-13, 2007
Light Meson Spectroscopy

SPECTRUM AND DECAYS OF MULTIQUARKS, INCLUDING $SU(3)_F$ BREAKING

F. Buccella
Dipartimento di Scienze Fisiche, Universitá di Napoli Federico II and INFN, Sezione di Napoli

Abstract

In the framework of a constituent quark model the spectrum of the lightest positive parity tetraquarks and of the pentaquarks of both parities is evaluated by assuming that the chromo-magnetic interaction plays the main role. A necessary condition for their decays into the "open door" channels selects the states easier to be detected. The comparison with the present experimental knowledge is very favourable.

1 Historical review: $SU(6)_{CS}$

This talk contains the results of a work on tetraquarks in collaboration with H. Högaasen, J. M. Richard and P. Sorba [1)] and on pentaquarks with M. Abud, D. Falcone, G. Ricciardi and F. Tramontano [2)].
More than thirthy years ago, short time after QCD was proposed as the theory

of strong interactions, De Rujula, Georgi and Glashow [3] have shown that the chromo-magnetic interaction:

$$H = -\sum_{i,j} C_{ij}\, \lambda_i \cdot \lambda_j\, \sigma_i \cdot \sigma_j \tag{1}$$

accounts for the mass splittings within the $SU(6)_{FS}$ [4] 56 multiplet:

$$M(\Delta) - M(N) = C_{qq}[C_6(70) - C_6(20) + 1] = 4C_{qq} \tag{2}$$

$$M(\Sigma) - M(\Lambda) = \frac{8}{3}(C_{qq} - C_{qs}). \tag{3}$$

They also predict:

$$M(\Xi) - M(\Sigma) = M(\Xi^*) - M(Y^*). \tag{4}$$

By applying the same concepts to the mesons, one gets:

$$M(\rho) - M(\pi^0) = C_{q\bar{q}}[C_6(35) - \frac{2}{3}] = \frac{16}{3}C_{q\bar{q}}. \tag{5}$$

Jaffe [5] proposed to consider mesons consisting of $2q$ and $2\bar{q}$ with the spectrum given by the chromo-magnetic interaction. Pauli principle relates the $SU(3)_F$ and $SU(6)_{CS}$ transformation properties of $2q$ and $2\bar{q}$:

$$2q : 6_F \times 15_{CS} + \bar{3}_F \times 21_{CS} \tag{6}$$

$$2\bar{q} : \bar{6}_F \times \overline{15}_{CS} + 3_F \times \overline{21}_{CS}. \tag{7}$$

To get light states one should have high $SU(6)_{CS}$ Casimir for $2q$ and $2\bar{q}$ and small for $2q2\bar{q}$ mesons. From the tensor products:

$$21 \times \overline{21} = 1 + 35 + 405 \tag{8}$$

$$15 \times \overline{15} = 1 + 35 + 189 \tag{9}$$

$$21 \times \overline{15} = 35 + 280 \tag{10}$$

$$15 \times \overline{21} = 35 + \overline{280} \tag{11}$$

and the values of the $SU(6)_{CS}$ Casimir:

$$C(6)\,(1) = 0 \tag{12}$$

$$C(6)\,(15) = 14/3 \tag{13}$$

$$C(6)\,(21) = 20/3 \quad (14)$$
$$C(6)\,(35) = 6 \quad (15)$$
$$C(6)\,(189) = 10 \quad (16)$$
$$C(6)\,(280) = C(6)\,(\overline{280}) = 12 \quad (17)$$
$$C(6)\,(405) = 14 \quad (18)$$

one gets the main features of the spectrum [1]. The spin singlets (0^+ scalars) are contained in the 1, 189, and 405 representations, the triplets (1^+ axials) in the 35, 280 and $\overline{280}$, the quintets (2^+) tensors in the 189 and 405. So we expect the lowest states to be a scalar nonet ($1_F + 8_F$) transforming with respect to $SU(6)_{CS}$ almost as the singlet contained in the tensor product $21 \times \overline{21}$. Another nonet and a 36-plet ($1_F + 8_F + 27_F$) of scalars and several ($8_F + 8_F + 10_F + \overline{10}_F$) axial states are expected at a higher mass. Another 36-plet of scalars is at still higher mass together with some axials and a nonet and a 36-plet of tensor states.

Up to now there is evidence for two scalar nonets with the isovector near in mass to the heavier isoscalar [6], a sort of "smoking gun" for the presence of hidden strangeness [7], and the ϕ ω resonance seen at BES [8] may belong to the heavier scalar 36-plet.

Jaffe [5] observed that some of these mesons may decay just through the separation of the constituents and called these final states "open door", for which it is reasonable to expect large couplings to the initial tetraquark; indeed the existence of the lightest $I = 0$ scalar has been for a long time controversial for its large width.

Recently a group theoretical necessary condition has been found [9] for "open door" channels, consisting in the $SU(6)_{CS}$ selection rule following from the transformation properties of the pseudoscalar (P) and vector (V) mesons, as a singlet (1) and an adjoint (35) representation, respectively. Therefore only the scalars, which are $SU(6)_{CS}$ singlets and the axials, which transform as a 35 may have "open door" decays into PP or PV [1]. In conclusion only the states, which transform as small $SU(6)_{CS}$ representations, have "open door" decays into PP or PV, while the heaviest, transforming as the $189, 280, \overline{280}$ and 405 representations, have "open door" decays only into VV. These considerations account for the fact that the lightest scalar multiplet are very broad, that the $f^0(1370)$ has been seen in the 4π channel [10] and the previously mentioned

1812 MeV resonance in the $\phi\ \omega$ channel.
Similar considerations may be applied to the pentaquarks, since the baryon octet (decuplet) transforms as a 70 (20) representation of $SU(6)_{CS}$: only the spin 1/2 (3/2) states transforming as a 70 (20) may have "open door" decays into B (B^*) P channels.

2 The spectrum of the pentaquarks

To construct a pentaquark one has to combine $4q$ in a 3 of colour to give, together with the $\bar{q}$, a colour singlet. Let first consider the negative parity states with all their constituents in S-wave, for which we have the mass formula for the $Y = 2$ states [11]:

$$\begin{aligned} m(s) &= \Sigma_{i=1,4}\, m_{q_i} + m_{\bar{s}} - C_{qq}\left[C_6(t) - \frac{1}{3}C_2(t) - \frac{26}{3}\right] \\ &\quad + C_{q\bar{s}}\left[C_6(p) - C_6(t) - \frac{1}{3}C_2(p) + \frac{1}{3}C_2(t) - \frac{4}{3}\right] \end{aligned} \tag{19}$$

which implies that, similarly to what happens for mesons, the lightest states correspond to high $SU(6)_{CS}$ Casimir for the tetraquark and as low as possible for the pentaquarks. Pauli principle relates the $SU(6)_{CS}$ and $SU(3)_F$ transformation properties of the $4q$'s, with the correspondances $210 \to 3$, $105 \to \bar{6}$, $105' \to 15$ and $\overline{15} \to 15'$. The terms proportional to $-C_{qq}$ and $C_{q\bar{s}}$ give contributions increasing with isospin and $C_6(p)$, respectively. If we consider the tensor products:

$$210 \times \bar{6} = 1134 + 70 + 56 \tag{20}$$

$$105' \times \bar{6} = 540 + 70 + 20 \tag{21}$$

we realize that the lowest $1/2^-$ ($3/2^-$) states will have their main components along the 70 (20) representation and therefore may have "open door" channels into $I = 0$ KN ($I = 1$ $K\Delta$) final states. These states, as it is the case for the $f^0(600)$, may be too broad to be easily seen, which makes us expect that the first states to be identified should be a D_{01} and a D_{15} with increasing mass, as it happened [12].
Positive parity states may be constructed with $4q$ in P-wave and the $\bar{q}$ in S-wave with respect to them [13] or with $4q$ in S-wave and the $\bar{q}$ in P-wave. In the first

case the presence of the orbital momentum of the $4q$ changes the relationship between the colour spin and flavour transformation properties.
For the positive parity states, the chromo-magnetic interaction between the $4q$ and the $\bar{q}$ either will be reduced by a factor two [14] or not considered and there will be a positive contribution from the orbital kinetic energy inversely proportional to the reduced mass of the involved constituents. Also a spin-orbit term will be present.
In conclusion we shall have for the $Y = 2$ states the mass formulas [11]:

$$\begin{aligned} m(p_1) &= \Sigma_{i=1,4}\, m_{q_i} + m_{\bar{s}} + \Delta m^1_{qq} + \Delta m^2_{qq} \\ &\quad + \frac{1}{2} C_{q\bar{s}} \left[C_6(p) - C_6(t) - \frac{1}{3} C_2(p) + \frac{1}{3} C_2(t) - \frac{4}{3} \right] \\ &\quad + K_1 \left(1 + \Sigma_{i=1,4}\, g_{1i}\, \vec{L}\cdot\vec{S}(q_i) \right) \end{aligned} \tag{22}$$

$$\begin{aligned} m(p_2) &= \Sigma_{i=1,4}\, m_{q_i} + m_{\bar{s}} - C_{qq} \left[C_6(t) - \frac{1}{3} C_2(t) - \frac{26}{3} \right] \\ &\quad + K_2 \left(1 + \Sigma_{i=1,4}\, g_{2i}\, \vec{L}\cdot\vec{S}(q_i) + \bar{g}\, \vec{L}\cdot\vec{S}(\bar{s}) \right) \end{aligned} \tag{23}$$

where $\Delta m^1_{qq} + \Delta m^2_{qq}$ is the contribution of the chromo-magnetic interaction within the two 2q clusters which depends on the colour and spin of the pair of quarks as reported in Table 1.

Table 1: *Chromomagnetic splittings for* $2q$ *states.*

$SU(3)_C \times SU(2)_S$	$\frac{\Delta m_{qq}}{C_{qq}}$
$(\bar{3}, 1)$	-2
$(6, 3)$	$-\frac{1}{3}$
$(\bar{3}, 3)$	$+\frac{2}{3}$
$(6, 1)$	$+1$

K_1 and K_2 are the kinetit term associated to the angular motion of the quarks and the spin-orbit term arises, as in electrodynamics, from the interaction of the quarks with the coloured current and the g's depend on the colour configuration.

For the other values of Y we take into account $SU(3)_F$ breaking with the proper constituent masses and with the giro-chromomagnetic factor for the strange quark smaller by the ratio $\frac{m_q}{m_s}$ with respect to the light quarks (u,d).
The positive parity states with $4q$ in S-wave and the $\bar{q}$ in P-wave have a spectrum characterized by the chromo-magnetic interation of the $4q$'s, which is the same than for negative parity states, the rotational kinetic term, which gives a positive contribution to their mass, and, instead of the chromo-magnetic interaction with the $\bar{q}$, the spin orbit term scatters around their masses.
For the positive parity states with $4q$ in P-wave, the interaction with the $\bar{q}$ provokes the eigenvalues of the mass to be mainly dictated by the $SU(6)_{CS}$ transformation properties of the pentaquarks with the consequence that the lightest states have their main components along the 70 (20) and angular momentum $1/2^+$ ($3/2^+$) with "open door" channels into a P and a baryon of the 56 of $SU(6)_{FS}$. Therefore we expect that the first positive pentaquarks have been found with $J^P = 1/2^+$, as again it has been the case. We may identify the resonances with mass [15, 16]:

$$M_{Roper} = 1365\, MeV \tag{24}$$

$$M_{\Theta^+} = 1540\, MeV \tag{25}$$

and [12, 17]:

$$M_{Z^*_{11}} = 1720\, MeV \tag{26}$$

$$M_{\Xi^{--}} = 1862\, MeV \tag{27}$$

as the $1/2^+$ states with $4q$ in P-wave and transforming as the $SU(3)_F$ $\bar{6}$ and 15 representations, respectively.
The negative parity states found in the ranges [12]:

$$M_{Z^*_{03}} = 1788 - 1854\, MeV \tag{28}$$

$$M_{Z^*_{15}} = 2074 - 2150\, MeV \tag{29}$$

may be identified as pentaquarks with all the constituents in S-wave.

3 Conclusion

The approach described here for the spectrum of the multiquark states is very promising.

The necessary condition found [9] for the "open door" decay channels [5] is an useful tool in the research of the states to be discovered.

References

1. F. Buccella , H. Högaasen, J.M. Richard and P. Sorba, Eur. Phys. J. C **49**, 743 (2007).
2. M. Abud, F. Buccella, D. Falcone, G. Ricciardi and F. Tramontano, (in preparation).
3. A. De Rújula, H. Georgi and S.L. Glashow, Phys. Rev. D **12**, 147 (1975).
4. F. Gursey and L.A. Radicati, Phys. Rev. Lett. **13**, 173 (1964).
5. R. L. Jaffe, Phys. Rev. D **17**, 1444 (1978).
6. The Particle Data Group Phys. Lett. B **592**, 1 (2004).
7. L. Maiani, F. Piccinini, A.D. Polosa, V. Riquer, Phys. Rev. D **71**, 014028 (2005) and Phys. Rev. D **72**, 031502 (2005);
   I. Bigi, L. Maiani, F. Piccinini, A.D. Polosa, V. Riquer, Phys. Rev. D **72**, 114016 (2005).
8. BES Collaboration, M. Ablikim *et al.*, Phys. Rev. Lett. **96**, 162002 (2006).
9. F. Buccella, Mod. Phys. Lett. A **21**, 831 (2006).
10. M. Gaspero Nucl. Phys. Rev. Lett. A **562**, 407 (1993).
11. F. Buccella, D. Falcone and F. Tramontano, Central Eur. J. Phys. **3**, 525 (2005).
12. R.A. Arndt and L. D. Roper Phys. Rev. D **31**, 2230 (1985);
    The Particle Data Group Phys. Lett. B **111**, 1 (1982);
    J.S. Hyslop, R.A. Arndt , L.D. Roper and R. L. Workman Phys. Rev. D **46**, 961 (1992).
13. R. L. Jaffe and F. Wilczek, Phys. Rev. Lett. **91**, 232003 (2003)
14. F. Buccella and P. Sorba, Mod. Phys. Lett. A **19**, 1547 (2004)

15. These Proceedings.

16. LEPS Collaboration, T. Nakano *et al.*, Phys. Rev. Lett. **91**, 012002 (2003);
DIANA Coll. V.V. Barmin *et al.*, Phys. Atom. Nucl. **66**, 1715 (2003) and Phys. Atom. Nucl. **70**, 35 (2007);
SVD Coll., A. Kubarovsky, arXiv:hep-ex/0610050v1.

17. NA49 Collaboration, C. Alt *et al.*, Phys. Rev. Lett. **92** 042003 (2004).

Frascati Physics Series Vol. XLVI (2007), pp. 749–756
HADRON07: XII Int. Conf. on Hadron Spectroscopy – Frascati, October 8-13, 2007
Heavy Ions

HEAVY FLAVOUR IN ALICE

Giuseppe Eugenio Bruno *for the* ALICE *Collaboration*
Dipartimento IA di Fisica dell'Università e
del Politecnico di Bari and INFN, Bari, Italy

Abstract

The production of heavy flavoured hadrons will allow to study the strongly interacting medium created in heavy ion collisions at LHC with probes of known mass and colour charge. The ALICE detector will be able to measure heavy flavour production down to low transverse momentum, combining leptonic and hadronic channels. The main physics motivations for the study of heavy flavour production at LHC energies and some examples of physics analyses developed so far by the ALICE heavy flavour working group are discussed.

1 Introduction

The LHC, designed to collide protons at a c.m.s. energy $\sqrt{s} = 14$ TeV, will also accelerate ions up to the same magnetic rigidity and allow the study of both symmetric systems (e.g. Pb–Pb) and asymmetric collisions, such as proton–nucleus (pA). In Table 1, we give examples of the c.m.s. energy and design

Table 1: *Examples of c.m.s. energies, design luminosities at the ALICE interaction region and geometrical cross sections for different collision systems in the LHC. Estimates of the production yields for charm and beauty* $\mathrm{Q\overline{Q}}$ *pairs are also given (for Pb-Pb collisions, in the centrality range corresponding to the most central 5% of the inelastic cross section).*

System	$\sqrt{s_{\mathrm{NN}}}$ (TeV)	L_0 ($\mathrm{cm^{-2}s^{-1}}$)	σ_{geom} (b)	$N^{\mathrm{c\overline{c}}}$	$N^{\mathrm{b\overline{b}}}$
pp	14.0	10^{31} [1]	0.07	0.16	0.0072
Pb–Pb	5.5	10^{27}	7.7	115	4.56
pPb	8.8	10^{29}	1.9	0.78	0.029

luminosity [1] at the ALICE interaction region for some collision systems. The typical yearly effective running times are of the order of 10^7 s for pp collisions and 10^6 s for the heavier systems. The expected yields for heavy-quark production, as obtained from a next-to-leading order perturbative QCD calculation [1)] including nuclear shadowing effects, are also reported in Table 1 [2)].

The study of quarkonia production in heavy ion collisions represents one of the most powerful methods to probe the nature of the medium the fireball is made of. In fact, quarkonia are sensitive to the collision dynamics at both short and long timescales, and are expected to be sensitive to plasma formation.

The measurement of open charm and open beauty production allows one to investigate the mechanisms of heavy-quark production, their propagation and, at low momenta, their hadronisation in the hot and dense medium formed in high-energy nucleus–nucleus collisions. The total open charm and open beauty cross sections are also needed as a reference to measure modifications in the quarkonia production rate. In fact, since at LHC energies heavy quarks are mainly produced through gluon–gluon fusion processes ($gg \rightarrow Q\bar{Q}$), the Drell-Yan process ($q\bar{q} \rightarrow l^+l^-$) does not provide an adequate reference, besides having a very small cross section at these energies, a direct measurement of the D and B mesons yields will provide a natural normalization for charmonia and bottomonia production. Finally, the measurement of B meson production is necessary in order to estimate the contribution of secondary J/Ψ (from B$\rightarrow$J/Ψ + X) to the total J/Ψ yield. The measurement of charm and beauty production

[1] Due to the limited rate capability of the ALICE detector, in pp collisions we must reduce the luminosity at our interaction region with respect to the LHC design value of 10^{34} $\mathrm{cm^{-2}s^{-1}}$ to a maximum of 10^{31} $\mathrm{cm^{-2}s^{-1}}$.

in pp and pA collisions, besides providing the necessary baseline for the study of medium effects in nucleus–nucleus collisions, is of great interest *per se*, as a test of both perturbative and nonperturbative QCD in a new energy domain.

2 Heavy-flavour detection in ALICE at LHC

The design of the ALICE apparatus [3)] will allow the detection of open heavy-flavour hadrons and quarkonia in the high-multiplicity environment of central Pb–Pb collisions at LHC energy, where up to few thousand charged particles might be produced per unit of rapidity. The heavy-flavour capability of the ALICE detector is provided by:

- Tracking; the Inner Tracking System (ITS), the Time Projection Chamber (TPC) and the Transition Radiation Detector (TRD), embedded in a magnetic field up to 0.5 T, will allow for track reconstruction in the pseudorapidity range $|\eta| < 0.9$ with an expected momentum resolution better than 2% for $p_{\rm t} < 20$ GeV/c and a transverse impact parameter[2] resolution better than 60 μm for $p_{\rm t} > 1$ GeV/c.

- Particle identification; charged hadrons (π, K, p) are identified via $\mathrm{d}E/\mathrm{d}x$ in the TPC and in the ITS and via time-of-flight measurements in the Time Of Flight (TOF) detector; electrons are separated from charged pions in the dedicated Transition Radiation Detector (TRD), and in the TPC; muons are identified in the muon spectrometer covering in acceptance the range $-4 < \eta < -2.5$.

Simulation studies [2)] have shown that ALICE has good potential for heavy-flavour physics. Among the main analyses in preparation there are:

- Quarkonia (section 3): ψ and Υ states in the $\mathrm{e^+e^-}$ ($|\eta| < 0.9$) and $\mu^+\mu^-$ ($-4 < \eta < -2.5$) channels.

- Open charm (section 4.1): fully reconstructed hadronic decays $\mathrm{D^0} \rightarrow \mathrm{K^-}\pi^+$, $\mathrm{D^+} \rightarrow \mathrm{K^-}\pi^+\pi^+$, $\mathrm{D_s^+} \rightarrow \mathrm{K^-K^+}\pi^+$ (under study), $\Lambda_{\rm c}^+ \rightarrow \mathrm{pK^-}\pi^+$ (under study), $\mathrm{D^0} \rightarrow \mathrm{K^-}\pi^+\pi^+\pi^-$ (under study) in $|\eta| < 0.9$.

[2]The transverse impact parameter, d_0, is defined as the distance of closest approach of the track to the interaction vertex, in the plane transverse to the beam direction.

- Open beauty (sections 4.2–4.4): inclusive single leptons $\mathrm{B} \rightarrow \mathrm{e} + X$ in $|\eta| < 0.9$ and $\mathrm{B} \rightarrow \mu + X$ in $-4 < \eta < -2.5$; inclusive displaced charmonia $\mathrm{B} \rightarrow \mathrm{J}/\psi\,(\rightarrow \mathrm{e}^{+}\mathrm{e}^{-}) + X$ in $|\eta| < 0.9$.

For all simulation studies, conservative values of charged-particle mid-rapidity density ($\mathrm{d}N_{\mathrm{ch}}/\mathrm{d}y = 6000$–$8000$) were assumed for central Pb–Pb collisions. In the following, we report the results of performance studies corresponding to the expected statistics collected by ALICE per LHC year: 10^7 central (0–5% σ^{inel}) Pb–Pb events and 10^9 pp events in the barrel detectors; the forward muon arm will collect about 4×10^8 central (0–5% σ^{inel}) Pb–Pb and 10^{12} pp events [2].

3 Quarkonia capabilities

ALICE can detect quarkonia in the $e^{+}e^{-}$ channel at central rapidity ($|\eta| < 1$) and in the $\mu^{+}\mu^{-}$ channel at forward rapidity ($-4 < \eta < -2.5$). For both channels the acceptance extends down to $p_{\mathrm{t}} = 0$, the minimum p_{t} for e and μ identification being about 1 GeV/c. The high p_{t} reach is expected to be 10 (20) GeV/c for the J/ψ in $\mathrm{e}^{+}\mathrm{e}^{-}$ ($\mu^{+}\mu^{-}$), for a one month Pb–Pb run at luminosity $L_0 = 5 \cdot 10^{27}\mathrm{cm}^{-2}\mathrm{s}^{-1}$. We emphasize the importance of separating the Υ, Υ' and Υ'', to probe the initial temperature of the medium; given that the mass difference between bottomonium states is about 400 MeV, a mass resolution of order 100 MeV at $M_{\ell^+\ell^-} \sim 10$ GeV, i.e. $\sigma_M/M \approx 1\%$, is required. This requirement is fulfilled for both dielectrons and dimuons, with a mass resolution of about 90 MeV. For illustration, in Figure 1 we show the simulated $\mathrm{l}^{-}\mathrm{l}^{+}$mass spectra in the Υ region after background subtraction [2].

4 Open charm and open beauty capabilities

4.1 Exclusive charm meson reconstruction

Among the most promising channels for open charm detection are the $\mathrm{D}^0 \rightarrow \mathrm{K}^{-}\pi^{+}$ ($c\tau \approx 120$ μm, branching ratio $\approx 3.8\%$) and $\mathrm{D}^{+} \rightarrow \mathrm{K}^{-}\pi^{+}\pi^{+}$ ($c\tau \approx 300$ μm, branching ratio $\approx 9.2\%$) decays. The detection strategy to cope with the large combinatorial background from the underlying event is based on the selection of displaced-vertex topologies, i.e. separation from the primary vertex of the tracks from the secondary vertex and good alignment between the reconstructed D meson momentum and flight-line [2, 4]. Invariant-mass analysis is used to extract the raw signal yield, to be then corrected for selection

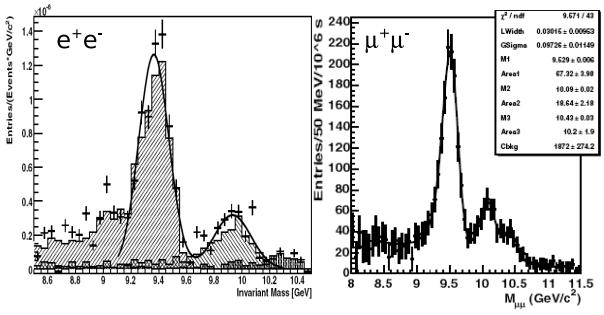

Figure 1: The signal of Υ states in central Pb–Pb collisions, as reconstructed by ALICE [2)], in the e^+e^- and in the $\mu^+\mu^-$ channel, in one month of data-taking.

and reconstruction efficiency and for detector acceptance. As shown in Figure 2 (left), the accessible $p_{\rm t}$ range for the $\rm D^0$ is 1–20 GeV/c in Pb–Pb and 0.5–20 GeV/c in pp, with statistical errors better than 15–20% at high $p_{\rm t}$. Similar capability is expected for the $\rm D^+$ (right-hand panel), though at present the statistical errors are estimated only in the range $1 < p_{\rm t} < 8$ GeV/c. In both cases the systematic errors (acceptance and efficiency corrections, centrality selection for Pb–Pb) are expected to be smaller than 20%.

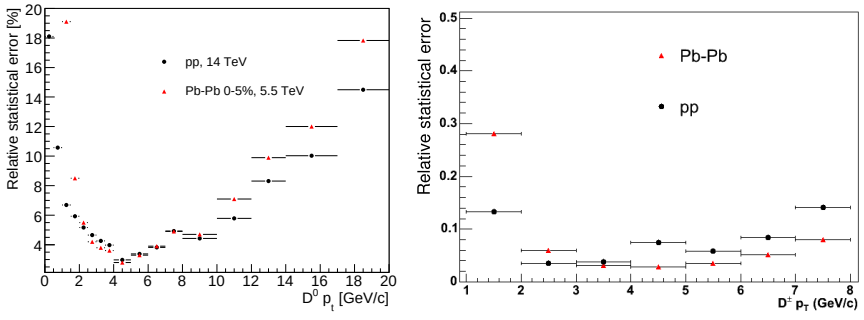

Figure 2: Expected relative statistical errors for the measurement in ALICE of the production cross sections of $\rm D^0$ in the $\rm K^-\pi^+$ channel (left) and $\rm D^+$ in the $\rm K^-\pi^+\pi^+$ channel (right), in 0–5% central Pb–Pb collisions and in pp collisions.

4.2 Beauty via single electrons.

The main sources of background electrons are: decays of D mesons; π^0 Dalitz decays and decays of light vector mesons (e.g., ρ and ω); conversions of photons in the beam pipe or in the inner detector layer and pions misidentified as electrons. Given that electrons from beauty have average impact parameter $d_0 \simeq 500$ μm and a hard $p_{\rm t}$ spectrum, it is possible to obtain a high-purity sample with a strategy that relies on: electron identification with a combined $\mathrm{d}E/\mathrm{d}x$ (TPC) and transition radiation (TRD) selection; impact parameter cuts to reduce the charm-decay component and reject misidentified $\pi^{\pm}$ and $\mathrm{e}^{\pm}$ from Dalitz decays and γ conversions. As an example, with $200 < d_0 < 600$ μm and $p_{\rm t} > 2$ GeV/c the expected signal purity of electrons from B decays is 80% and the statistics is 8×10^4 for 10^7 central Pb–Pb events, allowing the measurement of electron-level $p_{\rm t}$-differential cross section in the range $2 < p_{\rm t} < 20$ GeV/c with statistical errors smaller than 15% at high $p_{\rm t}$. Similar performance figures are expected for pp collisions [2].

4.3 Beauty via muons

B production in Pb–Pb collisions can be measured also in the ALICE muon spectrometer ($-4 < \eta < -2.5$) analyzing the single-muon $p_{\rm t}$ distribution [2]. The main backgrounds to the 'beauty muon' signal are $\pi^{\pm}$, $\mathrm{K}^{\pm}$ and charm decays. A cut $p_{\rm t} > 1.5$ GeV/c is applied to all reconstructed muons in order to increase the signal-to-background ratio. Then, a fit technique allows to extract a $p_{\rm t}$ distribution of muons from B decays. Since only minimal cuts are applied, the statistical errors are expected to be smaller than 5% up to muon $p_{\rm t} \approx 30$ GeV/c [2].

4.4 Beauty in the J/Ψ channel

Simulation studies are in progress to study the capability to separate J/Ψ of the B decay products from that of prompt origin. Such measurement can be performed by studying the separation from the main interaction vertex of the dilepton pairs in the J/ψ invariant mass region and it will also provide a measurement of the beauty $p_{\rm t}$-differential cross section down to $p_{\rm t} \approx 0$. The signed projection of the flight distance of J/Ψ on its transverse momentum, $L_{xy} = \vec{L} \cdot \vec{p}_{\rm T}(J/\Psi)/|p_{\rm T}|$, is a good measurement of the separation from the

main vertex. To reduce the dependence on the J/Ψ transverse momentum bin size and placement, the variable x is used instead of L_{xy}, $x = L_{xy} \cdot M(J/\Psi)/p_{\rm T}$, where the $M(J/\Psi)$ is taken as the known J/Ψ mass [5]. Expected distributions of x for 10^9 pp collisions are shown in Figure 3.

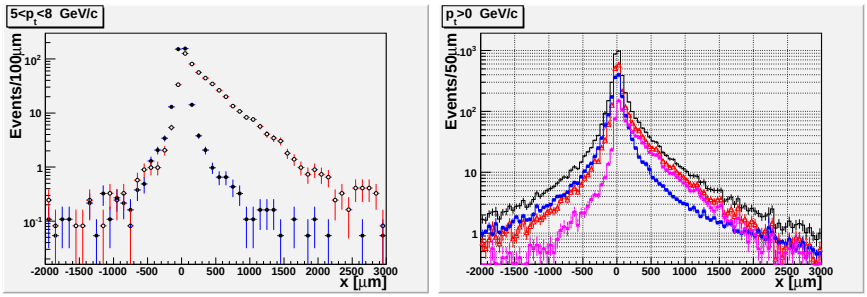

Figure 3: Distributions of the x variable, defined in the text, for $5 < p_{\rm t} < 8$ GeV/c (left) showed for secondary (open circles) and prompt (closed circles) J/Ψ, and for $p_{\rm t} > 0$ (right) showed for total J/Ψ (open triangles), secondary J/Ψ (closed triangles), total background (closed squares) and their sum (lines).

4.5 Nuclear modification factors

We investigated the possibility of using the charm and beauty measurements to study the high-$p_{\rm t}$ suppression induced by parton energy loss, by evaluating their nuclear modification factors $R_{\rm AA}(p_{\rm t}, \eta) = \frac{1}{\langle N_{\rm coll} \rangle} \cdot \frac{{\rm d}^2 N_{\rm AA}/{\rm d}p_{\rm t}{\rm d}\eta}{{\rm d}^2 N_{\rm pp}/{\rm d}p_{\rm t}{\rm d}\eta}$. The sensitivity to $R_{\rm AA}^{\rm D}$ and $R_{\rm AA}^{\rm e\ from\ B}$ is presented in Figure 4. Predictions [6] with and without the effect of the heavy-quark mass, for a medium transport coefficient $\hat{q}$ (a measurement of the medium density) in the range 25–100 GeV^2/fm, are also shown.

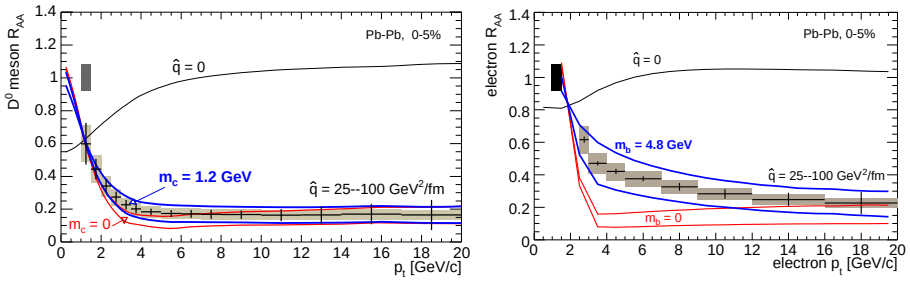

Figure 4: Nuclear modification factors for D^0 mesons (left) and for B-decay electrons (right). Errors corresponding to the centre of the prediction bands for massive quarks are shown: bars = statistical, shaded area = systematic.

5 Conclusions

We have discussed how heavy quarks, abundantly produced at LHC energies, will allow to address several issues at the heart of heavy-ion physics. They provide tools to probe the density (via parton energy loss and its predicted mass dependence) and the temperature (via successive dissociation patterns of quarkonia) of the high-density QCD medium formed in Pb–Pb collisions. The excellent tracking, vertexing and particle identification performance of ALICE will allow to explore deeply this rich phenomenology.

References

1. M. Mangano, P. Nason and G. Ridolfi, Nucl. Phys. B **373**, 295 (1992).
2. ALICE Coll. *PPR Vol. II*, J. Phys. G **32**, 1295 (2006).
3. ALICE Coll. *PPR Vol. I*, J. Phys. G **30**, 1517 (2004).
4. E. Bruna *et al.*, Preprint nucl-ex/0703005 (2007).
5. W.-M. Yao *et al.*, J. Phys. G **33**, 1 (2006).
6. N. Armesto *et al.*, Phys. Rev. D **71**, 054027 (2005).

Frascati Physics Series Vol. XLVI (2007), pp. 757
HADRON07: XII Int. Conf. on Hadron Spectroscopy – Frascati, October 8-13, 2007
Heavy Ions

QUARKONIA IN THE DECONFINED PHASE

W. Alberico
Affiliazione

Written contribution not received

Frascati Physics Series Vol. XLVI (2007), pp. 759–766
HADRON07: XII Int. Conf. on Hadron Spectroscopy – Frascati, October 8-13, 2007
Heavy Ions

ISOSPIN EFFECTS ON MESON PRODUCTION IN RELATIVISTIC HEAVY ION COLLISIONS

M. Di Toro, M. Colonna, G. Ferini, V. Greco, J. Rizzo
LNS-INFN and Physics-Astronomy Dept., Univ. of Catania, Italy
V. Baran
NIPNE-HH and Bucharest University, Romania
T. Gaitanos
Institut für Theoretische Physik, Universität Giessen, Germany
Liu Bo
IHEP, Beijing, China
G. Lalazissis, V. Prassa
Dept. of Theoretical Physics, Aristotle University, Thessaloniki, Greece
H. H. Wolter
Dept. für Physik, Universität München, Germany

Abstract

We show that the phenomenology of isospin effects on heavy ion reactions at intermediate energies (few *AGeV* range) is extremely rich and can allow a "direct" study of the covariant structure of the isovector interaction in a high density hadron medium. We work within a relativistic transport frame, beyond a cascade picture, consistently derived from effective Lagrangians, where isospin effects are accounted for in the mean field and collision terms. We show that rather sensitive observables are provided by the pion/kaon production (π^-/π^+, K^0/K^+ yields). Relevant non-equilibrium effects are stressed. The possibility of the transition to a mixed hadron-quark phase, at high baryon and isospin density, is finally suggested. Some signatures could come from an expected "neutron trapping" effect.

1 Introduction

Recently the development of new heavy ion facilities (radioactive beams) has driven the interest on the dynamical behaviour of asymmetric matter, [1]. Here we focus our attention on relativistic heavy ion collisions, that provide a unique terrestrial opportunity to probe the in-medium nuclear interaction in high density and high momentum regions. An effective Lagrangian approach to the hadron interacting system is extended to the isospin degree of freedom: within the same frame equilibrium properties (EoS, [2]) and transport dynamics can be consistently derived.

Within a covariant picture of the nuclear mean field, for the description of the symmetry energy at saturation (a_4 parameter of the Weizsäecker mass formula) (a) only the Lorentz vector ρ mesonic field, and (b) both, the vector ρ (repulsive) and scalar δ (attractive) effective fields [3, 4] can be included. In the latter case the competition between scalar and vector fields leads to a stiffer symmetry term at high density [3, 1]. We present here observable effects in the dynamics of heavy ion collisions. We focus our attention on the isospin content of meson production. We finally show that in the compression stage of isospin asymmetric collisions we can even enter a mixed deconfined phase.

2 Relativistic Transport

The starting point is a simple phenomenological version of the Non-Linear (with respect to the iso-scalar, Lorentz scalar σ field) effective nucleon-boson field theory, the Quantum-Hadro-Dynamics [2]. According to this picture the presence of the hadronic medium leads to effective masses and momenta $M^* = M + \Sigma_s$, $k^{*\mu} = k^\mu - \Sigma^\mu$, with Σ_s, Σ^μ scalar and vector self-energies. For asymmetric matter the self-energies are different for protons and neutrons, depending on the isovector meson contributions. We will call the corresponding models as $NL\rho$ and $NL\rho\delta$, respectively, and just NL the case without isovector interactions. For the more general $NL\rho\delta$ case the self-energies of protons and neutrons read:

$$\begin{aligned} \Sigma_s(p,n) &= -f_\sigma \sigma(\rho_s) \pm f_\delta \rho_{s3}, \\ \Sigma^\mu(p,n) &= f_\omega j^\mu \mp f_\rho j_3^\mu, \end{aligned} \tag{1}$$

(upper signs for neutrons), where $\rho_s = \rho_{sp} + \rho_{sn},\ j^\alpha = j_p^\alpha + j_n^\alpha, \rho_{s3} = \rho_{sp} - \rho_{sn},\ j_3^\alpha = j_p^\alpha - j_n^\alpha$ are the total and isospin scalar densities and currents and $f_{\sigma,\omega,\rho,\delta}$ are the coupling constants of the various mesonic fields. $\sigma(\rho_s)$ is the solution of the non linear equation for the σ field [3, 1].

For the description of heavy ion collisions we solve the covariant transport equation of the Boltzmann type within the Relativistic Landau Vlasov (RLV) method, using phase-space Gaussian test particles [5], and applying a Monte-Carlo procedure for the hard hadron collisions. The collision term includes elastic and inelastic processes involving the production/absorption of the $\Delta(1232MeV)$ and $N^*(1440MeV)$ resonances as well as their decays into pion channels, [6].

3 Isospin effects on pion and kaon production at intermediate energies

Kaon production has been proven to be a reliable observable for the high density EoS in the isoscalar sector [7, 8] Here we show that the $K^{0,+}$ production (in particular the K^0/K^+ yield ratio) can be also used to probe the isovector part of the EoS, [9, 10].

Using our RMF transport approach we analyze pion and kaon production in central $^{197}Au + ^{197}Au$ collisions in the $0.8 - 1.8\ AGeV$ beam energy range, comparing models giving the same "soft" EoS for symmetric matter and with different effective field choices for E_{sym}. We will use three Lagrangians with constant nucleon-meson couplings ($NL...$ type, see before) and one with density dependent couplings (DDF, see [4]), recently suggested for better nucleonic properties of neutron stars [11, 12].

Fig. 1 reports the temporal evolution of $\Delta^{\pm,0,++}$ resonances, pions ($\pi^{\pm,0}$) and kaons ($K^{+,0}$) for central Au+Au collisions at $1AGeV$. It is clear that, while the pion yield freezes out at times of the order of $50fm/c$, i.e. at the final stage of the reaction (and at low densities), kaon production occur within the very early (compression) stage, and the yield saturates at around $20fm/c$. From Fig. 1 we see that the pion results are weakly dependent on the isospin part of the nuclear mean field. However, a slight increase (decrease) in the π^- (π^+) multiplicity is observed when going from the NL (or DDF) to the $NL\rho$ and then to the $NL\rho\delta$ model, i.e. increasing the vector contribution f_ρ in the isovector channel. This trend is more pronounced for kaons, see the right

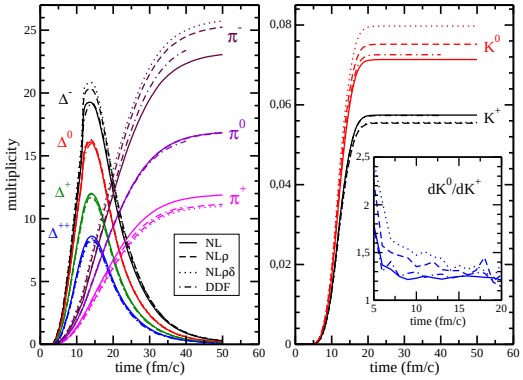

Figure 1: Time evolution of the $\Delta^{\pm,0,++}$ resonances and pions $\pi^{\pm,0}$ (left), and kaons ($K^{+,0}$ (right) for a central ($b = 0$ fm impact parameter) Au+Au collision at 1 AGeV incident energy. Transport calculation using the $NL, NL\rho, NL\rho\delta$ and DDF models for the iso-vector part of the nuclear EoS are shown. The inset contains the differential K^0/K^+ ratio as a function of the kaon emission time.

panel, due to the high density selection of the source and the proximity to the production threshold. Consistently, as shown in the insert, larger effects are expected for early emitted kaons, reflecting the early N/Z of the system.

When isovector fields are included the symmetry potential energy in neutron-rich matter is repulsive for neutrons and attractive for protons. In a HIC this leads to a fast, pre-equilibrium, emission of neutrons. Such a $mean\ field$ mechanism, often referred to as isospin fractionation [1)], is responsible for a reduction of the neutron to proton ratio during the high density phase, with direct consequences on particle production in inelastic NN collisions.

$Threshold$ effects represent a more subtle point. The energy conservation in a hadron collision in general has to be formulated in terms of the canonical momenta, i.e. for a reaction $1 + 2 \rightarrow 3 + 4$ as $s_{in} = (k_1^\mu + k_2^\mu)^2 = (k_3^\mu + k_4^\mu)^2 = s_{out}$. Since hadrons are propagating with effective (kinetic) momenta and masses, an equivalent relation should be formulated starting from the effective in-medium quantities $k^{*\mu} = k^\mu - \Sigma^\mu$ and $m^* = m + \Sigma_s$, where Σ_s and Σ^μ are the scalar and vector self-energies, Eqs.(1). The self-energy contributions will influence the particle production at the level of thresh-

olds as well as of the phase space available in the final channel. In fact the *threshold* effect is dominant and consequently the results are nicely sensitive to the covariant structure of the isovector fields. At each beam energy we see an increase of the π^-/π^+ and K^0/K^+ yield ratios with the models $NL \to DDF \to NL\rho \to NL\rho\delta$. The effect is larger for the K^0/K^+ compared to the π^-/π^+ ratio. This is due to the subthreshold production and to the fact that the isospin effect enters twice in the two-step production of kaons, see [9]. Interestingly the Iso-*EoS* effect for pions is increasing at lower energies, when approaching the production threshold.

We have to note that in a previous study of kaon production in excited nuclear matter the dependence of the K^0/K^+ yield ratio on the effective isovector interaction appears much larger (see Fig.8 of ref. [6]). The point is that in the non-equilibrium case of a heavy ion collision the asymmetry of the source where kaons are produced is in fact reduced by the $n \to p$ "transformation", due to the favored $nn \to p\Delta^-$ processes. This effect is almost absent at equilibrium due to the inverse transitions, see Fig.3 of ref. [6]. Moreover in infinite nuclear matter even the fast neutron emission is not present. This result clearly shows that chemical equilibrium models can lead to uncorrect results when used for transient states of an *open* system.

4 Testing Deconfinement at High Isospin Density

The hadronic matter is expected to undergo a phase transition to a deconfined phase of quarks and gluons at large densities and/or high temperatures. On very general grounds, the transition's critical densities are expected to depend on the isospin of the system, but no experimental tests of this dependence have been performed so far. In order to check the possibility of observing some precursor signals of a new physics even in collisions of stable nuclei at intermediate energies we have performed some event simulations for the collision of very heavy, neutron-rich, elements. We have chosen the reaction $^{238}U + ^{238}U$ (average proton fraction $Z/A = 0.39$) at 1 $AGeV$ and semicentral impact parameter $b = 7$ fm just to increase the neutron excess in the interacting region. In Fig. 2 we report the evolution of momentum distribution and baryon density in a space cell located in the c.m. of the system. We see that after about 10 fm/c a local equilibration is achieved. We have a unique Fermi distribution and from a simple fit we can evaluate the local temperature (black numbers

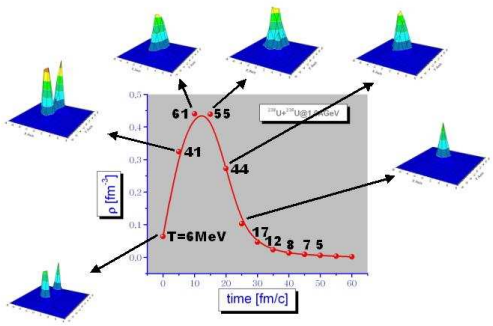

Figure 2: $^{238}U+^{238}U$, 1 $AGeV$, semicentral. Correlation between density, temperature, momentum thermalization inside a cubic cell, 2.5 fm wide, in the center of mass of the system.

in MeV). We note that a rather exotic nuclear matter is formed in a transient time of the order of 10 fm/c, with baryon density around $3-4\rho_0$, temperature $50-60$ MeV, energy density 500 MeV fm^{-3} and proton fraction between 0.35 and 0.40, likely inside the estimated mixed phase region.

In fact we can study the isospin dependence of the transition densities [13]. The structure of the mixed phase is obtained by imposing the Gibbs conditions [15] for chemical potentials and pressure and by requiring the conservation of the total baryon and isospin densities

$$\begin{aligned}
&\mu_B^{(H)} = \mu_B^{(Q)}\,, \quad \mu_3^{(H)} = \mu_3^{(Q)}\,,\\
&P^{(H)}(T,\mu_{B,3}^{(H)}) = P^{(Q)}(T,\mu_{B,3}^{(Q)})\,,\\
&\rho_B = (1-\chi)\rho_B^H + \chi\rho_B^Q\,,\\
&\rho_3 = (1-\chi)\rho_3^H + \chi\rho_3^Q\,,
\end{aligned} \tag{2}$$

where χ is the fraction of quark matter in the mixed phase. In this way we get the *binodal* surface which gives the phase coexistence region in the (T,ρ_B,ρ_3) space. For a fixed value of the conserved charge ρ_3 we will study the boundaries of the mixed phase region in the (T,ρ_B) plane. In the hadronic phase the charge chemical potential is given by $\mu_3 = 2E_{sym}(\rho_B)\frac{\rho_3}{\rho_B}$. Thus, we expect critical densities rather sensitive to the isovector channel in the hadronic EoS.

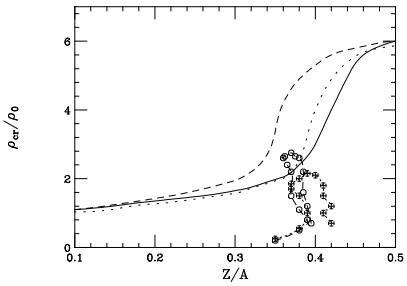

Figure 3: Variation of the transition density with proton fraction for various hadronic EoS parameterizations. Dotted line: $GM3$ RMF-model [14]; dashed line: $NL\rho$; solid line: $NL\rho\delta$. For the quark EoS: MIT bag model with $B^{1/4}$=150 MeV. The points represent the path followed in the interaction zone during a semi-central ^{132}Sn+^{132}Sn collision at 1 $AGeV$ (circles) and at 300 $AMeV$ (crosses).

In Fig. 3 we show the crossing density ρ_{cr} separating nuclear matter from the quark-nucleon mixed phase, as a function of the proton fraction Z/A. We can see the effect of the δ-coupling towards an *earlier* crossing due to the larger symmetry repulsion at high baryon densities. In the same figure we report the paths in the $(\rho, Z/A)$ plane followed in the c.m. region during the collision of the n-rich ^{132}Sn+^{132}Sn system, at different energies. At 300 $AMeV$ we are just reaching the border of the mixed phase, and we are well inside it at 1 $AGeV$. We expect a *neutron trapping* effect, supported by statistical fluctuations as well as by a symmetry energy difference in the two phases. In fact while in the hadron phase we have a large neutron potential repulsion (in particular in the $NL\rho\delta$ case), in the quark phase we only have the much smaller kinetic contribution. Observables related to such neutron "trapping" could be an inversion in the trend of the formation of neutron rich fragments and/or of the π^-/π^+, K^0/K^+ yield ratios for reaction products coming from high density regions, i.e. with large transverse momenta.

5 Perspectives

We have shown that meson production in n-rich heavy ions collisions at intermediate energies can bring new information on the isovector part of the in-medium interaction at high baryon densities. Important non-equilibrium effects for particle production are stressed. Finally the possibility of observing

precursor signals of the phase transition to a mixed hadron-quark matter at high baryon density is suggested.

Acknowledgements. We warmly thanks A.Drago and A.Lavagno for the intense collaboration on the mixed hadron-quark phase transition at high baryon and isospin density.

References

1. V.Baran, M.Colonna, V.Greco, M.Di Toro, *Phys. Rep.* **410** (2005) 335.
2. B. D. Serot, J. D. Walecka, Advances in Nuclear Physics, **16**, 1, eds. J. W. Negele, E. Vogt, (Plenum, N.Y., 1986).
3. B. Liu, V. Greco, V. Baran, M. Colonna, M. Di Toro, *Phys. Rev.* **C65** (2002) 045201.
4. T. Gaitanos, et al., *Nucl. Phys.* **A732** (2004) 24.
5. C. Fuchs. H.H. Wolter, *Nucl. Phys.* **A589** (1995) 732.
6. G. Ferini, M. Colonna, T. Gaitanos, M. Di Toro, *Nucl. Phys.* **A762** (2005) 147.
7. C. Fuchs, *Prog.Part.Nucl.Phys.* **56** 1-103 (2006).
8. C.Hartnack, H.Oeschler, J.Aichelin, *Phys. Rev. Lett.* **96** (2006) 012302.
9. G.Ferini et al., *Phys. Rev. Lett.* **97** (2006) 202301.
10. V.Prassa et al., *Nucl.Phys.* **A789** (2007) 311.
11. T.Klähn et al., *Phys. Rev.* **C74** (2006) 035802.
12. B.Liu et al., *Phys. Rev.* **C75** (2007) 048801.
13. M. Di Toro, A. Drago, T. Gaitanos, V. Greco, A. Lavagno, *Nucl. Phys.* **A775** (2006) 102.
14. N.K.Glendenning, S.A.Moszkowski, *Phys. Rev. Lett.* **67** (1991) 2414.
15. L.D.Landau, L.Lifshitz, *Statistical Physics*, Pergamon Press, Oxford 1969.

Frascati Physics Series Vol. XLVI (2007), pp. 767–774
HADRON07: XII Int. Conf. on Hadron Spectroscopy – Frascati, October 8-13, 2007
Heavy Ions

PHASE STRUCTURE, CRITICAL POINTS, AND SUSCEPTIBILITIES IN NAMBU-JONA-LASINIO TYPE MODELS

C. A de Sousa, Pedro Costa and M. C. Ruivo
Departamento de Física, Universidade de Coimbra, P - 3004 - 516 Coimbra, Portugal

Abstract

We investigate the chiral phase transition at finite temperature and chemical potential within SU(2) and SU(3) Nambu-Jona-Lasinio type models. The behavior of the baryon number susceptibility and the specific heat, in the vicinity of the critical end point, is studied. The class of the critical points is analyzed by calculating critical exponents.

1 Introduction

Strongly interacting matter at non-zero temperature and chemical potential is an exciting topic for physicists coming from different areas, either theoretical or experimental. One of the main goals in the heavy-ion physics program nowadays is to study the effects of several macroscopic phenomena occurring under extreme conditions. The discussion about the existence of a tricritical

point (TCP) or a critical end point (CEP) is also a topic of recent interest. As is well known, a TCP separates the first order transition at high chemical potentials from the second order transition at high temperatures. If the second order transition is replaced by a smooth crossover, a CEP which separates the two lines is found. At the CEP the phase transition is of second order and probably falls into the same universality class of the three-dimensional Ising model. The existence of the CEP in QCD was suggested at the end of the eighties [1], and its properties in the context of several models have been studied since then [2, 3, 4]. The most recent lattice results with $N_f = 2+1$ staggered quarks of physical masses indicate the location of the CEP at $T^{CEP} = 162 \pm 2\,\mathrm{MeV}$ and $\mu^{CEP} = 360 \pm 40\,\mathrm{MeV}$ [5], however its exact location is not yet known.

This point of the phase diagram is the special focus of the present contribution. Nambu-Jona-Lasinio (NJL) type models are used and the main goal is to locate the critical end point and confront the results with universality arguments.

We remark that most of the work done in this area has been performed with non strange quarks only. We will discuss the class of the critical points by including the analyzes in the chiral limit of both SU(2) and SU(3) versions of the NJL model.

The Lagrangian of the SU(3) NJL model [6, 7] is given by:

$$\begin{aligned} \mathcal{L} &= \bar{q}\,(i\partial\cdot\gamma - \hat{m})\,q + \frac{g_S}{2}\sum_{a=0}^{8}\Big[(\bar{q}\lambda^a q)^2 + (\bar{q}(i\gamma_5)\lambda^a q)^2\Big] \\ &+ g_D\Big[\det\big[\bar{q}(1+\gamma_5)q\big] + \det\big[\bar{q}(1-\gamma_5)q\big]\Big]\,. \end{aligned} \tag{1}$$

Using a standard hadronization procedure [8, 9], the baryonic thermodynamic potential, $\Omega(T, V, \mu_i)$, is obtained directly from the effective action. The baryon number susceptibility χ_B and the specific heat C describe, respectively, the response of the baryon density ρ_B and the entropy S with respect to the chemical potential μ_i and the temperature T:

$$\chi_B = \frac{1}{3}\sum_{i=u,d,s}\left(\frac{\partial\rho_i}{\partial\mu_i}\right)_T \quad \text{and} \quad C = \frac{T}{V}\left(\frac{\partial S}{\partial T}\right)_{N_i}\,. \tag{2}$$

These physical quantities are relevant observables to be studied in the context of possible signatures for chiral symmetry restoration.

Our model of strong interacting matter can simulate regions of a hot and dense fireball created in a heavy-ion collision. Since electrons and positrons are not involved in the strong interaction, we impose the condition $\mu_e = 0$. So, we naturally get the chemical equilibrium condition $\mu_u = \mu_d = \mu_s = \mu_B$ that will be used.

After this presentation of the model, we discuss the phase diagrams in sec. 2. The behavior of the baryon number susceptibility and the specific heat in the $T - \mu_B$ plane around the CEP is studied in sec. 3, as well as the corresponding critical exponents. Finally, we conclude in sec. 4 with a brief summary of our results.

2 Phase diagrams in SU(2) and SU(3) NJL models

In this section we analyze the phase diagrams in different conditions in the $T-\mu_B$ plane. Depending on the number of quark flavors $N_f = 2$ or $N_f = 3$, and on the masses of the quarks, different situations can occur and the transition from hadronic matter to QGP may be of first order, second order, or a crossover transition.

We start by analyzing the differences between the three-flavor NJL model and its simpler version in the SU(2) sector. The phase diagrams for both models are presented in fig. 1 as a function of μ_B and T.

Concerning the SU(2) model, and using physical values of the quark masses, $m_u = m_d = 6$ MeV, together with $\Lambda = 590$ MeV and $g_S\,\Lambda^2 = 2.435$, we find that the CEP is localized at $T^{CEP} = 79.9$ MeV and $\mu_B^{CEP} = 331.72$ MeV. We verified that, in the chiral limit, the transition is of second order at $\mu_B = 0$ and, as μ_B increases, the line of second order phase transition will end in a first order line at the TCP. The TCP is located at $\mu_B^{TCP} = 286.1$ MeV and $T^{TCP} = 112.1$ MeV.

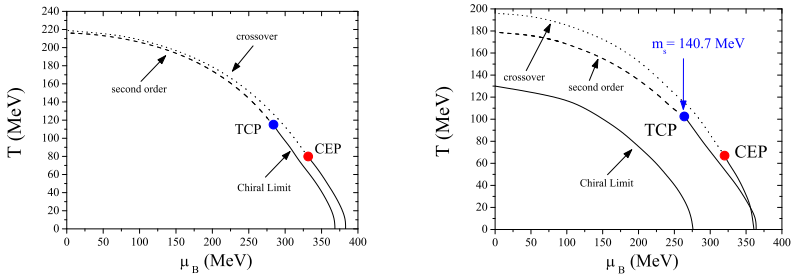

Figure 1: *Phase diagram in the SU(2) (left) and SU(3) (right) NJL models. The solid line represents the first order transition, the dashed the second order and the dotted the crossover transition.*

For the SU(3) NJL model, also in the chiral limit ($m_u = m_d = m_s = 0$), we verify that the phase diagram does not exhibit a TCP: chiral symmetry is restored via a first order transition for all baryonic chemical potentials and temperatures (see right panel of fig. 1). This pattern of chiral symmetry restoration remains for $m_u = m_d = 0$ and $m_s < m_s^{crit}$. In our model we found $m_s^{crit} = 18.3$ MeV for $m_u = m_d = 0$ [4]. When $m_s \geq m_s^{crit}$, at $\mu_B = 0$, the transition is second order and, as μ_B increases, the second order line will end in a first order line at the TCP. The TCP for $m_s = 140.7$ MeV is located at $\mu_B^{TCP} = 265.9$ MeV and $T^{TCP} = 100.5$ MeV. If we choose $m_u = m_d \neq 0$, instead of second order transition we have a smooth crossover which critical line will end in the first order line at the CEP. Using the set of parameters [7, 9]: $m_u = m_d = 5.5$ MeV, $m_s = 140.7$ MeV, $g_S\Lambda^2 = 3.67$, $g_D\Lambda^5 = -12.36$ and $\Lambda = 602.3$ MeV, this point is localized at $T^{CEP} = 67.7$ MeV and $\mu_B^{CEP} = 318.4$ MeV.

We point out that both situations are in agreement with what is expected at $\mu_B = 0$ [10]: the phase transition in the chiral limit is of second order for $N_f = 2$ and first order for $N_f \geq 3$.

3 Susceptibilities and critical exponents in the vicinity of the CEP

The phenomenological relevance of fluctuations around the CEP/TCP of QCD has been recognized by several authors.

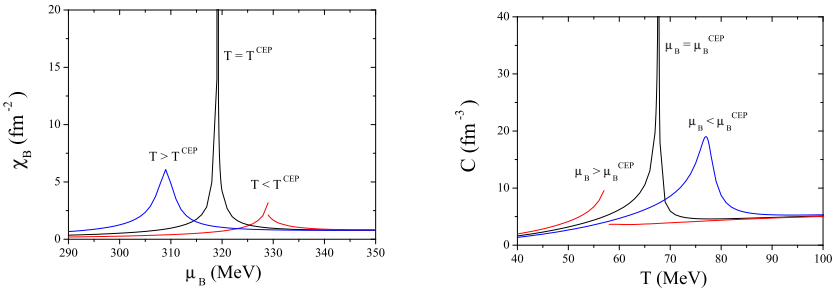

Figure 2: *Response functions in the SU(3) NJL model. Left panel: Baryon number susceptibility as a function of μ_B for different T around the CEP ($T^{CEP} = 67.7$ MeV and $T = T^{CEP} \pm 10$ MeV). Right panel: Specific heat as a function of T for different μ_B around the CEP ($\mu_B^{CEP} = 318.4$ MeV and $\mu_B = \mu_B^{CEP} \pm 10$ MeV).*

In the left panel of fig. 2, the baryon number susceptibility is plotted for three different temperatures around the CEP. For temperatures below T^{CEP} the phase transition is first order and, consequently, χ_B has a discontinuity. For $T = T^{CEP}$ the susceptibility diverges at $\mu_B = \mu_B^{CEP}$ (the slope of the baryon number density tends to infinity). For temperatures above T^{CEP}, in the crossover region, the discontinuity of χ_B disappears at the transition line. A similar behavior is found for the specific heat for three different chemical potentials around the CEP, as we can observe from the right panel of fig. 2. These calculations have been performed in the SU(3) NJL model, but the same qualitative behavior can be found in the SU(2) NJL version [4].

Summarizing, the baryon number susceptibility and the specific heat diverge at $T = T^{CEP}$ and $\mu = \mu^{CEP}$, respectively. [2, 3, 4] In order to make this statement more precise, we will focus on the values of a set of indices, the so-called critical exponents, which describe the behavior near the critical point of various quantities of interest (in our case ϵ and α are the critical exponents of χ_B and C, respectively). If the critical region of the CEP is small, it is expected that most of the fluctuations associated with the CEP will come from the mean field region around the CEP [2].

To a better understanding of the critical behavior of the system, we also analyze what happens in the SU(2) NJL model.

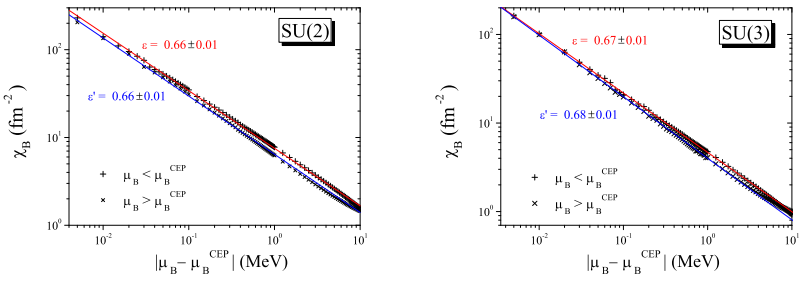

Figure 3: *Baryon number susceptibility as a function of* $|\mu_B - \mu_B^{CEP}|$ *at fixed temperature* $T = T^{CEP}$ *in SU(2) (left panel) and SU(3) (right panel) NJL models.*

To obtain the critical exponent $\epsilon(\epsilon')$ for the baryon number susceptibility, we will consider a path parallel to the μ_B-axis in the $T - \mu_B$ plane, from lower (higher) μ_B towards the critical μ_B^{CEP}, at fixed temperature $T = T^{CEP}$. To this purpose we consider a linear logarithmic fit of the type $\ln \chi_B = -\epsilon^{(\prime)} \ln |\mu_B - \mu_B^{CEP}| + c_1^{(\prime)}$, where the term c_1 (c_1') is independent of μ_B.

The values presented in fig. 3 for these critical exponents, calculated in both SU(2) and SU(3) NJL models, are consistent with the mean field theory prediction $\epsilon = 2/3$. This means that the size of the region is approximately the same independently of the direction of the path parallel to the μ_B-axis.

Paying now attention to the specific heat around the CEP, we have used a path parallel to the T-axis in the $T - \mu_B$ plane from lower/higher T towards T^{CEP} at fixed $\mu_B = \mu_B^{CEP}$. In fig. 4 we plot C as a function of T close to the CEP in a logarithmic scale for both SU(2) and SU(3) calculations. In this case we use a linear logarithmic fit, $\ln C = -\alpha \ln |T - T^{CEP}| + c_2$, where the term c_2 is independent of T.

Starting with the SU(2) case, we observe (see left panel of fig. 4), for $T < T^{CEP}$, that the slope of the fitting of data points changes for $|T - T^{CEP}|$ around 0.3 MeV. So we have a change from the critical exponent $\alpha = 0.59 \pm 0.01$ to $\alpha_1 = 0.45 \pm 0.01$. As pointed out in [2)], this change of the exponent can be interpreted as a crossover of different universality classes, with the CEP being affected by the TCP. It seems that the effect of the hidden TCP on the CEP is relevant for the specific heat contrarily to what happens to χ_B.

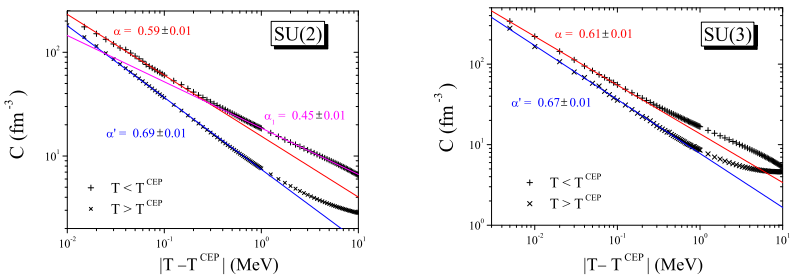

Figure 4: *Specific heat as a function of T for different values of μ_B around $\mu = \mu_B^{CEP}$ in SU(2) (left panel) and SU(3) (right panel) NJL models.*

We also observe that there is no clear evidence of change of the slope of the fitting of data points in the three-flavor NJL model (see fig. 4, right panel). In fact, now we only obtain a critical exponent $\alpha = 0.61 \pm 0.01$ when the critical point is approached from below. When the critical point is approached from above the trivial exponent $\alpha' = 0.67 \pm 0.01$ is obtained.

To justify the possible effect of the hidden TCP on the CEP, as suggested in [2, 3], we analyze the behavior of the specific heat around the TCP. We find nontrivial critical exponents $\alpha = 0.40 \pm 0.01$ and $\alpha = 0.45 \pm 0.01$, for SU(2) and SU(3) cases, respectively. This result, in spite of being close, is not in agreement with the respective mean field value ($\alpha = 1/2$). However, they can justify the crossing effect observed. We notice that the closest distance between the TCP and the CEP in the phase diagram occurs in the T-direction ($(T^{TCP} - T^{CEP}) < (\mu_B^{CEP} - \mu_B^{TCP})$), and is more clear in the SU(2) case.

4 Summary

We verified that our model calculation reproduces qualitative features of the QCD phase diagram at $\mu_B = 0$: for $m_i = 0$ the chiral transition is second-order for $N_f = 2$ and first-order for $N_f \geq 3$. Using realistic values for the current quark masses we find the location of the CEP in both SU(2) and SU(3) NJL models.

It was shown that the baryon number susceptibility and the specific heat diverge at the CEP. The critical exponents for χ_B around the CEP, in both

$N_f = 2$ and $N_f = 3$ NJL models, are consistent with the mean field values $\epsilon = \epsilon' = 2/3$. For the specific heat, the nontrivial values of α ($1/2 < \alpha < 2/3$) around the CEP can be interpreted as a crossover from a mean field tricritical exponent ($\alpha = 1/2$) to an Ising-like critical exponent ($\alpha = 2/3$).

A better insight to the difficult task of the analysis of the phase diagram of QCD can be provided by an extension of the NJL model where quarks interact with the temporal gluon field represented by the Polyakov loop dynamics.

Acknowledgments

Work supported by grant SFRH/BPD/23252/2005 from F.C.T. (P. Costa), Centro de Física Teórica and FCT under project POCI 2010/FP/63945/2005.

References

1. M. Asakawa *et al*, Nucl. Phys. A **504**, 668 (1989).
2. Y. Hatta *et al*, Phys. Rev. D **67**, 014028 (2003).
3. B.-J. Schaefer *et al*, Phys. Rev. D **75**, 085015 (2007).
4. P. Costa *et al*, Phys. Lett. B **647**,431 (2007); P. Costa *et al* to be published.
5. Z. Fodor *et al*, J. High Energy Phys. 0204, 050 (2004).
6. T. Hatsuda *et al*, Phys. Rept. **247**, 221 (1994).
7. P. Rehberg *et al*, Phys. Rev. C **53**, 410 (1996).
8. P. Costa *et al*, Phys. Rev. C **70**, 025204 (2004).
9. P. Costa *et al*, Phys. Rev. D **70**, 116013 (2004); Phys. Rev. D **71**, 116002 (2005); Phys. Lett. B **560**, 171 (2003); Phys. Lett. B **577**, 129 (2003).
10. R.D. Pisarski *et al*, Phys. Rev. D **29**, 338 (1984).

Frascati Physics Series Vol. XLVI (2007), pp. 775–782
HADRON07: XII Int. Conf. on Hadron Spectroscopy – Frascati, October 8-13, 2007
Heavy Ions

DIELECTRON SPECTROSCOPY AT 1-2 AGEV WITH HADES

Stefano Spataro for the HADES collaboration[‡]
II. Physikalisches Institut, Justus-Liebig-Universität, Gießen, Germany
INFN – Laboratori Nazionali del Sud, Catania, Italy
stefano.spataro@exp2.physik.uni-giessen.de

Abstract

The HADES spectrometer at GSI (Darmstadt) is investigating e^+ e^- pair production in p+p, p+A and A+A collisions. In this contribution we would like to highlight the physics motivations and the experiments performed so far, focusing mainly on the first results coming from ^{12}C+^{12}C collisions at 1 and 2 AGeV, and on preliminary results from p+p/d+p collisions at 1.25 AGeV.

1 Introduction

Models predict that hadron properties, such as mass and lifetime, depend on the temperature and the density of the ambient medium. While some hadronic many-body calculations predict a broadening of the meson in-medium spectral functions, other approaches predict a drop in meson masses related to chiral symmetry restoration [1, 2]. In this context dileptons are good penetrating

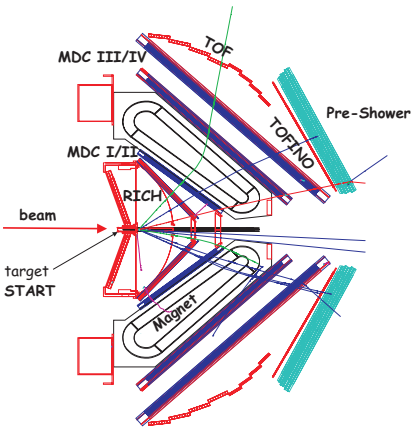

Figure 1: *Schematic layout of the HADES detector at GSI Darmstadt: a Ring Imaging Cherenkov detector (RICH), four planes of Multi-wire Drift Chambers (MDC) placed before and after a region of magnetic field, a Time-Of-Flight (TOF/TOFINO) system and a Pre-SHOWER detector.*

probes for hot and dense nuclear systems, because once produced they do not undergo the strong final state interaction, carrying information on the process and the local conditions.

Several experiments have focused on low mass lepton pairs, from bombarding energies of few AGeV, studied by the DLS experiment [3] at Bevalac, through the range of SPS energies (40-158 AGeV) at CERN studied by the CERES [4], HELIOS-3 [5] and NA60 [6] experiments, up to the high energies of the RHIC collider ($\sqrt{s_{NN}} = 200$ GeV) studied by the PHENIX experiment [7]. A dilepton enhancement was observed at the SPS and related to in-medium modifications of the ρ meson spectral function, but the excess yields found by DLS in C+C and Ca+Ca collisions at 1 AGeV could not be explained satisfactorily in the same way.

The High-Acceptance DiElectron Spectrometer HADES [8] at GSI operates in the energy regime of 1-2 AGeV (such as the DLS experiment), and has started a systematic investigation of e^+ e^- pair production in elementary and heavy ion collisions with improved resolution and higher statistics. The HADES setup has a 6-fold symmetry; it fully covers the azimuthal angle and the region between 18° and 85° in the polar angle. A cross section of HADES is shown in Fig. 1. Recent results from C+C at 1 and 2 AGeV will be discussed, with some considerations about the beam-energy dependence of pair yield. Moreover, preliminary distributions from p+p and d+p collisions will be shown as well, aiming at understanding the various components that contribute to the dilepton cocktails.

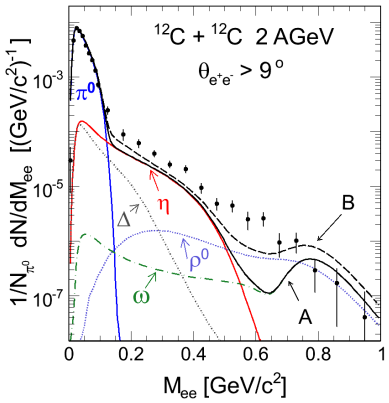

Figure 2: *Efficiency corrected dielectron invariant mass spectrum measured by HADES in C+C collisions at 2 AGeV (only statistical errors are depicted), in comparison with the cocktail expected from the superposition of the known long lived particles (cocktail A) and including even short-lived contributions (cocktail B), taken from* [9].

2 Dilepton production in C+C collisions

In order to verify and understand the dilepton production in light systems, we have done measurements of ^{12}C+^{12}C collisions at 1 and 2 AGeV. The same system was studied by the former DLS experiment at 1.04 GeV [3], and an excess over the known sources of dileptons was found in the 0.2-0.6 GeV/c^2 mass range.

The data at 2 AGeV [9] were taken with a partial tracking setup, resulting in modest resolution mode achieving mass resolution of about $\sigma_M/M \sim 9\%$. The readout was started by a first-level trigger decision requiring at least four hits in the TOF/TOFINO detectors, corresponding to $\sim 60\%$ of the total cross section, and a second-level decision with at least one lepton track in the event, to enhance the lepton content in the data stream.

Fig. 2 shows the invariant mass distribution of the signal e$^+$ e$^-$ pairs after subtraction of combinatorial background and efficiency corrections, normalized to the average number of charged pions $N_\pi = \frac{1}{2}(N_{\pi^+} + N_{\pi^-})$ extrapolated to 4π. Further details about the analysis can be found in [9]. At low masses (below 0.15 GeV/c^2) the spectrum is dominated by π° Dalitz decay pairs, whereas at higher masses η and Δ Dalitz decays are more prominent; the region around the ρ/ω pole masses is of particular interest to study in-medium modifications. A total of $\sim$ 23000 signal pairs was finally reconstructed ($\sim$ 2000 with M$_{ee} > 0.15$ GeV/c^2). The experimental spectrum was compared to a simulation cocktail

including all long-lived contributions (cocktail A in Fig. 2), such as free π and η meson decays whose production rates are constrained by experimental data [10], and ω decays estimated assuming m_t scaling. The cocktail well represents the data in the π° region, but undershoots at low pair masses calling for additional contributions. Such contributions are expected from the decays of short-lived resonances, mainly the $\Delta(1232)$ and the ρ, which were included in our cocktail B as long-dashed line (the Δ yield is scaled according to π production, while m_t scaling was used for the ρ). The simulation yield above π° is increased and the high mass region is filled by the ρ component, but still such type of simulation fails to reproduce well the data.

The same procedure was followed for the analysis of ^{12}C+^{12}C at 1 AGeV, detecting a total of $\sim$ 18000 signal pairs ($\sim$ 650 with $M_{ee} > 0.15$ GeV/c^2), and in this case the observed pair excess is much more pronounced than in the 2 AGeV data [11]. In order to quantify the excess yield, it is possible to evaluate the average pair enhancement above the known η Dalitz contribution in the η mass range M = 0.15-0.50 GeV/c^2. This ratio amounts to $F(2.0) = Y_{tot}/Y_\eta = 1.9 \pm 0.2(stat) \pm 0.3(sys) \pm 0.3(\eta)$ at 2 AGeV, while $F(1.0) = 6.8 \pm 0.6(stat) \pm 1.3(sys) \pm 2.0(\eta)$ at 1 AGeV, where the (η) error corresponds to the uncertainty from quoted errors of η multiplicity. It is interesting to compare the dependence of the excess pairs as a function of the bombarding energy with the neutral meson production in the C+C system, studied in the $\gamma\gamma$ decay channel [10]. Fig. 3 shows π° and η production with pair multiplicity from η Dalitz decays, together with the HADES excess pairs within the 0.15-0.50 GeV/c^2 mass range, and the DLS excess yield at 1.04 AGeV extrapolated assuming that the overall excess acceptance is close to the acceptance of η Dalitz pairs ($F(1.04) = 6.5 \pm 0.5(stat) \pm 2.1(sys) \pm 1.5(\eta)$). From the plot appears that the HADES and DLS data are in a good agreement around 1 AGeV, and that the evolution of the excess pairs as a function of beam energy seems to scale like the pion production, being very different from the energy dependence of η production. This would suggest that the physics mechanism of the pair excess is not so much connected to the excitations of higher energy resonances, but probably to low energy processes, such as Δ and low-mass tails of ρ resonance, and possibly bremsstrahlung processes as suggested in recent calculations [12]. Final conclusions can only be drawn after a proper analysis of elementary collisions, such as the HADES data from p+p and d+p runs.

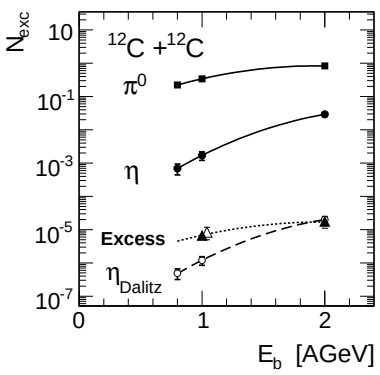

Figure 3: *Excess pair multiplicity in the mass range of 0.15-0.50 GeV/c^2 (full triangles: HADES, open triangles: DLS [3]) versus beam energy [11], together with the excitation functions of inclusive η (full circles) and π° (full squares) production from TAPS [10], as well as the η Dalitz decay contribution (open circles). Scaled down π° (dotted) and absolute η Dalitz (dashed) curves are shown for comparison.*

3 Dilepton production in elementary collisions

Measurements of pair production in p+p/d+p collisions aim at understanding the elementary production mechanisms of dileptons, before resolving in-medium effects in heavy-ion collisions. Indeed, our present knowledge of the hadron electromagnetic coupling is not so exhaustive, for example the Δ Dalitz decay has not been measured yet, as well as the nucleon-nucleon virtual bremsstrahlung in the HADES energy regime. Therefore, HADES has started a systematic investigation of this sector, with proton/deuteron beams on LH2 targets. The first run was p+p at 2.2 GeV bombarding energy, with the main goal of verifying the dielectron reconstruction efficiency by means of exclusive reconstruction of the well known hadronic ($\eta \to \pi^+\pi^-\pi^0$) and electromagnetic ($\eta \to e^+e^-\gamma$) η decay channels. Results were already discussed in [13].

In the low-energy range p+p and d+p collisions were studied at 1.25 AGeV, in order to check the contributions in the dilepton spectrum below the η production. In the p+p reactions the contribution from bremsstrahlung results almost negligible, so it is possible to isolate and study the Δ Dalitz decay via inclusive and exclusive analyses. Once knowing the Δ behavior at this energy, it is possible to use isospin arguments in order to subtract this term in quasi-free *pn* collisions in d+p data set, and to extract *pn* bremsstrahlung. For the d+p data, a forward wall was added into the HADES setup, to detect

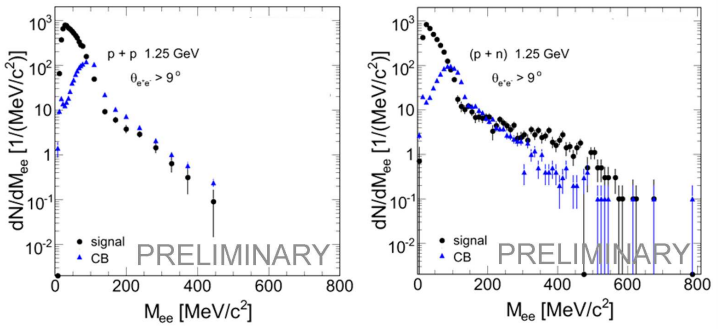

Figure 4: *Preliminary e^+ e^- mass spectra for p+p (left) and tagged pn (right) collisions at 1.25 AGeV, not corrected for efficiency. Signal pairs are shown (circles) after subraction of the combinatorial background (triangles).*

the spectator proton thus to tag the quasi-free *pn* reaction. Fig. 4 shows the preliminary invariant mass distributions of e^+ e^- signal pairs in p+p and *pn* reactions, not corrected for efficiency. In the p+p data we have collected $\sim$ 39000 signal pairs ($\sim$ 600 with $M_{ee} > 0.15$ GeV/c^2). The *pn* sample is derived from a preliminary on-line analysis and a total of $\sim$ 38000 signal pairs is estimated, that corresponds to about 50% of the expected statistics. The difference in the shape above π° mass may be related to isospin effects, but final conclusions can only be drawn once efficiency corrections are applied. Moreover, to draw conclusions on the Δ Dalitz branching ratio and form factor up to now unmeasured, a ppe^+e^- exclusive analysis is ongoing.

In a recent experiment we have also studied p+p collisions at 3.5 GeV, mainly focused on ω and ρ mesons production. The ω line shape is of particular importance for the next p+A experiment at the same energy, where it will be used as reference in order to study directly in-medium effects. From a preliminary analysis of online data we estimate few hundred ω mesons in the inclusive pair spectrum.

4 Summary and outlook

The HADES experiment is performing, with interesting results, a systematic study of dilepton production in elementary and ion collisions in the beam energy

range of few GeV. Currently, data on heavier systems (Ar+KCl) are being analyzed. In the near future, p+A collisions will be investigated to study medium modifications of ω production and, after an upgrade, the physics program will focus on dielectron production in heavy ion collisions and in pion induced experiments. After 2011 it is foreseen to install HADES at the new FAIR facility, which will allow to explore a new domain at beam energies up to 10 AGeV.

5 Acknowledgements

The collaboration gratefully acknowledges support by the following grants: BMBF 6MT238, 06GI179, 06F140, and 06DR135 (Germany); DFG cluster of excellence *Origin and Structure of the Universe*; GSI (TM-FR1, GI/ME3, OF/STR); GA ASCR IAA1048304 and MSMT LC7050 (Czech Republic); KBN 1P03B 056 29 (Poland); INFN (Italy); CNRS/IN2P3 (France); MCYT FPA2000-2041-C02-02 and XUGA PGID T02PXIC20605PN (Spain); UCY-10.3.11.12 (Cyprus); INTAS 05-1012-8861; EU contract RII3-CT-2004-506078.

References

1. R. Rapp and J. Wambach, Adv. Nucl. Phys. **25**, 1 (2000).
2. W. Cassing and E.L. Bratkovskaya, Phys. Rep. **308**, 65 (1999).
3. R.J. Porter et al., DLS Collaboration, Phys. Lett. **79**, 1229 (1997).
4. G. Agakichiev et al., CERES Collaboration, Eur. Phys. J. C **41**, 475 (2005).
5. M. Masera, HELIOS Collaboration, Nucl. Phys. A **590**, 93c (1995).
6. R. Arnaldi et al., NA60 Collaboration, Phys. Rev. Lett. **96**, 162302 (2006).
7. S. Afanasiev et al., PHENIX Collaboration, arXiv:0706.3034v1 [nucl-ex].
8. R. Schicker et al., HADES Collaboration, Nucl. Instr. Meth. A **380**, 586 (1996).
9. G. Agakichiev et al., HADES Collaboration, Phys. Rev. Lett. **98**, 052302 (2007).
10. R. Averbeck et al., TAPS Collaboration, Z. Phys. A **359**, 65 (1997); R. Holzmann et al., TAPS Collaboration, Phys. Rev. C **56**, R2920 (1997).

11. G. Agakichiev et al., HADES Collaboration, submitted to Phys. Lett B, arXiv:nucl-ex/0711.4281v1.

12. L. Kaptari and B. Kämpfer, Nucl. Phys. A **764**, 338 (2006).

13. S. Spataro et al., HADES Collaboration, Int. Jour. Mod. Phys. A **22**, 533 (2007).

‡The HADES Collaboration:

G. Agakishiev[8], C. Agodi[1], A. Balanda[3,e], G. Bellia[1,a], D. Belver[15], A. Belyaev[6], A. Blanco[2], M. Böhmer[11], J. L. Boyard[13], P. Braun-Munzinger[4], P. Cabanelas[15], E. Castro[15], S. Chernenko[6], T. Christ[11], M. Destefanis[8], J. Díaz[16], F. Dohrmann[5], A. Dybczak[3], T. Eberl[11], L. Fabbietti[11], O. Fateev[6], P. Finocchiaro[1], P. Fonte[2,b], J. Friese[11], I. Fröhlich[7], T. Galatyuk[4], J. A. Garzón[15], R. Gernhäuser[11], A. Gil[16], C. Gilardi[8], M. Golubeva[10], D. González-Díaz[4], E. Grosse[5,c], F. Guber[10], M. Heilmann[7], T. Hennino[13], R. Holzmann[4], A. Ierusalimov[6], I. Iori[9,d], A. Ivashkin[10], M. Jurkovic[11], B. Kämpfer[5], K. Kanaki[5], T. Karavicheva[10], D. Kirschner[8], I. Koenig[4], W. Koenig[4], B. W. Kolb[4], R. Kotte[5], A. Kozuch[3,e], A. Krása[14], F. Krizek[14], R. Krücken[11], W. Kühn[8], A. Kugler[14], A. Kurepin[10], J. Lamas-Valverde[15], S. Lang[4], J. S. Lange[8], K. Lapidus[10], L. Lopes[2], M. Lorenz[7], L. Maier[11], A. Mangiarotti[2], J. Marín[15], J. Markert[7], V. Metag[8], J. Micel[7], B. Michalska[3], D. Mishra[8], E. Morinière[13], J. Mousa[12], C. Müntz[7], L. Naumann[5], R. Novotny[8], J. Otwinowski[3], Y. C. Pachmayer[7], M. Palka[4], Y. Parpottas[12], V. Pechenov[8], O. Pechenova[8], T. Pérez Cavalcanti[8], J. Pietraszko[4], W. Przygoda[3,e], B. Ramstein[13], A. Reshetin[10], M. Roy-Stephan[13], A. Rustamov[4], A. Sadovsky[10], B. Sailer[11], P. Salabura[3], A. Schmah[4], R. Simon[4], Yu.G. Sobolev[14], S. Spataro[8], B. Spruck[8], H. Ströbele[7], J. Stroth[7,4], C. Sturm[7], M. Sudol[4], A. Tarantola[7], K. Teilab[7], P. Tlusty[14], M. Traxler[4], R. Trebacz[3], H. Tsertos[12], I. Veretenkin[10], V. Wagner[14], H. Wen[8], M. Wisniowski[3], T. Wojcik[3], J. Wüstenfeld[5], S. Yurevich[4], Y. Zanevsky[6], P. Zhou[5], P. Zumbruch[4]

[1] *Istituto Nazionale di Fisica Nucleare - Laboratori Nazionali del Sud, Catania, Italy*
[2] *LIP-Laboratório de Instrumentação e Física Experimental de Partículas, Coimbra, Portugal*
[3] *Smoluchowski Institute of Physics, Jagiellonian University of Cracow, Kraków, Poland*
[4] *Gesellschaft für Schwerionenforschung mbH, Darmstadt, Germany*
[5] *Institut für Strahlenphysik, Forschungszentrum Dresden-Rossendorf, Dresden, Germany*
[6] *Joint Institute of Nuclear Research, Dubna, Russia*
[7] *Institut für Kernphysik, Johann Wolfgang Goethe-Universität, Frankfurt, Germany*
[8] *II.Physikalisches Institut, Justus Liebig Universität Giessen, Giessen, Germany*
[9] *Istituto Nazionale di Fisica Nucleare, Sezione di Milano, Milano, Italy*
[10] *Institute for Nuclear Research, Russian Academy of Science, Moscow, Russia*
[11] *Physik Department E12, Technische Universität München, München, Germany*
[12] *Department of Physics, University of Cyprus, Nicosia, Cyprus*
[13] *Institut de Physique Nucléaire (UMR 8608), CNRS/IN2P3 - Universit Paris Sud, Orsay Cedex, France*
[14] *Nuclear Physics Institute, Academy of Sciences of Czech Republic, Rez, Czech Republic*
[15] *Departamento de Física de Partículas, University of Santiago de Compostela, Santiago de Compostela, Spain*
[16] *Instituto de Física Corpuscular, Universidad de Valencia-CSIC, Valencia, Spain*

Frascati Physics Series Vol. XLVI (2007), pp. 783–790
HADRON07: XII Int. Conf. on Hadron Spectroscopy – Frascati, October 8-13, 2007
Heavy Ions

RECENT STAR RESULTS ON HEAVY-FLAVOUR CORRELATION MEASUREMENTS USING LEADING ELECTRONS

André Mischke for the STAR Collaboration
Institute for Subatomic Physics, Utrecht University,
Princetonplein 5, 3584 CC Utrecht, the Netherlands.

Abstract

In this contribution first STAR measurement on two heavy-flavor particle correlations in p+p collisions at RHIC is presented. Heavy-flavor (charm and bottom) events are identified and separated on a statistical basis by the azimuthal correlation of their decay electrons and open charm mesons, which provide decisive information about the underlying production process. The azimuthal correlation distribution exhibits a two-peak structure which can be attributed to B decays on the near-side and predominantly charm pair production on the away-side. These assumptions are supported by dedicated simulations using PYTHIA and MC@NLO event generators. This novel correlation technique has the potential for comprehensive energy-loss measurements of heavy quarks in heavy-ion collisions.

1 Introduction

The investigation of heavy-flavor production in heavy-ion collisions provides key tests of parton energy-loss models and, thus, yields important information about the properties of the produced highly-dense QCD medium. Due to their large mass (m >1.2 GeV/c^2), heavy quarks are produced primarily in the early stage of the collision by hard scattering processes (large momentum transfer) and probe the complete space-time evolution of the medium. As recent RHIC measurements have shown [2)], heavy-quark production by initial state gluon fusion also dominates in heavy-ion collisions where many, in part overlapping nucleon-nucleon collisions occur. Heavy-quark production by thermal processes later in the collision is low since the expected energy available for particle production in the medium (≈0.5 GeV) is smaller than the energy needed to produce a heavy-quark pair (>2.4 GeV). Interaction processes of heavy quarks can be calculated in pQCD [3)] and their yields are sensitive to the initial gluon density [4)]. Theoretical models based on perturbative QCD predicted [5, 6)] that heavy quarks should experience smaller energy loss in the medium than light quarks when propagating through the extremely dense medium due to the mass-dependent suppression (called dead-cone effect). Charm and bottom mesons are currently identified by assuming that isolated electrons in the event stem from semi-leptonic decays of heavy-quark mesons. At large transverse momentum (p_{T}), this mechanism of electron production is dominant enough to reliably subtract other sources of electrons (conversions from photons and Dalitz decays). STAR measurements in central Au+Au collisions have shown [1)] that the electron yield from semi-leptonic heavy-quark decays exhibits an unexpectedly large suppression, suggesting substantial energy loss of heavy quarks in the produced medium. Surprisingly, the amount of suppression at high p_{T} is at the same level as observed for light-quark hadrons, which was not expected due to the dead-cone effect. Energy-loss models incorporating contributions from charm and bottom do not describe the observed suppression sufficiently (for a detailed discussion, see [1)]). Although it has been realized that energy loss by parton scattering is probably of comparable importance to energy loss by gluon radiation, the quantitative description of the data is still not satisfying. The remaining discrepancy between data and model calculations could indicate that the B dominance over D mesons starts at a higher p_{T} as expected. To verify this assumption an urgent need arises

to disentangle the D and B contribution to the non-photonic electron distribution experimentally. In this paper, we present a novel analysis technique to identify and separate charm and bottom quark events via leading electron azimuthal correlations with open charm mesons. The specific advantage of this correlation method, in contrast to the conventional heavy-quark measurements, is the possibility to efficiently trigger on heavy-quarks using their decay electrons. The STAR electromagnetic calorimeter provides a unique opportunity to identify electrons on the trigger level and, therefore, to select a sample of events with a large enhancement of heavy-flavor production. Moreover, this correlation method reduces significantly the combinatorial background in the reconstruction of D^0 mesons.

2 Heavy-flavor correlations

Flavor conservation implies that heavy quarks are produced in quark anti-quark pairs. A more detailed understanding of the underlying production process can be obtained from events in which both heavy-quark particles are detected. Due to momentum conservation, these heavy-quark pairs are correlated in relative azimuth ($\Delta\phi$) in the plane perpendicular to the colliding beams, leading to the characteristic back-to-back orientated sprays of particles. This correlation survives the fragmentation process to a large extent in p+p collisions. In this analysis, charm and bottom production events are identified using the characteristic decay topology of their jets. Charm quarks predominantly ($\approx$54%) hadronize directly and bottom quarks via B decays into D^0 mesons. The branching fraction for charm and bottom decays into electrons is $\approx$10%. While triggering on the so-called leading electron (trigger side), the balancing heavy quark, which is identified by the D^0 meson, can be used to identify the underlying production mechanisms (probe side). In addition, a charge-sign requirement on the trigger electron and decay Kaon provides a powerful tool to separate charm and bottom quark events. Fig. 1 illustrates the azimuthal correlation distribution for like- (left panel) and unlike-sign electron$-$Kaon pairs (right panel) obtained from PYTHIA simulations. On the left panel of Fig. 1, the near-side peak is dominated by D^0 mesons from B decays whereas the away-side peak stems mainly from charm pair production. By contrast, the away-side peak for unlike-sign electron$-$Kaon pairs (right panel) originates essentially from B decays only. Thus, the azimuthal correlation in combination with the charge-sign

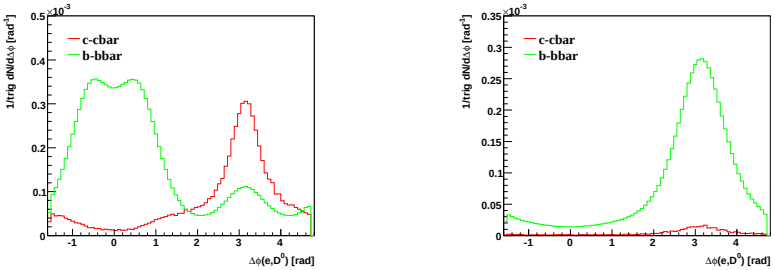

Figure 1: Azimuthal correlation distribution of non-photonic electrons and D^0 mesons for like-sign (left panel) and unlike-sign (right panel) electron−Kaon pairs obtained from PYTHIA simulations. The red (green) histogram depicts the charm (bottom) contribution for trigger electrons with $p_{\rm T} > 3$ GeV/c.

requirement allows the clear separation of charm and bottom quark events.

3 Data analysis

The analysis is based on Run VI p+p data taken at $\sqrt{s_{\rm NN}} = 200$ GeV by the STAR experiment at RHIC. Run VI provided the first dataset where the calorimeter was fully installed and operational. The integrated luminosity was 9 pb^{-1}, of those 1.2 million events were used after a cut on the collision vertex. The tight vertex cut is used to minimize the amount of material within the detector volume causing photon conversions. Particle identification via ionization energy loss and tracking over a large kinematical range with very good momentum resolution is performed by the Time Projection Chamber (TPC) [7] . The TPC has an acceptance of $|\eta| < 1.4$ and full azimuthal coverage. The STAR detector utilizes a barrel-electromagnetic calorimeter (BEMC) [8] as a leading particle (electrons and photons) trigger to study high $p_{\rm T}$ particle production. The calorimeter, situated behind the TPC, covers an acceptance of $|\eta| < 1$ and full azimuth. To enhance the high $p_{\rm T}$ range, a high-tower trigger was used with an energy threshold of 5.4 GeV for the highest energy in a BEMC cell.

The electron identification is performed by combining the information from the TPC and the BEMC (cell energy). Due to the finite momentum resolution of the calorimeter, only particles with $p_{\rm T} > 1.5$ GeV/c can be measured. A shower maximum detector, located at a depth of 5 radiation length inside

the calorimeter modules, measures the profile of an electromagnetic shower and the position of the shower maximum with high resolution $(\Delta\eta, \Delta\phi) = (0.007, 0.007)$. In contrast to hadrons, electrons deposit most of their energy in the BEMC cells. A cut on the shower profile size combined with a requirement on the ratio momentum-to-cell energy, $0 < p/E < 2$, reject a large amount of hadrons. The final electron sample is obtained by applying a momentum dependent cut on the ionization energy loss ($3.5 < dE/dx < 5.0$ keV/cm). The resulting hadron suppression factor is 10^5 at $p_{\rm T} = 2$ GeV/c and 10^2 at $p_{\rm T} = 7$ GeV/c. The electron purity is ≈100% up to $p_{\rm T} = 5$ GeV/c and decreases to 97% at $p_{\rm T} = 7$ GeV/c. Most of the electrons in the final state are originating from other sources than heavy-flavor decays. Photon conversions ($\gamma \rightarrow e^+e^-$) in the detector material between the interaction point and the TPC and neutral pion and η Dalitz decays ($\pi^0, \eta \rightarrow e^+e^-\gamma$) represent the dominant source of the so-called photonic electrons. Contributions from other decays, like ρ, ϕ and Ke3, are small and can be neglected. In this analysis, photonic electrons are identified and rejected based on invariant mass. Here, each electron candidate is combined with tracks which pass loose cuts on the ionization energy loss to preselect electron candidates [1)]. Electrons with an invariant mass of $m < 150$ MeV/c^2 are disregarded. The photonic background finding efficiency is estimated to be ≈70%. The ratio inclusive-to-photonic electrons is 1.35 at $p_{\rm T} = 3$ GeV/c and increases to 1.6 at $p_{\rm T} = 7$ GeV/c. About 6k non-photonic electrons, originating mostly from heavy-flavor decays, are used for the further analysis. The associated D^0 mesons are reconstructed via their hadronic decay channel $D^0 \rightarrow K^-\pi^+$ (B.R. 3.84%) by calculating the invariant mass of all oppositely charged TPC tracks in the same event. Moreover, negative tracks have to fullfil a dE/dx cut of $\pm 3\sigma$ around the Kaon band to enhance the Kaon candidate probability. Due to the high abundance of pions in the collisions, one usually has to handle a large combinatorial background of random pairs [9)]. In this analysis, however, only events with a non-photonic electron trigger are used for the D^0 reconstruction, which suppresses the combinatorial background. Furthermore, the Kaon candidates have to have the same charge sign as the non-photonic electrons (called like-sign electron−Kaon pairs). The resulting invariant mass distribution of Kaon-pion pairs shows a pronounced D^0 peak around the expected value (Fig. 2, left panel). The combinatorial background of random pairs is evaluated by combining all like-sign charged tracks in the

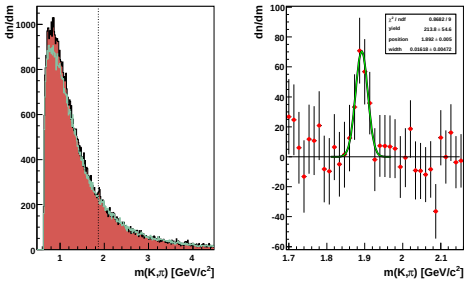

Figure 2: Left panel: Kaon-pion invariant mass distribution (red histogram) requiring a non-photonic electron trigger and the combinatorial background (green histogram). The dotted horizontal line indicates the expected D^0 mass. Right panel: Background subtracted invariant mass distribution. The solid line is a Gaussian fit to the data around the peak region.

same event. The discrepancy of the shape between the invariant mass and the combinatorial background distribution at lower masses can be understood in terms of jet particle correlations, which are not included in the background evaluation yet. It should be noted that the invariant mass distribution without a non-photonic electron trigger does not have a D^0 signal for the applied track quality cuts. Thus, the requirement of a non-photonic electron trigger allows suppressing the combinatorial background significantly (by a factor of $\approx$100 compared to earlier results [9]), yielding a signal-to-background ratio of $\approx$14% and a signal significance of about 4. The right panel of Fig. 2 illustrates the background subtracted invariant mass distribution. The peak position and width are determined using a Gaussian fit to the data. The measured peak position, $m = 1.892 \pm 0.005$ GeV/c^2, is slightly higher than the PDG value of 1.864 GeV/c^2, which can be explained by the finite momentum resolution of the TPC. The width of the signal, $\sigma_m = 16 \pm 5$ MeV/c^2, is found to be similar to earlier results and expectations from Monte-Carlo simulations [9]. Within statistical uncertainties, the D^0 and $\overline{D^0}$ yields are equal.

4 Results and discussion

The azimuthal angular ($\Delta\phi$) correlation is calculated between the transverse momentum of the non-photonic electrons and the associated charged hadron-

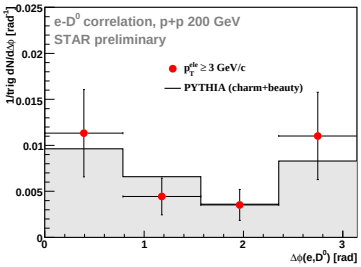

Figure 3: Azimuthal correlation distribution of non-photonic electrons and D^0 mesons (for like-sign electron−Kaon pairs) in p+p collisions at $\sqrt{s_{\rm NN}}$ = 200 GeV. Statistical errors are shown only. The grey histogram illustrates results from PYTHIA simulations, which are scaled by a factor of 2.86 to match the correlation distribution for unlike-sign electron−Kaon pairs.

pairs. The Kaon-pion invariant mass distribution is obtained for different $\Delta\phi$ bins, and the yield of the associated D^0 mesons is extracted as the area underneath a Gaussian fit to the signal. Fig. 3 shows the azimuthal correlation distribution of non-photonic electrons and D^0 mesons, which exhibits a near- and away-side correlation peak with similar yields. Comparisons to dedicated PYTHIA simulations have shown (Fig. 1, left panel) that the observed away-side correlation peak can be attributed to prompt charm pair production (≈70%) and B decays (≈30%). The near-side peak, by contrast, represents essentially contributions from B decays only. It has been shown [10] that higher order sub-processes like gluon splitting may have a significant contribution to the near-side azimuthal correlation. This contribution was estimated using MC@NLO simulation [11], which is a dedicated event generator with a realistic parton shower model. First results have demonstrated that the contribution from gluon splitting is small in the studied $p_{\rm T}$ range.

5 Summary and outlook

We present first two heavy-flavor particle correlation measurement at RHIC via non-photonic electron azimuthal correlations with open charm mesons in p+p collisions at $\sqrt{s_{\rm NN}}$ = 200 GeV, which allows the separation of charm and bottom production events. This correlation technique in combination with

the STAR inner tracker system will allow detailed energy-loss measurement of heavy quarks in heavy-ion collisions in the future.

6 Acknowledgements

We are grateful to Stefano Frixione (CERN) for providing the MC@NLO code and for very fruitfull discussions. This work is supported by a grant from the Netherlands Organization for Scientific Research (NWO).

References

1. B.I. Abelev *et al.*, Phys. Rev. Lett. **98**, 192301 (2007).
2. Y. Zhang *et al.*, J. Phys. **G32**, S529 (2006).
3. S. Frixione, M.L. Mangano, P. Nason, and G. Ridolfi, Adv. Ser. Direct. High Energy Phys. **15**, 609 (1998).
4. Z. Lin and M. Gyulassy, Phys. Rev. **C51**, 2177 (1995).
5. Y.L. Dokshitzer and D.E. Kharzeev, Phys. Lett. **B519**, 199 (2001).
6. M. Djordjevic, M. Gyulassy, and S. Wicks, Phys. Rev. Lett. **94**, 112301 (2005).
7. M. Anderson *et al.*, Nucl. Instr. Meth. **A499**, 659 (2003).
8. M. Beddo *et al.*, Nucl. Instr. Meth. **A499**, 725 (2003).
9. J. Adams *et al.*, Phys. Rev. Lett. **94**, 062301 (2005).
10. R.D. Field, Phys. Rev. **D65**, 094006; E. Norrbin and T. Sjöstrand, Eur. Phys. J. **C17**, 137 (2000).
11. S. Frixione and B.R. Webber, J. High Energy Phys. **0206**, 029 (2002); S. Frixione, P. Nason and B.R. Webber, J. High Energy Phys. **0308**, 007 (2003). The results are obtained from a private version of the MC@NLO code adapted to calculate charm production.

Frascati Physics Series Vol. XLVI (2007), pp. 791–798
HADRON07: XII Int. Conf. on Hadron Spectroscopy – Frascati, October 8-13, 2007
Heavy Ions

TOTAL CROSS-SECTION AND RAPIDITY GAP SURVIVAL PROBABILITY AT LHC

Andrea Achilli
INFN and Physics Department University of Perugia, I-06123 Perugia, Italy
Agnes Grau
Departamento de Fisica Teórica y del Cosmos Universidad de Granada, 18071 Granada, Spain
Giulia Pancheri
INFN Frascati National Laboratories, I-00044 Frascati, Italy
Yogendra N. Srivastava
INFN and Physics Department University of Perugia, I-06123 Perugia, Italy

Abstract

We present a model for the total cross-section which incorporates, (i) hard and soft gluon effects, (ii) satisfies the limits imposed by the Froissart bound and (iii) can be used to study other minimum bias effects such as the Survival Probability of Large Rapidity Gaps (SPLRG).

1 Introduction

In recent papers [1, 2] we have discussed how infra-red soft gluon emission, in conjunction with hard, perturbative QCD scatterings, allows us to give a quantitative description of the total hadronic cross section in the high energy limit. In particular, we obtain predictions for σ_{tot} as well as SPLRG's to be measured soon at the LHC. In our model, constraints imposed by the Froissart bound play a fundamental role.

2 Minijet cross-section

The original minijet model used perturbative QCD to obtain an expression for the total hadronic cross-section in terms of parton-parton hard scattering processes through the expression:

$$\sigma_{\rm jet}^{AB}(s, p_{tmin}) = \int_{p_{tmin}}^{\sqrt{s/2}} dp_t \int_{4p_t^2/s}^{1} dx_1 \int_{4p_t^2/(x_1 s)}^{1} dx_2 \sum_{i,j,k,l} f_{i|A}(x_1, p_t^2) f_{j|B}(x_2, p_t^2) \frac{d\hat{\sigma}_{ij}^{kl}(\hat{s})}{dp_t}. \tag{1}$$

This expression depends on the minimum transverse momentum allowed to the scattered partons with $p_{tmin} \approx (1-2)\ GeV$. We evaluated the minijet expression using various DGLAP evoluted, LO parametrizations available for the Partonic Density Functions $f_{i|A}$ [3] (PDFs), obtaining a cross-section which, however, rises too fast at high energies. We observed that values of the cross-section obtained from the minijet model at energies between 10 and 35 TeV could be parametrized with a power-law expression of the type:

$$\sigma = \sigma_1 \cdot (s/s_0)^{\epsilon} \tag{2}$$

with $s_0 = 1\ GeV^2$. The results of the fits obtained using different PDFs are presented in Table 1 and in Figure 1.

	σ_1 (mb)	ϵ
CTEQ	9 ± 1	0.30 ± 0.01
GRV	1.7 ± 0.7	0.41 ± 0.02
GRV98	1.8 ± 0.4	0.40 ± 0.01
MRST72	6.9 ± 0.9	0.31 ± 0.01
MRST73	7.3 ± 0.9	0.30 ± 0.01
MRST74	7.6 ± 0.9	0.31 ± 0.01
MRST75	7 ± 2	0.30 ± 0.01
MRST76	7.6 ± 0.6	0.32 ± 0.01

Table 1: parameters of the fits obtained with the function (2) on the values of the cross-section generated with the minijet model. For every fit, we have used points at 10, 15, 20 and 35 TeV assuming arbitrary errors on these point of 4%.

Were these mini-jet cross-sections used as such in a total cross-section calculation, they would show a violation of the Froissart bound ($\sigma_{tot} < C \log^2(s/s_0)$

as $s \to \infty$). The rise of the total cross section cannot be described considering only hard processes, it is necessary to invoke a formalism which ensures the satisfaction of unitarity. The proposed strategy is to embed these mini-jet cross-sections in an eikonal representation and obtain a more realistic behavior of the total cross-section through a saturation effect introduced by the impact parameter representation. In our model, we obtain this saturation through a non perturbative treatment of the soft processes which influence the high energy behaviour of σ_{tot}.

3 Model for total cross-section

In order to ameliorate our predictions for total cross-sections at high energy, soft processes have to be taken in account. Our model uses an eikonal formalism which implies multiple scattering and requires impact parameter distributions inside scattering particles. In the high energy limit, where (assuming, as is usual that) the real part of the eikonal goes to zero, the total cross-section is given by

$$\sigma_{tot} = 2 \int d^2\mathbf{b}[1 - e^{-n(b,s)/2}], \tag{3}$$

where $n(b,s) = n_{soft}(b,s) + n_{hard}(b,s)$ is the average number of partonic collisions which take place during the scattering, where the hard term in $n(b,s)$ is responsible for the growth of σ_{tot} at high energies. In it, there are contributions from all the partonic processes with $p_t > p_{tmin}$. Through $n_{soft}(b,s)$, it is possible to reproduce the right normalization at low energies [1, 2, 4, 5]. For $n_{soft/hard}(b,s)$ the function used is

$$n_{soft/hard}(b,s) = A_{BN}^{soft/hard}(b,s)\sigma_{soft/hard}(s) \tag{4}$$

where $\sigma_{hard} = \sigma_{jet}$ gives the rise of the total cross-section while $\sigma_{soft} = \sigma_0(1 + 2\epsilon/\sqrt{(}s))$ is a phenomenological expression with parameters $\sigma_0 = constant$ and $\epsilon = 0,1$ respectively for pp and $p\bar{p}$ processes. A_{BN} is an overlap function calculated considering contributions from the soft gluon emissions of the colliding partons. These emissions introduce an acollinearity between the particles and subtract energy for minijet production. The number of soft emissions increases with energy and tames the rise of the total cross section. The expression ob-

tained for A_{BN} is [6, 7, 8]

$$A_{BN}(b,s) = N \int d^2\mathbf{K}_\perp \; e^{-i\mathbf{K}_\perp \cdot \mathbf{b}} \frac{d^2P(\mathbf{K}_\perp)}{d^2\mathbf{K}_\perp} = \frac{e^{-h(b,q_{max})}}{\int d^2\mathbf{b} \; e^{-h(b,q_{max})}} \tag{5}$$

with N a normalization constant and

$$h(b,q_{max}) = (\frac{16}{3}) \int_0^{q_{max}} (\frac{\alpha_s(k_t^2)}{\pi})(\frac{dk_t}{k_t}) \log(\frac{2q_{\max}}{k_t})[1 - J_0(k_t b)] \tag{6}$$

In the last expression, the integration includes zero momentum values. In this infrared limit, the usual QCD-perturbative expression for α_s is not valid. We choose to use a phenomenological expression singular but integrable in the infrared limit:

$$\alpha_s(k_t^2) = (\frac{12\pi}{33 - 2N_f})\big(\frac{p}{\ln[1 + p(\frac{k_t}{\Lambda})^{2p}]}\big) \tag{7}$$

with $p < 1$ to have an integrable function in (6). More over, $p \geq 1/2$ will be shown in the fifth section.

4 Kinematical constraints on single gluon emission

The parameter q_{max} which appears in (6) is the maximum allowed transverse momentum of the gluon emitted from one of the colliding partons [9]. Kinematical considerations show that for a reaction of the kind:

$$q(p_1) + q(p_2) \rightarrow g(q) + jets(Q)$$

(where $q_{1,2}$, q and Q are the 4-momenta of the colliding partons of the gluon and of the family of jets respectively) the value of the maximum gluon transverse momentum is limited by kinematics to be a function of Q^2, the square of the c.m. jet energy and of $(p_1 + p_2)^2 = \hat{s}$:

$$q_{max} = \frac{\sqrt{\hat{s}}}{2}\left(1 - \frac{Q^2}{\hat{s}}\right) \tag{8}$$

So q_{max} should be calculated for every partonic subprocess with a given Q^2 and $\hat{s} = x_1 x_2 s$. In our model, we make a simplifying assumption, i.e. we consider a value of q_{max} averaged over all the subprocesses which could occur during an hadronic collision with energy $\sqrt{s}$ [5]:

$$q_{\max}(s) = \sqrt{\frac{s}{2}} \frac{\sum\limits_{i,j} \int \frac{dx_1}{x_1} \int \frac{dx_2}{x_2} \int_{z_{min}}^1 dz f_i(x_1) f_j(x_2) \sqrt{x_1 x_2}(1-z)}{\sum\limits_{i,j} \int \frac{dx_1}{x_1} \int \frac{dx_2}{x_2} \int_{z_{min}}^1 dz f_i(x_1) f_j(x_2)} \tag{9}$$

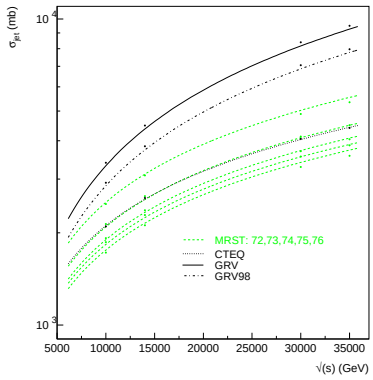

Figure 1: Fits obtained with the function (2) for the minijets cross-sections using various PDF parametrizations with $p_{tmin} = 1.15\ GeV$.

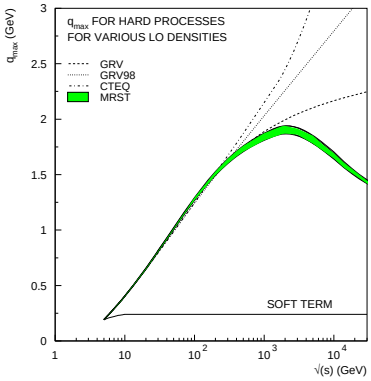

Figure 2: q_{max} values calculated from expression (9) using different PDF parametrization with $p_{tmin} = 1.15 GeV$.

with $z_{min} = 4p_{tmin}^2/(sx_1x_2)$. The partonic densities used here are the same used in (1). This averaged expression is a function of the energy of the hadronic process $\sqrt{s}$ and it also depends on p_{tmin} and on the parametrization used for the PDF. Expression (9) has been used only in the hard term of the model while for the soft part, we choose a set of phenomenological values, as shown in Figure 2, where q_{max} has been plotted as a function of the c.m. scattering energy $\sqrt{s}$ for different PDF's.

5 Restoration of the Froissart bound

In the extremely high energy limit, the expression (3) for total cross-section becomes

$$\sigma_T(s) \approx 2\pi \int_0^\infty db^2 [1 - e^{-n_{hard}(b,s)/2}]. \tag{10}$$

In this limit, we know from (2) that the rise of σ_{jet} is a power-law in s. To see the overall behaviour of n_{hard}, we turn to A_{hard} and take the limit, $k_t \to 0$ in (6). Since $d^3n(k) \propto \alpha_s(k_t^2)$, the infrared limit of α_s becomes crucial, and,

using (7), $\alpha_s(k_t) \approx (\frac{\Lambda}{k_t})^{2p}$. We see that, $h(b,s) \propto (b\bar{\Lambda})^{2p}$ and thus:

$$A_{hard}(b) \propto e^{-(b\bar{\Lambda})^{2p}} \tag{11}$$

and

$$n_{hard} \propto \left(\frac{s}{s_0}\right)^{\epsilon} e^{-(b\bar{\Lambda})^{2p}} \tag{12}$$

from which, the total cross-section in the high energy limit is given by

$$\sigma_T \rightarrow [\varepsilon \ln\left(\frac{s}{s_0}\right)]^{(1/p)} \tag{13}$$

The Froissart bound is thus restored for $p \geq 1/2$. With an appropriate choice of the parameter of the model we obtain a prediction [1)] of possible values for the total cross-section at LHC, shown in Figure 3, comparable with other phenomenological models developed in the past.

6 LRG Survival Probability

Our model has also been employed to calculate SPLRG [2)]. Using the probability of not having an inelastic collision

$$P_{no-inelastic} = |S|^2 = e^{-n(b,s)} \tag{14}$$

and considering only the soft part (to exclude hard interactions) of the overlap function $A(\mathbf{b}, q_{\max}^{soft})$ with $\int d^2\mathbf{b}\ A(\mathbf{b}, q_{\max}^{soft}) = 1$, the survival probability is given by:

$$< |S|^2 >= \int (d^2\mathbf{b})\ A(\mathbf{b}, q_{\max}^{soft})\ |S(b)|^2. \tag{15}$$

Our results are shown in Figure 4 and compared with those obtained from other models. It is gratifying to note that there is a reasonable consensus between various theoretical models lending firm support for the use of SPLRG in the arduous search of the Higgs boson.

References

1. R. M. Godbole, A. Grau, G. Pancheri and Y. N. Srivastava, Phys. Rev. D **72** (2005) 076001 [arXiv:hep-ph/0408355].

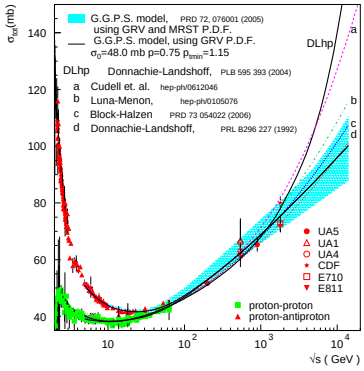

Figure 3: Models for total cross-section [11] compared with data [10] for different input parton densities and different models from [2].

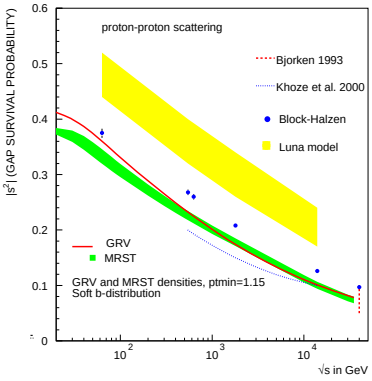

Figure 4: Models for survival probability of Large Rapidity Gaps [12] for different input parton densities and different models from [2].

2. A. Achilli, R. Hegde, R. M. Godbole, A. Grau, G. Pancheri and Y. Srivastava, Phys. Lett. B **659** (2008) 137-143 arXiv:0708.3626 [hep-ph]

3. M. Gluck, E. Reya, and A. Vogt, Z. Phys. **C53** (1992) 127–134; Z. Phys. **C67** (1995) 433–448; Eur. Phys. J. **C 5** (1998) 461–470; A. D. Martin, R. G. Roberts, W. J. Stirling, and R. S. Thorne, Phys. Lett. **B531** (2002) 216–224; H.L. Lai , J. Botts , J. Huston , J.G. Morfin , J.F. Owens , Jian-wei Qiu, W.K. Tung, H. Weerts, Phys.Rev. **D51** 4763-4782,1995.

4. A. Corsetti, G. Pancheri, Y. N. Srivastava and A. Grau, Phys. Lett. **382B** (1996) 282-288 [arXiv:hep-ph/9605314]

5. A. Grau, G. Pancheri and Y. N. Srivastava, Phys. Rev. D **60** (1999) 114020 [arXiv:hep-ph/9905228].

6. G. Pancheri-Srivastava and Y.N. Srivastava, Phys.Rev. **D15** (1977) 2915.

7. Y. L. Dokshitzer, D. I. D'Yakonov and S. I. Troyan, Phys. Lett. **79B** (1978) 269.

8. G. Parisi and R. Petronzio, Nucl. Phys. B **154** (1979) 427.

9. P. Chiappetta and M. Greco, Nucl. Phys. B **221** (1983) 269.

10. For total cross section data see:
W.-M. Yao *et al.* **PDG**, J. Phys. G. **33** (2006) 1; G. Arnison *et al.*, **UA1** Collaboration, Phys. Lett. **128B** (1983) 336; R. Battiston *et al.* **UA4** Collaboration, Phys. Lett. **B117** (1982) 126; C. Augier *et al.* **UA4/2** Collaboration, Phys. Lett. **B344** (1995) 451; M. Bozzo *et al.* **UA4** Collaboration, Phys. Lett. **147B** (1984) 392; G.J. Alner *et al.* **UA5** Collaboration, Z. Phys. **C32** (1986) 153; N. Amos *et. al.*, **E710** Collaboration, Phys. Rev. Lett. **68** (1992) 2433–2436; C. Avila *et. al.*, **E811** Collaboration, Phys. Lett. **B445** (1999) 419–422; F. Abe *et. al.*, **CDF** Collaboration, Phys. Rev. **D50** (1994) 5550–5561.

11. For total cross section models see:
M. M. Block and F. Halzen, Phys. Rev. D **73** (2006) 054022 [arXiv:hep-ph/0510238]; E. G. S. Luna and M. J. Menon, arXiv:hep-ph/0105076; J. R. Cudell and O. V. Selyugin, arXiv:hep-ph/0612046; A. Donnachie and P. V. Landshoff, Phys. Lett. B **296** (1992) 227 [arXiv:hep-ph/9209205]; A. Donnachie and P. V. Landshoff, Phys. Lett. B **595** (2004) 393 [arXiv:hep-ph/0402081]

12. For survival probability models see:
V. A. Khoze, A. D. Martin and M. G. Ryskin, Eur. Phys. J. C **14**, 525 (2000); M. M. Block and F. Halzen, Phys. Rev. D **63**, 114004 (2001); E. G. S. Luna, Phys. Lett. B **641**, 171 (2006); J. D. Bjorken, Phys. Rev. D **47** (1993) 101.

Frascati Physics Series Vol. XLVI (2007), pp. 799
HADRON07: XII Int. Conf. on Hadron Spectroscopy – Frascati, October 8-13, 2007
Heavy Ions

RESONANCE PHENOMENA IN HEAVY NUCLEI COLLISIONS AND STRUCTURIZATION OF THE POSITRON SPECTRUM

A. Glushkov
Odessa University, Head of Dept.

Written contribution not received

QUARKONIA STATES

Frascati Physics Series Vol. XLVI (2007), pp. 803–811
HADRON07: XII Int. Conf. on Hadron Spectroscopy – Frascati, October 8-13, 2007
Quarkonia States

HEAVY QUARKONIA IN LIGHT-FRONT QCD

Stanisław D. Głazek
Institute of Theoretical Physics, University of Warsaw, Poland

Abstract

This talk is based on results obtained for masses and wave functions of heavy quarkonia in a light-front Hamiltonian formulation of QCD with just one flavor of quarks using an ansatz for the mass-gap for gluons. Since the calculated spectra compare reasonably well with data, some further steps one can make are discussed.

1 Introduction

Discussion of heavy quarkonium dynamics in this talk is based on results for masses and wave functions obtained in Refs. [1, 2] in a relativistic (boost-invariant) Hamiltonian formulation of QCD. Steps involved in the calculation, starting with the Lagrangian for QCD, deriving the corresponding canonical

light-front (LF) Hamiltonian, carrying out the renormalization group procedure for effective particles (RGPEP) to obtain the quark and gluon operators at finite momentum scales, λ, deriving an effective Hamiltonian for heavy constituent quarks and gluons, H_λ, at momentum scales on the order of the quark mass, $\lambda_0 \sim m$, using an ansatz for the mass-gap for gluons, μ, to finesse a new Hamiltonian that acts only in the effective quark-antiquark Fock sector, $H_{\lambda_0 Q\bar{Q}}$, and solving numerically the resulting eigenvalue problem for $H_{\lambda_0 Q\bar{Q}}$, are described in the original literature (a condensed summary [3] is available).

Here, only one example of results for quarkonium masses obtained from $H_{\lambda_0 Q\bar{Q}}$ is quoted, to illustrate what happens in the simplest version of the LF approach to QCD. The key point is that the results do not depend on the ansatz μ and fit data reasonably well for the coupling constant expected from RGPEP, assuming it has a known value at $\lambda = M_Z$, and for the charm or bottom quark masses that have typically considered sizes. Then, the emerging recipe for the mass gap ansatz as a tool to facilitate numerical studies of effective quark and gluon dynamics is described. The ansatz is designed to be introduced only in the final stage of diagonalizing $H_{\lambda_0 Q\bar{Q}}$.

LF quantum field theory has a long history [4] with lots of modern developments [5] that cannot be duly reviewed here. As part of the progress, a conceptual outline of nonperturbative QCD in the LF frame was achieved [6] using the similarity renormalization group procedure [7, 8]. A confining logarithmic potential of order α in quark-antiquark sector has been discovered [9] and studied in heavy quarkonia [10, 11] and other systems [12, 13], but not using RGPEP [14]. Besides the work that led to Refs. [1, 2], distinct RGPEP applications in scattering theory [15] and gluonium [16] are relatively new. But there is a lot of work to do in LF QCD before it can be widely accepted as a viable alternative to lattice QCD [17]. The AdS/CFT method [18, 19] has not been connected with RGPEP in QCD yet.

2 Bottomonium masses as example

In the crudest version, H_λ is calculated using RGPEP to first order in α_{λ_0} in one flavor QCD, and $H_{\lambda_0 Q\bar{Q}}$ is then evaluated to the same order, using the ansatz μ for gluons in the effective quark-antiquark-gluon sector (see next section). The resulting eigenvalue problem does not depend on the ansatz μ and takes a form that satisfies requirements of rotational symmetry despite

that the LF reference frame distinguishes z-axis. For example, the eigenstates with quantum numbers of Υ are described by a 2×2 matrix wave function $\phi(\vec{k}\,) = \vec{b}(\vec{k}\,)\vec{\sigma}$, where ($\vec{s}$ is the polarization three-vector that determines the polarization state of the whole quarkonium in motion with arbitrary velocity)

$$b^m(\vec{k}\,) = \left[\delta^{mn}\,\frac{S(k)}{k} + \frac{1}{\sqrt{2}}\,\left(\delta^{mn} - 3\frac{k^m k^n}{k^2}\right)\,\frac{D(k)}{k}\right]\,s^n\,. \tag{1}$$

The matrix ϕ enters into the definition of a relativistic quantum state of a quarkonium with definite momentum and mass M,

$$|M, P^+, P^\perp, \vec{s}\rangle \;\;=\;\; \int [ij]\,(2\pi)^3 P^+ \delta^3(P - p_i - p_j)\,\chi_i^\dagger\,\phi(\vec{k}_{ij})\chi_j\,b^\dagger_{\lambda_0 i} d^\dagger_{\lambda_0 j}\,|0\rangle\,, \tag{2}$$

where i and j denote flavor, momentum, and spin quantum numbers (colors are combined to 0) of scale-dependent effective quarks that are created by operators $b^\dagger_{\lambda_0 i}$ and $d^\dagger_{\lambda_0 j}$ from the LF QCD vacuum. These LF operators depend on the scale λ (in ratio to Λ_{QCD} in the RGPEP scheme, and the quark mass). The relative momentum three-vector $\vec{k}_{ij}$ is defined using LF kinetic momentum variables and the quark mass corresponding to the scale λ_0. The eigenvalue equation satisfied by the S and D wave functions is written in terms of dimensionless momentum variables

$$\vec{p} = \vec{k}_{ij}/k_B\,, \tag{3}$$

where k_B denotes the strong Bohr momentum, $\alpha_{\lambda_0} m_{\lambda_0}/2$ (subscript λ_0 will be dropped from now on). Using $p = |\vec{p}\,|$, the radial equation can be written as

$$\left[\begin{array}{cc} h_{osc} & 0 \\ 0 & h_{osc} + k_p \frac{6}{p^2} \end{array}\right]\,\left[\begin{array}{c} S(p) \\ D(p) \end{array}\right] = \int_0^\infty dk\, f \frac{2pk}{\pi}\,\left[\begin{array}{cc} \mathcal{W}_{ss} & \mathcal{W}_{sd} \\ \mathcal{W}_{ds} & \mathcal{W}_{dd} \end{array}\right]\,\left[\begin{array}{c} S(k) \\ D(k) \end{array}\right] \tag{4}$$

with

$$h_{osc} \;\;=\;\; p^2 - k_p \partial_p^2 - x\,, \tag{5}$$

$$k_p \;\;=\;\; \frac{9}{128\,\sqrt{2\pi}}\,\left(\frac{\lambda_0^2}{\alpha\, m^2}\right)^3\,, \tag{6}$$

while the quarkonium mass eigenvalue is given by the eigenvalue x through

$$M = 2m\,\sqrt{1 + x\,\left(\frac{2}{3}\alpha\right)^2}\,. \tag{7}$$

Note that the eigenvalue is not energy in any specific frame of reference but the mass itself. The functions $\mathcal{W}_{ss}$, $\mathcal{W}_{sd}$, $\mathcal{W}_{ds}$, $\mathcal{W}_{dd}$ are given in the literature [2].

There is no quantitative trace of the gluon mass ansatz in this result. But there is a qualitatively new element in the form of a harmonic oscillator correction to the strong Coulomb potential (with LF Breit-Fermi terms).

Another qualitatively new element, a result of using RGPEP, is the form factor

$$f \;=\; \exp\left\{-\left[\frac{\mathcal{M}^2(p)-\mathcal{M}^2(k)}{\lambda_0^2}\right]^2\right\}, \tag{8}$$

where $\mathcal{M}$ denotes an invariant mass of a pair of free quarks. The form factor tempers the spin-dependent gluon exchange interaction. In particular, it regulates otherwise ultraviolet-divergent three-dimensional delta functions (in the position space formally associated with the momentum space of $\vec{k}$ via the Fourier transform), which are present in the functions $\mathcal{W}$ due to the relativistic spin effects.

One solves the eigenvalue equations for $b\bar{b}$ bound states, such as eq.4, assuming that α is given by the RGPEP evolution from the known value at $\lambda = M_Z$ down to λ_0. If $\alpha_{M_Z} = 0.12$, the lowest order RGPEP evolution of α_λ in QCD with only one flavor [20] produces $\alpha \sim 0.326$ at $\lambda_0 \sim 3.7$ GeV (about 30% smaller value is generated for 6 or 5 flavors). Less is known about the RGPEP evolution and value of the b-quark mass, m_b. Tab.1 shows masses of $b\bar{b}$ quarkonia obtained [2] when α and m_b are adjusted to reproduce masses of $\chi_1(1\mathrm{P})$ and $\chi_1(2\mathrm{P})$ at $\lambda_0 = 3697.67$ MeV.

If the RGPEP calculation of H_λ and subsequent reduction to $H_{\lambda Q\bar{Q}}$ were exact, there should be no dependence of the spectrum on λ. Once α and m_b are adjusted to observables at one scale, they evolve in some exact way, including the formation of bound states. But in this crudely simplified version of LF QCD, the RGPEP procedure is limited to order α and $H_{\lambda Q\bar{Q}}$ is finessed using an ansatz for the gluon mass gap μ. Therefore, one cannot change λ considerably using equations limited to order α and there is only a hope that in some small range of values of λ_0 the equations have a chance to work once the coupling constant and quark mass are given their right relativistic values [6, 22].

There is a characteristic pattern visible in the fourth column in tab.1: the greater the difference between a mass eigenvalue and the masses of quarkonia in the middle of the table, used to choose α and m_b, the greater the discrepancy

Table 1: Example of calculated masses (MeV) for $b\bar{b}$ states. The corresponding coupling constant and quark mass are $\alpha = 0.32595$ and $m_b = 4856.92$ MeV.

meson	theory	experiment [21]	difference
Υ10860	10725	10865 $\pm$8	-140
Υ10580	10464	10579.4 $\pm$1.2	-116
Υ3S	10382	10355.2 $\pm$0.5	27
$\chi_2$2P	10276	10268.65 $\pm$0.22$\pm$0.50	7
$\chi_1$2P	10256	10255.46 $\pm$0.22$\pm$0.50	0
$\chi_0$2P	10226	10232.5 $\pm$0.4 $\pm$0.5	-6
Υ2S	10012	10023.26 $\pm$0.31	-11
$\chi_2$1P	9912	9912.21 $\pm$0.26$\pm$0.31	-1
$\chi_1$1P	9893	9892.78 $\pm$0.26$\pm$0.31	0
$\chi_0$1P	9865	9859.44 $\pm$0.42$\pm$0.31	5
Υ1S	9551	9460.30 $\pm$0.26	91
η_b1S	9510	9300 $\pm$20 $\pm$20	210

between the crudely approximated theory and experiment. This should be expected. The most strongly bound states are sensitive to deviations of the effective potential from the Coulomb shape. For example, interactions order g^4 (or α^2), introduce δ-functions that are absent here because of the limitation to terms order g^2 in the RGPEP and two-quark reduction. Analogous 4th order δs and other singular corrections are known in QED. Here such terms should have much larger effect because the coupling constant is about 30 times larger then in QED (they have to be treated nonperturbatively). The least strongly bound states, those with largest masses, should not be described well without proper inclusion of gluons. The mass ansatz should fail to render interactions that are associated with gluons producing a linear potential at distances much larger than the strong Bohr radius.

3 Mass ansatz as a computational tool in QCD

The mass ansatz for virtual effective particles in Fock components that contain more such particles than just two in mesons, or three in baryons, deserves a comment for several reasons. One reason is that the ansatz may help improve the calculations for heavy quarkonia. Another reason is that it may lead to a possibility of calculating properties of baryons built from heavy quarks. The

third reason is that it may help in crossing the barrier that separates all small-coupling expansions in QCD from entering the region of quark masses much smaller than Λ_{QCD}.

The first two reasons concern the difficulty that precise numerical solutions of eigenvalue problems with coupled two-, three-, and more-particle sectors are hard to obtain. In this respect, the mass ansatz appears a candidate to mimic what happens in an infinite tower of the Fock components built from effective particles. Since the RGPEP form factors limit momentum transfers by λ, the spread of probability to sectors with many effective particles corresponding to the scale λ is tamed. But these sectors do influence the dynamics of the dominant sectors and some ansatz appears inevitable. The question is how to make it self-consistently. The basic idea is to drop all sectors above the highest included (in the sense of number of the effective particles), put in instead a mass ansatz in the highest Fock component, and see what happens in the dynamics of lower components. The next step is to increase the maximal number of effective particles by one and see if the same type of ansatz is producing the same answers. A small coupling expansion may constrain the options sufficiently for finding good candidates for suitable mass terms in the highest components.

The third reason that concerns light quarks is most speculative. It involves chiral symmetry, or rather the mechanism of its breaking. In LF Hamiltonian of QCD with small λ, there may exist finite terms that violate chiral symmetry and do not vanish in the limit of quark mass approaching zero [6]. At the same time, the LF vacuum state remains simple due to cutoffs imposed on the particle momentum components along the front. The question is how to find those terms in practice. LF power counting limits the structure of allowed terms but so far insufficiently for anybody to tackle the issue, even though the stakes are high.

From this point of view, the following observation is of interest. Consider a colorless state built from two effective gluons. They attract each other. Consider then that one of these gluons turns into a pair of quarks. These quarks are in an octet state and instead of attracting they repel each other. In perturbation theory, if the number of quark flavors is not too high, this is not dangerous and gluonic interactions sustain asymptotic freedom, generating infrared slavery. However, beyond perturbation theory, a pointlike creation of

a pair of quarks that repel each other by violent potentials may lead to an explosive behavior. Such behavior is entirely absent in QED because electrons attract anti-electrons and this effect slows down the growth of a pair, instead of accelerating it.

To be more specific, consider eq.4, in which the s-wave potential $\mathcal{W}_{ss}$ contains a term [2] that would be a δ-function if the form factor f did not smooth it out. This term is attractive in Υ. It is repulsive instead in the color octet states. When λ is comparable to the heavy quark mass, which means that α is small, the smallness of the coupling constant and form factor width produce an interaction that cannot compete significantly with the size of the quark mass. This is visible in tab.1. However, if the quarks are light, it is entirely unclear what will happen.

The situation is different than in the case of analogy between a gluonium and a helium atom with one doubly charged electron discussed in Ref. [22]. Here, two particles with the same charge are suddenly put on top of each other and large potential energy is created.

In the case of light quarks, the large terms are smoothed out by the RGPEP form factors f but their strength may be comparable with Λ_{QCD}. The central point is that in order to find out what happens due the explosive nature of color dynamics of effective particles beyond perturbation theory, one has to separate some sectors from a presumably decreasing but in principle infinite chain of them. This is what the mass ansatz facilitates. Thus, it opens a way to investigate interactions in the effective Hamiltonians that may be calculated perturbatively in RGPEP and then diagonalized nonperturbatively using computers. This way one can find out if the effective interactions may in principle be responsible for emergence of the constituent quark masses for quarks u, d, and s.

4 Conclusion

Tab.1 shows that the chance that LF Hamiltonian approach to QCD may apply in phenomenology of heavy quarkonia is not hopelessly small. Since the coupling constant one needs is order 1/3, and one may need even a smaller coupling constant when 4th order RGPEP is used, the approach stands ready for a more extended scrutiny. The reason it deserves to be checked is that it appears now to indicate a possibility that a single formulation of the entire

theory with quark masses much greater than Λ_{QCD} is conceivable with no need to combine different formulations for including information concerning different scales.

The harmonic potential finessed in the quark-antiquark sector using an ansatz for the gluon mass gap, leads to the eigenvalues M^2 that are proportional to the angular momentum of relative motion of quarks, like in the Regge trajectories. It is found that the oscillator frequencies are on the order of one inverse fermi, and the oscillator potential grows as the relative distance squared in fermis with a coefficient given by the quark mass. So, presumably, for states with masses greater than order 1 GeV above the ground states, the probability of emission of effective gluons increases and then formation of strings of gluons is favored if the gluons also have some oscillator force acting among them. For quantum gluons to form a string, each pair of the neighboring gluons must be held together stronger than by a linear potential. If it is capable of generating such effects, the LF Hamiltonian approach could thus lead to a quantum theory of the gluon string in QCD without ever introducing a nontrivial vacuum.

But the concept of mass ansatz in Fock sectors with one more effective particle than the maximal number treated nonperturbatively, is probably most interesting as a tool for finding out what happens when one attempts to solve eigenvalue equations for Hamiltonians that are evaluated using perturbative RGPEP in the case of canonical QCD with quark masses smaller than Λ_{QCD}. The idea discussed here is that effective particles in non-singlet color configurations may experience explosive potentials in the form of smoothed δ-functions that may cause effects order Λ_{QCD} per constituent. The ansatz for quark and gluon masses inserted in the highest sectors thus opens a possibility to generate concrete forms of such terms and to study them nonperturbatively. Nothing is known yet about what may come out from such studies.

5 Acknowledgements

I would like to thank Robert Perry for comments on the manuscript and acknowledge the outstanding hospitality of the organizers.

References

1. S. D. Głazek, Phys. Rev. D **69**, 065002 (2004).

2. S. D. Głazek, J. Młynik, Phys. Rev. D **74**, 105015 (2006).

3. S. D. Głazek, in: Continuous Advances in QCD 2006 (ed. M. Peloso and M. Shifman, Minneapolis, May 2006), 496 (World Scientific, 2007).

4. S. J. Brodsky et al., Phys. Rept. **301**, 299 (1998).

5. http://www.slac.stanford.edu/xorg/ilcac .

6. K. G. Wilson et al., Phys. Rev. D **49**, 6720 (1994).

7. S. D. Głazek, K. G. Wilson, Phys. Rev. D **48**, 5863 (1993).

8. S. D. Głazek, K. G. Wilson, Phys. Rev. D **49**, 4214 (1994).

9. R. J. Perry, in: Hadron Physics 94 (ed. V. E. Herscovitz et al., Gramado, April 1994), 120 (World Scientific, 1995); hep-th/9407056v2.

10. M. Brisudova, R. Perry, Phys. Rev. D **54**, 1831 (1996).

11. M. M. Brisudova et al., Phys. Rev. Lett. **78**, 1227 (1997).

12. B. H. Allen, R. J. Perry, Phys. Rev. D **62**, 025005 (2000).

13. R. D. Kylin, Ph.D. Thesis, The Ohio State University, 2001.

14. M. M. Brisudova, Mod. Phys. Lett. A **17**, 59 (2002).

15. M. Więckowski, hep-th/0511148.

16. T. Masłowski, PhD Thesis, University of Warsaw, 2005.

17. K. G. Wilson, Nucl. Phys. (Proc. Suppl.) **140**, 3 (2005).

18. S. J. Brodsky, G. F. de Teramond, Phys. Rev. Lett. **96**, 201601 (2006).

19. S. J. Brodsky et al., Phys. Rev. D **75**, 014003 (2007).

20. S. D. Głazek, Phys. Rev. D **63**, 116006 (2001).

21. Particle Data Group website, pdg.lbl.gov/2007/tables/mxxx.pdf

22. S. D. Głazek, K. G. Wilson, Phys. Rev. D **57**, 3558 (1998).

Frascati Physics Series Vol. XLVI (2007), pp. 813–820
HADRON07: XII Int. Conf. on Hadron Spectroscopy – Frascati, October 8-13, 2007
Quarkonia States

RECENT BES RESULTS ON CHARMONIUM DECAYS

Chang-Zheng Yuan
(for the BES Collaboration)
Institute of High Energy Physics, Beijing 100049, China

Abstract

In this talk, we present the recent results on charmonium decays from the BES experiment at the BEPC collider. The analyses are based on a 14 million $\psi(2S)$ events data sample. We report results on leptonic decays, hadronic decays, and radiative decays of $\psi(2S)$, as well as hadronic decays of χ_{cJ} states and rare or forbidden decays of J/ψ.

1 Introduction

We report the recent analyses on charmonium decays with the $\psi(2S)$ data collected with the BESII detector [1)] at the BEPC collider. The data sample has 14 million produced $\psi(2S)$ events [2)].

2 Branching fraction of $\psi(2S) \to \tau^+\tau^-$

The $\psi(2S)$ data provides an opportunity to compare the coupling of the photon to the three generation leptons by studying the leptonic decays $\psi(2S) \to e^+e^-$, $\mu^+\mu^-$, and $\tau^+\tau^-$. The leptonic decay branching fractions are described by the relation $B_{ee} \simeq B_{\mu\mu} \simeq B_{\tau\tau}/0.3885$, which are in good agreement with BESI measurement [3]. The branching fraction for $\psi(2S) \to \tau^+\tau^-$ is remeasured [4] with $\tau^+\tau^-$ pair reconstructed with their pure leptonic decays. At $\psi(2S)$ resonance, 1015 signal events are observed, and the QED process contributes 516 events measured with a data sample at $\sqrt{s} = 3.65$ GeV. The branching fraction is calculated to be $(0.310 \pm 0.021 \pm 0.038)\%$, where the first error is statistical and the second systematic. This improves the precision and the $e - \mu - \tau$ universality is tested at a higher level than at BESI.

3 $\psi(2S)$ radiative decays

Besides conventional meson and baryon states, QCD also predicts a rich spectrum of glueballs, hybrids, and multi-quark states in the 1.0 to 2.5 GeV/c^2 mass region. Therefore, searches for the evidence of these exotic states play an important role in testing QCD. The radiative decays of $\psi(2S)$ to hadrons are expected to contribute about 1% to the total $\psi(2S)$ decay width [5]. However, the measured channels only sum up to about 0.05% [6].

We measured the decays of $\psi(2S)$ into $\gamma p\overline{p}$, $\gamma 2(\pi^+\pi^-)$, $\gamma K^0_S K^+\pi^- + c.c.$, $\gamma K^+K^-\pi^+\pi^-$, $\gamma K^{*0}K^-\pi^+ + c.c.$, $\gamma K^{*0}\bar{K}^{*0}$, $\gamma\pi^+\pi^- p\overline{p}$, $\gamma 2(K^+K^-)$, $\gamma 3(\pi^+\pi^-)$, and $\gamma 2(\pi^+\pi^-)K^+K^-$, with the invariant mass of the hadrons (m_{hs}) less than 2.9 GeV/c^2 for each decay mode [7]. The differential branching fractions are shown in Fig. 1. The branching fractions below $m_{hs} < 2.9$ GeV/c^2 are given in Table 1, which sum up to 0.26% of the total $\psi(2S)$ decay width. We also analyzed $\psi(2S) \to \gamma\pi^+\pi^-$ and γK^+K^- modes to study the resonances in $\pi^+\pi^-$ and K^+K^- invariant mass spectrum. Significant signals for $f_2(1270)$ and $f_0(1710)$ were observed, but the low statistics prevent us from drawing solid conclusion on the other resonances [8].

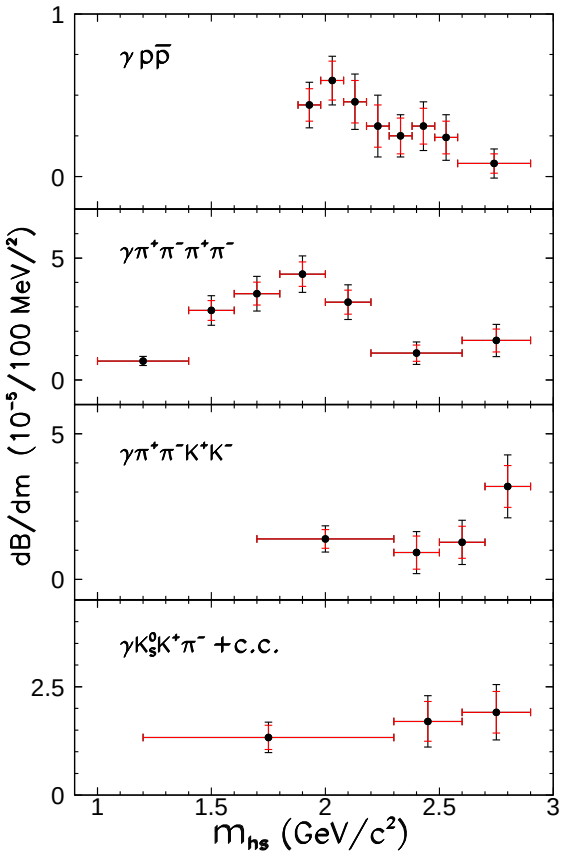

Figure 1: Differential branching fractions for $\psi(2S)$ decays into $\gamma p\overline{p}$, $\gamma 2(\pi^+\pi^-)$, $\gamma K^+K^-\pi^+\pi^-$, and $\gamma K^0_S K^+\pi^- + c.c.$ Here m_{hs} is the invariant mass of the hadrons in each final state. For each point, the smaller longitudinal error is the statistical error, while the bigger one is the quadratic sum of statistical and systematic errors.

Table 1: Branching fractions for $\psi(2S) \to \gamma + hadrons$ with $m_{hs} < 2.9$ GeV/c^2, where the upper limits are determined at the 90% C.L.

Mode	$\mathcal{B}(\times 10^{-5})$
$\gamma p\bar{p}$	2.9±0.4±0.4
$\gamma 2(\pi^+\pi^-)$	39.6±2.8±5.0
$\gamma K^0_S K^+\pi^- + c.c.$	25.6±3.6±3.6
$\gamma K^+K^-\pi^+\pi^-$	19.1±2.7±4.3
$\gamma K^{*0}K^+\pi^- + c.c.$	37.0±6.1±7.2
$\gamma K^{*0}\bar{K}^{*0}$	$24.0 \pm 4.5 \pm 5.0$
$\gamma\pi^+\pi^- p\bar{p}$	2.8±1.2±0.7
$\gamma K^+K^-K^+K^-$	< 4
$\gamma 3(\pi^+\pi^-)$	< 17
$\gamma 2(\pi^+\pi^-)K^+K^-$	< 22

4 $\psi(2S)$ hadronic decays

4.1 σ in $\psi(2S) \to \pi^+\pi^- J/\psi$

The process $\psi(2S) \to \pi^+\pi^- J/\psi$, $J/\psi \to \mu^+\mu^-$ is analyzed to study the $\pi^+\pi^-$ interaction [9].

We fit the data with two different models. For the first model, using four different Breit-Wigner parameterizations, the data can be well fitted with a σ term and a contact term. The final best estimate of the σ pole position is $(552^{+\ 84}_{-106}) - i(232^{+81}_{-72})$ MeV/c^2, where the errors cover the statistical and systematic errors, including the differences in the Breit-Wigner parameterizations.

We also fit our data according to the scheme in Ref. [10]. It is found that the $\pi\pi$ S-wave FSI plays a dominant role in $\psi(2S) \to \pi^+\pi^- J/\psi$, while the contribution from the contact term is small. The σ pole used in this fit, $469 - i203$ MeV/c^2 is consistent with the fits to the Breit-Wigner functions. This implies that, although the two theoretical schemes are very different, both of them find the σ meson at similar pole positions.

If the σ meson exists, the pole should occur universally in all $\pi\pi$ system with correct quantum numbers. Our analysis demonstrates that, in $\psi(2S) \to \pi^+\pi^- J/\psi$, one can still determine the pole location in good agreement with that obtained from $J/\psi \to \omega\pi^+\pi^-$ decay [11].

Table 2: Branching fractions for $\psi(2S)$ hadronic decays. Here Q_h is defined as $Q_h = \frac{\mathcal{B}(\psi(2S)\to h)}{\mathcal{B}(J/\psi\to h)}$, where $\mathcal{B}(J/\psi \to h)$s are taken from [6].

Mode: h	$\mathcal{B}(\times 10^{-4})$	$Q_h(\%)$
$p\overline{p}$	$3.36 \pm 0.09 \pm 0.25$	14.9 ± 1.4
$\Lambda\bar{\Lambda}$	$3.39 \pm 0.20 \pm 0.32$	16.7 ± 2.1
$\Sigma^0\bar{\Sigma}^0$	$2.35 \pm 0.36 \pm 0.32$	16.8 ± 3.6
$\Xi^-\Xi^+$	$3.03 \pm 0.40 \pm 0.32$	16.8 ± 4.7
$p\overline{p}\pi^0$	$1.32 \pm 0.10 \pm 0.15$	12.1 ± 1.9
$p\bar{n}\pi^-$	$2.45 \pm 0.11 \pm 0.21$	12.0 ± 1.5
$\bar{p}n\pi^+$	$2.52 \pm 0.12 \pm 0.22$	12.9 ± 1.7

4.2 Hadronic decays with Baryons in the final states

In perturbative QCD (pQCD), hadronic decays of both $\psi(2S)$ and J/ψ proceed dominantly via an annihilation of $c\bar{c}$ quarks into three gluons or one photon, followed by a hadronization process. This yields the so-called "12% rule", *i.e.* $Q_h \equiv \frac{B_{\psi(2S)\to h}}{B_{J/\psi\to h}} = \frac{B_{\psi(2S)\to e^+e^-}}{B_{J/\psi\to e^+e^-}} \simeq 12\%$. Table 2 summarizes recent measurements on $\psi(2S)$ decays at BES. For a number of $\psi(2S)$ decays Q_hs are in agreement with 12% within $1 \sim 2\sigma$.

The branching fractions of $\psi(2S)$ decays into octet baryon are measured [12] and listed in Table 2. For $\psi(2S) \to N\bar{N}\pi$ [13, 14], the ratio of the measured branching fractions is $\mathcal{B}(\psi(2S) \to p\overline{p}\pi^0) : \mathcal{B}(\psi(2S) \to p\bar{n}\pi^-) : \mathcal{B}(\psi(2S) \to \bar{p}p\pi^+) = 1 : 1.86 \pm 0.27 : 1.91 \pm 0.27$, which is consistent with the isospin symmetry prediction 1 : 2 : 2.

No $\psi(2S) \to \Lambda\overline{\Lambda}\pi^0$ and $\Lambda\overline{\Lambda}\eta$ are observed and the upper limits on the production rates are determined [15]. We also measure these two modes in J/ψ decays. In our analysis, it is found that $\Lambda\overline{\Lambda}\pi^0$ is seriously contaminated by $J/\psi \to \Sigma^0\pi^0\bar{\Lambda} + c.c.$ and $\Sigma^+\pi^-\bar{\Lambda} + c.c.$ After removing these backgrounds, no significant signal is observed for $J/\psi \to \Lambda\bar{\Lambda}\pi^0$, and the upper limit is determined to be $\mathcal{B}(J/\psi \to \Lambda\bar{\Lambda}\pi^0) < 0.64 \times 10^{-4}$ at the 90% C.L.; while the branching fraction of $J/\psi \to \Lambda\bar{\Lambda}\eta$ is determined to be $(2.62 \pm 0.60 \pm 0.44) \times 10^{-4}$. This indicates that $J/\psi \to \Lambda\bar{\Lambda}\pi^0$ is suppressed due to the isospin conservation, and the previous measurements by DM2 [16] and BESI [17] underestimate the background contribution.

5 $\chi_{cJ} \to$ three pseudoscalars

Decays of χ_{c0} and χ_{c2} into three pseudoscalars are suppressed by the spin-parity selection rule. We measured the branching fractions of χ_{c1} decays into $K^0_S K^+\pi^- + c.c.$ and $\eta\pi^+\pi^-$ and intermediate states involved [18].

$K^0_S K^+\pi^- + c.c.$ events are mainly produced via $K^*(892)$ intermediate state, and $\eta\pi^+\pi^-$ events via $f_2(1270)\eta$ and $a_0(980)\pi$. The branching fractions with these resonances are

$$\begin{aligned}
\mathcal{B}(\chi_{c1} \to K^*(892)^0\bar{K}^0 + c.c.) &= (1.1 \pm 0.4 \pm 0.1) \times 10^{-3},\\
\mathcal{B}(\chi_{c1} \to K^*(892)^+K^- + c.c.) &= (1.6 \pm 0.7 \pm 0.2) \times 10^{-3},\\
\mathcal{B}(\chi_{c1} \to f_2(1270)\eta) &= (3.0 \pm 0.7 \pm 0.5) \times 10^{-3},\\
\mathcal{B}(\chi_{c1} \to a_0(980)^+\pi^- + c.c. \to \eta\pi^+\pi^-) &= (2.0 \pm 0.5 \pm 0.5) \times 10^{-3}.
\end{aligned}$$

Except for $\chi_{c1} \to K^0_S K^+\pi^- + c.c.$, all other modes are the first observations.

6 Search for rare and forbidden decays

6.1 Upper limit on $\mathcal{B}(J/\psi \to \gamma\gamma)$

We searched for the C-parity violating decay, $J/\psi \to \gamma\gamma$ [19]. In a previous measurement [20], J/ψ produced directly in e^+e^- annihilation was used, and the upper limit measured is $\mathcal{B}(J/\psi \to \gamma\gamma) < 5 \times 10^{-4}$ at 90% C.L. In our analysis we studied this decay via $\psi(2S) \to \pi^+\pi^- J/\psi$, $J/\psi \to \gamma\gamma$. Therefore, the QED background is strongly suppressed since we observe a $\pi^+\pi^-$ pair plus two photons and do not base our search just on $\gamma\gamma$ invariant mass distribution.

The total number of events in the signal region is 52, the peaking background is 30.4 and the smooth background is 18.6. With the Bayesian method, the upper limit on the number of $J/\psi \to \gamma\gamma$ events is estimated to be 16 at the 90% C.L., in which the systematic errors have been taken into account. Therefore, the upper limit on $\mathcal{B}(J/\psi \to \gamma\gamma)$ is measured to be 2.2×10^{-5}. Our upper limit for the C-violating decay is about 20 times more stringent than the previous measurement. It indicates that there is no obvious C-parity violation.

6.2 Search for J/ψ decays into invisible particles

Invisible decays of quarkonium states such as J/ψ and Υ offer a window into what may lie beyond the standard model (SM) [21].

In order to detect invisible J/ψ decay, we use $\psi(2S) \to \pi^+\pi^- J/\psi$ and infer the presence of the J/ψ resonance from the J/ψ peak in the distribution of mass recoiling against the $\pi^+\pi^-$ [22]. A χ^2 fit is used to extract the number of J/ψ events in the $\pi^+\pi^-$ recoiling mass distribution in the range 3.0 GeV/c^2 < $M^{\rm recoil}_{\pi^+\pi^-}$ < 3.2 GeV/c^2. The function to describe the signal comes from the shape of the $\pi^+\pi^-$ recoiling mass spectrum from the control sample $\psi(2S) \to \pi^+\pi^- J/\psi$, $J/\psi \to \mu^+\mu^-$. The fit yields 6424 ± 137 events, which includes the contributions from both signal and peaking backgrounds, since they have the same probability density functions in the fit. After subtracting the expected backgrounds from the fitted yields, we get the number of events of $\psi(2S) \to \pi^+\pi^- J/\psi$, $J/\psi \to$ invisible to be 406 ± 385. The upper limit is determined to be $N^{J/\psi}_{UL} = 1045$ at the 90% C.L. from the Feldman-cousins frequentist approach. The upper limit on the ratio $\frac{\mathcal{B}(J/\psi \to \text{invisible})}{\mathcal{B}(J/\psi \to \mu^+\mu^-)}$ is 1.0×10^{-2} at 90% C.L. This measurement improves by a factor of 3.5 the bound on the product of the coupling of the U boson to the c-quark and LDM particles as described in Ref. [21].

7 Summary

Using the 14 M $\psi(2S)$ events sample taken with the BESII detector at the BEPC storage ring, BES experiment provided many interesting results in charmonium decays, including the observation of many $\psi(2S)$ radiative decays, some $\psi(2S)$ hadronic decays, χ_{cJ} decays, and the rare and forbidden J/ψ decays. These results shed light on the understanding of SM.

8 Acknowledgements

We thanks BES colleagues for the nice work presented in this talk. This work was supported in part by National Natural Science Foundation of China under Contract No. 10491303.

References

1. BES Collaboration, J. Z. Bai *et al.*, Nucl. Instrum. Meths. A **458**, 627 (2001).

2. X. H. Mo *et al.*, HEP&NP **28**, 455 (2004).

3. BES Collaboration, J. Z. Bai *et al.*, Phys. Rev. D **65**, 052004 (2002).
4. BES Collaboration, M. Ablikim *et al.*, Phys. Rev. D **74**, 112003 (2006).
5. P. Wang, C. Z. Yuan, and X. H. Mo, Phys. Rev. D **70**, 114014 (2004).
6. Particle Data Group, W.-M. Yao *et al.*, J. Phys. G **33**, 1 (2006).
7. BES Collaboration, M. Ablikim *et al.*, Phys. Rev. Lett. **99**, 011802 (2007).
8. BES Collaboration, M. Ablikim *et al.*, arXiv:0710.2324 [hep-ex].
9. BES Collaboration, M. Ablikim *et al.*, Phys. Lett. B **645**, 19 (2007).
10. F.K. Guo *et al.*, Nucl. Phys. A **761**, 269 (2005).
11. BES Collaboration, M. Ablikim *et al.*, Phys. Lett. B **598**, 149 (2004).
12. BES Collaboration, M. Ablikim *et al.*, Phys. Lett. B **648**, 149 (2007).
13. BES Collaboration, M. Ablikim *et al.*, Phys. Rev. D **71**, 072006 (2005).
14. BES Collaboration, M. Ablikim *et al.*, Phys. Rev. D **74**, 012004 (2006).
15. BES Collaboration, M. Ablikim *et al.*, Phys. Rev. D **76**, 092003 (2007).
16. DM2 Collaboration, P. Henrard *et al.*, Nucl. Phys. B **292**, 670 (1987).
17. BES Collaboration, J. Z. Bai *et al.*, Phys. Lett. B **424**, 213 (1998).
18. BES Collaboration, M. Ablikim *et al.*, Phys. Rev. D **74**, 072001 (2006).
19. BES Collaboration, M. Ablikim *et al.*, arXiv:0709.3371 [hep-ex].
20. W. Bartel *et al.*, Phys. Lett. B **66**, 489 (1977).
21. P. Fayet, Phys. Lett. B **84**, 421 (1979); P. Fayet, and J. Kaplan, Phys. Lett. B **269**, 213 (1991); B. McElrath, Phys. Rev. D **72**, 103508 (2005); P. Fayet, Phys. Rev. D **74**, 054034 (2006); P. Fayet, Phys. Rev. D **75**, 115017 (2007).
22. BES Collaboration, M. Ablikim *et al.*, arXiv:0710.0039 [hep-ex].

Frascati Physics Series Vol. XLVI (2007), pp. 821–828
HADRON07: XII Int. Conf. on Hadron Spectroscopy – Frascati, October 8-13, 2007
Quarkonia States

CHARMONIUM SPECTROSCOPY AT *BABAR*

Arafat Gabareen Mokhtar
Dept. of Physics Colorado State University
Fort Collins, CO 80523 USA

for the *BABAR* Collaboration

Abstract

The charmonium-like states, $Y(4260)$, $Y(4350)$, produced via initial state radiation, as well as the $X(3872)$, and $Y(3940)$, produced in B meson decays from the *BABAR* B-factory are reviewed. These mesons do not seem consistent with conventional charmonium models, and several alternate hypotheses have been proposed to explain these new discoveries.

1 Introduction

Several charmonium-like states have been discovered recently at the BELLE and *BABAR* B-factories. These new states have been observed in e^+e^- initial state radiation (ISR) interactions or in B-decays. The relevant Feynman diagrams representing ISR production and B-decay are shown in Fig. 1. In ISR events, a real photon is emitted from the incoming electron or positron

and subsequently the electron and positron annihilate to yield a virtual photon ($\gamma^\star$) which couples to a $c\bar{c}$ system with c.m. energy lower than the nominal value, and thus charmonia can be produced. In $\bar{B}$-decay, a W^- from the b-quark yields an $s\bar{c}$ system; the $\bar{c}$ combines with the c quark from b decay to produce a charmonium state, while the s quark and $\bar{q}$ spectator yield a strange meson.

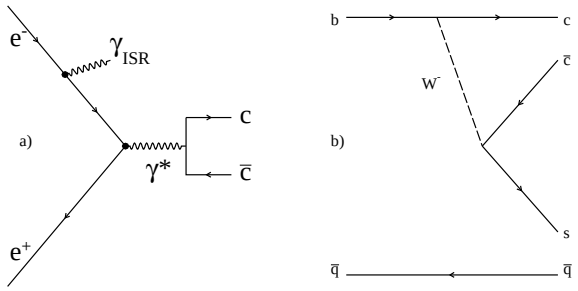

Figure 1: *Feynman diagrams representing charmonium production via a) ISR, b) $\bar{B}$ decay.*

The discovery of the charmonium-like state $X(3872) \to J/\psi\pi^+\pi^-$ was reported by the BELLE collaboration [1)], and confirmed by the CDF [2)], D0 [3)], and *BABAR* [4)] experiments. Since then several charmonium-like states have been discovered at the B-factories, however they do not seem consistent with conventional charmonium spectroscopy. Alternative explanations for these states have been proposed, such as molecules, 4-quark states, hybrids, etc.

In this report, we review briefly the latest results from the *BABAR* experiment concerning four of these charmonium-like states.

2 The $Y(4260)$

The $Y(4260) \to J/\psi\pi^+\pi^-$ was discovered by *BABAR* in the ISR reaction $e^+e^- \to \gamma_{ISR}J/\psi\pi^+\pi^-$ [5)] using 233 fb^{-1} of data, where detection of the ISR photon was not required. The $J/\psi\pi^+\pi^-$ mass distribution is shown in Fig. 2, where in the sub-figure a broader mass region shows the peak due to $\psi(2S) \to J/\psi\pi^+\pi^-$; an enhancement is observed at ~ 4.26 GeV/c^2. The mass region $3.8 < m_{J/\psi\pi^+\pi^-} < 5$ GeV/c^2 is fitted with a Breit-Wigner signal func-

tion and a second order polynomial background. The background from J/ψ side-band does not show any peaking structure. The number of signal events extracted from the fit is 125 ± 23, the mass is $M_Y = 4259 \pm 8^{+2}_{-6}$ MeV/c^2, and the width is $\Gamma_Y = 88 \pm 23^{+6}_{-4}$ MeV. The branching fraction obtained is $\Gamma_{Y,ee} * BF(Y(4260) \to J/\psi\pi^+\pi^-) = 5.5 \pm 1.0^{+0.8}_{-0.7}$ eV. At *BABAR*, no evidence was found for the processes $Y(4260) \to \phi\pi^+\pi^-$ [6], $Y(4260) \to D\bar{D}$ [7], and $Y(4260) \to p\bar{p}$ [8]. A search for the $Y(4260)$ resonance in B decay was carried out, and a 3σ effect was observed [9].

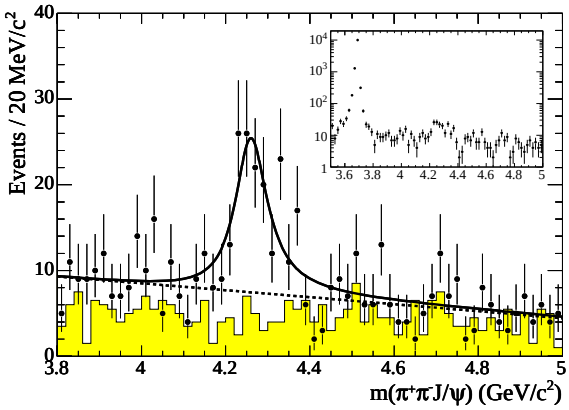

Figure 2: *The $J/\psi\pi^+\pi^-$ invariant mass distribution in the range $3.8 - 5.0$ GeV/c^2. The dots represent the data, the filled histogram shows the background from the J/ψ side-bands, the solid curve represents the fit result and the dashed line shows the background.*

3 The $Y(4350)$

In *BABAR*, a search for $Y(4260) \to \psi(2S)\pi^+\pi^-$ yielded instead evidence for a broad structure near ~ 4.3 GeV/c^2 [10]. This enhancement is not consistent with the $Y(4260)$ state. In Fig. 3, the $2(\pi^+\pi^-)J/\psi$ invariant mass is shown for the data (dots) and for the background (shaded histogram). The data points are fitted with a Breit-Wigner signal function with fixed mass and width [5] (dashed line), and again with mass and width as free parameters. The latter fit yields mass $m = 4324 \pm 23$ MeV/c^2, and width $\Gamma = 172 \pm 33$ MeV (statistical errors only). The $Y(4350)$ was confirmed by BELLE [11].

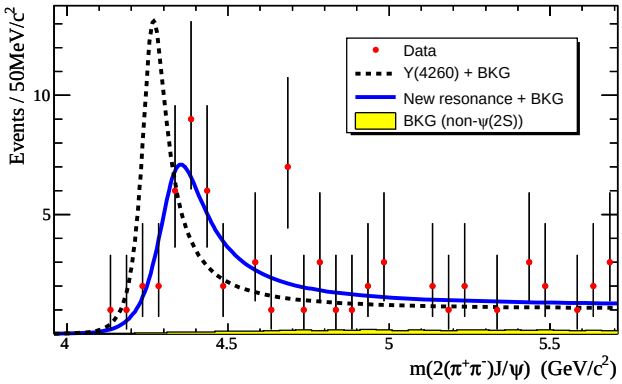

Figure 3: *The $2(\pi^+\pi^-)J/\psi$ invariant mass spectrum. The dots indicate the data and the shaded histogram represents the background. The solid curve shows the fit result with free mass and width parameters, while the dashed curve is obtained with the mass and width fixed to their $Y(4260)$ values* [5].

4 The $X(3872)$

The $X(3872)$ discovered by BELLE [1] was the first of the new charmonium-like states. Later CDF [2], D0 [3], and *BABAR* [4] confirmed the BELLE observation. In *BABAR*, a data sample of 211 fb^{-1} was analyzed to obtain the $J/\psi\pi^+\pi^-$ invariant mass in the region $3.8 - 3.95$ GeV/c^2 separately for charged and neutral B-candidates as shown in Fig. 4. The dots represent the data and the shaded histograms represent background. For charged B decay (Fig. 4(a)), a clear enhancement is observed for $m_{J/\psi\pi^+\pi^-} \sim 3870$ GeV/c^2. Statistically consistent behavior is observed for the neutral mode (Fig. 4(b)). The $X(3872)$ invariant mass obtained from the charged (neutral) B-mode is $m = 3871.3 \pm 0.6 \pm 0.1$ ($3868.6 \pm 1.2 \pm 0.2$) MeV/c^2, and the corresponding branching fraction values are $\mathcal{BF}(B^- \to X(J/\psi\pi^+\pi^-)K^-) = (10.1 \pm 2.5 \pm 1.0) \times 10^{-5}$ and $\mathcal{B}(B^0 \to X(J/\psi\pi^+\pi^-)K^0) = (5.1 \pm 2.8 \pm 0.7) \times 10^{-5}$ at 90% C.L.

In *BABAR*, no evidence for a charged partner of the $X(3872)$ was found [12], and so it is assumed that the $X(3872)$ has $I = 0$. Also *BABAR* [13] has confirmed the BELLE observation [14] of $X(3872) \to J/\psi\gamma$. In Fig. 5 we show the $J/\psi\gamma$ mass distribution obtained from *BABAR*, and a clear enhancement is observed at the $X(3872)$ mass. It follows that the $X(3872)$ has positive

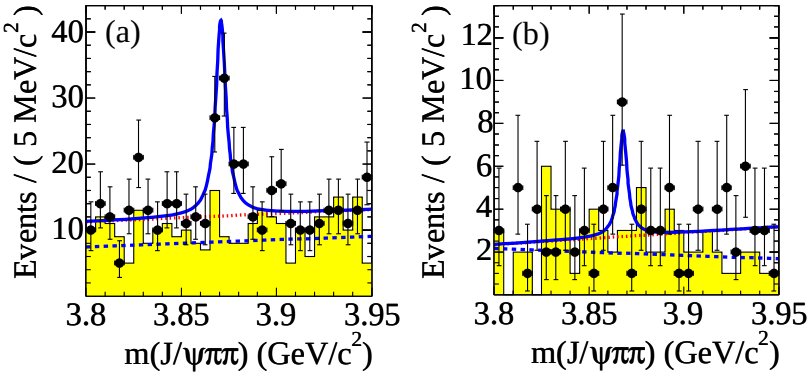

Figure 4: *The $J/\psi\pi^+\pi^-$ invariant mass distributions for charged (a) and neutral (b) B decay from BABAR. The dots represent the data, while the shaded histograms represent side-band background. The solid curves show the fit results, the dashed lines show combinatorial background, and the dotted lines represent the sum of combinatorial and peaking background contributions.*

C-parity.

Later both BELLE [15] and *BABAR* [16] have found evidence for the decay mode $X(3872) \to \bar{D}^{\star 0} D^0$. In Fig. 6, we show the $\bar{D}^{\star 0} D^0$ invariant mass as reported by *BABAR*. A clear enhancement near threshold is observed. The measured mass values from BELLE and *BABAR* are $3875.2 \pm 0.7^{+0.9}_{-1.8}$ MeV/c^2 and $3875.1^{+0.9}_{-0.7} \pm 0.5$ MeV/c^2, respectively. The difference between the mass value obtained in the $\bar{D}^{\star 0} D^0$ decay mode and that from PDG [17] is then $3.8^{+1.2}_{-2.0}$ MeV/c^2 from BELLE and $3.7^{+1.1}_{-0.9}$ MeV/c^2 from *BABAR*, indicating that the effect is real. This mass difference has received a lot of attention, although a simple explanation involving one unit of orbital angular momentum (and hence $J^P = 2^-$) has been proposed recently [18].

5 The $Y(3940)$

The $Y(3940)$ was first observed by the BELLE collaboration [19] in the decay process $B \to J/\psi\omega K$ using 253 fb^{-1} of data. The mass and width obtained for this resonance were $m = 3943 \pm 11 \pm 13$ MeV/c^2 and $\Gamma = 87 \pm 22 \pm 26$ MeV. In *BABAR* a data sample of 348 fb^{-1} is used to search for the $Y(3940)$ [20].

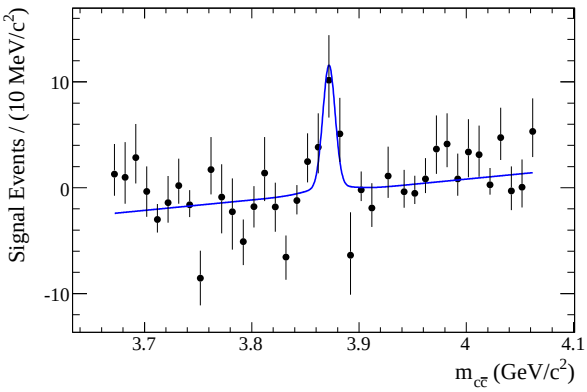

Figure 5: *The number of extracted signal events versus $m_{c\bar{c}}$ for the $X(3872)$ mass region. The solid curve represents the fit result.*

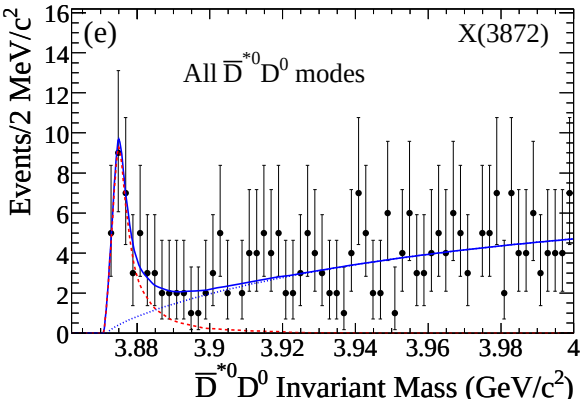

Figure 6: *The $\bar{D}^{*0}D^0$ invariant mass, where the solid curve shows the fit result and the dashed curves represent the signal and background contributions.*

Charged and the neutral B-decays are analyzed separately, and in the *BABAR* analysis finer mass binning was used on the basis of mass resolution studies. Signal events were corrected for acceptance and mass resolution effects. A significant enhancement is observed near threshold in the charged mode, and a statistically-limited, but consistent, signal is obtained in the neutral mode. In Fig. 7 we show the acceptance-corrected $J/\psi\omega$ mass distributions for the charged (Fig. 7(a)) and neutral (Fig. 7(b)) B decay modes, respectively. The data points are fitted with a Breit-Wigner signal function and a single Gaussian function for the non-resonant contribution. Good fits to the data are obtained, as shown by the solid curves.

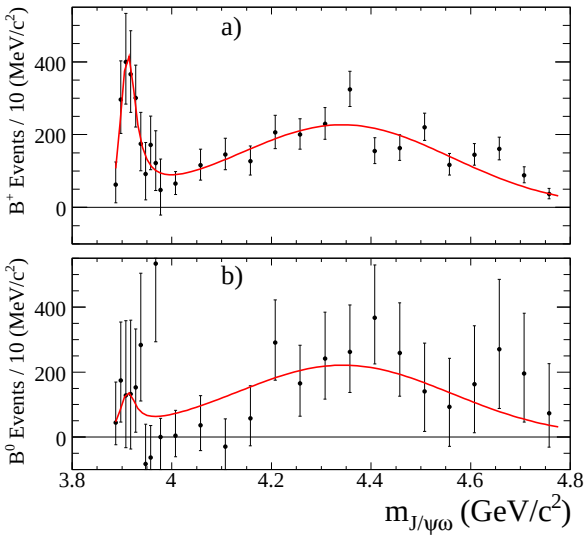

Figure 7: *The acceptance-corrected $J/\psi\omega$ mass distribution for (a) B^+ and (b) B^0 decay. The solid curves represent the fit results.*

The mass and width of the $Y(3940)$ are found to be $m = 3914.6^{+3.8}_{-3.4}(stat)^{+1.9}_{-1.9}(syst)$ MeV/c^2 and $\Gamma = 33^{+12}_{-8}(stat)^{+5}_{-5}(syst)$ MeV, respectively, with branching fractions for the charged and the neutral decay modes $\mathcal{BF}(B^+ \to YK^+) = (4.9^{+1.0}_{-1.0}(stat)^{+0.5}_{-0.5}(syst))\times 10^{-5}$, and $\mathcal{BF}(B^0 \to YK^0) = (1.5^{+1.4}_{-1.2}(stat)^{+0.2}_{-0.2}(syst)) \times 10^{-5}$; the latter has corresponding upper limit (95% C.L.) 3.9×10^{-5}.

6 Acknowledgments

The *BABAR* Collaboration acknowledges the extraordinary efforts of the PEPII collider group for providing the excellent luminosity. I should like to thank the Hadron07 conference organizers for a nice meeting at Frascati, and also Bill Dunwoodie and Walter Toki for useful comments.

References

1. S.-K. Choi *et al.*, Phys. Rev. Lett. **91**, 262001 (2003).
2. D. Acosta *et al.*, Phys. Rev. Lett. **93**, 072001 (2004).
3. V. M. Abazov *et al.*, Phys. Rev. Lett. **93**, 162002 (2004).
4. B. Aubert *et al.*, Phys. Rev. **D71**, 071103 (2005).
5. B. Aubert *et al.*, Phys. Rev. Lett. **95**, 142001 (2005).
6. B. Aubert *et al.*, Phys. Rev.**D 74**, 091103(R) (2006).
7. B. Aubert *et al.*, arXiv:0710.1371 [hep-ex], (2007).
8. B. Aubert *et al.*, Phys. Rev. **D 73**, 012005 (2006).
9. B. Aubert *et al.*, Phys. Rev. **D 73**, 011101 (2006).
10. B. Aubert *et al.*, Phys. Rev. Lett. **98**, 212001 (2007).
11. X. L. Wang *et al.*, Phys. Rev. Lett. **99**, 142002 (2007).
12. B. Aubert *et al.*, Phys. Rev. **D 71**, 031501 (2005).
13. B. Aubert *et al.*, Phys. Rev. **D 74**, 071101 (2006).
14. K. Abe *et al.*, arXiv:0505037 [hep-ex], (2005).
15. G. Gokhroo *et al.*, Phys. Rev. Lett. **97**, 162002 (2006).
16. B. Aubert *et al.*, arXiv:0708.1565 [hep-ex], (2007).
17. W.-M. Yao *et al.*, J. Phys. **G33**, 1 (2006).
18. W. Dunwoodie and V. Ziegler, arXiv:0710.5191 [hep-ex], (2007).
19. S.-K. Choi *et al.*, Phys. Rev. Lett. **94**, 182002 (2005).
20. B. Aubert *et al.*, arXiv:0711.2047 [hep-ex], (2007).

Frascati Physics Series Vol. XLVI (2007), pp. 829–836
HADRON07: XII Int. Conf. on Hadron Spectroscopy – Frascati, October 8-13, 2007
Quarkonia States

NEW RESULT ON $\Upsilon(5S)$ DECAY FROM BELLE — OBSERVATION OF "$\Upsilon(5S)$" $\to \Upsilon(1S)\pi^+\pi^-$, $\Upsilon(2S)\pi^+\pi^-$ —

George W.S. Hou (for the Belle Collaboration)
Department of Physics, National Taiwan University, Taipei, Taiwan 10617

Abstract

We report the observation of large signals in $e^+e^- \to \Upsilon(1S)\pi^+\pi^-$, $\Upsilon(2S)\pi^+\pi^-$ production on the $\Upsilon(5S)$ peak. The results are based on 21.7 fb^{-1} data collected with the Belle detector at the KEKB asymmetric energy e^+e^- collider. The pb level cross sections, or MeV level partial widths if interpreted as from the $\Upsilon(5S)$ itself, are anomalously large.

1 Motivation

The $\Upsilon(4S) \to \Upsilon(1S)\pi^+\pi^-$, $\Upsilon(2S)\pi^+\pi^-$ decays have recently been measured at the 10^{-4} level [1, 2]. Scaling by $\Gamma_{\Upsilon(4S)}/\Gamma_{\Upsilon(5S)}$, the branching ratios for $\Upsilon(5S)$ are expected at $\mathcal{O}(10^{-5})$, which calls for a dataset that is larger than on the $\Upsilon(4S)$. However, enhancement is possible. It was pointed out [3] in 2006 that the bottom counterpart of the $Y(4260)$ can be searched for at the B factories

via $\Upsilon\pi^+\pi^-$. The $Y(4260)$ was observed [4] by BaBar in $e^+e^- \to \gamma_{\rm ISR} J/\psi\pi^+\pi^-$, i.e. radiative return at $\Upsilon(4S)$ energy. It was confirmed by CLEO [5] via direct scan with much less data. By way of analogy, the "Y_b" can be searched for [3] in both $e^+e^- \to \gamma_{\rm ISR}\Upsilon\pi^+\pi^-$ on $\Upsilon(5S)$, or $e^+e^- \to \Upsilon\pi^+\pi^-$ direct scan.

We report the result of a study [6] using the 21.7 fb^{-1} data collected on the $\Upsilon(5S)$ by the Belle experiment at the KEKB e^+e^- collider.

2 $\Upsilon(4S),\ \Upsilon(3S) \to \Upsilon(1S)\pi^+\pi^-$ Template

The analysis is basically the same as those done previously with lower $\Upsilon(mS)$ states. We illustrate with $\Upsilon(4S)$ and $\Upsilon(3S)$ decays to gain familiarity.

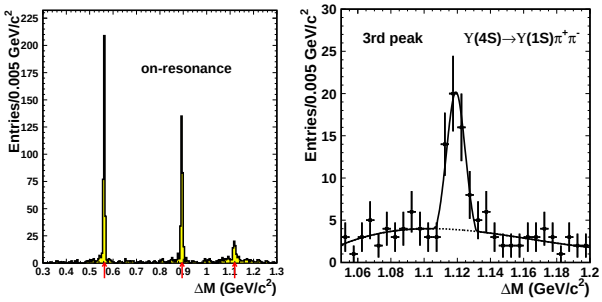

Figure 1: *a)* $\Delta M \equiv M_{\mu^+\mu^-\pi^+\pi^-} - M_{\mu^+\mu^-}$ *distribution* [2] *for* $M_{\mu^+\mu^-}$ *in* $\Upsilon(1S)$ *mass region; b) fit to signal and background of 3rd peak.*

We start with $\Upsilon(4S) \to \Upsilon(1S)\pi^+\pi^-$ based on 477 fb^{-1} of Belle data [2]. $\Upsilon(1S)$ candidates are reconstructed in $\mu^+\mu^-$ pairs. Together with an additional $\pi^+\pi^-$ pair, Fig. 1(a) projects events in the $\Upsilon(1S)$ band (3σ of resolution) onto $\Delta M \equiv M_{\mu^+\mu^-\pi^+\pi^-} - M_{\mu^+\mu^-}$. The first two peaks are from ISR return to $\Upsilon(2S)$ and $\Upsilon(3S)$, while the third peak from $\Upsilon(4S)$ is plotted in Fig. 1(b) with fitted signal and backgound. With better slow pion efficiencies, BaBar has observed [1] $\Upsilon(4S) \to \Upsilon(2S)\pi^+\pi^-$ as well.

Belle has studied $\Upsilon(3S) \to \Upsilon(1S)\pi^+\pi^-$ with 2.9 fb^{-1} data taken for the purpose [7] of dark matter search via $\Upsilon(3S) \to \pi^+\pi^- + nothing$ (using the $\pi^+\pi^-$ pair to tag $\Upsilon(1S) \to nothing$). The ΔM distribution and the $m_{\pi^+\pi^-}$

spectrum are plotted in Fig. 2. The result is in agreement with the study by CLEO [8] using 1.14 fb^{-1} data, which has resolved the decades-old problem of the double-peaked $m_{\pi\pi}$ spectrum for $\Upsilon(3S) \to \Upsilon(1S)\pi\pi$ by putting back a fit parameter that has been dropped in the past. We will not dwell further on this, however, as our purpose is to illustrate the analysis. The $\Upsilon(4S)$ and $\Upsilon(3S)$ studies provide useful crosschecks for our $\Upsilon(5S)$ study.

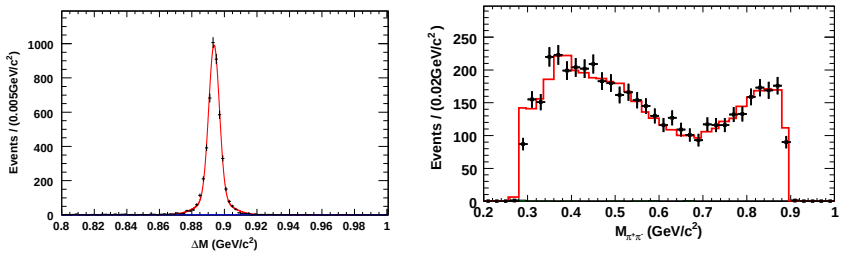

Figure 2: *a)* ΔM *distribution* [7] *for* $\Upsilon(3S) \to \Upsilon(1S)\pi^+\pi^-$ *with* $M_{\mu^+\mu^-}$ *in* $\Upsilon(1S)$ *mass region; b) dipion mass spectrum.*

3 $\Upsilon(5S)$ Dataset and $\Upsilon(nS)h^+h^-$ Event Selection

The $\Upsilon(5S)$ (called $\Upsilon(10860)$ by PDG [9]), was studied by CLEO and CUSB more than 20 years ago. After CLEO took 0.42 fb^{-1} data in 2003, Belle took an engineering run of 1.86 fb^{-1} in 2005 to study the feasibility of running on $\Upsilon(5S)$ for B_s physics. A year later, Belle took 21.7 fb^{-1} data on the $\Upsilon(5S)$ peak, which is the basis for our $\Upsilon(nS)h^+h^-$ ($h = \pi,\ K$) search.

Event selection is looser than the $\Upsilon(4S)$ study. One selects 4 prompt charged tracks, with no other charged tracks with $p_T > 100$ MeV/c^2. Calorimeter energy was not used, so photons are permitted. Two opposite sign tracks are identified as muons, and $M_{\mu^+\mu^-}$ is constrained within 3σ (150 MeV/c^2) of the nominal $\Upsilon(nS)$ mass. A major background is $\mu^+\mu^-e^+e^-$ from $\mu^+\mu^-\gamma$ with photon conversion. We impose a cut of $\cos\theta_{\pi\pi} < 0.95$ for the $\pi\pi$ opening angle, and use electron identification to reject $e^\pm$ that fake $\pi^\pm$. For $h = K$ case, active kaon identification is applied.

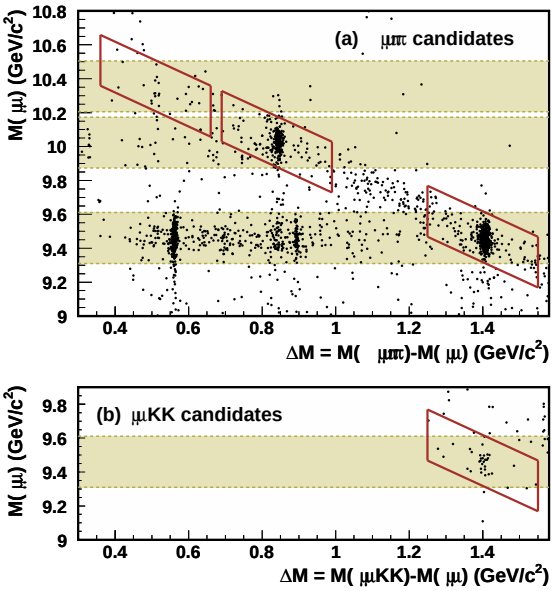

Figure 3: ΔM *vs* $M_{\mu^+\mu^-}$ *scatter plot* [6] *for a)* $\mu^+\mu^-\pi^+\pi^-$ *and b)* $\mu^+\mu^-K^+K^-$ *candidates on the* $\Upsilon(5S)$*. The bands are for* $M_{\mu^+\mu^-}$ *in* $\Upsilon(1S)$*,* $\Upsilon(2S)$*,* $\Upsilon(3S)$ *(*$\Upsilon(1S)$ *only for b)) mass regions. The signal box is as indicated.*

4 Results

The scatter plots of $e^+e^- \to \Upsilon(nS)\pi^+\pi^-$, $\Upsilon(1S)K^+K^-$ on the $\Upsilon(5S)$ peak are given in Fig. 3, where horizontal bands are for $|M_{\mu^+\mu^-} - M_{\Upsilon(nS)}| < 150$ MeV/c^2. Compared with square boxes in previous $\Upsilon(mS)$ analyses, the slanted signal box is better adapted to $\mu^+\mu^-\gamma$ conversion background.

We plot the ΔM projections for the $\Upsilon(1S)$ and $\Upsilon(2S)$ bands in Figs. 4(a) and 4(b), respectively. Scaling from Fig. 1(a) for 477 fb^{-1} on $\Upsilon(4S)$ peak, the absence of the $\Upsilon(4S)$ peak in Fig. 4(a) is to be expected. But with just 21.7 fb^{-1} data, this makes the large peaks at the $\Upsilon(5S)$ position, *in both* $\Upsilon(1S)\pi^+\pi^-$ *and* $\Upsilon(2S)\pi^+\pi^-$, rather striking. However, whether they are solely due to the $\Upsilon(5S)$ resonance needs to be proven, hence we shall denote it as "$\Upsilon(5S)$".

We have checked that the events near $\Delta M \sim 0.84$ GeV/c^2, below the

$\Upsilon(3S)$ peak, can be accounted for by $e^+e^- \to \Upsilon(2S)\pi^+\pi^-$ followed by $\Upsilon(2S) \to \Upsilon(1S) + X$, where X consists of photons. We therefore attribute the mild activity at 0.7 GeV/c^2 as likely due to some yet unmeasured $\Upsilon(2S)$ decays.

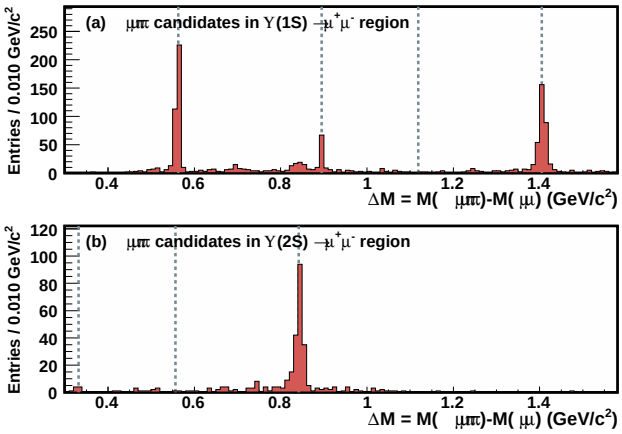

Figure 4: *ΔM distributions for a) $\Upsilon(1S)$ and b) $\Upsilon(2S)$ bands of Fig. 3(a). Dashed lines indicate $\Upsilon(2S)$ (for a) only), $\Upsilon(3S)$, $\Upsilon(4S)$, and $\Upsilon(5S)$.*

The ΔM distributions for the (slanted) signal boxes of Fig. 3 are plotted in Fig. 5. Note that Figs. 5(a) and (b) are not identical to the "$\Upsilon(5S)$"$\to \Upsilon(1S)\pi^+\pi^-$ and $\Upsilon(2S)\pi^+\pi^-$ peaks in Figs. 4(a) and (b). We perform an unbinned extended maximum likelihood fit, where the likelihood of the fit is

$$\mathcal{L}(N_s, N_b) = \frac{e^{-(N_s+N_b)}}{N!} \prod_{i=1}^{N} [N_s \cdot P_s(\Delta M_i) + N_b \cdot P_b(\Delta M_i)] \ , \qquad (1)$$

with N_s (N_b) the signal (background) yield, and P_s (P_b) the signal (background) probability density function (PDF), which is of double Gaussian (linear) form. The fitted signal and background are also shown in Fig. 5. Comparing with Fig. 1(b), the advantage of our choice for signal box is apparent. The extracted signal yields, as well as the significance, are given in Table 1.

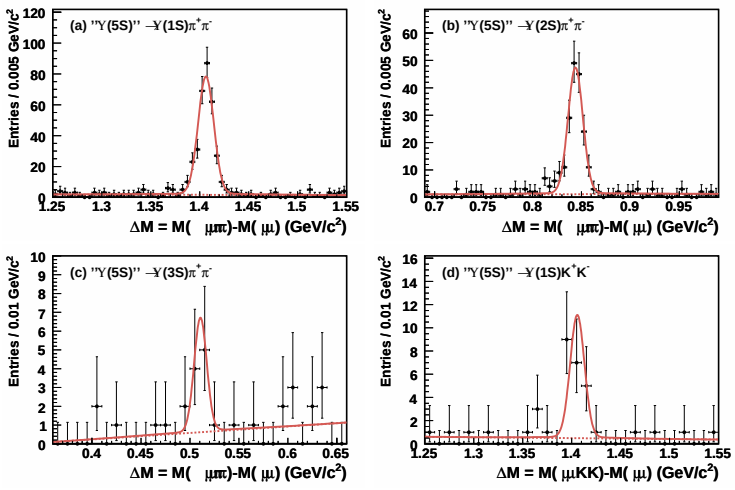

Figure 5: ΔM *distributions for the four signal regions of Fig. 3, together with the fitted signal (solid) and background (dashed).*

Table 1: *Signal yield (N_s), significance (Σ), reconstruction efficiency, and cross section (σ) for* $e^+e^- \to \Upsilon(nS)\pi^+\pi^-$, $\Upsilon(1S)K^+K^-$ *at* $\sqrt{s} = 10.87$ *GeV.*

Process	N_s	Σ	Eff.(%)	σ(pb)
$\Upsilon(1S)\pi^+\pi^-$	325^{+20}_{-19}	20σ	37.4	$1.60 \pm 0.10 \pm 0.12$
$\Upsilon(2S)\pi^+\pi^-$	186 ± 15	14σ	18.9	$2.33 \pm 0.19 \pm 0.31$
$\Upsilon(3S)\pi^+\pi^-$	$10.5^{+4.0}_{-3.3}$	3.2σ	1.5	$1.43^{+0.55}_{-0.45} \pm 0.19$
$\Upsilon(1S)K^+K^-$	$20.2^{+5.2}_{-4.5}$	4.9σ	20.3	$0.184^{+0.047}_{-0.041} \pm 0.028$

Since we have a few hundred $\Upsilon(1S)\pi^+\pi^-$ and $\Upsilon(2S)\pi^+\pi^-$ events, we give the $M_{\pi^+\pi^-}$ and $\cos\theta_{\rm HEL}$ distributions in Fig. 6, where $\theta_{\rm HEL}$ is the angle between π^- and "$\Upsilon(5S)$" momenta in the $\pi^+\pi^-$ rest frame (called θ_X in Ref. [8]). In Fig. 6, the open histogram is phase space, and the shaded histogram is the Brown-Cahn model [10]. Neither fit data well, hence efficiencies are estimated by re-weighted Monte-Carlo according to data. For "$\Upsilon(5S)$" $\to \Upsilon(3S)\pi^+\pi^-$ and $\Upsilon(1S)K^+K^-$, we still use the Brown-Cahn model for efficiency estimate because of limited statistics. The efficiencies are also given in Table 1. The cross

sections are normalized to the resonance cross section measured by Belle [11]. For a summary of systematic errors, see Ref. [6].

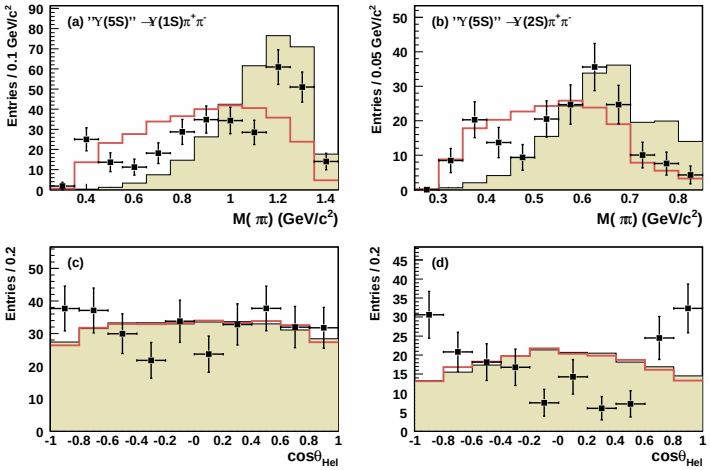

Figure 6: Background-subtracted a), b) $M_{\pi^+\pi^-}$ and c), d) $\cos\theta_{\rm Hel}$ distributions for $\Upsilon(1S)\pi^+\pi^-$, $\Upsilon(2S)\pi^+\pi^-$ events. The histograms are explained in the text.

5 Discussion and Conclusion

To appreciate the anomalous strength of the cross sections in Table 1, let us assume that it is solely due to the $\Upsilon(5S)$ resonance itself, i.e. "$\Upsilon(5S)$" = $\Upsilon(5S)$. Using PDG values, we find the branching fractions $\mathcal{B}(\Upsilon(5S) \to \Upsilon(1S)\pi^+\pi^-) = 0.53 \pm 0.03 \pm 0.05\%$ and $\mathcal{B}(\Upsilon(5S) \to \Upsilon(2S)\pi^+\pi^-) = 0.77 \pm 0.06 \pm 0.11\,\%$, and partial widths are $\Gamma(\Upsilon(5S) \to \Upsilon(1S)\pi^+\pi^-) = 0.58 \pm 0.04 \pm 0.09$ MeV and $\Gamma(\Upsilon(5S) \to \Upsilon(2S)\pi^+\pi^-) = 0.85 \pm 0.07 \pm 0.16$ MeV. These are two orders of magnitude (or more) higher than the $\Upsilon(2S)$, $\Upsilon(3S)$ and $\Upsilon(4S) \to \Upsilon(1S)\pi^+\pi^-$ partial widths of ~ 6 keV, 0.9 keV and 1.8 keV. It echoes the MeV level partial width of $Y(4260) \to J/\psi\pi^+\pi^-$, and a mechanism is needed.

But is it correct to assume "$\Upsilon(5S)$" = $\Upsilon(5S)$? The 21.7 fb^{-1} data was taken on the nominal $\Upsilon(5S)$ peak, and a single energy is not proof that the $\Upsilon(5S)$ is the sole source. Note that $\Gamma(\Upsilon(5S) \to e^+e^-) \simeq 0.31$ keV is similar

to $\Gamma(\Upsilon(4S) \to e^+e^-) \simeq 0.27$ keV, hence the $\Upsilon(5S)$ seems to be a normal bottomonium. From the fact that little radiative return activity is seen in Fig. 4 other than to $\Upsilon(2S)\pi^+\pi^-$ and $\Upsilon(3S)\pi^+\pi^-$, it could be that a Y_b state [3] lies above the $\Upsilon(5S)$. Only an energy scan could tell.

In the process of this analysis, it was uncovered that, while the signal yield of Fig. 1(b) for $\Upsilon(4S) \to \Upsilon(1S)\pi^+\pi^-$ is correct, the efficiency estimate [2] was erroneous. The new preliminary result of $\mathcal{B}(\Upsilon(4S) \to \Upsilon(1S)\pi^+\pi^-) = 1.06^{+0.18}_{-0.17} \pm 0.09 \times 10^{-4}$ is in better agreement with BaBar [1]. A revised publication would be forthcoming.

In conclusion, we observe anomalously large $e^+e^- \to \Upsilon(1S)\pi^+\pi^-$ and $\Upsilon(2S)\pi^+\pi^-$ on the $\Upsilon(5S)$ peak. If interpreted as coming from the $\Upsilon(5S)$ itself, the partial widths at 0.53 and 0.85 MeV are very large, analogous to $Y(4260) \to J/\psi\pi^+\pi^-$. Evidence is also reported for $e^+e^- \to \Upsilon(1S)K^+K^-$ and $\Upsilon(3S)\pi^+\pi^-$ at $\sqrt{s} \cong 10870$ MeV.

References

1. B. Aubert *et al.* [BaBar Collaboration], Phys. Rev. Lett. **96**, 232001 (2006).
2. A. Sokolov *et al.* [Belle Collaboration], Phys. Rev. D **75**, 071103 (2007).
3. W.S. Hou, Phys. Rev. D **74**, 017504 (2006).
4. B. Aubert *et al.* [BaBar Collaboration], Phys. Rev. Lett. **95**, 142001 (2005).
5. T.E. Coan *et al.* [CLEO Collaboration], Phys. Rev. Lett. **96**, 162003 (2006).
6. K.F. Chen *et al.* [Belle Collaboration], arXiv:0710.2577 [hep-ex].
7. O. Tajima *et al.* [Belle Collaboration], Phys. Rev. Lett. **98**, 132001 (2007).
8. D. Cronin-Hennessy *et al.* [CLEO Collaboration], Phys. Rev. D **76**, 072001 (2007).
9. Particle Data Group, http://pdg.lbl.gov/.
10. L.S. Brown and R.N. Cahn, Phys. Rev. Lett. **35**, 1 (1975).
11. A. Drutskoy *et al.* [Belle Collaboration], Phys. Rev. Lett. **98**, 052001 (2007).

Frascati Physics Series Vol. XLVI (2007), pp. 837
HADRON07: XII Int. Conf. on Hadron Spectroscopy – Frascati, October 8-13, 2007
Quarkonia States

CHARMONIUM AT HERA

D. Gladkov
Affiliazione

Written contribution not received

Frascati Physics Series Vol. XLVI (2007), pp. 839–846
HADRON07: XII Int. Conf. on Hadron Spectroscopy – Frascati, October 8-13, 2007
Quarkonia States

$X(3872)$ *vs* $X(3875)$

Yu.S.Kalashnikova
Institute of Theoretical and Experimental Physics,
117218, B.Cheremushkinskaya 25, Moscow, Russia

Abstract

The Flattè analysis is presented of the data on the near-threshold enhancement in the $D^0\bar{D}^0\pi^0$ mode, observed recently by the Belle Collaboration in the $B \to KD^0\bar{D}^0\pi^0$ decay. The Flatte parametrization is constrained with the data on the $X(3872)$ seen in the $\pi^+\pi^- J/\psi$ and $\pi^+\pi^-\pi^0 J/\psi$ modes. It is shown that the new Belle state can be understood as a manifestation of the $X(3872)$ resonance, if it is assumed that the $X(3872)$ is of a dynamical origin, being a virtual state in the $D^0 D^{*0}$ channel.

1 Introduction

The renaissance in charmonium spectroscopy has come with the discovery of the $X(3872)$ state [1)], the first one of a family of unexpected states found at B-factories. Most probable quantum numbers of the X is 1^{++}, though 2^{-+} is

not excluded, and, for both assignements, the mass is too low in comparison with quark model predictions. The discovery mode of the X is $J/\psi\pi^+\pi^-$, which, later on, was shown to come from $J/\psi\rho$, and the state was also seen in the $J/\psi\pi^+\pi^-\pi^0$ ($J/\psi\omega$) and $J/\psi\gamma$ modes [2], so considerable isospin violation is present.

The world average [3] for the mass of the $X(3872)$ is 3871.2 ± 0.5 MeV, very close to the $D\bar{D}^*$ threshold:

$$M_X - M(D^0\bar{D}^{*0}) = -0.6 \pm 0.6 \text{ MeV}. \quad (1)$$

Such threshold affinity has prompted the molecular interpretation of the X. Indeed, it was suggested many years ago [4] that the one–pion exchange could be responsible for the formation of near–threshold states in the D–meson systems. It was shown that in the 1^{++} $D\bar{D}^*$ system one–pion exchange is attractive, and calculations [5], [6] confirm this: with quite reasonable value of the $DD^*\pi$ coupling, the bound state appears in full analogy to the deuteron. Isospin violation appears in the molecular model due to an 8 MeV difference between the $D^0\bar{D}^{*0}$ and D^+D^{*-} thresholds.

One of competing models for the $X(3872)$ is the four–quark model [7]. In this model, two different neutral states exist, X_u with quark content $[cu][\bar{c}\bar{u}]$ and X_d with quark content $[cd][\bar{c}\bar{d}]$, and with masses differing by few MeV. Support of this model comes from new data reported by Belle [8] on the near–threshold enhancement in the $D^0\bar{D}^0\pi^0$ mode with the mass

$$M = 3875.2 \pm 0.7^{+0.3}_{-1.6} \pm 0.8 \text{ MeV}. \quad (2)$$

BaBar Collaboration [9] has observed the enhancement in the $D^0\bar{D}^0\pi^0$ *and* in the $D^0\bar{D}^0\gamma$ modes, with the mass of

$$M = 3875.6 \pm 0.7^{+1.4}_{-1.5} \pm 0.8 \text{ MeV}, \quad (3)$$

confirming the Belle result [8]. Thus the possibility should be considered seriously of the presence of two charmonium-like states, $X(3872)$ and $X(3875)$, surprisingly close to each other and to the $D^0\bar{D}^{*0}$ threshold, as required by the four–quark model.

Here, less exotic possibility is discussed, of a near–threshold peak in the $D^0\bar{D}^{*0}$ mass distribution being a consequence of strong coupling of the $X(3872)$ to the $D^0\bar{D}^{*0}$ continuum.

2 The Model

The data [8] on the decay $B \to K D^0 \bar{D}^0 \pi^0$ in the near–threshold region are analysed together with the data on the $\pi^+\pi^- J/\psi$ decay modes of the $X(3872)$ in the framework of Flattè-like parametrization of the near–threshold observables. The main assumtions are;

- The quantum numbers of the $X(3872)$ are 1^{++}
- $\pi^+\pi^- J/\psi$ ($\rho J/\psi$) and $\pi^+\pi^-\pi^0 J/\psi$ ($\omega J/\psi$) are the main decay modes of the $X(3872)$
- The underlying strong interaction conserves isospin, and all the isospin violation comes from the mass difference between charged and neutral $D\bar{D}^*$ thresholds. As no charged partners of the X is observed, we assume that the strong attraction takes place in the isosinglet $D\bar{D}^*$ channel

The $B \to K D^0 \bar{D}^0 \pi^0$ differential rate is parametrised as

$$\frac{dBr(B \to K D^0 \bar{D}^0 \pi^0)}{dE} = 0.62 \mathcal{B} \frac{1}{2\pi} \frac{g k_1}{|D(E)|^2}, \tag{4}$$

and $B \to K \pi^+ \pi^- J/\psi$ rate is given by

$$\frac{dBr(B \to K \pi^+ \pi^- J/\psi)}{dE} = \mathcal{B} \frac{1}{2\pi} \frac{\Gamma_{\pi^+\pi^- J/\psi}(E)}{|D(E)|^2}, \tag{5}$$

where

$$D(E) = \begin{cases} E - E_f - \frac{g\kappa_1}{2} - \frac{g\kappa_2}{2} + i\frac{\Gamma(E)}{2}, & E < 0 \\ E - E_f - \frac{g\kappa_2}{2} + i\left(\frac{gk_1}{2} + \frac{\Gamma(E)}{2}\right), & 0 < E < \delta \\ E - E_f + i\left(\frac{gk_1}{2} + \frac{gk_2}{2} + \frac{\Gamma(E)}{2}\right), & E > \delta \end{cases} \tag{6}$$

and

$$\delta = M(D^+ D^{*-}) - M(D^0 \bar{D}^{*0}) = 7.6 \text{ MeV},$$

$$k_1 = \sqrt{2\mu_1 E}, \quad \kappa_1 = \sqrt{-2\mu_1 E}, \quad k_2 = \sqrt{2\mu_2 (E-\delta)}, \quad \kappa_2 = \sqrt{2\mu_2(\delta - E)}.$$

Here μ_1 and μ_2 are the reduced masses in the $D^0\bar{D}^{*0}$ and D^+D^{*-} channels, respectively, and the energy E is defined relative to the $D^0\bar{D}^{*0}$ threshold. The

quantities E_f and g are Flattè parameters, and the factor $\mathcal{B}$ absorbes the short–ranged dynamics of the weak $B \to K$ transition. The coefficient 0.62 in Eq. (4) corresponds to the branching fraction [3)]

$$Br(D^{*0} \to D^0\pi^0) = (61.9 \pm 2.9)\%. \tag{7}$$

The term $i\Gamma/2$ in Eq. (6) accounts for non-$D\bar{D}^*$ modes:

$$\Gamma(E) = \Gamma_{\rho J/\psi}(E) + \Gamma_{\omega J/\psi}(E), \tag{8}$$

where $\Gamma_{\rho J/\psi}(E)$ and $\Gamma_{\omega J/\psi}(E)$ are calculated taking into account finite widths of ρ– and ω–mesons:

$$\Gamma_{\rho J/\psi(\omega J/\psi)}(E) = f_{\rho(\omega)} \int_{2m_\pi(3m_\pi)}^{M-m_{J/\psi}} \frac{dm}{2\pi} \frac{q(m)\Gamma_{\rho(\omega)}}{(m - m_{\rho(\omega)})^2 + \Gamma^2_{\rho(\omega)}/4}, \tag{9}$$

with f_ρ and f_ω being effective couplings, and q being the c.m. dipion/tripion momentum ($M = E + M(D^0\bar{D}^{*0})$).

The details of Flattè parametrization Eqs (4), (5) can be found in [10)].

3 Results

The data used in the analysis are taken from [1)] and [11)] ($\pi^+\pi^- J/\psi$ mode) and from [12)] ($D^0\bar{D}^0\pi^0$ mode). The analysis is performed for the data from charged B–meson decay mode only, as the signal from neutral B–meson decay is much less pronounced in all data sets. The ratio f_ρ/f_ω is constrained from the observed ratio of branching fractions [2)]

$$\frac{Br(X \to \pi^+\pi^-\pi^0 J/\psi)}{Br(X \to \pi^+\pi^- J/\psi)} = 1.0 \pm 0.4 \pm 0.3, \tag{10}$$

For the $D^0\bar{D}^0\pi^0$ data two different assumptions on the background were used. Namely, the combinatorial background was subtracted, and the rest of the background was taken as unrelated to the $D^0\bar{D}^{*0}$ mode (case A), and as completely due to the $D^0\bar{D}^{*0}$ mode (case B). With these assumptions, the background was evaluated from the Belle data off–peak.

The fit to the $\pi^+\pi^- J/\psi$ data alone requires a vanishing value of the $D\bar{D}^*$ coupling constant, $g = 0$, so that such solution cannot accommodate the $D^0\bar{D}^0\pi^0$ enhancement as a related phenomenon. Generally, a combined fit can

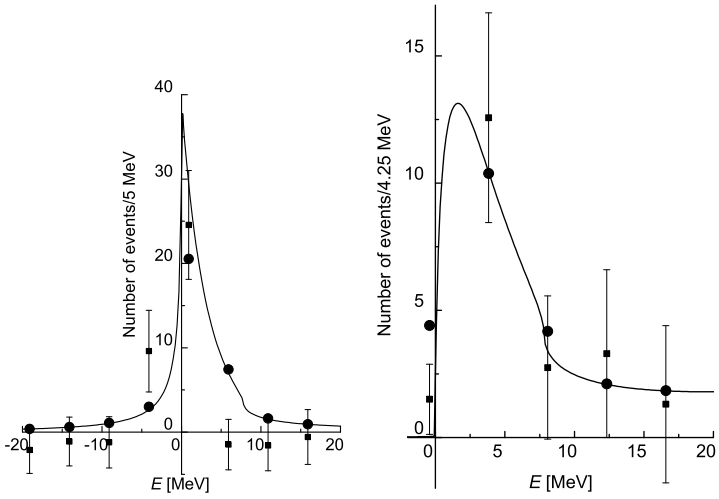

Figure 1: *Left: Fit to the differential rate for the $\pi^+\pi^- J/\psi$ channel measured by Belle* [1)]. *Right: Fit for the differential rate for the $D^0\bar{D}^0\pi^0$ channel measured by Belle* [12)] *using prescription A for the background. The distributions integrated over the bins are shown in each panel as filled dots, experimental data as filled squares with error bars.*

be achieved only if the $\pi^+\pi^- J/\psi$ distribution is peaked *exactly* at the $D^0\bar{D}^{*0}$ threshold, with the peak width (defined as the width at the peak half–height) close to the upper limits given by the experiment (2.3 MeV for Belle data, and 4.1 MeV for BaBar data). The values of the $D\bar{D}^*$ coupling constant g were found to be of the order of magnitude or larger than 0.3. With such values of g, the fits exhibit the scaling behaviour: they remain stable under the transformation

$$g \to \lambda g, \quad E_f \to \lambda E_f, \quad f_\rho \to \lambda f_\rho, \quad f_\omega \to \lambda f_\omega, \quad \mathcal{B} \to \lambda \mathcal{B}. \tag{11}$$

The representative example of our results is shown at Fig. 1 where the distributions for $\pi^+\pi^- J/\psi$ and $D^0\bar{D}^0\pi^0$ modes calculated for the case A are shown, together with $\pi^+\pi^- J/\psi$ distributions integrated over the 5 MeV bins, as in Refs [1)], and the $D^0\bar{D}^0\pi^0$ distributions integrated over the 4.25 MeV bins, as

in Ref. [12]. The corresponding set of Flattè parameters is

$$g = 0.3, \quad E_f = -11MeV, \quad \mathcal{B} = 1.1 \cdot 10^{-3}, \quad f_\rho = 0.007, \quad f_\omega = 0.036. \qquad (12)$$

The real part of the scattering length in the $D^0\bar{D}^{*0}$ channel in all the fits appears to be large and negative, and the imaginary part is much smaller. For example, the fit given by the set of parameters (12) yields the scattering length

$$a = (-3.98 - i0.46) \text{ fm}. \qquad (13)$$

This, together with the cusp in the $\pi^+\pi^- J/\psi$ mass distribution, signals the presence of a virtual state in the $D^0\bar{D}^{*0}$ channel. A large scattering length explains naturally the scaling behaviour of the Flattè parameters. Such kind of scaling was described in Ref. [13]: the scaling behaviour occurs if the scattering length approximation is operative. Indeed, scaling behaviour of the differential rates (4)–(5) takes place if it is possible to neglect the energy E in the expression (6) for the Flattè denominator $D(E)$. If the energy dependence of the charged D^+D^{*-} and non-$D\bar{D}^*$ channel contributions is neglected as well, this corresponds to the scattering length approximation.

4 Discussion

Both large scattering length and the scaling behaviour of the $D\bar{D}^*$ amplitude are consequences of the large value of the coupling constant of the state to the $D\bar{D}^*$ channel. As shown in Ref. [14], large coupling of the near–threshold state to the continuum channel points at a large dynamical $D\bar{D}^*$ component in the wavefunction. However, with negative scattering length, the X in our analysis appears to be a virtual state, not a bound one.

It is repeatedly claimed (see e.g. [15]) that large ratio of branching fractions,

$$\frac{Br(X \to D^0\bar{D}^0\pi^0)}{Br(X \to \pi^+\pi^- J/\psi)} \approx 9.7 \pm 3.4, \qquad (14)$$

following from the data [1], [11], [8] and [9], contradicts the molecular assignement for the X. This is based on a very simple observation, quantified in [6]: the bound–state decay into $D^0\bar{D}^0\pi^0$ occurs via $D^{*0} \to D^0\pi^0$ decay, and the corresponding rate is small because of tiny $D^{*0} \to D^0\pi^0$ width (about 40 keV). On the contrary, the phase space available for the $\pi^+\pi^- J/\psi$ mode is large.

While this is indeed the case for a bound–state decay, in B-decay the suppression is more moderate, as the $D^0\bar{D}^{*0}$ continuum provides the main contribution to the $D^0\bar{D}^0\pi^0$ rate. In the case of a virtual state it is much larger than for a bound state [10]. So the large ratio (14) tells that the X is a virtual state, similar to the $^1S_0$ nucleon–nucleon state rather than the $^3S_1$ deuteron bound state: the attraction in the $D^0\bar{D}^{*0}$ is strong, but not strong enough to form a bound state.

For a virtual state the $\pi^+\pi^- J/\psi$ line–shape differs drastically from the one given by a simple Breit–Wigner form: it displays a cusp with a width close to the limits imposed by the data analysis. Only considerable improvement in the experimental resolution could confirm or rule out this line–shape. In the latter case the scenario of two unrelated states, $X(3872)$ and $X(3875)$, would be quite plausible.

5 Acknowledgements

This work was supported by the Federal Agency for Atomic Energy of Russian Federation and by grants NSh-843.2006.2, DFG-436 RUS 113/820/0-1(R), RFFI-05-02-04012-NNIOa.

References

1. S. K. Choi *et al.* [Belle Collaboration], Phys. Rev. Lett. 91, 262001 (2003).
2. K.Abe *et al* [Belle Collaboration] arXiv:hep-ex/0505037
3. W.-M. Yao *et al* (Particle Data Group), J. Phys. G 33, 1 (2006).
4. M.B.Voloshin and L.B.Okun, JETP Lett.23 333 (1976); A.de Rujula, H.Georgi, and S.L.Glashow, Phys. Rev. Lett. 38 317 (1977)
5. N.A.Tornqvist, Phys. Rev. Lett. 67 556 (1991);
6. E.S.Swanson, Phys. Lett. B558 189 (2004)
7. L. Maiani, F. Piccinini, A.D. Polosa, V. Riquer, Phys.Rev. D71 014028L (2005); l. Maiani, A.D. Polosa, V. Riquer, arXiv:0707.3354.
8. G. Gokhroo *et al.* [Belle Collaboration], Phys. Rev. Lett. 97, 162002 (2006).

9. P. Grenier, *Charm and charmonium spectroscopy at B-factories*, Moriond QCD 2007, March 17th-24th.

10. C.Hanhart , Yu.S.Kalashnikova, A.E.Kudryavtsev, A.V.Nefediev, Phys. Rev. D76 034007 (2007).

11. B. Aubert *et al.* [BaBar Collaboration], Phys. Rev. D 73, 011101 (2006).

12. G. Majumder, http://belle.kek.jp/belle/talks/ICHEP2006/Majumber.ppt.

13. V. Baru, J. Haidenbauer, C. Hanhart, A. Kudryavtsev, and Ulf-G. Meißner, Eur. Phys. J. A **23**, 503 (2005).

14. V. Baru *et al*, Phys. Lett. B **586**, 53 (2004).

15. E. S. Swanson, Phys. Rep. **429**, 243 (2006).

Frascati Physics Series Vol. XLVI (2007), pp. 847–855
HADRON07: XII Int. Conf. on Hadron Spectroscopy – Frascati, October 8-13, 2007
Quarkonia States

SEARCH FOR THE RADIAL EXCITED STATES OF CHARMONIUM IN EXPERIMENTS USING LOW ENERGY ANTIPROTON BEAMS

M.Yu. Barabanov, A.S. Vodopianov, V.Kh. Dodokhov, V.A. Babkin
JINR, Veksler and Baldin Laboratory of High Energies
S.N. Chukanov, B.K. Nartov
Sobolev Institute of Mathematics, Siberian Branch of Russian Academy of Science
R.M.Yamaleev
JINR, Laboratory of Information Technologies

Abstract

The calculation of the spectrum of the radial excited states of charmonium in the relativistic spherical symmetric top for decay products was carried out. Using the integral formalism for hadron resonance decay products the widths of these states have been calculated. The values of masses and widths of charmonium are in good agreement with experimental data. Six new radial excited states of charmonium in mass region over $D\bar{D}$-threshold equals 3.73 GeV/c were predicted. Four of them (two scalar and two vector states) were experimentally revealed. The possibility of usage of antiproton beams with momentum ranging from 1 GeV/c to 15 GeV/c for studying of charmonium spectroscopy especially over $D\bar{D}$- threshold is discussed. The advantage of antiproton beams consists that in antiproton-proton annihilation the intensive appearance of particle-antiparticle pares is observed. This fact allows carry out spectroscopic researches with good statistics and high accuracy. Hence, the possibility of measuring of masses and widths of scalar and vector charmonium states with high accuracy is emerging.

1 Introduction

The fundamental understanding of strong interactions in the terms of QCD was greatly stimulated by discovery of the vector state of charmonium J/Ψ in 1974. Still the charmonium system is considered a powerful tool for careful understanding the nature of strong interaction. Nowadays the set of mesons and the baryons consisting of light quarks (u, d, s) is revealed. More then 100 states with widths ranging from 100 MeV to 400 MeV are known to exist in the mass interval from 1 GeV/c^2 to 2.5 GeV/c^2 [1]. The application of non-perturbative quantum chromodynamics methods are required for calculation of mass spectrum. The strong coupling constant α_s is large (> 0.7) (see fig.1)), and relativistic effects are significant [2], [3].

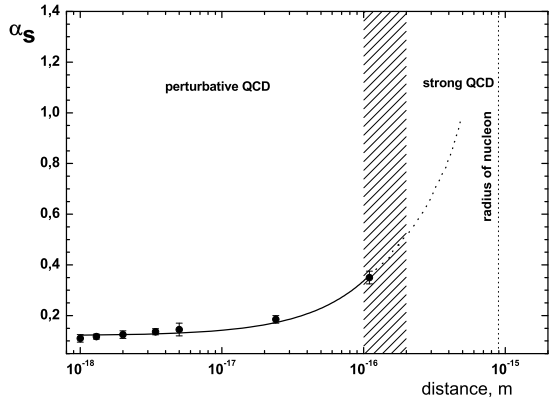

Figure 1: *Coupling strength constant α_s between two quarks as a function of their distance*

In this paper the system consisting of charmed quark and charmed anti-quark ($c\bar{c}$) - charmonium is considered. Until recently only few radial excited scalar and vector states of charmonium in the range of masses varying from 3 GeV/c^2 to 4.5 GeV/c^2 were revealed. Unlike light mesons and baryons they represent the narrow states with small widths and can be easily revealed in experiment. The strong coupling constant ($\alpha_s \approx 0.3$) is not too large, and relativistic effects are considered manageable ($< v^2/c^2 \approx 0.2 >$) [2], [3].

The possibility for study different scalar and vector charmonium states arises using low energy antiproton beams with the momentum ranging from 1 GeV/c to 15 GeV/c. The charmonium states with different quantum numbers

can be directly formed in proton-antiproton annihilation process. The precision of mass and width measurements of these states depends on the quality of antiproton beam [2), 3)]. It becomes possible extract the information about excited states of charmonium in such experiments which can be extremely useful for studies of the strong coupling nature.

The charmonium system has been investigated in great detail first in e^+e^- reactions, and afterwards on a restricted scale, but with high precision, in $p\bar{p}$-annihilations [2), 3)]. Despite these efforts a number of unsolved questions dealing with charmonium remain: radial excited scalar states of charmonium η_c (except the first radial excited state η_c') not found yet, h_c-state is poorly studied; properties of radial excited vector states of charmonium Ψ are poorly known; only few partial widths of ${}_3P^J$-states are known; little is known on charmonium states above the $D\bar{D}$-threshold.

In addition some of the measured widths in charmonium decays don't fit any theoretical scheme [2), 3)]. Therefore the additional experimental check or reconsideration of the according theoretical models need to be made [2), 3)]. More data on other decay modes and branch ratios are desirable in order to clarify the situation.

Of particular interest are the following decays of charmonium: $\Psi \to \rho\pi$, $\Psi \to$ baryon-antibarion, $\eta_c \to \rho\pi$, $\eta_c \to$ baryon-antybaryon (hadron helicity non-conserving processes); $\Psi \to \pi^+\pi^-$, $\omega\pi^0$, $\rho\pi$ (G-parity violation decays); $\Psi' \to \gamma\pi^0$, η,... (radiative decays); $\chi_{cJ} \to \rho\rho$, $\phi\phi$,...

Some of these decay channels were considered by our group. Based on the hadron resonance conception [4)] and relativistic spherical symmetric top model for decay products [5), 6)] we have calculated charmonium mass spectrum. Our calculations keep in with the already established radial excited states of charmonium (scalar and vector states). Six new scalar and vector states above the $D\bar{D}$-threshold were predicted. The charmonium mass spectrum up to bottom meson mass domain was investigated. To be sure that the predicted states can really exist and can be revealed in experiment, it was proposed to calculate their widths by using integral formalism for decay of hadronic resonance [7)] in analogy with α-decay theory [8)] and decay of resonant states in continuous spectrum of deformed nuclei [9)]. The results for the widths of the charmonium states are in good agreement with the experimentally established fact that charmonies are narrow states with the widths of the order of several tens MeV.

2 The relativistic spherical symmetric top model for the resonance decay products

According the papers [5) 6)] the dynamics of decaying resonance system (in this paper the radial excited states of charmonium decaying via the binary channels are considered) is defined with the set of $SU(2)$ groups generators. This group plays the fundamental role in quantization of energy (momentum) of the considered system. The authors have considered the mathematical aspects of the motion of a spining particle on the spherical surface S^3 embedded in four-dimensional Euclidean space. The radius R of sphere S^3 is a constant. The correspondence with tree-dimension of a real space is archived by transition to spherical surface S^3. The authors have shown, that two sets of generators of $SU(2)$ group define the motion equations of particles on the three-dimensional sphere S^3 in four-dimensional Euclidean space with the one-half spin. Later it was generalized for the particles with a spin equals unit [5) 6)]. In this approach any geometrical point allocated on sphere associates with the relativistic spherical symmetric top. The Hamiltonian of the considered system is formulated with the set of $SU(2)$ group generators. The particles formed over the resonance decay are described as a collection of two tops in the same quantum state, but differ with their mass. In this approach the collection of the definite resonance states with the same quantum numbers is interpreted as the radial excited states of the quantum system (the charmonium system in our case). Two decay products are only the objects to consider. There is no translational energy of the decay products, but the orbital kinetic energy is relevant for each of them. The spin rotational energy is described with the relativistic spherical symmetric top. Thus the resonance decay products are described as a collection of two tops in the same rotational state [5) 6)]. Therefore the decay channels may be joint to the groups with the properties of quantum objects. Inside each group the decay products momenta are quantized relatively characteristic length R. Thus we can consider the set of resonances as the states of relativistic quantum system.

Let us define the set of generators of SO(4) group

$$\vec{M} = [\vec{r}, \vec{p}], \vec{N} = R\vec{p} + \vec{r}\,(\vec{r}, \vec{p})\,/R, \tag{1}$$

where $\vec{r}$ and $\vec{p}$ - coordinate and momentum operators accordingly, $\vec{M}$ - angular momentum operator; $\vec{N}$ - dilatation operator, which defined on the sphere S^3 of the radius R.

The linear combinations of these orthonormal operators

$$\vec{\mu}_{\pm} = \left(\vec{M} \pm \vec{N}\right) \tag{2}$$

contribute two sets of generators of the $SU(2)$ group. Thus the $SU(2)$ group generates the action on a three-dimensional sphere S^3. This action consists of the translation with whirling around the direction of translation.

We get the Hamiltonian:

$$H = \frac{1}{2mR^2}\left\{2\hbar + (\vec{\mu}_{\pm}, \vec{\sigma})\right\}\left\{2\hbar + (\vec{\mu}_{\pm}, \vec{\sigma})\right\}, \tag{3}$$

where $\vec{\sigma}$ - is the spin operator, $\hbar$ - Plank constant, m - mass of the top. When $R \to \infty$ this Hamiltonian tends to the Pauli operator for the free particle motion:

$$R \to \infty : \ \vec{\mu}_{\pm}/R = \left(\vec{M} \pm \vec{N}\right)/R \to \pm\vec{p}$$

$$H = \frac{1}{2mR^2}\left\{2\hbar + (\vec{\mu}_{\pm}, \vec{\sigma})\right\}\left\{2\hbar + (\vec{\mu}_{\pm}, \vec{\sigma})\right\} \to \frac{1}{2m}\left(\vec{p}, \vec{\sigma}\right)^2. \tag{4}$$

The spectrum of the Hamiltonian is:

$$H\Psi_n = \frac{\hbar^2}{2mR^2}\left(n+1\right)^2\Psi_n, \ n = 0, 1, 2... \tag{5}$$

The wave function $\Psi_n = |LSJM_J\rangle$ was taken as eigenfunction of whole momentum $\vec{J}^2 = \left(\vec{\mu}_{\pm} + \vec{\sigma}\right)^2$ of the classical top.

In the framework of this approach in relativistic case the Hamiltonian of decaying resonance is defined with the equation:

$$H = \sqrt{m_a^2 + \frac{1}{R^2}\left((\vec{\mu}_{\pm}, \vec{\sigma}) + 2\hbar\right)^2} + +\sqrt{m_b^2 + \frac{1}{R^2}\left((\vec{\mu}_{\pm}, \vec{\sigma}) + 2\hbar\right)^2}, \tag{6}$$

where m_a and m_b are the masses of resonance decay products.

The spectrum of the Hamiltonian is:

$$E = \sqrt{m_a^2 + \frac{\hbar^2\left(n+1\right)^2}{R^2}} + \sqrt{m_b^2 + \frac{\hbar^2\left(n+1\right)^2}{R^2}}, n = 0, 1, 2... \tag{7}$$

Finally, the formula for the radial excited states of resonances can be written in the form:

$$E = \sqrt{m_a^2 + P_n^2} + \sqrt{m_b^2 + P_n^2} = \sqrt{m_a^2 + \left[n \cdot P_0\right]^2} + \sqrt{m_b^2 + \left[n \cdot P_0\right]^2} \tag{8}$$

where *Resonance* $\rightarrow a + b$ - is the binary decay channel of a resonance for two particles a and b (we used the system in which $\hbar = c = 1$), m_a, m_b - the masses of the decay products, P_0 - is the basic momentum. The momentum of relative motion of the resonance decay products P_n (particles a and b in a centre-of-mass system of decaying resonance) is quantized relatively P_0.

Table 1: *The spectrum of radial excited scalar states of charmonium and their widths. As basic there were taken two channels* $\pi^{\pm} \rightarrow \mu^{\pm}\nu_{\mu} \approx 100\%$ *and* $\Sigma^0 \rightarrow \Lambda\gamma \approx 100\%$.

Charmonium states	Quant. numbers $I^G\left(J^{PC}\right)$	Decay channel	M_{exp} MeV	M_{th} MeV	$\Gamma(M)_{exp}$ MeV	$\Gamma(M)_{th}$ MeV
$\eta_c\,(1S)$	$0^+\left(0^{-+}\right)$	$p\bar{p}$	2980.4±1.2	2974.86	25.5±3.4	18
$\eta_c\,(1S)$	$0^+\left(0^{-+}\right)$	$\rho^{\pm}\pi^{\mp}$	2980.4±1.2	2994.78	25.5±3.4	21
$\eta_c\,(1S)$	$0^+\left(0^{-+}\right)$	$\Sigma^0\bar{\Sigma}^0$	2980.4±1.2	2979.44	17.3±2.5	12
$\eta_c\,(2S)$	$0^+\left(0^{-+}\right)$	$p\bar{p}$	3638±4	3581.30	14±7	27
$\eta_c\,(2S)$	$0^+\left(0^{-+}\right)$	$\rho^{\pm}\pi^{\mp}$	3638±4	3625.00	14±7	20
$\eta_c\,(2S)$	$0^+\left(0^{-+}\right)$	$\Sigma^0\bar{\Sigma}^0$	3638±4	3586.30	14±7	16
$X\,(3940)$	$?^?\left(?^{??}\right)$	$p\bar{p}$	3936±14	3922.56	39±26	56
$X\,(3940)$	$?^?\left(?^{??}\right)$	$\rho^{\pm}\pi^{\mp}$	3936±14	3967.28	39±26	68
$X\,(3940)$	$?^?\left(?^{??}\right)$	$\Sigma^0\bar{\Sigma}^0$	3936±14	3930.82	39±26	46
$Y\,(4260)$	$?^?\left(?^{??}\right)$	$p\bar{p}$	4295±10	4305.18	133±26	94
$Y\,(4260)$	$?^?\left(?^{??}\right)$	$\rho^{\pm}\pi^{\mp}$	4295±10	4312.88	133±26	112
$Y\,(4260)$	$?^?\left(?^{??}\right)$	$\Sigma^0\bar{\Sigma}^0$	4259±8	4294.14	88±23	76

The authors have calculated mass spectrum of the radial excited states of charmonium. The basic momentum P_0 was taken from that decay channels which occur with $\approx 100\%$ probability. The masses of the decaying particles in these channels are known with high precision. Moreover, the charmonium states decay through the channel contains one (two) of these particles. Only several channels have $\approx 100\%$ decay probability [1)]. Most interesting are the following decay channels: $\pi^{\pm} \rightarrow \mu^{\pm}\nu_{\mu}, \Sigma^0 \rightarrow \Lambda\gamma$ (from these decay channels the basic momentum P_0 was taken).

We have considered the following decay channels of charmonium from the cited above $\Psi \rightarrow \pi\rho$, $\Psi \rightarrow \Sigma^0\bar{\Sigma}^0$; $\eta_c \rightarrow \pi\rho$, $\eta_c \rightarrow \Sigma^0\bar{\Sigma}^0$ (hadron helicity non-conserving process). The results of calculation are performed in Table 1 for the scalar and in Table 2 for the vector radial excited states of charmonium.

Application of the integral formalism for calculation of the widths of scalar and vector charmonium states gives the results which are in good agreement

Table 2: *The spectrum of radial excited vector states of charmonium and their widths. As basic there were taken two channels* $\pi^{\pm} \to \mu^{\pm}\nu_{\mu} \approx 100\%$ *and* $\Sigma^0 \to \Lambda\gamma \approx 100\%$.

Charmonium states	Quant. numbers $I^G\left(J^{PC}\right)$	Decay channel	M_{exp} MeV	M_{th} MeV	$\Gamma(M)_{exp}$ MeV	$\Gamma(M)_{th}$ MeV
$J/\Psi\,(1S)$	$0^-\left(1^{--}\right)$	$p\bar{p}$	3096.95±0.1	3092.50	0.099±0.012	0.096
$J/\Psi\,(1S)$	$0^-\left(1^{--}\right)$	$p\bar{p}$	3096.95±0.1	3102.40	0.099±0.012	0.096
$\Psi\,(2S)$	$0^-\left(1^{--}\right)$	$\rho^{\pm}\pi^{\mp}$	3685.98±0.09	3681.95	0.306±0.036	0.328
$\Psi\,(2S)$	$0^-\left(1^{--}\right)$	$\Sigma^0\bar{\Sigma^0}$	3685.98±0.09	3682.05	0.306±0.036	0.302
$\Psi\,(3770)$	$0^-\left(1^{--}\right)$	$p\bar{p}$	3770.0±2.4	3776.64	25.3±2.9	27
$\Psi\,(3770)$	$0^-\left(1^{--}\right)$	$p\bar{p}$	3770.0±2.4	3765.25	25.3±2.9	27
$\Psi\,(3836)$	$0^-\left(2^{--}\right)$	$\rho^{\pm}\pi^{\mp}$	3836±13	3853.25	24.0±5.0	0.48
$\Psi\,(3836)$	$0^-\left(2^{--}\right)$	$\Sigma^0\bar{\Sigma^0}$	3836±13	3813.63	24.0±5.0	0.41
$\Psi\,(4040)$	$0^-\left(1^{--}\right)$	$p\bar{p}$	4039±1	4045.80	52±10	56
$\Psi\,(4040)$	$0^-\left(1^{--}\right)$	$\rho^{\pm}\pi^{\mp}$	4039±1	4025.18	52±10	64
$\Psi\,(4040)$	$0^-\left(1^{--}\right)$	$\Sigma^0\bar{\Sigma^0}$	4039±1	4050.01	52±10	51
$\Psi\,(4160)$	$0^-\left(1^{--}\right)$	$p\bar{p}$	4153±3	4157.41	78±20	81
$\Psi\,(4160)$	$0^-\left(1^{--}\right)$	$\rho^{\pm}\pi^{\mp}$	4153±3	4140.10	78±20	92
$\Psi\,(4160)$	$0^-\left(1^{--}\right)$	$\Sigma^0\bar{\Sigma^0}$	4153±3	4171.24	78±20	68
$Y\,(4350)$	$0^-\left(1^{--}\right)$	$p\bar{p}$	4354±16	4348.12	106±19	110
$Y\,(4350)$	$0^-\left(1^{--}\right)$	$\rho^{\pm}\pi^{\mp}$	4354±16	4370.07	106±19	122
$Y\,(4350)$	$0^-\left(1^{--}\right)$	$\Sigma^0\bar{\Sigma^0}$	4354±16	4294.14	106±19	87
$\Psi\,(4415)$	$0^-\left(1^{--}\right)$	$p\bar{p}$	4421±4	4423.52	43±15	48
$\Psi\,(4415)$	$0^-\left(1^{--}\right)$	$\rho^{\pm}\pi^{\mp}$	4421±4	4428.34	43±15	59
$\Psi\,(4415)$	$0^-\left(1^{--}\right)$	$\Sigma^0\bar{\Sigma^0}$	4421±4	4418.22	43±15	38
$\Psi\,(4540)$	$?^?\left(?^{??}\right)$	$p\bar{p}$	—	4529.05	—	78
$\Psi\,(4540)$	$?^?\left(?^{??}\right)$	$\rho^{\pm}\pi^{\mp}$	—	4543.97	—	92
$\Psi\,(4540)$	$?^?\left(?^{??}\right)$	$\Sigma^0\bar{\Sigma^0}$	—	4544.57	—	70
$\Psi\,(4660)$	$?^?\left(?^{??}\right)$	$p\bar{p}$	4664±11	4679.60	48±15	106
$\Psi\,(4660)$	$?^?\left(?^{??}\right)$	$\rho^{\pm}\pi^{\mp}$	4664±11	4659.76	48±15	118
$\Psi\,(4660)$	$?^?\left(?^{??}\right)$	$\Sigma^0\bar{\Sigma^0}$	4664±11	4671.87	48±15	89
$\Psi\,(5060)$	$?^?\left(?^{??}\right)$	$p\bar{p}$	—	5059.92	—	108
$\Psi\,(5060)$	$?^?\left(?^{??}\right)$	$\rho^{\pm}\pi^{\mp}$	—	5066.28	—	126
$\Psi\,(5060)$	$?^?\left(?^{??}\right)$	$\Sigma^0\bar{\Sigma^0}$		5060.78	—	92

with the experimental data. Note that the values of partial widths in tables must be scaled for the branch ratio of the according channel. The calculated values of the widths one can also find in the Table 1 and Table 2.

3 Conclusion

The approach for calculation of mass spectrum of resonance radial excited states was proposed. In the framework of this approach the existing experimental data were described with high accuracy. The possibility of prediction for the new radial excited states of resonances appears.

The identical resonance decay channels can be joint into the groups characterized with parameter of dimension of length R_0 or, in other words, with basic momentum P_0. Inside each group these channels are classified by the quantum numbers $R_0 = \hbar/p_0$ and $n = p_n/p_0$. The characteristic length in the relativistic top model corresponds to a "predissociation" radius equivalent to the range of the potential determined the resonance decay.

The scalar and vector charmonium states have been analyzed. The possibility of the existence of their radial excited states was pointed. Two scalar and two vector radial excited states of charmonium were experimentally verified. Thus, there arises the possibility for the prediction of new radial excited charmonium states with quantum number determined beforehand.

The results of the researches point to the fact that charmonium spectroscopy studies are perspective in experiments using low energy antiproton beams with the momentum ranging from 1 GeV/c to 15 Gev/c.

References

1. Review of Particle Physics, Journal of Physics G: Nuclear and Particle Physics **33**, 1 (2006).
2. Letter of Intent: Construction of Glue/Charm-Factory at GSI, 1 (1999)
3. HESR-project, Contributions to the Scientific Case, 193 (1999)
4. F.A. Gareev *et al* EPAT, **27**, 97 (1996).
5. J. Keller *et al*, Advances in Applied Clifford Algebras **8**, 235 (1998).
6. J. Keller *et al*, Advances in Applied Clifford Algebras **8**, 255 (1998).

7. A.I. Baz *et al*, Scattering, reactions and decays in non-relativistic quantum mechanics, M.:Science, 1971.

8. S.G. Kadmenskiy *et al*, Alpha-decay and analogous nuclear reactions, M.: Energoatomizdat, 1985.

9. J.M. Bang *et al*, Nucl.Phys A **261**, 59 (1976).

Frascati Physics Series Vol. XLVI (2007), pp. 857-864
HADRON07: XII Int. Conf. on Hadron Spectroscopy – Frascati, October 8-13, 2007
Quarkonia States

SEARCHES FOR NEW PHYSICS IN THE TOP QUARK SAMPLES AT THE CDF EXPERIMENT

Luca Scodellaro for the CDF Collaboration
Instituto de Fisica de Cantabria, Avda Los Castros s/n, Santander, Spain

Abstract

Twelve years after the discovery of the top quark at Fermilab's Tevatron, we are now finally beginning to shed light on this peculiarly massive quark. With 1-1.7 fb^{-1} of integrated luminosity collected by the CDF detector, we are able to probe our knowledge of the top quark physics, and to search for signals of physics beyond the Standard Model. In this paper, we present results of measurements of top quark properties, as well as tests for the production mechanism of the top quark. We also describe CDF latest searches for beyond Standard Model couplings of the top quark. Finally, we present the most recent searches for direct production of new particles in the collected data samples.

1 Introduction

The discovery of the top quark in 1995 [1, 2] completed the third generation of fundamental fermions in the quark sector of the Standard Model (SM). Its

large mass, very close to the electroweak scale, results in a Yukawa coupling to the Higgs boson close to unity, suggesting a special role of the top quark in the electroweak symmetry breaking mechanism.

The CDF experiment studies proton-antiproton collisions produced at the Tevatron collider of Fermilab at a center-of-mass energy of $\sqrt{s} = 1.96$ TeV. The particles produced in the interactions are reconstructed through the CDF detector [3]. At the energies reached by the Tevatron, the top quark is produced mainly in top-antitop pairs via strong interaction. The production cross section predicted by the Standard Model is 6.7 ± 0.8 pb for a top mass of 175 GeV/c^2. Due to its short lifetime, the top quark decays before hadronizing into a W boson and a bottom quark with a branching ratio of almost 100%. The observed final states can therefore be classified according to the successive W decays into leptons or quarks.

The analyzes presented in this paper are based on two distinct samples which amount to an integrated luminosity of about 1-1.7 fb^{-1} . The lepton plus jets sample is collected by requiring one electron or muon with transverse energy $E_T > 20$ GeV, at least four jets with $E_T > 20$ GeV, with at least one of them tagged as coming from a bottom quark hadronization, and missing transverse energy $\not\!\!E_T > 20$ GeV to account for the undetected neutrino from W decay. These requests are aimed to select events where one W boson decays into quarks and the other one decays into leptons. The dilepton sample is selected by requiring two leptons (electrons or muons) with transverse energy $E_T > 20$ GeV, two jets with $E_T > 15$ GeV and missing transverse energy $\not\!\!E_T > 25$ GeV. These requests are aimed to select events where both W bosons decay leptonically. The $t\bar{t}$ production cross section has been measured in both samples with different techniques [4, 5]. Good agreement with SM prediction is observed. Sample composition is well understood, allowing for detailed searches for new phenomena.

This paper is organized as follow. In sec.2, we present the results of the measurements of some properties of the top quark and we discuss their implication in the SM. Sec.3 is dedicated to the investigation of the production mechanism of the top quark, while sec.4 describes the searches for beyond SM couplings of the top quark. Finally, in sec.5 we present the results of direct searches for exotic particles production in the top samples.

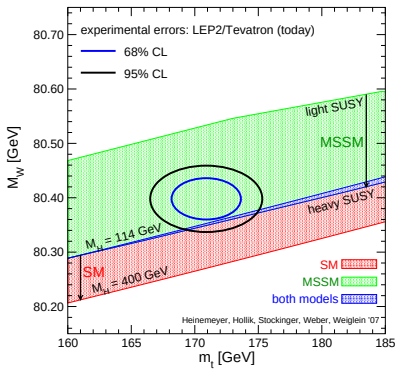

Figure 1: *SM and MSSM Higgs boson mass constraints in the m_t-M_W plane.*

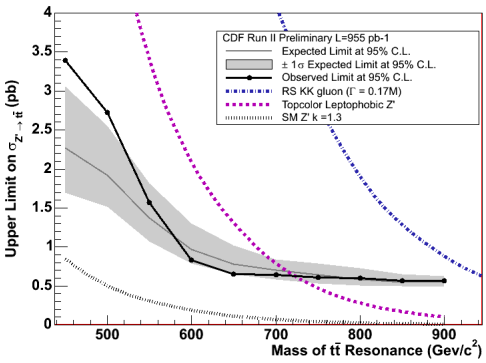

Figure 2: *Upper limits on the production cross section for $Z' \to t\bar{t}$ as a function of the Z' mass.*

2 Top Quark Properties

2.1 Top Quark Mass

The measurement of the top quark mass is a main goal for the Tevatron Run II. It requires to face several challenges such as a full final state reconstruction and a precise measurement of the energies of the jets and of the undetected neutrinos. A big effort has been put by the CDF collaboration to address these issues in the last years, finally leading to the best world measurement of the top mass, $m_t = 172.7 \pm 2.1$ GeV/c^2 [6]. Even without including this result, the most recent Tevatron combination reaches a precision of about 1% on the top mass, $m_t = 170.9 \pm 1.8$ GeV/c^2 [7]. Such a precise measurement of the top mass allows to constrain the mass of the Higgs boson through the radiative corrections to the mass of the W boson. Results are shown in fig.1 both for Standard Model and Minimal Supersymmetric Standard Model. Finally, the fit to electroweak parameter measurements tells us that the mass of the SM Higgs boson is lower than 144 GeV/c^2 at 95% CL.

2.2 Top Quark Charge

Fits to electroweak precision measurements seem to prefer a higher value for the top mass than measured. It has been suggested that the particle observed

at CDF is not the top quark but a fourth generation quark with charge $Q = -4/3$.In order to test this hypothesis, the charge of the observed particle has been reconstructed by looking to its decay products $t \to Wb$. By requiring the W boson to decay leptonically, we can directly measure its charge through the charge of the electron or muon. Indirect information on the charge of the b quark can be extracted from the charged tracks inside its hadronic jet. The observed charge distribution has been tested versus both $Q = +2/3$ ans $Q = -4/3$ hypotheses. Data are consistent with SM top hypothesis and allows to exclude the exotic quark at 87% CL [8].

2.3 Top Quark Width

The lifetime of the top quark in the SM is extremely short, $\tau_t \sim 4 \times 10^{-25}$ s. We can test this prediction by measuring the width Γ_t of the top quark by means of a template fit to the observed top mass spectrum, which is sensitive to the top width. By comparing the fitted value of top width to results from simulated experiments, we set an upper limit on the top quark width $\Gamma_t < 12.7$ GeV, which results on a lower limit on its lifetime $\tau_t > 5.2 \times 10^{-26}$ s [9].

3 Top Production Mechanism

3.1 Fraction of $t\bar{t}$ Events from Gluon Fusion

Top quark pairs in $p\bar{p}$ collisions at the energy reached at the Tevatron are expected to be produced from quark annihilation (85%) and gluon fusion (15%).A measurement of the fraction of $t\bar{t}$ events from gluon fusion can provide a test of perturbative QCD and reveal new mechanisms of production and decay of the top quark.

The CDF experiment measured the fraction $\sigma(gg \to t\bar{t})/\sigma(p\bar{p} \to t\bar{t})$ by using two different approaches. The first measurement relies on the fact that gluons tends to radiate gluons carrying a lower fraction of momentum of the initial parton with respect to quarks, leading to a higher number of tracks with low transverse momentum for $gg \to t\bar{t}$ events than for $q\bar{q} \to t\bar{t}$ production. The correlation between the average low p_T track multiplicity and the mean number of gluons is calibrated in control samples with different content of gluons, and used to build generic templates of low p_T track multiplicity for no-gluon and gluon-rich hypotheses. Fitting the track multiplicity observed

in the top samples by these templates, CDF found $\sigma(gg \to t\bar{t})/\sigma(p\bar{p} \to t\bar{t}) = 0.07 \pm 0.16$ [10].

The second measurement exploits the correlation in the spins of top and antitop, which tends to have the same sign in gluon fusion production and opposite sign in $q\bar{q}$ annihilation events. A neural network is used to discriminate different production processes. Information on the spin correlation is introduced by feeding the network with six angles between the products of the top decays. Data distribution is fitted to the neural network output shapes for simulated $t\bar{t}^{gg}$ and $t\bar{t}^{q\bar{q}}$ events, allowing to set an upper limit on the fraction of $t\bar{t}$ events from gluon fusion of $\sigma(gg \to t\bar{t})/\sigma(p\bar{p} \to t\bar{t}) < 0.33$ at 68% CL [11].

3.2 Forward-Backward Asymmetry

A forward-backward asymmetry in $t\bar{t}$ production can arise from interference in the production diagrams. In the SM, it is computed to be within 4-6% at NLO. The CDF collaboration measured the related charge asymmetry, which is defined as the difference between the top and antitop rapidities and can be measured in the lepton plus jets sample as the rapidity difference between the leptonically and the hadronically decaying tops multiplied by the charge of the electron or muon from W boson decay. The measured asymmetry is $A_{\Delta Y * Q} = 28 \pm 13(\text{stat}) \pm 5(\text{syst})\%$ [12], in agreement with SM NLO prediction.

4 Non-Standard Model Top Couplings

4.1 Right-Handed Weak Coupling

The SM only admits a V-A weak coupling of the top quark to the W boson. This prediction can be tested by measuring the W boson helicity in top decays: in the limit $m_b \to 0$, the b quark has left-handed polarization, forcing the W boson to assume longitudinal (70%) or left-handed (30%) polarization, while the right-handed polarization results to be forbidden.

The helicity of the W boson in top decays is measured in the lepton plus jets sample through the angle θ^* between the charged lepton and the reconstructed top quark in the rest frame of the leptonically decaying W boson. The generic form of the differential cross section can be written as

$$\frac{d\sigma}{d\,\cos\theta^*} \sim f^- \frac{3}{8}(1-\cos\theta^*)^2 + f^0 \frac{3}{4}(1-\cos^2\theta^*) + f^+ \frac{3}{8}(1+\cos\theta^*)^2, \quad (1)$$

where f^0, f^- and f^+ are the fraction of longitudinal, left-handed and right-handed polarized W bosons respectively. Two different fits of the observed $rmcos\theta^*$ distribution have been performed: a binned fit to the theoretical shapes corrected for efficiency and resolution effects, and an unbinned one to templates derived by Monte Carlo simulations. The two approaches give consistent results, and the measured fractions of differently polarized W bosons are in agreement with SM prediction. In particular, when assuming $f^0 = 0.7$ as in the SM, upper limits on the fraction of right-handed polarized W bosons are set at $f^+ < 0.12$ and $f^+ < 0.07$ at 95% CL for the two fitting techniques respectively [13, 14]. Yet another measurement has been realized by looking at the invariant mass of the charged lepton-bottom quark system in leptonically decaying top quarks: $M_{lb} \approx \frac{1}{2}(m_t^2 - M_W^2)\cos\theta^*$. An upper limit of $f^+ < 0.09$ at 95% CL has been derived by this approach [15].

4.2 Flavor Changing Neutral Current

The flavor changing neutral current decay $t \to Zq$ is highly suppressed in the SM, but a number of exotic models allow for a branching ratio up to few percent. CDF has recently performed a search for the process $t\bar{t} \to ZqWb$, where the successive decays $Z \to l^+l^-$ and $W \to q'\bar{q}$ provide a clean signature and a larger branching fraction of events respectively. A kinematic fit was used to reconstruct the events, and the fit χ^2 was used to discriminate background and signal events. No excess over SM expectation has been observed, and an upper limit of $BR(t \to Zq) < 10.6\%$ at 95% CL has been set [16], improving the previous world best limit $BR(t \to Zq) < 13.7\%$ set at LEP.

5 Searches for New Particles

5.1 $t\bar{t}$ Resonances

Top pair resonant production has been searched for in the $t\bar{t}$ invariant mass spectrum. A narrow Z′ resonance ($\Gamma_{Z'} \sim 1.2\% M_{Z'}$) with no interference with the s-channel of top pair production has been used as signal model. No excess over SM prediction has been observed, and upper limits on the production cross section as a function of Z′ mass (see fig.2) have been set at 95% CL [17].

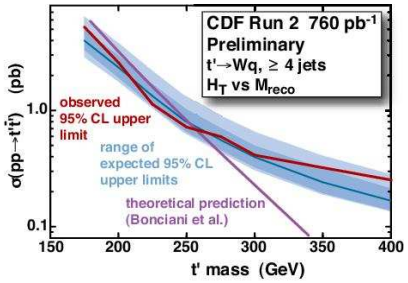

Figure 3: *Upper limits at 95% CL on the production rate for a massive t′ quark as a function of the t′ mass.*

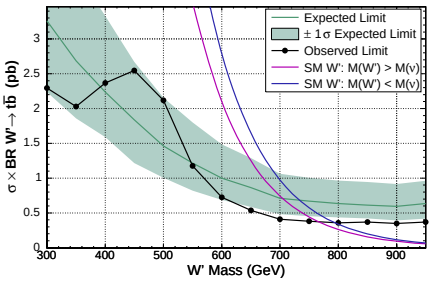

Figure 4: *Observed 95% CL upper limits on $\sigma(p\bar{p} \to W'X) \times BR(W' \to t\bar{b})$ as a function of W′ mass.*

5.2 Search for Massive $t' \to Wb$

A fourth generation of heavy fermions with $M_Z < m_f < M_H$ is compatible with electroweak precision measurement. CDF searched for pair production of massive top-like quarks t′ decaying into a W boson and a quark by looking at two distinct experimental signature: the sum of the transverse energy of all the objects in the event final states, and the reconstructed mass of the candidate t′ quark. Fitting the data to two-dimensional templates for signal and background simulated events, a 95% CL lower limit on the t′ mass has been set at $m_{t'} > 256$ GeV/c^2 [18], as shown in fig.3.

5.3 Heavy W′ Production

A W-like heavy boson decaying into a top and a bottom quarks would mimic the signature of a single top production. CDF searched for a heavy W′ production $q\bar{q}' \to W' \to t\bar{b} \to Wb\bar{b}$ in a sample of events selected by requiring a high-p_T charged lepton, large missing transverse energy but only two jets. No evidence for a W′ boson has been observed in the reconstructed $M_{Wb\bar{b}}$ mass spectrum, and 95% CL upper limits on W′ production and its couplings to fermions have been set [19] (see fig.4).

6 Conclusions

The top quark samples collected by the CDF detector in 1-1.7 fb^{-1} of $p\bar{p}$ collision data at the Tevatron collider have been established and well understood.

Lot of precision measurements and first results in searches for new physics have been achieved. No deviation from SM predictions have been so far observed, but CDF begins to have sensitivity to unexpected top quark properties and new phenomena in its top quark samples.

References

1. F. Abe *et al* (CDF Collaboration), Phys. Rev. Lett. **74**, 2626 (1995).
2. S. Abachi *et al* (D0 Collaboration), Phys. Rev. Lett. **74**, 2632 (1995).
3. D. Acosta *et al* (CDF Collaboration), Phys. Rev. D **71**, 032001 (2005).
4. CDF Collaboration, CDF Public Note 8795, (2007).
5. CDF Collaboration, CDF Public Note 8802, (2007).
6. CDF Collaboration, CDF Public Note 9025, (2007).
7. CDF and D0 Collaboration, arXiv:hep-ex/0703034v1, (2007).
8. CDF Collaboration, CDF Public Note 8967, (2007).
9. CDF Collaboration, CDF Public Note 8953, (2007).
10. CDF Collaboration, CDF Public Note 8724, (2007).
11. CDF Collaboration, CDF Public Note 8811, (2007).
12. CDF Collaboration, CDF Public Note 8963, (2007).
13. CDF Collaboration, CDF Public Note 8938, (2007).
14. CDF Collaboration, CDF Public Note 8971, (2007).
15. A. Abulencia *et al* (CDF Collaboration), Phys. Rev. Lett. **98**, 072001 (2007).
16. CDF Collaboration, CDF Public Note 8888, (2007).
17. CDF Collaboration, CDF Public Note 8675, (2007).
18. CDF Collaboration, CDF Public Note 8495, (2007).
19. CDF Collaboration, CDF Public Note 8747, (2007).

Frascati Physics Series Vol. XLVI (2007), pp. 865
HADRON07: XII Int. Conf. on Hadron Spectroscopy – Frascati, October 8-13, 2007
Quarkonia States

RECENT RESULTS ON D MESON AND ψ (3770) DECAYS AT BES

Gang Rong
Institute of High Energy Physics, Beijing, China

Written contribution not received

Frascati Physics Series Vol. XLVI (2007), pp. 867–873
HADRON07: XII Int. Conf. on Hadron Spectroscopy – Frascati, October 8-13, 2007
Quarkonia States

$\eta_b \to J/\psi\ J/\psi$ DECAY: THE LONG DISTANCE CONTRIBUTIONS

Pietro Santorelli
Dipartimento di Scienze Fisiche, Università "Federico II" and INFN, Napoli, Italy

Abstract

It has been argued long ago that η_b could be observed through the $\eta_b \to J/\psi(\to \mu^+\mu^-)J/\psi(\to \mu^+\mu^-)$ decay chain. Recent calculations indicate that the width of η_b into two J/ψ is almost three order of magnitude smaller than the one into the $D\overline{D^*}$. We study the effects of final state interactions due to the $D\overline{D^*}$ intermediate state on the $J/\psi\ J/\psi$ final state. We find that the inclusion of this contribution may enhance the short distance branching ratio of about two orders of magnitude.

About thirty years after the discovery of the $\Upsilon(1S)$ [1], no pseudoscalar $b\bar{b}$ states have been discovered. The experimental search of η_b has been done at CLEO [2], LEP [3, 4, 5] and CDF by using different decay processes. In the following we will focus our attention on the $\eta_b \to J/\psi\ J/\psi$ decay process to discover η_b and we will report the results obtained in [6].

Starting from the observed large width of $\eta_c \to \phi\phi$ the authors of ref. [7] suggested to detect η_b through the $\eta_b \to J/\psi\ J/\psi$ decay. By using scaling laws with heavy quark masses and the measured branching ratio of $\eta_c \to \phi\phi$ they

obtained [7]

$$\mathcal{B}r[\eta_b \to J/\psi\ J/\psi] \quad = \quad 7 \times 10^{-4\pm1}\,. \tag{1}$$

Following this suggestion, CDF Collaboration has searched for the $\eta_b \to J/\psi\ J/\psi \to 4\mu$ events in the full Run I data sample [8]. In the search window, where a background of 1.8 events is expected, a set of seven events are seen. This result seems confirm the predictions in eq. 1.
Recently, Maltoni and Polosa [9] criticize the scaling procedure adopted in ref. [7] whose validity should reside only in the domain of perturbative QCD. The non perturbative effects, which are dominant in $\eta_c \to \phi\phi$, as a consequence of its large branching fraction, cannot be rescaled by the same factor of the perturbative ones. In ref. [9] the inclusive decay rate of η_b to 4-charm states has been evaluated obtaining

$$\mathcal{B}r[\eta_b \to c\bar{c}c\bar{c}] = 1.8^{+2.3}_{-0.8} \times 10^{-5}\,, \tag{2}$$

where the upper value is even smaller than the lower limit on the corresponding exclusive process $\mathcal{B}r[\eta_b \to J/\psi\ J/\psi]$ estimated in ref. [7].

Jia [10], in the framework of color-singlet model, has performed an explicit calculation of the $\mathcal{B}r[\eta_b \to J/\psi\ J/\psi]$ obtaining

$$\mathcal{B}r[\eta_b \to J/\psi\ J/\psi] \quad \sim \quad (0.5 \div 6.6) \times 10^{-8}\,, \tag{3}$$

which is three order of magnitude smaller than the inclusive result in ref. [9]. The result in eq. 3 indicates that the cluster reported by CDF [8] is extremely unlikely to be associated with η_b. Moreover, the potential of discovering η_b through this decay mode is hopeless even in Tevatron Run II.
The $\eta_b \to D^{(*)}\overline{D^*}$ process has been suggested to detect η_b in [9], where the range $10^{-3} < \mathcal{B}r[\eta_b \to D\overline{D^*}] < 10^{-2}$ was predicted. On the contrary, in [10] was obtained

$$\begin{aligned} \mathcal{B}r[\eta_b \to D\overline{D^*}] \quad &\sim \quad 10^{-5}\,, \\ \mathcal{B}r[\eta_b \to D^*\overline{D^*}] \quad &\sim \quad 10^{-8}\,. \end{aligned} \tag{4}$$

In ref. [6] the following assumptions has been used

a) the short distance branching ratio of $\eta_b \to J/\psi\ J/\psi$ is too small to look at this channel to detect η_b ($\sim 10^{-8}$ [10]);

b) the branching ratio $\mathcal{B}r[\eta_b \to D\overline{D^*}]$ is of the order of 10^{-5} [10] or is in the range $10^{-3} \div 10^{-2}$ [9] [1];

c) the $\mathcal{B}r[\eta_b \to D^*\overline{D^*}]$ is negligible in comparison with $\mathcal{B}r[\eta_b \to D\overline{D^*}]$,

and we will consider the effect of $D\overline{D^*} \to J/\psi\, J/\psi$ rescattering (cfr fig. 1) which should dominate the long distance contribution to the decay under analysis. The dominance of $D\overline{D^*}$ intermediate state is a consequence of the large coupling of $D^{(*)}\overline{D^{(*)}}$ to J/ψ as result from quark model and QCD Sum Rules calculations (see later).

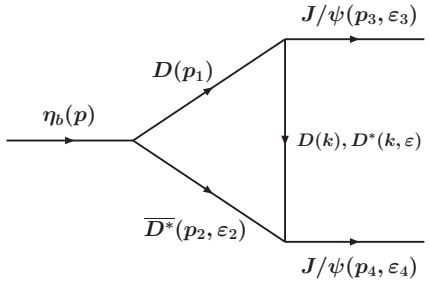

Figure 1: Long distance $t-$channel rescattering contributions to $\eta_b \to J/\psi\, J/\psi$.

The absorbitive part of the triangle graph in fig. 1 is given by

$$Abs(fig1) = \frac{1}{16\pi\, m_{\eta_b}\sqrt{m_{\eta_b}^2 - 4m_{J/\psi}^2}} \int_{t_m}^{t_M} dt\; \mathcal{A}(\eta_b \to D\overline{D^*})\mathcal{A}(D\overline{D^*} \to J/\psi J/\psi)$$
$$\equiv \left(\frac{A_{LD}}{m_{\eta_b}}\, g_{\eta_b DD^*}\right) \imath\, \varepsilon_{\alpha\beta\gamma\delta} p_3^\alpha p_4^\beta \epsilon_3^{*\gamma} \epsilon_4^{*\delta}\ , \qquad (5)$$

The integration domain is given by $[t_m, t_M] \approx [-60, -0.6]$ GeV^2.

The numerical values of the on-shell strong couplings $g_{JDD}(t), g_{JDD^*}(t)$ and $g_{JD^*D^*}(t)$[2] are taken from QCD Sum Rules [11], the Constituent Quark

[1] $\mathcal{B}r[\eta_b \to D\overline{D^*}]$ denotes the sum over the branching ratios of the three different charge assignment to the $D\overline{D^*}$ final state. In the following we assume, as in [9], they occur with the same probability of 1/3.

[2] We use dimensionless strong couplings in all cases. In particular our $g_{JDD^*}/m_{J/\psi}$ corresponds to $g_{JDD^*}(GeV^{-1})$ more used in literature.

Meson model [12] and a relativistic quark model [13] findings which are compatible each other. We use $(g_{JDD}, g_{JDD^*}, g_{JD^*D^*}) = (6, 12, 6)$. To take into account the off-shellness of the exchanged $D^{(*)}$ mesons in fig. 1 we have introduced the $t-$dependance of the couplings by means of the function

$$F(t) = \frac{\Lambda^2 - m^2_{D^{(*)}}}{\Lambda^2 - t}\,, \tag{6}$$

which satisfy QCD counting rules. Λ should be not far from the mass of the exchanged particle and should depends on the final state. However, a first-principles calculation of Λ doesn't exist. Thus, following the authors of [14] we write $\Lambda = m_R + \alpha\Lambda_{QCD}$, where m_R is the mass of the exchanged particle (D or D^*), $\Lambda_{QCD} = 220\ MeV$ and $\alpha \approx 2.2$ [14]; in the following we allow α to vary in the range $2.0 < \alpha < 2.4$.

It should be observed that we do not consider the contribution coming from the dispersive part of the diagram in fig. 1. In any case this contribution interferes with the short distance amplitude. Thus it can implies at most a larger branching ratio respect to the prediction we will give without considering it.

Using the definition in eq. 5, the full amplitude for the $\eta_b \to J/\psi\ J/\psi$ process can be written as

$$\begin{aligned}\mathcal{A}_f(\eta_b(p) \;\to\; & J/\psi(p_3,\varepsilon_3)\ J/\psi(p_4,\varepsilon_4)) = \\ & \imath\,\frac{g_{\eta_b JJ}}{m_{\eta_b}}\,\varepsilon_{\alpha\beta\gamma\delta} p_3^\alpha p_4^\beta \epsilon_3^{*\gamma}\epsilon_4^{*\delta}\left[1 + \ 3\ \frac{g_{\eta_b DD^*}}{g_{\eta_b JJ}}\imath\ A_{LD}\right]\,,\end{aligned} \tag{7}$$

where the factor 3 is due to the three different charge assignments to the $D\overline{D^*}$ intermediate state. In eq. 5 we have introduced the (on-shell) effective couplings $g_{\eta_b DD^*}$ and $g_{\eta_b JJ}$ defined by

$$\mathcal{A}(\eta_b(p) \to D(p_1)\ \overline{D^*}(p_2,\varepsilon_2)) \;=\; 2\ g_{\eta_b DD^*}(\varepsilon_2^*\cdot p)\,, \tag{8}$$

$$\mathcal{A}(\eta_b(p) \to J/\psi(p_3,\varepsilon_3)\ J/\psi(p_4,\varepsilon_4)) \;=\; \frac{\imath g_{\eta_b JJ}}{m_{\eta_b}}\varepsilon_{\alpha\beta\gamma\delta} p_3^\alpha p_4^\beta \varepsilon_3^{*\gamma}\varepsilon_4^{*\delta}\,, \tag{9}$$

and the ratio in eq. 7 is obtained in terms of the existing theoretical estimation of the $\mathcal{B}r[\eta_b \to D\overline{D^*}]/\mathcal{B}r[\eta_b \to J/\psi\ J/\psi] = (0.3/3.6)\times 10^{+3}(1 \text{ or } 10^{+2} \div 10^{+3})$, *i. e.* $g_{\eta_b DD^*}/g_{\eta_b JJ} \approx 1.1$ or $11 \div 35$. In fig. 2 the ratio $r = 3A_{LD}\ g_{\eta_b DD^*}/g_{\eta_b JJ}$ is plotted as a function of α for the allowed value (1.1) and the range ($11 \div 35$) of couplings ratio. Moreover, the dashed line is for $g_{\eta_b DD^*}/g_{\eta_b JJ} \approx 26$

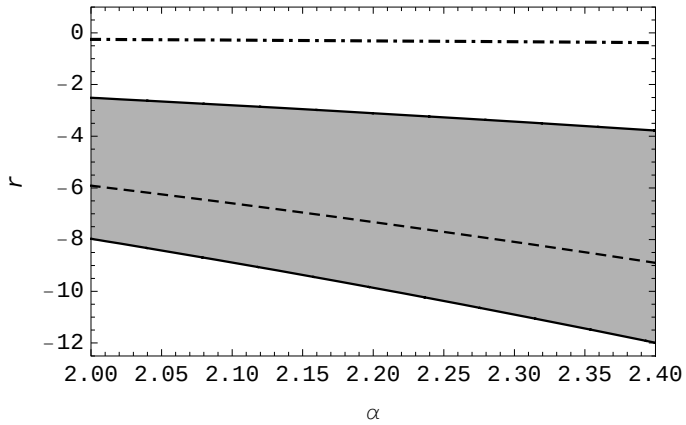

Figure 2: The ratio r (see text for definition) is plotted vs α for $g_{\eta_b DD^*}/g_{\eta_b JJ} \approx 1$ (dashed-dotted line) and $g_{\eta_b DD^*}/g_{\eta_b JJ} \approx 11 \div 35$ (solid lines). The dashed line correspond to $g_{\eta_b DD^*}/g_{\eta_b JJ} \approx 26$.

which corresponds the central value in the estimated range for $\mathcal{B}r[\eta_b \to D\overline{D^*}]$ estimated in ref. [9]. Looking at the figure 2 we see that the long distance absorbitive contribution coming from the graphs in fig. 1 is at the most about twelve times larger than the short distance amplitude.

It easy to show that, starting from the central value in eq. 3, we predict the branching ratio in the range $(3.6 \times 10^{-8} \div 9.6 \times 10^{-6})$, where the upper and the lower bound are obtained for $2.0 \leq \alpha \leq 2.4$ and $11 \leq g_{\eta_b DD^*}/g_{\eta_b JJ} \leq 35$.

As far as the number of events in full Tevatron Run I data (100 pb^{-1}) is concerned, one should take into account the $\mathcal{B}r[J/\psi \to \mu^+\mu^-] \approx 6\%$ [15] and the total cross section for η_b production at Tevatron energy, $\sigma_{tot}(\eta_b) = 2.5\ \mu b$ [9], obtaining between 0.03 and 8 produced events of $\eta_b \to J/\psi\ J/\psi$.

This is compatible with the experimental data from CDF Collaboration on the Run I dataset [8]. However, preliminary results from CDF Collaboration Run II data at 1.1 fb^{-1} [16] seems to be at odds with the previous findings. In fact, in the mass search window only 3 events have been observed. We are looking forward for the publication of the final results for a comparison. Note that for an integrated luminosity of 1.1 fb^{-1} we predict a range of events between 0.3 and 90. However, if we take into account the acceptance (± 0.6) and

efficiency for detecting muons (10%) this range becomes 0.002 to 0.6 events. Completely different is the case of LHC where large number of events are expected [10].

In conclusion, we have shown that, if the branching ratio of η_b into $D\overline{D^*}$ is large ($10^{-3} \div 10^{-2}$), the effect of final state interactions, *i. e.* the rescattering $D\overline{D^*} \to J/\psi\ J/\psi$, may increase the $\mathcal{B}r[\eta_b \to J/\psi\ J/\psi]$ of about two orders of magnitude. This result first of all call for a direct calculation of the $\eta_b \to D\overline{D^*}$ decay process and, in any case, it supports the experimental search of η_b by looking at its decay into $J/\psi\ J/\psi$, which has very clean signature.

References

1. S. W. Herb *et al.*, Phys. Rev. Lett. **39**, 252 (1977).
2. M. Artuso *et al.* [CLEO Collaboration], Phys. Rev. Lett. **94**, 032001 (2005) [arXiv:hep-ex/0411068].
3. A. Heister *et al.* [ALEPH Collaboration], Phys. Lett. B **530**, 56 (2002) [arXiv:hep-ex/0202011].
4. M. Levtchenko [L3 Collaboration], Nucl. Phys. Proc. Suppl. **126**, 260 (2004).
5. J. Abdallah [DELPHI Collaboration], Phys. Lett. B **634**, 340 (2006) [arXiv:hep-ex/0601042].
6. P. Santorelli, arXiv:hep-ph/0703232.
7. E. Braaten, S. Fleming and A. K. Leibovich, Phys. Rev. D **63** (2001) 094006 [arXiv:hep-ph/0008091].
8. J. Tseng [CDF collaboration], "Search for eta/b at CDF", FERMILAB-CONF-02-348-E;
9. F. Maltoni and A. D. Polosa, Phys. Rev. D **70** (2004) 054014 [arXiv:hep-ph/0405082].
10. Y. Jia, arXiv:hep-ph/0611130.

11. R. D. Matheus, F. S. Navarra, M. Nielsen and R. Rodrigues da Silva, Int. J. Mod. Phys. E **14** (2005) 555; M. E. Bracco, M. Chiapparini, F. S. Navarra and M. Nielsen, Phys. Lett. B **605** (2005) 326 [arXiv:hep-ph/0410071].

12. A. Deandrea, G. Nardulli and A. D. Polosa, Phys. Rev. D **68** (2003) 034002 [arXiv:hep-ph/0302273].

13. M. A. Ivanov and P. Santorelli, Phys. Lett. B **456** (1999) 248 [arXiv:hep-ph/9903446]; M. A. Ivanov, J. G. Korner and P. Santorelli, Phys. Rev. D **63**, 074010 (2001) [arXiv:hep-ph/0007169]; M. A. Ivanov, J. G. Korner and P. Santorelli, Phys. Rev. D **70** (2004) 014005 [arXiv:hep-ph/0311300]; M. A. Ivanov, J. G. Korner and P. Santorelli, Phys. Rev. D **71**, 094006 (2005) [Erratum-ibid. D **75**, 019901 (2007)] [arXiv:hep-ph/0501051]; M. A. Ivanov, J. G. Korner and P. Santorelli, Phys. Rev. D **73**, 054024 (2006) [arXiv:hep-ph/0602050].

14. H. Y. Cheng, C. K. Chua and A. Soni, Phys. Rev. D **71** (2005) 014030 [arXiv:hep-ph/0409317].

15. W. M. Yao *et al.* [Particle Data Group], J. Phys. G **33** (2006) 1.

16. M. Paulini (for CDF II and D0), Talk given at Heavy Quarks and Leptons, 16.10. - 20.10.2006 Munich, Germany;
see also *CDF public note # 8448*, August 18, 2006.

Frascati Physics Series Vol. XLVI (2007), pp. 877
HADRON07: XII Int. Conf. on Hadron Spectroscopy – Frascati, October 8-13, 2007
Low Energy QCD

EXPERIMENTAL STATUS OF $\pi\pi$ ISOSCALAR S-WAVE AT LOW ENERGY

F. Yndurain
Universidad Autonoma de Madrid

Written contribution not received

Frascati Physics Series Vol. XLVI (2007), pp. 879–886
HADRON07: XII Int. Conf. on Hadron Spectroscopy – Frascati, October 8-13, 2007
Low Energy QCD

$\pi\pi$ SCATTERING LENGTHS FROM KAON KE4 AND 3π DECAYS BY NA48/2

Massimo Lenti
INFN Sezione di Firenze
Via G.Sansone, 1 - 50019 Sesto F.no (FI) Italy

Abstract

The NA48/2 experiment at the CERN SPS has collected an unprecedented sample of $K^{\pm} \to \pi^{\pm}\pi^0\pi^0$ and $K^{\pm} \to \pi^+\pi^- e^{\pm}\nu$ decays. Both decays are important tools to study Chiral Perturbation Theory predictions and give access to $\pi\pi$ scattering lengths.

The NA48/2 experimental setup

The primary goal of the NA48/2 experiment at CERN is the search for direct CP violation in $K^{\pm} \to 3\pi$ decays [1)]. Data have been collected in 2003–04, providing samples of $\sim 4 \times 10^9$ $K^{\pm} \to 3\pi^{\pm}$ and $\sim 10^8$ $K^{\pm} \to \pi^{\pm}\pi^0\pi^0$ decays.

In the NA48/2 setup two simultaneous K^+ and K^- beams are produced by 400 GeV protons impinging on a 40 cm long Be target. Particles with a central momentum of 60 GeV/c and a momentum band of $\pm 3.8\%$ produced at

zero angle are selected by a system of dipole magnets forming an "achromat" with null total deflection, focusing quadrupoles, muon sweepers and collimators. With 7×10^{11} protons per burst of 4.5 s duration impinging on the target the positive (negative) beam flux at the entrance of the decay volume is 3.8×10^7 (2.5×10^7) particles per pulse, of which 5.7% (4.9%) are K^+ (K^-). The decay volume is a 114 m long vacuum tank.

Charged particles from $K^\pm$ decays are measured by a magnetic spectrometer consisting of four drift chambers and a large-aperture dipole magnet located between the second and third chamber. Charged particles are magnetically deflected in the horizontal plane by an angle corresponding to a transverse momentum kick of 120 MeV/c. The momentum resolution of the spectrometer is $\sigma(p)/p = 1.02\% \oplus 0.044\% p$ (p in GeV/c). The spectrometer is followed by a scintillator hodoscope consisting of two planes segmented into horizontal and vertical strips.

A liquid krypton calorimeter is used to reconstruct photons and electrons. It is an almost homogeneous ionization chamber with an active volume of 7 m^3 of liquid krypton, segmented transversally into 13248 projective cells of 2×2 cm^2 by a system of Cu-Be ribbon electrodes, and with no longitudinal segmentation. The calorimeter is $27X_0$ thick and has an energy resolution $\sigma(E)/E = 0.032/\sqrt{E} \oplus 0.09/E \oplus 0.0042$ (E in GeV). Spatial resolution for a single electromagnetic shower is $\sigma_x = \sigma_y = 0.42\%/\sqrt{E} \oplus 0.06$ cm for each transverse coordinate x, y. The ratio E/p between the energy E measured by the calorimeter and the momentum p measured by the spectrometer is used to separate charged pions from electrons.

A detailed description of the NA48 detector can be found elsewhere [2].

The Cusp effect and the measurement of $\pi\pi$ scattering lengths

A study of a partial sample of $K^\pm \to \pi^\pm\pi^0\pi^0$ decays corresponding to about 25% of the total sample revealed an anomaly in the $\pi^0\pi^0$ invariant mass (M_{00}) distribution in the region around $M_{00} = 2m_+$, where m_+ is the charged pion mass [3]. This anomaly, dubbed "cusp effect", never observed in previous experiments, was theoretically interpreted as an effect due mainly to the final state charge exchange scattering process $\pi^+\pi^- \to \pi^0\pi^0$ in $K^\pm \to 3\pi^\pm$ decay, and was shown to provide a precise determination of $a_0 - a_2$, where the a_I are the S-wave $\pi\pi$ scattering lengths in the isospin $I = 0$ and $I = 2$ states [4].

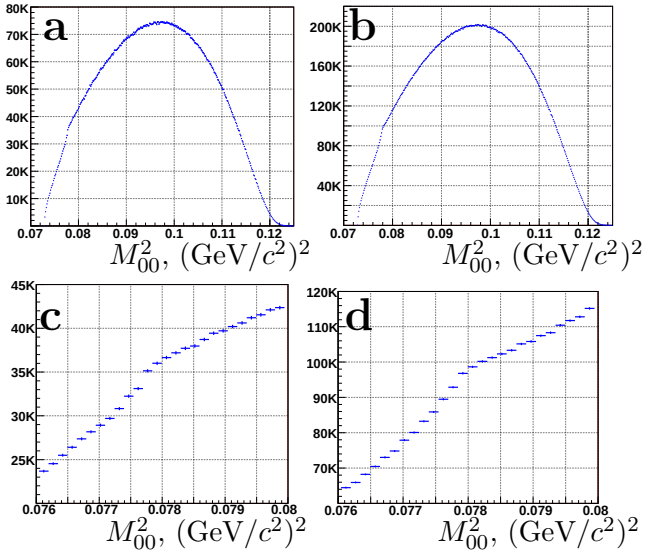

Figure 1: Reconstructed spectra of $\pi^0\pi^0$ invariant mass showing evidence for the cusp effect: the full kinematic range for (a) 2003 data (16.0×10^6 events), (b) 2004 data (43.6×10^6 events); zoomed threshold region for (c) 2003 data, (d) 2004 data. The 2003 plots correspond to the original discovery of the effect [3].

The reconstructed spectra of $\pi^0\pi^0$ invariant mass M_{00} for 2003 and 2004 data samples (totally 59.6×10^6 events) are presented in Fig. 1. The change of slope at $\pi^+\pi^-$ threshold is clearly visible. For description of this effect the $K^\pm \to \pi^\pm\pi^0\pi^0$ amplitude is presented as a sum of two terms $\mathcal{M} = \mathcal{M}_0 + \mathcal{M}_1$, where $\mathcal{M}_0$ is the "unperturbed" amplitude expressed as a polynomial expansion in terms of the kinematic variables $u = (s_3 - s_0)/m_+^2$ and $v = (s_1 - s_2)/m_+^2$, where $s_i = (P_K - P_i)^2$, P_K and P_i are 4-momenta of kaon and pions, and $i = 1, 2$ correspond to the two "even" (i.e. identical) pions:

$$\mathcal{M}_0(u, v) = \mathcal{M}_0(0, 0) \cdot (1 + g_0 u/2 + h' u^2/2 + k' v^2/2), \tag{1}$$

and $\mathcal{M}_1$ is a contribution from the $K^\pm \to 3\pi^\pm$ decay amplitude $\mathcal{M}_+$ through $\pi^+\pi^- \to \pi^0\pi^0$ charge exchange, which in the simplest case [4] is

$$\mathcal{M}_1 = -2 a_x m_+ \mathcal{M}_+ \sqrt{1 - (M_{00}/2m_+)^2}. \tag{2}$$

Here, in the limit of exact isospin symmetry, $a_x = (a_0 - a_2)/3$. The amplitude $\mathcal{M}_1$ changes from real to imaginary at the threshold $M_{00} = 2m_+$; as a consequence it interferes destructively with $\mathcal{M}_0$ below the threshold (leading to 13% integral depletion in this region), and adds quadratically above the threshold.

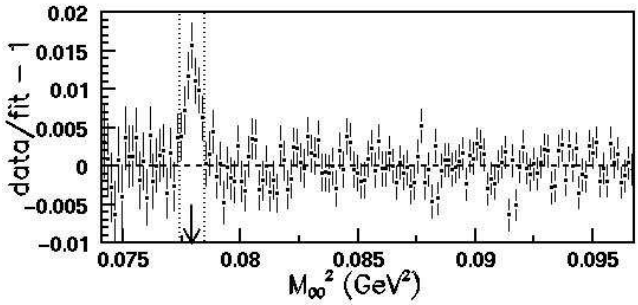

Figure 2: Deviation of the data spectrum from the fit result with statistical errors (combined 2003+2004 data set): $\Delta = Data/Fit - 1$. Good quality of the fit and an excess of events in the region of the threshold are demonstrated.

The model used for the present measurement is based on the formulation [5], which takes into account all rescattering processes at the one-loop and two-loop level. In this approach the matrix element of the $K^\pm \to \pi^\pm\pi^0\pi^0$ decay includes a number of additional terms depending on five S-wave $\pi\pi$ scattering lengths (corresponding to the processes $\pi^+\pi^- \to \pi^0\pi^0$, $\pi^+\pi^+ \to \pi^+\pi^+$, $\pi^+\pi^- \to \pi^+\pi^-$, $\pi^+\pi^0 \to \pi^+\pi^0$ and $\pi^0\pi^0 \to \pi^0\pi^0$) expressed as linear combinations of a_0 and a_2. In addition to [5], isospin breaking effects are taken into account introducing a single parameter $\epsilon = (m_+^2 - m_0^2)/m_+^2 = 0.065$ [6].

The fit to extract the scattering lengths and Dalitz plot slopes g_0, h' was performed in the M_{00} projection of the data using a full GEANT-based Monte Carlo simulation of the detector response. The used rescattering model does not include radiative corrections, which are particularly important at the threshold $M_{00} = 2m_+$, and contribute to formation of $\pi^+\pi^-$ atoms (pionium). Thus a group of seven bins near the threshold has been excluded from the fit. The quality of the fit (χ^2/NDF = 164/139 for 2003 analysis, and χ^2/NDF = 119/139 for 2004 analysis) illustrated in Fig. 2 shows an excess of events in this excluded region. This excess, being interpreted as due to pionium formation, yields the rate of pionium production $R = \Gamma(K^\pm \to \pi^+ A_{2\pi})/\Gamma(K^\pm \to 3\pi^\pm) = (1.82 \pm 0.21) \times 10^{-5}$, somewhat higher than a theoretical prediction [7].

Systematic uncertainties due to fitting technique, trigger efficiency, description of geometric acceptance and resolution, calorimeter non-linearity, and simulation of showers in the calorimeter have been evaluated. External uncertainties due to limited experimental knowledge of $\mathcal{M}_+/\mathcal{M}_0$ at the $\pi^+\pi^-$ threshold have been also considered. Stability checks with respect to decay vertex position, particle separations in the calorimeter front plane, and kaon sign have been performed. The measured scattering lengths are:

$$\begin{aligned}(a_0-a_2)m_+ &= 0.261 \pm 0.006_{\text{stat.}} \pm 0.003_{\text{syst.}} \pm 0.001_{\text{ext.}}\\ a_0 m_+ &= -0.037 \pm 0.013_{\text{stat.}} \pm 0.009_{\text{syst.}} \pm 0.002_{\text{ext.}}\end{aligned}$$

In addition, an uncertainty $\delta(a_0 - a_2) = 0.013$ has to be attributed to the result due to the precision of the theoretical model. The Dalitz plot slopes corresponding to the used model have been found to be

$$\begin{aligned}g_0 &= 0.649 \pm 0.003_{\text{stat.}} \pm 0.004_{\text{syst.}}\\ h' &= -0.047 \pm 0.007_{\text{stat.}} \pm 0.005_{\text{syst.}}\\ k' &= -0.0097 \pm 0.0003_{\text{stat.}} \pm 0.0008_{\text{syst.}}\end{aligned}$$

The K_{e4} decay analysis

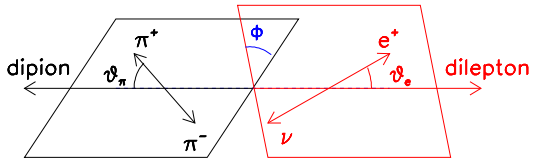

Figure 3: Topology of the charged Ke4 decay.

$K^\pm \to \pi^+\pi^- e^\pm \nu$ decays are of particular interest as they give access to the $\pi\pi$ phase shift $\delta = \delta_0^0 - \delta_1^1$ in absence of any other hadron. The measured variation of the phase shift with the invariant mass $M_{\pi\pi}$ near threshold can be related to a_0^0 and a_0^2 (the $\pi\pi$ s-wave scattering lengths for Isospin states 0 and 2) using dispersion relations and data at intermediate energies [8, 9, 10]. In the past years, only two experiments were able to collect large samples of K_{e4} decays [11, 12] and study their properties.

$K^\pm \to \pi^+\pi^- e^\pm \nu$ were selected in the 2003 data looking for three well reconstructed charged tracks, requiring two opposite sign pions and one electron

carrying the same charge as the total charge, identified from their E/p ratio. The level of background to signal is $\sim 0.5\%$ and has been cross-checked using Monte Carlo simulated events. The K_{e4} decay is fully described by the five kinematic Cabibbo-Maksymowicz variables: two invariant masses $M_{\pi\pi}$ and $M_{e\nu}$ and three angles θ_π, θ_e and Φ as shown in Figure 3. Three axial (F, G, R) and one vector (H) form factors contribute to the transition amplitude and can be developed in a partial wave expansion of s, p, d waves:

$$F = F_s\ e^{i\delta_s} + \ F_p\ e^{i\delta_p} cos\theta_\pi + .., \quad G = G_p\ e^{i\delta_g} + .., \quad H = H_p\ e^{i\delta_h} + ..$$

The form factor R is suppressed by a factor m_e^2/S_e and cannot be measured in K_{e4} decays. Neglecting d wave terms and assuming the same phase for $F_p,\ G_p,\ H_p$, only one phase $(\delta(q^2) = \delta_s - \delta_p)$ and 4 form factors are left, which are expanded further [13] in powers of $q^2 = ({M_{\pi\pi}}^2/4m_\pi^2) - 1$: $F_s = f_s(1. + f_s'/f_s\ q^2 + f_s''/f_s\ q^4 + ..),\ F_p = (f_p + ..),\ G_p = (g_p + g_p'\ q^2 + ..),\ H_p = (h_p + ..)$

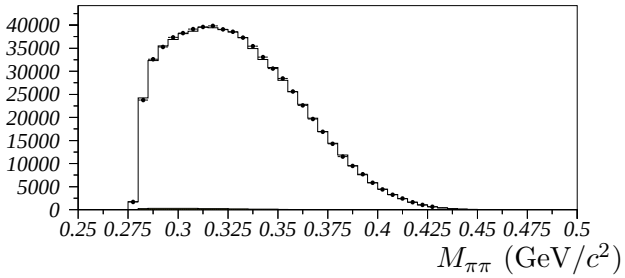

Figure 4: Reconstructed $\pi\pi$ mass in K_{e4} decays. Data are shown as symbols with error bars, simulation after fit as open histogram and background (hardly visible) from wrong sign events as shaded area.

From the data sample, a total of 15000 equi-populated bins are defined in the five-parameter space (10 along $M_{\pi\pi}$, 5 along $M_{e\nu}$, 5 along $cos\theta_\pi$, 5 along $cos\theta_e$ and 12 along Φ). Ten independent four-parameter fits are performed, one for each bin in $M_{\pi\pi}$. The set of form factors and the phase shift are used to minimize the differences summed over all bins between data events and predicted events from a detailed simulation. A particular attention was given to the acceptance and resolution in the five-variable space (see Figure 4 for $M_{\pi\pi}$). Radiative corrections, including Coulomb attraction between the two pions, were implemented using a dedicated generator code (PHOTOS).

Two series of fits are performed separately for the K^+ and K^- samples,

using the same $M_{\pi\pi}$ bins definition. The results are checked for consistency and then combined in each bin according to their statistical weight under the assumption of CP conservation (the ϕ distribution of K^+ decays is opposite to that of K^- decays with the same $|H_p|$ value). The Data/MC normalizations are rescaled to have a mean value equal to unity. A residual variation of F_s^2 with $S_e(= {M_{e\nu}}^2)$ suggests to measure the variation of the normalizations in the plane (q^2, $S_e/4m_\pi^2$). Polynomial in the dimensionless variable q^2 (and $S_e/4m_\pi^2$) are used to fit the form factor variations and the Universal Band center line constraint is used to deduce a value of the scattering length a_0^0.

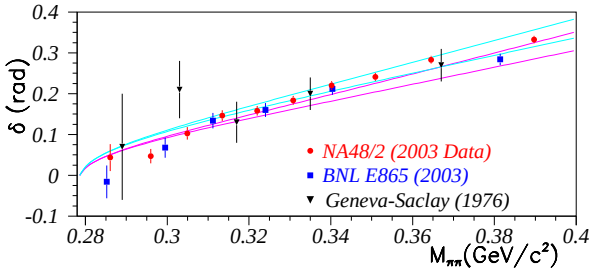

Figure 5: Phase shifts results from the three experiments. The top band is the prediction of the Roy equations for $a_0^0 = 0.26$, the lower band for $a_0^0 = 0.22$.

The fit results are given below (the first error is statistical, the second is systematic), including also a 2-parameter fit where both a_0^0 and a_0^2 are free:

$f'_s/f_s =$	0.172 ± 0.009 ± 0.006	$f''_s/f_s =$	-0.090 ± 0.009 ± 0.007
$f'_e/f_s =$	0.081 ± 0.008 ± 0.008	$f_p/f_s =$	-0.048 ± 0.004 ± 0.004
$g_p/f_s =$	0.873 ± 0.013 ± 0.012	$g'_p/f_s =$	0.081 ± 0.022 ± 0.014
$h_p/f_s =$	-0.411 ± 0.019 ± 0.007	a_0^0(1p) =	0.256 ± 0.006 ± 0.005
a_0^0(2p) =	0.233 ± 0.016 ± 0.007	a_0^2(2p) =	-0.047 ± 0.011 ± 0.004

Systematic uncertainty studies include comparison of two independent analyses, trigger efficiency, acceptance control, background contamination, electron mis-identification, implementation of radiative corrections and neglected S_e dependence of the form factors in the simulation. A comparison of NA48/2 phase shift results with those of previous experiments and the Universal Band predictions for two values of a_0^0 is shown in Figure 5: the data are in good agreement (apart from the highest energy point of E865) and favour large

values of a_0^0. Further theoretical developments [14] suggest that isospin symmetry breaking effects, neglected so far, should be considered when extracting $\pi\pi$ scattering lengths from phase measurements.

Conclusions

The cusp effect analysis in $K^\pm \to \pi^\pm\pi^0\pi^0$ decays, using the full 2003-2004 NA48/2 data sample, has been presented. The $K^\pm \to \pi^+\pi^- e^\pm\nu$ decay has been described using the 2003 NA48/2 data sample. $\pi\pi$ scattering length and decay form factors have been discussed in both decays.

References

1. J.R. Batley *et al.*, Phys. Lett. **B634** (2006) 474 and **B638** (2006) 22.
2. V. Fanti *et al.* (NA48), Nucl. Instrum. Methods **A574** (2007) 433.
3. J.R. Batley *et al.*, Phys. Lett. **B633** (2006) 173.
4. N. Cabibbo, Phys. Rev. Lett. **93** (2004) 121801.
5. N. Cabibbo and G. Isidori, JHEP **0503** (2005) 021.
6. K. Maltman and C.E. Wolfe, Phys. Lett. **B393** (1997) 19, erratum-ibid. **B424** (1998) 413. K. Knecht and R. Urech, Nucl. Phys. **B519** (1998) 329.
7. Z.K. Silagadze, JETP Lett. **60** (1994) 689.
8. S. Roy, Phys. Lett. **B36** (1971) 353.
9. B. Ananthanarayan, G. Colangelo, J. Gasser, H. Leutwyler, Phys. Rept. **353** (2001) 207.
10. S. Descotes, N. Fuchs, L. Girlanda, J. Stern, Eur. Phys. J. **C24** (2002) 469.
11. L. Rosselet et al., Phys. Rev.**D15** (1977) 574.
12. S. Pislak et al., Phys. Rev. Lett. **87** (2001) 221801,
    S. Pislak et al., Phys. Rev.**D67** (2003) 072004.
13. G. Amoros and J. Bijnens, J. Phys. **G25** (1999) 1607.
14. J. Gasser, Proceedings KAON 2007, Frascati, May 21-25, 2007.

Frascati Physics Series Vol. XLVI (2007), pp. 887–896
HADRON07: XII Int. Conf. on Hadron Spectroscopy – Frascati, October 8-13, 2007
Low Energy QCD

SEARCH FOR πK-ATOMS WITH DIRAC-II

Yves Allkofer*, C. Amsler, S. Horikawa, C. Regenfus, J. Rochet
Physik-Institut der Universität Zürich, CH-8057 Zürich, Switzerland†

Abstract

DIRAC II experiment searches for the electromagnetically bound system $K^+\pi^-$ (and $K^-\pi^+$) and will measure its lifetime. The latter is related to the S-wave $K\pi$ - scattering lengths which are of considerable interest to test chiral perturbation predictions involving the s-quark. There are large uncertainties in the $K\pi$ - scattering lengths which are obtained by extrapolation to low energies from the poorly known $K\pi$ isospin 1/2 and 3/2 phase shifts. The $K\pi$ atoms will be produced with 24 GeV/c protons from the CERN PS impinging on a target, and their dissociation products analysed by the DIRAC spectrometers. For particle identification the momentum distribution of π, K and p requires aerogel Čerenkov counters with a small index of refraction in the range 1.008 to 1.015. We will report on the status of the experiment.

* talk given by Y. Allkofer. *E-mail address:* Yves.Allkofer@cern.ch
† on behalf of the DIRAC collaboration

1 The DIRAC experiment and its upgrade

DIRAC is a running experiment at the CERN PS using a 24 GeV/c proton beam on a fixed Ni or Pt-target where *pionium*, a bound state between two opposite charged pions is produced. Up to now 15 000 pairs originating from pionium were detected, which leads to a precision of its lifetime τ of 10%. Including systematics and theoretical uncertainties one obtains,

$$\tau = (2.91^{+0.49}_{-0.62}) \cdot 10^{-15} s, \tag{1}$$

see ref. [1]. In this bound state the strong interaction between the two mesons changes the width (lifetime) of pionium. It can be shown, see ref. [2] that the lifetime can be expressed as a combination of the S-wave scattering lengths a_0^0 and a_2^0 for isospin 0 and 2 respectively,

$$\frac{1}{\tau} = \frac{2\alpha^3}{9} p^* |a_0^0 - a_2^0|^2 (1 + \delta), \tag{2}$$

where p^* is the π^0-momentum in the pionium system, α the fine structure constant and $\delta = (5.8 \pm 1.2) \cdot 10^{-2}$ accounts for corrections terms.

Chiral perturbation theory, (ChPT) describes the hadronic interactions according to the Standard Model at low energies i.e. below the chiral breaking symmetry which is slightly below 1 GeV/c. Very precise predictions are achieved, see ref. [3], for the $\pi\pi$ S-wave scattering length and hence for the pionium lifetime,

$$\tau = (2.9 \pm 0.1) \cdot 10^{-15} s. \tag{3}$$

The agreement between what has been measured by the DIRAC collaboration and the prediction using ChPT is very encouraging. Many efforts have been done to extend the 2 -flavor space to the 3-flavor space introducing the s-quark leading to a SU(3) ChPT. However, in contrast to the SU(2) ChPT the situation is much more confused. Already between different theoretical approaches there is no agreement anymore as shown in fig.1 where the dark shaded ellipse on the left are the results from ref. [4] based only on ChPT for the πK-scattering lengths combination and the light shaded ellipse on the right are the results from ref. [5] based on ChPT, together with Roy-Steiner dispersion relations.

From the experimental side the last results from scattering experiments were performed in the 70s based on the so called *one pion exchange* (OPE)

model. As an example, in ref. [6] the πK scattering lengths have been measured to be

$$m_\pi \cdot (a^0_{1/2} - a^0_{3/2}) = 0.475 \pm 0.013, \tag{4}$$

where 1/2 and 3/2 stand for the isospin. This result is far outside the range of fig.1.

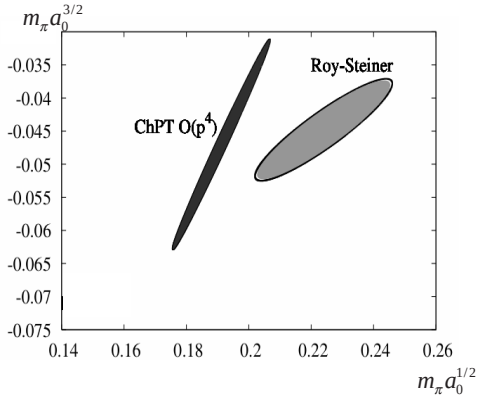

Figure 1: *Predicted S-wave πK-scattering length (isospin 1/2 and 3/2) using different theoretical approaches; the 95% C.L. ellipse obtained using ChPT, ref. [4], is shown on the left and the ellipse using the Roy-Steiner dispersion relations, ref. [5], is shown on the right.*

In order to clarify this situation it is crucial to perform a new experiment which aims to measure the πK-scattering length with small uncertainties. Similarly to pionium it is possible to relate the lifetime of πK-atoms to the corresponding S-wave scattering lengths,

$$\frac{1}{\tau} = \frac{8\alpha^3}{9} \left(\frac{M_\pi M_K}{M_\pi + M_K} \right)^2 p^* (a_{1/2} - a_{3/2})^2 (1 + \delta), \tag{5}$$

see ref. [7].

2 The upgrade to DIRAC II

The DIRAC II experiment aims to measure the lifetime of πK-atoms with a precision of 20%, leading to a determination of the πK-scattering length difference $|a^0_{1/2} - a^0_{3/2}|$ with an accuracy of about 10% which would be the

first test of the SU(3)-ChPT predictions in a model independent way. DIRAC II aims to measure simultaneously the lifetime of pionium in order to achieve 6% accuracy on the lifetime, leading to 3% on the scattering length difference $|a_0 - a_2|$. To obtain such a precise measurement the DIRAC-spectrometer had to be upgraded to reduce systematic errors and to improve the data collection efficiency. Also crucial for the observation of πK-atoms is the introduction of two new Čerenkov detectors for kaon identifications. The new spectrometer is shown in fig.2.

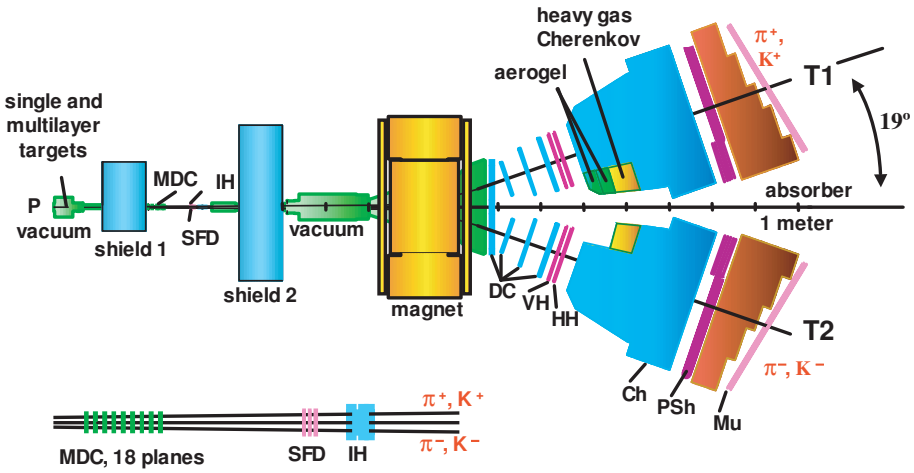

Figure 2: *DIRAC II upgraded spectrometer. From left to right : micro drift chambers (MDC), scintillating fiber detector (SFD), ionization hodoscope (IH), spectrometer magnet, drift chambers (DC), vertical and horizontal hodoscopes (VH,HH), aerogel Čerenkov detector, heavy gas Čerenkov detector, N_2-Čerenkov detector, preshower detector (PSh) and muon detector (Mu).*

2.1 Upgrade of the existing setup

A new tracker, the micro drift chambers (MDC) has been installed to improve track reconstruction upstream of the magnet. To detect atomic pairs immediately behind the magnet one has to distinguish two tracks with a very small opening angle. This task is fulfilled by this detector with a spatial resolution which is estimated to be around 22 μm for single tracks and less than 200 μm

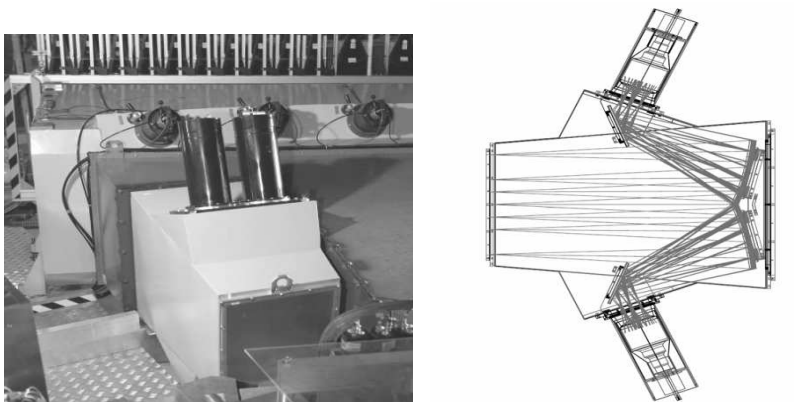

(a) (b)

Figure 3: *a) Photograph of the heavy gas Čerenkov detector installed in the negative spectrometer arm; b) Sketch of the inner part of the heavy gas detector showing the Čerenkov light propagation. The photons are first reflected backwards on a set of four spherical mirrors and then focused on the photocathod by flat mirrors.*

for double tracks, with a detection efficiency higher than 98%.

The scintillating-fiber detector (SFD) has also been upgraded. In the new detector fibers 0.27 mm in diameter are used instead of 0.5 mm in the previous version to improve the double-track resolution. Also, new readout electronics equipped with both ADC and TDC has been developed. The new TDC has 120 ps time resolution which is four times better than the old one.

New shielding has been installed, see fig.2 (shield 1 and 2), to reduce the number of accidentals. This allows to run with much higher primary beam intensity without increasing the deadtime of the detectors.

The vertical and horizontal hodoscopes (VH,HH) are located after the Drift Chambers (DC) which are DIRAC's main trackers. They have been enlarged to increase the aperture of the DIRAC spectrometer by 10% in the region where kaons from ionized πK-atoms are expected. Also at the very end of the spectrometer the muon detectors (Mu) have been enlarged for the same reason.

Electrons are rejected using two detectors, the N_2-Čerenkov detector (Ch) and the preshower detector (PSh). The Ch-detector had to be cut in the central

part to make room for the new aerogel and heavy gas Čerenkov detectors. This limits significantly the electron-rejection efficiency in this area. These losses have been compensated by a second layer of the PSh detector in the critical region and by reducing the sizes of the scintillator slabs by a factor of two. All

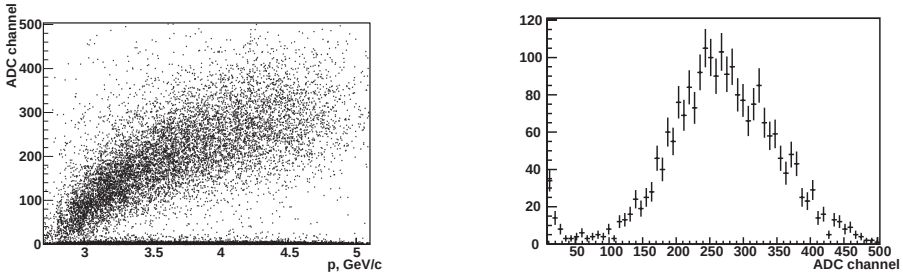

(a) (b)

Figure 4: *a) ADC channels vs. momentum for one of the four photomultipliers of the heavy gas Čerenkov detector; b) integrated pulse height spectrum for a pion momentum of* $p_\pi = 4$ *GeV/c.*

these modifications led to a detection efficiency increasing by a factor of more than two and to a strong reduction of systematic errors.

2.2 Kaon identification

Since kaon identification is crucial for the measurement of πK-atoms the two new Čerenkov detectors used for this purpose will be discussed more in detail in this section.

2.2.1 Heavy gas Čerenkov detector

The heavy gas Čerenkov detector shown in fig.3 detects pions and can be used in coincidence for the $\pi\pi$-atoms measurement to reduce systematics compared to earlier data (2001-2003), or in anti-coincidence for πK-atoms observation. The C_4F_{10} gas used as radiator is cleaned continuously through a recirculation system, see ref. [8], to achieve high purity. Each module is read out by four 5" photomultipliers (PM). Their response is shown in fig.4a) as a function of pion-momentum. The associated pulse height spectrum is shown in fig.4b).

Once calibrated the sum of all PMs leads to 20-25 photoelectrons and hence to a pion detection/rejection efficiency higher than 99.5% for $p_\pi \geq 4$GeV/c.

(a) (b)

Figure 5: *a) Photograph taken during the assembly of the two heavy aerogel modules illustrating the steps of the pyramid design; b) Side view of the pyramid design with the two PMs on the top and the bottom.*

2.2.2 Aerogel Čerenkov detector

The aerogel Čerenkov detector consists of three independent modules read out by two 5" PMs each. Because of the large momentum range to cover two refractive indices are used: $n = 1.015$ and $n = 1.008$. DIRAC requires to cover a large area, especially vertically. This implies the need for a more tricky design than is usual for ordinary threshold counters. In fact, the large distance between the two PMs of one module decreases strongly the number of collected photons and leads to a strong dependence on the impact position of the incoming particle: due to the strong absorption in aerogel, a track crossing close to one PM will give a better light collection efficiency than one crossing near the center of the counter. To compensate for this absorption the thickness of the radiator in the middle of the detector has been increased. This is the so-called *pyramid design*, see fig.5. To compensate for the small number of Čerenkov light in the $n = 1.008$ aerogel we developed a *sandwich* detector. It consists of alternating Tetratex (a diffusive reflector) layers coated with a wavelength shifter (WLS) and aerogel layers. Shifting UV-light to blue light reduces the absorption in aerogel which is strongly wavelength dependent, and also improves the detection efficiency of the PMs. The design is shown in fig.6 as well as the absorption and emission spectrum of p-terphenyl, the WLS we finally

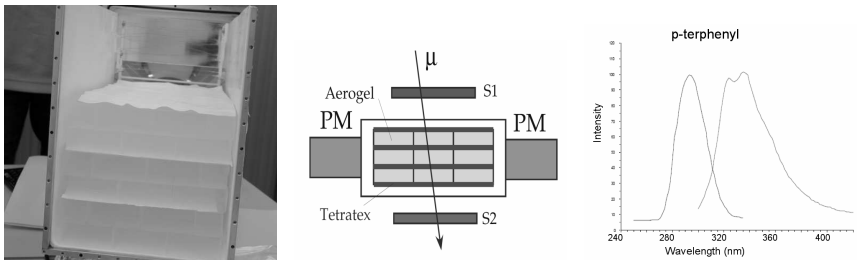

(a) (b) (c)

Figure 6: *a) Photograph taken during the assembly of the light aerogel module illustrating the wavelength shifter (WLS) coated Tetratex layers; b) Side view of the sandwich design alternating aerogel and WLS coated Tetratex; c) Absorption (on the left) and emission (on the right) spectrum of p-Terphenyl which was chosen as WLS.*

used. The final detector is shown in fig.7. The integrated pulse height spectrum for kaons is shown in fig.8 using the heavy gas detector in anticoincidence. For a proton rejection factor of typically 40 the kaon detection efficiency averaged over the full operating momentum range is estimated to lie above 85% for the $n = 1.008$ aerogel, and above 95% for the $n = 1.015$ one.

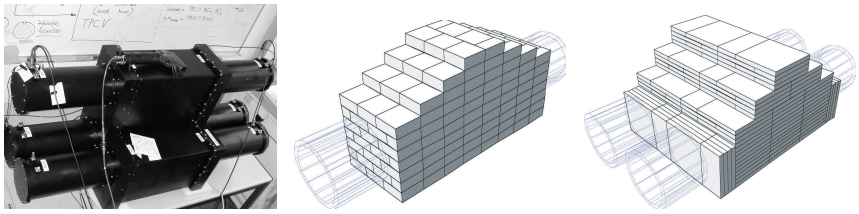

(a) (b) (c)

Figure 7: *Photograph of the final detector a) including the three modules during laboratory tests with cosmic rays. On the top a scintillating counter is used for triggering. The structure of the aerogel for the* $n = 1.008$ *and the two* $n = 1.015$ *modules is shown in b), respectively c).*

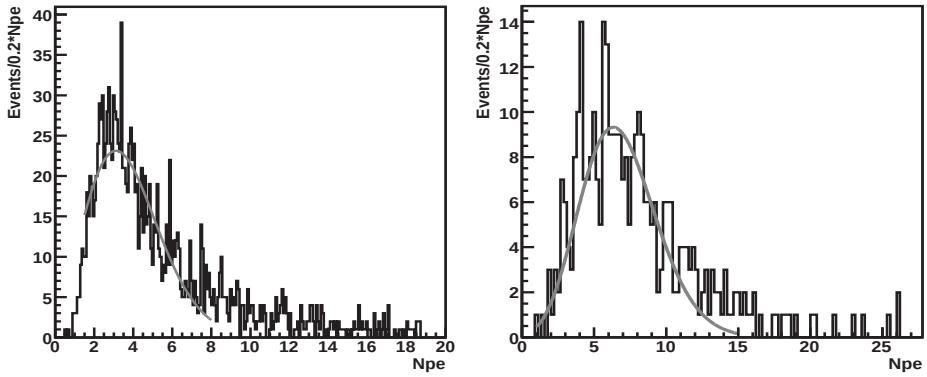

(a) (b)

Figure 8: *a) Integrated pulse height spectrum showing the kaon signals for the module with the* $n = 1.008$ *aerogel. b) Same spectrum for the* $n = 1.015$ *aerogel. For both the heavy gas detector is used in anti-coincidence for pion rejection.*

3 Outlook

The number of $\pi^- K^+$- and $K^- \pi^+$-atoms detected in 2007 run has been estimated as follows. The ratio between the number of ionized $\pi\pi$- and πK-atoms (including $\pi^- K^+$- and $K^- \pi^+$-atoms) was simulated to be 15 using FRITIOF 7.02, see ref. [9]. In 2001 we obtained 1600 $\pi\pi$-atoms per month. For 2007 this number has to be multiplied by a factor of two for the improved detection efficiency due to the spectrometer upgrade. This leads to 190 πK-atoms detected per month. The last correction comes from the different ionization probabilities for Ni (31%) and Pt-target (55%) used in 2001 and in 2007. We expect to detect about 1400 πK-atomic pairs during 4 months of data taking, which would lead to the observation of $\pi^- K^+$- and $K^- \pi^+$-atoms with a significance of more than 3 σ, taken the expected background into account.

References

1. B. Adeva *et al.* (DIRAC collaboration), Phys. Lett. **B619**, 50 (2005)
2. J. Gasser *et al.*, Phys. Rev. **D64**, 016008 (2001)
3. G. Colangelo *et al.*, Nucl. Phys. **B603**, 125 (2001)
4. V. Bernard *et al.*, Nucl. Phys. **B357**, 2757 (1991)
5. P. Buettiker *et al.*, Eur. Phys. J **C33**, 409 (2004)
6. P. Estabrooks *et al.*, Nucl. Phys. **B133**, 490 (1978)
7. J. Schweizer, Phys. Lett. **B587**,) 33 (2004)
8. Y. Allkofer *et al.*, Proc. 6th Int. Workshop on Ring Imaging Cherenkov Counters (RICH2007), Trieste, in print (2007)
9. B. Nilsson-Almquist, E. Stenlund, Com. Phys. Comm. **43**, 387 (1987).

Frascati Physics Series Vol. XLVI (2007), pp. 897–904
HADRON07: XII Int. Conf. on Hadron Spectroscopy – Frascati, October 8-13, 2007
Low Energy QCD

MEASUREMENT OF THE $\pi^+\pi^-$ ATOM LIFETIME AT DIRAC

V. Yazkov, on behalf of DIRAC Collaboration
Skobeltsyn Institute of Nuclear Physics of Moscow State University

Abstract

The measurement of the $\pi^+\pi^-$ atom lifetime with 10% precision provides, in a model independent way, the difference between the S-wave $\pi\pi$ scattering lengths for isospin 0 and 2, $|a_0 - a_2|$, with 5% accuracy. The scattering lengths a_0 and a_2 have been calculated in Chiral Perturbation Theory (ChPT) with a precision better than 2.5%. Therefore, such a measurement will be a sensitive check of the understanding of chiral symmetry breaking in QCD.

1 Introduction

Pionium or $A_{2\pi}$ is a hydrogen-like atom consisting of π^+ and π^- mesons. The $\pi^+\pi^-$ atom decays by strong interaction mainly into $\pi^0\pi^0$. The branching ratio of the alternative decay mode $A_{2\pi} \to 2\gamma$ is at the level of $4 \cdot 10^{-3}$. There is a

relation [1] between the width of $A_{2\pi}$ decay $\Gamma_{2\pi^0}$ and $\pi\pi$ scattering lengths for isospin 0 and 2: $\Gamma_{2\pi^0} = C \cdot |a_0 - a_2|^2$.

The scattering lengths a_0 and a_2 have been calculated in Chiral Perturbation Theory (ChPT) with a precision better than 2.5% [2]: $a_0 = 0.220 \pm 0.005$, $a_2 = -0.0444 \pm 0.0010$ and $a_0 - a_2 = 0.265 \pm 0.004$.

ChPT at next-to-leading order in isospin breaking provides correction to decay width $\Gamma^{NLO}_{2\pi^0} = \Gamma_{2\pi^0}(1 + \delta_\Gamma), \delta_\Gamma = (5.8 \pm 1.2)\%$. Using this correction the lifetime of $\pi^+\pi^-$ atoms is predicted [3] to be $\tau = (2.9 \pm 0.1) \cdot 10^{-15}$ s.

The goal of the DIRAC experiment at CERN (PS212) is to measure the pionium lifetime with 10% precision. Such a measurement provides in a model independent way the difference between the S-wave $\pi\pi$ scattering $|a_0 - a_2|$, with 5% accuracy. Therefore, such a measurement will be a sensitive check of the understanding of chiral symmetry breaking in QCD.

2 Method of lifetime measurement

The $A_{2\pi}$ are produced by Coulomb interaction in the final state of $\pi^+\pi^-$ pairs generated in proton-target interactions from fragmentation and strong decay ("short-lived" sources). For this cases the region of production being small as compared to the Bohr radius of the atom and, neglecting strong final state interaction, the cross section σ^n_A for production of atoms with principal quantum number n is proportional to the inclusive production cross section for pion pairs from "short lived" sources without Coulomb correlation (σ^0_s) [4]:

$$\frac{d\sigma^n_A}{d\vec{p_A}} = (2\pi)^2 \frac{E_A}{M_A} |\Psi^C_n(\vec{r^*} = 0)|^2 \frac{d^2\sigma^0_s}{d\vec{p_+} d\vec{p_-}}, \qquad (1)$$

with $\vec{p_A}$, E_A and M_A the momentum, energy and mass of the atom in the lab frame, respectively, and $\vec{p_+}$, $\vec{p_-}$ the momenta of the charged pions, and $|\Psi^C_n(\vec{r^*} = 0)|^2$ is the square of the Coulomb atomic wave function for zero distance $\vec{r^*}$ between them in the pair c.m. system.

Also $\pi^+\pi^-$ pairs from short-lived sources are generated in free state. Such pairs ("Coulomb pairs") are affected by Coulomb interaction, too. The number of produced atoms (N_A) is proportional to the number of "Coulomb pairs" (N^C) with low relative momenta ($N_A = K \cdot N^C$). The coefficient K is precisely calculable. And there are $\pi^+\pi^-$ pairs from long-lived sources (electromagnetically or weakly decaying mesons or baryons: $\eta, K^0_s, \ldots$). Such pairs, not affected

by final state interaction, are named "non-Coulomb pairs".

Another type of background is "accidental pairs" consisted of pions generated in two different proton-nucleus. They are also not affected by final state interaction.

After production $A_{2\pi}$ travel through the target and some of them are broken up due to their interaction with matter: "atomic pairs" are produced, characterized by small pair c.m. relative momenta $Q < 3$ MeV/c. These pairs are detected in the DIRAC setup. Other atoms annihilate into $\pi^0\pi^0$. Using experimentally measured number of "Coulomb" pairs it is possible to measure breakup probability $P_{\rm br}(\tau) = n_A/N_A = n_A/(K \cdot N_C)$.

The dependence of $P_{\rm br}$ on the lifetime τ is determined by the solution of differential transport equations [5]. In fig. 1 the lifetime dependence of $P_{\rm br}$ is presented for three different targets used in the DIRAC experiment. The nickel target provides the best statistical accuracy for the same running time.

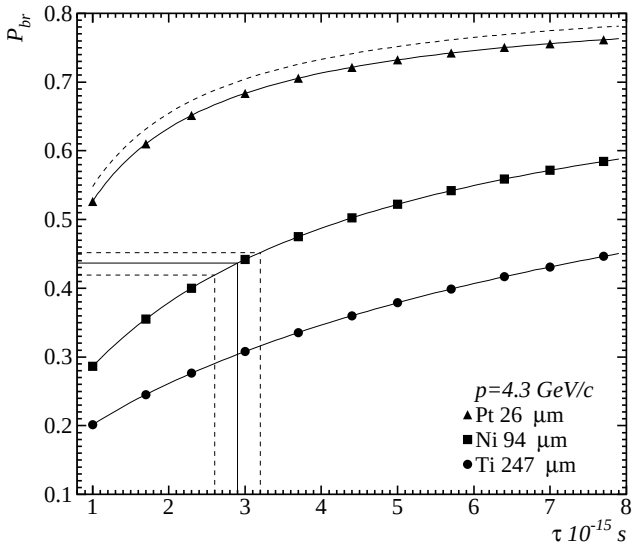

Figure 1: *Dependence of the breakup probability $P_{\rm br}$ on $A_{2\pi}$ lifetime for three targets used in the DIRAC experiment: platinum of 26 μm, nickel of 94 μm and titanium of 247 μm thickness.*

3 Experimental setup

The purpose of the DIRAC setup (Fig. 2) is to detect $\pi^+\pi^-$ pairs with small relative momenta [6]. This setup is located at the CERN T8 beam area (East Hall). It became operational at the end of 1998 and uses the 24 GeV proton beam from PS accelerator. During some periods in 2002 and 2003 there was 20 GeV proton beam.

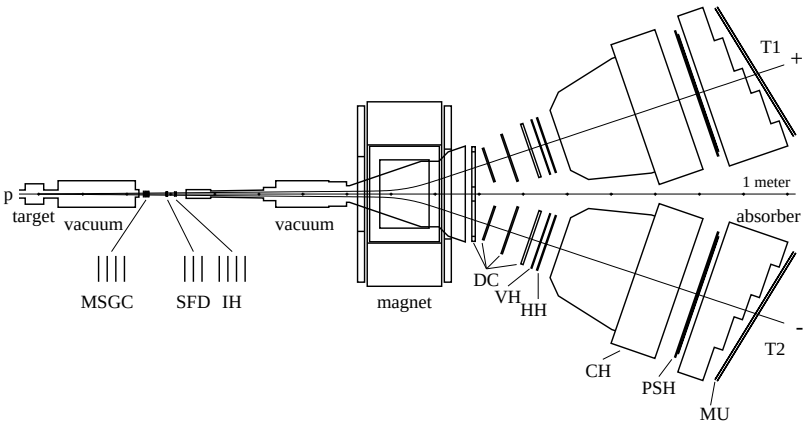

Figure 2: *DIRAC setup. MSGC are microstrip gas chambers, SFD is a scintillating fiber detector and IH is a scintillation ionization hodoscope. Downstream the spectrometer magnet there are two identical arms T1 and T2. Each arm consists of drift chambers (DC), vertical (VH) and horizontal (HH) scintillation hodoscopes, threshold Cherenkov counters (CH), shower detectors (PSH) and scintillation muon detectors (MU)*

4 Analysis

Experimental data collected in 2001, 2002, 2003 years was processed using measurement of drift chambers and X- and Y- planes of scintillation fiber detector. An experimental distribution of events dN/dQ over relative momentum Q is obtained (see fig.3a). Events which fit criterion $Q_T < 4$ MeV/c are selected. This distribution is a mixture of "atomic", "Coulomb" and "non-Coulomb" pairs. Admixture of "accidental" pairs is excluded using time measurements with vertical scintillation hodoscope.

The spectrometer including the target is fully simulated by GEANT-DIRAC [7], a GEANT3-based simulation code. The detector and trigger system response simulation are implemented in the DIRAC analysis code ARIANE [8]. The different event types are simulated according to the underlying physics.

Atoms are generated in S-states according to eq.1 using measured laboratory momentum distributions for pairs from short-lived sources. The "atomic" pairs are generated according to evolution of the atom while propagating through the target.

"Coulomb" pairs are generated according to $A_C(Q) \cdot Q^2$ using measured laboratory momentum distributions for short-lived pairs. The term Q^2 describes phase space modified by Coulomb interaction (Gamov-Sommerfeld factor) $A_C(Q) = (2\pi m_\pi \alpha/Q)/(1 - exp(-2\pi m_\pi \alpha/Q))$.

"Non-Coulomb" pairs, where at least one pion originates from the decay of a long-lived source do not undergo any final state interactions. Thus they are generated according to Q^2 using momentum distributions for long-lived sources (difference obtained from FRITIOF-6).

These simulated data sets are reconstructed with exactly the same procedures and cuts as used for experimental data.

Experimental distribution dN/dQ is fitted by a sum of simulated distribution of "atomic", "Coulomb" and "non-Coulomb" pairs. Contributions for each kind of pairs are free parameters of the fit. The result of fit is shown in fig.3.

Simulation shows that different projection of Q have different sensitivity to the systematic effects. Therefore the same analysis was repeated for distribution over absolute value of longitudinal projection $|Q_L|$ of relative momentum Q on the total pair momentum in the laboratory system (see fig.4).

5 Systematic errors

At the analysis of experimental data the next sources of systematic errors have been investigated:

1. The error in an estimation of multiple scattering in detectors and elements of the setup of experiment DIRAC.

2. An admixture of non-identified K^+K^- $\mathrm{p\overline{p}}$ pairs.

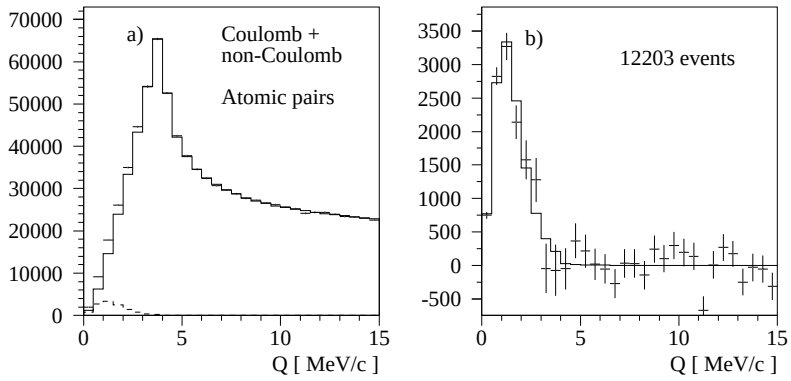

Figure 3: *a) Experimental distribution over Q (points with error bars); sum of distributions "Coulomb" and "non-Coulomb" pairs (solid) and "atomic" pairs (dashed). b) The difference of experimental distribution and a sum of background ("Coulomb" and "non-Coulomb") pairs (points with error bars) and simulated distribution of "atomic" pairs (solid).*

3. Final size of production region. Cross section of atom production eq.1 is calculated in approximation of point-like sources of pions. However there are correction due to finite size of production region and strong interaction in the final state [9].

4. Finite double-track resolution of fiber detector.

5. Presence of hits from background particles.

6. Accuracy of trigger system simulation.

Systematic errors are investigated for analysis of distributions over Q, $|Q_L|$ and two dimensional distribution over $(|Q_L|, Q_T)$. The values of statistical error, estimation of separate systematic errors and total systematic error are presented in tab.1. It is seen that the best analysis could be done using two dimensional distribution.

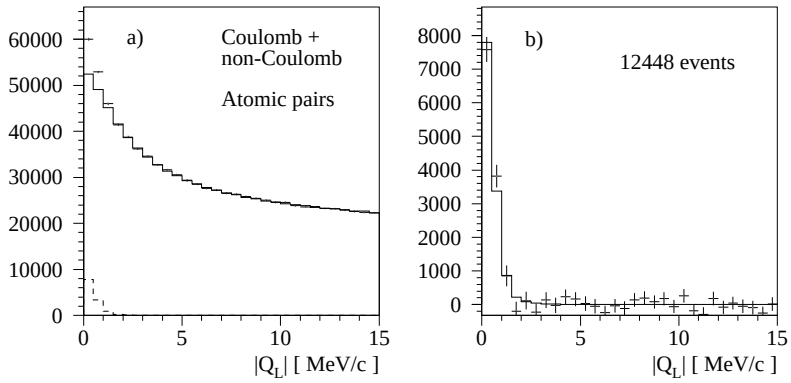

Figure 4: *a) Experimental distribution over $|Q_L|$ (points with error bars); sum of distributions "Coulomb" and "non-Coulomb" pairs (solid) and "atomic" pairs (dashed). b) The difference of experimental distribution and a sum of background ("Coulomb" and "non-Coulomb") pairs (points with error bars) and simulated distribution of "atomic" pairs (solid).*

6 Conclusion

Unfortunately these data have been analyzed very recently. Therefore collaboration is not ready to present final values of breakup probability and lifetime for $\pi^+\pi^-$ atom.

On the basis of breakup probability errors it is possible to expect that statistical error of lifetime τ is at the level $8.7 \div 12.2\%$ and systematic error of τ is at the level $3.3 \div 6.0\%$.

Therefore analysis of data collected in years 2001, 2002 and 2003 allows DIRAC experiment to achieve at least statistical accuracy better than 10%.

7 Acknowledgments

I would like to thank V. Brekhovskikh (IHEP) and M. Zhabitsky (JINR) for their help in preparing of presentation, all members of DIRAC collaboration

Table 1: *Estimation of relative errors of breakup probability for analysis with 3 variables.*

Error	δ_Q	$\delta_{\lvert Q_L\rvert}$	$\delta_{\lvert Q_L\rvert,Q_T}$
Statistical	0.031	0.044	0.031
Multiple scattering	0.018	0.008	0.014
Heavy particles admixture	0.001	0.008	0.001
Finite size effects	$^{+0.}_{-0.006}$	$^{+0.}_{-0.004}$	$^{+0.}_{-0.005}$
Double track resolution	0.009	0.001	0.003
Background particles	0.002	0.003	0.002
Trigger simulation	0.002	0.002	0.003
Total systematic	$^{+0.021}_{-0.022}$	0.012	$^{+0.015}_{-0.016}$

for there contribution to our joint research, and organizers of HADRON07 for invitation to make this report.

References

1. S.M. Bilenky *et al.*, Sov. J. Nucl. Phys. **10** (1969), p. 469.
2. G. Colangelo, *et al.*, Nucl. Phys. B **603** (2001), p. 125.
3. J. Gasser, *et al.*, Phys. Rev. D **64** (2001) 016008.
4. L.L. Nemenov, Sov. J. Nucl. Phys. **41** (1985), p. 629.
5. L.G. Afanasyev and A.V. Tarasov, Phys. At. Nucl. **59** (1996), p. 2130.
6. B. Adeva *et al.*, Nucl. Instrum. Methods A **515** (2003), p. 467.
7. O Gortchakov *et al.*, User guide (http://gortchak.home.cern.ch/gortchak/geant-dirac/montecarlo/instruction/instruct26.html)
8. D. Drijard *et al.*, The DIRAC offline user's guide (http://dirac.web.cern.ch/DIRAC/Userguide.html).
9. R. Lednicky, DIRAC note **2004-06** (nucl-th/0501065).

Frascati Physics Series Vol. XLVI (2007), pp. 905–912
HADRON07: XII Int. Conf. on Hadron Spectroscopy – Frascati, October 8-13, 2007
Low Energy QCD

RECENT KLOE RESULTS ON K_S/K_L DECAYS

Matteo Martini
INFN, Laboratori Nazionali di Frascati
On behalf of the KLOE collaboration *

Abstract

We present the measurements of the branching ratio for the $K_S \to \gamma\gamma$ and $K_S \to \pi e\nu\gamma$ decays, and a direct search for the $K_S \to e^+e^-$ decay carried out with the KLOE detector at DAΦNE.

* F. Ambrosino, A. Antonelli, M. Antonelli, F. Archilli, P. Beltrame, G. Bencivenni, S. Bertolucci, C. Bini, C. Bloise, S. Bocchetta, F. Bossi, P. Branchini, P. Campana, G. Capon, T. Capussela, F. Ceradini, F. Cesario, P. Ciambrone, F. Crucianelli, S. Conetti, E. De Lucia, A. De Santis, P. De Simone, G. De Zorzi, A. Denig, A. Di Domenico, C. Di Donato, B. Di Micco, M. Dreucci, G. Felici, M. L. Ferrer, S. Fiore, P. Franzini, C. Gatti, P. Gauzzi, S. Giovannella, E. Graziani, W. Kluge, V. Kulikov, G. Lanfranchi, J. Lee-Franzini, D. Leone, M. Martini, P. Massarotti, S. Meola, S. Miscetti, M. Moulson, S. Müller, F. Murtas, M. Napolitano, F. Nguyen, M. Palutan, E. Pasqualucci, A. Passeri, V. Patera, F. Perfetto, P. Santangelo, B. Sciascia, A. Sciubba, A. Sibidanov, T. Spadaro, M. Testa, L. Tortora, P. Valente, G. Venanzoni, R. Versaci.

1 The KLOE detector

The KLOE detector consists of a large cylindrical drift chamber, DC [1], of 4 m diameter and 3.3 m length filled with a helium-based gas mixture, surrounded by a lead-scintillating fiber calorimeter, EMC [2]. A superconducting coil around the EMC provides a 0.52 T magnetic field. The low-beta insertion quadrupoles are inside the apparatus and are surrounded by two compact tile calorimeters with veto purposes, QCAL [3].

The EMC is divided into a barrel and two endcaps covering 98% of the solid angle. Modules are read out at both ends by photomultipliers, PM, with a $\sim$ (4.4×4.4) cm^2 readout granularity, for a total of 2440 cells. Both amplitude and time information are obtained from the PMs. The signal amplitude measures the energy deposited in the modules and its time provides both the arrival time of particles and the position along the modules of the energy deposits. Cells close in time and space are grouped into a "calorimeter cluster". The cluster energy E is the sum of the cell energies. The cluster time T and position $\vec{R}$ are energy-weighted averages. Energy and time resolutions are $\sigma_E/E = 5.7\%/\sqrt{E\ (\mathrm{GeV})}$ and $\sigma_t = 57\ \mathrm{ps}/\sqrt{E\ (\mathrm{GeV})} \oplus 100\ \mathrm{ps}$, respectively. The photon detection efficiency is $\sim$ 90% at $E = 20$ MeV and reaches 100% above 70 MeV.

The QCAL is made of two tile calorimeters, $\sim$ 5 X_0 thick, surrounding the two sets of low-beta quadrupoles. The coverage in polar angle is $0.94 < |\cos\theta| < 0.99$. Each calorimeter consists of a sampling structure of lead and scintillator tiles arranged in 16 azimuthal sectors. The readout is by wavelength shifter fibers coupled to mesh photomultipliers. The fiber arrangement allows the measurement of the longitudinal coordinate by time differences.

Calorimeter signals are used for the trigger [4]. Two energy deposits with $E > 50$ MeV for the barrel and $E > 150$ MeV for the endcaps are required. Identification and rejection of cosmic-ray events are also performed at the trigger level.

A background identification algorithm, Filfo [5], mainly based on calorimeter clustering runs offline over all collected data to reject residual cosmic-ray, machine background and Bhabha events fragmenting on QCAL before running the whole reconstruction program.

2 Measurement of BR($K_S \to \gamma\gamma$)

A precise measurement of the $K_S \to \gamma\gamma$ decay rate is an important test of the predictions of Chiral Perturbation Theory (χPT). The decay amplitude of $K_S \to \gamma\gamma$ has been evaluated at the leading $O(p^4)$ order of χPT with a few percent precision [6] giving $BR(K_S \to \gamma\gamma) = 2.1{\times}10^{-6}$.
The more recent measurement of this decay, published from NA48 [7], indicates a branching ratio of 2.78×10^{-6} with a total uncertainty below 3%. This result differs from χPT $O(p^4)$ prediction of about 30% suggesting the presence of important contributions from higher order corrections.

In KLOE, K_S mesons are clearly tagged with an efficiency of ∼30% by identifying a K_L interaction in the calorimeter (K_L-crash in the following) which has a very distinctive signature given by a delayed ($\beta_K = 0.2$) energy cluster not associated to any track.

The main source of background for the $K_S \to \gamma\gamma$ decay is due to $K_S \to 2\pi^0$ events where two photons are not detected, either because outside the acceptance, or not reconstructed by the calorimeter. For the Monte Carlo simulation, MC, of the background, we use a production of $\phi \to K_S K_L$ decays corresponding to an equivalent luminosity of ~ 1.5 fb^{-1}. For the signal MC we use a production equivalent to ∼100 fb^{-1}. The data sample analyzed for this measurement corresponds to 1.9 fb^{-1}. In the simulation, the photon detection efficiency and resolutions have been tuned with data using a large sample of tagged photons in $\phi \to \pi^+\pi^-\pi^0$ events selected using only drift chamber information [5]. The interaction of the K_L in the main calorimeter is properly simulated.

To reject the main background from $K_S \to 2\pi^0$ decays, we count the number of prompt photons, N_γ with energy above 7 MeV produced in a large angular acceptance, $|cos(\theta)| < 0.93$. To improve the background rejection we also veto events from the small angle calorimeter, QCAL [3].

To improve the signal over background ratio we apply a kinematic fit ($N_{dof} = 7$) which imposes 4-momentum conservation on $\phi \to K_S K_L$ and $K_S \to \gamma\gamma$ decays, and $\beta = 1$ for each energy cluster. We reject events with $\chi^2_{fit} < 20$.

To estimate the signal, wee look at the two-dimensional distribution of the two-photon invariant mass, $M_{\gamma\gamma}$, and the opening angle between the two photons in the K_S center of mass system, $\theta^*_{\gamma\gamma}$. A binned max-likelihood fit to

the $M_{\gamma\gamma} - \theta^*_{\gamma\gamma}$ 2D distribution on data is done by using the MC shapes for signal and background.

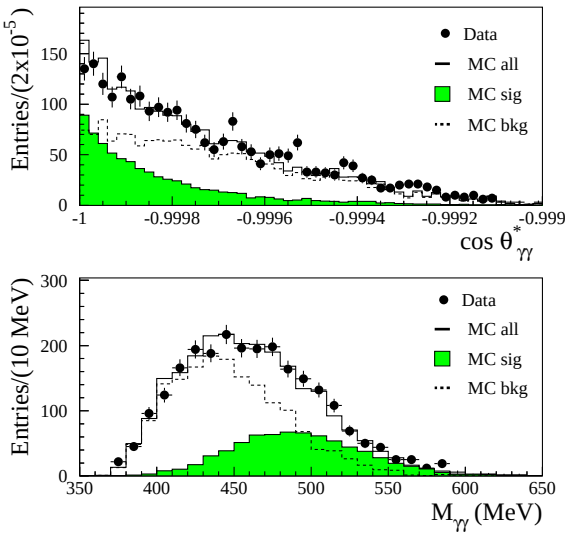

Figure 1: Distributions of $\cos(\theta^*_{\gamma\gamma})$ (a) and $M_{\gamma\gamma}$ (b) for the final sample.

Fig. 1 shows the fit result for the two-photon invariant mass and the angle distributions. The angle distribution for the signal has a shape more peaked around $\cos\theta^*_{\gamma\gamma}$ = -1 than for the background. The $M_{\gamma\gamma}$ distribution shows a gaussian shape around the K_S mass for the signal, while the background populates the low mass values. We count $N(2\gamma|tag) = 711 \pm 35$ signal events in a total of 2280 events.

As an independent check of the fit quality, we show in Fig. 2.a the χ^2 distribution for data and MC after minimization. A similar comparison is done also for the angular photon spectrum (Fig. 2.b), which clearly indicates the presence of a flat component due to signal, as expected by the two body decay of a spin 0 particle.

The branching ratio is normalized to the number of $K_S \to 2\pi^0$ events recorded in the same data sample by counting the K_S tagged events with

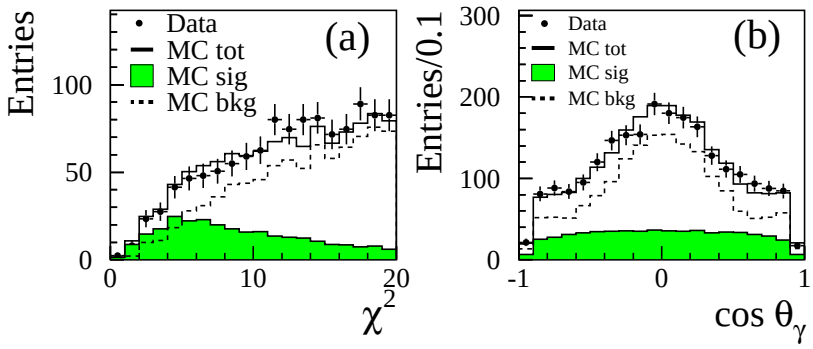

Figure 2: Distributions of χ^2 (a) and inclusive $\cos\theta_\gamma$ of the two photons in the event (b) for the final sample.

$N_\gamma = 4$.

The signal efficiency is the product of the efficiencies for the acceptance selection, the QCAL veto and the χ^2-cut:

$$\varepsilon(2\gamma|tag) = (50.55 \pm 0.15)\%$$

The number of $K_S \to 2\pi^0$ events after correcting for the selection efficiency is $(190.5 \pm 0.2) \times 10^6$. Using $\mathrm{BR}(K_S \to 2\pi^0) = (30.69 \pm 0.05)\%$ [8], we obtain:

$$BR(K_S \to \gamma\gamma) = (2.26 \pm 0.12(stat.) \pm 0.06(syst.)) \times 10^{-6}$$

where the second error includes the systematics due to fit procedure and to the small difference in energy scale between data and MC.

3 Direct search for $K_S \to e^+e^-$

The $K_S \to e^+e^-$ decay, like $K_L \to e^+e^-$ or $K_L \to \mu^+\mu^-$, is a flavour-changing neutral-current process, suppressed in the Standard Model and dominated by the two-photon intermediate state [9]. Using χPT to order $O(p^4)$, Ecker and

Pich evaluated the ratio $\Gamma(K_S \to e^+e^-)/\Gamma(K_S \to \gamma\gamma) = 8 \times 10^{-9}$ with 10% uncertainty [9]. Using the present average, $\mathrm{BR}(K_S \to \gamma\gamma) = (2.71 \pm 0.06) \times 10^{-6}$ [8], the Standard Model prediction is $\mathrm{BR}(K_S \to e^+e^-) \simeq 10^{-15}$.

K_S decays are tagged using the K_L-crash algorithm. $K_S \to e^+e^-$ events are selected requiring the presence of two tracks of opposite charge forming a vertex inside a cylinder centered on the origin of 4 cm radius and 10 cm length along the beam line. The track momenta and polar angles must satisfy the cuts $(120 < p < 350)$ MeV/c and $30^\circ < \theta < 150^\circ$. The tracks must also reach the calorimeter without spiralling, and have an associated cluster with $E > 50$ MeV.

The main backgrounds are $K_S \to \pi^+\pi^-$ decays where two pions are misidentified, and $\phi \to \pi^+\pi^-\pi^0$ decays where one prompt photon simulates K_L-crash and the other goes undetected. For the first, the M_{ee} invariant mass is peaked at low values: a cut $M_{ee} > 420$ MeV/c^2 rejects most of the background. To further reduce this contamination, we use an additional cut on the momentum evaluated in pion hypothesis, $P^* > 220$ MeV. To reject $\pi^+\pi^-\pi^0$ contamination, we impose a cut on the missing mass evaluated from ϕ momentum and from tracks momentum. After preselection we are left with $\sim 10^6$ events. To improve the signal and background separation, a χ^2-like variable is defined. To build this variable we use:

- Time of flight of the two particles
- E/p of both particles
- The distance between track impact point and the closest cluster

We normalize the relative fraction of background using the side bands.A signal box to select $K_S \to e^+e^-$ events can be conveniently defined in the χ^2-M_{ee} plane.

The signal box is chosen with an optimization procedure based on MC only. The boundaries are $(492 < M_{ee} < 504)$ MeV/c^2 and $\chi^2 < 20$, corresponding to a total signal efficiency of 55.8%.

Applying this selection to the data sample we obtain $N_{obs} = 3$. The background estimated from MC is $\mu_B = 7.1 \pm 3.6$, the value takes into account events fluctuations and normalization factors. The signal efficiency, given a K_L-crash, is $\varepsilon(e^+e^-|tag) = (55.8 \pm 0.3)\%$. Using a bayesian approach [10], we

evaluate the upper limit on the expected number of signal events $\mu_S < 4.3$ at 90% CL. The chosen interval for M_{ee} selects $K_S \to e^+e^-(\gamma)$ events with $E_\gamma <$ 6 MeV. Then we derive an upper limit for the branching ratio

$$BR(K_S \to e^+e^-(\gamma)\ ; E_\gamma < 6\ \text{MeV}) < 2.1 \times 10^{-8}$$

at 90% CL.

4 Measurement of BR($K_L \to \pi e\nu\gamma$)

The experimental measurements of this decay show a marginal disagreement from theoretical expectation. The ratio:

$$R = \frac{BR(Ke3\gamma, E^*_\gamma > 30MeV, \theta^*_{lep-\gamma})}{BR(Ke3(\gamma))}$$

has two possible components: radiation from electron bremsstrahlung, IB, and from weak vertex, DE. Due to the small electron mass, IB is dominant. The separation between IB and DE has never been measured before. For the first time, the DE contribution is measured. To disentangle the two contributions, the plane E^*_γ versus $\theta^*_{e-\gamma}$ is used. The variables are reconstructed by kinematic closure based on cluster position and tracking. The main background is constituted by $K_{\mu 3}$ and $\pi^+\pi^-\pi^0$ that are rejected using a "neural network" trained with the information from the electromagnetic calorimeter. Using a sample of 2×10^6 K_{e3} decays, KLOE obtain:

$$R = \frac{BR(K_L \to \pi e\nu\gamma)}{BR(K_L \pi e\nu)} = 0.924 \pm 0.023_{stat} \pm 0.016_{syst}$$

so confirming the disagreement with theory. According to [11], the spectrum can be parametrized as:

$$\frac{d\Gamma}{dE_\gamma} = \left(\frac{d\Gamma}{dE^*_\gamma}\right)_{IB} + \left[\langle X\rangle\, f\left(E^*_\gamma\right)\right]$$

We obtain: $\langle X\rangle = (2.3 \pm 1.3_{stat} \pm 1.4_{syst})$ That is in agreement with the theoretical expectation: $\langle X\rangle = -1.2 \pm 0.4$.

References

1. KLOE collaboration, M. Adinolfi *et al.*, Nucl. Inst. Meth. A 488 (2002), 51.
2. KLOE collaboration, M. Adinolfi *et al.*, Nucl. Inst. Meth. A 482 (2002), 364.
3. KLOE collaboration, M. Adinolfi *et al.*, Nucl. Inst. Meth. A 483 (2002), 649.
4. KLOE collaboration, M. Adinolfi *et al.*, Nucl. Inst. Meth. A 492 (2002), 134.
5. KLOE collaboration, F. Ambrosino *et al.*, Nucl. Inst. Meth. A 534 (2004), 403.
6. G. D'Ambrosio, D. Espriu, Phys. Lett. B175 (1986), 237.
7. J. R. Batley, *at al.*, Phys. Lett. B551 (2003), 7.
8. W.-M. Yao et al., J. Phys. J. G 33 (2006) 1.
9. G. Ecker and A. Pich, Nucl. Phys. B366 (1991) 189.
10. O. Helene, Nucl. Instr. Meth. 212 (1983) 319.
11. J. Gasser *et al.*, Eur. Phys. J. 40C (2005) 205.

Frascati Physics Series Vol. XLVI (2007), pp. 913
HADRON07: XII Int. Conf. on Hadron Spectroscopy – Frascati, October 8-13, 2007
Low Energy QCD

CHIRAL SYMMETRY AND STRINGS

L. Glozman
Institute for Physics, Theoretical Physics Branch, University of Graz

Written contribution not received

Frascati Physics Series Vol. XLVI (2007), pp. 915–922
HADRON07: XII Int. Conf. on Hadron Spectroscopy – Frascati, October 8-13, 2007
Low Energy QCD

THE LARGE DEGENERACY OF EXCITED HADRONS AND QUARK MODELS

P. Bicudo
Dep. Física and CFTP, Instituto Superior Técnico,
Av. Rovisco Pais, 1049-001 Lisboa, Portugal

Abstract

The pattern of a large approximate degeneracy of the excited hadron spectra (larger than the chiral restoration degeneracy) is present in the recent experimental report of Bugg. We review how the Coulomb Gauge chiral invariant and confining Bethe-Salpeter equation simplifies in the case of very excited quark-antiquark mesons. The resulting meson spectrum is solved, and the excited chiral restoration is recovered, for all mesons with $J > 0$. Applying the ultra-relativistic simplification to a linear equal-time potential, linear Regge trajectories are obtained, for both angular and radial excitations. The spectrum is also compared with the semi-classical Bohr-Sommerfeld quantization relation. However the excited angular and radial spectra do not coincide exactly. We then search, with the classical Bertrand theorem, for central potentials producing always classical closed orbits with the ultra-relativistic kinetic energy. We find that no such potential exists, and this implies that no exact larger degeneracy can be obtained in our equal-time framework, with a single principal quantum number comparable to the non-relativistic Coulomb or harmonic oscillator potentials.

1 Introduction

Here we address the question, is it possible to build an equal-time quark model, with linear trajectories, with excited chiral symmetry, and, also, with a principal quantum number [1]?

In the recent report of Bugg [2] a large degeneracy emerges from the spectra of the angularly and radially excited resonances produced in $p\bar{p}$ annihilation by the Crystal Ball collaboration at LEAR in CERN. Moreover, excited baryons have also been observed by the Crystal Barrel collaboration at ELSA [3]. This degeneracy may be the third remarkable pattern of the excited spectra of hadronic resonances. A long time ago, Chew an Fautschi remarked the existence of linear Regge trajectories for angularly excited mesons. A similar linear aligning of excited resonances was also reported for radial excitations. Recently, there has been a new revival of the chiral symmetric quark models, [4, 5] by Glozman *et al.* [6, 7] and other authors, who have been systematically researching the degeneracy of chiral partners in excited resonances, both in models and in lattice QCD.

We adopt the framework of the Coulomb gauge confinement, of the mass gap equation, and of the equal-time Bethe-Salpeter equation. In Section II we review and expand earlier work on chiral symmetry breaking and mesonic boundstates. In Section III we solve the equation with the method of the double diagonalization of the equal time hamiltonian. We then address in Section IV the large degeneracy, where both radial and angular excitations are degenerate. We conclude in Section V.

2 Quark mass gap and boundstates in equal time

A simple harmonic equal-time confining quark-quark potential, [5, 8, 9] . can be approximately derived from QCD up to the first cumulant order, of two gluons.

For excited mesons with $j > 0$, the spectrum in table 1 is very well approximated by the solutions of the pair of Schrödinger-like equations,

$$\left[-\frac{d^2}{dk^2} + 2k - \frac{1}{k^2} + \frac{j(j+1)}{k^2}\right] \nu(k) \quad = \quad M\nu(k) \tag{1}$$

Table 1: *Masses of the first angular and radial excitations of the different light-light tachyons and mesons in the chiral limit of a vanishing quark mass m. Each column includes both positive and negative parity degenerate states, except for the pseudoscalar and scalar tachyonic states, which are simply avoided with a sufficiently large constituent quark mass. The meson masses are separated in two different families with the same J because two different Salpeter equations (1) and (2) exist for each J.*

n	Pse	Sca	j=1	j=1	j=2	j=2	j=3	j=3
0	$\frac{2\times10^{-1}i}{m^2}$	$\frac{3\times10^{-2}i}{m^2}$	3.71	4.59	6.15	6.45	7.65	7.84
1	$\frac{2\times10^{-3}i}{m^2}$	$\frac{3\times10^{-4}i}{m^2}$	6.49	7.15	8.43	8.69	9.72	9.89
2	$\frac{2\times10^{-5}i}{m^2}$	$\frac{3\times10^{-6}i}{m^2}$	8.76	9.32	10.45	10.68	11.61	11.76
3	$\frac{2\times10^{-7}i}{m^2}$	$\frac{3\times10^{-8}i}{m^2}$	10.77	11.27	12.30	12.51	13.38	13.52
4	$\frac{2\times10^{-9}i}{m^2}$	$\frac{3\times10^{-10}i}{m^2}$	12.61	13.08	14.05	14.25	15.12	15.26

$$\left[-\frac{d^2}{dk^2}+2k-\frac{2}{k^2}+\frac{j(j+1)}{k^2}\right]\nu(k) \quad = \quad M\nu(k) \tag{2}$$

obtained when the negative energy component ν^- are neglected in the full Salpeter equations.

3 Linear Regge trajectories and semi-classical quantization with the linear potential

Our simple results of eq. (1) and eq. (2) are extended to a linear potential [10, 11], to get the linear Regge trajectories. Both from the quark modelling of the heavy quarkonium, and from Lattice QCD static potentials, it is suggested that the long range confining quark potential is linear. Continuing with the limit where $\frac{m}{k}\to 0$, and aiming at large total angular momenta j, we assume for the radial equation, the minimal extension of eq. (1) and eq. (2) of Section II for a linear potential,

$$(2\,p+\sigma\;r)\,\nu = E\nu\;, \tag{3}$$

where, in momentum space, the position r is an operator,

$$\widehat{r}=\sqrt{-\frac{d^2}{dp^2}+\frac{j(j+1)}{p^2}}\;, \tag{4}$$

Table 2: *Masses of the light-light mesons, in dimensionless units of $\sigma = 1$, computed with the ultra-relativistic equal time chiral degenerate Schrödinger equation (3). The $j = 0$ mesons are distant from the experimental spectrum, but chiral degeneracy is theoretically plausible for the very excited mesons.*

j	n=0	n=1	n=2	n=3	n=4	n=5	n=6	n=7	n=8
0	3.16	4.71	5.89	6.87	7.73	8.51	9.21	9.87	10.49
1	4.22	5.46	6.48	7.38	8.17	8.90	9.58	10.21	10.81
2	5.08	6.13	7.05	7.87	8.61	9.30	9.95	10.56	11.13
3	5.81	6.74	7.58	8.34	9.04	9.70	10.31	10.90	11.45
4	6.46	7.31	8.08	8.79	9.45	10.08	10.67	11.23	11.77
5	7.05	7.83	8.55	9.22	9.86	10.45	11.02	11.56	12.08
6	7.60	8.32	9.00	9.64	10.24	10.82	11.36	11.89	12.39
7	8.11	8.79	9.43	10.04	10.62	11.17	11.70	12.21	12.70
8	8.59	9.23	9.84	10.43	10.98	11.51	12.03	12.52	12.99
9	9.04	9.65	10.24	10.80	11.33	11.85	12.34	12.82	13.29
10	9.47	10.06	10.62	11.16	11.68	12.18	12.66	13.12	13.58
11	9.88	10.45	10.99	11.51	12.01	12.49	12.96	13.42	13.86
12	10.28	10.82	11.35	11.85	12.34	12.81	13.26	13.71	14.14
13	10.66	11.19	11.69	12.18	12.65	13.11	13.56	13.99	14.41

neglecting now the terms $\frac{-1}{k^2}$ or $\frac{-2}{k^2}$. In configuration space, r is the c-number and the operator is the momentum p, replaced in eq. (3) by

$$\widehat{p} = \sqrt{-\frac{d^2}{dr^2} + \frac{j(j+1)}{r^2}} \ . \tag{5}$$

Again, the usual centrifugal barrier for spinless particles is extended for fermions in the chiral restoration limit substituting $\mathbf{L}^2$ by $\mathbf{J}^2$, consistent with the result of Section II.

The numerical solutions are shown in Table 2. In Fig. 1 and in Fig. 2 we graphically demonstrate that the angular excitations and the radial excitations of this simple spectrum are disposed in linear Regge trajectories,

$$\begin{aligned} j &\simeq \alpha_0 + \alpha M^2 \ , \\ n &\simeq \beta_0 + \beta M^2 \ . \end{aligned} \tag{6}$$

This agrees qualitatively with the experimental spectrum [2], where the linear Regge trajectories are also present. As anticipated, in the limit of large excitations, our trajectories are also parallel to the ones of Wagenbrunn and Glozman [7].

Interestingly, with the semi-classical Bohr-Sommerfeld quantization relation, and in our units of $\hbar = c = \sigma = 1$, we get for the Regge slopes respectively,

$$\begin{aligned} \alpha &= \frac{1}{8} , \\ \beta &= \frac{1}{4\pi} , \end{aligned} \tag{7}$$

in excelent agreement with the slopes of Figs. 1 and 2, and with the slopes of the recent Bethe-Salpeter calculation of Wagenbrunn and Glozman [7].

The important point we want to stress is that we find quantitative discrepancies with the experiment, although our theoretical result show linear Regge trajectories and comply the chiral degeneracy. In particular, experimentally, the radial and agular slopes defined in eq. (6) should be almost identical [2],

$$\begin{aligned} \alpha_{\rm exp} &= 0.877 \text{ GeV}^{-2} , \\ \beta_{\rm exp} &= 0.855 \text{ GeV}^{-2} , \end{aligned} \tag{8}$$

while our theoretical slopes, depicted in Figs. 1 and 2 and semi-classically computed in eq. (7), differ by $\pi/2$. Moreover the meson masses in Table 2 do not exactly comply with the large degeneracy emerging in the observations of Bugg. Identical slopes would be necessary to reproduce this large experimental degeneracy.

4 Using classical closed orbits to search for a potential with a principal quantum number

To try to solve the large degeneracy problem, it is then natural to extend our simple linear potential $\sigma\, r$ of eq. (3) to a wider class of hadronic potentials. We ask for a a spectrum with a principal quantum number, similar to the non-relativistic spectra of the Coulomb potential or of the harmonic oscillator potential, where the principal quantum numbers are respectively $n + l + 1$ and $2n + l + \frac{3}{2}$. The difference here is that our kinetic energy is the ultra-relativistic one $T = 2\, p\, c$ whereas in the non-relativistic case $T = \frac{p^2}{2\mu}$.

Notice that in the non-relativistic case, classical closed orbits coincide with a quantum principal number. We can also address this problem searching for classical closed orbits with an ultra-relativistic kinetic energy. When all the classical orbits are closed then the Hermann-Jacobi-Laplace-Runge-Lenz vector is conserved, because this vector does not precess. In the Hamilton-Jacobi

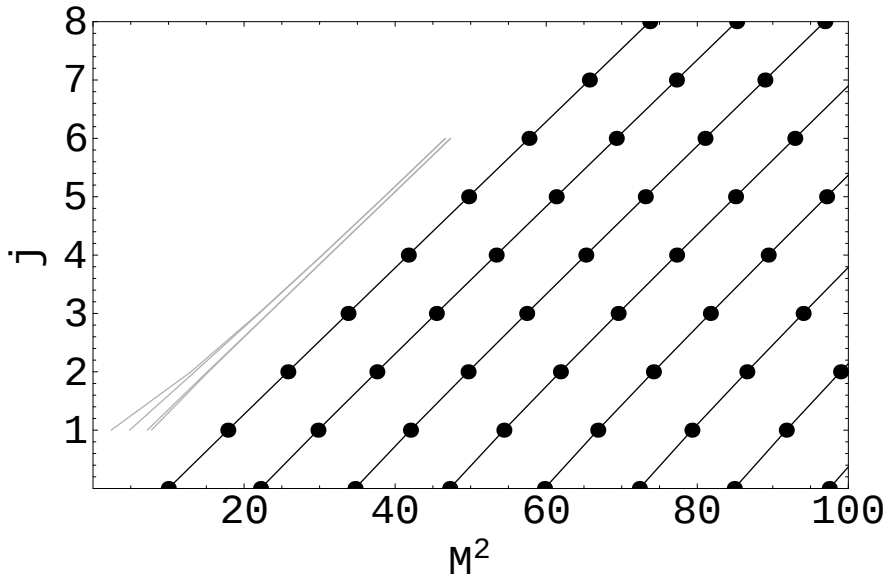

Figure 1: We show the quasi-linear Regge trajectories, of j as a function of M^2. Each line corresponds to a fixed radial n, increasing from left to right. The M are the masses of the light-light mesons, in dimensionless units of $\sigma = 1$, computed with the ultra-relativistic equal time chiral degenerate Schrödinger equation (3). In grey we also show the trajectories with $n = 0$ and starting at $j = 1$ of Ref. [7].

formalism, this vector commutes with the hamiltonian. The same commutation then also occurs in the quantum Schrödinger formalism, the formalism we are using now. Then a larger symmetry group, including the angular momentum and the Hermann-Jacobi-Laplace-Runge-Lenz vector exists. Finally this implies that a principal quantum number exists. For simplicity we consider a kinetic energy $T = p\,c$ and a general potential $V(r)$, used for a single particle in a central potential, comparable to our two-body problem in the centre of mass frame.

Unfortunately, this restricts the class of possible potentials,

$$\frac{d}{du}J|_{u=u_0} = 1 - \beta^2 = \frac{f^2(\frac{1}{u_0})}{c^2 L^2 {u_0}^2} - 2 + \frac{u_0}{f_0}\frac{df(\frac{1}{u_0})}{du_0} \tag{9}$$

and the problem here is that, unlike in the non-relativistic limit, the equation

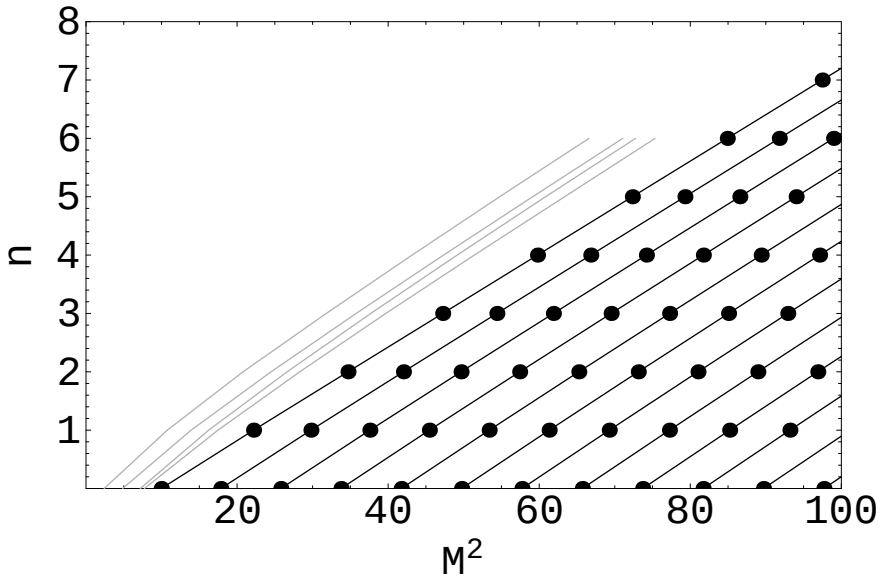

Figure 2: We show we show the quasi-linear Regge trajectories, of n as a function of M^2. Each line corresponds to a fixed angular j, increasing from left to right. The M are the masses of the light-light mesons, in dimensionless units of $\sigma = 1$, computed with the ultra-relativistic equal time chiral degenerate Schrödinger equation (3). In grey we also show the trajectories with $j = 1$ of Ref. [7].

still depends on the parameter cL, and thus the closed orbits are possible, but there is no potential for which all orbits are closed, since the closing depends on cL.

5 Conclusion

The most ambitious approach to the large degeneracy consists in asking for a model with a principal quantum number.

We start with a semi-relativistic chiral invariant quark model, with relativistic kinetic energy, with negative energy components, but with an instantaneous potential. For excited states all the different spin-tensor potentials merge and we arrive at a schrödinger-like ultra-relativistic potential quark model with

a simple $\mathbf{J}^2$ dependence, leading to the chiral degeneracy of the excited spectra. This schrödinger-like quark model is conveniently simple to show that the linear potential, well known for a spectrum with linear Regge trajectories, fails to reproduce the large degeneracy. We also find that this large symmetry does not exist, neither for the linear potential nor for any other central potential, in our ultra-relativistic and instantaneous framework.

References

1. P. Bicudo, Phys. Rev. D **76**, 094005 (2007) [arXiv:hep-ph/0703114].
2. D. V. Bugg, Phys. Rept. **397**, 257 (2004) [arXiv:hep-ex/0412045].
3. U.Thoma, "Recent results from the Crystal Barrel experiment at ELSA," presented at the International Workshop XXXIV on Gross Properties of Nuclei and Nuclear Excitations, Hirschegg, (2007)
4. A. Le Yaouanc, L. Oliver, S. Ono, O. Pene and J. C. Raynal, Phys. Rev. D **31**, 137 (1985).
5. P. Bicudo and J. E. Ribeiro, Phys. Rev. D **42**, 1611 (1990); Phys. Rev. D **42**, 1625; Phys. Rev. D **42**, 1635.
6. L. Y. Glozman, Phys. Rept. **444**, 1 (2007) [arXiv:hep-ph/0701081].
7. R. F. Wagenbrunn and L. Y. Glozman, Phys. Rev. D **75**, 036007 (2007) [arXiv:hep-ph/0701039];
8. P. Bicudo, Phys. Rev. D **74**, 036008 (2006) [arXiv:hep-ph/0512041].
9. P. Bicudo, Phys. Rev. D **74**, 065001 (2006) [arXiv:hep-ph/0606189].
10. P. Bicudo, J. E. Ribeiro and J. Rodrigues, Phys. Rev. C **52**, 2144 (1995).
11. F. J. Llanes-Estrada and S. R. Cotanch, Phys. Rev. Lett. **84**, 1102 (2000) [arXiv:hep-ph/9906359].
12. P. J. A. Bicudo and A. V. Nefediev, Phys. Rev. D **68**, 065021 (2003) [arXiv:hep-ph/0307302].

HEAVY MESON SPECTROSCOPY

Frascati Physics Series Vol. XLVI (2007), pp. 925
HADRON07: XII Int. Conf. on Hadron Spectroscopy – Frascati, October 8-13, 2007
Heavy Meson Spectroscopy

DYNAMICALLY GENERATED OPEN AND HIDDEN CHARM MESON SYSTEMS

Daniel Gamermann
IFIC- Universidad de Valencia

Written contribution not received

Frascati Physics Series Vol. XLVI (2007), pp. 927
HADRON07: XII Int. Conf. on Hadron Spectroscopy – Frascati, October 8-13, 2007
Heavy Meson Spectroscopy

BOTTOMONIUM MASSES, DECAY RATES AND SCALAR CHARGE RADII

J. N Pandya
Department of Physics, Veer Narmad South Gujarat University
Surat 395 007, INDIA

Written contribution not received

Frascati Physics Series Vol. XLVI (2007), pp. 929–936
HADRON07: XII Int. Conf. on Hadron Spectroscopy – Frascati, October 8-13, 2007
Heavy Meson Spectroscopy

OPEN FLAVOR CHARMED MESONS

P. C. Vinodkumar,
*Department of Physics, Sardar Patel University,
Vallabh Vidyanagar-388 120,Gujarat, India.
Ajay Kumar Rai,
Department of Applied Sciences and Humanities,
SVNIT, Surat-395 007,Gujarat, India.
*Bhavin Patel,
Jignesh Pandya,
Department of Physics, Veer Narmad South Gujarat University,
Surat-395 007,Gujarat, India.

Abstract

We present here recent results on the investigations of the mass spectrum (S-states and P-states), decay constants, decay widths and life time of the D, D_s,and $B_c$mesons within the framework of phenomenological potential models.We also present the binding energy and the masses of the di-meson molecular systems with one or more charm meson combinations. Many of the newly found experimental open charm states are identified with the orbital excitations of the conventional open charm mesons while others like X(3872), Y(3930), $D_{sJ}(2632, 2700)$ *etc.*, are identified as molecular like states.

1 Introduction

The study of spectroscopy and the decay properties of the heavy flavour mesonic states provides us useful information about the dynamics of quarks and gluons at the hadronic scale. The remarkable progress at the experimental side, with various high energy machines such as LHC, B-factories, Tevatron, ARGUS collaborations, CLEO etc for the study of hadrons has opened up new challenges in the theoretical understanding of heavy flavour hadrons. In order to understand the structure of the newly observed zoo of open flavour meson resonances [1, 2, 3, 4] in the energy range of 2-5 GeV, it is necessary to analyze their spectroscopic properties and decay modes based on theoretical models. Many of these states could be the excited charmed mesonic states while for many other states the possibility of multi-quark or molecular like structures are being proposed. Thus, the main objective of the present talk includes the study of spectroscopy and the decay properties of the open flavour charm mesons. We study these open charm states as the excited states of the conventional quark-antiquark systems within the frame work of a potential model [5, 6].

We also study, following the molecular interpretation of some of the recently observed meson states, the binding energy and the ground state masses of di-hadronic molecules [7, 8]. For the binding energy of the di-hadronic state, we consider a large r ($r \to \infty$) limit of the confined gluon propagator employed in our earlier study on N-N integrations. [9]

2 Theoretical methodology: A Potential Scheme

For the light-heavy flavour bound system of $q\overline{Q}$ or $\overline{q}Q$ we treat the heavy-quark (Q=c, b) non-relativistically and the light-quark (q = u, d, s) relativistically within the mesonic system. The Hamiltonian for the case be written as [6]

$$H = M + \frac{p^2}{2m} + \sqrt{p^2 + m^2} + V(r) + V_{S_{\bar{Q}} \cdot S_q}(r) + V_{L \cdot S}(r) \tag{1}$$

Where M is the heavy quark mass, m is the light quark mass, p is the relative momentum of each quark, V(r) is the confined part of the quark- antiquark potential, $V_{S_{\bar{Q}} \cdot S_q}(r)$ and $V_{L \cdot S}(r)$ are the spin-spin and spin orbital part of the interaction. Here we consider

$$V(r) = \frac{-\alpha_c}{r} + Ar^{\nu} \tag{2}$$

where $\alpha_c = \frac{4}{3}\alpha_s$, α_s being the strong running coupling constant, A and ν are the potential parameters. For computing the hyperfine and spin-orbit splitting, we consider the spin dependent part of the usual OGEP given by [10]

$$V_{S_{\bar{Q}}\cdot S_q}(r) = \frac{2}{3}\frac{\alpha_c}{M_{\bar{Q}}m_q}\ \vec{S_{\bar{Q}}}\cdot\vec{S_q}\ 4\pi\delta(\vec{r}), \quad V_{L\cdot S}(r) = \frac{\alpha_c}{M_{\bar{Q}}m_q}\ \frac{\vec{L}\cdot\vec{S}}{r^3} \tag{3}$$

We employ the harmonic oscillator wave function and use the virial theorem, to get the energy expression from the hamiltonian defined by Eqn.(1). Here μ is the wave function parameter determined using the variational method. The parameters used here are $m_{u/d} = 0.360\ GeV$,$m_s = 0.5\ GeV$, $m_c = 1.41\ GeV$, $m_b = 4.88\ GeV$, $\alpha_c = 0.48$ (for open charm meson) and $\alpha_c = 0.36$ (for open beauty-charm meson). The computed S and P wave mass spectrum of D, D_s and B_c mesons are tabulated in Table 1 alongwith the experimental and other theoretical results.

3 The decay constants and Lifetime of the open charm mesons

The decay constant of the mesons is an important parameter in the determination of the leptonic, non-leptonic weak decay processes. It is related to the wave function at the origin through Van-Royen-Weisskoff formula. Incorporating a first order QCD correction factor, we compute them using the relation [11]

$$f_P^2 = \frac{12\left|\Psi_P(0)\right|^2}{M_P}C^2(\alpha_s),\ \text{where}C^2(\alpha_s) = 1 - \frac{\alpha_s}{\pi}\left[2 - \frac{M_Q - m_q}{M_Q + m_q}\ ln\frac{M_Q}{m_Q}\right] \tag{4}$$

where M_P is the ground state mass of the pseudoscalar states.

In the spectator approximation [6, 12] the inclusive widths of b and c quarks decay are given by

$$\Gamma(b \to X) = \frac{9\ G_F^2\left|V_{Q\bar{Q}}\right|^2 m_b^5}{192\pi^3}, \quad \Gamma(c \to X) = \frac{5\ G_F^2\left|V_{Q\bar{q}}\right|^2 m_c^5}{192\pi^3} \tag{5}$$

and width of the annihilation channel is computed using the expression given by [6, 12]

$$\Gamma(Anni) = \frac{G_F^2}{8\pi}\left|V_{Q\bar{q}}\right|^2 f_P^2 M_P \sum_i m_i^2\left(1 - \frac{m_i^2}{M_P^2}\right)^2 C_i \tag{6}$$

Table 1: *S-Wave and P-Wave Masses (in MeV)*

	ν	1^1S_0	$1\ ^3S_1$	$1\ ^3P_0$	$1\ ^3P_1$	1^1P_1	$1\ ^3P_2$	2^1S_0	$2\ ^3S_1$
D	0.5	1922	1992	2195	2203	2210	2218	2286	2294
	1.0	1912	1993	2347	2367	2390	2414	2580	2639
	1.5	1905	2003	2388	2435	2481	2527	2599	2709
	Expt.	1864	2006	–	–	–	–	–	–
	Ebert	1875	2009	2414	2438	2459	2501	2579	2629
	Pandya	1815	1909	2385	2417	2449	2481	2653	2690
D_s	0.5	2042	2089	2353	2364	2375	2386	2466	2476
	1.0	2003	2104	2512	2544	2576	2608	2813	2847
	1.5	1937	2135	2607	2678	2750	2821	3149	3228
	Expt.	1969	2112	–	–	2535	2574	–	–
	Ebert	1981	2111	2508	2515	2560	2569	2670	2716
	Pandya	2009	2110	2385	2417	2449	2481	2778	2280
B_c	1.0	6349	6373	6715	6726	6738	6749	6821	6855
	Lattice	6280	6321	6727	6743	6765	6783	6960	6990
	ALV	6356	6397	6673	–	–	6751	6888	6910
	EFG	6270	6332	6699	6734	6749	6762	6835	7072

Expt. [3], ALV [12], EFG [13], Pandya [14], Lattice [15], Ebert [16]

where $C_i = 1$ for the $\tau\nu_\tau$ channel and $C_i = 3\left|V_{Q\bar{q}}\right|^2$ for $Q\bar{q}$, and m_i is the mass of the heaviest fermions. Here$|V_{Q\bar{q}}|$ and $\left|V_{Q\bar{Q}}\right|$ are the respective CKM Matrix, where numerical values are obtained from [3]. The total width of the $Q\overline{q}$ meson decay is the addition of partial widths *i.e.* $\Gamma(total) = \Gamma(Q \to X) + \Gamma(Anni)$. In the case of the B_c meson, both the heavy quark , b and c under go the decay and the total width is obtained as $\Gamma_{total}(B_c) = \Gamma(b \to c)+\Gamma(c \to X)+\Gamma(Anni)$. The computed pseudoscalar decay constants with and without the correction factor $C^2(\alpha_s)$, the total width and lifetime of D, D_s and B_c mesons are listed in Table 2 along with other model predictions and experimental values.

4 Di-hadrons as molecular states

The low-lying di-hadronic molecular system consisting of di-meson tetra quark states are treated here by assuming non-relativistic. Hamiltonian given by

$$H = M + \frac{P^2}{2\mu} + V(R_{12}) + V_{SD}(S_1S_2) \tag{7}$$

Table 2: *Decay constants (f_P) and lifetime of meson.*

System	ν	f_P MeV	$f_P(cor.)$ MeV	$\Gamma(total)$ $10^{-4}eV$	τ ps
D	0.5	231	157	6.126	1.074
	1.0	250	170	6.142	1.072
	1.5	276	187	6.167	1.067
	Expt.	–	–	–	1.040±0.007
	Penin	–	195±20	–	–
	Ebert	–	243±25	–	–
D_s	0.5	218	156	9.148	0.719
	1.0	321	229	12.630	0.521
	1.5	451	322	18.515	0.356
	Expt.	–	–	–	0.500±0.007
	Heister	–	285	–	–
B_c	1.0	–	556	13.86	0.47
	Expt.	–	–	–	$0.46^{+0.18}_{-0.16}$

Expt. [3], Ebert [13], Penin [17], Heister [18]

where $M = m_{h_1} + m_{h_2}$, m_{h_1} and m_{h_2} are masses of the hadrons, μ is the reduced mass, P is the relative momentum of the two hadrons and $V(R_{12})$ is the residual (molecular) interaction potential between the two hadrons given by the asymptotic expression ($r \to \infty$) of the confined one gluon exchange interaction (COGEP) given by [9]

$$V(R_{12}) = \frac{-k_{mol}}{R_{12}} e^{-C^2 \ R_{12}^2/2} \tag{8}$$

where k_{mol} is the residual strength of the strong interaction coupling and C is the effective colour screening parameter of the confined gluons. Using a trial wave function given by

$$\psi(R_{12}) = \left(4\frac{\Omega^{3/2}}{\sqrt{\pi}}\right)^{1/2} e^{-\Omega \ \ R_{12}^2/2} \tag{9}$$

By minimizing the expectation value of H, the ground state molecule energy is obtained as

$$E(\Omega) = M + \frac{3\Omega}{4\mu} - \frac{4k_{mol}\Omega^{3/2}}{c^2 + 2\Omega} + \frac{8}{9}\frac{\alpha_s}{m_{h_1} m_{h_2}} \ \vec{S}_1 \ \cdot \vec{S}_2 \ |\psi(0)|^2 \tag{10}$$

Table 3: *Low-lying masses of Multiquarks as di-hadronic molecule*

Systems $h_1 - h_2$	J^{PC}	Ω GeV^2	ψ $GeV^{3/2}$	BE GeV	Mass GeV	Expt [3] GeV	Others GeV
π-D	0^{++}	0.0186	0.0757	0.022	2.027	–	–
π-D^*	1^{+-}	0.0188	0.0762	0.022	2.169	–	–
K-D	0^{++}	0.1415	0.3465	0.015	2.344	$D_{sJ}(2.317)$	–
K-D^*	1^{+-}	0.1455	0.3539	0.016	2.485	$D_{sJ}(2.460)$	–
ρ -D	1^{+-}	0.2684	0.5602	0.033	2.603	–	–
K^*-D	1^{+-}	0.3265	0.6489	0.039	2.718	$D_{sJ}(2.700)$	–
	0^{++}	0.2795	0.5775	0.235	2.543	–	–
ρ -D^*	1^{++}	–	–	0.134	2.644	–	–
	2^{++}	–	–	0.064	2.845	–	–
	0^{++}	0.3420	0.6718	0.158	2.624	$D_{sJ}(2.632)$	–
K^*-D^*	1^{++}	–	–	0.040	2.741	–	–
	2^{++}	–	–	0.077	2.976	–	–
D-D	0^{++}	0.3568	0.6935	0.008	3.738	–	3.723 [19]
D-D^*	1^{+-}	0.3810	0.7285	0.006	3.878	X(3.870)	3.876 [20]
	0^{++}	0.4081	0.7670	0.084	3.930	–	–
D^*-D^*	1^{++}	–	–	0.040	3.974	–	–
	2^{++}	–	–	0.048	4.062	$\psi(4.040)$	3.968 [21]

Here, we have added the spin-hyperfine contribution separately. The binding energy of the di-mesons as $BE = |m_{h_1} + m_{h_2} - E|$ and the parameters $k_{mol} =$ 0.45. and c=1.25 GeV are employed to compute the binding energy (BE) at the charmed sector. The computed masses and binding energies of the di-meson systems are tabulated in Table 3.

5 Conclusion and Discussion:

The properties of open charm mesons *vis a vis* D, D_s and B_c are investigated by us using an effective static quark-antiquark interaction potential of the form $-\frac{\alpha_c}{r} + Ar^{\nu}$. We found that the potential form with $\nu = 1.0$ is consistent with the experimental results of the light-heavy flavour mesons. The relativistic treatment of light flavour and non relativistic treatment of heavy

flavour seem to be justifiable in light of the successful prediction of the various properties of light-heavy flavour mesons. In the case of B_c-meson study, the non-relativistic treatment for both the heavy quarks yields better result. The S-wave and P-wave masses, decay constants f_P,the decay widths and life time of D, D_s and B_c mesons are studied within the potential scheme with $0.5 \leq \nu < 2$. The recently observed $D_{s1}(2536)$ and $D^*_{sJ}(2857)$ are found to be the 1^3P_1 and 2^3S_1 states predicted in our model with $\nu = 1.0$ Other predicted excited states are expected to be identified and observed in future experiments.

The pseudoscalar decay constant f_P predicted without the correction terms $C^2(\alpha_s)$ of Eqn.(4) in our model with potential indeax $\nu = 1$ is found to be in better agreement with the experimental values of $f_{D^+} = 222.6 \pm 16 MeV$ of CLEO collaboration [22] and the predicted value of $321 MeV$ for f_{D_s} is within the error bar of the experimental result of $283 \pm 17 \pm 7 \pm 14$ MeV by BaBar collaboration [1]. However, the PDG average value for f_{D_s} is 267 ± 33 MeV [3]. The ratio of $\frac{f_{D_s}}{f_D}$ in our case is 1.34 with the correction factor, while that with out correction factor is 1.28 which is in accordance with the Lattice results of $1.24 \pm 0.01 \pm 0.07$ [23]. The lifetime predictions of 1.07 ps for D and 0.52 ps for D_s mesons are in good agreement with the respective experimental result of 1.04 ± 0.007 ps of $D^{\pm}$ and 0.5 ± 0.007 ps with $\nu = 1.0$.

The exotic states such as $X(3872)$, $D_{SJ}(2317, 2460, 2632, 2700$ and $2860)$, $\psi(4040)$ etc are identified as the low lying di-mesonic molecular states at the charm sector as shown in Table 3. Though there exist many attempts, the zoo of open flavour mesonic states continues to pose challenges to both experimental analysis and theoretical predictions.

Acknowledgement: Part of this work is done with a financial support from DST, Government of India, under a Major Research Project **SR/S2/HEP-20/2006**.

References

1. Aubert B et al. (BABAR Collaboration), Phys. Rev. Lett. **98**, 122011 (2007); Phys. Rev. Lett. **97** 222001 (2006).

2. D. Besson et al. (CLEO Collaboration), Phys. Rev. **D 68**, 032002 (2003).
3. W. M. Yao et al., (Partcle Data Group) J. Phys. **G 33**, 1 (2006).
4. Antimo Palano, Nucl. Phys. **B 156**,105 (2006).
5. Ajay Kumar Rai, R H Parmar and P C Vinodkumar, Jnl. Phys G. **28**,2275-2280 (2002).
6. Ajay Kumar Rai and P C Vinodkumar, Pramana J. Phys. **66**(2006).
7. P Colangelo et al., Mod. Phys. Lett. **A 19**, 2083(2004).
8. Ajay Kumar Rai, Jignesh Pandya and P C Vinodkumar, Nucl. Phys. **A782**, 406-409 (2007).
9. Khadkikar S B and Vijayakumar K B , Phys. Lett. **B 254**, (1991).
10. S. S. Gershtein et al.,Phys. Rev **D51**, 3613(1995).
11. E. Braaten and S. Fleming Phys. Rev **D 52**, 181 (1995).
12. A Abd El-Hady et al., Phys. Rev **D 59**, 094001 (1999).
13. D. Ebert, R. N. Faustov and V. O. Galkin, Phys. Rev. **D 67**, 5663 (2003).
14. J. N. Pandya and P. C. Vinodkumar, Pramana J. Phys. **57**, 821 (2001).
15. C T H Davies et al., Phys. Lett. **B 382**, 131 (1996).
16. D. Ebert, R. N. Faustov and V. O. Galkin, Phys. Rev. **D 57**, 014027 (1998).
17. A. A. Penin et al., Phys. Rev. **D 65**, 054006 (2002).
18. A. Heister et al.,ALEPH Collaboration Phys.Lett.**B 528**,1(2002).
19. L. Maiani, et al., Phuys. Rev. **D 71**, 014028 (2005).
20. D. Jane and M. Rosina, Few-Body Systems **35**, 175 (2004) .
21. D. Ebert, R. N. Faustov and V. O. Galkin, Phys. Lett. **B 634**, 21 (2006).
22. Artuso M et al.,Phys. Rev. Lett.**95**, 251801 (2005).
23. Aubin C et al.,Phys. Rev. Lett.**95**, 122002 (2005).

Frascati Physics Series Vol. XLVI (2007), pp. 937–944
HADRON07: XII Int. Conf. on Hadron Spectroscopy – Frascati, October 8-13, 2007
Heavy Meson Spectroscopy

DECAYS OF $D^*_{s0}(2317)$ AND $D_{s1}(2460)$ MESONS

Valery E. Lyubovitskij, Amand Faessler, Thomas Gutsche
Institut für Theoretische Physik, Universität Tübingen,
Auf der Morgenstelle 14, D-72076 Tübingen, Germany

Abstract

We discuss a possible interpretation of $D^*_{s0}(2317)$, $D_{s1}(2460)$, $B^*_{s0}(5725)$ and $B_{s1}(5778)$ mesons as hadronic molecules. Using an effective Lagrangian approach we calculate their weak, strong and radiative decays. The new impact of molecular structure of these states is the presence of $u(d)$ quarks in K, $D^{(*)}$ and $B^{(*)}$ mesons which give rise to the direct strong isospin-violating transitions $D^*_{s0}(B^*_{s0}) \to D_s(B_s)+\pi^0$ and $D_{s1}(B_{s1}) \to D^*_s(B^*_s)+\pi^0$ in addition to the modes generated by $\eta - \pi^0$ mixing as was considered before in the literature.

1 Introduction

Nowadays there is strong interest to study newly observed mesons and baryons in the context of a hadronic molecule interpretation [1]. As stressed for example in Ref. [2] the scalar $D_{s0}^*(2317)$ and axial $D_{s1}(2460)$ mesons could be candidates for a scalar DK and a axial D^*K molecule because of a relatively small binding energy of ~ 50 MeV. These states were discovered and confirmed just a few years ago by the Collaborations BABAR at SLAC, CLEO at CESR and Belle at KEKB [3]. In the interpretation of these experiments it was suggested that the $D_{s0}^*(2317)$ and $D_{s1}(2460)$ mesons are the P-wave charm-strange quark states with spin-parity quantum numbers $J^P = 0^+$ and $J^P = 1^+$, respectively.

The next important question concerns the possible structure of $D_{s0}^*(2317)$ and $D_{s1}(2460)$ mesons. The simplest interpretation of these states is that they are the missing $j_s = 1/2$ (the angular momentum of the s-quark) members of the $c\bar{s}$ $L = 1$ multiplet. However, this standard quark model scenario is in disagreement with experimental observation since the $D_{s0}^*(2317)$ and $D_{s1}(2460)$ states are narrower and their masses are lower when compared to theoretical (see e.g. discussion in Ref. [1]). Therefore, in addition to the standard quark-antiquark picture alternative interpretation of the $D_{s0}^*(2317)$ and $D_{s1}(2460)$ mesons have been suggested: four-quark states, mixing of two- and four-quark states, two-diquark states and two-meson molecular states. Up to now strong and radiative decays of the $D_{s0}^*(2317)$ and $D_{s1}(2460)$ mesons have been calculated using different approaches [4]- [25]: quark models, effective Lagrangian approaches, QCD sum rules, lattice QCD, etc.

A new feature related to the molecular $D^{(*)}K$ structure of the $D_{s0}^*(2317)$ and $D_{s1}(2460)$ mesons is that the presence of $u(d)$ quarks in the $D^{(*)}$ and K mesons gives rise to a direct strong isospin-violating transitions $D_{s0}^* \to D_s\pi^0$ and $D_{s1} \to D_s^*\pi^0$ in addition to the decay mechanism induced by $\eta - \pi^0$ mixing as considered previously.

In present paper we will consider the strong, radiative and leptonic decays of the $D_{s0}^*(2317)$ and $D_{s1}(2460)$ meson using an effective Lagrangian approach. The approach is based on the hypothesis that the D_{s0}^* and D_{s1} are a bound state of D, K and D^*, K mesons, respectively. In other words we investigate the position that D_{s0}^* and D_{s1} are (DK) and (D^*K) hadronic molecules. Their couplings to the constituents are described by the effective Lagrangians. The

corresponding coupling constants $g_{D^*_{s0}DK}$ and $g_{D_{s1}D^*K}$ are determined by the compositeness condition $Z = 0$ [26, 27], which implies that the renormalization constant of the hadron wave function is set equal to zero. Note, that this condition was originally applied to the study of the deuteron as bound state of proton and neutron [26]. Then it was extensively used in the low-energy hadron phenomenology as the master equation for the treatment of mesons and baryons as bound states of light and heavy constituent quarks (see Refs. [27, 28]). Recently the compositeness condition was used to study the light scalar mesons a_0 and f_0 as $K\bar{K}$ molecules [29]. A new impact of the molecular structure of the $D^*_{s0}(2317)$ and $D_{s1}(2460)$ mesons is that the presence of $u(d)$ quarks in the D^* and K meson gives rise to the direct strong isospin-violating transitions $D^*_{s0} \to D_s\pi^0$ and $D_{s1} \to D^*_s\pi^0$ in addition to the decay induced by $\eta - \pi^0$ mixing considered before in the literature. We show that the direct transition dominates over the $\eta - \pi^0$ mixing transitions. The obtained results for the partial decay widths are consistent with previous calculations. Also we extend our formalism to the bottom sector: $B^*_{s0}(5725)$ and $B_{s1}(5778)$ states.

2 Approach: basic notions and results

In this section we briefly discuss the formalism for the study of the hadronic molecules. As example, we consider $D^{*\pm}_{s0}(2317)$ mesons as a bound state of D and K mesons. Extension to other states is straightforward. First of all we specify the quantum numbers of the $D^{*\pm}_{s0}(2317)$ mesons. We use the current results for the quantum numbers of isospin, spin and parity: $I(J^P) = 0(0^+)$ and mass $m_{D^*_{s0}} = 2.3173$ GeV [3]. Our framework is based on an effective interaction Lagrangian describing the coupling between the $D^*_{s0}(2317)$ meson and their constituents - D and K mesons:

$$\mathcal{L}_{D^*_{s0}}(x) = g_{D^*_{s0}} D^{*-}_{s0}(x) \int dy \Phi_{D^*_{s0}}(y^2) D(x + w_{KD} y) K(x - w_{DK} y) + \text{H.c.} \quad (1)$$

where D and K are the corresponding meson doublets, $w_{ij} = m_i/(m_i + m_j)$ is the kinematical variable, m_D and m_K are the masses of D and K mesons. The correlation function $\Phi_{D^*_{s0}}$ characterizes the finite size of the $D^*_{s0}(2317)$ meson as a D K bound state and depends on the relative Jacobi coordinate y with x being the center of mass (CM) coordinate. In numerical calculations we employ the Gaussian form of $\Phi_{D^*_{s0}}$. Its Fourier transform reads

as $\tilde{\Phi}_{D^*_{s0}}(p_E^2) = \exp(-p_E^2/\Lambda^2_{D^*_{s0}})$, where p_E is the Euclidean Jacobi momentum. Here $\Lambda_{D^*_{s0}}$ is a size parameter, which parametrizes the distribution of D and K mesons inside the D^*_{s0} molecule. The coupling constant $g_{D^*_{s0}}$ is determined by the compositeness condition [26, 27], which implies that the renormalization constant of the hadron wave function is set equal to zero: $Z_{D^*_{s0}} = 1 - \Sigma'_{D^*_{s0}}(m^2_{D^*_{s0}}) = 0$, where $\Sigma'_{D^*_{s0}}$ is the derivative of the D^*_{s0} meson mass operator. This condition was originally applied to the study of the deuteron as a bound state of proton and neutron [26]. Then it was extensively used in low-energy hadron phenomenology as the master equation for the treatment of mesons and baryons as bound states of light and heavy constituent quarks [27, 28].

Effective Lagrangian (1) is the starting point for the study of the decays of hadronic molecules. It defines the transition of the molecule into their constituents. Then we should specify the Lagrangian which describes the interaction of the constituents with external fields (hadrons and gauge bosons) and the diagrams which contribute to the matrix elements of physical processes. All further details can be found in Refs. [21]- [23]. Below in Tables 1 – 4 we display our results for the strong and radiative decay widths and their ratios $R_{D^*_{s0}} = \Gamma(D^*_{s0} \to D^*_s\gamma/\Gamma(D^*_{s0} \to D_s\pi)$ and $R_{D_{s1}} = \Gamma(D_{s1} \to D_s\gamma)/\Gamma(D_{s1} \to D^*_s\pi)$, including extension to bottom sector, and compare them with the predictions of other approaches. Also we present our results for the leptonic decay constants: $f_{D^*_{s0}} = 67.1$ MeV and $f_{D_{s1}} = 144.5$ MeV.

3 Summary

We studied the new charm-strange mesons $D^*_{s0}(2317)$ and $D_{s1}(2460)$ in the hadronic molecule interpretation, considering a DK and D^*K bound states, respectively. Using an effective Lagrangian approach we calculated their weak, strong and radiative decays. A new impact of their molecular structure is that the presence of $u(d)$ quarks in the $D^{(*)}$ and K meson loops gives rise to a direct strong isospin-violating transition $D^*_{s0} \to D_s\pi^0$ and $D_{s1} \to D^*_s\pi^0$ in addition to the decay mechanism induced by $\eta - \pi^0$ mixing as was considered before in the literature. Also we extend our formalism to the bottom sector: $B^*_{s0}(5725)$ and $B_{s1}(5778)$ states.

Table 1: Strong decay widths in keV.

Approach	$\Gamma(D_{s0}^* \to D_s\pi)$	$\Gamma(D_{s1} \to D_s^*\pi)$
Ref. [14]	6 ± 2	
Ref. [7]	7 ± 1	7 ± 1
Ref. [18]	8.69	11.41
Ref. [6]	10	10
Ref. [8]	16	32
Ref. [5]	21.5	21.5
Ref. [17]	32	35
Ref. [13]	39 ± 5	43 ± 8
Ref. [4]	$10 - 100$	
Ref. [9]	155 ± 70	155 ± 70
Ref. [10]	129 ± 43	187 ± 73
Ref. [25]	140	140
Our results [21, 23]	$46.7 - 75$	$50.1 - 79.2$

Table 2: Radiative decay widths in keV.

Approach	$\Gamma(D_{s0}^* \to D_s^*\gamma)$	$\Gamma(D_{s1} \to D_s\gamma)$
Ref. [8]	0.2	
Ref. [24]	0.49	
Ref. [7]	0.85 ± 0.05	
Ref. [12]	1	≤ 7.3
Ref. [15]	≈ 1.1	$0.6 - 2.9$
Ref. [20]	$1.3 - 9.9$	$5.5 - 31.2$
Ref. [10]	≤ 1.4	≈ 2
Ref. [16]	1.6	6.7
Ref. [5]	1.74	5.08
Ref. [6]	1.9	6.2
Ref. [11]	$4 - 6$	$19 - 29$
Ref. [25]	< 7	$\simeq 43.6$
Ref. [9]	21	93
Our results [21, 23]	$0.47 - 0.63$	$2.37 - 3.73$

Table 3: Ratios

Approach	$R_{D^*_{s0}}$	$R_{D_{s1}}$
Ref. [8]	0.01	
Ref. [10]	≤ 0.02	0.01 - 0.02
Ref. [25]	< 0.05	$\simeq 0.31$
Ref. [5]	0.08	0.24
Ref. [11]	$0.11 - 0.14$	
Ref. [6]	0.19	0.62
Ref. [9]	0.09 - 0.25	0.41 - 1.09
Ref. [16]	0.16	0.67
Data [3]	≤ 0.059	0.44 ± 0.09
Our results [21, 23]	$\simeq 0.01$	$\simeq 0.05$

Table 4: Decay widths of $B^*_{s0}(5725)$ and $B_{s1}(5778)$ in keV.

Approach	$\Gamma(B^*_{s0} \to B_s\pi)$	$\Gamma(B_{s1} \to B^*_s\pi)$	$\Gamma(B^*_{s0} \to B^*_s\gamma)$	$\Gamma(B_{s1} \to B_s\gamma)$
Refs. [18, 19]	7.92	10.36		
Our results	$52.9 - 87.1$	$53.4 - 87.5$	$1.54 - 2.04$	$1.04 - 1.22$

Acknowledgments

This work was supported by the DFG (contracts FA67/31-1 and GRK683). This research is also the part of the EU Integrated Infrastructure Initiative Hadronphysics project under contract number RII3-CT-2004-506078 and President grant of Russia "Scientific Schools" No. 5103.2006.2.

References

1. J.L. Rosner, Phys. Rev. **D74**, 076006 (2006)
2. T. Barnes, F.E. Close and H. J. Lipkin, Phys. Rev. **D68**, 054006 (2003)
3. W.M. Yao *et al.* [Particle Data Group], J. Phys. **G33**, 1 (2006)
4. H.Y. Cheng and W.S. Hou, Phys. Lett. **B566**, 193 (2003)

5. W.A. Bardeen, E.J. Eichten and C.T. Hill, Phys. Rev. **D68**, 054024 (2003)

6. S. Godfrey, Phys. Lett.**B568**, 254 (2003)

7. P. Colangelo and F. De Fazio, Phys. Lett. **B570**, 180 (2003)

8. Fayyazuddin and Riazuddin, Phys. Rev. **D69**, 114008 (2004)

9. S. Ishida, M. Ishida, T. Komada, T. Maeda, M. Oda, K. Yamada and I. Yamauchi, AIP Conf. Proc. **717**, 716 (2004)

10. Y.I. Azimov and K. Goeke, Eur. Phys. J. **A21**, 501 (2004)

11. P. Colangelo, F. De Fazio and A. Ozpineci, Phys. Rev. D **D72**, 074004 (2005)

12. F.E. Close and E.S. Swanson, Phys. Rev. D **D72**, 094004 (2005)

13. W. Wei, P.Z. Huang and S.L. Zhu, Phys. Rev. **D73**, 034004 (2006)

14. M. Nielsen, Phys. Lett. **B634**, 35 (2006)

15. X. Liu, Y.M. Yu, S.M. Zhao and X.Q. Li, Eur. Phys. J. **C47**, 445 (2006)

16. J. Vijande, F. Fernandez and A. Valcarce, Phys. Rev. D **D73**, 034002 (2006) [Erratum-ibid. D **74**, 059903 (2006)]

17. J. Lu, X.L. Chen, W.Z. Deng and S.L. Zhu, Phys. Rev. D **73**, 054012 (2006)

18. F.K. Guo, P.N. Shen, H.C. Chiang and R.G. Ping, Phys. Lett. B **B641**, 278 (2006)

19. F.K. Guo, P.N. Shen and H.C. Chiang, Phys. Lett. **B647**, 133 (2007)

20. Z.G. Wang, Phys. Rev. **D75**, 034013 (2007)

21. A. Faessler, T. Gutsche, V.E. Lyubovitskij and Y.L. Ma, Phys. Rev. **D76**, 014005 (2007)

22. A. Faessler, T. Gutsche, S. Kovalenko and V.E. Lyubovitskij, Phys. Rev. **D76**, 014003 (2007)

23. A. Faessler, T. Gutsche, V.E. Lyubovitskij and Y.L. Ma, arXiv:0709.3946 [hep-ph], Phys. Rev. **D76** (in print)

24. D. Gamermann, L.R. Dai and E. Oset, arXiv:0709.2339 [hep-ph]

25. M.F.M. Lutz and M. Soyeur, arXiv:0710.1545 [hep-ph]

26. S. Weinberg, Phys. Rev. **130**, 776 (1963); A. Salam, Nuovo Cim. **25**, 224 (1962)

27. G.V. Efimov and M.A. Ivanov, *The Quark Confinement Model of Hadrons*, (IOP Publishing, Bristol & Philadelphia, 1993)

28. M.A. Ivanov, M.P. Locher and V.E. Lyubovitskij, Few Body Syst. **21**, 131 (1996); M.A. Ivanov, V.E. Lyubovitskij, J.G. Körner and P. Kroll, Phys. Rev. **D56**, 348 (1997); A. Faessler, T. Gutsche, M.A. Ivanov, V.E. Lyubovitskij and P. Wang, Phys. Rev. **D68**, 014011 (2003); A. Faessler, T. Gutsche, M.A. Ivanov, J.G. Korner, V.E. Lyubovitskij, D. Nicmorus and K. Pumsa-ard, Phys. Rev. **D73**, 094013 (2006); A. Faessler, T. Gutsche, B.R. Holstein, V.E. Lyubovitskij, D. Nicmorus and K. Pumsa-ard, Phys. Rev. **D74**, 074010 (2006)

29. V. Baru, J. Haidenbauer, C. Hanhart, Yu. Kalashnikova and A.E. Kudryavtsev, Phys. Lett. **B586**, 53 (2004); C. Hanhart, Yu.S. Kalashnikova, A.E. Kudryavtsev and A.V. Nefediev, Phys. Rev. **D75**, 074015 (2007)

Frascati Physics Series Vol. XLVI (2007), pp. 945–952
HADRON07: XII Int. Conf. on Hadron Spectroscopy – Frascati, October 8-13, 2007
Heavy Meson Spectroscopy

CHARM PHYSICS: HINTS FOR A MATURE DESCRIPTION OF HADRONS

A. Valcarce
Departamento de Física Fundamental, Universidad de Salamanca, Spain
J. Vijande
Departamento de Física Teórica, Universidad de Valencia, Spain
N. Barnea
The Racah Institute of Physics, The Hebrew University, Jerusalem, Israel

Abstract

The physics of charm has become one of the best laboratories exposing the limitations of the naive constituent quark model and also giving hints into a more mature description of hadron spectroscopy. Recent discoveries are a challenge that have revolutionized our understanding of the hadron spectra. In this talk we address the study of many-quark components in charmonium spectra. To make the physics clear we also discuss exotic many-quark systems.

More than thirty years after the so-called November revolution [1], heavy meson spectroscopy is being again a challenge. The formerly comfortable world of heavy meson espectroscopy is being severely tested by new experiments [2]. This challenging situation arose in the open-charm sector with the discovery of the $D_{sJ}^*(2317)$, the $D_{sJ}(2460)$ and the $D_0^*(2308)$ mesons. All of them are positive parity states with masses smaller than expectations from quark potential

models, and in the first two cases also smaller widths. In general, one could say that the area phenomenologically understood in the open-charm meson spectrum extends to states where the $q\bar{q}$ pair is in relative $S-$wave. In the positive parity sector, $P-$wave states, is where the problems arise. This has been said as an example where naive quark models are probably too naive [3]. Out of the many explanations suggested for these states, the unquenching of the naive quark model has been successful [4]. When a $q\bar{q}$ pair occurs in a $P-$wave but can couple to hadron pairs in $S-$wave the latter will distort the $q\bar{q}$ picture. In the examples mentioned above, the 0^+ and 1^+ $c\bar{s}$ states predicted above the $DK(D^*K)$ thresholds couple to the continuum. This mixes $DK(D^*K)$ components in the wave function. This idea can be easily formulated in terms of a meson wave-function described by

$$|\psi\rangle = \sum_i \alpha_i \, |q\bar{q}\rangle_i + \sum_j \beta_j \, |qq\bar{q}\bar{q}\rangle_j \tag{1}$$

where q stands for quark degrees of freedom and the coefficients α_i and β_j take into account the possible admixture of four-quark components in the standard $q\bar{q}$ picture.

This explanation has open the discussion about the presence of compact four-quark states in charmonium spectroscopy. This is an old idea long ago advocated to explain the proliferation of light-scalar mesons [5]. In the case of charmonium spectroscopy, some members of the new hadronic zoo may fit in the simple quark model description as $q\bar{q}$ pairs ($X(3940)$, $Y(3940)$, and $Z(3940)$ may fit into the χ_{c0}, χ_{c1}, and χ_{c2} quark model structure) others appear to be more elusive ($X(3872)$ and $Y(4260)$).

The debate has been open with special emphasis on the nature of the $X(3872)$. Since it was first reported by Belle in 2003 [6] it has gradually become the flagship of a new armada of states whose properties make their identification as traditional $q\bar{q}$ states unlikely. In this heterogeneous group we could include states like the $Y(2460)$ reported by $BABAR$, and the aforementioned $D_{sJ}(2317)$ and $D_{sJ}(2460)$ reported by $BABAR$ and CLEO. An average mass of 3871.2±0.5 MeV and a narrow width of less than 2.3 MeV have been reported for the $X(3872)$. Note the vicinity of this state to the $D^0\overline{D^{*0}}$ threshold, $M(D^0\,\overline{D^{*0}}) = 3871.2 \pm 1.2$ MeV. With respect to the $X(3872)$ quantum numbers, neither D0 nor $BABAR$ have been able to offer a clear prediction. Its isovector nature has been excluded by $BABAR$ due to the negative

Table 1: *$c\bar{c}n\bar{n}$ results.*

	CQC		BCN	
$J^{PC}(K_{\max})$	E_{4q}	Δ_E	E_{4q}	Δ_E
0^{++} (24)	3779	+34	3249	+75
0^{+-} (22)	4224	+64	3778	+140
1^{++} (20)	3786	+41	3808	+153
1^{+-} (22)	3728	+45	3319	+86
2^{++} (26)	3774	+29	3897	+23
2^{+-} (28)	4214	+54	4328	+32
1^{-+} (19)	3829	+84	3331	+157
1^{--} (19)	3969	+97	3732	+94
0^{-+} (17)	3839	+94	3760	+105
0^{--} (17)	3791	+108	3405	+172
2^{-+} (21)	3820	+75	3929	+55
2^{--} (21)	4054	+52	4092	+52

results in the search for a charged partner in the decay $B \to X(3872)^- K$, $X(3872)^- \to J/\psi\pi^-\pi^0$ [7]. CDF has studied the $X(3872)$ J^{PC} quantum numbers using dipion invariant mass distribution and angular analysis, obtaining that only the assignments 1^{++} and 2^{-+} are able to describe data [8]. On the other hand, recent studies by Belle combining angular and kinematic properties of the $\pi^+\pi^-$ invariant mass strongly favor a $J^{PC} = 1^{++}$ state, and the observation of the $X(3872) \to D^0\overline{D^0}\pi^0$ also prefers the 1^{++} assignment compared to the 2^{-+} [9]. Therefore, although some caution is still required until better statistic is obtained [10], an isoscalar $J^{PC} = 1^{++}$ state seems to be the best candidate to describe the properties of the $X(3872)$.

To study the possible existence of four-quark states in the charmonium spectrum we have solved exactly the four-body Schrödinger equation using the hyperspherical harmonic (HH) formalism [11]. We have used two standard quark-quark interaction models: a potential containing a linear confinement and a Fermi-Breit one-gluon exchange interaction (BCN), and a potential containing besides boson exchanges between the light quarks (CQC). The model parameters have been tuned in the meson and baryon spectra. To make the physics clear we have solved simultaneously two different type of systems: the cryptoexotic $c\bar{c}n\bar{n}$ and the flavor exotic $cc\bar{n}\bar{n}$, where n stands for a light u or d quark. The results are reported in Tables 1 and 2, indicating the quantum

Table 2: *$cc\bar{n}\bar{n}$ results.*

		CQC			
	$J^P(K_{\max})$	E_{4q}	Δ_E	R_{4q}	$R_{4q}/(r_{2q}^1+r_{2q}^2)$
I=0	0^+ (28)	4441	+15	0.624	>1
	1^+ (24)	3861	−76	0.367	0.808
	2^+ (30)	4526	+27	0.987	>1
	0^- (21)	3996	+59	0.739	>1
	1^- (21)	3938	+66	0.726	>1
	2^- (21)	4052	+50	0.817	>1
I=1	0^+ (28)	3905	+50	0.817	>1
	1^+ (24)	3972	+33	0.752	>1
	2^+ (30)	4025	+22	0.879	>1
	0^- (21)	4004	+67	0.814	>1
	1^- (21)	4427	+1	0.516	0.876
	2^- (21)	4461	−38	0.465	0.766

numbers of the state studied, J^{PC}, the maximum value of the grand angular momentum used in the HH expansion, K_{max}, and the energy difference between the mass of the four-quark state, E_{4q}, and that of the lowest two-meson threshold calculated with the same potential model, Δ_E. For the $cc\bar{n}\bar{n}$ system we have also calculated the radius of the four-quark state, R_{4q}, and its ratio to the sum of the radii of the lowest two-meson threshold, $R_{4q}/(r_{2q}^1+r_{2q}^2)$. As can be seen in Table 1, in the case of the $c\bar{c}n\bar{n}$ there appear no bound states for any set of quantum numbers, including the suggested assignments of the $X(3872)$: 1^{++} and 2^{-+}. The situation is different for the $cc\bar{n}\bar{n}$ where we observe the existence of bound states. It is particularly interesting the $J^P=1^+$ channel, that it is bound both with the CQC and the BCN models. For the $c\bar{c}n\bar{n}$ system, independently of the quark-quark interaction and the quantum numbers considered, the system evolves to a well separated two-meson state. This is clearly seen in the energy, approaching the corresponding two free-meson threshold, and also in the probabilities of the different color components of the wave function and in the radius. We illustrate the convergence plotting in Fig. 1 the energy of the $J^{PC}=1^{++}$ state as a function of K. It can be observed how the BCN 1^{++} state does not converge to the lowest threshold for small values of K, being affected by the presence of an intermediate $J/\psi\,\omega|_S$ threshold with an energy of 3874 MeV. Once sufficiently large values of K are considered

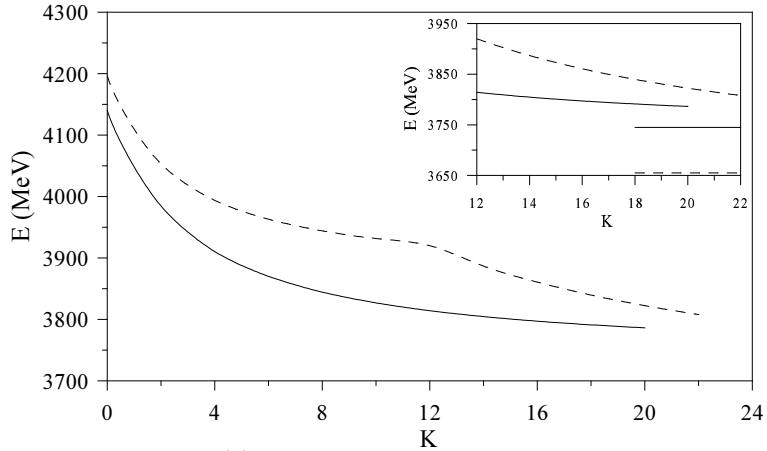

Figure 1: *Energy of the* 1^{++} *state using the CQC (solid line) and BCN models (dashed line) as a function of* K*. The insert in the upper-right corner magnifies the large values of* K *to show the convergence to the corresponding threshold showed by a straight line.*

the system follows the usual convergence to the lowest threshold (see insert in Fig. 1). The dashed line of Fig. 2 illustrates how the system evolves to two singlet color mesons, whose separation increases with K. Thus, in any manner one can claim for the existence of a bound state for the $c\bar{c}n\bar{n}$ system.

A completely different behavior is observed in Table 2. Here, there are some particular quantum numbers where the energy is quickly stabilized below the theoretical threshold. For example, the solid line in Fig. 2 illustrates how the radius of the 1^+ $cc\bar{n}\bar{n}$ state is stable, and it is smaller than the sum of the radius of the two-meson threshold. We obtain $r_{4q} = 0.37$ fm compared to $r_{M_1} + r_{M_2} = 0.44$ fm for the 1^+ state. The analysis of the color components in the wave function is involved in this case. One cannot directly conclude the presence of octet-octet components in the wave function, because the octet-octet color component in the $(c_1\bar{n}_3)(c_2\bar{n}_4)$ basis can be re-expressed as a singlet-singlet color component in the $(c_1\bar{n}_4)(c_2\bar{n}_3)$ coupling, being the same physical system due to the identity of the two quarks and the two antiquarks. The actual interest and the capability of some experiments [12] to detect double charmed states makes this prediction a primary objective to help in the understanding

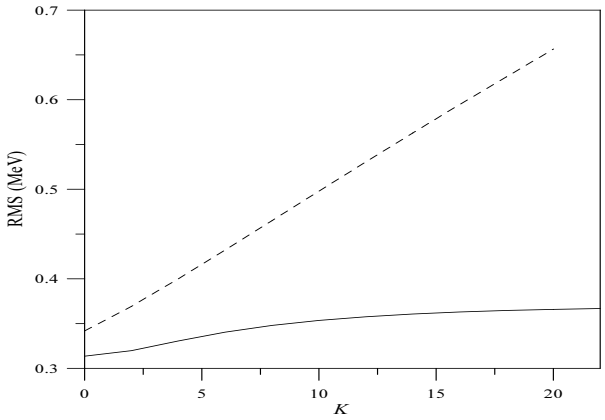

Figure 2: *Evolution with K of the radius (RMS) of the $c\bar{c}n\bar{n}$ $J^{PC} = 1^{++}$ state (dashed line) and the $cc\bar{n}\bar{n}$ $J^{P} = 1^{+}$ state (solid line) for the CQC model.*

of QCD dynamics.

There is an important difference between the two physical systems studied. While for the $c\bar{c}n\bar{n}$ there are two allowed physical *decay channels*, $(c\bar{c})(n\bar{n})$ and $(c\bar{n})(\bar{c}n)$, for the $cc\bar{n}\bar{n}$ only one physical system contains the possible final states, $(c\bar{n})(c\bar{n})$. This has important consequences if both systems (two- and four-quark states) are described within the same two-body Hamiltonian, the $c\bar{c}n\bar{n}$ will hardly present bound states, because the system will reorder itself to become the lightest two-meson state, either $(c\bar{c})(n\bar{n})$ or $(c\bar{n})(\bar{c}n)$. In other words, if the attraction is provided by the interaction between particles i and j, it does also contribute to the asymptotic two-meson state. This does not happen for the $cc\bar{n}\bar{n}$ if the interaction between, for example, the two quarks is strongly attractive. In this case there is no asymptotic two-meson state including such attraction, and therefore the system will bind.

Once all possible quantum numbers of the $X(3872)$ have been analyzed and discarded very few alternatives remain. If this state is experimentally proved to be a compact four-quark state this will point either to the existence of non two-body forces or to the emergence of strongly bound diquark structures within the tetraquark. Both possibilities are appealing, does the interaction

becomes more involved with the number of quark or does the Hilbert space becomes simpler? On the one hand, some lattice QCD collaborations [13] have reported the important role played by three- and four-quark interactions within the confinement (the $Y-$ and $H-$shape). On the other hand, diquark correlations have been proposed to play a relevant role in several aspects of QCD, from baryon spectroscopy to scaling violation [14]. The spontaneous formation of diquark components can be checked within our formalism. The four-quark state can be explicitly written in the $(cn)(\bar{c}\bar{n})$ coupling to isolate the diquark-antidiquark configurations. In the case of $J^{PC} = 1^{++}$ only two components of the wave function have the proper quantum numbers to be identified with a diquark, being their total probability less than 3%. Therefore, it is clear that without any further hypothesis two-body potentials do not favor the presence of diquarks and any description of these states in terms of diquark-antidiquark components would be selecting a restricted Hilbert space.

Finally, our conclusions can be made more general. If we have an N-quark system described by two-body interactions in such a way that there exists a subset of quarks that cannot make up a physical subsystem, then one may expect the existence of N-quark bound states by means of central two-body potentials. If this is not true one will hardly find $N-$quark bound states [15]. For the particular case of the tetraquarks, this conclusion is exact if the confinement is described by the first $SU(3)$ Casimir operator, because when the system is split into two-mesons the confining contribution from the two isolated mesons is the same as in the four-quark system. The contribution of three-body color forces [16] would interfere in the simple comparison of the asymptotic and the compact states. Another possibility in the same line would be a modification of the Hilbert space. If for some reason particular components of the four-quark system (diquarks) would be favored against others, the system could be compact [17]. Lattice QCD calculations [18] confirm the phenomenological expectation that QCD dynamics favors the formation of good diquarks [5], i.e., in the scalar positive parity channel. However, they are large objects whose relevance to hadron structure is still under study. All these alternatives will allow to manage the four-quark system without affecting the threshold and thus they may allow to generate any solution.

This work has been partially funded by MCyT under Contract No. FPA2007-65748 and by JCyL under Contract No. SA016A07.

References

1. J.D. Bjorken, The November Revolution: A Theorist Reminisces, in: A Collection of Summary Talks in High Energy Physics (ed. J.D. Bjorken), p. 229 (World Scientific, New York, 2003).
2. J.L. Rosner, J. Phys. Conf. Ser. **69**, 012002 (2007).
3. F. Close, Rumsfeld Hadrons, in Proceedings of 5th Flavor Physics and CP Violation Conference, Bled, Slovenia, 12-16 May 2007, p. 20.
4. J. Vijande, F. Fernández, A. Valcarce, Phys. Rev. D. **73**, 034002 (2006).
5. R.L. Jaffe, Phys. Rept. **409**, 1 (2005).
6. Belle Collaboration, S.-K. Choi *et al*, Phys. Rev. Lett. **91**, 262001 (2003).
7. *BABAR* Collaboration, A. Aubert *et al*, Phys. Rev. D **71** 031501R (2005).
8. CDF Collaboration, A. Abulencia *et al*, Phys. Rev. Lett. **96**, 102002 (2006).
9. Belle Collaboration, G. Gokhroo *et al*, Phys. Rev. Lett. **97**, 162002 (2006).
10. K.K. Seth, AIP Conf. Proc. **814**, 13 (2006).
11. J. Vijande, E. Weissman, N. Barnea, A. Valcarce, Phys. Rev. D **76**, 094022 (2007).
12. SELEX Collaboration, A. Ocherashvili *et al*, Phys. Lett. B **628**, 18 (2005).
13. F. Okiharu, H. Suganuma, T.T. Takahashi, Phys. Rev. D **72**, 014505 (2005);
14. R. Jaffe, F. Wilczek, Phys. Rev. Lett. **91**, 232003 (2003);
15. H.J. Lipkin, Phy. Lett. **58B**, 97 (1975).
16. V. Dmitrašinović, Phys. Rev. D **67**, 114007 (2003).
17. L. Maiani *et al*, Phys. Rev. Lett. **93**, 212002 (2004).
18. C. Alexandrou, Ph. de Forcrand, B. Lucini, Phys. Rev. Lett. **97**, 222002 (2006).

Frascati Physics Series Vol. XLVI (2007), pp. 953–958
HADRON07: XII Int. Conf. on Hadron Spectroscopy – Frascati, October 8-13, 2007
Heavy Meson Spectroscopy

EXCITED BOTTOM MESON IN CONSTITUENT QUARK MODEL

F. Fernández, A. Valcarce
Departamento de Física Fundamental, Universidad de Salamanca, Spain
J. Vijande
Departamento de Física Teórica, Universidad de Valencia, Spain

Abstract

L=1 excited bottom meson states are studied as a mixture of conventional P wave quark-antiquark states and four-quark components. A similar picture has been successfully used to describe the D_J and D_{sJ} open charm mesons. The four-quark components shift the masses of some positive parity B_{sJ} states below their corresponding isospin preserving two-meson threshold and therefore they are expected to be narrow. The other positive parity states agree with the recently measured B meson states by CDF and D0 collaboration

The spectroscopy of L=1 excited bottom mesons has received a renewed interest in the last years. Recently, D0 and CDF Collaborations have reported several results on the spectroscopy of orbitally excited bottom mesons [1)]. CDF quotes two states, B_1 and B_2^*, with masses $M(B_1) = 5734 \pm 3 \pm 2$ MeV and $M(B_2^*) = 5738 \pm 6 \pm 1$ MeV, while D0 also found the same states but with slightly different masses, $M(B_1) = 5720.8 \pm 2.5 \pm 5.3$ and $M(B_2^*) - M(B_1) = 25.2 \pm 3.0 \pm 1.1$ MeV. In the strange sector CDF reported two narrow B_{s1} and

B^*_{s2} states with masses $M(B_{s1}) = 5829.4$ MeV and $M(B^*_{s2}) = 5839$ MeV while D0 measured only the B^*_{s2}, obtaining a mass of $5839.1 \pm 1.4 \pm 1.5$ MeV. These data confirm the findings of the L3 Collaboration [2] which reported the first measurement of the mass and width of the B'_1 and B^*_2 mesons, $5670 \pm 10 \pm 13$ and $5768 \pm 5 \pm 6$ MeV, respectively.

Heavy-light mesons play in QCD a similar role as the hydrogen atom in QED. This analogy provides a simple way to make predictions for their excited states. In the limit $M_Q \to \infty$ heavy-light mesons can be characterized by the spin of the heavy quark, S_Q, the total angular momentum of the light quark, $\vec{j_q} = \vec{S_q} + \vec{L}$, and the total angular momentum, $\vec{J} = \vec{S_Q} + \vec{j_q}$. For P wave excited states there appear two degenerate doublets: one corresponding to $j_q = 1/2$, and the other to $j_q = 3/2$, with quantum numbers $J^P = 0^+, 1^+$ and $J^P = 1^+, 2^+$, respectively. For the dominant two-meson decays, states with $j_q = 1/2$ can only decay via an S wave transition, whereas the $j_q = 3/2$ states undergo a D wave transition. Therefore the decay widths are expected to be much broader for $j_q = 1/2$ than $j_q = 3/2$ states. We denote the $J^P = (0^+, 1^+)_{j_q=1/2}$ states as $(A^*_0, A^{'}_1)$ and the $J^P = (1^+, 2^+)_{j_q=3/2}$ states as (A_1, A^*_2), with $A = B$ (for $b\overline{n}$ states, where n stands for a light u or d quark) or B_s (for $b\overline{s}$ states).

The two states measured by D0 and CDF collaborations should correspond with the narrow doublet. Although the other two states are predicted to be broad our experience from the open charm sector shows that in these particular states one can expect contributions from $qq\bar{q}\bar{q}$ ($L = 1, S = 1, 0$) components. Physical mesons are easily identified with $q\bar{q}$ states when virtual quarks loops are not important. This is the case of the pseudoscalar and vector mesons due to the P-wave nature of the loop dressing. On the contrary in the scalar sector the $q\bar{q}$ pair is in a P-wave state, whereas the contributing quark loops are in an S-wave. In this case the coupling between $q\bar{q}$ pairs and $qq\bar{q}\bar{q}$ structures may be relevant.

In the present work we have extended to the bottom sector the analysis done on Ref. [3] for open-charm mesons. In this referebce we show that the D_{sJ} system, including the new experimental states, can be explained as a coupled system of $q\bar{q}$ and $qq\bar{q}\bar{q}$ components. Based on this results we will extend our study to excited P wave open-beauty mesons. The model is based on the assumption that the constituent quark mass appears as a consequence of the spontaneous breaking of the original QCD $SU(3)_L \otimes SU(3)_R$ chiral symme-

try at some momentum scale, which is the most important nonperturbative phenomenon for hadron structure at low energies. In this domain of momenta quarks are quasiparticles with a constituent mass interacting through scalar and pseudoscalar boson-exchange potentials. Beyond the chiral symmetry breaking scale one expects the dynamics being governed by QCD perturbative effects. They are taken into account through the one-gluon-exchange potential [4]. The confining interaction is taken from lattice simulations being a linear potential screened at large distances due to quark-pair creation. Therefore, hadrons are described in this scheme as clusters of confined quarks and antiquarks interacting trough gluon and boson exchanges. In the heavy quark sector chiral symmetry is explicitly broken and the boson modes are absent. Explicit expressions for the qq and $q\bar{q}$ potentials are given in [5].

Using this model we have solved the Schrödinger equation for the two- and four-body problems. The two-body case has been solved exactly, while to solve the four-body case we have used a variational method with a radial trial wave function taken as the most general combination of generalized gaussians [6]. This wave function includes all possible flavor-spin-color channels that contribute to a given configuration. Details of these wave functions can be found in Ref. [7]. The two and four quark sector are coupled perturbatively

Let us first compare the experimental results with the predictions of our model for the $b\bar{n}$ and $b\bar{s}$ quark pairs. In Table 1 it can be seen that the model nicely reproduces the known experimental data. The two states which have not been measured, $(A_0^*, A_1^{'})$ lie above the $BK = 5774$ MeV and $B^*K = 5820$ MeV thresholds for the strange sector, and above the $B\pi = 5417$ MeV threshold for the non-strange one.

Once the mixing of the $q\bar{q}$ pairs with the $bq\bar{q}\bar{q}$ states is considered, the $J^P = 0^+$ and 1^+ states acquire almost a 30% of four-quark component (see Table 2). Without being dominant, this component is the responsible for shifting the mass of the unmixed states below the BK and B^*K thresholds. Being both states below their isospin-preserving two-meson threshold, the only allowed strong decays to $B_s^*\pi$ would violate isospin and are expected to be narrow, of the order of a few keV. A second $b\bar{s}$ $J = 1^+$ resonance appears at $M = 5857$ MeV, with almost 99% of $q\bar{q}$ component which may correspond with the new B_{s1} state reported by CDF with a mass around 5829 MeV. The fourth state appears at 6174 MeV. A similar calculation in the non-strange sector

Table 1: $b\overline{s}$ and $b\overline{n}$ quark model (QM) masses, in MeV. Experimental data (Exp.) are taken from Ref. [8], except for the states denoted by a dagger that have been taken from Ref. [1] and by a double dagger from Ref. [2].

$nL\ J^P$	QM ($b\bar{s}$)	Exp.	QM ($b\bar{n}$)	Exp.
$1S\ 0^-$	5355	5369.6±2.4	5281	5279.2±0.5
$1S\ 1^-$	5400	5416.6±3.5	5321	5325.0±0.6
$1P\ 0^+$	5838	–	5848	–
$1P\ 1^+$	5837 5869	$5829.4\pm0.2\pm0.6^\dagger$	5768 5876	$5734\pm3\pm2^\dagger$ $5720.8\pm2.5\pm5.3^\dagger$ $5670\pm10\pm13^{\dagger\dagger}$
$1P\ 2^+$	5853	$5839.6\pm0.4\pm0,5^\dagger$ $5839.1\pm1.4\pm1.5^\dagger$	5786	$5738\pm6\pm1^\dagger$ $5746.0\pm2.5\pm5.3^\dagger$ $5768\pm5\pm6^{\dagger\dagger}$

Table 2: Masses (QM), in MeV, and probability of the different wave function components for B_s mesons once the mixing between $q\bar{q}$ and $qq\bar{q}\bar{q}$ configurations is considered.

$I=0$						$I=1/2$		
$J^P=0^+$			$J^P=1^+$			$J^P=0^+$		
QM	5679	6174	QM	5713	5857	QM	5615	6086
P($bn\bar{s}\bar{n}$)	0.30	0.51	P($bn\bar{s}\bar{n}$)	0.24	~ 0.01	P($bn\bar{n}\bar{n}$)	0.48	0.46
P($b\bar{s}_{1^3P}$)	0.69	0.26	P($b\bar{s}_{1^1P}$)	0.74	~ 0.01	P($b\bar{n}_{1P}$)	0.51	0.47
P($b\bar{s}_{2^3P}$)	~ 0.01	0.23	P($b\bar{s}_{1^3P}$)	~ 0.01	0.99	P($b\bar{n}_{2P}$)	~ 0.01	0.07

is much more involved and we can only predict the existence of a B_0^* state with $M = 5615$ MeV and 48% of four-quark component and 51% of $b\bar{n}$ pair. The lowest state, representing the B_0^*, is 200 MeV above the isospin preserving threshold $B\pi$, therefore it would be broad. The orthogonal state appears higher in energy, at 6086 MeV, also with an important four-quark component.

Although the L3 collaboration do not give explicitly the masses of the B_0^* and B_1 mesons, they are constrained by the relations $M(B_2^*) - M(B_1) \approx M(B_1') - M(B_0^*) \approx 12$ MeV. This allows to estimate the masses of the B_0^* and B_1 mesons from the experimental data reported for the B_1' and B_2^* mesons, obtaining $M(B_0^*) \approx 5658$ MeV and $M(B_1) \approx 5756$ MeV. The B_1 mass value agrees with the recent measurement of CDF and D0 Collaborations [1] and

with our prediction (see Table 1) whereas the B_0^* mass is very close to the $I = 1/2$, $J^P = 0^+$ state with a 48% of four-quark component (see Table 2). Furthermore L3 Collaboration observes an excess of events above the expected background in the $B\pi$ mass spectrum in the region 5.9-6.0 GeV, which fits within our second $I = 1/2$, $J^P = 0^+$ mixed state at 6086 MeV. The L3 data may be therefore indicating that the $L = 1$ excited B mesons show the same behavior as the corresponding excited states in the open charm sector

Electromagnetic decay widths would be an important diagnostic tool to understand the nature of these states. The mixing among the 1^3P_1 $c\overline{s}$ 1^1P_1 $c\overline{s}$ and the four quark component in the 1^+ state generates a very small 1^3P_1 $c\overline{s}$ probability. The electromagnetic decay of the 1^1P_1 $c\overline{s}$ component to the 1^- state is forbidden whereas the transition from the four-quark component to the meson-photon state does only occur for very particular component of the tetraquark wave function: the one where the light quark-antiquark pair is in a color singlet, spin one isospin zero state, with a very small probability for the 1^+ state. Then we found a very large value (of the order of 100) for the ratio $\frac{1^+\to 0^-+\gamma}{1^+\to 1^-+\gamma}$ due to the small 1^3P_1 $c\overline{s}$ probability of the 1^+ state. This value would provide an experimental signature of the proposed structure

In summary we have calculated the $L = 1$ excited B mesons in terms of two- and four-quark components based in our experience on the open-charm mesons. Our results for the B_{s1}^* and B^*s2 mesons agree with the recently measured B states by CDF and D0 Collaborations. In addition we predict the existence of two resonances, B_{s0}^* and B_{s1}', with almost 30% of four-quark component, which lie below the BK and B^*K thresholds, respectively. Thus, the only allowed strong decays would violate isospin and the resonances must be narrow. In the non-strange sector we do not found such narrow resonances but our results give support to the L3 Collaboration findings. Therefore the mixing between two and four-quark components, which explains the unexpected low masses of $D_{sJ}^*(2317)$ and $D_{sJ}(2460)$ open-charm states, would also play a relevant role in the open-beauty sector.

We encourage experimentalists to find these two narrow resonances in the B_s sector that would show the importance of multiquark states in the of the open-bottom and open-charm sectors.

This work has been partially funded by Ministerio de Ciencia y Tecnología

under Contract No. FPA2004-05616, by Junta de Castilla y León under Contract No. SA016A07.

References

1. M. Paulini (CDF and D0 Collaborations), arXiv:hep-ex/0702047.
2. M. Acciarri *et al.* (L3 Collaboration), Phys. Lett. B **465**, 323 (1999).
3. J. Vijande, F. Fernández, and A. Valcarce, Phys. Rev. D **73**, 034002 (2006).
4. A. de Rújula, H. Georgi, and S.L. Glashow, Phys. Rev. D **12**, 147 (1975).
5. J. Vijande, F. Fernández, and A. Valcarce, J. Phys. G **31**, 481 (2005).
6. Y. Suzuki and K. Varga, Lect. Notes Phys. **M54**, 1 (1998).
7. J. Vijande, F. Fernandez, A. Valcarce, and B. Silvestre-Brac, Eur. Phys. J. A **19**, 383 (2004).
8. W.M. Yao *et al.* (Particle Data Group), J. Phys. G **33**, 1 (2006).

Frascati Physics Series Vol. XLVI (2007), pp. 959–966
HADRON07: XII Int. Conf. on Hadron Spectroscopy – Frascati, October 8-13, 2007
Heavy Meson Spectroscopy

DALITZ PLOT ANALYSES AT CLEO-C

Paras Naik
Carleton University, Ottawa, Ontario, Canada K1S 5B6
Liming Zhang
Syracuse University, Syracuse, New York, USA 13244
Norman Lowrey
University of Illinois at Urbana-Champaign, Urbana, Illinois, USA 61801
CLEO Collaboration
LEPP, Ithaca, New York, USA 14853

Abstract

We present several recent analyses of Dalitz plots from the CLEO-c experiment, including published and preliminary analyses of $D^+ \to \pi^-\pi^+\pi^+$, $D^+ \to K^-\pi^+\pi^+$, and $D^0 \to K^0_{S,L}\pi^+\pi^-$ decays. More information on these analyses can be found in References [1, 2, 3]. New preliminary analyses we present include a search for CP asymmetry in $D^+ \to K^+K^-\pi^+$ decays and a Dalitz plot analysis of $D^0 \to K^0_S\pi^0\pi^0$.

We report on a search for the CP asymmetry in the singly Cabibbo-suppressed decay $D^+ \to K^+K^-\pi^+$ using a data sample of 572 pb^{-1} accumulated with the CLEO-c detector and taken at the $e^+e^- \to \psi(3770)$ resonance. We have searched for CP asymmetries using a Dalitz plot based analysis that determines the amplitudes and relative phases of the intermediate states.

We also use a 281 pb^{-1} CLEO-c data sample taken at the $e^+e^- \to \psi(3770)$ resonance to study the $D^0 \to K^0_S\pi^0\pi^0$ Dalitz plot. Our nominal fit includes the K^0_S, $K^*(892)$, $f_0(980)$, $f_0(1370)$, and $K^*(1680)$ resonances.

1 Search for CP asymmetry in $D^+ \to K^+K^-\pi^+$ Decays

Singly Cabibbo-suppressed (SCS) D-meson decays are predicted in the Standard Model (SM) to exhibit CP-violating charge asymmetries smaller than the order of 10^{-3}. Direct CP violation in SCS decays could arise from the interference between tree-level and penguin processes. Doubly Cabibbo-suppressed and Cabibbo-favored (CF) decays are expected to be CP invariant in the SM due to the lack of contribution from penguin processes. Measurements of CP asymmetries in SCS processes greater than $\mathcal{O}(10^{-3})$ would be evidence of physics beyond the SM [4].

We define two variables: the energy difference $\Delta E \equiv \sum_i E_i - E_{\rm beam}$ and the beam-constrained mass $m_{\rm BC} \equiv \sqrt{E^2_{\rm beam} - |\sum_i \vec{P}_i|^2}$, where E_i, $\vec{P}_i$ are the energy and momentum of each D decay product, and $E_{\rm beam}$ is the beam energy. We define a signal box corresponding to 2.5 standard deviations in each variable, and remove multiple candidates in each event by choosing the candidate that gives the smallest $|\Delta E|$. We obtain 13693 ± 137 $D^+ \to K^+K^-\pi^+$ signal candidates. To reduce smearing effects introduced by the detector, a mass constraint fit for the D^+ candidate is applied to obtain the mass squared variables, $m^2_{K^+\pi^+}$ and $m^2_{K^-\pi^+}$, for the $D^+ \to K^+K^-\pi^+$ Dalitz plot (DP) shown in Figure 1(a).

The decay amplitude as a function of DP variables is expressed as a sum of two-body matrix elements and one non-resonant (NR) decay amplitude [5]. For most resonances, the matrix element is parameterized by Breit-Wigner shapes that take into account D meson and intermediate resonance form factors and angular dependence. For the $f_0(980)$ we use a Flatté function [6]. For the $a_0(980)$, we use the function in Ref. [7]. We choose the same phase conventions for the intermediate resonances as the E687 Collaboration [8]. A fit fraction (FF), the integral of a single component divided by the sum of all components, is reported for each intermediate resonance to allow for more meaningful comparisons between results.

For D^+ decays to $K^-\pi^+$ S-wave states, we consider three amplitude models. One model uses a coherent sum of a uniform non-resonant term and Breit-Wigner term for the $K^*_0(1430)$ resonance. The second model only uses a Breit-Wigner term for the $K^*_0(1430)$ resonance. The third model uses the LASS amplitude for $K^-\pi^+ \to K^-\pi^+$ elastic scattering [9, 10]. We present

results only for the third model, although the first model provides a similar fit.

Figure 1: *The results of fitting the* $D^+ \to K^+K^-\pi^+$ *data for Model three. (a) The scatter plot for squared mass of* $K^-\pi^+$ *versus* $K^+\pi^+$ *and the projections onto squared mass of (b)* $K^-\pi^+$ *(c)* $K^+\pi^+$ *and (d)* K^+K^- *for both fit (curve) and data (points) are shown. The dashed line shows the background contribution.*

We determine the detection efficiency as a function of the two DP variables by fitting a signal MC sample generated with a flat distribution in the phase space. We use a fit to the events in the ΔE sideband ($24 < |\Delta E| < 42$ MeV and $|m_{\rm BC} - m_{D^+}| < 9$ MeV/c^2) to describe the background distribution of the DP. Having information for both the background and efficiency, as well as the fraction of signal events in the signal region, we fit the data in the DP to extract the amplitudes and phases of any contributing intermediate resonances. We perform an unbinned maximum likelihood fit. The signal fraction f is $f_0 = (84.1 \pm 0.2)\%$, constrained in the fit to be within its error σ_f obtained from the fit to the $m_{\rm BC}$ distribution. We begin by fitting the DP with all known resonances that may possibly contribute to this decay. We determine

Table 1: *The fit results in Model three. The errors shown are statistical, experimental systematic, and modeling systematic respectively.*

Component	Amplitude	Phase (°)	Fit Fraction (%)
$\overline{K}^*(892)^0K^+$	1(fixed)	0(fixed)	$23.9 \pm 0.6^{+0.1+0.9}_{-0.3-0.4}$
$K^-\pi^+(S)K^+$	$4.53 \pm 0.16^{+0.22+0.31}_{-0.01-0.23}$	$21 \pm 3^{+0+7}_{-6-2}$	$53 \pm 3^{+5+8}_{-0-5}$
$a_0(980)\pi^+$	$0.74 \pm 0.09^{+0.03+0.16}_{-0.01-0.39}$	$96 \pm 7^{+0+4}_{-4-15}$	$1.7 \pm 0.4^{+0.1+1.3}_{-0.0-0.6}$
$\phi(1020)\pi^+$	$1.23 \pm 0.02^{+0.00+0.01}_{-0.00-0.02}$	$-148 \pm 3^{+1+5}_{-1-3}$	$28.0 \pm 0.5^{+0.0}_{-0.4} \pm 0.5$
$f_2(1270)\pi^+$	$0.91 \pm 0.13^{+0.03+0.11}_{-0.01-0.24}$	$20 \pm 6^{+5+9}_{-0-11}$	$0.9 \pm 0.2^{+0.1}_{-0.0} \pm 0.2$
$a_0(1450)\pi^+$	$1.36 \pm 0.10^{+0.20+0.45}_{-0.01-0.25}$	$116 \pm 5^{+1+13}_{-5-10}$	$3.4 \pm 0.5^{+1.0+2.5}_{-0.0-1.2}$
$\phi(1680)\pi^+$	$2.6 \pm 0.3^{+0.2+0.6}_{-0.0-0.7}$	$-96 \pm 10^{+0+17}_{-16-12}$	$0.89 \pm 0.18^{+0.15+0.3}_{-0.02-0.2}$
$\overline{K}^*_2(1430)^0K^+$	$3.5 \pm 1.0^{+1.6+1.6}_{-0.0-2.6}$	$-156 \pm 6^{+1+30}_{-0-8}$	$2.1 \pm 1.2^{+2.4+2.2}_{-0.0-1.3}$

which resonances are to be included by maximizing the fit confidence level (C.L.). The procedure is to add all possible resonances, then subsequently remove those which do not contribute significantly, or worsen our C.L. The projections of the DP for the fit to Model three are shown in Figures 1(b-d). The results of the fit amplitudes, phases, and fractions including errors are shown in Table 1 for Model three.

Table 2: *A_{CP} for each component of the fit using $D^\pm$ samples in Model three. The errors for fit fractions and phases are statistical only, and those for A_{CP} are statistical, experimental systematic, and modeling systematic respectively.*

Component j	$A_{CP\,j}(\%)$
$\overline{K}^*(892)^0K^+$	$-0.1 \pm 2.9^{+2.3+0.7}_{-0.4-0.4}$
$K^-\pi^+(S)K^+$	$-1 \pm 5^{+1+6}_{-2-4}$
$a_0(980)\pi^+$	$-11 \pm 23^{+4+24}_{-9-6}$
$\phi(1020)\pi^+$	$-3.0 \pm 1.9^{+0.1+0.2}_{-0.2-0.3}$
$f_2(1270)\pi^+$	$4 \pm 25^{+3+22}_{-4-46}$
$a_0(1450)\pi^+$	$-18 \pm 14^{+0+16}_{-8-9}$
$\phi(1680)\pi^+$	$-9 \pm 21^{+22+7}_{-4-3}$
$\overline{K}^*_2(1430)^0K^+$	$69 \pm 51^{+1+8}_{-28-41}$

To search for CP violation in this model, we fit the D^+ and D^- samples independently. We use the same background fraction and PDF as those used in the fit to the total sample, but different coefficients for efficiency functions which are obtained from signal MC of $D^\pm$ decays. The calculated CP asymmetry, $A_{CP\,j} \equiv \frac{FF_{j\,D^+} - FF_{j\,D^-}}{FF_{j\,D^+} + FF_{j\,D^-}}$, is shown for each resonance j in Table 2.

2 Dalitz Plot Analysis of $D^0 \to K^0_S\pi^0\pi^0$ Decays

The PDG [11] has little information on the $D^0 \to K^0_S\pi^0\pi^0$ decay. In addition to providing a more comprehensive study of the $D^0 \to K^0_S\pi^0\pi^0$ decay, this DP analysis seems like a good place to look for the low mass $\pi\pi$ S-wave signature of the σ. The $K^0_S\pi^+\pi^-$ mode is much cleaner and has better statistics, but the ρ^0 resonance overlaps the region where we would expect to find the low mass S-wave signature. Using CLEO-c data, we eliminate nearly all of the background by doing a double-tagged analysis, where both D mesons are completely reconstructed.

We have analyzed 281 pb^{-1} of CLEO-c data taken on the $e^+e^- \to \psi(3770)$ resonance. In a double-tagged analysis, both D mesons are reconstructed. For our double-tagged analysis, we consider candidates with one D reconstructed as $K^0_S\pi^0\pi^0$, and the other D reconstructed using any of the following decay modes (charge conjugation is implied throughout this analysis): $\overline{D^0} \to K^+\pi^-$, $\overline{D^0} \to K^+\pi^-\pi^0$, $\overline{D^0} \to K^+\pi^-\pi^+\pi^-$. In a single-tagged analysis, we reconstruct only one D meson in the event, which decays to $K^0_S\pi^0\pi^0$.

Table 3: $D^0 \to K^0_S\pi^0\pi^0$ *signal yield, number of candidates, and signal fraction*

Result	Double Tag	Single Tag
Signal Yield	257 ± 17	1884 ± 56
Total Candidates	276	2548
Signal Fraction	0.931 ± 0.062	0.739 ± 0.022

To reduce 2π background that fakes a K^0_S, we enforce a 2σ enhanced flight significance selection criteria on our K^0_S candidates. To reduce the $K\pi\pi^0$ background, we require $|dE/dx_{pion}| < 3\sigma$ and $dE/dx_{kaon} < -2\sigma$ for both K^0_S daughter pions. We use the same particle identification selection criteria for double-tagged and single-tagged analyses. We apply a 2σ selection criteria on the reconstructed K^0_S mass. After enforcing our selection criteria on the K^0_S mass, we apply a 2σ selection criteria on ΔE. We additionally apply a 2σ cut on the beam constrained mass. For each event that has more than one candidate, we require the following: For the double-tagged data, we take the average of the signal beam constrained mass and the tagged beam constrained mass, and we select whichever candidate's average is closest to the nominal D

mass. For the single-tagged data, we select the candidate with ΔE closest to zero. Table 3 shows our signal yield and signal fraction.

For this analysis, we define our DP variables as follows: $x \equiv$ larger $m^2_{K^0_S\pi^0}$, $y \equiv m^2_{\pi^0\pi^0}$, $z \equiv$ smaller $m^2_{K^0_S\pi^0}$. When fitting such a Dalitz plot, we must take into account the fact that the two π^0 final state particles are indistinguishable, so we explicitly symmetrize the functions we use in x and z.

To study the efficiency of reconstructing our signal, we generate 100000 signal Monte Carlo events distributed uniformly across the Dalitz plot phase space. Half of these events force the D^0 to decay directly into $K^0_S\pi^0\pi^0$ and the $\overline{D}^0$ to decay into neutrinos. The other half of these events force the $\overline{D}^0$ to decay directly into our signal mode and the D^0 to decay into neutrinos. We fit the efficiency over the Dalitz plot to a third-order polynomial explicitly symmetric in x and z. To fit for the background, we use a sideband from single-tagged data which is centered $5\sigma_{m_{D^0}}$ lower in m_{BC} than the signal region, with the same width as that of the signal region, and has the appropriate range in ΔE which conserves the boundaries of the signal DP. We use this background shape for the double-tagged data as well as for the single-tagged data. We fit the background events to a third-order polynomial explicitly symmetric in x and z, plus a non-interfering $K^*(892)$ Breit-Wigner in both x and z.

The signal is parameterized with an isobar model that has four interfering resonances plus one non-interfering resonance. To enforce the symmetry requirement in the DP, we include each K^* resonance as an x resonance and a z resonance, while using the same amplitude and phase for the x contribution and z contribution. The parameters for the K^0_S, $K^*(892)$, and $K^*(1680)$ come from the PDG [11]. The parameters for the $f_0(980)$ are approximated from a BES paper [12]. The parameters for the $f_0(1370)$ come from Reference [13].

Figure 2(a) displays the DP from the double-tagged data. To fit this DP with an unbinned maximum likelihood fitter, we fix the signal fraction to 0.931 as determined from the beam constrained mass distribution. The fit also fixes the efficiency parameters and background parameters as determined from the signal Monte Carlo and sideband. The fit determines the amplitudes and phases of the resonances and calculates the fit fractions. Figure 2(b) shows the fit results.

To estimate systematic errors, we use the technique developed by Jim Wiss and Rob Gardner [14]. Using this technique, the systematic errors are

Figure 2: *(a) Dalitz plot of the double-tagged data (2 entries per candidate, second entry has x and z swapped) and (b) fits to the double-tagged x+z projection and double-tagged y projection.*

essentially independent of the number of systematic sources considered [14]. Table 4 gives our preliminary results. We are currently extending our analysis to the full available CLEO-c $\psi(3770)$ data sample, and studying the effects of using a σ or κ S-wave to possibly improve our fit.

3 Acknowledgements

We would like to thank David Asner, David Cinabro, Mikhail Dubrovin, Qing He, Mats Selen, Ed Thorndike, Eric White, our paper committees, and the rest of the CLEO-c Dalitz Plot Analysis Working Group for their insight, comments, and suggestions.

References

1. M. Dubrovin *et al*, Phys. Rev. D **76**, 012001 (2007).
2. M. Dubrovin, hep-ex/0707.3060 (2007)
3. E.J. White and Q. He, hep-ex/0711.2285 (2007)
4. Y. Grossman, A. L. Kagan, Y. Nir, Phys. Rev. D **75**, 036008 (2007).
5. S. Kopp *et al.* (CLEO Collaboration), Phys. Rev. D **63**, 092001 (2001).
6. E. M. Aitala *et al.* (E791 Collaboration), Phys. Rev. Lett. **86**, 765 (2001).

Table 4: *Final results including systematic errors. The first error is statistical. The second error is systematic arising from our selection criteria. The third error is systematic arising from our signal model.*

resonance		double tag
K^0_S	Fit Fraction	$0.026 \pm 0.023 \pm 0.003 \pm 0.001$
	Amplitude	$0.101 \pm 0.029 \pm 0.009 \pm 0.004$
	Effective Width	$0.0046 \pm 0.0011 \pm 0.0001 \pm 0.0001$
$K^*(892)$	Fit Fraction	$0.542 \pm 0.054 \pm 0.030 \pm 0.053$
	Amplitude	1 (fixed)
	Phase (°)	0 (fixed)
$f_0(980)$	Fit Fraction	$0.090 \pm 0.032 \pm 0.009 \pm 0.027$
	Amplitude	$1.50 \pm 0.27 \pm 0.10 \pm 0.20$
	Phase (°)	$12 \pm 17 \pm 14 \pm 8$
$f_0(1370)$	Fit Fraction	$0.238 \pm 0.071 \pm 0.047 \pm 0.086$
	Amplitude	$2.77 \pm 0.45 \pm 0.30 \pm 0.66$
	Phase (°)	$344 \pm 10 \pm 10 \pm 18$
$K^*(1680)$	Fit Fraction	$0.114 \pm 0.027 \pm 0.021 \pm 0.032$
	Amplitude	$4.55 \pm 0.68 \pm 0.49 \pm 0.59$
	Phase (°)	$97 \pm 20 \pm 17 \pm 13$

7. A. Abele *et al.*, Phys. Rev. D **57**, 3860 (1998).

8. P. L. Frabetti *et al.* (E687 Collaboration), Phys. Lett. B **351**, 591 (1995).

9. D. Aston *et al.* (LASS Collaboration), Nucl. Phys. B **296**, 493 (1988).

10. B. Aubert *et al.* (BABAR Collaboration), Phys. Rev. D **76**, 011102(R) (2007).

11. W. M. Yao *et al.* (Particle Data Group Collaboration), Journal of Physics G **33**, 1 (2006) and 2007 partial update for edition 2008.

12. M. Ablikim, *et al.*, BES Collab., Phys. Lett. B **607** (2005) 243.

13. A. Kirk, hep-ph/0009168 (2000).

14. Jim Wiss, Rob Gardner, "Estimating Systematic Errors", unpublished (1994).

Frascati Physics Series Vol. XLVI (2007), pp. 967–982
HADRON07: XII Int. Conf. on Hadron Spectroscopy – Frascati, October 8-13, 2007
Heavy Meson Spectroscopy

CHARMED MESON DALITZ PLOT ANALYSES AT *BABAR*

Kalanand Mishra *
(for the *BABAR* collaboration)
University of Cincinnati, Cincinnati, Ohio 45221, USA

Abstract

We report recent results of the Dalitz plot analyses of D and D_S decays performed by the *BABAR* collaboration, and point out some of the important applications of these results.

1 Introduction

The amplitudes describing D and D_s meson weak decays into final states with three pseudo-scalers are dominated by intermediate resonances that lead to highly nonuniform intensity distributions in the available phase space. The results of the Dalitz plot analysis of these decays are playing increasingly important role in flavor physics, particularly in the extraction of the *CP*-violating phase $\gamma = \arg\left(-V_{ud}V_{ub}^*/V_{cd}V_{cb}^*\right)$ of the quark mixing (*i.e.,* CKM) matrix by exploiting interference structure in the D Dalitz plot from the decay $B^\pm \to DK^\pm$ [1] and in the measurement of D^0–$\overline{D}^0$ mixing parameters.

2 Detector

We perform these analyses using e^+e^- collision data collected at and around 10.58 GeV center-of-mass (CM) energy with the *BABAR* detector [2] at the PEP-II storage ring. Tracking of charged particles is provided by silicon detector and a drift chamber operating in a 1.5-T magnetic field. Particle types are identified using specific ionization energy loss measurements in the two tracking devices and Cherenkov photons detected in a ring-imaging detector. The energy of photons and electrons is measured with an electromagnetic calorimeter. In case of neutral D-meson decays, we distinguish D^0 from $\overline{D}^0$ by reconstructing the decays $D^{*+} \to D^0\pi^+$ and $D^{*-} \to \overline{D}^0\pi^-$. For each decay mode, we estimate the signal efficiency as a function of position in the Dalitz plot using simulated signal events generated uniformly in the available phase space, subjected to the same reconstruction procedure applied to the data, and corrected for differences in particle-identification rates in data and simulation.

3 Dalitz plot parametrization

The complex quantum mechanical amplitude $\mathcal{A}$ that describes decays to three particles A, B and C in the final state can be characterized as a coherent sum of all relevant quasi-two-body $D/D_s \to (r \to AB)C$ isobar model resonances, $\mathcal{A} = \sum_r a_r e^{i\phi_r} A_r(s)$. Here $s = m^2_{AB}$, and A_r is the resonance amplitude. We obtain the coefficients a_r and ϕ_r from a likelihood fit. The probability density function for signal events is $|\mathcal{A}|^2$.

Unless stated otherwise, for S-, P-, and D-wave (spin = 0, 1, and 2, respectively) resonant states we use the Breit-Wigner amplitude:

$$A_{BW}(s) = \mathcal{M}_L(s,p)\,\frac{1}{M_0^2 - s - iM_0\Gamma(s)}, \quad (1)$$

$$\Gamma(s) = \Gamma_0\Big(\frac{M_0}{\sqrt{s}}\Big)\Big(\frac{p}{p_0}\Big)^{2L+1}\Big[\frac{\mathcal{F}_L(p)}{\mathcal{F}_L(p_0)}\Big]^2, \quad (2)$$

where M_0 (Γ_0) is the resonance mass (width) [3], L is the angular momentum quantum number, p is the momentum of either daughter in the resonance rest frame, and p_0 is the value of p when s = M_0^2. The function $\mathcal{F}_L$ is the Blatt-Weisskopf barrier factor [4]: $\mathcal{F}_0 = 1$, $\mathcal{F}_1 = 1/\sqrt{1+Rp^2}$, and $\mathcal{F}_2 = 1/\sqrt{9+3Rp^2+Rp^4}$, where we take the meson radial parameter R to be

1.5 GeV^{-1}. The quantity $\mathcal{M}_L$ is the spin part of the amplitude: $\mathcal{M}_0$ = constant, $\mathcal{M}_1 \propto -2\vec{p_A}.\vec{p_C}$, and $\mathcal{M}_2 \propto \frac{4}{3}\left[3(\vec{p_A}.\vec{p_C})^2 - |\vec{p_A}|^2.|\vec{p_C}|^2\right]$, where $\vec{p_i}$ is the 3-momentum of particle i in the resonance rest frame. The fit fraction for a resonant process r is defined as $f_r \equiv \int |a_r A_r|^2 \, d\tau / \int |\mathcal{A}|^2 \, d\tau$, where $d\tau$ is a phase-space element. Due to interference among the contributing amplitudes, the f_r do not sum to one in general. In all cases, we model small incoherent background empirically from data.

4 Angular moments

For D and D_s decays to three spinless particles, the Dalitz plot uniquely represents the kinematics of the final state. The angular distributions provide further information on the detailed event-density variations in various regions of the phase space in a different form. We define the helicity angle θ_H for decays $D^0 \to (r \to AB)C$ as the angle between the momentum of A in the AB rest frame and the momentum of AB in D^0 rest frame. The moments of the cosine of the helicity angle, $Y_l^0(\cos\theta_H)$, are defined as the efficiency-corrected invariant mass distributions of events when weighted by spherical harmonic functions

$$Y_l^0(\theta_H) = \sqrt{\frac{1}{2\pi}}\ P_l(m), \tag{3}$$

where m is the invariant mass of the AB system and the P_l are Legendre polynomials of order l:

$$\int_{-1}^{1} P_l(x)\ P_n(x)\ dx = \delta_{ln}. \tag{4}$$

These angular moments have an obvious physical significance. Since spherical harmonic functions are the eigen-functions of the angular momentum, the Dalitz plot of a three-body decay can be represented by the sum of an infinite number of spherical harmonic moments in any two-body channel. In a region of the Dalitz plot where S- and P-waves in a single channel dominate, their amplitudes are given by the following Legendre polynomial moments,

$$P_0 = \frac{|S|^2 + |P|^2}{\sqrt{2}}, \qquad P_1 = \sqrt{2}|S||P|\ \cos\theta_{SP}, \qquad P_2 = \sqrt{\frac{2}{5}}\ |P|^2, \tag{5}$$

where $|S|$ and $|P|$ are, respectively, the magnitudes of the S- and P-wave amplitudes, and $\theta_{SP} = \theta_S - \theta_P$ is the relative phase between them. It is worth

noting that this partial-wave analysis is valid, in the absence of higher spin states, only if no interference occurs from the crossing channels.

5 Dalitz plot analysis of $D^0 \to K^-K^+\pi^0$

The $K^\pm\pi^0$ systems from the decay $D^0 \to K^-K^+\pi^0$ [5] can provide information on the $K\pi$ S-wave amplitude in the mass range 0.6–1.4 GeV/c^2, and hence on the possible existence of the $\kappa(800)$, reported to date only in the neutral state ($\kappa^0 \to K^-\pi^+$) [6]. If the κ has isospin 1/2, it should be observable also in the charged states. Results of the present analysis can be an input for extracting the CKM phase γ by exploiting interference in the Dalitz plot from the decay $B^\pm \to D^0_{K^-K^+\pi^0}K^\pm$ [1].

We perform the analysis on 385 fb^{-1} data using the same event-selection criteria as in our measurement of the branching ratio of the decay $D^0 \to K^-K^+\pi^0$ [7]. To minimize uncertainty from background shape, we choose a high purity (∼98%) sample using $1855 < m_{D^0} < 1875$ MeV/c^2, and find 11278±110 signal events. The Dalitz plot for these events is shown in Fig. 1(a).

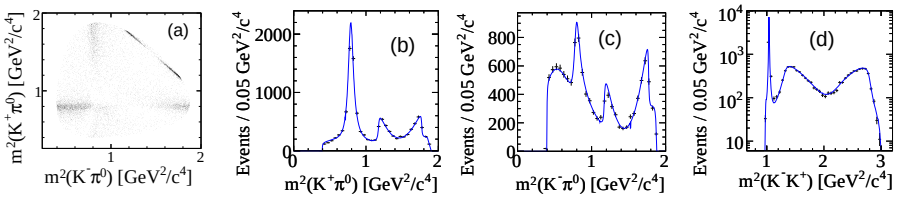

Figure 1: *Dalitz plot for $D^0 \to K^-K^+\pi^0$ [9] data (a), and the corresponding squared invariant mass projections (b–d). In plots (b–d), the dots with error bars are data points and the solid lines correspond to the best isobar fit models.*

For D^0 decays to $K^\pm\pi^0$ S-wave states, we consider three amplitude models: LASS amplitude for $K^-\pi^+ \to K^-\pi^+$ elastic scattering [8, 9], the E-791 results for the $K^-\pi^+$ S-wave amplitude from a partial-wave analysis of the decay $D^+ \to K^-\pi^+\pi^+$ [10], and a coherent sum of a uniform nonresonant term plus Breit-Wigner terms for $\kappa(800)$ and $K_0^*(1430)$ resonances.

In Fig. 2 we compare the $K\pi$ S-wave amplitude from the E-791 analysis [10] to the LASS amplitude. The LASS $K\pi$ S-wave amplitude gives the best agreement with data and we use it in our nominal fits (χ^2 probability 62%).

The $K\pi$ S-wave modeled by the combination of $\kappa(800)$ (with parameters taken from Ref. [6]), a nonresonant term and $K_0^*(1430)$ has a smaller fit probability (χ^2 probability $< 5\%$). The best fit with this model (χ^2 probability 13%) yields a charged κ of mass (870 ± 30) MeV/c^2, and width (150 ± 20) MeV/c^2, significantly different from those reported in Ref. [6] for the neutral state. This does not support the hypothesis that production of a charged, scalar κ is being observed. The E-791 amplitude [10] describes the data well, except near threshold. We use it to estimate systematic uncertainty in our results.

We describe the D^0 decay to a K^-K^+ S-wave state by a coupled-channel Breit-Wigner amplitude for the $f_0(980)$ and $a_0(980)$ resonances, with their respective couplings to $\pi\pi$, $K\bar{K}$ and $\eta\pi$, $K\bar{K}$ final states [9]. Only the high mass tails of $f_0(980)$ and $a_0(980)$ are observable, as shown in Fig. 3.

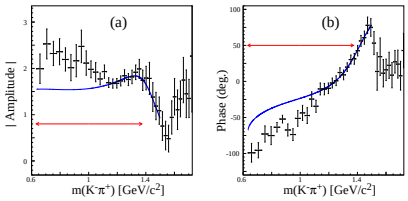

Figure 2: *LASS (solid line) and E-791 (dots with error bars) $K\pi$ S-wave amplitude (a) and phase (b). The double headed arrow indicates the mass range available in $D^0 \to K^-K^+\pi^0$.*

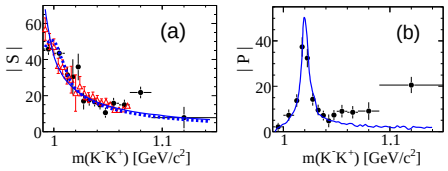

Figure 3: *The phase-space-corrected K^-K^+ S- and P-wave amplitudes, $|S|$ and $|P|$, respectively. (a) Lineshapes for (solid line) $f_0(980)$, and (broken line) $a_0(980)$. (b) Lineshape for $\phi(1020)$ (solid line). In each plot, solid circles with error bars correspond to values obtained from the model-independent analysis. In (a), the open triangles correspond to values obtained from the decay $D^0 \to K^-K^+\bar{K}^0$.*

We find that two different isobar models describe the data well. Both yield almost identical behavior in invariant mass (Fig. 1b–1d) and angular distribution (Fig. 4). The dominance of $D^0 \to K^{*+}K^-$ over $D^0 \to K^{*-}K^+$ suggests that, in tree-level diagrams, the form factor for D^0 coupling to K^{*-} is suppressed compared to the corresponding K^- coupling. While the measured fit fraction for $D^0 \to K^{*+}K^-$ agrees well with a phenomenological prediction [11] based on a large SU(3) symmetry breaking, the corresponding results for $D^0 \to K^{*-}K^+$ and the color-suppressed $D^0 \to \phi\pi^0$ decays differ signifi-

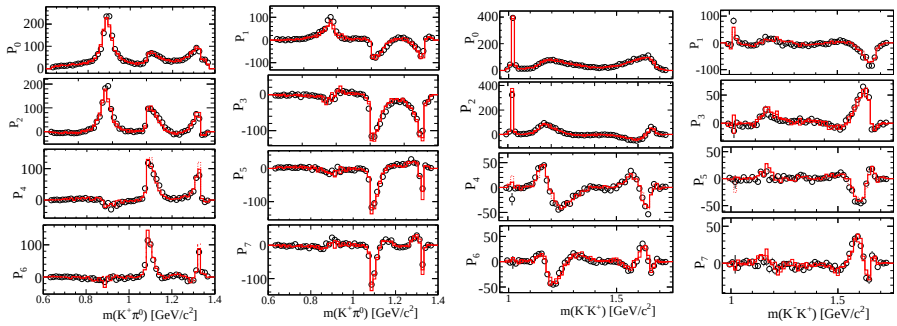

Figure 4: *Legendre polynomials moments for the $K^+\pi^0$ (columns I, II) and K^-K^+ (columns III, IV) channels of $D^0 \to K^-K^+\pi^0$. The circles with error bars are data points and the curves are derived from the fit functions.*

Table 1: *The results obtained from the $D^0 \to K^-K^+\pi^0$ Dalitz plot fit* [9]. *The errors are statistical and systematic, respectively. We show the $a_0(980)$ contribution, when it is included in place of the $f_0(980)$, in square brackets.*

	Model I		
State	Amplitude, a_r	Phase, ϕ_r (°)	Fraction, f_r (%)
$K^*(892)^+$	1.0 (fixed)	0.0 (fixed)	45.2±0.8±0.6
$K^*(1410)^+$	2.29±0.37±0.20	86.7±12.0±9.6	3.7±1.1±1.1
$K^+\pi^0(S)$	1.76±0.36±0.18	-179.8±21.3±12.3	16.3±3.4±2.1
$\phi(1020)$	0.69±0.01±0.02	-20.7±13.6±9.3	19.3±0.6±0.4
$f_0(980)$	0.51±0.07±0.04	-177.5±13.7±8.6	6.7±1.4±1.2
$[a_0(980)^0]$	[0.48±0.08±0.04]	[-154.0±14.1±8.6]	[6.0±1.8±1.2]
$f_2'(1525)$	1.11±0.38±0.28	-18.7±19.3±13.6	0.08±0.04±0.05
$K^*(892)^-$	0.601±0.011±0.011	-37.0±1.9±2.2	16.0±0.8±0.6
$K^*(1410)^-$	2.63±0.51±0.47	-172.0±6.6±6.2	4.8±1.8±1.2
$K^-\pi^0(S)$	0.70±0.27±0.24	133.2±22.5±25.2	2.7±1.4±0.8
	Model II		
$K^*(892)^+$	1.0 (fixed)	0.0 (fixed)	44.4±0.8±0.6
$K^*(1410)^+$			
$K^+\pi^0(S)$	3.66±0.11±0.09	-148.0±2.0±2.8	71.1±3.7±1.9
$\phi(1020)$	0.70±0.01±0.02	18.0±3.7±3.6	19.4±0.6±0.5
$f_0(980)$	0.64±0.04±0.03	-60.8±2.5±3.0	10.5±1.1±1.2
$[a_0(980)^0]$	[0.68±0.06±0.03]	[-38.5±4.3±3.0]	[11.0±1.5±1.2]
$f_2'(1525)$			
$K^*(892)^-$	0.597±0.013±0.009	-34.1±1.9±2.2	15.9±0.7±0.6
$K^*(1410)^-$			
$K^-\pi^0(S)$	0.85±0.09±0.11	108.4±7.8±8.9	3.9±0.9±1.0

cantly. It appears from Table 1 that the $K^+\pi^0$ S-wave amplitude can absorb any $K^*(1410)$ and $f_2'(1525)$ if those are not in the model. The other components are quite well established, independent of the model. From Table 1, the strong phase difference, δ_D, between the $\overline{D}^0$ and D^0 decays to $K^*(892)^+K^-$ state and their amplitude ratio, r_D, are given by: $\delta_D = -35.5^\circ \pm 1.9^\circ$ (stat) $\pm 2.2^\circ$ (syst) and $r_D = 0.599 \pm 0.013$ (stat) $\pm$ 0.011 (syst) [9]. Systematic uncertainties in quantities in Table 1 arise from experimental effects (*e.g.,* efficiency parameters, background shape, particle-identification), and also from uncertainty in the nature of the models used to describe the data (*e.g., $K\pi$ S*-wave amplitude and resonance parameters).

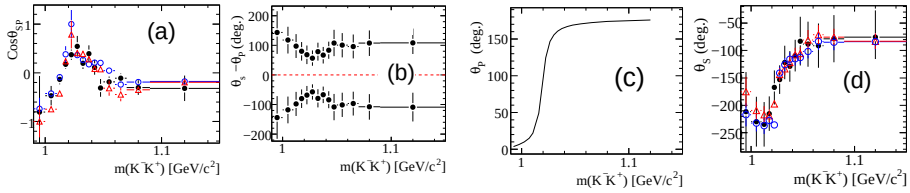

Figure 5: *Results of the partial-wave analysis of the K^-K^+ system. (a) Cosine of relative phase $\theta_{SP} = \theta_S - \theta_P$, (b) two solutions for θ_{SP}, (c) P-wave phase for $\phi(1020)$, and (d) S-wave phase derived from the upper solution in (b). Solid bullets are data points, and open circles and open triangles correspond, respectively, to isobar models I, II.*

We show the Legendre polynomials moments in Fig. 4 for the $K^+\pi^0$ and K^-K^+ channels, for $l = 0 - 7$. We use the relations of Eq. 5 to evaluate $|S|$ and $|P|$ shown in Fig. 3, and θ_{SP} shown in Fig. 5, for the K^-K^+ channel in the mass range $m_{K^-K^+} < 1.15$ GeV/c^2. The measured values of $|S|$ agree well with those obtained in the analysis of the decay $D^0 \to K^-K^+\bar{K}^0$ [12] and also with either the $f_0(980)$ or the $a_0(980)$ lineshape. The measured values of $|P|$ are consistent with a Breit-Wigner lineshape for $\phi(1020)$.

6 Dalitz plot analysis of $D^0 \to \pi^-\pi^+\pi^0$

An important component of the program to study *CP* violation is the measurement of the angle γ of the unitarity triangle related to the Cabibbo-Kobayashi-Maskawa quark mixing matrix. The decays $B \to D^{(*)0}K^{(*)}$ can be used to measure γ with essentially no hadronic uncertainties, exploiting interference

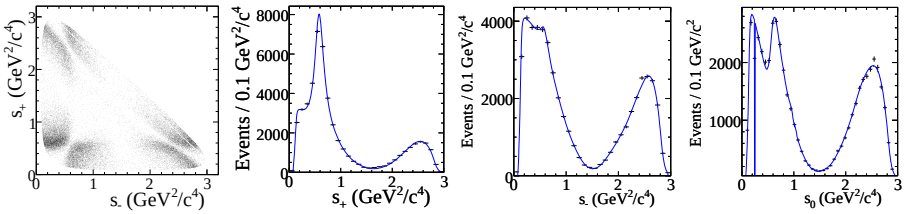

Figure 6: *Dalitz plot and invariant mass-squared projections for the* $D^0 \to \pi^-\pi^+\pi^0$ *decay excluding* $D^0 \to K^0_s\pi^0$.

between $b \to u\overline{c}s$ and $b \to c\overline{u}s$ decay amplitudes. The most effective method to measure γ has turned out to be the analysis of the D-decay Dalitz plot distribution in $B^\pm \to DK^\pm$ with multi-body D decays [13]. This method has only been used with the Cabibbo-favored decay $D \to K^0_S\pi^+\pi^-$ [14, 15]. We perform the first *CP*-violation study of $B^\pm \to DK^\pm$ using a multibody, Cabibbo-suppressed D decay, $D \to \pi^+\pi^-\pi^0$.

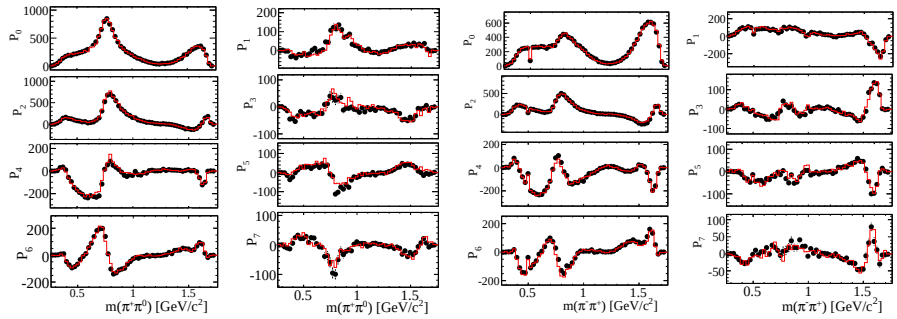

Figure 7: *Legendre polynomials moments for the* $\pi^+\pi^0$ *(columns I, II) and* $\pi^-\pi^+$ *(columns III, IV) channels of* $D^0 \to \pi^-\pi^+\pi^0$. *The circles with error bars are data points and the curves are derived from the fit functions.*

We determine the parameters a_r, ϕ_r, and f_r by fitting a large sample of D^0 and $\overline{D}^0$ mesons, flavor-tagged through their production in the decay $D^{*+} \to D^0\pi^+$ [7]. Of the D candidates in the signal region $1848 < m_{D^0} < 1880$ MeV/c^2, we obtain from the fit 44780 ± 250 signal and 830 ± 70 background events.

Table 2 summarizes the results of this fit, with systematic errors ob-

tained by varying the masses and widths of the $\rho(1700)$ and σ resonances and the form factors, and also varying the signal efficiency parameters to account for uncertainties in reconstruction and particle identification. The Dalitz plot distribution of the data is shown in Fig. 6(a-d). The distribution is marked by three destructively interfering $\rho\pi$ amplitudes, suggesting a final state dominated by $I = 0$ [16]. We show the Legendre polynomials moments in Fig. 7 for the $\pi^+\pi^0$ and $\pi^-\pi^+$ channels, for $l = 0 - 7$. The agreement between data and fit is again excellent. Unlike in case of the decay $D^0 \to K^-K^+\pi^0$, we cannot use the relations of Eq. 5 to evaluate $|S|$ and $|P|$, and θ_{SP} in any of the two-body $\pi\pi$ channels because of the contributions from cross-channels in the entire available mass-range.

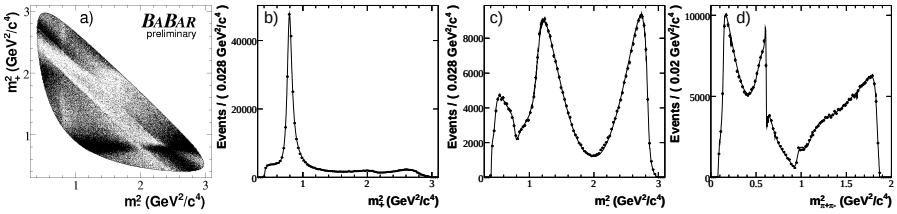

Figure 8: *(a) The* $\bar{D}^0 \to K^0_S\pi^-\pi^+$ *Dalitz distribution from* $D^{*-} \to \bar{D}^0\pi^-$ *events, and projections on (b)* $m^2_+ = m^2_{K^0_S\pi^+}$*, (c)* $m^2_- = m^2_{K^0_S\pi^-}$*, and (d)* $m^2_{\pi^+\pi^-}$*.* $D^0 \to K^0_S\pi^+\pi^-$ *from* $D^{*+} \to D^0\pi^+$ *events are also included. The curves are the model fit projections.*

7 Dalitz plot analysis of $D^0 \to K^0_S\pi^+\pi^-$

The Dalitz plot analysis of the decay $D^0 \to K^0_S\pi^+\pi^-$ is also motivated by its application to the measurement of CKM phase γ [17]. We determine the $D^0 \to K^0_S\pi^+\pi^-$ decay amplitude from an unbinned maximum-likelihood fit to the Dalitz plot distribution of a high-purity ($\sim 98\%$) D^0 sample from 390328 $D^{*+} \to D^0\pi^+$ decays reconstructed in 270 fb^{-1} of data, shown in Fig. 8. The decay amplitude is expressed as a coherent sum of two-body resonant terms and a uniform non-resonant contribution. For $r = \rho(770)$ and $\rho(1450)$ we use the functional form suggested in Ref. [18], while the remaining resonances are parameterized by a spin-dependent relativistic Breit-Wigner distribution. The model consists of 13 resonances leading to 16 two-body decay amplitudes

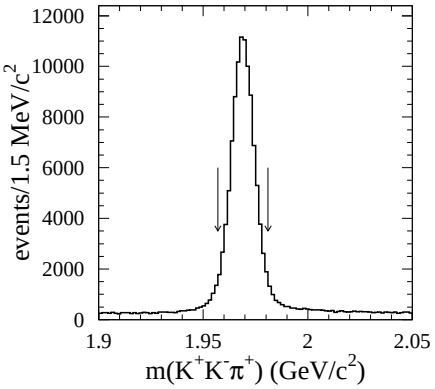

Figure 9: *The invariant mass distribution of the reconstructed D_S candidate in the decay $D_s^+ \to K^+K^-\pi^+$. For the Dalitz plot analysis we use events in the mass window shown by vertical arrows. The results are preliminary.*

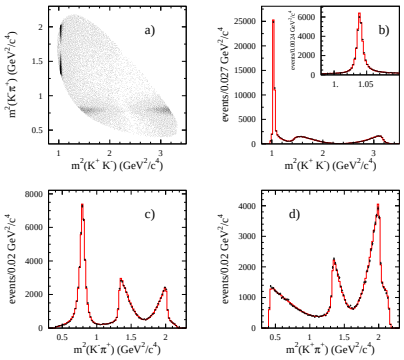

Figure 10: *(a) The $D_s^+ \to K^+K^-\pi^+$ Dalitz distribution, and projections on (b) $m^2_{K^+K^-}$, (c) $m^2_{K^-\pi^+}$, and (d) $m^2_{K^+\pi^+}$. The curves are the model fit projections. The results are preliminary.*

and phases (see Table 3), plus the non-resonant contribution, and accounts for efficiency variations across the Dalitz plane and the small background contribution.

All the resonances considered in this model are well established except for the two scalar $\pi\pi$ resonances, σ and σ', whose masses and widths are obtained from our sample [19]. Their addition to the model is motivated by an improvement in the description of the data. The possible absence of the σ and σ' resonances is considered in the evaluation of the systematic errors. In this respect, the K-matrix formalism [20] provides a direct way of imposing the unitarity constraint that is not guaranteed in the case of the Breit-Wigner parametrization and is suited to the study of broad and overlapping resonances in multi-channel decays. We use the K-matrix method to parameterize the $\pi\pi$ S-wave states, avoiding the need to introduce the two σ scalars. A description of this alternative parametrization can be found in Ref. [21].

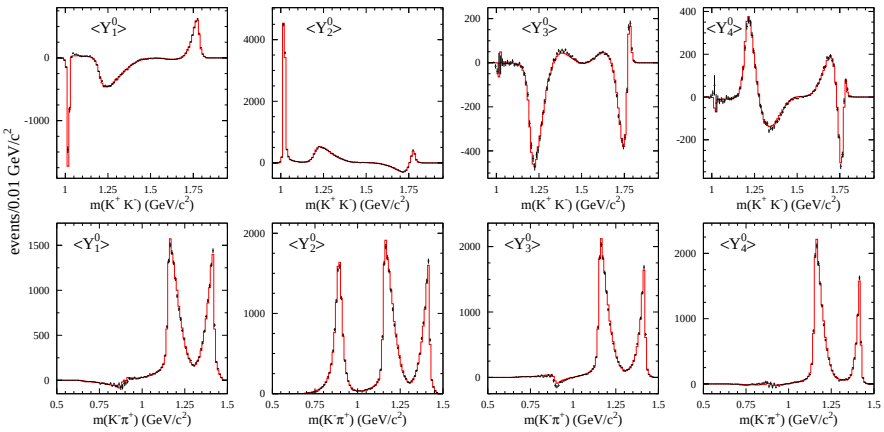

Figure 11: *Legendre polynomials moments for the K^+K^- (top) and $K^-\pi^+$ (bottom) channels of $D_s^+ \to K^+K^-\pi^+$. The dots with error bars are data points and the curves are derived from the fit functions. The results are preliminary.*

8 Dalitz plot analysis of $D_s^+ \to K^+K^-\pi^+$

We study the decay $D_s^+ \to K^+K^-\pi^+$ using a data sample of 240 fb^{-1}. We focus particularly on the measurement of the relative decay rates $\frac{\mathcal{B}(D_s^+\to\phi\pi^+)}{\mathcal{B}(D_s^+\to K^+K^-\pi^+)}$ and $\frac{\mathcal{B}(D_s^+\to\bar{K}^{*0}(892)K^+)}{\mathcal{B}(D_s^+\to K^+K^-\pi^+)}$.

The decay $D_s^+ \to \phi(1020)\pi^+$ is frequently used as the D_s^+ reference decay mode. The improvement in the measurements of these ratios is therefore important. A previous Dalitz plot analysis of this decay used $\sim$ 700 signal events [22]. We perform the present analysis using a number of signal events more than two orders of magnitude larger.

We reconstruct the decay by fitting the three charged tracks in the event to a common vertex, requiring the χ^2 probability to be greater than 0.1%. We cleanly remove a small background from the decay $D^{*+} \to D^0_{K^+K^-}\pi^+$ by requiring $m_{K^+K^-} < 1.85$ GeV/c^2. In Fig. 9 we show the invariant mass distribution of the reconstructed D_s^+ candidate in the decay $D_s^+ \to K^+K^-\pi^+$. For the Dalitz plot analysis, we use events in the $\pm 2\sigma$ mass window of the reconstructed D_s^+ candidate. We parametrize the incoherent background shape empirically using the events in the sidebands. In the signal region, we find 100850 signal events with a purity of about 95%.

Table 2: *The results obtained from the* $D^0 \to \pi^-\pi^+\pi^0$ *Dalitz plot fit* [1)]. *The errors are statistical and systematic, respectively. We take the mass (width) of the* σ *meson to be 400 (600)* MeV/c^2.

State	a_r (%)	ϕ_r (°)	f_r(%)
$\rho(770)^+$	100	0	67.8±0.0±0.6
$\rho(770)^0$	58.8±0.6±0.2	16.2±0.6±0.4	26.2±0.5±1.1
$\rho(770)^-$	71.4±0.8±0.3	−2.0±0.6±0.6	34.6±0.8±0.3
$\rho(1450)^+$	21±6±13	−146±18±24	0.11±0.07±0.12
$\rho(1450)^0$	33±6±4	10±8±13	0.30±0.11±0.07
$\rho(1450)^-$	82±5±4	16±3±3	1.79±0.22±0.12
$\rho(1700)^+$	225±18±14	−17±2±3	4.1±0.7±0.7
$\rho(1700)^0$	251±15±13	−17±2±2	5.0±0.6±1.0
$\rho(1700)^-$	200±11±7	−50±3±3	3.2±0.4±0.6
$f_0(980)$	1.50±0.12±0.17	−59±5±4	0.25±0.04±0.04
$f_0(1370)$	6.3±0.9±0.9	156±9±6	0.37±0.11±0.09
$f_0(1500)$	5.8±0.6±0.6	12±9±4	0.39±0.08±0.07
$f_0(1710)$	11.2±1.4±1.7	51±8±7	0.31±0.07±0.08
$f_2(1270)$	104±3±21	−171±3±4	1.32±0.08±0.10
$\sigma(400)$	6.9±0.6±1.2	8±4±8	0.82±0.10±0.10
Non-Res	57±7±8	−11±4±2	0.84±0.21±0.12

The Dalitz plot for the $D_s^+ \to K^+K^-\pi^+$ events is shown in Fig. 10. In the K^+K^- threshold region, a strong $\phi(1020)$ signal can be observed, together with a rather broad structure indicating the presence of the $f_0(980)$ and $a_0(980)$ S-wave resonances. A strong $K^{*0}(890)$ signal can also be seen. We perform an unbinned maximum likelihood fit to determine the relative amplitudes and phases of intermediate resonant and non-resonant states. The complex amplitude coefficient for each of the contributing states is measured with respect to $\overline{K}^{*0}K^+$. We summarize the fit results in Table 4 showing fit-fractions, amplitudes, and phases of the contributing resonances. The projections of the Dalitz plot variables in data and the ones from the fit results are shown in Fig. 10. Further tests on the fit quality can be estimated using Y_L^0 angular moments. These moments are shown for the K^+K^- and $K^-\pi^+$ channels in Fig. 11. The agreement between the data and fit is excellent. We find a rather large contribution from the $f_0(980)\pi^+$, but with a large systematic uncertainty due primarily to a poor knowledge of the shape parameters of $f_0(980)$ and higher f_0 states.

From the fit-fraction values reported in Table 4, we make the following

Table 3: *Complex amplitudes $a_r e^{i\phi_r}$ and fit fractions of the different components ($K_S\pi^-$, $K_S\pi^+$, and $\pi^+\pi^-$ resonances) obtained from the fit of the $D^0 \to K_S\pi^+\pi^-$ Dalitz distribution from $D^{*+} \to D^0\pi^+$ events. Errors are statistical only.*

Component	$Re\{a_r e^{i\phi_r}\}$	$Im\{a_r e^{i\phi_r}\}$	f_r (%)
$K^*(892)^-$	-1.223 ± 0.011	1.3461 ± 0.0096	58.1
$K_0^*(1430)^-$	-1.698 ± 0.022	-0.576 ± 0.024	6.7
$K_2^*(1430)^-$	-0.834 ± 0.021	0.931 ± 0.022	6.3
$K^*(1410)^-$	-0.248 ± 0.038	-0.108 ± 0.031	0.1
$K^*(1680)^-$	-1.285 ± 0.014	0.205 ± 0.013	0.6
$K^*(892)^+$	0.0997 ± 0.0036	-0.1271 ± 0.0034	0.5
$K_0^*(1430)^+$	-0.027 ± 0.016	-0.076 ± 0.017	0.0
$K_2^*(1430)^+$	0.019 ± 0.017	0.177 ± 0.018	0.1
$\rho(770)$	1	0	21.6
$\omega(782)$	-0.02194 ± 0.00099	0.03942 ± 0.00066	0.7
$f_2(1270)$	-0.699 ± 0.018	0.387 ± 0.018	2.1
$\rho(1450)$	0.253 ± 0.038	0.036 ± 0.055	0.1
Non-res	-0.99 ± 0.19	3.82 ± 0.13	8.5
$f_0(980)$	0.4465 ± 0.0057	0.2572 ± 0.0081	6.4
$f_0(1370)$	0.95 ± 0.11	-1.619 ± 0.011	2.0
σ	1.28 ± 0.02	0.273 ± 0.024	7.6
σ'	0.290 ± 0.010	-0.0655 ± 0.0098	0.9

preliminary measurements:

$$\frac{\mathcal{B}(D_s^+ \to \phi\pi^+)}{\mathcal{B}(D_s^+ \to K^+K^-\pi^+)} = 0.379 \pm 0.002\ (\text{stat}) \pm 0.018\ (\text{syst}),$$

$$\frac{\mathcal{B}(D_s^+ \to \bar{K}^{*0}(892)K^+)}{\mathcal{B}(D_s^+ \to K^+K^-\pi^+)} = 0.487 \pm 0.002\ (\text{stat}) \pm 0.016\ (\text{syst}).$$

9 Conclusions

we have studied the amplitudes of the decays $D^0 \to K^-K^+\pi^0$, $D^0 \to \pi^-\pi^+\pi^0$, $D^0 \to K_S^0\pi^+\pi^-$, and $D_s^+ \to K^+K^-\pi^+$. Using $D^0 \to K^-K^+\pi^0$ Dalitz plot analysis, we measure the strong phase difference between the $\overline{D}^0$ and D^0 decays to $K^*(892)^+K^-$ and their amplitude ratio, which will be useful in the measurement of the CKM phase γ. We observe contributions from the $K\pi$ and K^-K^+ scalar and vector amplitudes, and analyze their angular moments. We find no evidence for charged κ, nor for higher spin states. We also perform a partial-wave analysis of the K^-K^+ system in a limited mass range. We measure the

Table 4: *The results obtained from the $D_s^+ \to K^+K^-\pi^+$ Dalitz plot fit, listing fit-fractions, amplitudes and phases. The errors are statistical and systematic, respectively. The results are preliminary.*

Decay Mode	Decay fraction(%)	Amplitude	Phase(radians)
$\bar{K}^*(892)^0K^+$	48.7±0.2±1.6	1.(Fixed)	0.(Fixed)
$\phi(1020)\pi^+$	37.9±0.2±1.8	1.081±0.006±0.049	2.56±0.02±0.38
$f_0(980)\pi^+$	35±1±14	4.6±0.1±1.6	−1.04±0.04±0.48
$\bar{K}_0^*(1430)^0K^+$	2.0±0.2±3.3	1.07±0.06±0.73	−1.37±0.05±0.81
$f_0(1710)\pi^+$	2.0±0.1±1.0	0.83±0.02±0.18	−2.11±0.05±0.42
$f_0(1370)\pi^+$	6.3±0.6±4.8	1.74±0.09±1.05	−2.6±0.1±1.1
$\bar{K}_0^*(1430)^0K^+$	0.17±0.05±0.30	0.43±0.05±0.34	−2.5±0.1±0.3
$f_2(1270)\pi^+$	0.18±0.03±0.40	0.40±0.04±0.35	0.3±0.2±0.5

magnitudes and phases of the components of the $D^0 \to \pi^+\pi^-\pi^0$ decay amplitude, which we use in constraining the CKM phase γ using $B^\pm \to D_{\pi^+\pi^-\pi^0}K^\pm$. We measure the amplitudes of the neutral D-meson decays to the $K_s^0\pi^-\pi^+$ final state and use the results as input in the measurement of γ using the decay $B^\mp \to D^{(*)}_{K_s^0\pi^-\pi^+}K^\mp$. Finally we parametrize the amplitudes of the $D_s^+ \to K^+K^-\pi^+$ Dalitz plot and perform precision measurements of the relative decay rates $\frac{\mathcal{B}(D_s^+\to\phi\pi^+)}{\mathcal{B}(D_s^+\to K^+K^-\pi^+)}$ and $\frac{\mathcal{B}(D_s^+\to\bar{K}^{*0}(892)K^+)}{\mathcal{B}(D_s^+\to K^+K^-\pi^+)}$.

Acknowledgements

We are grateful for the excellent luminosity and machine conditions provided by our PEP-II colleagues, and for the substantial dedicated effort from the computing organizations that support *BABAR*. This work is supported by the United States Department of Energy and National Science Foundation.

References

1. B. Aubert *et al.* [BaBar Collaboration], Phys. Rev. Lett. **99**, 251801 (2007) [arXiv:hep-ex/0703037].

2. B. Aubert *et al.* (*BABAR* Collaboration), Nucl. Instr. and Methods **A479**, 1 (2002).

3. W. -M. Yao *et al.* (PDG), J. Phys. **G33**, 1 (2006).

4. J.M. Blatt and W.F. Weisskopf, Theoretical Nuclear Physics, John Wiley & Sons, New York, 1952.

5. Reference to the charge-conjugate decay is implied throughout. The initial state referred to is D^0, not $\overline{D}^0$.

6. E.M. Aitala *et al.* (E-791 Collaboration), Phys. Rev. Lett. **89**, 121801 (2002).

7. B. Aubert *et al.* (*BABAR* Collaboration), Phys. Rev. **D74**, 091102 (2006).

8. D. Aston *et al.* (LASS Collaboration), Nucl. Phys. **B296**, 493 (1988); W.M. Dunwoodie, private communication.

9. B. Aubert *et al.* (*BABAR* Collaboration), Phys. Rev. **D76**, 011102 (R)(2007).

10. E.M. Aitala *et al.* (E-791 Collaboration), Phys. Rev. **D73**, 032004 (2006); B.T. Meadows, private communication.

11. F. Buccella *et al.*, Phys. Rev. **D51**, 3478 (1995).

12. B. Aubert *et al.* (*BABAR* Collaboration), Phys. Rev. **D72**, 052008 (2005).

13. We use the symbol D to indicate any linear combination of a D^0 and a $\overline{D}^0$ meson state.

14. A. Poluektov *et al.* (Belle Collaboration), Phys. Rev. **D73**, 112009 (2006).

15. B. Aubert *et al.* (*BABAR* Collaboration), Phys. Rev. Lett. **95**, 121802 (2005).

16. C. Zemach, Phys. Rev. **133**, B1201 (1964).

17. B. Aubert *et al.* (*BABAR* Collaboration), hep-ex/0607104.

18. G.J. Gounaris and J.J. Sakurai, Phys. Rev. Lett. 21, 244 (1968).

19. The σ and σ' masses and widths are determined from the data. We find (in MeV/c^2) $M_\sigma = 490\pm6$, $\Gamma_\sigma = 406\pm11$, $M_{\sigma'} = 1024\pm4$, and $\Gamma_{\sigma'} = 89\pm7$. Errors are statistical.

20. E. P. Wigner, Phys. Rev. 70, 15 (1946); S. U. Chung *et al.*, Ann. Phys. 4, 404 (1995); I. J. R. Aitchison, Nucl. Phys. **A** 189, 417 (1972).

21. B. Aubert *et al.* (*BABAR* Collaboration), hep-ex/0507101.

22. P.L. Frabetti *et al.* (E687 Collaboration), Phys. Lett. **B351**, 591 (1995).

Frascati Physics Series Vol. XLVI (2007), pp. 983–1001
HADRON07: XII Int. Conf. on Hadron Spectroscopy – Frascati, October 8-13, 2007
Heavy Meson Spectroscopy

D^0- $\overline{D}^0$ MIXING ANALYSES AT *BABAR*

Rolf Andreassen*
(for the *BABAR* collaboration)
University of Cincinnati, Cincinnati, Ohio 45221, USA

Abstract

We summarise results of analyses of D meson mixing parameters performed by the *BABAR* collaboration.

1 Introduction

Understanding D meson (charm) mixing is an important step in measuring CP violation in the charm sector. It also fills in a gap between the well-measured cases of K [1)] and B [2, 3)] system mixing, both of which have down-type quarks in the intermediate state, where charm mixing has up-type quarks. Since mixing in the D^0 system is expected to be small in the Standard Model [4)] (modulo the hard-to-predict effects of long-distance interactions [5)]), charm mixing also offers a chance to observe New Physics either through CP violation in mixing [6)] or a large mass difference between the D mass eigenstates [5)]. In this proceeding, we summarise the result of four different approaches to

measuring the D mixing parameters at *BABAR*, involving the decays $D^0 \to K^+ \pi^-$ [7], $D^0 \to K^+ K^-$ or $\pi^+ \pi^-$ [8], $D^0 \to K^+ \pi^- \pi^0$ [9], and $D^0 \to K^+ \pi^- \pi^+ \pi^-$ [10].

2 Detector

We present analyses of e^+e^- collisions at a center-of-mass (CM) energy of 10.58, collected at the *BABAR* detector at the PEP-II storage ring. Particle identification is done by dE/dx measurements from two tracking detectors and from measuring Cherenkov angles in a ring-imaging detector. D mesons are tagged by reconstructing $D^{*+} \to D^0 \pi^+$ and $D^{*-} \to \overline{D}^0 \pi^-$ decays, and assigning flavour according to the charge of the slow pion.

3 Formalism and notation

D mesons are produced in pure flavour eigenstates, $|D^0\rangle$ or $|\overline{D}^0\rangle$. These flavour eigenstates are not equal to the mass and lifetime eigenstates

$$\begin{aligned} |D_1\rangle &= p|D^0\rangle + q|\overline{D}^0\rangle \\ |D_2\rangle &= p|D^0\rangle - q|\overline{D}^0\rangle \end{aligned}$$

by which they propagate and decay. Therefore, a particle produced as a D^0 may become a $\overline{D}^0$ before its decay. The process is governed by the mass and lifetime differences of the D_1 and D_2 states; these decay according to

$$\begin{aligned} |D_1(t)\rangle &= e^{-i(m_1 - i\Gamma_1/2)t}|D_1\rangle \\ |D_2(t)\rangle &= e^{-i(m_2 - i\Gamma_2/2)t}|D_2\rangle \end{aligned}$$

where m_i, Γ_i are the mass and width of the D_i state. We define

$$\begin{aligned} \Delta M &= m_1 - m_2 \\ \Delta\Gamma &= \Gamma_1 - \Gamma_2 \\ \Gamma &= (\Gamma_1 + \Gamma_2)/2 \\ x &= \Delta M/\Gamma \\ y &= \Delta\Gamma/2\Gamma \\ R_M &= (x^2 + y^2)/2 \end{aligned}$$

The quantities x and y are collectively referred to as mixing parameters. Estimates within the Standard Model vary from 10^{-4} (counting only short-distance effects) to as high as 1%. Establishing the presence of New Physics requires either $x >> y$, or *CP* violation [5].

4 Experimental approach

The studies considered here use a common apparatus for tagging D mesons as either D^0 or $\overline{D}^0$, and for measuring their decay times. In particular, by considering only D mesons from $D^* \to D^0\ \pi_s$, we can use the charge of the slow pion π_s to determine the production flavour of the D^0, and measure its flight length from the decay vertices of the D^* and D^0 particles.We make use of the mass of D^0 candidates (m_{D^0}) and the mass difference Δm between D^0 and D^* candidates to extract our signal yields, and to define sidebands for background studies. Figure 1 shows distributions of these quantities for the $D^0 \to K^-\ \pi^+$ analysis, which may be considered typical.

For historical reasons, D mesons whose decay flavour matches their production flavour (e.g. $D^{*+} \to D^0\ \pi^+$ with $D^0 \to K^-\ \pi^+$) are called 'right-sign' (RS), while the opposite case is referred to as 'wrong-sign' (WS). Wrong-sign decays may come about either through mixing or through doubly-Cabibbo-suppressed (DCS) Feynmann diagrams. To distinguish the two cases, we use the decay-time distribution, as will be shown for each decay mode.

In addition to these two sources of wrong-sign events, there is the case where a correctly reconstructed D^0 is matched with a pion not from a D^* decay to produce a spurious D^*; this is referred to as the "mistag" background. Another source of background is D mesons reconstructed with the correct tracks, but wrong particle assigments, or with tracks missing; this is the "bad D^0" or "mis-reconstructed charm" background. Finally there is background from combinatorics.

5 $D^0 \to K^+\ \pi^-$

In the limit of small mixing and *CP* conservation, the decay-time distribution for wrong-sign decays of mesons produced as D^0 may be approximated as

$$\frac{T_{\rm WS}(t)}{e^{-\Gamma t}} \quad \propto \quad R_D + y'\sqrt{R_D}(\Gamma t) + \frac{1}{4}(x'^2 + y'^2)(\Gamma t)^2 \qquad (1)$$

where x' and y' are related to x and y by

$$\begin{aligned} x' &= x\cos\delta_{K\pi} + y\sin\delta_{K\pi} \\ y' &= y\cos\delta_{K\pi} - x\sin\delta_{K\pi}. \end{aligned}$$

The angle $\delta_{K\pi}$ is the strong phase between Cabibbo-favoured (CF) and DCS decays. The quantity R_D is the amplitude, in the absence of mixing, for the D^0 to decay by a DCS process; the term quadratic in t is the amplitude, in the absence of DCS processes, for the D^0 to mix and then decay as a $\overline{D}^0$; and the term linear in t is the interference term between these two processes.

We apply Equation 1 in two ways: The first is to enforce *CP* conservation by fitting both D^0 and $\overline{D}^0$ samples together. The second is to search for *CP* violation by doing two fits, calculating x'^2 and y' for D^0 and $\overline{D}^0$ separately.

We use 384 fb^{-1} of e^+e^- data, pairing tracks of opposite charge to make D^0 candidates, and then pairing these with slow pion tracks to make D^* candidates. The phase space available for slow pions is small; we require their momentum to be greater than 0.1 GeV/c in the lab frame, and less than 0.45 GeV/c in the CM frame. We fit the full decay chain, constraining the D^* to come from the beam spot, the D^0 and slow pion to come from a common vertex, and the $K^\mp$ and $\pi^\pm$ to come from a different common vertex. We reject candidates if the χ^2 probability of this fit is less than 0.1%. The D^0 decay time and error on the decay time are taken from this fit; candidates whose decay-time error exceeds 0.5 ps are assumed to be badly reconstructed, and thrown away, and we also require that the decay time be between -2 and 4 ps. We further require the CM momentum of D^0 candidates to be at least 2.5 GeV/c, which suppresses backgrounds from B-meson decays and combinatorics. Where multiple D^* candidates share tracks, we use only the candidate with the highest χ^2 probability from the fit. With these criteria, our samples consist of 1,229,000 RS and 64,000 WS D^0 and $\overline{D}^0$ candidates. Figure 1 shows their distribution in $m_{K\pi}$ and Δm.

We extract the mixing parameters using an unbinned, extended maximum-likelihood fit, which proceeds in three stages. The first step is to fit the $m_{K\pi} - \Delta m$ distributions to extract shape parameters in these variables; these are then fixed in subsequent fits. Next we fit the RS sample to extract the D^0 lifetime and resolution functions, using the $m_{K\pi} - \Delta m$ parameters from the previous step to separate the components. Finally we fit the WS sample for the

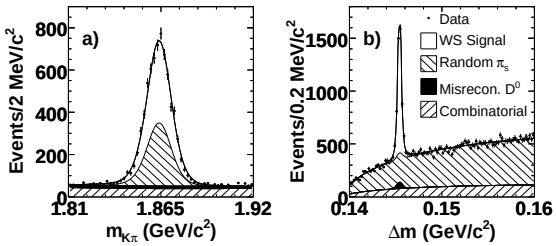

Figure 1: *a)* $m_{K\pi}$ *for wrong-sign (WS) candidates with* $0.1445 < \Delta m < 0.1465\,\mathrm{GeV}/c^2$*, and b)* Δm *for WS candidates with* $1.843 < m_{K\pi} < 1.883\,\mathrm{GeV}/c^2$*. The fitted PDFs are overlaid.*

mixing parameters using three different models. The first model assumes no *CP* violation and no mixing; the second permits mixing, but not *CP* violation; the third allows both mixing and *CP* violation.

The $m_{K\pi} - \Delta m$ distributions are fitted to a sum of four PDFs, one each for signal, mistags, bad D^0 and combinatorial background. Of these, the signal peaks in both $m_{K\pi}$ and Δm. The mistagged events - correctly reconstructed D^0 with a pion not from a D^* decay - peak in $m_{K\pi}$ but not in Δm. Bad D^0 events have a D^0 with one or more daughters missing, or assigned the wrong particle hypothesis; they peak in Δm but not in $m_{K\pi}$. Finally, combinatorial background does not peak in either variable. Figure 1 shows these various shapes. The signal peak contains $1,141,500 \pm 1,200$ candidates for the RS sample, and $4,030 \pm 90$ for the WS.

We describe the decay-time distribution of the RS signal with an exponential convolved with a sum of three Gaussians, whose widths are proportional to the measured event-by-event error on the decay time. The combinatorial background is described by a sum of two Gaussians, one of which has a power-law tail; the mistag background is described by the same PDF as the signal, because the slow pion has little influence on the vertex fit. For the WS signal, we use Equation 1, convolved with the resolution function determined by the RS fit. Figure 2 shows the data, overlaid by these various PDFs. From inspection, it is clear that the fit allowing mixing describes the data better than the one which imposes zero mixing.

Figure 3 shows the likelihood contours of the mixing parameters from the

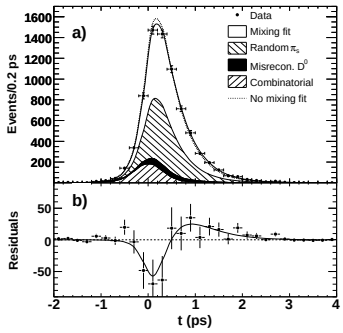

Figure 2: *a) Projections of the proper-time distribution of combined D^0 and $\overline{D}^0$ WS candidates and fit result integrated over the signal region $1.843 < m_{K\pi} < 1.883$ GeV/c^2 and $0.1445 < \Delta m < 0.1465$ GeV/c^2. The result of the fit allowing (not allowing) mixing but not CP violation is overlaid as a solid (dashed) curve. b) The points represent the difference between the data and the no-mixing fit. The solid curve shows the difference between fits with and without mixing. The difference between the mixing-allowed fit and the data is therefore the difference between the solid curve and the points, or essentially zero.*

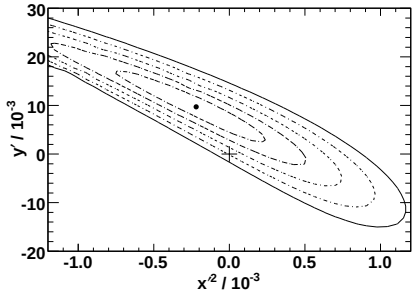

Figure 3: *The central value (point) and confidence-level (CL) contours for $1 - CL = 0.317$ (1σ), 4.55×10^{-2} (2σ), 2.70×10^{-3} (3σ), 6.33×10^{-5} (4σ) and 5.73×10^{-7} (5σ), calculated from the change in the value of $-2 \ln \mathcal{L}$ compared with its value at the minimum. Systematic uncertainties are included. The no-mixing point is shown as a plus sign (+).*

fit allowing mixing but not *CP* violation, including systematic uncertainties. The point of maximum probability is in the unphysical region where x'^2 is negative; adjusting for this by moving to the most likely point in the physical region, $x'^2 = 0$, $y' = 6.4 \times 10^{-3}$, we find that $-2\Delta \ln \mathcal{L}$ is 23.2 units between the most likely physical point and the point of no mixing. Including the systematic uncertainties, we thus find mixing at a significance of 3.9 σ. Table 1 shows the results of our fits in more detail; we find no evidence for *CP* violation, as shown by the asymmetry $A_D = (R_D^+ - R_D^-)/(R_D^+ + R_D^-)$ where subscript '+' indicates only the D^0 sample was used, and '−' indicates the $\overline{D}^0$ sample.

Table 1: *Results from the different fits. The first uncertainty listed is statistical and the second systematic.*

Fit type	Parameter	Fit Results ($/10^{-3}$)
No *CP* viol. or mixing	R_D	$3.53 \pm 0.08 \pm 0.04$
No *CP* violation	R_D	$3.03 \pm 0.16 \pm 0.10$
	x'^2	$-0.22 \pm 0.30 \pm 0.21$
	y'	$9.7 \pm 4.4 \pm 3.1$
CP violation allowed	R_D	$3.03 \pm 0.16 \pm 0.10$
	A_D	$-21 \pm 52 \pm 15$
	x'^{2+}	$-0.24 \pm 0.43 \pm 0.30$
	y'^{+}	$9.8 \pm 6.4 \pm 4.5$
	x'^{2-}	$-0.20 \pm 0.41 \pm 0.29$
	y'^{-}	$9.6 \pm 6.1 \pm 4.3$

We evaluate systematic uncertainties from three sources: Variations in the fit model, in the selection criteria, and in our procedure for dealing with track-sharing D^* candidates. The most significant source of systematic uncertainty in R_D and the mixing parameters is from the fit model for the long-lived background component caused by other D decays in the signal region, followed by the presence of a non-zero mean in the time-resolution function, caused by small misalignments in the detector. For the asymmetry A_D, the dominant contribution is uncertainty in modeling the differences between K^+ and K^- absorption in the detector.

6 $D^0 \to K^+K^-$ or $\pi^+\,\pi^-$

For D mesons decaying to *CP* eigenstates, mixing changes the decay time distribution in such a way that we may, to a good approximation, consider the decays exponential with changed lifetimes ([11])

$$\begin{aligned}\tau^+ &= \tau^0\left[1+|q/p|\,(y\cos\phi_f - x\sin\phi_f)\right]^{-1}\\ \tau^- &= \tau^0\left[1+|p/q|\,(y\cos\phi_f + x\sin\phi_f)\right]^{-1}\end{aligned}$$

where τ^0 is the lifetime for decays to final states which are not *CP* eigenstates, and τ^+ (τ^-) is the lifetime for D^0 ($\overline{D}^0$) decays to *CP*-even states. We can combine the three lifetimes into quantities

$$\begin{aligned}y_{CP} &= \tau^0/\langle\tau\rangle - 1\\ \Delta Y &= \left(\tau^0 A_\tau\right)/\langle\tau\rangle.\end{aligned}$$

Here ϕ_f is the *CP*-violating phase $\phi_f = \arg(q\overline{A}_f/pA_f)$, A_f ($\overline{A}_f$) being the amplitude for D^0 ($\overline{D}^0$) decaying to the final state f. $\langle\tau\rangle$ is the average of τ^+ and τ^-, and A_τ is their asymmetry $(\tau^+ - \tau^-)\,/\,(\tau^+ + \tau^-)$. In the absence of mixing, both y_{CP} and ΔY are zero. In the absence of *CP* violation in the interference of mixing and decay (ie, $\phi_f = 0$), ΔY is zero and $y_{CP} = y$.

For this analysis, we use 384 fb^{-1} of *BABAR* data, and measure the lifetimes for the *CP*-even decays[1] $D^0 \to K^+\,K^-$ and $D^0 \to \pi^+\,\pi^-$, and for $D^0 \to K^-\,\pi^+$, which is not a *CP* eigenstate and thus gives our τ^0.

In addition to particle identification requirements, the cosine of the helicity angle (defined as the angle between the momentum of the positively charged D^0 daughter in the D^0 rest frame, and the D^0's momentum in the lab frame) is required less than 0.7; this suppresses combinatorial backgrounds. D^0 candidates are then combined with pions to produce D^* candidates. Electrons are rejected by combining pion candidates with each other track in the event and vetoing those which form a good photon conversion or pion Dalitz decay, as well as by $\mathrm{d}E/\mathrm{d}x$ measurements. The requirements for slow pions and the vertex fit of the D^* are the same as for the $D^0 \to K^-\,\pi^+$ analysis (Section 5).

Figure 4 shows the mass distributions of D^0 candidates; Table 2 shows the yield and purity of the samples, calculated using events within a 15 MeV/c^2

[1] Charge conjugation is implied throughout unless otherwise noted.

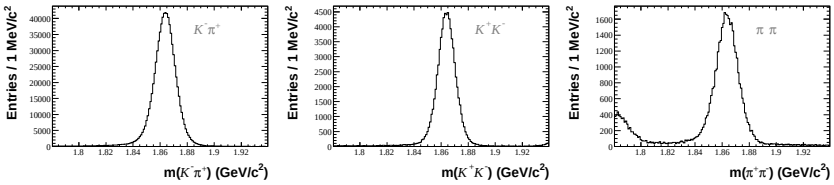

Figure 4: *Reconstructed D^0 mass distributions for the three D^0 samples, within ± 0.8 MeV/c^2 of the Δm peak.*

Table 2: *Sample sizes and purities.*

Sample	Size	Purity (%)
$K^-\pi^+$	730,880	99.9
K^-K^+	69,696	99.6
$\pi^-\pi^+$	30,679	98.0

D^0 mass and 0.8 MeV/c^2 Δm window. We fit the decay time distributions of these samples using an unbinned maximum likelihood fit to all five decay modes simultaneously, using separate PDFs for signal decays, mistagged events, mis-reconstructed charm events, and combinatorial background.

As with the $D^0 \to K^-\,\pi^+$ study, we model the decay-time distribution of signal events using a simple exponential convolved with a sum of three Gaussians for the resolution. Each Gaussian has a width proportional to the event-by-event error on the measured decay time; their mean is common, and allowed to be offset from zero to account for any effects of detector mis-alignment. Mistagged events - that is, events with a correctly reconstructed D^0, but wrongly assigned slow pion - account for about 0.4% of the sample; of these, half will have the wrong flavour assignment to the D^0. However, they have the same decay-time distribution and resolution as true signal. Hence we model these events using the signal PDF, but reversing the flavour assignment.

Mis-reconstructed charm events have an exponential decay-time distribution, which we convolve with a single Gaussian. The fraction of such events is obtained from simulation, which we check by comparing data and Monte Carlo in the sidebands $1.89 < m_{D^0} < 1.92\,\mathrm{GeV}/c^2$ and $0.151 < \Delta m < 0.159\,\mathrm{GeV}/c^2$.

We estimate the charm background as $(0.009 \pm 0.002)\%$ of events in the signal region for $D^0 \to K^- \pi^+$, $(0.2 \pm 0.1)\%$ for $D^0 \to K^+ K^-$, and $(0.15 \pm 0.15)\%$ for $D^0 \to \pi^+ \pi^-$. For combinatorial background, we model the decay-time distribution as the sum of a Gaussian and a modified Gaussian with a power-law tail, the latter accounting for a long-lived component. Each decay mode has its own shape for combinatorial background, the shapes being determined from fits to the sideband regions; the fraction of this background is again estimated from Monte Carlo with uncertainties derived from comparison of MC and data. We find $(0.032 \pm 0.003)\%$ in the $D^0 \to K^- \pi^+$ mode, $(0.16 \pm 0.02)\%$ in $D^0 \to K^+ K^-$, and $(1.8 \pm 0.2)\%$ in $D^0 \to \pi^+ \pi^-$.

We consider several sources of systematic error, including variations of the signal and background models, changes to the event selection, and detector effects. We vary the models by changing the signal PDF shape and size, as well as the position of the signal box. We also test our resolution model by forcing the common mean of the three Gaussians to zero, and by allowing it to float separately for different bins of the D^0 polar angle. Of these effects, the largest systematic uncertainty derives from widening the D^0 mass window, which increases the amount of badly-reconstructed signal events in the sample.

We vary the mis-reconstructed charm model by changing its fraction in the fit, by varying its effective lifetime, by using a different sideband region, and by using a decay time distribution obtained from Monte Carlo instead of the sideband data. Due to the purity of the data, these effects are all small, the largest being from varying the background fraction in the $D^0 \to \pi^+ \pi^-$ mode, where the purity is worst.

We vary our event selection criteria in two ways: By throwing out or keeping all multiple candidates (as opposed to selecting the candidate with the best χ^2 probability for its vertex fit), and by changing the acceptable range of errors on decay times. The last, which changes the amount of poorly reconstructed signal events, has the largest effect.

Finally, we consider effects of our understanding of the detector by repeating our analysis with different misalignment parameters. This changes our fitted lifetimes by up to 3 fs; but since the lifetimes change by similar amounts, and we are considering ratios of lifetimes, the effect on the mixing parameters is small. All these systematic effects are summarised in Table 3.

The results of these decay-time fits are shown in Table 4. From the

Table 3: *Summary of systematic uncertainties on y_{CP} and ΔY, separately for KK and $\pi^+\pi^-$ and averaged over the two CP modes, in percent.*

	$\sigma_{y_{CP}}$ (%)			$\sigma_{\Delta Y}$ (%)		
Systematic	KK	$\pi^+\pi^-$	Avg.	KK	$\pi^+\pi^-$	Avg.
Signal model	0.130	0.059	0.085	0.072	0.265	0.062
Charm bkg	0.062	0.037	0.043	0.001	0.002	0.001
Comb. bkg	0.019	0.142	0.045	0.001	0.005	0.002
Selection criteria	0.068	0.178	0.046	0.083	0.172	0.011
Detector model	0.064	0.080	0.064	0.054	0.040	0.054
Quadrature sum	0.172	0.251	0.132	0.122	0.318	0.083

measured lifetimes, we extract

$$\begin{aligned} y_{CP} &= 1.24 \pm 0.39(\text{stat}) \pm 0.13(\text{syst})]\% \\ \Delta Y &= [-0.26 \pm 0.36(\text{stat}) \pm 0.08(\text{syst})]\% \end{aligned}$$

which is evidence for D^0-$\overline{D}^0$ mixing at the 3-sigma level, and consistent with CP conservation. This amount of D^0-$\overline{D}^0$ mixing is consistent with Standard Model predictions.

Table 4: *Measured lifetimes for the different decay modes. Uncertainties are statistical only.*

Mode	Lifetime (fs)
$D^0 \to K^- \pi^+$	409.33 ± 0.70
D^0 $(D^{*+}) \to K^+ K^-$	401.28 ± 2.47
D^0 $(D^{*-}) \to K^+ K^-$	404.47 ± 2.52
D^0 $(D^{*+}) \to \pi^+ \pi^-$	407.64 ± 3.68
D^0 $(D^{*-}) \to \pi^+ \pi^-$	407.26 ± 3.73

7 $D^0 \to K^+ \pi^- \pi^0$

For the case of D^0 decays to three-body final states, we can modify Equation 1 to give a decay-time distribution for each point in the decay phase space:

$$\begin{aligned}\mathcal{A}(P,t) &= e^{-\Gamma t}\Big[|\overline{A_P}|^2 \\ &\quad +|\overline{A_P}||A_P|\,(y''\cos\delta_P - x''\sin\delta_P)\,\Gamma t \\ &\quad +|A_P|^2(x''^2+y''^2)(\Gamma t)^2\Big].\end{aligned} \tag{2}$$

In analogy with Equation 1, $\overline{A_P}$ is the amplitude (in the absence of mixing) for D^0 mesons to decay by a DCS process to the point P on the Dalitz plot. The term quadratic in time is the amplitude (in the absence of DCS processes) for the D^0 to mix before its decay, and then decay to the point D by a CF process. Within this term, the factor A_P is the amplitude for the CF decay, while the remaining factors are the mixing amplitude. The term linear in time is the interference between the DCS and mixing terms. The quantity δ_P is the phase of the intermediate states in the decay, relative to some reference resonance. As with the $D^0 \to K^-\ \pi^+$ case, an unknown strong phase $\delta_{K\pi\pi^0}$ between CF and DCS decays prevents us measuring x and y directly; instead we are sensitive to

$$\begin{aligned}x'' &= x\cos\delta_{K\pi\pi^0} + y\sin\delta_{K\pi\pi^0} \\ y'' &= y\cos\delta_{K\pi\pi^0} - x\sin\delta_{K\pi\pi^0}.\end{aligned}$$

As with the previous two analyses, we use 384 fb^{-1} of *BABAR* data, reconstructing $D^0 \to K^-\ \pi^+\ \pi^0$ candidates from two oppositely-charged tracks and two photon candidates with energy at least 100 MeV. The π^0 candidate is required to have a lab momentum of at least 350 MeV/c, and a mass-constrained fit probability of at least 1%. The slow pion is required to have a momentum transverse to the beam axis of at least 120 MeV/c, and the D^0 candidate to have a CM momentum of at least 2.4 GeV/c. As in the previous two analyses, we extract the D^0 decay time, with error, from a vertex fit constraining the D^* to the beam spot; this fit is required to have a χ^2 probability of at least 1%.

Figure 5 shows the $m_{K\pi\pi}$ and Δm distributions that result from these criteria. We fit these distributions as described for the $D^0 \to K^-\ \pi^+$ study in Section 5; the fit to the WS sample uses shape parameters from the RS

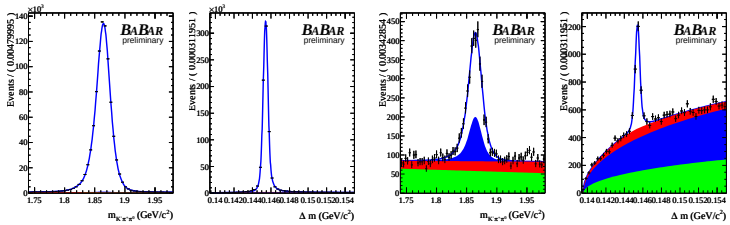

Figure 5: *(Distributions of RS (top) and WS (bottom) data (points with error bars) with fitted PDFs (dashed line) overlaid. The $m_{K\pi\pi}$ distribution (left) requires $0.145 < \Delta m < 0.146\,\mathrm{GeV}/c^2$; the Δm distribution (right) requires $1.85 < m_{K\pi\pi} < 1.88 gevcc$. The white regions represent signal events, the light gray (blue) misassociated $\pi_s^{\pm}$ events, the medium gray (red) correctly associated $\pi_s^{\pm}$ with misreconstructed D^0 events, and the dark gray (green) remaining combinatorial background.*

fit, suppressing the associated systematics. Table 5 shows the yields for each component.

Table 5: *Number of RS and WS events of signal and background in the m_{D^0} and Δm signal region.*

Category	N events (RS)	N events (WS)
Signal	639802 ± 1538	1483 ± 56
Combinatoric	1537 ± 57	499 ± 57
Mistag	2384 ± 57	765 ± 29
Bad D^0	3117 ± 93	227 ± 75

We compute the quantity A_P in Equation 2, the time-independent amplitude of CF decays to the point P on the Dalitz plot, by fitting the RS Dalitz plot to an isobar model, using the signal and background fractions obtained in the fit to the $m_{K\pi\pi} - \Delta m$ distribution. The background PDF is empirically determined from the $m_{K\pi\pi} - \Delta m$ sidebands, and its fraction is set to the background fraction derived from the $m_{K\pi\pi} - \Delta m$ fit.

With A_P (or more accurately, the phases and amplitudes for intermediate resonances from which A_P can be calculated) known, we then go on to fit the WS sample simultaneously to the Dalitz plot. We thereby determine $\overline{A_P}$, and the decay-time distribution, to extract the mixing parameters. The

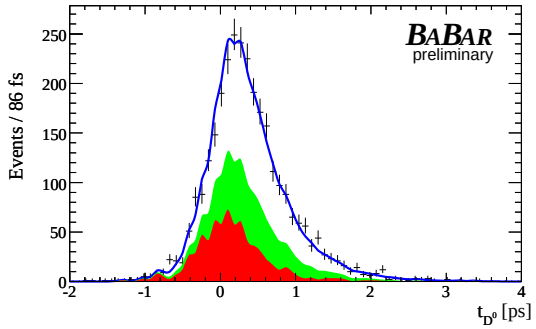

Figure 6: *WS D^0 decay-time distribution (crosses) with fit (solid blue line) overlaid. The green and red regions show the mistag and (combinatoric+bad-D^0) backgrounds respectively. These backgrounds are taken from sideband data, which accounts for their jagged shape.*

signal decay-time PDF is taken as Equation 2 convolved with a sum of three Gaussians, as described for the previous two analyses; the parameters of the Gaussians are extracted from a fit to the RS decay-time distribution, and fixed in the WS fit. For the background components, mistagged events are described by the RS parameters, since they contain correctly reconstructed D^0 mesons; the other two background components are described empirically using the sidebands. Figure 6 shows the WS fit projected to the decay time. From this we extract $x'' = 2.39 \pm 0.61$ (stat.) $\pm$ 0.32 (syst.)% and y'' = -0.14 $\pm$ 0.60 (stat.) $\pm$ 0.40 (syst.) %. This excludes the no-mixing hypothesis at the 99% confidence level.

8 $D^0 \to K^+ \pi^- \pi^+ \pi^-$

As in the case of $D^0 \to K^- \pi^+ \pi^0$, the four-body final state $K^+ \pi^- \pi^+ \pi^-$ has a decay-time distribution which varies across the phase space. However, since the phase space is enlarged by one dimension, and the data sample for this analysis is smaller, we do not fit for a decay time at each phase-space point. Instead we integrate across phase space to get a WS to RS decay-rate ratio of

$$\frac{\Gamma_{\rm WS}(t)}{\Gamma_{\rm RS}(t)} = \tilde{R}_D + \alpha\tilde{y}'\sqrt{\tilde{R}_D}(\Gamma t) + \frac{1}{4}(\tilde{x}'^2 + \tilde{y}'^2)(\Gamma t)^2 \quad (3)$$

where a tilde indicates integration over phase space. The quantity α is a suppression factor accounting for strong-phase variation across phase space; in effect it measures the amount of information we lose by the integration procedure. As in the $D^0 \to K^-\,\pi^+$ analysis, $\tilde{R}_D$ is the amplitude for doubly-Cabibbo-suppressed decays, the term quadratic in time is the amplitude for mixed decays, and the term linear in time is the interference between the two. Again we account for an unknown strong phase by using variables

$$\begin{aligned} \tilde{x}' &= x\cos\tilde{\delta} + y\sin\tilde{\delta} \\ \tilde{y}' &= y\cos\tilde{\delta} - x\sin\tilde{\delta} \end{aligned}$$

where $\tilde{\delta}$ is the strong phase difference integrated across phase space. Equation 3 assumes *CP* conservation. To account for possible *CP* violation in interference between DCS and mixed contributions, we introduce the integrated *CP*-violation phase $\tilde{\phi}$, and parametrise *CP* violation in the mixing itself with $|p/q|$. This allows us to make the substitutions

$$\begin{aligned} \alpha\tilde{y} &\to |p/q|^{\pm 1}\left(\alpha\tilde{y}'\cos\tilde{\phi} \pm \beta\tilde{x}'\sin\tilde{\phi}\right) \\ \left(x^2+y^2\right) &\to |p/q|^{\pm 2}\left(x^2+y^2\right) \end{aligned}$$

in Equation 3, applying plus signs for the D^0 sample and minus signs for $\overline{D}^0$. β is an information-loss parameter analogous to α, in this case accounting for phase-space variation in ϕ.

This analysis uses a 230.4 fb^{-1} *BABAR* dataset. The reconstruction procedure is analogous to that of the previous three analyses, the main difference being the requirement that neither pion pair have an invariant mass within 20 MeV/c^2 of the K^0_S mass of 0.4977 GeV/c^2. We demand a D^0 CM momentum requirement of at least 2.4 GeV/c. Two vertex fits are performed, one for the D^0 candidate, required to have a χ^2 probability of at least 0.5%, and one for the full D^* decay tree. For the latter, from which we derive our decay-time value and error, the D^* is constrained to come from the beam-spot, and the probability is required to be at least 1%. The mean σ_t for signal events is 0.29 ps; events with $\sigma_t > 0.5$ ps are rejected. The signal yields are calculated from a fit to the $(m_{K3\pi}, \Delta m)$ distribution; Table 6 shows the results.

The $(m_{K3\pi}, \Delta m)$ fit which extracts the signal yields also determines shape parameters for those two variables; these are then used in a three-dimensional fit which also includes the time distribution. The decay time function for RS

Table 6: *Signal yields determined by the two-dimensional fit to the* $(m_{K3\pi}, \Delta m)$ *distributions for the WS and RS samples. Uncertainties are calculated from the fit.*

	D^0	$\overline{D}^0$
WS	$(1.162 \pm 0.053) \times 10^3$	$(1.040 \pm 0.051) \times 10^3$
RS	$(3.511 \pm 0.006) \times 10^5$	$(3.492 \pm 0.006) \times 10^5$

Table 7: *Summary of results.*

Mode	Lum. [fb^{-1}]	Mixing	*CP* violation
$D^0 \to K^-\ \pi^+$	384	3.9 σ	No evidence
$D^0 \to K^-\ K^+$ or $\pi^+\ \pi^-$	384	3.0 σ	No evidence
$D^0 \to K^-\ \pi^+\ \pi^0$	384	Excl. NM at 99% CL	No evidence
$D^0 \to K^-\ \pi^+\ \pi^-\ \pi^+$	230.4	Cons. with NM at 4.3% CL	No evidence

events is a simple exponential convolved with a double Gaussian, with widths proportional to σ_t and separate means. For mistagged events we use the RS decay-time PDF; for mis-reconstructed D^0 component we use the signal PDF; and for combinatorial background a Gaussian with a power-law tail. We fit the RS sample to determine the D^0 lifetime and the time-resolution parameters, which are then held fixed in the fit to the WS sample. We allow yields and background shape parameters to vary. Figure 7 shows the WS decay-time distribution and fit. Figure 8 shows contours of constant likelihood in the (R_D, R_M) plane; we find $R_M = (0.019^{+0.016}_{-0.015} \pm 0.002)\%$ assuming *CP* conservation, and $R_M = (0.017^{+0.017}_{-0.016} \pm 0.003)\%$ with *CP* violation allowed. There is no significant difference between the D^0 and $\overline{D}^0$ samples in the *CP*-allowed fit.

To extract a consistency with the no-mixing hypothesis from these contours is not quite straightforward, because the linear term in Equation 3 becomes unconstrained as R_M approaches zero. We therefore estimate the consistency of our data with no-mixing using a frequentist method; we generate 1000 data sets of 76300 events each, setting the mixing parameters to zero in the generation. We then apply our fit procedure to these sets; in 43 cases we find an R_M equal to or greater than for the data. We therefore conclude that our data are consistent with no-mixing only at the 4.3% confidence level.

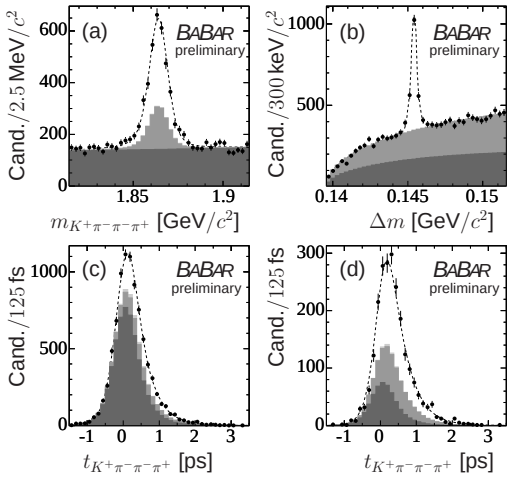

Figure 7: *Distributions of WS data with fitted PDF overlaid. The light gray shows mis-reconstructed charm, the medium gray shows mistagged events, and the dark gray shows combinatorial background.*

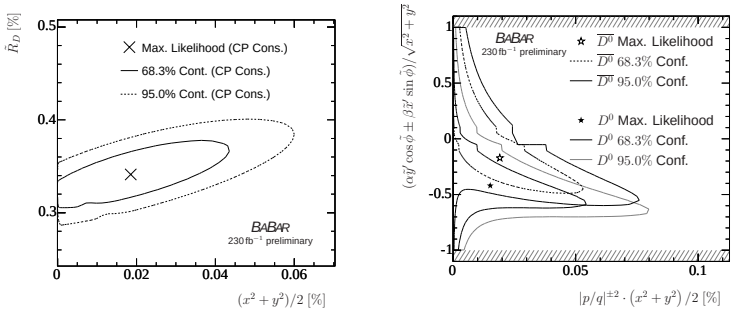

Figure 8: *Left: Contours of constant* $\Delta \ln \mathcal{L} = 1.15, 3.0$ *in terms of the doubly Cabibbo-suppressed amplitude and the time-integrated mixing rate. Right: Contours of constant* $\Delta \ln \mathcal{L} = 1.15, 3.0$ *in terms of the normalized interference term and the integrated mixing rate, for the* D^0 *and* $\overline{D}^0$ *samples separately. The hatched regions are physically forbidden.*

We investigate systematic uncertainties from four sources, listed in order of decreasing significance. First is the σ_t threshold, which we increase from 0.5 to 0.6 ps. Second is the decay-time resolution function; we change this by fixing one of the Gaussian widths to be exactly equal to σ_t, letting the other constant of proportionality float as before. Third, the $m_{K3\pi}$ distribution of the background is changed from exponential to a second-order polynomial. And fourth, we use the nominal value of the D^0 lifetime instead of the one obtained from our RS fit. Taken all together, these uncertainties are smaller than the statistical uncertainty by a factor of five.

9 Summary and outlook

BABAR has found evidence for mixing in several channels, as summarised in Table 7. With the total *BABAR* luminosity expected to reach 750 fb^{-1} before shutdown, or nearly twice the largest amount used in these studies, we expect to be able to improve these measurements of the D mixing parameters, and to add other channels as well.

10 Acknowledgements

We are grateful for the excellent luminosity and machine conditions provided by our PEP-II colleagues, and for the substantial dedicated effort from the computing organizations that support *BABAR*. The collaborating institutions wish to thank SLAC for its support and kind hospitality. This work is supported by DOE and NSF (USA), NSERC (Canada), CEA and CNRS-IN2P3 (France), BMBF and DFG (Germany), INFN (Italy), FOM (The Netherlands), NFR (Norway), MES (Russia), MEC (Spain), and STFC (United Kingdom). Individuals have received support from the Marie Curie EIF (European Union) and the A. P. Sloan Foundation.

References

1. K. Lande, E. T. Booth, J. Impeduglia, L. M. Lederman, and W. Chinowsky, Phys. Rev. **103**, 1901 (1956);

2. C. Albajar et al. (UA1 Collaboration), Phys. Lett. **B186**, 247 (1987); H. Albrecht et al. (ARGUS Collaboration), Phys. Lett. **B192**, 245 (1987).

3. V. M. Abazov et al. (D0 Collaboration), Phys. Rev. Lett. **97**, 021802 (2006); A. Abulencia et al. (CDF Collaboration), Phys. Rev. Lett. **97**, 242003 (2006a).

4. S. Bianco, F. L. Fabbri, D. Benson, and I. Bigi, Riv. Nuovo Cim. **26N7**, 1 (2003); G. Burdman and I. Shipsey, Ann. Rev. Nucl. Part. Sci. **53**, 431 (2003).

5. L. Wolfenstein, Phys. Lett. **B164**, 170 (1985); J. F. Donoghue, E. Golowich, B. R. Holstein, and J. Trampetic, Phys. Rev. **D33**, 179 (1986); I. I. Y. Bigi and N. G. Uraltsev, Nucl. Phys. **B592**, 92 (2001); A. F. Falk, Y. Grossman, Z. Ligeti, and A. A. Petrov, Phys. Rev. **D65**, 054034 (2002); A. F. Falk, Y. Grossman, Z. Ligeti, Y. Nir, and A. A. Petrov, Phys. Rev. **D69**, 114021 (2004); A. A. Petrov, Int. J. Mod. Phys. **A21**, 5686 (2006).

6. Blaylock et. al.(1995) Phys. Lett. **volume B355** pages 555 year 1995 hep-ph/9504306

7. B. Aubert *et. al.*, (*BABAR* Collaboration), "Evidence for D^0-$\overline{D}^0$ Mixing", submitted to Phys. Rev. Lett, arXiv:hep-ex/0703020v1

8. B. Aubert *et. al.*, (*BABAR* Collaboration), "Measurement of D^0-$\overline{D}^0$ mixing using the ratio of lifetimes for the decays $D^0 \to K^-\ \pi^+$, $K^-\ K^+$, and $\pi^-\ \pi^+$", submitted to Phys. Rev. D - Rap. Comm.

9. B. Aubert *et. al.*, (*BABAR* Collaboration), "Search for mixing in $D^0 \to K^+\ \pi^-\ \pi^0$", given at Lepton-Photon 2007.

10. B. Aubert *et. al.*, (*BABAR* Collaboration), "Search for D^0-antiD^0 mixing in the decays $D^0 \to K^+\ \pi^-\ \pi^+\ \pi^-$", given at ICHEP 2006, arXiv:hep-ex/0607090

11. Bergmann et. al.(2000) Phys. Lett. **volume B486** pages 418 year 2000 hep-ph/0005181

Frascati Physics Series Vol. XLVI (2007), pp. 1003–1010
HADRON07: XII Int. Conf. on Hadron Spectroscopy – Frascati, October 8-13, 2007
Heavy Meson Spectroscopy

CHARM SPECTROSCOPY AT *BABAR*

Vincent Poireau
LAPP, IN2P3/CNRS et Université de Savoie, Annecy-Le-Vieux, France

Abstract

We present a mini-review on charm spectroscopy at the *BABAR* experiment. We first report on the $c\bar{s}$ meson spectrum, and present precise measurements of the $D_{s1}(2536)$ meson as well as the properties of the many new states discovered since 2003 ($D^*_{s0}(2317)$, $D_{s1}(2460)$, $D^*_{sJ}(2860)$, and $D_{sJ}(2700)$ mesons). We then discuss about charmed baryons observed recently in the *BABAR* experiment: Ω_c^0 and Ω_c^{*0} css baryons, $\Lambda_c(2940)^+$ udc baryon and the Ξ_c usc/dsc baryons.

1 Introduction

Observations of a long list of new meson and baryon resonances have been recently reported by the *BABAR*, Belle and CLEO experiments. We present here the new resonances observed in the $c\bar{s}$ and charmed baryon sectors by the *BABAR* experiment.

In this short review, we do not present results on $c\bar{u}$ and $c\bar{d}$ resonances (D, D^*, D^{**} mesons) and on $c\bar{c}$ states (charmonium or charmonium-like state).

Analyzes presented here were performed using data collected at the $\Upsilon(4S)$ resonance with the *BABAR* detector [1], located at the PEP-II asymmetric

energy e^+e^- collider. From 1999 to 2007, the *BABAR* experiment recorded a luminosity of 432 fb^{-1} at the $\Upsilon(4S)$ peak and 45 fb^{-1} at 40 MeV below the peak. This corresponds to about 475.10^6 $B\bar{B}$ pairs and 620.10^6 $c\bar{c}$ pairs. The analyzes presented here use only a subset of the total recorded luminosity.

2 $c\bar{s}$ mesons

Before 2003, only four $c\bar{s}$ mesons were known: two S-wave mesons, D_s ($J^P = 0^-$) and D_s^* (1^-), and two P-wave mesons, $D_{s1}(2536)$ (1^+) and $D_{s2}(2573)$ (2^+). The masses predicted by the potential model [2] were in good agreement with the measured masses. The potential model predicted also two other broad states (width of a few hundred of MeV) at masses between 2.4 and 2.6 GeV/c^2.

2.1 $D_{s1}(2536)$ meson

With the discovery of additional $c\bar{s}$ mesons, a comprehensive knowledge of all known D_s mesons is mandatory. As of 2006, the properties of the $D_{s1}(2536)$ meson were not perfectly known: the width was determined to be less than 2.3 MeV at 90% confidence level, and the quantum numbers were only inferred.

In Ref. [3], a high precision measurement of the mass and of the width was performed, using events in the $c\bar{c}$ continuum. Reconstructing inclusively the decay $D_{s1}(2536) \to D^{*+}K_S^0$, with $D^{*+} \to D^0\pi^+$ and D^0 decaying either to $K^-\pi^+$ or to $K^-\pi^+\pi^-\pi^+$, one obtain a mass of $(2534.85 \pm 0.02 \pm 0.40)$ MeV/c^2 (where the first error is statistical and the second is systematic). The error on the mass is dominated by the uncertainty on the D^{*+} mass. Furthermore, the width was measured at a value of $(1.03 \pm 0.05 \pm 0.12)$ MeV. This is the first time that a direct measurement of the width is given, rather than just an upper limit.

Additionally, in another analysis [4], the $D_{s1}(2536)$ meson was reconstructed exclusively in B decays, with $B \to D^{(*)}D_{s1}(2536)$ (8 modes in total) followed by $D_{s1}(2536) \to D^*K$. A total of 182 ± 19 events is seen, which gives an observation at the 12σ significance level (where σ is the 68% C.L. standard deviation). With this method, a mass of $(2534.78 \pm 0.31 \pm 0.40)$ MeV/c^2 is obtained, in good agreement with the inclusive measurement. The exclusive reconstruction allows to determine the J^P quantum number: fits to the helicity distribution in the data favor the quantum number $J = 1$ while $J = 2$ is

disfavored. More statistics is needed to conclude definitely and determine the parity P.

2.2 $D^*_{s0}(2317)$ and $D_{s1}(2460)$ mesons

In 2003, two new resonances were discovered by the *BABAR* and CLEO experiments: the $D^*_{s0}(2317)$ and $D_{s1}(2460)$ mesons [5]. These two resonances are very narrow, and have masses well below what was predicted by the potential model (the $D^*_{s0}(2317)$ and $D_{s1}(2460)$ mesons were predicted to lie above the DK and D^*K threshold, respectively, but have been observed below these thresholds). These states are very well known experimentally: masses are measured with an error below 2 MeV/c^2, 95% confidence level upper limits on widths are about 4 MeV ; J^P quantum numbers (0^+ and 1^+ for $D^*_{s0}(2317)$ and $D_{s1}(2460)$ respectively), decay modes and branching fractions are also well measured. Despite a good knowledge of these states, their theoretical interpretation is still unclear. One obvious possibility is to identify these two resonances with the 0^+ and 1^+ $c\bar{s}$ states, although it is difficult to fit these resonances within the potential model. Other interpretations have been proposed: four quark states, DK molecules or $D\pi$ atoms [6].

2.3 $D^*_{sJ}(2860)$ meson

The $D^*_{sJ}(2860)$ resonance was discovered by *BABAR* in 2006 [7], looking in the $c\bar{c}$ continuum: $e^+e^- \to D^0K^+X$ and $e^+e^- \to D^+K^0_sX$, where we consider the decays $D^0 \to K^-\pi^+, K^-\pi^+\pi^0$ and $D^+ \to K^-\pi^+\pi^+$ and where X could be anything. A clear peak is observed in the DK invariant mass for the sum of these 3 modes, with a mass of $(2856.6 \pm 1.5 \pm 5.0)$ MeV/c^2 and a width of $(47 \pm 7 \pm 10)$ MeV. This signal is seen with a statistical significance above 8σ. Although this resonance is observed with a high significance, no other experiments have yet confirmed this state. Given that this resonance decays to two pseudoscalars, the J^P quantum number should be 0^+, 1^-, 2^+, etc. Different interpretations have been proposed, inside the $c\bar{s}$ scheme: this state could be a radial excitation of the $D^*_{s0}(2317)$, but other possibilities are not ruled out [8].

2.4 $D_{sJ}(2700)$ meson

In the same analysis, *BABAR* reported a broad enhancement, named $X(2690)$, at a mass of $(2688 \pm 4 \pm 3)$ MeV/c^2 and a width of $(112 \pm 7 \pm 36)$ MeV. A new state, the $D_{sJ}(2700)$, was reported independently by Belle at a similar mass, with a J^P quantum number equal to 1^-, looking at $B^+ \to \bar{D}^0 D^0 K^+$ events [9]. Since the $X(2690)$ and $D_{sJ}(2700)$ mesons have the same decay modes and that the mass and width are consistent with each other, it is reasonable to think that they are indeed the same state.

BABAR performed an exclusive analysis [9], looking at events where B decays to $\bar{D}^{(*)} D^{(*)} K$. Thanks to the many final states studied, this analysis has the advantage to be able to look at four $D^0 K^+$ invariant mass distributions as well as four $D^+ K^0_s$ invariant mass distributions. Adding these final states together, a clear resonant enhancement is seen around a mass of 2700 MeV/c^2. Furthermore, adding the four $D^{*0} K^+$ and four $D^{*+} K^0_s$ invariant mass distributions together, a similar enhancement is observed around a mass of 2700 MeV/c^2. No precise measurement was given by this preliminary analysis yet.

The potential model predicts the 2^3S_1 $c\bar{s}$ state at a mass of 2720 MeV/c^2. Also, from chiral symmetry considerations, a $1^+ - 1^-$ doublet of states has been predicted. If the 1^+ state is identified as the $D_{s1}(2536)$, the mass predicted for the 1^- state is (2721 ± 10) MeV/c^2 [10].

3 Charmed baryons

The production and decay of singly-charmed baryons are largely unexplored and provide an interesting environment to study the dynamics of quark-gluon interactions. All nine ground states with $J^P = 1/2^+$ and all six ground states with $J^P = 3/2^+$ are now observed (the last missing state, Ω_c^{*0}, was discovered by *BABAR* in 2006). Several orbitally excited states have already been seen as well. The spin and parity of each of these excited single-charm baryons are assigned based on a comparison of the measured masses and natural widths with predictions of theoretical models.

3.1 Ω_c^0 and Ω_c^{*0} baryons

The Ω_c^0 baryon, a *css* state with $J^P = 1/2^+$, was observed by *BABAR* [11] decaying to four hadronic modes: $\Omega_c^0 \to \Omega^-\pi^+$ (with a significance of 18σ), $\Omega_c^0 \to \Omega^-\pi^+\pi^0$ (5.1σ), $\Omega_c^0 \to \Omega^-\pi^+\pi^+\pi^-$ (4.2σ) and $\Omega_c^0 \to \Xi^- K^-\pi^+\pi^+$ (4.3σ). The ratios of branching fractions were measured, significantly improving upon the previous values. The p^* spectrum of Ω_c^0 was also measured in order to study the production rates in both $c\bar{c}$ and $B\bar{B}$ events, using only the $\Omega^-\pi^+$ final state. This analysis find comparable production rates of Ω_c^0 baryons from the continuum and from B meson decays. This is the first observation of this baryon in B decays.

Recently, *BABAR* discovered [12] the *css* ground state with $J^P = 3/2^+$, the Ω_c^{*0} baryon. This baryon was observed with a significance of 5.2σ in the decay to $\Omega_c^0\gamma$, combining the four decay modes of the Ω_c^0 cited in the previous paragraph. The difference of mass between Ω_c^{*0} and Ω_c^0 was measured to be $(70.8 \pm 1.0 \pm 1.1)$ MeV/c^2. A non-relativistic QCD effective field theory calculation predicts the mass difference to be in the range 50-73 MeV/c^2, while a lattice calculation gives a mass difference equal to (94 ± 10) MeV/c^2 [13].

The ratio of inclusive production cross-section was determined to be

$$\frac{\sigma(e^+e^- \to \Omega_c^{*0} X, x_p(\Omega_c^{*0}) > 0.5)}{\sigma(e^+e^- \to \Omega_c^0 X, x_p(\Omega_c^0) > 0.5)} = 1.01 \pm 0.23 \pm 0.11, \qquad (1)$$

where the scaled momentum $x_p = p^*/p^*_{\rm max}$ of the Ω_c^{*0} (Ω_c^0) is required to be greater than 0.5 in the numerator (denominator) cross-section.

3.2 $\Lambda_c(2940)^+$ baryon

A search for charmed baryons decaying to D^0p was performed [14] and revealed two states: the $\Lambda_c(2880)^+$ baryon and a previously unobserved state, the $\Lambda_c(2940)^+$. This is the first observation of charmed baryons decaying to a D meson and a light baryon.

The $\Lambda_c(2880)^+$ baryon was previously observed [15] by the CLEO experiment in the $\Lambda_c\pi^+\pi^-$ decay mode, with a mass of (2880.9 ± 2.3) MeV/c^2 and a width less than 8 MeV at 90% confidence level. Using *BABAR* data in the D^0p channel leads to much more precise values, in particular with the first measurement of the width of the $\Lambda_c(2880)^+$: $m = (2881.9 \pm 0.1 \pm 0.5)$ MeV/c^2

and $\Gamma = (5.8 \pm 1.5 \pm 1.1)$ MeV. The existence of the decay $D^0 p$ rules out various interpretations of this baryon [16].

The new baryon $\Lambda_c(2940)^+$ is observed with a significance above 7σ, with a mass of $(2939.8 \pm 1.3 \pm 1.0)$ MeV/c^2 and an intrinsic width of $(17.5 \pm 5.2 \pm 5.9)$ MeV. This new state could be interpreted as a *udc* baryon. To determine if this new state belongs to an isotriplet (analogous to Σ_c^0 and Σ_c^{++}), a search for doubly-charged partner was performed, looking at the decay mode $D^+ p$. No signal corresponding to either the $\Lambda_c(2880)^+$ or $\Lambda_c(2940)^+$ baryon was observed, which shows that both states are isoscalar.

3.3 $\Xi_c(2980)^+$, $\Xi_c(3077)^{+/0}$, $\Xi_c(3055)^+$ and $\Xi_c(3123)^+$ baryons

The *BABAR* experiment searched [17] for the excited charm-strange baryons $\Xi_c(2980)^+$ and $\Xi_c(3077)^{+/0}$, discovered previously by the Belle collaboration [18]. *BABAR* confirms the states $\Xi_c(2980)^+$, $\Xi_c(3077)^{+/0}$, looking at the $\Lambda_c^+ K^- \pi^+$ and $\Lambda_c^+ K_S^0 \pi^-$ final states, with $\Lambda_c^+ \to pK^-\pi^+$, pK_S^0, $pK_S^0\pi^-\pi^+$, $\Lambda\pi^+$, $\Lambda\pi^+\pi^-\pi^+$. The $\Xi_c(2980)^+$ baryon is observed at a mass of $(2969.3 \pm 2.2 \pm 1.7)$ MeV/c^2 with a width of $(27 \pm 8 \pm 2)$ MeV. The $\Xi_c(3077)^+$ is seen at a mass of $(3077.0 \pm 0.4 \pm 0.2)$ MeV/c^2 with an intrinsic width of $(5.5 \pm 1.3 \pm 0.6)$ MeV. *BABAR* confirmed also the $\Xi_c(3077)^0$ state at a mass of $(3079.3 \pm 1.1 \pm 0.2)$ MeV/c^2 with a width of $(5.9 \pm 2.3 \pm 1.5)$ MeV. These results are in good agreement with the values given by Belle, except for the $\Xi_c(2980)^+$ baryon where the difference could be explained by the fact that *BABAR* incorporates phase space effect near the threshold and takes into account decays to $\Sigma_c(2455)^{++}K^-$.

In addition to these confirmations, *BABAR* discovered a new baryon, the $\Xi_c(3055)^+$, and found an evidence for the $\Xi_c(3123)^+$ baryon. The $\Xi_c(3055)^+$ and $\Xi_c(3123)^+$ signals are observed only in $\Sigma_c(2455)^+K^-$ and $\Sigma_c(2520)^+K^-$ intermediate-resonant decays, respectively. The $\Xi_c(3055)^+$ is seen with a 6.4σ significance, with a mass of $(3054.2 \pm 1.2 \pm 0.5)$ MeV/c^2 and a width of $(17 \pm 6 \pm 11)$ MeV, while the $\Xi_c(3123)^+$ is observed with a 3.6σ significance at a mass of $(3122.9 \pm 1.3 \pm 0.3)$ MeV/c^2 and with a width of $(4.4 \pm 3.4 \pm 1.7)$ MeV.

These baryons have same or similar decay channels as the double-charm baryon, but are identified as single-charm based on the measured masses, natural widths and charges of the members of the isospin doublet. In the current state of knowledge, it is difficult to assign a spin-parity to these baryons. More theoretical and experimental work is needed to clarify the properties of these

states.

4 Conclusion

Although no new resonances were discovered in many years, *BABAR* gave an impressive list of new results since 1999. In the $c\bar{s}$ sector, the $D^*_{s0}(2317)$ and $D_{s1}(2460)$ mesons are now very well known experimentally, but no definite interpretation was given theoretically. The $D^*_{sJ}(2860)$ and $D_{sJ}(2700)$ mesons were discovered recently and need more experimental inputs. Many new charmed baryon states were observed by *BABAR*. Thanks to the discovery of the Ω_c^{*0}, all ground states are now established. A lot of excited states have been observed, and probably many of them have yet to be discovered. The production rate, the decay channels and the measured properties (masses, widths) of these excited states will help to understand the internal quark dynamics.

A lot of analyzes are still in progress with the current data set in *BABAR*: more decay modes for the resonances presented here are being investigated. *BABAR* is taking data until the end of 2008, which is the promise of more surprises to arise.

5 Acknowledgements

The author is very grateful to the organizers of the HADRON 2007 conference for their support and all efforts in making this venue successful.

We are also grateful for the excellent luminosity and machine conditions provided by our PEP-II colleagues, and for the substantial dedicated effort from the computing organizations that support *BABAR*.

References

1. B. Aubert *et al.* (*BABAR* Collaboration), Nucl. Instrum. Meth. **A 479** 1 (2002).
2. S. Godfrey and N. Isgur, Phys. Rev. **D 32** 189 (1985).
3. B. Aubert *et al.* (*BABAR* Collaboration), arXiv:hep-ex/0607084 (2006).
4. B. Aubert *et al.* (*BABAR* Collaboration), arXiv:0708.1565 (2007).

5. S.K. Choi *et al.* (Belle Collaboration), Phys. Rev. Lett. **91** 262001(2003) ; B. Aubert *et al.* (*BABAR* Collaboration), Phys. Rev. **D74** 032007 (2006).

6. H-Y Cheng and W-S Hou, Phys. Lett. **B566** 193 (2003) ; T. Barnes, F. E. Close, and H. J. Lipkin, Phys. Rev. **D68** 054006 (2003) ; A. Szczepaniak, Phys. Lett. **B567** 23 (2003).

7. B. Aubert *et al.* (*BABAR* Collaboration), Phys. Rev. Lett. **97** 222001 (2006).

8. E. van Beveren, and G. Rupp, Phys. Rev. Lett. **97** 202001 (2006) ; P. Colangelo, F. De Fazio, and S. Nicotri, Phys. Lett. **B642** 48 (2006).

9. J. Brodzicka *et al.* (Belle Collaboration), arXiv:0707.3491 (2007) ; B. Aubert *et al.* (*BABAR* Collaboration), preliminary (2007).

10. M. A. Nowak, M. Rho, and I. Zahed, Phys. Polon. **B 35**, 2377 (2004).

11. B. Aubert *et al.* (*BABAR* Collaboration), Phys. Rev. Lett. **99** 062001 (2007).

12. B. Aubert *et al.* (*BABAR* Collaboration), Phys. Rev. Lett. **97** 232001 (2006).

13. N. Mathur *et al.*, Phys. Rev. Lett. **B592**, 1 (2004) ; R. M. Woloshyn, Nucl. Phys. Proc. Suppl. **93**, 38 (2001).

14. B. Aubert *et al.* (*BABAR* Collaboration), Phys. Rev. Lett. **98**, 012001 (2007).

15. M. Artuso *et al.* (CLEO), Phys. Rev. Lett. **86**, 4479 (2001).

16. A. E. Blechman, A. F. Falk, D. Pirjol, and J. M. Yelton, Phys. Rev. **D67**, 074033 (2003).

17. B. Aubert *et al.* (*BABAR* Collaboration), arXiv:hep-ex/0607042 (2006) ; B. Aubert *et al.* (*BABAR* Collaboration), preliminary (2007).

18. R. Chistov *et al.* (Belle Collaboration), arXiv:hep-ex/0606051 (2006).

Frascati Physics Series Vol. XLVI (2007), pp. 1011–1018
HADRON07: XII Int. Conf. on Hadron Spectroscopy – Frascati, October 8-13, 2007
Heavy Meson Spectroscopy

SEMILEPTONIC DECAYS AT *BABAR*

Michael Mazur
(representing the *BABAR* Collaboration)
INFN Pisa, Largo Pontecorvo 3, I-56127, Pisa, Italy

Abstract

We present the results of several recent measurements of semileptonic B meson decays with the *BABAR* detector. Charmless semileptonic decays $B \to X_u \ell^- \overline{\nu}_\ell$ are studied in three kinematic regions, leading to measurements of the partial branching fraction and the CKM matrix element $|V_{ub}|$. We measure the partial width of $\overline{B}^0 \to X_u \ell^- \overline{\nu}_\ell$ at high lepton momentum spectrum and set limits on isospin-violating contributions to charmless semileptonic decays. We present a study of $B^- \to D^{*0} e^- \overline{\nu}_e$ decays, including measurements of the form factors and $|V_{cb}|$. Branching fractions of $B \to D \ell^- \overline{\nu}_\ell$, $D^* \ell^- \overline{\nu}_\ell$, and $D^{(*)} \ell^- \overline{\nu}_\ell$ decays are measured to help quantify the role of D^{**} decays in the inclusive semileptonic decay rates. We present measurements of the branching fractions of $B \to D \tau^- \overline{\nu}_\tau$ and $B \to D^* \tau^- \overline{\nu}_\tau$ which are potentially sensitive to contributions from a charged Higgs boson.

1 Introduction

Semileptonic decays provide an excellent laboratory in which to study electroweak physics, QCD, and to search for physics beyond the Standard Model.

We present the results of five analyses of semileptonic B meson decays.

We analyze data collected with the *BABAR* detector [1)] at the PEP-II collider. The analyses presented here are based on about 380M $e^+e^- \to B\overline{B}$ pairs, except for the analyses of $B^- \to D^{*0}e^-\overline{\nu}_e$ and $B \to D^{(*)}\tau^-\overline{\nu}_\tau$, which are based on 230M $B\overline{B}$ pairs. Because semileptonic decays involve one or more neutrinos in the final state, the kinematic information is incomplete; four of the analyses presented here use the tagging techniques described below to reconstruct one of the two B mesons in the event and improve the kinematic constraints on the second.

1.1 Semileptonic $B_{\rm tag}$ Reconstruction

We partially reconstruct neutral $B_{\rm tag}$ candidates in the mode $\overline{B}^0 \to D^{*+}\ell^-\overline{\nu}_\ell$[1] by identifying the prompt lepton and the low-momentum pion coming from $D^{*+} \to D^0\pi^+$ decay. We identify B candidates using $m^2_{\nu,{\rm tag}}$, the squared missing mass of the $B_{\rm tag}$ candidate, assuming that a D^0 meson was produced parallel to the π^+; for correctly reconstructed events, $m^2_{\nu,{\rm tag}}$ peaks at zero. The large $\overline{B}^0 \to D^{*+}\ell^-\overline{\nu}_\ell$ branching fraction and the partial reconstruction technique result in a large tagging efficiency.

1.2 Hadronic $B_{\rm tag}$ Reconstruction

We fully reconstruct $B_{\rm tag}$ candidates in 1114 hadronic final states $B_{\rm tag} \to D^{(*)}Y^\pm$, where the $Y^\pm$ system may consist of up to six light hadrons ($\pi^\pm$, π^0, $K^\pm$, and K^0_S). $B_{\rm tag}$ candidates are identified using two kinematic variables, $m_{\rm ES} = \sqrt{s/4 - |\mathbf{p}_{\rm tag}|^2}$ and $\Delta E = E_{\rm tag} - \sqrt{s}/2$, where $\sqrt{s}$ is the total e^+e^- energy and $\mathbf{p}_{\rm tag}$ ($E_{\rm tag}$) is the $B_{\rm tag}$ momentum (energy), all defined in the e^+e^- center-of-mass frame. We reconstruct $B_{\rm tag}$ candidates in about 0.3% to 0.5% of $B\overline{B}$ events. While this efficiency is rather small, the technique allows for the determination of the momentum, charge, and flavor of the second B meson in the event, providing powerful background rejection constraints.

2 Inclusive $B \to X_u\ell^-\overline{\nu}_\ell$ and $|V_{ub}|$

Precision measurement of the CKM matrix element $|V_{ub}|$ is one of the main goals of the B-factory physics program since, together with the angle β, $|V_{ub}|$

[1] Charge conjugate processes are implied throughout this document.

helps to determine the apex of the unitarity triangle [2]. The main experimental challenge is the separation of $B \to X_u \ell^- \overline{\nu}_\ell$ signal events from charmed $B \to X_c \ell^- \overline{\nu}_\ell$ backgrounds which are about 50 times more common, which can be achieved in restricted regions of phase space. A variety of QCD calculations are available to extrapolate $|V_{ub}|$ from measurements of the charmless branching fraction in these phase space regions [3, 4, 5].

We measure the partial branching fractions for $B \to X_u \ell^- \overline{\nu}_\ell$ in three regions of phase space where charm background is suppressed. We use three kinematic variables to distinguish signal events from $B \to X_c \ell^- \overline{\nu}_\ell$ background: M_X, the invariant mass of the hadronic system; q^2, the invariant mass squared of the lepton-neutrino system; and $P_+ \equiv E_X - |\mathbf{p}_X|$, the light-cone component of the hadronic final state momentum along the jet direction, where E_X and $\mathbf{p}_X$ are the energy and momentum of the hadronic system in the B rest frame.

One B meson is fully reconstructed as described in Section 1.2. Semileptonic decays are identified by a single identified electron or muon with momentum $|\mathbf{p}^*_\ell| > 1$ GeV/c in the rest frame of the recoiling B meson. The track and photon candidates remaining after reconstructing the $B_{\rm tag}$ and ℓ^- candidates are associated with the X system, and the missing four-momentum $p_{\rm miss} \equiv p_{e^+e^-} - p_{B_{\rm tag}} - p_X - p_\ell$ is required to be consistent with a single neutrino: $m^2_{\rm miss} \equiv p^2_{\rm miss} < 0.5$ GeV$^2/c^4$. We suppress charm background by rejecting events with identified kaons in the X system and events which are kinematically consistent with $B \to D^* \ell^- \overline{\nu}_\ell$ decays.

We subtract combinatorial backgrounds by fitting the distributions of $B_{\rm tag}$ $m_{\rm ES}$ in bins of the three kinematic variables M_X, P_+, and q^2. We then perform three separate fits to the resulting kinematic distributions in order to distinguish signal events from background. The results are normalized to the total semileptonic decay width to give partial branching fractions and, using three different theoretical predictions, we present measurements of $|V_{ub}|$, all of which are summarized in Table 1. The dominant systematic uncertainties are due to Monte Carlo statistics and reconstruction efficiency. The total error on $|V_{ub}|$ is less than 10%, and these measurements are each compatible with the current world average [6]. More details are available in [7].

Table 1: *Summary of measured partial branching fractions and values of $|V_{ub}|$ for three kinematic cuts. The first error is statistical and the second is systematic; for $\Delta\mathcal{B}$, the third error represents the theoretical error on the efficiency, while for $|V_{ub}|$, it represents the extrapolation to the full decay width.*

Kinematic region	$\Delta\mathcal{B}(B \to X_u \ell^- \overline{\nu}_\ell)$ (10^{-3})	$\lvert V_{ub}\rvert$ (10^{-3})
$M_X < 1.55$ GeV/c^2	$1.18 \pm 0.09 \pm 0.07 \pm 0.01$	$4.27 \pm 0.16 \pm 0.13 \pm 0.30$ [3)] $4.56 \pm 0.17 \pm 0.14 \pm 0.32$ [4)]
$P_+ < 0.66$ GeV/c^2	$0.95 \pm 0.10 \pm 0.08 \pm 0.01$	$3.88 \pm 0.19 \pm 0.16 \pm 0.28$ [3)] $3.99 \pm 0.20 \pm 0.16 \pm 0.24$ [4)]
$M_X < 1.7$ GeV/c^2, $q^2 > 8.0$ GeV^2/c^4	$0.76 \pm 0.08 \pm 0.07 \pm 0.02$	$4.48 \pm 0.22 \pm 0.19 \pm 0.30$ [3)] $4.53 \pm 0.22 \pm 0.19 \pm 0.25$ [4)] $4.81 \pm 0.23 \pm 0.20 \pm 0.36$ [5)]

3 Isospin Violation in $B \to X_u \ell^- \overline{\nu}_\ell$ Decays

As experimental precision in $|V_{ub}|$ measurements increases, higher-order effects in the theoretical calculations become increasingly important. One such effect is weak annihilation [8)] — the annihilation of a $b\overline{u}$ quark pair to a $\ell^- \overline{\nu}_\ell$ pair — which should be observable as a violation of isospin symmetry (it only occurs for charged B mesons) at high lepton momentum.

We measure the rate of inclusive $\overline{B}^0 \to X_u \ell^- \overline{\nu}_\ell$ decays using $\Upsilon(4S) \to B^0\overline{B}^0$ events tagged by the partial reconstruction technique described in Section 1.1. By comparing the results with a previously published untagged measurement (including both charged and neutral B decays), we set limits on isospin-violating processes. We select events with a high-momentum lepton in the recoil of a tag B and apply cuts to reduce the background from $B \to X_c \ell^- \overline{\nu}_\ell$ decays. We extract signal yields by fitting the tag-side $m^2_{\nu,\mathrm{tag}}$ distribution and by subtracting the remaining backgrounds, obtaining a partial branching fraction in the lepton momentum interval $2.3 < p_\ell < 2.6$ GeV/c of $\Delta\mathcal{B}(\overline{B}^0 \to X_u \ell^- \overline{\nu}_\ell) = (1.30 \pm 0.21 \pm 0.07) \times 10^{-4}$. The dominant systematic uncertainties come from Monte Carlo statistics and lepton misidentification.

By comparing this to the untagged result [9)], we obtain the ratio $R^{-/0} \equiv \Delta\Gamma(B^-)/\Delta\Gamma(\overline{B}^0) = 1.18 \pm 0.35 \pm 0.17$, indicating no evidence for isospin vi-

olation. We place a 90% C.L. on the weak annihilation contribution to inclusive charmless semileptonic decays, $|\Gamma_{\rm WA}|/\Gamma_u < 3.8\%/f_{\rm WA}$, where $f_{\rm WA}$ represents the fraction of weak annihilation in the selected momentum interval 2.3–2.6 GeV/c. This result is consistent with results from the CLEO Collaboration [10]. More details are available in [11].

4 Study of $B^- \to D^{*0} e^- \overline{\nu}_e$ Decays

The differential decay width for the exclusive decay $B \to D^* \ell^- \overline{\nu}_\ell$ is given by

$$\frac{\mathrm{d}\Gamma}{\mathrm{d}w}(B \to D^* \ell^- \overline{\nu}_\ell) = \frac{G_F^2 |V_{cb}|^2}{48\pi^3} \mathcal{F}^2(w) \mathcal{G}(w) \ , \qquad (1)$$

where w is the Lorentz boost of the D^* in the B rest frame, $\mathcal{G}(w)$ is a phase-space factor, and $\mathcal{F}(w)$ is a form factor describing the hadronic part of the interaction and which can be calculated precisely at $w = 1$. By studying the decay rate, we can extract $|V_{cb}|$ as well as information about the strong force from the w-dependence of the form factor. The neutral B decay $\overline{B}^0 \to D^{*+} \ell^- \overline{\nu}_\ell$ has been extensively studied, while only two measurements exist for the charged B decay [6, 12]; inconsistencies still remain between the various measurements, which a new measurement of the charged mode would help resolve.

We select $B^- \to D^{*0} e^- \overline{\nu}_e$ candidates by pairing high-momentum electrons with D^{*0} candidates reconstructed as $D^{*0} \to D^0 \pi^0$, $D^0 \to K^- \pi^+$. Signal events are distinguished from background by using two variables: the mass difference $\delta m \equiv m(K^- \pi^+ \pi^0) - m(K^- \pi^+)$ and $\cos\theta_{\rm BY} \equiv (2E_B E_Y - m_B^2 - m_Y^2)/2p_B p_Y$, where Y represents the $D^{*0} e^-$ system. A maximum likelihood fit is performed to the three-dimensional distribution of (δm, $\cos\theta_{\rm BY}$, w) to extract $\mathcal{F}(1)|V_{cb}|$ and the form factor slope parameter, $\rho^2_{A_1}$ [13]. The dominant systematic uncertainties are due to the soft π^0 reconstruction efficiency and the branching fraction of $D^{*0} \to D^0 \pi^0$.

We obtain the results $\mathcal{F}(1)|V_{cb}| = (36.3 \pm 0.6 \pm 1.4) \times 10^{-3}$, $\rho^2_{A_1} = 1.15 \pm 0.06 \pm 0.08$, and, by integrating over w, we obtain the total branching fraction $\mathcal{B}(B^- \to D^{*0} e^- \overline{\nu}_e) = (5.71 \pm 0.08 \pm 0.41)\%$. Using $\mathcal{F}(1) = 0.919 \pm 0.033$ [14], we obtain $|V_{cb}| = (39.5 \pm 0.6 \pm 2.0) \times 10^{-3}$, in good agreement with the average from $\overline{B}^0 \to D^{*+} \ell^- \overline{\nu}_\ell$ decays [6] and with results obtained in inclusive $B \to X_c \ell^- \overline{\nu}_\ell$ decays [15]. More details are available in [16].

Table 2: *Branching fraction measurements of* $B \to D/D^*/D^{**}\ell^-\overline{\nu}_\ell$ *decays.*

Mode	$\mathcal{B}(B^-)[\%]$	$\mathcal{B}(\overline{B}^0)[\%]$
$D\ell^-\overline{\nu}_\ell$	$2.33 \pm 0.09 \pm 0.08$	$2.21 \pm 0.11 \pm 0.09$
$D^*\ell^-\overline{\nu}_\ell$	$5.83 \pm 0.15 \pm 0.28$	$5.49 \pm 0.16 \pm 0.23$
$D\pi\ell^-\overline{\nu}_\ell$	$0.42 \pm 0.06 \pm 0.03$	$0.43 \pm 0.08 \pm 0.03$
$D^*\pi\ell^-\overline{\nu}_\ell$	$0.59 \pm 0.05 \pm 0.04$	$0.48 \pm 0.08 \pm 0.04$

5 $B \to D/D^*/D^{**}\ell^-\overline{\nu}_\ell$

The determination of the individual exclusive branching fractions of $B \to X_c\ell^-\overline{\nu}_\ell$ decays is important to help understand the dynamics of semileptonic decays, as well as in understanding backgrounds in measurements of $|V_{ub}|$ and $|V_{cb}|$. Measurements of these branching fractions have been performed by several experiments using different techniques [12], but the various measurements are somewhat inconsistent. In order to help understand this, we measure the branching fractions of $B \to D\ell^-\overline{\nu}_\ell$, $B \to D^*\ell^-\overline{\nu}_\ell$, $B \to D\pi\ell^-\overline{\nu}_\ell$ and $B \to D^*\pi\ell^-\overline{\nu}_\ell$ for both charged and neutral B mesons.

We select semileptonic B decays by reconstructing a $D^{(*)}\ell^-$, $D^{(*)+}\pi^-\ell^-$, or $D^{(*)0}\pi^+\ell^-$ system in the recoil of a fully reconstructed $B_{\rm tag}$. We require that there be no additional particles in the event, and we extract signals by fitting distributions of $m^2_{\rm miss}$, where correctly reconstructed events peak at $m^2_{\rm miss} = 0$. The fit results are summarized in Table 2. The dominant systematic uncertainties are due to the $D^{(*)}$ branching fractions, $B_{\rm tag}$ selection, and charged track reconstruction efficiency. These measurements are consistent with but more precise than existing measurements [12, 16, 17], and are consistent with the assumption of isospin symmetry. More details are available in [18].

6 $B \to D/D^*\tau^-\overline{\nu}_\tau$

Semileptonic decays to τ leptons provide a new source of information on SM processes as well as a window into physics beyond the SM [19] since the large τ mass gives sensitivity to a charged Higgs boson, but are experimentally challenging since the τ decays and the final state contains multiple neutrinos.

We measure the branching fractions of four decay modes: $B^- \to D^0\tau^-\overline{\nu}_\tau$, $B^- \to D^{*0}\tau^-\overline{\nu}_\tau$, $\overline{B}^0 \to D^+\tau^-\overline{\nu}_\tau$, and $\overline{B}^0 \to D^{*+}\tau^-\overline{\nu}_\tau$, using the leptonic τ

decays $\tau^- \to \ell^- \overline{\nu}_\ell \nu_\tau$. We reconstruct a $D^{(*)}$ meson and a light lepton in the recoil of a fully reconstructed $B_{\rm tag}$, and require that there be no other particles in the event. The signal is extracted using a maximum likelihood fit to the distributions of $m^2_{\rm miss}$ and $|\mathbf{p}^*_\ell|$; the dominant backgrounds $B \to D^{(*)} \ell^- \overline{\nu}_\ell$ have only one neutrino and peak in $m^2_{\rm miss}$ near zero, while three-neutrino signal events tend to have large $m^2_{\rm miss}$. The fit is performed simultaneously for all four $D^{(*)}$ modes, as well as in four control samples designed to constrain the feed-down background from $B \to D^{**} \ell^- \overline{\nu}_\ell$ events. The fit gives both signal yields and $B \to D^{(*)} \ell^- \overline{\nu}_\ell$ background yields, allowing us to measure the branching ratios $R \equiv \mathcal{B}(B \to D^{(*)} \tau^- \overline{\nu}_\tau)/\mathcal{B}(B \to D^{(*)} \ell^- \overline{\nu}_\ell)$. We normalize these ratios to previously measured light leptonic modes [12]. The dominant systematic uncertainties are due to the parameterization of the fit PDFs and the composition of combinatorial backgrounds.

Combining charged and neutral B results, we measure the branching ratios $R(D) = (41.6 \pm 11.7 \pm 5.2)\%$ and $R(D^*) = (29.7 \pm 5.6 \pm 1.8)\%$, with significances 3.6σ and 6.2σ, respectively. These correspond to absolute branching fractions for the $\overline{B}^0$ of $\mathcal{B}(\overline{B}^0 \to D^+ \tau^- \overline{\nu}_\tau) = (0.86 \pm 0.24 \pm 0.11 \pm 0.06)\%$ and $\mathcal{B}(\overline{B}^0 \to D^{*+} \tau^- \overline{\nu}_\tau) = (1.62 \pm 0.31 \pm 0.10 \pm 0.05)\%$, where the third error is due to the normalization mode. This represents the first evidence for $B \to D \tau^- \overline{\nu}_\tau$ decays, while the $B \to D^* \tau^- \overline{\nu}_\tau$ result is consistent with a recent Belle measurement [20]. More details are available in [21].

7 Summary

We have presented the preliminary results of five analyses of semileptonic B meson decays at *BABAR*. The results include improved measurements of semileptonic B branching fractions and CKM parameters $|V_{ub}|$ and $|V_{cb}|$, a search for isospin violation, a measurement of the $B \to D^*$ form factor, and a search for new physics in $B \to D^{(*)} \tau^- \overline{\nu}_\tau$ decays.

References

1. B. Aubert *et al.* (*BABAR* Collab.), Nucl. Instrum. Methods Phys. Res., Sect. A **479** 1 (2002).

2. N. Cabibbo, Phys. Rev. Lett. **10** 531 (1963); M. Kobayashi and T. Maskawa, Prog. Theor. Phys. **49**, 652 (1973).

3. B. O. Lange, M. Neubert, and G. Paz, Phys. Rev. D **72** 073006 (2005).
4. J. R. Andersen and E. Gardi, JHEP **0601** 097 (2006).
5. C.W. Bauer, Z. Ligeti, and M. Luke, Phys. Rev. D **64** 113004 (2001).
6. E. Barberio *et al.* (HFAG), arXiv:0704.3575 (2007).
7. B. Aubert *et al.* (*BABAR* Collab.), arXiv:0708.3702, submitted to Phys. Rev. Lett.
8. I.I. Bigi and N.G. Uraltsev, Nucl. Phys. B **423** 33 (1994); M. Neubert and C.T. Sachrajda, Nucl. Phys. B **483** 3339 (1997); M.B. Voloshin, Phys. Lett. B **515** 74 (2001); A.K. Leibovich, Z. Ligeti, and M.B. Wise, Phys. Lett. B **539** 242 (2002).
9. B. Aubert *et al.* (*BABAR* Collab.), Phys. Rev. D **73** 012006 (2006).
10. J.L. Rosner *et al.* (CLEO Collab.), Phys. Rev. Lett. **96** 121801 (2006).
11. B. Aubert *et al.* (*BABAR* Collab.), arXiv:0708.1753.
12. W.-M. Yao *et al.* (PDG), J. Phys. G: Nucl. Part. Phys. **33** 1 (2006).
13. I. Caprini, L. Lellouch, and M. Neubert, Nucl. Phys. B **530** 153 (1998).
14. S. Hashimoto *et al.*, Phys. Rev. D **66** 014503 (2002).
15. O. Buchmüller and H. Flächer, Phys. Rev. D **73** 073008 (2006).
16. B. Aubert *et al.* (*BABAR* Collab.), arXiv:0707.2655.
17. D. Liventsev *et al.* (Belle Collab.), Phys. Rev. D **72** 051009 (2005).
18. B. Aubert *et al.* (*BABAR* Collab.), arXiv:0708.1738
19. J.G. Körner and G.A. Schuler, Z. Phys. C **46** 93 (1990); A.F. Falk *et al.*, Phys. Lett. B **326** 145 (1994); D.S. Hwang and D.-W. Kim, Eur. Phys. Jour. C **14** 271 (2000); M. Tanaka, Z. Phys. C **67** 321 (1995); C.-H. Chen and C.-Q. Geng, JHEP **0610** 053 (2006).
20. A. Matyja *et al.* (Belle Collab.), Phys. Rev. Lett. **99** 191807 (2007).
21. B. Aubert *et al.* (*BABAR* Collab.), arXiv:0709.1698, to appear in Phys. Rev. Lett.

Frascati Physics Series Vol. XLVI (2007), pp. 1019
HADRON07: XII Int. Conf. on Hadron Spectroscopy – Frascati, October 8-13, 2007
Heavy Meson Spectroscopy

$\eta - \eta'$ MIXING FROM ELECTROMAGNETIC TRANSITIONS TO WEAK DECAYS OF CHARM AND BEAUTY HADRONS

C. Di Donato
INFN Napoli

Written contribution not received

Frascati Physics Series Vol. XLVI (2007), pp. 1021–1028
HADRON07: XII Int. Conf. on Hadron Spectroscopy – Frascati, October 8-13, 2007
Heavy Meson Spectroscopy

DETERMINATION OF THE b-QUARK MASS AND NONPERTURBATIVE PARAMETERS IN SEMILEPTONIC AND RADIATIVE PENGUIN DECAYS AT *BABAR*

Kerstin Tackmann (on behalf of the *BABAR* collaboration)
University of California, Berkeley and Lawrence Berkeley National Laboratory
Berkeley, CA 94720, USA

Abstract

Knowing the mass of the b-quark is essential to the study of the structure and decays of B mesons as well as to future tests of the Higgs mechanism of mass generation. We present recent preliminary measurements of the b-quark mass and related nonperturbative parameters from moments of kinematic distributions in charmed and charmless semileptonic and radiative penguin B decays. Their determination from charmless semileptonic B decays is the first measurement in this mode. The data were collected by the *BABAR* detector at the PEP-II asymmetric-energy e^+e^-–collider at the Stanford Linear Accelerator Center at a center-of-momentum energy of 10.58 GeV.

1 Introduction

An important goal of the B-physics program is the precise measurement of the CKM matrix [1] elements $|V_{cb}|$ and $|V_{ub}|$. The most accurate determinations are obtained from semileptonic decays $B \to X_c \ell\nu$ and $B \to X_u \ell\nu$, respectively.

Generally, two different approaches can be used: The hadronic state $X_{c,u}$ can be reconstructed either in specific exclusive modes, or inclusively by summing over all possible hadronic final states. The inclusive determinations rely on an Operator Product Expansion (OPE) in inverse powers of the b-quark mass m_b [2]. At second order in the expansion, two nonperturbative parameters arise, which describe the kinetic energy and the chromomagnetic moment of the b quark inside the B meson. In the kinetic scheme, they are denoted by μ_π^2 and μ_G^2, respectively. Two more parameters arise at third order, ρ_D^3 and ρ_{LS}^3. In the kinetic scheme, short- and long-distance contributions are separated by a hard cutoff μ and the b-quark mass and nonperturbative parameters are given at $\mu = 1\,\mathrm{GeV}$.

The mass m_b and the nonperturbative parameters can be determined from the study of kinematic distributions in semileptonic and radiative penguin B decays.

Precise measurements of m_b are needed both to reduce the uncertainty of inclusive determinations of $|V_{ub}|$, as well as for studying New Physics effects in the Higgs sector at future experiments.

Here, we present recent determinations of m_b and higher-order nonperturbative parameters from charm and charmless semileptonic and radiative penguin B decays at the *BABAR* experiment [3].

2 The Recoil Method

In all analyses presented, $\Upsilon(4S) \to B\bar{B}$ decays are tagged by reconstructing one B meson (B_{reco}) fully in hadronic modes, $B_{\mathrm{reco}} \to D^{(*)}Y^{\pm}$. The $Y^{\pm}$ system is composed of hadrons with a total charge of ± 1, $Y^{\pm} = n_1\pi^{\pm} + n_2K^{\pm} + n_3K_S + n_4\pi^0$, with $n_1 + n_2 \leq 5$, $n_3 \leq 2$, $n_4 \leq 2$. We test the kinematic consistency of B_{reco} candidates with two variables, $m_{\mathrm{ES}} = \sqrt{s/4 - \vec{p}_B^{\,2}}$ and $\Delta E = E_B - \sqrt{s}/2$. Here, $\sqrt{s}$ is the invariant mass of the e^+e^- system and E_B and $\vec{p}_B$ denote the energy and momentum of the B_{reco} candidate in the $\Upsilon(4S)$ frame. We require ΔE to be 0 within three standard deviations. In events with multiple B_{reco} candidates we retain the candidate reconstructed in the mode with highest purity as estimated from the ratio of signal over background for events with $m_{\mathrm{ES}} > 5.27\,\mathrm{GeV}$ on Monte Carlo simulation (MC).

By fully reconstructing one of the B mesons in the event, the charge, flavor and momentum of the second B can be inferred. All particles that are

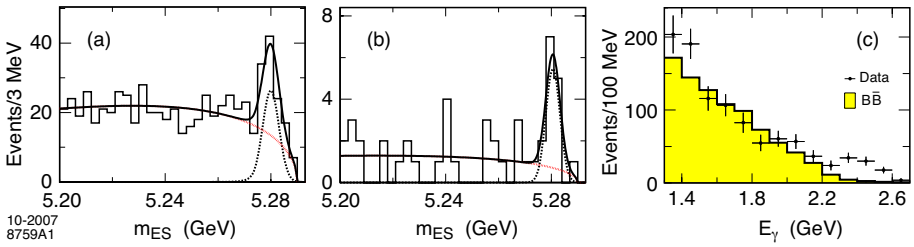

Figure 1: *Fits in $B \to X_s\gamma$ to $m_{\rm ES}$ for two E_γ regions. The dashed curve shows the signal, the solid grey (red) curve the background as given by the fit. The solid black curve shows the sum of signal and background. a) $1.6\,{\rm GeV} < E_\gamma < 1.7\,{\rm GeV}$ for charged B events and b) $2.3\,{\rm GeV} < E_\gamma < 2.4\,{\rm GeV}$ for neutral B events. c) The measured photon energy spectrum before subtraction of backgrounds. Points show the data spectrum, the shaded histogram shows the $B\bar{B}$ backgrounds, where the shape is taken from MC.*

not used in the reconstruction of the $B_{\rm reco}$ are assigned to the decay of the signal B. The efficiency to reconstruct a $B_{\rm reco}$ candidate is 0.3% (0.5%) for $B^0\bar{B}^0$ (B^+B^-) events.

We use fits to the $m_{\rm ES}$ distribution to subtract the combinatorial background from $B\bar{B}$ events and and the background from continuum ($e^+e^- \to q\bar{q}, q = u, d, s, c$) events. The backgrounds are modeled with a threshold function [4] and the signal is described by a Gaussian function joined with an exponential tail to describe photon energy loss [5]. Examples from the measurement in radiative penguin decays are shown in Fig. 1 (a) and (b).

3 Radiative Penguin Decays

The first and second moments of the photon energy spectrum in radiative penguin decays, $B \to X_s\gamma$, are used for a preliminary determination of m_b and μ_π^2 [6]. The moments are extracted as a function of the lower cut on the photon energy, $E_\gamma^{\rm min}$, measured in the rest frame of the signal B. The full reconstruction of the second B in the event results in an improved signal purity and different systematic uncertainties, but lower statistics, than alternative methods.

The measurement is based on a sample of 232 million $B\bar{B}$ pairs. Events

with a well reconstructed, high energy photon are selected if the photon is not compatible with originating from the decay of a π^0 or η, or a $\rho^\pm \to \pi^\pm\pi^0$ decay assuming that the second photon from the π^0 decay was lost. Continuum background is suppressed by using a Fisher discriminant that makes use of the difference between event topologies in $B\bar{B}$ and continuum events.

The E_γ spectrum is measured in bins of 100 MeV and is shown in Fig. 1 (c). The region $1.3\,\mathrm{GeV} < E_\gamma < 1.9\,\mathrm{GeV}$ is used to normalize the backgrounds, the largest part of which consists of photons from unreconstructed π^0 or η decays. The backgrounds are extrapolated into the signal region, $E_\gamma > 1.9\,\mathrm{GeV}$, the shape of the backgrounds is taken from MC. The signal region contains 119 ± 22 $B \to X\gamma$ events over an estimated background of 145 ± 9 events. The measured photon spectrum is corrected for efficiency, which varies with E_γ, and resolution effects. First and second central moments, $\langle E_\gamma \rangle$ and $\langle E_\gamma^2 \rangle - \langle E_\gamma \rangle^2$, as a function of E_γ^{min} are extracted from the corrected spectrum. The moments for $E_\gamma^{\mathrm{min}} \leq 2.0\,\mathrm{GeV}$ are used to determine $m_b = 4.46^{+0.21}_{-0.23}\,\mathrm{GeV}$ and $\mu_\pi^2 = 0.64^{+0.39}_{-0.38}\,\mathrm{GeV}^2$ in the kinetic scheme with a correlation of $\rho = -0.94$.

4 Charm Semileptonic B Decays

Moments of the hadronic mass and lepton energy spectra in $B \to X_c\ell\nu$ decays are used for a preliminary extraction of m_b, the charm-quark mass m_c, nonperturbative parameters and $|V_{cb}|$ [7]. We present moments of the hadronic mass $\langle m_X^k \rangle$, $k = 1..6$, which use a larger data set than the previous measurement and new measurements of the mixed hadronic mass-energy moments $\langle n_X^k \rangle$, $k = 2, 4, 6$. n_X is defined by $n_X^2 = m_X^2 c^4 - 2\bar{\Lambda}E_X + \bar{\Lambda}^2$, where m_X is the mass and E_X the energy of the inclusive X_c system in the B rest frame and $\bar{\Lambda} = 0.65\,\mathrm{GeV}$. The mixed moments are expected to yield a more precise determination of higher order nonperturbative parameters. The moments are extracted as a function of a lower cut on the lepton energy between 0.8 GeV and 1.9 GeV in the signal B rest frame.

The measurement is based on a sample of 232 million $B\bar{B}$ pairs. After reconstructing the B_{reco} and identifying the lepton, where both electrons and muons are used, the hadronic system is reconstructed from the remaining tracks and neutral energy depositions in the event. A kinematic fit imposing energy-momentum conservation and the missing energy and momentum in the event to be consistent with coming from one neutrino is performed to improve the

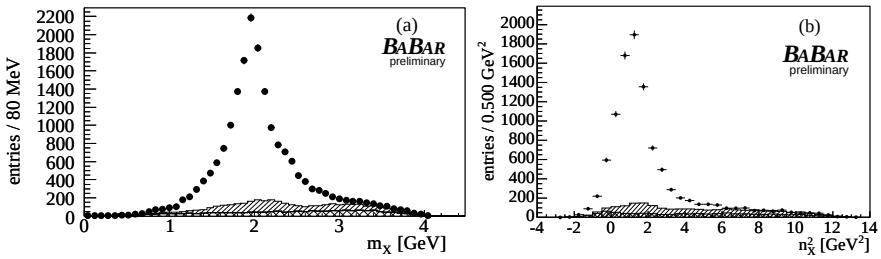

Figure 2: *a) The measured hadronic mass spectrum and b) the measured n_X spectrum for $E_l > 0.8\,\mathrm{GeV}$ in the B rest frame. Tag-side backgrounds are indicated by the hatched histogram, signal-side backgrounds by the cross-hatched histogram.*

resolution in the hadronic variables. The hadronic mass and mixed hadronic mass-energy spectra are shown in Fig. 2. The moments are extracted directly from the kinematically fitted hadronic masses and energies and are corrected for the effect of lost particles. The main contribution to the systematic uncertainties on the moments arise from the impact of the reconstruction efficiencies of neutral particles on the inclusive event reconstruction.

A combined fit is performed to hadronic mass moments, lepton energy moments [8] in $B \to X_c \ell\nu$ decays and photon energy moments in $B \to X_s\gamma$ decays [9] and yields $m_b = (4.552 \pm 0.055)\,\mathrm{GeV}$, $m_c = (1.070 \pm 0.085)\,\mathrm{GeV}$ (correlation $\rho_{m_b m_c} = 0.96$), $\mu_\pi^2 = (0.471 \pm 0.070)\,\mathrm{GeV}^2$, $\mu_G^2 = (0.330 \pm 0.060)\,\mathrm{GeV}^2$, $\rho_D^3 = (0.220 \pm 0.047)\,\mathrm{GeV}^3$ and $\rho_{LS}^3 = (-0.159 \pm 0.095)\,\mathrm{GeV}^3$ in the kinetic scheme.

5 Charmless Semileptonic B Decays

Moments of the hadronic mass spectrum in $B \to X_u \ell\nu$ decays are used for a preliminary extraction of m_b, μ_π^2 and ρ_D^3. Their determination in $B \to X_u \ell\nu$ allows for a test of the theoretical framework used for the extraction of $|V_{ub}|$ in the same channel in which $|V_{ub}|$ is determined. The hadronic mass moments are measured with an upper cut on the hadronic mass to reduce experimental uncertainties.

The measurement is based on a sample of 383 million $B\bar{B}$ pairs. After

reconstructing the $B_{\rm reco}$ and identifying the lepton, where both electrons and muons with a minimum energy of $E_\ell = 1\,\mathrm{GeV}$ in the B rest frame are used, the hadronic system is reconstructed from the remaining tracks and neutral energy depositions in the event. Vetos on identified $K^\pm$, reconstructed K_S and partically reconstructed $D^{*\pm}$ are employed to suppress the dominant background from $B \to X_c\ell\nu$ events. The remaining $B \to X_c\ell\nu$ and non-semileptonic backgrounds are subtracted by a fit to the hadronic mass spectrum (Fig. 3 (a)). The full m_X^2 region contains 1027 ± 176 signal events. The background-subtracted spectrum is unfolded for detector acceptance, efficiency and resolution effects (Fig. 3 (b)) and the first and second and third central moments are extracted from the unfolded spectrum for $m_X^2 < 6.4\,\mathrm{GeV}^2$:

$$\begin{aligned}
\langle m_X^2 \rangle &= (1.96 \pm 0.34(\mathrm{stat}) \pm 0.53(\mathrm{syst}))\,\mathrm{GeV}^2 \\
\langle (m_X^2)^2 - \langle m_X^2 \rangle^2 \rangle &= (1.92 \pm 0.59(\mathrm{stat}) \pm 0.87(\mathrm{syst}))\,\mathrm{GeV}^4 \\
\langle (m_X^2)^3 - \langle m_X^2 \rangle^3 \rangle &= (1.79 \pm 0.62(\mathrm{stat}) \pm 0.78(\mathrm{syst}))\,\mathrm{GeV}^6
\end{aligned}$$

with correlation coefficients $\rho_{12} = 0.99$, $\rho_{23} = 0.94$ and $\rho_{13} = 0.88$. The main systematic uncertainties arise from the control of the $B \to X_c\ell\nu$ background.

A fit of these moments to predictions in the kinetic scheme [10] yields

$$\begin{aligned}
m_b &= (4.604 \pm 0.125(\mathrm{stat}) \pm 0.193(\mathrm{syst}) \pm 0.097(\mathrm{theo}))\,\mathrm{GeV} \\
\mu_\pi^2 &= (0.398 \pm 0.135(\mathrm{stat}) \pm 0.195(\mathrm{syst}) \pm 0.036(\mathrm{theo}))\,\mathrm{GeV}^2 \\
\rho_D^3 &= (0.102 \pm 0.017(\mathrm{stat}) \pm 0.021(\mathrm{syst}) \pm 0.066(\mathrm{theo}))\,\mathrm{GeV}^3.
\end{aligned}$$

with correlation coefficients $\rho_{m_b\mu_\pi^2} = -0.99$, $\rho_{\mu_\pi^2\rho_D^3} = 0.57$ and $\rho_{m_b\rho_D^3} = -0.59$.

6 Summary

We presented preliminary determinations of the b-quark mass m_b and nonperturbative parameters from charmed and charmless semileptonic and radiative penguin B decays at *BABAR*. The determination in charmless semileptonic B decays has been performed for the first time. The results for m_b and μ_π^2 are summarized in Table 1 and compared in Fig. 4. The determinations in the different channels are consistent within the quoted uncertainties and with earlier determinations [11].

Work supported in part by the Department of Energy contract DE-AC02-76SF00515.

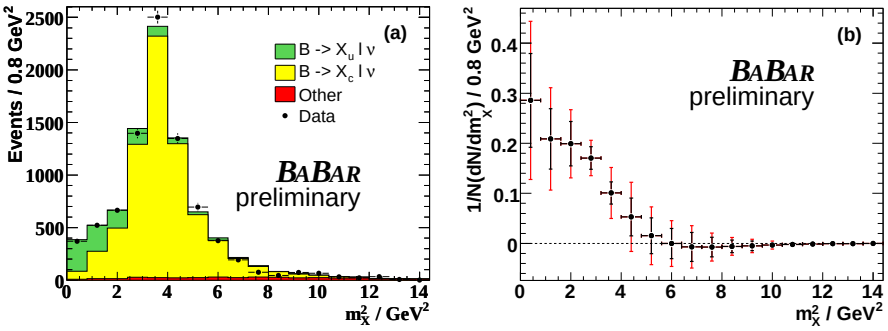

Figure 3: *a) The measured hadronic mass spectrum before subtraction of $B \to X_c \ell \nu$ and non-semileptonic backgrounds. b) Unfolded hadronic mass spectrum in $B \to X_u \ell \nu$. The inner error bars show the statistical uncertainties only.*

Table 1: *Results for m_b and μ_π^2 in the kinetic scheme and their correlations.*

	m_b/ GeV	μ_π^2/ GeV^2	ρ
$B \to X_s\gamma$ [6]	$4.46^{+0.21}_{-0.23}$	$0.64^{+0.39}_{-0.38}$	-0.94
$B \to X_c \ell \nu$ [7] [8] and $B \to X_s \gamma$ [9]	4.552 ± 0.055	0.471 ± 0.070	-0.56
$B \to X_u \ell \nu$	4.604 ± 0.250	0.398 ± 0.240	-0.99

References

1. N. Cabibbo, Phys. Rev. Lett. **10**, 531 (1963). M. Kobayashi and T. Maskawa, Prog. Theor. Phys. **49**, 652 (1973).

2. I. I. Y. Bigi, M. A. Shifman, N. G. Uraltsev and A. I. Vainshtein, Phys. Rev. Lett. **71**, 496 (1993) [arXiv:hep-ph/9304225]. J. Chay, H. Georgi and B. Grinstein, Phys. Lett. B **247**, 399 (1990). A. V. Manohar and M. B. Wise, Phys. Rev. D **49**, 1310 (1994) [arXiv:hep-ph/9308246].

3. B. Aubert *et al.* [BABAR Collaboration], Nucl. Instrum. Meth. A **479**, 1 (2002) [arXiv:hep-ex/0105044].

4. ARGUS Collaboration, H. Albrecht *et al.*, Z. Phys. C **48**, 543 (1990).

5. T. Skwarnicki, DESY-F31-86-02.

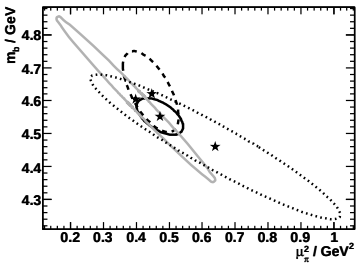

Figure 4: *Results from the recent BABAR analyses presented in the m_b–μ_π^2 plane in the kinetic scheme. The dotted ellipse shows the result of the presented $B \to X_s\gamma$ analysis [6], the dashed ellipse the result from $B \to X_c\ell\nu$ decays [7, 8], the black solid ellipse the result from its combination with earlier $B \to X_s\gamma$ measurements [9] and the solid grey ellipse the result from $B \to X_u\ell\nu$ decays.*

6. B. Aubert *et al.* [BABAR Collaboration], arXiv:0711.4889 [hep-ex]. Submitted to Phys. Rev. D.

7. B. Aubert *et al.* [BABAR Collaboration], arXiv:0707.2670 [hep-ex].

8. B. Aubert *et al.* [BABAR Collaboration], Phys. Rev. D **69**, 111104 (2004) [arXiv:hep-ex/0403030].

9. B. Aubert *et al.* [BABAR Collaboration], Phys. Rev. D **72**, 052004 (2005) [arXiv:hep-ex/0508004]. B. Aubert *et al.* [BaBar Collaboration], Phys. Rev. Lett. **97**, 171803 (2006) [arXiv:hep-ex/0607071].

10. P. Gambino, G. Ossola and N. Uraltsev, JHEP **0509**, 010 (2005) [arXiv:hep-ph/0505091].

11. C. W. Bauer, Z. Ligeti, M. Luke, A. V. Manohar and M. Trott, Phys. Rev. D **70**, 094017 (2004) [arXiv:hep-ph/0408002]. O. Buchmüller and H. Flächer, Phys. Rev. D **73**, 073008 (2006) [arXiv:hep-ph/0507253]. K. Abe *et al.* [BELLE Collaboration], arXiv:hep-ex/0611047.

Frascati Physics Series Vol. XLVI (2007), pp. 1029–1036
HADRON07: XII Int. Conf. on Hadron Spectroscopy – Frascati, October 8-13, 2007
Heavy Meson Spectroscopy

RADIATIVE PENGUIN DECAYS AT BABAR

Minghui Lu (on behalf of BaBar collaboration)
University of Oregon, Eugene, OR 97403, USA

Abstract

A review of recent measurements of $b \to s\gamma$ and $b \to d\gamma$ radiative penguin decays at BaBar is presented.

1 Introduction

In the Standard Model (SM), $b \to s$ and $b \to d$ transitions are flavor changing neutral current (FCNC) transitions and can not proceed at tree level. Thus radiative decays like $B \to X_s\gamma$ and $B \to X_d\gamma$ proceed primarily through a one loop Feynman diagram known as penguin diagram. Because of this, these radiative decays are rare, with branching fractions on the order of 10^{-6} to 10^{-4}. For the same reason, any significant difference in branching fraction measurements of these channels could indicate new physics beyond standard model.

In the past few years, BaBar detector [1] has collected more than $400 fb^{-1}$ data, which makes it possible to study these rare radiative penguin decays extensively. The analysis covered in this paper will include both inclusive and exclusive measurements. The relevant theoretical framework is Operator Product Expansion (OPE) [2]. The OPE framework provides parton-level predictions, so the connection to the experimental observables requires further non-perturbative corrections. For inclusive decays, heavy-quark expansion and quark-hadron duality can keep non-perturbative corrections under control, allowing direct interpretation of the measurement of the inclusive decay rates. However, the experimental measurement is difficult due to large backgrounds. For exclusive decays, the calculation of form factors introduces significant uncertainties, though the measurements are experimentally clean.

2 $b \to s\gamma$

2.1 Inclusive $b \to s\gamma$

The Photon spectrum is usually measured in the inclusive $b \to s\gamma$ decays. The latest theoretical calculations on $B \to X_s\gamma$ branching fraction in the standard model at the next-to-next-to-leading order (NNLO) in QCD gave about 7% uncertainty [3], while the world average performed by the Heavy Quark Flavor Averaging Group [4] for $E_\gamma > 1.6$ GeV reads

$$B(\bar{B} \to X_s\gamma) = (3.55 \pm 0.24^{+0.009}_{-0.10} \pm 0.03) \times 10^{-4}. \quad (1)$$

An important observation is that the shape of the photon spectrum, which is not sensitive to physics beyond the standard model, can be used to determine HQE parameters [5] [6]. These parameters can then be used to reduce the error in the extraction of the CKM matrix elements $|V_{ub}|$ and $|V_{cb}|$ from semi-leptonic B decays. The details will not be covered in this article.

BaBar has published two inclusive $b \to s\gamma$ measurements, one a fully inclusive analysis with lepton tag [7], the other from a sum of exclusive final states [8]. These two measurements were based on 88 million $B\bar{B}$ events. In this paper, a new method, called recoil method, is used to measure the $B \to X_s\gamma$ branching fraction and photon spectrum based on 232 million $B\bar{B}$ events. In this method, we fully reconstruct the recoiling B meson in its hadronic decay modes $B \to D^{(*)}X^{\pm}$, where X is composed of relevant π and K with total

charge of ± 1. The signal can then be extracted in bins of photon energy by fitting the beam constrained mass $m_{ES} = \sqrt{((E^*_{beam})^2 - (P^*_B)^2)}$, where $*$ denotes the center of mass frame. By fully reconstructing the recoil B, the charge andmomentum of the signal B can be determined and thus the CP asymmetry can be derived. The photon spectrum can also be measured directly in the B rest frame. The disadvantage of this method is that the reconstruction efficiency of the recoiled B is low, about 0.3% in this case.

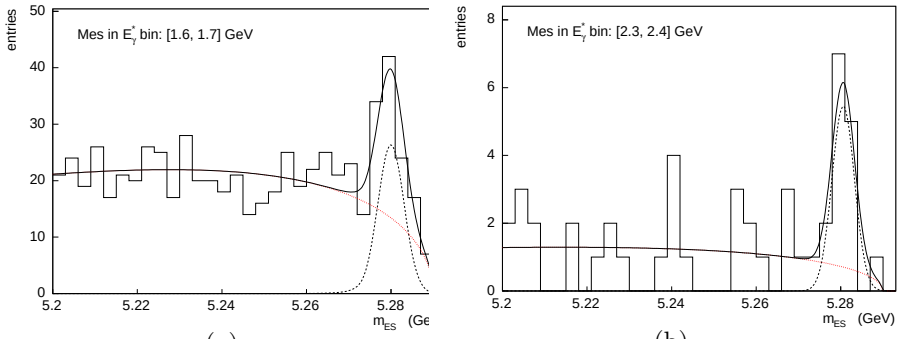

(a) (b)

Figure 1: Fits to the distribution of the m_{ES} for two E_γ regions. The dashed curve shows the CB term and the dotted curve is the Argus term, corresponding to B and non-B events, respectively; the solid curve is their sum. (a) $1.6\,GeV < E_\gamma < 1.7\,GeV$ for the charged B sample. (b) $2.3\,GeV < E_\gamma < 2.4\,GeV$ for the neutral B sample.

The photon with energy greater than 1.3GeV in B rest frame is selected. The high energy photons are vetoed if they originated from a π^0 or η. Furthermore, the event is rejected if the candidate photon combined with a $\pi^\pm$ is consistent with a $\rho^\pm \to \pi^\pm\pi^0$ decay. The continuum background is suppressed by using a Fisher discriminant that combines 12 variables related to the different event decay topologies of $B\bar{B}$ and continuum events. After event selection, we divide the event sample into 14 intervals of photon energy, each is 100 MeV wide. Then a binned maximum likelihood fit was performed to the m_{ES} distribution to determine the signal yield (See fig.2.1 for examples). The photon spectrum is measured in bins of the 100 MeV and is shown in fig.2. After sub-

tracting the background events and applying the selection efficiency correction and photon resolution correction, the corrected photon spectrum is obtained and the partial branching fraction is shown in fig.2. Taking into account the systematics, the partial branching fraction is,

$$B(\bar{B} \to X_s\gamma) = (3.66 \pm 0.85_{stat} \pm 0.59_{syst}) \times 10^{-4}. \quad (2)$$

By extrapolating [9] to $E_\gamma > 1.6$GeV, the branching fraction becomes,

$$B(\bar{B} \to X_s\gamma) = (3.91 \pm 0.91_{stat} \pm 0.64_{syst}) \times 10^{-4}. \quad (3)$$

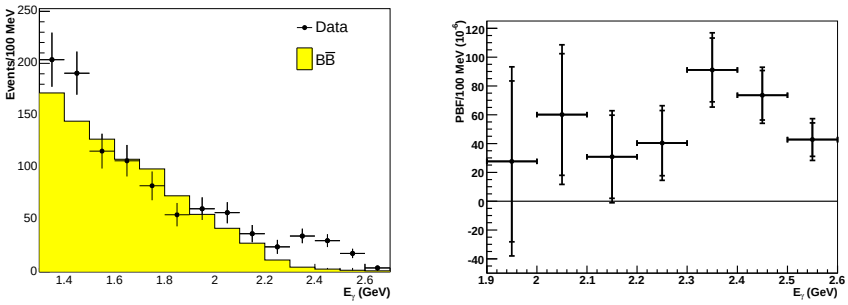

(a) (b)

Figure 2: (a) The measured numbers of B events as a function of photon energy. The points are from data; the histogram is from a $B\bar{B}$ MC sample which excludes the signal decay $B \to X\gamma$. (b)The partial branching fractions $(1/\Gamma_B)(d\Gamma/dE_\gamma)$ with statistical and total error.

2.2 Exclusive $b \to s\gamma$

In this paper, I will mainly discuss the measurement of the time-dependent CP asymmetry in $B^0 \to K^{*0}\gamma$ decays.

The radiative decay $b \to s\gamma$ proceeds at leading order through a loop diagram involving a virtual W^- boson and t quark in standard model. Possible interference between the direct decay $B^0 \to K^{*0}(K_S\pi^0)\gamma$ and the decay via B^0 mixing, $B^0 \to \bar{B}^0 \to K^{*0}\gamma$, is suppressed by the order of $\frac{m_s}{m_b}$ due to helicity. SM predictions of the CP asymmetry due to interference between mixing and

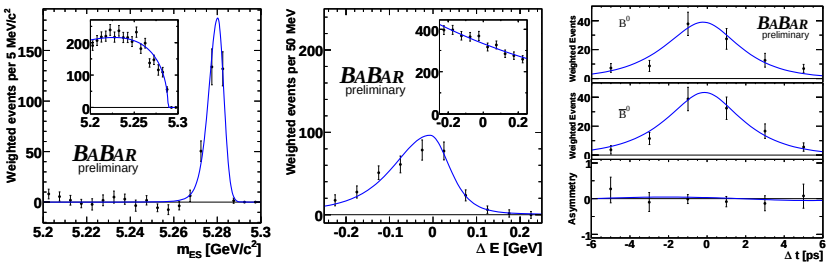

(a) (b) (c)

Figure 3: Signal and background (inset) distributions for m_{ES} (left) and ΔE (middle). Signal distribution for δt (right), with B_{tag} tagged as B^0 (top) or $\bar{B}^0$ (center), and the asymmetry (bottom). The curves represent the PDFs for signal decays in the likelihood fit, normalized to the final fit result.

decay are expected to be about -0.02 [10], but it could be larger if higher order QCD effect is taken into account [11].

Time-dependent CP asymmetries are determined by fitting distribution

$$\mathcal{P}_{\pm}(\Delta t) = \frac{e^{-|\Delta t|/\tau_B}}{4\tau_B} \times [1 \pm S_f \sin(\Delta m_d \Delta t) \mp C_f \cos(\Delta m_d \Delta t)]\,, \qquad (4)$$

where the upper and lower signs correspond to the tag-side B having flavor B^0 and $\bar{B}^0$ respectively, τ_B is the B^0 lifetime, and Δm_d is the $B^0 - \bar{B}^0$ mixing frequency. The C_f coefficient is associated with the difference in decay amplitudes for $B^0 \to f$ and $\bar{B}^0 \to f$, while the S_f coefficient involves interference between the $B^0 - \bar{B}^0$ mixing and decay amplitudes.

We updated this measurement of the time-dependent CP Asymmetry in $B^0 \to K^{*0}\gamma$ based on 431 million $B\bar{B}$ events collected at BABAR. Photon quality cuts and π^0/η veto were applied to select the primary photon. K^* candidates were selected based on kinetic and angular constraints. The signal B^0 decays were identified by using m_{ES} and ΔE. We determine the proper time difference between B_{sig} and B_{tag} from the spatial separation between their decay vertices. The signal yields and CP asymmetry were extracted from an unbinned likelihood fit to m_{ES}, ΔE, L_2/L_0, $m(K^0_S\pi^0)$, flavor tag, Δt, and $\sigma\Delta t$ (see fig.3).

The dominant systematics were from $B\bar{B}$ background, fit bias and the

selection of PDF. Combining all, we found 316 ± 22 signal events with

$$S_{K^*\gamma} = -0.08 \pm 0.31 \pm 0.05$$

and

$$C_{K^*\gamma} = -0.15 \pm 0.17 \pm 0.03,$$

where the first error is statistical and the second systematic. We found our preliminary results to be consistent with our previous result [12], as well as with the standard model expectation.

3 $b \to d\gamma$

Compared to $b \to s\gamma$, the amplitude of $b \to d\gamma$ is suppressed by the ratio of the CKM matrix elements $|V_{td}/V_{ts}|$, thus it is more difficult to observe. Its branching ratio is typically around the order of 10^{-6}. Previous measurements of the exclusive decays $B^+ \to \rho^+\gamma$, $B^0 \to \rho^0\gamma$, and $B^0 \to \omega\gamma$ by the Belle [13] and BaBar [14] experiments found branching fractions are in good agreement with SM predictions [15]. With large uncertainties associated with the exclusive measurements, there is a strong motivation to extend the experimental study to additional final states and different regions of the hadronic mass spectrum. In this paper we report the first study of $b \to d\gamma$ transitions using a sum of seven exclusive $X_d\gamma$ final states in the hadronic mass range $1.0 < M(X_d) < 1.8$GeV.

We exclusively reconstruct seven $b \to d\gamma$ decay modes with up to four charged pions and one neutral pion or eta in the final state, which accounts for 50% $b \to d\gamma$ cross section in this region. The events from continuum that contain a high enrgy photon from π^0 or η decays or from initial-state radiation will be rejected. We also reject $B \to X_d\pi^0$, $B \to X_d\eta$ and $B \to X_s\gamma$ from combinatorial B decays. Then a Neural Net is used to further reduce continuum background.

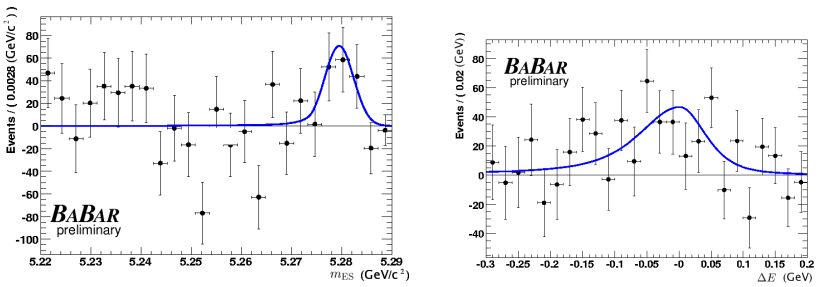

(a) (b)

Figure 4: Signal distributions of m_{ES} (left) and ΔE (right) for $B \to X_d\gamma$ in the range $1.0 < M(X_d) < 1.8\text{GeV}/c^2$ with the background subtraction as described in the text. The curves represent the PDFs used in the fit, normalized to the fitted yield.

The signal content of the data is determined by means of a two-dimensional unbinned maximum likelihood fit to the ΔE and m_{ES} distributions (see fig.4). We find 178 ± 53 signal events. The dominant systematics are from Neural net efficiency, PDF shapes, fit bias and the B background normalization. The effect of the X_d fragmentation model by JETSET is also assessed. After combining the fit results and the uncertainties, we obtain the partial branching fraction $\sum_{X_d=1}^{7} B(B \to X_d\gamma)|_{(1.0<M(X_d)<1.8\text{GeV}/c^2)} = (3.1 \pm 0.9^{+0.6}_{-0.5} \pm 0.5) \cdot 10^{-6}$, where the uncertainties are statistical, systematic and model respectively. Including statistical and systematic uncertainties only, this corresponds to a signal significance of 3.1σ.

This analysis can be extended to the mass region $0.6 < M(X_d) < 1.0\text{GeV}$ for its non-resonant contribution. Then the extraction of the ratio can be performed by comparing the branching fraction of $b \to d\gamma$ and $b \to s\gamma$ in a more inclusive way to reduce theoretical uncertainties.

4 Summary

We have presented the latest measurements from radiative penguin decays at BaBar. The current measurements have not shown significant deviations from

standard model, the more data collected at B factories and the improved analysis techniques will certainly add more stringent constraints on new physics search.

References

1. B. Aubert *et al*(BABAR Collaboration), Nucl. Instrum. Methods A **479**, 1 (2002).
2. t. Hurth, Rev. Mod. Phys. **75**, 1159 (2003).
3. T. Becher *et al*, Phys. Rev. Lett. **98**, 022003 (2007); M. Misiak *et al*, Phys. Rev. Lett. **98**, 022002 (2007).
4. E. Barberio *et al*, arXiv:0704.3575 (2007).
5. D. Benson *et al*, Nucl. Phys. B**710**, 371(2005).
6. B. Lange *et al*, Phys. Rev. D**72**, 073006 (2005).
7. B. Aubert *et al* (BABAR Collaboration), Phys. Rev. Lett. **97**, 171803 (2006).
8. B. Aubert *et al* (BABAR Collaboration), Phys. Rev. D**72**, 052004 (2005).
9. O. Buchmueller *et al*, Phys. Rev. D**73**, 073008 (2007).
10. P. Ball *et al*, Phys. Lett. B**642**, 478 (2006).
11. B. Grinstein *et al*, Phys. Rev. D 73, 014013 (2006).
12. B. Aubert *et al* (BABAR Collaboration), Phys. Rev. D**72**, 051103 (2005).
13. D. Mohapatra *et al.* (Belle Collaboration), Phys. Rev Lett. **96**, 221601 (2006).
14. B. Aubert *et al.* (BABAR Collaboration), Phys. Rev. Lett. **98**, 151802 (2007).
15. P. Ball *et al*, Phys. Rev. D**75**, 054004 (2007).

Frascati Physics Series Vol. XLVI (2007), pp. 1037
HADRON07: XII Int. Conf. on Hadron Spectroscopy – Frascati, October 8-13, 2007
Heavy Meson Spectroscopy

LEPTONIC DECAYS AT BaBaR

E. Salvati
University of Massachusetts

Written contribution not received

Frascati Physics Series Vol. XLVI (2007), pp. 1039–1046
HADRON07: XII Int. Conf. on Hadron Spectroscopy – Frascati, October 8-13, 2007
Heavy Meson Spectroscopy

CHARMLESS HADRONIC B DECAYS AT *BABAR*

Gagan B. Mohanty
Representing the *BABAR* Collaboration
Department of Physics, University of Warwick, Coventry, United Kingdom

Abstract

We report recent measurements of branching fractions and charge asymmetries of charmless hadronic B decays using the data collected with the *BABAR* detector at the PEP-II asymmetric energy e^+e^- collider.

1 Introduction

B meson decays to hadronic final states without a charm quark are an important probe of the Standard Model (SM) of particle physics. The so-called charmless decays play a key role in testing the Cabibbo-Kobayashi-Maskawa (CKM) predictions of charge-parity (CP) violation, with sensitivity to the three angles α, β and γ of the Unitarity Triangle. The dominant contributors to this class of B decays are "penguin" decays mediated by $b \to s$ and $b \to d$ process involving a virtual loop with the emission of a gluon and the CKM-suppressed $b \to u$ tree diagram. Due to the presence of an extra strange quark, the first

diagram contributes only to final states containing an odd number of kaons; while the latter two result in final states with no, or an even number of, kaons. Penguin decays provide an ideal environment to look for new physics (NP) with possible contributions from non-SM particles in the loop, while the interference between tree and penguin amplitudes (of comparable magnitudes) allows to search for direct *CP* violation [1]. Furthermore, studies of these decay processes can be used to constrain varieties of theoretical models of B decays based on factorization, perturbative QCD, and SU(3) flavor symmetry.

In these proceedings, we summarize most recent results on charmless hadronic B decays [2] culminating in three-body, quasi-two-body (Q2B), or other multibody final states; studied using e^+e^- collision data collected with the *BABAR* detector [3] near the $\Upsilon(4S)$ resonance. The results should be considered preliminary, unless a journal reference is given.

2 Analysis Method

The challenge in studying charmless hadronic B decays is to extract a small signal (typical branching fraction is of the order of 10^{-6}) out of a sea of background events. The continuum light-quark production, $e^+e^- \to q\overline{q}\,(q = u, d, s, c)$, forms the most dominant background component. It is suppressed by exploiting the difference in event topology - B mesons are produced almost at rest resulting in a spherical event, while the light-quark pairs tend to have a jetlike shape owing to the large available kinetic energy - and by utilizing flavor and decay-time information of B meson candidates. Particle identification plays a crucial role in separating charged pions from kaon track candidates. This becomes particularly important against the background emanating from B decays with similar hadronic final states. Backgrounds from final states with charm quarks are suppressed by invariant-mass vetoes on charmonia and D mesons. The signal yield is extracted by performing an unbinned maximum-likelihood (ML) fit to event-shape variables (usually combined to a Fisher discriminant $\mathcal{F}$ or an artificial Neural Network NN), and kinematic quantities that make use of precise beam-energy information and energy-momentum conservation. The kinematic variables are the difference ΔE between the energy of the reconstructed B candidate and the beam energy ($E_{\rm beam}$), and the beam-energy substituted mass $m_{\rm ES} \equiv \sqrt{E^2_{\rm beam} - \mathbf{p}^2_B}$, where $\mathbf{p}_B$ is the momentum of the B candidate [here all quantities are calculated in the $\Upsilon(4S)$ rest frame]. Where

available, the invariant-mass and angular variables of Q2B resonances are used to further enhance background suppression. For signal modes with a significant yield, the *CP* violation or charge asymmetry is measured using $A_{CP} = \frac{N_{\overline{B}} - N_B}{N_{\overline{B}} + N_B}$, where $N_{\overline{B}}$ and N_B correspond to the number of $\overline{B}$ ($\overline{B}^0$ or B^-) and B (B^0 or B^+) decays detected in the inclusive yield, respectively.

3 Experimental Results

3.1 Three-body Decay $B^+ \to K^+K^-\pi^+$

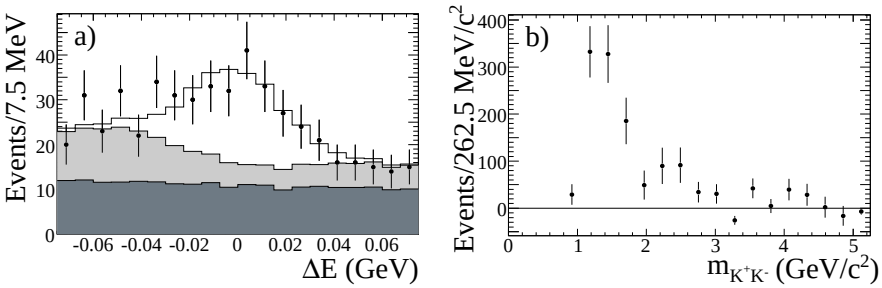

Figure 1: *a) ΔE projection of $B^+ \to K^+K^-\pi^+$ candidate events and b) Efficiency-corrected $m_{K^+K^-}$ distribution of the $K^+K^-\pi^+$ signal candidates with $m_{K^+\pi^-} > 1.5\,\mathrm{GeV}/c^2$.*

Using 383 million $B\overline{B}$ pairs recorded by *BABAR*, we report the first observation of charmless hadronic decays of charged B mesons to the final state $K^+K^-\pi^+$ [4]. We observe in total 429 ± 43 signal events with a significance of 9.6 standard deviation (σ), and measure the inclusive branching fraction [5] $\mathcal{B}(B^+ \to K^+K^-\pi^+) = [5.0 \pm 0.5(\mathrm{stat}) \pm 0.5(\mathrm{syst})] \times 10^{-6}$. Figure 1(a) shows the ΔE distribution of selected candidate events, following a signal-enhancing requirement on the likelihood ratio which is formed out of m_{ES} and NN variables. Points show the data, the dark filled histogram shows the $q\overline{q}$ background and the light filled histogram shows the $B\overline{B}$ background. Approximately half of the signal events appear to originate from a broad structure peaking near 1.5 GeV/c^2 in the K^+K^- invariant mass distribution (see Figure 1(b)). This structure is reminiscent of similar states observed in Dalitz plot analyses of $B^+ \to K^+K^-K^+$ [6] and $B^0 \to K^0_S K^+K^-$ [7], and is likely to be of great

interest for the understanding of low energy hadronic bound states [8]. Results on the $K^-\pi^+$ mass spectrum are in reasonable agreement with a dedicated Q2B analysis [9] that has put the most stringent upper limit (UL) on $B^+ \to \overline{K}^{*0}(892)K^+$ and a first UL on $B^+ \to \overline{K}_0^{*0}(1430)K^+$ at 1.1×10^{-6} and 2.2×10^{-6}, respectively (all quoted ULs are computed at 90 % confidence level). The measured charge asymmetry is found to be consistent with zero.

3.2 Vector-Vector Decay $B^0 \to K^{*0}\overline{K}^{*0}$

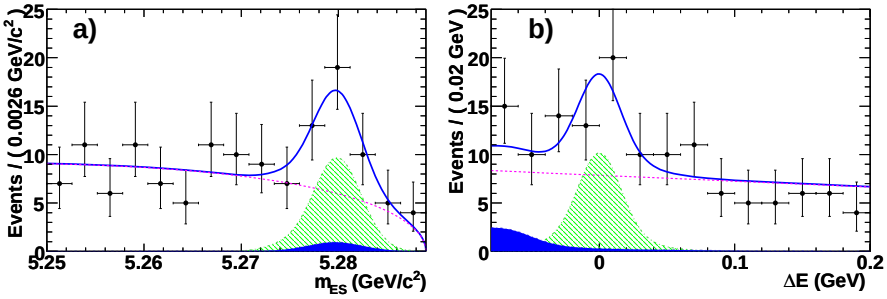

Figure 2: *Projections of a) $m_{\rm ES}$ and b) ΔE of candidate events in the $B^0 \to K^{*0}\overline{K}^{*0}$ decays.*

We report the observation of the $b \to d$ penguin-dominated vector-vector decay $B^0 \to K^{*0}\overline{K}^{*0}$ at $6\,\sigma$ significance [10] with a sample of 383 million $B\overline{B}$ pairs. Figure 2 shows $m_{\rm ES}$ and ΔE projections of candidate events with a requirement on the signal-to-background likelihood ratio, calculated excluding the plotted variable. Points with error bars show the data, the solid line shows the projection for signal-plus-background, the dashed line is the continuum background, the hatched region is the signal, and the shaded region is the $B\overline{B}$ background. Performing a simultaneous likelihood fit we determine the branching fraction $\mathcal{B}(B^0 \to K^{*0}\overline{K}^{*0}) = [1.28^{+0.35}_{-0.30}(\text{stat}) \pm 0.11(\text{syst})] \times 10^{-6}$, and the fraction of longitudinal polarization $f_L = 0.80^{+0.10}_{-0.12}(\text{stat}) \pm 0.06(\text{syst})$. The branching fraction measurement is consistent with theoretical predictions [11]. The measured f_L value agrees with the model expectation of QCD factorization [12], which predicts it to be ~ 0.9 in the vector-vector decay of a pseudoscalar (B^0 here). We have also improved the existing UL on the SM-suppressed decay

$B^0 \to K^{*0}K^{*0}$ by two orders of magnitude to 4.1×10^{-7}.

3.3 Decays involving a Vector and two Pseudoscalars

Using a data sample of 383 million $\Upsilon(4S) \to B\overline{B}$ events, we measure the branching fractions and *CP* violation asymmetries [13] of hadronic decays $B^0 \to K^{*0}h^+h'^-$, where h and h' refers to either a kaon or a pion. The K^{*0} is detected via its self-tagging decay mode $K^{*0} \to K^+\pi^-$. Table 1 summarizes results of these measurements. We have made three new observations in the final states $K^{*0}K^+K^-$, $K^{*0}\pi^+\pi^-$ and $K^{*0}\pi^+K^-$. In the SM-suppressed decay $B^0 \to K^{*0}K^+\pi^-$, where a branching fraction comparable to or larger than that of the $K^{*0}\pi^+K^-$ mode would be a signature of NP, no signal is observed and a first UL is set at 2.2×10^{-6}. We find no evidence for *CP* violation in these $B^0 \to K^{*0}h^+h'^-$ decays.

Table 1: *Measured signal yields, branching fractions ($\mathcal{B}$), significance (S) and CP violation asymmetries (for the significant modes) of $B^0 \to K^{*0}(892)h^+h'^-$. The first uncertainty is statistical and the second is systematic.*

$B^0 \to$ Mode	Signal yield	$\mathcal{B}(\times 10^{-6})$	$S(\sigma)$	A_{CP}
$K^{*0}K^+K^-$	984 ± 46	$27.5 \pm 1.3 \pm 2.2$	> 10	$0.01 \pm 0.05 \pm 0.02$
$K^{*0}\pi^+K^-$	183 ± 42.4	$4.6 \pm 1.1 \pm 0.8$	5.3	$0.22 \pm 0.33 \pm 0.20$
$K^{*0}K^+\pi^-$	18.8 ± 29.4	< 2.2	0.9	–
$K^{*0}\pi^+\pi^-$	2019 ± 108	$54.5 \pm 2.9 \pm 4.3$	> 10	$0.07 \pm 0.04 \pm 0.03$

3.4 Axial-vector and Pseudoscalar Modes

We report results of a first search for B meson decays to final states with an axial-vector meson, $b_1(1235)$, and a pseudoscalar meson (pion or kaon), carried out with a data sample containing 382 million $B\overline{B}$ pairs. In the quark model the b_1 is the $I^G = 1^+$ member of the $J^{PC} = 1^{+-}$, $^1P_1$ nonet. Its mass and width are (1229.5 ± 3.2) MeV/c^2 and (142 ± 9) MeV, respectively, and the dominant decay is to $\omega(782)\pi$ [14]. By performing an extended ML fit to ΔE, $m_{\rm ES}$, $\mathcal{F}$, and reconstructed invariant masses of the b_1 and ω resonances [15], we find clear signals for $B^+ \to b_1^0\pi^+$, $B^+ \to b_1^0K^+$, $B^0 \to b_1^\mp\pi^\pm$ and $B^0 \to b_1^-K^+$. Table 2 summarizes the signal yield, branching fraction, significance and charge asymmetry of these four decay modes.

Measured branching fractions and charge asymmetries agree with QCD factorization predictions [16]. Observations in the $B \to b_1 K$ modes, if confirmed with higher precision, would indicate a sizable weak annihilation contribution to these modes [16]. Furthermore, the measurement of an asymmetry parameter, $\Gamma(B^0 \to b_1^+\pi^-)/\Gamma(B^0 \to b_1^-\pi^+) = -0.01 \pm 0.12$ in the decays $B^0 \to b_1^{\mp}\pi^{\pm}$ agrees well with G-parity suppression [17].

Table 2: *Measured signal yields, branching fractions ($\mathcal{B}$), significance (S) and direct CP asymmetries of $B \to b_1(1235)h$ where $h = K/\pi$. The first uncertainty is statistical and the second is systematic.*

Decay mode	Signal yield	$\mathcal{B}(\times 10^{-6})$	$S(\sigma)$	A_{CP}
$B^+ \to b_1^0\pi^+$	178^{+39}_{-37}	$6.7 \pm 1.7 \pm 1.0$	4.0	$0.05 \pm 0.16 \pm 0.02$
$B^+ \to b_1^0 K^+$	219^{+38}_{-36}	$9.1 \pm 1.7 \pm 1.0$	5.3	$-0.46 \pm 0.20 \pm 0.02$
$B^0 \to b_1^{\mp}\pi^{\pm}$	387^{+41}_{-39}	$10.9 \pm 1.2 \pm 0.9$	8.9	$-0.05 \pm 0.10 \pm 0.02$
$B^0 \to b_1^- K^+$	267^{+33}_{-32}	$7.4 \pm 1.0 \pm 1.0$	6.1	$-0.07 \pm 0.12 \pm 0.02$

Moving on to another axial-vector state $a_1(1260)$, which is the $I^G = 1^-$ state of the $J^{PC} = 1^{++}$, $^3P_1$ nonet, we report evidence of two decay modes containing pions in the final state [18] and two observations in kaon modes [19]. For pion modes the analysis comprises a smaller dataset containing 232 million $B\overline{B}$ pairs, while in kaon modes we have utilized 383 million $\Upsilon(4S) \to B\overline{B}$ events. Here the a_1 meson is reconstructed via its most dominant decay to three pions. Neglecting contributions from isoscalars, such as the σ meson, to the two-pion state; we assume $\mathcal{B}(a_1^{\pm}(1260) \to \pi^{\pm}\pi^+\pi^-)$ is equal to $\mathcal{B}(a_1^{\pm}(1260) \to \pi^{\pm}\pi^0\pi^0)$ and $\mathcal{B}(a_1^{\pm}(1260) \to (3\pi)^{\pm}) = 100\%$. The three-pion decay is also considered as the only possible decay mode for neutral a_1 mesons. These assumptions help in translating the product of $\mathcal{B}(B \to a_1(1260)h)$ and $\mathcal{B}(a_1(1260) \to 3\pi)$ into the former. Table 3 summarizes this branching fraction measurement in the decays $B^+ \to a_1^+\pi^0$, $B^+ \to a_1^0\pi^+$, $B^+ \to a_1^+ K^0$ and $B^0 \to a_1^- K^+$ along with the assorted signal yield and significance. Measured branching fractions are in reasonable agreement with factorization model predictions [20]. In the case of kaon modes, we find no evidence for direct *CP* violation.

Table 3: *Measured signal yields, branching fractions ($\mathcal{B}$) and significance (S) of $B \to a_1(1260)h$ where $h = K/\pi$. The first uncertainty is statistical and the second is systematic.*

Decay mode	Signal yield	$\mathcal{B}(\times 10^{-6})$	$S(\sigma)$
$B^+ \to a_1^+\pi^0$	459 ± 78	$26.4 \pm 5.4 \pm 4.1$	4.2
$B^+ \to a_1^0\pi^+$	382 ± 79	$20.4 \pm 4.7 \pm 3.4$	3.8
$B^+ \to a_1^+K^0$	241 ± 32	$34.9 \pm 5.0 \pm 4.4$	6.2
$B^0 \to a_1^-K^+$	272 ± 44	$16.3 \pm 2.9 \pm 2.3$	5.1

4 Conclusions

BABAR is pioneering several new measurements in charmless hadronic B decays that probe the SM in two orthogonal directions - the weak interaction by measuring the CKM angles [21)], and the strong interaction by exploring low-lying hadronic bound states and by providing precision tests of QCD models. We eagerly look forward to the last run, which together with data taken during the year 2006-2007 and not used in the presented results, would double the dataset. This will be crucial for realizing other rare hadronic decay modes such as $B^+ \to K_S^0 K_S^0 \pi^+$ within our reach.

5 Acknowledgments

It is a pleasure to thank the organizers of the HADRON07 conference for a job well-done! This work is supported in part by the Science and Technology Facilities Council of the United Kingdom, and the US Department of Energy under contract number DE-AC02-76SF00515.

References

1. Direct *CP* violation has been demonstrated convincingly by both *BABAR* and Belle experiments in the decay $B^0 \to K^+\pi^-$. Please refer to:
   B. Aubert *et al.* [*BABAR* Collab.], Phys. Rev. Lett. **93**, 131801 (2004);
   Y. Chao *et al.* [Belle Collab.], Phys. Rev. Lett. **93**, 191802 (2004); and
   B. Aubert *et al.* [*BABAR* Collab.], Phys. Rev. Lett. **99**, 021603 (2007).

2. Unless explicitly stated otherwise, charge-conjugate states are assumed throughout.

3. B. Aubert *et al.* [*BABAR* Collab.], Nucl. Instrum. Meth. A **479**, 1 (2002).

4. B. Aubert *et al.* [*BABAR* Collab.], Phys. Rev. Lett. **99**, 221801 (2007).

5. M. Pivk and F.R. Le Diberder, Nucl. Instrum. Meth. A **555**, 356 (2005).

6. A. Garmash *et al.* [Belle Collab.], Phys. Rev. D **71**, 092003 (2005); and B. Aubert *et al.* [*BABAR* Collab.], Phys. Rev. D **74**, 032003 (2006).

7. B. Aubert *et al.* [*BABAR* Collab.], Phys. Rev. Lett. **99**, 161802 (2007).

8. E. Klempt and A. Zaitsev, **arXiv:0708.4016** [hep-ph].

9. B. Aubert *et al.* [*BABAR* Collab.], Phys. Rev. D **76**, 0711031 (2007).

10. B. Aubert *et al.* [*BABAR* Collab.], **arXiv:0708.2248** [hep-ex].

11. M. Beneke, J. Rohrer, and D. Yang, Nucl. Phys. B **774**, 64 (2007).

12. A. Ali, J.G. Korner, G. Kramer, and J. Willrodt, Z. Phys. C **1**, 269 (1979); M. Suzuki, Phys. Rev. D **66**, 054018 (2002).

13. B. Aubert *et al.* [*BABAR* Collab.], Phys. Rev. D **76**, 071104 (2007).

14. Y.-M. Yao *et al.* [Particle Data Group], J. Phys. G **33**, 1 (2006).

15. B. Aubert *et al.* [*BABAR* Collab.], **arXiv:0707.4561** [hep-ex].

16. H.-Y. Cheng and K.-C. Yang, **arXiv:0709.0137** [hep-ph].

17. S. Weinberg, Phys. Rev. **112**, 1375 (1958).

18. B. Aubert *et al.* [*BABAR* Collab.], **arXiv:0708.0050** [hep-ex].

19. B. Aubert *et al.* [*BABAR* Collab.], **arXiv:0709.4165** [hep-ex].

20. V. Laporta, G. Nardulli, and T.N. Pham, Phys. Rev. D **74**, 054035 (2006); Erratum-ibid. D **76**, 079903 (2007).

21. S. Emery in these proceedings.

Frascati Physics Series Vol. XLVI (2007), pp. 1047–1054
HADRON07: XII Int. Conf. on Hadron Spectroscopy – Frascati, October 8-13, 2007
Heavy Meson Spectroscopy

DETERMINATION OF THE ANGLES OF THE UNITARITY TRIANGLE AT *BABAR*

Sandrine Emery-Schrenk
Representing the *BABAR* collaboration
CEA-Saclay, DAPNIA/SPP, Gif-sur-Yvette, France

Abstract

We report recent measurements of the three angles of the unitarity triangle using the data collected with the *BABAR* detector at the PEP-II asymmetric energy e^+e^- collider.

1 Introduction

In the Standard Model, CP violation arises from the complex quark mixing CKM matrix, described in the Wolfenstein parametrization as:

$$V_{CKM} = \begin{pmatrix} V_{ud} & V_{us} & V_{ub} \\ V_{cd} & V_{cs} & V_{cb} \\ V_{td} & V_{ts} & V_{tb} \end{pmatrix} = \begin{pmatrix} 1-\frac{\lambda^2}{2} & \lambda & A\lambda^3(\rho - i\eta) \\ -\lambda & 1-\frac{\lambda^2}{2} & A\lambda^2 \\ A\lambda^3(1-\rho-i\eta) & -A\lambda^2 & 1 \end{pmatrix} \quad (1)$$

The unitarity of the CKM matrix results in a triangle in the (ρ, η) plane (Fig. 1). Overconstraining the triangle by measurements of the angles and sides tests the unitarity of the CKM matrix and the validity of the Standard Model.

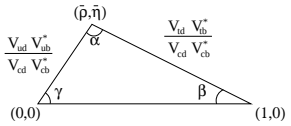

Figure 1: *Unitarity triangle.*

The β (ϕ_1) angle is the phase of V_{td}, involved in $B^0 - \bar{B}^0$ mixing; the γ (ϕ_3) angle is the phase of V_{ub}, involved in the $b \to u$ charmless decays. Measurements of $\alpha = \pi - \beta - \gamma$ (ϕ_2) use processes involving both $B^0 - \bar{B}^0$ mixing and $b \to u$ transitions. In these proceedings, we summarize the most recent measurements at *BABAR* of the angles β, α, and γ (in order of increasing measurement difficulty). The results should be considered preliminary unless a journal reference is given. Most results are based on the analysis of 383 millions $b\overline{b}$ pairs. Charge-conjugate states are assumed throughout for B decays.

2 Methodology

The angles of the unitarity triangle are measured using CP violating processes in which amplitudes with different CKM phases interfere. Most measurements of β and α exploit the interference between the decay of a B^0 directly to a CP eigenstate (f_{CP}) and the decay of a B^0 first oscillating to a $\bar{B}^0$ and then decaying into the CP eigenstate. Measuring the time-dependent CP asymmetry (Eq. 2) allows the extraction of $S_{f_{CP}}$ and $C_{f_{CP}}$, which are functions (Eq. 3) of $\lambda_{f_{CP}}$, the product of a -2β phase term from B mixing times the ratio of the amplitudes $\bar{A}_{f_{CP}}$ and $A_{f_{CP}}$ of the $\bar{B}^0$ and B^0 decays to f_{CP}.

$$A_{f_{CP}} = \frac{\Gamma(\bar{B}^0) - \Gamma(B^0)}{\Gamma(\bar{B}^0) + \Gamma(B^0)} = S_{f_{CP}} \sin(\Delta m_d \Delta t) - C_{f_{CP}} \cos(\Delta m_d \Delta t) \qquad (2)$$

$$\lambda_{f_{CP}} \approx e^{-2i\beta} \times \frac{\bar{A}_{f_{CP}}}{A_{f_{CP}}}, \quad S_{f_{CP}} = \frac{2\Im(\lambda_{f_{CP}})}{1+|\lambda_{f_{CP}}|^2}, \quad C_{f_{CP}} = \frac{1-|\lambda_{f_{CP}}|^2}{1+|\lambda_{f_{CP}}|^2} \qquad (3)$$

If only one decay diagram is involved in the $B^0 \to f_{CP}$ decay, Eq. 3 reduces to:

$$C_{f_{CP}} = 0, \quad S_{f_{CP}} = -\sin(2 \times [\beta + \phi_{CKM}]) \tag{4}$$

where ϕ_{CKM} is the CKM phase in the decay amplitude $A_{f_{CP}}$, and is equal to zero (γ) for $b \to c$ ($b \to u$) transitions used for β (α) measurements.

Measurements of α are more difficult due to the low branching fraction of the charmless $b \to u$ tree transitions, and to non-negligible penguin $b \to d$ diagrams involving a different CKM phase (and a source of direct CP violation). Only an effective value α_{eff} is measured.

$$C_{f_{CP}} \neq, 0 \quad S_{f_{CP}} = \sqrt{1 - C^2_{f_{CP}}} \times \sin(2\alpha_{eff}) \tag{5}$$

More details on charmless B decays and penguins diagrams can be found in [1]. $B^0 - \bar{B}^0$ pairs are produced at the $\Upsilon(4S)$ resonance in a coherent state. To measure the CP asymmetry, we reconstruct one B meson into a useful decay channel for an angle measurement, while the other B is used to tag the flavor at production. The difference between the two B mesons decay times is reconstructed using the difference in decay flight ($\Delta z \approx 250\mu m$, $\sigma_{\Delta z} \approx 170\mu m$) along the beams direction, neglecting transverse flight.

3 Measurements of the β angle

The golden decay channels $B^0 \to$ charmonium [J/Ψ, Ψ', χ_c, η_c] $K^0_{S,L}$ (CP eigenstates) are dominated by a color-suppressed $b \to c$ tree diagram. Their relatively high branching ratio ($\approx 10^{-3}$) and the absence of direct CP violation allows the simple extraction of $S = -\eta_f \sin(2\beta)$ from the CP asymmetry measurement (Eqs. 2, 4), where η_f is the CP eigenvalue of the final state. These analyses at *BABAR* allow an accurate measurement of $\sin(2\beta) = 0.714 \pm 0.032 \pm 0.018$ [2].

To resolve the $\pi - 2\beta$ ambiguity in $\sin(2\beta)$, different analyses constrain the value of $\cos(2\beta)$. The $\cos(2\beta)$ term in the time-dependent and full angular analysis of the $J/\Psi K^{*0}$ decay appears in the interference between CP-odd and CP-even amplitudes: $\cos(2\beta) = 3.32^{+0.76}_{-0.96}(stat) \pm 0.27(syst)$ [3]. A time-dependent analysis of the $D^* D^* K^0_S$ mode also constrains $\cos(2\beta) > 0$ @ 94% C.L [4]. The most recent result is the time-dependent Dalitz analysis [5] of the

$D^0(\bar{D}^0) \to K^0_S\pi^+\pi^-$ decay, from the $B^0(\bar{B}^0)$ decay to $D^0(\bar{D}^0)h^0 = \pi^0, \eta, \eta', \omega$. The analysis is sensitive to $\sin(2\beta)$ and $\cos(2\beta)$ [6] due to the interference between the D^0 and $\bar{D}^0$ decays and yields $\cos(2\beta) > 0$ @ 86% C.L [7].

Some channels contain additional loop diagrams that are negligible in the Standard Model. Measuring an effective value $\sin(2\beta)_{eff}$ different from the golden mode value is an indication of new physics. Such channels are $B^0 \to D^+D^-$ [8], $B^0 \to D^{*+}D^{*-}$ [9], and $B^0 \to D^{(*)0}_{CP}h^0$ [10]. Recently published results do not indicate any significant direct CP violation, or any $\sin(2\beta)_{eff}$ deviation from the golden mode.

Several $b \to sq\bar{q}$ penguin modes analyses were updated recently at both *BABAR* and Belle and are summarized in [11]. The average $\sin(2\beta)_{eff}$ over the penguin modes was 2.5 σ away from the golden mode $\sin(2\beta)$ value at the time of the winter 2007 conferences. But now, for *BABAR* $\sin(2\beta)_{eff} = 0.67 \pm 0.04$ (<1 σ deviation). This is mostly due to the new time-dependent Dalitz analysis of the $B^0 \to K^0_S\pi^+\pi^-$ decay [12]. We fit the phase and magnitude for each component's amplitude ($K^{*+}(892)\pi^-$, $K^{*+}(1430)\pi^-$, $K^0_S\rho^0$, $K^0_S f_0$, non-resonant) and derive the quasi-two-body parameters C and S (Eq. 2) for the various components. For $K^0_S f_0$, $\eta_{CP}S = 0.94^{+0.02}_{-0.07}(stat)^{+0.04}_{-0.05}(syst)$ is the largest deviation from the golden mode. But the errors must be handled with caution, as a constraint to remain in the physical bound was added.

4 Measurements of the α angle.

Similar analyses of the time-dependent CP asymmetry of $b \to u$ transitions to $\pi^+\pi^-$ [13] and $\rho^+\rho^-$ [14] CP final states only allow an effective measurement (α_{eff}) of α (Sec. 2) due to penguin pollution. The difference $\alpha - \alpha_{eff}$ is constrained with an isospin analysis [15] using the measured branching fractions and the CP parameters of the other $\pi\pi$ ($\rho\rho$) modes. Neglecting the electroweak penguins contribution, the $u \leftrightarrow d$ $SU(2)$ symmetry leads to relationships between the amplitudes of the different $\pi\pi$ ($\rho\rho$) modes. The more complicated $\rho\rho$ vector-vector modes are advantageous since the $\rho^+\rho^-$ branching fraction is 5 times higher than for $\pi^+\pi^-$. The $\rho^+\rho^-$ is almost 100% longitudinally polarized (CP-even state), so only the longitudinal components are used in the isospin analysis and the penguin pollution rate is less than for $\pi^+\pi^-$. Moreover, the C and S CP parameters extracted from the $\rho^0\rho^0$ time-dependent analysis provide additional constraints to the isospin analysis (Fig. 2.b). Results from the new

isospin analyses of the $\pi\pi$ [16] and $\rho\rho$ [17] modes are shown on Fig. 2.

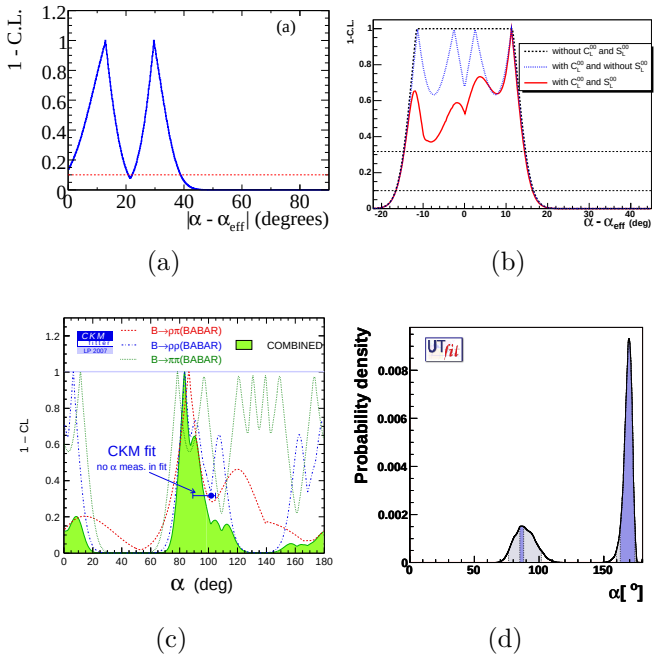

Figure 2: (a) $|\alpha - \alpha_{eff}|$ *scan from* $\pi\pi$ *analyses.* (b) $|\alpha - \alpha_{eff}|$ *scan from* $\rho\rho$ *analyses.* (c) α *scan from CKMFitter frequentist approach* [20]. (d) α *scan from UTFit Bayesian approach* [21]. *The use of* $SU(3)$ *flavor symmetry excludes the* α *solutions from isospin analysis near zero.*

Another approach for constraining α is the time-dependant Dalitz analysis of the $B^0 \to (\rho\pi)^0 \to \pi^+\pi^-\pi^0$ [18], which is directly sensitive to α unlike the $\sin(2\alpha_{eff})$ measurements presenting multiple ambiguities from the $\sin(2\alpha_{eff})$ measurement and the isospin analysis. Recently published *BABAR* results [19] are also shown in Fig.2.c.

The $a_1\pi$ mode also allows an accurate measurement of $\alpha_{eff}^{a_1\pi} = 78.6 \pm 7.3^\circ$ [22]. The available measurements of $K_1\pi$ and $a_1 K$ branching fractions [23] and the use of flavour symmetry will allow one to constrain $\alpha - \alpha_{eff}$ [24].

5 Measurements of the γ angle.

The time-dependent analysis of $B^0 \to D^{(*)+}\pi^{-,+}$ (or $\rho^{-,+}$) decays allows the measurement of $sin(2\beta+\gamma)$ [25].

The most recent γ results are from the analysis of $B^+ \to D^{(*)0}K^{(*)+}$ decays which are sensitive to γ due to the interference between two tree diagrams: one color favored $B^+ \to \bar{D}^{(*)0}K^{(*)+}$ $b \to c$ transition and a small (color and CKM) suppressed $B^+ \to D^{(*)0}K^{(*)+}$ $b \to u$ contribution carrying a CKM γ phase. Methods are based on D^0 decay modes for which the D^0 and the $\bar{D}^0$ can not be distinguished: the D^0 or $\bar{D}^0$ can decay into CP eigenstates (GLW method [26]), into the wrong sign $K^+\pi^-$ final state (ADS method [27]), or into three bodies such as $K^0_S\pi^+\pi^-$ in which case a Dalitz analysis is performed (GGSZ method [28]). The challenge of these methods is to disentangle the electroweak part carrying information on γ from the hadronic uncertainties from the B and D meson decays. The GLW method allows one to eliminate the hadronic uncertainties from the D decay, but the interference term is small since the magnitudes of the amplitudes of the tree diagrams involved are very different. The interference is larger using the ADS method since the large $B^+ \to \bar{D}^{(*)0}K^{(*)+}$ amplitude is combined with the small doubly Cabbibbo suppressed D decay, but hadronic uncertainties come from both the B and the D decay. In that sense the different methods complement each other. The best method may be the Dalitz GGSZ analysis.

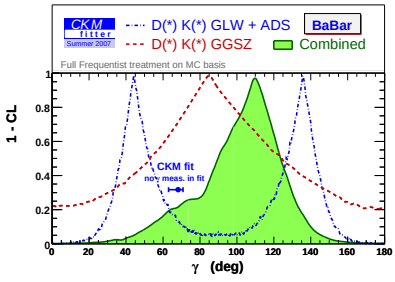

Figure 3: *Gamma scan summary for BABAR results from CKMFitter.*

Only the GLW method was updated recently at *BABAR* [29]. The studied

CP-even (CP-odd) D^0 decay modes are K^+K^- and $\pi^+\pi^-$ ($K^0\pi^0$ and $K^0\omega$). The direct CP asymmetry measured between the B^+ and B^- decays for CP-even D decays $A_{CP+} = 0.35 \pm 0.09(stat) \pm 0.05(syst)$ is significantly different from zero. All results are summarized in [11] and shown in Fig. 3.

6 Conclusion

The results of the angles (β, α, γ) of the unitarity triangle are consistent [20, 21] with Belle results, and with other CKM constraints such as the measurement of ϵ_K, the length of the sides of the unitarity triangle determined from the measurements of Δm_d, Δm_s, $|V_{ub}|$, etc.

References

1. Gagan B. Mohanty, Charmless Hadronic B Decays, these proceedings.
2. *BABAR* Collab., B. Aubert *et al.*, Phys. Rev. Lett. **99**, 171803 (2007).
3. *BABAR* Collab., B. Aubert *et al.*, Phys. Rev. D **71**, 032005 (2005).
4. *BABAR* Collab., B. Aubert *et al.*, Phys. Rev. D **74**, 091101 (2006).
5. Kalanand Mishra, these proceedings.
6. *BABAR* Collab., B. Aubert *et al.*, arXiv:hep-ph/0503174
7. *BABAR* Collab., B. Aubert *et al.*, arXiv:0708.1544 (2007).
8. *BABAR* Collab., B. Aubert *et al.*, Phys. Rev. Lett. **99**, 071801 (2007).
9. *BABAR* Collab., B. Aubert *et al.*, arXiv:0708.1549 (2007).
10. *BABAR* Collab., B. Aubert *et al.*, Phys. Rev. Lett. **99**, 081801 (2007).
11. Heavy Flavor Averaging Group (HFAG), Summer 2007 results, http://slac.stanford.edu/xorg/hfag/triangle/summer2007/
12. *BABAR* Collab., B. Aubert *et al.*, arXiv:0708.2097 (2007).
13. *BABAR* Collab., B. Aubert *et al.*, Phys. Rev. Lett. **99**, 021603 (2007); Phys. Rev. D **75**, 012008 (2007).

14. *BABAR* Collab., B. Aubert *et al.*, Phys. Rev. D **76**, 052007 (2007).

15. Gronau and London, Phys. Rev. Lett. **65**, 3381 (1990).

16. *BABAR* Collab., B. Aubert *et al.*, arXiv:0707.2798 (2007); Phys. Rev. Lett. **97**, 261601 (2006).

17. *BABAR* Collab., B. Aubert *et al.*, arXiv:0708.1630v1 (2007).

18. Synder and Quinn, Phys. Rev. D **48**, 2139 (1993).

19. *BABAR* Collab., B. Aubert *et al.*, Phys. Rev. D **76**, 012004 (2007).

20. CKMFitter Group, Eur. Phys. Jour. C**41** 1-131 (2005); online update at http://ckmfitter.in2p3.fr

21. UTFit Collab., Phys. Rev. Lett. **97** 151803 (2006); online update at http://utfit.roma1.infn.it/ ; hep-ph/0701204 for α.

22. *BABAR* Collab., B. Aubert *et al.*, Phys. Lett. **98**, 181803 (2007).

23. *BABAR* Collab., B. Aubert *et al.*, arXiv:0709.4165 (2007) ($a_1 K$ results); F. Blanc, talk at Moriond QCD (2007) ($K_1 \pi$ results).

24. Gronau and Zupan, Phys. Rev. D **73**, 057502 (2006).

25. *BABAR* Collab., B. Aubert *et al.*, Phys. Rev. D **71**, 112003 (2005); Phys. Rev. D **73**, 111101 (2006).

26. Gronau and London, Phys. Lett. B253, 483 (1991); Gronau and Wyler, Phys. Lett. B265, 172 (1991); Dunietz, Phys. Lett. B270, 75 (1991).

27. Atwood, Dunietz and Soni, Phys. Rev. Lett. **78**, 3257 (1997); hep-ph/0409281.

28. Atwood, Dunietz and Soni, Phys. Rev. D **63** 036005 (2001); Giri, Grossman, Soffer, Zupan Phys. Rev. D **68**, 054018 (2003).

29. *BABAR* Collab., B. Aubert *et al.*, arXiv:0708.1534 (2007).

Frascati Physics Series Vol. XLVI (2007), pp. 1055–1062
HADRON07: XII Int. Conf. on Hadron Spectroscopy – Frascati, October 8-13, 2007
Heavy Meson Spectroscopy

STUDY OF STRUCTURE OF THE MASS GAP BETWEEN TWO SPIN MULTIPLETS

Takayuki Matsuki
Tokyo Kasei University, 1-18-1 Kaga, Itabashi, Tokyo 173-8602, JAPAN
Toshiyuki Morii
Kobe University, Nada, Kobe 657-8501, JAPAN
Kazutaka Sudoh
High Energy Accel. Res. Org., Tsukuba, Ibaraki 305-0801, JAPAN

Abstract

Studying our semirelativistic potential model and the numerical results, which succeeds in predicting and reproducing recently discovered higher resonances of D, D_s, B, and B_s, we find a simple expression for the mass gap between two spin multiplets of heavy-light mesons, $(0^-, 1^-)$ and $(0^+, 1^+)$. The mass gap between chiral partners defined by $\Delta M = M(0^+) - M(0^-)$ and/or $M(1^+) - M(1^-)$ is given by $\Delta M = M(0^+) - M(0^-) = M(1^+) - M(1^-) \approx \Lambda_{\rm Q} - m_q$ in the limit of heavy quark symmetry. We also study the case including $1/m_Q$ corrections.

1 Introduction

The discovery of the narrow D_{sJ} particles by BaBar [1)] and CLEO [2)] and soon confirmed by Belle [3)] immediately reminded people an effective theory

approach proposed by Nowak et al. and others [4, 5, 6, 7]. From this effective theory, they derived the Goldberger-Treiman relation for the mass gap between chiral partners $0^+(1^+)$ and $0^-(1^-)$ instead of the heavy meson mass itself and predicted the mass gap to be around $\Delta M = g_\pi f_\pi \approx 349$ MeV, where g_π is the coupling constant for $0^+ \to 0^- + \pi$ and f_π is the pion decay constant.

Since this mass gap between chiral partners in the case of D_s agrees well with the experiments (around 350 MeV), people thought that underling physics may be explained by their $SU(3)$ effective Lagrangian [8, 9]. However, when $(0^+, 1^+)$ for D meson were found by Belle and FOCUS, and later reanalyzed by CLEO, their explanation needs to be modified. Furthermore, what they originally predicted could not be identified as any of heavy meson multiplets for D, D_s, B, and B_s. In other words, the forumula can be applied equally for any of these heavy meson multiplets. Thus, it is required to find the mass gap formula, if it exists, which agrees well with the experiments and explains the physical ground of its formula.

In this paper, using our semirelativistic potential model, we first give our formula for the mass gap between chiral partners $0^+(1^+)$ and $0^-(1^-)$ for *any* heavy meson, D, D_s, B, and B_s, among which the known mass gaps, i.e., the ones for D and D_s, agree well with the experiments although there is some ambiguities for D meson data. Next we show how this mass gap depends on a light quark mass m_q for $q = u, d$, and s, where we neglect the difference between u and d quarks. Our formula naturally explain that the mass gap for D is larger than that for D_s and predict the mass gaps for B and B_s.

2 Semirelativistic Quark Potential Model and Structure of Mass Gap

Mass for the heavy meson X with the spin and parity, j^P, is expressed in our formulation as [12]

$$M_X(j^P) = m_Q + E_0^k(m_q) + O\left(1/m_Q\right), \tag{1}$$

where the quantum number k is related to the total angular momentum j and the parity P for a heavy meson as

$$j = |k| - 1 \ \text{ or } \ |k|, \quad P = \frac{k}{|k|}(-1)^{|k|+1}, \quad E_0^k(m_q) = E_0(j^P, m_q). \tag{2}$$

To begin with, we study the heavy meson mass without $1/m_Q$ corrections so that we can see the essence of the mass gap. States with the same $|k|$ value are degenerate in a pure chiral limit and without confining scalar potential, which is defined as $m_q \to 0$ and $S(r) \to 0$ [13]. We consider the scenario that a chiral symmetry breaking and a confinement take place in two steps. First the degeneracy is broken due to gluon fields when $S(r)$ is turned on and confines quarks into heavy mesons but keeping vanishing light quark mass intact. In fact, in this limit our model gives the mass gap between two spin multiplets $\Delta M \approx 300$ MeV as follows;

$$\begin{aligned} \Delta M &= E_0(1^+,0) - E_0(1^-,0) = E_0(0^+,0) - E_0(0^-,0) \\ &= 295.1 \text{ MeV} \quad \text{for } D, \text{ and } D_s, \\ &= 309.2 \text{ MeV} \quad \text{for } B, \text{ and } B_s, \end{aligned} \tag{3}$$

This gap is mainly due to gluon fields which confines quarks into heavy mesons. It is interesting that obtained values are close to $\Lambda_{\rm QCD} \approx 300$ MeV. Next, turning on a light quark mass which explicitly breaks a chiral symmetry, we have $SU(3)$ flavor breaking pattern of the mass levels, i.e., mass of D becomes different from that of D_s with the same value of j^P. Since we assume $m_u = m_d$, there still remains $SU(2)$ iso-spin symmetry. Note that even after chiral symmetry is broken, there is still degeneracy between members of a spin multiplet due to the heavy quark symmetry, i.e., $SU(2)_f \times SU(2)_{\rm spin}$ symmetry, with $SU(2)_f$ rotational flavor symmetry and $SU(2)_{\rm spin}$ rotational spin symmetry. By using the optimal values of parameters in Ref. [14], which is listed in Table 1, degenerate masses without $1/m_Q$ corrections for $D,\ D_s$ and $B,\ B_s$ mesons are calculated and presented in Table 2. Furthermore, by changing m_q from 0 to 0.2 GeV, we have calculated the m_q dependence of ΔM_0 and have obtained Fig. 1, in which ΔM_0 is linearly decreasing with m_q. From Fig. 1, we find that the mass gap between two spin multiplets for a heavy meson X can be written as

$$\Delta M_0 = M_X(0^+) - M_X(0^-) = M_X(1^+) - M_X(1^-) = g_0 \Lambda_{\rm Q} - g_1 m_q, \tag{4}$$

$$\Lambda_Q = 300 \text{ MeV}, \begin{cases} g_0 = 0.9836,\ g_1 = 1.080, & \text{for } D/D_s \\ g_0 = 1.017,\ g_1 = 1.089, & \text{for } B/B_s \end{cases}, \tag{5}$$

where the values of g_0, and g_1 are estimated by fitting the optimal line with Fig. 1. Since both g_0 and g_1 are very close to 1, we conclude that the mass

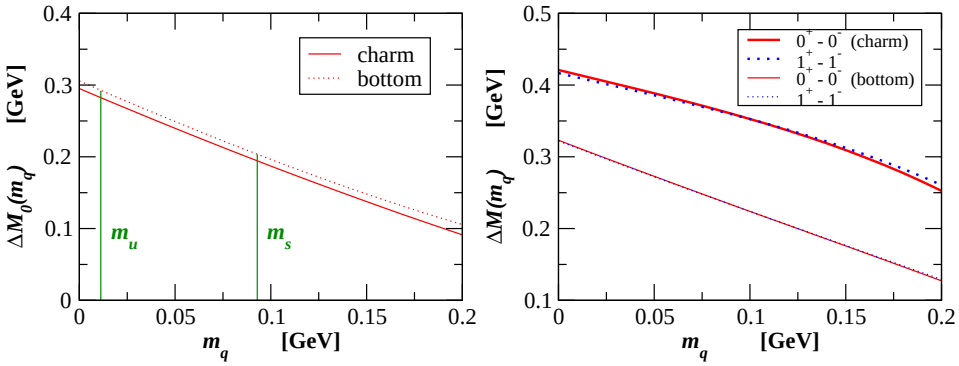

Figure 1: Plots of the mass gap between two spin multiplets. Light quark mass dependence is given. The horizontal axis is light quark mass m_q and the vertical axis is the mass gap. Both the heavy quark limit ΔM_0 (Left) and the one with $1/m_Q$ corrections ΔM(Right) are given.

gap is essentially given by

$$\Delta M_0 = \Lambda_Q - m_q \tag{6}$$

Though the physical ground of this result is out of scope at present, Eq. (6) is serious, since it is very different from the one of an effective theory approach which gives the relation,

$$\Delta M_0 = g_\pi \left(\langle \sigma \rangle + m_q \right). \tag{7}$$

where g_π is the Yukawa coupling constant between the heavy meson and a chiral multiplet and is taken to be $g_\pi = 3.73$ in [8], and $\langle \sigma \rangle = f_\pi$. This expression is obtained in the heavy quark symmetric limit and should be compared with our Eq. (6). Instead of minus sign for the term m_q that we obtained, the authors of [5] obtained plus sign as shown in the above equation. The same result is obtained even if we use the nonlinear Σ model [8]. The result given by Eq. (6) is exact when $\mathcal{O}\left(1/m_Q\right)$ terms are neglected. As we will see later, since $1/m_Q$ corrections are nearly equal to each other for two spin doublets, the above equation (6) between two spin multiplets holds approximately even with $1/m_Q$ corrections.

The reason why the mass gap can be written like Eq. (5) or (6) is explained in our formulation. (See the details in Refs. [11] and [12].)

Table 1: Optimal values of parameters.

Params.	α_s^c	α_s^b	a (GeV^{-1})	b (GeV)
	0.261±0.001	0.393±0.003	1.939±0.002	0.0749±0.0020
	$m_{u,d}$ (GeV)	m_s (GeV)	m_c (GeV)	m_b (GeV)
	0.0112±0.0019	0.0929±0.0021	1.032±0.005	4.639±0.005
	# of data	# of parameter	total χ^2/d.o.f	
	18	8	107.55	

Table 2: Degenerate masses of model calculations and their mass gap between $0^+(1^+)$ and $0^-(1^-)$ for $n = 1$.

	$M_0(D)$	$M_0(D_s)$	$M_0(B)$	$M_0(B_s)$
$0^-/1^-$	1784	1900	5277	5394
$0^+/1^+$	2067	2095	5570	5598
$0^+(1^+) - 0^-(1^-)$	283	195	293	204

3 $1/m_Q$ Corrections

Next let us study the case when $1/m_Q$ corrections to the mass gap are taken into account. Part of the results is given in [15]. In Table 3, we give our numerical results in the cases of $n = 1$ and $n = 2$ (radial excitations). Values in brackets are taken from the experiments. Our values seem to agree with the experimental ones though the fit is not as good as the case for the absolute values of heavy meson masses. We assume the form of the mass gap with the $1/m_Q$ corrections as follows.

$$\Delta M = \Delta M_0 + \frac{c + d \cdot m_q}{m_Q}. \tag{8}$$

Using Eq.(4) for D and D_s mesons, i.e. $\Delta M_0 = g_0\Lambda_{\rm Q} - g_1 m_q = 295.1 - 1.080 m_q$, we obtain the values of the parameters c and d for D/D_s mesons given in Table 3, which are given by

$$c = 1.28 \times 10^5 \text{ MeV}^2, \quad d = 4.26 \times 10^2 \text{ MeV}. \tag{9}$$

The term c/m_Q lifts the constant $g_0\Lambda_Q$ about 100 MeV and the term d/m_Q gives deviation from -1 to the coefficient for m_q in the case of D/D_s.

Applying this formula, Eq. (8), to the case for B/B_s with $m_Q = m_b$, we obtain the mass gap as follows.

$$B(0^+) - B(0^-) \quad \approx \quad B(1^+) - B(1^-) \approx 322,$$

Table 3: Model calculations of the mass gap. Values in brackets are taken from the experiments. Units are MeV.

Mass gap ($n=1$)	$\Delta M(D)$	$\Delta M(D_s)$	$\Delta M(B)$	$\Delta M(B_s)$
$0^+ - 0^-$	414 (441)	358 (348)	322	239
$1^+ - 1^-$	410 (419)	357 (348)	320	242

$(n=2)$	$\Delta M(D)$	$\Delta M(D_s)$	$\Delta M(B)$	$\Delta M(B_s)$
$0^+ - 0^-$	308	274	206	160
$1^+ - 1^-$	350	327	216	171

$$B_s(0^+) - B_s(0^-) \quad \approx \quad B_s(1^+) - B_s(1^-) \approx 240 \quad \text{MeV}, \tag{10}$$

which should be compared with our model calculations, 321 and 241 MeV, in Table 3. Thus the linear dependence of the mass gap on m_q is also supported in the case where the $1/m_Q$ corrections are taken into account. The calculated m_q dependence of ΔM with $1/m_Q$ corrections is presented in Fig. 2, for $0 < m_q < 0.2$GeV.

4 Miscellaneous Phenomena

Global Flavor $SU(3)$ Recovery – Looking at the mass levels of 0^+ and 1^+ states for the D and D_s mesons, one finds that mass differences between D and D_s becomes smaller compared with those of the 0^- and 1^- states. This can be seen from Table 4 and was first discussed in Ref. [16] by Dmitrašinović. He claimed that considering D_{sJ} as a four-quark state, one can regard this phenomena as flavor $SU(3)$ recovery. However, in our interpretation, this is not so as we have seen that this is caused by the mass gap dependency on a light quark mass, m_q, as shown in Fig. 1. That is, when the mass of D meson is elevated largely from the $0^-/1^-$ state to the $0^+/1^+$ state, the mass of D_s meson is elevated by about 100 MeV smaller than that of $0^-/1^-$ as one can see from Fig. 1. In our interpretation, the $SU(3)$ is not recovered since the light quark masses of $m_u = m_d$ and m_s do not change their magnitudes when the transition from $0^-/1^-$ to $0^+/1^+$ occurs, and their values remain to be $m_{u(d)} = 11.2$ MeV and $m_s = 92.9$ MeV, respectively, as presented in Table 1.

Mass Gap of Heavy Baryons – When we apply our formula to the heavy-light baryons which include two heavy quarks, (ccs), (ccu), (bcs), (bcu), (bbs),

Table 4: D/D_s meson mass spectra for both the calculated and experimentally observed ones. Units are MeV.

$^{2s+1}L_J(J^P)$	$M_{\rm calc}(D)$	$M_{\rm obs}(D)$	$M_{\rm calc}(D_s)$	$M_{\rm obs}(D_s)$
$^1S_0(0^-)$	1869	1867	1967	1969
$^3S_1(1^-)$	2011	2008	2110	2112
$^3P_0(0^+)$	2283	2308	2325	2317
$"^3P_1"(1^+)$	2421	2427	2467	2460

Table 5: B/B_s meson mass spectra for both the calculated and experimentally observed ones. Units are MeV.

$^{2s+1}L_J(J^P)$	$M_{\rm calc}(B)$	$M_{\rm obs}(B)$	$M_{\rm calc}(B_s)$	$M_{\rm obs}(B_s)$
$^1S_0(0^-)$	5270	5279	5378	5369
$^3S_1(1^-)$	5329	5325	5440	–
$^3P_0(0^+)$	5592	–	5617	–
$"^3P_1"(1^+)$	5649	–	5682	–

and (bbu), mass gaps between two pairs of baryons, like (ccs) and (ccu), will be given by Eq. (6) in the heavy quark symmetric limit and by Eq. (8) with $1/m_Q$ corrections where we have to replace m_Q with $m_{Q_1} + m_{Q_2}$. Here the isospin symmetry is respected since in our model $m_u = m_d$. This speculation is legitimized since QQ pair can be considered to be 3^* expression in the color $SU(3)$ space so that the baryon like QQq can be regarded as a heavy-light meson and our arguments expanded in this paper can be applied [17, 18].

References

1. BaBar Collaboration, B. Aubert *et al.*, Phys. Rev. Lett. **90**, 242001 (2003).
2. CLEO Collaboration, D. Besson *et al.*, Phys. Rev. D **68**, 032002 (2003);
3. Belle Collaboration, P. Krokovny *et al.*, Phys. Rev. Lett. **91**, 262002 (2003); Y. Mikami *et al.*, Phys. Rev. Lett. **92**, 012002 (2004).
4. M. A. Nowak *et al.*, Phys. Rev. D **48**, 4370 (1993).
5. W. A. Bardeen *et al.*, Phys. Rev. D **49**, 409 (1994).
6. D. Ebert *et al.*, Nucl. Phys. B **434**, 619 (1995); Phys. Lett. B **388**, 154 (1996).

7. A. Deandrea *et al.*, Phys. Rev. D **58**, 034004 (1998).
8. W. A. Bardeen *et al.*, Phys. Rev. D **68**, 054024 (2003).
9. M. Harada *et al.*, Phys. Rev. D **70**, 074002 (2004).
10. Belle Collaboration, K. Abe *et al.*, Phys. Rev. D **69**, 112002 (2004).
11. T. Matsuki *et al.*, hep-ph/0710.0325, to be published in Phys. Lett. B.
12. T. Matsuki *et al.*, Phys. Rev. D **56**, 5646 (1997).
13. T. Matsuki *et al.*, Phys. Lett. B **606**, 329 (2005). hep-ph/0408326.
14. T. Matsuki *et al.*, Prog. Theor. Phys. **117**, 1077 (2007).
15. T. Matsuki *et al.*, Eur. Phys. J. C **31**, 701 (2007).
16. V. Dmitrašinović, Phys. Rev. Lett. **94**, 162002 (2005).
17. M. Savage *et al.*, Phys. Lett. B **248**, 177 (1990).
18. T. Ito *et al.*, Z. Phys. C **59**, 57 (1993).

Frascati Physics Series Vol. XLVI (2007), pp. 1063
HADRON07: XII Int. Conf. on Hadron Spectroscopy – Frascati, October 8-13, 2007
Heavy Meson Spectroscopy

STUDY OF X(3872) FROM B_c DECAYS

Cai-Dian Lu
University of Massachusetts

Written contribution not received

Frascati Physics Series Vol. XLVI (2007), pp. 1065–1072
HADRON07: XII Int. Conf. on Hadron Spectroscopy – Frascati, October 8-13, 2007
Heavy Meson Spectroscopy

BARYONS AND MESONS WITH BEAUTY AND CHARM

Gary R. Goldstein
Tufts University, Medford, MA 02155 USA
Kameshwar C. Wali
Syracuse University, Syracuse, NY 13244-1130 USA

Abstract

Recent experimental findings of several mesons and baryons with *beauty* and *charm* as flavors remind us of the days when strangeness was discovered, and how its inclusion led to SU(3)-flavor symmetry with enormous success in the classification of the "proliferated" states into SU(3) multiplets. In this talk, we venture into the past and, applying the same techniques, predict some new *beauty*- and *charm*- flavored hadrons. If these new states are confirmed experimentally, it may provide a useful phenomenological model for classifying numerous states that are found to be in the PDG data.

1 Introduction

Several dedicated accelerators have been exploring the spectrum of *beauty* or *bottom* and *charm* hadrons over the last several years. There have been new

states discovered at the Fermilab Tevatron as well. This conference has presented exciting data on new beauty and charm states. Particularly interesting and puzzling are the sightings of new neutral *quarkonium* states. In some instances, the continued *absence* of pseudoscalar quarkonium states is notable. Baryons were covered also, in several presentations, and summarized by K. Seth [1]. Some of these new states were long anticipated. Some are unexpected and not yet understood. There are still unanswered questions about these states.

In the following we will present some new ideas about grouping this plethora of charm and beauty hadrons, along the lines of the original SU(3) of flavor. We will choose new flavor groups for charm and beauty, determine the mass spectra for some of the surmised group representations, investigate mixing and propose a U-spin approach to the SU3)$_{charm}$ sector.

2 Conventional SU(3)$_{flavor}$ Review

It is well known that Gell-Mann's and Ne'eman's eightfold way [2] had immense success in classifiying the then known mesons and baryons into SU(3) octets and decouplets. had immense success. First order perturbation in explicit symmetry breaking, surprising at first sight because of large mass differences, led to dramatic predictions such as the existence of the pseudoscalar meson η and the strange baryon Ω. Combined with Cabibbo's explanation of the weak decays in terms of a mixing angle, and numerous other successes, this led to the quark model and quantum chromodynamics as the theory of strong interactions.

The subsequent discoveries of baryons and mesons having flavors other than strangeness (charm, beauty and top) raises an interesting, hypothetical question: to what extent the success of broken SU(3) flavor symmetry stretches beyond the strange quark mass? With this in mind, we investigate the predictions of SU(3) flavor symmetries with *beauty* and *charm* instead of *strangeness* as the heavy flavor. We use the Gell-Mann-Okubo mass formulas to relate the masses and predict new states to be discovered.

The generic mass formulas in the case of strange baryons and mesons based on an explicit symmetry breaking term that transforms like an **octet** are as follows:

Baryons:

$$3M_\Lambda + M_\Sigma = 2(M_N + M_\Xi) \tag{1}$$

Mesons(pseudoscalar):

$$3m_{\eta_8}^2 + m_\pi^2 = 4m_K^2 \tag{2}$$

and similarly for the vectors, $\omega_8, \rho, K*$.

The spin 3/2 decouplet members $(N^*, \Sigma^*, \Xi^*, \Omega)$ obey an equal spacing rule.

Also, in our analysis, we need the standard single-octet mixing angle. In the case of the generic pseudoscalar octet, the singlet and octet states are governed by the equations;

$$\begin{aligned} |\eta\rangle &= |\eta_8\rangle cos\theta + |\eta_1\rangle sin\theta \\ |\eta'\rangle &= -|\eta_8\rangle sin\theta + |\eta_1\rangle cos\theta \end{aligned} \tag{3}$$

On the other hand, the physical masses are related by the equations,

$$\begin{aligned} M_{\eta_8} &= M_\eta cos^2(\theta) + M_{\eta'} sin^2(\theta), \\ M_{\eta_1} &= M_\eta sin^2(\theta) + M_{\eta'} cos^2(\theta) \end{aligned} \tag{4}$$

Recall how these mass breaking and mixing *ansätze* are applied in the ordinary octet/singlet pseudoscalar mesons. The GMO formula for mesons, Eq. 2, gives M(η_8)= 566.7 MeV. Then Eq. 4 can be solved to yield θ=-12.5° and M(η_1) = 938.6 MeV . There are other approaches to obtaining the mixing angle, particularly through comparison of η and π^0 into $\gamma\gamma$ decays. We will keep the value here, for consistency with the following applications of mixing and symmetry breaking. In recent years there have been efforts to determine the magnitude of mixing of gluonic degrees of freedom into the canonical quark mixing. At this conference evidence was presented that the gluonic modes played an insignificant role in the development of the η, η' mixing [3]. This will guide our choices below.

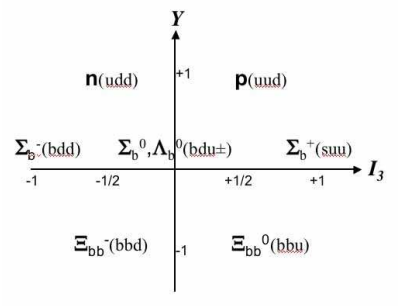

Figure 1: *Spin* $\frac{1}{2}$ *baryon octet representation of* $SU(3)_B$.

3 Mesons with Beauty

We now posit a new symmetry, $\mathrm{SU}(3)_B$, in which the conventional assignments of flavor are altered by replacing the *s-flavor* by *b-flavor*. Then for the meson representations as shown in Fig. 2, $B^{\pm}$, B^0 and $\bar{B}^0$ are the natural counterparts to the $K^{\pm}$, K^0 and $\bar{K}^0$, forming iso-doublet components of an octet along with $\pi^{\pm}$ and η_B, η'_B. We apply this to the pseudoscalars.

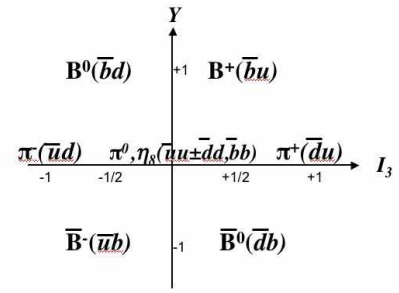

Figure 2: *Pseudoscalar meson octet representation of* $SU(3)_B$.

From Particle Data Group listings [4] the masses are

$$M(B^{\pm}) = 5279 \pm 0.5\,\mathrm{MeV}$$
$$M(B^{0}) = 5279 \pm 0.5\,\mathrm{MeV}$$
$$M(\eta'_B) = 9300 \pm 20\,\mathrm{MeV} \tag{5}$$

Note that we choose the unconfirmed 9300 state to be the η'_B. This is in the vicinity of the expected state, although it has not been settled upon experimentally [5]. We would expect a lower mass state to contain the u and d flavors in this octet. Using these values and the GMO formula of Eq. 2, we obtain

$$M(\eta_{B8}) = 6095.1\,\mathrm{MeV}. \tag{6}$$

Now from the masses of η_{B8} and our assumed η'_B, along with the pseudoscalar mixing angle we determine the lower mass physical η_B,

$$M(\eta_B) = 5938\,\mathrm{MeV} \text{ and } \mathrm{M}(\eta_{\mathrm{B1}}) = 9142\,\mathrm{MeV}. \tag{7}$$

Note that if we let the η'_B mass go to 9400, just 60 MeV below the Υ, the η_B drops by only 5 MeV. The η_B predicted should be observable; a neutral $J^{PC} = 0^{-+}$ with significant hidden *beauty* at a mass well below the Υ. Given the admixture of hidden u and d flavors there are many open decay channels, so decay width will be very broad. Its production via $\Upsilon \to \gamma + \eta_B$ should be quite striking.

We will not apply the symmetry to the vector mesons. There the mixing angle for the usual flavor SU(3) octet is quite close to the ideal value, for which the ϕ is purely a hidden strange state ($\bar{s}s$), satisfying the Zweig rule for its decays. This is true for the ground state charmonium and bottomonium vector mesons as well.

4 Baryons with Beauty

The following baryonic states have been experimentally established:
Spin $\frac{1}{2}$ b-Baryons:
Λ_b^0(5620 MeV); Σ_b^-(5816 MeV); Σ_b^+(5808 MeV)
Spin $\frac{3}{2}$ b-Baryons:
Σ_b*(5829 MeV); $\Sigma_b^0 - \Delta = 4597$ MeV.
Again we replace *s-flavor* with *b-flavor* to form SU(3)$_B$. Using the GMO linear

formula Eq. 1 (with N as the member of the Octet), and using the values for $\Lambda_b^0(5620)$ and the average of $\Sigma_b^-(5816$ MeV); $\Sigma_b^+(5808$ MeV) we find, $M_{\Xi_{bb}}^{0,-} =$ 10,400 MeV.

Using the decuplet equal spacing rule (N* or Δ as the member) for the spin 3/2 representation, we predict the masses of the other two members, $M(\Xi_{bb}^*)$=10,426 MeV and $M(\Omega_{bbb})$=15,023 MeV. These predictions await experimental discovery of these multiple beauty states, perhaps at the Tevatron.

5 Charm and SU(3) Multiplets

The above $SU(3)_B$ multiplets were obtained by substituting the $b-$flavor for the $s-$flavor. What about the $c-$flavor, with associated charge $+2/3$? It makes some sense to replace $u-$flavor by *charm* to form $SU(3)_C$. Then, however, the normal octet assignments for the mesons would involve large mass breaking for equal hypercharge Y states, *i.e.* fixed "I-spin" states. On the other hand, we know that there is smaller splitting among equal charm states. This suggests that the octet for (c,d,s) flavors be a "U-spin" octet. The states are assigned with charge on the vertical axis and U_3 on the horizontal axis, as indicated by flavor labels in Fig. 3 for pseudoscalars.

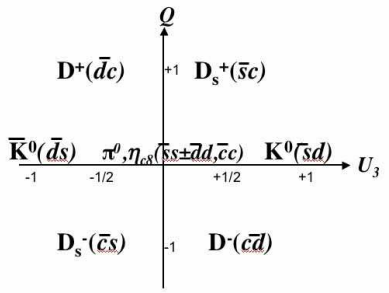

Figure 3: *U-spin pseudoscalar meson octet representation of* $SU(3)_c$.

The masses of these pseudoscalars are:

$$M(D^+[\bar{d}c]) = 1869\text{MeV} \quad \text{M}(\text{D}_\text{s}^+[\bar{\text{s}}\text{c}]) = 1968\text{MeV}$$
$$M(\bar{K}^0[\bar{d}s]) = 498\text{MeV} = \text{M}(\text{K}^0[\bar{\text{s}}\text{d}]). \tag{8}$$

Taking the average for D^+ and D_s^+ and applying the GMO formula Eq. 2, we obtain an η_{c8} mass of 2197.1 MeV. What about the physical η states? There is a signal at 2100 MeV [4] that we can associate with the lower mass state η_c (not to be confused with the state at 2980 MeV). Then with the same pseudoscalar mixing angle of 12.5°, we obtain high mass states

$$M(\eta_c') = 4171\,\text{MeV and M}(\eta_{c1}) = 4074\,\text{MeV}. \tag{9}$$

It is worth noting that for a somewhat larger mixing angle of 19.4° the η_c' would drop down to 2980 MeV, where the known charmonium pseudoscalar lies. But the anchor here remains the tentative η_c at 2100 MeV. If this state is established to be a *bone fide* 0^{-+}, it will be a state with significant hidden charm.

Charmed baryons in this $\text{SU}(3)_C$ scheme fall into octets and anti-decuplets. We will not deal with the decuplet, since there are very few established $\frac{3}{2}^+$ charmed baryons. For the octet of Fig. 4, we can use the mass breaking as for the mesons. The U-spin multiplets are preserved, although within each U-spin multiplet there is some breaking, albeit smaller than the breaking from one charm level to the next. The $\Omega_{cc}(scc)^+$ has not been reported, but there is a signal for $\Xi_{cc}(dcc)^+$ at 3519 GeV. This can be considered as the "anchor" state for the mass breaking. Using this mass along with $M(\Sigma_c^0) = 2454$ GeV, $M(\Omega_c^0) = 2698$ GeV and two states $M(\Xi_c^0) = 2471$ GeV and 2578 GeV, we evaluate the GMO formula to obtain the Ω_{cc}^+ mass at 3953 GeV. This puts the charm 2 state within reach, experimentally.

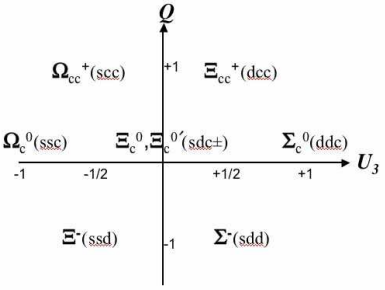

Figure 4: *U-spin and Spin* $\frac{1}{2}$ *baryon octet representation of* $SU(3)_b$.

Finally, in the list of tentative meson and baryon states [4] there are other possible candidates for our "anchor" states. In conventional quark model assignments these intermediate mass states fall through the cracks. They may very well be evidence of residual SU(3) symmetries that codify mass breaking more readily than the conventional view. This would not invalidate the conventional non-relativistic quark models, based on QCD expectations, and their extensive agreements with data. Nor would the existence of intermediate mass states demonstrate the correctness of the $SU(3)_{flavor}$ that we considered here. However the $SU(3)_{B\,\mathrm{or}\,C}$ would provide a useful phenomenological model of mass breaking among the heavy flavor hadrons.

In this talk we have concentrated on the mass spectrum [6]. We could extend our analysis to include decays, which will yield some new relations based on our novel $SU(3)_{flavor}$ assignments. This is work for the future.

6 Acknowledgements

We appreciate the suggestions of Sheldon Stone. This work is supported in part by funds provided by the U.S. Department of Energy (D.O.E.); G.R.G. #DE-FG02-92ER40702; and K.C.W. #DE-FG02-85ER402.

References

1. K. Seth summary talk, "Hadron07", Frascati 2007.
2. M. Gell-Mann and Y.Ne'eman, "The Eightfold Way", Benjamin, N.Y. (1964), and references therein.
3. R. Escribano, "'On the Gluon Content of the η and η' mesons, presentation, Hadron07.
4. W.-M. Yao, *et al.*, Particle Data Group, "Review of Particle Physics", Jour. of Phys. **G 33**, 1 (2006).
5. T.K. Pedlar, "Recent Results in Bottomonium Spectroscopy", arXiv:hep-ex/0702011.
6. G.R. Goldstein and K.C. Wali, arXiv:hep-ph/0705.4525, for more details.

Frascati Physics Series Vol. XLVI (2007), pp. 1073–1078
HADRON07: XII Int. Conf. on Hadron Spectroscopy – Frascati, October 8-13, 2007
Heavy Meson Spectroscopy

FEASIBILITY STUDY FOR THE B_C MESON AT CMS

Aafke C. Kraan
INFN Pisa, Polo Fibonacci Largo B. Pontecorvo, 3 - 56127 Pisa, Italy

Abstract

In this talk the prospects to measure the mass and lifetime of the B_c meson at CMS are discussed. Using the channel $B_c \to J/\psi\pi$ 120 B_c events are expected to be selected in the first 1 fb^{-1} of data. The expected accuracy of the mass measurement is 2.0(stat.)$\pm$14.9(syst.) MeV/c^2, and the accuracy on the lifetime is 0.044(stat.) $\pm$ 0.010(syst.) ps.

1 B-physics at CMS

The Compact Muon Solenoid (CMS) experiment is scheduled to start data taking in 2008 at the Large Hadron Collider (LHC) at CERN, where two 7 TeV proton beams will be collided head-on, resulting in collisions at a centre-of-mass energy of 14 TeV. The high luminosity data samples expected to be collected at CMS and the high energy reach will offer entirely new opportunities for B-physics studies. Measurements for B-physics in CMS will generally rely on

B-hadron decays into final states containing a J/ψ-meson, leading to two muons for which dedicated triggers exist. The most relevant subdetectors in CMS for many B-physics studies are the silicon tracker, providing momentum and vertex measurements, and the muon chambers, for muon identification and momentum measurements, both having a large acceptance ($|\eta| < 2.5$) and high precision.

2 The B_c-meson

The B_c meson is the ground state of a charm and bottom quark-anti-quark pair: $B_c^+ = \bar{b}c$ or $B_c^- = b\bar{c}$ [1]. Unlike heavy-light quark systems as B_u, B_d or B_s, the dynamics of the B_c meson can be treated in a non-relativistic expansion just like the heavy quarkonia $c\bar{c}$ and $b\bar{b}$. At the same time, and contrary to the $c\bar{c}$ and $b\bar{b}$ ground states, the B_c meson carries flavour, leading to different heavy quark dynamics. Given the fact that no top-mesons exist, it is the only heavy-heavy quark system carrying flavour, making it a unique system.

2.1 Theory predictions

B_c production Many uncertainties exist in calculations for the B_c production cross section at the LHC [2, 3]. Just like production of $b\bar{b}$ and $c\bar{c}$, B_c production involves hard perturbative QCD (for the hard production of a $c\bar{c}$ and $b\bar{b}$ pair), and soft non-perturbative QCD (to describe the soft non-relativistic binding of the heavy quarks into a colour singlet bound state). Since the production involves the creation of both a $b\bar{b}$ and a $c\bar{c}$-pair, the production rate is predicted to be smaller ($\sim 10^{-1}$) than that for bottomonia and charmonia, where only one heavy quark pair is needed. The production cross section is also smaller ($\sim 10^{-3}$) than that of the lighter B-mesons like B_u, B_d and B_s because the creation of a $c\bar{c}$-pairs is suppressed in comparison with that of light quark pairs. The B_c production cross section at LHC is at least an order of magnitude larger than that at the Tevatron.

B_c mass Different theoretical predictions exist for the mass of the B_c meson. Traditionally non-relativistic potential models for heavy quark bound states were used to predict the mass of the B_c meson, giving values in the range 6.2–6.4 GeV [4] with large uncertainties. More recent NNLO calculations [5] predict the mass to be around 6.3 GeV with uncertainties of about 20 MeV. Even

smaller uncertainties are obtained by calculations based on lattice QCD [6], with unquenched lattice calculations predicting a value of 6.304 ± 0.012 GeV.

$\mathbf{B_c}$ decay The B_c-meson being the ground state, it decays via weak interactions only. As a consequence it has a much longer lifetime than the $b\bar{b}$ and $c\bar{c}$ states. On the other hand, since either quarks can participate in the decay, the B_c meson has a shorter lifetime than the lighter B-mesons. There are three classes of B_c^+ decays:

1. the $\bar{b}$ quark decays weakly while the c-quark is spectator,
2. the c-quark decays weakly while the $\bar{b}$-quark is spectator,
3. the annihilation channel $B_c^+ \to \ell\nu_\ell / c\bar{s}/u\bar{s}$. with $\ell = e, \mu, \tau$

The first class leads to final states like $J/\psi\ell\nu_\ell$ or $J/\psi\pi$. Since the semileptonic mode is not fully reconstructable due to the missing neutrino, the hadronic mode is more suitable for a precise mass measurement, and is used in this analysis. The expected branching ratio for $B_c \to J/\psi\pi$ is 13–16% [8].

The second and third class both lead to final states which are experimentally much harder to detect.

The predicted branching ratios [7, 8] for the first class of decays are 19.6–25.0%, for the second class 64.3–72.0% and for the third 8.4–9.9%, all predictions agreeing within errors. For the B_c lifetime predictions range from 0.4–0.7, the most accurate prediction being $\tau[B_c^+] = 0.48 \pm 0.05$ ps [7].

3 Current experimental measurements

The first observation of the B_c meson was made by CDF in Run 1 [9] in the channel $B_c \to J/\psi\ell\nu_\ell$. Based on 20 signal events the B_c mass was measured to be $6.40 \pm 0.39 \pm 0.13$ GeV/c^2, and the lifetime $0.46^{+0.18}_{-0.16}$(stat) ± 0.03(syst) ps. The best mass measurement has been performed recently by CDF [11] in the $B_c \to J/\psi\pi$ channel; using 2.2 pb^{-1} of data the B_c mass was found to be 6274.1 ± 3.2(stat.)± 2.6(syst.)MeV/c^2, with 80 signal events. The best measurement for the B_c lifetime was recently reported by D0 [12], based on 1.4 fb^{-1} of data the lifetime was found to be $0.444^{+0.039}_{-0.036}$(stat)$^{+0.039}_{-0.034}$(syst) ps.

4 Event generation

Details of the analysis described below can be found elsewhere [13], and only a short summary is given here. The BCVEGPY generator [2] is used to generate B_c events, followed by hadronisation with PYTHIA. Fig.**??**(left) shows the differential cross section as function of the P_T of the B_c meson. At generator level the B_c meson is required to have $P_T > 10$ GeV and $|\eta < 2.0|$, the muons must have $P_T > 4$ GeV and $|\eta| < 2.2$, and the pion must have $P_T > 2$ GeV and $|\eta| < 2.4$. All J/ψ's were forced to decay into $\mu^+\mu^-$, the branching ratio of which is 5.93%. In total 5.2×10^4 events are generated corresponding to 29.2 fb^{-1}.

Generated backgrounds processes include events with light B-hadrons decays, prompt J/ψ's, $b\bar{b} \to \mu^+\mu^- X$, $c\bar{c} \to \mu^+\mu^- X$, W+jets, Z+jets and general QCD processes.

5 Event selection

Signal events are characterised by two muons from the J/ψ and a charged pion track, all coming from a displaced vertex due to the long-lived B_c. No trigger study has been performed, but the selection efficiency of the trigger requirements and offline reconstruction is expected to be similar. The offline selection is as follows. First J/ψ candidates are selected by requiring 2 muons with $P_T > 4$ GeV and $|\eta| < 2.2$ with opposite charge, from the same vertex, and having an invariant mass between 3.0 and 3.2 GeV. Secondly, pion candidates are selected by requiring a third track coming from the same vertex as the 2 muons with $P_T > 2$ GeV and $|\eta| < 2.4$, but not being a lepton. To reject prompt J/ψ background, the events are required to have a proper decay length $L_{xy}^{PDL} > 60\mu$m, a significance $L_{xy}/\sigma_{xy} > 2.5$ and a small opening angle θ between the vector from primary to secondary vertex and the momentum vector of the reconstructed B_c: $\cos\theta > 0.8$. The invariant mass distribution is given in Fig.**??** (right). Finally the invariant mass of B_c candidates is required to be between 6.25 and 6.55 GeV. The selection efficiency for B_c events is 6.9%. In 1 fb^{-1} 120 ± 11 signal events are expected, and 2.6 ± 0.4 background events, dominated by light B-mesons and QCD background.

6 Kinematic fit

Using a kinematic fit the 2 muon tracks were constrained to have an invariant mass equal to that of the J/ψ (3.096 GeV), and the third track of the pion was imposed to come from the same same vertex as the two muon tracks. Fig. 1(left)

shows the resulting invariant mass distribution. While the input mass in the Monte Carlo events was 6400 MeV, the fitted mass value is 6402 ± 2 MeV, and the width of the peak is 22 MeV. To extract the B_c lifetime a binned likelihood fit was performed, resulting in $c\tau = 148.8 \pm 13.1 \mu$m while the input value was 150μm.

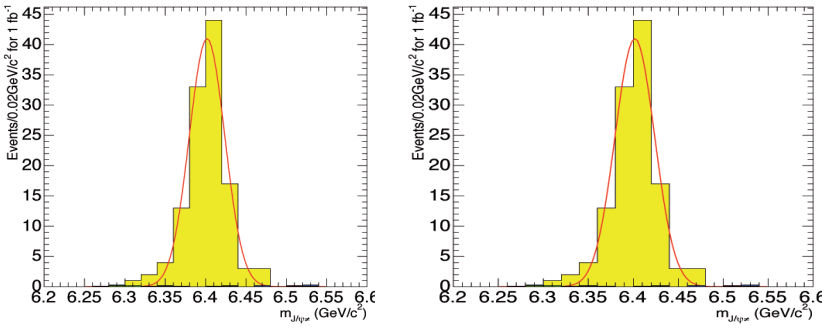

Figure 1: *Left: the invariant mass of the $J/\psi\pi$. Right: proper decay length distribution.*

7 Systematic errors

For the B_c mass the dominant systematic errors are the momentum scale uncertainty and the momentum resolution, resulting in a total systematic error of 14.9 MeV. Although these systematic sources also dominate in the CDF measurement [11], this is much larger than the 2.6 MeV quoted there. The reason is that the procedure to determine the error is very conservative, and it is based on a worst case scenario for a misaligned detector. Also, no control samples have been used so far. Only real data will allow for a realistic estimate of this kind of systematic errors, and with real data the $B^- \to J/\psi K^-$ control sample can be used as reference, expected to decrease the systematic errors significantly. For the lifetime the dominant contributions are the vertex uncertainty, theoretical uncertainties and the momentum resolution; the total systematic error being 3.0μm, representing again a highly conservative estimate.

8 Acknowledgements

Thanks to Urs Langenegger and Gigi Rolandi for comments on this manuscript.

References

1. Charge conjugation is implied everywhere.
2. C.-H. Chang *etal*, Eur. Phys. J. **C38**, 267 (2004)
3. A.V. Berezhnoi *etal*, Phys. Atom. Nucl.**60**, 1729 (1997); J.P. Gouz *etal*, Phys. Atom. Nucl. **67**, 1559 (2004)
4. E.J. Eichten and C. Quigg, Phys. Rev. **D49**, 5845 (1994); S.S. Gershtein, V.V. Kiselev *etal*, Phys. Rev. **D**51, 3613 (1995), W. Kwong and J. Rosner, Phys. Rev. **D**44, 212 (1991)
5. See e.g. N. Brambilla *etal*, Phys. Rev. **D65**, 03400 (2002)
6. H.P. Shanahan *etal*, Phys. Lett. **B453**, 289 (1999), I.F. Allison *etal*, Phys. Rev. Lett. **94**, 172001 (2005)
7. See e.g. V.V. Kiselev, hep-ph/0211021
8. CERN Yellow Report, CERN-2005-005, hep-ph/0412158, p262 and refs.
9. CDF collaboration, Phys. Rev. Lett. **81**, 2432 (1998)
10. CDF collaboration, Phys. Rev. Lett. **96**, 082002 (2006)
11. CDF collaboration, public CDF-note 8004, July 2007
12. D0 collaboration, public D0-note 5524-CONF, October 2007
13. X.W. Meng, J.Q. Tao, G.M. Chen, CMS NOTE 2006/118

Frascati Physics Series Vol. XLVI (2007), pp. 1079
HADRON07: XII Int. Conf. on Hadron Spectroscopy – Frascati, October 8-13, 2007
Heavy Meson Spectroscopy

DOUBLE FLAVOR VIOLATING TOP QUARK DECAYS $t \to \mu_i \tau^{\pm} \mu^{\mp}$ IN EFFECTIVE THEORIES

C. Pagliarone
Universitá di Cassino and INFN di Pisa

Written contribution not received

HADRON STRUCTURE

Frascati Physics Series Vol. XLVI (2007), pp. 1083–1090
HADRON07: XII Int. Conf. on Hadron Spectroscopy – Frascati, October 8-13, 2007
Hadron Structure

MEASUREMENT OF THE $\gamma n(p) \to K^+\Sigma^-(p)$ AT JEFFERSON LAB

Sergio Anefalos Pereira
Laboratori Nazionali di Frascati-INFN
Via E. Fermi,40 -I 00044 Frascati (Roma), Italy

Abstract

A comprehensive study of the electromagnetic strangeness production has been undertaken at Thomas Jefferson National Accelerator Facility (Jefferson Lab). The preliminary analysis results of the measurement of the $\gamma n(p) \to K^+\Sigma^-(p)$ will be reported. These data were collected with CLAS detector using incident photon beam energy in the range from 0.8 to 3.6 GeV and a liquid-deuterium target.

1 Physical Motivation

The measurement of the spectrum of excited baryons and their decay amplitudes is very important to understand the nucleon structure. Of special interest is the search for "missing resonances" predicted by the SU(6)xO(3) symmetry of constituent quark model [1)], but not found experimentally.

The question is if some dynamical aspect of hadronic structure may act to restrict the quark models spectrum of states to something closer to what

has been already observed (for instance models using alternative symmetries predict fewer states [2]) or if these "missing resonances" decay preferably in other channel than π N, and so not well studied so far.

The PDG compilation [3] gives poorly-known $K\Lambda$ couplings for only five well-established resonances, and no $K\Sigma$ couplings for any resonance. The most representative model calculation of the KY photoproduction, the Kaon-MAID code [4], includes only three N^* states, the $S_{11}(1650)$, the $P_{11}(1710)$ and the $P_{13}(1720)$ for $K\Lambda$, and just the $S_{31}(1900)$ and the $P_{31}(1910)$ resonances for $K\Sigma$. Additional good quality photoproduction data of these channels is essential to see what additional resonance formation and decay information can be obtained.

For the $\gamma N \to KY$ reaction, there are six elementary amplitude: $\gamma n \to K^0\Lambda$, $\gamma n \to K^0\Sigma^0$, $\gamma n \to K^+\Sigma^-$, $\gamma p \to K^+\Lambda$, $\gamma p \to K^+\Sigma^0$, $\gamma p \to K^0\Sigma^+$. While there are total and differential cross section data for all γp reactions [5, 6, 7, 8], for the γn channels only differential cross section data for the $\gamma n \to K^+\Sigma^-$ channel, and in a limited energy and angular range [9], are available.

2 CLAS detector at Jefferson Lab

The CLAS detector in Hall B at Jefferson Lab [10] is designed to measure exclusive reactions with multi-particle final states. It is built around six superconducting coils producing a toroidal magnetic field, that naturally separate the detector into six sectors, each functioning as an independent magnetic spectrometer. Each sector is instrumented with 3 sets of multi-wire drift chambers for track reconstruction and one layer of scintillator counters (SC), covering the angular range from 8° to 140°, for time-of-flight measurements. The forward region ($8° \leq \theta \leq 45°$) contains gas-filled threshold Cerenkov counters and lead-scintillator sandwich-type electromagnetic calorimeters (EC) for particle identification. For two CLAS sectors the coverage of the electromagnetic calorimeters is extended up to polar angles of 70°. The Hall-B hosts also a tagger spectrometer with which is possible tag photons with energies in the range 20% - 95% of the electron energy and with a resolutions $\sim 0.1\%$.

The present data (g10 experiment) were collected during a two-month period in early 2004 using the CLAS detector and the Hall B photon tagging system. The incident electron beam energy was E_0=3.767 GeV, producing

tagged photons in the range from 0.8 to 3.6 GeV. The photon beam was directed onto a 24-cm long liquid-deuterium target. The trigger required two charged particles detected in coincidence with a tagged photon. The CLAS torus magnet was run at two settings, low field (2250 Amps) and high field (3375 Amps), each for about half of the run period. The low field setting has slightly better acceptance at forward angles, but worse momentum resolution. An integrated luminosity of about 30 pb^{-1} for each torus magnet configuration was collected here.

3 Analysis Procedure

In this exclusive measurement, K^+, π^- and n are detected by CLAS while the spectator proton is identified as missing particle. The diagram of the reaction is shown in Fig. 1. The Σ^- in the $\gamma n \to K^+\pi^- nX$ is identified calculating the invariant mass of pion and neutron, M($\pi^- n$). The key points of this channel are the correct identification of K^+ and neutron.

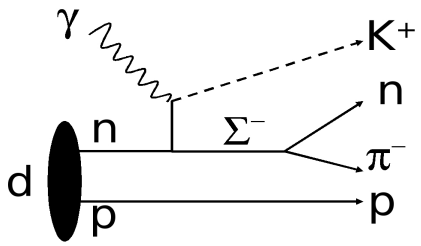

Figure 1: *The reaction diagram of the* $\gamma n(p) \to K^+\pi^- n(p)$ *channel.*

Charged-particle reconstruction requires both particle tracking and TOF. The tracking information is used to determine the particle momentum (p) and flight path and the TOF gives particle velocity (β) when combined with flight-path information. The momentum and velocity information are combined to give the particle mass. In order to correctly identify the K^+, several cuts are applied. Among the three detected particles, only the kaon is produced in the initial interaction (π^- and n are produced from Σ^- decay) so it should

be in time with the photon. Then a cut on the difference between the time obtained when the kaon is created and the time when the photon has interacted is applied. Another cut used is on the difference between the kaon β measured from TOF and the one calculated from momentum. Also a study on the kaon mass in function of the kaon momentum, k_p, has shown that for $k_p \leq 0.5$ GeV/c, the kaon mass peak is not clear. So kaons with momentum less than 0.5 GeV/c are rejected. The kaon β distribution versus the K^+ momentum before and after all cuts applied is shown in Fig. 2.

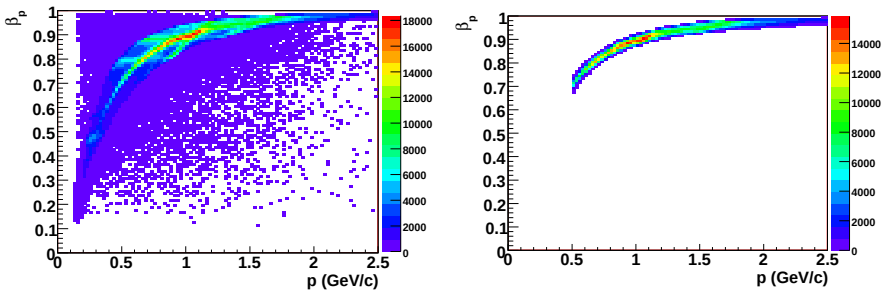

Figure 2: *The left plot shows the Kaon β distribution versus the Kaon momentum before cuts applied. The right plot shows the distribution after applying all the cuts described in the text.*

The missing particle is identified as $MM(K^+\pi^-n)$ in the reaction $\gamma n \rightarrow K^+\pi^-nX$. Because the proton doesn't participate to the reaction, a cut on the missing particle momentum, $p_{miss} \leq 0.25 GeV/c$, is then applied, as shown in Fig. 3. After K^+ selection and missing momentum cut, the Σ^- is identified as the $M(\pi^-n)$.

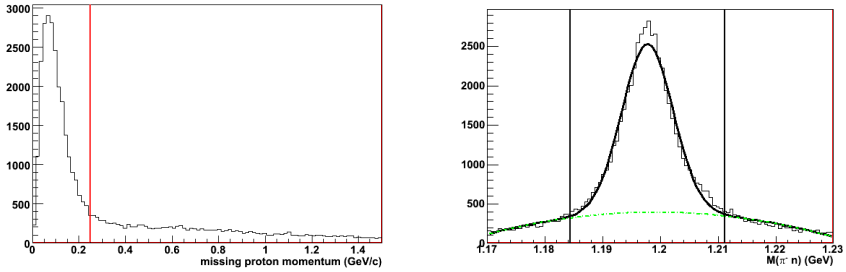

Figure 3: *The left plot shows the missing momentum distribution in* $\gamma n \rightarrow K^+\pi^- nX$. *The vertical line represents the missing momentum cut applied,* $p_{miss} \leq 0.25 GeV/c$. *The right plot shows the invariant mass of* $M(\pi^- n)$. *The Gaussian fit (black full curve) gives a mass of 1.198 GeV, which is in good agreement with PDG value (1.197 GeV). The second order polynomial (green dashed curve) fits the background. The two vertical lines represent the* 3σ *cut on the Gaussian fit.*

3.1 Background Subtraction

After all cuts are applied, the misidentified events under the peak must be subtracted. The background subtraction is done fitting the Σ^- invariant mass distributions, in 100 MeV E_γ bins from 1.1 to 3.6 GeV, with a Gaussian (black full curves) plus a second order polynomial (green dashed curves), as seen in Fig. 4. The Gaussian fits the peak and the polynomial fits the background. The horizontal lines are the 3σ cuts on the Gaussian fit. The real Σ^- events are defined as the number of events within 3σ cut and above the polynomial fit.

3.2 Preliminary Yield and Efficiency calculation

After background subtraction, the yield is extracted. Monte Carlo simulation is used to calculate the efficiency. The binning for the following results are 200 MeV in E_γ and 0.2 in K^+ CosΘ in the center-of-mass frame. The preliminary results of efficiency and extracted yield are shown in Fig. 5.

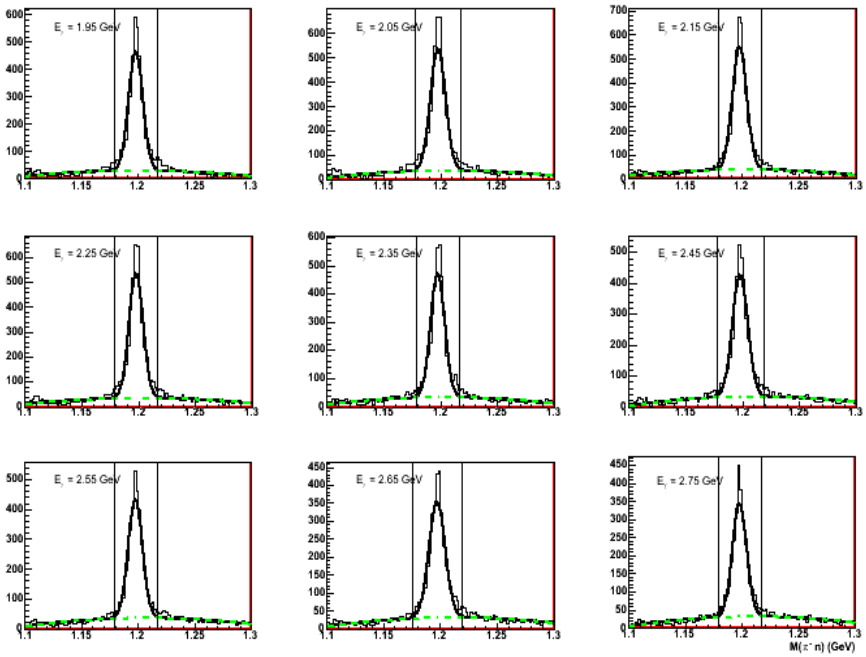

Figure 4: *The background subtraction is done fitting the Σ^- invariant mass distributions, in 100 MeV E_γ bins. Here, only 9 E_γ bins are shown (from 1.95 to 2.75 GeV). A Gaussian (black full curves) plus a second order polynomial (green dashed curves) are used to fit the peak and the background, respectively.*

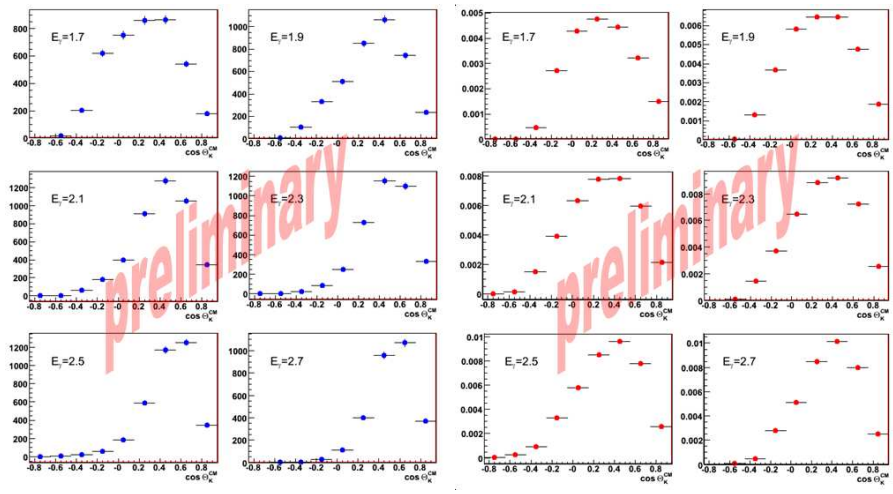

Figure 5: *The blue circles show the preliminary yield after background subtraction versus cosine of K^+ angle in the center-of-mass frame for six E_γ bins. The red circles show the efficiency, obtained from Monte Carlo calculation, versus cosine of K^+ angle in the center-of-mass frame.*

The normalized yield (corrected by efficiency) is shown in Fig. 6. The preliminary results are shown for twelve E_γ bins.

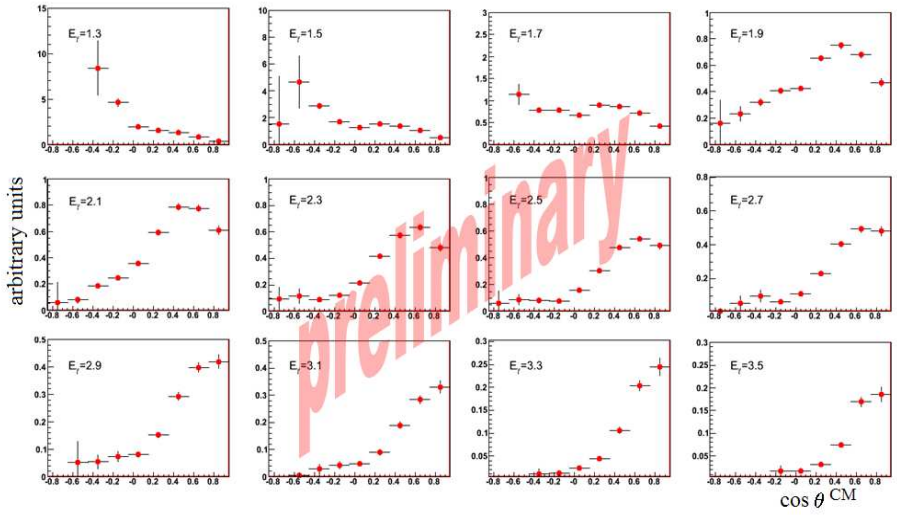

Figure 6: *The preliminary normalized yield are shown. The energy range basically covers all kinematic region from 1.2 to 3.6 GeV (the Σ^- production threshold is around 1.1 GeV).*

4 Summary

It is very important to investigate baryon resonances which decay into KY in the final state in order to study the lack of the predicted resonances. There are almost no experimental data on neutrons and the study of $\gamma n \to K + \Sigma^-$ reaction channel using the CLAS G10 data will provide a set of results in $\gamma - n$ interactions in a wide E_γ range from 1.1 to 3.6 GeV and angular range from 10 to 140 deg. in laboratory frame. The preliminary results has shown that the studied channel can be well identified and the yield corrected by the efficiency was extracted.

References

1. S. Capstick, Phys. Rev. D **34**, 2809 (1986).
2. R. E. Cutkosky and R. E. Hendrick, Phys. Rev. D **16**, 2902 (1977).
3. S. Eidelman *et al*, Phys. Lett. B **592**, 1 (2004).
4. T. Mart, C. Bennhold, H. Haberzettl and L. Tiator, "KaonMAID 2000" at www.kph.uni-mainz.de/MAID/kaon/kaonmaid.html.
5. R. Bradford *et al*, Phys. Rev. C **73**, 035202 (2006).
6. K.-H. Glander *et al*, Eur. Phys. J. A **19**, 251 (2004).
7. ABBHHM Collaboration, Phys. Rev. **175**, 1669 (1968).
8. C. Bennhold *et al*, Nucl. Phys. A **639**, 209c (1998).
9. H. Kohri *et al*, Phys. Rev. Lett. **97**, 082003 (2006).
10. B. A. Mecking *et al*, Nucl. Instr. and Meth. A **503**, 513 (2003)

Frascati Physics Series Vol. XLVI (2007), pp. 1091
HADRON07: XII Int. Conf. on Hadron Spectroscopy – Frascati, October 8-13, 2007
Hadron Structure

g8b EXPERIMENT AT JLAB: PHOTOPRODUCTION OF ϕ MESON

J. Salamanca
Idaho State University

Written contribution not received

Frascati Physics Series Vol. XLVI (2007), pp. 1093
HADRON07: XII Int. Conf. on Hadron Spectroscopy – Frascati, October 8-13, 2007
Hadron Structure

HADRON MODIFICATION IN NUCLEAR MATTER AT CLAS

C. Djalali
University of South Carolina

Written contribution not received

Frascati Physics Series Vol. XLVI (2007), pp. 1095–1100
HADRON07: XII Int. Conf. on Hadron Spectroscopy – Frascati, October 8-13, 2007
Hdron Structure

EXPERIMENTAL TEST OF THE HADRON STRUCTURE IN THE POLARISED BINARY *hadron − hadron* SCATTERING REACTIONS

A. I. Machavariani
High Energy Physics Institute of Tbilisi State University,
University str. 9, Tbilisi 380086, Georgia
Joint Institute for Nuclear Research,
Dubna, Moscow region 141980, Russia
Institute für Theoretische Physik
der Univesität Tübingen, Tübingen D-72076, Germany

Abstract

The sufficient dependence on the azimuthal angle ϕ of the binary hadron-hadron scattering amplitude is considered as a test of the structure of the scattering particles, because *the structureless particles* by the binary reactions are located on the same plane and consequently, the cross sections and polarisation observables of the *point-like* hadron-hadron binary scattering reactions are independent on the azimuthal angle ϕ.

Present theoretical description of the NN, πN, γN and other binary hadron-hadron scattering reactions is performed in the framework of the concept of the point-like particles, where any state of a hadron is constructed as a point-like object with definite mass, momenta and quantum numbers only. In particular the asymptotic particles in the quantum field theory and in the collision theory are considered as structureless objects which are completely

described by three-momenta, mass and quantum numbers. Afterwards the scattering amplitude and all of the observables are expressed via the mass, three-momenta and quantum numbers of asymptotic particles. The same is valid in the general field-theoretical formulations with the quark-gluon degrees of freedom [1, 2, 3, 4, 5, 6, 7], where hadrons are constructed as quark bound (or cluster) states and the asymptotic composed particle states satisfy the same conditions as the asymptotic states of the structureless (point-like) particles. *Moreover in the present experiments particles are also observed as point-like objects with definite momenta and quantum numbers.*

On the other hand nowadays hadrons are defined as quark-gluon clusters or bound states and the hadron-hadron interaction at the $1GeV$ energy region is determined as an interaction with overlapping of hadrons. This overlapping or contact interaction implies the essential contributions from the ingredient quark exchange. Therefore the intermediate states of the considered hadron interaction are constructed by the many-body $3q+3q \Longrightarrow 3q'+3q'$ interaction. This many body interaction can not be located in a single plane to the contrary with any binary reaction of the point-like objects. The cross section and polarisation observables of the binary hadron-hadron scattering reaction for the point-like hadrons are independent of the azimuthal angle ϕ, because the corresponding reaction for the two point-like objects is located on the single plane. Thus the nontrivial ϕ dependence of the binary hadron-hadron scattering amplitudes represents the model-independent kinematical test of the hadron structure. In order to demonstrate this let me consider the elastic NN scattering amplitude, where every nucleon is described via the definite mass, spin, isospin and four-momentum $q_p = (\sqrt{m_N^2 + \mathbf{q}_p{}^2}, \mathbf{q}_p)$. The most general NN scattering amplitude has a form [8, 9]

$$f(E,\theta,\phi) \equiv F(s,t,\phi) = a(E,\theta) + b(E,\theta)\Big(\mathbf{s_1}\cdot\mathbf{n}\Big)\Big(\mathbf{s_2}\cdot\mathbf{n}\Big)$$
$$+c(E,\theta)\Big(\mathbf{s_1}\cdot\mathbf{m}\Big)\Big(\mathbf{s_2}\cdot\mathbf{m}\Big)$$
$$+d(E,\theta)\Big(\mathbf{s_1}\cdot\mathbf{l}\Big)\Big(\mathbf{s_2}\cdot\mathbf{l}\Big) + e(E,\theta)\Big((\mathbf{s_1}+\mathbf{s_2})\cdot\mathbf{n}\Big) \qquad (1)$$

In this expression the dependence on the azimuthal angle ϕ is isolated via the dependence on the unit vector $\mathbf{n}$, where the mutually orthogonal unit vectors $\mathbf{n} = (\mathbf{p}'\times\mathbf{p})/|(\mathbf{p}'\times\mathbf{p})|$, $\mathbf{m} = (\mathbf{p}'-\mathbf{p})/|(\mathbf{p}'-\mathbf{p})|$; and $\mathbf{l} = (\mathbf{p}'+\mathbf{p})/|(\mathbf{p}'+\mathbf{p})|$

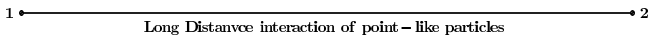

Figure 1: *A long-distance criteria of the point-like particles with weak interaction potential* $|V(1,2)| << M_1(M_2)$.

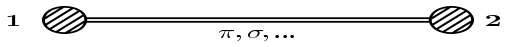

Figure 2: *Particle exchange interaction when* $|V(1,2)| \leq M_1(M_2)$.

forms the basis in the 3D momentum space and $\mathbf{p} = \mathbf{q}_1 = -\mathbf{q}_2$ and $\mathbf{p}' = \mathbf{q}'_1 = -\mathbf{q}'_2$ denote the three-momenta of the initial and final nucleons in the c.m. frame.

The NN scattering amplitude (1) determines all 24 polarisation observables via the amplitudes a, b, c, d, e which are depending on the NN energy E and the scattering angle θ (or on the Mandelstam variables s, t) only [8, 9, 10]. Thus the cross sections and polarisation observables of the point-like nucleons are independent on the azimuthal angle ϕ i.e. this binary NN scattering observables are degenerated over the the azimuthal angle ϕ.

An usual criteria of the point-like objects is so called long-distance condition of the interacting objects, when the interaction potential is much more smaller as the masses of these particles as it is depicted in Fig. 1. This condition was fulfilled for the low energy (nonrelativistic) NN scattering reaction [8], where the NN potential $V(1,2)$ is independent on the $\mathbf{n} \cdot \sigma$ and $|V(1,2)| << m_N$.

In the intermediate energy region ($E_{NN} \sim 0.5GeV$) the NN potential is comparable with the mass of nucleon m_N and $V_{NN} \sim m_N$. Therefore in this energy region nucleon is not more a point-like object (Fig. 2). The structure

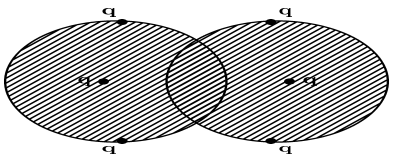

Figure 3: *Overlapping, or contact, or quark exchange interaction of two nucleons, where instead of NN potential appears the $6q$ or more complicated interaction potential between fractals of nucleons.*

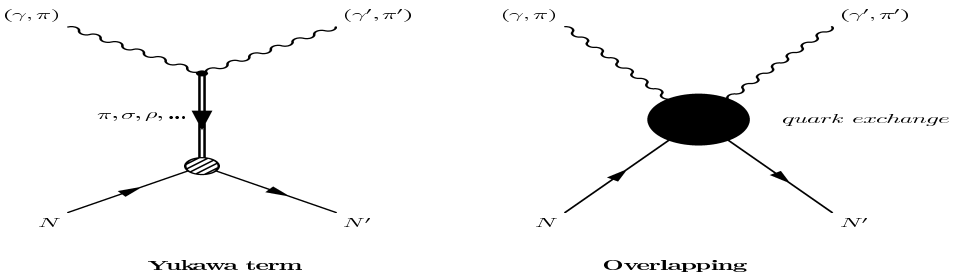

[1]

Figure 4: *The off shell particle exchange and overlapping, or contact, or quark exchange interaction diagrams of two nucleons.*

effects of nucleons in the NN reactions are essential according to the accepted interpretation in the energy region $E \sim m_N \sim 1GeV$), where the contact or overlapping or quark exchange contributions are comparable or larger as the mass of nucleon (Fig. 3). A construction of the NN potential which is depending on the $\mathbf{n} \cdot \sigma$ variables will be considered in our forthcoming papers.

The unified field-theoretical formulation of the hadron-hadron interaction problems with and without quark degrees of freedom, performed in the framework of the $3D$ time-ordered approach [5, 6, 7], allows to separate the meson exchange contributions from the (Fig. 4A) from the quark-gluon exchange

diagrams (Fig. 4B).

The overlapping, or contact, or quark exchange interactions (Fig. 3 and 4B) requires to consider hadrons as a composite particles. In this case in the intermediate states one has to take into account the strong interaction of the many-body $(6q, ...)$ systems which must destroy the scattering-plane degeneracy of the binary hadron-hadron interactions, i.e. the NN amplitude obtains a nontrivial dependence on the azimuthal ϕ angle. The general dependence on ϕ of the NN scattering amplitude implies the following form of the NN amplitude

$$f_{composed}(E,\theta,\phi) = a(E,\theta,\phi) + b(E,\theta,\phi)\Big(\mathbf{s_1}\cdot\mathbf{n}\Big)\Big(\mathbf{s_2}\cdot\mathbf{n}\Big)$$
$$+c(E,\theta,\phi)\Big(\mathbf{s_1}\cdot\mathbf{m}\Big)\Big(\mathbf{s_2}\cdot\mathbf{m}\Big) + d(E,\theta,\phi)\Big(\mathbf{s_1}\cdot\mathbf{l}\Big)\Big(\mathbf{s_2}\cdot\mathbf{l}\Big)$$
$$+e(E,\theta,\phi)\Big((\mathbf{s_1}+\mathbf{s_2})\cdot\mathbf{n}\Big)... \qquad (2)$$

The expression (2) predicts an essential dependence on ϕ of the NN polarisation observables. The quark-gluon exchange terms change the spin-orientation of the interacted particles, Therefore the essential ϕ-dependence generates the dependence over the hadron size parameter which indicates the nontrivial distribution of the final particles in the different scattering-planes.

It must be noted that the considered above effects can be not included in the usual form-factors of hadrons, because the well known form-factors are depending only on the four-momentum transfer $t = (p' - p)^2$ and not on ϕ. For example the form-factor of pion is

$$< \mathbf{p}'|j_\mu(0)|\mathbf{p} >= \frac{(p'+p)_\mu}{2m_\pi}F(t) \qquad (3)$$

The experimental evidence of the proton structure effects can be done by a measurement of the following quantity by the fixed E *and* θ:

$$\Big[\lambda_\pm(\phi)\Big]_{fixed\ E\ and\ \theta} = \Big[A_{nooo}\frac{d\sigma_{pp\to p'p'}}{d\Omega} \pm \Big(A_{nooo}\frac{d\sigma_{pp\to p'p'}}{d\Omega}\Big)_{\phi=0}\Big]_{fixed\ E\ and\ \theta}$$
$$= Re\Big(a^*(E,\theta,\phi)e(E,\theta,\phi)\Big) \pm Re\Big(a^*(E,\theta,\phi=0)e(E,\theta,\phi=0)\Big) \qquad (4)$$

The most promising energy region for determination of the $\lambda(\phi)$ parameter is $E \sim 1 - 2GeV$, where the quark structure effects are nowadays indisputable.

The essential dependence on the azimuthal ϕ-angle of the binary scattering observables is the necessity condition of the structure for the interacted hadrons. This means that the ϕ independence of the polarised observables of the $1+2 \Longrightarrow 1'+2'$ reaction indicates the structureless nature of the scattered particles.

References

1. K. Huang and H. A. Weldon, Phys. Rev. **D11** (1975) 257.
2. R. Haag, Phys. Rev. **112** (1958) 669.
3. K. Nishijima, Phys. Rev. **111** (1958) 995.
4. W. Zimmermann, Nuovo Cim. **10** (1958) 598.
5. A. I. Machavariani, Fiz. Elem. Chastits At Yadra **24** (1993) 731; A. I. Machavariani, Few-Body Phys. **14** (1993) 59.
6. A. I. Machavariani, A. J. Buchmann, Amand Faessler, and G. A. Emelyanenko, Ann. of. Phys. **253** (1997) 149.
7. A. I. Machavariani, Amand Faessler and A. J. Buchmann. Nucl. Phys. **A646** (1999) 231; (Erratum **A686** (2001) 601).
8. M. L. Goldberger and M. Watson, Collision Theory. (New York-London-Sydney, John Wiley and Sns.) 1965.
9. P. La France and P. Winternitz, J. De Phys. **41**(1980) 1391.
10. A. I. Machavariani, U. Straub and Amand Faessler. Nucl. Phys.**A548** (1992) 592.

Frascati Physics Series Vol. XLVI (2007), pp. 1101
HADRON07: XII Int. Conf. on Hadron Spectroscopy – Frascati, October 8-13, 2007
Hadron Structure

SPACELIKE AND TIMELIKE NUCLEON FORM FACTORS WITHIN LIGHT-FRONT DYNAMICS

G. Salmè
Istituto Nazionale di Fisica Nucleare, Sezione di Roma, Roma, Italy

Written contribution not received

Frascati Physics Series Vol. XLVI (2007), pp. 1103-1108
HADRON07: XII Int. Conf. on Hadron Spectroscopy – Frascati, October 8-13, 2007
Hadron Structure

ELECTROMAGNETIC DECAYS OF VECTOR MESONS IN A COVARIANT MODEL

Silvia Pisano
Università di Roma "Sapienza", Rome, Italy
Tobias Frederico
ITA-CTA, São José dos Campos, São Paulo, Brazil
Emanuele Pace
Università di Roma and INFN "Tor Vergata", Rome, Italy
Giovanni Salmè
INFN Sezione di Roma, Rome, Italy

Abstract

A fully covariant model for describing the electromagnetic decay of Vector Mesons, both in light and in heavy sectors, is presented. The main ingredients of our approach are i) an Ansatz for the Bethe-Salpeter vertex for Vector Mesons, and ii) a Mandelstam-like formula for the electromagnetic decay constant. The free parameters of our approach are fixed through a comparison with the transverse momentum distribution obtained within a Light-Front Hamiltonian Dynamics framework with constituent quarks. Preliminary results for both the decays constants and the probability of the valence component are shown.

1 Introduction

Aim of this contribution is to present a fully covariant model for describing the electromagnetic (em) decay of Vector Mesons (VM's), both in light and heavy

sectors. To this end, a simple analytic form for the Bethe-Salpeter (BS) amplitude of VM's is adopted in order to perform without any further approximation the calculations of the decay constants. Moreover, with such an Ansatz one can easily evaluate the so-called transverse momentum distribution of a constituent inside the VM (see de Melo et al [1)] for the pion case), that plays an essential role for fixing the value of the parameters appearing in our approach, and in turn for including some non perturbative inputs in our analytical Ansatz. A possible form of the BS amplitude for an interacting $q\bar{q}$ system with $J = 1$, can be written as follows

$$\Psi_\lambda(k,P) = S(k,m_1)\ [\epsilon_\lambda(P)\cdot V(P)]\ \Lambda_{VM}(k,k-P)\ S(k-P,m_2) \quad (1)$$

where $S(p,m)$ is the Dirac propagator of a constituent with mass m, P^μ the four-momentum of a VM with mass $P^2 = M^2$, $\epsilon^\mu_\lambda(P)$ its polarization four-vector, λ the helicity, $V^\mu(k,k-P)$ the Dirac structure of the amplitude and $\Lambda_{VM}(k,k-P)$ the momentum dependence of the BS amplitude. In particular, the adopted covariant form for the Dirac structure is the familiar one (transverse to P^μ), viz

$$V^\mu(P) = \frac{M}{M+m_1+m_2}\ \left[\gamma^\mu - \frac{P^\mu \not{P}}{M^2} + \imath\frac{1}{M}\ \sigma^{\mu\nu}P_\nu\right] \quad (2)$$

that in the limit of non interacting system leads to the Melosh Rotations for a $^3S_1$ system [2, 3)], as expected. For the present preliminary calculations, the momentum dependence has the following simple form with single poles, viz

$$\Lambda_{VM}(k,k-P) = \mathcal{N}\ \left[k^2 - m_1^2 + (P-k)^2 - m_2^2\right]\ \times$$
$$\Pi_{i=1,3}\frac{1}{\left[k^2 - m^2_{R_i} + \imath\epsilon\right]\left[(P-k)^2 - m^2_{R_i} + \imath\epsilon\right]} \quad (3)$$

where m_{R_i}, $i = 1,2,3$ are the free parameters of our Ansatz (to be determined as described below), $\mathcal{N}$ the normalization factor, that can be derived by imposing the standard normalization for the Bethe-Salpeter amplitude, in Impulse Approximation (i.e. with free propagators for the constituents). The form chosen for $\Lambda_{VM}(k,k-P)$ allows one both to implement the correct symmetry under the exchange of the quark momenta (for equal mass constituents) and to avoid any free propagation of the constituents (cf the numerator in Eq. (3)).

To determine m_{R_i} in Eq. (3), we first define the constituent transverse momentum distribution inside the VM, $n(k_\perp)$, along the same guidelines

adopted by de Melo et al. [1] for the pion, within a Light-Front Hamiltonian Dynamics approach. In a frame where $\mathbf{P}_\perp = \mathbf{0}$, one has

$$n(k_\perp) = \frac{N_c}{P_{q\bar{q}}(2\pi)^3\,[P^+]^2}\int_0^{2\pi} d\theta_{\hat{k}_\perp}\int_0^1 \frac{d\xi\ M_0^2}{\xi(1-\xi)}\ |\Phi(\xi,\mathbf{k}_\perp;m_{R_i})|^2 \quad (4)$$

where N_c is the number of colors, $k_\perp = |\mathbf{k}_\perp|$ and $\Phi(\xi,\mathbf{k}_\perp;m_{R_i})$ is the valence wave function associated to a given BS amplitude, see, e.g., Huang and Karmanov [4] and Frederico et al [3]. In Eq. (4), the probability $P_{q\bar{q}}$ of the valence component reads

$$P_{q\bar{q}} = \frac{N_c}{(2\pi)^3\,[P^+]^2}\int_0^1 \frac{d\xi}{\xi\ (1-\xi)}\int d\mathbf{k}_\perp M_0^2\ |\Phi(\xi,\mathbf{k}_\perp;m_{R_i})|^2 \quad (5)$$

Finally, $n(k_\perp)$ is normalized as: $\int k_\perp\ dk_\perp\ n(k_\perp) = 1$.

In spite of the simple form assumed for Λ_{VM}, one can nicely fit the constituent transverse momentum distributions obtained within 3-D approaches, that i) retain only the valence component of the VM's and ii) are able to yield a reasonable description of the spectrum. In this work we have extracted the parameters m_{Ri} in Eq. (4) by fitting $n(k_\perp)$ to the corresponding quantity obtained from i) a Harmonic Oscillator model (see, e.g. Figs. 1 and 2), ii) the Godfrey-Isgur model [5] and iii) an adapted version of the model by Salcedo et al [6] (ITA model).

2 The Mandelstam formula for em decay constant

In order to evaluate the em decays constants, f_V, we adopted a Mandelstam-like formula [7] (see also de Melo et al. [8])). The starting point is the *macroscopic* definition of f_V, through the transition matrix element of the em current for a given neutral VM, viz

$$\langle 0|J^\mu(0)|P,\lambda\rangle = \imath\sqrt{2}f_V\epsilon_\lambda^\mu \quad (6)$$

The decay constant f_V is related to the em decay width as follows

$$\Gamma_{e^+e^-} = \frac{8\pi\alpha^2}{3}\frac{|f_V|^2}{M^3} \quad (7)$$

In our model, the transition matrix element in Eq. (6) can be approximated *microscopically à la* Mandelstam through

$$\langle 0|J^\mu(0)|P,\lambda\rangle = \mathcal{F}_{VM}\ \frac{N_c\mathcal{N}}{(2\pi)^4}\int d^4k \frac{\Lambda_{VM}(k,k-P,m_1,m_2)}{(k^2-m_1^2+\imath\epsilon)\ [(P-k)^2-m_2^2+\imath\epsilon]}\ \times$$

Table 1: *Preliminary VM em decay widths within the Harmonic Oscillator model. Adopted quark masses:* $m_u = 0.310$ *GeV,* $m_s = 0.460$ *GeV,* $m_c = 1.749$ *GeV,* $m_b = 5.068$ *GeV,*

VM	m_{VM} (MeV)	$P_{q\bar{q}}$	$\Gamma^{th}_{e^+e^-}$ (keV)	$\Gamma^{exp}_{e^+e^-}$ (keV)
ρ	775.5 ± 0.4	0.884	10.328	7.02 ± 0.11
ϕ	1019.460 ± 0.019	0.961	1.582	1.32 ± 0.06
J/ψ	3096.916 ± 0.011	0.787	1.572	5.55 ± 0.14

Table 2: *Preliminary VM em decay widths within the Godfrey-Isgur* [5] *model,* $m_u = 0.220$ *GeV,* $m_s = 0.419$ *GeV,* $m_c = 1.628$ *GeV,* $m_b = 4.977$ *GeV.*

VM	m_{VM} (MeV)	$P_{q\bar{q}}$	$\Gamma^{th}_{e^+e^-}$ (KeV)	$\Gamma^{exp}_{e^+e^-}$ (keV)
ρ	775.5 ± 0.4	0.411	18.098	7.02 ± 0.11
ϕ	1019.460 ± 0.019	0.906	3.733	1.32 ± 0.06
J/ψ	3096.916 ± 0.011	0.908	5.911	5.55 ± 0.14

$$\mathrm{Tr}[\epsilon_\lambda(P) \cdot V(P)\ (\not{k} - \not{P} + m_2)\gamma^\mu(\not{k} + m_1)] \tag{8}$$

where

$$\mathcal{F}_\rho = \frac{(Q_u - Q_d)}{\sqrt{2}} \qquad \mathcal{F}_\phi = Q_s \qquad \mathcal{F}_{J/\Psi} = Q_c$$

with Q_i the quark charge. In Tabs. 1, 2, 3, the preliminary results for both valence probability, $P_{q\bar{q}}$, and em decay widths, $\Gamma_{e^+e^-}$ are shown. Even if a more refined evaluations are in progress, some comments are in order: i) for the Harmonic Oscillator model the light meson decay widths can be reasonably well described (in the light sector the confining interaction is quite relevant), while the J/ψ one is largely underestimated; ii) for the Godfrey-Isgur model [5], the heavy sector is well reproduced, while the light sector is overestimated, and this appears correlated to the poor estimate of the valence probability (work in progress suggests that an Ansatz for the BS amplitude with a more rich structure substantially improves the comparison); iii) for the adapted version of the ITA model [6] the same pattern of the Harmonic Oscillator case has been found, even if more dynamical contents are present in this model.

Table 3: *Preliminary VM em decay widths within an adapted version of the ITA model.* [6]. *Adopted quark masses:* $m_u = 0.334$ *GeV,* $m_s = 0.460$ *GeV,* $m_c = 1.791$ *GeV,* $m_b = 4.679$ *GeV.*

VM	m_{VM} (MeV)	$P_{q\bar{q}}$	$\Gamma^{th}_{e^+e^-}$ (keV)	$\Gamma^{exp}_{e^+e^-}$ (keV)
ρ	775.5 ± 0.4	0.913	7.548	7.02 ± 0.11
ϕ	1019.460 ± 0.019	0.995	1.294	1.32 ± 0.06
J/ψ	3096.916 ± 0.011	0.726	1.250	5.55 ± 0.14

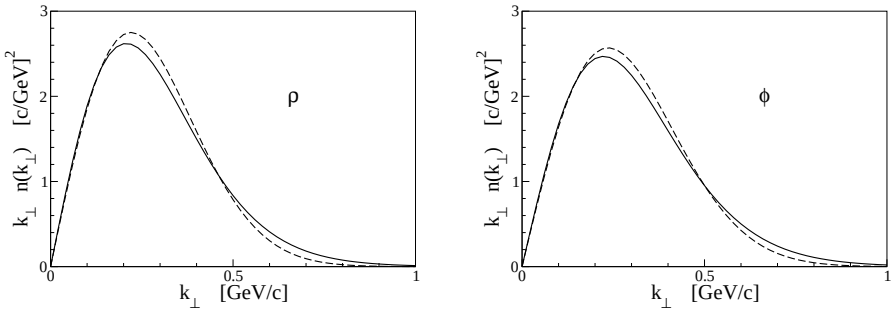

Figure 1: *Transverse momentum distributions for a constituent inside* ρ *and* ϕ *vs the quark transverse momentum. Dashed line: Harmonic Oscillator model. Solid line: fit by using the analytic Ansatz in Eq. (3)*

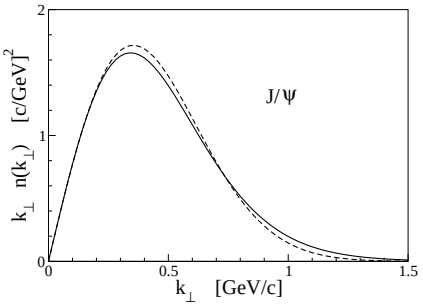

Figure 2: *The same as in Fig. 1, but for* J/ψ.

3 Conclusions

In this contribution we have presented the main ingredients of our model for evaluating both the em decay width of the ground states of VM's and the probability of the valence component of the state. In our fully covariant model, a simple, analytic Ansatz for the BS amplitude is proposed, and the three parameters, m_{Ri}, for each neutral VM, are determined through a fitting procedure, based on the transverse momentum distribution of a constituent inside a given VM, obtained within a Light-Front Hamiltonian Dynamics framework. From this first comparisons between our results and the experimental data, one could argue that two different regimes occur in the light (ρ, ϕ) and in the heavy sector (J/ψ). From the theoretical side, indeed, the Harmonic Oscillator and the adapted ITA [6)] models seem to better reproduce the light mesons (cf Tab. 1, 2) while for the heavy sector the Godfrey-Isgur model [5)] seems to work better (cf. Tab. 3).

The work in progress will substantially improve the present calculations, in two respect: both introducing a more refined Ansatz for the BS amplitude and extending our investigation to the em decay of the Υ.

References

1. J. P. B. C. de Melo, T. Frederico, E. Pace and G. Salmè, Nucl. Phys. **A 707**, 399 (2002).
2. W. Jaus, Phys. Rev. **D 44**, 2851 (1991).
3. T. Frederico, E. Pace, S. Pisano and G. Salmè to be published.
4. Dae Sung Hwang and V. A. Karmanov, Nucl. Phys. **B 696**, 413 (2004).
5. S. Godfrey and N. Isgur, Phys. Rev. **D 32**, 189 (1985).
6. L. A. M. Salcedo, J. P. B. C. de Melo, D. Hadjimichel and T. Frederico, Eur. Phys. Jour. **27** 213 (2006).
7. S. Mandelstam, Proc. Royal Soc. (London) **A233**, 248 (1956).
8. J. P. B. C. de Melo, T. Frederico, E. Pace and G. Salmè, Phys. Rev. **D 73**, 074013 (2006).

Frascati Physics Series Vol. XLVI (2007), pp. 1109–1116
HADRON07: XII Int. Conf. on Hadron Spectroscopy – Frascati, October 8-13, 2007
Hadron Structure

SYSTEMATIC ERRORS OF BOUND-STATE PARAMETERS EXTRACTED BY MEANS OF SVZ SUM RULES

Wolfgang Lucha
Institute for High Energy Physics, Austrian Academy of Sciences, Nikolsdorfergasse 18, A-1050, Vienna, Austria
Dmitri Melikhov
Institute for High Energy Physics, Austrian Academy of Sciences, Nikolsdorfergasse 18, A-1050, Vienna, Austria
and
Nuclear Physics Institute, Moscow State University, 119991, Moscow, Russia
Silvano Simula
INFN, Sezione di Roma III, Via della Vasca Navale 84, I-00146, Roma, Italy

Abstract

This talk presents the results of our study of systematic errors of the ground-state parameters obtained by Shifman–Vainshtein–Zakharov (SVZ) sum rules. We use the harmonic-oscillator potential model as an example: in this case we know the exact solution for the polarization operator, which allows us to obtain both the OPE to any order and the parameters (masses and decay constants) of the bound states. We extract the parameters of the ground state by making use of the standard procedures of the method of QCD sum rules, and compare the obtained results with their known exact values. We show that if the continuum contribution to the polarization operator is not known and is modelled by some effective continuum threshold, the standard procedures adopted in sum rules do not allow one to gain control over the systematic errors of the extracted ground-state parameters.

A QCD sum-rule calculation of hadron parameters [1] involves two steps: one first constructs the operator product expansion (OPE) series for a relevant correlator and then extracts the parameters of the ground state by a numerical procedure. Each of these steps leads to certain uncertainties in the final result.

The first step lies entirely within QCD and, in the case of SVZ sum rules, allows for a rigorous treatment of the uncertainties: the correlator is not known precisely because of uncertainties in quark masses, condensates, α_s, etc., but all corresponding errors in the correlator may be controlled. [Complications arising in light-cone sum rules are discussed in our second talk [2].]

The second step lies beyond QCD: even if several terms of the OPE for the correlator were known precisely, the hadronic parameters might be extracted by a sum rule only within some error, which may be treated as a systematic error of the method.

Here we present the results of our recent study of systematic uncertainties of the sum-rule procedures [3, 4]. To this end, a quantum-mechanical harmonic-oscillator (HO) potential model is a perfect tool: in this case both the spectrum of bound states (i.e., masses and wave functions) and the exact correlator (and hence its OPE to any order) are known precisely. Therefore, one may apply the sum-rule machinery for extracting parameters of the ground state and test the accuracy of the extracted values by comparing with the known exact results. In this way the accuracy of the method can be probed. For a detailed discussion of various aspects of sum rules in quantum mechanics, we refer to Refs. [5–9].

To illustrate the essential features of the QCD calculation, we consider a non-relativistic model with a confining potential,

$$V(r) = \frac{m\omega^2 \mathbf{r}^2}{2}, \qquad r = |\mathbf{r}|, \tag{1}$$

and analyze the Borel transform $\Pi(\mu)$ of the polarization operator $\Pi(E)$, which gives the evolution operator in the imaginary time $1/\mu$:

$$\Pi(\mu) = \left(\frac{2\pi}{m}\right)^{3/2} \left\langle \mathbf{r}_f = \mathbf{0} \left| \exp\left(-\frac{H}{\mu}\right) \right| \mathbf{r}_i = \mathbf{0} \right\rangle . \tag{2}$$

For the HO potential (1), the exact analytic expression for $\Pi(\mu)$ is well known:

$$\Pi(\mu) = \left(\frac{\omega}{\sinh(\omega/\mu)}\right)^{3/2} . \tag{3}$$

Expanding the above expression in inverse powers of μ, we get the OPE series

$$\begin{aligned}\Pi_{\rm OPE}(\mu) &\equiv \Pi_0(\mu)+\Pi_1(\mu)+\Pi_2(\mu)+\cdots \\ &= \mu^{3/2}\left(1-\frac{\omega^2}{4\mu^2}+\frac{19}{480}\frac{\omega^4}{\mu^4}+\cdots\right); \end{aligned} \tag{4}$$

higher power corrections may be derived from the exact result (3).

The "phenomenological" representation for $\Pi(\mu)$ is obtained by using the basis of hadronic eigenstates of the model, namely,

$$\Pi(\mu)=\sum_{n=0}^{\infty} R_n \exp\left(-\frac{E_n}{\mu}\right), \tag{5}$$

where E_n is the energy of the nth bound state and R_n [the square of the leptonic decay constant of the nth bound state] is given by

$$R_n=\left(\frac{2\pi}{m}\right)^{3/2}|\Psi_n(\mathbf{r}=\mathbf{0})|^2. \tag{6}$$

For the lowest states, one finds from (3)

$$E_0=\frac{3}{2}\omega,\ R_0=2\sqrt{2}\omega^{3/2}, \qquad E_1=\frac{7}{2}\omega,\ R_1=3\sqrt{2}\omega^{3/2}, \qquad \ldots. \tag{7}$$

The sum rule is just the equality of the correlator calculated in the "quark" basis and in the "hadron" basis:

$$\begin{aligned} &R_0\exp\left(-\frac{E_0}{\mu}\right)+\int\limits_{z_{\rm cont}}^{\infty}{\rm d}z\,\rho_{\rm phen}(z)\exp\left(-\frac{z}{\mu}\right) \\ &\qquad=\int\limits_0^{\infty}{\rm d}z\,\rho_0(z)\exp\left(-\frac{z}{\mu}\right)+\mu^{3/2}\left(-\frac{\omega^2}{4\mu^2}+\frac{19}{480}\frac{\omega^4}{\mu^4}+\cdots\right). \end{aligned} \tag{8}$$

Following Ref. [1], we use explicit expressions for the power corrections, but for the zeroth-order free-particle term we use its expression in terms of the spectral integral.

Let us introduce an "effective" continuum threshold $z_{\rm eff}(\mu)$, different from the physical μ-independent continuum threshold $z_{\rm cont}$, by the relation

$$\Pi_{\rm cont}(\mu)=\int\limits_{z_{\rm cont}}^{\infty}{\rm d}z\,\rho_{\rm phen}(z)\exp\left(-\frac{z}{\mu}\right)=\int\limits_{z_{\rm eff}(\mu)}^{\infty}{\rm d}z\,\rho_0(z)\exp\left(-\frac{z}{\mu}\right). \tag{9}$$

The spectral densities $\rho_{\rm phen}(z)$ and $\rho_0(z)$ are different functions. Thus the two sides of (9) can be equal to each other only if the effective continuum threshold, $z_{\rm eff}(\mu)$, depends on μ in an appropriate way. In our model, we can calculate $\Pi_{\rm cont}$ precisely and, therefore, we can obtain the function $z_{\rm eff}(\mu)$ by solving (9). In the general case of an actual QCD sum-rule analysis, the effective continuum threshold is not known and constitutes one of the essential fitting parameters.

Making use of (9), we now rewrite the sum rule (8) in the form

$$R_0 \exp\left(-\frac{E_0}{\mu}\right) = \Pi(\mu, z_{\rm eff}(\mu)), \tag{10}$$

where the cut correlator $\Pi(\mu, z_{\rm eff}(\mu))$ reads

$$\begin{aligned}&\Pi(\mu, z_{\rm eff}(\mu))\\ &\quad\equiv \frac{2}{\sqrt{\pi}} \int\limits_0^{z_{\rm eff}(\mu)} {\rm d}z\, \sqrt{z} \exp\left(-\frac{z}{\mu}\right) + \mu^{3/2}\left(-\frac{\omega^2}{4\mu^2} + \frac{19}{480}\frac{\omega^4}{\mu^4} + \cdots\right).\end{aligned} \tag{11}$$

As is obvious from (10), the cut correlator satisfies the equation

$$-\frac{{\rm d}\log\Pi(\mu, z_{\rm eff}(\mu))}{{\rm d}(1/\mu)} = E_0. \tag{12}$$

The cut correlator $\Pi(\mu, z_{\rm eff}(\mu))$ is the quantity that actually governs the extraction of the ground-state parameters.

The "fiducial" [1)] range of μ is defined as the range where, on the one hand, the OPE reproduces the exact expression with better than some chosen accuracy (for instance, within, say, 0.5%) and, on the other hand, the ground state is expected to give a sizable contribution to the correlator. If we include only the first three power corrections (that is, Π_1, Π_2, and Π_3) we must require $\omega/\mu < 1.2$. Since we know the ground-state parameters, we fix $\omega/\mu > 0.7$, where the ground state contributes more than 60% of the full correlator. So our fiducial range is $0.7 < \omega/\mu < 1.2$.

We shall be interested in situations where the hadronic continuum is *not* known — which is typical for heavy-hadron physics and in the discussion of the properties of exotic hadrons. Can we extract the ground-state parameters?

We denote the values of the ground-state parameters extracted from the sum rule (10) by E and R. The notations E_0 and R_0 are reserved for the exact values. In many interesting cases the ground-state energy may be determined,

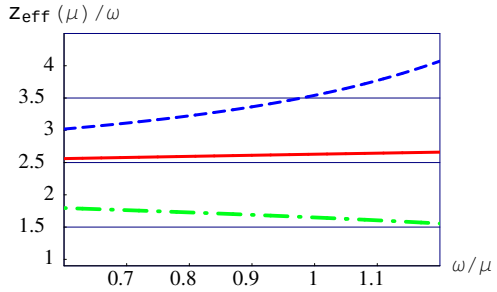

Figure 1: The effective continuum threshold $z_{\rm eff}(\mu)$ obtained by solving (8) for $E = E_0$ and $R = 0.7R_0$ [long-dashed (blue) line], $R = R_0$ [solid (red) line] and $R = 1.15R_0$ [dash-dotted (green) line].

e.g., from experiment. However, setting $E = E_0$ does not help: still, for any R within a broad range, one finds a function $z_{\rm eff}(\mu, R)$ [Fig. 1] which solves the sum rule (10) *exactly*. Therefore, we conclude that *in a limited range of μ the OPE alone cannot say much about the ground-state parameters*. What really matters is the continuum contribution, or, equivalently, $z_{\rm eff}(\mu)$. Only by making some assumptions about $z_{\rm eff}(\mu)$ one is able to extract R.

Typically, one assumes $z_{\rm eff}(\mu)$ to be constant and imposes some criteria to fix its value. Rigorously speaking, a *constant* effective continuum threshold $z_{\rm eff}(\mu) = z_c = \text{const}$ is incompatible with the sum rule (10). Nevertheless, such an Ansatz may work well, especially in our HO model: As seen from Fig. 1, the exact $z_{\rm eff}(\mu)$ is almost flat in the fiducial interval. Therefore, the HO model represents a very favorable situation for applying the QCD sum-rule machinery.

Now, how to determine z_c? A widely used procedure [10] is to calculate

$$E(\mu, z_c) \equiv -\frac{\mathrm{d}\log\Pi(\mu, z_c)}{\mathrm{d}(1/\mu)}, \tag{13}$$

which now depends on μ due to approximating $z_{\rm eff}(\mu)$ by a constant. Then, one determines μ_0 and z_c as the solution to the system of equations

$$E(\mu_0, z_c) = E_0, \qquad \frac{\partial}{\partial\mu} E(\mu, z_c)\Big|_{\mu=\mu_0} = 0, \tag{14}$$

yielding $z_c = 2.454\,\omega$, $\mu_0/\omega = 1$ [Fig. 2]. Finally, one takes the value $R(\mu_0, z_c)$ as the sum-rule estimate for the quantity R. The error of R is usually obtained

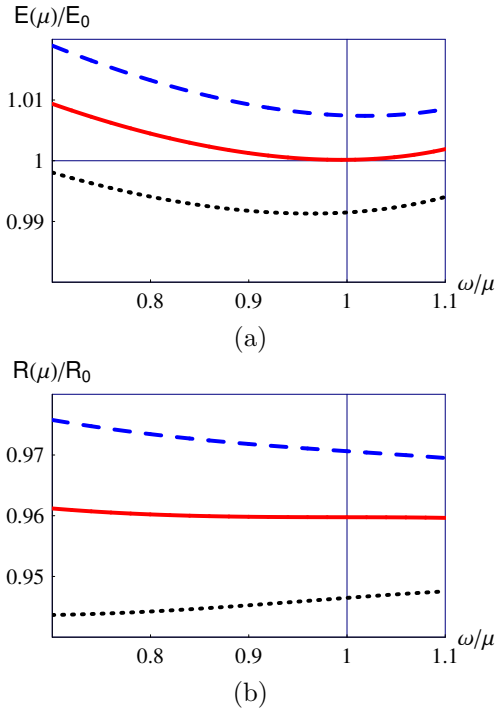

Figure 2: Constant effective continuum threshold z_c: $E(\mu)$ for three different values of z_c (a) and the corresponding $R(\mu)$ (b).

by looking at the range covered by $R(\mu, z_c)$ when one allows for a variation of μ within the fiducial range. Following this procedure, one obtains in our case a good central-value estimate: $R/R_0 = 0.96$. Since $R(\mu, z_c)$ is extremely stable in the fiducial range, one expects its true value to be rather close to the extracted value and, accordingly, assigns a very small error to the sum-rule estimate.

Note, however, a dangerous point: (i) a perfect description of $\Pi(\mu)$ with an accuracy better than 1%, (ii) a deviation of $E(\mu, z_c)$ from E_0 at the level of only 1%, and (iii) an extreme stability of $R(\mu)$ in the entire fiducial range conspire to lead to a 4% error in the extracted value of R! Clearly, this error could not be guessed on the basis of the other numbers obtained, and it would be wrong to try to estimate the error from, e.g., the range covered by R when varying the Borel parameter μ within the fiducial interval.

Let us summarize the lessons we have learnt from the above investigation:

1. The knowledge of the correlator to any accuracy within a limited range of the Borel parameter μ is not sufficient for an extraction of the ground-state parameters since rather different models for the correlator, generically of the form of a ground state plus an effective continuum, lead to the same correlator.

2. Modelling the hadron continuum by a *constant* effective continuum threshold z_c allows one to determine the value of z_c by, e.g., requiring the average energy $E(\mu)$ to be close to E_0 in the region of stability of the sum rule. In the model under discussion this leads to a good estimate, $R/R_0 = 0.96$, with almost μ-independent R. The unpleasant feature of this extraction procedure is that the deviation of R from R_0 is much larger than the variations of $E(\mu)$ and $R(\mu)$ over the fiducial interval of μ. In particular, it would be wrong to assign the systematic error on the basis of the range covered by $R(\mu)$ when μ is varied within the fiducial interval. This means that the standard procedures adopted in QCD sum rules do not allow one to control the systematic errors. Consequently, no rigorous systematic errors for hadronic parameters extracted by sum rules can be provided. Let us also stress that the independence of the extracted values of the hadron parameters from the Borel mass μ does not guarantee the extraction of their true values.

Finally, in the model under consideration sum rules provide a rather good estimate for R_0, even though its error cannot be determined on the basis of the standard procedures adopted in sum-rule analyses. This may be a consequence of the following features of the model: (i) a large gap between ground state and the first excitation contributing to the sum rule; (ii) an almost constant exact effective continuum threshold. Whether or not the same good accuracy may be achieved in QCD, where the features mentioned above are absent, is not obvious at all and requires more detailed investigations.

We would like to point out that with respect to the problem of assigning systematic errors to the extracted hadron parameters, the method of QCD sum rules faces very similar problems as the application of approaches based on the constituent quark picture: for instance, the relativistic dispersion approach [11] yields very successful predictions for the form factors of exclusive D decays and provides many predictions for the form factors of weak decays of B mesons [12]. However, assigning rigorous errors to these predictions could not be done so far.

Acknowledgements. We thank R. Bertlmann, B. Grinstein, and B. Stech for interesting discussions and inspiring comments, and the Austrian Science Fund (FWF) for financial support under project P17692.

References

1. M. Shifman, A. Vainshtein, and V. Zakharov, Nucl. Phys. B **147**, 385 (1979).
2. W. Lucha, D. Melikhov, and S. Simula, "Systematic errors of transition form factors extracted by means of light-cone sum rules", arXiv:0712.0178.
3. W. Lucha, D. Melikhov, and S. Simula, Phys. Rev. D **76**, 036002 (2007); Phys. Lett. B **657**, 148 (2007).
4. W. Lucha, D. Melikhov, and S. Simula, Phys. Rev. D **75**, 096002 (2007); W. Lucha and D. Melikhov, Phys. Rev. D **73**, 054009 (2006); Phys. Atom. Nucl. **70**, 891 (2007).
5. V. Novikov, M. Shifman, A. Vainshtein, and V. Zakharov, Nucl. Phys. B **237**, 525 (1984).
6. A. I. Vainshtein, V. I. Zakharov, V. A. Novikov, and M. A. Shifman, Sov. J. Nucl. Phys. **32**, 840 (1980).
7. V. A. Novikov *et al.*, Phys. Rep. **41**, 1 (1978); M. B. Voloshin, Nucl. Phys. B **154**, 365 (1979); J. S. Bell and R. Bertlmann, Nucl. Phys. B **177**, 218 (1981); Nucl. Phys. B **187**, 285 (1981); V. A. Novikov, M. A. Shifman, A. I. Vainshtein, and V. I. Zakharov, Nucl. Phys. B **191**, 301 (1981).
8. A. Le Yaouanc *et al.*, Phys. Rev. D **62**, 074007 (2000); Phys. Lett. B **488**, 153 (2000); Phys. Lett. B **517**, 135 (2001).
9. D. Melikhov and S. Simula, Phys. Rev. D **62**, 074012 (2000).
10. M. Jamin and B. Lange, Phys. Rev. D **65**, 056005 (2002).
11. D. Melikhov, Phys. Rev. D **53**, 2460 (1996); Phys. Rev. D **56**, 7089 (1997); Eur. Phys. J. direct **C4**, 2 (2002) [hep-ph/0110087]; D. Melikhov and S. Simula, Eur. Phys. J. C **37**, 437 (2004).
12. D. Melikhov and B. Stech, Phys. Rev. D **62**, 014006 (2000).

Frascati Physics Series Vol. XLVI (2007), pp. 1117–1126
HADRON07: XII Int. Conf. on Hadron Spectroscopy – Frascati, October 8-13, 2007
Hadron Structure

NEW RESULTS ON EXCLUSIVE ϕ^0 AND ρ^0 VECTOR MESON PRODUCTION AT HERMES

Witold Augustyniak (on behalf of HERMES collaboration)
Soltan Institute for Nuclear Studies Dep.I 69 Hoza, 00-681 Warsaw, Poland

Abstract

The exclusive diffractive production of light vector mesons (ρ^0, ϕ^0) on hydrogen and deuterium targets in the HERMES kinematic region of $0.5 < Q^2 < 7$ GeV^2 and $3.0 < W < 6.3$ GeV is described. Spin density matrix elements (SDMEs) have been determined for exclusive ρ^0 and ϕ^0 production. New results on kinematic dependences of SDMEs on Q^2 and t' are presented. Violation of s-Channel Helicity Conservation (SCHC) is observed on several non-zero values of SDMEs for ρ^0, but not for ϕ^0. An indication of a contribution of unnatural parity-exchange amplitudes for exclusive ρ^0 production is observed for proton data and presented via the relations of several SDMEs as a functions of Q^2, t' and x_{Bj}.

1 Introduction

The results of the experimental studies of exclusive electroproduction of ρ^0 and ϕ^0 vector mesons are presented. The experiment was performed with a beam energy of 27.5 GeV for fixed hydrogen or deuterium targets.
The reaction $e+N \to e'+VM+N$ in the lowest order is equivalent to $\gamma^*+N \to VM+N$. Therefore, such processes can be described by characteristics typical for virtual photons: virtuality Q^2, polarization and energy of the photon as well as ϵ the polarization parameter expresing the ratio of the longitudinal to transverse fluxes.
In the proton rest frame, vector meson production at high energy can be seen to occur in three distinct steps ordered in time: the virtual photon breaks up into a quark and antiquark pair; the quark-antiquark pair interacts hard with the target; the scattered quark-antiquark pair forms the final state of vector meson. The scattering process on the proton occurs on a much shorter time scale than the fluctuation of the photon into a $q\bar{q}$ pair or the vector meson formation time, allowing the treatment of the scattering as a perturbation. The resulting amplitude can be factorized:

$$A = \Phi^*_{\gamma^* \to q\bar{q}} \otimes A_{q\bar{q}+p \to q\bar{q}+p} \otimes \Phi_{q\bar{q} \to V}. \tag{1}$$

The first term represents the amplitude for the fluctuation of a virtual photon into a $q\bar{q}$ pair. The last term describes the recombination of the final, scattered hadronic state into vector meson. The middle term corresponds to the short distance amplitude for the scattering of the hadronic state off the target. This term can be calculated by pQCD models describing an exchange of a colourless system and the structure of the nucleon. The possibility of factorization and calculation of the cross section by pQCD as well as the prediction of the cross section to be proportional to the square of the gluon density in hadrons have been shown in the papers of S.J. Brodsky *et al.* [1)] and L. Frankfurt *et al.* [2)]. The extension of factorization and possibility to use Generalized Parton Distributions (GPDs) to describe the structure of nucleon has been done by Collins *et al.* [3)]. Additionally, the authors state that the amplitude for production of longitudinally polarized vector mesons depends on the unpolarized parton densities. The amplitude for transversely polarized vector mesons depends only on the transversity densities. The amplitude for the production of pseudoscalar mesons depends only on the helicity densities. For these reasons the studies of

electroproduction of vector mesons are an important tool for the investigation of the nucleon structure.
Here, the experimental sets of 23 SDME's are presented and the Schilling-Wolf [6] representation is used. From the SDME's we may make conclusions about helicity conservation (SCHC), and about the exchange system having natural or unnatural parity. The natural parity exchange (NPE) indicates that the interaction is mediated by a 'particle of natural' parity $J^P = 0^+, 1^-, 2^+, ...$ like ρ^0, ω, A_2 or of 'unnatural' parity (UPE) $J^P = 0^-, 1^+, ...$ like π, a_1, b_1.
The dependences of SDME's on Q^2 and t' are also discussed.

2 Detection of ϕ^0 and ρ^0 vector mesons

The decay products of vector mesons: $\rho^0 \to \pi^+\pi^-$ ($\sim 100\%$) and $\phi^0 \to K^+K^-$ ($\sim 49\%$) were detected by the HERMES spectrometer [4]. The ρ^0 mesons were identified by requiring for its invariant mass the condition: $0.6 < M_{\pi\pi} < 1$GeV. The contribution to the background from as π's misidentified K's from a ϕ^0 is suppressed by requiring $M_{KK} > 1.04$ GeV.
In the case of ϕ^0 mesons the condition for the invariant mass is $0.99 < M_{KK} < 1.04$GeV and the identification of kaons was imposed using the RICH [5].

3 Spin Density Matrix Elements

The Spin Density Matrix Elements (SDME) are described, e.g., in Refs. [6, 7, 8]. Here, only main definitions, necessary for the interpretation of the experimental results, are presented. The same symbols as in the above mentioned papers are used. The matrix $\rho^\alpha_{\lambda_V\lambda_{V'}}$ contains also information on polarization:

$$\rho^\alpha_{\lambda_V\lambda_{V'}} = \frac{1}{2N_\alpha} \sum_{\lambda_\gamma \lambda'_V} T_{\lambda_V\lambda_\gamma} \Sigma^\alpha_{\lambda_\gamma\lambda'_\gamma} T^*_{\lambda'_\gamma\lambda'_\gamma}, \qquad (2)$$

where $\Sigma^\alpha_{\lambda_\gamma\lambda'_\gamma}$ are nine Hermitian matrices defining the photon polarization: upper index $\alpha = 0$ represents the unpolarised transverse photon, $\alpha = 1, 2$ two directions of lineary polarised photons, $\alpha = 3$ circular polarization, and $\alpha = 5 - 8$ provide the information about transverse/longitudinal interferences. The $\rho^\alpha_{\lambda_V\lambda_{V'}}$ matrices have the following symmetry with respect to index α:

$$\rho^\alpha_{-\lambda-\lambda'} = \begin{cases} (-1)^{\lambda-\lambda'}\rho^\alpha_{\lambda\lambda'}, & \text{for } \alpha = 0,1,4,5,8 \\ -(-1)^{\lambda-\lambda'}\rho^\alpha_{\lambda\lambda'}, & \text{for } \alpha = 2,3,6,7, \end{cases}$$

thus reducing the number of independent terms.

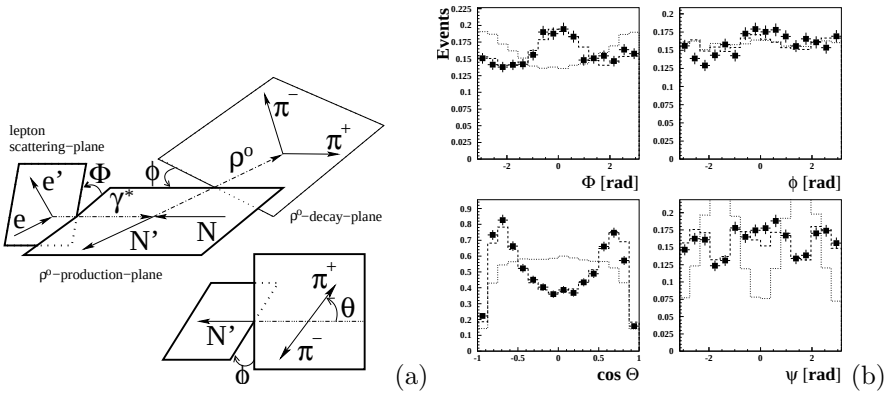

Figure 1: *a) Definition of the angles in the process $\gamma^* N \to \rho^0 N$. The angle Φ is the angle between the scattering and the production planes, determined in the 'hadronic' center-of-mass system of virtual photon and target nucleon: the θ and ϕ are the polar and azimuthal angles of π^+ (K^+) in the vector meson rest frame. b) Angular distributions in Φ, ϕ, cos(θ) and $\psi = \Phi - \phi$ for a typical sample of ρ^0 data. The two lines indicate the Monte Carlo input distributions with initial set of parameters (dotted) and the result of the 23 parametrs fit (dashed) defined as the SDME's.*

In Refs. [6, 7, 8] two frames, defined in Fig. 1(a), were chosen: the rest frame of the vector meson to describe the angular distributions of its decay products in terms of cos(θ) and ϕ, and the 'hadronic' center-of-mass system of the virtual photon and target nucleon in which the angle Φ defined as the angle between the the scattering and production planes. The angles determined in the experiment are also shown in Fig. 1(a). The set of typical angular distributions is shown in Fig. 1(b). The distribution W(cos(θ),ϕ,Φ,r^α_{ij}) [6] is measured in the experiment and defined by a set r^α_{ij} of matrix elements ρ^α_{ik}: $r^{04}_{ik} = \frac{\rho^0_{ik}+\epsilon R\rho^4_{ik}}{1+\epsilon R}$, $r^\alpha_{ik} = \frac{\rho^0_{ik}}{1+\epsilon R}$ (α=1,2,3) and $r^\alpha_{ik} = \sqrt{(}R)\frac{\rho^0_{ik}}{1+\epsilon R}$ (α=5,6,7,8). In these formulae parameter R is the ratio of the longitudinal to transverse cross sections: $R = \frac{\sigma_L}{\sigma_T}$. The distribution W(cos(θ),ϕ,Φ,r^α_{ij}) for an unpolarised lepton beam is determined by a set of 15 r^α_{ik} parameters, i.e., for α up to 6. For the measurement with a polarised lepton beam, the W distributions are determined

by a set of 8 r^{α}_{ik} parameters, i.e., for α= 7 and 8.
The sets of 23 SDME's for the data samples selected by Q^2 and t' have been determined. The parameters r^{α}_{ij} have been determined from a fit of Monte Carlo distributions to experimental 3-dimensional distributions. The initial uniform MC distributions were subjected to successive reweighting by changing the parameters r^{α}_{ij}.

4 Results

The 23 measured SDME's presented in Fig. 2 are subdivided into five classes. Class A contains SDME's dominated by helicity-conserving amplitudes T_{00} and T_{11} describing the transitions $\gamma^*_L \rightarrow \rho_L(\phi_L)$ and $\gamma^*_T \rightarrow \rho_T(\phi_T)$, respectively. Class B: SDME's describing the interference between the two main amplitudes T_{00} and T_{11}. Class C: $\gamma^*_T \rightarrow V_L$ contains the terms with T_{01} but no terms with quadratic $|T_{01}|^2$. Class D: $\gamma^*_L \rightarrow V_T$ contains terms opposite to those transitions in class C. And the last class E describes the transitions $\gamma^*_T \rightarrow V_{-T}$. In the case of natural parity transition the hierarchy relations among the transitions are expressed by

$$|T_{00}| \sim |T_{11}| \gg |T_{01}| > |T_{01}| \sim |T_{1-1}|. \tag{3}$$

For that reason, elements that are more sensitive to spin-flip and that are easier to observe, are elements like $r^5_{00} \sim \mathrm{Re}\{T_{00}T^*_{01}\}$ rather than elements like $r^1_{00} = |T_{01}|^2$

The elements belonging to class A in the ρ^0 and ϕ^0 cases are similar. The elements of class B describe the interference of the dominating amplitudes defined by the phase δ

$$\tan(\delta) = \frac{Re\{r^5_{10}\} - Im\{r^6_{10}\}}{Re\{r^8_{10}\} + Im\{r^7_{10}\}}. \tag{4}$$

The values determined are $\delta_\phi = 33.0^0 \pm 7.4^0_{stat}$, $\delta_\rho = 28.1^0 \pm 2.8^0_{stat} \pm 3.7^0_{sys}$ in the case of proton and $24.4^0 \pm 5.2^0_{stat} \pm 2.1^0_{sys}$ in the case of deuteron.
The values of elements for ϕ^0 mesons belonging to class C, D and E fluctuate near zero indicating that only the SCHC mechanism is observed. For ρ^0 mesons the elements with non-zero values belonging to classes C, D, E indicate that there exists also a production mechanism with non-conservation of s-channel helicity.

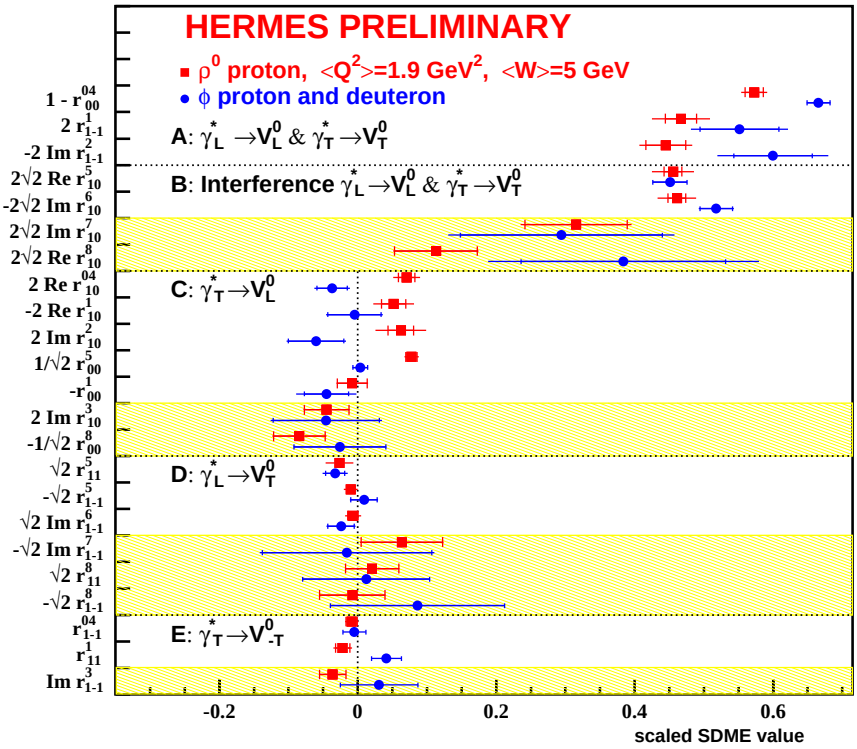

Figure 2: *The 23 SDME's extracted for ρ^0 production on proton (squares) and ϕ^0 meson production on proton and deuteron (circles) in the entire HERMES kinematics with $\langle x \rangle = 0.08$, $\langle Q^2 \rangle = 1.9 GeV^2$, $\langle t' \rangle = 0.13 GeV^2$. The SDME's are renormalized to represent leading contribution of the corresponding amplitude. The inner error bars represent the statistical uncertainties, while the outer ones indicate the statistical and systematic uncertainties added in quadrature. The unshaded (shaded) areas indicate beam-polarization independent (dependent) SDME's. The vertical dashed line at zero corresponds to SDME's expected to be zero under the hypothesis of SCHC.*

5 Unnatural-Parity Exchange

Without assuming SCHC, the hypothesis of natural parity exchange in the t channel alone leads to following sum rules: $U_1 = 1 - r^{04}_{00} - 2r^{04}_{1-1} - 2r^{1}_{11} - 2r^{1}_{1-1} =$

0, $U_2 = r^5_{11} + r^5_{1-1} = 0$ and $U_3 = r^8_{11} + r^8_{1-1} = 0$. These signatures for ρ^0 and ϕ^0 mesons are presented in Fig. 3(a) and Fig. 3(b). In the case of ϕ^0 mesons all signatures fluctuate near zero indicating that the machanism of unnatural parity exchange does not contribute. In the case of ρ^0, a nonzero result is found.

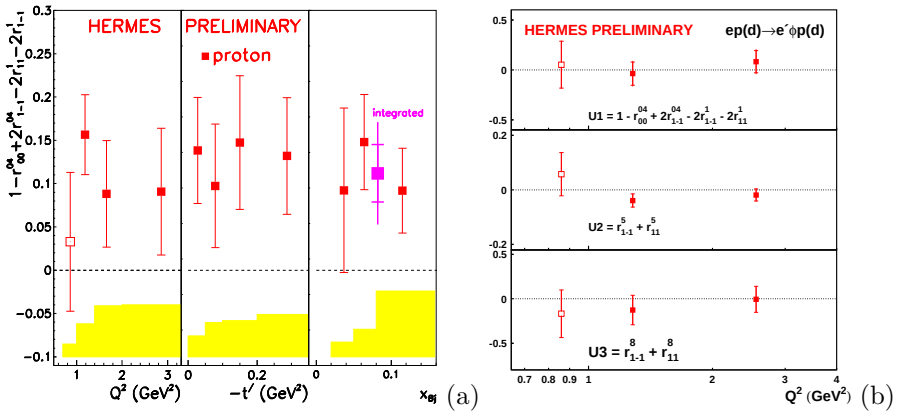

Figure 3: *a) The dependences of signature existing for unnatural parity exchange* $U_1 = 1 - r^{04}_{00} + 2r^{04}_{1-1} - 2r^1_{11} - 2r^1_{1-1}$ *on* Q^2*, t', and* x_{Bj}*. The first* Q^2*-bin* ($Q^2 < 1.0 GeV^2$)*, indicated by an open square, is not included in the t' and* x_{Bj} *dependences. b) The three signatures* U_1*,* U_2 *and* U_3 *for* ϕ^0 *mesons.*

6 Dependences of SDME's on Q^2 and t'

In the previous section the signatures constructed from SDME's were presented as functions of Q^2, t', and x_{Bj}. In this section the dependences of SDME's on Q^2 and t' are discussed. The set of SDME's is limited to 15 elements. The elements determining the sign of phase are omitted. The elements are ordered in a way different from that in Fig. 2. In Fig. 4 the dependences of SDME's on Q^2 are presented. One can see a dependence on Q^2 of the elements related to SCHC: r^{04}_{00}, r^1_{1-1}, Im $\{r^2_{1-1}\}$, Re$\{r^5_{10}\}$ and Im$\{r^6_{10}\}$. In this figure the dependences for proton and deuteron targets are presented. No difference between the two targets is observed.

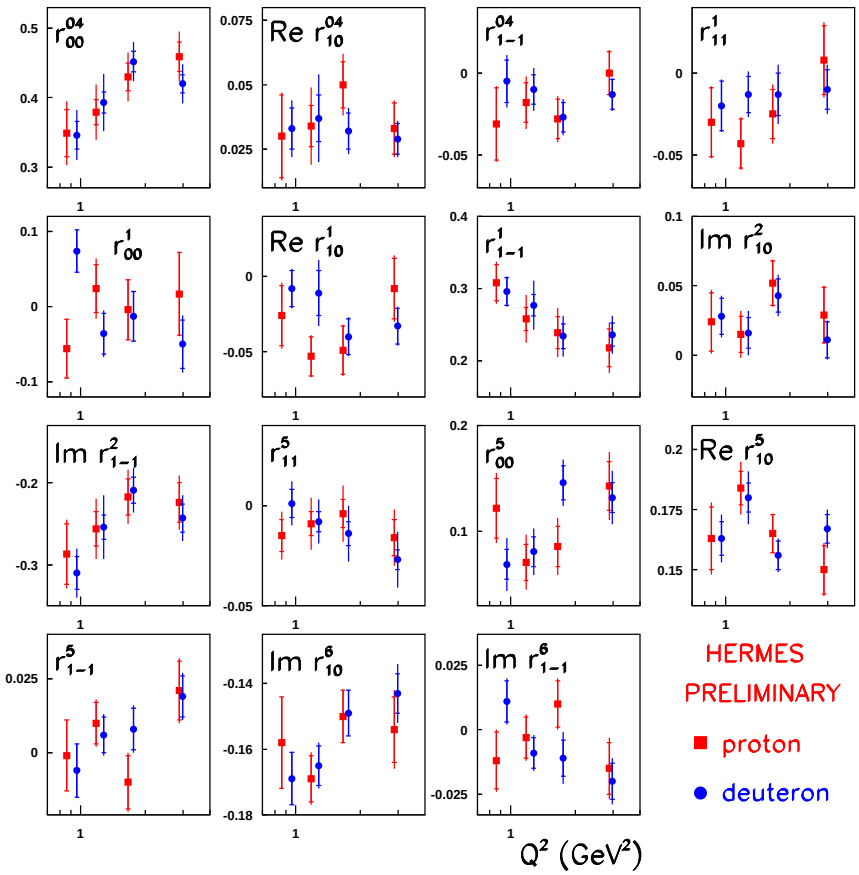

Figure 4: *The dependences of the ρ^0 mesons SDME's on Q^2 for proton and deuteron targets .*

In Fig. 5 the dependences on t' are presented. The much more interesting here are the elements related to amplitudes describing the single spin flip, $\gamma^*_T \to V_L$: Re$\{r^{04}_{10}\}$, Re$\{r^{1}_{10}\}$, Im $\{r^{2}_{10}\}$ and r^{5}_{00}. This subset describes the so-called strong spin flip transition. The dependences are easily seen. But for the second subset, defined by the transition $\gamma^*_L \to V_T$ and elements r^{5}_{11}, r^{5}_{1-1}, as well as Im$\{r^{6}_{1-1}\}$, the dependences are weaker. Similar to the previously presented Q^2 dependences also here no differences between proton and deuteron targets

are observed.

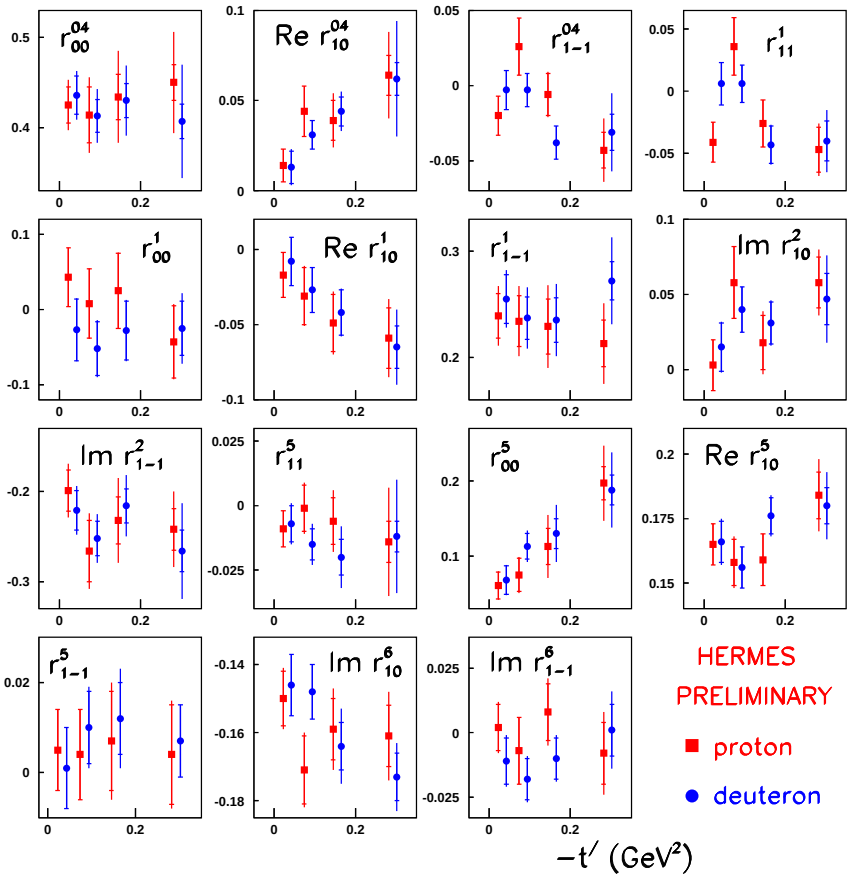

Figure 5: *The dependences of the ρ^0 mesons SDME's on t' for proton and deutron targets.*

7 Summary

The SDME's were determined for ρ^0 and ϕ^0 vector mesons. It was found that the SCHC mechanism with NPE is dominating. In the case of ρ^0 mesons the non-conservation SCHC transitions–particulary for $\gamma^* \to \rho_L$–and an UPE

signal is observed. The dependences on Q^2 of elements corresponding to SCHC in the case of ϕ^0 and ρ^0 are similar. The similarity is also observed for the interference phases between amplitudes T_{00} and T_{11}. In both cases the observed values of the phase were found to lie in the range of $\delta \sim 20^0 - 30^0$. Using data with polarized beam the positive sign of the phase was determined. Monotonic dependences on t' were also observed for elements belonging to class C.

References

1. S.J. Brodsky *et al.*, Phys. Rev. **D 50**, 3134 (1994).
2. L. Frankfurt *et al.*, Phys. Rev. **D 54**, 3194 (1996).
3. J.C. Collins *et al.*, Phys. Rev. **D 56**, 2982 (1997).
4. K. Ackerstaff *et al.*, NIM **A 417**, 230 (1998).
5. N. Akopov *et al.*, NIM **A 479**, 511 (2002).
6. K. Schilling *et al.*, Nucl. Phys **B 15**, 397 (1970).
7. K. Schilling *et al.*, Nucl. Phys **B 61**, 381 (1973).
8. H. Fraas *et al.*, Ann. Phys. **87**, 417 (1974).

Frascati Physics Series Vol. XLVI (2007), pp. 1127–1134
HADRON07: XII Int. Conf. on Hadron Spectroscopy – Frascati, October 8-13, 2007
Hadron Structure

DEEPLY VIRTUAL COMPTON SCATTERING AND GENERALIZED PARTON DISTRIBUTIONS AT CLAS

Silvia Niccolai
IPN Orsay
for the CLAS Collaboration

Abstract

The exclusive electroproduction of real photons and mesons at high momentum transfer allows us to access the Generalized Parton Distributions (GPDs). The formalism of the GPDs provides a unified description of hadronic structure in terms of quark and gluonic degrees of freedom. In particular, Deeply Virtual Compton scattering (DVCS), $ep \to e'p'\gamma$, is one of the key reactions to determine the GPDs experimentally, as it is the simplest process that can be described in terms of GPDs. A dedicated experiment to study DVCS has been carried out in Hall B at Jefferson Lab. Beam-spin asymmetries, resulting from the interference of the Bethe-Heitler process and DVCS have been extracted over the widest kinematic range ever accessed for this reaction ($1 < Q^2 < 4.6$ (GeV/c)^2, $0.09 < -t < 1.8$ (GeV/c)^2, $0.1 < x_B < 0.58$). In this paper, the results obtained experimentally are shown and compared to GPD parametrizations.

1 GPDs and DVCS

The Generalized Parton Distributions (GPDs), introduced nearly a decade ago, have emerged as a universal tool to describe hadrons, and nucleons in particular, in terms of their elementary consituents, the quarks and the gluons [1, 2, 3, 4, 5]. The GPDs, which generalize the features of form factors and ordinary parton distributions, describe the correlations between partons in quantum states of different (or same) helicity, longitudinal momentum, and transverse position. They also can give access, via the Ji's sum rule [3], to the contribution to the nucleon spin coming from the orbital angular momentum of the quarks. There are four different GPDs for the nucleon: H, E (the two spin-independent GPDs), $\tilde{H}$, $\tilde{E}$ (the two spin-dependent GPDs), and they can be measured in exclusive hard reactions.

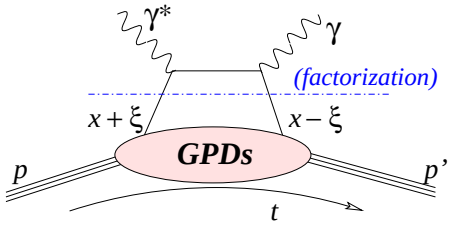

Figure 1: *Leading-order "handbag diagram" for DVCS. x is the average longitudinal momentum fraction of the active quark in the initial and final states, while 2ξ is their difference ($\xi \simeq x_B/(2-x_B)$, where x_B is the Bjorken scaling variable). $t = (p'-p)^2$ is the squared four-momentum trasfered to the target.*

Deeply Virtual Compton scattering (DVCS), $ep \to e'p'\gamma$, is the simplest process to access GPDs. In the Bjorken regime (high γ^* virtuality Q^2, small squared momentum transfered to the nucleon t) and at leading twist, this mechanism (Fig. 1) corresponds to the absorption of a virtual photon by a quark carrying the longitudinal momentum fraction $x+\xi$. The struck quark emits a real photon and goes back in the nucleon with the longitudinal momentum fraction $x-\xi$. The amplitude for DVCS is factorized [2, 3] into a hard-scattering part (exactly calculable in pQCD) and a non-perturbative part, representing the

soft structure of the nucleon, parametrized by the GPDs, which will depend on the three kinematic variables x, ξ and t.
The DVCS amplitude interferes with the amplitude for Bethe-Heitler (BH), the process where the real photon is emitted either by the incoming or the scattered electron (Fig. 2). Although these two reactions are experimentally indistinguishable, the BH is known and exactly calculable via the electromagnetic form factors. Furthermore, their different sensitivity to the polarization of the beam or of the target can also be positively exploited.

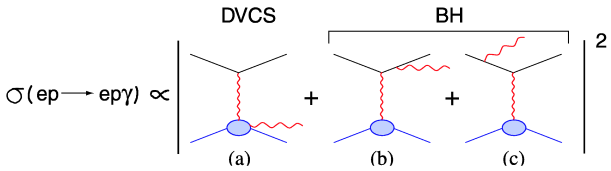

Figure 2: *The $ep \to e'p'\gamma$ cross section is the sum of the DVCS and the Bethe-Heitler process (where the photon is emitted by either the incoming or the outgoing electron).*

On the one hand, the unpolarized cross section for this process can be written as

$$\frac{d\sigma}{dQ^2 dx_B dt d\phi} \propto |T_{BH}|^2 + |T_{DVCS}|^2 + I, \quad (1)$$

where I is the interference term. The sum on the right-hand side is dominated - at least for the electron-beam energies accessible at Jefferson Lab, where $|T_{BH}|^2 >> |T_{DVCS}|^2$ - by the contribution of the Bethe-Heitler process, $|T_{BH}|^2$.
On the other hand, the helicity-dependent cross-section difference, which can be written as

$$\frac{d\sigma^+}{dQ^2 dx_B dt d\phi} - \frac{d\sigma^-}{dQ^2 dx_B dt d\phi} \propto T_{BH} \cdot Im[T_{DVCS}] \propto a \cdot \sin\phi + b \cdot \sin 2\phi, \quad (2)$$

where "+" and "-" correspond to the two opposite beam helicities, is directly proportional to the interference term, and thus to the imaginary part of the DVCS amplitude. The DVCS-BH interference term can be decomposed in $sin\phi$

and $\sin 2\phi$ terms (where ϕ is the angle between the leptonic and the hadronic planes), whose coefficients are proportional to integrals of GPDs [6]. At twist-2, which corresponds to the "handbag" approximation, the $\sin\phi$ term is expected to be dominant.
After a few first promising observations in non-dedicated experiments of DVCS asymmetries (beam spin [7, 8] and longitudinal target spin [9]) showing $\sin\phi$ dominance, a recent precise dedicated experiment [10] gave indications that scaling is achieved in this process at relatively modest Q^2 values. In the dedicated CLAS experiment here reported, the first systematic and precise exploration of the $ep \to e'p'\gamma$ over the widest phase-space covered so far has been achieved.

2 The experiment

The experiment (e1-dvcs) was performed at Jefferson Lab during two months in the spring of 2005, using the Hall B CLAS detector [11] and a 5.775 GeV longitudinally-polarized electron beam, delivered by the CEBAF accelerator, which impinged on a 2.5-cm-long liquid-hydrogen target. All the three particles in the $ep\gamma$ final state were detected in CLAS. In order to increase the acceptance of the detector for the DVCS-BH photons, mostly emitted at forward angles, a new inner calorimeter (IC), made up of 424 lead-tungstate crystals - each 16 cm long and having 2.1 cm^2 square section -, was added to the standard CLAS configuration [12]. After selecting the $ep\gamma$ events and applying the standard CLAS fiducial cuts to exclude the least efficient areas of the detector, kinematic cuts (on the trasverse missing momentum, on the missing energy, and on the cone angle between the measured and calculated photon) were applied in order to ensure exclusivity. The remaining background, due to the $ep\pi^0$ events where only one of the two decay photons was detected which survived the exclusivity cuts, was estimated, using Monte-Carlo simulations and detected $ep\pi^0 \to e'p'\gamma\gamma$ events. The contamination due to π^0 events so estimated varies between 1 and 25% depending on the kinematics [12].

3 Results

In order to extract beam-spin asymmetries, the selected data sample was divided into 13 bins in the (Q^2, x_B) plane (Fig. 3, left), in 5 bins in $-t$ (from

0.09 GeV^2/c^2 up to 1.8 GeV^2/c^2), and in 12 bins in ϕ, each 30^o wide [12]. The beam-spin asymmetry was then calculated, for each bin, as

$$A = \frac{N^+ - N^-}{P(N^+ + N^-)}, \tag{3}$$

where $N^{+(-)}$ is the number of $ep\gamma$ events for positive (negative) beam helicity, and P is the beam polarization ($P = 0.794$ in average for this experiment), and then fitted with the function

$$A = \frac{a \sin\phi}{(1 + c\cos\phi)}. \tag{4}$$

represented by red long-dashed curve in Fig. 3, right side. The terms in the denominator in Eq. 4 arise from the ϕ expansion of the unpolarized DVCS-BH cross section (Eq. 1) [6].

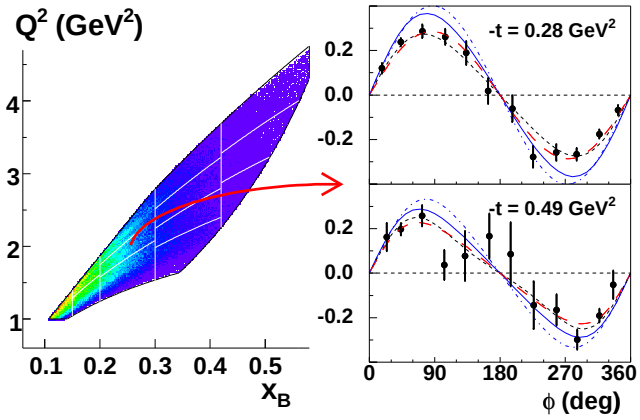

Figure 3: *Left: kinematic coverage and binning in the (Q^2, x_B) plane. Right: beam-spin asymmetry as a function of ϕ for 2 of the 62 (Q^2, x_B, t) bins. The red long-dashed curve corresponds to the fit with Eq. 4. The black dashed curve is a Regge calculation [14]. The blue curves correspond to the GPD calculation of Ref. [13] at twist-2 (solid) and twist-3 (dot-dashed) levels, with the contribution of the GPD H only.*

The parameter a, corresponding to the asymmetry at 90^o, appears to be dominant with respect to c at the lowest $-t$ values. Its evolution as a function of $-t$ for each (Q^2, x_b) is plotted in Fig. 4.

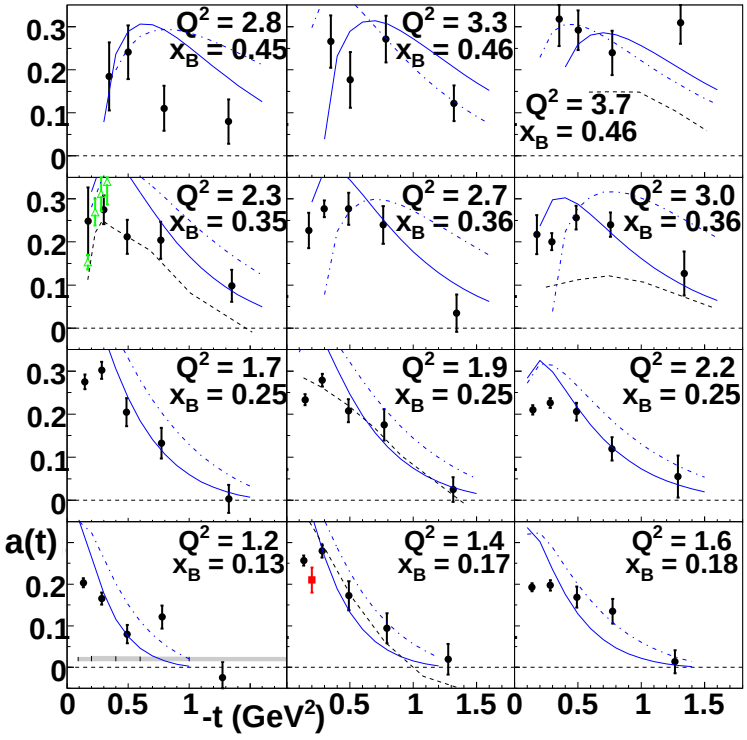

Figure 4: *The parameters $a = A(90^o)$ is plotted, as a function of $-t$, for each (Q^2, x_B) bin. The black points represent this work, the green and the red ones are the results, respectively, from Ref.* [10] *and Ref.* [7]*. The curves are described in the caption of Fig. 3*

The obtained values of $a(t)$, which are in good agreement with the previous CLAS result [7] and with the more recent points from Hall A [10], have been compared to the predictions of a GPD parametrization [13]. In this model, only the contribution of the GPD H was retained. H is here described with a double-distribution with Regge-inspired t slope plus a D-term calculated

within the chiral-soliton model [13]. This model overestimates the experimental asymmetries at low t, expecially at low values of Q^2 and x_B.
The data have also been compared to Regge calculations based on meson exchange, in which DVCS is viewed as ρ production followed by $\rho-\gamma$ coupling in vacuum or in the nucleon field [14]. This calculation, shown as a dashed curve in Figs. 3 and 4, is in fair agreement with the experiment in some kinematic bins.
The meaning of a possible dual description for DVCS (handbag vs. meson exchange) remains to be investigated.

4 Summary and perspectives

The most extensive data set for DVCS up to date was obtained with the CLAS detector in the e1-dvcs experiment. Beam-spin asymmetries, as a function of Q^2, x_b, t and ϕ were extracted in the valence quark region. The measured kinematic dependences will put strong constraints on any DVCS model, and in particular on the Generalized Parton Distributions of the nucleon.
The e1-dvcs data used to extract the presented beam-spin asymmetries are also under analysis to obtain unpolarized DVCS cross sections and polarized cross section differences [15]. Analyses to extract cross sections for various meson electroproduction channels ($ep \to e'p'\pi^0$, $ep \to e'p'\eta$, $ep \to e'n\rho^+$) are underway as well, and they will provide constraints for models on the flavor decomposition of GPDs.
In the near future, an experiment to measure DVCS on a longitudinally polarized target is scheduled to run in the Hall B for the second half of 2008: it will be mainly focused in the extraction of target-spin asymmetries (which are sensitive to a different combination of GPDs compared to the beam-spin asymmetries), but it will also allow, for the first time, to obtain double-spin (beam and target) asymmetries, linked to the *real part* of the DVCS amplitude.
For the future at longer term, measurements of GPDs via DVCS and meson electroproduction will be among the main subjects of the program driving the 12 GeV upgrade for the CEBAF accelerator and the new CLAS12 detector.

References

1. D. Muller, D. Robaschik, B. Geyer, F.M. Dittes, and J. Horejsi, Fortschr. Phys. 42, 101 (1994).
2. A.V. Radyushkin, Phys. Rev. D **56**, 5524 (1997).
3. X.-D. Ji, Phys. Rev. Lett. **78**, 610 (1997).
4. M. Burkardt, Phys. Rev. D **62**, 071503 (2000).
5. M. Diehl, Eur. Phys. J. C **25**, 223 (2002).
6. A.V. Belitski, D. Muller, and A. Kirchner, Nucl. Phys. **B629**, 323 (2002).
7. S. Stepanyan *et al* (CLAS), Phys. Rev. Lett. **87**, 182002 (2001).
8. A. Airapetian *et al* (HERMES), Phys. Rev. Lett. **87**, 182001 (2001).
9. S. Chen *et al* (CLAS), Phys. Rev. Lett. **97**, 072002 (2006).
10. C. Munoz Camacho *et al*, Phys. Rev. Lett. **97**, 262002 (2006).
11. B.A. Mecking *et al*, Nucl. Instr. Meth. **A503**, 513 (2003).
12. F.X. Girod *et al* (CLAS), hep-ph: 0711.4805, submitted to Phys. Rev. Lett. (2007).
13. A.V. Radyushkin, in *At the Frontier of Particle Physics - Handbook of QCD*, M. Shifman Ed. (World Scientific, Singapore 2001), p. 1037; M. Guidal, M.V. Polyakov, and M. Vanderhaeghen, Phys. Rev. D **72**, 054013 (2005); K. Goeke, M.V. Polyakov, and M. Vanderhaeghen, Prog. Part. Nucl. Phys. **47**, 401 (2001).
14. J.M. Laget, arXiv:0708.1250 hep-ph (2007).
15. H.S. Jo, Ph.D. Thesis, Université Paris Sud, Orsay, France (2007).

Frascati Physics Series Vol. XLVI (2007), pp. 1135–1142
HADRON07: XII Int. Conf. on Hadron Spectroscopy – Frascati, October 8-13, 2007
Hadron Structure

LATEST HERMES RESULTS ON HARD-EXCLUSIVE PROCESSES

Tibor Keri on behalf of the HERMES collaboration
Justus-Liebig-Universität Giessen

Abstract

Hard exclusive processes provide unique access to Generalized Parton Distributions, which extend our description of the nucleon structure beyond the standard parton distributions. The Deeply Virtual Compton Scattering process and the hard-exclusive ρ^0 production are used to access the total angular momentum of quarks J_q. By comparing the HERMES result and the theoretical predications based on Generalized Parton Distributions, a model-dependent constraint on J_u and J_d has been obtained.

1 Introduction

The nucleon spin S_z can be schematically decomposite into the contributions [1)].

$$S_z = \frac{1}{2} = \frac{1}{2}\Delta\Sigma + L_q + \Delta G + L_g \tag{1}$$

$\Delta\Sigma$ is the contribution by the quark spin. The measured value is about $\frac{1}{3}$. First measurements of the contribution by the gluon spin ΔG indicate a value of the order of 0.1. The orbital angular momentum contributions by quarks L_q and gluons L_g are unknown so far. The total orbital angular momentum of the nucleon can be separated into the quark contribution $J_q = \frac{1}{2}\Delta\Sigma + L_q$ and the gluon contribution $J_g = \Delta G + L_g$. Using hard-exclusive reactions, HERMES was able to extract first model dependent results on J_q.

2 The HERMES forward spectrometer

The HERMES experiment [2)] is one of the four experiments in the Hadron Electron Ring Anlage (HERA) at Deutsche Electron Sychrotron (DESY) in Hamburg / Germany. HERA consists off two parallel synchrotron rings for protons and e^-/e^+-leptons. The 27.5 GeV lepton beam is self-polarizing due to the Sokolov-Ternov effect with an average polarization of around 55%. The HERMES experiment is running with H-, D-, N- and noble gases as fixed gas target. The gas target can be polarized in longitudinal or transverse direction. Together with the longitudinally or transversely polarized lepton beam accurate and unique studies are possible to access the budget of the nucleon spin. The spectrometer has a very highly efficient particle identification (PID) by a Ring Imaging Cherenkov Detector and a Transition Radiation Detector. The leptons and photons are detected by a preshower detector and an electromagnetic calorimeter. Drift chambers and proportional chambers are used for tracking. The recoiling particles is not detected. The events selection for exclusivity is done by missing mass kinematic calculation.

3 Nucleon spin budget

As the spin contribution by quarks and gluons does not match the nucleon spin budget, access to the orbital angular momentum of quarks and gluons is necessary. The HERMES experiment has a wide range of physics program to investigate the nucleon spin contribution [3)]. A promising way to access the missing information are the Generalized Parton Distributions (GPD) [4)].

Table 1: *Generalized Parton Distributions*

unpolarized	polarized	nucleon helicity
$H(x,\xi,t)$	$\tilde{H}(x,\xi,t)$	conserved
$E(x,\xi,t)$	$\tilde{E}(x,\xi,t)$	flipped

3.1 GPD formalism

The Form Factors (FF) of the nucleon as measured in elastic scattering as function of target momentum transfer t can be interpreted in terms of transverse positions of quarks in the nucleon. The longitudinal momentum distribution of quarks is accessible via Deep Inelastic Scattering and is parameterized in Parton Distribution Functions (PDF) as function of target momentum fraction x. In the GPD a combination of transverse position and longitudinal momentum distribution is accessible via hard-exclusive processes. These distributions H, E, $\tilde{H}$, $\tilde{E}$ (see tab.1) are functions of x, t and of the skewedness ξ. The first moments of GPD are the FF, while the GPD in the limit $t \to 0$ describes the PDF. The Ji sum rule (see eq.2) relates the GPD to the total angular momentums for quarks and gluons.

$$J_{q,g} = \lim_{t\to 0} \int_{-1}^{+1} dx\ x[H_{q,g}(x,\xi,t) + E_{q,g}(x,\xi,t)] \tag{2}$$

Hard exclusive processes in deep inelastic lepton scattering provide access to the unknown GPD of the nucleon. The different final states make different GPD accessible. For example, vector meson production gives access to H and E, while pseudoscalar meson production provides access to $\tilde{H}$, $\tilde{E}$. Deeply Virtual Compton Scattering (DVCS) enables to access all four GPD and is the simplest and cleanest way to access the GPD.

3.2 The Hard-Exclusive DVCS Process

The final state of DVCS is indistinguishable of the Bethe Heitler process (BH). The total cross section is the coherent sum:

$$d\sigma \propto |\tau_{BH} + \tau_{DVCS}|^2 = |\tau_{BH}|^2 + |\tau_{DVCS}|^2 + |\tau^*_{BH}\tau_{DVCS} + \tau^*_{DVCS}\tau_{BH}| \tag{3}$$

While $|\tau_{BH}|^2$ can be calculated in QED in terms of the Dirac and the Pauli form factors F_1 and F_2, $|\tau_{DVCS}|^2$ is parameterizable in terms of Compton Form

Factors $\mathcal{H}$, $\mathcal{E}$, $\tilde{\mathcal{H}}$, $\tilde{\mathcal{E}}$, which are convolutions of the GPD H, E, $\tilde{H}$, $\tilde{E}$. Due to kinematics, fixed target experiments like HERMES and JLab have access to the interference term by azimuthal asymmetries and provide linear combinations of the DVCS amplitudes in magnitude and phase. Combining data with different charges C and helicity P allows the decomposition of the interference term I (see eq.4) in Fourier sums that depend on different GPD. Fig.1(a) shows the definition of the azimuthal angle ϕ and the polarisation angle ϕ_S, which will be needed later.

$$I = |\tau^*_{BH}\tau_{DVCS} + \tau^*_{DVCS}\tau_{BH}| \propto C(c_0 + \sum_n c_n \cos n\phi + P(s_n \sin n\phi)) \quad (4)$$

By combining longitudinally polarized beam data with different helicity the GPD $\mathcal{I}m(\mathcal{H})$ is accessible by cross section asymmetries $A_{LU} \propto \mathcal{I}m(\mathcal{H}) \sin\phi$. For an unpolarized proton target this yields $A_{LU}^{\sin\phi} = -0.18 \pm 0.03(stat.) \pm 0.03(sys.)$ for $< -t >= 0.18\text{GeV}^2$, $< x >= 0.12$ and $< Q^2 >= 2.5\text{GeV}^2$. Currently a reanalysis with over 20 times more data is in progress.

Unique at HERA is the possibility to measure the beam charge asymmetry. By combining e^-- and e^+-beam data the GPD $\mathcal{R}e(\mathcal{H})$ is accessible by $A_C \propto \mathcal{R}e(\mathcal{H}) \cos\phi$. For proton $A_C^{\cos\phi}$ is $0.063 \pm 0.029(stat.) \pm 0.026(sys.)$. Here a first separation of different GPD can be achieved. Comparison of VGG-calculations with four different setups disfavors the Regge-model with D-term (see fig.1(b)). Ten times more data is used for the reanalysis.

With the longitudinal target spin asymmetry access to $\mathcal{I}m(\tilde{\mathcal{H}})$ by $A_{UL} \propto \mathcal{I}m(\tilde{\mathcal{H}}) \sin\phi$ is possible. A_{UL} for proton is $-0.071 \pm 0.034(stat.)$. Here appear an unexpected $\sin 2\phi$ dependence by more than 3σ from zero. A possible reason is a π^0 background contamination. A more accurate reanalysis is planned. For deuterium the result is consistent with zero.

In case of target transverse spin asymmetry (TTSA) the GPD E is not suppressed. The amplitude A_{UT} (see eq.5) is given by

$$A_{UT} \propto \mathcal{I}m\left[F_2\mathcal{H} - F_1\mathcal{E}\right](\sin\phi - \phi_S\cos\phi) + \mathcal{I}m\left[F_2\tilde{\mathcal{H}} - F_1\tilde{\mathcal{E}}\right](\cos\phi - \phi_S\sin\phi). \quad (5)$$

The $A_{UT}^{\cos\phi-\phi_S\sin\phi}$ term has a very weak dependence to J_u with the assumption of $J_d = 0$, while the $A_{UT}^{\sin\phi-\phi_S\cos\phi}$ term has a strong dependence on J_u (see fig.2(a)). With the Ji sum rule (see eq.2) a first model dependent constraint on the total angular momentum of quarks by p-DVCS is accessible.

The complementary measurements by n-DVCS at JLab Hall A give another model dependent constraint (see fig.2(b)) [7]. Several other QCD-calculations yield results which are close to these results on the total angular momentum contribution of u- and d-quarks to the nucleon spin budget.

3.3 *Hard Exclusive ρ^0 production*

Hard Exclusive ρ^0 production probes quark and gluon content of the nucleon by the same order of α_S and in linear dependence of GPD [5]. As GPD H and especially GPD E are not suppressed in TTSA, this gives an alternative to access the total angular momentum of quarks and of gluons. The factorization is only proven for longitudinal photons and is therefore challenging. Longitudinal and transverse ρ^0 contributions to the cross section have different dependency on θ^*, which is the polar angle of decay π^+ in the ρ^0 rest frame. The event selection requires exactly one scattered beam lepton, two oppositely charged pions and exclusivity by the missing mass method. Even with 10% background contamination from semi-inclusive pion production, limited acceptance and experimental resolution the result is in good agreement with the result from DVCS. The current results seems to favor a positive J_u (see fig.3(a)). The challenging quantification of J_u by hard exclusive meson production processes is improved by currently fast developments in theory.

4 Recoil Detector

In order to improve exclusivity, t-resolution and suppression of background the HERMES experiment was upgraded with a Recoil Detector (RD) [6]. Intensive Monte Carlo studies including hard exclusive processes like DVCS and BH have been carried out in the design of the detector. The momentum range for recoiling particles lies between 50MeV/c and 1.5GeV/c. The polar angle of the recoil proton is below $\pi/2$ with respect to the beam axis. A detector covering this angular range suppresses background contamination from 5% to far below 1% for semi-inclusive processes and from 11% to below 1% for associated BH-processes.

The RD (see fig.3(b)) consists off three sub-detectors; a Silicon Strip Detector (SSD), a Scintillating Fiber Tracker (SFT) and a Photon Detector (PD). The SSD, which is located in the beam vacuum to detect very low momentum

particles, consists of two layers with in total 16 Tigre-sensors, each with an active area of 99*99mm^2, 300μm thick and 756μm strip pitch. The SFT consists of two barrels each with two parallel layers and two stereo layers of scintillating fibers. The angle between parallel fibers and stereo fibers is 10^o. These two sub-detectors achieve PID and momentum reconstruction between 100MeV/c and 1.5GeV/c. The PD is a tungsten-scintillator calorimeter with three layers of fibers with parallel, $+45^o$ and -45^o inclination for PID and gamma ray detection. An additional feature of the PD is the Cosmic Trigger for alignment and calibration measurements.

Although the RD is not perfectly understood yet, the available tools to look at hard-exclusive processes are already working very well. Full tracking with alignment to the HERMES forward spectrometer is implemented. Several track reconstruction algorithms are available to make cross checks. The residuals of the starting vertex reconstruction are about 33μm for real data and about 27μm for MC data. The current tracking efficiency for MC data is above 98%. Major topics like time dependent noise corrections, calibrations and beam geometry corrections are already working very fine. A highly dedicated group improves the understanding of RD rapidly further. During the 16 month of data taking 13k (7.4M) events as DVCS (DIS)-candidates for proton and 3k (1.5M) events for deuterium with e^- beam with SFT-only has been collected. With e^+ beam 60k (40M) events for proton and 15k (10M) events for deuterium are on tapes.

5 Conclusions

The aim is to show the pioneering work to understand the spin budget of the nucleon investigated by the HERMES experiment and others. The Generalized Parton Distribution model is used to access the total angular momentum of the quarks by the Deeply Virtual Compton Scattering process and by ρ^0 meson production. Both hard exclusive processes give different access to a first model dependent constraint on the J_u and J_d (see fig. 2(b)).

The successful update in 2005 and data taking of the HERMES experiment together with the Recoil Detector improves the exclusivity and suppresses the background drastically. The informations gained by the study of the Recoil Detector will be used to reanalyze previous data to improve the current results.

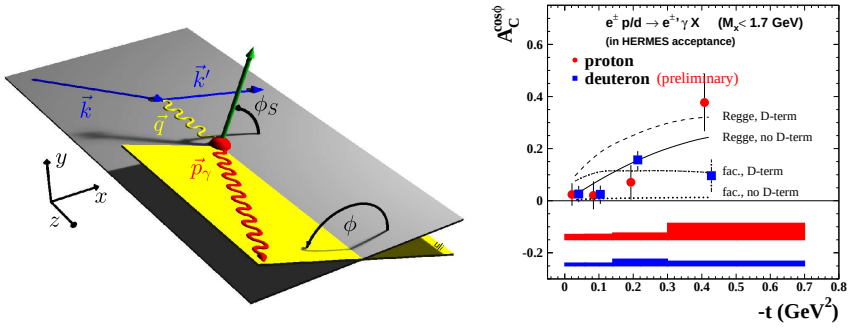

(a) (b)

Figure 1: *(a) Definition of ϕ and ϕ_S. (b) The $\cos\phi$ amplitude of the beam-charge asymmetry on proton and on unpolarized or spin-averaged polarized deuterium as a function of $-t$ at average values of $< x >= 0.10$ and $< Q^2 >= 2.5 GeV^2$. The GPD model calculations use a factorized or a Regge-inspired t-dependence with or without a D-term contribution.*

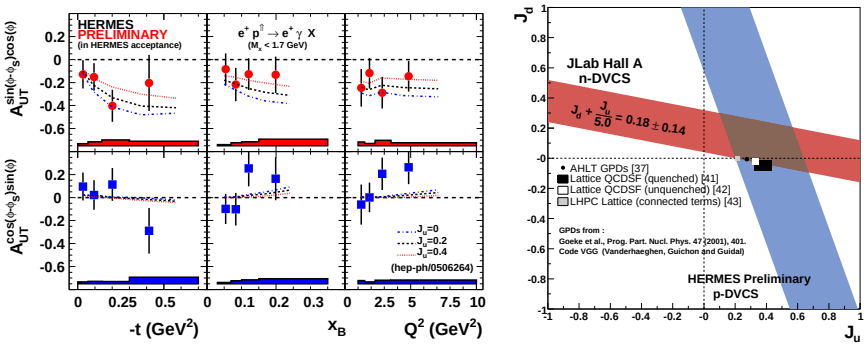

(a) (b)

Figure 2: *(a) The $\sin\phi - \phi_S \cos\phi$ amplitude (upper) and the $\cos\phi - \phi_S \sin\phi$ amplitude (lower) of the transverse target-spin asymmetry as a function of $-t$, x_B and Q^2 in comparison with theoretical predictions. (b) Model dependent constraint on the u- and d-quark total angular momentum J_u and J_d based on p-data by HERMES and n-data by JLab Hall A with some Lattice QCD calculations.*

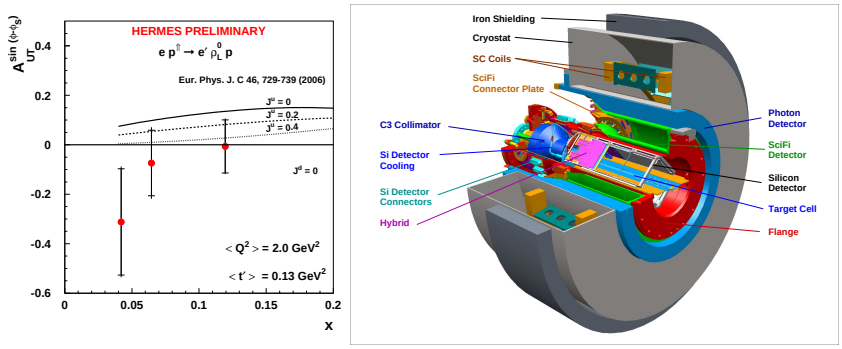

(a) (b)

Figure 3: *(a) x_B dependences of $A_{UT}^{\sin\phi-\phi_S}$ moment of the TTSA of exclusive production of ρ_L^0 mesons compared to the model calculations. The error bars represent the total error. (b) The 3D model of the HERMES Recoil Detector.*

6 Acknowledgments

We gratefully acknowledge the DESY management for its support, the staff at DESY, our national funding agency BMBF and the EU for financial support. The author want to thank the HERMES collaboration for the fine support.

References

1. HERMES, A. Airapetian, *et al.*, arXiv:9907020v1 [hep-ex] (1999)
2. HERMES, K. Ackerstaff, *et al.*, Nucl. Instrum. Meth. **A417**,230 (1998)
3. HERMES, M. Düren, *et al.*, this volume (2007)
4. HERMES, F. Ellinghaus, *et al.*, arXiv:0710.5768v1 [hep-ex] (2007)
5. HERMES, A. Rostomyan, *et al.*, arXiv:0707.2486v1 [hep-ex] (2007)
6. HERMES, N. Pickert, *et al.*, Nucl. Instrum. Meth. **A 581**, 504, (2007)
7. HERMES, Z. Ye, *et al.*, arXiv:0606061v1 [hep-ex] (2006)
   JLab Hall A, M. Mazouz, *et al.*, arXiv:0709.0450v1 [nucl-ex] (2007)

Frascati Physics Series Vol. XLVI (2007), pp. 1143
HADRON07: XII Int. Conf. on Hadron Spectroscopy – Frascati, October 8-13, 2007
Hadron Structure

STUDY OF THE LOW ENERGY INTERACTION OF HADRONS AT COSY-11

R. Czyzykiewicz
Jagellonian University

Written contribution not received

Frascati Physics Series Vol. XLVI (2007), pp. 1145–1152
HADRON07: XII Int. Conf. on Hadron Spectroscopy – Frascati, October 8-13, 2007
Hadron Structure

SYSTEMATIC ERRORS OF TRANSITION FORM FACTORS EXTRACTED BY MEANS OF LIGHT-CONE SUM RULES

Wolfgang Lucha
Institute for High Energy Physics, Austrian Academy of Sciences, Nikolsdorfergasse 18, A-1050, Vienna, Austria
Dmitri Melikhov
Institute for High Energy Physics, Austrian Academy of Sciences, Nikolsdorfergasse 18, A-1050, Vienna, Austria
and
Nuclear Physics Institute, Moscow State University, 119992, Moscow, Russia
Silvano Simula
INFN, Sezione di Roma III, Via della Vasca Navale 84, I-00146, Roma, Italy

Abstract

This talk presents results of our study of heavy-to-light transition form factors extracted with the help of light-cone sum rules. We employ a model with scalar particles interacting via massless-boson exchange and study the heavy-to-light correlator, relevant for the extraction of the transition form factor. We calculate this correlator in two different ways: by making use of the Bethe–Salpeter wave function of the light bound state and by making use of the light-cone expansion. This allows us to calculate the full correlator and separately the light-cone contribution to it. In this way we show that the off-light cone contributions are not suppressed compared to the light-cone one by any large parameter. Numerically, the difference between the value of the form factor extracted from the full correlator and from the light-cone contribution to this correlator is found to be about 20–30% in a wide range of masses of the particles involved in the decay process.

In a previous talk [1] (see also Ref. [2] for details) we have shown that the hadron parameters can be extracted from sum rules only with some accuracy, which lies beyond the control of the standard procedure adopted in the method of sum rules, even if the correlator in a limited range of the Borel parameter is known *precisely*. In the light-cone sum-rule analysis of hadron form factors, the relevant correlator is not known precisely and is obtained as an expansion near the light cone (LC) [3]. This entails additional uncertainties in the extraction of hadron parameters, in this case, of the form factors. This talk reports the results of our recent systematic analysis of off-light-cone effects in sum rules for heavy-to-light form factors [4].

The effects are investigated in a model involving scalar constituents. We consider two types of scalar "quarks", viz., heavy quarks Q of mass m_Q and light quarks φ of mass m, and study the weak transition of the heavy scalar "meson" $M_Q(Q\varphi)$ to the light "meson" $M(\varphi\varphi)$ induced by the weak heavy-to-light $Q \to \varphi$ quark transition. The analysis of this model is technically simpler but allows one to study some essential features of the corresponding QCD case.

For calculating the correlator of interest, we need the Bethe–Salpeter (BS) amplitude of the light meson, defined by

$$\Psi_{\rm BS}(x,p') = \langle 0|T\varphi(x)\varphi(0)|M(p')\rangle = \Psi(x^2, xp', p'^2 = M^2). \tag{1}$$

As a function of xp', this amplitude may be represented by the Fourier integral

$$\Psi_{\rm BS}(x,p') = \int\limits_0^1 {\rm d}\xi \exp(-{\rm i}\xi p'x) K(x^2,\xi), \tag{2}$$

where the ξ-integration runs from 0 to 1. The kernel $K(x^2,\xi)$ may be expanded near the light cone $x^2 = 0$:

$$K(x^2,\xi) = \phi_0(\xi) + x^2\,\phi_1\left(\xi, \log(-x^2)\right) + {\rm O}(x^4). \tag{3}$$

It is convenient to use the parametrization of $K(x^2,\xi)$ proposed by Nakanishi [5]

$$K(x^2,\xi) = \frac{1}{(2\pi)^4{\rm i}} \int\limits_0^\infty {\rm d}z\, G(z,\xi) \int \frac{{\rm d}^4k' \exp(-{\rm i}k'x)}{[\,z + m^2 - \xi(1-\xi)M^2 - k'^2 - {\rm i}0]^3}, \tag{4}$$

where $G(z,\xi)$ exhibits no singularities in the integration regions in z and ξ. The function $G(z,\xi)$ may be obtained as the solution of an equation obtained from the BS equation for $\Psi_{\rm BS}(x,p')$. The LC distribution amplitudes ϕ_i

can be expressed in terms of $G(z,\xi)$. For instance, the light-cone distribution amplitude reads

$$\phi_0(\xi) \quad = \quad \frac{1}{32\pi^2}\int\limits_0^\infty \mathrm{d}z\,\frac{G(z,\xi)}{z+m^2-\xi(1-\xi)M^2}. \tag{5}$$

For interactions dominated by exchange of a massless boson at small distances, the solution of the BS equation in the ladder approximation takes the form [6)]

$$G(z,\xi)=\delta(z)G(\xi), \qquad G(\xi)=\xi(1-\xi)f(\xi), \tag{6}$$

where $f(\xi)$ is nonzero at the end-points. In this case, all distribution amplitudes exhibit the same end-point behaviour, namely,

$$\phi_0(\xi)\simeq\xi, \qquad \phi_1(\xi)\simeq\xi, \qquad \ldots. \tag{7}$$

Now, to extract the $M_Q\to M$ transition form factor, we analyze the correlator

$$\Gamma(p^2,q^2)=\mathrm{i}\int \mathrm{d}^4x\exp(\mathrm{i}px)\langle 0|T\varphi(x)Q(x)Q(0)\varphi(0)|M(p')\rangle. \tag{8}$$

We should (i) write this correlator as a dispersion representation in p^2

$$\Gamma_{\rm th}(p^2,q^2)=\int\frac{\mathrm{d}s}{s-p^2-\mathrm{i}0}\Delta_{\rm th}(s,q^2), \tag{9}$$

(ii) perform the Borel transform $p^2\to\mu^2$ which gives

$$\Gamma_{\rm th}(p^2,q^2)\to\hat{\Gamma}_{\rm th}(\mu^2,q^2)=\int \mathrm{d}s\exp\left(-s/2\mu^2\right)\Delta_{\rm th}(s,q^2), \tag{10}$$

and (iii) cut the correlator at an effective continuum threshold $s=s_0$ getting

$$\hat{\Gamma}_{\rm th}(\mu^2,q^2,s_0)=\int \mathrm{d}s\,\theta(s<s_0)\,\exp\left(-s/2\mu^2\right)\Delta_{\rm th}(s,q^2). \tag{11}$$

The form factor is related to the cut correlator by

$$f_{M_Q}\,F_{M_Q\to M}(q^2)=\exp\left(M_Q^2/2\mu^2\right)\hat{\Gamma}_{\rm th}\left(\mu^2,q^2,s_0(\mu^2,q^2)\right), \tag{12}$$

where f_{M_Q} is the decay constant of the heavy meson M_Q and $s_0(\mu^2,q^2)$ is an effective continuum threshold, dependent on both q^2 and μ^2.

For large m_Q and for $q^2 \ll m_Q^2$, up to terms power-suppressed by $1/m_Q^2$, the correlator reads [4]

$$\Gamma_{\rm th}(p^2,q^2) = \int \frac{{\rm d}^4k\,{\rm d}^4x}{(2\pi)^4} e^{{\rm i}x(p-k)} \frac{1}{m_Q^2-k^2-{\rm i}0} \langle 0|T\varphi(x)\varphi(0)|M(p')\rangle. \qquad (13)$$

In order to calculate this correlator, we may proceed along two different lines.
I. Express the correlator in terms of the BS amplitude $\Psi_{\rm BS}$ in momentum space:

$$\Gamma_{\rm th}(p^2,q^2) = \frac{1}{(2\pi)^4} \int {\rm d}^4k \frac{\Psi_{\rm BS}(k,p')}{m_Q^2-(p-k)^2-{\rm i}0}. \qquad (14)$$

It is then straightforward to calculate $\Delta_{\rm th}(s,q^2)$ in terms of the kernel $G(z,\xi)$. The corresponding explicit expression for $\Gamma_{\rm th}$ may be found in Ref. [4].
II. Use the light-cone expansion of $\Psi_{\rm BS}(x,p')$:

$$\Gamma_{\rm th}(p^2,q^2) = \int \frac{{\rm d}^4k\,{\rm d}^4x}{(2\pi)^4} e^{{\rm i}x(p-k)} \frac{1}{m_Q^2-k^2-{\rm i}0} \sum_{n=0}^{\infty} (x^2)^n \int\limits_0^1 {\rm d}\xi e^{-{\rm i}p'x\xi} \phi_n(\xi), \qquad (15)$$

with the functions $\phi_i(\xi)$ related to $G(z,\xi)$.

Let us introduce the following quantities: the binding energy of the heavy hadron ε_Q by $M_Q = m_Q + \varepsilon_Q$; a new Borel parameter β by $\mu^2 = m_Q\beta$; a new effective continuum threshold δ by $s_0 = (m_Q+\delta)^2$, such that $\varepsilon < \delta < \beta$. The parameters ε, δ, and β remain finite in the limit $m_Q \to \infty$. Hereafter, the light-meson mass is set equal to zero: $M = 0$. We consider the case $q^2 = 0$, and suppress the argument q^2 in the correlators.

The uncut Borel image (*not* related to the form factor of interest) reads

$$e^{\frac{M_Q^2}{2m_Q\beta}} \hat\Gamma_{\rm th}(\beta) = \int\limits_0^1 \frac{d\xi}{1-\xi} \left[\phi_0(\xi) - \frac{1}{\beta^2}\frac{\phi_1(\xi)}{(1-\xi)^2} + \cdots\right] \exp\left(-\frac{m_Q\xi}{2\beta(1-\xi)}\right). \qquad (16)$$

For large m_Q, the integral is saturated by region of small $\xi = O(\beta/m_Q)$.

The cut Borel image, i.e. the l.h.s. of (12) which yields the heavy-to-light form factor, takes the form [one should be careful with the surface terms when applying the cut in the dispersion representation, see details in ref.[4]]:

$$e^{\frac{M_Q^2}{2m_Q\beta}} \hat\Gamma_{\rm th}(\beta,\delta) = \int\limits_0^{\xi_0} \frac{d\xi}{1-\xi} \left[\phi_0(\xi) - \frac{\phi_1(\xi)}{\beta^2(1-\xi)^2} + \cdots\right] \exp\left(-\frac{m_Q\xi}{2\beta(1-\xi)}\right)$$
$$-4\exp\left(\frac{\varepsilon_Q-\delta}{\beta}\right)\left[\frac{\phi_1(\xi_0)}{m_Q^2} + \frac{\phi_1(\xi_0)}{2m_Q\beta} + \frac{\phi_1'(\xi_0)}{m_Q^2}\right] + \cdots, \qquad (17)$$

where $\xi_0 = 2\delta/m_Q$ and $\cdots$ stand for the contributions of terms corresponding to $n \geq 2$ and of terms power-suppressed for large m_Q.

Let us now address an important question: Are the off-LC contributions (which represent one of the higher-twist effects) suppressed compared to the light-cone contribution?

In the *uncut* correlator, the off-LC terms are suppressed by powers of the parameter $1/\beta$ (but remain of the same order in $1/m_Q$ as the LC contribution).

For the *cut* correlator, however, the situation is quite different because of the presence of surface terms. We may consider the following cases: $\delta, m \ll \beta$, while $m_Q \to \infty$ and $\delta, m \ll m_Q$, while $\beta \to \infty$. Due to the end-point behaviour of the distribution amplitudes (7), in both cases the contributions of the terms $n = 0, 1, \ldots$ have the same order. Therefore we conclude that *for the realistic case of interactions dominated by massless-boson exchange at short distances, the off-LC contributions are not suppressed compared to the LC contribution by any large parameter.*

Next, we give numerical estimates. Fig. 1 shows results for beauty-meson decay, with $M_Q = 5.27$ GeV, $m_Q = 4.8$ GeV, and $m = 150$ MeV. The discussion of the relevant parameter values and further examples may be found in Ref. [4].

Hereafter, the $n = 0$ contribution to the correlator in Eq. (15) is referred to as the light-cone correlator; $\Delta_{\rm LC}(s)$ is the corresponding spectral density.

Taking into account that the end-point region is essential for the transition form factors, we can without loss of generality take the kernel of the form $G(z, \xi) = m^2 \delta(z) \xi(1 - \xi)$. It is then straightforward to calculate the spectral densities $\Delta_{\rm th}$ and $\Delta_{\rm LC}$ [cf. Fig. 1]. It is important that the thresholds in $\Delta_{\rm th}$ and $\Delta_{\rm LC}$ do not coincide: in the light-cone spectral density the threshold is m_Q^2 whereas in the full spectral density it is $(m_Q + m)^2$. The region near the threshold provides the main contribution to the cut Borel-transformed correlator. The mismatch of the thresholds is responsible for the nonvanishing of the off-light-cone effects in the cut correlator.

The effective continuum threshold δ is the quantity which determines to a great extent the values of hadron observables extracted from the sum rule [2]. We fix δ by a standard procedure: we require that, for both LC and full spectral densities,

$$\langle s(\beta, \delta) \rangle = M_Q^2. \tag{18}$$

This equation may be used as the definition of the implicit function $\delta(\beta)$. We,

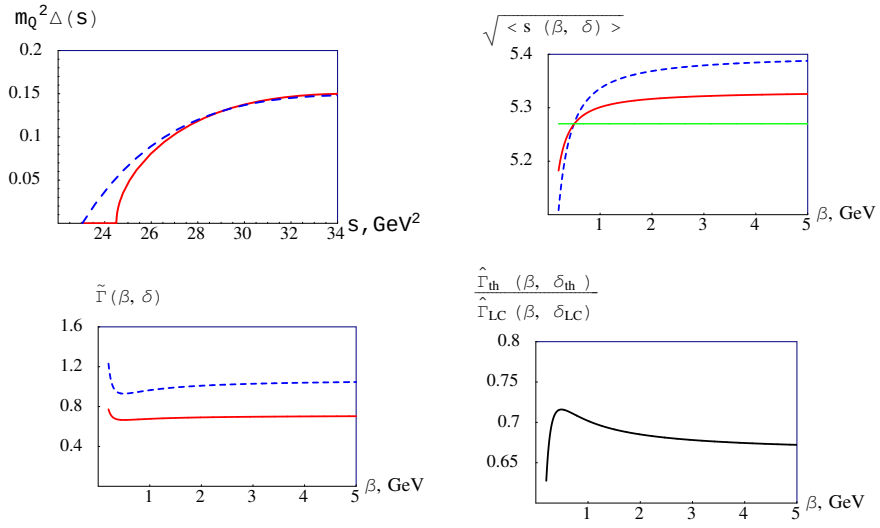

Figure 1: Plots for the parameters corresponding to beauty-meson decay $m_Q = 4.8$ GeV, $m = 150$ MeV, $\delta_{\rm LC} = 0.96$ GeV, and $\delta_{\rm th} = 0.79$ GeV. *Upper left panel*: Spectral densities $m_Q^2\Delta_{\rm th}(s)$ (solid red line) and $m_Q^2\Delta_{\rm LC}(s)$ (dashed blue line). *Upper right panel*: $\sqrt{\langle s\rangle_{\rm th}}$ (solid red line) and $\sqrt{\langle s\rangle_{\rm LC}}$ vs. β (dashed blue line). The horizontal (green) line locates $M_Q = 5.27$ GeV. *Lower left panel*: $\widetilde{\Gamma}(\beta,\delta) = m_Q^2 \exp\left(M_Q^2/(2\mu^2)\right)\hat{\Gamma}(\mu^2, s_0)$ vs. β: $\widetilde{\Gamma}_{\rm th}(\beta,\delta_{\rm th})$ (solid red line) and $\widetilde{\Gamma}_{\rm LC}(\beta,\delta_{\rm LC})$ (dashed blue line). *Lower right panel*: The ratio $\hat{\Gamma}_{\rm th}(\beta,\delta_{\rm th})/\hat{\Gamma}_{\rm LC}(\beta,\delta_{\rm LC})$ vs. β.

however, proceed in a different way: we do not consider the β-dependent $\delta_{\rm th}$ and $\delta_{\rm LC}$, but determine constant values $\delta_{\rm th}$ and $\delta_{\rm LC}$ such that relation (18) is satisfied for some specific value of β. Here, δ is fixed from

$$\sqrt{\langle s\rangle_{\rm LC}} = \sqrt{\langle s\rangle_{\rm th}} = M_Q \tag{19}$$

for $\beta = 0.5$ GeV; this gives $\delta_{\rm LC} = 0.96$ GeV and $\delta_{\rm th} = 0.79$ GeV.

As can be seen from the plots, the light-cone contribution to the correlator considerably exceeds the full correlator. Obviously, the difference between these two quantities is just the contribution of the off-LC terms in the LC expansion of the correlator. This difference is to a large extent of pure "kinematical" origin, related to the mismatch between the thresholds in $\Delta_{\rm th}$ and $\Delta_{\rm LC}$.

The main results of the present analysis may be summarized as follows:

1. The difference between the cut full correlator and the LC contribution to the latter is always nonvanishing, since the off-LC contributions are not suppressed by any large parameter compared to the LC one. *In heavy-to-light decays, there exists no rigorous theoretical limit in which the cut LC correlator coincides with the cut full correlator.*

2. The light-cone contribution provides *numerically* the bulk of the cut full correlator, the contribution of the off-LC terms being always negative. Thus, the light-cone correlator systematically *overestimates* the full correlator, the difference at small q^2 being $20 \div 30\%$.

3. The Borel curves for the full and the LC correlators turn out to be of similar shapes. Such a similarity of the Borel curves implies that the systematic difference between the correlators cannot be diminished by any relevant choice of the criterion for extracting the heavy-to-light form factor.

Finally, let us point out the following: Although the model discussed here differs, in many aspects, from QCD, it mimics correctly those features which are essential for the effects discussed. Therefore, many of the results derived in this work hold also for QCD. In particular, the following relationship between the light-cone and the full correlators for large values of m_Q and μ is valid in QCD:

$$\frac{\hat{\Gamma}_{\rm th}(\mu^2, q^2 = 0, \delta)}{\hat{\Gamma}_{\rm LC}(\mu^2, q^2 = 0, \delta)} = 1 - {\rm O}\left(\frac{\Lambda_{\rm QCD}}{\delta}\right). \tag{20}$$

For numerical estimates, we used parameter values relevant for B and D decays. We therefore believe that also the numerical estimates for off-LC effects (one of the higher-twist effects) obtained in this work provide a realistic estimate for higher-twist effects in QCD.

Thus, our analysis suggests a sizeable contribution to heavy-to-light correlators, related to higher-twist effects in QCD. This contribution is hard to control in the method of light-cone sum rules because higher-twist distribution amplitudes are not known with sufficient accuracy. Therefore, one might expect sizeable errors in the heavy-to-light form factors, related to higher-twist effects. [These errors arise in addition to the systematic errors related to the procedure of extracting hadron observables from a correlator discussed in our first talk [1)]]. The effect is larger for decays of heavy mesons containing the strange quark, i.e., of B_s and D_s, than for the decays of B and D mesons.

The off-LC and other higher-twist effects in weak decays of heavy mesons in QCD deserve a detailed investigation: for the method of light-cone sum rules the corresponding distribution amplitudes are "external" objects and should be provided by other nonperturbative methods. In particular, the combination of light-cone sum rules with approaches based on the constituent quark picture [7], which successfully describe heavy-meson decays, might be fruitful. Moreover, it seems promising to apply different versions of QCD sum rules to transition form factors [8]; this may be helpful in understanding the genuine uncertainties of the form factors extracted from the light-cone sum rules.

Acknowledgements. D. M. would like to thank the Austrian Science Fund (FWF) for support under project P17692.

References

1. W. Lucha, D. Melikhov, and S. Simula, "Systematic errors of bound-state parameters extracted by means of SVZ sum rules", arXiv:0712.0177.
2. W. Lucha, D. Melikhov, and S. Simula, Phys. Rev. D **76**, 036002 (2007); Phys. Lett. B **657**, 148 (2007); W. Lucha and D. Melikhov, Phys. Rev. D **73**, 054009 (2006); Phys. Atom. Nucl. **70**, 891 (2007).
3. I. I. Balitsky, V. M. Braun, and A. V. Kolesnichenko, Nucl. Phys. B **312**, 509 (1989); V. M. Braun and I. Filyanov, Z. Phys. C **44**, 157 (1989); V. I. Chernyak and I. R. Zhitnitsky, Nucl. Phys. B **345**, 137 (1990); P. Ball and V. M. Braun, Phys. Rev. D **58**, 094016 (1998).
4. W. Lucha, D. Melikhov, and S. Simula, Phys. Rev. D **75**, 096002 (2007).
5. N. Nakanishi, Phys. Rev. **130**, 1230 (1963).
6. V. A. Karmanov and J. Carbonell, Eur. Phys. J. A **27**, 1 (2006).
7. D. Melikhov, Phys. Rev. D **53**, 2460 (1996); Phys. Rev. D **56**, 7089 (1997); Eur. Phys. J. direct **C4**, 2 (2002) [hep-ph/0110087]; D. Melikhov and S. Simula, Eur. Phys. J. C **37**, 437 (2004); D. Melikhov and B. Stech, Phys. Rev. D **62**, 014006 (2000).
8. V. Braguta, W. Lucha, and D. Melikhov, arXiv:0710.5461 [hep-ph].

Frascati Physics Series Vol. XLVI (2007), pp. 1153–1160
HADRON07: XII Int. Conf. on Hadron Spectroscopy – Frascati, October 8-13, 2007
Hadron Structure

MEASUREMENT OF THE PION POLARISABILITY AT COMPASS

Jan Friedrich
Technische Universität München

for the COMPASS collaboration

Abstract

The COMPASS experiment at CERN has investigated Primakoff reactions of 190 GeV/c pions with the Coulomb field of various target nuclei, predominatly lead, in a pilot run in the year 2004. The photoproduction process $\pi^- Z \to \pi^- Z\gamma$ is related to Compton scattering on the pion, and gives access to the electric and magnetic polarisabilities, α_π and β_π. The unique feature of the COMPASS setup to measure the equivalent reaction with identified muons during the same beam time allows for a reliable treatment of systematic apparative effects. In a first analysis, the value $\alpha_\pi = 2.5 \pm 1.7_{\mathrm{stat}} \pm 0.6_{\mathrm{sys}} \cdot 10^{-4}$ fm^3 was obtained, assuming $\alpha_\pi = -\beta_\pi$ on theoretical reasons.

1 Introduction

The electromagnetic polarisability of the pion is a longstanding challenge in strong interaction physics, being on one hand a well-defined and much scruti-

Table 1: *Experimental situation of the pion polarisabilities.*

	$\alpha_\pi + \beta_\pi$	$\alpha_\pi - \beta_\pi$ $[10^{-4}\,\mathrm{fm}^3]$
$e^+e^- \to e^+e^-\pi^+\pi^-$		
Mark II [4]	$0.22 \pm 0.07 \pm 0.04$	4.8 ± 1.0
CELLO [3]	$0.33 \pm 0.06 \pm 0.01$	
$\gamma p \to n\pi^+\gamma$		
MAMI [5]		$11.6 \pm 1.5 \pm 3.0 \pm 0.5$
$\pi^- Z \to Z\pi^-\gamma$		
Serpukhov [6]	$1.8 \pm 3.1 \pm 2.5$	12.3 ± 2.6

nised quantity of the theory, on the other hand difficult to measure experimentally, due to the short lifetime of the pion. It is a decisive quantity for chiral perturbation theory (χPT), as the low momentum limit can be realised in Compton scattering, and an unambigious prediction derived from the radiative pion decay can be provided, $\alpha_\pi = 2.93 \pm 0.5 \cdot 10^{-4}$ fm^3 and $\beta_\pi = 2.77 \pm 0.5 \cdot 10^{-4}$ fm^3 [1]. Other theoretical approaches based on sum rules or quark confinement models predict mostly the polarisabilities tending to higher values, up to a factor 3, see [2] for an overview.

The experimental situation is also not conclusive, cf. Tab. 1. Early measurements, as the Serpukhov experiment, have supported a comparatively high value for the polarisabilities, confirmed by the recent MAMI measurement, while experiments on photon-photon reactions found reasonable agreement with the χPT calculation. A new measurement with high statistics and controlled systemtics is highly eligible.

2 Primakoff measurements with COMPASS

COMPASS [7] has been set up as multi-purpose fixed-target experiment with advanced LHC generation detectors and data acquisition at the CERN super proton synchrotron. Up to present time, mostly a 160 GeV/c tertiary muon beam has been used to study deep inelastic scattering on the nucleon. During 4 weeks of the beam time in the year 2004, the beam was changed to 190 GeV/c negative pions, and the spectrometer was optimized for the detection of soft hadronic reactions, namely diffractive dissociation and Primakoff processes.

The experimental technique for observing Primakoff reactions bases on a special property following from the Weizsäcker-Williams ansatz, where the nuclear Coulomb field is decomposed into quasi-real photons, which interact with the incoming particles. Consequently, the cross section for reactions with the nuclear electric field is factorised into the equivalent photon density and a real photon scattering cross section,

$$\frac{d^3\sigma}{dQ^2 d\omega d\cos\vartheta} = \frac{\alpha_f Z^2}{\pi\omega} \cdot \frac{Q^2 - Q^2_{\min}}{Q^4} \cdot \left|F_Z(Q^2)\right|^2 \frac{d\sigma_{\gamma\pi}(\omega,\vartheta)}{d\cos\vartheta} \tag{1}$$

with α_f the fine structure constant, ω the photon energy and ϑ the photon scattering angle in the π rest frame. Since the cross section is proportional to Z^2, a heavy target such as lead is favourable for a high yield, despite the larger radiative corrections. The Q^2 range of interest is limited, such that the nuclear form factor contribution is $|F_Z|^2 \approx 1$. The Q^{-4} term, arising from the photon propagator, leads to a steep fall of the differential cross section with increasing Q^2, and the Primakoff reaction appears as peak at very small values in the Q^2 spectrum, making it experimentally distinguishable from competing reactions and combinatorial background. For the Compton scattering process [8],

$$\frac{d\sigma_{\gamma\pi}}{d\Omega} = \left(\frac{d\sigma_{\gamma\pi}}{d\Omega}\right)_B - \frac{\alpha_f m_\pi^3 s_-^2}{4 s_1^2 (s_+ + z s_-)} \left[(1-z)^2(\alpha_\pi - \beta_\pi) + \frac{s_1^2}{m_\pi^4}(1+z)^2(\alpha_\pi + \beta_\pi)\right] \tag{2}$$

where the Born cross section is

$$\left(\frac{d\sigma_{\gamma\pi}}{d\Omega}\right)_B = \frac{\alpha_f^2}{2 s_1} \cdot \left[1 + \left(\frac{s_- + z s_+}{s_+ + z s_-}\right)^2\right] \tag{3}$$

and s_1 the squared total energy in the $\gamma\pi$ centre of momentum system and $s_\pm = s_1 \pm m_\pi^2$.

Due to the small momentum transfer to the nucleus in these reactions, the scattered pion as well as the produced photon leave the interaction point under small angles of less than a few mrad. The photons in forward direction with $E_\gamma > 40$ are observed in an electromagnetic calorimeter, which also served as trigger. The incoming and outgoing pions were measured in silicon tracker detectors with a resolution of about $10\mu m$.

3 Data Analysis

The event selection required exactly one outgoing track of high quality and measured momentum, and one cluster in the calorimeter with an energy higher than 7 GeV. While the exclusivity of the reaction can not be ensured by the cut on the total energy balance, $E_\pi - E_{\pi'} - E_\gamma$ <25 GeV, a clear signature of Primakoff reactions is seen in the Q^2 spectrum, cf. Fig. 1.

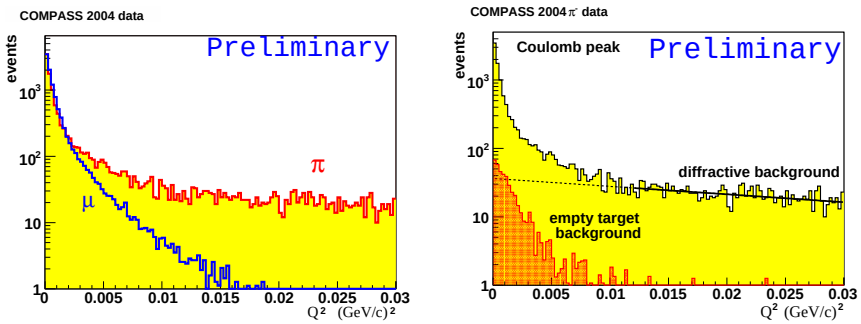

Figure 1: *Reconstructed Q^2 spectrum, showing the steep rise at small values due to Primakoff reactions. Left plot: The spectrum observed with pion beam is compared to the muon control measurement. It is seen that the contributions at higher Q^2 values are only present in the pion case, proving their origin in the additional hadronic reactions. The right plot indicates how the statistical weights are obtained in order to subtract higher-Q^2 (labelled diffractive background) and empty target contributions.*

The Primakoff events are selected with $Q^2 < 6.5 \cdot 10^{-3}$ GeV$^2/c^2$, and the non-Primakoff fraction under the peak is estimated by an extrapolation of an exponential function fitted to the Q^2 spectrum in the range $2 - 10 \cdot 10^{-2}$ GeV$^2/c^2$. The observed $\pi\gamma$-mass spectrum is presented in Fig. 2, where also the removal of background due to beam kaon decays (with a non-observed soft photon in $K^- \to \pi^-\pi^0$), is demonstrated. The mass is cut at $3.75 \cdot m_\pi$, just below the region where ρ contributions set in.

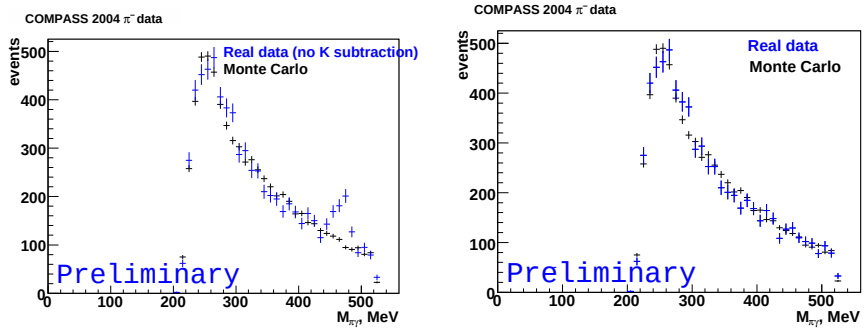

Figure 2: *The non-corrected $M_{\pi\gamma}$ spectrum shows a contribution from K decays (left), which disappear after proper "empty target" subtraction (right).*

Although most of the statistics was collected with lead target, some beam time was devoted to measure the Primakoff reaction also on carbon and copper targets. The observed Primakoff reactions show the expected Z^2-dependence of Eq. 1.

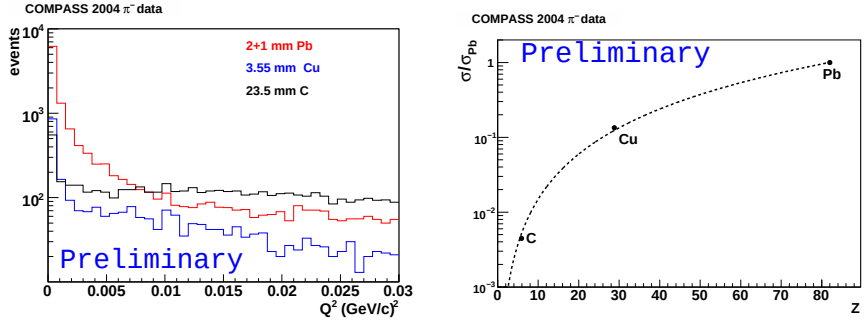

Figure 3: *Measurements of targets with different Z nuclei have all shown the characteristic Primakoff peak (left). After extracting the peak strength and normalizing to the lead luminosity, the Z^2 dependence of the Primakoff cross section is seen (right).*

In order to extract the polarisability contribution, the differential cross

section $d\sigma(\alpha_\pi, \beta_\pi)/dx$ is compared to the case α_π=β_π=0 of a "non-polarisable pion". Only the dependence of the relative photon energy[1] $x = E_\gamma/E_{\mathrm{Beam}}$ was investigated so far, which necessitates to make the assumption $\alpha_\pi = -\beta_\pi$, and consequently in the following only the dependence $d\sigma(\beta_\pi)/dx$ is studied.

Presently only a part of the statistics with a segmented lead target of 2+1 mm thickness was investigated, resulting in about 7500 Primakoff events. The acceptance of the apparatus is estimated using a Primakoff event generator (POLARIS [9]) and a Monte Carlo simulation by a GEANT description of the COMPASS setup. The resulting acceptance curve is depicted in Fig. 4 for both the pion and the muon beam cases, validating by the similar behaviour the estimate of systematic effects on the pion data from the interpretation of the muon data. Also, the increasing importance of the K^- ("empty target") subtraction at higher photon energies is apparent.

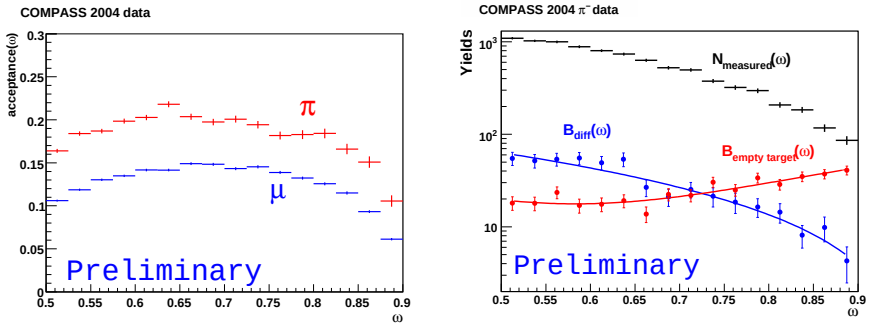

Figure 4: *The acceptance of the COMPASS spectrometer for Primakoff Compton scattering, depending on the relative outgoing photon energy (left), and the distributions of the previously discussed background contributions (right).*

In addition to the simulated acceptance correction, which was obtained using the one-photon Born approximation, the respective factors for radiative corrections were applied to the extent they have been derived up to now [10]. The resulting ratios $R = d\sigma(\beta_\pi)/d\sigma(\beta_\pi = 0)$ are given in Fig. 5. It appears that a signal with the correct sign and magnitude is observed for the pion, taking

[1] the relative photon energy is denoted "ω" in the figures

the χPT prediction as a scale, while the muon data are in good agreement with the expectation of no polarisability signal. From its statistical error, an upper limit for the apparative systematic error $< 0.6 \cdot 10^{-4}\mathrm{fm}^3$ can be derived.

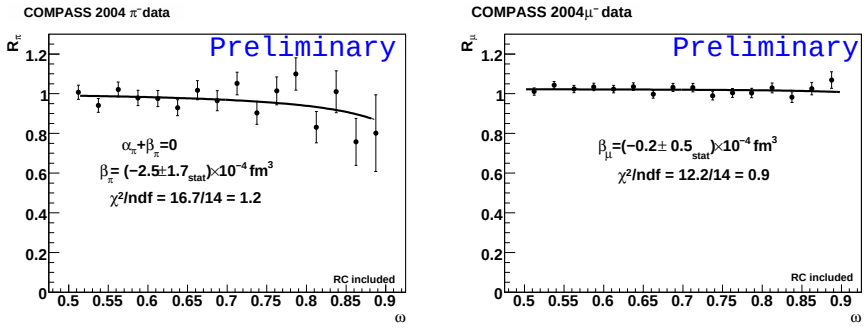

Figure 5: *Extraction of the pion magnetic polarisability β_π by its influence on the cross section shape at high relative outgoing photon energies (left). The control measurement with muon beam is shown on the right plot, giving an estimate for the apparative systematic uncertainty of the obtained result.*

4 Conclusions

The present analysis of the 2004 pion beam data demonstrates the capability of COMPASS to settle the experimental uncertainty of the pion polarisability, provided the necessary refinements of the analysis are taken on. With the full 2004 statistics evaluated, a firm estimate will be possible for a future Primakoff COMPASS data taking, including an independent extraction of α_π and β_π.

This work is supported by BMBF, the Maier-Leibnitz Laboratory of the Munich universities and the Cluster of Excellence EXC153.

References

1. J. Gasser, M.A. Ivanov, M.E. Sainio, Nucl. Phys. **B745**, 84 (2006).
2. J. Portolés, M.R. Pennington, Second DAΦNE Handbook (1999).
3. The CELLO collaboration, Z. Phys. **C56**, 381 (1992).

4. MARKII collaboration, Phys. Rev. **D42**, 1350 (1990), Phys. Lett. **B277**, 158 (1992).

5. J. Ahrens *et al.*, Eur. Phys. J. **A23**, 113 (2005).

6. Y.M. Antipov *et al.*, Phys. Lett. **B121**, 445 (1983), Z. Phys. **C26**, 495 (1985).

7. The COMPASS collaboration, CERN proposal SPSLC96-14 and Nucl. Instrum. Meth. **A577**, 455 (2007).

8. D. Drechsel, L. Fil'kov, Z. Phys. **A349**, 177 (1994).

9. M. Buenerd, Nucl. Instrum. Meth. **A361**, 111 (1995).

10. A. Arbuzov, arXiv:0710.3639v1[hep-ph].

Frascati Physics Series Vol. XLVI (2007), pp. 1161–1170
HADRON07: XII Int. Conf. on Hadron Spectroscopy – Frascati, October 8-13, 2007
Hadron Structure

LATEST HERMES RESULTS ON TRANSVERSE-SPIN EFFECTS IN HADRON STRUCTURE AND FORMATION

Luciano Libero Pappalardo
(On behalf of the HERMES Collaboration)
Universita' degli Studi di Ferrara
Via Saragat, 1, 44100 Ferrara, Italy

Abstract

Transverse target single spin asymmetries in semi inclusive deep inelastic scattering allow to study the so-called Collins and Sivers mechanisms. The first one connects the poorly known foundamental transversity distribution function, describing the transverse spin-polarization of quarks in a transversely polarized proton, to the Collins fragmentation function, describing spin-orbit correlations in the hadron formation process. The second one is sensitive to the Sivers function, which correlates the intrinsic transverse momentum of quarks with the proton's spin orientation and is related to the orbital angular momentum of quarks. Preliminary results on azimuthal single target-spin asymmetries in semi inclusive electroproduction of pions and kaons at the HERMES experiment are presented. The full data set collected with a transversely polarized hydrogen target was analyzed providing the HERMES most precise results on the Collins and Sivers azimuthal moments.

1 The leading-twist parton distribution functions

After integrating over the quark transverse momentum p_T, three parton distribution functions are needed at leading twist for a complete description of the momentum and spin distributions of the quarks within the nucleon. Two of these have been experimentally explored in some detail. The first one is the well known *momentum distribution* $q\left(x, Q^2\right)$, reflecting, in a frame in which the nucleon has a very high momentum, the probability to find quarks carrying a fraction x of the nucleon momentum at photon virtuality Q^2, regardless of their spin orientation. The second one is the *helicity distribution* $\Delta q\left(x, Q^2\right)$ reflecting, in the helicity basis, the difference in probabilities to find, in a longitudinally polarized nucleon, quarks with their spin aligned and anti-aligned to the spin of the nucleon [1)]. In a basis of transverse spin eigenstates, the third distribution function, known as *transversity* [2, 3)], reflects the difference in probabilities to find, in a transversely polarized nucleon, quarks with their spin aligned and anti-aligned to the spin of the nucleon. This quantity has no probabilistic interpretation in the helicity basis, where it is related to a forward scattering amplitude involving helicity flip of both quark and target nucleon ($N^{\Rightarrow}q^{\leftarrow} \rightarrow N^{\Leftarrow}q^{\rightarrow}$). Since hard interactions conserve chirality, chiral-odd transversity has so far remained unmeasured in inclusive processes.

2 The Collins and Sivers mechanisms

At HERMES azimuthal Single Target-Spin Asymmetries (SSA) in Semi-Inclusive Deeply Inelastic Scattering (SIDIS) on a transversely polarized proton target are investigated. In such events the scattered lepton is detected in coincidence with at least one of the hadrons produced in the fragmentation of the struck quark. This allows, in particular, to access the so-called *Collins moments*, in which transversity is convoluted with the chiral-odd *Collins fragmentation function*, thus restoring chirality conservation. The Collins function describes the correlation between the transverse spin of the struck quark and the transverse momentum $P_{h\perp}$ of the produced hadron [4)]. The transverse polarization of the struck quark can indeed influence the transverse (with respect to the virtual photon direction) component of the hadron momentum, leading to a left-right asymmetry in the momentum distribution of the produced hadrons (*Collins mechanism*). However, similar asymmetries might also arise from a

completely different mechanism involving a correlation between the transverse polarization of the target nucleon and the transverse momentum p_T of quarks (*Sivers mechanism*) [5]. This correlation is accounted for by the naïve T-odd Sivers distribution function $f_{1T}^{\perp}$, which, being related to a forward scattering amplitude involving helicity flip of only the target nucleon ($N^{\Rightarrow}q^{\leftarrow} \to N^{\Leftarrow}q^{\leftarrow}$), must involve orbital angular momentum of the quarks [6, 7]. The so-called *Sivers moments*, which are proportional to a convolution of the Sivers function with the unpolarized fragmentation function, are also accessible at HERMES in SIDIS.

3 The HERMES experiment

The data analyzed was recorded during the 2002–2005 running period of the HERMES experiment using a transversely nuclear-polarized hydrogen gas target internal to the $E = 27.6$ GeV HERA positron/electron storage ring at DESY. Being interested in the extraction of azimuthal moments which are independent on the beam polarization, the two beam helicity states were combined resulting in a vanishing net beam polarization. The open-ended target cell was fed by an atomic-beam source [8] based on Stern-Gerlach separation and RF transitions of hyperfine states. The nuclear polarization of the atoms was flipped at $1 - 3$ min time intervals, while both this polarization and the atomic fraction inside the target cell were continuously measured. The average value of the proton polarization was $\langle P_z \rangle = 0.74 \pm 0.06$.
Scattered leptons and any coincident hadrons were detected by the HERMES spectrometer [9], whose acceptance spans the vertical and horizontal scattering-angle ranges $40 < |\theta_y| < 140$ mrad and $|\theta_x| < 170$ mrad. Leptons are identified with an efficiency exceeding 98% and a hadron contamination of less than 1% using an electromagnetic calorimeter, a transition-radiation detector, a preshower scintillation counter and a dual radiators RICH. In particular the RICH allows to identify the charged hadrons ($\pi^{\pm}, K^{\pm}, p$) in the momentum range 2 GeV $< P_h <$ 15 GeV. An unfolding algorithm, based on a Monte Carlo simulation of the RICH detector, is used to estimate the contamination and efficiency of the hadron identification, which represent the main contributions to the systematic error on our results.

4 Extraction of Collins and Sivers moments

Events were selected subject to the kinematic requirements $W^2 > 10$ GeV^2, $0.1 < y < 0.95$ and $Q^2 > 1$ GeV^2, where W is the invariant mass of the initial photon-nucleon system and y is the fractional beam energy transfer to the target. Coincident hadrons were accepted if $0.2 < z < 0.7$ and $\theta_{\gamma^* h} > 0.02$ rad, where z is the energy fraction of the hadron and $\theta_{\gamma^* h}$ is the angle between the directions of the virtual photon and the hadron.
For each hadron type h, the cross section asymmetry with respect to the target polarization was evaluated as:

$$A_{UT}^{h}\left(\phi,\phi_S\right) = \frac{1}{\langle P_z\rangle}\frac{N_h^{\Uparrow}\left(\phi,\phi_S\right) + N_h^{\Downarrow}\left(\phi,\phi_S\right)}{N_h^{\Uparrow}\left(\phi,\phi_S\right) - N_h^{\Downarrow}\left(\phi,\phi_S\right)} \ , \tag{1}$$

were $N_h^{\Uparrow(\Downarrow)}$ represents the semi-inclusive yield in the target spin state "$\Uparrow$ ($\Downarrow$)" for a hadron type h, and ϕ and ϕ_S are two azimuthal angles, defined with respect to the lepton scattering plane, as shown in Figure 1.

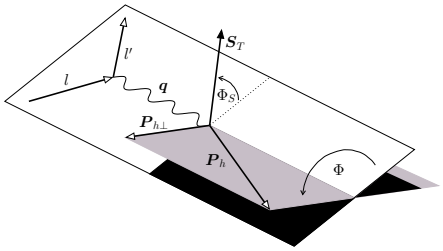

Figure 1: *Kinematics of semi-inclusive DIS on a transversely polarized target.*

The cross section asymmetry (1) can be expanded in terms of azimuthal moments. Each of these moments is characterized by a specific azimuthal modulation, expressed in terms of the *sine* or the *cosine* of different combinations of the azimuthal angles ϕ and ϕ_S. In particular the Collins moment is modulated by $\sin(\phi+\phi_S)$ whereas the Sivers moment is modulated by $\sin(\phi-\phi_S)$. Thanks to their different azimuthal modulations, these moments can be disantangled and extracted separately.
In 2005 the HERMES Collaboration published a first evidence of non-zero Collins and Sivers moments for charged pions [10]. The results, based on a lim-

ited data sample (2002-2003 running period), were extracted in a least-squares fit of the cross-section asymmetry (1). The Collins and Sivers moments have now been extracted using the full HERMES data set on a transversely polarized hydrogen target, resulting in a substantial increase of the statistical precision. Furthermore these moments have also been extracted for neutral pions and charged kaons. Due to the relatively poor statistics for kaons, which would have produced non reliable fit results in some azimuthal (ϕ, ϕ_S) bins, a new fit method was adopted for all the hadron types, based on an unbinned, with respect to ϕ and ϕ_S, Maximum Likelihood approach. The corresponding Likelihood function is based on the following Probability Density Function:

$$\begin{aligned} F = 1 + P_z \cdot \Big[& 2\langle sin(\phi + \phi_S)\rangle^h_{UT} \; sin(\phi + \phi_S) \; + \\ & 2\langle sin(\phi - \phi_S)\rangle^h_{UT} \; sin(\phi - \phi_S) \; + \\ & 2\langle sin(3\phi - \phi_S)\rangle^h_{UT} \; sin(3\phi - \phi_S) \; + \\ & 2\langle sin(2\phi - \phi_S)\rangle^h_{UT} \; sin(2\phi - \phi_S) \; + \\ & 2\langle sin(\phi_S)\rangle^h_{UT} \; sin(\phi_S) \Big] \; . \end{aligned} \tag{2}$$

Here the indices U and T stand for Unpolarized beam and Transversely polarized target, respectively. In addition to the Collins and Sivers amplitudes, three other sine modulations are included as they were found to influence the fit results: the leading twist amplitude $\langle sin(3\phi - \phi_S)\rangle^h_{UT}$ and two twist-three amplitudes $\langle sin(2\phi - \phi_S)\rangle^h_{UT}$ and $\langle sin(\phi_S)\rangle^h_{UT}$.

The preliminary results for the Collins and Sivers moments for charged pions are reported in Figure 2 as a function of x, z and $P_{h\perp}$. The shaded bands in the figure represent the maximal systematic uncertainty, which include contributions from acceptance effects, instrumental smearing, QED radiation and hadron misidentification. A common 8.1% scale uncertainty is due to the target polarization uncertainty. Concerning the Collins moments, the results show a significantly positive (negative) amplitude for π^+ (π^-). These results confirm the previously published ones [10] and demonstrate that both the transversity distribution and the Collins fragmentation function are non-zero. The fragmentation is said to be *favoured* if the produced hadron contains an *up* quark as a valence quark (e.g. π^+) and *unfavoured* in the opposite case (e.g. π^-).

The unexpectedly high negative amplitude for π^- thus suggests a disfavoured Collins function with a magnitude similar to that of the favoured one but with

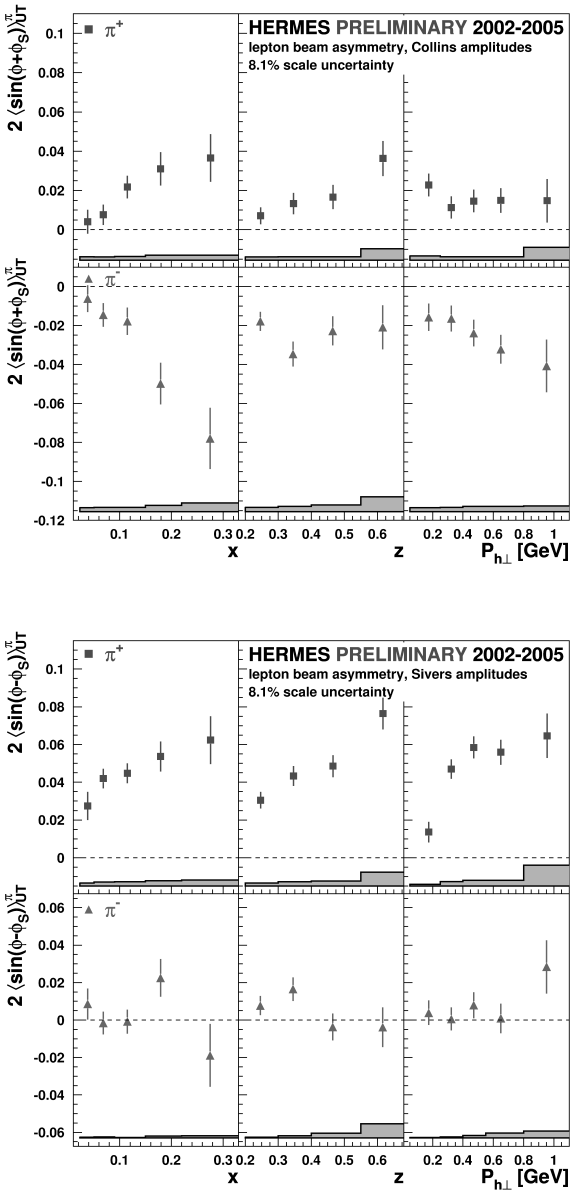

Figure 2: *Collins (upper plot) and Sivers (lower plot) moments for π^+ (upper panels) and π^- (lover panels) as a function of x, z and $P_{h\perp}$.*

opposite sign. Concerning the Sivers moments, the results show a significantly positive amplitude for π^+, which clearly demonstrates that also the Sivers function is non-zero, and an amplitude consistent with zero for π^-. In particular, the former result implyies the existence of a non zero orbital angular momentum of the quarks within the nucleon, which is one of the still unmeasured possible contributions to the nucleon spin [7].

The isospin symmetry has to hold for the π-meson triplet also at the azimuthal moments level. In particular, concerning the Collins and Sivers moments, the following isospin relation holds:

$$\langle sin(\phi \pm \phi_S)\rangle_{UT}^{\pi^+} + C \cdot \langle sin(\phi \pm \phi_S)\rangle_{UT}^{\pi^-} - (1+C) \cdot \langle sin(\phi \pm \phi_S)\rangle_{UT}^{\pi^0} = 0 \ , \quad (3)$$

where C represents the unpolarized cross-section ratio for semi-inclusive negative and positive pion production ($C = \sigma_{UU}^{\pi^-}/\sigma_{UU}^{\pi^+}$). In order to test this relation, which represents an important consistency check of our results, the Collins and Sivers moments were also extracted for π^0, as shown in Figure 3.

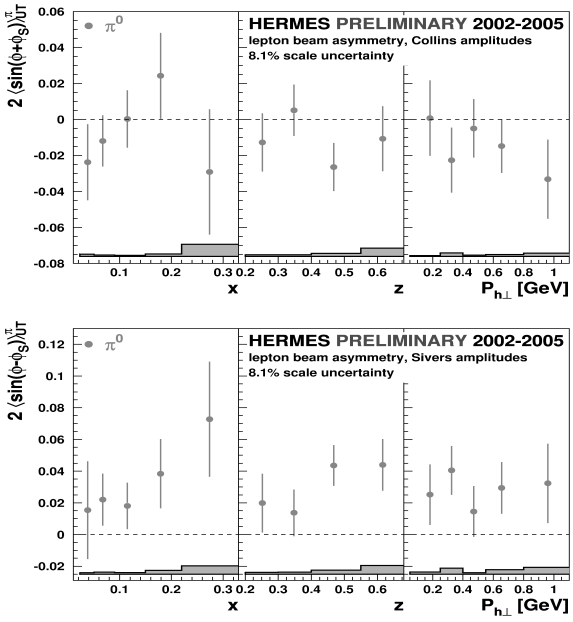

Figure 3: *Collins and Sivers moments for π^0 as a function of x, z and $P_{h\perp}$.*

The results show a Collins amplitude consistent with zero and a Sivers amplitude slightly positive. As expected, the magnitude of these amplitudes is intermediate compared to the corresponding amplitudes for π^+ and π^-, fulfilling the isospin relation (3).
In order to probe the contribution of the sea quarks, the Collins and Sivers moments were also extracted for charged kaons. For comparison the results are plotted in Figure 4 and Figure 5 together with those of the charged pions.

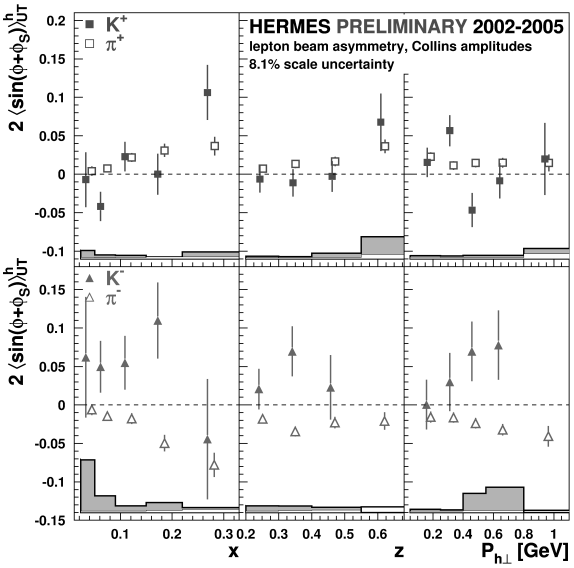

Figure 4: *Collins moments for K^+ (upper panels) and K^- (lower panels) as a function of x, z and $P_{h\perp}$. For comparison, the kaon results (full dots) are presented together with the pions results (open dots).*

The Collins moments are compatible within the statistical accuracy for π^+ and K^+, while are of opposite sign for K^- and π^-. However, there is no reason to expect a similar amplitude for K^- and π^-, being the K^- a fully sea object ($K^- \equiv (\bar{u}s)$).
The amplitude for K^+ is roughly twice as big as that for π^+ concerning the Sivers moments. Since the valence content of these two mesons differs only in the anti-quark involved, this observation appears to suggest a significant Sivers

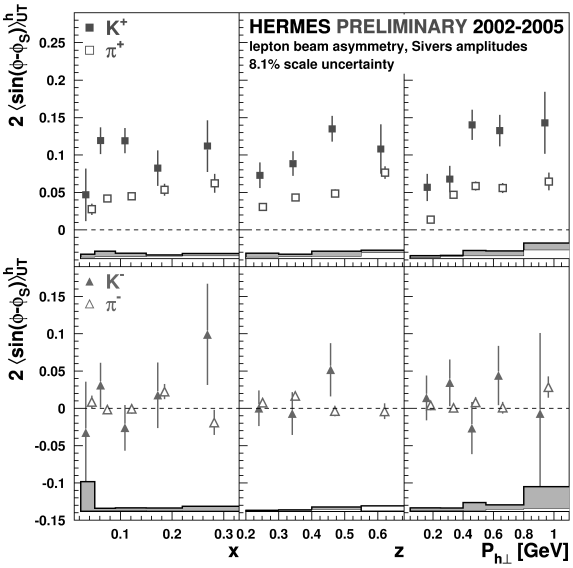

Figure 5: *Sivers moments for K^+ (upper panels) and K^- (lower panels) as a function of x, z and $P_{h\perp}$. For comparison, the kaon results (full dots) are presented together with the pions results (open dots).*

function for the proton sea quarks.

5 Conclusions

Azimuthal single target-spin asymmetries in semi-inclusive electroproduction of pions and kaons were measured at HERMES in deeply inelastic scattering of positrons and electrons on a transversely polarized hydrogen target. Significant amplitudes for both the Collins and the Sivers mechanisms were observed indicating the existence of non-zero distribution and fragmentation functions relevant for the description of the transverse degrees of freedom of the nucleon.

References

1. A. Airapetian *et al* (HERMES), Phys. Rev. **D71**, 012003 (2005).

2. J.P. Ralston and D.E. Soper, Nucl. Phys. **B152**, 109 (1979).

3. V. Barone, A. Drago and G. Ratcliffe, Physics Reports **359**, 1-168 (2002).
4. J.C. Collins, Nucl. Phys. **B396**, 161 (1993).
5. D.W. Sivers, Phys. Rev D **41**, 83 (1990).
6. S.J. Brodsky, D.S. Hwang and I. Schmidt, Phys. Lett. **B530**, (2002).
7. M. Burkardt, Phys. Rev. **D66**, 114005 (2002).
8. A. Airapetian *et al* (HERMES), Nucl. Instr. and Meth. **A540**, 68 (2005).
9. K. Ackerstaff *et al.* (HERMES), Nucl. Inst. & Meth. **A 417**, 230 (1998).
10. A. Airapetian *et al* (HERMES), Phys. Rev. Lett. **94**, 012002 (2005).

Frascati Physics Series Vol. XLVI (2007), pp. 1171–1178
HADRON07: XII Int. Conf. on Hadron Spectroscopy – Frascati, October 8-13, 2007
Hadron Structure

π^o ELECTROPRODUCTION AND TRANSVERSITY

Simonetta Liuti, Saeed Ahmad
University of Virginia, Charlottesville, VA 22904, USA
Gary R. Goldstein
Tufts University, Medford, MA 02155, USA
Leonard Gamberg
Pennsylvania State University, Penn State Berks, Reading, PA 19610, USA

Abstract

Exclusive π^o electroproduction and related processes are suggested to investigate the chiral odd transversity distributions of quarks in the transversely polarized nucleon, $h_1(x)$, and its first moment, the tensor charge. The connection between a description based on partonic degrees of freedom, given in terms of generalized parton distributions, and Regge phenomenology is explored.

1 Introduction

Most of the information on the partonic structure of hadrons has been traditionally obtained through inclusive deep inelastic experiments. With an appropriate selection of probes and reactions, accurate measurements conducted through the years allowed one to map out in detail the different components

of proton structure, the Parton Distribution Functions (PDFs) in a wide kinematical region of the four-momentum transfer, Q^2, and of the longitudinal momentum fraction of the proton's momentum, x_{Bj}. An inclusive/exclusive connection in lepton-nucleon scattering was advocated [1], although studies of the partonic structure through exclusive measurements remained ambiguous in establishing the regime of four-momentum transfer in which such a description should be valid. A new avenue was recently suggested in view of the factorization properties of new types of exclusive processes, namely Deeply Virtual Compton Scattering (DVCS), Deeply Virtual Meson Production (DVMP), and related crossed-channel reactions. The soft matrix elements, identified with Generalized Parton Distributions (GPDs), can describe both the intrinsic motion of partons and their coordinate space representation (see [2, 3] for reviews). It is at present an outstanding problem to be able to reconcile and properly connect the newly suggested QCD-based picture with the hadronic description of hard exclusive reactions based on Regge theory. The latter is well known to predict a vast number of observations at large s, and small t, corresponding to the $x_{Bj} \to 0$ limit of inclusive Deep Inelastic Scattering (DIS). Initial studies of the correspondence between the regime expected to be dominated by Regge exchanges and the partonic description in DVCS and DVMP were performed in [4, 5] where it was claimed that the "leading Regge trajectories should dominate the amplitudes for exclusive leptoproduction". Therefore one might think of the hard exclusive process as probing the deep inelastic structure of a t-channel exchange target, or the mesonic cloud. On the other side, it was pointed out in Ref. [6] that the model used in [4, 5] might disagree with the perturbative QCD scaling violation pattern, which was recently observed in a particular (large W^2) kinematical regime. A formalism using the conformal moments of the nucleon GPDs was instead introduced with a non-perturbative input based on Regge ansätze.

Whether or not specific models are seemingly able to reproduce the current trend of data it is important to determine the physical origin of the hadronic structure that is detectable with hard exclusive scattering experiments aiming to shed light on the complementary picture where hadron structure at this transition regime emerges through QCD dynamics.

In this context we analyze a specific class of exclusive reactions, namely π^o electroproduction with the goal of obtaining a relation between experimental

observables and the tensor charge.

2 Tensor Charge and Transversity

The chiral odd transversity distribution of quarks in the transversely polarized nucleon, $h_1(x)$, and its first moment, the tensor charge, δq, are defined as

$$\begin{aligned} \langle PS \mid \overline{\psi}\, \sigma^{\mu\nu}\, \psi \mid PS \rangle &= \delta q\, \overline{U}(P,S) \sigma^{\mu\nu} U(P,S) \\ &\equiv \delta q\, 2\,(P^\mu S^\nu - P^\nu S^\mu)\,, \end{aligned} \tag{1}$$

and

$$h_1(x_{Bj}, Q^2) = \Phi^\Gamma = \int dp^-\, d^2\mathbf{p_T}\, \mathrm{Tr}\,\{\Gamma\Phi\}\,|_{\mathrm{x_{Bj}P^+=p^+}}, \tag{2}$$

with $\Gamma = i\sigma^{i+}\gamma_5$, and $\Phi(x;P,S)$ being the correlation function defining the matrix element for the DIS process [7].
Notice that in the helicity basis [8] h_1 corresponds to the off-diagonal quark chirality matrix elements

$$h_1 = \Phi_{+L,-R} + \Phi_{-R,+L} = q^\uparrow(x_{Bj}, Q^2) - q^\downarrow(x_{Bj}, Q^2) \tag{3}$$

originally introduced in [9, 10] where the subscripts $\Lambda\lambda, \Lambda'\lambda'$ refer to the helicities of the proton (Λ, Λ'), and of the struck quark (λ, λ'). The connection between tensor charge and transversity is given by [7]:

$$\delta q = \int_0^1 h_1(x_{Bj}, Q^2)\, dx_{Bj} \tag{4}$$

In a non-relativistic scenario $h_1(x_{Bj}, Q^2)$ would coincide with the distribution of longitudinally polarized quarks in a longitudinally polarized proton, $g_1(x_{Bj}, Q^2)$. Its dynamical origin is therefore related to the relativistic motion of quarks in the nucleon.

Many attempts have been made to connect the tensor charge to measurable processes, the most successful of which have been through semi-inclusive DIS [11]. Various theoretical approaches to modeling these quantities have been taken: from QCD Sum rules [12] to Lattice QCD [13] to phenomenological studies [14]. One particular approach to predicting the nucleon's tensor

charges, δu and δd has been the work of Gamberg and Goldstein [16]. The tensor charges were calculated using approximate SU(6) $\otimes$ O(3) symmetry among the light axial vector mesons, an axial vector dominance hypothesis, and a generalization with re-scattering. This formalism which is based upon t-channel exchange is reminiscent of Regge Cut models on the one hand, depicted in Fig. 1, and the the large s, small t (large u) $q\overline{q}$ pair (or to a t-channel exchange) or ERBL region of DVMP on the other hand, depicted in Fig. 2.

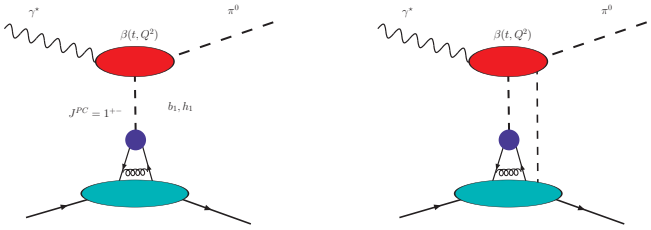

Figure 1: *The factorized Regge pole contribution to* π^0 *scattering is depicted.*

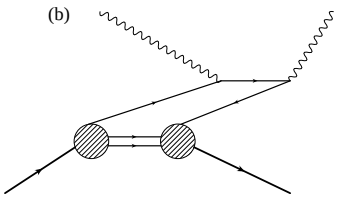

Figure 2: *Leading order diagram for DVCS in the ERBL* [1, 15] *region where a* $q\overline{q}$ *pair is first produced from the nucleon and subsequently interacts with the photons.*

This scheme yielded values for u and d quark tensor charges dependent on transverse momentum factors interpreted as transverse momentum transfer $\Delta_\perp^2$ of the quarks in the nucleon. $\Delta_\perp^2$ dependence suggests that re-scattering loop corrections must be present in single spin asymmetries in exclusive pion production [17, 16]. This approach left two open questions. First, the poles

in momentum transfer t are quite far removed from the relevant $t \to 0$ limit. Secondly, the charges depend on average values of the constituent transverse momenta, $\langle k_T^2 \rangle$. To address these questions and to develop a deeper understanding of the partonic underpinnings of transversity, we addressed them using the connection between GPDs and transversity recently studied in [18].

Note that $H_T(x,\xi,t)$, the Generalized Parton Distribution for transversity can be written as the off forward quark-target scattering amplitude, $A_{\Lambda\lambda,\Lambda'\lambda'}$,

$$H_T(X,\zeta,t) = A_{++,--} + A_{--,++}, \tag{5}$$

where $H_T(x,\xi,t)$ has the following properties:

$$\int H_T(x,\xi,t)\,dx = A_{T,10}(t) \tag{6}$$

$$H_T(x,0,0) = h_1(x) \tag{7}$$

and the form factor $A_{T,10}(t)$ gives the tensor charge for $t \to 0$.[1]

In order to investigate more extensively the tensor charge and the possible mechanisms at work in both the partonic and hadronic pictures exclusive electroproduction of π^0 and η on both proton and neutron targets, can be used where a more direct connection between theoretical quantities and observables can be established.

3 Extraction of Tensor Charge from Data

We propose a dynamical mechanism for the process $\gamma^* P \to \pi^0(\eta) P'$ that allows for a direct extraction of the tensor charge from experiment. The cross section for π^o electroproduction reads

$$\begin{aligned} \frac{d\sigma}{dt\,d\phi} &\propto L_{\mu\nu}^{h=\pi^o} W^{\mu\nu} \\ &= \left(\frac{d\sigma_T}{dt} + \epsilon\frac{d\sigma_L}{dt}\right) + \epsilon\frac{d\sigma_{TT}}{dt}\cos 2\phi + \sqrt{2\epsilon(\epsilon+1)}\frac{d\sigma_{LT}}{dt}\cos\phi. \end{aligned} \tag{8}$$

$L_{\mu\nu}^{h=\pi^o}$ is the leptonic tensor, or polarization density matrix, and

$$W^{\mu\nu} = \sum_f J_\mu J_\nu^* \delta(E_i - E_f) \tag{9}$$

[1] Notice that $A_{\Lambda\lambda,\Lambda'\lambda'}$, reduces to $\Phi_{\Lambda\lambda,\Lambda'\lambda'}$, Eq.(3), in the forward limit.

where the sum is carried out over all final states, and J_μ is the matrix element of the proton electromagnetic current operator between the initial and final states. Note that the quantity

$$\frac{d\sigma_{TT}}{dt} = W_{yy} - W_{xx} \equiv 2\Re e(J_1 J_{-1}*) \quad (10)$$

can also be written in terms of the helicity amplitudes introduced in Section 2. $d\sigma_{TT}/dt$ enables us to access the tensor charge by taking the $t \to 0$ limit of the only non-flip helicity amplitude for the process. This is in fact proportional to a combination of unnatural parity exchanges (see Fig.1) that provide the quantum numbers in the t-channel that are necessary to produce a chirality flip and emit the π^o. Notice that other quantities that provide similar information such as the target transverse polarization asymmetry, A_{UT}, can be considered. These will be discussed in detail in a forthcoming publication.

In this contribution we present preliminary results using both the hadronic and the partonic descriptions, the latter obtained by implementing a recent GPD parametrization [19]. A practical extraction of the tensor charge can be obtained by noticing that in either the hadronic or in the partonic, GPD-type, description of *e.g.* $d\sigma_{TT}/dt$, the tensor charges for the different isospin components might be treated as parameters related to the normalization of H_T. Therefore our models can be used to constrain the range of values allowed by the data.

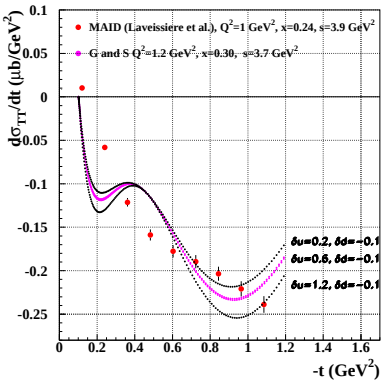

Figure 3: *Experimental determination of the tensor charge for u and d quarks, δu and δd, using MAID data on $d\sigma_{TT}/dt$* [20]. *The suggested extraction method is explained in the text.*

As an example in Fig. 3 we show a comparison of our Regge model with the MAID [20] parametrization of pion electroproduction data at $s = 4$ GeV^2 and $Q^2 \approx 1$ GeV^2. The different curves were obtained by varying the values of the tensor charge entering the normalization of the different t-channel exchanges. We expect a variety of new flavor sensitive observables to be extracted from data in the near future using both unpolarized data and asymmetries from transversely polarized proton and deuteron data on π^o and η production at the higher values of s available at Jefferson Lab. This analysis promises to be a rich area of experimental exploration in the near future.

4 Conclusions

We presented our preliminary results on an alternative method to extract the tensor charge, and its related GPDs from experimental observables such as the structure function $d\sigma_{TT}/dt$ in unpolarized exclusive π^o electroproduction. Our study uses both a Regge model, and a diquark scheme for the transverse GPD, H_T, which include as parameters the isospin dependent tensor charges.

A feasibility study with members of the Hall B collaboration at Jefferson Lab is in progress.

References

1. G. P. Lepage and S. J. Brodsky, Phys. Lett. **B87**, 359 (1979)
2. M. Diehl, Phys. Rept. **388**, 41 (2003).
3. A. V. Belitsky and A. V. Radyushkin, Phys. Rept. **418**, 1 (2005)
4. A. P. Szczepaniak and J. T. Londergan, Phys. Lett. B **643**, 17 (2006)
5. A. P. Szczepaniak, J. T. Londergan and F. J. Llanes-Estrada, arXiv:0707.1239 [hep-ph].
6. K. Kumericki, D. Mueller, K. Passek-Kumericki, arXiv:0710.5649.
7. R. L. Jaffe and X. Ji, Phys. Rev. Lett. **67** 552 (1991)
8. M. Boglione and P.J. Mulders, Phys. Rev. **D60**, 054007 (1999)
9. G. R. Goldstein and M. J. Moravcsik, Annals Phys. **98**, 128 (1976)
10. J. Ralston and D. Soper, Nucl. Phys. **B152** 109 (1979)
11. L. Pappalardo, *these proceedings*.
12. H. He and X. Ji, Phys. Rev. **D52** 2960, 1995.
13. M. Gockeler *et al*, [QCDSF Collaboration], Phys. Rev. Lett. **98**, 222001 (2007)
14. M. Anselmino *et al.*, Phys. Rev. **D75**, 054032, (2007)
15. A. V. Efremov and A. V. Radyushkin, Phys. Lett. **B94**, 245 (1980).
16. L. P. Gamberg and G. R. Goldstein, Phys. Rev. Lett. **87**, 242001 (2001)
17. G. R. Goldstein and J. F. Owens, Phys. Rev. D **7** (1973) 865.
18. M. Diehl and Ph. Hagler, Eur. Phys. J. C **44**, 87 (2005).
19. S. Ahmad, H. Honkanen, S. Liuti and S. K. Taneja, Phys. Rev. D **75**, 094003 (2007); *ibid* arXiv:0708.0268.
20. D. Drechsel, S.S. Kamalov, L. Tiator, Nucl. Phys. A645 (1999) 145-174.

Frascati Physics Series Vol. XLVI (2007), pp. 1179–1186
HADRON07: XII Int. Conf. on Hadron Spectroscopy – Frascati, October 8-13, 2007
Hadron Structure

TRANSVERSITY AND SIDIS AT CLAS

H. Avakian
Jefferson Lab
P. Rossi
Laboratori Nazionali di Frascati

Abstract

Transverse Momentum Dependent (TMD) parton distributions were introduced to describe both longitudinal and transverse momentum distributions of partons. Great progress has been made in the last years in measurements of different Single Spin Asymmetries (SSAs) in semi-inclusive processes providing access to TMDs. Here we present an overview of ongoing TMD studies at Jefferson Lab with CLAS and program planned with CLAS and CLAS12.

1 Introduction

The spin structure of the nucleon has been of particular interest since the EMC [1)] measurements, subsequently confirmed by a number of other experiments [2, 3, 4, 5, 6, 7)], implied that the helicity of the constituent quarks account for only a fraction of the nucleon spin. Possible interpretations of

this result include significant polarization of either the strange sea (negatively polarized) or gluons (positively polarized) and the contribution of the orbital momentum of quarks. The semi-inclusive deep inelastic scattering (SIDIS) experiments, when a hadron is detected in coincidence with the scattered lepton provide access to spin-orbit correlations. Observables are spin azimuthal asymmetries, and in particular single spin azimuthal asymmetries (SSAs), of the detected hadron, which are due to the correlation between the quark transverse momentum and the spin of the quark/nucleon. Measurements of SSAs in SIDIS provide access to a list of novel distribution functions, namely Transverse Momentum Dependent distribution functions (TMDs) which contain information on the parton transverse momentum.

2 Transverse Momentum Dependent Distributions Functions

Significant progress has been made recently in understanding the role of partonic initial and final state interactions [8, 9, 10]. The interaction between the active parton in the hadron and the spectators leads to gauge-invariant transverse momentum dependent (TMD) parton distributions [8, 9, 10, 11, 12]. Furthermore, QCD factorization for semi-inclusive deep inelastic scattering at low transverse momentum in the current-fragmentation region has been established in Refs. [13, 14]. This new framework provides a rigorous basis to study the TMD parton distributions from SIDIS data using different spin-dependent and independent observables. TMDs are probability densities for finding a (polarized) parton with a longitudinal momentum fraction x and transverse momentum $\vec{k}_T$ in a (polarized) nucleon (see Table 1). The diagonal elements of the table are the partonic momentum, longitudinal and transverse spin distribution functions. Off-diagonal elements require non-zero orbital angular momentum and are related to the wave function overlap of L=0 and L=1 Fock states of the nucleon [15]. The TMDs $f_{1T}^{\perp}$ and $h_1^{\perp}$, which are related to the imaginary part of the interference of wave functions for different orbital momentum states and are known as the Sivers and Boer-Mulders functions [16, 17, 18, 9, 10, 11], describe unpolarized quarks in the transversely polarized nucleon and transversely polarized quarks in the unpolarized nucleon respectively. This functions parameterize the correlations between the transverse momentum of quarks and the spin of a transversely polarized target or the transverse spin of the quark, respectively. They require both orbital angular momentum, as well as non-

Table 1: *Leading-twist transverse momentum-dependent distribution functions. U, L, and T stand for transitions of unpolarized, longitudinally polarized, and transversely polarized nucleons (rows) to corresponding quarks (columns).*

N/q	U	L	T
U	$\mathbf{f_1}$		$h_1^\perp$
L		$\mathbf{g_1}$	$h_{1L}^\perp$
T	$f_{1T}^\perp$	g_{1T}	$\mathbf{h_1}$ $h_{1T}^\perp$

trivial phases from the final state interaction, that survive in the Bjorken limit.

Similar quantities arise in the hadronization process. One particular case is the Collins T-odd fragmentation function $H_1^\perp$ [19] describing fragmentation of transversely polarized quarks into unpolarized hadrons.

3 SIDIS at JLab with CLAS and CLAS12

Measurements of SSAs in SIDIS kinematics have been done at Jefferson Lab using a 5.7 GeV electron beam and the CEBAF Large Acceptance Spectrometer (CLAS) [20]. Scattering of longitudinally polarized electrons off a polarized NH_3 and ND_3 targets was studies over a wide range of kinematics. The average beam polarization was $\sim 73\%$ and the average target polarization for NH_3 (ND_3) was $\sim 70\%$ ($\sim 30\%$). The scattered electrons and pions were detected in CLAS. In the DIS kinematics ($Q^2 > 1\ GeV^2$, $W^2 > 4\ GeV^2$), ~ 8 millions π^+ have been detected in the $y < 0.85$, $z > 0.4$ range.

3.1 Single Spin Asymmetry with Longitudinally Polarized Target

Spin-orbit correlations in SIDIS with a longitudinally polarized target give raise to the Mulders leading-twist distribution function $h_{1L}^\perp$. It is related to the real part of the interference of wave functions for different orbital momentum states, and describes transversely polarized quarks in the longitudinally polarized nucleon. For a longitudinally polarized target the only azimuthal asymmetry arising in leading order is the $\sin 2\phi$ moment,

$$\sigma_{UL}^{\sin 2\phi} \propto S_L 2(1-y) \sin 2\phi \sum_{q,\bar{q}} e_q^2 x h_{1L}^{\perp q}(x) H_1^{\perp q}(z). \quad (1)$$

where ϕ is the azimuthal angles of the hadron and x, y, z define the fractions of the proton momentum carried by the struck quark, electron momentum carried by the virtual photon and the virtual photon momentum carried by the final state hadron, respectively. The physics of σ_{UL}, which involves the Collins fragmentation function $H_1^\perp$ and Mulders distribution function $h_{1L}^\perp$, was first discussed by Kotzinian and Mulders in 1996 [22, 23, 24].

A recent measurement of the $\sin 2\phi$ moment of σ_{UL} by HERMES [25] is consistent with zero. A measurably large asymmetry has been predicted only at large x ($x > 0.2$), a region well-covered by JLab [26, 27].

Indeed, the kinematic dependence of the SSA for π^+, measured from the CLAS EG1 data set at 6 GeV [28] is consistent with predictions [21] (see fig.1). The curve is the result of the calculation by Efremov et al. [21], using $h_{1L}^\perp$ from the chiral quark soliton model evolved to Q^2=1.5 GeV^2. Current statistical errors for π^-, and in particular π^0, are large and do not allow strong conclusions from the measured SSAs. Data at 6 GeV with ten times higher statistics will be soon available at CLAS allowing statistically significant measurement of the $\sin 2\phi$ moment. The projected results are shown in fig.1.

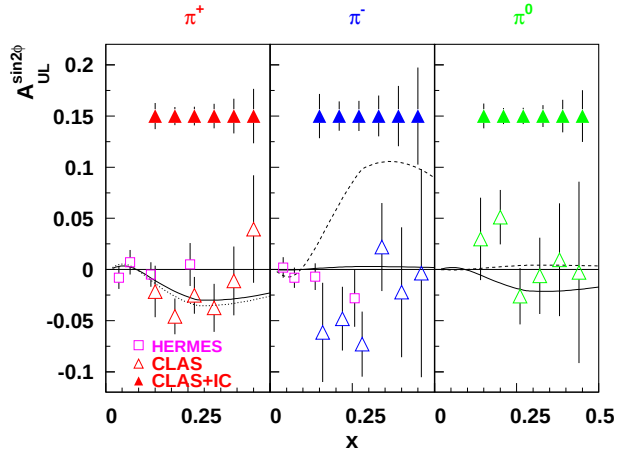

Figure 1: *The projected x-dependence of the target SSA at 6 GeV. The triangles illustrate the expected statistical accuracy. The open squares and triangles show the existing measurements of the Mulders TMD from HERMES and the* CLAS *5.7 GeV EG1 data sets, respectively. The curves are calculated using Ref.* [21].

3.1.1 *Double Spin Asimmetry and Flavour Decomposition*

The data with longitudinally polarized beam and target provides important information input for flavor decomposition through measurement of double spin asymmetries, sensitive to the ratio of helicity and momentum distributions. There are indications that the double-spin asymmetry (see fig.2) at small P_T tends to increase for π^- and decrease for π^+. A possible interpretation of the P_T-dependence of the double spin asymmetry may involve different widths of transverse momentum distributions of quarks with different flavor and polarization [29] resulting from a different orbital structure of quarks polarized in the direction of the proton spin and opposite to it [30, 31].

Detailed measurements of A_{LL} and its $\cos\phi$ moment as a function of P_T in different bins in x, z, Q^2 proposed for `CLAS12` (see projected results in fig.2) will allow study of the flavor dependence of transverse momentum distributions.

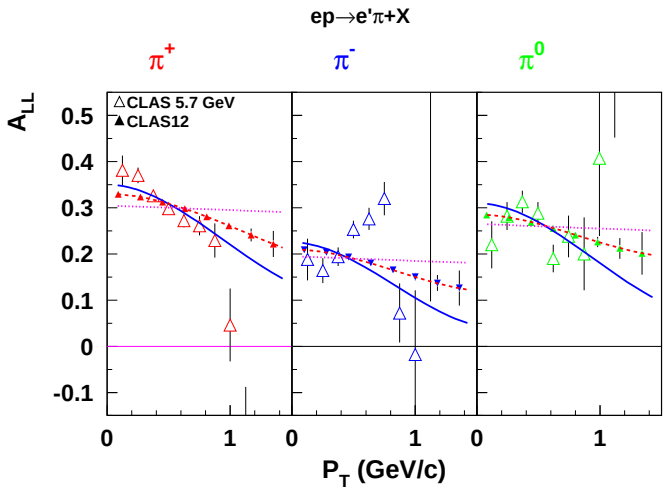

Figure 2: *The double spin asymmetry A_{LL} as a function of the transverse momentum of hadrons, P_T, averaged in the $0.4 < z < 0.7$ range.Open and full triangles are preliminary CLAS data at 5.7 GeV and projected results at 11 GeV, respectively. Curves are predictions from* [29]

3.2 Single Spin Asymmetry with Transversely Polarized Target

For transversely polarized target and unpolarized beam one of the leading twist contribution to the cross section is

$$\sigma_{UT}^{Collins} \quad \propto \quad (1-y)\sin(\phi+\phi_S)\sum_{q,\bar{q}} e_q^2 x h_1(x) H_1^{\perp q}(z) \tag{2}$$

where ϕ_S is the azimuthal angle of the transverse spin in the photon frame. The leading-twist transversity distribution h_1 [32, 33] and its first moment, the tensor charge, are as fundamental for understanding of the spin structure of the nucleon as are the helicity distribution g_1 and the axial vector charge. The transversity distribution h_1 is charge conjugation odd. It does not mix with gluons and for non-relativistic quarks it is equal to the helicity distribution g_1. Thus, it probes the relativistic nature of quarks and it has a very different Q^2 evolution than g_1.

In the last few years, first results on transverse SSAs have become available [34, 35]. HERMES measurements for the first time directly indicated significant azimuthal moments generated both by Collins (fig. 3) and Sivers effects. Measurements with CLAS12 are planned and projected results are shown in fig. 3)

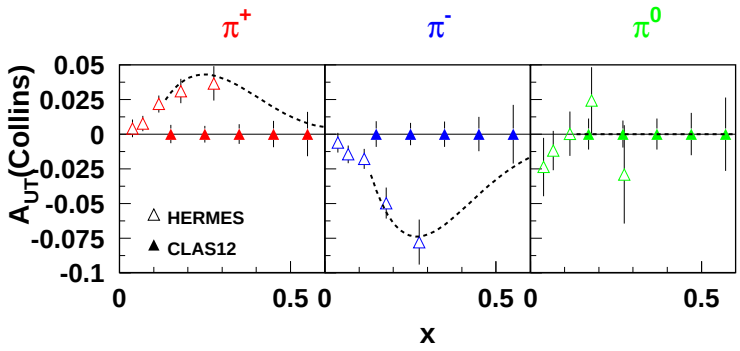

Figure 3: *Projected transverse spin asymmetry from the Collins effect* ($A_{UT}^{\sin(\phi+\phi_S)}$) *in single* π *production with* CLAS *at 11 GeV. Curves represent predictions by Anselmino and collaborators.* [36]

4 Conclusion

Measured single and double spin asymmetries for all pions in a large range of kinematic variables (x_B, Q^2, z, $P_\perp$, and ϕ) combined with measurements with unpolarized targets will provide detailed information on the flavor and polarization dependence of the transverse momentum distributions of quarks in the valence region. These studies are underway at Jefferson Lab using the CLAS detector and they are also important part of the 12 GeV physics program to be carried out with the `CLAS12` detector.

References

1. J. Ashman *et al*, Phys. Lett. **B206**, 364 (1988).
2. D. Adams *et al*, Phys. Rev. **D56**, 5330 (1997).
3. K. Abe *et al*, Phys. Rev. **D58**, 112003 (1998).
4. P. Anthony *et al*, Phys. Lett. **B458**, 529 (1999).
5. K. Ackerstaff *et al*, Phys. Lett. **B464**, 123 (1999).
6. A. Airapetian*et al*, Phys. Rev. **D71**, 012003 (2005).
7. R. Fatemi *et al*, Phys. Rev. Lett. **91**, 222002 (2003).
8. S.J. Brodsky, D.S. Hwang *and* I. Schmidt, Phys. Lett. **B530**, 99 (2002).
9. J.C. Collins, Phys. Lett. **B536**, 43 (2002).
10. X. Ji *and* F. Yuan, Phys. Lett. **B543**, 66 (2002).
11. A. V. Belitsky, X. Ji *and* F. Yuan, Nucl. Phys. **B656**, 165 (2003).
12. D. Boer, P.J. Mulders *and* F. Pijlman, Nucl. Phys. **B667**, 201 (2003).
13. X. Ji, J. Ma *and* F. Yuan, Phys. Rev. **D71**, 034005 (2005).
14. J.C. Collins *and* A. Metz, Phys. Rev. Lett. **93**, 252001 (2004).
15. X. Ji, J.-P. Ma *and* F. Yuan, Nucl. Phys. **B652**, 383 (2003).
16. D.W. Sivers, Phys. Rev. **D43**, 261 (1991).

17. M. Anselmino *and* F. Murgia, Phys. Lett. **B442**, 470 (1998).

18. S.J. Brodsky, D.S. Hwang *and* I. Schmidt, Nucl. Phys. **B642**, 344 (2002).

19. J.C. Collins, Nucl. Phys. **B396**, 161 (1993).

20. B. Mecking *et*, Nucl. Instr. Meth. **A503**, 513 (2003).

21. A.V. Efremov, K. Goeke *and* P. Schweitzer, Czech. J. Phys. **55**, A189 (2005).

22. P.J. Mulders *and* R.D. Tangerman, Nucl. Phys. B**461**, 197 (1996).

23. A. Kotzinian, Nucl. Phys. **B441**, 234 (1995).

24. A. Kotzinian *and* P.J. Mulders, Phys. Rev. **D54**, 1229 (1996).

25. A. Airapetian *et al*, Phys. Rev. Lett. **84**, 4047 (2000).

26. A.V. Efremov, Goeke K. *and* P. Schweitzer, Phys. Rev. **D67**, 114014 (2003).

27. H. Avakian, A. V. Efremov, K. Goeke, A. Metz, P. Schweitzer and T. Teckentrup, arXiv:0709.3253 [hep-ph].

28. H. Avakian, P. Bosted, V. Burkert *and* L. Elouadrhiri, AIP Conf. Proc. **792**, 945 (2005).

29. M. Anselmino, A. Efremov, A. Kotzinian *and* B. Parsamyan, Phys.Rev. **D74**, 074015 (2006).

30. S.J. Brodsky *and* S.D. Drell, Phys. Rev. **D22**, 2236 (1980).

31. S.J. Brodsky, M. Burkardt *and* I. Schmidt, Nucl. Phys. **B441**, 197 (1995).

32. J.P. Ralston *and* D.E. Soper, Nucl. Phys. **B152**, 109 (1979).

33. R.L. Jaffe *and* X. Ji, Nucl. Phys. **B375**, 527 (1992).

34. A. Airapetian *al*, Phys. Rev. Lett. **94**, 012002 (2005).

35. V.Y. Alexakhin *et al*, Phys. Rev. Lett. **94**, 202002 (2005).

36. M. Anselmino *et al*, Phys. Rev. **D75**, 054032 (2007).

Frascati Physics Series Vol. XLVI (2007), pp. 1187–1190
HADRON07: XII Int. Conf. on Hadron Spectroscopy – Frascati, October 8-13, 2007
Hadron Structure

LATEST HERMES RESULTS ON THE HELICITY SUBSTRUCTURE OF THE NUCLEON

Riccardo Fabbri,
on behalf of the HERMES Collaboration,
DESY, 22607 Hamburg, Germany

Abstract

The HERMES experiment at DESY aims to study the spin structure of the nucleon. An overview of the final results for the structure function g_1 and of the recent results for the gluon polarization is given.

1 Introduction

In recent years, a major goal in the study of QCD has been the detailed investigation of the spin structure of the nucleon. The nucleon helicity can be decomposed conceptually into the contributions from its constituents according to the relation

$$S_z^N = \frac{1}{2} = \frac{1}{2}\Delta\Sigma + \Delta G + L_z^q + L_z^g \ . \tag{1}$$

Here $\Delta\Sigma$ (ΔG) and L_z^q (L_z^g) represent the quark (gluon) spin and orbital angular momentum, respectively.

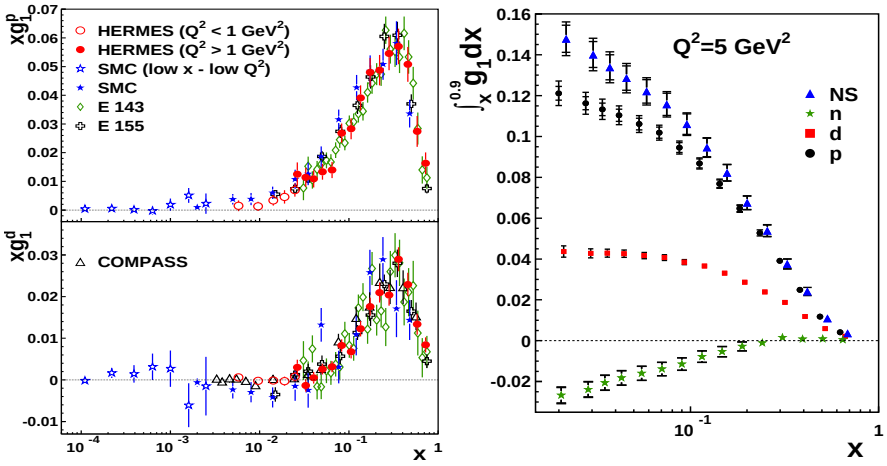

Figure 1: Left panel: the HERMES results for xg_1 vs x for the proton and the deuteron are compared to previously published data. Right panel: the integral of g_1 over the range $0.021 < x < 0.900$ is shown as a function of the low-x limit of integration.

The HERMES experiment [1)] is located at the laboratory DESY in Hamburg, Germany. In 1996-2000 HERMES has taken data using a gaseous longitudinally polarized hydrogen or deuterium target, internal to the 27.6 GeV HERA longitudinally polarized positron or electron beam.

2 Spin Structure Function g_1 and Quark Helicity

Polarized structure functions g_1, depending on the Bjorken variable x and on the scale Q^2, have been extracted from double-spin asymmetries of cross section in the inclusive DIS process $\vec{e} + \vec{N} \rightarrow e + X$ [2)]. The final HERMES results for $g_1^{p,d}$ from all the data accumulated with longitudinally polarized hydrogen and deuterium targets are presented in the left panel of Fig. 1, and compared to previously published data. The accuracy of the HERMES proton data is comparable to the most precise published measurements (at SLAC and CERN) in the same x range, while the deuteron data provide the most precise determination of g_1^d in the intermediate x range.

The right panel of Fig. 1 shows the integrals of the g_1 for proton, deuteron, and neutron over the range $0.021 < x < 0.900$, corresponding to the event selection $Q^2 > 1$ GeV^2, as a function of the low-x limit of integration. Using

the partonic distribution evolution, all the data points have been evaluated at the common scale $Q^2 = 5$ GeV^2. The deuteron integral appears to saturate at $x < 0.04$. Based on the assumed saturation of the integral of g_1^d, and using the axial charge a_8 as external input, the flavour-singlet axial charge a_0 has been determined from the data to be $0.330 \pm 0.025(exp.) \pm 0.011(theo.) \pm 0.028(evol.)$ at NNL order in the strong coupling constant α_S. In the *modified minimal subtraction* ($\overline{MS}$) scheme, which was used in this analysis, the charge a_0 can be interpreted as the contribution $\Delta\Sigma$ of the quark spin to the nucleon helicity. The HERMES data suggest a substantial fractional contribution of the quark helicity to the nucleon helicity, and that a major contribution from the gluon helicity and/or orbital angular momentum of quarks and gluons is needed.

3 The Gluon Helicity Distribution

A direct LO, model dependent extraction of the gluon polarization $\Delta g/g(x, Q^2)$ has been performed by studying double-spin asymmetries $A_\parallel$of the cross section for single charged hadron production in the process $\vec{e} + \vec{d} \rightarrow h^\pm X$ [3]. The high statistics data sample of hadrons vetoed by the scattered beam particle was used. In the accessed kinematic region, the scale dependence of $\Delta g/g$ is expected to vary slowly, and was not considered.

The asymmetry arises from a superposition of different subprocesses contributing to the production of hadrons at a given transverse momentum p_T (with respect to the beam direction). The asymmetry has been measured in different p_T bins, applying the cut $p_T > 1$ GeV to enhance the gluon-induced subprocess contribution. To relate the measured asymmetry to the gluon polarization, information on the various subprocess contributions to the hadron production is needed. Their corresponding asymmetries A_i and relative weights R_i were obtained from Monte Carlo simulation using Pythia 6.2 and parameterizations of the polarized parton distributions of the nucleon and the photon.

The extracted gluon-induced asymmetry $A^{Sg} = (A_\parallel - R_{Bg}A^{Bg})/R_{Sg}$ contains a convolution of $\Delta g(x)/g(x)$ with the hard subprocess cross section over the x-range covered by the data. Two methods have been applied to extract the gluon polarization out of the convolution A^{Sg}. Method I assumes that $\Delta g(x)/g(x)$ is constant in the measured x range, resulting in the extracted value $\Delta g(x)/g(x)_{|I} = 0.078 \pm 0.034(stat.) \pm 0.011(exp.syst.) \pm^{+0.125}_{-0.082}$ $(model\ syst.)$ at $\langle x \rangle_{|I} = 0.204$ and scale 1.35 GeV^2. Method II employes a functionl form

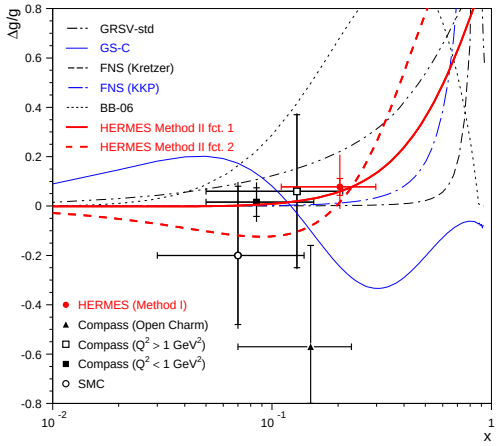

Figure 2: HERMES results (closed circle and thickest lines) for the gluon polarization $\Delta g(x)/g(x)$ determined using the two methods described in the text. Also shown are the results from COMPASS and SMC, and several NLO QCD fits.

for $\Delta g(x)/g(x)$, which is used to calculate the gluon-induced asymmetry A^{Sg} for each p_T bin. The function parameters are determined by minimizing χ^2 for the difference $(A_{\parallel} - R_{Bg}A^{Bg}) - R_{Sg}A^{Sg}$, using all bins in p_T. A second functional form is used to estimate the additional systematical uncertainty originating from the fitting procedure. The results from the two methods are shown in Fig. 2, together with previous determinations of $\Delta g(x)/g(x)$ [4], and are compared to different parameterizations obtained from NLO QCD fits. The HERMES data favour a small gluon polarization (at LO) in the accessed x-range.

References

1. HERMES Collaboration, K. Ackerstaff et al., Nucl. Inst. and Methods **A 417** (1998) 230.
2. HERMES Collaboration, A. Airapetian et al., Phys. Rev. **D 75**, 012007 (2007).
3. P. Liebing, on behalf of the HERMES Collaboration, Proc. 17th International Spin Physics Symposium, AIP Conf. Proc. 915, 331 (2006).
4. K. Kurek, on behalf of the COMPASS Collaboration, Proc. 14th International Workshop on Deep Inelastic Scattering and QCD; COMPASS Collaboration, E. S. Ageev, et al., Phys. Lett. **B 633** 25 (2006); SMC Collaboration, B. Adeva, et al., Phys. Rev. **D 70** 012002 (2004).

Frascati Physics Series Vol. XLVI (2007), pp. 1191–1196
HADRON07: XII Int. Conf. on Hadron Spectroscopy – Frascati, October 8-13, 2007
Hadron Structure

CALCULATION OF NULEONS F_2 STRUCTURE FUNCTIONS USING RADIATIVE GLUONS AND MESON CLOUD MODEL IN LIGHT-CONE FRAME

F. Zamani
Department of Physics, Villanova University
800 East Lancaster Avenue, Villanova, PA 19085, USA

Abstract

In our previous works [1-5], using a quark-diquark model along with meson cloud, we investigated F_2 and g_1 structure function. Our work has shown that it is necessary for the core nucleon to have a spin-1 diquark component. In this work we will use superposition of spin-0 and spin-1 diquarks as the core nucleon to calculate quark distribution functions. Then, using pQCD, an initial gluon distribution is generated inside the core nucleon. The physical nucleon is assumed to be a superposition of the bare nucleon plus the virtual light-cone Fock states of the baryon-meson pairs. The initial distributions are evolved using DGLAP equations. The F_2 structure functions calculated from the evolved distributions are compared with NMC and Zeus results along with a CTEQ fit. Also, we will show that the meson cloud is a contributing factor to sea quark asymmetry and to Gottfried sum-rule violation.

1 Formulation

1.1 Proton Wavefunction:

We start with writing the wave function of the nucleon as $\Psi = \Phi\chi\phi$, where Φ, χ and ϕ are the flavor, spin and momentum distributions, respectively. We are going to consider three different wave functions for the core nucleon. Set-1 and Set-3 are quark-diquark system. For set-1 we assume that the nucleon is a quark-diquark system with spin-0 diquark and for Set-3 a superposition of spin-0 and spin-1 diquarks [1]:

$$\begin{aligned}
\Psi_1 \quad = \tfrac{A}{\sqrt{2}}[\quad & uud(\chi^{\rho 1}\phi_1^{\lambda 1} + \chi^{\rho 2}\phi_1^{\lambda 2}) - udu(\chi^{\rho 1}\phi_1^{\lambda 1} - \chi^{\rho 3}\phi_1^{\lambda 3}) - \\
& duu(\chi^{\rho 2}\phi_1^{\lambda 2} + \chi^{\rho 3}\phi_1^{\lambda 3})] + \\
\tfrac{B}{\sqrt{6}}[\quad & uud(\chi^{\rho 1}\phi_1^{\rho 1} + \chi^{\rho 2}\phi_1^{\rho 2} - 2\chi^{\rho 3}\phi_1^{\rho 3}) + \\
& udu(\chi^{\rho 1}\phi_1^{\rho 1} - 2\chi^{\rho 2}\phi_1^{\rho 2} + \chi^{\rho 3}\phi_1^{\rho 3}) + \\
& duu(-2\chi^{\rho 1}\phi_1^{\rho 1} + \chi^{\rho 2}\phi_1^{\rho 2} + \chi^{\rho 3}\phi_1^{\rho 3})] + \\
\tfrac{C}{\sqrt{2}}[\quad & uud(\chi^{\lambda 1}\phi_1^{\rho 1} + \chi^{\lambda 2}\phi_1^{\rho 2}) - udu(\chi^{\lambda 1}\phi_1^{\rho 1} - \chi^{\lambda 3}\phi_1^{\rho 3}) - \\
& duu(\chi^{\lambda 2}\phi_1^{\rho 2} + \chi^{\lambda 3}\phi_1^{\rho 3})] + \\
\tfrac{D}{\sqrt{6}}[\quad & uud(\chi^{\lambda 1}\phi_1^{\lambda 1} + \chi^{\lambda 2}\phi_1^{\lambda 2} - 2\chi^{\lambda 3}\phi_1^{\lambda 3}) + \\
& udu(\chi^{\lambda 1}\phi_1^{\lambda 1} - 2\chi^{\lambda 2}\phi_1^{\lambda 2} + \chi^{\lambda 3}\phi_1^{\lambda 3}) + \\
& duu(-2\chi^{\lambda 1}\phi_1^{\lambda 1} + \chi^{\lambda 2}\phi_1^{\lambda 2} + \chi^{\lambda 3}\phi_1^{\lambda 3})]. \qquad (1)
\end{aligned}$$

For Set-2, we assume that there is no clustering of the quarks inside the nucleon [6]:

$$\Psi_2 = \frac{-1}{\sqrt{3}}(uud\chi^{\lambda 3} + udu\chi^{\lambda 2} + duu\chi^{\lambda 1})\phi_2. \qquad (2)$$

For Set-1 we use $A = .9798$, $B = -.2$, $C = 0.0$ and $D = 0.0$ in Eq.(1). Equation (2) is used for set-2. For Set 3 we choose $A = -0.7874$, $B = 0.0$, $C = 0.0$, and $D = -0.6164$ in Eq.(1). Also, in Eqs. (1) and (2), u and d represent the up and down flavor. χ^{ρ_i}, and χ^{λ_i} with $i = 1, 2, 3$ represent the Melosh transformed spin wave functions [7].

1.2 Radiative Gluons:

Having constructed the wavefunction for the core nucleon, we know introduce gluons inside the nucleon. Following the work done by Barone and collaborators

[8], one can consider a transition $v(x) \rightarrow q(x) \ + g(x)$, where $v(x)$ is the initial valence quark distribution in quark model and g(x) is the gluon distribution generated in the process. Knowing $v(x)$, one can calculate $q(x)$ and $g(x)$ in the following way:

$$\begin{aligned} q(x,Q_1^2) &= v(x)[1-\int_0^1 dy G(1-y,Q_1^2,0)] + \\ &\int_x^1 \frac{dy}{y} G(1-y,Q_1^2,0)[v(\frac{x}{y}) - yv(x)], \end{aligned} \tag{3}$$

$$\tilde{g}(x,Q_1^2,0) = \int_x^1 \frac{dy}{y} v(\frac{x}{y}) G(y,Q_1^2,0), \tag{4}$$

where $G(x,Q_1^2,0)$ is the flux of gluons generated from the target quark:

$$G(x,Q_1^2,0) = \frac{4}{3}\int_0^{Q_1^2} d^2\vec{k}\ \frac{\alpha_s(\vec{k}^2)}{2\pi} V(-k_g^2) \frac{([1+(1-x)^2]\vec{k}^2 + x^4 m_f^2)}{x[\vec{k}^2 + (1-x)\mu_G^2 + x^2 m_f^2]^2}, \tag{5}$$

where $-k_G^2$ is the gluon's virtuality

$$-k_G^2 = \frac{\vec{k}^2 + x^2 m_f^2}{(1-x)}, \tag{6}$$

$V(\vec{k})$ is the vertex function related to the charge form factor of the nucleon:

$$V(\vec{k}) = 1 - F_{charge}(3\vec{k}^2), \tag{7}$$

m_f is the mass of the quark with flavor f, and μ_G is the effective mass of gluons introduce so that the color forces do not propagate beyond the confinement radius and is taken to be about $145MeV$.

To perform the next step of evolution from Q_1^2 to Q_2^2, $(Q_2^2 > Q_1^2)$, one repeats the above procedure by replacing $v(x) \rightarrow q(x,Q_1^2)$and $G(x,Q_1^2,0) \rightarrow G(x,Q_2^2,Q_1^2)$ which lead to new gluon distribution

$$g(x,Q_2^2) = \tilde{g}(x,Q_2^2,Q_1^2) + \tilde{g}(x,Q_1^2,0), \tag{8}$$

and obviously these along with Eq.(3) will lead to $q(x,Q_2^2)$. This procedure can be repeated in small steps until one reaches the desired final Q^2, which in our case is 0.5 GeV^2. In our case, at this stage we have introduced about six gluons that carry about 27% of the nucleon's momentum. The next step is to introduce meson cloud at this momentum transfer and evolve the distributions to the final momentum transfer.

1.3 Meson cloud model in light-cone frame:

Using the convolution model, one can decompose the physical nucleon in terms of the core nucleon and intermediate, virtual meson-baryon states [1-5, and the references therein]:

$$\mid N\rangle = Z^{1/2}[\mid N\rangle_{bare} + \sum_{BM} \beta_{BM} \mid BM\rangle], \tag{9}$$

where Z is the probability of the physical nucleon being in the core state, BM stands for a virtual baryon-meson state and β_{BM} is the probability amplitude for the physical nucleon being in BM state. The summation in Eq. (14), in general, includes all physically possible pairs from the meson octet and baryon octet and decuplet. In terms of the quark distributions one can write:

$$q_N(x) = Z[q_{N,core}(x) + \sum_{MB} \alpha_{MB}(\int_x^1 n_{MB} q_M(\frac{x}{y})\frac{dy}{y} + \int_x^1 n_{BM} q_B(\frac{x}{y})\frac{dy}{y})], \tag{10}$$

where x is the fraction of the total momentum of the nucleon being carried by the quark, q, α_{MB} are spin-flavor Clebsch-Gordan coefficients, n_{MB} and n_{BM} ,the splitting functions, are the probabilities of the nucleon being in state of MB or BM respectively, y is the fraction of the momentum being carried by the meson(baryon) in $n_{MB}(y)(n_{BM}(y))$. The splitting functions can be expressed in the following way [9,10]:

$$n_{BM}(y, k_\perp^2) = \frac{1}{4\pi^2}\frac{m_N m_B}{y(1-y)}\frac{\mid V_{IMF}(y, k_\perp^2)\mid^2 \mid \Gamma_{BM}(y, k_\perp^2)\mid^2}{[m_N^2 - M_{BM}^2(y, k_\perp^2)]^2}, \tag{11}$$

where $V_{IMF}(y, k_\perp^2)$ is the vertex function and $\Gamma_{BM}(y, k_\perp^2)$ is the vertex form factor. Having the splitting function one can calculate the initial dressed polarized quark distributions. These distributions can be evolved using the DGLAP equations [11-13]. Using the evolved distributions we can calculate F_2 structure functions for proton and neutron and evaluate the Gottfried sum rule (GSR), which is [14]:

$$\int_0^1 \frac{dx}{x}[F_{2p}(x, Q^2) - F_{2n}(x, Q^2)] = \frac{1}{3}. \tag{12}$$

2 Results and discussion

We have studied the impact of radiative gluons on core u-quark distribution. As a result of this radiative process there is noticeable reduction in the peak value of the distribution and a shift of the peak value to lower x values.

As a result of this radiative process there is noticeable reduction in the peak value of the distribution and a shift of the peak value to lower x values.

We have also studied the evolved xu-valence and xd-valence distributions. All data have been evolved to $Q_f^2 = 70GeV^2$.

Having the distribution functions we can calculate the F_2 structure function for proton and neutron [1]. These produce the results for F_{2p} and F_{2n}

The $F_{2p} - F_{2n}$ and F_{2n}/F_{2p}, respectively have been studied as well[1].

From the results one can see that set-3g model specially the one that includes vector meson cloud has a better agreement with CTEQ6M fit. Figs. 4 and 5 shows that our results are in rather good agreement with ZEUS, NMC and CTEQ6M results all the way down to low x value of about 0.02. Below $x = 0.02$ the model starts to depart from observation. One final note about Figs. 4-7 is that they are generated using pseudoscalar mesons along with the corresponding baryon octets and decuplets. Having the structure function we can calculate the GSR using Eq. 12. The results are presented in 2.

Table 1: GSR results for this work, NMC [15], ZEUS [16,17], and CTEQ6M 5-flavor [18] at $Q^2 = 70\ GeV^2$.

	Set-3g	Set-2g	Set-1g	NMC	ZEUS	CTEQ6M-5f
GSR	0.265	0.266	0.277	0.212	0.232	0.236

In Table 1 we see that our model does predict the violation of GSR but to a lesser degree than NMC, ZEUS results and CTEQ6M fit. Again, set-3g has a better agreement with observation and CTEQ6M fit. It would be interesting to find out the contribution of vector mesons to the GSR violation.

To summarize, we used a quark-diquark model for the core nucleon. We considered three different wavefunctions for the core nucleon. Two were two variations of quark-diquark model and the third represented a case with no diquark inside the nucleon. The two diquark cases considered were one with only spin-0 diquark and the other a superposition of spin-0 and spin-1 diquark.

We introduced gluons through a radiative process. In the final step the meson cloud was introduced and the distributions were evolved to the final momentum transfer. Both diquark models had a reasonably good agreement with experimental results for F_2 structure functions down to x about 0.02 specially the case that considered spin-1 diquark. Our calculations also showed that the meson cloud is a source of sea quark asymmetry which leads to the GSR violation. However, the degree of violation is less than observation. One could improve on this by introducing the vector meson component of the meson cloud which is the next step of our research.

3 References

1- F. Zamani, Phys. Rev. **C74** (2006) 035204-1.
2- F. Zamani, Nucl. Phys. **A755** (2005)365.
3- F. Zamani, Phys. Rev. **C68**, 055202-1 (2003).
4- F. Zamani and D. Saranchak, Phys. Rev. **C63**, 065202-1 (2001).
5- F. Zamani, Phys. Rev. **C58**, 3641 (1998).
6- F. Schlumpf, Ph.D. thesis, University of Zurich, (1992).
7- H.J. Melosh, Phys. Rev. **D9**, 1095 (1974).
8- V. Barone, M. Genovese, N. N. Nikolaev, E. Predazzi and B. G. Zakharov, Int. J. Mod. Phys. **A8**, 2779 (1993).
9- V.R. Zoller, Z.Phys. **C53**, 443 (1992).
10- J. Speth and A. W. Thomas, Adv. Nucl. Phys. **24**,83 (1997).
11- V. N. Gribov and L. N. Lipatov, Sov. J. Nucl. Phys., **15**, 438 (1972).
12- G. Altarelli and G. Parisi, Nucl. Phys. **B126**(1977)298.
13- Yu. L. Dokshitzer, Sov. Phys. JETP **46**, 641 (1977).
14- K. Gottfried, Phys. Rev. Lett. **18**, 1174 (1967).
15- P. Amaudruz *et al.*, Phys. Lett. **B295**, 166 (1992).
16- S. Chekanov *et al.*, Phys. Rev. **D 67**, 012007 (2003).
17- J. Rautenberg, Ph.D. thesis, University of Bonn, (2004).
18- J. Pumplin, D. R. Stump, J. Huston, H. L. Lai, P. Nadolsky, and W. K. Tung, JHEP **0207**, 012 (2002).

Frascati Physics Series Vol. XLVI (2007), pp. 1199–1206
HADRON07: XII Int. Conf. on Hadron Spectroscopy – Frascati, October 8-13, 2007
Hadrons in Matter

PRECISE MEASUREMENT OF KAONIC HELIUM ATOMS X-RAYS

M. Iio[a], G. Beer[b], H. Bhang[c], P. Buehler[d], M. Cargnelli[d], J. Chiba[e], S. Choi[c] C. Curceanu[f], Y. Fukuda[g], C. Guaraldo[f], T. Hanaki[e], R. S. Hayano[h], A. Hirtl[d], M. Iliescu[f], T. Ishikawa[h], S. Ishimoto[i], T. Ishiwatari[d], M. Iwai[i], K. Itahashi[a], M. Iwasaki[a], B. Juhasz[d], P. Kienle[d,j], J. Marton[d], Y. Matsuda[a] H. Ohnishi[a], S. Okada[a], H. Outa[a], D. Pietreanu[f], F. Sakuma[a], M. Sato[a] P. Schmid[d], D. Sirghi[f], F. Sirghi[f], S. Suzuki[i], T. Suzuki[a], H. Tatsuno[h], D. Tomono[a], E. Widmann[d], T. Yamazaki[a,h], H. Yim[c] and J. Zmeskal[d]

[a] *RIKEN Nishina Center, RIKEN, Wako-shi, Saitama 351-0198, Japan*
[b] *University of Victoria, Box 3055, Victoria, British Columbia, Canada*
[c] *Seoul National University, Kwanak-gu, Seoul 151-742, South Korea*
[d] *Stefan Meyer Institut für subatomare Physik, 1090 Vienna, Austria*
[e] *Tokyo University of Science, Noda-shi, Chiba 278-8510, Japan*
[f] *Laboratori Nazionali di Frascati dell' INFN, Frascati, Italy*
[g] *Tokyo Institute of Technology, Meguro-ku, Tokyo 152-8551, Japan*
[h] *The university of Tokyo, Hongo, Bunkyo-ku, Tokyo 113-0033, Japan*
[i] *KEK(High Energy Accelerator Research Organization), Ibaraki, Japan*
[j] *Technische Universiät at München, 85748, Garching, Germany*

Abstract

We performed an accurate and clean measurement of the kaonic-^{4}He Balmer-series x-rays at KEK-PS [E570]. The $2p$-level strong-interaction shift was estimated to be $2 \pm 2(stat) \pm 2(syst)$ eV in agreement with most theories, thus solving the long-standing kaonic helium puzzle. For the near future, we are planning an experiment to measure the x-rays of kaonic-^{3}He at J-PARC [E17]. Crucial information for the isospin dependent $\bar{K}$-nucleus strong interaction at the low energy limit will be provided by the E17 experiment.

1 Introduction

The strong-interaction energy-level shift and width of kaonic atoms were measured for understanding of the $\bar{K}$-nucleus interaction in the low energy limit. The experimental data of most kaonic atoms except helium and oxygen were

in good agreement with the fitting by the optical-potential models [1]. The $2p$-level shift and width of kaonic-^{4}He have been measured in the past by three experiments. The average of the shift, determined by the past three kaonic-^{4}He x-rays measurements, was $\sim$40 eV large shift [2] [3] [4], while a majority of theoretical calculations suggested very small shift below 1 eV [5] [6] [7]. As to this discrepancy, there has been a long debate, the so-called "kaonic helium puzzle". On the other hand, Akaishi and Yamazaki predicted a large $2p$-level shift ($\mid \Delta E_{2p} \mid \sim$10 eV) of kaonic-^{4}He and kaonic-^{3}He atoms [8] by their theoretical framework of a "deeply-bound kaonic nuclear system" [9]. Therefore precise measurement of the $2p$ energy level shift of kaonic helium atoms has been long awaited.

In the present experiment at KEK [E570], we have performed a measurement of the Balmer-series x-rays of kaonic-^{4}He with a precision of $\sim$2 eV (statistical), thus a definitive answer has been provided to this long-standing puzzle. It is extremely important to measure the $2p$ shifts of both kaonic-^{4}He and kaonic-^{3}He in order to confirm or not the isospin dependence of Akaishi's prediction [8]. We therefore plan to measure the x-rays of kaonic-^{3}He at J-PARC [E17] using a similar technique to that of E570.

2 E570 experiment

The E570 experiment was performed at the K5 beamline of the KEK 12 GeV proton synchrotron in October, 2005 (cycle 1) and December, 2005 (cycle 2). The E570 experimental apparatus was essentially no different from the KEK-PS E549 experiment performed on the same beamline for one month from the end of May, 2005 [10], except for the inclusion of silicon drift x-ray detectors (SDD) and energy calibration foils in the superfluid liquid ^{4}He target system. Figure 1 shows a schematic view of the experimental setup around the target. The kaonic-^{4}He atom was generated by negatively-charged kaons stopped inside the superfluid ^{4}He target cell (cylindrical shape 15 cm long and 20 cm in diameter at a density of 0.145 g/cm^3). Incident kaons with momentum $\sim$650 MeV/c were degraded in carbon degraders, counted with beamline counters, and tracked by a beamline drift chamber. The energy losses of the incident particles were measured by a scintillation counter named T0.

In E570, a significant improvement over the past experiments was achieved by incorporating the following:

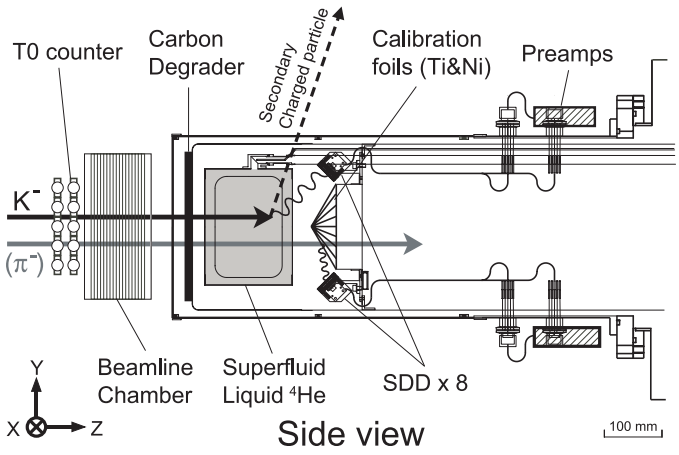

Figure 1: *A schematic side view of the E570 setup around the cylindrical target with the x-ray detection system. Eight SDDs are mounted on holders tilted at a 45 degree angle to the beam center in an annular-shaped pattern. Fan-shaped high-purity titanium and nickel foils are put alternately on a cone-shaped support located on the beam axis.*

2.1 Silicon drift x-ray detector

For this experiment, Silicon Drift Detectors (SDDs) produced by KETEK [11] were adopted for energy resolution improvement of x-ray detection. Each SDD has an effective area of 100 mm^2 and a 260 μm-thick active layer. The temperature of the SDDs was kept at $\sim$85 K during the experimental period by a connection to the thermal-radiation shield for the helium target cooled by liquid nitrogen. Typical energy resolution is 190 eV (FWHM) at 6.4 keV, which is about twice as good as that of the Si(Li) x-ray detectors used in the previous three experiments. The time resolution is about 160 nsec (rms).

In the SDD, the electrons produced by an x-ray hit drift radially toward the central anode where they are collected. The small anode size (and hence small capacitance) is essential to realize the good energy resolution despite the large effective area. The small anode area also makes it possible to reduce the active layer thickness, while the capacitance is still kept small. The thin active layer helps to reduce continuum background caused by the Compton scattering occurring inside the detector.

2.2 Cuts for reducing background events

The X-ray events coming from the kaonic-^{4}He transitions were selected by the reaction vertices reconstructed from an incident kaon track and a second charged particle track which come from the liquid ^{4}He target, which is called the "fiducial volume cut". Moreover, in-flight kaon decay/reaction events were rejected by applying a correlation cut between the z-coordinate of the reaction vertex and the energy loss in T0. As a result, a good signal-to-noise ratio of $\sim$4 was achieved, which is about 5 times better than that of the past experiments.

2.3 In-beam energy calibration

The energy calibration was done by using characteristic x-rays induced by beam particles on high-purity titanium and nickel foils placed just behind the target cell. The energy of the kaonic-^{4}He $3d \rightarrow 2p$ x-ray, $\sim$6.4 keV, lies between these characteristic x-ray energies of 4.5 keV(Ti) and 7.5 keV(Ni). To obtain high-statistics energy calibration spectra, we accumulated SDD self-triggered events together with the stopped-K^- triggered events, which provide high-accuracy in-situ calibration spectra. To avoid detecting the background characteristic x-rays from other than the titanium and nickel, high-purity aluminum foils were placed on all objects in the view of the SDDs.

3 Analysis and result of E570

A typical x-ray spectrum for SDD self-triggered events is shown in Figure 2(a). Characteristic x-ray peaks of titanium and nickel were obtained with high statistics. Time-dependent gain drift was corrected about every 20 hours. The energy scale was calibrated by K_α lines of titanium and nickel with well-known energies. Figure 3 (a), (b) respectively show the stopped-K^- triggered-event x-ray spectra taken in October, 2005 (cycle 1) and December, 2005(cycle 2). These spectra had cuts applied to reduce background events, kaonic-^{4}He $3d \rightarrow 2p$, $4d \rightarrow 2p$ and $5d \rightarrow 2p$ transitions are clearly observed, while the titanium and nickel x-ray peaks are greatly suppressed.

To fit the spectra containing kaonic-^{4}He x-ray peaks, a convolution of a Gaussian (representing the detector response) and a Lorentz function (representing the natural width), a "Voigt function", was adopted as the main-peak function, where as a Gaussian response was employed as a main-peak func-

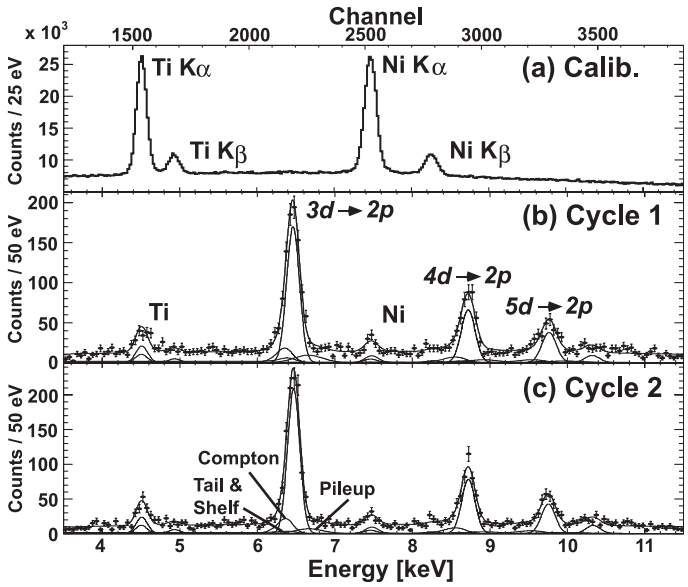

Figure 2: *(a) A typical x-ray spectrum for self-triggered events which provides high-statistics energy-calibration information. (b), (c) Measured x-ray spectra for stopped-K^- events obtained from the runs in October, 2005 (cycle 1) and December, 2005 (cycle 2) respectively. A fit line is also shown for each spectrum, along with individual functions of the fit.*

tion for fitting the characteristic x-ray peaks since their natural width is much less than the energy resolution of the SDDs. A low-energy tail structure due to Compton scattering must be taken into account to obtain an x-ray peak position with a precision of a few eV. The effects were studied by simulating the x-ray data with GEANT4 including an extension package for Low-Energy Compton Scattering (LECS). Using spectrum analysis, we established that pileup effects due to the high-rate beam conditions were non-negligible. The spectral function due to the pileup events could be estimated by waveform analysis using Flash ADC data. As a result, the measured values of the kaonic-^{4}He x-ray transition energy are given in Table 1 with only statistical errors. In this table, we also tabulate the EM values updated from Refs. [2) 3) 4)] by Koike [12)] using the latest kaon mass given by the particle data group (PDG) [13)].

Table 1: *Measured and EM calculated* [12] *kaonic-*^{4}*He x-ray energies of* $3d \rightarrow 2p$*,* $4d \rightarrow 2p$ *and* $5d \rightarrow 2p$ *transitions. The quoted error is purely statistical.*

Transition	$3d \rightarrow 2p$	$4d \rightarrow 2p$	$5d \rightarrow 2p$
Measured energy (eV)	6466.7 ± 2.5	8723.3 ± 4.6	9760.1 ± 7.7
EM calc. energy (eV)	6463.5	8721.7	9766.8

Since the strong-interaction shifts are negligibly small for the levels with a principal quantum number n larger than two, the $2p$-level shift ΔE_{2p} can be derived from the Balmer-series x-ray energies using the equation:

$$\Delta E_{2p} = (E_{(n,d)} - E_{(2,d)}) - (E^{EM}_{(n,d)} - E^{EM}_{(2,d)}) \quad (1)$$

where $E_{(n,d)} - E_{(2,d)}$ and $E^{EM}_{(n,d)} - E^{EM}_{(2,d)}$ correspond to the measured and calculated EM x-ray energies, respectively. Taking the average of the $2p$-level shifts of the three lines, we obtained the shift as:

$$\Delta E_{2p} = 2 \pm 2(stat) \pm 2(syst)eV. \quad (2)$$

This value is consistent with 0 in agreement with most theories [5] [6] [7]. To conclude, $2p$-level shift was determined by using silicon drift detectors which lead to a much improved energy resolution and signal-to-noise ratio compared to the Si(Li) x-ray detectors used in the past experiments. Our careful and precise result excludes the earlier claim of a large shift of about ∼40 eV. Therefore, "long-standing kaonic helium puzzle" has been solved. We have already published these results in Physics Letters B [14].

4 J-PARC E17 experiment

The measurement of the $2p$-level shifts of both kaonic-^{4}He and kaonic-^{3}He not only provide the crucial information on the isospin-dependent $\bar{K}$-nucleus strong-interaction at the low energy limit, but also are extremely important in order to understand the basis of the Akaishi-Yamazaki prediction of "deeply-bound kaonic nuclei". Unlike the case of kaonic-^{4}He, no data exist yet on the kaonic-^{3}He x-rays. Therefore, we are planning an experiment to measure the x-rays of the kaonic-^{3}He at J-PARC [E17] [15].

The E17 experiment will be performed at the K1.8BR beamline of the J-PARC 50 GeV proton synchrotron. The principle of the E17 experiment

is the same as that of E570. We stop negatively-charged kaons in a liquid helium target, and observe x-rays with silicon drift detectors. Incoming kaons and charged particles emitted from the K^--reaction vertices are tracked. This experiment is closely related to another experiment "A search for deeply-bound kaonic nuclear states by in-flight $^3He(K^-, n)$ reaction"[E15] [16]. Both of these experiments address the question of deeply-bound kaonic states, and there is a large overlap of the collaboration members. Both experiments will use the same beamline, Cylindrical Detector System (CDS) and liquid ^{3}He target. At the present stage of the preparation, the CDS and target used by both experiments have been conceptually developed. To start an experiment in winter, 2009, we are also advancing the development of the beamline detectors for stopped-K^- experiments and the preamps of the SDDs.

5 Summary

Kaonic-^{4}He Balmer-series x-rays were measured with a precision of $\sim$2 eV (statistical) at the KEK-PS K5 beamline. The kaonic-^{4}He atom x-ray energy of the $3d \rightarrow 2p$ transition was determined to be $6467 \pm 3(stat) \pm 2(syst)$ eV. The $2p$-level strong interaction shift was deduced as $\Delta E_{2p} = 2 \pm 2(stat) \pm 2(syst)$ eV. A precise measurement of kaonic-^{3}He x-rays is planned for the J-PARC K1.8BR beamline. At present, some devices for the experiment have been developed. E17 experiment will start in January, 2009 at the earliest.

6 Acknowledgements

We are grateful to the KEK staff members of the beam channel group, accelerator group, cryogenics group, and electronics group, for support of the present experiment. We acknowledge T. Koike who made an electromagnetic calculation of the kaonic helium atomic states. This research was supported by KEK, RIKEN, SMI and Grant-in-Aid for Scientific Research from the Ministry of Education of Japan, Nos. 17340087, 14102005 and 17070007.

References

1. C.J. Batty, E. Friedman, A. Gal, Phys. Rep. **287** (1997) 386.
2. C.E. Wiegand, R. Pehl, Phys. Rev. Lett. **27** (1971) 1410.

3. C.J. Batty, *et al.*, Nucl. Phys. A **326** (1979) 445.

4. S. Baird, *et al.*, Nucl. Phys. A **392** (1983) 297.

5. C.J. Batty, Nucl. Phys. A **508** (1990) 89c.

6. S. Hirenzaki, Y. Okumura, H. Toki, E. Oset, A. Ramos, Phys. Rev. C **61** (2000) 055205.

7. E. Friedman, private communication.

8. Y. Akaishi, in: Proceedings for International Conference on Exotic Atoms (EXA05), Austrian Academy of Sciences Press, Vienna, 2005, p. 45.

9. Y. Akaishi and T. Yamazaki, Phys. Rev. C **65** (2002) 044005.

10. M. Sato, *et al.*, arXiv: 0708.2968, Phys. Lett. B, in press.

11. http://www.ketek.net.

12. T. Koike, in preparation.

13. W.-M. Yao, *et al.*, J. Phys. G **33** (2006) 1.

14. S. Okada, *et al.*, Phys. Lett. B **653** (2007) 387-391.

15. R.S. Hayano, *et al.*, Proposal of J-PARC 50-GeV PS "Precision spectroscopy of Kaonic Helium 3 $3d \rightarrow 2p$ X-rays", 2006.

16. M. Iwasaki, *et al.*, Proposal of J-PARC 50-GeV PS "A search for deeply-bound kaonic nuclear states by in-flight $^3He(K^-, n)$ reaction", (2006).

Frascati Physics Series Vol. XLVI (2007), pp. 1207–1214
HADRON07: XII Int. Conf. on Hadron Spectroscopy – Frascati, October 8-13, 2007
Hadrons in Matter

THE SIDDHARTA EXPERIMENT: KAONIC HYDROGEN AND DEUTERIUM X-RAY SPECTROSCOPY

T. Ishiwatari[a] M. Bazzi[b], G. Beer[c], s L. Bombelli[d], A.M. Bragadireanu[b,e], M. Cargnelli[a], M. Catitti[b], C. Curceanu (Petrascu)[b,e], C. Fiorini[d], T. Frizzi[d], F. Ghio[f], B. Girolami[f], C. Guaraldo[b], R.S. Hayano[g], M. Iliescu[b,e], M. Iwasaki[h], P. Kienle[a,i], P. Lechner[j], P. Levi Sandri[b], A. Longoni[d], V. Lucherini[b], J. Marton[a], K. Nikolics[a], D. Pietreanu[b], T. Ponta[e], D.L. Sirghi[b,e], F. Sirghi[b,e], H. Soltau[j], L. Struder[k], H. Tatsuno[g], O. Vazquez Doce[b], E. Widmann[a], J. Zmeskal[a]

[a] *Stefan Meyer Institut für subatomare Physik, Vienna, Austria*
[b] *INFN, Laboratori Nationali di Frascati, Frascati (Roma), Italy*
[c] *Dep. of Phys. and Astro., Uni. of Victoria, Victoria B.C., Canada*
[d] *Politechno di Milano, Sez. di Elettronica, Milano, Italy*
[e] *IFIN-HH, Magurele, Bucharest, Romania*
[f] *INFN Sez. di Roma I and Inst. Superiore di Sanita, Roma, Italy*
[g] *Univ. of Tokyo, Tokyo, Japan*
[h] *RIKEN, The Inst. of Phys. and Chem. Research, Saitama, Japan*
[i] *Tech. Univ. München, Phsik Dep., Garching, Germany*
[j] *PNSensors GmbH, München, Germany*
[k] *MPI for Extraterrestrial Physics, Garching, Germany*

Abstract

The SIDDHARTA experiment will determine the most accurate values of the strong-interaction shift and width in kaonic hydrogen, and will perform the first measurement of the kaonic deuterium X-ray lines, using the time correlation between the kaon and kaonic X-ray,which will suppress the asynchronous background by 2-3 orders of magnitude compared to DEAR. New large-area silicon drift detectors (SDDs) were developed specially designed for the kaonic X-ray spectroscopy in the SIDDHARTA experiment. With these measurements, precise values of the isospin-dependent antikaon-nucleon scattering lengths will be extracted, thus opening a new insight in the low-energy kaon nucleon interaction.

1 Introduction

Determination of the shift and width of kaonic hydrogen and deuterium ground state is one of the highest priorities in kaon physics researches. The shift and width of kaonic hydrogen and deuterium are related to the scattering lengths by the Deser formula. Determining the isospin dependent scattering lengths provide the fundamental low-energy QCD physics: for example, SU(3) chiral symmetry, $\bar{K}N$ sigma-term, and nature of $\Lambda(1405)$, as well as $S^0(3115)$ and $S^+(3140)$, which have been recently studied both in experiments and theories.

Difficulties of precise determination of the kaonic X-ray energy and width lie in a high-background condition on available kaon beams and small X-ray yields (a few % for kaonic hydrogen; below 1% for kaonic deuterium). To overcome these difficulties, an X-ray detection system, having high background rejection capability, large-area detectors, and good resolution both in energy and timing, is required.

In the SIDDHARTA experiment, large area silicon drift detectors (SDDs), which have good resolution both in energy and timing, were developed specially designed for the kaonic X-ray spectroscopy. Using the kaon and SDD signal timing, the shift and width both of kaonic hydrogen and deuterium will be precisely determined. In this paper, the working progress of the SIDDHARTA experiment, as well as the recently performed kaonic atom experiments, is described briefly.

2 Historical overview of the kaonic hydrogen X-ray measurements

Measurements of the kaonic hydrogen Kα line ($2p \rightarrow 1s$ transition) were not successful for a long time. From '70s to '80s, three experimental groups observed the week kaonic hydrogen X-ray signals and obtained the attractive shift and width [1]. However, compared to the data of scattering experiments, the shift values determined from the kaonic hydrogen X-rays have a large discrepancy: even the sign of the shift values does not agree. This discrepancy was called "kaonic hydrogen puzzle", and it was a long-standing problem [2].

The first clear observation of the kaonic hydrogen X-rays was performed by the KpX group at KEK (Japan) [2]. The KpX group used a gaseous hydrogen target, although an efficiency for kaons to stop the target decreases. The problem in the kaonic hydrogen experiments before the KpX group was

due to kaon absorption from high n states caused by the Stark effect. In this experiment, Si(Li) X-ray detectors were used to detect the kaonic X-rays. The Si(Li) detectors have good time resolution, but energy resolution is insufficient to determine the shift and width accurately.

The DEAR group subsequently measured the kaonic hydrogen X-rays using a gaseous hydrogen target [3]. The most accurate values of the shift and width of kaonic hydrogen 1s state were obtained. In the DEAR experiment, charge coupled devices (CCDs) were used to detect the kaonic X-rays. The CCDs have good energy resolution, but time resolution is insufficient. The experimental setup and results of the DEAR experiment will be summarized in Section 3.

The KpX and DEAR experiment show that the shift of the kaonic hydrogen 1s state is repulsive. It agrees with the sign obtained from the scattering data for the first time. Thus, the kaonic hydrogen puzzle is found to be due to the insufficient measurements of the kaonic hydrogen X-rays, which are mainly due to the Stark effect that causes significant decrease of the X-ray yield in case of high density targets.

Theoretical studies of the $\bar{K}N$ interaction using the KpX and DEAR results have been progressed with many authors. However, the errors of both the experiments are still large to obtain much improved information on the $\bar{K}N$ physics. An accurate determination of the kaonic hydrogen shift and width is now one of the important experiments. In addition, only the isospin average of the scattering lengths can be obtained from the kaonic hydrogen data. To obtain the isospin 0 and 1 term of the scattering lengths independently, the determination of the shift and width of the kaonic deuterium 1s state is required, as well as the values of the kaonic hydrogen 1s state [4].

3 The DEAR experiment and results

The latest experiment of the kaonic hydrogen X-ray measurement was performed by DEAR [3]. Here, it would be worthwhile to describe the DEAR experiment briefly, since the new experiment by the SIDDHARTA group will be performed with a similar setup except for the X-ray detection system.

The DEAR experiment was performed at DAΦNE, which is an electron-positron collider optimized to produce ϕ mesons at reset. The ϕ mesons decay into back-to-back correlated K^+K^- pairs with a branching ratio of 50%. Thus,

the K^-'s produced in the DAΦNE machine have the following characteristics: low-momentum, monochromatic, and low hadronic background. These characteristics are suited for kaonic atom production [4].

The DEAR experimental setup consists of a pressured gaseous target, charge coupled-devices (CCDs) as an X-ray detector, and the kaon monitor [3]. The density of the target gas was selected as 2.1g/l (0.03 of liquid hydrogen density) to optimize the kaonic hydrogen X-ray yields, taking the kaon stopping efficiency in the target and the Stark effect into account. The kaonic X-rays were detected by 16 CCDs [5]. The CCDs consist of a large number of small sized pixel arrays with a thin depletion layer of 30 μm. In the DEAR experiment, a type of CCD55-30 (EEV) was selected after the tests of several types. In our application, the CCDs were cooled down to 165 K to optimize the energy resolution. The CCDs gave good energy resolution ($\sim$150 eV at 6 keV), although there is no time resolution.

The kaonic hydrogen X-ray measurement [3] was performed, just after the success of the kaonic nitrogen measurements [6]. The kaonic hydrogen data of about 58 pb^{-1} were accumulated. The kaonic hydrogen X-ray lines were clearly observed. The signal-to-background was about 1:70. The shift and width of the kaonic hydrogen 1s state was obtained from the fit of the kaonic lines. The shift is $-194 \pm 37 \pm 6$ eV, and the width is $249 \pm 111 \pm 30$ eV [3].

Although the DEAR experiment obtained the most accurate values of the shift and width of the kaonic hydrogen 1s state, the signal-to-background ratio was not sufficient to obtain much precise values. A detail CCD data analysis shows that the background events on the energy spectra originate from MIPs (minimum ionizing particle) creating a small sized events [5]. These events can be rejected using time information of an X-ray detector, since the MIPs are generated from the electron/positron beams and are not correlated to the K^+K^- production. To significantly improve the signal-to-background ratio, a breakthrough using X-ray detectors having good time resolution is necessary.

4 The SIDDHARTA experiment

The SIDDHARTA experiment brings a new phase in the study of kaonic atoms at DAΦNE. In the SIDDHARTA experiment, large-area silicon drift detectors (SDDs) employed for the measurement of the X-ray energy and timing to overcome the problem of the signal-to-background ratio [7]. SDDs, initially

developed as position sensitive detectors, are nowadays used for X-ray spectroscopy. SDDs have good resolution both in energy and timing. The energy resolution of SDDs is the same order as CCDs, and the time resolution is of the same order as Si(Li) [7].

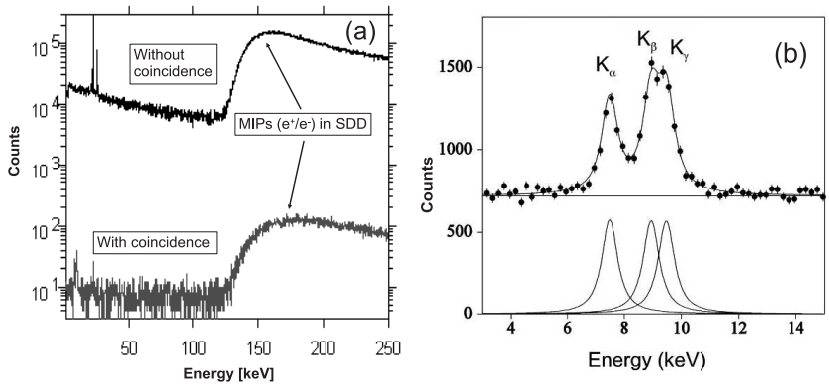

Figure 1: (a) Expected background suppression using the triple coincidence of K^+, K^-, and X-ray signal. (b) Expected kaonic deuterium X-ray energy spectra.

We are developing a new type of 1 cm^2 SDDs specially designed for SIDDHARTA, performed partially under the Joint Research Activity JRA 10 of the I3 project "Study of strongly interacting matter (HadronPhysics)" within FP6 of the EU. The SDDs will provide excellent background suppression by using the time correlation between the kaonic X-rays and the back-to-back correlated K^+K^- pairs produced by the DAΦNE electron-positron collider. The time resolution of the SDDs allows us to detect the kaonic X-rays in coincidence with the back-to-back correlated K^+K^- pairs.

There are two background sources in DAΦNE: backgrounds synchronous and asynchronous to the K^+K^- production, respectively [8]. The main source is asynchronous background, which is due to electromagnetic showers originating from e^+e^- lost from the beam pipes, the Touschek effect, and the interaction with the residual gas. The asynchronous background was the main components of the background events on the DEAR spectra. The synchronous background, originating from particles produced by ϕ decay, and secondary

particles produced by kaon reactions as well as the decay particles of kaons, is small. Therefore, the events related to the charged-kaon production are selected only by demanding a triple coincidence of K^+, K^-, and X-ray signal, so that the asynchronous background is rejected.

The Monte Carlo simulations show that a S/N ratio of 5:1 is expected for the kaonic hydrogen measurement. With the data of 400 pb^{-1}, a precision of 2.5 eV for the shift and 5.0 eV for the width can be obtained. For kaonic deuterium, a S/N ratio of about 1:1 is estimated, assuming a yield of 0.002 for the Kα and a width of 630 eV. With the data of 600 pb^{-1}, a precision of about 15 eV for the energy shift and 40 eV for the width can be obtained.

5 Status of the SIDDHARTA experiment

The target system, kaon trigger system, and X-ray detection system have been tested. In particular, many studies of the SDDs are dedicated. Each SDD is examined by the optical inspection, DC current measurement, and spectroscopic tests, which check the SDD product quality, and provide specification of each SDD for the optimal working voltages.

The test measurements of the SDDs using both the radioactive sources and the high energy electron beam were performed at the beam test facility (BTF). These test measurements are very important, since the SDDs can be tested in a similar environment as the DAΦNE interaction point. One of the tests was concentrated to the measurements of the SDD time resolution and the capability of background suppression.

BTF provides the electron beam with 50 Hz. The electrons passed through scintillators installed in the beam line and hit on lead radiators, which generated high energy γ-rays and electrons. These secondary particles hit on the SDDs were detected. The X-rays from the radioactive source were measured simultaneously.

The time difference between the scintillator signals and SDD signals were measured, which provide the SDD time resolution, since the time resolution of the scintillators is negligible compared to that of the SDDs. The spectra of the SDD time resolution is shown in Fig. 2. The time resolution of 720 ns (FWHM) at -120 degree was obtained. The background suppression capability in the X-ray energy spectra was also measured using the SDD time information. The suppression factor was obtained to be $(4.6 \pm 0.5) \cdot 10^{-5}$ with an efficiency

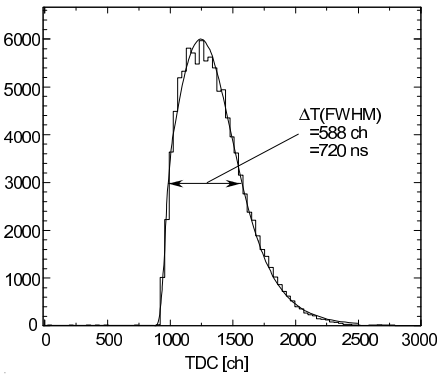

Figure 2: Time resolution of the SIDDHARTA 1 cm^2 SDD measured at BTF.

of 98% coincidence events with the trigger rate of 50 Hz.

The SIDDHARTA experiment will be started from 2008. The strategy of this experiment is as follows. In the first stage, tuning and optimization of the setup using a nitrogen gas target will be performed, where about data of 100 pb^{-1} will be spent. After the confirmation of the setup including the kaonic nitrogen X-ray detection, the hydrogen measurement will be started, and collecting data of 400 pb^{-1}, an accuracy of a few eV in the shift can be obtained. In the last stage, the measurement of kaonic deuterium will be dedicated, and data of about 600 pb^{-1} will be accumulated. As further target materials, the measurements of the kaonic helium-3 and helium-4 X-rays will be performed.

Before starting the full SIDDHARTA setup, the DAY-1 experiment using a smaller setup will be be performed from 2007, where a reduced number (8-12) of the SDDs are installed. A new beam collision scheme and new beam optics are studied to increase the luminosity and decrease the background from the electron/positron beams. In addition to the beam studies, performance tests and background measurements of the SDDs are performed, as well as studies of the degrader configurations to optimize the kaon stopping efficiency in the target. A nitrogen gas target will be used for the DAY-1 experiment, since the kaonic nitrogen X-ray yields are known to be high (about 50%) [6], and the kaonic nitrogen data can be compared to the DEAR data, which provide

improvement of the background condition from the DEAR runs. Within 3 days of measurements, assuming a luminosity of 10 pb^{-1}/day, about 4000 X-rays of kaonic nitrogen atoms will be collected, and a lot of indispensable information for the SIDDHARTA experiment will be obtained from short time measurements. Therefore, the DAY-1 experiment will give us a promise of the success of the SIDDHARTA experiment.

6 Conclusions

The SIDDHARTA experiment will obtain the most accurate values of the shift and width of the kaonic hydrogen ground state with an accuracy of a few eV, and the first determination of the kaonic deuterium shift and width will be performed. In addition, the kaonic ^{3}He and ^{4}He X-rays could be measured. Therefore, the results of the SIDDHARTA experiment will provide us with the most reliable data for the light kaonic atoms, and the SIDDHARTA data will lead to tremendously significant development of the low-energy $\bar{K}N$ physics.

Acknowledgements

Part of this work was supported by "Transnational Access to Research Infrastructureh (TARI), HadronPhysics I3, Contract No. RII3-CT-2004-506078.

References

1. J.D. Davis *et al.*, Phys. Lett. B 83 (1979) 55; M. Izycki *et al.*, Z. Physik A 279 (1980) 11; P.M. Bird *et al.*, Nucl. Phys. A 404 (1983) 482.
2. M. Iwasaki *et al.*, Phys. Rev. Lett. 78 (1997) 3067.
3. G. Beer *et al.*, Phys. Rev. Lett. 94 (2005) 212302.
4. S. Bianco *et al.*, Riv. Nuovo Cimento 22 (1999) 1.
5. T. Ishiwatari *et al.*, Nucl. Instr. and Meth. A 556 (2006) 509.
6. T. Ishiwatari *et al.*, Phys. Lett. B 593 (2004) 48.
7. T. Ishiwatari, Nucl. Instr. and Meth. A 581 (2007) 326.
8. C. Curceanu (Petrascu) *et al.*, Eur. Phys. J. A 31 (2007) 537.

Frascati Physics Series Vol. XLVI (2007), pp. 1215–1224
HADRON07: XII Int. Conf. on Hadron Spectroscopy – Frascati, October 8-13, 2007
Hadrons in Matter

STUDY OF THE (K^+,K^0) REACTION ON MEDIUM LIGHT NUCLEI CLOSE TO THRESHOLD

The FINUDA Collaboration *

* M. Agnello[a], G. Beer[b], L. Benussi[c], M. Bertani[c], H.C. Bhang[d], S. Bianco[c], G. Bonomi[e], E. Botta[f], M. Bregant[g], T. Bressani[f], S. Bufalino[f], L. Busso[h], D. Calvo[i], P. Camerini[g], M. Caponero[j], P. Cerello[i], B. Dalena[k], G. D'Erasmo[k], F. De Mori[f], D. Di Santo[k], D. Elia[l], F.L. Fabbri[c], D. Faso[h], A. Feliciello[i], A. Filippi[i], V. Filippini[m,+], R.A. Fini[l], E. M. Fiore[k], H. Fujioka[n], P. Gianotti[c], N. Grion[o], O. Hartmann[c], A. Krasnoperov[p], V. Lenti[l], V. Lucherini[c], V. Manzari[l], S. Marcello[f], T. Maruta[n], N. Mirfakhrai[q], O. Morra[r], T. Nagae[s], H. Outa[t], E. Pace[c], M. Pallotta[c], M. Palomba[k], A. Pantaleo[l], A. Panzarasa[m], V. Paticchio[l], S. Piano[o], F. Pompili[c], R. Rui[g], G. Simonetti[k], H. So[d], V. Tereshchenko[p], S. Tomassini[c], A. Toyoda[s], R. Wheadon[i], A. Zenoni[e]. [a] *Dip. di Fisica, Politecnico di Torino and INFN Sez. di Torino, Italy;* [b] *Univ. of Victoria, Canada;* [c] *Laboratori Nazionali di Frascati dell'INFN, Frascati, Italy;* [d] *Dep. of Physics, Seoul National University, South Korea;* [e] *Dip. di Meccanica, Univ. di Brescia and INFN Sez. di Pavia, Italy;* [f] *Dip. di Fisica Sperimentale, Univ. di Torino and INFN Sez. di Torino, Italy;* [g] *Dip. di Fisica, Univ. di Trieste and INFN Sez. di Trieste, Italy;* [h] *Dip. di Fisica Generale, Univ. di Torino and INFN Sez. di Torino, Italy;* [i] *INFN Sez. di Torino, Italy;* [j] *ENEA, Frascati, Italy;* [k] *Dip. di Fisica, Univ. di Bari and INFN Sez. di Bari, Italy;* [l] *INFN Sez. di Bari, Italy;* [m] *INFN Sez. di Pavia, Italy;* [n] *Dep. of Physics, Univ. of Tokyo, Japan;* [o] *INFN Sez. di Trieste, Italy;* [p] *Joint Inst. for Nuclear Physics, Dubna, Russia;* [q] *Dep. of Physics, Shahid Beheshty University of Teheran, Iran;* [r] *INAF-IFSI Sez. di Torino and INFN Sez. di Torino, Italy;* [s] *KEK, Tsukuba, Ibaraki, Japan;* [t] *RIKEN, Wako, Saitama, Japan.*
+ *This paper is dedicated to the memory of our colleague and friend Valerio Filippini*

Abstract

The ability of the FINUDA spectrometer, operated at the DAΦNE collider at LNF, to explore the K^+ charge exchange reaction on medium-light nuclei from about 100 MeV/c down to threshold has been proved by searching for K^0_S. The analysis of the $\sim$200 pb^{-1} data collected in 2003-2004 on ^{7}Li allows us to set an upper limit for the total cross section at such a low momentum. This analysis together with the results foreseen for the second FINUDA run are discussed here.

1 Introduction

The charge exchange reaction induced by low energy K^+ was intensively studied in the fifties and early sixties using emulsions, bubble chambers and counter experiments [1)], while in the following years it gave rise only to a sporadic interest [2)]. The reason was that a low momentum K^+ has no access to states containing hyperons, differently from K^- (see [3)]), and its interaction probability was hence thought to simply be smoothly decreasing at low momenta. Later, more refined experiments focused only on higher energies to search for possible $S = +1$ resonances [4)]. When it was understood that the relative weakness of the K^+ strong interaction with nucleons could probe the distribution of quarks in nuclei [5)], an intense phase of studies devoted to this item started at intermediate energies to compare K^+-nucleus interactions with those on deuterons [6)], and look for possible evidence of strange quark content in nucleons and nuclei. Then these studies again subsided, until the very recent upsurge of activity related to the *pentaquark* search [7)] (and references therein).

The inelastic charge exchange reaction (K^+,K^0) on ^{7}Li has been experimentally investigated close to threshold with the FINUDA spectrometer at the e^+,e^- collider DAΦNE by searching for K^0_S decay. It is the first time that this process has been studied at such low momentum. An upper limit of 2.0 mb (at 95% confidence level) has been measured for the total cross section [8)]. In the following the analysis and the results from the first FINUDA run are described and the expected events on second run targets are reported.

2 The FINUDA experiment at DAΦNE

The DAΦNE collider, described in detail in Ref. [9], is a source of K^+,K^- pairs via the decay of a $\Phi(1020)$ meson created in the collision of 510 MeV e^+,e^- beams. The charged kaons, coming from Φ decay at rest, are emitted back-to-back with a momentum of 127 MeV/c, slightly modulated in the radial plane by the tiny outward *boost* ($\approx$ 13 MeV/c) of the decaying Φ due to the small crossing angle of the e^+,e^- beams ($\approx$ 12.5;15 mrad for first and second run, respectively) (see Fig.1).

FINUDA is a high acceptance, high resolution, non-focusing magnetic spectrometer consisting of a superconducting solenoid (B = 1 T) located around the thin (500 μm) Be beam pipe of DAΦNE, which includes several tracking detectors and two scintillator barrels. A full description of the apparatus and of its performance evaluated with the data of the first run is given in Ref. [10]. The FINUDA vertex region is shown in Fig.1, for the first (a) and

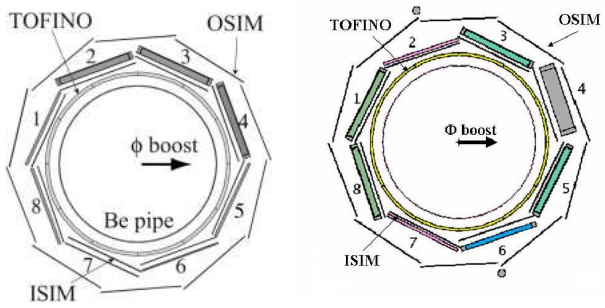

(a) (b)

Figure 1: *The FINUDA vertex-target region. The Be pipe, the inner thin scintillator barrel (TOFINO), the ISIM and OSIM Si-microstrip detectors and the eight targets (numbered from 1 to 8) are shown for the first (a) and for the second (b) run (see text for details). The bold arrow indicates the direction of* Φ *boost.*

second (b) run respectively. For the first data taking the following targets were used: three natural C (slots 1,5,8), two ^{6}Li (enriched to 90%) (slots 2,3), one of ^{7}Li (slot 4), one ^{27}Al (slot 6), and one natural V (slot 7). For the second

one, the same two ^{6}Li (slot 1,8), two ^{7}Li (slot 3,5), two ^{9}Be, one of ^{13}C and ^{16}O targets were chosen.

3 Identifying the (K^+,K^0) reaction with the FINUDA spectrometer

In this analysis, we selected events originated from the K^+ interactions with the FINUDA targets. Such events are collected using the same trigger of the Hypernuclear data taking (described in [10], [11]). Almost all the K^+ entering the FINUDA targets are brought to rest and then decay: a check of the performance of both the spectrometer and the reconstruction-analysis code is performed by using the $K_{\mu 2}$ and $K_{\pi 2}$ decays of stopped K^+, producing a 236 MeV/c μ^+, and a 205 MeV/c π^+, respectively [10]. The elementary reaction $K^+ + n \rightarrow K^0_S + p$ can occur inside the nuclei of the FINUDA targets. Indeed, the elementary process cannot be studied experimentally on free neutrons and existing data were thus obtained mainly on deuterium targets. This means that the effective threshold of the reaction (*i.e.* the minimum kaon momentum value) increases with respect to that of the elementary one (63.8 MeV/c), depending on the selected nucleus. The K^+ produced by DAΦNE have a maximum momentum of $\approx$ 130 MeV/c for kaons whose direction is parallel to the outward boost. After crossing the beam pipe and the FINUDA inner detectors, they reach the targets in slots 4 and 5 mainly with momenta $\approx$ 100 MeV. This means that the reaction under study can be below threshold on several nuclei. Moreover, due to the low momentum of the K^+, also the Coulomb barrier plays a role in the probability of K^+ interaction on nuclei, that it is expected to increase with the Z of the target nucleus. Fig.2 shows the momentum threshold Q of the (K^+, K^0) reaction for a selection of different nuclei. As a result, in the FINUDA first run, the reaction was accessible only to the ^{7}Li target, while in the second one, it was possible on the ^{7}Li, the ^{13}C and the ^{2}H of $^{2}H_2O$ targets. In Fig. 3a) the simulated K^+ momentum entering these FINUDA targets is shown with the thresholds (arrows) for the accessible charge exchange reactions:

$$K^+ + {}^{7}Li \rightarrow K^0_S + {}^{7}Be \quad (1)$$

$$K^+ + {}^{13}C \rightarrow K^0_S + {}^{13}N \quad (2)$$

$$K^+ + {}^{2}H \rightarrow K^0_S + p + p \quad (3)$$

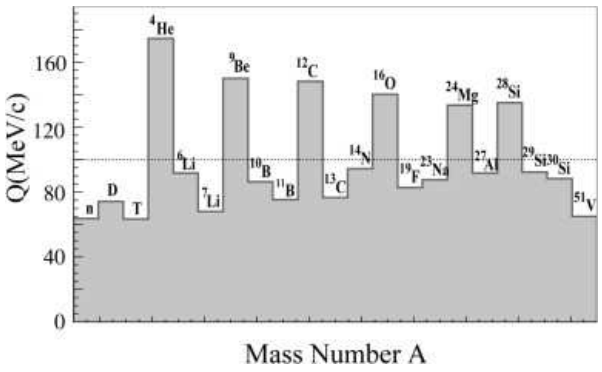

Figure 2: *The Q-values (in MeV/c) for the threshold of the reaction* (K^+, K^0) *for several nuclei according to their mass number A. The horizontal line indicates the maximum* K^+ *momentum reachable on the FINUDA targets.*

FINUDA can detect K^0_S from Φ decay by its decay in π^+ π^- (B.R. = 0.69) [13]. Fig. 3b) shows the simulated momentum distribution of K^0_S produced in the (K^+,K^0) reaction for the K^+ momentum distribution shown in Fig.3a) due to kinematic constraints only and considering the final nuclei ^{7}Be, and ^{13}N in their ground state. Fig. 4 shows the momentum distribution of the π^+, π^- coming from the decay of the K^0_S whose momentum is shown in figure 3.

3.1 Electromagnetic Background and signal region

The main source of background is the K^+ decay at rest into π^+, π^0. It produces, with a rather high BR of ≈21%, π^+, π^0 pairs whose topologies and momenta are similar to those of the π^+, π^- pairs from K^0_S decay. The π^0 decays immediately, mainly into $\gamma\gamma$. One of the γ rays can be emitted in the same direction of the π^0, and crossing the target material can then create an e^+e^- pair. If the e^- is also forward emitted, the topology and momentum of this event are similar to those from the $K^0_S \to \pi^+\pi^-$ decay.

The presence of this background has been proven in Ref. [8] both by a Monte Carlo simulation (see bottom of Fig.3 in Ref. [8]) and experimentally. At the momenta involved, FINUDA cannot discriminate between an e^- and a π^-, hence this background is very insidious. We studied the possible contamination from this reaction by using the FINUDA Monte Carlo program. We generated

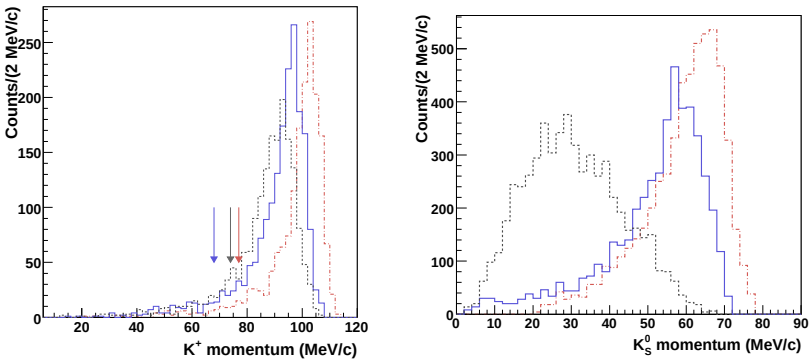

(a) (b)

Figure 3: *Simulation of the momentum distribution of K^+ entering the FINUDA targets (a) and of the produced K^0_S (b) from (K^+,K^0) reaction on the three target nuclei, the arrows on figure (a) show the threshold for the (K^+,K^0) reaction on the corresponding nucleus: ^{13}C (dashed-dot line), ^{7}Li (full line) and ^{2}H (dashed line).*

a number of $K^+ \to \pi^+\pi^0$ decays comparable with the experimentally measured number of stopped K^+, and then we examined the distributions in relative angle and invariant mass of the resulting π^+e^- events in the hypothesis they represent $\pi^+\pi^-$ pairs. From this study it is possible to define, at 95% confidence level, a background free region in the relative angle versus invariant mass distribution between 176 and 180 degrees and between 494 and 502 MeV/c^2, respectively.

4 Results ad discussion

The number of K^0_S, coming from the (K^+,K^0) reaction is related to the cross section by the effective integrated luminosity and the FINUDA efficiency to detect (π^+, π^-) pairs from K^0_S decay according to (4).

$$\int N_{ev} = \sigma_{K^0_S} \cdot \varepsilon \cdot \int \mathcal{L} \tag{4}$$

where ε is estimated by a Monte Carlo simulation to be $\approx$0.12. The experimental effective integrated luminosity for the (K^+, K^0) reaction in each FINUDA

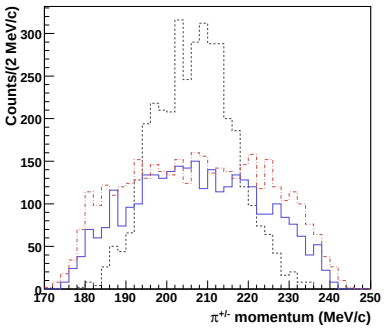

Figure 4: *Simulation of the momentum distribution of pions from the K^0_S of the (K^+,K^0) reaction on the three target nuclei: ^{13}C (dashed-dot line), ^7Li (full line) and ^2H (dashed line).*

target has been evaluated as follow:

$$\int \mathcal{L} = \Phi_{Keff} \cdot N_0 \cdot \rho \cdot \frac{< t >}{A} \tag{5}$$

where Φ_{Keff} is the number of K^+ entering the target with the momentum above the reaction threshold, N_0 is the Avogadro's number, ρ is the target material density, $< t >$ is the K^+ path length in the target and A is the mass number of the target nucleus. The value of $< t >$ and the fraction of K^+ above threshold are evaluated with the FINUDA Monte Carlo program. Then the latter is used to scale the number of stopped kaons from the data in order to obtain Φ_{Keff}.

From the analysis of the first set of FINUDA data, in which the reaction (K^+, K^0) was accessible only to the ^{7}Li target, no event was found. The effective integrated luminosity for ^{7}Li target in the first FINUDA run was 8.71×10^{27} cm^{-2}, hence with the related collected statistics we achieved a sensitivity of $\approx$1 mb per event. Table 1 shows the effective integrated luminosity for each target above threshold of the second FINUDA run and the expected events considering a 1 mb cross section.

The result of the first FINUDA run indicates that the cross section near threshold for ^{7}Li(K$^+$,K^0)^{7}Be is less than 2 mb with a probability of $\approx$95%. No previous measurements of this cross section exist on whichever nuclei, deuterons

Table 1: *Effective integrated luminosity per each target above threshold of the second FINUDA run and expected events per $\sigma_{K^0_S}$ 1 mb.*

Nuclear target	Eff. $\int \mathcal{L}$ (cm^{-2})	Expected Events / 1 mb
^{7}Li (slot 3)	1.13617×10^{29}	~ 13.6
^{1}3C (slot 4)	1.42054×10^{29}	~ 17
^{7}Li (slot 5)	1.66538×10^{29}	~ 12
^{2}H (slot 6)	2.81157×10^{28}	~ 5

included. A compilation of the existing cross section data and the calculations up to 800 MeV/c K^+ laboratory momenta are shown in Fig.5. The experimental data were extracted from measurements on deuterium or on heavier nuclei. As one can see, in the low momentum region, the available data or calculations are very old and go down to a minimum momentum twice bigger than that accessible to FINUDA.

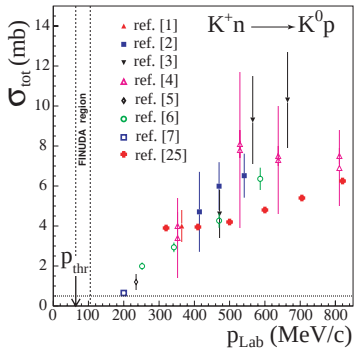

Figure 5: *Existing data and calculations of the total cross section of the elementary charge exchange reaction $K^+ + n \rightarrow K^0 + p$ below 800 MeV/c K^+ laboratory momentum* [8]. *The momentum threshold and the region explored by FINUDA are also indicated. The horizontal dotted line shows the 0.5 mb cross section level.*

At low momentum the relationship between the (K^+, K^0) cross section on nuclei and that of the elementary process is not trivial. The most relevant effect is the Pauli exclusion principle. At higher laboratory momenta (from

300 MeV/c up to the threshold for pion emission) Pauli blocking becomes progressively less effective; in such a momentum region the K^+ interaction cross section with nuclei becomes (within 10%) proportional to the number of nucleons in the nucleus *volume* [13]. We put two limiting expectations for the possible value of the cross section of (K^+, K^0) on Li near threshold: an upper one equal to the corresponding cross section for the elementary process multiplied by the number of neutrons in the target (i.e. no Pauli damping) as in the 500-800 MeV/c momentum region; and a lower one equal to the cross section of the corresponding elementary process. Taking $\approx$ 0.5 mb as the estimate for the elementary cross section near threshold (Fig.5) and assuming that the *volume* approximation is valid, we get for $^7Li(K^+, K^0)^7Be$ cross section an upper bound value of $\approx$2 mb. The interval ($\leq$0.5 mb - 2.0 mb) is compatible with the FINUDA result confirming, for the first time experimentally, a smooth and rather low cross section on nuclei (or, at least for ^{7}Li) in this momentum region.

References

1. J.E.Lannutti *et al.*, Phys. Rev.**109**, 2121 (1958); M.N.Whitehead *et al.*, Phys. Rev. **118**, 300 (1960); B.Sechi Zorn and G.T.Zorn, Phys. Rev. **120**, 1898 (1960); W.Slater *et al.*, Phys. Rev. Lett. **7**, 378 (1961); V.J.Stenger *et al.*, Phys. Rev. **134**, B1111 (1964).

2. R.G.Glasser *et al.*, Phys. Rev. D **15**, 1200 (1977); M.J.Paez and R.H.Landau, Phys. Rev. C **24**, 2689 (1981).

3. N.Kaiser, P.B.Siegel, W.Weise, Nucl. Phys. A **594**, 325 (1995); B.Borasoy, R.Nissler, W.Weise, arXiv:hep-ph/0505239 v1, 27 May 2005; E.Oset and A.Ramos, Nucl. Phys. A **635**, 99 (1998).

4. R.L.Cool *et al.*, Phys. Rev. D **1**, 1887 (1970); T.Bowen *et al.*, Phys. Rev. D **7**, 22 (1973); A.S.Carroll *et al.*, Phys. Lett. B **45**, 531 (1973).

5. P.B.Siegel, W.B.Kaufmann, W.R.Gibbs, Phys. Rev. C **31**, 2184 (1985)

6. G.E.Brown *et al.*, Phys. Rev. Lett. **26**, 2723 (1988); W.Weise, Il Nuovo Cimento, **102A**, 265 (1989); E.Piasetzky, Il Nuovo Cimento, **102A**, 282 (1989); Y.Mardor *et al.*, Phys. Rev. Lett. **65**, 2110 (1990); J.C.Caillon and

J.Labarsouque, Phys. Rev. C **45**, 2503 (1992); S.V.Akulinichev, Phys. Rev. Lett. **68**, 290 (1992); J.C.Caillon and J.Labarsouque, Phys. Lett. B **295**, 21 (1992); R.A.Krauss *et al.*, Phys. Rev. C **46**, 655 (1992); R.Weiss *et al.*, Phys. Rev. C **49**, 2569 (1994).

7. S.Kabana, arXiv:hep-ex/0503019 v1, 10 Mar 2005 and references therein; A.Gal and E.Friedman, Phys. Rev. Lett. **94**, 072301 (2005); A.Sibirtsev *et al.*, Eur. Phys. J. A **23**, 491 (2005).
8. M.Agnello *et al.*, Phys. Lett. B **649**, 25 (2007).
9. C.Milardi *et al.*,*DAΦNE operation with the FINUDA Experiment*, in Proc. of 9th European Particle Accelerator Conference (EPAC 2004), Lucerne, Switzerland, 5-9 July 2004, p. 233.
10. M.Agnello *et al.*, Phys. Lett. B **622**, (2005) 35.
11. M.Agnello *et al.*, Phys. Rev. Lett. **94**, (2005) 212303.
12. M.Agnello *et al.*, Phys. Lett. B **654**,(2007) 80.
13. M.Agnello *et al.*, Nucl. Phys. A **754** (2005) 399c.

Frascati Physics Series Vol. XLVI (2007), pp. 1225–1234
HADRON07: XII Int. Conf. on Hadron Spectroscopy – Frascati, October 8-13, 2007
Hadrons in Matter

MEASUREMENT WITH HIGH RESOLUTION OF THE PROTON SPECTRA FROM THE NON-MESONIC WEAK DECAY OF ${}^{5}_{\Lambda}$He, ${}^{7}_{\Lambda}$Li AND ${}^{12}_{\Lambda}$C

The FINUDA Collaboration *

* M. Agnello[a], G. Beer[b], L. Benussi[c], M. Bertani[c], H.C. Bhang[d], S. Bianco[c], G. Bonomi[e], E. Botta[f], M. Bregant[g], T. Bressani[f], S. Bufalino[f], L. Busso[h], D. Calvo[i], P. Camerini[g], M. Caponero[j], P. Cerello[i], B. Dalena[k], G. D'Erasmo[k], F. De Mori[f], D. Di Santo[k], D. Elia[l], F.L. Fabbri[c], D. Faso[h], A. Feliciello[i], A. Filippi[i], V. Filippini[m,+], R.A. Fini[l], E. M. Fiore[k], H. Fujioka[n], P. Gianotti[c], N. Grion[o], O. Hartmann[c], A. Krasnoperov[p], V. Lenti[l], V. Lucherini[c], V. Manzari[l], S. Marcello[f], T. Maruta[n], N. Mirfakhrai[q], O. Morra[r], T. Nagae[s], H. Outa[t], E. Pace[c], M. Pallotta[c], M. Palomba[k], A. Pantaleo[l], A. Panzarasa[m], V. Paticchio[l], S. Piano[o], F. Pompili[c], R. Rui[g], G. Simonetti[k], H. So[d], V. Tereshchenko[p], S. Tomassini[c], A. Toyoda[s], R. Wheadon[i], A. Zenoni[e]. [a] *Dip. di Fisica, Politecnico di Torino and INFN Sez. di Torino, Italy;* [b] *Univ. of Victoria, Canada;* [c] *Laboratori Nazionali di Frascati dell'INFN, Frascati, Italy;* [d] *Dep. of Physics, Seoul National University, South Korea;* [e] *Dip. di Meccanica, Univ. di Brescia and INFN Sez. di Pavia, Italy;* [f] *Dip. di Fisica Sperimentale, Univ. di Torino and INFN Sez. di Torino, Italy;* [g] *Dip. di Fisica, Univ. di Trieste and INFN Sez. di Trieste, Italy;* [h] *Dip. di Fisica Generale, Univ. di Torino and INFN Sez. di Torino, Italy;* [i] *INFN Sez. di Torino, Italy;* [j] *ENEA, Frascati, Italy;* [k] *Dip. di Fisica, Univ. di Bari and INFN Sez. di Bari, Italy;* [l] *INFN Sez. di Bari, Italy;* [m] *INFN Sez. di Pavia, Italy;* [n] *Dep. of Physics, Univ. of Tokyo, Japan;* [o] *INFN Sez. di Trieste, Italy;* [p] *Joint Inst. for Nuclear Physics, Dubna, Russia;* [q] *Dep. of Physics, Shahid Beheshty University of Teheran, Iran;* [r] *INAF-IFSI Sez. di Torino and INFN Sez. di Torino, Italy;* [s] *KEK, Tsukuba, Ibaraki, Japan;* [t] *RIKEN, Wako, Saitama, Japan.*

Abstract

The aim of this work is to present the latest experimental results obtained with the FINUDA experiment, installed at the collider DAΦNE at Laboratori Nazionali di Frascati, from the study of the NMWD for ^{6}Li, ^{7}Li and ^{12}C targets. Proton spectra will be presented for the NMWD of $^{5}_{\Lambda}$He, $^{7}_{\Lambda}$Li and $^{12}_{\Lambda}$C hypernuclei. In particular the proton spectrum following the weak decay of $^{7}_{\Lambda}$Li has been never studied before.

1 Introduction

The importance of the non-mesonic weak decays (NMWD) of Hypernuclei has been recognized from the early days of hypernuclear physics [1], but for several decades the item was scarcely studied experimentally, due to the hardness of obtaining reasonable event rates. Only in the last few years a considerable effort was performed at KEK by the SKS Collaboration and measurements of several observables, like lifetimes, neutron and proton spectra, coincidence spectra and polarization were measured with reasonable precision. A quite recent experimental review is due to Outa [2]. Also from the theoretical side a clever effort has been performed, in close correlation with the flow of the experimental data coming out. Reviews on the theoretical progress are due to Alberico and Garbarino [3].

As a result of these efforts, a reasonable qualitative agreement between theory and experiment was achieved on some items, but not on others. In particular Bauer *et. al* [4] noticed a strong disagreement concerning the partial proton decay widths Γ_p for the $\Lambda n \rightarrow np$ process in nuclei. These considerations lead us to analyze carefully the proton spectra following the NM decay of Hypernuclei in the data collected with the FINUDA spectrometer at DAΦNE [5]. In a previous paper [6] we presented our results concerning $^{12}_{\Lambda}$C, obtained from the analysis of the data collected in the 2003-2004 run; we present here preliminary results from the analysis of the above data on $^{12}_{\Lambda}$C with an improved code of analysis, as well as of new data collected in the 2006-2007 run on targets of ^{6}Li and ^{7}Li.

2 Experimental method and analysis techniques

The FINUDA detector has been described in a previous pubblication [7], and we recall here only a few relevant features. Hypernuclei are produced by the reaction

$$K^-_{stop} +^A Z \rightarrow^A_\Lambda Z + \pi^- \tag{1}$$

induced by the low-energy (16 MeV) K^- from the $\phi(1020)$-decay produced at the DAΦNE ϕ-factory. FINUDA consists of several subdetectors (Si-microstrip detectors, low mass drift chambers, straw tubes, scintillators) arranged to provide the hypernucleus formation vertex, with a spatial resolution of 30 μm, and the tracking of the charged particles from the vertex, with a resolution of $\sim$0.6% FWMH for pions and 1.2% for protons. The detectors are arranged in a cylindrical geometry centered around the colliding beams (e^+,e^-) axis, in a magnetic field provided by a superconducting solenoid of 1 T, homogeneous within 1% and the total solid angle of detection is 2π sr. Compared with the analysis performed in [6] , the more significant improvements are:

1. the reconstruction of the trajectories of the charged particles, previously done by requiring 4 hits in the tracking detectors (*long tracks*), now is done also requiring 3 hits (*short tracks*). This improvement allowed to recover the losses in statistics (inefficiencies of the detectors), as well as to lower the low energy cut on the proton spectra from 25 to 15 MeV.

2. the particle identification was performed not only taking into account the information from the Si-microstrip detectors but also using the drift chambers information.

3. the distance between the K^- interaction vertex of reaction (1) and the π^- extrapolated track point was required to be less than 3 mm, allowing a powerful cleaning of the spectra from the background due to the physical processes, mainly Σ^- decay in flight from the reactions:

$$K^- + (np) \rightarrow \Sigma^- + p \qquad\qquad \Sigma^- \rightarrow p + \pi^- \tag{2}$$

which is one of the limiting feature to the use of reaction (1).

4. the acceptance, whose precise knowledge is of paramount importance for the determination of the proton spectra in particular near the threshold of 15 MeV, was evaluated passing the simulated events (protons emitted isotropically from 100 to 600 MeV/c, from the nuclear targets) through the full reconstruction chain used for the real events. Geometrical effects, efficiency of the FINUDA pattern recognition, trigger requests and quality cuts were then taken into proper account. We remark that in the analysis reported previously only geometrical effects were taken into account.

3 Experimental results

3.1 *^{6}Li targets*

The results reported here correspond to a total of $\sim$21$\times$ 10^6 K^- stopped in the two ^{6}Li targets used in the 2006-2007 run. ^{6}Li is the only nuclear target for which reaction (1) does not lead to a bound hypernucleus. As a matter of fact $^6_\Lambda$Li is unbound and decays immediately into $^5_\Lambda$He + p. In the spectrum of π^- from (1) on a ^{6}Li target, a peak appears at 275 MeV/c and it is the signature of the $^5_\Lambda$He formation. Fig.1(a) shows the π^- momentum spectrum in coincidence with a proton. By selecting the π^- in the range from 272 to 278 MeV/c (black area in Fig.1(a)) we obtain the proton spectrum shown in Fig.1(b) (dots). It exhibits a double humped camel-back shape; the hump at 80 MeV is due to the protons from the NM weak decay of $^5_\Lambda$He, that one at 120 MeV to reaction (2). A similar structure, but with a less pronounced second hump was observed for $^{12}_\Lambda$C, and will be reported for $^7_\Lambda$Li. The case of $^6_\Lambda$Li is special, since it exhibits a peculiar (α+d) cluster structure. We observed clearly such an effect in a previous analysis on the (K^-np) absorption process on ^{6}Li [8]. For ^{6}Li we modeled the (K^-np) absorption process contribution by using the quasi-d momentum distributions calculated by [10]. The hatched histogram in Fig1(a) shows the π^- spectrum from such a simulation; the two π^- spectra of Fig1(a) are normalized to the same area beyond 278 MeV/c. The black squares in Fig.1(b) indicate the spectrum of the protons from reaction (2) emitted in coincidence with a π^- in the range 272-278 MeV/c, i.e. the background. The second hump is nicely reproduced. Fig.1(c) shows the difference between the two spectra of Fig.1(b). We will discuss such a spectrum after the discussion on the ^{7}Li targets, which is related.

3.2 ^{7}Li *targets*

The results discussed here correspond to a total of $\sim 13 \times 10^{6}$ K^{-} stopped in the two ^{7}Li targets used in the 2006-2007 run. Fig. 2(a) shows the π^{-} spectrum in coincidence with a proton. By selecting the π^{-} in the range from 272 to 278 MeV/c (hatched area in Fig.2(a)) corresponding to the formation of $^{7}_{\Lambda}$Li in the ground state, we obtain the proton spectrum of Fig2(b) (black dots) which shows a maximum at 80 MeV, with a shoulder around 120 MeV. In order to subtract the contribution from the reaction (2), we used an approach similar to that adopted for ^{6}Li, apart the modeling of the internal motion of the (np) pair, taken from conventional models of the nucleon internal momenta and not from a peculiar cluster structure.

The hatched histogram in Fig2(a) shows the π^{-} spectrum from this source, normalized at the same area beyond 278 MeV/c. The dots in Fig. 2(b) indicate the spectrum of the protons from reaction (1) emitted in coincidence with a π^{-} in the momentum range 272-278 MeV/c. Fig. 2(c) shows the difference between the two spectra. The spectrum looks like a peak centered at 80 MeV, as expected from NM decays, with a low energy tail that can be attributed to final state interaction and/or two nucleons $\Lambda + (np) \rightarrow nnp$ induced decays [9].

A closer inspection to Fig.2(a) indicate a hint for a peak at 269 MeV/c (inset of Fig.2(a)), which does not show up in the inclusive π^{-} spectrum, but only if a proton in coincidence is required. It corresponds to the formation of the ($^{5}_{\Lambda}$He+d) system. If true the proton spectrum should be that measured for the ^{6}Li targets. By selecting the π^{-} from 267 to 271 MeV/c we obtain a final spectrum which is very same, within the errors, of that measured for ^{6}Li, and reported in Fig3(a), superimposed. We have omitted all the intermediate steps of the analysis, fully similar to the previous one. By adding the two spectra we obtain the final spectrum of protons from $^{5}_{\Lambda}$He NM decays, represented in Fig.3(b).

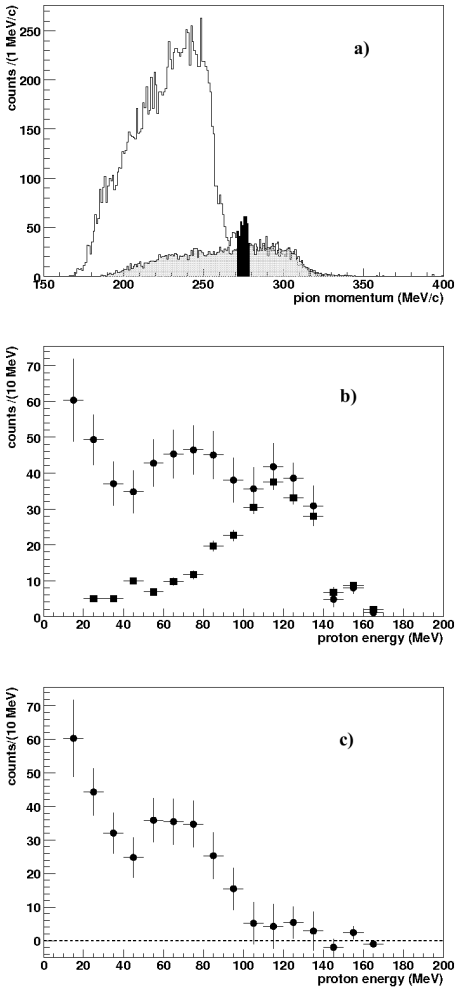

Figure 1: a): π^- spectrum for events with an additional proton track, from the two ^{6}Li targets; the region selected in black evidences the *g.s.* region and superimposed (hatched histogram) the contribution to the spectrum from the K^-np channel. b): Energy spectrum of the proton coming from the background absorption process (squares) superimposed to the acceptance corrected proton spectrum obtained from the data (dots) for the $^5_\Lambda$He. c): Proton energy spectrum coming from the NMWD of $^5_\Lambda$He after the background subtraction.

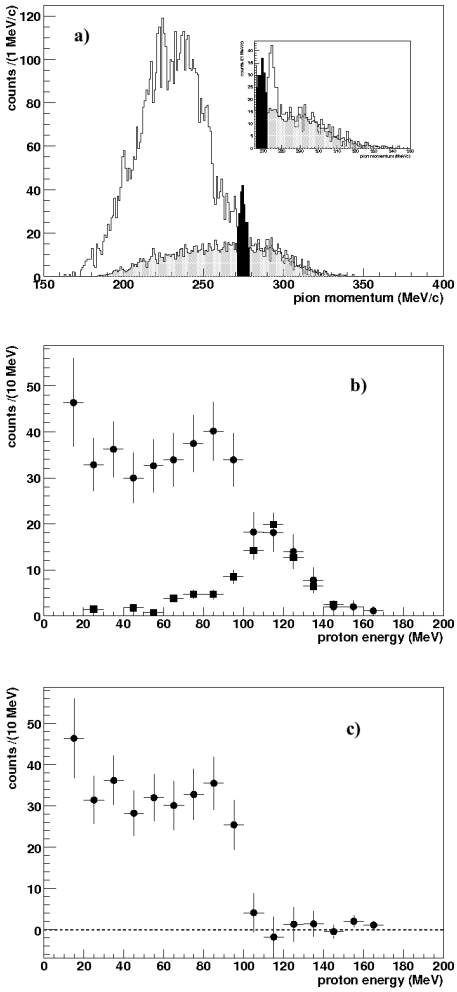

Figure 2: a): π^- spectrum for events with an additional proton track, from the two ^{7}Li targets; the black region correspond to the interval choosen for the *g.s.* and superimposed (hatched histogram) the contribution to the spectrum from the $K^- np$ absorption reaction. b): Energy spectrum of the proton coming from the background (squares) superimposed to the acceptance corrected proton spectrum obtained from the data (dots) for the $^7_\Lambda$Li. c):Proton energy spectrum coming from the NMWD of $^7_\Lambda$Li after the background subtraction.

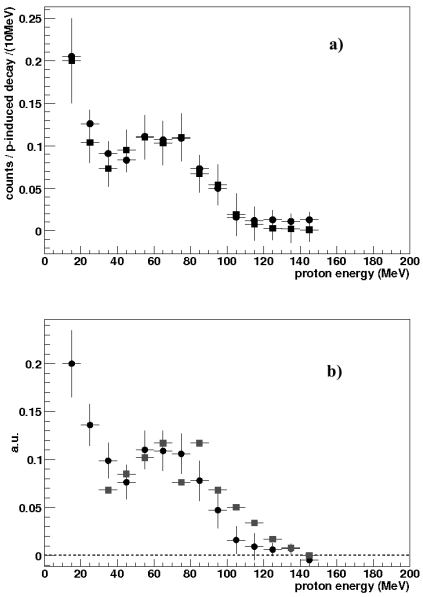

Figure 3: a): Proton energy spectrum of ${}^{5}_{\Lambda}$He obtained from ^{7}Li targets analysis (squares) and the one obtained with the analysis of ^{6}Li targets (dots). The two spectra are normalized to area beyond 15 MeV. b): (black dots) FINUDA proton spectrum from induced proton non mesonic weak decay for ${}^{5}_{\Lambda}$He; squares: result achieved for the ${}^{5}_{\Lambda}He$ at the KEK experiments; the two spectra are normalized to area beyond 35 MeV.

3.3 ^{12}C *targets*

The analysis of the spectra of protons emitted from ${}^{12}_{\Lambda}$C in the ground state was carried out as in Ref. [6], but with the improvements of the reconstruction code described in Sec.2. We omit for sake of brevity the intermediate analysis steps, and we present only the final result, shown by Fig.4.

3.4 Results and Discussion

The partial decay rates Γ_p we measured and reported in Tab. 1 and are calculated for protons of energy greater than 15 MeV. Then they must be considered

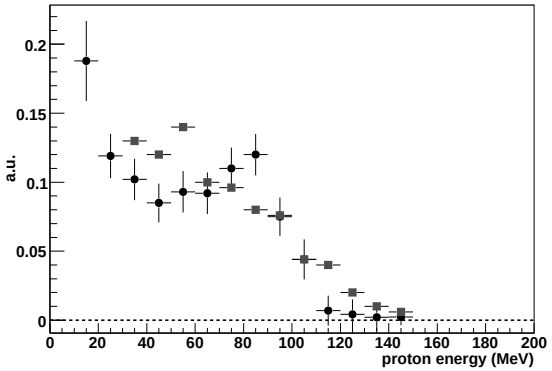

Figure 4: Black dots: FINUDA proton spectrum from induced proton non mesonic weak decay for ${}^{12}_{\Lambda}C_{g.s.}$; squares: result achieved for ${}^{12}_{\Lambda}C_{g.s.}$ at the KEK experiments; the two spectra are normalized to area beyond 35 MeV.

only as lower bounds for the Γ_p. The comparison with previous existing data by SKS [11] is reported in Fig.3(b) and 4. The grey squares repesent the KEK data. In order to compare the shapes of the spectra, we have normalized to area the spectra by FINUDA and by SKS beyond 35 MeV. Whereas there is a consistency for the spectra from ${}^{5}_{\Lambda}$He (the Kolmogorov-Smirnov test provides a confidence level of 75%), the spectra for ${}^{12}_{\Lambda}$C are fully inconsistent (the Kolmogorov-Smirnov test provides a confidence level of 5%). Work is in progress in order to compare the experimental results with the theoretical predictions. At present our conclusion is that the proton spectra show the " memory of the free reaction $\Lambda + p \rightarrow np$ " (peak at 80 MeV); a result which is naively expected on simple grounds. The low energy tail can be attributed to FSI or two nucleon absorption processes [3].

References

1. W.B. Cheston and H. Primakoff , Phys. Rev. **92**, (1953) 1537.

2. H. Outa in Hadron Physics-Proceedings of the International School of Physics of Enrico Fermi, Course CLVIII, edited by T. Bressani, A. Filippi, U. Wiedner (SIF, Bologna; IOS Press, Amsterdam, 2005), p.219;

Target material	**Hypernucleus**	Γ_p (units of Γ_Λ)
^{7}Li and ^{6}Li	$^{5}_{\Lambda}$He	0.26±0.1
^{7}Li	$^{7}_{\Lambda}$Li	0.37±0.09
^{12}C	$^{12}_{\Lambda}$C	0.43±0.07

Table 1: Γ_p values calculated for the proton induced decay of the studied hypernuclei. The errors reported in the table are statistical only.

3. W. M. Alberico and G. Garbarino, Phys. Rep. **369**, (2002) 1;in Hadron Physics-Proceedings of the International School of Physics of Enrico Fermi, Course CLVIII, edited by T. Bressani, A. Filippi, U. Wiedner (SIF, Bologna; IOS Press, Amsterdam, 2005), p.125;

4. E. Bauer, G. Garbarino, A. Parreno and A. Ramos arXiv:nucl-th/0602066;

5. FINUDA Collaboration (M. Agnello *et.al*), Phys. Letter B. **622**, (2005) 35;

6. FINUDA Collaboration (M. Agnello *et.al*), Eur. Phys. J. A **33**, (2007) 251-254;

7. FINUDA Collaboration (M. Agnello *et.al*), Nucl. Instrum. and Methods A **570**, (2007) 205;

8. FINUDA Collaboration (M. Agnello *et.al*), Nucl. Phys. A **775**, (2006) 35;

9. Alberico, W.M. and Garbarino, G., *Phys. Rep.*,**369**, (2002), 1;

10. T. Yamazaki and Y. Akaishi, Nucl. Phys. A **792**, 229 (2007);

11. S. Okada *et al.*, Phys. Lett. B, **597** (2004) 249;

Frascati Physics Series Vol. XLVI (2007), pp. 1235–1242
HADRON07: XII Int. Conf. on Hadron Spectroscopy – Frascati, October 8-13, 2007
Hadrons in Matter

STUDY OF HYPERNUCLEI WITH HEAVY ION BEAMS (HYPHI) AT GSI - EXPERIMENTAL DESIGN AND CURRENT STATUS

S. Minami, P. Achenbach, J. Pochodzalla
Institut für Kernphysik, Johannes Gutenberg-Universität, D-55099 Mainz, Germany
S. Bianchin, V. Bondar, O. Borodina, J. Hoffmann, M. Kavatsyuk, N. Kurz, O. Lepyoshkina, W. Ott, C. Rappold, T.R. Saito, W. Trautmann, F. Zenke
GSI-Darmstadt, D-64291 Darmstadt, Germany
D. Nakajima
Department of Physics, University of Tokyo, Bunkyo 113-0033, Japan
S. Ajimura
RCNP, Osaka University, Ibaraki 567-0047, Japan
T. Fukuda, Y. Mizoi
Osaka Electro-Communication University, Neyagawa 572-8530, Japan
Y. Hayashi, T. Hiraiwa, M. Moritsu, T. Nagae, K. Tanida
Department of Physics, Kyoto University, Kyoto 606-8502, Japan
T. Mochizuki, A. Sakaguchi
Graduate School of Science, Osaka University, Toyonaka 560-0043, Japan

Abstract

The HypHI project aims to study various exotic hypernuclei produced by nuclear collisions with stable heavy ion beams and rare isotope beams, and to measure magnetic moments of hypernuclei for the first time. Currently the first experiment is in preparation, which is to establish the experimental method by detecting light hypernuclei produced by a 2.0 A GeV ^{6}Li beam impinging on a carbon target. The detector system has been designed with the help of Monte Carlo simulations, and construction and test of the detector system are in progress. The results of the simulations and the performance of the detector system will be described.

1 Introduction

Λ hypernuclei have been mainly studied by means of meson induced production reactions, (K^-,π^-) and (π^+,K^+), by which hypernuclei are formed from

target nuclei by changing a neutron in nuclei into a Λ-hyperon. The produced species are, therefore, confined to a region around the β-stability line. Recently experiments to create Λ hypernuclei with neutron excess have been carried out with (e,e' K^+) reactions at Jefferson Lab [2] and with (π^-,K^+) double charge exchange reactions at KEK [3]. These experiments can produce neutron-rich Λ hypernuclei which were not accessible before, however the produced hypernuclei are still in the vicinity of the β-stability line and are restricted by the availability of target materials. The HypHI project [1] aims at studying hypernuclei produced in projectile fragments by nuclear collisions, with which one can expect the formation of various hypernuclei. The usage of rare isotope (RI) beams will increase probability to produce exotic hypernuclei far from β-stability. The production of Λ hypernuclei at projectile fragment region has been discussed by coalescence models [7]. In the models, hypernuclei are formed from projectile fragments picking up hyperons created by nucleon-nucleon collisions in the overlap region. Heavy ion beams of up to 2 A GeV are available at GSI, and the fragment separator (FRS) can be used for experiments with RI-beams. Λ hypernuclei with a Lorentz factor γ ∼3 produced with a 2 A GeV beam will decay about 20 cm in average behind the target assuming a typical lifetime of 0.2 nsec. The feature of the long mean decay paths is suitable for precise lifetime measurements as well as energy measurements of decay particles because of decay vertices located outside of the target. The long mean decay paths also permit the direct measurement of magnetic moments, envisaged with stable heavy ion beams of 20 A GeV from the future FAIR facility at GSI.

The experimental study of hypernuclear production via a heavy ion collision was started at the LBL Bevalac in 1975 with a beam of ^{16}O at 2.1 A GeV reacting with a polyethylene target [5]. The authors claimed to have observed more than 20 hypernuclear events, however, without clear identification and cross section of 2±1 μb which is one order of magnitude larger than theoretical estimates. A similar experiment was performed at Dubna a decade later, utilizing a carbon target and beams of ^{3}He,^{4}He,^{6}Li and ^{7}Li, with energies ranging from 2.2 to 5.14 A GeV [6]. The main detector was a streamer chamber placed in a magnetic field of 0.9 T and events in the chamber were photographed by three cameras. The measured production cross sections of the $^3_\Lambda$H and $^4_\Lambda$H are 0.2 (+0.3-0.15) μb and 0.3 (+0.3-0.15) μb, respectively, which agree with the cross sections calculated with coalescence models. The results

are, however, with large errors because of small statistics. The HypHI project has started with a pilot experiment (Phase 0) as feasibility study including the confirmation of the cross sections measured at Dubna.

2 The Phase 0 experiment

In the Phase 0 experiment, a feasibility of hypernuclear spectroscopy with heavy ion beams will be demonstrated by identifying mesonic decays of the lightest hypernuclei, ${}^{3}_{\Lambda}\mathrm{H} \rightarrow {}^{3}\mathrm{He} + \pi^-$, ${}^{4}_{\Lambda}\mathrm{H} \rightarrow {}^{4}\mathrm{He} + \pi^-$ and ${}^{5}_{\Lambda}\mathrm{He} \rightarrow {}^{4}\mathrm{He} + \mathrm{p} + \pi^-$ produced as projectile fragments by collisions of a ${}^{6}\mathrm{Li}$ beam of 2 A GeV and a ${}^{12}\mathrm{C}$ target [4]. The detector system has been designed to track decay

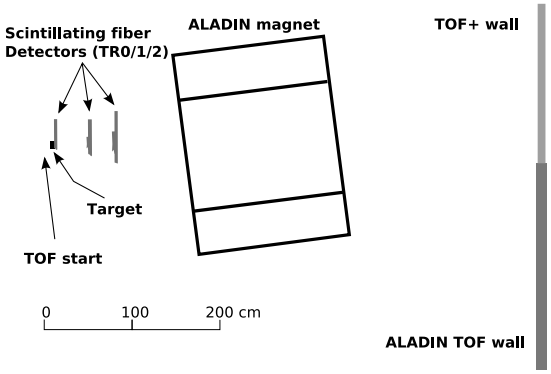

Figure 1: The detector setup for the Phase 0 experiment.

products of hypernuclei in a dipole magnetic field to reconstruct their invariant mass. The decay vertex behind the target as an unique signature of hypernuclei will be used for background reduction at the online triggering stage and also during offline analysis. Figure 1 shows the detector setup, which consists of 3 layers of scintillating fiber (SciFi) detectors, TR0, TR1 and TR2, TOF-start and TOF-walls, the ALADIN-TOF wall for the detection of negatively charged particles and the TOF+ wall for positively charged particles, to deduce velocity, energy deposit and position information, and the ALADIN dipole magnet with a magnetic field of 0.7 T to analyze the particle momenta. Each layer of SciFi detector consists of x- and y-plates, which are placed perpendicular to each other to give horizontal and vertical position information. In addition to this setup, two drift chambers are planed to be placed between TR1 and TR2, and

Table 1: Position and size of the detectors used in the simulations. The center of the target is located at the origin of the coordinate system. For x and y directions, the size and the coordinate values of the start- and end-points of their coverages are listed.

Detector	Position and size (mm)				
	x		y		z
TR0	50	(-25 ; 25)	50	(-25 ; 25)	27.2
TR1	110	(-30 ; 80)	60	(-30 ; 30)	400
TR2	200	(-50 ; 150)	120	(-60 ; 60)	700
ALADIN-TOF	2300	(-2500 ; -200)	1000	(-500 ; 500)	5500
TOF+	1750	(-175 ; 1575)	2000	(-1000 ; 1000)	5500

behind the dipole magnet. They are not used for results reported in this paper.

2.1 Monte Carlo simulation

The Phase 0 experiment has been designed with the help of Monte Carlo (MC) simulations. Hadronic reactions at the target were simulated with the ultra-relativistic quantum molecular dynamics model (UrQMD) [8], and projectile fragments were formed by binding nucleons with projectile rapidity. Geant4 was used to simulate reactions of outgoing particles from the target through the detector system. The size and position of detectors used in the simulations are listed in Table 1. In the case of ${}^{4}_{\Lambda}$H, resulting momentum resolutions of particles from the decay of ${}^{4}_{\Lambda}$H are 320 MeV/c in σ for α and 8.2 MeV/c for π^-. The spatial resolutions of decay vertices was found to be 5 mm in σ along the beam axis, and 0.3 mm along axes perpendicular to the beam. Background processes and events with ${}^{4}_{\Lambda}$H are simulated separately and normalized assuming a production cross section of ${}^{4}_{\Lambda}$H is 0.1 μb. The reconstructed invariant mass spectrum is shown in Figure 2, in which a clear peak with a width of 3.0 MeV/c^2 in σ can be observed on top of a broad background. It is planned to use a beam intensity of 10^7 particles per second and a target thickness of 8 g/cm^2, which will give a few thousand reconstructed ${}^{4}_{\Lambda}$H events per week. The estimated yield is high enough to measure production cross sections with sufficient accuracy and to demonstrate the feasibility of the project.

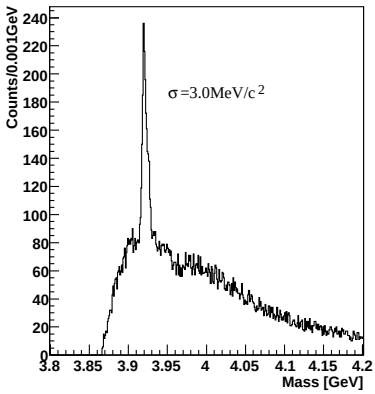

Figure 2: The invariant mass spectrum for ${}^{4}_{\Lambda}$H.

2.2 Trigger system

An efficient trigger system is essential because of the expected high reaction rate. The data acquisition (DAQ) system and the electronics used for the experiment constrain the trigger decisions to be reached within 500 nsec with a rate of less than 3 kHz. The trigger system was designed to use only detectors with fast signal output, SciFi detector and TOF walls made of plastic scintillator. There are 3 functions in the trigger system, and the most important function is 'vertex trigger' to select events with decay vertices in a decay volume located between TR0 and TR1, which can be achieved by requesting special hit patterns on TR0, TR1 and TR2. Hit patterns are examined for x axis and y axis separately for simplicity. The effects of both axes are listed as 'X_Vertex' and 'Y_Vertex' in Table 2 and also the combined effect is shown as 'X_Vertex & Y_Vertex'. The decay modes of interest contain α and π^- in the final state which reach the corresponding TOF-walls. The other functions are to request at least one hit with large energy deposit by α at TOF+ and at least one hit at ALADIN-TOF. Trigger rates have been studied by MC simulation. The efficiency of ${}^{4}_{\Lambda}$H events and the factors of background reduction are listed in Table 2. For the case of background, we only use UrQMD output as input to GEANT4 to simulate hadronic reactions in the target. About 40% of the beam is estimated to cause hadronic reactions. The trigger system with 'full trigger functions' will, therefore, produce triggers with a rate of 0.7 kHz under

the condition that the rate of ^{6}Li beam is 10^7 /sec, which fulfills the constraint given by DAQ. It is also shown that the efficiency to select $^4_\Lambda$H is kept as high as 7.0%, taking the inefficiency of the detector system into account.

Table 2: The efficiency for $^4_\Lambda$H events and the factors of background reduction are listed for each trigger function.

Trigger	$^4_\Lambda$H Efficiency (%)	Background Reduction (%)
X_Vertex	34.	10.
Y_Vertex	30.	8.0
X_Vertex & Y_Vertex	14.	1.7
ALADIN-TOF	28.	15.
TOF+	94.	14.
Full trigger functions	7.0	0.017

2.3 R&D of detectors and electronics

The Phase 0 experiment will be performed at Cave-C at GSI, where the ALADIN magnet and ALADIN-TOF are presently located. New developments for Phase 0 are the SciFi detectors, the TOF+ wall and related electronics, especially VUPROM1 for the fast trigger decision. Prototype detectors for SciFi detector and TOF+ have been constructed and tested with scattered particles from collisions of a 2 A GeV Ni beam with a ^{12}C target. In addition to spacial resolution to measure decay vertices, energy resolution at TR0 is also important to distinguish background events with α and Λ, because they simulate a decay vertex by weak mesonic decay of Λ and could have the same final state by missing one proton. The production of α occurs at the target for the case of the background and behind TR0 for the case of signal. The detection of α at TR0 by energy deposit is, therefore, useful to reduce the background. Figure 3 shows ΔE spectra for proton, α, Li and Be measured by the prototype SciFi detector. The peak of αs is sufficiently separated from that of protons.

The TOF+ wall will be used for the trigger decision by selecting energy deposit by α. The trigger will be made by a newly developed logic module, VUPROM1, a 1-unit-wide VME 6U module with programmable logic devices (PLDs) and a digital signal processor (DSP). The PLD, Virtex-4 manufactured

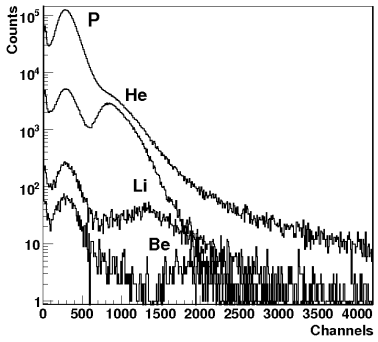

Figure 3: ΔE spectra for proton, α, Li and Be measured by the SciFi detector.

by Xilinx corp. is capable to be operated with a clock of 400 MHz frequency. Analog signals from TOF+ are fed to a comparator and the output from comparator to VUPROM1 for measurements of time over threshold (TOT) which is expected to depend on energy deposit. A plot of charge measured by charge sensitive ADC versus TOT by VUPROM1 is shown in the left panel in Figure 4, and a clear correlation can be observed. The right histogram shows TOT spectra of all events and for events after applying a cut to enhance α. One can observe a peak by α after the cut which is well separated from the proton peak in the ungated spectrum. A large fraction of events without α on TOF+ can be rejected on the trigger level by selecting pulse width of α by VUPROM1.

3 Summary

A heavy ion collision is a promising way to extend our knowledge of Λ hypernuclei to the neutron-rich and proton-rich sides. The long decay path enables precise measurements of decay properties and direct measurement of magnetic moments. The existing experimental information is, however, still scarce so that one needs to start with an experiment to establish feasibility. Phase 0 of the HypHI project is designed to measure production cross sections of light hypernuclei with statistics of a few thousands. MC simulations have been performed to design the detector system. The resulting invariant mass spectrum showed a clear peak by signal above the background. Trigger algorithms

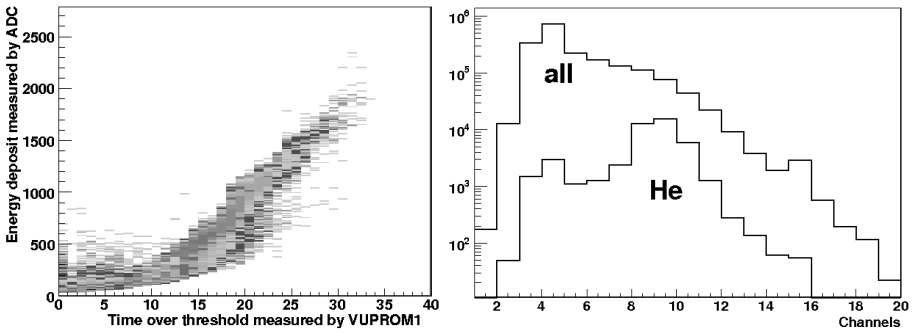

Figure 4: Left) Energy deposit measured by ADC vs TOT by VUPROM1. One channel of VUPROM1 corresponds to 2.5 nsec. Right) TOT spectra measured by VUPROM1 with all events and events after applying a cut to enhance α.

have been designed to fulfill the requirements presented by the DAQ system. Prototype detectors, SciFi detector and TOF+, have been constructed, and VUPROM1, the electronic module for a fast trigger output, have been developed. Tests of prototype detectors demonstrated expected performance.

References

1. T.R. Saito *et al.*, Proc. The IX Int. Conf. on Hypernuclear and Strange Particle Physics (HYP2006), Springer-Verlag (2007) 171.
2. T. Miyoshi, *et al.*, Phys. Rev. Lett. **90** (2003) 232502.
3. P.K. Saha, *et al.*, Phys. Rev. Lett. **94** (2005) 052502.
4. The HypHI collaboration, A proposal of the HypHI Phase 0 experiment, submitted to GSI PAC EA33 with a realization as S319.
5. K.J. Nield, *et al.*, Phys. Rev., **C13** (1976) 1263.
6. A.U. Abdurakhimov, *et al.*, Nuovo Cimento **A102** (1989) 645; S. Avramenko, *et al.*, Nucl. Phys. **A547** (1992) 95c.
7. M. Wakai, H. Bando and M. Sano, Phys. Rev., **C38** (1988) 748.
8. M. Bleicher, *et al.*, J. Phys. G **25** (1999) 1859.

Frascati Physics Series Vol. XLVI (2007), pp. 1243–1250
HADRON07: XII Int. Conf. on Hadron Spectroscopy – Frascati, October 8-13, 2007
Hadrons in Matter

PARTICLE IDENTIFICATION AT $\bar{P}ANDA$: RECIPES AND PHYSICS APPLICATIONS

C. Sfienti, R. Hohler, D. Lehmann, K. Peters,
G. Schepers, L. Schmitt, C. Schwarz
GSI, Planckstraße 1, D-64291 Darmstadt, Germany
P. Achenbach, J. Pochodzalla, A. Sanchez Lorente
Johannes Gutenberg-Universität, J.J.Becher-Weg 45, D-55099 Mainz, Germany
D. Bettoni, V. Carassiti, A. Cecchi
INFN-Ferrara, Via Paradiso 12, I-44100, Ferrara, Italy

on behalf of the $\bar{P}ANDA$ Collaboration

Abstract

Though fifty years have already passed since the discovery of the first hypernuclear events, studies of hypernuclei are still at the forefront of nuclear physics. Due to the large yield of hyperon-antihyperon pairs produced at $\bar{P}ANDA$ a large-scale production of single- and double-hypernuclei under unique experimental conditions will be feasible.
Particle identification (PID) is an essential requirement for such a unique physics program. Highly luminous beams require detector systems with exceptional capabilities. Having to deal with an extremely wide range of particles and momenta, at a rate of $2 \cdot 10^7/s$ with up to 10 reaction products, different PID methods will be exploited.

1 Introduction

Hadron and nuclear physics with antiprotons are among the main scientific motivations of the future Facility for Antiproton and Ion Research (FAIR) at Darmstadt (Germany). Therefore the High Energy Storage Ring (HESR) was designed to deliver cooled antiproton beams of unprecedented intensity and quality in the energy range of 1.5 GeV to 15 GeV.
Antiproton beams in this energy regime will provide access to the heavier strange and charm quarks and to a large production of gluons, offering a broad range of investigations from the study of quantum chromodynamics to the test of fundamental symmetries. Among the various research issues addressed by the $\bar{P}ANDA$ experiment [1)] the study of double-hypernuclei and hyperatoms by means of γ-spectroscopy with Ge-detectors will offer a unique tool to investigate YN and YY interactions.
To accomplish such ambitious goals a high performance Particle Identification (PID) for hadrons and leptons over a large range of solid angle and momenta is mandatory.

2 Hypernuclei and Hyperatoms in $\bar{P}ANDA$

Hypernuclei represent the first step towards an extension of the periodic system into the sector of strangeness thus adding a third dimension to our evolving picture of nuclei. They provide a large variety of new and exciting perspectives [2)].
On one hand the hyperon embedded in a nuclear system may serve as a sensitive probe for the nuclear structure and its possible modification due to the presence of the hyperon. On the other hand, the strange quark offers the unique opportunity to trace an individual quark without the need to resolve individual partonic degrees of freedom in a hadronic system. Also properties of hyperons may change dramatically if implanted inside a nucleus. Thus a nucleus may serve as a laboratory offering a unique possibility to study basic properties of hyperons and strange exotic objects.
Because of the low energy release of only 28 MeV in a conversion of a Ξ^- and a proton into a Λ pair, attempts to produce $\Lambda\Lambda$-hypernuclei are generally based on the Ξ^- capture reaction. The world supply of data on $\Lambda\Lambda$-hypernuclei is very limited [2)]. Even the high precision of emulsion data does not allow an

unequivocal interpretation of the deduced values for the effective binding energy between two Λ particles and hence for the strength of the $\Lambda\Lambda$-interaction. Clearly a drawback common to all theoretical investigations is the lack of high resolution and systematic data on multi-hypernuclei and their level structure. Thanks to the use of $\bar{p}$ beams, the large yield of hyperon-antihyperon pairs produced at these energies and the skilful combination of experimental techniques, copious production of single and double hypernuclei at $\bar{P}ANDA$ is expected. The precision γ-spectroscopy of these exotic nuclei and the study of their weak decays will provide a large variety of new and exciting perspectives ranging from genuine hypernuclear states with new symmetries not available in ordinary nuclei, over non-mesonic weak decays which offer the unique chance to study the interplay of the quark-exchange and meson-exchange aspects of the baryon-baryon forces, up to the possibility to study basic properties of hyperons and strange exotic objects.

For the measurements of double-hypernuclei (Fig. 1) and Ω-atoms a nuclear target will be used. In order to minimize the background from associated particles, the production of hypernuclei and hyperatoms at $\bar{P}ANDA$ will use $\Xi\bar{\Xi}$ and $\Omega\bar{\Omega}$ pair production close to threshold in antiproton nucleus collisions. The trigger will be based on the detection of high momentum antihyperons at small angles or of positive kaons produced by the antihyperons absorbed in the primary target nuclei. The $2K^+$ trigger will provide significantly higher count rates but requires the detection of rather low momentum kaons of a few hundreds MeV/c.

The second ingredient of the experiment is the deceleration of the Ξ^- inside the nucleus and subsequent absorption in a secondary active target. The geometry of this solid-state micro-tracker is determined by the short mean life of the Ξ^-. In order to track the stopped Ξ^- and the charged fragments resulting from the decay of the produced hypernuclei, it is planned to sandwich the absorber with solid state pixel or strip detectors.

As a third element, an efficient germanium γ-array is required. This array will be mounted at the backward angle outside of the superconducting solenoid magnet [1)]. Because of the expected high background rate due to hadronic reactions at the target new fast readout electronics is presently being developed for the Ge-detectors.

With these three ingredients we will be able to reconstruct approximately 3000

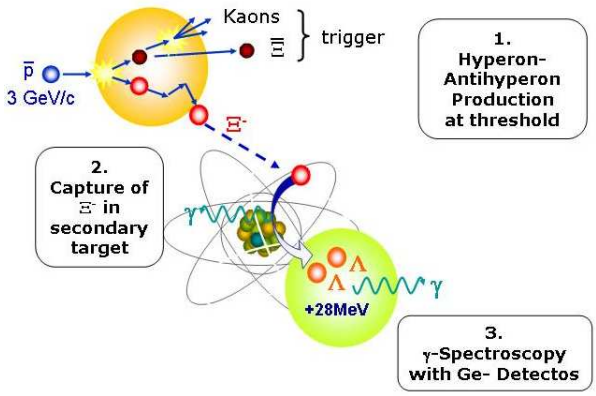

Figure 1: *Various steps of the proposed reaction in case of double-hypernucleus production.*

stopped Ξ^- per day with the unique $\bar{\Xi}^+$ trigger. By applying the kaon trigger we will exceed this number by up to two orders of magnitude thus providing a few 10^5 Ξ^- per day. At this rate, high resolution γ-spectroscopy of double-hypernuclei will become possible for the first time.

3 Particle IDentification in $\bar{P}ANDA$

To accomplish the ambitious goals of the $\bar{P}ANDA$ physics programs a nearly full coverage of the solid angle together with good particle identification in the momentum range from 200 MeV/c up to more than 10 GeV/c (Fig. 2 shows as illustrative example the decay $J/\psi \rightarrow K^+K^-\gamma$) and high energy and angular resolutions for charged particles and photons is mandatory .
Particle identification for charged hadrons (p, $\pi^{\pm}, K^{\pm}$) will be accomplished using a combination of Cherenkov type detectors, covering the high-momentum range, and of TOF counters and a novel TPC foreseen for lower momenta. Time of flight can be partly exploited, since a scintillator barrel in the target spectrometer and a scintillator wall after the dipole magnet with very good time resolution can measure the relative timing of charged particles. However, no start detector is foreseen. The energy loss within the trackers will also be used for particle identification below 1 GeV/c since the individual charge is

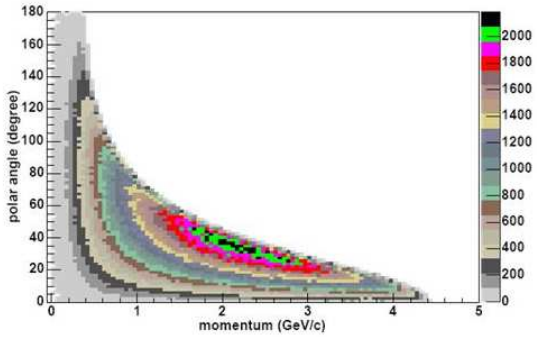

Figure 2: *Angular distribution .vs. momentum of radiative decays of resonances in formation experiments like* $J/\psi \to K^+K^-\ \gamma$.

obtained by analog readout or time-over-threshold measurement.

High precision electromagnetic calorimetry for neutral particle and electron identification is required over a large energy range from a few MeV up to several GeV. Lead-tungstate has been chosen for the calorimeters due to its good resolution, fast response and high density allowing a compact setup. The detection system will be complemented by muon detectors located outside the magnet yokes.

The main part of charged particles is identified by various Cherenkov detectors. The $\bar{P}ANDA$ target spectrometer (Fig. 3 (a)) is almost hermetically sealed to avoid solid angle gaps. Moreover to keep material volume low the spectrometer is designed compact with only little space for the single detector subsystems. The possibility of using thin radiators and placing the readout elements outside the acceptance favors the use of DIRC[1] designs as Cherenkov imaging detectors for particle identification.

Charged particles in a medium with index of refraction n, propagating with velocity $v > c/n$, emit radiation at an angle $\Theta_C = \arccos(1/n\beta)$. If the index of refraction $n > \sqrt{2}$ then the radiator bar acts also as a light guide and Cherenkov photons trapped in the bar are reflected internally preserving the absolute value of the angle at each reflection. Thus, the mass of the detected

[1]Detection of Internally Reflected Cherenkov light.

particle can be determined by combining the velocity information determined from Θ_C with momentum information from the tracking detectors. Due to the strong variation of the typical particle momentum with polar angle, the particle identification can be achieved using two systems of Cherenkov detectors in the target spectrometer. A barrel shaped DIRC with bar radiators will cover the central region, and a disc DIRC will be located in the forward endcap part.
For the latter, two readout concepts are investigated: measuring the photon time-of-propagation in a multi wavelength band Disc-DIRC [3], or measuring angles in a focussing lightguide dispersion-correcting Disc-DIRC [4].
Since $\bar{P}ANDA$ is a fixed-target experiment, the distribution of kaons is forward peaked and will be detected mainly in the endcap DIRC and the forward part of the barrel DIRC.

4 The Barrel-DIRC detector

The charged PID in the barrel section of the target spectrometer has to work in a strong magnetic field of B $\approx$ 2 T within the solenoid. Additionally, it cannot take too much radial space, since it is surrounded by an electromagnetic calorimeter. The detection of momenta up to several GeV/c can be performed by a setup as realized in the BaBar detector [5]. This barrel DIRC will detect kaons from 22^o to approx. 120^o due to the kaon threshold for Cherenkov light. Particles in this angular range are relatively slow, so that one can use materials with high refraction indices (like SiO_2 n=1.47) favoring the internal reflection of photons. As a first approach a version of the installed BaBar detector scaled down in size was envisaged. Since the photon detector uses a pin hole focus, the diameter of the photo-multiplier tubes (PMTs) has to match the light-exit geometry of the radiator slabs. In addition, the distance between PMT and radiator exit must be large compared to the lateral dimensions of the radiator cross section to produce a sharp image. Due to the smaller radius of the $\bar{P}ANDA$ radiator barrel, the number of PMTs is reduced compared to the BaBar setup. A sketch of this scaled down detector is shown in Fig. 3 (b).
While a DIRC as it exists at BaBar would fulfill the charged PID requirements of the $\bar{P}ANDA$ detector, we initiate the development of a smaller photon detector easier to integrate within the complete detector setup [6]. In particular a photon detector coupled with a small air gap to the radiator slabs with focussing lenses is the favored scenario. This reduces image distortions, sorts out

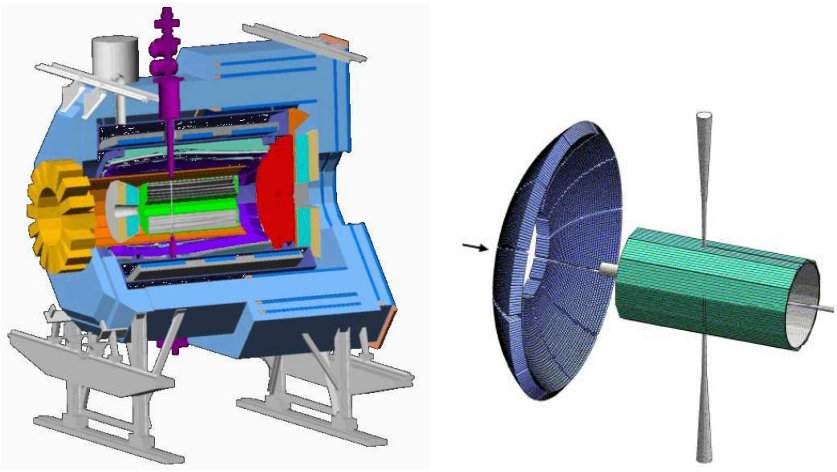

(a) (b)

Figure 3: *a) $\bar{P}ANDA$ target spectrometer. The Barrel and the Endcap DIRC detector positions are shown in light and dark yellow (color online). b) The $\bar{P}ANDA$ barrel DIRC as a version of the BaBar-DIRC scaled down in size: The beam comes from the left as indicated by the arrow. On the right the radiator barrel is crossed vertically by the target pipe of a cluster-jet or a pellet target. Centered within the barrel a piece of the beam pipe is visible. In the forward direction the ends of the radiators are covered with a mirror reflecting the Cherenkov light back towards the photon detector. On the left the $\approx$ 7000 PMTs of the photon detector are shown. The coupling between the end of the radiator slabs, a water box, is not shown.*

large angle photons deteriorating the Cherenkov image and allows also for a more simple integration of the photon detector in the full setup (see Fig. 3 a): Due to the air gap the photon detector can be easily removed and reconnected. Efforts are taken to produce a small-scale prototype.
Meanwhile several photon detector types are tested, to determine whether they stand high magnetic fields above 1 Tesla and high photon rates [7]. Microchannel plate photomultiplier tubes have shown to be promising candidates: they offer a gain high enough for single photon detection combined with a sufficiently low dark count rate in the kHz regime. Their time resolution is excellent and they stand high magnetic fields.

5 Conclusions and Outlook

The development of high resolution γ-spectroscopy with Ge-detectors of single-Λ hypernuclei during the past years put hypernuclei studies again in the forefront of nuclear physics. Combining a high luminosity antiproton beam with a novel solid-state tracking system and a high-rate Ge-array, γ-spectroscopy of $\Lambda\Lambda$-hypernuclei and hyperatoms will become feasible at the $\bar{P}ANDA$ experiment of the future international accelerator facility at GSI.
The high antiproton rates expected for the $\bar{P}ANDA$ experiment require novel detectors. Current Research and Development addresses also the point that the proposed detector components have to stand a high-radiation environment [8)] especially in the forward direction posing a challenge for each material. We propose several DIRC detector designs for PID that fit into the limited available space of the target spectrometer and with increased performance over currently running DIRC models meet, the physics requirements.

References

1. A. Rotondi, *et al.*, this proceeding.
2. for the most recent review on the subject see
   Proc. IX International Conference on Hypernuclear and Strange Particle Physics, edts. J. Pochodzalla and Th. Walcher, SIF and Springer-Verlag Berlin Heidelberg (2007) and Eur. Phys. J. A **33**, Number 3 (2007).
3. P. Schönmeier, *et al.*, in: Proc. Sixth International Workshop on Ring Imaging Cherenkov Counters, (2007) to appear in Nucl. Instr. Meth. A.
4. K. Föhl, *et al.*, *ibidem.*
5. R. Aleksan, *et al.*, Nucl. Inst. Meth. A **397**, 261 (1997).
6. C. Schwarz, *et al.*, in: Proc. Sixth International Workshop on Ring Imaging Cherenkov Counters, (2007) to appear in Nucl. Instr. Meth. A.
7. A. Lehmann, *et al.*, *ibidem.*
8. M. Hoeck, *et al.*, *ibidem.*

Frascati Physics Series Vol. XLVI (2007), pp. 1251–1258
HADRON07: XII Int. Conf. on Hadron Spectroscopy – Frascati, October 8-13, 2007
Hadrons in Matter

SELF-CONSISTENT COUPLED-CHANNEL APPROACH TO D AND $\bar{D}$ IN HOT DENSE MATTER

Laura Tolós
FIAS. J.W.Goethe-Universität.
Ruth-Moufang-Str. 1, 60438 Frankfurt (M), Germany
Angels Ramos
Dept. d'Estructura i Constituents de la Matèria. Universitat de Barcelona.
Diagonal 647, 08028 Barcelona, Spain
Tetsuro Mizutani
Department of Physics, Virginia Polytechnic Institute and State University.
Blacksburg, VA 24061, USA

Abstract

A self-consistent coupled-channel approach is used to study the properties of D and $\bar{D}$ mesons in hot dense matter. The starting point is a broken SU(4) s-wave Tomozawa-Weinberg DN ($\bar{D}N$) interaction supplemented by an attractive isoscalar-scalar term. The Pauli blocking effects, baryon mean-field bindings, and π and open-charm meson self-energies are incorporated in dense matter at finite temperature. In the DN sector, the dynamically generated $\tilde{\Lambda}_c$ and $\tilde{\Sigma}_c$ resonances remain close to their free space position while acquiring a remarkable width because of the thermal smearing of Pauli blocking. Therefore, the D meson spectral density shows a single pronounced quasiparticle peak close to the free mass, that broadens with increasing density, and a low energy tail associated to smeared $\tilde{\Lambda}_c N^{-1}$, $\tilde{\Sigma}_c N^{-1}$ configurations. In the $\bar{D}N$ case, the low-density approximation to the repulsive $\bar{D}$ self-energy is found unreliable already at subsaturation densities. From this study we speculate the possible existence of D-mesic nuclei. We also discuss the consequences for J/Ψ suppression at FAIR.

Over the last years there has been a growing interest in the open (D, $\bar{D}$) and hidden (e.g. J/Ψ) charmed mesons within the context of relativistic nucleus-nucleus collisions. In particular, J/Ψ supression was predicted as a clear signature of the formation of the quark-gluon plasma (QGP) [1].

The future CBM (Compressed Baryon Matter) experiment of the FAIR (Facility for Antiproton and Ion Research) project at GSI will investigate, among others, the possible modifications of the properties of open and hidden charmed mesons in a hot and dense baryonic environment. The in-medium modification of the $D(\bar{D})$ mesons may explain the J/Ψ suppression in an hadronic environment, on the basis of a mass reduction of $D(\bar{D})$ in the nuclear medium [2, 3]. Furthermore, this reduction in mass was thought to provoke possible $D^0, D^-, \bar{D^o}$ bound states in heavy nuclei such as Pb [2].

However, a self-consistent coupled-channel meson-baryon approach in nuclear medium is found essential due to the strong coupling among the DN and other meson-baryon channels [4, 5, 6, 7], which induces the appearance of dynamically-generated resonances close to threshold.

In the present article, we pursue a coupled-channel study of the spectral properties of D and $\bar{D}$ mesons in nuclear matter at finite temperatures by extending the result of Ref. [7] to finite temperature. Then our finding is used to discuss the possibility of D-mesic nuclei as well as to examine the possible implications in the J/Ψ suppression at FAIR.

Self-consistent coupled-channel approach for D and $\bar{D}$ mesons

The D and $\bar{D}$ self-energies at finite temperature are obtained from a self-consistent coupled-channel calculation taking, as bare interaction (V), a type of broken SU(4) s-wave Tomozawa-Weinberg (TW) interaction supplemented by an attractive isoscalar-scalar term (Σ_{DN}). The multi-channel transition matrix T

$$T = V + V\ G\ T \tag{1}$$

is solved using a cutoff regularization [7], which is fixed by reproducing the position and the width of the $I = 0$ $\Lambda_c(2593)$ resonance. As a result, a new Σ_c resonance in the $I = 1$ channel is generated around 2800 MeV.

The in-medium solution at finite temperature is obtained by incorporating the corresponding medium modifications in the loop function G. We incorpo-

rate Pauli blocking effects, mean-field bindings of baryons via a temperature-dependent $\sigma - \omega$ model, and π and open-charm meson self-energies in the intermediate propagators (see Ref. [8]).

The D ($\bar{D}$) self-energy is obtained self-consistently summing the in-medium $T_{D(\bar{D})N}$ amplitudes over the thermal nucleon Fermi distribution, $n(\vec{q},T)$, as

$$\Pi_{D(\bar{D})}(q_0,\vec{q},T) = \int \frac{d^3p}{(2\pi)^3}\, n(\vec{p},T)\, [T^{(I=0)}_{D(\bar{D})N}(P_0,\vec{P},T) + 3T^{(I=1)}_{D(\bar{D})N}(P_0,\vec{P},T)] \ , \quad (2)$$

where $P_0 = q_0 + E_N(\vec{p},T)$ and $\vec{P} = \vec{q} + \vec{p}$ are the total energy and momentum of the $D(\bar{D})N$ pair in the nuclear matter rest frame, and the values (q_0,$\vec{q}$) and (E_N,$\vec{p}$) stand for the energy and momentum of the $D(\bar{D})$ meson and nucleon, respectively, also in this frame. The in-medium spectral density then reads

$$S_{D(\bar{D})}(q_0,\vec{q},T) = -\frac{1}{\pi}\frac{\mathrm{Im}\,\Pi_{D(\bar{D})}(q_0,\vec{q},T)}{\mid q_0^2 - \vec{q}^{\,2} - m^2_{D(\bar{D})} - \Pi_{D(\bar{D})}(q_0,\vec{q},T)\mid^2} \ . \quad (3)$$

Open charm in hot dense matter

Fig. 1 shows the behavior of the in-medium $I = 0$ $\Lambda_c(2593)$ and $I = 1$ $\Sigma_c(2770)$ resonances, denoted as $\tilde{\Lambda}_c$ and $\tilde{\Sigma}_c$, respectively, for three different self-consistent calculations: i) the self-consistent dressing of D mesons only (dotted lines), ii) adding the mean-field binding of baryons (MFB) (dash-dotted lines) and iii) including MFB and the pion self-energy dressing (PD) (solid lines). We consider two models: the thick lines correspond to model A ($\Sigma_{DN} \neq 0$) while the thin-dashed lines refer to case (iii) within model B ($\Sigma_{DN} = 0$).

The inclusion of medium modifications at $T = 0$ lowers the position of the $\tilde{\Lambda}_c$ and $\tilde{\Sigma}_c$ resonances with respect to their free values, in particular with the inclusion of MFB. Their widths, which increase due to $\tilde{Y}_c N \to \pi N \Lambda_c, \pi N \Sigma_c$ processes, differ according to the phase space available. In contrast to the $\bar{K}N$ results [9, 10], the PD induces a small effect in the resonances because of reduced charm-exchange channel couplings. Still it is seen in the positions and widths through the absorption of these resonances by one and two nucleon processes when the pion self-energy is incorporated. On the other hand, models A and B show qualitatively similar features.

Finite temperature results in the reduction of the Pauli blocking effects due to the smearing of the Fermi surface. Both resonances move up in energy

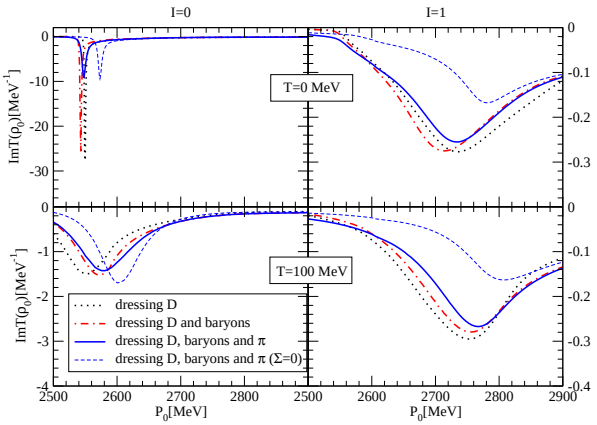

Figure 1: $I = 0$ $\tilde{\Lambda}_c$ and $I = 1$ $\tilde{\Sigma}_c$ resonances in a hot medium.

closer to their free position while they are smoothen out, as seen previously in [5]. At $T = 100$ MeV, $\tilde{\Lambda}_c$ is at 2579 MeV and $\tilde{\Sigma}_c$ at 2767 MeV for model A, while model B generates both resonances at higher energies: $\tilde{\Lambda}_c$ at 2602 MeV and $\tilde{\Sigma}_c$ at 2807 MeV.

We display in Fig. 2 the D meson spectral function at zero momentum obtained in cases (i) to (iii) for model A (thick lines) and in case (iii) for model B (thin line) at saturation density, $\rho_0 = 0.17$ fm^{-3}. Two peaks appear in the spectral density at $T = 0$. The lower one corresponds to the $\tilde{\Lambda}_c N^{-1}$ excitations, whereas the higher one is the quasi(D)-particle peak mixed with the $\tilde{\Sigma}_c N^{-1}$ state. The lower energy mode goes up by about 50 MeV relative to (i) when MFB effects are included. The reason is that the meson requires to carry more energy to excite the $\tilde{\Lambda}_c$ in order to compensate for the attraction felt by the nucleon. The same effect is observed for the $\tilde{\Sigma}_c N^{-1}$ configuration that mixes with the quasiparticle peak. As expected, the PD does not alter much the position of $\tilde{\Lambda}_c N^{-1}$ excitation or the quasiparticle peak. For model B (case (iii) only), the absence of the Σ_{DN} term moves the $\tilde{\Lambda}_c N^{-1}$ excitation closer to the quasiparticle peak, while the latter completely mixes with the $\tilde{\Sigma}_c N^{-1}$ excitation.

Finite temperature effects result in the dilution of those structures with increasing temperature while the quasiparticle peak gets closer to its free value

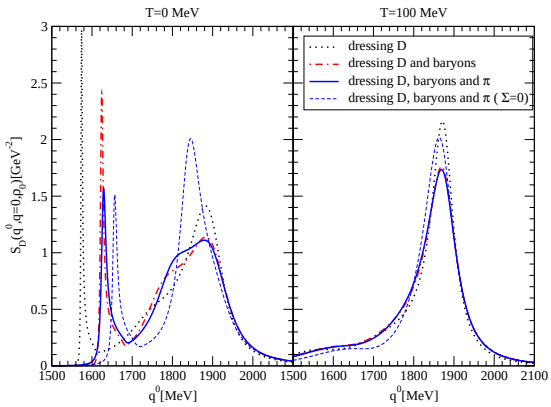

Figure 2: The $q = 0$ D meson spectral function at ρ_0 for $T = 0, 100$ MeV

and it becomes narrower. This is due to the fact that the self-energy receives contributions from DN pairs at higher momentum where the interaction is weaker.

The evolution of the spectral function with temperature is seen in Fig. 3 for two densities, ρ_0 and $2\rho_0$, and two momenta, $q = 0$ MeV/c and $q = 450$ MeV/c, in case (iii) for model A. As in the previous figure, we observe how the $\tilde{\Lambda}_c N^{-1}$ and $\tilde{\Sigma}_c N^{-1}$ structures dissolve with increasing temperature, while the quasiparticle peak becomes narrower and moves closer to its free value position. The widening of the quasiparticle peak for larger nuclear density may be understood as due to enhancement of collision and absorption processes. The $\tilde{\Lambda}_c N^{-1}$ mode moves down in energy with increasing density due to the lowering in the position of the $\tilde{\Lambda}_c$ resonance induced by the more attractive Σ_{DN} term in model A.

With regard to the $\bar{D}N$ sector, we first study the effective $\bar{D}N$ interaction in free space and, in particular, the $\bar{D}N$ scattering lengths. For model A (B) those are $a^{I=0} = 0.61$ (0) fm and $a^{I=1} = -0.26$ (-0.29) fm. The zero value of the $I = 0$ scattering length for model B is due to the vanishing coupling coefficient of the corresponding pure TW $\bar{D}N$ interaction. This is in contrast to the repulsive $I = 0$ scattering length reported in [6], while agreement is found in the $I = 1$ contribution. In the case of model A, the non-zero value of the $I = 0$ scattering length is due to the magnitude of the Σ_{DN} term. Our

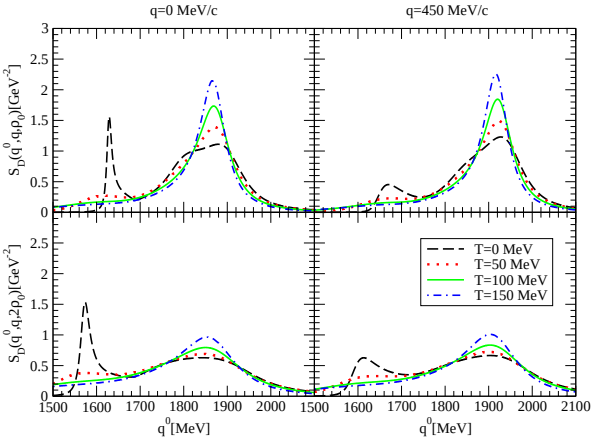

Figure 3: The evolution of the D meson spectral function with temperature

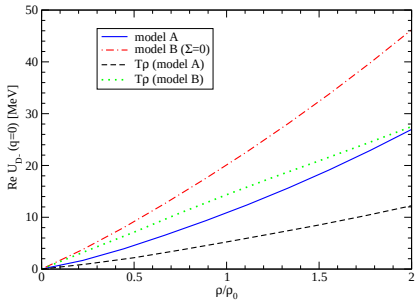

Figure 4: $\bar{D}$ mass shift and the low-density approximation

results are consistent with those of a recent calculation based on meson- and one-gluon exchanges [11].

Next, we display the $\bar{D}$ mass shift in cold nuclear matter in Fig. 4. For both A and B models, the mass shift is repulsive due to the $I = 1$ dominant component. However, despite the absence of resonances in the $\bar{D}N$ interaction, the low-density $T\rho$ approximation breaks down at relatively low densities, so it is not applicable at saturation density.

The comparison between D and $\bar{D}$ optical potentials at $q = 0$ MeV/c as

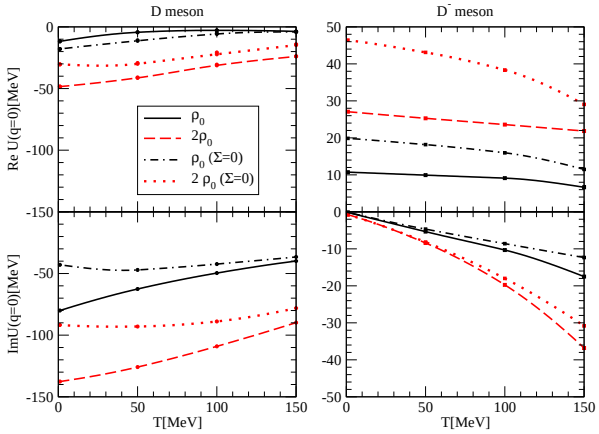

Figure 5: The D and $\bar{D}$ potentials as function of temperature

functions of temperature for two different densities (ρ_0 and $2\rho_0$) is shown in Fig. 5. For model A (B) at $T = 0$ and ρ_0, the D meson feels an attractive potential of -12 (-18) MeV while the $\bar{D}$ feels a repulsion of 11 (20) MeV. A similar shift for D meson mass is obtained in Ref. [5]. The temperature dependence of the repulsive real part of the $\bar{D}$ optical potential is very weak, while the imaginary part increases steadily due to the increase in the collisional width. The picture is somewhat different for the D meson due to the overlap of the quasiparticle peak with the $\tilde{\Sigma}_c N^{-1}$ mode. Furthermore, the in-medium behavior of the $\tilde{\Sigma}_c N^{-1}$ mode is determinant for understanding the effect of the Σ_{DN} term on the D meson potential.

Taking into account our results, we might look at the question of possible $\bar{D}$ bound states discussed in [2]. While D^- -mesic atoms can always be bound by the Coulomb interaction, no strongly bound nuclear states or even bound $\bar{D}^0$ nuclear systems are expected due to the repulsive $\bar{D}$-nucleus optical potential at zero momentum. In the charm $C = 1$ sector, an experimental observation of bound D nuclear states is ruled out by the moderate attraction and large width found for the D meson optical potential.

With respect to the J/Ψ suppression, the in-medium $\bar{D}$ mass is seen to increase by about $10 - 20$ MeV whereas the tail of the quasiparticle peak of the D spectral function extends to lower "mass" due to the thermally spread

$\tilde{Y}_c N^{-1}$. Nevertheless, it is very unlikely that this lower tail extends as far down by 600 MeV with sufficient strength to influence the J/Ψ production . So the only way for the J/Ψ suppression to take place is by cutting its supply from the excited charmonia: $\chi_{c\ell}(1P)$ or Ψ', which will be strongly absorbed in the medium by multi-nucleon processes.

1 Acknowledgments

This work is partly supported by contracts MRTN-CT-2006-035482 (FLAVIAnet, EU), RII3-CT-2004-506078 (HadronPhysics, EU), by FIS2005-03142 (MEC, Spain), 2005SGR-00343 (Generalitat de Catalunya), ANBest-P and BNBest-BMBF 98/NKBF98 (Germany).

References

1. T. Matsui and H. Satz, *Phys. Lett.* **B178**, 416 (1986).
2. K. Tsushima, D. H. Lu, A. W. Thomas, K. Saito and R. H. Landau, *Phys. Rev.* **C59**, 2824 (1999)
3. A. Sibirtsev, K. Tsushima and A. W. Thomas, *Eur. Phys. J.* **A6**, 351 (1999); A. Hayashigaki, *Phys. Lett.* **B487**, 96 (2000); A. Mishra, E. L. Bratkovskaya, J. Schaffner-Bielich, S. Schramm and H. Stöcker, *Phys. Rev.* **C70**, 044904 (2004).
4. L. Tolos, J. Schaffner-Bielich and A. Mishra, *Phys. Rev.* **C70**, 025203 (2004).
5. L. Tolos, J. Schaffner-Bielich and H. Stöcker, *Phys. Lett.* **B635**, 85 (2006).
6. M. F. M. Lutz and C. L. Korpa, *Phys. Lett.* **B633**, 43 (2006).
7. T. Mizutani and A. Ramos, *Phys. Rev* **C74**, 065201 (2006).
8. L. Tolos, A. Ramos and T. Mizutani, *arXiv:nucl-th/0710.2684*.
9. A. Ramos and E. Oset, *Nucl. Phys.* **A671**, 481 (2000)
10. L. Tolos, A. Ramos and A. Polls, *Phys. Rev.* **C65**, 054907 (2002)
11. J. Haidenbauer, G. Krein, U. G. Meissner and A. Sibirtsev, *Eur. Phys. J.* **A33**, 107 (2007).

Frascati Physics Series Vol. XLVI (2007), pp. 1259–1265
HADRON07: XII Int. Conf. on Hadron Spectroscopy – Frascati, October 8-13, 2007
Hadrons in Matter

BOUND KAON APPROACH FOR THE ppK^- SYSTEM IN THE SKYRME MODEL

T. Nishikawa
Department of Physics, Tokyo Institute of Technology,
2-12-1, Oh-Okayama, Meguro, Tokyo 152-8551, Japan
Y. Kondo
Kokugakuin University, Higashi, Shibuya, Tokyo 150-8440, Japan

Abstract

The bound states of a negative charged kaon (K^-) and two-proton (pp) is investigated in the Skyrme model. We describe the ppK^- system as two-Skyrmion around which a kaon field fluctuates. The two-Skyrmion is projected onto $(pp)_{S=0}$ state using the method of collective coordinate quantization. We find that the energy of K^- can be considerably small, and that ppK^- is a molecular state. The binding energy of the ppK^- is estimated in the Born-Oppenheimer approximation to be $B.E. = 104 - 126$ MeV. The mean pp distance is $\sqrt{\langle r_{pp}^2 \rangle} = 1.6 - 1.8$ fm.

1 Introduction

For recent years, lots of theoretical or experimental efforts to explore the possibility of $\bar{K}$ (anti-kaon)-nucleus bound states, "$\bar{K}$-nuclei", [1)] have been made. Up to now, no firm evidences to show their existence are known. Although the report by FINUDA collaboration [2)] suggests the existence of the ppK^- bound states (p and K^- denote the proton and the negative charged kaon,

respectively.), the interpretation of the results are still unclear. We expect that more clear evidence will be seen in the future experiment planned at J-PARC [3]. On the other hand, theoretical studies of ppK^- have been performed by several groups: variational method with a phenomenological $\bar{K}N$ interaction [1] and Fadeev approach [4, 5]. An attempt to describe the $\bar{K}$-nuclei as $\Lambda(1405)$ hyper nuclei has also been made in Ref. [6].

In the present work, we investigate the issue of the kaonic nuclei from completely different point of view, the large N_c QCD [7]. In such hypothetical world, QCD reduces to a weakly interacting meson theory and baryons emerge as topological solitons of the meson field [8]. The topological soliton of the pion field, called "Skyrmion", behaves like a nucleon [9, 10]. Hyperons can be well described as bound states of $\bar{K}$ and a Skyrmion [11, 12].

We describe the ppK^- system as two-Skyrmion around which a kaon field fluctuates [13]. The two-Skyrmion is projected onto the spin-singlet proton-proton state using the method of collective coordinate quantization. We derive the equation of motion for the kaon fluctuating around the Skyrmions at fixed positions. Then we obtain the energy of the kaon as a function of the pp relative distance. Next, we solve the dynamics of the pp radial motion to estimate the binding energy of the ppK^-. The possible structure of the ppK^- state is also discussed.

2 Behavior of K^- coupled to pp

First, we derive the equation of motion for K^- coupled to pp. The action of the Skyrme model is given by

$$\Gamma = \int d^4x \left\{ \frac{F_\pi^2}{16} \mathrm{tr}(\partial_\mu U^\dagger \partial^\mu U) + \frac{1}{32e^2} \mathrm{tr}\left[\partial_\mu U U^\dagger, \partial_\nu U U^\dagger\right]^2 \right\} + \Gamma_{\mathrm{SB}} + \Gamma_{\mathrm{WZW}}, \quad (1)$$

where U is the chiral SU(3) field built out of the eight Nambu-Goldstone bosons. Γ_{SB} is the symmetry breaking term [12] and Γ_{WZW} the Wess-Zumino-Witten anomaly action [14]. The pion decay constant, F_π, and the arbitrary constant, e, are determined later. We put the following ansatz for the chiral field,

$$U = U(1) U_K U(2), \quad (2)$$

where $U(1)$ and $U(2)$ are the fields of the baryon number $B = 1$ SU(2) Skyrmions fixed at the positions whose relative distance is R. U_K is the field

carrying strangeness given by

$$U_K = \exp\left[i\frac{2\sqrt{2}}{F_K}\begin{pmatrix} \mathbf{0} & K \\ K^\dagger & \mathbf{0} \end{pmatrix}\right], \tag{3}$$

where F_K is the kaon decay constant and K the usual kaon isodoublet. The two Skyrmions are rotated independently in the space of SU(2) collective coordinate as $U(1) \to A_1(t)U(1)A_1(t)^\dagger$ and $U(2) \to A_2(t)U(2)A_2(t)^\dagger$, where $A_i(t)$ is the collective coordinate. We substitute the ansatz into the action, Eq.(1), expand it to the second order in K and neglect the terms suppressed by $1/N_c$. Thus we obtain the Lagrangian for the kaon field under the background of $B = 2$ Skyrmion. Note that the form of KNN interaction is unambiguously determined once the ansatz for U is given. The two-Skyrmion is projected onto the spin-singlet pp state by taking an expectation value of the kaon Lagrangian with the $(pp)_{S=0}$ wave function in the space of the collective coordinate. The direction of the distance vector, $\boldsymbol{R}$, joining the two Skyrmions is averaged. Then the background field becomes spherical, which allows us to perform the spherical partial wave analysis by setting the kaon field as $K(\boldsymbol{r}, t) = k(r)Y_{lm}(\theta, \phi)$. Variation with respect to $k(r)$ gives the equation of motion for the kaon.

We solve the kaon's equation of motion numerically. We take the chiral limit, $m_\pi = 0$. For the kaon mass and the ratio of the decay constant, the empirical values are used: $m_K = 495$ MeV, $F_K/F_\pi = 1.23$. For F_π and the Skyrme parameter, e, we examine two choices (i) Set I: fitted to N and Δ masses, $F_\pi = 129.0$ MeV and $e = 5.45$ [10], (ii) Set II: fitted to Δ and $\Lambda(1405)$ masses, $F_\pi = 129.7$ MeV and $e = 5.0$. The calculated spectrum of low-lying baryons [12] is displayed in Table 1.

The left panel of Figure.1 shows the energy of K^- as a function of the pp relative distance, R. We can see the dependence on the choice of the parameter is weak. Looking at the S-wave channel, the binding of the kaon is extremely strong for smaller distance, *i.e.* $R \lesssim 1.0\,\mathrm{fm}$. As R is increased, the binding becomes looser. However, at $R = 2.0\,\mathrm{fm}$, for instance, which is close to the average inter NN distance in normal nuclei, the binding is still deep: the binding energy is about 140 MeV.

In Figure 2, we plot the distribution of K^- in S-wave, varying R. The baryon number density is also plotted. At $R = 1.5\,\mathrm{fm}$, K^- is centered between the two protons. The distribution for relatively larger separation, $R \gtrsim 2.0\,\mathrm{fm}$, is characteristic to molecular orbital states [13, 15]. This is expected from the

Table 1: *Calculated masses of low-lying baryons* [12]. *In Set I,* F_π *and* e *are adjusted so as to reproduce masses of the nucleon and the* Δ. *In Set II, they are fitted to* $\Delta(1232)$ *and* $\Lambda(1405)$.

I	J^P	Set I	Set II	observed state
1/2	$1/2^+$	fitted	1003	N(939)
3/2	$3/2^+$	fitted	fitted	$\Delta(1232)$
0	$1/2^+$	1105	1202	$\Lambda(1116)$
0	$1/2^-$	1325	fitted	$\Lambda(1405)$
1	$1/2^+$	1203	1295	$\Sigma(1193)$
1	$3/2^+$	1349	1384	$\Sigma(1385)$
1/2	$1/2^+$	1332	1471	$\Xi(1318)$

fact that the potential acting on the kaon is a double-well potential which is most attractive at the proton's respective position. Then K^- experiences the strong attraction from pp without increase of the kinetic energy. Therefore, it is quite natural that the binding of K^- to two-proton is stronger than to one proton.

3 pp radial motion

We assume that the pp radial motion is governed by the Hamiltonian, $H = T_{NN}(R) + V_{NN}(R) + \omega_{L=0}(R) - m_K$, where T_{NN} is the kinetic energy and the nucleon is regarded as a non relativistic point like particle. $V_{NN}(R)$ is the state-independent part of the NN potential obtained from the product of $B = 1$ Skyrmion [16]. Within the product ansatz, the attraction of the nuclear force in medium range cannot be produced [17]. $\omega_{L=0}(R)$ is the S-wave kaon's energy obtained in the previous section. $V_{NN}(R)+\omega_{L=0}(R)-m_K$ can be regarded as the effective pp potential in the ppK^- system. We show the behavior of the potential terms in the right panel of Figure 1. The attractive potential generated by bound kaon (lower curve), $\omega_{L=0}(R) - m_K$, is so strong that it overcomes the strongly repulsive $V_{NN}(R)$ (upper curve). As a result, the effective pp potential in the ppK^- system (middel curve) is strongly attractive in the medium range.

The energy of the ppK^- state is obtained by solving the Schrödinger

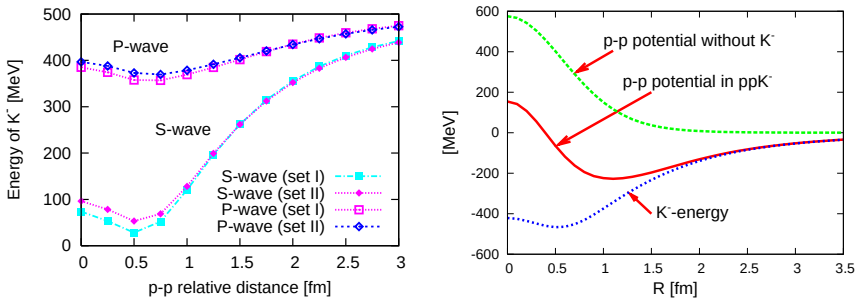

Figure 1: Left: Energy of S- and P-wave K^- as functions of the proton-proton relative distance, R. Right: The upper curve is the pp potential in the absence of K^-, $V_{NN}(R)$. The lower one is the energy of the S-wave K^- with m_K subtracted. The middle one corresponds to their sum, the effective pp potential in the ppK^- system. The parameter set I is adopted.

Table 2: *Energy (MeV) of the ppK^- bound state relative to $2M_N+m_K$ ("total") and its decomposition into the NN kinetic energy ($\langle T_{NN}\rangle$), the NN potential energy ($\langle V_{NN}\rangle$), and the kaon's energy ($\langle\omega_{L=0}-m_K\rangle$). The average inter pp distance (fm), $\sqrt{\langle r_{NN}^2\rangle}$, is also shown.*

parameter set	$\langle T_{NN}\rangle$	$\langle V_{NN}\rangle$	$\langle\omega_{L=0}-m_K\rangle$	total	$\sqrt{\langle r_{NN}^2\rangle}$
set I	42.0	74.5	-239.2	-125.5	1.63
set II	36.2	73.7	-211.3	-104.0	1.80

equation. In Table 2, we diplay the energy of ppK^- bound state relative to $2M_N + m_K$ and its decomposition into the NN kinetic and potential energies and the kaon's energy. The mean pp distance is also shown. $\langle\mathcal{O}\rangle$ denotes the expectation value of $\mathcal{O}$. Our result of the ppK^- binding energy is $104-126$ MeV. The smallness of the NN kinetic energy may imply that the Born-Oppenheimer approximation is not so poor. The mean pp distance is $1.6-1.8$ fm, which is smaller than or comparable with the average NN distance in normal nuclei.

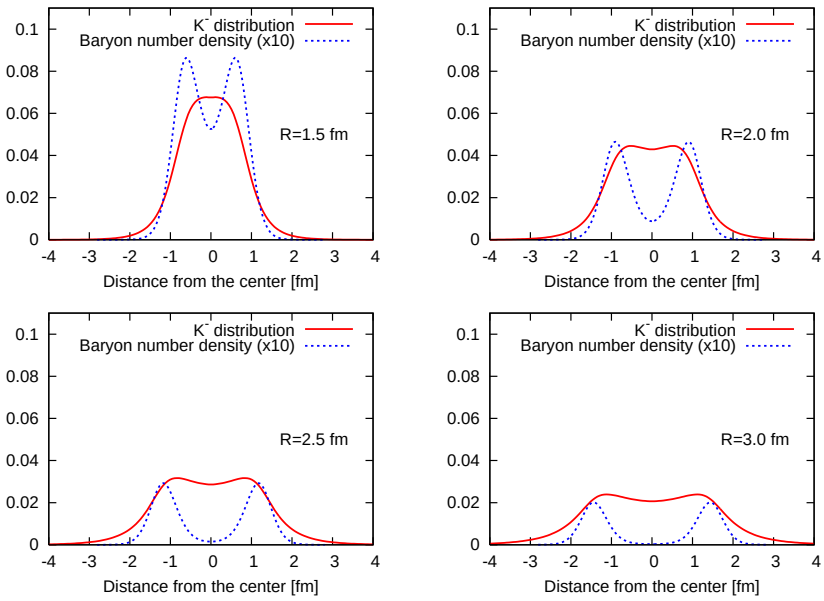

Figure 2: S-wave K^- distribution and baryon number density for the pp relative distance, $R = 1.5$, 2.0, 2.5 and 3.0 fm. Both are in unit of eF_π. The horizontal axis is the distance from the center. The baryon number density is multiplied by a factor 10. For F_π and e, set I is adopted.

4 Summary

We have explored the possibility of the K^- and two-proton bound state, ppK^-, in the topological soliton model. The ppK^- state can be realized as a very deeply bound and compact state, whose binding energy is $B_{ppK^-} = 104 - 126$ MeV and the mean pp distance is $\sqrt{\langle r_{NN}^2 \rangle} = 1.6 - 1.8$ fm.

The deep binding of the ppK^- state is attributed to the extremely strong attractive potential produced by K^-. The attraction cancels the repulsive pp potential and makes ppK^- deeply bound. Recently, Akaishi and Yamazaki has given an essentially the same argument in the context of a three-body variational calculation with the realistic NN potential and the phenomenological $\bar{K}N$ potential [15]. It is very intriguing that both of the Skyrme model and the phenomenological approach show a similar tendency.

5 Acknowledgment

This work was supported in part by the 21st Century COE Program at Tokyo Institute of Technology "Nanometer-Scale Quantum Physics" from the Ministry of Education, Culture, Sports, Science and Technology, Japan.

References

1. Y. Akaishi and T. Yamazaki, Phys. Rev. **C65**, 044005 (2002).
2. M. Agnello *et al.*, Phys. Rev. Lett. **94**, 212303 (2005).
3. T. Koike and T. Harada, Phys. Lett. **B652**, 262 (2007).
4. N.V. Shevchenko, A. Gal and J. Mares, Phys. Rev. Lett. **98**, 082301 (2007).
5. Y. Ikeda and T. Sato, Phys. Rev. **C76**, 035203 (2007).
6. A. Arai, M. Oka and S. Yasui, `arXiv:0705.3936`.
7. G. t'Hooft, Nucl. Phys. **B72**, 461 (1974).
8. E. Witten, Nucl. Phys. **B160**, 57 (1979).
9. T.H.R. Skyrme, Proc. Roy. Soc. **A260**, 127 (1961).
10. G.S. Adkins, C.R. Nappi and E. Witten, Nucl. Phys. **B233**, 109 (1984).
11. C.G. Callan, K. Hornbostel and I. Klebanov, Phys. Lett. **B202**, 269 (1988).
12. M. Rho, D.O. Riska and N.N. Scoccola, Z. Phys. **A341**, 343 (1992).
13. T. Nishikawa and Y. Kondo, Physica **E40**, 406 (2007); `hep-ph/0703100`; `arXiv:0710.0948`.
14. E. Witten, Nucl. Phys. **B223**, 422 (1983).
15. Y. Akaishi and T. Yamazaki, Proc. Jpn. Academy, Series B, Vol.83 (2007) 144.
16. H. Yabu and K. Ando, Prog. Theor. Phys. **74**, 750 (1985).
17. M. Oka and A. Hosaka, Ann. Rev. Nucl. Part. Sci. **42**, 333 (1992) and references therein.

Frascati Physics Series Vol. XLVI (2007), pp. 1267–1274
HADRON07: XII Int. Conf. on Hadron Spectroscopy – Frascati, October 8-13, 2007
Hadrons in Matter

A SEARCH FOR STRANGE TRIBARYONS IN THE ^{4}He($K^-_{stopped}$, N) REACTIONS

M. Sato[a], H. Bhang[b], J. Chiba[c], Seonho Choi[b], Y. Fukuda[d], T. Hanaki[c], R. S. Hayano[e], M. Iio[a], T. Ishikawa[e], S. Ishimoto[f], T. Ishiwatari[g], K. Itahashi[a], M. Iwai[f], M. Iwasaki[a,d], P. Kienle[g,h], J. H. Kim[i], Y. Matsuda[a], H. Ohnishi[a], S. Okada[a], H. Outa[a], S. Suzuki[f], T. Suzuki[a], D. Tomono[a], E. Widmann[f], T. Yamazaki[a,e], H. Yim[b],

[a] *RIKEN Nishina Center,RIKEN, Japan*
[b] *Department of Physics, Seoul National University, South Korea*
[c] *Department of Physics, Tokyo University of Science, Japan*
[d] *Department of Physics, Tokyo Institute of Technology, Japan*
[e] *Department of Physics, The University of Tokyo, Japan*
[f] *High Energy Accelerator Research Organization (KEK), Japan*
[g] *Stefan Meyer Institut für subatomare Physik, Österreichische Akademie der Wissenschaften, Austria*
[h] *Physik Department, Technische Universität München, Germany*
[i] *Korea Research Institute of Standards and Science (KRISS), South Korea*

Abstract

We have measured a nucleon energy from the stopped K^- reaction on ^{4}He to search for the strange tribaryon states at KEK 12-GeV PS. In the obtained missing mass spectrum from the ^{4}He($K^-_{stopped}$, p) reaction, no significant narrow peak structure was observed. The 95 % C. L. upper limits for the formation branching ratio of the tribaryon states with strangeness -1, charge 0 and isospin 1 was determined to be $(0.4 \sim 6) \times 10^{-4}$, $(0.2 \sim 6) \times 10^{-3}$ and $(0.06 \sim 5) \times 10^{-2}/(\textit{stopped } K^-)$ for an assumed width of 0, 20 and 40 MeV/c^2, respectively.

1 Introduction

A theoretical prediction by Akaishi and Yamazaki on deeply-bound kaonic nuclear states [1)] has provoked many activities both theoretically and experimentally. A recent KEK experiment (KEK-PS E471), whose original motivation

was to search for a deeply-bound K^- state in ^{3}He, reported a peak structure in the proton missing mass spectrum [2]. This state was denoted as strange tribaryon, $S^0(3115)$, and can be interpreted as a signal from a formation of deeply-bound K^- nuclei. In E471, another candidate for the tribaryon state, $S^+(3140)$, was indicated in the neutron spectrum [3, 4], but the statistical significance was insufficient for a definitive evidence on its existence. Theoretical interpretations were still controversial [5, 6, 7] and the urgent confirmation and further investigation was eagerly required for the understanding of the nature of these states.

We performed a new measurement called E549 with the following purposes; (1) confirmation of the $S^0(3115)$ and $S^+(3140)$ states and determine the width and formation yield precisely, (2) search for other candidates of the strange tribaryon states and (3) derive the isospin dependence of the strange tribaryon states by comparing the results from proton and neutron measurements.

In this paper, we would like to concentrate on the results of the proton spectroscopy due to limitations of space, and the results on the neutron measurement will be given in a paper to follow.

2 KEK-PS E549 experiment

The experiment E549 was performed at the K5 beam line in the KEK 12-GeV proton synchrotron in May 2005. A schematic drawing of the experimental setup was illustrated in Fig. 1. We adopted the $^4\mathrm{He}(K^-_{stopped},\ N)$ reaction to search for the strange tribaryon states. A separated K^- beam with 650 MeV/c was degraded in a carbon degrader and stopped inside a super-fluid ^{4}He target. The beam timing and trajectory were measured by a beam defining counter (T0) and a tracking drift chamber (BLC). Nucleon energies from the $^4\mathrm{He}(K^-_{stopped},\ N)$ reaction were measured by mean of time-of-flight (TOF) method.

The E549 experimental setup was mostly based on that for E471 [8], but a significant improvement was taken so as to achieve higher energy resolution and statistics compared with E471, because the experimental setup for E471 was optimized for the neutron measurement. We installed dedicated TOF counters ($\mathrm{P_{start}}$ and $\mathrm{P_{stop}}$) and a tracking chamber (PDC). For the precise yield estimation, all the data for the proton spectroscopy was taken with inclusive

condition, i.e. coincidence between incident K^- timing and a hit signal on TOF counters. We accumulated data corresponding to $(1.03 \pm 0.15) \times 10^8$ stopped K^- inside the helium target.

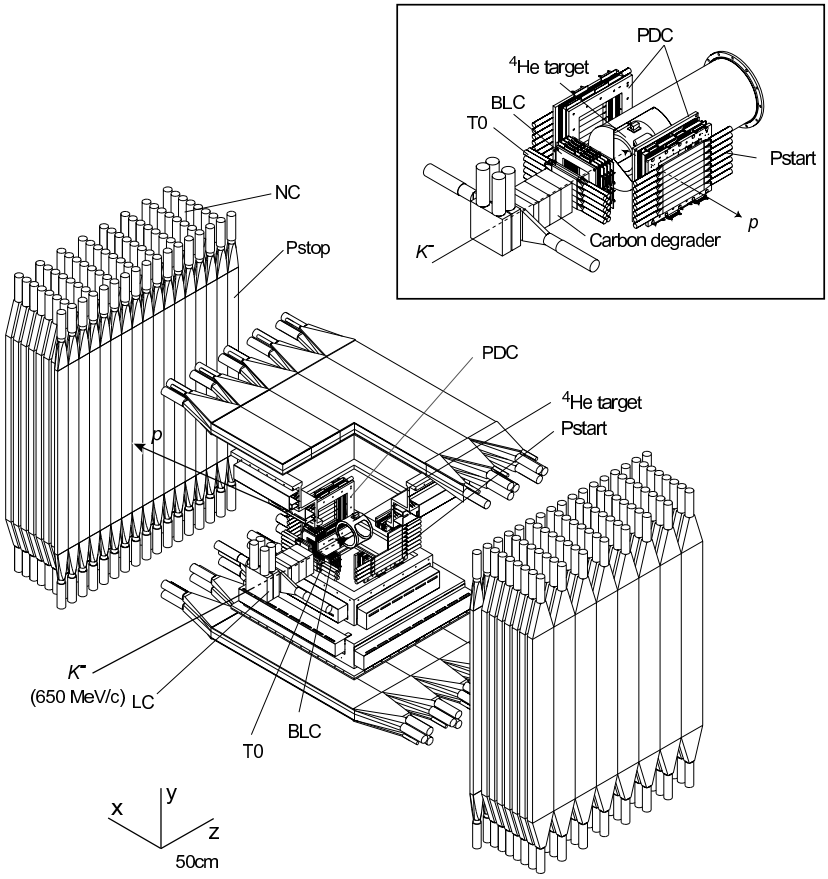

Figure 1: A schematic view of the E549 experimental setup. T0: beam timing counter, BLC:beamline drift chamber, P_{start} and P_{stop}: TOF start and stop counters, PDC: proton drift chamber, and NC: neutron counter array.

3 Analysis and Results

For the check of the detector performance and its long-term stability, we use the decay fraction of K^-s stopped in ^{4}He. It is well-known that a few percent of stopped K^- in liquid helium form long-lived atomic states, which is called as *metastable* states [10, 11]. Since the partial lifetime of these states (τ_{meta} = 59 ± 4 ns) is much longer than the free kaon lifetime, K^-s trapped in the metastable state can decay freely. The decay fraction and the effective lifetime of K^- in the metastable state was measured to be 3.5 ± 0.5 % and 10.24 ± 0.11 ns, respectively, in a past KEK experiment [10]. We used these values in the present analysis. In the decay products of K^-s, a monochromatic muon from the $K^-_{\mu 2}$ decay ($K^- \to \mu^- \overline{\nu}_\mu$) was used to estimate the timing resolution for the present TOF system. To see the $K^-_{\mu 2}$ decay component clearly, we applied the reaction timing analysis. The reaction timing, T_{react}, was defined by the timing difference between the stopped K^- and the outgoing charged particle. Then, by selecting the large T_{react} events, we can only observe the decay components of the K^-s in the metastable state.

Figure 2 (a) shows the $1/\beta$ spectrum with delayed timing selection of $T_{react} > 2$ ns. We can see clear three peaks attributed to the electrons ($1/\beta \sim 1$), μ^-'s from the $K^-_{\mu 2}$ decay ($1/\beta \sim 1.1$) and π^-'s from the $K^-_{\pi 2}$ decay ($1/\beta \sim 1.22$), respectively. The timing resolution was determined by the width of μ^- peak to be 0.020 in σ. This resolution was twice better than that of E471 and the resulting missing mass resolution was plotted in the upper part of Fig. 3 taking into account uncertainties from the energy loss straggling and multiple scattering of protons from the reaction vertex to the TOF counters.

Protons from the stopped K^- reaction were clearly identified by the correlation between the particle velocity ($1/\beta$) and the total energy. Figure 2(b) shows the correlation plot between the $1/\beta$ and the total light output in P_{stop} and NC. The proton events were selected by applying a correlation cut as shown in the figure, and defined by the events lying within the region between two solid lines.

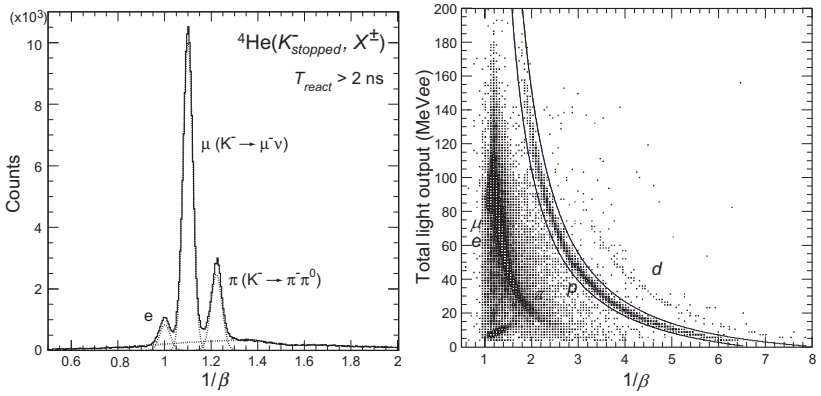

(a) (b)

Figure 2: a) 1β spectrum from the ^{4}He($K^-_{stopped}$, $X^\pm$) reaction. The resulting fitting lines were overlaid. b) A criteria for proton identification. Protons were defined the events lying between two lines.

Figure 3 shows the missing spectrum from the inclusive ^{4}He($K^-_{stopped}$, p) reaction together with a scale for the proton momentum. The abscissa and ordinate show the missing mass and proton yield per number of stopped K^-, respectively. A closeup of the low mass region was shown in the inset. The vertical lines represent mass threshold of possible decay modes of a strange tribaryon state. As shown in the spectrum, there was no peak structure throughout the missing mass spectrum.

To quantify the search results, we derived upper limits for the formation branching ratio of narrow strange tribaryon states from the obtained missing mass spectrum. The spectrum was fitted with a Voigt peak function (convolution of a Gaussian and a Lorentzian) with an assumed width and mass and a smooth polynomial background function. Then the obtained peak yield and its error was converted to upper limits with the 95 % confidence level with "unified" method advocated by Feldman and Cousins [12]. Figure 4 shows the upper limits for the formation branching ratio of the strange tribaryon state with assumed with of 0 (solid), 20 (dashed) and 40 (dotted) MeV/c^2, respectively

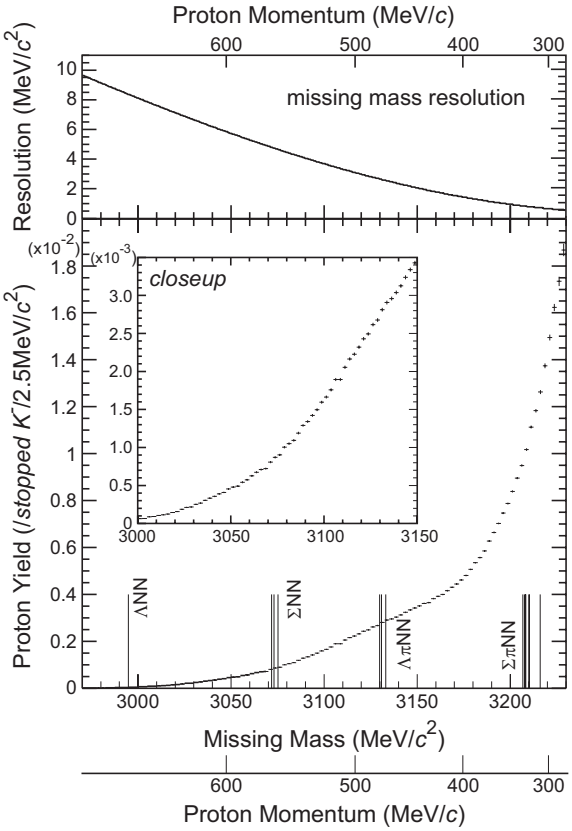

Figure 3: The missing mass spectrum from the ^{4}He($K^-_{stopped}$, p) reaction.

This result was quite inconsistent with that of E471. We studied the cause of this discrepancy and found a possible cause of a fake peak formation by an erroneous time-walk correction [9].

The present missing mass analysis from the stopped K^- reaction was only sensitive for states with a narrow width, because the background shape was not known well due to the unsatisfactory knowledge on the $\overline{K}N$ interaction. An experimental search for a broad state may become possible by exclusive measurements.

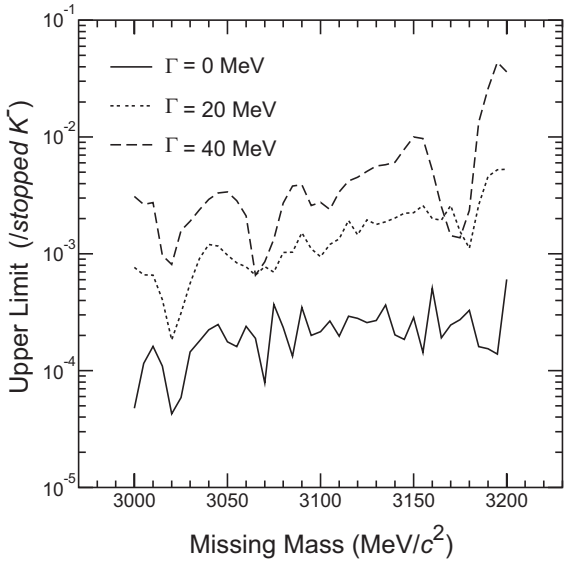

Figure 4: Upper limits for the formation branching ratio of a strange tribaryon state at the 95 % C.L. as a function of the missing mass. Solid, dotted and dashed curves corresponds to the assumed width of $\Gamma = 0, 20$ and 40 MeV/c^2, respectively

4 Conclusion

We have measured the nucleon energy from the ^{4}He($K^-_{stopped}$, N) reaction at the KEK 12 GeV PS. In the proton spectroscopy, we achieved twice better missing mass resolution and much higher statistics than those of E471. In the obtained missing mass spectrum, no significant narrow peak structure was observed. We have derived the upper limits for the formation branching ratio of the strange tribaryon states with the quantum number of strangeness -1, charge 0 and isospin 1 in the mass range of 3000 to 3200 MeV/c^2. They were determined with a 95 % confidence level to be $(0.4 \sim 6)\times10^{-4}$, $(0.2 \sim 6)\times10^{-3}$ and $(0.06 \sim 5) \times 10^{-2}/(stopped\ K^-)$ for an assumed width of 0, 20 and 40 MeV/c^2, respectively. From this result, a large formation branching ratio (order of 1 %/($stopped\ K^-$)) of a narrow tribaryon state, including S^0(3115), is clearly

excluded [13].

5 Acknowledgements

We are grateful to all of the staff in KEK-PS for their continuous support of the present experiment. This research was partially supported by RIKEN, KEK and Grand-in-Aid for Scientific Research (S), 14102005 of the Ministry of Education, Science, Sports and Culture of Japan.

References

1. Y. Akaishi and T. Yamazaki, Phys. Rev. C 65 (2002) 044005.
2. T. Suzuki et al., Phys. Lett. B 597 (2004) 263.
3. M. Iwasaki et al., arXiv:nucl-ex/0310018.
4. T. Suzuki et al., Nucl. Phys. A754 (2005) 375c.
5. Y. Akaishi, A. Dote and T. Yamazaki, Phys. Lett. B 613 (2005) 140.
6. Y. Maezawa et al., Prog. Theor. Phys. 114 (2005) 317.
7. E. Oset and H. Toki, Phys. Rev. C 74:015207, 2006.
8. M. Iwasaki et al., Nucl. Inst. Meth. A 473 (2001) 286.
9. M. Iwasaki et al., arXiv: 0706.0297[nucl-ex], Proceedings of The IX International Conference on Hypernuclear and Strange Particle Physics (HYP06), Mainz, Germany (2006) edited by J. Pochodzalla and Th. Walcher Springer Berlin.
10. T. Yamazaki et al., Phys. Rev. Lett. 63 (1989) 1590.
11. H. Outa, Doctoral Dissertation, University of Tokyo (2003).
12. G. J. Feldman and R. D. Cousins, Phys. Rev. D 57 (1998) 3873.
13. M. Sato et al., Phys. Lett. B, in press; arXiv:0708.2968[nucl-ex].

Frascati Physics Series Vol. XLVI (2007), pp. 1275–1282
HADRON07: XII Int. Conf. on Hadron Spectroscopy – Frascati, October 8-13, 2007
Hadrons in Matter

DOUBLE STRANGENESS PRODUCTION IN $\overline{p}^4He$ ANNIHILATION AT REST

G. Bendiscioli, L. Lavezzi, P. Montagna, A. Rotondi
Dipartimento di Fisica Nucleare e Teorica dell'Università di Pavia and INFN Sezione di Pavia, via Bassi 6, 27100 Pavia, Italy
A. Fontana, A. Panzarasa, P. Salvini
INFN Sezione di Pavia, via Bassi 6, 27100 Pavia, Italy
T. Bressani
Dipartimento di Fisica Nucleare e Teorica dell'Università di Torino and INFN Sezione di Torino, via P.Giuria 1, 10133 Torino, Italy

Abstract

Events with production of two positive kaons are observed in $\overline{p}^4He$ annihilations at rest into four and five prongs. K^+ pairs are produced associated to Σ pairs, $\Lambda\Sigma$ pairs and ΛK^- pairs. Lower limits for the yields are measured. The events could be the signature of different production mechanisms like rescattering cascades and quark-gluon plasma or bound $2K^-$-few nucleon system formation and decay. Even though the statistics is very small, signatures compatible with the formation of bound systems ($2K^-2n$) are discussed.

1 Introduction

Some kaon-nucleon potential models [1, 2, 3] predict a strong attraction in the I=0 isospin state, which could allow the existence of antikaon-nucleon bound states (usually referred to as DBKS, deeply bound kaon states). In Refs. [4, 5]

the binding energies and widths of S=-2 bound systems are discussed and the binding of two $\overline{K}$ turns out to be stronger than that of one $\overline{K}$. These DBKS are expected to be produced in collisional capture processes or in antinucleon-nucleon annihilations, as the several s-quarks produced in case of quark-gluon plasma formation would act as seeds for kaon clusters production. Several potential models are founded on a potential depth which is dependent on the nuclear medium density [6, 7], so that the DBKS observation should be favored in heavy nuclei. In general the DBKS production is connected with the possible existence of multinucleon bound states and the possibility that a high-density nuclear medium will be created around the $\overline{K}$ cluster. Such conditions could be reproduced even in the antiproton annihilation on a light nucleus like ^4He [8], as the existence of annihilation with involvement of more than one nucleon has been proved in [9] and the antiproton annihilation on helium nucleus is a strong source of strangeness production [10].

Following [11, 12] , kaonic bound states could be revealed indirectly by the production of K^+ pairs. Indeed the creation of two $\overline{s}$ quarks (i.e. two K^+) has to be accompanied by the creation of a s-quark pair, which in turn materialize in a pair of antistrange particles (antikaons or hyperons). In the antiproton-nucleon annihilation at rest the total energy available is equal to two nucleon masses ($\approx$ 1876 MeV) , so that the $2K^+2K^-$ final state (total mass of $\approx$ 1974MeV) is forbidden. Instead, the antiproton annihilation on a nucleus with involvement of more than one nucleon allows the production of hyperons, which can be detected through their decay modes. In particular, the $\overline{p}$-nucleus annihilation at rest events with two K^+ in the final state are allowed as the kaon pair can be produced associated with a pair of strange dibaryons or a DBKS with S=-2. We stress that, on the contrary, events with two K^- production are forbidden. We looked for $\overline{p}^4He$ annihilation reactions with two K^+ and with two K^- production : the former are signals for possible DBKS production while the reactions with K^- pair production , clearly "fake" events, are used for background subtraction. Indeed the observation of events with two K^- in the final state is due to wrong mass identification: as the percentage of misidentification of K^- and K^+ must be the same, the number of $2K^-$ events allows an estimate of the amount of wrong $2K^+$.

The data were collected by the Obelix experiment, exposed to the antiproton beam of the LEAR accelerator at CERN. The apparatus, described

Table 1: $\overline{p}^4He$ *annihilation reactions into four and five prongs with two* K^+ *production with their energy thresholds. In the table n means neutron and* p_s *spectator proton (with momentum* $< 300MeV/c$*, not detected). In the last column the number of detectable final state particles (charged mesons and protons with momentum* $> 300MeV/c$*) is reported.*

Intermediate and Final states	E_{MeV}	
$2K^+\Lambda\Lambda 2\pi^- p_s \rightarrow 2K^+(n\pi^0)(n\pi^0)2\pi^- p_s \rightarrow 2K^+2\pi^- X$	4436	4
$2K^+\Sigma^-\Sigma^- p_s \rightarrow 2K^+(n\pi^-)(n\pi^-)p_s \rightarrow 2K^+2\pi^- X$	4320	4
$2K^+K^0\Lambda\pi^- 2n \rightarrow 2K^+(p\pi^-)\pi^- 2nK^0 \rightarrow 2K^+2\pi^- pX$	4619	5
$2K^+\Lambda\Lambda\pi^- n \rightarrow 2K^+(n\pi^0)(p\pi^-)\pi^- n \rightarrow 2K^+2\pi^- pX$	4298	5
$2K^+\Lambda\Lambda 2\pi^-\pi^+ n \rightarrow 2K^+(n\pi^0)(n\pi^0)2\pi^-\pi^+ n \rightarrow 2K^+2\pi^-\pi^+ X$	4437	5
$2K^+\Sigma^-\Sigma^+\pi^- n \rightarrow 2K^+(n\pi^-)(n\pi^+)\pi^- n \rightarrow 2K^+2\pi^-\pi^+ X$	4461	5
$2K^+\Sigma^-\Lambda n \rightarrow 2K^+(n\pi^-)(p\pi^-)n \rightarrow 2K^+2\pi^- pX$	4240	5
$2K^+K^-\Lambda 2n \rightarrow 2K^+K^-(p\pi^-)n \rightarrow 2K^+K^-\pi^- pX$	4476	5

in [13, 14], included two scintillator barrels for time-of-flight measurements separated by a magnetic spectrometer for momentum, trajectory length and specific ionization measurements.

2 Data Analysis

We restricted our analysis on the $\overline{p}^4He$ annihilation channels allowed by strangeness and energy conservation ($E_{tot} \approx 4666$MeV) into four and five prongs, i.e. the reactions listed in tab.1. We stress that the second reaction in tab.1 does not necessarily include neutral mesons production in the final states.

The data sample consisted in a total of 238 746 annihilation events into four prongs (two negative and two positive, connected to the annihilation vertex) and 47 299 annihilation into five prongs (two negative and three positive connected to the vertex). It must be taken into account that the apparatus had a limited acceptance in the low momentum region: taking into account the minimum momentum measured by the spectrometer and the energy loss between the vertex and the four jet drift chambers the momentum threshold is of $\approx 100\ MeV/c$ for pions , $\approx 150\ MeV/c$ for charged kaons and $\approx 300\ MeV/c$ for protons. The data analysis goes through three crucial points: the charged kaons identification , over the huge pion background (charged kaons are $\approx 1\%$ of the total of charged prongs), the selection of events with $2K^+$ production

and the selection of the "fake" events with $2K^-$ production and, at last, the background subtraction to get the real number of $2K^+$ events.

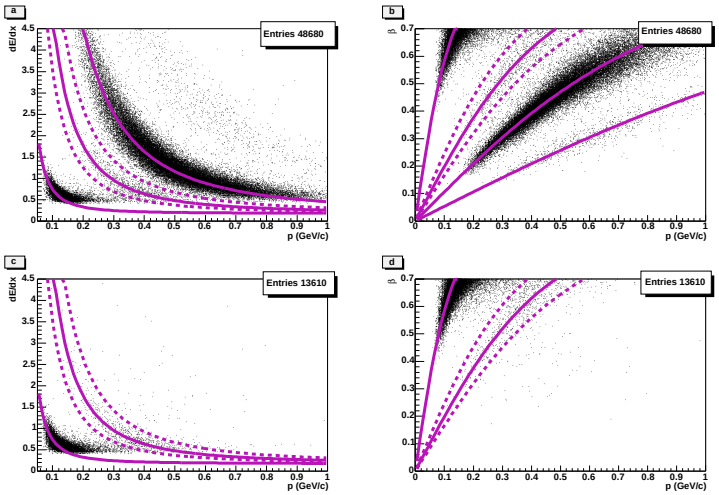

Figure 1: Track distributions for positively (a,b) and negatively (c,d) charged particles in four-prong events after the dE/dxvs.β and $\beta < 0.7$ cut. Different particles accumulate around their corresponding theoretical lines: solid lines are drawn for pions, kaons and protons mass hypothesis in (a), with the deuton mass hypothesis in (b) and for pion and kaon mass only in (c) and (d). Kaons fall between the dotted lines in β and dE/dx distributions.

The complete description for charged particles identification has already been described in ref. [10]. Kaons identification is performed by the independent measurements of momentum (p), specific energy loss (dE/dx) and velocity (β) from time-of-flight measurement. These quantities must satisfy the following correlations:

$$\frac{dE}{dx} = \frac{4\pi N z^2 e^4 Z c^2}{m_e \beta^2 A} \left[\ln \left(\frac{2 m_e c^2 \beta^2}{I(1-\beta^2)} \right) - \beta^2 \right] \tag{1}$$

$$\beta = \frac{p}{\sqrt{M^2 + p^2}} = \frac{p}{E} \tag{2}$$

$$\frac{dE}{dx} = \left(\frac{4\pi N z^2 e^4 Z}{m_e A}\right) \frac{p^2 + M^2}{p^2} \left[\ln\left(\frac{2m_e \frac{p^2}{p^2+M^2}}{I(1 - \frac{p^2}{p^2+M^2})}\right) - \frac{p^2}{p^2 + M^2}\right] \qquad (3)$$

where M is the "unknown" mass to be recognized. As the first relation is independent of the mass, supposing relatively small measurement errors, the data of all tracks distribute close to the same functional line. The other two relations depend on the mass, describing the family of lines shown in fig.1.

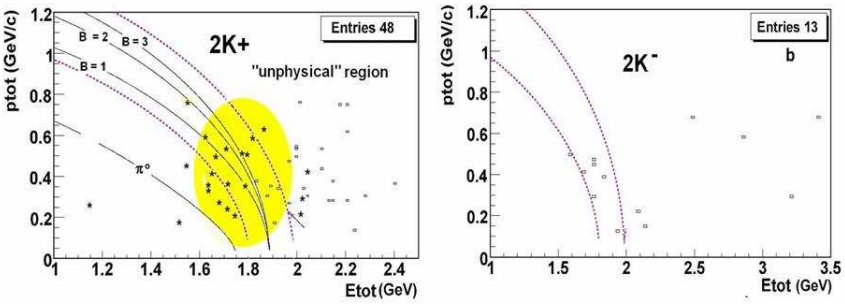

Figure 2: Four prong events. P_{tot} vs. E_{tot} for the $2\pi^- 2K^+$ events (a) and for the $2K^- 2\pi^+$ background (b) events. The full lines correspond to annihilation with barionic number equal to 1,2,3 in the initial state (annihilation over two,three and four nucleons) and the bands between dotted lines enclose mostly the region without neutral meson production.

In order to pick up the kaons we resorted at first to Eq. 1 selecting tracks with values of β and dE/dx around the ideal line, than we excluded tracks with $\beta > 0.7$. This last cut was done in order to select tracks in a β region where kaon production is maximum: indeed from bubble chamber experiments the number of kaons over this β region strongly decreases (see [15]). After this selection kaon tracks are the ones falling in the band inside the dotted lines of figs.1. The K^+ pair is expected to be produced in case of annihilation with involvement of more than one nucleon, so that we selected events according to the energy and momentum conservation laws , taking into account that the total initial energy E_0 may vary from two nucleon masses ($2m_N$) in case of

single nucleon annihilation (initial barionic number B=0) to a maximum of five nucleon masses for the annihilation involving four nucleons (B=3). Neglecting the Fermi motion, we can write the following implicit relationship between the total measured momentum (P_{tot}) and the total measured energy (E_{tot}) as a function of the initial energy E_0 and of the invariant mass of the unseen particles M_U (mainly neutrals or particles escaping the apparatus solid angle acceptance).

$$P_{tot} = \sqrt{(E_o - E_{tot})^2 - M_U} \tag{4}$$

Eq.4 draws a line for a each E_0 value (i.e. each B value) and for $M_U = 0$ in the P_{tot} vs. E_{tot} plane. Annihilation reactions are represented as points located in different regions of this plane: the region at right-hand side of the B=3 line is not physical in the ideal case, when neglecting the nucleon Fermi motion, annihilations on one nucleon concentrate in one point at $E_{tot} = 2m_N$ and events with neutral mesons production distribute on the left-hand side of the B=1 line. Of course the experimental data distribution will be spread around the theoretical lines, as the Fermi motion could be partly delivered to the annihilation mesons, as can be seen in [16] comparing the pion momentum distribution for annihilation on ^4He (extended up to $\approx 700 MeV/c$) and on H (extended up to $\approx 500 MeV/c$). We report here figures and comments relative to the four prong events analysis: details on the five prong events analysis can be found in Ref. [16]. After kaon identification the $2\pi^- 2K^+ X$ event distribution in the P_{tot} vs. E_{tot} plane can be seen in fig.2, together with the corresponding background $2\pi^+ 2K^- X$ event distribution. Even after background subtraction a number of events in fig.2a remains in the non-physical region. On the other hand, as discussed before, the lines are drawn neglecting the nucleons Fermi motion and we stress that a high Fermi momentum means a small interaction distance, which agrees with the idea of an annihilation on a bag of several nucleons. Another interesting point is that the region corresponding to events with neutral meson production is nearly empty: this means that mainly the second reaction in Tab.1 and not the first one is produced. To extract the number of "true" $2K^+$ events we evaluated the difference between the number of observed $2K^+ 2\pi^-$ events and the number of $2K^- 2\pi^+$ events corrected for the K^- defect R=87% (estimated from the ratio $2K+$ / $2K^-$ for events on hydrogen collected by the same experiment).

$$N(2K^+ 2\pi^- X)_{true} = N(2K^+ 2\pi^- X)_{observed} - RN(2K^- 2\pi^+ X)_{observed} \tag{5}$$

The yield lower limits are deduced considering the total $\overline{p}^4He$ annihilation frequency into four and five prongs from [17].

$$Y_{(2K^+2\pi^-2np_s)} = (0.172\pm0.038)10^{-4} \quad Y_{(2K^+\pi^+2\pi^-3n)} = (2.71\pm0.047)10^{-4} \quad (6)$$

$$Y_{(2K^+p2\pi^-2n)} = (1.21 \pm 0.29)10^{-4} \quad Y_{(2K^+K^-p\pi^-2n)} = (0.28 \pm 0.14)10^{-4} \quad (7)$$

3 Conclusions

For the first time the $2K^+$ production in $\overline{p}^4He$ annihilation was observed. Neverthless, the existence of bound kaon-antikaon system does not come straightforward, as different production mechanisms could be invoked.

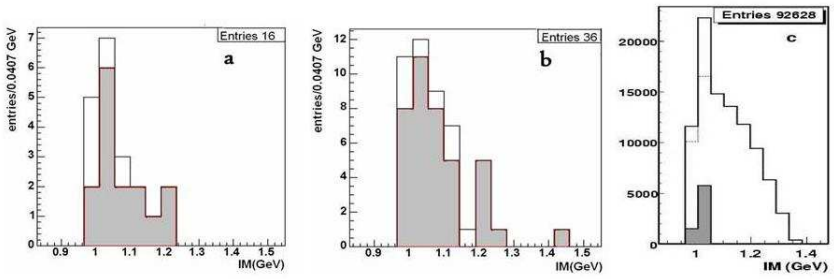

Figure 3: $2K^+$ invariant mass for all four prong selected events (a) and for events with prong momentum $< 400MeV/c$ (b). Montecarlo distribution (c) for all events (solid line) and momentum cut (dotted) for uncorrelated particles and with $\approx 10\%$ contribution from a bound system of B=150MeV (grey).

In particular double positive kaons production could come from rescattering cascades, from formation and decay of a quark gluon plasma other than of a DBKS. Some indications about the production mechanisms could be obtained looking at the $2K^+$ invariant mass distributions. Extended comments on this topic are to be found in [16]: in this proceeding we reported only the main results. Comparing the $2K^+$ experimental invariant mass distribution with the same distribution coming from a Montecarlo of events generated with the hypothesis of four uncorrelated particles production ($\overline{p}^4He \rightarrow 2K^+\Sigma^-\Sigma^-$) or of DBKS production ($\overline{p}^4He \rightarrow 2K^+X$, $X = (2K^-2n)_B$) we appreciate that the four prong data are compatible with a small contribution ($\approx 10\%$) from

a bound system with $B \approx 150 MeV$ (see fig.3). In a similar way can be shown that five prong events data are compatible with about 50% contribution from a $(2K^- 2n)$ bound system of binding energy around 150MeV. Our final conclusions are that events with $2K^+$ production are observed in $\overline{p}^4He$ annihilation at rest into four and five prongs and that the $2K^+$ invariant mass distributions are compatible with the idea that a bound kaon state with strangeness S=-2 is produced. Nevertheless the statistics is small and we cannot exclude other production mechanisms.

References

1. Y.Akaishi,T.Yamazaki,Phys.Rev **C65**,044005 (2002).
2. T.Yamazaki,Y.Akaishi,Phys.Lett. **B535**, 70 (2002).
3. A.Dote' et al.,Phys.Lett. **B590** , 391c (2005).
4. T.Yamazaki et al.,Phys.Lett. **B587** , 167 (2004).
5. A.Dote' et al.,Nucl.Phys. **A754** , 391c (2005).
6. J.Mares et al.,Nucl.Phys. **A770** , 84 (2006).
7. C.J.Batty et al.,Phys.Rep. **287** , 385 (1997).
8. G.Bendiscioli et al,Nucl.Phys. **A789** , 222 (2007).
9. P.Salvini et al.,Nucl.Phys. **A760** , 349 (2005).
10. A.Panzarasa et al.,Nucl.Phys. **A747** , 448 (2005).
11. W.Weise,arXiv:nucl-th/0507058 v1(2005).
12. P.Kienle,Int.Jour.Mod.Phys. **A22** , 365 (2007).
13. A.Adamo et al.,Nucl.Phys. **A569** , 761 (1994).
14. A.Adamo et al.,Proc. of the Workshop on N$\overline{N}$ Interaction, Moscow (1991).
15. J.Roy, Proc. of the 4th Int. Symp. on $\overline{N}N$ Interaction, Syracuse (1975).
16. G.Bendiscioli et al., Nucl.Phys. **A797** , 109 (2007).
17. F.Balestra et al,Nuovo Cimento **A100** , 323 (1988).

Frascati Physics Series Vol. XLVI (2007), pp. 1283–1292
HADRON07: XII Int. Conf. on Hadron Spectroscopy – Frascati, October 8-13, 2007
Hadrons in Matter

SEARCHES FOR MULTIBARYON STATES WITH Λ HYPERON SYSTEMS IN pA COLLISION AT 10 GeV/c

P. Zh. Aslanyan
Joint Institute for Nuclear Research, Dubna, Russia
and Yerevan State of University
V.N. Emelyanenko
Joint Institute for Nuclear Research

Abstract

Experimental data as a stereo photographs from the 2m propane bubble chamber LHE, JINR have been analyzed for exotic multibaryon metastable and stable states searches. A number of peculiarities were found in the effective mass spectra of $\Lambda\pi^{\pm}$,$\Lambda\pi^{+}\pi^{-}$, Λp, Λpp, $\Lambda p\pi$,$\Lambda\Lambda$ and ΛK^{0}_{S} subsystems. The observed well known $\Sigma^{*+}(1385)$,$\Lambda^{*}(1600)$ and $K^{*\pm}(892)$resonances are good tests for this method. The width of $\Sigma^{*-}(1385)$ for p+A reaction is two time larger than that presented in PDG. The $\Lambda\pi^{-}$ spectrum showed an enhancement in the mass range of 1345 MeV/c^2 which is interpreted as a stopped Ξ^{-} in the nucleus. The cross section of stopped Ξ^{-} production is ≈ 8 times larger than obtained by fritiof model with same experimental conditions.

1 Prewiew

There are a few actual problems of nuclear and particle physics which are concerning subject of this report [1)]- [7)]. These are following: in-medium modification of hadrons, the origin of hadron masses, the restoration of chiral symmetry, the confinement of quarks in hadrons, the structure of neutron stars. Strange multi-baryonic clusters are an exiting possibility to explore the properties of cold dense baryonic matter and non-perturbative QCD. Multi-quark states, glueballs and hybrids have been searched for experimentally for a very long time, but none is established

2 Experiment

The full experimental information of more than 700000 stereo photographs are used to select of events by V^0 channel [1)].The momentum resolution charged particles are found to be $< \Delta P/P >$=2.1 % for stopped particles and $< \Delta P/P >$=9.8 %, for nonstopped particles. The mean values of measurement errors for the depth and azimuthal angles are equal to $\leq$0.5 degrees. The masses of the identified 8657-events with Λ hyperon 4122-events with K_s^0 meson are consistent with their PDG values [1)].The experimental total cross sections are equal to 13.3 and 4.6 mb for Λ and K_s^0 production in the p+C collisions at 10 GeV/c. Protons can be identified by relative ionazation over the following momentum range: $0.150 < P < 0.900$ GeV/c.

The background has been obtained by methods: polynomial function, mixing angle and by FRITIOF model [4)]. The statistical significance of resonance peaks were calculated as NP $/\sqrt{NB}$, where NB is the number of counts in the background under the peak and NP is the number of counts in the peak above background.

3 (Λ, π^+) and (Λ, π^-) spectra

The $\Lambda\pi^+$- effective mass distribution for all 15444 combinations with bin size of 13 MeV/c^2 in Fig.1a has shown [5)]- [7)]. The resonance with similar decay properties for $\Sigma^{*+}(1382) \rightarrow \Lambda\pi^+$ identified which was a good test for this method. The decay width is equal to $\Gamma \approx 45$ MeV/c^2. $\Delta M/M = 0.7$ in range of $\Sigma^{*+}(1382)$ invariant mass. The cross section of $\Sigma^{*+}(1382)$ production (540

exp. events) is approximately equal to 0.9 mb for p+C interaction.

The $\Lambda\pi^-$- effective mass distribution for all 6730 combinations with bin sizes of 18 and 12 MeV/c^2 in Fig.1b,2a has shown. The solid curve(Fig.1b) is the sum of the background (by the polynomial method) and 1 Breit-Wigner resonance($\chi^2/N.D.F. = 39/54$). There is significant enhancement in the mass range of 1372 MeV/c^2 with 11.3 S.D.,Γ =93 MeV/c^2. The cross sectio of Σ^{*-} production (≈680 events) is equal to ≈ 1.3 mb at 10 GeV/c for p+C interaction. The width for Σ^{*-} observed ≈2 times larger than PDG value. A possible explanation is nuclear medium effects on invariant mass spectra of hadrons decaying in nuclei [9].

Fig. 2a shows $\Lambda\pi^-$ effective mass distribution with bin size of 12 MeV/c^2, where there are significant enhancements in mass regions of 1345(3.0 S.D.) and 1480(3.2) too. The solid curve(Fig.2a) is the sum of the background and 1 Breit-Wigner resonance ($\chi^2/N.D.F. = 109/88$). The background (dashed)curve is the sum of the six -order polynomial and 1 Breit-Wigner function with parameters for identified resonance $\Sigma^{*-}(1385)$(Fig.1b). There are negligible enhancements in mass regions of 1410, 1520 and 1600 MeV/c^2. The cross section of Ξ^-- production (≈60 events) stopped in nuclear medium is equal to 315 μb at 10 GeV/c for p+propane interaction. The observed number events with Ξ^- by weak decay channel is equal to 8 (w=$1/e_\Lambda$ =5.3, where is a full geometrical weight of registered for Λs) [2].Then experimental cross section for identified Ξ^- by weak decay channel [2] is equal to 44μb and 11.7μb in p+propane and p+C collisions, respectively, which are conformed with FRITIOF calculation. The observed experimental cross section for stopped Ξ^-(60 events) is 8 times larger than the cross section which is obtained by fritiof model with same experimental conditions. The width of $\Sigma^{*-}(1385)$ for p+A reaction is two time larger than that presented in PDG.Figures shows that there is observed $\Sigma^{*-}(1480)$ correlation which is agreed with report from SVD2 collaboration too.

4 (Λ, p) and (Λ, p, p) spectra

Fig. 2b) shows the invariant mass for all Λp 13103 combinations with bin size of 15 MeV/c^2 ([3]) . There are enhancements in mass regions of 2100, 2150, 2225 and 2353 MeV/c^2(Fig.2b). There are many published articles [3]- [7]for the (Λp)invariant mass with identified protons in momentum range of 0.350< P_p < 0.900 GeV/c. There are significant enhancements in mass regions of 2100, 2175,

2285 and 2353 MeV/c^2.Their excess above background by the second method is 6.9, 4.9, 3.8 and 2.9 S.D., respectively. There is also a small peak in 2225(2.2 S.D.) MeV/c^2 mass region.

Fig.2c shows the invariant mass of 4011(Λp)combinations with bin size 15 MeV/c^2 for stopped protons in momentum range of 0.14< P_p < 0.30 GeV/c.The dashed curve is the sum of the 8-order polynomial and 4 Breit-Wigner curves with χ^2 = 30/25 from fits(Table 1). A significant peak at invariant mass 2220 MeV/c^2 (6.1 S.D.), B_K 120 MeV was specially stressed by Professor T. Yamazaki on μCF2007, Dubna, June-19-2007 that is conform with KNC model [8] prediction by channel of $K^- pp \to \Lambda$p .

The Λp effective mass distribution for 2025 combinations with relativistic protons over a momentum of P >1.65 GeV/c is shown in Fig.2d . The solid curve is the 6-order polynomial function(χ^2/n.d.f=205/73). There are significant enhancements in mass regions of 2155(2.6 S.D.), 2225(4.7 S.D., with Γ=23 MeV/c^2), 2280(4.2 S.D.), 2363(3.6 S.D.) and 2650 MeV/c^2(3.7 S.D.). These observed peaks for combinations with relativistic protons P >1.65 GeV/c agreed with peaks for combination with identified protons and with stopped protons(Table 1).

The Λpp effective mass distribution for 3401 combinations for identified protons with a momentum of P_p <0.9 GeV/c is shown in Fig. 3a) [5]- [7]. The solid curve is the 6-order polynomial function(χ^2/n.d.f=245/58, Fig.3a). The backgrounds for analysis of the experimental data are based on FRITIOF and the polynomial method. There is significant enhancements in mass regions of 3145 MeV/c^2(6.1 S.D.) and with width 40 MeV/c^2. There are small enhancements in mass regions of 3225(3.3 S.D.), 3325(5.1 S.D.), 3440(3.9 S.D) and 3652MeV/c^2(2.6 S.D.)(Table 1). These peaks from Λp and Λpp spectra were partly conformed with experimental results from FOPI(GSI), FINUDA(INFN), OBELIX(CERN) and E471(KEK).

5 (Λ, Λ) spectrum

There is observed significant enhancement in mass region of 2360(4.5 S.D.) Mev/c^2 for (Λ, Λ) spectrum in Fig. 3b)(137 combination). This peak is conformed with theoretical predictions and with earlier published result from neutron exposure by PBC method with very poor statistics too. There is small

enhancement in mass range of 2525 Mev/c^2(3.0 S.D.) too(Table 1).

6 (Λ, p, π^-) spectrum

The (Λ, p, π^-) effective mass distribution (Fig. 3c) for 2975 combinations for identified protons in momentum range of P <0.9 GeV/c can taken by the 6-order polynomial function which is satisfactory described the experimental data with $\chi^2/(N.D.F.)$=1. But the background by FRITIOF model do not describe the experimental distribution. The sum of BW (with mass 2520 MeV/c^2 and experimental width 280 MeV/c^2) and FRITIOF model for $\Lambda p\pi^-$ effective mass distribution is satisfactory described the experimental data too. Therefore one of probably interpretation of this peak that it can be reflection from phase space distribution too. Earlier published result about observation of resonance with mass 2495 MeV/c^2 and width 200 MeV/c^2 for $\Lambda p\pi^-$ spectrum by PBC method for neutron exposure(7 GeV/c) is not uniquely conformed.

7 (Λ, π^+, π^-) spectrum

The $\Lambda\pi^+\pi^-$ effective mass distribution for all 3476 combinations with bin size 36 MeV/c^2 has shown in Fig. 3d. The dashed curve is the the background by the polynomial method.There are significant enhancement in mass region of $\Lambda^*(1600)$(5.5 S.D., Γ_e=80 MeV/c^2,ΔM=25 MeV/c^2) with width 55 (from PDG). There are small enhancements in mass regions of $\Lambda^*(1520)$(3.5 S.D.),$\Lambda^*(1690)$(3.8 S.D.) and $\Lambda^*(1800)$(2.8 S.D.) MeV/c^2 which are interpreted as a reflection from resonances of $\Lambda^*(1520)$, $\Lambda^*(1690)$ and $\Lambda^*(1800)$ from PDG. There are not observed exotic states which were earlier observed and published for $\Lambda\pi^+\pi^+$ spectrum (in mass ranges of 1704,2071,2604 Mev/c^2)with small statistic in neutron exposure by PBC method [10].

8 Conclusion

•The invariant massspectra of $\Lambda\pi^+$, $\Lambda\pi^+\pi^-$ and $K^0_s\pi^\pm$ have shown well known resonances from PDG as $\Sigma^{*+}(1385)$,$\Lambda^*(1520), \Lambda^*(1600), \Lambda^*(1690)$ and $K^{*\pm}$(892) which are a good test for this method.

• A number of important peculiarities were observed in pA $\rightarrow \Lambda(K^0_S)$ X reactions in the effective mass spectrum for exotic states with decay modes (Table 1) [4]- [7] : $(\Lambda, \pi), (\Lambda, \pi^+, \pi^-), (\Lambda, p), (\Lambda, p, p), (\Lambda, \Lambda), \Lambda, p, \pi^-), (\Lambda, K^0_s)$ and

$K_s^0\pi^{\pm}$.

• Particulary peaks for (Λ, p) and (Λ, p, p) spectra are in agreement with experimental data from the reports of FOPI, E471(KEK), OBELIX, FINUDA collaborations, but there are some inconstancy by widths.

9 Acknowledgements

The work was partly supported by the grant of RFBR 07-02-08644 and org. committee of International Conference HADRON, Frascati,INFN, 8-12 October, 2007.

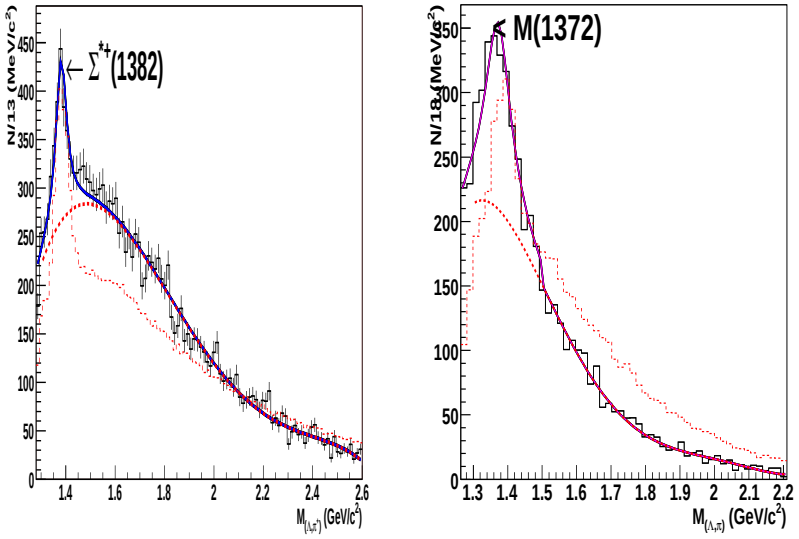

(a) (b)

Figure 1: *a)The $\Lambda\pi^+$ - spectrum; b)All $\Lambda\pi^-$ comb with bin size of 18 MeV/c^2. The simulated events by FRITIOF is the dashed histogram. The background is the dashed curve.*

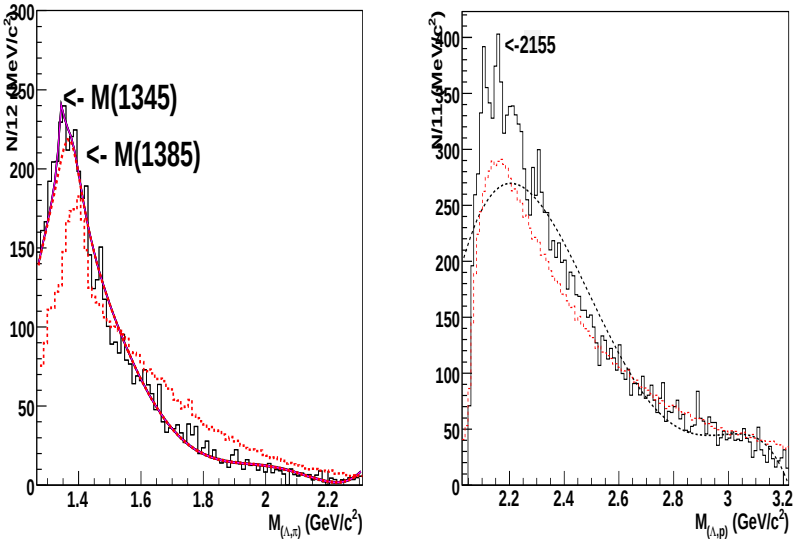

(a) (b)

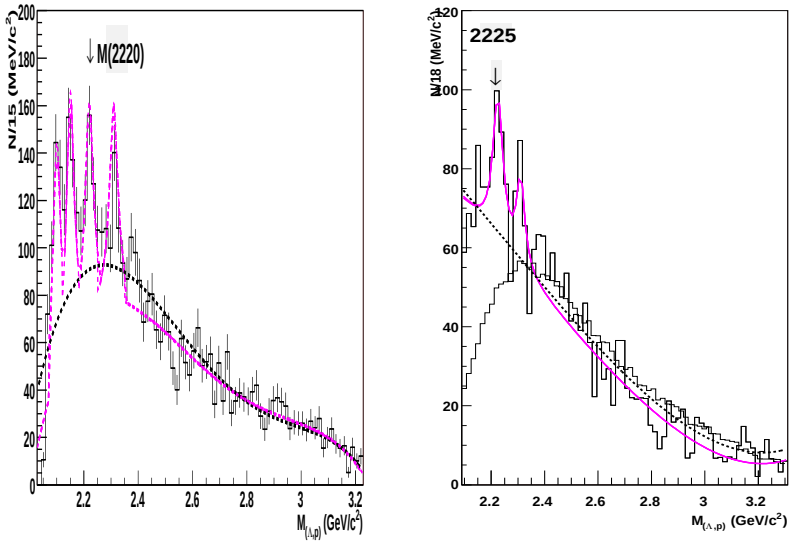

(c) (d)

Figure 2: *a) $\Lambda\pi^-$ spectrum with bin size of 12 MeV/c^2.b)All comb for the Λp spectrum; c)Λp spectrum with stopped protons in momentum range of 0.14< P_p <0.30 GeV/c;d) Λp spectrum for relativistic positive tracks in range of P_p >1.65 GeV/c. The dashed histogram is simulated events by FRITIOF.*

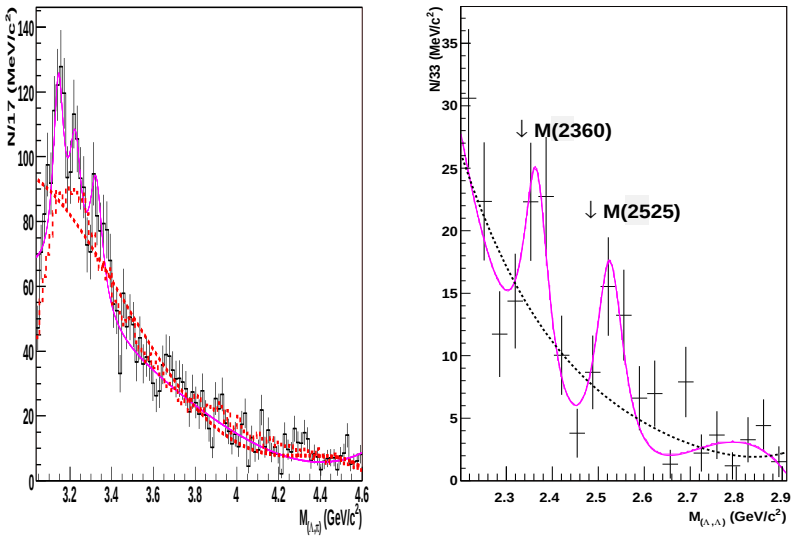

(a) (b)

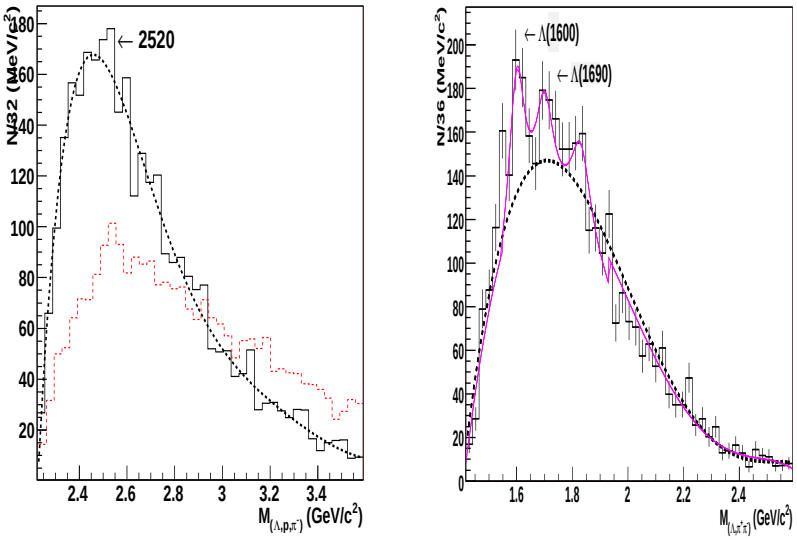

(c) (d)

Figure 3: a)Λpp spectrum with identified protons P_p <0.9 GeV/c; b)$\Lambda\Lambda$ spectruma) c)$\Lambda\pi^- p$ spectrum with identified protons P_p <0.9 GeV/c; d)$\Lambda\pi^+\pi^-$ spectrum for positive tracks in momentum range of $P_{\pi+}$ <0.9 GeV/c. The dashed histogram is simulated events by FRITIOF. The experimental background is the dased curve.

Table 1: *The effective mass , width(*Γ*) and S.D. for observed exotic strange resonances in p+ propane collisions.*

Λp	2100	24	5.7
	2150	19	5.7
	2220	23	6.1
	2310	30	3.7
	2380	32	3.5
Λpp	3145	40	6.1
	3225	50	3.3
	3325	53	4.8
$\Lambda\Lambda$	2365	55	4.5
	2525	63	3.0
ΛK_s^0	1750	14±6	5.6
	1795	26±15	3.3
$K_s^0\pi^\pm$	890	50	6.0-8.2
	780-800	10	2.5-4.2
	720-730	30-125	4.1-15.2
	1060	-	7.2

References

1. P.Zh. Aslanyan et al.,Phys. of Part. and Nuclei Letters, Vol. 4, No. 1,pp. 99-108, 2007. JINR Commun.,E1-2005-150, 2005.
2. P.Z. Aslanyan, JINR Commun.,E-2001-265,2002.
3. P.Z. Aslanyan et al., Proc. Conf. on LEAP05,May 16-22, Bonn, 2005; AIP,v. 796, p.195, ISBN 0-7354-0284-1.
4. P.Zh. Aslanyan et al.,Physics of Particles and Nuclei Letters, Vol. 3, No. 5,pp. 331-334, 2006.JINR Commun.,E1-2005-149, 2005.
5. P.Z. Aslanyan et. al., Proc. XVIII ISHEPP, Dubna,September 25-30, 2006. Proc. , Spin'06, October 2-7, Kyoto, Japan 2006, ISBN 978-0-7354-0423-6,AIP, v.915.ArXiv:hep-ex/0610086v1.
6. P.Z. Aslanyan,Proc. IUTP'07,Schladming,Austria, 25-3 March, 2007.
7. P.Z. Aslanyan,Proc. on Int. Confereence Hadron Structure, Bratislava, 2-8 September,2007; ArXiv:hep/ex-0710.4322v2.

8. T.Yamazaki, Y.Akaishi,Phys.Lett. B535,70,2002.

9. T.Yamazaki, Y.Akaishi,Phys.Lett. B453,p.p.1-6,1999.

10. B.A. Shahbazian et al., Nucl. Physics, A374(1982),p. 73c-93.c.

11. M. Agnello et al., Phys. Rev. Lett. 94, 212303 (2005). M. Agnello et al., arXiv: 0708.3614v1 (2007).

12. T. Suzuki et al., Phys.Lett. B 597, 263 (2004). M. Iwasaki et al., arXiv: nucl-ex/0310018v2.T. Suzuki et al., arXiv: 0709.0996v2.

13. N. Herrmann, Proceedings EXA05 (2006).

14. G. Bendiscioli et al., Nucl. Phys. A 789, 222 (2007).

Frascati Physics Series Vol. XLVI (2007), pp. 1293–1298
HADRON07: XII Int. Conf. on Hadron Spectroscopy – Frascati, October 8-13, 2007
Hadrons in Matter

THE AMADEUS EXPERIMENT: STUDY OF THE KAONIC NUCLEAR CLUSTERS AT DAΦNE

Oton Vazquez Doce
LNF-INFN, Via Enrico Fermi 40, 00044 Frascati (Roma), Italy
on behalf of the AMADEUS collaboration

Abstract

The AMADEUS experiment will perform the first complete experimental study of the case of the so-called deeply bound kaonic nuclear states. Such a study has deep consequences in a still open sector of the strangeness hadronic/nuclear physics: how the hadron masses and hadron interactions change in the nuclear medium with consequences on the structure of cold dense hadronic matter. AMADEUS will perform exclusive - full acceptance - measurements, all particles in the formation and decay processes of deeply bound nuclear clusters will be detected.

1 The AMADEUS scientific case: Kaonic clusters

The change of the hadron masses and hadron interactions in the nuclear medium and the structure of cold dense hadronic matter are hot topics of hadron physics today. These important, yet unsolved, problems will be the research field of AMADEUS [1)].

AMADEUS will search for antikaon-mediated deeply bound nuclear states, which could represent the ideal conditions for investigating the way in which the spontaneous and explicit chiral symmetry breaking pattern of low-energy QCD occur in the nuclear environment.

Such states were predicted by Wycech [2] some time ago; now the availability of experimental facilities for studying these kind of exotic nuclei has triggered a vivid discussion, initiated with the publication of the paper by Akaishi and Yamazaki [3], where a phenomenological strongly attractive $\bar{K}N$ potential is used favouring the existence of nuclear bound states of kaons in nuclei, while contracting the core of the resulting kaonic nucleus, producing a cold and dense nuclear system.

The possible formation of a deeply bound kaonic nuclear state (DBKNS) could provide information concerning the modification of the kaon mass and of the $\bar{K}N$ interaction in the nuclear medium, with many important consequences in hadronic and nuclear physics:

- such compact exotic nuclear systems might get formed with binding energies so large ($\sim$100 MeV) that their widths turn out rather narrow, since the $\Sigma\pi$ decay channel is energetically closed and, additionally, the $\Lambda\pi$ channel is forbidden by isospin selection rule;
- high-density cold nuclear matter might be formed around K^-, which could provide information concerning a modification of the kaon mass and of the $\bar{K}N$ interaction in the nuclear medium;
- empirical information could be obtained on whether kaon condensation can occur in nuclear matter, with implications in astrophysics: neutron stars, strange stars.
- nuclear dynamics under extreme conditions (nuclear compressibility, etc) could be investigated.

2 The framework of AMADEUS

There exist, actually, several different theoretical approaches to the problem, bringing arguments either for, or against the existence of the deeply bound kaonic nuclear states. In between the two extremes of the theoretical debate, there are as well predictions of shallower potentials than those which lead to the kaonic clusters [4]. Currently, the intense theoretical debate undergoing

shows even more the importance of the AMADEUS physics case and reinforces the need to perform it in the near future.

From the experimental point of view, several approaches have been followed since first experimental indications of the formation of tribaryonic states K^-ppn and K^-pnn were found at KEK [5] [6], although the last was lately not confirmed [7]. Other facilities allowed to study the problem bringing new data to the field, as it was made by FINUDA at DAΦNE [8], at GSI [9] and at BNL-AGS [10]; data from older, not dedicated, experiments were reanalyzed as well [11] [12]. What emerges, however, is an experimental status of the DBKNS search with few, low statistics and not complete results, which are, rightly, not easy to be attributed to a DBKNS interpretation, since other scenarios cannot be excluded.

From the theoretical and experimental status of these studies arises the need to perform in the future new dedicated experiments, which should attack the DBKNS search both in formation and in the decay processes, as completely as possible. New dedicated experiments are planned at J-PARC, FOPI, GSI, and, of course, AMADEUS at an upgraded DAΦNE.

3 Performing AMADEUS at DAΦNE

The new proposal, AMADEUS at DAΦNE, has the goal to perform, for the first time, a systematic and complete spectroscopic study of deeply bound kaonic nuclei, both in formation and in the decay processes. Moreover, AMADEUS aims to perform other types of measurements as: elastic and inelastic kaon interactions on various nuclei, obtaining important information for a better understanding of the undergoing processes. These high precision measurements will be achieved by implementing the KLOE detector with an inner AMADEUS-dedicated setup, containing a cryogenic target and a trigger system.

The planned upgrade of DAΦNE will reach a luminosity as high as 10^{33} cm^{-2} s^{-1} [13], delivering an integrated luminosity of about 10 fb^{-1} per year, equipped with the dedicated 4π detector KLOE [14] complemented with the AMADEUS apparatus will become the top level scientific center to study DBKNS using K^- induced processes at rest. In the left part of Fig. 1 the location of AMADEUS setup within KLOE detector is shown.

For the integration of the AMADEUS setup within KLOE a solution which is presently under study is to use a half-toroidal target placed around

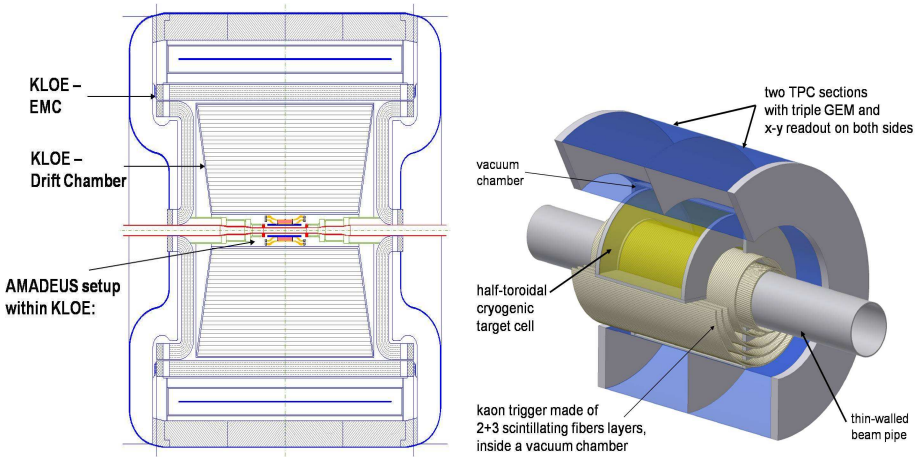

Figure 1: AMADEUS setup implementation position inside KLOE detector (left), and detail of the central region (right).

the beam pipe and surrounding the interaction region. The beam pipe can be a thin-walled aluminum pipe with carbon fiber reinforcement. A degrader which might be an active one, i.e. a scintillator (or scintillating fiber) detector is placed around the pipe just in front of the target. This detector is essential, delivering an optimal trigger condition by making use of the back-to-back topology of the kaons generated from the Φ-decay.

A Phase-1 of AMADEUS experiment was already proposed [15] together with a luminosity request and a physics program. The AMADEUS first phase program foresees the investigation of the most basic antikaon-mediated clusters, namely:

- kaonic dibaryon state ppK$^-$, produced via ^{3}He (stopped K, n) reaction;
- kaonic 3-baryon states ppnK$^-$ and pnnK$^-$, produced via ^{4}He (stopped K$^-$, n/p) reactions.

The search for these DBKNS will be performed by the process of K^- stopped in high-density gaseous ^{3}He and ^{4}He targets, measuring their binding energies and their widths. The processes for the case of a ^{4}He target are shown in Fig. 2. The luminosity request of this first phase of AMADEUS is of 4 fb^{-1}.

Lately, the KLOE detector capability to reconstruct hyperons with a very good resolution, ideal for DBKNS studies, was proven as one of the first output

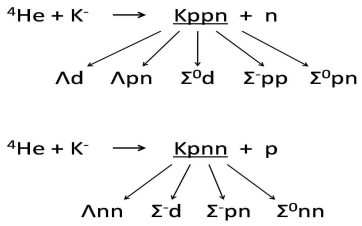

Figure 2: Kaonic tribaryonic clusters formation and decay channels in K^- stopped in ^{4}He processes.

of the fruitful collaboration between the AMADEUS and the KLOE groups. Preliminary results of the analysis of a sample of the 2005 KLOE data searching for hadronic interactions of the K^- in the ^{4}He gas of the KLOE Drift Chambers [16] has been presented, showing the capabilities in performing nuclear physics measurements with the KLOE detector. An excellent invariant mass resolution, FWHM $\sim$ 1 MeV/c^2, has been found in the reconstruction of the decay of $\Lambda(1116)$ hyperon into proton and negative pion. Also a good performance of KLOE setup detecting neutrons has been recently proved by kloNe group [17].

After this first phase, a second phase of AMADEUS will follow, with an upgraded setup and with a higher luminosity request, where DBKNS complete and systematic spectroscopy will be performed also in heavier targets as Li, B, Be and C. An inner tracker should be eventually installed inside the DC of KLOE (two possible solutions are being considered, either cylindrical GEM detectors or a TPC-GEM combination, see right part of Fig. 1) in order either to reduce the background and/or to perform more refined (better resolution) dedicated measurements. With this second phase the complete scientific program of AMADEUS will be covered:

- determination of binding energies, decay widths and quantum numbers of all states, including excited ones,
- measurement of the spin-orbit interaction,
- determination of partial widths of kaonic nuclear states by observation of all decay channels,
- Dalitz analysis of the 3-body decays of the kaonic nuclei will reflect the

momentum wave functions and the angular momentum transfer, so one can study the size of kaonic nuclei and assign spin and parity to the decaying state,

- obtain, as a by-product, information concerning the multi-nucleon absorption mode.

AMADEUS plans as well to perform other more "classical" measurements, by no mean less important. Such measurements are being longly awaited and are extremly important in hadronic physics and in astrophysics.

References

1. AMADEUS Letter of Intent, **http://www.lnf.infn.it/esperimenti/siddharta/LOI_AMADEUS_March2006.pdf**
2. S. Wycech, Nucl. Phys. A **450**, 399c (1986).
3. Y. Akaishi and T. Yamazaki, Phys. Rev. C **65**, 044005 (2002).
4. W. Weise, **nucl-th/0701035**.
5. T. Suzuki et al., Phys. Lett. B **597**, 263 (2004).
6. M. Iwasaki et al., arXiv: **nucl-ex/0310018v2**.
7. M. Iwasaki, plenary talk **HYP06**, Mainz (2006).
8. M. Agnello et al., Phys. Rev. Lett. **94**, 212303 (2005).
9. N. Herrmann, Proceedings **EXA05** (2006).
10. T. Kishimoto et al., Nucl. Phys. A **754**, 383c (2005).
11. G. Bendiscioli et al., Nucl. Phys. A **789**, 222 (2007).
12. P. Aslanyan in Miniproceedings of the International Workshop on Exotic Hadronic Atoms, Trento, **hep-ph/0610201** (2006).
13. http://www.lnf.infn.it/acceleratori/upgradeslide/20060606_drago.pdf.
14. M. Adinolfi et al., Nucl. Instr. Meth. A **488**, 51-73 (2002).
15. The AMADEUS collaboration, LNF preprint, **LNF07/24(IR)** (2007).
16. M. Cargnelli, C. Petrascu, O. Vazquez Doce and KLOE K-charged group, KLOE memo **337** (2007); presentation on 35th LNF Scientific Committee, **http://www.lnf.infn.it/committee/talks/35CurceanuDoce.ppt**.
17. M. Anelli et al., Nucl. Instr. Meth. A **581**, 368 (2007).

FUTURE FACILITIES

Frascati Physics Series Vol. XLVI (2007), pp. 1457–1466
HADRON07: XII Int. Conf. on Hadron Spectroscopy – Frascati, October 8-13, 2007
Future Facilities

FUTURE PROSPECTS ON HIGH RESOLUTION HYPERNUCLEAR γ-RAY SPECTROSCOPY AT FRASCATI *

E. Botta
Dipartimento di Fisica Sperimentale, Universita' degli Studi di Torino e Istituto Nazionale di Fisica Nucleare, Sezione di Torino
Via P. Giuria 1, 10125 Torino, Italy
A. Feliciello
Istituto Nazionale di Fisica Nucleare, Sezione di Torino
Via P. Giuria 1, 10125 Torino, Italy

Abstract

The DAΦNE e^+e^- collider, the Φ-factory operating at present at the INFN National Laboratories of Frascati (Italy), is the unconventional playground where the FINUDA Collaboration is successfully carrying on its hypernuclear study program. In view of a possible machine luminosity upgrade, it has been proposed to improve the present FINUDA spectrometer with γ-ray detection capability: a powerful and complete experimental setup dedicated to hypernuclear physics would be realized.

1 Introduction

Strangeness is playing a more and more important rôle in modern physics. Several interesting phenomena are in fact induced by or tagged by the detection

* The activity has been partially granted by Progetti di Ricerca di Interesse Nazionale 2005 of the Italian Government (Hypergamma program).

of strange particles. The central point of the strangeness nuclear physics is the insertion of an explicit strangeness content into a nucleus. The investigation of such an exotic system called *hypernucleus*, where one or more *nucleons* have been replaced by one or more *hyperons*, allows to address a rich spectrum of physics topics ranging from genuine nuclear physics to particle physics.

Spectroscopy of S = -1 hypernuclei (single Λ-hypernuclei) represents the only practical way to access information about the *hyperon-nucleon* interaction at low energy that is a fundamental ingredient for a complete understanding of the baryon-baryon force in the SU(3) framework.

On the other side the observation of the Λ-hypernucleus decay modes offers the unique opportunity to look at the four baryon, strangeness changing, weak vertex. In addition the determination of the relative weights of the different decay channels represented a long standing puzzle. Complete reviews about Λ-hypernucleus spectroscopy and decay can be found in Refs. [1)].

Finally, the *hyperon* can be considered like a probe testing the nuclear structure to put in evidence its possible modifications, but it is also possible to study how the nuclear medium affects the properties of the embedded strange particles.

2 Physics motivations

Despite the strong interest and the great discovery potential of strange nuclear physics, the level of understanding of the field is not completely satisfactory. One of the reasons is represented by the limitations of the experimental apparatuses as far as energy resolution and angular acceptance are concerned.

γ-ray spectroscopy is a consolidated technique that allowed to get a deep insight into the nuclear structure. Unfortunately this methodology could not be applied to hypernuclear physics for long time: low beam intensity and high level of contaminating hadronic particles prevented the use of High Purity Germanium detectors (HPGe). Only in the last few years the improvement of the beam characteristics allowed to use HPGe crystals and to make a spectacular step forward in hypernuclear physics, pushing down the energy resolution on the low-lying hypernuclear levels from $\sim$ 1 MeV [2)] to $\sim$ 2 keV [3)].

These precise measurements allowed for the first time to determine the strength of the spin-dependent terms of the phenomenological expression for the $\Lambda\mathcal{N}$ interaction potential [4)].

In addition a wide spectrum of new physics topics could be now addressed as well. Of particular interest is the measurement of the possible energy level splitting due to the $\Lambda\mathcal{N}$ spin orbit interaction, in order to check whether this effect is really much weaker than in the $\mathcal{N}\mathcal{N}$ case [5].
Moreover the presence of the Λ *hyperon* can induce several effects on the host nucleus (changes of both size and shape, modification of cluster structure, manifestation on new symmetries or changes of *nucleon* collective motions). These phenomena are observable by looking at the value of the reduced probability of electric quadrupole γ-ray transitions ($B(E2)$). One of the most spectacular effects, observed so far in what is called impurity nuclear physics, is the shrinking of the nucleus core. In the case of ${}^{7}_{\Lambda}Li$ a reduction of about 20% with respect to the ${}^{6}Li$ radius has been inferred [6]. Such a behavior can be considered a precursor of matter condensation induced by strange particles. In addition, this so called glue-like rôle of the Λ makes possible to search for neutron rich Λ-hypernuclei, that is for nuclear systems with really extreme neutron to proton ratios [7]. As far as the medium effect is concerned, the determination of the g-factor of a Λ particle embedded into a nucleus can be done through precise measurements of the reduced transition probability of the Λ spin-flip $M1$ transitions ($B(M1)$).

However even large and sophisticated HPGe detector arrays are not sufficient in itself to carry on exhaustive and definitive hypernuclear physics studies. This is essentially due to the fact that the high excited energy region of the hypernucleus spectrum cannot be explored by means of γ-ray spectroscopy. As a matter of fact all the experiments based on this new approach foresee a combined use of both γ-ray detectors and magnetic spectrometers [3, 8], but the two kind of devices are just put one in front of the other, without a real integration in a single apparatus.

This consideration led to propose a modification of the FINUDA spectrometer in order to setup a real complete and unique apparatus dedicated to hypernuclear physics [9].

3 The FINUDA spectrometer upgrading

At DAΦNEsingle Λ-hypernuclei are produced by stopping in very thin nuclear targets the very low-energy K^- following the main ϕ resonance decay, through

the reaction:

$$K^-_{stop} + {}^A Z \rightarrow {}^A_\Lambda Z + \pi^-. \quad (1)$$

The outgoing, low-momentum ($\leq 270\ MeV/c$), π^- are detected by the FINUDA apparatus. The various sub-detectors are housed inside the coil of a superconducting solenoid, providing a highly homogeneous magnetic field of 1.0 T. The detector features a momentum resolution from 0.5 to 1.5% fwhm, depending on the mass and momentum of the charged particles, an angular acceptance close to 2π sr and good particle identification. It is composed of three parts from the beam axis outward: the *interaction/target region* composed of a 12-thin-slab scintillator array ($\sigma \sim 250$ ps), an octagonal array of silicon microstrip ($\sigma \sim 30\mu$m) and the target system, the *external tracking device* composed of a decagonal array of silicon microstrip ($\sigma \sim 30\mu$m), two octagonal arrays of $He - iC_4H_{10}$ filled low mass drift chambers ($\sigma \sim 150\mu$m) and a stereo straw tube detector ($\sigma \sim 150\mu$m) and, finally, the *external time of flight detector*, a barrel of 72 scintillator slabs ($\sigma \sim 350$ ps). The whole tracker is immersed in a He atmosphere to minimize the Coulomb multiple scattering contribution to the momentum resolution for low momentum charged particles. Further details about the FINUDA experiment and its physics program can be found in Refs. [10]. The general philosophy underlaying the FINUDA upgrade is to add to the present apparatus the capability of detecting γ-rays emitted during the deexcitation of the produced hypernuclei, without renouncing to the key features that make FINUDA one of the most complete and performing magnetic spectrometer ever dedicated to hypernuclear physics studies. In order to fulfill this ambitious goal one has several experimental challenges to cope with.

The first, central question to be answered is whether encapsulated HPGe crystals can be safely operated for long periods immersed into a strong (≥ 1 T) magnetic field. Up to now these devices have been only seldomly used in such conditions and their behavior was not well known. The main concern is represented by a possible enhancement of the Penning effect due to the longer path of electrons in the magnetic field: their interaction with the residual gas within the capsule may cause secondary ionization, producing eventually fatal discharges. Another question is whether some of the components of the standard readout electronics coupled to γ-ray detectors, carrying quite large currents, can suffer by the Hall effect. The increased drift path of charge carriers

inside the crystal has an important impact also on the charge collection time, on the rise time of the output signal and, in the end, on the energy resolution of HPGe detectors. Trapping and detrapping phenomena can contribute to this effect as well. Being the recent progress in hypernuclear studies essentially determined just by the excellent energy resolution of such detectors, the second step was to understand to what extent their performance is affected.

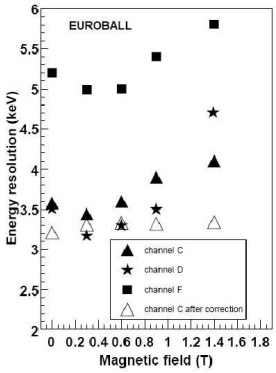

Figure 1: Measured energy resolution (FWHM) of the Euroball cluster detector operated into magnetic field for the ^{60}Co 1332 keV γ-line (from Ref. [13]).

In order to look for a quantitative answer to these two issues, an extensive R&D project has been carried out within a Joint Research Activity (I3HP-JRA6/HyperGamma) of the European Union Sixth Framework Programme (FP6). Two existing γ-ray detectors have been put inside a magnetic field up to 1.6 T, almost parallel to the drift electric field (tilt angle of 0 rad): the Versatile and Efficient GAmma (VEGA) [11] super-segmented-clover detector and the Euroball Cluster detector [12]. The experimental results obtained so far have been summarized in Ref. [13]. Fig.1 shows that the energy resolution of the EUROBALL detector is nicely preserved up to 1 T, that actually is the nominal magnetic field value of the FINUDA spectrometer; similar results have been reported for the VEGA detector.

Being the FINUDA experiment run at a collider, the apparatus must be operated for periods usually longer than 6 months without possibility of intervention on it. In order to be prepared to use HPGe detectors in such unusual conditions, a further long duration test devoted to monitor eventual, long-term

effects of magnetic field is currently being carried on. After approximately one year of operation neither energy resolution worsening nor efficiency losses have been observed.

Another challenging aspect of this project is the use of HPGe crystals, which are intrinsically slow detectors, in an experiment with high counting-rates. At DAΦNE the main source of physical electromagnetic background is represented by *photons* resulting from decay of π^0's, following the ϕ resonance disintegration chain. Its intensity depends of course on the DAΦNE luminosity: at 1.0×10^{32} cm^{-2} s^{-1} we can expect a rate of few hundred Hz, to be increased by the contribution of the machine induced background.

A way to overtake the problem of pile-up events relies on the development of a dedicated electronics (pre-amplifier and spectroscopic amplifier) [1)]. A possible alternative strategy is represented by the careful analysis of the shape of the signal picked up at the exit of the preamplifier and recorded by means of a fast flash ADC (FADC).

Due to the type of electronic currently associated with the Euroball-like encapsulated HPGe crystals, that is resistor reset preamplifier, the Hyper-Gamma Collaboration has investigated the performance of the Moving Window Deconvolution (MWD) algorithm [14)]. The leading idea is to attempt to process the preamplifier output through several MWD filters with different duration lengths, running simultaneously (Multi MWD, MMWD) to choose on-line the most suitable filter length event by event in order to achieve the maximum energy resolution. Some preliminary tests were performed in order to understand to what extent the proposed signal processing scheme is effective. An Euroball type HPGe crystal was exposed to ^{22}Na, ^{57}Co and ^{60}Co γ-ray sources in a series of measurements with 1.5, 34 and 110 kHz counting rates. The first results obtained for the ^{60}Co 1332 keV γ-line are very encouraging [15)].

Once clarified these fundamental points, the HyperGamma Collaboration started to study the mechanical integration of a HPGe crystal array within a collider-type apparatus like FINUDA. It is worthwhile to remind that the very exciting results achieved by exploiting the γ-ray spectroscopy technique [3)], were obtained by installing the HPGe detector array upstream a single arm magnetic spectrometer. The same geometrical configuration will be implemented also for the new experimental E13 setup at J-PARC [8)]. This "serial" coupling is by far simpler than the insertion of a new sub-detector in the heart

of a complex spectrometer, not originally designed to host these additional devices. So the FINUDA simulation program was extensively used to carefully model every detail in order to achieve the best possible detector performance.

The definitive breakthrough was determined by the idea of abandoning the traditional way of cooling the HPGe crystals by quite large liquid Nitrogen dewars. Very recently, different models of electromechanical refrigerator have been made available on the market, thus allowing a more compact and flexible arrangements of HPGe crystal arrays. After some tests on the cooling effectiveness of these new devices, it has been possible to design a new compact cryostat, capable of hosting a row of three Euroball-like HPGe capsules. This way the additional sub-detector essentially consists of an arm supporting the "linear" cryostat that mechanically fits in the gap between the two FINUDA drift chamber arrays. No original components need to be removed and, moreover, the integrity of the chamber containing the He atmosphere is completely preserved. Figure 2 shows a sketch of the final FINUDA setup proposed for the hypernuclear γ-ray spectroscopy program at DAΦNE. The fraction of the solid angle coverage lost is of $\sim$18%. The reduced dimensions of the described

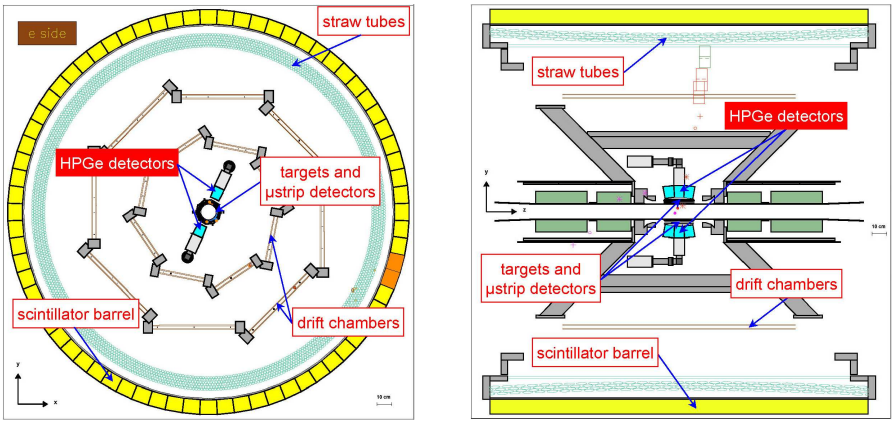

Figure 2: Schematic frontal (left) and lateral (right) cross sections of the modified FINUDA apparatus.

arrangement from one side and the negligible level of hadronic background in DAΦNE on the other will allow to place the γ-ray detectors really close to the nuclear targets. On the contrary, at hadron machines, in order to minimize

the radiation damage on the HPGe crystals, it is mandatory to install the γ-ray detectors relatively away ($\sim$15 cm) from the beam line and then from the target where the hypernuclei are created. In addition the linear extension of the triple γ-ray detector array has been designed in order to exactly match the longitudinal dimension of the FINUDA nuclear targets, covering an angular region $\Delta\Omega \sim 12\%$ of 4π sr. This way it has been possible to maximize the overall spectrometer performance both in terms of angular acceptance and efficiency. A comparison between the proposed E13 and the FINUDA experimental apparatuses allows to understand why the two approaches would be complementary. The solution adopted for the next generation experiment at J-PARC privileges the γ-ray detection: the Hyperball-J detector, a renewed and improved version of the former Hyperball HPGe array , surrounds the interaction target, with a solid angle coverage $\Delta\Omega = 27$–35% of 4π sr, while the acceptance for charged particles which follow the hypernucleus creation is very limited ($\Delta\Omega \sim$110 msr of the SKS spectrometer).

The current DAΦNE peak luminosity value is 1.6×10^{32} cm^{-2} s^{-1} and $\sim$9 pb^{-1} per day were delivered on average to the FINUDA experiment. Very recently an upgrading plan has been presented [16]. It foresees a partial machine component replacement and a new design for the interaction regions, characterized by a larger beam crossing angle. Thanks to the implementation of the "crab waist" collision scheme, it should be possible to reach a top luminosity value of $\sim 0.5 \times 10^{33}$ cm^{-2} s^{-1} (and, hopefully, of 10^{33} cm^{-2} s^{-1}) by the end of year 2007.

On the basis of what it has been experimentally observed during the previous FINUDA data taking periods, it is known that an integrated luminosity of 500 pb^{-1} corresponds to $\sim 2.5 \times 10^4$ detected hypernuclear events from the ${}^{12}_{\Lambda}$C ground state. By taking into account the FINUDA reduced acceptance ($\sim$82% of the present one), the fraction of solid angle covered by two arms, carrying a triple γ-ray detector array each, ($\sim$12% of 4π sr) and the estimated HPGe crystal efficiency ($\sim$10%) one can infer that, with a similar integrated luminosity, it will be possible to observe $\sim 1.5 \times 10^3$ γ-ray transitions. This number nicely agrees with the expectation for the J-PARC hypernuclear experiments with stopped K^- [17].

4 Conclusions

The HyperGamma Collaboration successfully accomplished its commitments. Following the encouraging results obtained by JRA6, a new R&D activity started, granted by the PRIN 2005 Project of the Italian Government. The main aim is to extend the previous measurements, operating HPGe detectors in stronger magnetic fields, even tilted with respect to the drift electric field. At this moment a complete set of measurements has been performed at the SOLE magnet of the INFN Laboratori Nazionali del Sud (Catania, Italy), with a coaxial n-type crystal in a set-up allowing to vary the tilt angle from $\pi/2$ rad, the worst situation for the Lorentz force influence, to $\sim \pi/4$ rad. Magnetic field up to 2.5 T has been used.

References

1. O. Hashimoto and H. Tamura, *Progr. Part. Nucl. Phys.* **57** (2006) 564.
   H.Outa in *Proc. of Intern. School of Physics "Enrico Fermi"*, Course CLVIII, Hadron Physics, Varenna (CO), Italy, 22 June - 2 July, 2004, Eds. T. Bressani, U. Wiedner and A. Filippi (IOS Press, Amsterdam, 2005), p. 219-258.

2. M. Agnello *et al.*, *Phys. Lett. B* **622** (2005) 35.

3. H. Tamura *et al.*, *Nucl. Phys. A* **691** (2001) 86c.

4. R.H. Dalitz and A. Gal, *Ann. Phys.* **116** (1978) 67.
   D.J. Millener *et al.*, *Phys. Rev. C* **31** (1985) 499.
   D.J. Millener, *Nucl. Phys. A* **754** (2005) 48c.

5. T. Nagae, *Nucl. Phys. A* **691** (2001) 76c.
   N. Kaiser and W. Weise, *Phys. Rev. C* **71** (2005) 015203.

6. K. Tanida *et al.*, *Phys. Rev. Lett.* **86** (2001) 1982.

7. L. Majling, *Nucl. Phys. A* **585** (1995) 211.
   M. Agnello *et al.*, *Phys. Lett. B* **640** (2006) 145.

8. Y. Fujii *et al.*, *Gamma-ray spectroscopy of light hypernuclei*, Proposal for J-PARC 50 GeV Proton Synchrotron (KEK, Tsukuba 2006) 1.

9. A. Feliciello, *Proc. of Workshop on e^+e^- in the 1–2 GeV range: physics and accelerators prospects*, Alghero (SS), Italy, September 10–13, 2003, eConf C0309101: FRWP001.
T. Bressani, E. Botta, A. Feliciello and V. Paticchio, Nucl. Phys. A **754** (2005) 410c.

10. The FINUDA Collaboration, *FINUDA: a detector for nuclear physics at DAΦNE*, LNF-93/021 (SIS-LNF, Frascati 1993) 1
The FINUDA Collaboration, *FINUDA technical report*, LNF-95/024 (SIS-LNF, Frascati 1995) 1

11. J. Gerl *et al.*, *VEGA: a proposal for Versatile and Efficient GAmma-detectors*, GSI Report (GSI, Darmstadt 1998) 1.

12. J. Eberth *et al.*, *Nucl. Instr. Meth. A* **369** (1996) 135.

13. A. Sanchez Lorente *et al.*, *Nucl. Instr. Meth. A* **573** (2007) 410.

14. A. Georgiev and W. Gast, *IEEE Trans. Nucl. Sci.* **NS-40** (1993) 770.
J. Stein *et al.*, *Nucl. Instr. Meth. B* **113** (1994) 141.
A. Georgiev, W. Gast and R.M. Lieder, *IEEE Trans. Nucl. Sci.* **NS-41** (1994) 1116.

15. M. Kavatsyuk *et al.*, GSI Scientific Report 2006, GSI Darmstadt (2007)

16. P. Raimondi *et al.*, Proc. of Particle Accelerator Conference (PAC 07), Albuquerque, New Mexico, June 25-29, 2007, p. 1469.

17. K. Imai *et al.*, *New Generation Spectroscopy of Hadron Many-Body Systems with Strangeness S = -2 and -1*, Letter of Intent (KEK, Tsukuba 2002) 1.

Frascati Physics Series Vol. XLVI (2007), pp. 1467–1475
HADRON07: XII Int. Conf. on Hadron Spectroscopy – Frascati, October 8-13, 2007
Future Facilities

THE PHYSICS CASE OF KLOE-2

P. Moskal for the KLOE-2 Collaboration
Institute of Physics, Jagellonian University, Cracow, Poland

Abstract

Selected issues of the research programme for continuing the experimentation by means of the KLOE apparatus equipped with the inner tracker and the $\gamma\gamma$ taggers at the DAΦNE e^+e^- collider upgraded in luminosity and energy are briefly presented.

1 Introduction

The Accelerator Division of the INFN Frascati Laboratory is currently commissioning the new e^+e^- interaction region, based on the *crabbed waist* scheme [5)], designed in order to increase the collider luminosity up to an order of magnitude, from $\sim 10^{32}$ cm^{-1}s^{-2} to $\sim 10^{33}$ cm^{-1}s^{-2}. In parallel the KLOE detection facility is being upgraded by new components in order to improve its tracking and clustering capabilities as well as in order to tag $\gamma\gamma$ fusion processes. For the detailed description of the detector upgrade the interested reader is referred to the proceedings of D. Domenici [1)]. Hereafter we will concentrate on some of the physics aspects of the KLOE-2 research programme which in part will be a natural continuation of the measurements of the kaon properties conducted with unique precision by the KLOE collaboration[1].

[1]To taste the flavor of the copious physics results achieved by KLOE we refer the reader to the recent reviews [2), 3), 4)].

The basic motivation of the KLOE-2 experiment is the test of fundamental symmetries and Quantum Mechanics coherence of the neutral kaon system, and the search for phenomena beyond the Standard Model. Thanks to the luminosity and energy upgrade of DAΦNE , as well as the planned installation of new detectors, the successor of KLOE, the KLOE-2 experiment, will be able to improve the accuracy of the measurement of the K_S mesons and to study the time evolution of the entangled pairs of neutral kaons with an unprecedented precision. The KLOE-2 group aims also at the significant improvement of the sensitivity of the tests of the discrete symmetries in the decays of K, η and η' mesons beyond the presently achieved limits. In some cases like e.g. the tests of P, C, or CP symmetries an improvement by two orders of magnitude is expected with an integrated luminosity of 50 fb^{-1} to be achieved within 3-4 years of data taking. Among other issues we intend also to test lepton universality, search for the quantum decoherence effects in the evolution of the entangled KK pairs originating from the decays of the ϕ meson, to study the structure of the scalar mesons, and search for the univocal signal from the σ meson produced in the fusion of gamma quanta. We intend also to measure the hadronic cross sections in the energy range from 1 to 2.5 GeV with the precision of 1% which is needed for the evaluation of the contribution of the hadron vacuum polarisation to the muon magnetic anomaly a_μ and to the variation of the fine structure constant with the momentum transfer.

In the rest of the report, due to the space limitation, we will give account of only a few of the above mentioned physics aspects. For a more comprehensive description of the vast KLOE-2 physics programme the interested reader is referred to the Expression of Interest for the continuation of the experimentation with the KLOE apparatus at DAΦNE [6].

2 Quantum Interferometry and CPT tests

CPT invariance is a fundamental theorem in the framework of quantum field theory (QFT), as a consequence of Lorenz invariance, unitarity and locality. In several quantum gravity (QG) models, however, CPT can be violated via some mechanism which can also violate standard Quantum Mechanics (QM). In a recent review Bernabeu, Ellis, Mavromatos, Nanopoulos and Papavassiliou [7] discuss the theoretical motivations for possible CPT violations and the unique role played by the entagled neutral kaon pairs produced at DAΦNE in precision tests of the CPT symmetry.

As an example of this incredible precision reachable with neutral kaons, we take the model by Ellis, Hagelin, Nanopoulos and Srednicki (EHNS) which introduces three CPT and QM-violating real parameters α, β and γ [8]. On phenomenological grounds, they are expected to be $O(m_K^2/M_{Pl})$ $\sim 2\times 10^{-20}$GeV

at most, since $M_{Pl} \sim 10^{19}$ GeV, the Plank mass. Interestingly enough, this model give rise to observable effects in the behaviour of entagled neutral meson systems, as shown also in [9], that can be experimentally tested.

KLOE has already published competitive results on these issues [10], based on a statistics of $\sim$400 pb^{-1}, and is now on the way of updating them using the full data sample. The analysis makes use of correlated $K_L^0 - K_S^0$ pairs, by measuring the relative distance of their decay point into two charged pions.

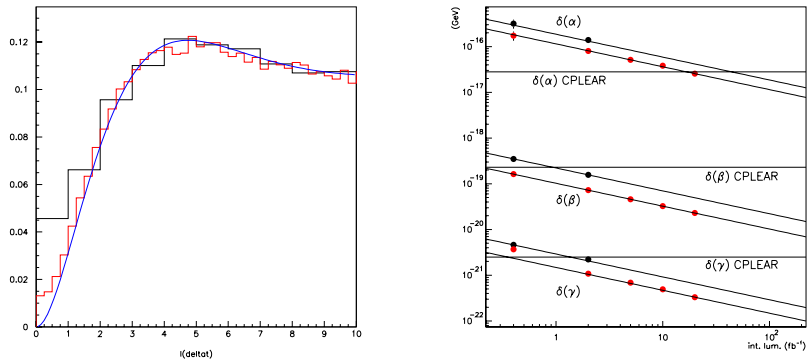

Figure 1: *(left) Distribution of the time interval between the decays of kaons for the* $\phi \to K_S K_L \to \pi^+\pi^-\pi^+\pi^-$ *events. Result obtained with the present KLOE resolution* $\sigma_{\Delta t} \approx 0.9\ \tau_S$ *is compared with the distribution expected by KLOE-2 with* $\sigma_{\Delta t} \approx 0.25\,\tau_S$*, and with the ideal case (solid line). (right) Limits on the CPT violating parameters* α*,* β*, and* γ *obtainable by KLOE-2 as a function of the integrated luminosity.*

Figure 1 shows results of the feasibility test of the studies of the possible decoherence phenomena of the entangled neutral kaon pairs conducted by the KLOE group and the potential limits that can be obtained by KLOE-2 on α, β, and γ as a function of the integrated luminosity. Results are presented for a detector both with and without the insertion of an inner tracker with vertex resolution of 0.25 τ_S (to be compared with the present KLOE vertex resolution, 0.9 τ_S). In the figure are also given results from CPLEAR [11]. Without entering too much into the details, it is clear that with a reasonable integrated luminosity, KLOE-2 can set the best limits on these parameters. Moreover, the more interesting region below the Plank limit can be explored also for the parameter β as soon as $\int Ldt \geq$ 5-10 fb^{-1}.

3 CP Violation

The study of CP violation in kaon decays has been the main motivation for the construction of KLOE and DAΦNE. The aimed precision on $\mathrm{Re}\,(\epsilon'/\epsilon)$ of a few parts in ten thousand was not achieved because of statistical limitation. At the new machine, this can be obtained both via the measurement of the four separate branching ratios and via interferometry (which allows also the measurement of $\mathrm{Im}\,(\epsilon'/\epsilon)$).

Concerning the first technique, it is important to remember that KLOE has already measured the ratio of the charged to neutral two-pion decays of the K_S^0 with a precision of 0.2% [12]. Moreover, $\mathrm{BR}(K_L^0 \to \pi^+\pi^-)$ has been measured with a precision of 1%, using ∼1/5 of the acquired statistics [13]. Taking into account the 1/6 factor in the double ratio formula, the key missing ingredient for the measurement of $\mathrm{Re}\,(\epsilon'/\epsilon)$ is $\mathrm{BR}(K_L^0 \to \pi^0\pi^0)$ for which one can obtain an accuracy of few per mil with an integral luminosity ≥10 fb^{-1}.

A direct consequence of CP violation in the kaon sector is the prediction $\mathrm{BR}(K_S^0 \to 3\pi^0) \sim 2 \times 10^{-9}$. This decay has however never been observed. The best limit comes from KLOE $\mathrm{BR}(K_S^0 \to 3\pi^0) < 1.2 \times 10^{-7}$, based on a statistics of ∼400 pb^{-1} [14]. The KLOE-2 with the integrated luminosity of 50 fb^{-1} can reduce the upper limit by a factor of 100 or perhaps even observe the signal for the first time.

As far as the η meson is concerned it has been argued [15] that some unconventional CP-violation mechanism could induce an angular asymmetry of the production plane of the e^+e^- pair with respect to that of the $\pi^+\pi^-$ pair, for the decay $\eta \to e^+e^-\pi^+\pi^-$. This asymmetry, A_η, can be as large as ∼1%, while in the Standard Model it is negligible. KLOE has started an analysis of this decay channel, with very promising results. A signal of several hundreds events is clearly seen in a subsample of about 600 pb^{-1}, to be compared with the two previous measurements, which are based on 7 and 16 events [16]. With the present KLOE statistics a sensitivity on A_η of order few per cent can be reached. It has to be underlined that, due to the low average momentum of the four tracks, acceptance in this case is a key issue. The insertion of the inner tracker would therefore be extremely beneficial, and would allow us to reach a sensitivity down to the per mil level.

4 Tests of P and C symmetries

P and C are believed to be exact symmetries of strong and electromagnetic interactions. Tests of their validity have been published by KLOE by setting the limits $\mathrm{BR}(\eta \to \pi^+\pi^-) < 1.3 \times 10^{-5}$ and $\mathrm{BR}(\eta \to 3\gamma) < 1.6 \times 10^{-5}$, on the

basis of $\sim$400 pb^{-1} of data [17], [18]. The previous limits can be taken down to the 10^{-7} level, which would be among the best limits on P and C conservation ever set in elementary particle decays [19]. It is worth noting that for the first decay channel the experimental improvements are expected to come mainly from the increase in luminosity, while in the second case an additional handle can come from the insertion of the low-theta gamma vetos. Figure 2 presents the capability of the KLOE detector for the clear identification of the η meson via the detection of the monoenergetic photons from the $\phi \to \eta\gamma$ decay.

5 Precise measurement of V_{us}

In the recent years, flavor physics and in particular the precise determination of the CKM matrix elements has received great attention. Deviations from unitarity of the CKM matrix would signal presence of physics beyond the Standard Model. The test of unitarity of the first row of the CKM matrix reads:

$$|V_{ud}|^2 + |V_{us}|^2 + |V_{ub}|^2 = (0.9737 \pm 0.0003)^2 + (0.2255 \pm 0.0013)^2 + 0(10^{-5}) \quad (1)$$

where the value of V_{us} is largely dominated by KLOE results. KLOE is in fact the experiment that has provided the most experimental inputs for this determination: branching ratios, lifetimes, form factors [20], [21].

From the inspection of the above equation, it is clear that a more precise test of unitarity requires a measurement of V_{us} at the per mil level. At present the largest uncertainty on V_{us} comes from the error on the theoretical calculation of $f_+(0)$, the kaon form factor at zero momentum transfer, which is known with a precision of 0.5% . Recent progress of lattice QCD, however, suggests the possibility that this error can be soon reduced by a considerable factor, moving therefore the attention to the experimental side.

KLOE-2 is natural for performing these precision experiments. For instance, we could easily improve on the measurement of the K^0_L and $K^\pm$ lifetimes. Also, we can precisely measure the K^0_S semileptonic decays. KLOE has published the best determination of this branching ratio [21] BR$(K^0_S \to \pi e\nu) = (7.046 \pm 0.091) \cdot 10^{-4}$, based on 400 pb^{-1} of data. Most of the systematics scale with statistics, thus one can expect this branching ratio to be determined with a precision approximately scaling with the square root of luminosity, reaching the 0.2% level at around 20 fb^{-1}. The advantage here, with respect to the use of the more copious semileptonic K^0_L decays, is that the K^0_S lifetime is already known with a precision of a few parts in ten thousands.

6 Lepton Flavor Violation

In the Standard Model, the ratio $R_K = \Gamma(K_{e2})/\Gamma(K_{\mu 2})$ can be calculated with great accuracy. We have

$$R_K^{SM} = (2.472 \pm 0.001) \times 10^{-5} \quad (2)$$

In a SUSY framework, however, violations of lepton universality can be expected in K_{l2} decays, inducing deviations from the prediction above at the level of up to few per mil [22].

Experimental knowledge of R_K has been poor so far. Recently, however, the NA48/2 Collaboration has presented results based on two separate samples of about 4000 observed K_{e2} events each. The group continues the studies with the goal of obtaining a precision on R_K of few parts in a thousand. Also KLOE has presented a preliminary result, based on about 8000 events, obtained analyzing a large fraction of the acquired statistics. Both the KLOE and the NA48/2 result confirm the SM at the percent level.

The KLOE result demonstrates the capability of KLOE-2 of reaching a precision comparable to the one foreseen for NA48/2, with an integrated luminosity of $\geq$20 fb^{-1}. This is extremely relevant, since the two experiments have totally different systematics.

7 Low energy QCD

There still exists no analytical method for the description of QCD at low energy. However, new techinques have been developed to systematically perform QCD inspired calculations on the strong and electromagnetic interactions of the pseudoscalar meson, in the framework of an effective theory, the Chiral Perturbation Theory (ChPT) [23]. Such a theory is based on a perturbative expansion in terms of the momenta of the involved mesons. The price to pay is the rapid increase in the number of free parameters, to be determined experimentally, as the perturbative order increases.

At present, calculations are being done up to the order p^4, and the question arises on what can be the contribution coming from the next-to leading order corrections. This issue can be addressed experimentally, by precision measurements of several K, η and η' decay channels, most of which are at present controversial. For instance, KLOE has measured BR($K_S^0 \to \gamma\gamma$) = $(2.27 \pm 0.13^{+0.03}_{-0.04}) \times 10^{-6}$, a result which differs by more than three sigmas from NA48 and is in perfect agreement with $O(p^4)$ ChPT expectations (see figure 2).

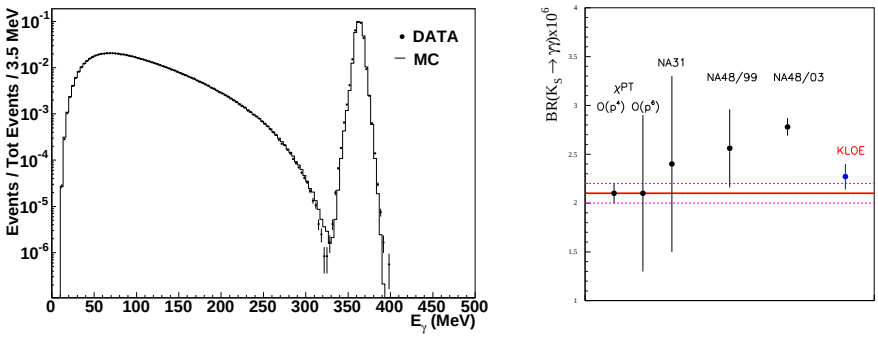

Figure 2: *(left) Photon spectrum for events* $\phi \to \eta\gamma \to \pi^0\pi^0\pi^0\gamma$*, showing the 363-MeV tagging photon well separated from those from* π^0 *decay. (right) Experimental results from KLOE and NA48 for the decay* $K_S^0 \to \gamma\gamma$*. The two measurements are in disagreement by more than 3 sigmas. KLOE is in agreement with* $O(p^4)$ *ChPT calculations, while NA48 suggests a relevant contribution from* $O(p^6)$ *terms*

However, this measurement is limited by statistics and by the presence of a large background of $K_S^0 \to 2\pi^0$ events with two lost photons. A large improvement on background rejection (almost a factor three) is expected by building a dedicated photon-veto detector in the low-θ region, down to 8-10°. Analogous improvement is foreseen also for the $\eta \to \pi^0\gamma\gamma$ decay. This last decay is particularly interesting since in ChPT all lower level contributions are suppressed, so that it provides a window for $O(p^6)$ effects. Recent results from Crystal Ball and KLOE are in good agreement with ChPT, however the $M_{\gamma\gamma}$ spectrum, which is of interest for the theory, has never been measured, because of the large background coming from $\eta \to 3\pi^0$ decays. In this case any sizeable improvement in cluster reconstruction, obtained also by the upgrade of the EmC readout, has an impact on the final sensitivity.

8 Studies on the nature of the Scalar Mesons

The nature of the lowest mass scalar mesons is a long standing question. On the one hand, evidence of the lowest mass states is still experimentally weak, on the other the very important issue of the s-quark content of the f_0 and a_0 is not fully understood. This latter point has been widely investigated by KLOE, using the radiative decays $\phi \to \pi^+\pi^-\gamma, \pi^0\pi^0\gamma, \eta\pi^0\gamma$ [24]. In this case, however, the couplings of the two mesons with kaons (g_{fkk}, g_{akk}), have to be determined

indirectly, using some phenomenological model. A more direct measurement of these two couplings can be done searching for the much rarer decay chains $\phi \to (f_0, a_0)\gamma \to K\overline{K}\gamma$. KLOE has searched for these decays, setting the preliminary limit $B(f_0, a_0 \to K\overline{K}) < 1.8{\times}10^{-8}$. This limit is at the border of where one could reasonably expect to see the signal and start making sensible statements about g_{fkk} and g_{akk}. It is therefore of utmost importance for the KLOE-2 group to increase the data sample for the above mentioned processes.

References

1. D. Domenici *et al*, these proceedings
2. J. Lee-Franzini, P. Franzini, e-Print: hep-ex/0702016
3. C. Bloise, AIP Conf. Proc. **950**, 192 (2007).
4. F. Ambrosino *et al*, e-Print: hep-ex/0603056v2.
5. D. Alesini *et al*, LNF-06/33 (IR), (2006)
6. http://www.lnf.infn.it/lnfadmin/direzione/KLOE2-LoI.pdf
7. J. Bernabeu, J. Ellis, N.E. Mavromatos, D.V. Nanopoulos and J. Papavassiliou, arXiv:hep-ph/0607322, contribution to the DAΦNE Handbook of neutral kaon interferometry (to be published)
8. J. Ellis, J.S. Hagelin, D.V. Nanopoulos, M. Srednicki, Nucl. Phys. B **241**, 381 (1984)
9. P. Huet, M. Peskin, Nucl. Phys. B **434**, 3 (1995)
10. F. Ambrosino *et al* (KLOE Collaboration) Phys. Lett. B **642**, 315 (2006)
11. A. Adler *et al* (CPLEAR Collaboration), Phys. Lett. B **364** 239 (1995)
12. F. Ambrosino *et al* (KLOE Collaboration), Eur. Phys. J. C **48**, 767 (2006)
13. F. Ambrosino *et al* (KLOE Collaboration), Phys. Lett. B **638**, 140 (2006)
14. F. Ambrosino *et al* (KLOE Collaboration), Phys. Lett. B **619**, 61 (2005)
15. Dao-Neng Gao, Mod. Phys. Lett.A **17**, 1583 (2002)
16. R.R. Akhmetshin *et al* (CMD-2 Collaboration), Phys. Lett. B **501**, 191 (2001); Chr. Bargholtz *et al* (WASA Collaboration), Phys. Lett. B **644**, 299 (2006)

17. F. Ambrosino *et al* (KLOE Collaboration), Phys. Lett. B **606**, 276 (2005)

18. A. Aloisio *et al* (KLOE Collaboration), Phys. Lett. B **591**, 49 (2004)

19. M. Yao *et al* (Particle Data Group), Journal of Physics G **33**, 1 (2006)

20. F. Ambrosino *et al* (KLOE Collaboration), Phys. Lett. B **626**, 15 (2005);
F. Ambrosino *et al* (KLOE Collaboration), Phys. Lett. B **632**, 43 (2006);
F. Ambrosino *et al* (KLOE Collaboration), Phys. Lett. B **632**, 76 (2006);
F. Ambrosino *et al* (KLOE Collaboration), Phys. Lett. B **636**, 166 (2006)

21. F. Ambrosino *et al* (KLOE Collaboration), Phys. Lett. B **636**, 173 (2006)

22. A. Masiero, P. Paradisi, R. Petronzio, Phys. Rev. D **74**, 011701(R) (2006)

23. J. Gasser and H. Leutwyler, Annals Phys. **158**, 142 (1984)

24. A. Aloisio *et al* (KLOE Collaboration) Phys. Lett. B **536**, 209 (2002);
F. Ambrosino *et al* (KLOE Collaboration) Phys. Lett. B **634**, 148 (2006)

Frascati Physics Series Vol. XLVI (2007), pp. 1477–1484
HADRON07: XII Int. Conf. on Hadron Spectroscopy – Frascati, October 8-13, 2007
Future Facilities

THE UPGRADE OF THE KLOE DETECTOR:KLOE2

Danilo Domenici
Laboratori Nazionali di Frascati - INFN
Via Enrico Fermi 40, I-00044 Frascati, Italy

Abstract

The KLOE experimental activity is planned to continue at the DAFNE e^+e^- machine upgraded in luminosity and energy. The challenge is to improve the systematics at the level demanded by the increase of the integrated luminosity to 50 fb^{-1} in 3÷4 years of running period.

The vast physics program, mainly focused K_S, η, kaon interferometry, charged kaon decays, requires an optimization of the apparatus for the detection of low energy events produced close to the interaction point.

Besides a normal revision of some subsystem (Drift Chamber, FEE, DAQ, online/offline) the evolution of the KLOE apparatus includes a revisited Calorimeter system (new readout of the main calorimeter, new low angle crystal calorimeter, new QCAL) and the insertions of two new subdetectors, a $\gamma\gamma$ tagger and a new Inner Tracker. An overview of KLOE2 will be given, and the status of the various R&D of the upgrades will be reported.

1 The KLOE detetctor

KLOE [1)] (K LOng Experiment) is a multi-purpose detector optimized for the K_L physics. It is composed by two major subdetectors: a Drift Chamber (DC) and an Electromagnetic Calorimeter (EMC).

The DC is a huge device (2 m radius, 4 m length) operating in a 5.2 kG magnetic field with an ultra-light He/CO_2 gas mixture. The total 55000 stereo wires (field and sensing) provide a momentum resolution $\sigma(p_T)/p_T \simeq 0.4\%$.

The EMC is composed by Lead foils with scintillating fibers embedded. The barrel and the two end-caps account for a 98% coverage of the total solid angle. The main performances are a good energy resolution ($\sigma_E/E \simeq 5.7\%/\sqrt{E(GeV)}$) and an excellent time resolution ($\sigma_T \simeq 54ps/\sqrt{E(GeV)} \oplus 50ps$) needed both by the trigger and by the μ/π discrimination, performed with the time of flight measurement.

2 KLOE2 highlights

KLOE2 will exploit the capability of the upgraded DAFNE e^+e^- machine, that with the new Crab Waist interaction region and other re-designed parts should gain a factor of $5 \div 7$ in luminosity [2]. The test of the accelerator has started in November 2007 and the first results are expected for the spring of 2008. The plan is to deliver a total integrated luminosity of 50 fb^{-1} in a $3 \div 4$ years period of data taking at the Φ peak energy (1020 MeV).

A vast physics program [3] can be successfully accomplished with such a statistics, allowing to reach significant sensitivities for the study of K_S, η, η' rare decays, neutral kaon interferometry and lepton universality test. An option for a run at a higher energy ($1 < \sqrt{s} < 2.5$ GeV) is foreseen as well, to complete a multihadronic cross section measurement and $\gamma\gamma$ physics programs.

The roll-in [4] has been proposed to be performed in two steps: in the Step0 (end of 2008) the present detector will be operated with minimal upgrades for a reliable and efficient run; in the Step1 (end of 2009) all the major hardware upgrades will be implemented, aiming to a long period data taking.

3 KLOE2 hardware upgrades

KLOE2 will operate with the present main subdetectors (DC and EMC) and a reduced magnetic field (3 kG) to enhance the sensitivity for low momentum tracks. Moreover an extensive hardware upgrade plan is foreseen:

- a new readout of the present calorimeter;
- a new low angle crystal calorimeter (C-CAL);

- a new calorimeter around the quadrupoles (Q-CAL);
- a new $\gamma\gamma$ tagger detector;
- a new ultra-light Inner Tracker (IT).

3.1 The upgrade of Calorimeter readout

Two options exist for the upgrade of the Calorimeter readout. The first consists in the replacement of the existing phototubes with multianode, position sensitive devices. This would fairly improve the photon cluster resolution, but would require an enormous installation effort since much of the detector should be dismounted and machined in order to properly couple the new phototubes to the modules. The second option plans to substitute the present phototubes the corresponding new version, with a Quantum Efficiency increased from 20% to 40%. This would lead to a 30% increase in time resolution (from $\sigma_{\mathrm{T}} \simeq 54\mathrm{ps}/\sqrt{\mathrm{E(GeV)}}$ to $\sigma_{\mathrm{T}} \simeq 38\mathrm{ps}/\sqrt{\mathrm{E(GeV)}}$), as well as a 30% increase in spatial resolution along the fiber (z) direction and a slighter increase in energy resolution. Fig.1 shows the resulting improvement in the π/μ discrimination measurement. The HQE option has the unique advantage of avoiding any mechanical intervention on the modules, but such devices are still in a development stage and the availability could represent an issue.

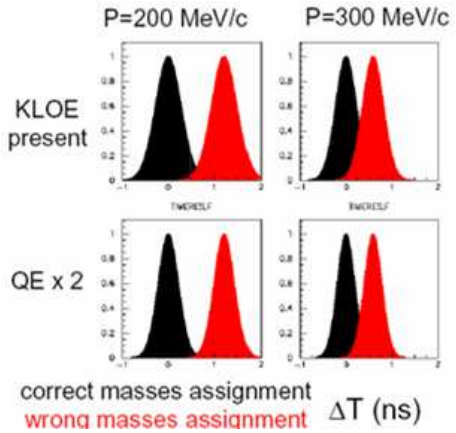

Figure 1: *Improvement in the π/μ discrimination power with a high quantum efficiency for two tracks at 200 and 300 MeV/c. Above the present discrimiation power, below the improvement with the a doubled Quantum Efficiency of the photomultipliers.*

3.2 The low angle crystal calorimeter

The new position of Quad1 improves the acceptance of the EMC from 21° to 18°, thus suggesting not to insert any detector above this angle, to leave the photons be reconstructed by the end-caps. However few calorimeter crystals can be inserted in the region down to 8°, in order to improve the acceptance for photons coming from η and K_S decays. (see Fig. 2). The requirements the CCAL should have in order to profitably work as a photon veto are: a minimum length of 8 X_0; a high light yield; the ability of reconstruct the transverse position; a good time resolution to survive the accidental rate from machine background and separate prompt photons. A valuable choice would be the use of LYSO crystals readout by APD.

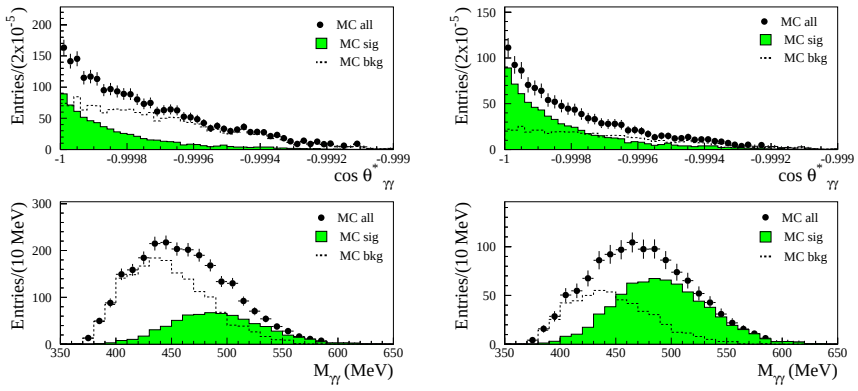

(a) (b)

Figure 2: *a) Reconstruction of angle (above) and invariant mass (below) of a $K_S \to \gamma\gamma$ decay over the $K_S \to \pi^0\pi^0$ background; b) the improvement with the CCAL photon veto.*

3.3 The QCAL

The existing QCAL (Quadrupole Calorimeter) is placed around the Quads and is composed by 15 layers of Lead and scintillating fibers, readout by wavelength shifter (WLS) fibers optically coupled in open air. It was installed to increase the acceptance for photons, mainly for a precision measurement of the impact position of the photons from the K_L decays in the Drift Chamber, for a fine $K_L \to 3\pi^0/K_L \to 2\pi^0$ discrimination. It is no more compatible with the completely revisited geometry of the interaction region and will be dismissed.

Nevertheless the same motivations that drove its operation still suggest to have the new Quads instrumented. The proposed solution is a detector made of square tiles (5x5 cm^2) of plastic scintillator (BC-408) and Lead layers for a total radiation length of 5 X_0. The readout of the single tile is performed with WLS fibers (Kuraray Y11-200) embedded in circular grooves coupled to Silicon Photomultipliers (SiPM).

3.4 The $\gamma\gamma$ tagger

The tagger detector measures the displacement from the main orbit of the scattered e^+e^- events ($e^+e^- \rightarrow e^+e^-\gamma^*\gamma^* \rightarrow e^+e^-X$). The energy of the electrons is measured as well. Two stations are needed in order to obtain information about the whole spectrum of the electrons: one very close to the interaction point, for $E_e < 160$ MeV, and another at a further point, for $160 < E_e < 200$ MeV. Each station of the tagger is composed by modules or micro-strip Silicon detectors and plastic scintillator tiles, readout by conventional photomultiplier tubes.

4 The Inner Tracker

The motivation for the addition of an Inner Tracker in KLOE apparatus is the optimization for the physics coming from the interaction region, namely for a fine reconstruction of the K_S, η and η' decay products.

The detector requirements are:

1. $\sigma_{r\phi} \simeq 200$ μm and $\sigma_Z \simeq 500$ μm spatial resolutions;
2. 5 kHz/cm^2 rate capability;
3. $\sim 1.5\%$ X_0 overall material budget.

Preliminary simulation studies [5] have shown that a detector with such characteristics would noticeably improve the reconstruction capability of KLOE: in the case of a π track from a $K_S \rightarrow \pi\pi$ decay, for instance, the sigma of the difference between the reconstructed and Montecarlo x-coordinates of the vertex decreases from 4.9 mm to 1.9 mm.

The Inner Tracker (IT) will be inserted in the available space inside the KLOE Drift Chamber. It is composed by five independent tracking layers (L1-L5), each providing a 2-D point space measurement of the track. The innermost layer will be placed at 15 cm from the beam line, corresponding to 20 τ_S in order not to spoil the K_LK_S interference. The outermost layer will be placed at 25 cm from the beam line, just inside the internal wall of the Drift Chamber. Each layer is a cylindrical GEM (Gas Electron Multiplier [6]) detector. This innovative technology allows to have an ultra-light, full sensitive detector fulfilling the stringent requirement on the material budget, needed

to minimize the multiple scattering effect for low-momentum tracks. In fact the detector is composed by thin (50 μm) polyimide foils Copper clad, acting as cathode, readout anode and multiplication stage. Moreover the high rate capability of the GEM (up to 50 MHz/cm^2 [7]) measured) makes this detectors suitable to be placed near the interaction point of a high-luminosity collider machine.

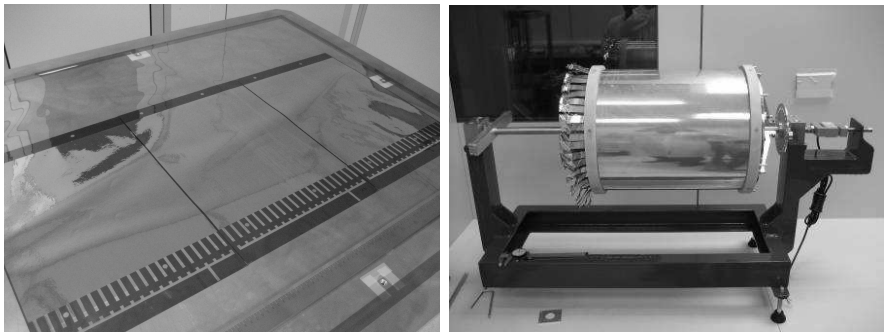

(a) (b)

Figure 3: *a) one of the large (960x352 cm^2) GEM foils used for one prototype; b) the final detector mounted on the stretching system.*

The R&D studies on cylindrical GEM started in 2006 with the construction of a small size prototype (diameter 9 cm and length 25 cm), and continued in 2007 with a new full size prototype with similar dimensions of the IT Layer1: same diameter (300 mm) but a reduced active length (352 mm). Several difficulties have been overcome in the assembly of the prototypes, and innovative construction techniques have been profitably exploited, as the design without hard frames within the active area, and the mechanical stretching of the chamber to confer structural rigidity [8].

Both chambers have been operated with a Ar/CO_2 gas mixture and successfully tested with an X-ray gun up to a gain of 10^4. The extensive test program proceeds in the next months with X-rays, cosmic rays and test beams,

in order to fully characterize the detectors. A study on different gas mixtures (e.g. $Ar/i-C_4H_{10}/CF_4$) is scheduled as well.

5 Conclusions

The KLOE detector is ready to take up the challenge given by the next 50 fb^{-1} of integrated luminosity delivered by the upgraded DAFNE accelerator, in Frascati.

Complex hardware improvements are planned both to reduce the systematics and to open new physics channels. A new readout system for the Electromagnetic Calorimeter, and a new Crystal-Calorimeter and QCAL, will be devoted to improve the overall γ detection efficiency. A new Tagger will open the way to profitable $\gamma\gamma$ physics. In order to optimize the reconstruction capability for the decays near the interaction point a new Inner Tracker will be inserted inside the Drift Chamber.

It is based on the novel technique of fully cylindrical GEM detector. The positive, though not exhaustive results obtained with the two prototypes built, have been proved valid the basic idea of the detector, representing a completely new step in the development of tracking devices with gas detectors.

References

1. KLOE Collaboration, preprint LNF-93/002(IR) 1993.
2. D. Alesini *et al.*, preprint LNF-06/33(IR) 2006.
3. KLOE2 Letter of Intent. `http://www.lnf.infn.it/kloe/kloe2/LoI/LoI.pdf`
4. F. Bossi *et al.*, preprint LNF-07/19(IR) 2007.
5. V. Patera. Private communication.
6. F. Sauli, Nucl.Instr.Meth. **A386** (1997) 531.
7. M. Alfonsi *et al.*, Nucl.Instr.Meth. **A518** (2004) 106.
8. G. Bencivenni *et al.*, NSS-MIC07 Conference Record.

Frascati Physics Series Vol. XLVI (2007), pp. 1485
HADRON07: XII Int. Conf. on Hadron Spectroscopy – Frascati, October 8-13, 2007
Future Facilities

HIDDEN AND OPEN CHARM AT PANDA

T. Stockmanns
Forschungszentrum Jlich, Institut für Kernphysik I

Written contribution not received

Frascati Physics Series Vol. XLVI (2007), pp. 1487–1494
HADRON07: XII Int. Conf. on Hadron Spectroscopy – Frascati, October 8-13, 2007
Future Facilities

THE PHYSICS CASE OF THE SUPERB FACILITY

A. Bevan
Particle Physics Research Center, Queen Mary University of London, Mile End Road, London, E1 4NS, United Kingdom.

Abstract

The physics case of the SuperB facility with design luminosity of 10^{36} $\mathrm{cm}^{-2}\mathrm{s}^{-1}$ is compelling. Such a facility has a rich and varied potential to probe physics beyond the Standard Model. These new physics constraints are obtained through the study of the rare or Standard Model forbidden decays of $B_{u,d,s}$, D and τ particles. The highlights of this wide-ranging physics programme are discussed in these proceedings.

1 Introduction

A conceptual design report of a next generation e^+e^- collider capable of delivering 100 times the luminosity of the current B factories has recently been compiled [1]. This report forms the basis of the physics motivation, detector, and accelerator designs for the next generation B factory at an e^+e^- collider. Details of the accelerator and detector designs are discussed elsewhere [2]. Data taking could commence as early as 2015 if the project is approved in the next few years. By this time, the LHC will have produced the results of direct

searches for SUSY, Higgs particles and many other new physics (NP) scenarios, as well as providing precision measurements of CP violation and the CKM mechanism for quark mixing in $B_{u,d,s}$ decays. The focus of high energy physics at that time will either be to understand the nature of any new particles found at the LHC, or to try and indirectly constrain possible high energy new particles by looking for virtual contributions to increasingly rare decays. If new particles exist they can contribute significantly at loop level to many rare B, D and τ decays. If this occurs, we may measure observables that differ from Standard Model (SM) expectations. Precision measurements of branching fractions, CP, and other asymmetries in many different rare decays can be used to elucidate the flavor structure of new particles and distinguish between different NP scenarios. Some NP scenarios introduce new particles at low energies (few GeV) which can be observed directly at SuperB. In short, the main aim of the SuperB facility is to search for and elucidate the behavior of NP.

2 B Phyiscs

2.1 Measurements of $\sin(2\beta_{\rm eff})$

Since the discovery of CP violation in the decay of B mesons through $b \to c\bar{c}s$ transitions, an industry has developed in performing alternate measurements of $\sin 2\beta$ in other processes (these are measurements of $\sin(2\beta_{\rm eff})$). In the presence of new physics, one can measure CP asymmetries that are significantly different from the SM expectation which is $\sin 2\beta$ measured in $b \to c\bar{c}s$ transitions. Measurements of $\sin(2\beta_{\rm eff})$ are performed in decays with $b \to s$ and $b \to d$ transitions. Loop dominated rare decays can receive significant contributions from new physics, and large effects have been ruled out by current measurements (See Figure 1). The general trend of measurements shows that $\sin(2\beta_{\rm eff}) < \sin(2\beta)$. In addition to the experimental uncertainties on the measurement of $\sin(2\beta_{\rm eff})$, there are theoretical uncertainties on the SM prediction in each decay mode. The first thing to note when considering theoretical uncertainties is that different decay modes have different expected shifts that are known with different levels of precision. As a result, it is not correct to average all of the $\sin(2\beta_{\rm eff})$ measurements and compare this average with the reference from $b \to c\bar{c}s$ transitions, although in practice this comparison is often made. You really have to perform a precision measurement for each mode, and then

make the comparison. Ideally when you make such a comparison, you want the experimental and theoretical uncertainties to be similar. There is insufficient statistics available at the existing B factories to do this comparison correctly. The most precise estimates of the SM uncertainty on $\Delta S = \sin(2\beta_{\rm eff}) - \sin(2\beta)$ are of the order of a percent for $B \to \eta' K^0$, $B \to K^+K^-K^0$, and $B \to 3K^0_S$ decays [3]. SuperB will be able to experimentally measure $\sin(2\beta_{\rm eff})$ to one percent with $75ab^{-1}$, thus enabling a comparison at the few percent level between $\sin(2\beta_{\rm eff})$ and $\sin(2\beta)$.

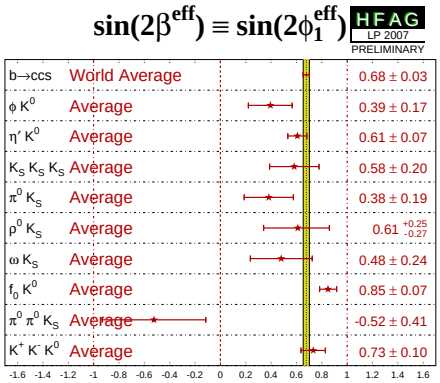

Figure 1: *The distribution of* $\sin(2\beta_{\rm eff})$ *measured in* $b \to s$ *penguin decays, along with the reference measurement of* $\sin(2\beta)$ *from* $b \to c\bar{c}s$ *decays*

2.2 New Physics in Mixing

In the SM we know that B_d and B_s mesons mix. It is possible to model new physics in mixing by allowing for an arbitrary NP amplitude to also contribute to the box diagram, and search for the effect of NP by comparing data to the ratio of the NP+SM contribution to that of the SM [4], i.e.

$$C_{B_d} e^{i\phi_{B_d}} = \frac{< B^0 | \mathcal{H}_{NP+SM} | \overline{B}^0 >}{< B^0 | \mathcal{H}_{SM} | \overline{B}^0 >}. \qquad (1)$$

The SM prediction is for $C_{B_d} = 1$ and $\phi_{B_d} = 0$, so any deviation from this would signify NP. It is possible to constrain C_{B_d} and ϕ_{B_d} using the available data, and extrapolate to SuperB as shown in Figure 2.

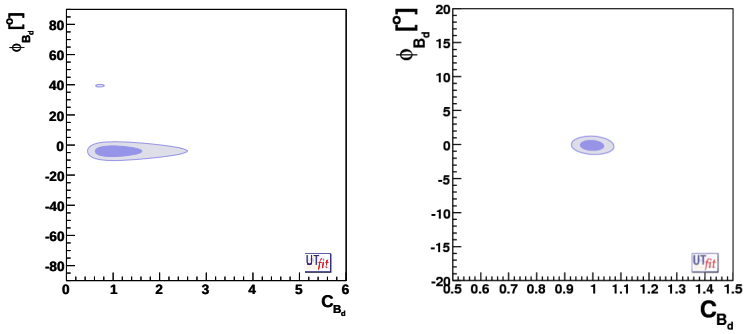

(a) (b)

Figure 2: *The distribution of $C_{B_d} = 1$ vs $\phi_{B_d} = 0$ obtained a) from current measurements, and b) obtained with 75ab^{-1} of data from a SuperB factory.*

2.3 Minimal Flavor Violation

One set of NP models that is popular assumes that there are no new flavor couplings. The corollary of this is that all CP violation is described by the SM Yukawa couplings. Models of this type are called Minimal Flavor Violation (MFV) models, examples of these are Higgs doublet, MSSM and large extra dimension models. Within the realm of MFV models we can still use the SuperB experiment to tell us about the nature of NP. For example, it is possible to use $B^+ \to \tau^+\nu$ decays to constrain the mass of the charged Higgs m_{H^+} as a function of the Higgs vacuum expectation value, $\tan\beta$ in 2HDM or MSSM (See Figure 3). In 2HDM, the branching fraction of $B^+ \to \tau^+\nu$ can be enhanced or suppressed by a factor r_H which has the form $(1 - \tan^2\beta[m_B^2/m_{H^+}^2])^2$ [5], and the corresponding factor for MSSM is $(1 - \tan^2\beta[m_B^2/m_{H^+}^2]/[1 + \epsilon_0 \tan\beta])^2$ where $\epsilon_0 \sim 0.01$ [6]. Other decay modes, including $D^+ \to \tau^+\nu$, $\mu^+\nu$, and

$b \to s\gamma$ can be used to constrain the charged Higgs mass in a similar way. The worst case scenario of MFV suggests that SuperB would be sensitive to new particles with masses up to 600 GeV.

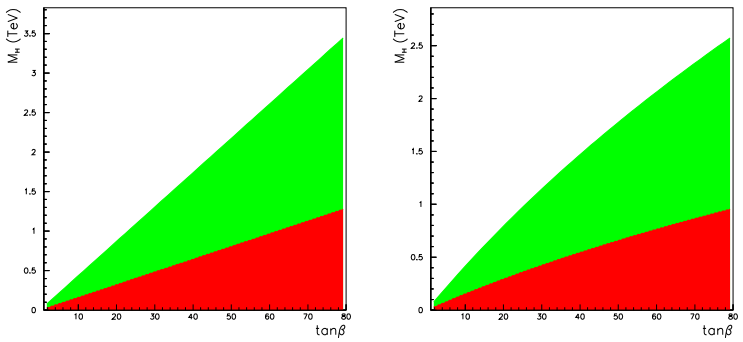

(a) (b)

Figure 3: *The distribution the mass of the charged Higgs vs* $\tan\beta$ *in a) 2HDM and b) MSSM. The red band is what could be excluded by the current B factories with a data sample of* $2ab^{-1}$*, and the green band is what could be excluded using* $75ab^{-1}$ *of data from a SuperB factory assuming that the measured* $B^+ \to \tau^+\nu$ *branching fraction has the standard model value.*

2.4 Other Searches for New Physics

In contrast to the MFV scenario described above, we can think of a more generalized SUSY scenario. Given that quarks and neutrinos can change type or mix, it is natural to consider that their super-partners would also have non-trivial flavor couplings and would mix. If this is not true, then the NP extension to the SM would have a fine-tuned and unnatural behavior. We can already rule out large new physics contributions to B and kaon physics, but CP violation is small in the SM, so we should not expect to see large $\mathcal{O}(1)$ NP effects, and should be content to search for small CP violation effects from NP. The simplest model of this type is MSSM with squark mixing matrices.

Combinations of observables measurable at SuperB can be combined to provide non-trivial constraints on the real and imaginary parts of these squark mixing parameters. For example, Figure 4 shows the constraint that SuperB can put on the complex parameter $(\delta^d_{2,3})_{LR}$ with a data sample of $75ab^{-1}$, where the d indicates a quark, the indices $2,3$ indicate mixing between the second and third squark generations and the LR indicates a left-right helicity for the SUSY partner quarks. The measurements of the branching fractions of $b \to s\gamma$ (green) and $b \to sl^+l^-$ (cyan), with the CP asymmetry in $b \to s\gamma$ (magenta) are combined (blue) to constrain the real and imaginary parts of $(\delta^d_{2,3})_{LR}$. SuperB has a sensitivity > 100 TeV for this type of NP model [7]. Other examples of constraints squark mixing parameters are described in [1].

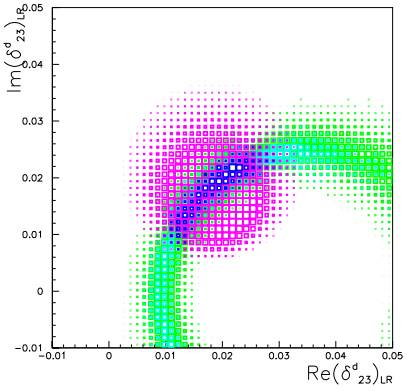

Figure 4: *The distribution constraint on the real vs imaginary part of* $(\delta^d_{2,3})_{LR}$ *obtainable at SuperB using the constraints described in the text.*

There are also models of NP that predict light new particles (Higgs or dark matter candidates). If such particles exist, then it would be possible to create them directly at a SuperB factory. Some of these models are described further in [1].

3 D Phyiscs

Given the recent observation that D^0 mesons mix, we now know that the plethora of observables that one can use to search for CP violation in B decays also exists in D decays. As with B meson decays, the pattern of observables (the branching fractions, CP asymmetries and other observables) in the decays of charm decays can be used to constrain NP scenarios. Work is ongoing to understand how to use these correlations in charm decays to constrain NP.

4 τ Phyiscs

Many NP scenarios have couplings that represent lepton flavor violation (LFV). Such a decay would give an unmistakable signal in the detector, and would mark the start of a new era in particle physics. The current best limits from searches for signals of LFV are $\mathcal{O}(10^{-7})$ [8]. These limits are an order of magnitude away from upper bounds in many new physics scenarios [9]. A SuperB facility would provide sufficient statistics to find LFV at the level of such predictions, or push upper limits down to $\mathcal{O}(10^{-9}$ to $10^{-10})$.

The decays of τ leptons proceed via a single amplitude. If a non-zero CP asymmetry is measured in any τ decay, then this is a clear signal of new physics. There have been many proposed searches for CP violation in τ decays [10]. When doing such searches, one has to decouple the possible effects of CP violation in any final state kaons, and the difference between K^+ and K^- interactions in the detector.

It is possible to test CPT by comparing the ratio of lifetimes of the τ^+ and τ^-. Any deviation from one would indicate CPT violation. The expected statistical precision of such a test is at the level of $\mathcal{O}(10^{-4})$. If this precision were to be achieved, then the lifetime ratio test in τ decays would be comparable to that in μ decays [11].

5 Conclusion

The SuperB facility has the potential to indirectly search for NP at energy scales far beyond the reach of the direct searches at the LHC. The ability to probe flavor couplings in NP scenarios up to several hundred TeV means that results from SuperB will be of general interest, and complimentary to the LHC

physics programme over the next few decades. There are two possible scenarios: (i) If the LHC discovers new particles, it will be possible to measure their basic properties such as mass and width at ATLAS and CMS. However, in order to fully understand these new particles, one needs to understand their flavor dynamics as well. The flavor dynamics of new physics can be probed well above the TeV scale at SuperB. (ii) If the LHC doesn't discover any new particles, then it is important to probe ever increasing energy scales. Again, SuperB can probe well above the TeV scale while indirectly searching for new physics. The correlations of flavor related observables measured at SuperB can help us distinguish between the multitude of NP scenarios being proposed today. Without this set of measurements from SuperB, we may not be able to resolve between many of the plausible NP scenarios that exist. These proceedings discuss the core of the physics programme of SuperB, and the interested reader will find a more comprehensive treatment in Ref. [1)]. More discussion on exploiting correlations between measurements of flavor observables to distinguish between NP models can be found in Ref [12)].

References

1. M. Bona *et al*, arXive:0709.0451 [hep-ex].
2. F. Forti, and E. Paoloni in these proceedings.
3. See Section 2.1.1 of Ref. [1)] and references therein.
4. M. Bona *et al*, [UT fit collaboration], hep-ph/0509219.
5. W. S. Hou, Phys. Rev. D **48** 2342 (1993).
6. A. G. Akeroyd and S. Recksiegel, J. Phys. G **29** 2311 (2003).
7. L. Silvestrini, Contribution to the SuperB IV workshop, Rome (2006).
8. B. Aubert *et al*, Phys. Rev. Lett. **95** 041802 (2005).
9. See Section 2.2.1 of Ref. [1)] and references therein.
10. See Section 2.2.3 of Ref. [1)] and references therein.
11. W. M. Yao *et al.*, J. Phys. G **33** 1 (2006).
12. J. Hewett *et al.*, SLAC-R-709.

Frascati Physics Series Vol. XLVI (2007), pp. 1495–1500
HADRON07: XII Int. Conf. on Hadron Spectroscopy – Frascati, October 8-13, 2007
Future Facilities

Super$B$: DETECTOR FOR A VERY HIGH LUMINOSITY ELECTRON POSITRON COLLIDER $\Upsilon(4S)$ PEAK

Eugenio Paoloni
I.N.F.N. sezione di Pisa & Università di Pisa
on behalf of the Super$B$ Conceptual Design Report authors

Abstract

Super$B$ is a proposal for a second generation Bfactory, i.e. an energy asymmetric e^+e^- collider operating at the $\Upsilon(4S)$ resonance peak with a design luminosity in excess of $10^{36}/\,\mathrm{cm}^2/\,\mathrm{s}$. Super$B$ is also the detector that will collect the events produced by such a machine. Both these components will be quickly sketched in the following.

1 Overview

The origin of electroweak symmetry breaking and the search for extensions of the Standard Model (SM) will be the main themes of the saga of particle physics research in the next decade.

The Large Hadron Collider, whose operations should start in May 2008, will soon commence his quest for the Higgs boson. It will also begin extensive searches for phenomena beyond the SM that will end, if Nature is gentle with us, with the production and observation of new particles.

This is not, however, the only way to look for New Physics (NP): new particles can reveal themselves through virtual effects in decays or production of

the SM ones. The high-precision measurements in the sector of heavy flavoured SM particles ($B, \tau, D,$) represent a second viable path to the discovery of NP, where it would be not reachable at the LHC energy, and to the investigation on the nature of the new particles, where already discovered by the LHC.

Super$B$ [1] mission will be to produce and record roughly one thousand B pairs per second and an equivalent rate of τ pairs and charmed particles in order to study with unprecedented accuracy and sensitivity their phenomenology aiming to discover (or study) the NP as shown in the Francesco Forti's talk at this very same conference and extensively described in the first chapter of the Super$B$ Conceptual Design Report (CDR) [1].

In the following sections the Super$B$ collider concept will be sketched out along with the Super$B$ detector.

2 The Super$B$ collider

Super$B$ is an energy asymmetric e^+e^- collider operating at the $\Upsilon(4S)$ resonance peak with a design luminosity in excess of $10^{36}/\,\mathrm{cm}^2/\,\mathrm{s}$ (cfr. the second chapter of the Super$B$ CDR [1]). Such a collider would produce an integrated luminosity of at least $15{,}000\,\mathrm{fb}^{-1}$ ($15\,\mathrm{ab}^{-1}$) in a running year ($1.5\times10^7\,\mathrm{s}$). This correspond to roughly 15 billions B pairs, 14 billions τ pairs and 19 billions $e^+e^- \to c\bar{c}$ events per running year. A novel collider concept based on strong vertical final focusing, large Piwinsky angle collision scheme and low emittance storage rings had been developed and studied to achieve an increase by a factor 100 of the luminosity with respect to the present generation of B factories without a significant increase of the beam currents and hence without a significant increase of the needed wall-plug power.

3 Backgrounds

The machine backgrounds rate caused by beam particles scattered by residual gas molecules in the vacuum chambers scales with the beams currents, hence it is not a source of concern. A careful design of masks and collimators will keep the rate of this component of the background at a manageable level like in the present B factories. The same argument holds for synchrotron radiation produced by dipoles and off axis quadrupoles near the IP.

The rate of the background produced through beam-beam scattering at

Table 1: Luminosity scaling background processes compared with respect the $\Upsilon(4S)$ production cross section

Process	Cross section	Evt. / crossing
$e^+e^- \to e^+e^-\gamma \quad E_\gamma/E_{beam} > 1\%$	~ 340 mbarn	~ 680
$e^+e^- \to e^+e^-e^+e^-$	~ 7.3 mbarn	~ 15
$e^+e^- \to e^+e^-$ (in the detector)	~ 30 nbarn	$\sim 30 \times 10^{-6}$
$e^+e^- \to e^+e^-$		
$e^+e^- \to \Upsilon(4S)$	~ 1 nbarn	$\sim 1 \times 10^{-6}$

the Interaction Point (IP) scales instead with the luminosity and is expected to be the dominant contribution to the total background rate.

The physical processes raising major concerns are the QED ones: radiative Bhabha ($e^+e^- \to e^+e^-\gamma$) and pair production ($e^+e^- \to e^+e^-e^+e^-$) whose cross section is reported in tab. 1. The impact of these backgrounds had been evaluated using the BBBrem [2] and Diag36 [3] generators in conjunction with a full Geant4 simulation of the detector and of the final focus magnets. A careful design of the optical dispersion function near the IP in conjunction with a properly designed tungsten shielding prevent radiative Bhabha particles to impinge in the detector sensitive volumes.

Pair production will affect mostly the inner vertex detector requiring a finely segmented detector with fast read-out able to cope with a $5\,\mathrm{MHz/\,cm^2}$ hit rate.

4 The Super$B$ detector

The Super$B$ detector concept is based on the current *BABAR* detector with those modifications required to operate at a luminosity of $10^{36}/\,\mathrm{cm^2/\,s}$ and with a reduced center-of mass boost.

The current *BABAR* detector is shown in Fig. 1. *BABAR* consists of a tracking system with a 5 layer double-sided silicon strip vertex tracker (SVT) and a 40 layer drift chamber (DCH) inside a 1.5T magnetic field, a Cherenkov detector with quartz bar radiators (DIRC), an electromagnetic calorimeter (EMC) consisting of 6580 CsI(Tl) crystals and an instrumented flux-return (IFR) comprised of both limited streamer tube (LST) and resistive plate chamber (RPC) detectors for K^0_L detection and μ identification.

The Super$B$ detector concept reuses a number of components from *BABAR*:

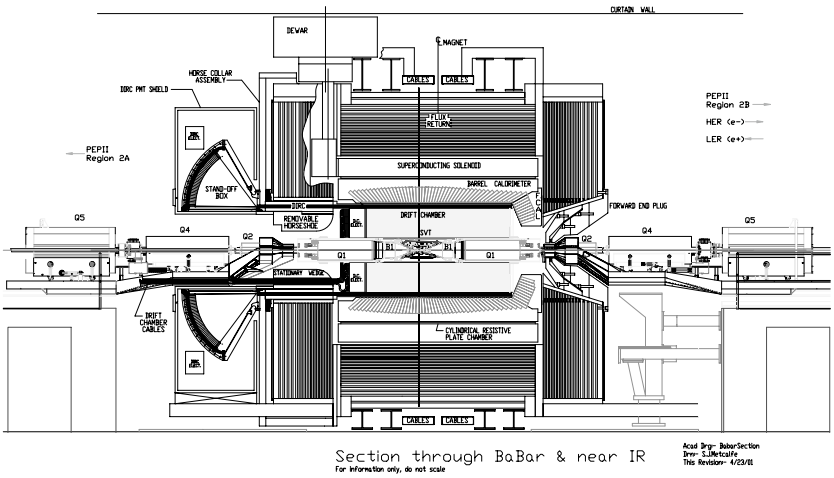

Figure 1: The current *BABAR* detector.

the flux-return steel, the superconducting coil, the barrel of the EMC and the quartz bars of the DIRC. The flux-return will be augmented with additional absorber to increase the number of interactions lengths for muons to roughly 7λ. The DIRC readout will be replaced with either faster PMTs in the current water tank or multi-channel plate (MCP) photon detectors in a focusing configuration to reduce the impact of beam related backgrounds and improve performance. The forward EMC will feature cerium-doped LSO (lutetium orthosilicate) or LYSO (lutetium yttrium orthosilicate) crystals, hereafter referred to as L(Y)SO crystals, which have a much shorter scintillation time constant, and lower Moliére radius and better radiation hardness than the current CsI(Tl) crystals, again for reduced sensitivity to beam backgrounds and better position resolution.

The tracking detectors for Super$B$ will be new. The current SVT cannot operate at $\mathcal{L} = 10^{36}/\,\mathrm{cm}^2/sec$, and the DCH has reached the end of its design lifetime and must be replaced at the end of *BABAR* operation. To maintain sufficient Δt resolution for time-dependent *CP* violation measurements with the Super$B$ boost of $\beta\gamma = 0.28$, the vertex resolution will be improved by reducing the radius of the beam pipe, placing the inner-most layer of the SVT at a radius

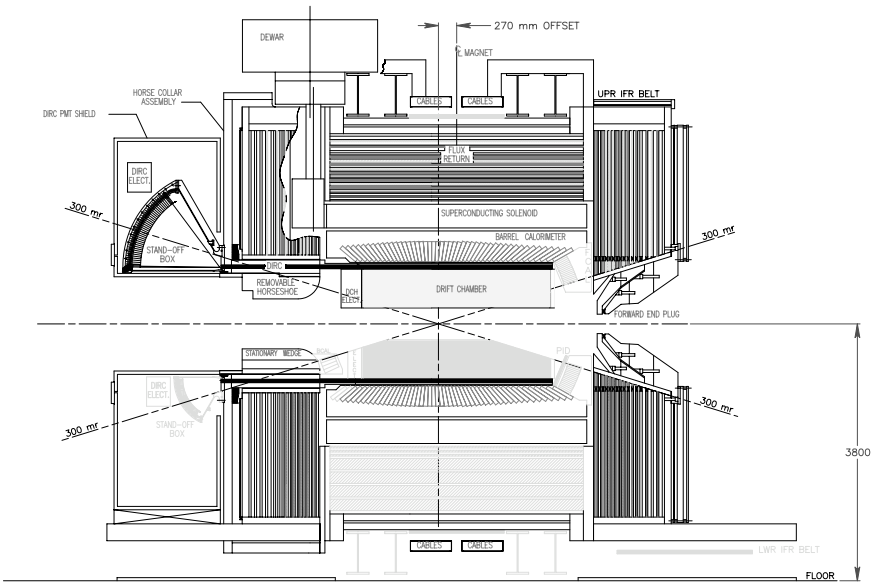

Figure 2: Concept for the Super$B$ detector. The upper half shows the baseline concept, and the bottom half adds a number of detector optional configurations.

of roughly 1.2 cm. This innermost layer of the SVT will be constructed of either silicon striplets or Monolithic Active Pixel Sensors (MAPS [4]), depending on the estimated occupancy from beam-related backgrounds. Likewise the cell size and geometry of the DCH will be driven by occupancy considerations. To improve the hermeticity of the detector Super$B$ may also include a backwards EMC detector also consisting of L(Y)SO crystals and forward and backward particle identification systems using either a time-of-flight (TOF) or an Aerogel RICH (ARich) detector.

The Super B detector concept is shown in Fig. 2. The top portion of this elevation view shows the minimal set of new detector components, with the most reuse of current *BABAR* detector components; the bottom half shows the configuration of new components required to cope with higher beam backgrounds and to achieve greater hermiticity.

5 Conclusions

A general purposes detector able to collect $\mathcal{O}(10^{10})$ $e^+e^- \rightarrow \Upsilon(4S)$ events per Snowmass year had been quickly presented along with the machine able to produce such a huge sample and the physical motivation for such big effort. The interested reader can find detailed information on all these subjects in the Super B CDR [1)], a 453 page book available from INFN Publishing Services,INFN-Pisa, L.go Pontecorvo,3, I-56127, Pisa, Italy.

References

1. M. Bona *et al.*,"Super B: A High-Luminosity Asymmetric e^+e^- Super Flavor Factory. Conceptual Design Report," arXiv:0709.0451 [hep-ex].
2. R. Kleiss and H. Burkhardt, Comput. Phys. Commun. **81**, 372 (1994).
3. F. A. Berends, P. H. Daverveldt and R. Kleiss, "Monte Carlo Simulation of Two Photon Processes. 2. Complete Lowest Order Calculations for Four Lepton Production Processes in electron Positron Collisions," Comput. Phys. Commun. **40** (1986) 285.
4. S. Bettarini *et al.*, Nucl. Instrum. Meth. A **572**, 277 (2007).

Frascati Physics Series Vol. XLVI (2007), pp. 1501
HADRON07: XII Int. Conf. on Hadron Spectroscopy – Frascati, October 8-13, 2007
Future Facilities

THE PHYSICS CASE OF ILC

B. Mele
Laboratori Nazionali di Frascati, Italy

Written contribution not received

Frascati Physics Series Vol. XLVI (2007), pp. 1503–1510
HADRON07: XII Int. Conf. on Hadron Spectroscopy – Frascati, October 8-13, 2007
Future Facilities

DETECTOR DESIGN FOR ILC

Alessandro Calcaterra
Laboratori Nazionali di Frascati dell'INFN

Abstract

The International Linear Collider will allow a final and firm establishment of the status of the Higgs sector in the Standard Model, besides opening the way to new physics as well. But the experimental difficulties will be so great that a new generation of detectors and techniques will be required, different from and better than those characteristic of the LEP/SLD era. This paper describes very briefly some of the problems presented to charged- and neutral-particle detection and analysis at the ILC, and ways, explored at this time, to eventually overcome them.

1 The ILC and its promise for Physics

The International Linear Collider [1)] will be an accelerator of unprecedented complexity. The total center-of-mass energy will span the range from 200

to 500 GeV, possibly up to a maximum of 1 TeV, with a relative resolution on the beam energy of order 0.1%(apart from the beamsstrahlung tail). The luminosity, driven by the target of integrating 500 fb^{-1} in the first 4 years of operation, must reach $2 \times 10^{34}\text{cm}^{-2}\text{s}^{-1}$ with an efficiency of over 75%, and this implies extremely small transverse beam dimensions: 0.6 μm (horizontal) by O(10 nm)(vertical).

As the SLC experience has shown, the sensitivity in the measurement of electroweak asymmetries will be amplified by polarizing the electron beam to 80%, and if possible also the positron beam; the polarization will be measured for every pulse with a resolution of less than 1%.

The machine, schematically shown in fig. 1, will emit a train of 3000 bunches 1 ms long every 200 ms. During a train, electronics on the detector will store data for every bunch; the time between trains will be used to zero-suppress data, perform feature extraction and transfer the results to the outside world.

The single most interesting item of ILC physics [2)] will be the complete study and classification of Higgs boson decays; by "complete" it's meant that only the cleanliness of the initial state at the ILC will allow not just the discovery of "Higgs" mass enhancements in several channels, but also the spin measurement, and the demonstration that the coupling strength scales with the masses of decay particles.

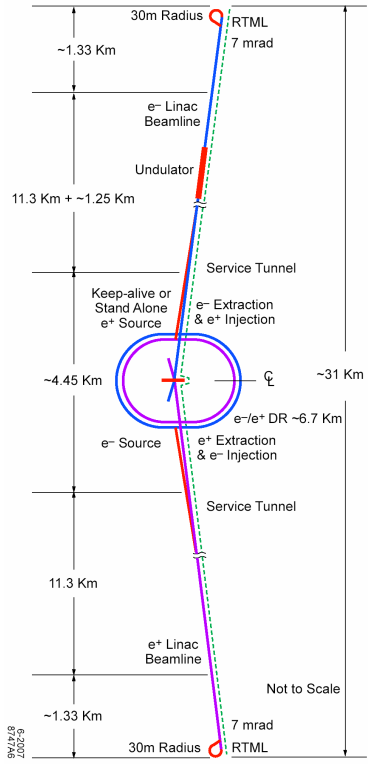

Figure 1: *A schematic layout of the ILC.*

2 Challenges to detection and analysis

ILC physics will be a physics of jets, rather than of particles: a vertex detector will not only find and fit vertices, but will also give a global measurement of jet flavor, via reconstruction of entire decay chains of secondary and tertiary heavy quark vertices.

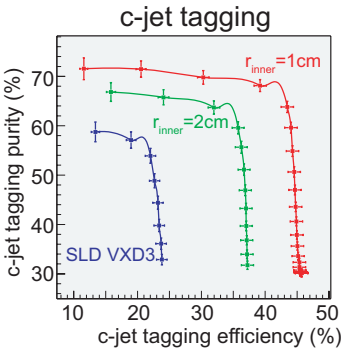

Figure 2: *Charm Tagging efficiency and purity.*

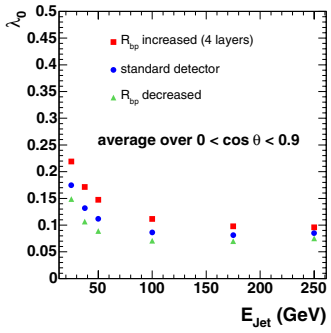

Figure 3: B^0 *vertex charge misreconstruction probability.*

To achieve this, one of the many essential necessities is minimization of the beam pipe radius: fig. 2 shows how the efficiency/purity for charm tagging at the vertex detector level improves, going from a state-of-the-art vertex detector of the past, to ones having smaller radii; and fig. 3 gives the probability of misreconstructing a B^0 for a $B^{\pm}$ as a function of the B jet energy and beam pipe radius.

Challenges posed to tracking are also very hard: the measurement believed to be most sensitive to the Higgs mass is the dilepton mass recoiling against the Z in events $e^+e^- \rightarrow ZH$ with $Z \rightarrow \ell^+ \ell^-$: reconstructing the Z mass, one obtains from 4-momentum conservation $M_h^2 = s + M_Z^2 - 2E_Z\sqrt{s}$. In the formula both the tracking and the beam energy are equally important: with the charged momentum resolution given by $\Delta P_t/P_t = a \times P_t + b$, one sees in fig. 4, from a study using 500 fb^{-1} at 350 GeV, that deterioration of the Higgs mass measurement by a factor 3 appears if the high-momentum component of the error (relating to the $B \times R^2$ factor) is not kept small.

If detectors at ILC are to identify particle jets as a whole, then calorimetry

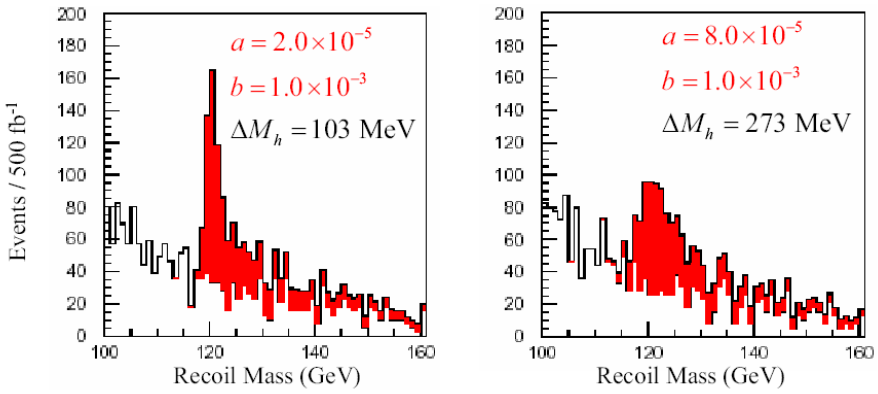

Figure 4: *Higgs recoil mass spectra for different tracker resolution parameters.*

must be able to cleanly separate Z and W bosons also in their decays to hadron jet pairs, simply measuring the total jet energy: fig. 5 shows on the left the separation of ZZ events from WW ones for a single-hadron energy resolution of $60\%/\sqrt{E(GeV)}$ (left), typical of LEP/SLD calorimeters, and of $30\%/\sqrt{E(GeV)}$ (right), the target resolution for calorimetry at ILC.

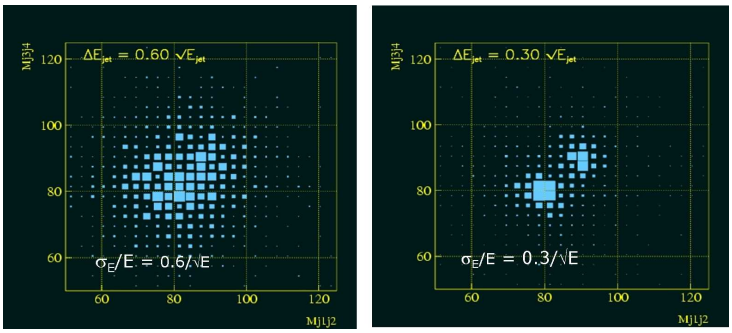

Figure 5: *Higgs di-jet invariant mass for different jet-energy resolution.*

It's not possible to give even a sketch of the set of requirements posed by ILC physics to detectors in such a short space; the reader wanting a complete view must consult ref. [1)].

3 Present developments and ideas

The first period of work dedicated to the study of detector ideas for ILC has ended in the summer of 2007 with the presentation of 3 different, but almost conventional detector concepts, plus an ambitious novel design called the "4^{th} concept" and work has now started, aiming at bringing together the separate concepts into a single proposal, called for now the ILD.

The 3 first concepts differ essentially for the choice of whether to favour a high B field in a relatively small tracking volume ("SiD" concept), or the opposite ("GLD"), or a compromise between the two ("LDC"); the SiD group has proposed the idea of an all-Silicon, integrated tracking volume, shown in fig. 6, while the other two have chosen more usual TPC's. All concepts take pains to implement as complete as possible hermeticity by having secondary tracking and calorimetric detectors covering every dead area of the apparatus.

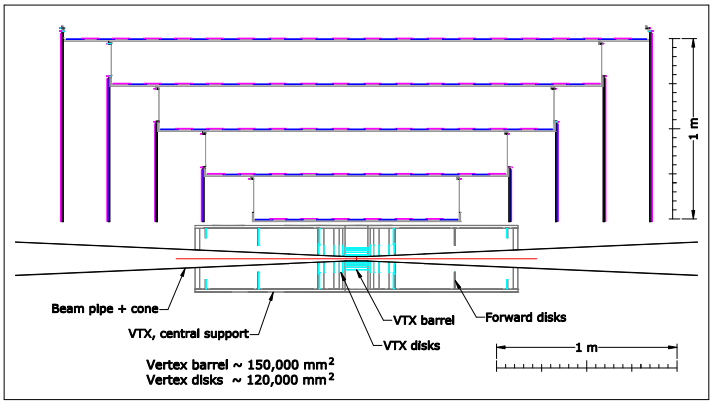

Figure 6: *The SiD concept of integrated tracking.*

For calorimetry, the 3 "conventional" concepts have proposed different sampling devices for the electromagnetic sections (highly segmented W-Si for SiD and LDC, W-scintillator for GLD) and the hadronic ones (Fe-RPC for SiD, Fe-scintillator with SiPM readout for LDC, Pb-scintillator for GLD). The necessity to minimize the radial thickness of all calorimetry (included at ILC in the magnetized volume) is the reason behind the extensive use of Tungsten as

an absorber; besides, the small Molière radius of W will lead to better lateral confinement of e.-m. showers.

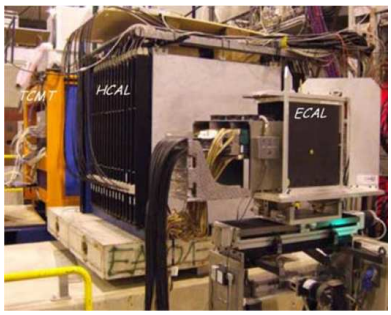

Figure 7: *The CALICE test beam calorimeter.*

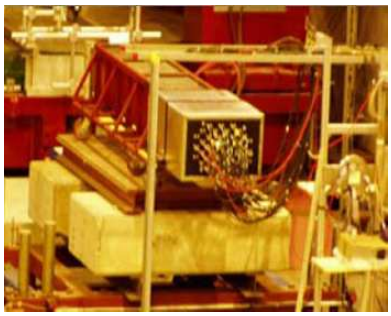

Figure 8: *The DRM test readout module.*

The CALICE collaboration has built a cubic-meter prototype of the proposed LDC calorimeter containing almost 10000 analog channels; each one is a small($\sim$ 3 x 3 x 0.5 cm^3) scintillator tile coupled to a Silicon photomultiplier (SiPM). This prototype, shown in fig. 7, is currently taking test-beam data.

Why this high level of granularity? The only techniques promising (for now) an error of $\sim 30\%/\sqrt{E}$ for the shower energy are those based on "Particle Flow Analysis" (PFA). The core of this idea is that every component of a shower must be measured in the detector best suited: tracking chambers for charged particles, ECAL for electrons, and HCAL for neutrals. Hence, the need to associate as correctly as possible every cluster of energy to the correct category. It may be shown that, with PFA, the biggest contribution to the error is not due to HCAL single-particle resolution, but rather to confusion in this assignment; that can only be reduced by increasing detector segmentation.

The "4^{th}" concept has made a different choice for calorimetry; the absorber is instrumented simultaneously with a dual-readout system of fibers. One system, sensitive to Čerenkov light, will measure the energy of the electromagnetic component of showers; the second one, common scintillating fibers, will measure the both the e.-m. and hadronic components. In this way, one will correctly gauge the mixture, and weigh away relative fluctuations.

A prototype of this DREAM calorimeter already exists, is taking test-beam data, and is shown in fig. 8.

4 Expected performance

ILC Monte Carlo studies are by now accurately predicting the expected performance of ILC detectors and techniques. For vertexing, fig. 9 shows a promising efficiency/purity plot from a full simulation of $Z \rightarrow q\overline{q}$ events at the Z pole in the LDC detector, using the SLD topological vertexing algorithm.

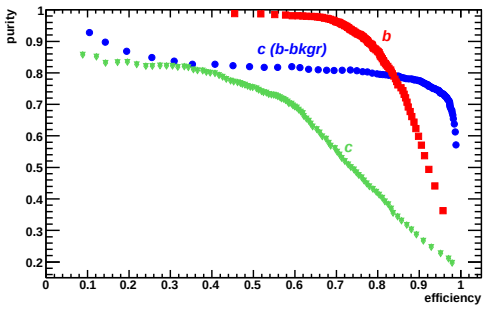

Figure 9: *Vertex flavor tagging from LDC full simulation.*

Fig. 10 illustrates how the tracking efficiency ($t\overline{t} \rightarrow$ 6 jets at 500 GeV) is better than 95% in the LDC simulation, and fig.11 shows that jet resolution in the GLD detector is very close to the ILC target of $30\%/\sqrt{E(GeV)}$ for events $Z \rightarrow$ light quarks at the Z pole.

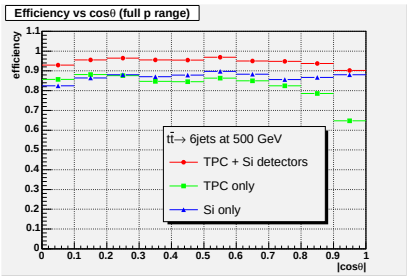

Figure 10: *Tracking efficiency with LDC.*

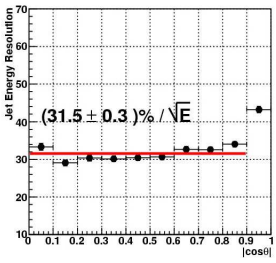

Figure 11: *Calorimetry resolution in GLD.*

Subdetector performance from full simulations of technology already existent, just scaled up to ILC-size detectors, is indeed getting closer to the

requirements from physics. But how will this closeness maps to physically interesting measurements? In fig.12 we see an LDC analysis of the Higgs mass recoiling against a dilepton pair from the Z: the background from the ILC is from a parameterization, both $Z\rightarrow e^+e^-$ and $Z\rightarrow \mu^+$ μm events are included, and $50\,\mathrm{fb}^{-1}$ of data at a total energy of 250 GeV have been used. The benefit of running near to the threshold for ZH production is apparent in the narrowness of the H peak, only 70 MeV.

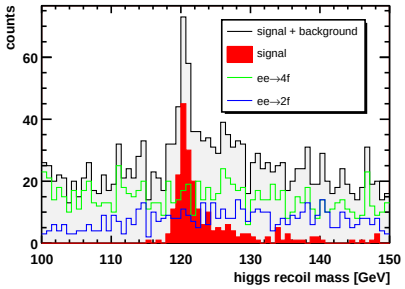

Figure 12: *Higgs dilepton mass (LDC).*

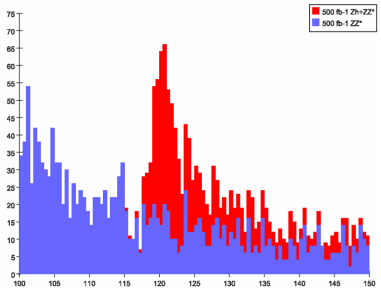

Figure 13: *Higgs dimuon mass (SiD).*

Fig. 13 shows a similar analysis from the SiD group of $500\,\mathrm{fb}^{-1}$ of data taken above ZH threshold, at 350 GeV in the center of mass; only dimuon events from the Z have been used, and the background from ILC is fully simulated. It is evident that, in spite of a bigger data sample, the worsened efficiency from charged tracking translates into a mass peak 135 MeV wide.

The ILC community has by now produced an impressive amount of work, aimed at making both the ILC itself and its detector (the ILD) a definite reality. One can start to see a near future in which the ILC and ILD will offer the possibility to test the Standard Model to its very limits, and possibly beyond.

References

1. The material presented in this talk is freely available at the ILC document repository: `http://www.linearcollider.org/wiki`

2. A review of ILC physics is given by B. Mele in these Proceedings.

BARYON SPECTROSCOPY

Frascati Physics Series Vol. XLVI (2007), pp. 1301–1308
HADRON07: XII Int. Conf. on Hadron Spectroscopy – Frascati, October 8-13, 2007
Baryon Spectroscopy

BARYON REGGE TRAJECTORIES IN THE LIGHT OF THE $1/N_c$ EXPANSION OF QCD

J. L. Goity
Department of Physics, Hampton University,
Hampton, VA 23668, USA
Thomas Jefferson National Accelerator Facility,
Newport News, VA 23606, USA
N. Matagne
University of Liège, Institute of Physics B5,
Sart Tilman, B-4000 Liège 1, Belgium

Abstract

This proceeding summarizes the analysis of the baryon Regge trajectories we made in the $1/N_c$ approach of QCD. By considering the evolution of the spin-flavor singlet component of the masses with respect to the angular momentum, we found two distinct and remarkably linear Regge trajectories for symmetric and for mixed symmetric spin-flavor multiplets.

In the low energy regime, typical of baryon spectroscopy, QCD is a non-perturbative theory in the strong coupling. This makes a first-principles treatment of the theory very difficult. There is, however, an expansion which provides profound insight, in particular in the mentioned non-perturbative regime. That expansion naturally arises from the large N_c limit of QCD [1)], where N_c is the number of colors: the expansion in powers of $1/N_c$ furnishes an ordering principle for studying QCD in the non-perturbative regime, and in particular for implementing effective theories to study mesons and baryons.

In baryons, the large N_c limit gives rise to a contracted SU($2N_f$) symmetry (N_f is the number of light flavors, equal to 3 in what follows) [2], which allows for a very efficient implementation of a systematic $1/N_c$ expansion of the various observables (baryon masses, axial vector currents, etc). The expansion can be built in terms of operator products involving the generators of spin-flavor SU(6) [3]. The operator products are ordered in powers of $1/N_c$ and are accompanied by unknown effective coefficients which are determined by the QCD dynamics. In the spirit of effective theories, those coefficients are determined by fitting to experimental data, or possibly to lattice QCD data.

For excited baryons, the usual approach is to assume an exact SU(6)$\times$O(3) symmetry in the large N_c limit. This symmetry is however not exact, because it is broken, for mixed symmetric spin-flavor multiplets, at $\mathcal{O}(N_c^0)$ by spin-orbit interactions [4]. However, the observed smallness of these interactions justify the assumption that there is an approximate O(3) symmetry around which one can implement the $1/N_c$ expansion. Following this scheme, the $1/N_c$ expansion of QCD was succesfully applied to study baryon masses of various excited multiplets [5], and strong [6] and electromagnetic [7] transitions. More recently, compatibility between $1/N_c$ expansion and quark models has been investigated [8].

A well known result in hadron spectroscopy are the approximately linear dependences of the square of hadron masses with the angular momentum, known as Regge trajectories. In this talk, a new assessment of the baryon Regge trajectories in the light of the $1/N_c$ expansion is discussed. This new assessment is based on analyzing the evolution of the effective coefficients in the mass operators as a function of the quantum number ℓ associated with the O(3) group [9].

From the analysis of excited multiplets in the $1/N_c$ expansion, it appears that the main features of the spectrum can be described by a few operators, namely the spin-flavor singlet operator of $\mathcal{O}(N_c)$, the hyperfine interaction and the strangeness operator; for some multiplets, the hyperfine SU(3) breaking operator is also needed, although it plays no role in our discussion here. The idea is to take only those dominant mass operators, defined in a consistent fashion across different multiplets in such a way that the comparison of their coefficients has physical significance (this requires some modifications to the operators [5] as one goes from symmetric to mixed symmetric spin-flavor repre-

sentations). In addition to limiting the operator basis as mentioned above, we neglect effects of state mixing within and between multiplets. This assumption is a consistent approximation justified by several previous analyses, and further strengthened by the results reported here. For ground state baryons, the mass formula reads:

$$\hat{M}_{\rm GS} = N_c\, c_1 \mathbb{1} + \frac{1}{N_c} c_{\rm HF} \left(\hat{S}^2 - \frac{3}{4} N_c \right) - c_{\mathcal{S}}\, \hat{\mathcal{S}} + \frac{1}{N_c} c_4 \left(\hat{I}^2 - \hat{S}^2 - \frac{1}{4} \hat{\mathcal{S}}^2 \right), \quad (1)$$

where $\hat{S}$ and $\hat{I}$ are the spin and isospin operators respectively, and $\hat{\mathcal{S}}$ is the strangeness operator. The hyperfine term is defined in such a way that the one-body pieces are removed and the hyperfine SU(3) breaking operator does not contain terms linear in the strangeness operator.

For the excited multiplets, the group theory can be easily carried out if one keeps in mind the Hartree picture of the baryon, consisting of a ground state core composed of $N_c - 1$ quarks and an excited quark. Keeping only the operators which are dominant, the excited baryon mass formula becomes:

$$\begin{aligned} \hat{M}' &= N_c\, c_1 \mathbb{1} + \frac{c_{\rm HF}}{N_c} \left(\hat{S}^{c^2} - \frac{3}{4}(N_c - 1)\mathbb{1} \right) - c_{\mathcal{S}}\, \hat{\mathcal{S}} \\ &\quad + \frac{4\, c_4}{3 N_c} \left(\sqrt{3} \hat{S}^c \cdot \hat{G}_8^c - \frac{1}{2} \hat{S}^{c^2} - \frac{1}{8} N_c \hat{\mathcal{S}}^c \right), \end{aligned} \quad (2)$$

where the c upper label indicates that the operator acts only on the core (the last term is a hyperfine SU(3) breaking operator which is only important the $[\mathbf{56}, 2^+]$ multiplet). The matrix elements of the excited baryon mass operator in the $[\mathbf{56}, \ell]$ and $[\mathbf{70}, \ell]$ multiplets are given explicitly in [9].

The dynamical coefficients are obtained by fitting to the empirical masses taken from the Particle Data Group [10]. Tables I and II show the results of the fits for the different multiplets. For high excitations ($\ell > 4$), the identification of resonances as belonging to a definite SU(6)×O(3) multiplet is unclear and the ones we suggest here are based on Ref. [11]. For some multiplets, the χ^2 of the fit is quite large because the masses are known with sufficient precision for the absence of the operators being neglected to be noticed, *e.g.* spin-orbit interaction.

The evolution of the coefficient c_1 from multiplet to multiplet is the main focus here. We can define Regge trajectories for this coefficient by plotting $(N_c\, c_1)^2$ vs ℓ. These are, therefore, the Regge trajectories for the spin-flavor

singlet component of the baryon masses. The plot shown in Fig. 1 displays two separate and distinct Regge trajectories corresponding to the **56**-plet and the **70**-plet SU(6) states . The separation between the two trajectories can be explained in the Hartree picture as a result of the exchange interaction between the excited quark and the core, which are $\mathcal{O}(1)$ and $\mathcal{O}(1/N_c)$ for **56**-plets and **70**-plets respectively. The trajectories can be summarized by linear fits (in units of GeV^2):

$$\begin{aligned} \left(3\,c_1\left([\mathbf{56},\ell]\right)\right)^2 &= (1.179 \pm 0.003) + (1.05 \pm 0.01)\,\ell, \\ \left(3\,c_1\left([\mathbf{70},\ell]\right)\right)^2 &= (1.34 \pm 0.02) + (1.18 \pm 0.02)\,\ell. \end{aligned} \tag{3}$$

The main point of this analysis is that the spin-flavor singlet contributions to baryon masses can be arranged in almost perfectly linear Regge trajectories, which clearly select between the symmetric and the mixed symmetric spin-flavor states. This way of presenting Regge trajectories, instead of the usual one in terms of the physical masses, which include all other contributions breaking spin-flavor symmetry, seems to be the appropriate one. One can, in particular, easily verify that including hyperfine effects is sufficient to blur the picture to the point that the two separate trajectories cannot be clearly distinguished. One example of a clear conclusion one can draw from this analysis is the following one: since the two distinct Regge trajectories would most likely be indistinguishable if important mixing of **56**-plet and **70**-plet states would take place, one can make the strong conjecture that such mixings are most likely small.

For the other contributions to the masses, the evolution of the coefficients is less precise and is not expected to follow a regular Regge pattern. The coefficient associated with the hyperfine interaction seems to increase with the excitation but the uncertainty is large for baryons with $\ell > 2$. The increasing of the hyperfine interaction with ℓ is an interesting effect, which may have an explanation in the quark-diquark picture of baryons. Such an effect would be explained if the diquark suffers a reduction in size as ℓ increases, a picture that is intuitively plausible in flux-tube quark models of baryons. Finally, for the strangeness coefficient $c_{\mathcal{S}}$ one would expect a similar value for all multiplets. Although this cannot be confirmed by the analyses because the uncertainty in its determination is in general rather large, the results are consistent with that expectation.

Table 1: *Empirical and theoretical masses and the fitted effective coefficients for the* **56***-plets.*

Multiplet	Baryon	Name, status	Exp. [MeV]	Th. [MeV]	c_1 [MeV]	$c_{\rm HF}$ [MeV]	$c_{\mathcal{S}}$ [MeV]	c_4 [MeV]	$\chi^2_{\rm dof}$
$[\mathbf{56}, 0^+]$	$\mathrm{N}_{1/2}$	N(939)****	939 ± 1	939 ± 2	362 ± 1	295 ± 3	208 ± 3	90 ± 5	9.1
	$\Lambda_{1/2}$	Λ(1116)****	1116 ± 1	1117 ± 1					
	${}^8\Sigma_{1/2}$	Σ(1193)****	1192 ± 4	1177 ± 4					
	${}^8\Xi_{1/2}$	Ξ(1318)****	1318 ± 3	1325 ± 4					
	$\Delta_{3/2}$	Δ(1232)****	1232 ± 1	1233 ± 2					
	${}^{10}\Sigma_{3/2}$	Σ(1385)****	1383 ± 3	1381 ± 1					
	${}^{10}\Xi_{3/2}$	Ξ(1530)****	1532 ± 1	1529 ± 2					
	$\Omega_{3/2}$	Ω(1672)****	1672 ± 2	1677 ± 2					
$[\mathbf{56}, 2^+]$	$\mathrm{N}_{3/2}$	N(1720)****	1700 ± 50	1682 ± 18	603 ± 5	767 ± 66	233 ± 46	416 ± 124	1.9
	$\Lambda_{3/2}$	Λ(1890)****	1880 ± 30	1822 ± 11					
	$\mathrm{N}_{5/2}$	N(1680)****	1683 ± 8	1682 ± 17					
	$\Lambda_{5/2}$	Λ(1820)****	1820 ± 5	1822 ± 11					
	${}^8\Sigma_{5/2}$	Σ(1915)****	1918 ± 18	1915 ± 38					
	$\Delta_{1/2}$	Δ(1910)****	1895 ± 25	1938 ± 18					
	$\Delta_{3/2}$	Δ(1920)***	1935 ± 35	1938 ± 18					
	$\Delta_{5/2}$	Δ(1905)****	1895 ± 25	1938 ± 18					
	$\Delta_{7/2}$	Δ(1950)****	1950 ± 10	1938 ± 18					
	${}^{10}\Sigma_{7/2}$	Σ(2030)****	2033 ± 8	2032 ± 18					
$[\mathbf{56}, 4^+]$	$\mathrm{N}_{9/2}$	N(2220)****	2245 ± 65	2245 ± 92	770 ± 20	398 ± 372	110 ± 94		0.13
	$\Lambda_{9/2}$	Λ(2350)***	2355 ± 15	2355 ± 21					
	$\Delta_{7/2}$	Δ(2390)*	2387 ± 88	2378 ± 84					
	$\Delta_{9/2}$	Δ(2300)*	2318 ± 132	2378 ± 84					
	$\Delta_{11/2}$	Δ(2420)*	2400 ± 100	2378 ± 84					
$[\mathbf{56}, 6^+]$	$\mathrm{N}_{13/2}$	N(2700)**	2806 ± 207	2806 ± 207	954 ± 40	342 ± 720			
	$\Delta_{15/2}$	Δ(2950)**	2920 ± 122	2920 ± 122					

Table 2: *Empirical and theoretical masses and the fitted effective coefficients for the* **70***-plets.*

Multiplet	Baryon	Name, status	Exp. [MeV]	Th. [MeV]	c_1 [MeV]	$c_{\rm HF}$ [MeV]	$c_{\mathcal{S}}$ [MeV]	$\chi^2_{\rm dof}$
$[\mathbf{70}, 1^-]$	$\mathrm{N}_{1/2}$	N(1535)****	1538 ± 18	1513 ± 14	529 ± 5	443 ± 19	148 ± 13	61
	${}^8\Lambda_{1/2}$	Λ(1670)****	1670 ± 10	1662 ± 6				
	$\mathrm{N}_{3/2}$	N(1520)****	1523 ± 8	1513 ± 14				
	${}^8\Lambda_{3/2}$	Λ(1690)****	1690 ± 5	1662 ± 6				
	${}^8\Sigma_{3/2}$	Σ(1670)****	1675 ± 10	1662 ± 6				
	${}^8\Xi_{3/2}$	Ξ(1820)***	1823 ± 5	1810 ± 15				
	$\mathrm{N}'_{1/2}$	N(1650)****	1660 ± 20	1661 ± 17				
	${}^8\Lambda'_{1/2}$	Λ(1800)***	1785 ± 65	1809 ± 12				
	${}^8\Sigma'_{1/2}$	Σ(1750)***	1765 ± 35	1809 ± 12				
	$\mathrm{N}'_{3/2}$	N(1700)***	1700 ± 50	1661 ± 17				
	$\mathrm{N}'_{5/2}$	N(1675)****	1678 ± 8	1661 ± 17				
	${}^8\Lambda'_{5/2}$	Λ(1830)****	1820 ± 10	1809 ± 12				
	${}^8\Sigma'_{5/2}$	Σ(1775)****	1775 ± 5	1809 ± 12				
	$\Delta_{1/2}$	Δ(1620)****	1645 ± 30	1661 ± 17				
	$\Delta_{3/2}$	Δ(1700)****	1720 ± 50	1661 ± 17				
	${}^1\Lambda_{1/2}$	Λ(1405)****	1407 ± 4	1514 ± 4				
	${}^1\Lambda_{3/2}$	Λ(1520)****	1520 ± 1	1514 ± 4				
$[\mathbf{70}, 2^+]$	$\mathrm{N}'_{1/2}$	N(2100)*	1926 ± 26	1987 ± 50	640 ± 16	400 (input)	120 ± 86	0.03
	$\mathrm{N}'_{5/2}$	N(2000)**	1981 ± 200	1987 ± 50				
	$\Lambda'_{5/2}$	Λ(2110)***	2112 ± 40	2108 ± 71				
	$\mathrm{N}'_{7/2}$	N(1990)**	2016 ± 104	1987 ± 50				
	$\Lambda'_{7/2}$	Λ(2020)*	2094 ± 78	2108 ± 71				
	$\Delta_{5/2}$	Δ(2000)**	1976 ± 237	1987 ± 50				
$[\mathbf{70}, 3^-]$	$\mathrm{N}_{5/2}$	N(2200)**	2057 ± 180	2153 ± 67	731 ± 17	249 ± 315	30 ± 159	0.15
	$\mathrm{N}_{7/2}$	N(2190)****	2160 ± 49	2153 ± 67				
	$\mathrm{N}'_{9/2}$	N(2250)****	2239 ± 76	2236 ± 81				
	$\Delta_{7/2}$	Δ(2200)*	2232 ± 87	2236 ± 81				
	${}^1\Lambda_{7/2}$	Λ(2100)****	2100 ± 20	2100 ± 28				
$[\mathbf{70}, 5^-]$	$\mathrm{N}_{11/2}$	N(2600)***	2638 ± 97		900 ± 20			

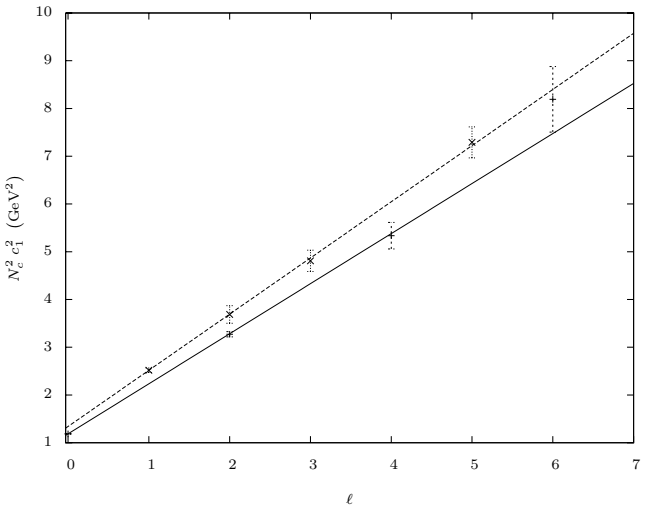

Figure 1: $(N_c\ c_1)^2$ vs ℓ for the **56**-plets (+) and the **70**-plets ($\times$) with the respective linear Regge trajectories from the fit shown in Eqn. (3).

References

1. G. 't Hooft, Nucl. Phys. **72**, 461 (1974); E. Witten, Nucl. Phys. **B160**, 57 (1979).

2. J. L. Gervais, B. Sakita, Phys. Rev. Lett. **52**, 87 (1984); Phys. Rev. **D30**, 1795 (1984); R. Dashen, A. V. Manohar, Phys. Lett. **B315**, 425 (1993); R. Dashen, A. V. Manohar, Phys. Lett. **B315**, 438 (1993).

3. R. Dashen, E. Jenkins, A. V. Manohar, Phys. Rev. **D51**, 3697 (1995).

4. J. L. Goity, Phys. Lett. **B414**, 140 (1997).

5. D. Pirjol, T. M. Yan, Phys. Rev. **D57**, 1449 (1998); D. Pirjol, T. M. Yan, Phys. Rev. **D57**, 5434 (1998); C. E. Carlson, C. D. Carone, J. L. Goity, R. F. Lebed, Phys. Lett. **B438**, 327 (1998); C. E. Carlson, C. D. Carone, J. L. Goity, R. F. Lebed, Phys. Rev. **D59**, 114008 (1999); C. L. Schat, J. L. Goity, N. N. Scoccola, Phys. Rev. Lett. **88**, 102002 (2002); J. L. Goity, C. L. Schat, N. N. Scoccola, Phys. Rev. **D66**, 114014 (2002); J. L. Goity, C. L. Schat, N. N. Scoccola, Phys. Lett. **B564**, 83 (2003); J. L. Goity, C. L. Schat and

N. N. Scoccola, Phys. Lett. **B564**, 83 (2003); N. Matagne and Fl. Stancu, Phys. Lett. **B631**, 7 (2005); N. Matagne, Fl. Stancu, Phys. Rev. **D74**, 034014 (2006).

6. C. E. Carlson, C. D. Carone, Phys. Lett. **B484**, 260 (2000); J. L. Goity, C. L. Schat, N. N. Scoccola, Phys. Rev. **D71**, 034016 (2005); J. L. Goity, N. N. Scoccola, Phys. Rev. **D72**, 034024 (2005).

7. C. E. Carlson, C. D. Carone, Phys. Rev. **D58**, 053005 (1998); C. E. Carlson, C. D. Carone, Phys. Lett. **B441**, 363 (1998); J. L. Goity, N. N. Scoccola, Phys. Rev. Lett. **99**, 062002 (2007); N. N. Scoccola, J. L. Goity, N. Matagne, arXiv:0711.4203 [hep-ph].

8. C. Semay, F. Buisseret, N. Matagne, F. Stancu, Phys. Rev. **D75**, 096001 (2007); C. Semay, F. Buisseret, F. Stancu, arXiv:0708.3291 [hep-ph].

9. J. L. Goity, N. Matagne, Phys. Lett. **B655**, 223 (2007).

10. Particle Data Group, W.-M. Yao et al., J. Phys. **G33**, 1 (2006).

11. E. Klempt, arXiv:nucl-ex/0203002.

Frascati Physics Series Vol. XLVI (2007), pp. 1309–1316
HADRON07: XII Int. Conf. on Hadron Spectroscopy – Frascati, October 8-13, 2007
Baryon Spectroscopy

PROPERTIES OF BARYON RESONANCES AND STRONG DECAYS

T. Melde and W. Plessas
Institute for Physics, Theoretical Physics, Universitätsplatz 5, Graz, Austria

Abstract

We report on the theoretical description of strong baryon decay processes within relativistic constituent quark models. Results for the π-, η- and K- decays of low lying light and strange baryon resonances are discussed in the Goldstone boson exchange constituent quark model along the point-form spectator-model leading to Poincaré-invariant partial decay widths. The results follow a systematics that, together with the invariant mass eigenvalues, spin- and flavour-structure and spatial distributions, allows for a consistent classification of the mass-eigenstates and identification with the experimentally observed baryon resonances.

1 Introduction

Modern constituent quark models (CQMs) reproduce the masses of the light and strange baryon ground and resonance states below about 2 GeV fairly

well [1]. However, in some cases disturbing discrepancies remain, like for example the $\Lambda(1405)$ resonance, whose mass cannot be explained by any CQM relying only on three-quark configurations. Other considerable uncertainties appear also in the Σ and Ξ excitation spectra, mainly due to a limited experimental data base.

The theoretical description of strong decays of light and strange baryon resonances remains a considerable challenge. So far, mostly nonrelativistic CQM calculations have been applied and the theoretical results for partial decay widths in these models greatly scatter around the experimental data [2, 3, 4, 5, 6]. While some experimental results are reproduced, it has proven difficult to explain others that grossly overestimate the measured ones. Furthermore, in the development of the decay models sometimes ad-hoc parametrizations (leading beyond the CQMs) have been introduced in order to fit the data. This makes it rather difficult to compare the various models with each other. Not surprisingly, the theoretical situation remains far from presenting a consistent picture.

Recently, we performed covariant calculations of the π, η, and K decay widths employing relativistic CQMs within the so-called point-form spectator model (PFSM) [7, 8, 9] attaining a completely different pattern for the theoretical results. In most cases, the covariant results systematically underestimate the experimental data. It also is clear that relativity plays an immense role as the nonrelativistic reduction causes large effects. In particular, the truncations in the spin-coupling terms and the neglect of Lorentz boosts introduced large changes in the theoretical predictions. Interestingly, these changes can explain the variations observed in the nonrelativistic calculations. It is noteworthy, that the Bonn group reached similar results for relativistic decay widths obtained with an instanton-induced CQM in the framework of the Bethe-Salpeter equation [10, 11]. Consequently, one can argue that the relativistic decay calculations produce a systematic pattern of the results. This allows for a more detailed investigation of the flavor multiplet classification of baryons in a relativistic CQM. In the following we show some of the implications with regard to hyperon resonances.

Table 1: *Classification of flavor octet baryons. The superscripts denote the percentages of octet content in the mass eigenstates as calculated with the GBE CQM* [15].

$(LS)J^P$				
$(0\frac{1}{2})\frac{1}{2}^+$	$N(939)^{100}$	$\Lambda(1116)^{100}$	$\Sigma(1193)^{100}$	$\Xi(1318)^{100}$
$(0\frac{1}{2})\frac{1}{2}^+$	$N(1440)^{100}$	$\Lambda(1600)^{96}$	$\Sigma(1660)^{100}$	$\Xi(1690)^{100}$
$(0\frac{1}{2})\frac{1}{2}^+$	$N(1710)^{100}$		$\Sigma(1880)^{99}$	
$(1\frac{1}{2})\frac{1}{2}^-$	$N(1535)^{100}$	$\Lambda(1670)^{72}$	$\Sigma(1560)^{94}$	
$(1\frac{3}{2})\frac{1}{2}^-$	$N(1650)^{100}$	$\Lambda(1800)^{100}$	$\Sigma(1620)^{100}$	
$(1\frac{1}{2})\frac{3}{2}^-$	$N(1520)^{100}$	$\Lambda(1690)^{72}$	$\Sigma(1670)^{94}$	$\Xi(1820)^{97}$
$(1\frac{3}{2})\frac{3}{2}^-$	$N(1700)^{100}$		$\Sigma(1940)^{100}$	
$(1\frac{3}{2})\frac{5}{2}^-$	$N(1675)^{100}$	$\Lambda(1830)^{100}$	$\Sigma(1775)^{100}$	$\Xi(1950)^{100}$

2 Systematics of strong decays

The comprehensive relativistic studies of π, η, and K decay widths [7, 8, 9] suggest a classification of light and strange baryon resonances into $SU(3)$ flavor multiplets as presented in Tables 1 and 2. Clearly, in most cases the octet and decuplet assignments agree with the ones by the PDG [12], but there also are some important differences. The $\Lambda(1810)$ is identified as a flavor singlet, not as an octet. Also, the $\Sigma(1620)$ belongs to the octet involving the $N(1650)$ in our classification. The $\Xi(1690)$ is assigned to the octet involving $N(1440)$, the $\Sigma(1560)$ falls into the octet involving $N(1535)$, the $\Sigma(1940)$ is assigned to the octet involving $N(1700)$, and the $\Xi(1690)$ as well as $\Xi(1950)$ are members of the octets involving $N(1440)$ and $N(1675)$, respectively. With the exception of the $\Lambda(1810)$ these assignments are congruent to a phenomenological classification by Guzey and Polyakov [13]. However, the identification of the $\Lambda(1810)$ as a flavor singlet is supported by the study of Matagne and Stancu [14]. While most assignments are rather well established, the Σ assignments for $J^P = \frac{1}{2}^-$ excitations should still be taken with some care, as these resonances are not all sufficiently well constrained by experiment. Improved experimental data in this sector could be very helpful to discriminate between the different theoretical models.

In Fig. 1 the relativistic results for the partial decay widths of octet

Table 2: *Classification of flavor decuplet baryons. The superscripts denote the percentages of decuplet content in the mass eigenstates as calculated with the GBE CQM* [15].

$(LS)J^P$				
$(0\frac{3}{2})\frac{3}{2}^+$	$\Delta(1232)^{100}$	$\Sigma(1385)^{100}$	$\Xi(1530)^{100}$	$\Omega(1672)^{100}$
$(0\frac{3}{2})\frac{3}{2}^+$	$\Delta(1600)^{100}$	$\Sigma(1690)^{99}$		
$(1\frac{1}{2})\frac{1}{2}^-$	$\Delta(1620)^{100}$	$\Sigma(1750)^{94}$		
$(1\frac{1}{2})\frac{3}{2}^-$	$\Delta(1700)^{100}$			

baryon resonances are given for specific decay channels. Instead of using the absolute values, we present the predictions relative to the magnitudes of the experimental data. Overall, in each one of the octets (labeled by the contained nucleon member) the theoretical widths systematically underestimate the experiments by similar amounts. However, it is also important to understand reasons for the exceptions. Clearly, the relative partial widths of $\Lambda(1670) \to \Sigma\pi$ and $\Lambda(1690) \to \Sigma\pi$ are too large compared to the others in these multiplets. The reason for this behaviour can be explained by the large admixtures of flavour singlet contributions in the corresponding eigenstates (see Table 1). The $N(1710) \to N\pi$ decay width also appears to be unusually large. In this case, the reason is not yet particularly clear, and one might suspect a deficiency in the theory and/or experiment. The $N(1650) \to N\eta$ is another exception, but this particular decay mode represents a notorious difficulty for CQMs and should not be too worrisome. The remaining results in the η channel seem to have rather large relative partial decay widths, but one should keep in mind that they are normed to phenomenological partial decay widths that are basically zero.

The $J^P = \frac{1}{2}^-$ sector of the Σ resonances is particularly interesting, because the CQMs produce three lower-lying eigenstates, while the PDG reports only one established resonance (with at least three-star), namely the $\Sigma(1750)$. Its partial width for the decay into $\Sigma\pi$ is supposed to be rather small [12], but the theoretical decay predictions of the lowest $J^P = \frac{1}{2}^-$ Σ eigenstates for this decay mode turn out to be rather big [8]. Such a behaviour would not agree with the general pattern observed in Fig. 1. Consequently, the identification of these eigenstates as the $\Sigma(1750)$ appears troublesome. The PDG also reports

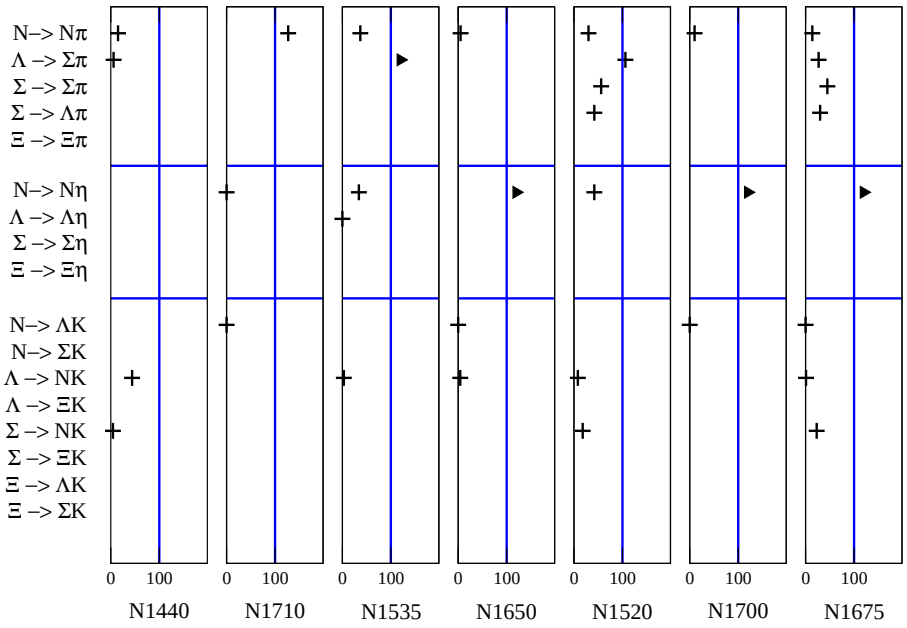

Figure 1: Covariant predictions for π, η, and K partial decay widths of octet baryon resonances by the GBE CQM [15] according to refs. [7, 8, 9]. Only established resonances (with at least three-star status) are included. The theoretical results (marked by crosses) are given as percentages of the best estimates for experimental widths reported by the PDG [12]. The multiplets are denoted by their nucleon members and follow the assignment in Table 1

two more Σ resonances lying below the $\Sigma(1750)$, but only with two-star status. The $\Sigma(1620)$ with a J^P assignment of $\frac{1}{2}^-$ and the $\Sigma(1560)$ without a definite J^P assignment are therefore candidates for the identification of the two lowest-lying eigenstates. Interpreting these two mass eigenstates as the $\Sigma(1560)$ and the $\Sigma(1620)$ and the third eigenstate as the $\Sigma(1750)$ again leads to a consistent pattern of the partial decay widths [8]. Consequently, the $\Sigma(1560)$ and the $\Sigma(1620)$ are assigned to the flavor octets as given in Table 1. However, the third eigenstate, $\Sigma(1750)$, now falls into the decuplet (cf. Table 2). We should not that this classification can be further substantiated by a more detailed investigation of baryon resonance wave functions considering their specific spin-, flavor- and spatial structures as resulting from the relativistic CQMs.

3 Conclusions and outlook

Recent relativistic results for strong decay widths of baryon resonances have produced a completely different pattern of CQM predictions. In particular, the magnitudes of the various partial decay widths are generally too small and not compatible with phenomenology. So far, we have merely considered the direct predictions of CQMs without any additional fitting of the results. However, improving the theoretical description through additional ad-hoc fit parameters might not lead to a better understanding of the underlying physics. Especially, as the findings obtained within the PFSM approach [7, 8, 9] are surprisingly similar to the ones in the framework of the Bethe-Salpeter equation [10, 11]. Clearly, the observed defects suggest missing contributions in the theoretical models. In this respect, one must bear in mind that the baryon ground and resonance states are all described as bound three-quark eigenstates of the invariant mass operator. Thus they have zero widths and in principle cannot decay. The decay amplitudes are merely calculated as transition matrix elements between the bound states. Consequently, the shortcomings should not be really surprising. For a more concise understanding of the strong decays one now must think of improvements in the description of the resonance states and the decay operator.

The PFSM provides the simplest relativistic decay mechanism, as it reduces to the elementary emission model in the nonrelativistic limit [8]. However, it is not a mere one-body operator but effectively includes many-body contributions [16, 17]. Certainly the point-form calculation is manifestly co-

variant and already contains all relativistic effects according to the spectator-model construction. Additional studies along this line, employing different quark-meson couplings, could provide further insights. Ultimately, however, improvements of the decay operator might be necessary that go beyond the spectator model.

Another step towards improvements consists in an extension of CQMs to include explicit couplings to the decay channels. In such a framework, the baryon states will receive a finite width leading to a more realistic description of the excited resonances. Of course, such a procedure will not only have an effect on the widths, but also modify the (real) mass values (cf., e.g., refs. [18, 19]). As a result a complete reconstruction of the CQMs might be necessary.

4 Acknowledgements

This work was supported by the Austrian Science Fund FWF, Project P19035. Valuable contributions to this manuscript have been made by B. Sengl and R. F. Wagenbrunn.

References

1. W. Plessas, Few-Body Syst. Suppl. **15**, 139 (2003).
2. F. Stancu and P. Stassart, Phys. Rev. D **39**, 343 (1989).
3. S. Capstick and W. Roberts, Phys. Rev. D **47**, 1994 (1993).
4. A. Krassnigg *et al.*, Few Body Syst. Suppl. **10**, 391 (1999).
5. W. Plessas *et al.*, Few Body Syst. Suppl. **11**, 29 (1999).
6. L. Theussl, R. F. Wagenbrunn, B. Desplanques, and W. Plessas, Eur. Phys. J. A **12**, 91 (2001).
7. T. Melde, W. Plessas, and R. F. Wagenbrunn, Phys. Rev. C **72**, 015207 (2005); Erratum, Phys. Rev. C **74**, 069901 (2006).
8. T. Melde, W. Plessas, and B. Sengl, Phys. Rev. C **76**, 025204 (2007).
9. B. Sengl, T. Melde, and W. Plessas, Phys. Rev. D **76**, 054008 (2007).

10. B. Metsch, AIP Conf. Proc. **717**, 646 (2004).

11. S. Migura, Ph.D. thesis, University of Bonn, Bonn, Germany, 2007.

12. W.-M. Yao *et al.*, Journal of Physics G **33**, 1+ (2006).

13. V. Guzey and M. V. Polyakov, hep-ph/0512355 (2005).

14. N. Matagne and F. Stancu, Phys. Rev. D **74**, 034014 (2006).

15. L. Y. Glozman, W. Plessas, K. Varga, and R. F. Wagenbrunn, Phys. Rev. D **58**, 094030 (1998).

16. T. Melde, L. Canton, W. Plessas, and R. F. Wagenbrunn, Eur. Phys. J. A **25**, 97 (2005).

17. T. Melde *et al.*, Phys. Rev. D **76**, 074020 (2007).

18. F. Gross and Y. Surya, Phys. Rev. C **47**, 703 (1993).

19. Y. Surya and F. Gross, Phys. Rev. C **53**, 2422 (1996).

Frascati Physics Series Vol. XLVI (2007), pp. 1317–1324
HADRON07: XII Int. Conf. on Hadron Spectroscopy – Frascati, October 8-13, 2007
Baryon Spectroscopy

PHOTOPRODUCTION OF NEUTRAL MESONS WITH CB-ELSA/TAPS

Volker Crede for the CB-ELSA/TAPS Collaboration
Florida State University, Tallahassee, U.S.A.

Abstract

The CsI(Tl) Crystal Barrel calorimeter at ELSA, University of Bonn, Germany, is the ideal instrument to study various multi-photon final states over the full dynamical range. For the data presented at this conference, the Two-Armed Photon Spectrometer (TAPS) was placed in the forward direction, serving as a fast trigger and increasing the overall angular coverage to essentially the full 4π solid angle. Preliminary differential cross sections for the reactions $\gamma p \to p\eta$ and $\gamma p \to p\eta'$ have been determined. The η meson has been studied in its two neutral decay modes ($\eta \to 3\pi^0 \to 6\gamma$ and $\eta \to 2\gamma$) for incoming photon energies in the range of $E_\gamma = 850 - 2500$ MeV. The η' meson has been identified in its neutral decay mode into $2\pi^0\eta \to 6\gamma$ for a photon energy range of $E_\gamma = 1500 - 2500$ MeV. Both the η and η' photoproduction data cover the full angular range ($-1 < \cos\theta^{cms}_{meson} < 1$). The new data show overall good agreement with recently published data from CB-ELSA and CLAS. Above $E_\gamma > 1.9$ GeV in the η' differential cross sections, a discrepancy in the absolute normalization between CLAS and CB-ELSA/TAPS is observed.

1 Introduction

The mass spectrum of hadron resonances is clearly organized according to flavor content, spin and parity. For intermediate and long-distance phenomena such as hadron properties, the full complexity of QCD emerges, including nonlinearity and confinement, and is a strong obstacle to understanding hadronic phenomena at a fundamental level. Lattice-QCD studies are making progress towards the solution of the QCD Lagrangian in the low-energy regime and for bound states, but more development is required. In the mean time, quark models have been developed to predict the properties of hadronic states. Thus, the primary goals of hadron physics are to determine the relevant degrees of freedom at different scales, to relate them to each other, and ultimately to the parameters and fundamental fields of QCD.

Models based on three constituent quark degrees of freedom predict many more states in the baryon mass spectra than have been seen experimentally. Consequently, these states are called *unobserved* or *missing*. The majority of known non-strange baryon resonances stems from πN scattering experiments. Model calculations show that for some of the missing states the πN couplings are small, but that these states should be observed in photoproduction experiments, thus providing a sensitive tool to study hadron properties. Baryon resonances have large, overlapping widths. Photoproduction of η and η' mesons has the distinct advantage of serving as an isospin filter. Both the η and η' meson have isospin $I = 0$ and for this reason, isospin conservation guarantees that the Nη and Nη' final states can only be reached via formation of N* resonances. Contributions from Δ^* states with $I = 3/2$ are excluded.

2 Experimental Setup

The data presented at the HADRON 2007 conference were accumulated in October/November of 2002 at the electron accelerator facility ELSA in Bonn (Germany) with the experimental setup shown in Fig. 1. Electrons extracted from ELSA hit a primary radiation target with an energy of 3.18 GeV and produced bremsstrahlung. The corresponding energy of the photons ($E_\gamma = E_0 - E_{e^-}$) was determined in a tagging system by the deflection of the scattered electrons in a magnetic field. This detector provided a tagged beam in the photon energy range from 0.8 GeV up to 2.5 GeV. The CsI(Tl) Crystal-Barrel

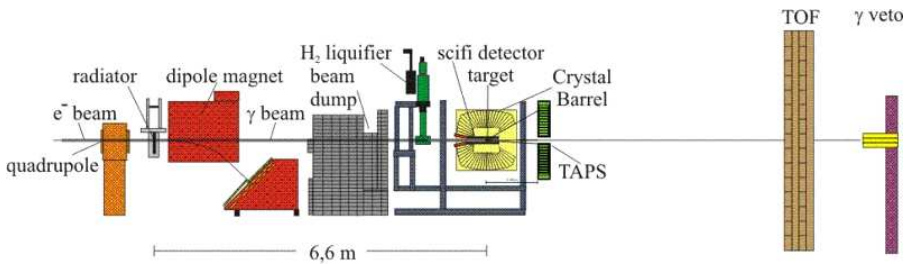

Figure 1: Experimental configuration of the CB-ELSA/TAPS experiment

calorimeter in combination with the BaF_2 TAPS forward wall covered about 98 % of the 4π solid angle. The TAPS detector had fast trigger capabilities and provided high granularity in the forward direction. This experimental configuration is an ideal instrument to study various multi-photon final states over the full dynamical range. The photoproduction target in the center of the Crystal-Barrel (5 cm in length, 3 cm in diameter) was filled with liquid hydrogen. It was surrounded by a scintillating fibre detector which provided an intersection point of a charged particle's trajectory with the detector and hence helped identify clusters of charged particles in the Crystal Barrel.

3 Data Reconstruction

Events with two and six photons were required to reconstruct the η meson in its $\gamma\gamma$ and $3\pi^0$ decay, respectively. The left side of Fig. 2 shows the $\gamma\gamma$ invariant mass spectrum after a 10^{-2} confidence-level cut in a kinematic fit enforcing energy and momentum conservation. Since the proton is identified but not used as input for the kinematic fit, its momentum is determined by kinematic fitting, resulting in only one kinematic constraint. The η meson is observed above a very small residual background. The second distribution in Fig. 2 shows the $3\pi^0$ invariant mass spectrum. The pion mass was imposed for three $\gamma\gamma$ pairs in the kinematic fit, resulting in four constraints. The data were selected with a 10^{-3} confidence-level cut. Again, the η is observed above very little background. Residual background events under the $\eta_{\gamma\gamma}$ and $\eta_{3\pi^0}$ peaks were subtracted using side bins. The right side of Fig. 2 shows a clear peak for the η' meson reconstructed from its neutral decay into $\pi^0\pi^0\eta$. A 10^{-2}

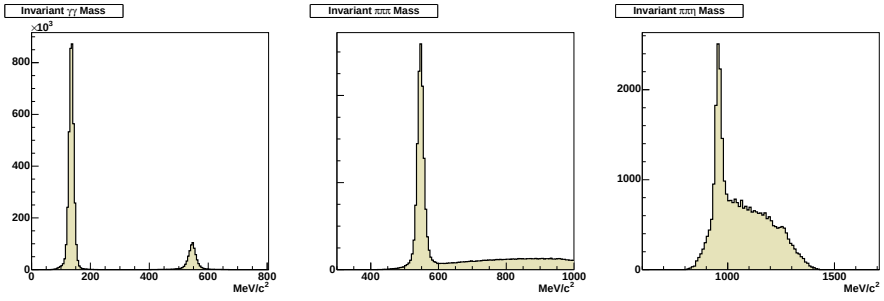

Figure 2: Invariant mass spectra indicating the excellent quality of the data. The π^0 and the η peaks in the $\gamma\gamma$ spectrum (left plot) are essentially background free. The $3\pi^0$ distribution (center) shows some residual background of about 5 % under the η peak. The $\pi^0\pi^0\eta$ distribution (right plot) shows a clear peak for the η' meson.

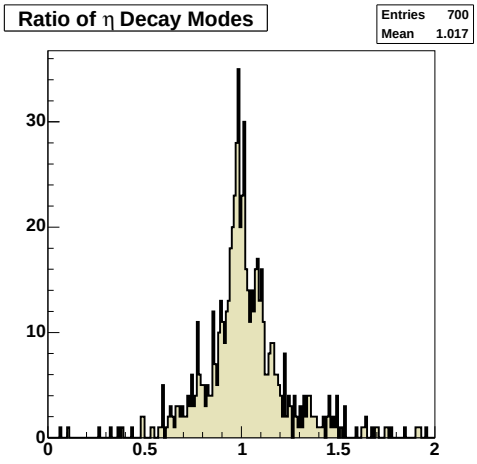

Figure 3: Plotted is the bin-wise ratio of the two independently extracted η cross sections from the decay into $3\pi^0$ and two photons, respectively. The distribution shows the overall good understanding of the detection efficiency. The two different η cross sections have been averaged in Fig. 4 and 5.

confidence-level cut was applied to a $\pi^0\eta 2\gamma$ hypothesis and the η' identified via a cut on the pion mass in the remaining invariant $\gamma\gamma$ mass spectrum.

The detector acceptance was determined from GEANT-based Monte-Carlo simulations. The overall good understanding of the detection efficiency can be seen in Fig. 3. Shown is the bin-wise ratio of the two independently extracted η cross sections from the decay into $3\pi^0$ (six-photon final state) and two photons, respectively. Consequently, the two different η cross sections have been averaged in the following (Fig. 4 and 5). The photon flux was determined by a χ^2 fit of the π^0 cross section from the same data sample to previously published CB-ELSA π^0 data [1)]. The good agreement between the 2γ- and 6γ-final states for a known cross section provides an important cross check for 4γ-final states like $p\pi^0\pi^0$ and $p\pi^0\eta$.

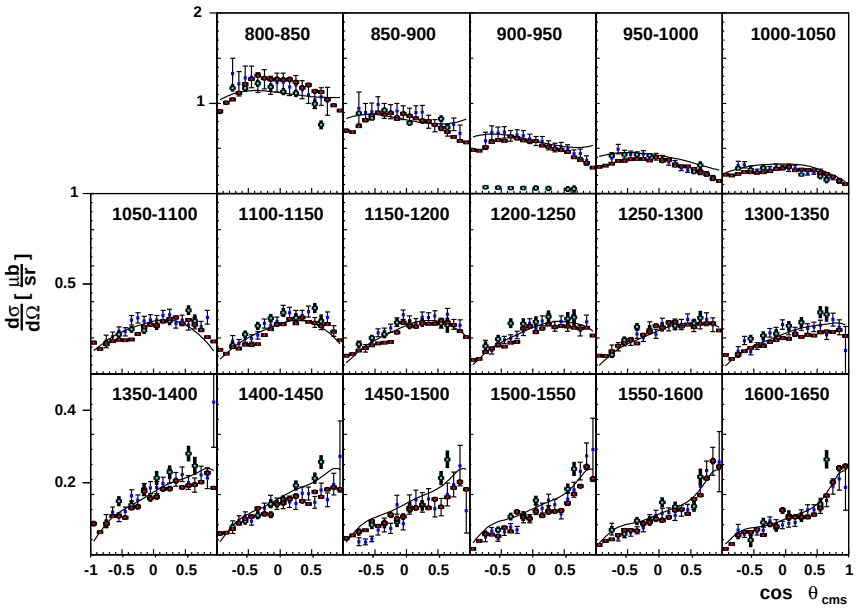

Figure 4: Preliminary cross sections for $\gamma p \rightarrow p\eta$. See text for details.

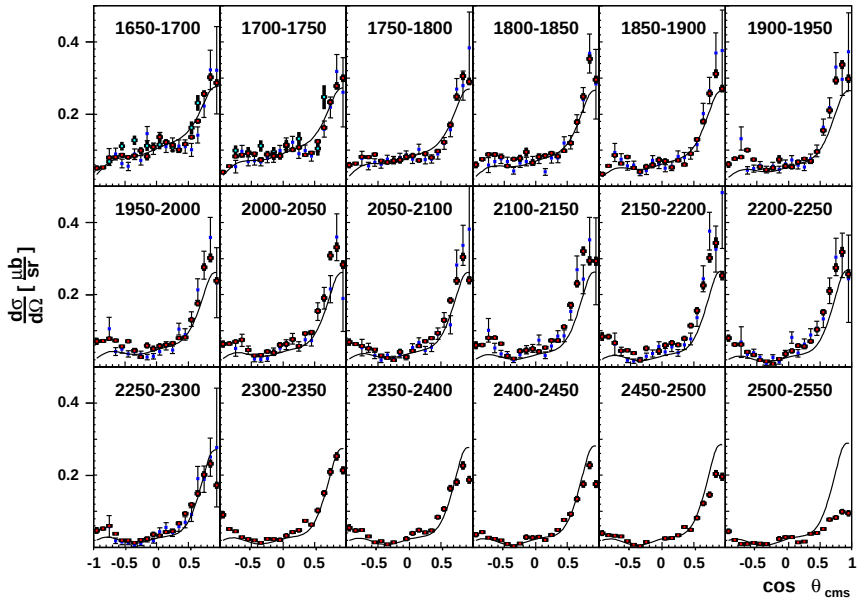

Figure 5: Preliminary cross sections for $\gamma p \to p\eta$. See text for dtails.

3.1 Preliminary Results on η Photoproudction

Fig. 4 shows preliminary differential cross sections for the reaction $\gamma p \to p\eta$ for incoming photon energies between 0.8 and 1.65 GeV in 50 MeV-wide bins of the incoming photon energy. Fig. 5 shows differential cross sections for the same reaction for incoming photon energies between 1.65 and 2.5 GeV. Shown in both figures are the new CB-ELSA/TAPS data points superimposed on recent data from CLAS [2)] and CB-ELSA [3)]. The solid line represents the latest SAID solution. The CB-ELSA/TAPS data are in good agreement with previously determined and published cross sections. More important, they cover the full angular range of the meson in the center-of-mass system: $-1 < \cos\theta_\eta^{cms} < 1$. Resonance production is observed up to high energies. The rise of the cross section in the very forward direction is generally associated with the production of η mesons in the t-channel. A partial wave analysis to identify resonance contributions is in preparation.

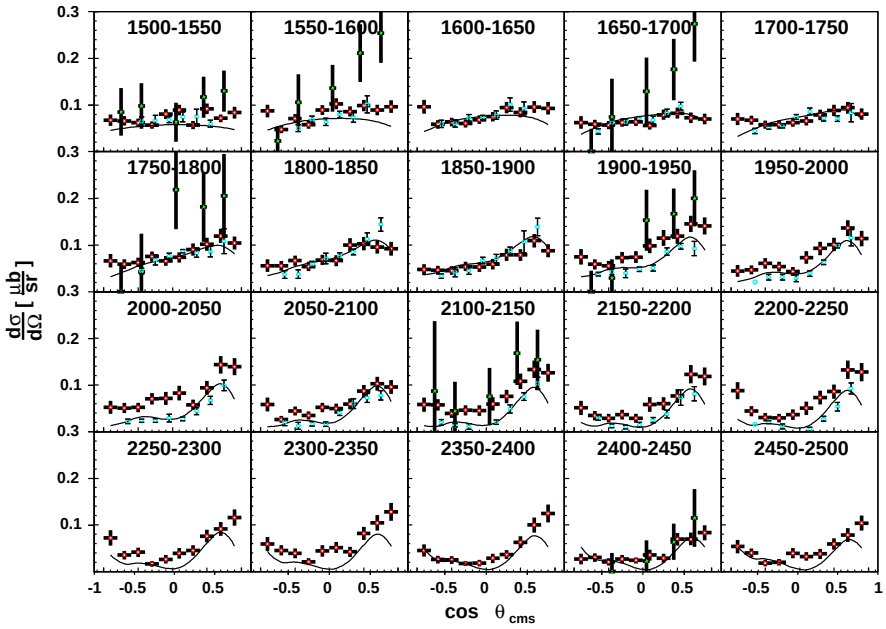

Figure 6: Preliminary differential cross sections for the reaction $\gamma p \rightarrow p\eta'$ for incoming photon energies between 1.5 and 2.5 GeV. Shown are the CB-ELSA/TAPS data points superimposed on recent data from CLAS and a very low-statistics sample from SAPHIR.

4 Preliminary Results on η' Photoproduction

Differential cross sections for the reaction $\gamma p \rightarrow p\eta'$ have been determined for a tagged photon beam with energies from 1525 to 2475 MeV (Fig. 6). The η' is identified in its all-neutral decay to $\pi^0\pi^0\eta$ (Fig. 2, right side). For the first time again, the extracted cross sections cover the full angular range. These data should continue to prove quite useful in guiding future experimental and theoretical investigations of the structure of the nucleon. Shown also in Fig. 6 are results from the SAPHIR experiment [4)] and recent results from the CLAS collaboration [5)]. There is good overall agreement of the angular distributions between the new CB-ELSA/TAPS and the CLAS data. However,

a discrepancy in the absolute normalization of about a factor of 2 seems to occur at an incoming photon energy of 1900 MeV and beyond. The SAPHIR results are based on only 250 events and show large error bars. The linear forward rise was originally consistent with a coherent excitation of two resonances, S_{11} and P_{11}, with masses of 1897 and 1986 MeV, respectively. Analyses of the CLAS data suggest a strong coupling of the $N\eta'$ channel to both the $N(1535)S_{11}$ and $N(1710)P_{11}$ resonances and the importance of $J = 3/2$ states in the process.

5 Summary and Conclusion

The CB-ELSA collaboration recently reported evidence for a new $N(2070)D_{15}$ resonance in η photoproduction data [3]. The isobar analysis of these data, which also included other data sets, found eleven nucleon resonances that couple to $p\eta$ and identified three dominant contributions to this channel: $N(1535)S_{11}$, $N(1720)P_{13}$, and $N(2070)D_{15}$. A new partial wave analysis is in preparation to confirm these findings on the basis of the new CB-ELSA/TAPS data presented here.

6 Acknowledgements

I would like to thank the technical staff at ELSA and all participating institutions for valuable advise and contributions to the analysis. I acknowledge financial support from the National Science Foundation.

References

1. H. van Pee *et al.* [CB-ELSA Collaboration], Eur. Phys. J. A **31**, 61 (2007) [arXiv:0704.1776 [nucl-ex]].
2. M. Dugger *et al.* [CLAS Collaboration], Phys. Rev. Lett. **89**, 222002 (2002) [Erratum-ibid. **89**, 249904 (2002)].
3. V. Crede *et al.* [CB-ELSA Collaboration], Phys. Rev. Lett. **94**, 012004 (2005) [arXiv:hep-ex/0311045].
4. R. Plotzke *et al.* [SAPHIR Collaboration], Phys. Lett. B **444** (1998) 555.
5. M. Dugger *et al.* [CLAS Collaboration], Phys. Rev. Lett. **96** (2006) 062001, [Erratum-ibid. **96** (2006) 169905]

Frascati Physics Series Vol. XLVI (2007), pp. 1325–1332
HADRON07: XII Int. Conf. on Hadron Spectroscopy – Frascati, October 8-13, 2007
Baryon Spectroscopy

EVIDENCE FOR NEW RESONANCES IN THE COMBINED ANALYSIS OF RECENT HYPERON PHOTOPRODUCTION DATA

V.A. Nikonov
Helmholtz-Institut für Strahlen- und Kernphysik, Uni-Bonn, Germany
Petersburg Nuclear Physics Institute, Gatchina, Russia

Abstract

A partial wave analysis of data on photoproduction of hyperons including single and double polarization observables is presented. The large spin transfer probability reported by the CLAS collaboration can be successfully described within an isobar partial wave analysis.

The new CLAS data on hyperon photoproduction [1)] show a remarkably large spin transfer probability. In the reactions $\gamma p \to \Lambda K^+$ and $\gamma p \to \Sigma K^+$ using a circularly polarized photon beam, the polarizations of the Λ and Σ hyperons were monitored by measurements of their decay angular distributions. For photons with helicity $h_\gamma = 1$, the magnitude of the Λ polarization vector was found to be close to unity, 1.01 ± 0.02 when integrated over all production angles and all center-of-mass energies W. For Σ photoproduction, the polarization was determined to be 0.82 ± 0.03 (again integrated over all energies and

angles), still a remarkably large value. The polarization was determined from the expression $\sqrt{C_x^2 + C_z^2 + P^2}$, where C_z is the projection of the hyperon spin onto the photon beam axis, P the spin projection on the normal-to-the-reaction plane, and C_x the spin projection in the center-of-mass frame onto the third axis. The measurement of polarization effects for both Λ and Σ hyperons is particularly useful. The ud pair in the Λ is antisymmetric in both spin and flavour; the ud quark carries no spin, and the Λ polarization vector is given by the direction of the spin of the strange quark. In the Σ hyperon, the ud quark is in a spin-1 state and points into the direction of the Σ spin while the spin of the strange quark is opposite to it.

Independently of the question if the polarization phenomena require an interpretation on the quark or on the hadron level, the large polarization seems to contradict an isobar picture of the process in which intermediate N^*'s and Δ^*'s play a dominant role. It is therefore important to see if the data are compatible with such an isobar interpretation or not.

1 Data and fits

The data used in this analysis comprise differential cross section for $\gamma p \to K^+\Lambda$, $K^+\Sigma^0$, Σ^+K^0 including their recoil polarization and the photon beam asymmetry, and the recent spin transfer measurements [1, 2, 3, 4, 5, 6, 7, 8]. Data are included from the SAID data base [9, 10, 11, 12, 13, 14, 15, 16, 17] on photoproduction of π^0 and η with measurements of differential cross sections, beam and target asymmetries and recoil polarization. We did not use the $K^+\Sigma^0$ recoil polarization data from [5] since they have larger errors and a smaller energy range than the CLAS data.

The fit also used data on photo-induced $2\pi^0$ production [18, 19] and $\pi^0\eta$ [20] and the recent BNL data on $\pi^- p \to n\pi^0\pi^0$ [21] in an event-based likelihood fit. $2\cdot\ln\mathcal{L}$ was added to the pseudo-χ^2 function. The data essentially determined the contributions of isobars to the $N\pi\pi$ and $N\pi\eta$ final state and are not discussed here further. Details can be found in [18, 19, 20].

Data on πN elastic data from the SAID data base [22] were used for those partial waves which are described by a K-matrix.

Two separate classes of solutions were found, giving rather different isobar contributions. These will be compared in the discussion of the data. The two classes of solutions will be called solution 1 and 2, respectively.

New resonance is added to describe the new CLAS data, the $N(1900)P_{13}$, for which so far, evidence had been weak only. It is surprising that the new very significant data on C_x and C_z are well described by introducing just one single resonance to the model. Compared to our previous analysis [23, 24], the $\Delta(1600)P_{33}$ and $N(1710)P_{11}$ have been introduced when the data on two-pion production and the elastic πN scattering amplitude were included in the fit [18, 19]. Here, just $N(1900)P_{13}$ was added. We also tried to introduce additional resonances, one by one, in the $1/2^{\pm}$, $3/2^{\pm}$, $5/2^{\pm}$, $7/2^{\pm}$, $9/2^{\pm}$ partial waves, without finding a significant improvement.

The $\gamma p \to K^+\Lambda$ differential cross section was measured recently by CLAS with large statistics [2]. The total cross section does not show a narrow peak in the $\gamma p \to K^+\Lambda$ cross section at 1700 MeV as suggested by older data [3, 4] but for which we did not find a physical interpretation in our previous fits [23, 24]. The SAPHIR data are still included using a relative normalisation function as described in [24]. The total cross section seems to be better described by solution 1. However, the quality of the description of the angular distributions is very similar for both solutions; discrepancies in the total cross sections are due to the extrapolation into regions where no data exist. Hence, the total cross section cannot be used to favor solution 1 over solution 2. Note, that the total cross section is calculated as sum of the measured differential cross sections and the integrated fit result for the angular region where data are not available.

Fig. 1 shows the data on C_x and C_z and the fit obtained with solution 1 and 2. This is the data which gave the surprising large value for the spin transfer probability from the circularly polarized photon in the initial state to the final state hyperon. For both observables a very satisfactory agreement between data and fit is achieved. Small deviations show up in two mass slices in the 2.1 GeV mass region. These should however not be over-interpreted. $C_x^2 + C_z^2 + P^2$ is constrained by unity; in the corresponding mass- and $\cos\Theta_K$ bins, C_z^2 and the recoil polarization are sizable pointing at a statistical fluctuation beyond the physical limits. Of course, a fit must not follow data into not allowed regions.

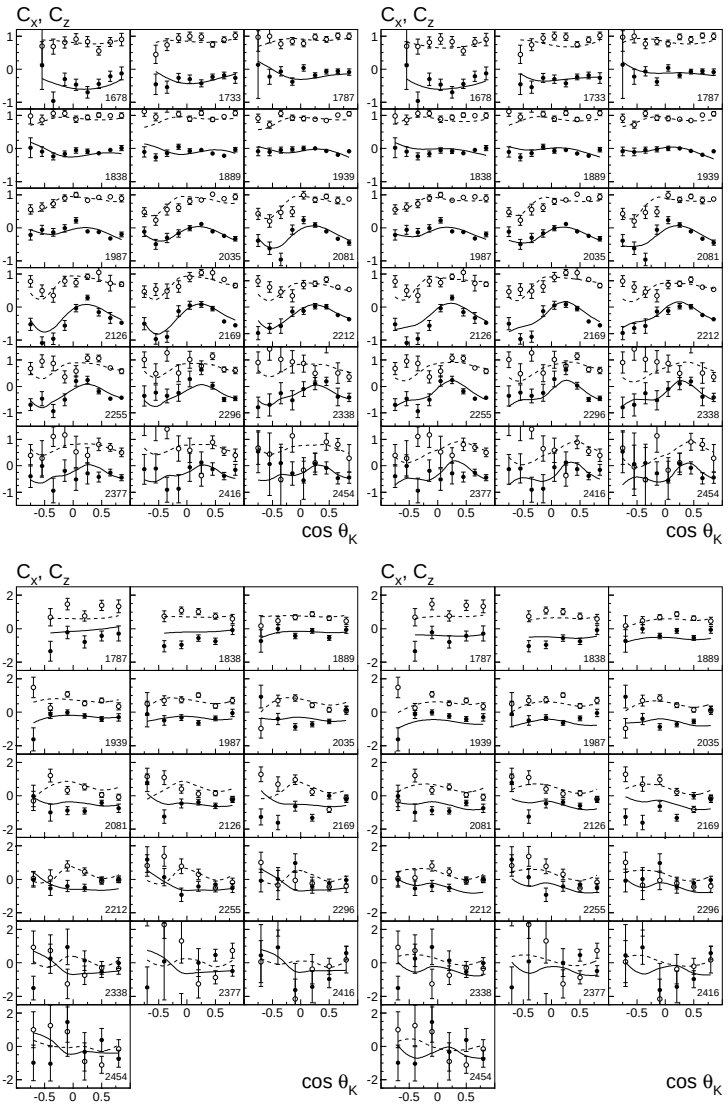

Figure 1: *Double polarization observables C_x (black circle) and C_z (open circle) for $\gamma p \to K^+\Lambda$ (top panel) and $\gamma p \to K^+\Sigma^0$ (bottom panel)* [1]*. The solid and dashed curves are results of our fit obtained with solution 1 (left) and solution 2 (right) for C_x and C_z, respectively.*

2 Evidence for the $N(1900)P_{13}$

The fits described in this paper used a number of new reactions, and a variety of different results were obtained. The reaction $\gamma p \to p\pi^0\pi^0$ was studied by the CBELSA collaboration [18]. The analysis returned decays of baryon resonances in the third resonance region into $p\pi^0\pi^0$ via different isobars like $\Delta(1232)\pi$, $N(\pi\pi)_{\mathrm{S-wave}}$, $N(1440)\pi$, and others. In connection with precise low-energy data on $\gamma p \to p\pi^0\pi^0$ of the A2/TAPS collaboration at MAMI, properties of the Roper resonance were derived [19]. The reaction $\gamma p \to p\pi^0\eta$ [20] required introduction of a $\Delta(1940)D_{33}$ which is suggested to form, jointly with $\Delta(1900)S_{31}$ and $\Delta(1930)D_{35}$, a triplet of resonances at a rather low mass, incompatible with quark model calculations. The new CLAS data on C_x and C_z require introduction of a $N(1900)P_{13}$ resonance; without it no good description of the data was reached [25].

The effect of removing the $N(1900)P_{13}$ resonance from the fit can be seen in figure 1 of [25]. The fit quality changes by $\chi^2_{\mathrm{tot}} = 1540$ units. The $N(1900)P_{13}$ was replaced by resonances with other quantum numbers. Replacing it by an S_{11} {or D_{15}} state, χ^2_{2b} changed by 950 {970} only. Using P_{11} quantum numbers (instead of P_{13}) gave $\Delta\chi^2_{\mathrm{2b}} = 205$ only. An F_{15} state improved χ^2_{2b} marginally; introducing F_{17} and G_{17} did not improve the fit. A resonance with P_{33} quantum numbers provided a change in χ^2_{2b} which was smaller by a factor 2 than the one found for a P_{13} state.

In a final step, the P_{13} was parameterized as 3-pole 8-channel K-matrix with πN, ηN, $\Delta(1232)\pi$ (P and F-waves), $N\sigma$, $D_{13}(1520)\pi$ (S-wave), $K\Lambda$ and $K\Sigma$ channels. This resulted in the fit solutions 1 and 2 which both are compatible with a large body of data. Both solutions are compatible with elastic πN scattering. Real and imaginary part of the P_{13} partial wave [22] are satisfactorily described for invariant masses up to 2.4 GeV. From the fit, properties of resonances in the P_{13}-wave were derived. The lowest-mass pole is identified with the established $N(1720)P_{13}$, the second pole with the badly known $N(1900)P_{13}$. A third pole is introduced at about 2200 MeV. It improves the quality of the fit in the high-mass region but its quantum numbers cannot be deduced safely from the present data base.

The first P_{13} state was found to be much broader than suggested by most other analyses [26]. However, the only analysis taking $N\pi\pi$ data into account gives a width of (380 ± 180) MeV [27]. The most recent analysis of

elastic scattering data [22] gave a 355 MeV width. The elastic width of the $N(1720)P_{13}$ (≈ 45 MeV) is even narrower than the $N(1680)F_{15}$ elastic width ≈ 85 MeV). Given the large spread of pole positions reported in [26], we do not think that our result is in conflict with previous work.

3 Discussion

Triggered by the measurement of the spin transfer coefficients C_x and C_z we have refitted data on single π, η, K^0 and K^+ photoproduction. Besides C_x and C_z the new data on unpolarised differential cross section for $\gamma N \to K^+\Lambda$, $\gamma N \to K^+\Sigma^0$, and $K^0\Sigma^+$ photoproduction, and double pion production data were added to the combined analysis. The refit was motivated by the bad prediction of the spin transfer coefficients with our previous partial wave analysis. All data sets can be described well after introducing a $N(1900)P_{13}$ resonance. Its mass and width are estimated to 1915 ± 50 MeV and 180 ± 50 MeV, respectively. This result covers the two K-matrix solutions found here: in the first one, the pole position of the second P_{13} state is located at $1870 - i\,85$ MeV and in the second solution at $1960 - i88$ MeV. The reason for the ambiguity is likely connected with the existence of a P_{11} state with similar mass and width.

Even though the description of all distributions is very reasonable, the two solutions have remarkably different isobar contributions. In solution 1, the P_{13} partial wave shows a significant double structure (not present in solution 2). The S_{11} wave is much stronger in solution 2.

The new P_{13} state [25] also improves the description of the $\gamma p \to K^+\Sigma^0$ reaction. However the effect from introducing this state is much smaller here. Actually, in our previous analysis, the double polarization data of this channel were already described much better than those for $\gamma p \to K\Lambda$ (see figures in [1]); a fully satisfactory description was already achieved after a slight readjustment of the fit parameters. Nevertheless, the P_{13} state definitely improved the description and provided a noticeable signal in the $\gamma p \to K^+\Sigma^0$ total cross section. Differential and total cross sections had already been described successfully when a P_{11} state was introduced at 1840 MeV [24]. When both states, P_{11} and P_{13}, were introduced, they share about equal contributions to this cross section. The statistical significance for two states was however not convincing. So, at the end, only one resonance was introduced in [24]; the likelihood favoured P_{11} quantum numbers.

Although a qualitatively good description of all fitted observables was obtained, both solutions have some local problems.

The partial wave analysis presented here demonstrates that the CLAS findings, that the Λ (and Σ) hyperons are produced 100% (or 80%) polarized, can be described quantitatively in the conventional picture where intermediate resonances strongly contribute to the dynamics of the reactions. Even in the case of large non-resonant contribution baryon resonances still play an important role in the dynamics of the process. On the other hand, the analysis also shows that even data sets comprising various high-statistics differential cross sections, beam, target and recoil asymmetries, double polarization observables, and data which resolve the two isospin contributions (by a simultaneous analysis of the $p\pi^0$ and $n\pi^+$, the $K^+\Sigma^0$ and the $K^0\Sigma^+$ as well as the isospin selective $p\eta$ and $K^+\Lambda$ channels) are still not yet sufficient to converge into a unique solution. Systematic measurements with further double polarization observables – as being planned and carried out at several laboratories – are urgently needed.

The work was supported by the DFG within the SFB/TR16 and by a FFE grant of the Research Center Jülich. This work is also supported by RFBR 07-02-01196-a.

References

1. R. Bradford *et al.*, Phys. Rev. C **75** (2007) 035205.
2. R. Bradford *et al.*, Phys. Rev. C **73** (2006) 035202.
3. K. H. Glander *et al.*, Eur. Phys. J. A **19** (2004) 251.
4. J. W. C. McNabb *et al.*, Phys. Rev. C **69** (2004) 042201.
5. A. Lleres *et al.*, Eur. Phys. J. A **31** (2007) 79.
6. R. G. T. Zegers *et al.*, Phys. Rev. Lett. **91** (2003) 092001.
7. R. Lawall *et al.*, Eur. Phys. J. A **24** (2005) 275.
8. R. Castelijns *et al.*, "Nucleon resonance decay by the $K^0\Sigma^+$ channel," arXiv:nucl-ex/0702033.
9. O. Bartholomy *et al.*, Phys. Rev. Lett. **94** (2005) 012003.

10. O. Bartalini *et al.*, Eur. Phys. J. A **26** (2005) 399.

11. A. A. Belyaev *et al.*, Nucl. Phys. B **213** (1983) 201.

12. R.A. Arndt *et al.*, http://gwdac.phys.gwu.edu.
R. Beck *et al.*, Phys. Rev. Lett. **78** (1997) 606.
D. Rebreyend *et al.*,Nucl. Phys. A **663** (2000) 436.

13. K. H. Althoff *et al.*, Z. Phys. C **18** (1983) 199.
E. J. Durwen, BONN-IR-80-7 (1980).
K. Buechler *et al.*, Nucl. Phys. A **570** (1994) 580.

14. V. Crede *et al.*, Phys. Rev. Lett. **94** (2005) 012004.

15. B. Krusche *et al.*, Phys. Rev. Lett. **74** (1995) 3736.

16. J. Ajaka *et al.*, Phys. Rev. Lett. **81** (1998) 1797.

17. O. Bartalini *et al.*, "Measurement of η photoproduction on the proton from threshold to 1500 MeV," arXiv:0707.1385 [nucl-ex].

18. U. Thoma *et al.*, "N^* and Δ^* decays into $N\pi^0\pi^0$", arXiv:0707.3592.

19. A.V. Sarantsev *et al.*, "New results on the Roper resonance and of the P_{11} partial wave", arXiv:0707.3591.

20. I. Horn *et al.*, "Evidence for the $\Delta D_{33}(1940)$ resonance from $\gamma p \to p\pi^0\eta$ photoproduction",

21. S. Prakhov *et al.*, Phys. Rev. C **69** (2004) 045202.

22. R. A. Arndt, W. J. Briscoe, I. I. Strakovsky and R. L. Workman, Phys. Rev. C **74**, 045205 (2006)

23. A.V. Anisovich *et al.*, Eur. Phys. J. A **25** (2005) 427.

24. A. V. Sarantsev, V. A. Nikonov, A. V. Anisovich, E. Klempt and U. Thoma, Eur. Phys. J. A **25** (2005) 441.

25. V.A. Nikonov *et al.*, "Further evidence for $N(1900)P_{13}$ from photoproduction of hyperons", arXiv:0707.3600.

26. W. M. Yao *et al.* [Particle Data Group], J. Phys. G **33** (2006) 1.

27. D. M. Manley and E. M. Saleski, Phys. Rev. D **45** (1992) 4002.

Frascati Physics Series Vol. XLVI (2007), pp. 1333–1340
HADRON07: XII Int. Conf. on Hadron Spectroscopy – Frascati, October 8-13, 2007
Baryon Spectroscopy

PARTIAL WAVE ANALYSIS IN THE BONN-GATCHINA FRAMEWORK

A. V. Anisovich
HISKP, Universität Bonn, D-53115 Bonn

Abstract

Partial wave amplitudes for production and decay of baryon resonances are constructed in the framework of the operator expansion method. The approach is applied to the partial wave analysis of a large data set. A number of new baryon states is observed in the analysis and their properties are discussed.

1 Introduction

Most information about baryons comes from pion- and photon-induced production of single mesons. However the experience from meson spectroscopy shows that excited states decay dominantly into multi-body channels and are not observed reliably in the elastic cross section. Thus reactions with three or more final states provide rich information about the properties of hadronic resonances.

The task to extract pole positions and residues from multi-body final states is however not a simple one. Main problems can be traced to the large interference effects between different isobars and to contributions from singularities related to multi-body interactions. In our method, singularities in the reaction can be classified, resonances which are closest to the physical region can be taken into account accurately. Other contributions can be parameterized in an efficient way.

One of the key points in this approach is the operator decomposition method which provides a tool for a universal construction of partial wave amplitudes for reactions with two– and many–body final states.

2 The structure of fermion propagator

The angular dependence of the single-meson-production amplitude via an intermediate resonance with $J = n + 1/2$ has the general form [1), 2)]:

$$\bar{u}(q_1)\tilde{N}^{\pm}_{\alpha_1\ldots\alpha_n}(q^{\perp})F^{\alpha_1\ldots\alpha_n}_{\beta_1\ldots\beta_n}(P)V^{(i\pm)\mu}_{\beta_1\ldots\beta_n}(k^{\perp})u(k_1)\varepsilon_{\mu}\ . \tag{1}$$

Here q_1 and k_1 are the momenta of the nucleon in the πN and γN channel and $q^{\perp}$ and $k^{\perp}$ are the components of the relative momenta which are orthogonal to the total momentum of the resonance. The fermion propagator has the structure:

$$F^{\mu_1\ldots\mu_n}_{\nu_1\ldots\nu_n}(p) = (m+\hat{p})O^{\mu_1\ldots\mu_n}_{\alpha_1\ldots\alpha_n}T^{\alpha_1\ldots\alpha_L}_{\beta_1\ldots\beta_L}O^{\beta_1\ldots\beta_L}_{\nu_1\ldots\nu_L} \tag{2}$$

Here $(m+\hat{p})$ corresponds to the propagator for a fermion with $J = 1/2$. The operator $T^{\mu_1\ldots\mu_L}_{\nu_1\ldots\nu_L}$ describes the tensor structure of the propagator. It is equal to 1 for a $J = 1/2$ particle and is proportional to $g^{\perp}_{\mu\nu} - \gamma^{\perp}_{\mu}\gamma^{\perp}_{\nu}/3$ for a particle with spin $J = 3/2$ ($\gamma^{\perp}_{\mu} = g^{\perp}_{\mu\nu}\gamma_{\nu}$).

$$\begin{aligned} T^{\alpha_1\ldots\alpha_L}_{\beta_1\ldots\beta_L} &= \frac{L+1}{2L+1}\big(g^{\perp}_{\alpha_1\beta_1} - \frac{L}{L+1}\sigma^{\perp}_{\alpha_1\beta_1}\big)\prod_{i=2}^{L} g^{\perp}_{\alpha_i\beta_i}, \\ \sigma^{\perp}_{\mu\nu} &= \frac{1}{2}(\gamma^{\perp}_{\mu}\gamma^{\perp}_{\nu} - \gamma^{\perp}_{\nu}\gamma^{\perp}_{\mu}) \end{aligned} \tag{3}$$

The operators which describe the decay of a baryon state into the πN system are the following

$$\begin{aligned} N^{+}_{\mu_1\ldots\mu_n}(k^{\perp}) &= X^{(L)}_{\mu_1\ldots\mu_n}(k^{\perp})\ . \\ N^{-}_{\mu_1\ldots\mu_n}(k^{\perp}) &= i\gamma_5\gamma_{\nu}X^{(n+1)}_{\nu\mu_1\ldots\mu_n}(k^{\perp})\ . \end{aligned} \tag{4}$$

The decay of the states into γN is described by the following operators:

$$\begin{aligned} V^{(1+)\mu}_{\alpha_1\ldots\alpha_L}(k^\perp) &= \gamma_\mu i\gamma_5 X^{(L)}_{\alpha_1\ldots\alpha_L}(k^\perp)\,, \\ V^{(2+)\mu}_{\alpha_1\ldots\alpha_L}(k^\perp) &= \gamma_\nu i\gamma_5 X^{(L+2)}_{\mu\nu\alpha_1\ldots\alpha_L}(k^\perp)\,, \\ V^{(3+)\mu}_{\alpha_1\ldots\alpha_L}(k^\perp) &= \gamma_\nu i\gamma_5 X^{(L)}_{\nu\alpha_1\ldots\alpha_{L-1}}(k^\perp) g^\perp_{\mu\alpha_L}\,. \end{aligned} \tag{5}$$

$$\begin{aligned} V^{(1-)\mu}_{\alpha_1\ldots\alpha_{L-1}}(k^\perp) &= \gamma_\xi\gamma_\mu X^{(L)}_{\xi\alpha_1\ldots\alpha_{L-1}}(k^\perp)\,, \\ V^{(2-)\mu}_{\alpha_1\ldots\alpha_{L-1}}(k^\perp) &= X^{(L)}_{\mu\alpha_1\ldots\alpha_{L-1}}(k^\perp)\,, \\ V^{(3-)\mu}_{\alpha_1\ldots\alpha_{L-1}}(k^\perp) &= X^{(L-2)}_{\alpha_2\ldots\alpha_{L-1}}(k^\perp) g^\perp_{\alpha_1\mu}\,. \end{aligned} \tag{6}$$

3 The partial wave formalism

In our approach high-spin resonances are described by relativistic multi-channel Breit-Wigner amplitudes and important partial waves with low total spin ($J < 5/2$) are described in the framework of the K-matrix/P-vector approach. The amplitude for elastic scattering is given by

$$\hat{A}(s) \;=\; \hat{K}\,(\hat{I} \;-\; i\hat{\rho}\hat{K})^{-1}\,, \tag{7}$$

where the phase space matrix $\hat{\rho}$ is a diagonal matrix. The photoproduction amplitude can be written in the P-vector approach. The P-vector amplitude is then given by

$$A_a \;=\; \hat{P}_b\,(\hat{I} \;-\; i\hat{\rho}\hat{K})^{-1}_{ba}\,. \tag{8}$$

The production vector $\hat{P}$ and the K-matrix $\hat{K}$ have the following parameterizations:

$$K_{ab} \;=\; \sum_\alpha \frac{g^{(\alpha)}_a g^{(\alpha)}_b}{M^2_\alpha - s} \;+\; f_{ab}, \quad P_b \;=\; \sum_\alpha \frac{g^{(\alpha)}_{\gamma\mathrm{N}} g^{(\alpha)}_b}{M^2_\alpha - s} \;+\; \tilde{f}_b \tag{9}$$

where M_α, $g^{(\alpha)}_a$ and $g^{(\alpha)}_{\gamma\mathrm{N}}$ are the mass, coupling constant and photo-coupling of the resonance α; f_{ab} describes direct non-resonant transition processes from an initial state a to a final state b. The production process may have a non-resonant contribution due to $\tilde{f}_b$. In general, these non-resonant contributions are functions of s. For all partial waves except S_{11}, it is sufficient to assume f_{ab} and $\tilde{f}_b$ to be constants.

Table 1: *Hyperon photoproduction data used in the partial wave analysis and* χ^2 *for solutions 1 and 2.*

Observable	N_{data}	w_i	$\frac{\chi^2}{N_{\mathrm{data}}}$	$\frac{\chi^2}{N_{\mathrm{data}}}$	Ref.
			Sol. 1	Sol. 2	
$C_x(\gamma\mathrm{p} \to \Lambda\mathrm{K}^+)$	160	5	1.71	1.66	7)
$C_z(\gamma\mathrm{p} \to \Lambda\mathrm{K}^+)$	160	7	1.95	2.34	7)
$\sigma(\gamma\mathrm{p} \to \Lambda\mathrm{K}^+)$	1377	5	2.02	1.99	8)
$\sigma(\gamma\mathrm{p} \to \Lambda\mathrm{K}^+)$	720	1	1.53	1.55	12)
$\mathrm{P}(\gamma\mathrm{p} \to \Lambda\mathrm{K}^+)$	202	6.5	1.65	2.28	13)
$\mathrm{P}(\gamma\mathrm{p} \to \Lambda\mathrm{K}^+)$	66	3	2.89	1.05	14)
$\Sigma(\gamma\mathrm{p} \to \Lambda\mathrm{K}^+)$	66	5	2.19	2.85	14)
$\Sigma(\gamma\mathrm{p} \to \Lambda\mathrm{K}^+)$	45	10	1.98	1.82	15)
$C_x(\gamma\mathrm{p} \to \Sigma^0\mathrm{K}^+)$	94	5	2.70	3.50	7)
$C_z(\gamma\mathrm{p} \to \Sigma^0\mathrm{K}^+)$	94	5	2.77	2.24	7)
$\sigma(\gamma\mathrm{p} \to \Sigma^0\mathrm{K}^+)$	1280	3	2.10	2.19	8)
$\sigma(\gamma\mathrm{p} \to \Sigma^0\mathrm{K}^+)$	660	1	1.33	1.41	12)
$\mathrm{P}(\gamma\mathrm{p} \to \Sigma^0\mathrm{K}^+)$	95	6	1.58	1.94	13)
$\Sigma(\gamma\mathrm{p} \to \Sigma^0\mathrm{K}^+)$	42	5	1.04	1.34	14)
$\Sigma(\gamma\mathrm{p} \to \Sigma^0\mathrm{K}^+)$	45	10	0.62	0.76	15)
$\sigma(\gamma\mathrm{p} \to \Sigma^+\mathrm{K}^0)$	48	2.3	3.51	3.41	13)
$\sigma(\gamma\mathrm{p} \to \Sigma^+\mathrm{K}^0)$	120	5	0.98	1.09	16)
$\sigma(\gamma\mathrm{p} \to \Sigma^+\mathrm{K}^0)$	72	5	1.17	0.77	17)

Table 2: *Single π and η production data used in the partial wave analysis and χ^2 for solutions 1 and 2.*

Observable	N_{data}	w_i	$\frac{\chi^2}{N_{\mathrm{data}}}$	$\frac{\chi^2}{N_{\mathrm{data}}}$	Ref.
			Sol. 1	Sol. 2	
$\sigma(\gamma\mathrm{p} \to \mathrm{p}\pi^0)$	1106	7	0.99	1.03	18)
$\sigma(\gamma\mathrm{p} \to \mathrm{p}\pi^0)$	861	3	3.22	2.44	19)
$\Sigma(\gamma\mathrm{p} \to \mathrm{p}\pi^0)$	469	2.3	3.75	3.35	19)
$\Sigma(\gamma\mathrm{p} \to \mathrm{p}\pi^0)$	593	2.3	2.13	2.20	20)
$\mathrm{P}(\gamma\mathrm{p} \to \mathrm{p}\pi^0)$	594	3	2.58	2.54	21)
$\mathrm{T}(\gamma\mathrm{p} \to \mathrm{p}\pi^0)$	380	3	3.85	3.90	21)
$\sigma(\gamma\mathrm{p} \to \mathrm{n}\pi^+)$	1583	2.8	1.07	1.27	22)
$\sigma(\gamma\mathrm{p} \to \mathrm{p}\eta)$	667	30	0.84	0.77	23)
$\sigma(\gamma\mathrm{p} \to \mathrm{p}\eta)$	100	7	1.69	1.97	24)
$\Sigma(\gamma\mathrm{p} \to \mathrm{p}\eta)$	51	10	1.82	1.91	25)
$\Sigma(\gamma\mathrm{p} \to \mathrm{p}\eta)$	100	10	2.11	2.24	26)
$\gamma \to p2\pi^0$	160k	3	likelihood fit		3)
$\gamma \to p\pi^0\eta$	16k	5	likelihood fit		5)
$\pi^- p \to n2\pi^0$	180k	2.5-4	likelihood fit		6)
$P_{11}(\pi N \to N\pi)$	110	20	1.60	1.74	11)
$P_{13}(\pi N \to N\pi)$	134	10	3.78	2.83	11)
$S_{11}(\pi N \to N\pi)$	126	30	1.86	1.84	11)
$D_{33}(\pi N \to N\pi)$	108	12	1.88	2.69	11)

Table 3: *Properties of $N(1440)P_{11}$. The left column lists mass, width, partial widths of the Breit-Wigner resonance; the right column pole position and squared couplings to the final state at the pole position.*

M	=	$1436 \pm 15\,\mathrm{MeV}$	$\mathrm{M_{pole}}$	=	$1371 \pm 7\,\mathrm{MeV}$
Γ	=	$335 \pm 40\,\mathrm{MeV}$	Γ_{pole}	=	$192 \pm 20\,\mathrm{MeV}$
$\Gamma_{\pi N}$	=	$205 \pm 25\,\mathrm{MeV}$	$g_{\pi N}$	=	$(0.51 \pm 0.05) \cdot e^{-i\pi \frac{(35\pm5)}{180}}$
$\Gamma_{\sigma N}$	=	$71 \pm 17\,\mathrm{MeV}$	$g_{\sigma N}$	=	$(0.82 \pm 0.16) \cdot e^{-i\pi \frac{(20\pm13)}{180}}$
$\Gamma_{\pi\Delta}$	=	$59 \pm 15\,\mathrm{MeV}$	$g_{\pi\Delta}$	=	$(-0.57 \pm 0.08) \cdot e^{i\pi \frac{(25\pm20)}{180}}$
	T-matrix: $A_{1/2} = 0.055 \pm 0.020\,\mathrm{GeV}$			$\phi = (70 \pm 30)^\circ$	

4 Data and fits

The data used in this analysis are listed in Tables 1 and 2. The fit also used data on photo-induced $2\pi^0$ production [3, 4], $\pi^0\eta$ [5] and the recent BNL data on $\pi^- p \to n\pi^0\pi^0$ [6] in an event-based likelihood fit.

The fit uses 14 N^* and 7 Δ resonances. The background is described by reggeized t–channel π, $\rho\,(\omega)$, K and K^* exchanges and by baryon exchanges in the s– and u–channels. Fits were performed using a pseudo-χ^2 function

$$\chi^2_{\mathrm{tot}} = \chi^2_{\mathrm{2b}} \; - \; 2\ln\mathcal{L}\;, \quad \chi^2_{\mathrm{2b}} = \frac{\sum w_i \chi_i^2}{\sum w_i\, N_i} \sum N_i\;, \tag{10}$$

where the N_i are given as N_{data} (per channel) in the second and the weights in the third column of Tables 1 and 2. The data were fitted with weights w_i which ensure that low-statistics data are described reasonably well.

The P_{13} wave is described by a three-pole multi-channel K-matrix which we interpret as $N(1720)P_{13}$, $N(1900)P_{13}$, and $N(2200)P_{13}$. The $N(1900)P_{13}$ resonance is required [27], [28] due to the inclusion of the CLAS spin transfer measurements in hyperon photoproduction [7]. The $N(2200)P_{13}$ was already needed to fit single-pion photoproduction [9].

The P_{33} wave is represented by a two-pole two-channel K-matrix. The low energy part of pion photoproduction is described by the $\Delta(1232)$ state even though non-resonant contributions were needed to get a good fit. The

quality of the description of the elastic amplitude improved dramatically by introduction of a second pole. The first K-matrix pole has 1231 ± 4 MeV mass and helicity couplings $a_{1/2} = -0.125 \pm 0.008$ and $a_{3/2} = -0.267 \pm 0.010$. The pole position in the complex energy plane was found to be $M = 1205 \pm 4$ MeV and $2 \times Im = 92 \pm 10$ MeV. The second K-matrix pole was not very stable and varied between 1650 and 1800 MeV. The T-matrix pole showed better stability, and gave $M = 1550 \pm 40$ MeV and $\Gamma = 290 \pm 60$ MeV.

The two S_{11} resonances are treated as coupled–channel $5 \otimes 5$ K-matrix including $N\pi$, $N\eta$, $K\Lambda$, $K\Sigma$, and $\Delta\pi$ as channels. The $N\sigma$ or the $N\rho$ decay mode were added as 6^{th} channel for part of the fits. The first K-matrix pole varied over a wide range in different fits, from 1100 to 1480 MeV . The physical amplitude exhibited, however, a stable pole at M_{pole}=1508^{+10}_{-30}-i(83±8) MeV. The second K-matrix pole always converged to 1715 ± 30 MeV T-matrix pole at 1645 ± 15 MeV . Introduction of an additional pole did not lead to a significant improvement in the fit.

The P_{11} partial wave is largely non-resonant. Two P_{11} resonances were needed to describe this partial wave, the Roper resonance and a second one situated in the region The properties of the $N(1440)P_{11}$ resonance determined here are listed in Table 3. The Breit-Wigner parameters are deduced by the method given in [4].

References

1. A.V. Anisovich *et al.*, Eur. Phys. J. A **24** (2005) 111.
2. A.V. Anisovich and A.V. Sarantsev, Eur. Phys. J. A **30** (2006) 427.
3. U. Thoma *et al.*, arXiv:0707.3592.
4. A.V. Sarantsev *et al.*, arXiv:0707.3591.
5. I. Horn *et al.*, "Evidence for the $\Delta D_{33}(1940)$ resonance from $\gamma p \to p\pi^0\eta$ photoproduction",
6. S. Prakhov *et al.*, Phys. Rev. C **69** (2004) 045202.
7. R. Bradford *et al.*, Phys. Rev. C **75** (2007) 035205.
8. R. Bradford *et al.*, Phys. Rev. C **73** (2006) 035202.

9. A.V. Anisovich *et al.*, Eur. Phys. J. A **25** (2005) 427.

10. A. V. Sarantsev, V. A. Nikonov, A. V. Anisovich, E. Klempt and U. Thoma, Eur. Phys. J. A **25** (2005) 441.

11. R. A. Arndt, W. J. Briscoe, I. I. Strakovsky and R. L. Workman, Phys. Rev. C **74**, 045205 (2006)

12. K. H. Glander *et al.*, Eur. Phys. J. A **19** (2004) 251.

13. J. W. C. McNabb *et al.*, Phys. Rev. C **69** (2004) 042201.

14. A. Lleres *et al.*, Eur. Phys. J. A **31** (2007) 79.

15. R. G. T. Zegers *et al.*, Phys. Rev. Lett. **91** (2003) 092001.

16. R. Lawall *et al.*, Eur. Phys. J. A **24** (2005) 275.

17. R. Castelijns *et al.*, arXiv:nucl-ex/0702033.

18. O. Bartholomy *et al.*, Phys. Rev. Lett. **94** (2005) 012003.

19. O. Bartalini *et al.*, Eur. Phys. J. A **26** (2005) 399.

20. A. A. Belyaev *et al.*, Nucl. Phys. B **213** (1983) 201.

21. R.A. Arndt *et al.*, http://gwdac.phys.gwu.edu.
R. Beck *et al.*, Phys. Rev. Lett. **78** (1997) 606.
D. Rebreyend *et al.*,Nucl. Phys. A **663** (2000) 436.

22. K. H. Althoff *et al.*, Z. Phys. C **18** (1983) 199.
E. J. Durwen, BONN-IR-80-7 (1980).
K. Buechler *et al.*, Nucl. Phys. A **570** (1994) 580.

23. V. Crede *et al.*, Phys. Rev. Lett. **94** (2005) 012004.

24. B. Krusche *et al.*, Phys. Rev. Lett. **74** (1995) 3736.

25. J. Ajaka *et al.*, Phys. Rev. Lett. **81** (1998) 1797.

26. O. Bartalini *et al.*, arXiv:0707.1385 [nucl-ex].

27. A.V. Anisovich *et al.*, arXiv:0707.3596.

28. V.A. Nikonov *et al.*, arXiv:0707.3600.

Frascati Physics Series Vol. XLVI (2007), pp. 1341–1348
HADRON07: XII Int. Conf. on Hadron Spectroscopy – Frascati, October 8-13, 2007
Baryon Spectroscopy

LIGHT HADRON SPECTRUM IN THE INSTANTON LIQUID MODEL

P. Faccioli and M.Traini
Dipartimento di Fisica, Università degli Studi di Trento and I.N.F.N.
M. Cristoforetti,
Physik Department, Technische Universität München
M.C. Tichy,
Insitut für Theoretische Physik, Universität Tübingen,
Dipartimento di Fisica, Università degli Studi di Trento

Abstract

We review our recent study the role played by the chiral interactions in the lowest-lying sector of the light hadron spectrum, based on the Interacting Instanton Liquid Model (IILM). We discuss how the ordering of the lowest meson and baryon excitations is explained by the structure of the instanton-induced quark-quark and gluon-gluon interaction. We focus on the pion, nucleon, vector- and axial-vector mesons, and on the scalar glueball. We find that all these hadrons are bound in this model and have realistic masses.

1 Introduction

The spectrum of the lightest hadrons encodes information about the way the $u-$ and $d-$ quarks interact with gluons, at different distance scales. The ~ 400 MeV splitting between parity partners, e.g. vector- and axial-vector-

mesons, suggests that the interactions associated with the spontaneous breaking of chiral symmetry are very important in the low-lying sector of the spectrum. Similarly, the large splitting between the pion and the η' implies that topological interactions related to the axial anomaly are giving significant contribution. On the other hand, splitting between parity-partners is much reduced for higher resonances, and there have been claims that chiral symmetry may even be restored, up in the spectrum [1].

A qualitative and constituent-quark-model inspired explanation for the observed structure of the light-hadron spectrum is the following. The wave-function of the ground-state hadrons and of the lowest resonances is narrower than that of the higher excitations. Consequently, quarks in low-lying states and low-lying resonances are on average relatively close to each other and therefore are rather insensitive to the long-distance, confining part of the quark-quark interaction. On the other hand, they are very sensitive to the non-perturbative correlations which take place at the intermediate distance scales, $\sim 1/\Lambda_\chi \sim 0.2 - 0.3$ fm, where Λ_χ is the scale associated to chiral symmetry breaking. Conversely, up in the spectrum, the hadron wave-function extends for larger distances and quarks begin to experience the effect of the confining forces, which take place at the QCD scale $1/\Lambda_{QCD} \sim 1$ fm.

Based on such a discussion, two questions emerge naturally: (i) what is the microscopic origin of the interactions associated with the spontaneous breaking of chiral symmetry? (ii) are any of the light hadrons completely dominated by such chiral forces, to a point that they would exist even if confining correlations were completely removed? In this talk, I will review our recent attempts to address these questions in the context of the Interacting Instanton Liquid Model.

It has long been argued that instantons of size $\sim$ 0.3 fm represent the main vacuum gauge field configurations responsible for the non-perturbative dynamics at the chiral scale [2]. Recent lattice studies [3] have provided strong evidence in support of such an hypothesis. As a consequence of the spontaneous breaking of chiral symmetry, quark propagating in the instanton vacuum develop an effective mass of $\sim 350-400$ MeV, hence this model provides a connection between current and constituent quark.

The main drawback of the instanton models is that they do not provide confinement. On the one hand, this is a serious problem. It implies that instan-

tons cannot be the only important non-perturbative gauge field fluctuations in the vacuum. On the other hand, just because of such a flew, the instanton models represent a convenient framework in which the effect of chiral symmetry breaking can be disentangled from that of confinement and the questions listed above can be addressed.

2 The instanton-induced interaction in the different hadrons

The interaction generated by instantons is not equally important in all hadrons. Due to the specific quantum-number structure of the 't Hooft vertex, and of the instanton gauge field there are channels in which the instanton effect come at leading order in the instanton vacuum diluteness, $\kappa \sim 0.1$ and channels in which they come at sub-leading orders. This feature of the model is very important as it provides a natural explanation to a number of observed phenomena [4]: for example, it explains the well-known $\Delta\ I = 1/2$ rule for non-leptonic hyperon decays, or the early set-in of the perturbative regime in $\gamma\gamma^* \to \pi$ transition form factor, relative to the strongly non pertrubative behavior of the space-like pion form factor [5].

As far as the hadron spectrum is concerned, the structure of the instanton-induced interaction correctly accounts for the ordering of the lowest-lying states, i.e. where we expect chiral forces to be important. In fact, leading instanton forces are most attractive in the pion, but are suppressed in the ρ-meson and A_1-meson and are even repulsive in the η'-meson. Similarly, they are very strong and attractive in the nucleon and are suppressed in the Δ-isobar. Remarkably, the same dynamical mechanism can explain also the ordering of the lightest glueball excitations observed in lattice QCD simulations, with strong attraction in the scalar channel, suppression in the tensor channel and repulsion in the speudo-scalar channel.

3 Hadron Mass Calculation in the IILM

In the IILM, the QCD path integral over all possible gluon field configurations is replaced by

$$\mathcal{Z}_{QCD} \simeq \mathcal{Z}_{ILM} = \sum_{N_+,N_-} \frac{1}{N_+!N_-!} \int \prod_i^{N_++N_-} \mathrm{d}\Omega_i d(\rho_i) e^{-S_{int}} \prod_i^{N_f} \det(iD + im_f) \tag{1}$$

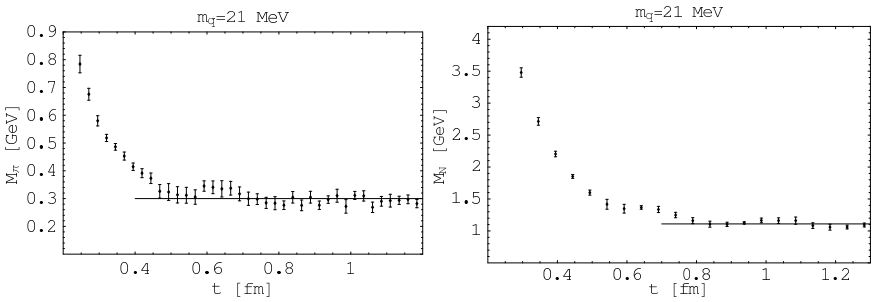

Figure 1: Typical effective mass plots obtained in the IILM and used to extract the pion (left panel) and nucleon (right panel) masses.

Here, $\mathrm{d}\Omega_i = \mathrm{d}U_i \mathrm{d}^4 z_i \mathrm{d}\rho_i$ is the measure in the space of collective coordinates, color orientation, position and size, associated with the single instantons. Quantum fluctuations are included in Gaussian approximation, through the semi-classical instanton amplitude $d(\rho_i)$. S_{int} is a bosonic interaction between pseudo-particles which includes a phenomenological short-range repulsive core required to remove large-sized instantons from the vacuum. In the formulation of the model we have considered [6], the strength of such a repulsion is the only phenomenological parameter, which has to be tuned to reproduce observations.

In a field-theoretic framework, the information about the hadron spectrum is encoded in the two-point Euclidean correlation functions,

$$G_H(\tau) = \int \mathrm{d}^3\underline{x} \langle 0|T[j_H(\underline{x},\tau)\overline{j}_H(\underline{0},0)|0\rangle, \tag{2}$$

where J_H is an operator which excites states of hadrons with quantum number of the hadron H. Once such a correlation function has been evaluated, the mass of lowest-lying stable hadron can then be extracted from the plateau in the large Euclidean time limit of the effective mass, i.e. using

$$M_H = \lim_{\tau\to\infty} M_H^{eff}(\tau) \qquad M_H^{eff}(\tau) = \frac{1}{\Delta\tau} \ln \frac{G_H(\tau)}{G_H(\tau+\Delta\tau)}.$$

The pion and the nucleon are the two hadrons in which the instanton-induced interaction is most intense. Typical effective mass plots obtained from IILM

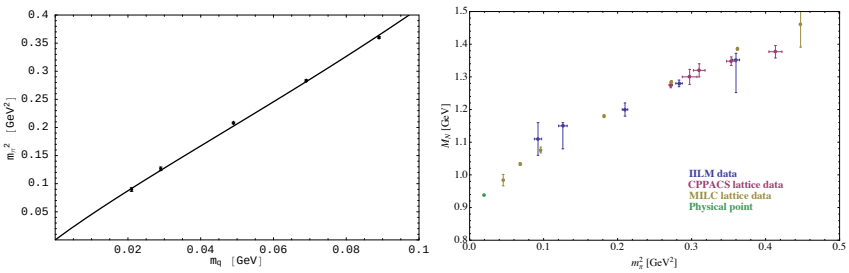

Figure 2: Left Panel: The pion mass as a function of the quark mass obtained in the IILM and compared with the extrapolation formula derived from chiral perturbation theory. Right Panel: The nucleon mass as a function of the pion mass squared obtained in IILM and in lattice calculations.

calculations [6] are shown in Fig. 2 and are indistinguishable from those obtained in lattice QCD simulations. They clearly display a plateau, which is the signature for the existence of a bound-state. We have extracted the hadron masses corresponding to five different values of the quark mass in the range $20 < m_q < 90$ MeV. The behavior of the pion (nucleon) mass with m_q (m_π^2) is presented in Fig.3. We have fitted the chiral behavior of the pion mass on the quark mass using the extrapolation formula obtained to $\mathcal{O}(p^2)$ from chiral perturbation theory. This leads to low-energy effective coefficients $f_0 = 85$ MeV and $\langle \bar{q}q \rangle = (-259\text{MeV})^3$, in excellent agreement with phenomenology. On the other hand, the calculated nucleon masses at different values of the pion mass agree very well with the available results of lattice QCD simulations.

Extracting information about the mass of the unstable vector and axial-vector meson resonances from the effective mass plot analysis is much harder than in the case of ground-state hadrons. In fact, if the quark mass is sufficiently small, the effective mass does not converge to the mass of the lowest resonance, but to the invariant mass of the decay products, at threshold. In order to be able to extract the masses of ρ and A_1 mesons from IILM correlations functions, the expected specific functional form of their effective mass was investigated in detail in [7], by using the experimental information about their spectral function, available from ALEPH. In Fig. 3 we compare the expected

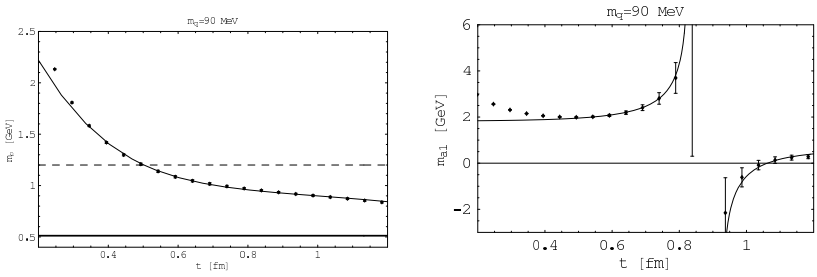

Figure 3: The effective mass plot for the ρ-meson (left panel) and A_1 meson (right panel) evaluated in the IILM (points) and compared with the behavior expected from the structure of the spectral function (line). The significance of the thick line and of the dashed line is explained in the original paper [7)]

shape of the effective mass (line) with the points obtained in the IILM and find agreement. Note that the singularity in the axial-vector channel arises from the interference of the pion and axial-vector contributions and therefore represent a clean evidence that both such states exist in the instanton vacuum.

On the other hand, we have found that the calculated mass are almost 30% larger than the experimental value. This fact can be interpreted as a signature that in such systems confinement begins to play an important role.

We conclude this section by mentioning our recent calculation of the mass of the scalar glueball, in the instanon vacuum [8)]. While numerical calculations completely analog to the ones performed for the nucleon and pion are in presently progress, here we discuss our recent results based on the Single Instanton Approximation (SIA) [9)].

The SIA follows from the observation that the contribution of a single pseudo-particle to a generic matrix element is very strong near its center, but decreases rapidly away from it. Hence, if the liquid is sufficiently dilute, short-sized correlation functions are saturated by the contribution a *single* pseudo-particle in the ensemble, the one closest to the endpoints of the correlator.

The main advantage of the SIA is that it allows to obtain predictions from analytic calculations, rather than from Monte Carlo numerical simulations. The prize to pay is that the SIA can be used to compute correlation functions with

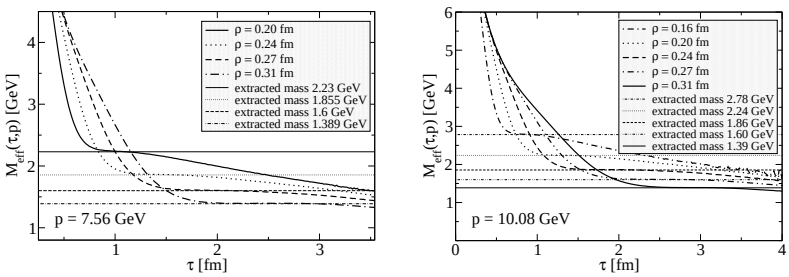

Figure 4: The effective mass plot for the ρ-meson (left panel) and A_1 meson (right panel) evaluated in the IILM (points) and compared with the behavior expected from the structure of the spectral function (solid line).

external momenta larger than ~ 1 GeV and for Euclidean times smaller thant ~ 1 fm.

In order to be able to use the SIA, it is convenient to introduce a *momentum-dependent effective mass*,

$$M_{eff}(\tau,\mathbf{p}) = \sqrt{E^2_{eff}(\tau,\mathbf{p}) - \mathbf{p}^2}, \qquad E_{eff}(\tau,\mathbf{p}) = -\frac{d}{d\tau}\log G_S(\tau,\mathbf{p}). \qquad (3)$$

If the lowest scalar glueball excitation in the spectrum is a single-particle bound-state, then in the large Euclidean time limit $M_{eff}(\tau,\mathbf{p})$ must stop depending on τ and on $\mathbf{p}$ and converge to the glueball's mass: $\lim_{\tau\to\infty} M_{eff}(\tau,\mathbf{p}) = M_{0^{++}}$.

Results for the SIA momentum-dependent effective mass $M_{eff}(\tau,\mathbf{p})$ are reported in Fig. 4, which shows how the effective mass plot calculated at two different momenta, in a range of different average instanton sizes. These plots clearly show that there exist a range of Euclidean times for which the momentum-dependent effective mass becomes independent on both momentum and Euclidean time. The scalar glueball mass predicted by the model is $M_{O^{++}} = 1.290 - 1.420$ GeV, in good agreement with the recent results of lattice calculations of Meyer and Teper [10] $M^{latt.}_{0^{++}} = 1475(30)_{stat.}(65)_{sys.}$ MeV.

4 Conclusions

In this talk, we have reviewed our recent attempts to use the IILM to understand how much of the hadron spectrum can be understood in terms of interactions which occur at the chiral symmetry breaking scale. We have found that nucleon, pion, vector- and axial- vector mesons as well as the lightest scalar glueball can be bound and have realistic masses, even in the absence of confinement. These results complement previous studies, in which it was shown that also the electro-weak structure of light hadrons can be well understood in this model.

References

1. L. Ya. Glozman, [arXiv: hep-ph/0701081]
2. E.V.Shuryak, Nucl. Phys. **B214** (1982), 237. D. Diakonov and V. Petrov: Nucl. Phys. **B245** (1984), 259.
3. C. Gattringer, Phys. Rev. Lett. **88** (2002), 221601. C. Gattringer *et al.*, Nucl. Phys. **B617** (2001) 101. P. Faccioli and T. A. De Grand, Phys. Rev. Lett. **91** (2003), 182001.
4. P.Faccioli, Int. J. Mod. Phys. **A20** (2005): 4615.
5. M. Cristoforetti *et al.* Phys. Rev. **D70** (2004) 054016. P. Faccioli, A. Schwenk and E.V. Shuryak, Phys. Rev. **D67** (2003) 113009.
6. M.Cristoforetti, P.Faccioli, J.Negele and M.Traini, Phys. Rev. **D75** (2007), 034008.
7. M.Cristoforetti, P.Faccioli and M.Traini Phys. Rev. **D75** (2007), 054024.
8. C.M.Tichy and P.Faccioli, [arXiv:0711.3829 (hep-ph)]
9. P. Faccioli and E.V. Shuryak, Phys. Rev. **D64** (2002) 114020. P.Faccioli, Phys. Rev. **D65** (2002) 094014.
10. H. B. Meyer and M. J. Teper, Phys. Lett. B **605** (2005), 344

Frascati Physics Series Vol. XLVI (2007), pp. 1349–1356
HADRON07: XII Int. Conf. on Hadron Spectroscopy – Frascati, October 8-13, 2007
Baryon Spectroscopy

BARYON, HEAVY STABLE PARTICLE AND STRANGE MESON PRODUCTION

Karin Daum
Bergische Universität Wuppertal, Gaußstrasse 20,D-42097 Wuppertal, Germany *

Abstract

Results on particle production in *ep* scattering at HERA are presented. The fragmentation into charged particles in deep-inelastic *ep* scattering is investigated. Proton and deuteron production is studied and the data on differential cross sections, the baryon-to-meson ratios and Bose-Einstein correlations of neutral and charged strange hadrons are summarized.

1 Introduction

The study of particle production provides valuable insights into parton fragmentation and hadronisation processes and thereby sheds light on the non-perturbative regime of Quantum Chromodynamics (QCD). The comparison of

* Permanent address: DESY, Notkestrasse 85, D-22607 Hamburg, Germany; e-mail:daum@mail.desy.de

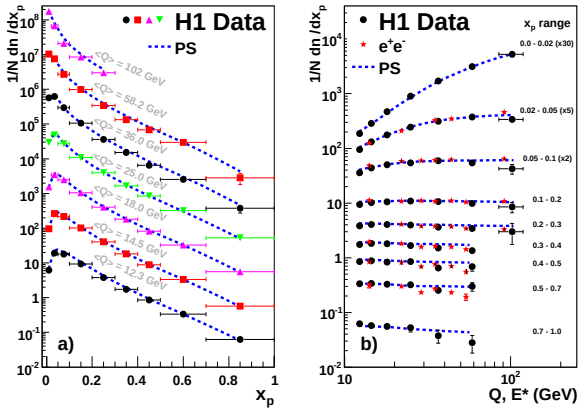

Figure 1: *Charged particle fragmentation function (a) as a function of x_p in bins of Q and b) as a function of Q in bins of x_p together with e^+e^- results.*

the results obtained in *ep* scattering at HERA to e^+e^- annihilation data makes it possible to test the universality of QCD in the particle formation process.

2 Inclusive Particle Production

In deep-inelastic *ep* scattering (DIS) the charged particle momentum spectrum is measured in the current hemisphere of the Breit-frame [1)], where the photon virtuality, Q, can be related to the momentum of the scattered parton. The influence from QCD processes absent in e^+e^- annihilation is reduced by requiring 100 GeV^2 $< Q^2 <$10000 GeV^2. Fig.1 shows the charged hadron momentum distribution scaled by $Q/2$ [2)] in comparison to the charged particles fragmentation function from e^+e^--annihilation [3)] for which half the centre-of-mass energy $E^*/2$ is the relevant scale. The agreement observed between *ep*- and e^+e^--data supports the concept of quark fragmentation universality.

3 (Anti)Deuteron Production in DIS

The fragmentation to light stable nuclei, such as deuterons (d), is poorly understood. In the coalescence model [4)] the d production rate is given by the

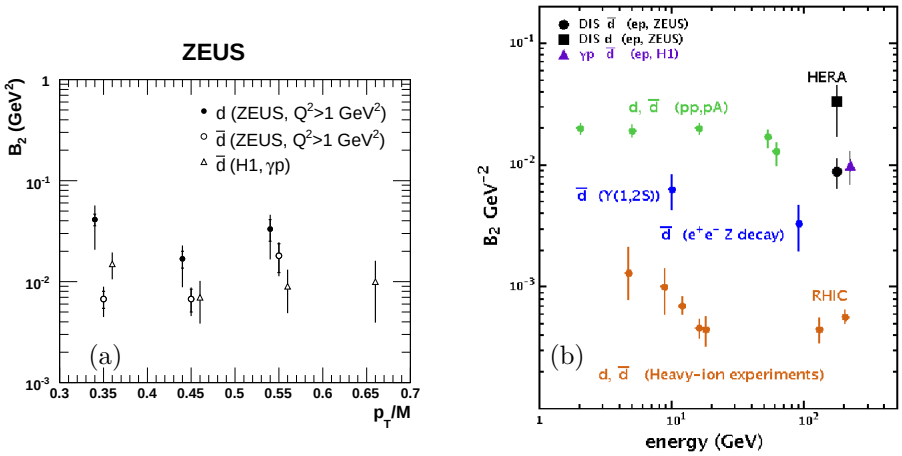

Figure 2: *Coalescence parameter B_2 for $d(\overline{d})$: (a) as a function of p_T/M from ep collisions at HERA and (b) for different scattering processes.*

overlap of its wave function with those of its constituents, the proton (p) and neutron (n). By assuming isospin invariance the invariant d cross section is proportional to the square of the invariant p cross section, where the proportionality, the coalescence parameter B_2, corresponds to the inverse volume of the fragmentation region for d formation.

Fig. 2a shows the measurements on B_2 for d and $\overline{d}$ as a function of p_T/M from ep collisions at HERA. The results obtained for $\overline{d}$ in DIS [5] and in photoproduction (γp) [6] agree within the errors. However, the results for d production are systematically above the $\overline{d}$ data. Fig. 2b summarizes the B_2 results from various high energy scattering processes [7]. Large variations in B_2 are observed which clearly indicates that $d(\overline{d})$ production cannot be understood as universal within this model.

4 Strange Hadron Production

The study of strange hadron production at particle colliders yields information on the strangeness content of the QCD vacuum and on the effect of the relatively large bare strange quark mass on particle formation. In the current fragmentation models this is accounted for by introducing a single parameter - the

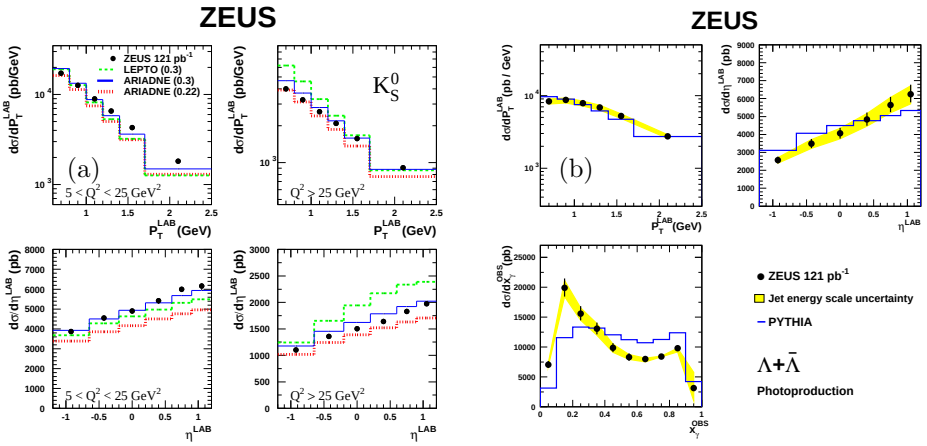

Figure 3: *Differential production cross sections of (a) K^0_S in DIS as a function of p_T^{lab} and η^{lab} and (b) of $\Lambda(\overline{\Lambda})$ in γp as a function of p_T^{lab}, η^{lab} and x_γ^{obs}.*

strangeness suppression factor λ_s. This parameter may be accessed quite easily in e^+e^- annihilation analyses because the contribution from $e^+e^- \to s\overline{s}$ is well known. In ep scattering the situation is more complex since the strangeness contribution to the proton structure F_2 has considerable uncertainties.

Fig. 3 shows the differential cross sections for the production of K^0_s mesons in DIS and of Λ baryons in γp in ep collisions at HERA [8]. The DIS cross sections are compared to absolute predictions of ARIADNE [9] and LEPTO [10] MC calculations. The γp cross sections are compared to the PYTHIA [11] predictions normalized to the cross section observed in data. In DIS reasonable agreement with data is observed for ARIADNE when setting $\lambda_s = 0.3$ as preferred by e^+e^- data [12]. Previous ep data [13] were favouring $\lambda_s = 0.22$ which leads to a less satisfactory description of the data presented here. The LEPTO MC with $\lambda_s = 0.3$ disagrees with data. In γp, PYTHIA with multiple interactions yields an adequate description of the shapes of the measured cross sections in p_T^{lab} and in η^{lab}. However, it fails to reproduce the x_γ^{obs} distribution which measures the momentum fraction carried by the photon entering the hard subprocess. Especially at small x_γ^{obs} the description is poor.

The formation of baryons in the fragmentation process is yet not well understood. In ep collisions the possible rôle of the incident proton's baryon

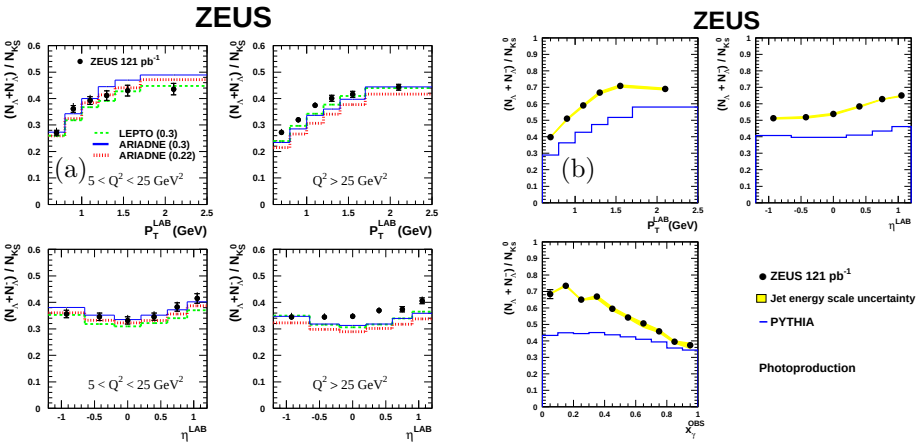

Figure 4: *Strange baryon-to-meson ratio (a) in DIS as a function of* p_T^{lab} *and* η^{lab} *and (b) in* γp *as a function of* p_T^{lab}, η^{lab} *and* x_γ^{obs}.

number on final state baryon formation is of specific interest. The study of the strange baryon-to-meson ratio, defined as $\mathcal{R} = (N(\Lambda) + N(\overline{\Lambda}))/N(K_s^0)$, may provide deeper insight into this process.

Fig. 4 shows the strange baryon-to-meson ratio in DIS and γp in comparison to the model expectations. In DIS the overall agreement of ARIADNE using $\lambda_s = 0.3$ with the data is better than about 10%. At low Q^2 the agreement is even better. The $\mathcal{R}$ value varies between about 0.2 and 0.5. This compares well to the e^+e^- annihilation results, where $\mathcal{R}$ lies in the range of 0.2 to 0.4 [14] for 10 GeV< $\sqrt{s}$ <200 GeV. In γp significantly larger values for $\mathcal{R}$ are observed. At small x_γ^{obs} values of $\mathcal{R} \approx 0.7$ are reached, while in the region of direct photoproduction, i.e. $x_\gamma^{obs} \approx 1$, it approaches 0.4 consistent with the observations in DIS and in e^+e^- annihilation. The rise at low x_γ^{obs} is not reproduced by the PYTHIA model suggesting a lack of understanding of strange baryon formation in the multi-parton environment at small x_γ^{obs}.

5 Bose-Einstein Correlations of Strange Mesons

Due to the symmetrization of the two-particle wave function the production of identical bosons is expected to be enhanced at small distances in phase space.

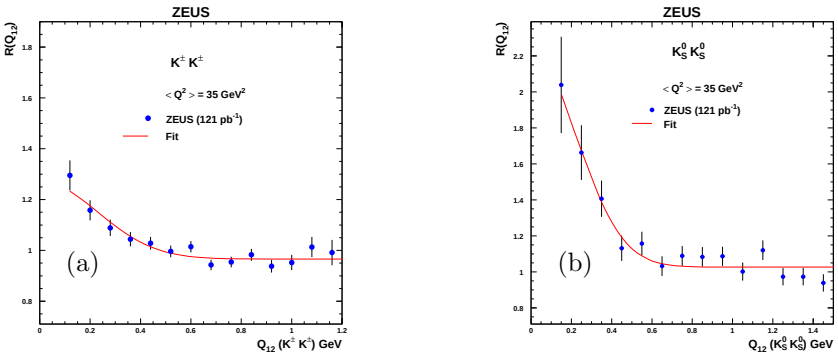

Figure 5: *The correlation function of (a) $K^{\pm}K^{\pm}$ and (b) of $K^0_sK^0_s$ pairs.*

This effect is called Bose-Einstein correlations (BEC). It allows determining the size of the particle formation region. Using the four-momentum difference $Q_{12} = \sqrt{-(p_1 - p_2)^2}$ and assuming a static source with a Gaussian density distribution, the correlation function can be written as [15]

$$R(Q_{12}) = 1 + \lambda \exp(-r^2 Q_{12}^2). \quad (1)$$

Here λ denotes the strength of the BEC and r is the radius of the formation region.

Fig. 5 shows the two-particle correlation $R(Q_{12})$ for $K^{\pm}K^{\pm}$ and for $K^0_sK^0_s$ pairs in DIS at HERA [16] together with the result from a fit according to eqn. 1. In both samples a strong rise in the correlation function towards small values of Q_{12} is observed. This is a clear sign of BEC in case of the $K^{\pm}K^{\pm}$ sample. For the $K^0_sK^0_s$ pairs a complication arises from the fact that the strange quantum number of K^0_s mesons is undetermined. Therefore, contaminations from $f_0(980)$ decaying to $K^0\overline{K}^0$ are possible. After this effect is taken into account the $K^0_sK^0_s$ data still show evidence for the presence of BEC, however with reduced significance.

A compilation of the correlation radius r from DIS and e^+e^- annihilation measurements at LEP [17] is given in fig. 6 for different boson pairs. Within the uncertainties r agrees very well for the different processes, meson pairs and particle charges. This suggests that the particle formation region for pseudo-scalar mesons is universal.

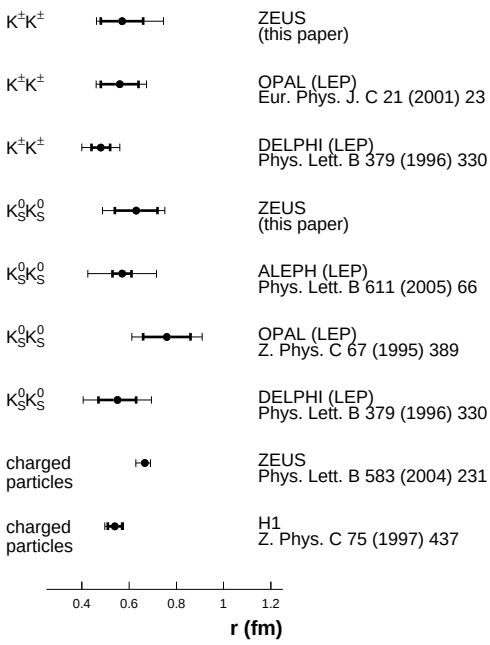

Figure 6: *Comparison of DIS and LEP results on r from BEC studies.*

6 Conclusions

Results on particle production in *ep* collisions at HERA have been presented and compared to data from other scattering processes. Universality has been observed for the inclusive charged particle production within current uncertainties. Strange meson production could be understood within the models in most of the phase space suggesting the strangeness suppression factor λ_s being process independent. The analysis of BEC shows universality of the formation region for pseudo-scalar mesons.

The results on strange baryon-to-meson ratio uncovers a lack of understanding of the fragmentation to strange baryons in the multi-parton environment at small x_γ^{obs}. The results from different processes on the deuteron formation region are found to be inconsistent within the coalescence model.

References

1. R.P. Feynman,"Photon-Hadron Interactions", (Benjamin, N.Y., 1972).
2. F.D. Aaron *et al* [H1], Phys.Lett. B **654**, 148 (2007).
3. A. Peterson *et al* [MARK II], Phys. Rev. D**37**, 1, (1989); W. Braunschweig *et al* [TASSO], Z. Phys. C **47**, 187 (1990); Y.K. Li *et al* [AMY], Phys. Rev. D **41**, 2675 (1990); P.D. Acton *et al* [OPAL], Z. Phys. C **53**, 539 (1992); P. Abreu *et al* [DELPHI], Phys. Lett. B **311**, 408 (1993).
4. S.T. Buttler, C.A. Pearson, Phys. Rev. **129**, 836 (1963).
5. S. Chekanov *et al* [ZEUS], Nucl. Phys. B **786**, 181 (2007).
6. A. Aktas *et al* [H1], Eur. Phys. J. C **36**, 413 (2004).
7. See for instance Refs.1-11 in [5)].
8. S. Chekanov *et al* [ZEUS], Eur. Phys. J. C **51**, 1 (2007).
9. L. Lönblad, Comp. Phys. Comm. **71**, 15 (1992).
10. G. Ingelmann *et al*, Comp. Phys. Comm. **101**, 108 (1997).
11. T. Sjöstrand *et al*, Comp. Phys. Comm. **135**, 238 (2001).
12. P.D. Acton *et al* [OPAL], Z. Phys. C**56**, 521 (1992); R. Akers *et al* [OPAL], Z. Phys. C **68**, 1 (1995); D. Busculic *et al* [ALEPH], Z. Phys. C **69**, 379 (1996); P. Abreu *et al* [DELPHI], Z. Phys. C **73**, 61 (1996).
13. S. Chekanov *et al* [ZEUS], Phys. Lett. B **553**, 141 (2002).
14. Particle Data Group, S.Eidelmann *et al*, Phys. Lett. B**592**, 1 (2004).
15. G. Goldhaber *et al*, Phys. Rev. **120**, 300 (1960).
16. S. Chekanov *et al* [ZEUS], Phys. Lett. B **652**, 1 (2007).
17. S. Schael *et al* [ALEPH], Phys. Lett. B **611**, 66 (2005); S. Abreu *et al* [DELPHI], Phys. Lett. B **379**, 330 (1996); G. Abbiendi *et al* [OPAL], Eur. Phys. J. C **21**, 23 (2001); R. Akers *et al* [OPAL], Z. Phys. C **67**, 389 (1995).

Frascati Physics Series Vol. XLVI (2007), pp. 1357
HADRON07: XII Int. Conf. on Hadron Spectroscopy – Frascati, October 8-13, 2007
Baryon Spectroscopy

BARYON ISOSPIN MASS SPLITTING

L.-H. Chan
Luisiana State University

Written contribution not received

Frascati Physics Series Vol. XLVI (2007), pp. 1359–1366
HADRON07: XII Int. Conf. on Hadron Spectroscopy – Frascati, October 8-13, 2007
Baryon Spectroscopy

LINEAR MASS RULES AND HADRONIC SHELLS: THE BARYONS

Paolo Palazzi
particlez.org

Abstract

The meson mass system is multilinear. This result, combined with a stability analysis of the meson spectrum indicative of shell structure, implies that meson shells are geometrically similar to nuclear shells. In addition, the meson mass rules suggest solid-phase bound states on an fcc lattice, possibly with stable leptons as constituents. The preliminary baryon mass systematics shows compatible linear quantization rules, while the baryonic shell sequence corresponds to a lower constituent density, and starts only at shell 3. The baryonic number might be related to a different lattice organization.

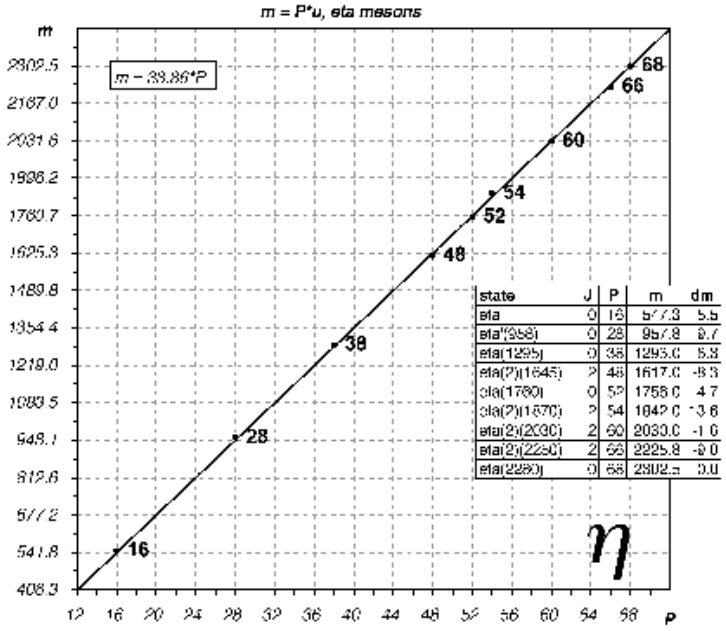

Figure 1: *Mass multiplicity plot for the η mesons: $m_{\rm i} = u * P_{\rm i}$, with the mass unit u and the even integer multiplicities $P_{\rm i}$ obtained by minimization.*

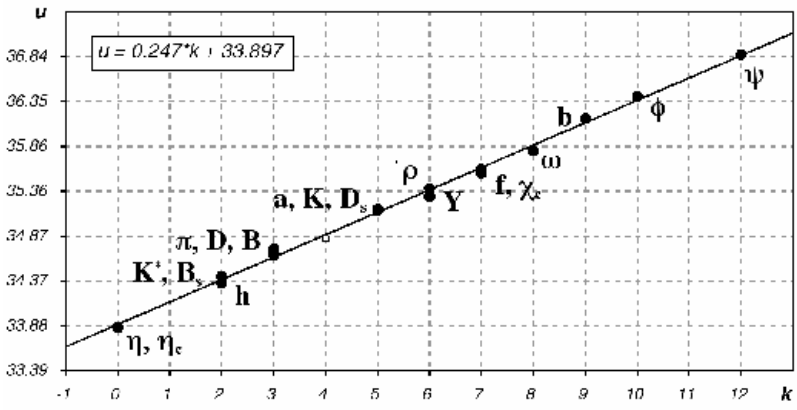

Figure 2: *Meson mass unit grid $u_{\rm k} = u_0 + k*du, k = [0..12]$; q-qbar asymmetric families with labels above the line, q-qbar symmetric below.*

1 State of the art

The cognitive landscape of particle physics is patchy. Quarks define an accurate and mysterious CKM chemistry and a plausible but incomplete classification scheme, and their identification with the constituents seen in deep-inelastic scattering experiments is problematic. The quark model is still schematic as in the days of Gell-Mann, and the masses of hadrons cannot be derived from quark masses and binding energies. Even more surprisingly, no comprehensive hadronic mass rules are yet part of the accepted body of knowledge.

The standard model is not really satisfactory, and the trend is to go "beyond" it by adding more rather than looking elsewhere. The approach of the present author is to attack the problems of mass rules and hadron models with an open mind, by analyzing the hadron spectrum in the hope of extracting new or not well established regularities which may suggest alternative viewpoints.

2 Mass rules and the mesons

The mass of a bound state is its more fundamental parameter, corresponding to its total energy, and it is surprising that with so many hadron masses, and so many phenomenologists over so many years, there are no established mass rules. Few authors research this field, and publishing such results is problematic: "there are no mass rules, and if you think you found one, you are a crackpot!". Actually the rules are linear and have been known for more than 50 years, although in an approximate formulation.

Y. Nambu observed in 1952 that meson masses are even multiples of a mass unit u of about 35 MeV/c^2, baryons (and also unstable leptons) odd multiples, so that mass differences among similar particles are quantized by 70 MeV/c^2 [1]. M. H. Mac Gregor studied this property extensively [2, 3] and few other authors mentioned it also. Recently this rule has been reassessed by the present author for all the mesons listed by the PDG, grouped by quark composition and J^{PC}, with evaluation of its significance by Montecarlo [4, 5].

This analysis shows that the rule is statistically significant separately for each group and with slightly different values of u (see for example the η mesons in fig.1). For certain groups u is linearly spin dependent, and the different base values of u for the various meson groups are linearly quantized on a grid of 12 intervals, and are strongly correlated with the quantum numbers (fig.2).

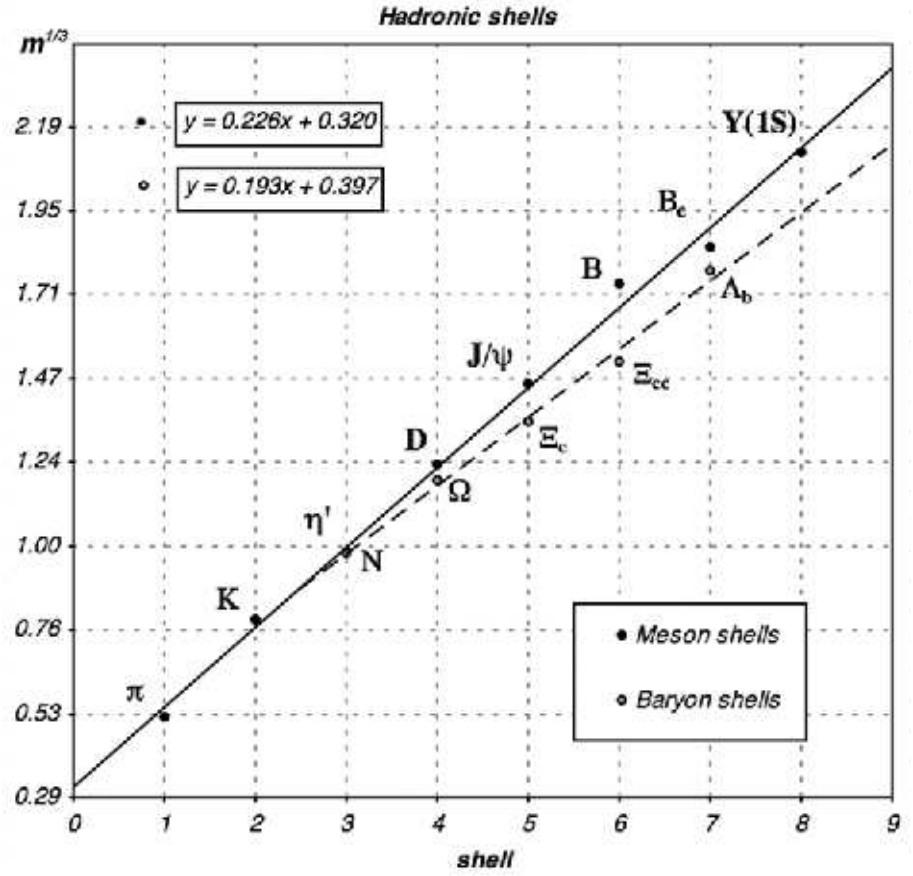

Figure 3: *Hadronic shells, expressed as the cuberoot of the mass (in GeV/c^2) versus shell number. Compared to the mesons, the baryonic shells start only at shell 3, and grow with a lower slope.*

3 Hadronic shells

In atoms and in nuclei, stability is organized with shells, which can be expressed with alignments of the 1/3 power of the total number of constituents of the most stable configurations. Atomic shells show as the cube root of Z for the inert gases charted vs the shell number. Nuclear stability is related mostly to the neutronic magic number series, but with a derived sequence based on the atomic number A = Z + N, stability can be expressed in a similar way [6].

Through the linear mass rules mentioned previously, hadrons can be probed for shell organization. By analyzing the distribution of particle lifetimes as a function of the mass, stability peaks are recognized separately for mesons and for baryons [6], and indeed the cube roots of their masses follow two distinct alignments (fig.3). Postulating that one 35 MeV/c^2 mass unit corresponds to one constituent, the mass and the number of constituents are proportional, giving a strong indication that hadrons may be shell structured.

4 Meson shells

The mesonic shells expressed with the number of constituents are geometrically very similar to nuclear shells: the shell population sequences are almost identical, doubly-magic-equivalent states are present only up to shell 3, and there are also clear indications of sub-shells [7]. The mesonic shell sequence is correlated with the quark composition up to b-bbar in shell 8, and no states are present around the mass values of the hypothetical subsequent shells.

In this context the mesonic mass quantization patterns are compatible with solid-phase partonic bound states on an fcc lattice, with light spin-1/2 partons of charge 0, +1 and -1 coupled anti-ferromagnetically with positive binding energy [7]. Given these constraints, a possible choice for the constituents in agreement with these results (and the only one with non-fictitious particles), are the stable leptons, as proposed by A. O. Barut in a different context, with short-distance electromagnetism acting as the strong interaction [8].

In this unconventional scenario, suggested by the results extracted from the whole meson spectrum, in first approximation there is no dynamic in the bound state, nor any need for color. Mesons are unstable elastic crystals of stable leptons, and at least half of the mysterious parameters of the standard model are no longer needed [7]. What about the baryons?

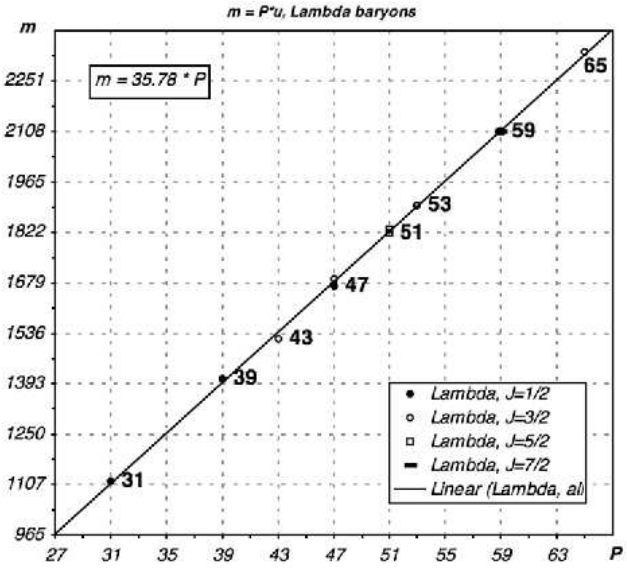

Figure 4: *Mass multiplicity plot for the* Λ *baryons:* $m_{\rm i} = u * P_{\rm i}$*, with the mass unit* u *and the odd integer multiplicities* $P_{\rm i}$ *obtained by minimization.*

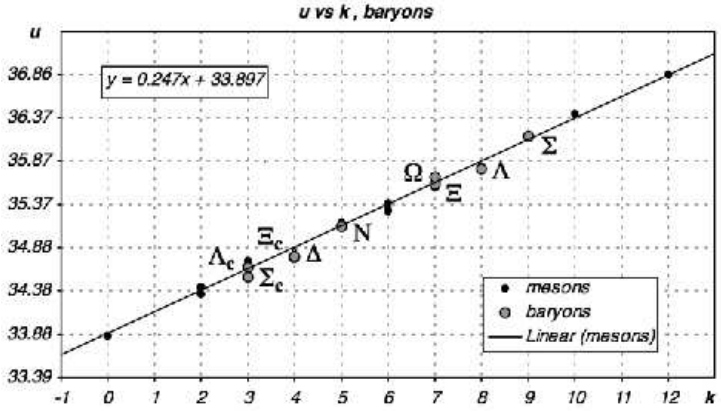

Figure 5: *Baryon mass units plotted on top of the meson grid* $u_{\rm k} = u_0 + k * du, k$ *= [0..12] of fig. 2. Only positions 3,4,5 and 7,8,9 are occupied, respectively by unflavored or charmed baryons, and strange ones.*

5 Baryon mass rules

The same automatic analysis procedure used for mesons can be applied to the baryons, fitting the masses with odd multiples of the same mass unit after grouping the states by quark composition and J^{PC}. For certain baryon families, such as the N and the Δ, the PDG record of each state must be carefully inspected to detect possible mergers of separate states which are close in mass. The complete analysis with all the fits and their statistical significance will be published separately in an extensive report [9]. The results show that the baryon mass rules are very similar to the mesons, but for the odd rather than even multiplicity.

For certain baryon families u is spin dependent with the same coefficient as the mesons. The graph of fig.4 is the multiplicity fit for the Λ baryons, showing no spin dependence. The resulting mass units for the various baryon families can be charted on the same u-grid as the mesons, and show a remarkable pattern (fig.5). Unflavored and charmed baryons occupy positions 3,4 and 5 on the grid, while strange baryons sit at locations 7,8 and 9. Also an amazing sequence of equally spaced Θ^+ baryons [10] (of which only one is listed by the PDG and considered dubious), follows the same periodicity rule with a mass unit of 35.89 MeV/c^2 sharply on mark 8 of the u-grid [11].

6 Baryon shells

By comparing the meson and baryon shell plots from fig.3 it appears that the first baryonic shell is number 3, and that the constituent density of baryonic shells is lower than the mesonic ones. These clues, and the odd mass multiplicity of the baryons, indicate that the baryon lattice organization is different, centered, less dense and also such that only at shell 3 and above the structures are cohesive. Various possible solutions compatible with the constituent count of the various shells are currently being investigated. The radial charge density distribution of the proton and the neutron [12], and the shape of the p-p elastic cross-section [13] also indicate that the nucleon is structured in three layers.

This line of research is incomplete, and a lot remains to be done. If it were to be confirmed, particle physics would loose much of its glamour, and become more structural, along the lines of nuclear physics.

7 Acknowledgements

I am grateful to Petros Aslanyan, Norman Cook, Simone Giani and Malcolm Mac Gregor for interesting discussions.

References

1. Y. Nambu, An Empirical Mass Spectrum of Elementary Particles, Prog. Theor. Phys. **7**, 131 (1952).
2. M. H. Mac Gregor, Models for Particles, Lett. Nuovo Cim. **7**, 211 (1970).
3. M. H. Mac Gregor, Electron generation of leptons and hadrons with reciprocal alpha-quantized lifetimes and masses, *Int.J.Mod.Phys.* **A20**, 719 and 2893 (2005).
4. P. Palazzi, The Meson Mass System, Int. J. Mod. Phys. **A22**, 2-3, 546 (2007).
5. P. Palazzi, Patterns in the Meson Mass Spectrum, *http://particlez.org* , p3a-2004-001 (2004).
6. P. Palazzi, Particles and Shells, *http://cdsweb.cern.ch*, CERN-OPEN-2003-006 (2003).
7. P. Palazzi, Meson Shells, *http://particlez.org* , p3a-2005-001 (2005).
8. A. O. Barut, Stable Particles as Building Blocks of Matter, Surveys High Energ.Phys. **1**, 113 (1980).
9. P. Palazzi, The Baryon Mass System, in preparation.
10. P. Zh. Aslanyan *et al.*, Observation of S=+1 narrow resonances in K^0_s p from p+C_3H_8 collision at 10 GeV/c, Nucl.Phys. **A755**, 375 (2005);
11. P. Palazzi, Seven at One Blow, *http://particlez.org* , p3a-2005-005 (2005).
12. R. M. Littauer, H. F. Schopper, R. R. Wilson, Structure of the Proton and Neutron, Phys. Rev. Letters **7**, 144 (1961).
13. M.M. Islam, R.J. Luddy and A.V. Produkin, pp Elastic Scattering at LHC and Nucleon Structure, Mod. Phys. Lett., **A18**, 743 (2003)

Frascati Physics Series Vol. XLVI (2007), pp. 1367–1374
HADRON07: XII Int. Conf. on Hadron Spectroscopy – Frascati, October 8-13, 2007
Baryon Spectroscopy

BARYON SPECTROSCOPY IN CONSTITUENT QUARK MODELS

J. Vijande
Departamento de Física Teórica e IFIC. Universidad de Valencia - CSIC, Spain
A. Valcarce
Departamento de Física Fundamental, Universidad de Salamanca, Spain
P. Gonzalez
Departamento de Física Teórica e IFIC. Universidad de Valencia - CSIC, Spain
H. Garcilazo
Escuela Superior de Física y Matemáticas, Instituto Politécnico Nacional, Mexico.

Abstract

We present a study of the baryon spectra for all flavor sectors within a constituent quark model. We address some of the outstanding problems in baryon spectroscopy, as for example the spin splitting evolution for te different flavor sectors, the flavor independence of confinement and the missing state problem.

1 The light sector

The complexity of Quantum Chromodynamics (QCD), the quantum field theory of the strong interaction, has prevented so far a rigorous deduction of its predictions even for the simplest hadronic systems. In the meantime while lattice QCD starts providing reliable results, QCD-inspired models are useful tools to get some insight into many of the phenomena of the hadronic world. One

of the central issues to be addressed is a quantitative description of the low-energy phenomena, from the baryon-baryon interaction to the baryon spectra, still one of the major challenges in hadronic physics.

Nowadays, we have at our disposal realistic quark models accounting for most part of the one- and two-body low-energy hadron phenomenology. Among the quark models found in the literature [1], the ambitious project of a simultaneous description of the baryon-baryon interaction and the hadron spectra in all the flavor sectors has only been undertaken by the constituent quark model of Ref. [2]. The success in describing the properties of the strange and non-strange one and two-hadron systems encourages its use as a guideline in order to assign parity and spin quantum numbers to already determined baryon states as well as to predict still non-observed resonances.

The results we are going to present have been obtained by solving exactly the Schrödinger equation by the Faddeev method in momentum space. The results are of similar quality to others present in the literature based on models specifically designed for the study of the baryon spectra [3]. In the constituent quark model used in this work the hyperfine splitting is shared between pseudoscalar forces and perturbative QCD contributions, provided by the one-gluon exchange. In Table 1 we give the contribution of different pieces of the interacting hamiltonian to the energy of several octet and decuplet baryons. One observes that the hyperfine splittings are controlled by the one-gluon exchange (OGE) and one-pion exchange (OPE) [one-kaon exchange (OKE)] potentials in the non-strange [strange] sector. The OGE and OPE generate almost the experimental hyperfine splitting, the one-eta (OEE) and one-sigma exchange (OSE) given a final small tune. The expectation value of the OPE flavor operator for two light quarks is replaced by the similar effect of the OKE when a light and a strange quarks are involved. They enhance in a similar way the hyperfine splitting produced by the OGE. The important effect of the OGE is observed when Table 1 is compared to Table II of Ref. [4]. The contribution of the pseudoscalar forces is much smaller in our case, generating decuplet-octet mass differences of the order of $100-200$ MeV, the remaining mass difference given by the OGE.

Table 1: Eigenvalue, in MeV, of the kinetic energy combined with different contributions of the interacting potential. The subindexes in the potential stand for: $1 = CON$, $2 = 1+OGE$, $3 = 1+OPE$, $4 = 2+OPE$, $5 = 3+OKE$, $6 = 5+OEE$, $7 = 6+OSE$. Experimental date is taken from the PDG.

State	V_1	V_2	V_3	V_4	V_5	V_6	V_7	Exp.
$N(1/2^+)$	1534	1254	1407	969	969	1030	939	939
$\Delta(3/2^+)$	1534	1314	1510	1291	1291	1283	1232	1232
$N^*(1/2^+)$	1787	1601	1716	1448	1448	1479	1435	1420–1470
$N(1/2^-)$	1722	1530	1675	1422	1422	1447	1411	1515–1525
$\Sigma(1/2^+)$	1679	1417	1674	1408	1326	1229	1213	1192.642±0.024
$\Sigma(3/2^+)$	1679	1462	1673	1454	1437	1438	1382	1383.7±1.0
$\Sigma^*(1/2^+)$	1983	1757	1931	1752	1703	1688	1644	1630–1690
$\Sigma(1/2^-)$	1859	1677	1854	1671	1645	1634	1598	≈ 1620
$\Lambda(1/2^+)$	1679	1405	1600	1225	1171	1217	1122	1115.683±0.006
$\Xi(1/2^+)$	1819	1557	1819	1557	1472	1446	1351	1321.31±0.13
$\Omega(3/2^+)$	1955	1743	1955	1743	1743	1728	1650	1672.45±0.29

2 The missing state problem

Constituent quark models of baryon structure are based on the assumption of effective quark degrees of freedom so that a baryon is a three-quark color-singlet state. Lattice QCD in the quenched approximation shows out a qq confining potential linearly rising with the interquark distance [5]. This potential produces an infinite discrete hadron spectrum. The implementation of this confining force with OGE and/or Goldstone boson exchanges derived from chiral symmetry breaking, or other effective interactions, turns out to be fruitful in the construction of quark potential models providing a precise description of baryon spectroscopy. However an outstanding problem remains unsolved: all models predict a proliferation of baryon states at excitation energies above 1 GeV which are not experimentally observed as resonances. This difference between the quark model prediction and the data about the number of physical resonances is known as the missing resonance problem.

Unquenched lattice QCD points out a string breaking in the static potential between two quarks [5] what should be properly incorporated in the

phenomenological description of the high energy hadronic spectrum. The spontaneous creation of a quark-antiquark pair at the breaking point may give rise to a breakup of the color flux tube between two quarks in such a way that the quark-quark potential does not rise with the interquark distance but it reaches a maximum saturation value. The simplest quark-quark screened potential, containing confinement and one-gluon exchange terms, reads:

$$V(r_{ij}) = \frac{1}{2}\left[\overline{\sigma} r_{ij} - \frac{\overline{\kappa}}{r_{ij}} + \frac{\hbar^2 \overline{\kappa_\sigma}}{m_i m_j c^2} \frac{e^{-r_{ij}/\overline{r_0}}}{\overline{r_0}^2 r_{ij}} (\vec{\sigma_i} \cdot \vec{\sigma_j})\right] \left(\frac{1 - e^{-\mu\ r_{ij}}}{\mu\ r_{ij}}\right) + \frac{\overline{M_0}}{3} \quad (1)$$

where r_{ij} is the interquark distance, $m_{i,j}$ the masses of the constituent quarks, $\vec{\sigma}_{i,j}$ the spin Pauli operators, and $\overline{M_0}$ is a constant. The screening multiplicative factor appears between parenthesis on the right hand side. μ, the screening parameter, is the inverse of the saturation distance and its effective value is fitted together with the other parameters, $\overline{\sigma}$, $\overline{\kappa}$, and $\overline{\kappa_\sigma}$, to the spectrum.

For nonstrange baryons the model predicts quite approximately the number and ordering of the experimental states up to a mass of 2.3 GeV [6, 7].

More recent lattice calculations [5] show that the $Q\overline{Q}$ potential saturates sharply for a breaking distance of the order of 1.25 fm corresponding to a saturation energy of about twice the B meson ($Q\overline{q}$) mass, indicating that the formation of two heavy-light subsystems is energetically favored. A saturated quark-quark potential incorporating this effect can be parametrized as:

$$V(r_{ij}) = \begin{cases} V_{sr}(r_{ij}) & r_{ij} < r_{sat} \\ \sigma r_{sat} & r_{ij} \geq r_{sat} \end{cases} , \quad (2)$$

where

$$V_{sr}(r_{ij}) = \frac{1}{2}\left[\sigma r_{ij} - \frac{\kappa}{r_{ij}} + \frac{\hbar^2 \kappa_\sigma}{m_i m_j c^2} \frac{e^{-r_{ij}/r_0}}{r_0^2 r_{ij}} (\vec{\sigma_i} \cdot \vec{\sigma_j})\right] + \frac{M_0}{3} \quad (3)$$

whose parameters are given in Ref. [8]. The calculation of the spectrum proceeds exactly in the same manner as in Ref. [6], to which we refer for technical details. It is worth to remark that the presence, in the three-body problem, of two-body thresholds (for only one quark to be released), apart from the absolute three-body ones (saturation energy), may represent further constraints in the applicability limit of the model to any particular channel. The results obtained are represented in Fig. 1. As in Ref. [6] we have also included the predicted states close above the thresholds.

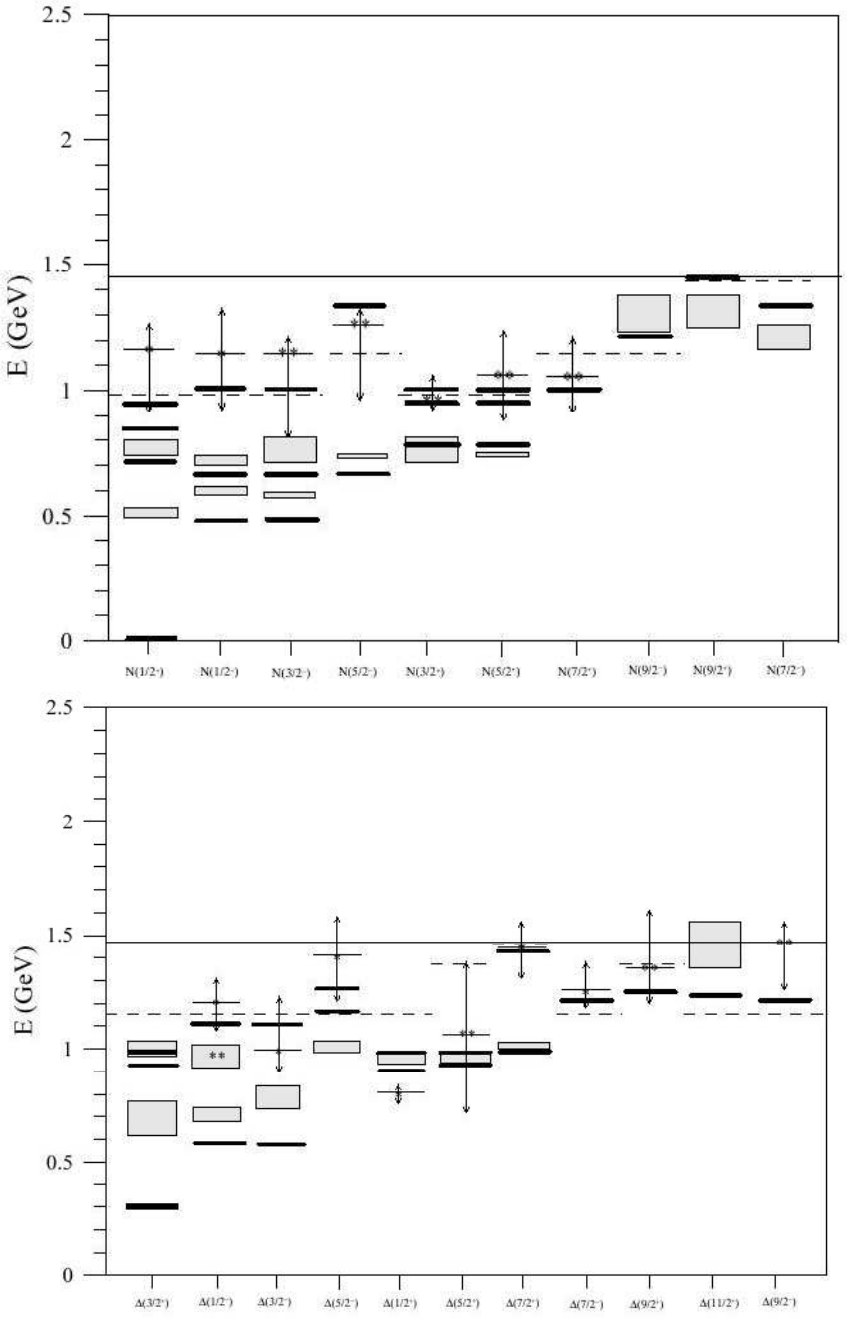

Figure 1: Relative energy nucleon (upper part) and Δ (lower part) spectra for the screened potential of Eq. (2) with the parameters of Ref. [6]. The thick solid lines represent our results. The shaded region, whose size stands for the experimental uncertainty, represents the experimental data for those states cataloged as $(***)$ or $(****)$ states in the Particle Data Book. Experimental data cataloged as $(*)$ or $(**)$ states are shown by short thin solid lines with stars over them and by vertical lines with arrows standing for the experimental uncertainties. Finally, we show by a dashed line the $1q$ ionization threshold and by a long thin solid line the total threshold.

The quality of the description of the light baryon spectra is remarkable since apart from keeping the same level of quality than in the low and medium-lying spectrum a perfect one to one correspondence between our predicted states and the experimental resonances for any J^P is obtained. Similar results are obtained using the screeend potential given in Eq.1. The number and ordering of states remains unaltered. The sharp potential tends quite generally to push upward the highest energy states. In other words the screened potential is quite similar to the closest physical approach to a nonscreened potential, represented by the sharp interaction, that takes effectively into account the effect of the baryon decay to open channels in order to select the observed resonances.

3 The heavy sector

Since the discovery at BNL [9] and posterior confirmation at Fermilab [10] of the existence of charmed baryons in the late 70's, an increasing interest on heavy baryon spectroscopy arose. It became evident that baryons containing heavy flavors c or b could play an important role in our understanding of QCD. Since then, several new hadrons containing a single charm or bottom quark have been identified [11]. While the mass of these particles is usually measured as part of the discovery process, other quantum numbers such as the spin or parity have often proved to be more elusive. For heavy baryons, no spin or parity quantum numbers of a given state have been measured directly. Therefore, a powerful guideline for assigning quantum numbers to new states or even to indicate new states to look for is required by experiment.

Several criteria can be chosen to fit the confinement strength in the baryon spectra, being the most usual ones to fit the energy splitting between the nucleon and its first radial excitation (roper resonance) or to fit the splitting with its lowest orbital excitation (negative parity). We show the differences using both criteria in Fig. 2. On the left hand side we show the spectra obtained in the first case, named [A], and on the right hand side the results obtained for the later, named [B]. A better agreement is observed with the model reproducing the orbital excitations of the light baryon sector [12]. There is no experimental state that we do not predict and there is no low-lying theoretical resonance that has not been observed. The recently discovered $\Sigma_c(2800)$ [13] would correspond to an orbital excitation with $J^P = 1/2^-$ or $3/2^-$, any other correspondence

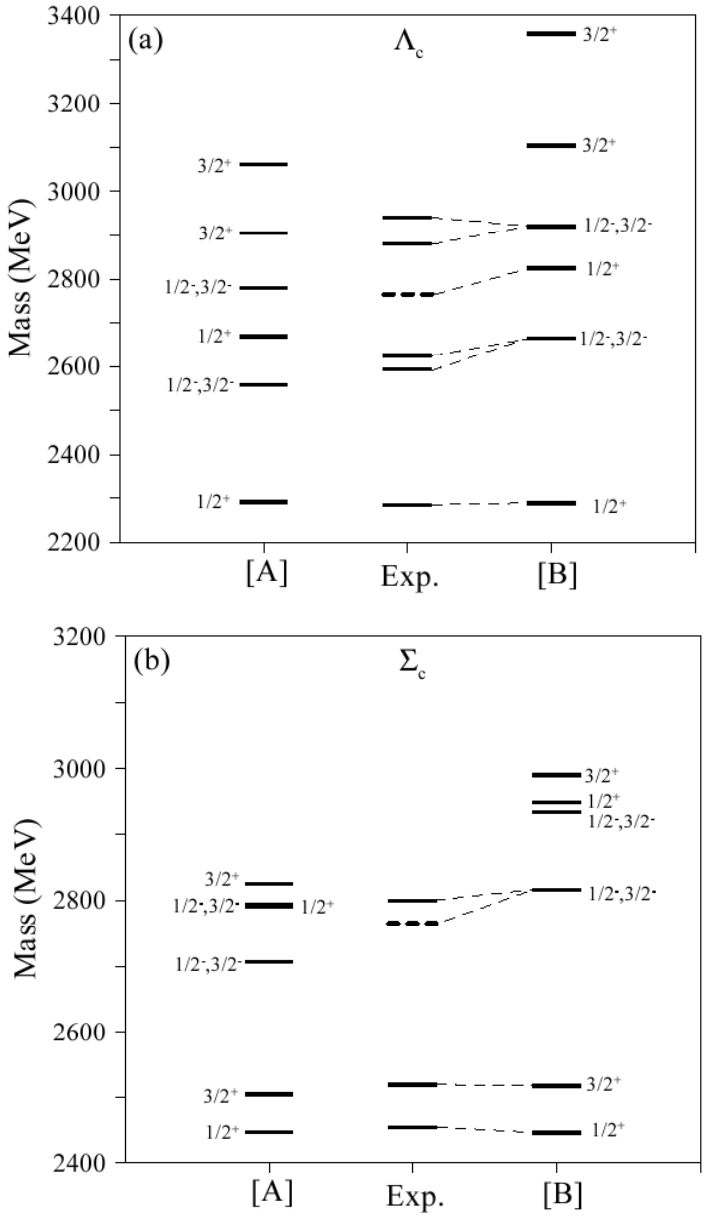

Figure 2: (a) Spectra of Λ_c for two different confinement strengths compared to experiment. (b) Same as (a) for Σ_c states.

being definitively excluded. For Λ_c baryons, the recently confirmed as a Λ_c state, $\Lambda_c(2880)$ [14], and the new state $\Lambda_c(2940)$ [14] may constitute the second orbital excitation of the Λ_c baryon. Finally, there is an state with a mass of 2765 MeV reported in Ref. [15] as a possible Λ_c or Σ_c state and also observed in Ref. [13]. While the first reference (and also the PDG) are not able to decide between a Λ_c or a Σ_c state, the second one prefers a Λ_c assignment. As seen in Fig. 2, this state may constitute the second member of the first orbital excitation of Σ_c states or the first radial excitation of Λ_c baryons. An experimental effort to confirm the existence of this state and its decay modes would help on the symbiotic process between experiment and theory to disentangle the details of the structure of heavy baryons.

References

1. A. Valcarce, *et al*, Rep. Prog. Phys. **68**, 965 (2005).
2. J. Vijande, F. Fernández, and A. Valcarce, J. Phys. G **31**, 481 (2005).
3. A. Valcarce, H. Garcilazo, J. Vijande, Phys. Rev. C**72**, 025206 (2005).
4. M. Furuichi and K. Shimizu, Phys. Rev. C **65**, 025201 (2002).
5. SESAM Coll., G.S. Bali, *et al*, Phys. Rev. D **71**, 114513 (2005).
6. J. Vijande, *et al*, Phys. Rev. D **69**, 074019 (2004).
7. P. González, *et al*, Phys. Rev. D **68**, 034007 (2003).
8. P. González, *et al*, Eur. Phys. J. A**29**, 235 (2006).
9. E.G. Cazzoli *et al.*, Phys. Rev. Lett. **34**, 1125 (1975).
10. C. Baltay *et al.*, Phys. Rev. Lett. **42**, 1721 (1979).
11. W.-M. Yao *et al.*, J. Phys. G **33**, 1 (2006).
12. H. Garcilazo, J. Vijande, A. Valcarce, J. Phys. G**34**, 961 (2007).
13. Belle Coll., R. Mizuk *et al.*, Phys. Rev. Lett. **94**, 122002 (2005).
14. BABAR Coll., B. Aubert *et al.*, Phys. Rev. Lett. **98**, 122011 (2007).
15. CLEO Coll., M. Artuso *et al.*, Phys. Rev. Lett. **86**, 4479 (2001).

Frascati Physics Series Vol. XLVI (2007), pp. 1375–1382
HADRON07: XII Int. Conf. on Hadron Spectroscopy – Frascati, October 8-13, 2007
Baryon Spectroscopy

LIGHT-QUARK BARYON ANOMALIES

P. González
Departamento de Física Teórica e IFIC. Universidad de Valencia - CSIC, Spain
J. Vijande
Departamento de Física Teórica e IFIC. Universidad de Valencia - CSIC, Spain
A. Valcarce
Departamento de Física Fundamental, Universidad de Salamanca, Spain

Abstract

We show that the coupling of $S-$wave meson-baryon channels to three-quark states may induce significant mass shifts. This mechanism can explain the "anomalous" masses found for some light-quark baryons. It also suggests a way to improve the extraction of baryon resonances from data analyses.

1 The low lying light-quark baryon spectrum: anomalies.

Non relativistic or relativized quark models describe quite reasonably the light-quark baryon spectrum below 1.9 GeV excitation energy [1, 2, 3, 4, 5, 6, 7, 8, 9, 10]. This means that the masses of all the well established resonances rated four stars $(****)$ in the PDG book [11], with the exception in most models of the Roper resonance $N_{P_{11}}(1440)$, are well reproduced ($\lesssim 100$ MeV difference with the PDG average value). Regarding $(***), (**)$ and $(*)$ baryons the situation

is much less favourable specially for $\Delta's$ as can be checked for instance in Fig. 1 for the particular model of reference [3].

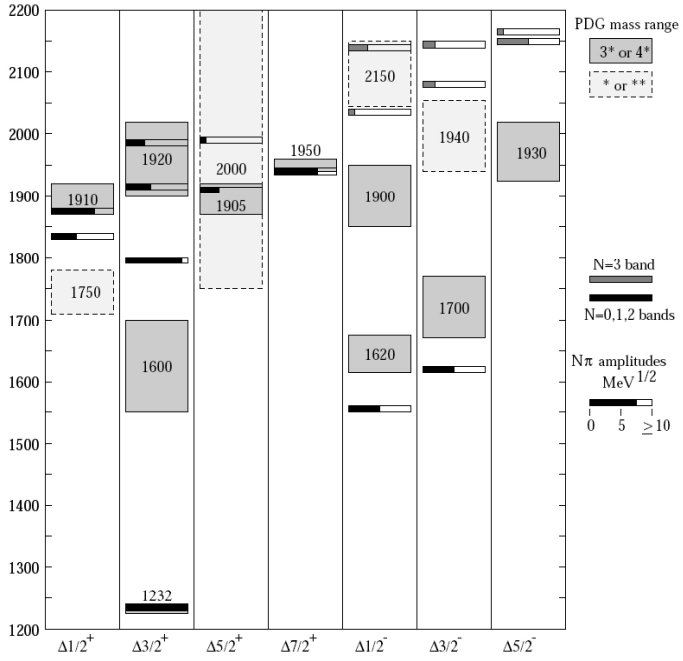

Figure 1: Delta spectrum taken from reference [9]. Predicted masses from reference [3] are shown as bars and compared to the range of central values for resonance masses from the PDG review (shown as boxes). $N\pi$ decay amplitudes are also indicated.

The important point is that although the predictions for the baryon masses are model dependent there are some cases, $\Delta_{P_{31}}(1750)(*)$, $\Delta_{P_{33}}(1600)(**)$, $\Delta_{S_{31}}(1900)(**)$, $\Delta_{D_{33}}(1940)(*)$ and $\Delta_{D_{35}}(1930)$, where the discrepancy between the predictions and the average PDG masses follows a systematic in the sense that i) it is very significant ($\gtrsim$ 80 MeV) for all quark models based on two-quark interactions [1, 2, 3, 4, 7, 8, 9, 10] and ii) it always corresponds to an overprediction. We shall call anomalies these overpredicted–mass resonances. The list of identified anomalous deltas could even be enlarged by a $\Delta_{F_{35}}(\sim 1720)$ which would correspond to the lowest energy state of $\Delta(5/2^+)$.

This resonance is not catalogued as such in the PDG book. On the contrary it appears a quite bizarre $\Delta_{F_{35}}(2000)(**)$ with average mass obtained from three different data analyses, two of them [12, 13] reporting a mass about 1720 ($\pm$60) MeV and the other [14] giving a quite different value of 2200 ± 125 MeV. Then by considering them as two differentiated resonances the $\Delta_{F_{35}}(\sim 1720)$ would be a clear candidate for an anomaly. On the other hand in the nucleon sector the most prominent candidate for an anomaly is $N_{P_{11}}(1440)$ despite its correct mass description in some *ad hoc* models [8]. In the strange Λ sector an outstanding overpredicted mass state is the $\Lambda_{S_{01}}(1405)(****)$.

The description of most anomalies improves a lot when considering models incorporating three-quark as well as two-quark interactions. Figs. 2 and 3 show the predicted delta spectrum from two of these models [5, 6].

In Ref. [5] a three-quark *two-sigma* exchange is proposed to complement the two-quark confining plus one-gluon exchange potentials. In Ref. [6] baryons appear as vibrations and rotations of a three-quark *Y-shaped string*-like configuration. A look at the figures show that both models are able to reproduce well (within the present day experimental uncertainty interval) the masses of all the delta anomalies with the exception of the proposed $\Delta_{F_{35}}(\sim 1720)$. Notice also that in Fig. 2 the mass prediction for the lowest $\Delta(1/2^+)$ resonance, $\sim$ 1750 MeV, in perfect agreement with the current $\Delta_{P_{31}}(1750)(*)$, is far away from a $\Delta(1/2^+)$ resonance at 1550 MeV drawn at the figure which appeared in the PDG book at the time reference [5] was published. Unfortunately these three-quark descriptions, successful for deltas, fail for $\Lambda_{S_{01}}(1405)$: Ref. [5] predicts a mass of 1550 MeV and Ref. [6] 1640 MeV. This can be understood by realizing that the energy systematic of these models is such that the energy step associated to a radial excitation like $\Delta_{P_{33}}(1600)(***)$ and $N_{P_{11}}(1440)$ or to a quark Pauli blocked configuration like $\Delta_{P_{31}}(1750)(*), \Delta_{S_{31}}(1900)(**), \Delta_{D_{33}}(1940)(*)$ and $\Delta_{D_{35}}(1930)$ [15], gets reduced to approximately half of its value with respect to quark models containing only two-quark interactions. This reduction makes possible the agreement with data. On the contrary the predictions for regular-step states do not vary significantly with respect to two-quark models. This explains why the $\Lambda_{S_{01}}(1405)$ is out of the systematic as it would be the $\Delta_{F_{35}}(\sim 1720)$.

On the other hand the anomalous character of $\Lambda_{S_{01}}(1405)$ has motivated a lot of studies being mostly interpreted, at the hadron level, as a $N\overline{K}$ un-

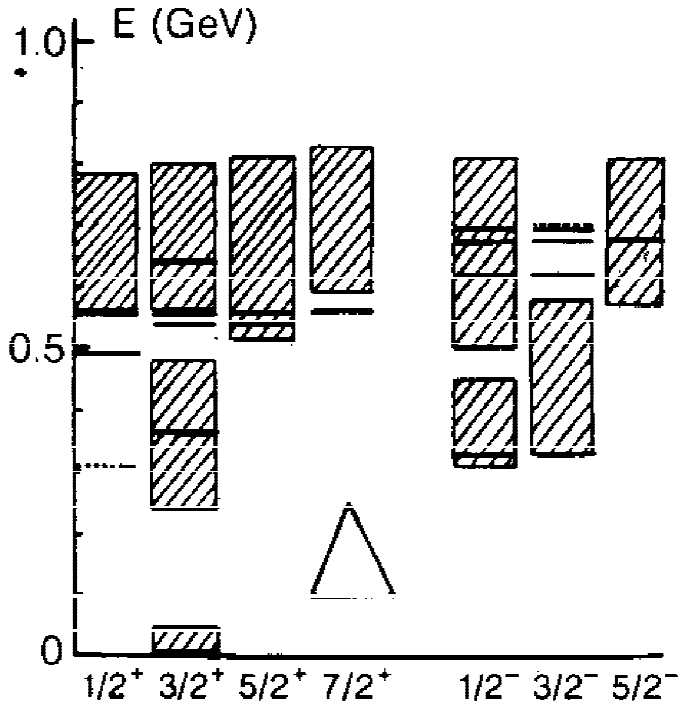

Figure 2: Delta spectrum from reference [5]. Predicted masses from reference [6] are shown as bars and compared to the range of central values for resonance masses from the PDG review (shown as boxes).

stable (quasi)bound system (in the chiral unitary approximation one of the poles couples mostly to $N\overline{K}$) [16]. Alternatively, at the quark level, the identification of the lowest $\Lambda(1/2^-)$ state in two-quark interaction models (mass about 1550 MeV) with $\Lambda_{S_{01}}(1405)$ has been suggested, the difference in mass being attributed to the mass shift induced by its strong coupling to the $S-$ wave $N\overline{K}$ channel (threshold at 1435 MeV) [17]. Very recently a quantitative confirmation of this idea has been obtained within a specific quark model framework [18]. Let us remark that although these explanations are formulated in terms of different degrees of freedom (hadrons or quarks) they may be somehow equivalent through the effectiveness of parameters, cutoffs,...

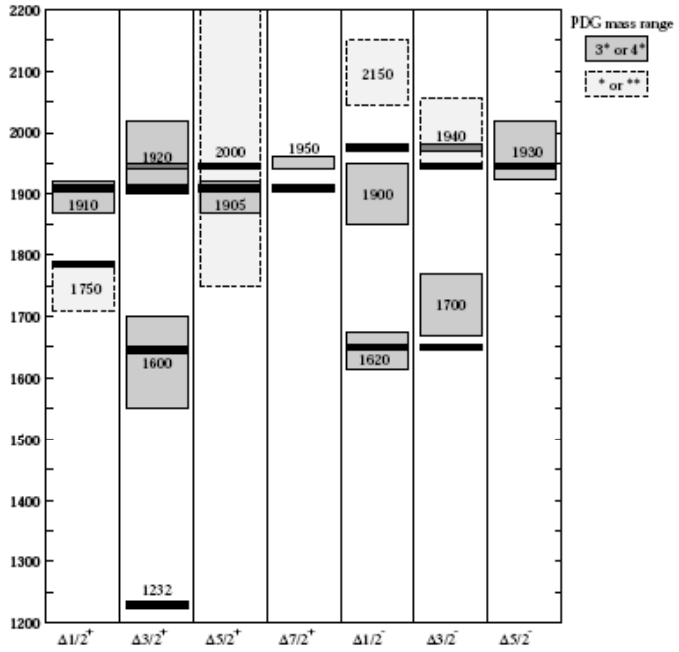

Figure 3: Delta spectrum taken from reference [9]. Solid lines indicate the masses predicted by the model. Experimental data are shown through their full width; uncertain channels are denoted by dashed lines.

Since the consideration of the coupling to the $S-$ wave $N\overline{K}$ channel, with threshold below the two-quark interaction prediction but above the experimental mass of the resonance, is essential to get a right description of $\Lambda_{S_{01}}(1405)$ in all cases we wonder whether a similar physical mechanism could be at work for other anomalies.

First we centre on $\Delta_{F_{35}}(\sim 1720)$ for which no plausible explanation, at the quark and hadron levels, has been pursued yet. Two-quark interaction models predict the mass of the lowest $\Delta(5/2^+)$ state to be about 1910 MeV. It is very nice to verify the presence of the $S-$ wave $\pi N_{D_{15}}(1675)$ threshold at 1815 MeV, 100 MeV below the "two-quark" mass and 65 MeV above data, since this channel couples to $\Delta(5/2^+)$. So the $\Delta_{F_{35}}(\sim 1720)$ could well be the non-strange analogous of the $\Lambda_{S_{01}}(1405)$.

Second we deal with the radial excitations $\Delta_{P_{33}}(1600)(***)$ and $N_{P_{11}}(1440)$ $(****)$. In the case of the Roper resonance $N_{P_{11}}(1440)$ ("two-quark" mass prediction about 1650 MeV) it is known the relevant role played by the $S-$wave σN channel (threshold at $\sim$ 1540 MeV) not only at the theoretical level to explain the $N_{P_{11}}(1440)$ in a couple meson-baryon channel scheme [19] but also at the experimental level where its implementation as an effective inelastic channel makes feasible the extraction of the resonance in some data analyses [12, 13]. For the $\Delta_{P_{33}}(1600)$ ("two-quark" mass prediction about 1750 MeV) the $S-$wave $\pi N_{D_{13}}(1520)$ channel (threshold at 1660 MeV) could play a similar role.

Third we treat the resonances associated to quark Pauli blocked configurations , $\Delta_{S_{31}}(1900)(**), \Delta_{D_{33}}(1940)(*)$, $\Delta_{D_{35}}(1930)$ and $\Delta_{P_{31}}(1750)(*)$. The first three share the same quark configuration ("two-quark" mass prediction about 2200 MeV) and the possible coupling to the $S-$wave $\rho\Delta$ channel (threshold at 2002 MeV) [15]. For the fourth one the "two-quark" mass is about 1875 MeV with a possible coupling to $\pi\Delta_{S_{31}}(1620)$ ($S-$wave threshold at 1760 MeV).

Therefore we find for all the anomalies without exception $S-$wave meson-baryon channels possibly coupling to the corresponding "two-quark" configurations. To put this qualitative analyses on a more sound basis we next perform a quantitative model calculation.

2 Meson-baryon threshold effects

To evaluate the effect of the presence of meson-baryon thresholds as the ones identified above in the description of the anomalies we shall consider the two-level problem with hamiltonian matrix

$$[H] = \begin{pmatrix} \langle\Psi_{3q}|H_c|\Psi_{3q}\rangle & \langle\Psi_{3q}|H_{int}|\Psi_{mB}\rangle \\ \langle\Psi_{mB}|H_{int}|\Psi_{3q}\rangle & \langle\Psi_{mB}|H_f|\Psi_{mB}\rangle \end{pmatrix} \approx \begin{pmatrix} M_{3q^{2b}} & a \\ a^* & M_m + M_B \end{pmatrix} \tag{1}$$

where H_c, H_f and H_{int} are the "two-quark", the free and the coupling interaction hamiltonians respectively. a, parametrizing the coupling, is fitted phenomenologically.

The results obtained for $a = 75$ MeV for all the anomalies are shown in Table 1. The improvement with respect to the "two-quark" predictions is

PDG Resonance	Predicted mass	Experiment
$\Delta_{P_{33}}(1600)(***)$	1626	1550–1650
$N_{P_{11}}(1440)(****)$	1465	1410–1470
$\Delta_{D_{35}}(1930)(***)$	1978	1900–2020
$\Delta_{D_{33}}(1940)(*)$	1962	1840–2040
$\Delta_{D_{31}}(1900)(*)$	1946	1850–1950
$\Delta_{P_{31}}(1750)(*)$	1714	1660–1780
$\Delta_{F_{35}}(\approx 1720)(N.C.)$	1782	1660–1785
$\Lambda_{S_{01}}(1405)(****)$	1397	1400–1410

Table 1: Predicted masses, (MeV), for the anomalies. Experimental data taken from Ref. [11].

astonishing. All the predicted masses lye within the experimental uncertainty interval. This seems to confirm the meson-baryon coupling to three quark components as the physical mechanism underlying the anomalous nature of the mentioned resonances. Furthermore the use of the involved meson-baryon channels as effective inelastic channels in data analyses could result in an improvement in the experimental identification and extraction of the anomalies.

This work has been partially funded by Ministerio de Ciencia y Tecnología under Contract No. FPA2007-65748-C02 and by European Integrated Infrastructure Iniciative 506078.

References

1. N. Isgur and G. Karl, Phys. Lett. **72B**, 109 (1977); Phys. Rev. D **19**, 2653 (1979).
2. B. Silvestre-Brac and C. Gignoux, Phys. Rev. D **32**, 743 (1985).
3. S. Capstick and N. Isgur, Phys. Rev. D **34**, 2809 (1986).
4. R. Sartor and Fl. Stancu, Phys. Rev. D **31**, 128 (1985); Fl. Stancu and P. Stassart, Phys. Lett. B **269**, 243 (1991).
5. B. Desplanques, C. Gignoux, B. Silvestre-Brac, P. González, J. Navarro and S. Noguera, Z. Phys. A **343**, 331 (1992).

6. R. Bijker, F. Iachello and A. Leviatan, Ann. Phys. **236**, 69 (1994).

7. Y.-B. Dong, J.-C Su and S.-S. Wu, J. Phys. G **20**, 73 (1994).

8. L.Ya. Glozman and D.O. Riska, Phys. Rep. **268**, 263 (1996); L.Ya. Glozman, W. Plessas, K. Varga and R.F. Wagenbrunn, Phys. Rev. D **58**, 094030 (1998).

9. S. Capstick and W. Roberts, Prog. Part. Nucl. Phys. **45**, S241 (2000) and references therein.

10. A. Valcarce, F. Fernández, P. González, and V. Vento, Phys. Lett. B **367**, 35 (1996); A. Valcarce, H. Garcilazo and J. Vijande, Phys. Rev. C **72**, 025206 (2005).

11. W.-M. Yao *et al.*, J. Phys. G **33**, 1 (2006).

12. D.M. Manley and E.M. Saleski, Phys. Rev. D **45**, 4002 (1992).

13. T.P. Vrana, S.A. Dytman and T.-S.H. Lee, Phys. Rep. **328**, 181 (2000).

14. R.E. Cutkosky, C.P. Forsyth, J.B. Babcock, R.L. Kelly and R.E. Hendrick, Proceedings of the IV Intenational Conference on Baryon Resonances (Baryon 1980), edited by N. Isgur, Toronto 1980.

15. P. González, J. Vijande and A. Valcarce, work in preparation.

16. A. Müller-Groeling, K. Holinde and J. Speth, Nucl. Phys. A **513**, 557 (1990); D. Jido, J.A. Oller, E. Oset, A. Ramos and U.G. Meissner, Nucl. Phys. A **755**, 669 (2005); and references therein.

17. S. Pakvasa and S.F. Tuan, Phys. Lett. B **459**, 301 (1999) and references therein.

18. S. Takeuchi and K. Shimizu, Phys. Rev. C **76**, 035204 (2007).

19. O. Krehl, C. Hanhart, S. Krewald and J. Speth, Phys. Rev. C **62**, 025207 (2000); C. Schütz, J. Haidenbauer, J. Speth and J.W. Durso, Phys. Rev. C **57**, 1464 (1998).

Frascati Physics Series Vol. XLVI (2007), pp. 1383–1393
HADRON07: XII Int. Conf. on Hadron Spectroscopy – Frascati, October 8-13, 2007
Baryon Spectroscopy

DYNAMICAL EIGHTFOLD WAY AND CONFINEMENT IN STRONGLY COUPLED LATTICE QCD

Paulo A. Faria da Veiga*, Michael O'Carroll
Departamento de Matemática Aplicada e Estatística, ICMC-USP,
C.P. 668, 13560-970 São Carlos SP, Brazil
Antônio Francisco Neto
Núcleo de Física, Campus Prof. Alberto Carvalho - UFS
49500-000 Itabaiana SE, Brazil

Abstract

We review our recent work validating the Eightfold Way exactly. We consider 3-flavor lattice QCD in the strong-coupling regime (small hopping parameter $\kappa > 0$ and much smaller gauge coupling $\beta > 0$) and in an imaginary-time functional integral formulation. By analyzing the subspace of the quantum mechanical Hilbert space with odd (even) number of fermions, we obtain from the dynamics the exact baryon (meson) spectrum. Using spectral representations for the 2-point functions, the hadron states are detected by isolated dispersion curves in the energy-momentum spectrum. A correlation subtraction method ensures that these hadron states are the only spectrum up to near a two-particle threshold. Hence, we do show confinement up to near the two-meson threshold. The asymptotic baryon (meson) masses are $-3\ln\kappa$ ($-2\ln\kappa$), and are given by *convergent* expansions in κ and β. The form of the dispersion curves is also obtained. Within the baryon octet (decuplet) all the masses are equal, but there is an $\mathcal{O}(\kappa^6)$ octet-decuplet baryon mass splitting. All mesonic masses within the pseudoscalar (vector) mesons are also the same but there is an $\mathcal{O}(\kappa^4)$ pseudoscalar-vector meson mass splitting. A new linear time reflection symmetry is employed to derive some of the results.

1 Introduction and Results

In [1], a quark model with three flavors and an $SU(3)_f$ flavor symmetry was introduced to classify the known hadrons by an eightfold way scheme. An $SU(3)_c$ local gauge model of quarks and gluons and color dynamics was later proposed, the well-known Quantum Chromodynamics (QCD), as the model for strong interactions. Perturbation theory was successfully used for high-energy phenomena but not at low energies. To understand the low-lying energy-momentum (E-M) spectrum and confinement in QCD a lattice approximation in an imaginary-time functional integral formulation was introduced in [2]. Soon, the use of the lattice became a powerful tool in different contexts, to determine the particle content of the model and to answer questions which were not attainable using perturbation theory. For instance, several accomplishments in the strong coupling expansion are found in [3, 4, 5, 6] and numerical simulations on the lattice, which acquired a very important status, are e.g. reported in [7]. In a mathematically rigorous treatment, a physical Hilbert space $\mathcal{H}$ and E-M operators are constructed for the lattice QCD in [8]. A Feynman-Kac (F-K) formula is also established.

In a series of papers [9, 10, 11], we determined the low-lying E-M spectrum of increasingly complex $SU(3)_c$ lattice QCD models in the strong coupling regime, i.e. with a hopping parameter κ and plaquette coupling $\beta = 1/g_0^2$ satisfying $0 < \beta \ll \kappa \ll 1$. We obtained the one-hadron and the two-hadron bound-state spectra, up to a two-particle energy threshold. The reason for working in this region of parameters is that the hadron spectrum is the low-lying spectrum; baryons have asymptotic mass $\approx -3\ln\kappa$ and the meson mass is $\approx -2\ln\kappa$. If $0 < \kappa \ll \beta \ll 1$, the low-lying spectrum consists of only glueballs [12] of mass $\approx -4\ln\beta$ and their excitations.

Here, we review the results of our papers [13, 14]. We obtain the low-lying spectrum *exactly* in the $SU(3)_c$ lattice QCD model with 3 flavors, in $3+1$ dimensions and in the strong coupling regime. We validate the Gell-Mann and Ne'eman eightfold way directly from the quark-gluon dynamics. Besides, we show that the spectrum associated with the eightfold way baryon (meson) states is the *only* spectrum in the subspace $\mathcal{H}_{odd}$ ($\mathcal{H}_{even}$) of the underlying Hilbert space $\mathcal{H}$ of vectors with an odd (even) number of fermions, up to the meson-baryon (meson-meson) energy threshold of $\approx -5\ln\kappa$ ($\approx -4\ln\kappa$). Since the hadronic local composite fields are $SU(3)_c$ gauge invariant, we show

confinement up to the meson-meson threshold. No guesswork is made in our dynamical treatment regarding the form of the hadron composite fields.

Besides the usual $\mathrm{SU}(3)_f$ quantum numbers (total hypercharge Y, quadratic Casimir C_2, total isospin I and its 3rd component I_3), the basic excitations of our model also carry spin labels. The total spin operator J and its z-component J_z are defined using $\pi/2$ rotations about the spatial coordinate axes and agree with the infinitesimal generators of the continuum for improper zero-momentum meson states.

Regarding the baryons, we show the existence of 56 states associated with the eightfold way baryons and their anti-particles. They form the $J = 1/2$ flavor octet ($C_2 = 3$) and the $J = 3/2$ decuplet ($C_2 = 6$). Anti-baryons and baryons have the same spectral properties by charge conjugation. For the mesons, there are 36 states which can be grouped into three flavor nonets associated with the vector mesons ($J = 1$) and one nonet associated with the pseudo-scalar mesons ($J = 0$). Each nonet decomposes into an $\mathrm{SU}(3)_f$ singlet ($C_2 = 0$) and octet ($C_2 = 3$). Charge conjugation leaves invariant each of the singlets and octets. Hence, these multiplets contain their antiparticles.

All the hadrons are detected by *isolated dispersion curves* $w(\vec{p})$, $\vec{p} = (p^1, p^2, p^3) \in \mathbf{T}^3 \equiv (-\pi, \pi]^3$, in the E-M spectrum. For $\beta = 0$, we obtain

$$w(\kappa, \vec{p}) = -3 \ln \kappa - 3\kappa^3/4 + \kappa^3 \sum_{j=1,2,3} (1 - \cos p^j)/4 + \kappa^6 r(\kappa, \vec{p}) \,, \qquad (1)$$

for the baryons, with $r(0, \vec{p}) \neq 0$. For the mesons, we have

$$w(\vec{p}) = -2 \ln \kappa - 3\kappa^2/2 + \kappa^2 \sum_{j=1,2,3} (1 - \cos p^j)/2 + \kappa^4 r(\kappa, \vec{p}) \,. \qquad (2)$$

In Eq. (1), for the octet, $r(\kappa, \vec{p})$ is jointly analytic in κ and in each p^j, for small $|\Im m p^j|$. A new linear symmetry called *time reflection*, in contrast with the ordinary antilinear time reversal, is used to define a spin flip symmetry in the lower (upper) indices. This symmetry is employed to show that all octet dispersion curves are identical, and the four decuplet dispersion curves are pairwise identical (depend only on $|J_z|$). The $\beta = 0$ baryon masses have all the form $M = -3 \ln \kappa - 3\kappa^3/4 + \kappa^6 r(\kappa)$, with $r(\kappa)$ real analytic. We show a partial restoration of the continuous rotational symmetry at zero spatial momentum [15] which implies a same $r(\kappa)$ for all members of the octet (decuplet).

So, there is no mass splitting within the octet (decuplet), but there is an octet-decuplet mass difference of $3\kappa^6/4 + \mathcal{O}(\kappa^7)$, at $\beta = 0$, which persists for $\beta \neq 0$.

In Eq. (2), $|r(\kappa, \vec{p})| \leq$ const. For the pseudo-scalar mesons $r(\kappa, \vec{p})$ is jointly analytic in κ and p^j, for $|\kappa|$ and $|\Im m p^j|$ small. The meson masses are given by $m(\kappa) = -2\ln\kappa - 3\kappa^2/2 + \kappa^4 r(\kappa)$, with $r(0) \neq 0$ and $r(\kappa)$ real analytic; they are also analytic in β. For a fixed nonet, the mass of the vector mesons are independent of J_z and are all equal within each octet. All singlet masses are also equal for the vector mesons. For $\beta = 0$, up to and including $\mathcal{O}(\kappa^4)$, for each nonet, the masses of the octet and the singlet are equal. All members of each octet have identical dispersions. Other dispersion curves may differ. Indeed, there is a pseudo-scalar, vector meson mass splitting (between $J = 0, 1$) given by $2\kappa^4 + \mathcal{O}(\kappa^6)$, at $\beta = 0$, which persists for $\beta \neq 0$.

2 Model and Spectral Analysis

Our lattice QCD model partition function is $Z = \int e^{-S(\psi,\bar{\psi},g)}\, d\psi\, d\bar{\psi}\, d\mu(g)$, and for $F(\bar{\psi}, \psi, g)$, the normalized correlations are

$$\langle\, F\,\rangle = \frac{1}{Z} \int F(\bar{\psi}, \psi, g)\, e^{-S(\psi,\bar{\psi},g)}\, d\psi\, d\bar{\psi}\, d\mu(g)\,. \tag{3}$$

The $\mathrm{SU}(3)_f$ and gauge-invariant action $S \equiv S(\psi, \bar{\psi}, g)$ is Wilson's action [3]

$$\begin{aligned} S \;=\; & \tfrac{\kappa}{2} \sum \bar{\psi}_{a,\alpha,f}(u) \Gamma^{\sigma e^\mu}_{\alpha\beta} (g_{u,u+\sigma e^\mu})_{ab} \psi_{b,\beta,f}(u + \sigma e^\mu) \\ & + \textstyle\sum_{u \in \mathbb{Z}^4_o} \bar{\psi}_{a,\alpha,f}(u) M_{\alpha\beta} \psi_{a,\beta,f}(u) - \frac{1}{g_0^2} \sum_p \chi(g_p)\,. \end{aligned} \tag{4}$$

Here, besides summation over $\alpha, \beta = 1, 2, 3, 4$ (spin), $a = 1, 2, 3$ (color) and $f = 1, 2, 3 \equiv u, d, s$ (isospin), the first sum is over $u = (u^0, \vec{u}) = (u^0, u^1, u^2, u^3) \in \mathbb{Z}^4_o \equiv \{\pm 1/2, \pm 3/2, \pm 5/2 ...\} \times \mathbb{Z}^3$, $\sigma = \pm 1$ and $\mu = 0, 1, 2, 3$. 0 is the time direction and the 3 is the z-direction. e^μ is the μ-direction unit vector. At a site $u \in \mathbb{Z}^4_o$, $\hat{\psi}_{a\alpha f}(u)$ are Grassmann fields (the hat meaning the presence or absence of a bar). $\alpha = 1, 2$ are *upper* spin indices and $\alpha = 3, 4 \equiv +, -$ are *lower* ones. For each nearest neighbor oriented bond $< u, u \pm e^\mu >$ there is an $\mathrm{SU}(3)_c$ matrix $U(g_{u,u\pm e^\mu})$ parametrized by $g_{u,u\pm e^\mu} \in \mathrm{SU}(3)_c$, with $U(g_{u,u+e^\mu})^{-1} = U(g_{u+e^\mu,u})$. We drop the U from the notation. To each oriented plaquette p there is a plaquette variable $\chi(U(g_p))$ where $U(g_p)$ is the orientation-ordered product of $\mathrm{SU}(3)_c$ matrices, and χ is $\Re e\,(\mathrm{trace})$. $M \equiv M(m, \kappa) = \mathbb{1}$, by choosing the bare quark mass $m = 1 - 2\kappa$. Also, we

take $\Gamma^{\pm e^\mu} = -\mathbb{1} \pm \gamma^\mu$, where $\gamma^0 = \begin{pmatrix} \mathbb{1} & 0 \\ 0 & -\mathbb{1} \end{pmatrix}$, $\gamma^{j=1,2,3} = \begin{pmatrix} 0 & i\sigma^j \\ -i\sigma^j & 0 \end{pmatrix}$ are Dirac matrices obeying $\{\gamma_\mu, \gamma_\nu\} = 2\delta_{\mu\nu}\mathbb{1}$, where σ^j are Pauli matrices. $d\mu(g)$ is the product measure over non-oriented bonds of normalized $\mathrm{SU}(3)_c$ Haar measures. The Grassmann integrals are Berezin integrals; for $\kappa = 0$, $\langle \psi_{\ell_1}(x)\, \bar{\psi}_{\ell_2}(y)\rangle = \delta_{\alpha_1,\alpha_2}\delta_{a_1 a_2}\delta_{f_1 f_2}\delta(x-y)$, and Wicks theorem applies.

The physical quantum mechanical Hilbert space $\mathcal{H}$ and the E-M operators H and P^j, $j = 1,2,3$, are defined as in [8, 9]. Polymer expansion methods [8, 16] ensure the thermodynamic limit of correlations exists (below we work in this limit), and truncated correlations have exponential tree decay. The limiting correlations are lattice translational invariant and extend to analytic functions in κ and β. For gauge-invariant F and G restricted to $u^0 = 1/2$, we have the F-K formula

$$(G, \check{T}_0^{x^0}\check{T}_1^{x^1}\check{T}_2^{x^2}\check{T}_3^{x^3}F)_{\mathcal{H}} = \langle [T_0^{x^0}\vec{T}^{\vec{x}}F]\Theta G\rangle \ , \tag{5}$$

where $T_0^{x^0}$, $T_i^{x^i}$, $i = 1,2,3$, denote translation of the functions of Grassmann and gauge variables by $x^0 \geq 0$, $\vec{x} = (x^1, x^2, x^3) \in \mathbb{Z}^3$, $T^{\vec{x}} = T_1^{x^1}T_2^{x^2}T_3^{x^3}$ and Θ is an antilinear, order reversing operator which involves time reflection [8]. In Eq. (5), we do not distinguish between Grassmann, gauge variables (rhs) and the associated vectors in $\mathcal{H}$ (lhs). As linear operators in $\mathcal{H}$, $\check{T}_{\mu=0,1,2,3}$ are mutually commuting; $\check{T}_0$ is self-adjoint, with $-1 \leq \check{T}_0 \leq 1$, and $\check{T}_{j=1,2,3}$ are unitary. So, $\check{T}_j = e^{iP^j}$ defines the self-adjoint momentum operator $\vec{P} = (P^1, P^2, P^3)$ with spectral points $\vec{p} \in \mathbf{T}^3$ and $\check{T}_0^2 = e^{-2H} \geq 0$ defines the energy operator $H \geq 0$. We call a point in the E-M spectrum with $\vec{p} = \vec{0}$ a mass. Also, we let $\mathcal{E}(\lambda^0, \vec{\lambda})$ be the product of the spectral families of $\check{T}_0$, P^1, P^2, P^3.

Besides the $\mathrm{SU}(3)_f$ flavor and $\mathrm{SU}(3)_c$ local gauge symmetries, the symmetries [9] of charge conjugation $\mathcal{C}$, parity $\mathcal{P}$, $\pi/2$ rotations about the spatial axes and coordinate reflections are extensively used.

Due to the lack of space, below we concentrate on $\mathcal{H}_{odd} \subset \mathcal{H}$ and the baryon spectrum. (Although more delicate[1], the analysis for the mesons in $\mathcal{H}_{even} \subset \mathcal{H}$ is similar.) To show the existence of baryons up to $\approx -5\ln\kappa$,

[1]The baryon fields are $\sim \psi\psi\psi$ and are automatically truncated. The meson fields are $\sim \bar{\psi}\psi$ and truncation of the 2-meson function must be explicitly implemented to eliminate the vacuum state. For this, we adopt the method of duplicate field variables of [17] which complicates the analysis a bit.

we define a matrix-valued 2-point function $G(u,v) \equiv G(u-v)$. This 2-point function has a spectral representation obtained from the F-K formula and the spectral representations of the E-M operators. Its Fourier transform $\tilde{G}(p) = \sum_{x\in\mathbb{Z}^4} G(x)e^{-ip.x}$, $p = (p^0, \vec{p})$, has a representation which allows us to relate momentum space singularities on the $\Im m p^0$ axis to points in the E-M spectrum.

It ought to be emphasized that any claimed spectral results derived from a 2-point correlation *without* a spectral representation is *not* reliable. First, a relation between this correlation and the E-M operators must be established. It is unfortunate that this basic requirement is not always satisfied! Only showing exponential decay of correlations, in principle, says nothing about the spectrum. Even when the associated decay rate is in the spectrum, we learn nothing about the spectrum *above* this point or about the nature of the spectrum. An isolated state is needed to characterize a particle.

We now sketch how our results are obtained. $\tilde{G}(p)$ has a strip of analyticity in $\Im m p^0$ which is $|\Im m p^0| \leq -(3-\epsilon)\ln\kappa$, $0 < \epsilon \ll 1$, leading to

$$|G(u,v)| \leq \text{const}\, \kappa^{3|u-v|}\,, \tag{6}$$

with $|u-v| \equiv |u^0 - v^0| + |\vec{u}-\vec{v}|$, $|\vec{u}-\vec{v}| = \sum_{i=1,2,3} |u^i - v^i|$. To show that there are isolated baryon and antibaryon dispersion curves up to $\approx -5\ln\kappa$, we consider the inverse $\tilde{\Gamma}(p) = \tilde{G}(p)^{-1}$. For fixed $\vec{p}$, κ and β, we show that

$$\tilde{\Gamma}^{-1}(p) = \{\text{cof}\,[\tilde{\Gamma}(p)]\}^t / \det\tilde{\Gamma}(p)\,, \tag{7}$$

provides a meromorphic extension of $\tilde{G}(p)$ in p^0. (This is a key point!) Thus, the singularities of $\tilde{G}(p)$ are zeroes of $\det\tilde{\Gamma}(p)$. The dispersions $w(\vec{p})$ verify

$$\det\tilde{\Gamma}(p^0 = iw(\vec{p}), \vec{p}, \kappa) = 0\,. \tag{8}$$

That $\tilde{\Gamma}(p)^{-1}$ does provide a meromorphic extension of $\tilde{G}(p)$ follows from the faster temporal falloff of $\Gamma(x = u - v)$, the convolution inverse of G. Namely,

$$|\Gamma_{\ell_1\ell_2}(u,v)| \leq \text{const}\,|\kappa|^{3+5(|u^0-v^0|-1)+3|\vec{u}-\vec{v}|}\,, \tag{9}$$

for $|u^0 - v^0| \geq 1$. The faster falloff of $\Gamma(x)$ gives us analyticity in $|\Im m p^0| \leq -(5-\epsilon)\ln\kappa$, and implies the zeros of $\det\tilde{\Gamma}(p)$ are *isolated*, for each $\vec{p}$, κ and β. To find the number and behavior of the particle dispersion curves, we need the short distance, low κ order behavior of Γ, which follows from that of G.

By using the hyperplane decoupling method [9, 11], we find from the dynamics that the normalized baryon excitations fields are given by (with the simultaneous presence or absence of bars and taking *only* lower spin indices)

$$\hat{B}_{\vec{\alpha}\vec{f}}(x) = \epsilon_{abc}\,\hat{\psi}_{a\alpha_1 f_1}(x)\hat{\psi}_{b\alpha_2 f_2}(x)\hat{\psi}_{c\alpha_3 f_3}(x)/[n_{\vec{\alpha}\vec{f}}]\,. \tag{10}$$

$n_{\vec{\alpha}\vec{f}}$ is chosen such that, for coincident points, $\langle B_{\vec{\alpha}\vec{f}}\bar{B}_{\vec{\alpha}'\vec{f}'}\rangle^{(0)} = -\delta_{\vec{\alpha}\vec{\alpha}'}\delta_{\vec{f}\vec{f}'}$.

With this composite field, the 2-baryon function we use to detect baryons, for all u and v, is given by (χ here is the Heaviside function)

$$G_{\ell_1\ell_2}(u,v) = \langle B_{\ell_1}(u)\bar{B}_{\ell_2}(v)\rangle\,\chi_{u^0\le v^0} - \langle \bar{B}_{\ell_1}(u)B_{\ell_2}(v)\rangle^*\,\chi_{u^0>v^0}\,, \tag{11}$$

where the $\ell = (\vec{\alpha}\vec{f})$, and we suppress the lower spin indices. Letting $G = G_d + G_n$, where $G_{d,\ell_1\ell_2}(u,v) = G_{\ell_1\ell_2}(u,u)\delta_{\ell_1\ell_2}\delta_{uv}$ is the diagonal part of G, we define Γ by the Neumann series $\Gamma \equiv (G_d+G_n)^{-1} = \sum_{k=0}^{\infty} G_d^{-1}(-G_nG_d^{-1})^k$, which converges by the bound of Eq. (6).

To relate points in the E-M spectrum to singularities of $\tilde{G}_{\ell_1\ell_2}(p)$ on the $\Im m p^0$ axis, we first use the F-K formula to obtain a spectral representation, with $\bar{B}_\ell \equiv \bar{B}_\ell(1/2,\vec{0})$ and $x = v-u \in \mathbb{Z}^4$, $x^0 \neq 0$,

$$\begin{aligned} G_{\ell_1\ell_2}(x) &= -(\bar{B}_{\ell_1}, \check{T}^{|x^0|}\check{T}^{\vec{x}}\bar{B}_{\ell_2})_{\mathcal{H}} \\ &= -\int_{-1}^{1}\int_{\mathbb{T}^3}(\lambda^0)^{|x^0|-1}e^{-i\vec{\lambda}.\vec{x}}d_\lambda(\bar{B}_{\ell_1},\mathcal{E}(\lambda^0,\vec{\lambda})\bar{B}_{\ell_2})_{\mathcal{H}}\,, \end{aligned} \tag{12}$$

which is an even function of $\vec{x}$ by the $\mathcal{P}$ symmetry. For the Fourier transform, after separating out the $x^0 = 0$ contribution, we get

$$\tilde{G}_{\ell_1\ell_2}(p) \;=\; \tilde{G}_{\ell_1\ell_2}(\vec{p}) - (2\pi)^3\int_{-1}^{1} f(p^0,\lambda^0)d_{\lambda^0}\alpha_{\vec{p},\ell_1\ell_2}(\lambda^0)\,, \tag{13}$$

with $f(x,y) \equiv (e^{ix}-y)^{-1} + (e^{-ix}-y)^{-1}$, where $d_{\lambda^0}\alpha_{\vec{p},\ell_1\ell_2}(\lambda^0) = \int_{\mathbb{T}^3}\delta(\vec{p}-\vec{\lambda})$ $d_{\lambda^0}d_{\vec{\lambda}}(\bar{B}_{\ell_1},\mathcal{E}(\lambda^0,\vec{\lambda})\bar{B}_{\ell_2})_{\mathcal{H}}$, and we have set $\tilde{G}(\vec{p}) = \sum_{\vec{x}} e^{-i\vec{p}.\vec{x}}G(x^0=0,\vec{x})$.

As seen from Eq. (13), singularities on the $\Im m\, p^0$ axis are spectral points and are contained in the zeroes of $\det\tilde{\Gamma}(p)$.

We consider first the determination of the baryon masses (i.e. $\vec{p}=\vec{0}$). We pass to a basis where $\tilde{\Gamma}(p^0,\vec{p}=\vec{0})$ is diagonal. The diagonalization is achieved by exploiting the $\mathrm{SU}(3)_f$ symmetry, and passing to the eightfold way baryon particle basis. The new basis and the individual spin and isospin basis we have used hitherto are related by an orthogonal transformation. The octet and the decuplet basis are the usual ones from the continuum [1]. Applying the

$SU(3)_f$ symmetry reduces $\tilde{\Gamma}(p)$ to a block form with 8 identical 2×2 blocks associated with the octet, and 10 identical 4×4 blocks associated with the decuplet. Using $\pi/2$ rotations about e^3, $\tilde{\Gamma}(p)$ is diagonal at $\vec{p} = \vec{0}$; and by e^1 reflections the elements only depend on $|J_z|$. However, the partial restoration of continuous rotational symmetry at zero spatial momentum [15] shows that the masses are independent of J_z. The determinant factorizes, and we consider one of the 56 typical factors (for which we omit all indices).

Next, we employ the auxiliary function method [16] to determine convergent expansions for the baryon octet and the decuplet masses, and the $\mathcal{O}(\kappa^6)$ octet-decuplet mass splitting. Our method works for all $\beta \ll \kappa \ll 1$, but here we analyze only the leading $\beta = 0$ case, for simplicity. As the mass $\nearrow \infty$ as $\kappa \searrow 0$, the usual implicit function theorem does not apply to solve Eq. (8) at $\vec{p} = \vec{0}$. We make a nonlinear transformation from p^0 to $w = -1 - c_3(\vec{p})\kappa^3 + \kappa^3 e^{-ip^0}$, with $c_3(\vec{p}) = -\sum_{j=1,2,3} \cos p^j/4$, and introduce an auxiliary function $H(w,\kappa)$ such that $\tilde{\Gamma}(p^0,\vec{p}) = H(w = -1 - c_3(\vec{p})\kappa^3 + \kappa^3 e^{-ip^0}, \kappa)$. With this, the nonsingular part of the mass $M + 3\ln\kappa$ is brought from infinity to close to $w = 0$, as $\kappa \searrow 0$. Using $\mathcal{T}$ and $\mathcal{P}$ $[\Gamma(x^0,\vec{x}) = \Gamma(-x^0,\vec{x})]$, we have

$$\begin{aligned} H(w,\kappa) \;=\; & \textstyle\sum_{\vec{x}} \Gamma(x^0 = 0, \vec{x}) e^{-i\vec{p}.\vec{x}} + \sum_{\vec{x}, n=1,2\ldots} \Gamma(n,\vec{x}) \\ & \times \left[\left(\tfrac{1+w+c_3(\vec{p})\kappa^3}{\kappa^3} \right)^n + \left(\tfrac{\kappa^3}{1+w+c_3(\vec{p})\kappa^3} \right)^n \right] e^{-i\vec{p}.\vec{x}}. \end{aligned} \tag{14}$$

The bound on Γ of Eq. (9) guarantees that $H(w,\kappa)$ is jointly analytic in κ and w, $|\kappa|$, $|w| \ll 1$. To control the mass to $\mathcal{O}(\kappa^6)$, we need the low κ order short distance behavior of $\Gamma(x)$, which follows from that of $G(x)$. Precisely, we need $\Gamma(x^0 = n, \vec{x})/\kappa^{3n})$ up to and including $\mathcal{O}(\kappa^6)$. At $\kappa = 0$, $G(x = 0) = -1$ implies $\Gamma(x = 0) = -1$, and $G(x = e^0) = -\kappa^3 + \mathcal{O}(\kappa^4)$ implies $\Gamma(x = e^0) = \kappa^3 + \mathcal{O}(\kappa^4)$. Other contributions follow from the coefficients of the κ expansion of G. Namely, there are contributions arising from non-intersecting paths connecting the point 0 to x and paths that emit and absorb a meson. Using these short-distance results, after a lengthy calculation, we find

$$H(w,\kappa) = w + \frac{\kappa^6}{1+w} + a_6\kappa^6 + b\kappa^6 + \kappa^6 \sum_{n=1,\ldots,4} c'_{3n+6}(1+w)^n + h(w,\kappa)\kappa^7\,, \tag{15}$$

with the same b and c's for the octet and the decuplet, and $h(w,\kappa)$ jointly analytic in w and κ. The term $a_6\kappa^6$ comes from $x = \epsilon e^i + \epsilon' e^j$, $ij = 12, 13, 23$, $\epsilon, \epsilon' = \pm 1$, which we call *spatial angles*. a_6 is equal to $a_o = 3/8$ ($a_d = -3/8$) for

the octet (decuplet) and gives the mass splitting $M_d - M_o = 3\kappa^6/4 + \mathcal{O}(\kappa^7)$. As $H(0,0) = 0$ and $[\partial H/\partial w](0,0) = 1$, the analytic implicit function theorem implies that $H(w,\kappa) = 0$ has the analytic solution $w(\kappa) = -a_6\kappa^6 - b'\kappa^6 + \mathcal{O}(\kappa^7)$, with $b' = b + 1 + \sum_{n=1,\ldots,4} c'_{3n+6}$.

For $\beta \neq 0$, the arguments above hold since $H(w,\kappa,\beta)$ is jointly analytic in w, κ, and β and $[\partial H/\partial w](w = 0, \kappa = 0, \beta = 0) = 1 \neq 0$. $w(\kappa,\beta)$ is jointly analytic in κ and β. The non-singular contribution to the mass is also jointly analytic in κ and β. In particular, the mass splitting persists for $0 < \beta \ll \kappa$.

For the $\vec{p} \neq \vec{0}$ dispersion curves, the 2×2 and the 4×4 blocks of $\tilde{\Gamma}(p)$ still have a complicated structure even after the use of the usual well known symmetries. However, we have found a new local symmetry of spin flip $\mathcal{F}_s$, which is a composition of $\mathcal{T}$, $\mathcal{C}$ and a nonlocal, linear time reflection, and which we use to simplify $\tilde{\Gamma}(p)$. The action of $\mathcal{F}_s$ on single Fermi fields is such that $\hat{\psi}_1 \to \hat{\psi}_2$, $\hat{\psi}_2 \to -\hat{\psi}_1$, $\hat{\psi}_3 \to \hat{\psi}_4$ and $\hat{\psi}_4 \to -\hat{\psi}_3$. For functions of the gauge fields, $f(g_{xy}) \to \bar{f}(g^*_{xy})$. With this, the action of Eq. (4) is *termwise invariant* and we have a symmetry of the system satisfying $\langle F \rangle = \langle \mathcal{F}_s F \rangle^*$.

For the 2×2 block of G of the octet, using $\mathcal{F}_s$ shows that the blocks are diagonal and a multiple of the identity. The identical dispersion curves $w(\vec{p})$ can be obtained by using the auxiliary function method as before. For the 4×4 decuplet blocks, $\mathcal{F}_s$ simplifies the matrix $\tilde{\Gamma}(\vec{p})$ but it is *not* diagonal. We have not been able to apply the auxiliary function method. However, we can use a Rouché theorem [16] argument (principle of the argument), to show that there are exactly four pairwise identical solutions for each fixed $\vec{p}$.

The above analysis shows the existence of baryons in the subspace of $\mathcal{H}$ generated by the baryon fields. To extend the results to the whole $\mathcal{H}_{odd}$, up to near the meson-baryon threshold of $\approx -5 \ln \kappa$, we use $G(x)$ to define a generalized subtracted 2-point function $\mathcal{G}(x)$ and show that $\tilde{\mathcal{G}}(p)$ is regular in $|\Im m p^0| \leq -(5 - \epsilon) \ln \kappa$, showing an upper mass gap property.

3 Conclusions

We have validated the eightfold way in strongly coupled lattice QCD with 3 flavors, by showing the energy-momentum spectrum consists exactly of the eightfold way hadrons up to near the meson-meson threshold, showing confinement up to near this threshold. The determination of the one-hadron spectrum is a necessary step to analyze the existence of bound states. With our method

we can access the hadron-hadron spectrum, and should be able to help in clarifying fundamental open questions as e.g. the existence of certain tetraquark and pentaquark states as e.g. meson-meson and meson-baryon bound-states.

This work was supported by CNPq and FAPESP. PAFdV thanks the organizers of the Hadron07 Conference for inviting him to give a talk.

References

1. M. Gell-Mann, Y. Ne'eman, *The Eightfold Way* (Benjamin, New York, 1964). D. Griffiths, *Introduction to Elementary Particles* (John Wiley & Sons, New York, 1987).

2. K. Wilson, Phys. Rev. **D10**, 2445 (1974).

3. K. Wilson, in *New Phenomena in Subnuclear Physics*, Part A, ed. by A. Zichichi (Plenum Press, New York, 1977).

4. T. Banks *et al.*, Phys. Rev. **D 15**, 1111 (1977). J. Fröhlich, C. King, Nucl. Phys **B 290**, 157 (1987). I. Montvay, Rev. Mod. Phys. **59**, 263 (1987). F. Myhrer, J. Wroldsen, Rev. Mod. Phys. **60**, 629 (1988). D. Schreiber, Phys. Rev. **D 48**, 5393 (1993). M. Creutz, Nucl. Phys. **B** (Proc. Suppl.) **94** 219 (2001). R. Machleidt, Nucl. Phys. **A 689**, 11c (2001). R. Machleidt *et al.*, Phys. Rep. **149**, 1 (1987).

5. J.Hoek, N. Kawamoto, J.Smit, Nucl. Phys. **B 199**, 495 (1982). J.Hoek, J.Smit, Nucl. Phys. **B 263**, 129 (1986).

6. M. Creutz, *Quarks, Gluons and Lattices* (Cambridge University Press, Cambridge, 1983). I. Montvay, G. Münster, *Quantum Fields on a Lattice* (Cambridge University Press, Cambridge, 1997).

7. H.R. Fiebig *et al.*, Nucl. Phys. Proc. Suppl. **53**, 804 (1997). C. Stewart, R. Koniuk, Phys. Rev. **D 57**, 5581 (1998). H.R. Fiebig, H. Markum, in *International Review of Nuclear Physics*, ed. by A.M. Green (World Scientific, Singapoure, 2003). Ph. de Forcrand, S. Kim, Phys. Lett. **B 645**, 339 (2007). M.J. Savage, arXiv:nucl-th/0601001.

8. K. Osterwalder, E. Seiler, Ann. Phys. (NY) **110**, 440 (1978). E. Seiler, Lect. Notes in Phys. **159** (Springer, New York, 1982).

9. P.A. Faria da Veiga, M. O'Carroll, R. Schor, Commun. Math. Phys. **245**, 383 (2004).

10. P.A. Faria da Veiga, M. O'Carroll, R. Schor, Phys. Rev. **D 67**, 017501 (2003). A.F. Neto, P.A. Faria da Veiga, M. O'Carroll, J. Math. Phys. **45**, 628 (2004). P.A. Faria da Veiga, M. O'Carroll, R. Schor, Phys. Rev. **D 68**, 037501 (2003). P.A. Faria da Veiga, M. O'Carroll, A.F. Neto, Phys. Rev. **D 69**, 097501 (2004). P.A. Faria da Veiga, M. O'Carroll, Phys. Rev. **D 71**, 017503 (2005). P.A. Faria da Veiga, M. O'Carroll, A.F. Neto, Phys. Rev. **D 72**, 034507 (2005). P.A. Faria da Veiga, M. O'Carroll, Phys. Lett. **B 643**, 109 (2006).

11. P.A. Faria da Veiga, M. O'Carroll, Phys. Rev. **D 75**, 074503 (2007).

12. R. Schor, Nucl. Phys. **B 222**, 71 (1983); **B 231**, 321 (1984).

13. P.A. Faria da Veiga, M. O'Carroll, *Eightfold Way From Dynamical First Principles in Strongly Coupled Lattice QCD*, J. Math. Phys. (2007), to appear. *Exact Dynamical Eightfold Way Baryon Spectrum and Confinement in Strongly Coupled Lattice QCD* (2007), submitted.

14. A.F. Neto, M. O'Carroll, P.A. Faria da Veiga, *Dynamical Eightfold Way Mesons in Strongly Coupled Lattice QCD* (2007), submitted. *Mesonic Eightfold Way From Dynamics in Lattice QCD With Strongly Coupling* (2007), submitted.

15. M. Hamermesh, *Group Theory and Its Application to Physical Problems* (Addison-Wesley, Reading MA, 1962). J. Calloway, *Quantum Theory of the Solid State*, Part A (Academic Press, New York, 1974).

16. B. Simon, *Statistical Mechanics of Lattice Models* (Princeton University Press, Princeton, 1994).

17. J. Glimm and A. Jaffe, *Quantum Physics: A Functional Integral Point of View* (Springer Verlag, New York, 1986).

Frascati Physics Series Vol. XLVI (2007), pp. 1395–1402
HADRON07: XII Int. Conf. on Hadron Spectroscopy – Frascati, October 8-13, 2007
Baryon Spectroscopy

MESON-BARYON SCATTERING AND RESONANCES WITH STRANGENESS -1

J. A. Oller
Departamento de Física, Universidad de Murcia, E-30071 Murcia, Spain

Abstract

Meson-baryon interactions in S-wave with strangeness -1 are studied. This is a sector populated by plenty of resonances interacting in several two-body coupled channels. We consider a large set of experimental data, where the recent experiments have reached a remarkable accuracy. This requires a sound theoretical description to account for all the data and we employ Unitary Chiral Perturbation Theory up to and including $\mathcal{O}(p^2)$. The spectroscopy of our solutions is studied within this approach, discussing the rise of the two $\Lambda(1405)$ resonances and of the $\Lambda(1670)$, $\Lambda(1800)$, $\Sigma(1480)$, $\Sigma(1620)$ and $\Sigma(1750)$.

1 Introduction

The study of strangeness -1 meson-baryon dynamics comprising the $\bar{K}N$ plus coupled channels, has been renewed both from theoretical and experimental sides. Experimentally, we have new exciting data like the increasing improvement in precision of the measurement of the $\alpha-$line of kaonic hydrogen accomplished recently by DEAR [1)], and its foreseen better determination, with an expected error of a few eV, by the DEAR/SIDDHARTA Collaboration [2)]. This has established a challenge to theory in order to match such precision.

In this respect, ref. [3] provides an improvement over the traditional Deser formula for relating scattering at threshold with the spectroscopy of hadronic atoms [4]. In addition, one needs a good scattering amplitude to be implemented in this equation. The study of strangeness -1 meson-baryon scattering has a long history. In recent years it has received a lot of attention from the application of SU(3) baryon Chiral Perturbation Theory (CHPT) to this sector together with a unitarization procedure, see e.g., [5, 6, 7, 8, 9]. The importance of including the data measured with remarkable precision by the Crystal Ball Collaboration, for the reactions $K^- p \to \eta\Lambda$ [10] and $\pi^0\pi^0\Sigma^0$ [11] was remarked in ref. [12]. We will report here about the series of works [8, 9] on meson-baryon CHPT. Recently, we also presented the first full and minimal SU(3) CHPT meson-baryon Lagrangians to $\mathcal{O}(p^3)$ in ref. [13]. The study of $K^- p$ plus coupled channel interactions offers, from the theoretical point of view, a very challenging test ground for chiral effective field theories of QCD since one has there a good amount of experimental data, Goldstone bosons dynamics and large and explicit SU(3) breaking. In addition, this sector shows a very rich spectroscopy with many I=0, 1 S-wave resonances that will be the object of our study as well.

2 Formalism and Results

A general meson-baryon partial wave in coupled channels can be written in matrix notation as [5],

$$T = [1 + \mathcal{K}g]^{-1}\,\mathcal{K}\ , \tag{1}$$

where g is a diagonal matrix that comprises the unitarity bubble for every channel and $\mathcal{K}$ is the interaction kernel that is determined from meson-baryon CHPT. This is accomplished by performing a power expansion of T calculated from CHPT and then matched, order by order, with the chiral expansion of eq.(1),

$$T_1 + T_2 + T_3 + \mathcal{O}(p^4) = \mathcal{K}_1 + \mathcal{K}_2 + \mathcal{K}_3 - \mathcal{K}_1 \cdot g \cdot \mathcal{K}_1 + \mathcal{O}(p^4)\ , \tag{2}$$

taking into account that g is of chiral order one. We calculate $\mathcal{K}$ up to $\mathcal{O}(p^2)$, $\mathcal{K}_1 = T_1$ and $\mathcal{K}_2 = T_2$. The lowest order result, T_1, contains the seagull, direct and crossed exchange diagrams, while the next-to-leading order amplitudes, T_2, come from pure contact interactions. Once the kernel $\mathcal{K} = T_1 + T_2$ has been calculated, we insert it in eq.(1) and evaluate the S-wave amplitudes.

In ref. [8] a large set of meson-baryon scattering data was fitted which was enlarged in ref. [9] including new precise ones from the Crystal Ball Collaboration. Since we are just considering the S-wave amplitudes, we include in the fits those data points for the several K^-p cross sections with laboratory frame K^- three-momentum $p_K \leq 0.2$ GeV. This also enhances the sensitivity to the lowest energy region in which we are particularly interested. The number of data points included in each fit, without the data for the energy shift and width of kaonic hydrogen, is 97. Unless the opposite is stated, we also include in the fits the DEAR measurement of the shift and width of the $1s$ kaonic hydrogen energy level [1],

$$\Delta E = 193 \pm 37(stat) \pm 6(syst.)\ \text{eV}\ ,\ \Gamma = 249 \pm 111(stat.) \pm 39(syst.)\ \text{eV}\,, \quad (3)$$

which is around a factor of two more precise than the KEK previous measurement [14], $\Delta E = 323 \pm 63 \pm 11$ eV and $\Gamma = 407 \pm 208 \pm 100$ eV. We further constrain our fits by computing at $\mathcal{O}(p^2)$ in baryon SU(3) CHPT several πN observables with the values of the low energy constants involved in the fit. We calculate at $\mathcal{O}(p^2)$: a^+_{0+}, the isospin-even pion-nucleon S-wave scattering length, $\sigma_{\pi N}$, the pion-nucleon σ term, and m_0, from the value of the proton mass m_p. In this way we fix three of our free parameters. Ref. [9] included further data from recent experiments of the Crystal Ball Collaboration [10, 11]. As noted in ref. [9] these data cannot be reproduced from the fits given in ref. [8] and then new fits were considered in the former reference that from the beginning include the data from [10, 11]. As in ref. [8] two type of fits were found. The so called A-type fits, second column in table 1, that together with scattering data also reproduce the DEAR measurement on kaonic hydrogen. The others are the B-type fits, third column of table 1, that reproduce the former but not the latter. In fig.1 and table 2, second column, we show the reproduction of the data by the A-type fits and in fig.2 and table 2, third column, the same is done for the B-type fits. The lowest order fit is also shown in fig.2.

One also observes a factor of 2 of difference between the K^-p scattering lengths of the A- and B-type fits. So, if finally the DEAR measurement [1] is confirmed by the results of the DEAR/SIDDHARTA Collaboration [2], it would give rise to an important step forward in the knowledge of kaon-nucleon interactions. This difference in the scattering lengths makes also that only the A-type fits have a pattern of isospin violation in the calculations of the shift and width of kaonic hydrogen of expected size [3]. For the B-type fits the isospin violations turn out to be rather large, 30%, while for the A-type ones

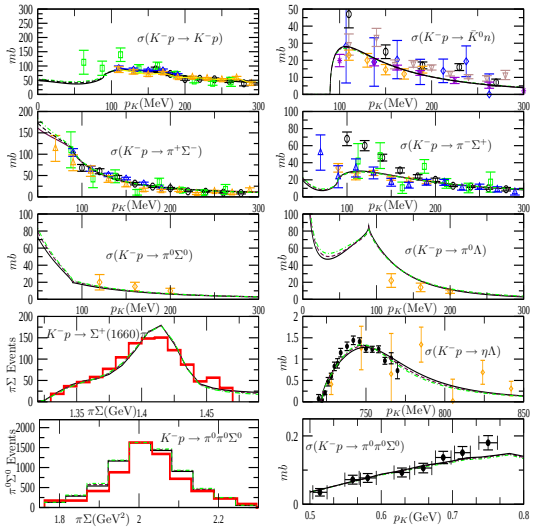

Figure 1: *The solid lines correspond to the $\sigma = 40^*$ MeV fit, the dashed lines to the 30^* MeV fit, and the dash-dotted curves to the 20^* MeV one of the A-type fits of ref.* [9]. *The different lines can be barely distinguished. For experimental references see ref.* [9].

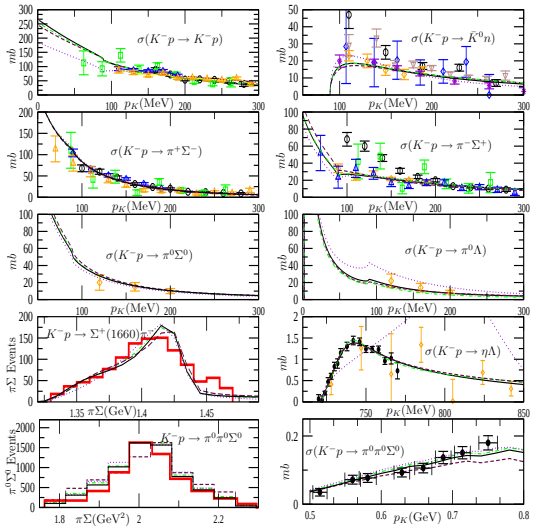

Figure 2: *The notation is like in fig.1 but for the B-type fits, with the additional dotted lines for the $\mathcal{O}(p)$ fit. For experimental references see ref.* [9].

Table 1: *A- and B-type fits, third and fourth columns, respectively, for a enforced* $\sigma_{\pi N} = 20$ *MeV. For precise definitions of the parameters* f, b_0, b_D, b_F, b_i *and* a_i *see ref.* [9]. *Three between the parameters* b_0, b_D, b_F *and* b_i *are fixed.*

Units	Parameters	A-type	B-type
MeV	f	75.2	95.8
GeV^{-1}	b_0	-0.615	-0.201
GeV^{-1}	b_D	$+0.818$	-0.005
GeV^{-1}	b_F	-0.114	-0.133
GeV^{-1}	b_1	$+0.660$	$+0.122$
GeV^{-1}	b_2	$+1.144$	-0.080
GeV^{-1}	b_3	-0.297	-0.533
GeV^{-1}	b_4	-1.048	$+0.028$
	a_1	-1.786	$+4.037$
	a_2	-0.519	-2.063
	a_5	-1.185	-1.131
	a_7	-5.251	-3.488
	a_8	-1.316	-0.347
	a_9	-1.186	-1.767

Table 2: *Table of results for the A- and B-type fits, second and third columns, respectively, given in table 1. The* $\sigma_{\pi N}$ *value enforced in the fits is 20 MeV.* ΔE *and* Γ *are calculated employing ref.* [3], *while* ΔE_D *and* Γ_D *are calculated with the Deser formula* [4].

	A-type	B-type
γ	2.36	2.34
R_c	0.629	0.643
R_n	0.168	0.160
ΔE (eV)	194	436
Γ (eV)	324	614
ΔE_D (eV)	204	418
Γ_D (eV)	361	848
a_{K^-p} (fm)	$-0.49 + i\,0.44$	$-1.01 + i\,1.03$
a_0 (fm)	$-1.07 + i\,0.53$	$-1.75 + i\,1.15$
a_1 (fm)	$0.44 + i\,0.15$	$-0.13 + i\,0.39$
$\delta_{\pi\Lambda}(\Xi)$ ($^\circ$)	3.4	-1.4
m_0 (GeV)	1.2	1.1
a^+_{0+} $(10^{-2} \cdot M_\pi^{-1})$	-2.0	-0.5

it is only 14%. Another interesting fact is that the values of the scattering lengths are rather independent of the values given to the sigma terms [8, 9]. The value for the f (the weak decay constant in the SU(3) chiral limit of the lightest pseudoscalars) in table 1 for the fit I is close to 80 MeV, the value given by the MILC Collaboration [15].

3 Spectroscopy

We show in tables 3 and 4 the I=0 and 1 poles, respectively, corresponding to the so-called fit I of ref. [9], similar to the one given in third column in table 1 but with $\sigma_{\pi N} = 40$ MeV. By passing continuously from one Riemann sheet to the other some of the poles in the tables with the same isospin are connected and represent the same resonance. One observes poles corresponding to the $\Lambda(1405)$, $\Lambda(1670)$ and $\Lambda(1800)$ in good agreement with the mass and width given to those resonances in the PDG [16]. In addition, there is a lighter resonance around 1310 MeV, not quoted in the PDG, and this has to do with the so called two $\Lambda(1405)$ resonances, although for fit I it appears much lighter than in ref. [6]. For I=1 one has the $\Sigma(1750)$ resonance. Fit I amplitudes also show in I=1 a broad bump at around 1.6 GeV corresponding to the $\Sigma(1620)$. There are also other poles around the $\bar{K}N$ threshold which mix up giving rise to a clear bump structure from 1.4 to 1.45 GeV. Finally, we also observe an I=2 pole for fit I at $1722 - i\,181$ MeV.

Regarding the I=0, 1 poles positions for the fit II of ref. [9], similar to that in the fourth column of table 1 but with $\sigma_{\pi N} = 40$ MeV, there are also poles corresponding to the $\Lambda(1405)$, $\Lambda(1670)$ but not for the $\Lambda(1800)$. There is no $\Sigma(1750)$ resonance either and the bumps for the $\Sigma(1620)$ have disappeared in several amplitudes. One also observes poles for $I = 1$ close to the $\bar{K}N$ threshold, although the resonant structure is much less prominent than in fit I.

In summary, we have reviewed the works of refs. [8, 9]. We have shown two type of fits that agree with scattering experimental data but only the A-type ones agree with the DEAR measurement of kaonic hydrogen [1]. These latter fits are also those that offer a remarkable agreement with spectroscopic information [16].

Table 3: *Fit I, I=0 Poles. The pole positions are given in MeV and the couplings in GeV. The symbol $|\gamma_{MB}|_0$ is the modulus of the coupling of the corresponding pole to the state with definite isospin.*

Re(Pole)	-Im(Pole)	Sheet	
$\lvert\gamma_{\pi\Sigma}\rvert_0$	$\lvert\gamma_{\bar{K}N}\rvert_0$	$\lvert\gamma_{\eta\Lambda}\rvert$	$\lvert\gamma_{K\Xi}\rvert_0$
1301	13	1RS	
1.12	5.83	0.41	2.11
1309	13	2RS	
3.66	4.46	0.21	3.05
1414	23	2RS	
4.24	4.87	0.85	9.35
1388	17	3RS	
3.81	1.33	0.42	9.55
1676	10	3RS	
1.28	1.67	2.19	5.29
1673	18	4RS	
1.26	1.82	2.13	5.32
1825	49	5RS	
2.29	2.10	0.89	7.43

Table 4: *Fit I, I=1 Poles. The notation is similar to that in table 3.*

Re(Pole)	-Im(Pole)	Sheet		
$\lvert\gamma_{\pi\Lambda}\rvert$	$\lvert\gamma_{\pi\Sigma}\rvert_1$	$\lvert\gamma_{\bar{K}N}\rvert_1$	$\lvert\gamma_{\eta\Sigma}\rvert$	$\lvert\gamma_{K\Xi}\rvert_1$
1425	2RS			
1.35	1.66	3.92	4.23	2.98
1468	2RS			
2.80	5.96	8.74	10.66	2.48
1433	3RS			
0.65	0.80	1.58	5.82	2.14
1720	4RS			
1.82	1.21	0.95	6.78	5.31
1769	6RS			
2.65	0.61	2.48	3.32	4.22
1340	3-4RS			
1.33	5.50	1.58	3.28	1.20
1395	3-4RS			
2.08	1.49	1.24	7.63	3.97

References

1. G. Beer *et al.* [DEAR Collaboration], Phys. Rev. Lett. **94**, 212302 (2005).

2. D. L. Sirghi and F. Sirghi, (DEAR/SIDDHARTA Collaboration), The physics of kaonic atoms at DAFNE, http://www.lnf.infn.it/esperimenti/dear/DEAR_RPR.pdf.

3. U.-G. Meißner, U. Raha and A. Rusetsky, Eur. Phys. J. **C35**, 349 (2004).

4. S. Deser *et al.*, Phys. Rev. **96**, 774 (1954); T. L. Trueman, Nucl. Phys. **26**, 57 (1961).

5. J. A. Oller and U.-G. Meißner, Phys. Lett. **B500**, 263 (2000).

6. D. Jido, J. A. Oller, E. Oset, A. Ramos and U.-G. Meißner, Nucl. Phys. **A725**, 181 (2003).

7. B. Borasoy, R. Nissler and W. Weise, Phys. Rev. Lett. **94**, 213401 (2005); Ibid. **96**, 199201 (2006); Eur. Phys. J. **A25**, 79 (2005); Phys. Rev. **C74**, 055201 (2006).

8. J. A. Oller, J. Prades and M. Verbeni, Phys. Rev. Lett. **95**, 172502 (2005); Phys. Rev. Lett. **96** 199202 (2006).

9. J. A. Oller, Eur. Phys. J. **A28**, 63 (2006).

10. A. Starostin *et al.* [Crystal Ball Collaboration], Phys. Rev. **C64**, 055205 (2001).

11. S. Prakhov *et al.* [Crystal Ball Collaboration], Phys. Rev. **C70**, 034605 (2004).

12. V. K. Magas, E. Oset and A. Ramos, Phys. Rev. Lett. **95**, 052301 (2005).

13. J. A. Oller, M. Verbeni and J. Prades, J. High Energy Phys **09**, 079 (2006); (E)-hep-ph/0701096; M. Frink, U.-G. Meißner, Eur. Phys. J. **A29**, 255 (2006).

14. M. Iwasaki *et al.*, Phys. Rev. Lett. **78**, 3067 (1997); Phys. Rev. **C58**, 2366 (1998).

15. C. Aubin *et al.* [MILC Collaboration], Phys. Rev. **D70** 114501 (2004).

16. W. M. Yao *et al.* [Particle Data Group], J. Phys. **G33** 1 (2006).

Frascati Physics Series Vol. XLVI (2007), pp. 1403–1414
HADRON07: XII Int. Conf. on Hadron Spectroscopy – Frascati, October 8-13, 2007
Baryon Spectroscopy

SEARCH FOR AN EXOTIC Θ^+ BARYON IN $\nu_\mu N$ IN THE NOMAD EXPERIMENT

Vincenzo Cavasinni[1], Dmitry Naumov[2], Oleg Samoylov[2]
[1] University of Pisa and Istituto Nazionale di Fisica Nucleare, Pisa, Italy
[2] Joint Institute for Nuclear Research, Dubna, Russia
Contact e-mail: samoylov@nusun.jinr.ru
(On behalf of the NOMAD Collaboration)

Abstract

A search for exotic Θ^+ baryon via $\Theta^+ \to pK^0_S$ decay mode in the NOMAD muon neutrino DIS data is reported. The special background generation procedure was developed. The proton identification criteria are tuned to maximize the sensitivity to the Θ^+ signal as a function of x_F which allows to study the Θ^+ production mechanism. We do not observe any evidence for the Θ^+ state in the NOMAD data. We provide an upper limit on Θ^+ production rate at 90% CL as 2.13 per 1000 of neutrino interactions.

1 Introduction

Since 2003 during three years an intense experimental activity has been carried out to search for exotic baryon states with charge and flavor requiring a minimal valence quark configuration of four quarks and one antiquark (such states are often referred to as "pentaquarks"). Searches for exotic baryon states have a

$\sim$ 30 year history, but a theoretical paper by Diakonov, Petrov and Polyakov [1] has triggered practically all recent activity.

The LEPS Collaboration was the first to report the observation of the Θ^+ ($uudd\bar{s}$) state with positive strangeness [2]. Then confirmations followed from many experiments. A narrow peak in the invariant mass distributions of pK^0_S or nK^+ pairs with a mass of $\simeq 1530 - 1540$ MeV/c^2 and a width of less than 25 MeV/c^2 was observed in all these experiments with significances of 4-8 σ's. However, after this initial flurry of positive results, negative results, in particular from high statistics experiments, started to dominate the field. Possible explanations for such a controversial experimental situation could be ascribed to specific production mechanisms yielding pentaquarks only for specific initial state particles. However, the CLAS experiment at Jefferson Lab has recently reported the results of a new analysis of photon–deuterium interactions with a statistics six times larger than the earlier event sample which showed a positive result. In this new analysis no Θ^+ peak was seen. A review of the experimental evidence for and against the existence of pentaquarks is presented in [3]. Recent theoretical status of pentaquarks is published here [4].

This article describes a search for the lightest member of the antidecuplet of exotic baryons, Θ^+, in the decay channel $\Theta^+ \to p + K^0_S$ from a large sample of neutrino interactions recorded in the NOMAD experiment at CERN.

2 The NOMAD detector

The large sample of neutrino interactions, about 1.5 millions, measured in NOMAD together with the good reconstruction quality of individual tracks, offer an excellent opportunity to search for $\Theta^+ \to p + K^0_S$. The NOMAD detector [5] consisted of an active target of 44 drift chambers, with a total fiducial mass of 2.7 tons, located in a 0.4 Tesla dipole magnetic field, as shown in Fig. 1.

The drift chambers, made of low Z material (mainly Carbon) served the double role of a nearly isoscalar target for neutrino interactions and of the tracking medium. The average density of the drift chamber volume was 0.1 g/cm^3. These chambers provided an overall efficiency for charged track reconstruction of better than 95% and a momentum resolution of approximately 3.5% in the momentum range of interest (less than 10 GeV/c). Reconstructed tracks were used to determine the event topology (the assignment of tracks to vertices), to reconstruct the vertex position and the track parameters at each vertex and, finally, to identify the vertex type (primary, secondary, V^0, etc.). A transition radiation detector placed at the end of the active target was used for particle identification. A lead-glass electromagnetic calorimeter

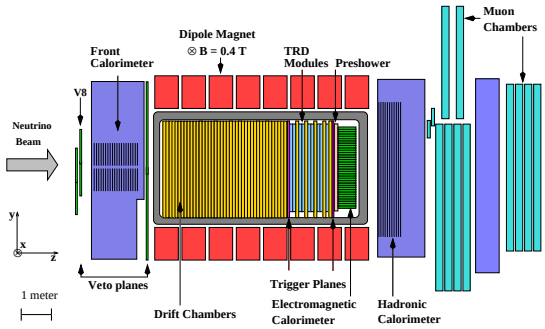

Figure 1: A sideview of the NOMAD detector.

located downstream of the tracking region provided an energy resolution of $3.2\%/\sqrt{E[\mathrm{GeV}]} \oplus 1\%$ for electromagnetic showers and was crucial to measure the total energy flow in neutrino interactions. In addition, an iron absorber and a set of muon chambers located after the electromagnetic calorimeter were used for muon identification, providing a muon detection efficiency of 97% for momenta greater than 5 GeV/c.

Neutral strange particles were reconstructed and identified with high efficiency and purity using the V^0-like signature of their decays [6]. Proton identification needed further development for the search presented here using information from the drift chambers, transition radiation detector and electromagnetic calorimeter.

The NOMAD Monte Carlo simulation (MC) is based on LEPTO 6.1 [7] and JETSET 7.4 [8] generators for neutrino interactions, and on a GEANT [9] based program for the detector response. The relevant JETSET parameters have been tuned in order to reproduce the yields of strange particles measured in ν_μ CC interactions in NOMAD [6]. To define the parton content of the nucleon for the cross-section calculation we have used the parton density distributions parametrized in [10].

3 Event selection

We have analysed neutrino–nucleon interactions of both charged (CC) and neutral current (NC) types. These events are selected with the requirements:

– The reconstructed primary vertex should be within a fiducial volume (FV) defined by $|x, y| < 120$ cm, $5 < z < 395$ cm (see Fig. 1 for the definition of the NOMAD coordinate system)

– There should be at least two charged tracks originating from the primary vertex;

– The visible hadronic energy should be larger than 3 GeV.

The ν_μ CC events are identified requiring in addition:

– The presence of an identified muon from the primary vertex.

The NC sample contains a contamination of about 30% from unidentified CC events. However, we do not apply further rejection against this background in order not to reduce the statistics. The event purity for the ν_μ CC selection is 99.6%. The total sample amounts to about 1.5 million neutrino events (see Table 1).

	CC	NC	CC+NC
N_{obs}	785232	393539	1178771
N_{corr}	1017664	481269	1498933

Table 1: Statistics of observed (N_{obs}) and efficiency corrected (N_{corr}) neutrino CC and NC events in the data.

3.1 K^0_S identification

K^0_S mesons are identified through their V^0-like decay $K^0_S \to \pi^+\pi^-$ using a kinematic constrained fit [6]. With a purity of 97% we identify 15934 and 7657 K^0_S mesons in the CC and NC samples respectively, thus yielding a total statistics of more than 23k K^0_S's. The reconstructed $K^0_S \to \pi^+\pi^-$ invariant mass distribution in the ν_μ CC (left) and ν_μ NC (right) subsamples are shown in Fig. 2. The two distributions have the same K^0_S mass mean value, 497.9 MeV/c^2, in agreement with the PDG value, and a width compatible with the expected experimental resolution of $\sim$9.5 MeV/c^2.

3.2 Proton reconstruction

The identification of protons is the most difficult part of the present analysis. As the NOMAD experiment does not include a dedicated detector for proton identification, we developed a special procedure for this purpose. The main background in the proton selection is the π^+ contamination since pions are about 2.5 times more abundant than protons. However the π^+ contamination can be suppressed exploiting the differences in the behaviour of protons and pions propagating through the NOMAD detector. We use three sub-detectors which can provide substantial rejection factors against pions:

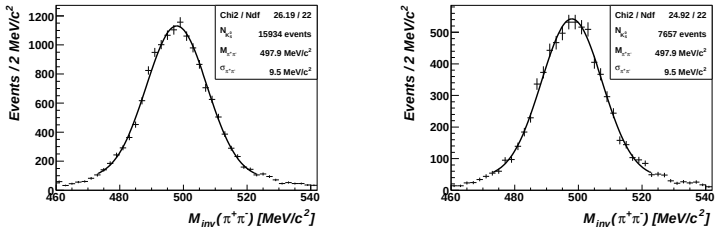

Figure 2: Reconstructed $K^0_S \to \pi^+\pi^-$ invariant mass distribution in the ν_μ CC (left) and ν_μ NC (right) subsamples of the data.

1. *The Drift Chambers (DC).* A low energy proton ranges out faster than a pion of the same momentum. Thus a correlation between the particle momentum and its path length can be used as a discriminator between protons and pions. The momentum interval of applicability of this method is below 600 MeV/c.

2. *The Transition Radiation Detector (TRD).* The energy deposition of protons and pions in the TRD is very different due to the larger proton ionization loss for momenta below 1 GeV/c, allowing a good pion–proton separation in this momentum interval. A modest discrimination is also possible for momenta above 3 GeV/c because of relativistic rise effects.

3. *The Electromagnetic Calorimeter (ECAL).* The proton sample can be cleaned further by taking into account the different Cherenkov light emission of protons and pions of the same momentum.

4 The background

Random K^0_S–proton pairs produce combinatorial background in the K^0_Sp invariant mass ($M(K^0_S p) \equiv M$) distribution. Understanding the shape of this background is crucial in the search for a possible Θ^+ signal. We studied this background in three different ways:

1. MC events contain no Θ^+ and could be used, therefore,to study the background for this analysis. However, the small fraction of proton–K^0_S pairs with an invariant mass in the interesting mass region would require a very large sample of MC events to reduce statistical fluctuations.

2. We combined protons and $K^{0\prime}_S s$ from different events in the data, thus making *fake pairs*, paying special attention that the original data dis-

tributions of multiplicity, proton and kaon momenta, and their relative opening angle, were well reproduced in the final *fake pair* sample.

3. A polynomial fit to the M distribution of the data themselves, excluding the Θ^+ mass region, can also be used to describe the background for the Θ^+ search.

Fig. 3 shows the invariant mass distributions of combinations of a positively charged track, assumed to be a proton, and a K^0_S for the data and for the fake pair background, without using proton identification and with "optimal" proton identification. The "signal" interval $1510 < M < 1550$ MeV/c^2 is *excluded* in the data. There is good agreement between the shapes of the data and background distributions. Polynomial fits of the data excluding the "signal" interval $1510 < M < 1550$ MeV/c^2 is also shown as dashed curves. There is a reasonable agreement of the background shapes obtained by *fake pair* procedure and by a polynomial fit of the data.

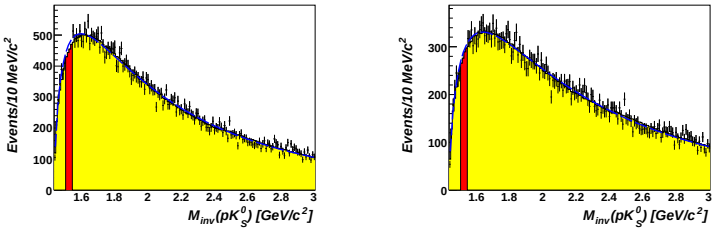

Figure 3: Invariant mass distribution of pairs of one positively charged track (assumed to be a proton) and a K^0_S for the data (points with error bars) and for the fake pair background (shadowed area). (Left) Proton identification has not been used. (Right) "Optimal" proton identification. Data in the "signal" region ($1510 < M < 1550$ MeV/c^2) are not shown. Dashed curve is fit of the data by a polynomial excluding the "signal" region.

5 Θ^+ analysis tools

5.1 The proton identification strategy

The Θ^+ signal is expected to appear as a narrow peak in the invariant mass distribution of K^0_S–proton pairs. K^0_S are identified using their V^0-like signature (see Sec. 3.1). To separate protons from π^+, for each positively charged track we build likelihoods under the proton and π^+ hypothesis using the information

from DC, TRD, and ECAL (see Sec. 3.2), and we take their ratios $\mathcal{L}_{DC}$, $\mathcal{L}_{TRD}$, $\mathcal{L}_{ECAL}$:

$$\begin{array}{ll} \mathcal{L}_{DC}(p, L), & L - \text{ track length} \\ \mathcal{L}_{TRD}(p, \epsilon_{TRD}), & \epsilon_{TRD} - \text{ energy release in TRD} \\ \mathcal{L}_{ECAL}(p, \epsilon_{ECAL}), & \epsilon_{ECAL} - \text{ energy release in ECAL} \\ & p - \text{ track momentum.} \end{array} \quad (1)$$

We optimize the cuts for the proton identification likelihood ratios maximizing the sensitivity to the expected Θ^+ signal. These "optimal" cuts are not necessarily those which maximize the purity of the proton sample.

The best approach for tuning the proton identification cuts would be to maximize the sensitivity using a detailed Monte Carlo for Θ^+ production. However, given the poor knowledge on the properties of this particle, there is no available MC generator describing the production of exotic baryons. We create, therefore, "fake" Θ^+ states in the NOMAD event generator by using pairs of protons and K^0_S with invariant mass close to the mass of Θ^+ state. However, in this approach the momentum distribution of these "fake" Θ^+ states is determined by the momentum distribution of protons and K^0_S from the primary vertex. This can result in wrong "optimal" cuts if the true momentum distribution of Θ^+ particles is very different. We try to avoid this problem by subdividing the original MC sample into several narrow bins of x_F and optimizing the cuts for *each* x_F interval independently. The x_F variable is defined as the ratio of the longitudinal projection of the Θ^+ momentum on the hadronic jet momentum to the hadronic jet energy in the hadronic center-of-mass frame. The variable x_F is in the range $(-1, 1)$ with negative (positive) values often called the *target (current)* fragmentation regions.

5.2 The pK^0_S mass resolution

The expected mass resolution of the pK^0_S pair is estimated as follows.

- For MC events we calculate the invariant masses of the generated and reconstructed pK^0_S pairs, and we fit the distribution of the difference between the two values by a Gaussian whose width is taken as the mass resolution (method "A").
- Using the measured momenta of the proton ($\vec{p}_1$) and of the K^0_S ($\vec{p}_2$),

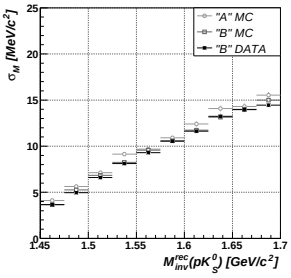

Figure 4: *The expected invariant mass resolution of proton+K^0_Spair as a function of the invariant mass for three different approaches: "A", "B MC" and "B DATA" (see text for details).*

the angle θ between $\vec{p}_1$ and $\vec{p}_2$, and the associated errors $\sigma(\vec{p}_1)$ and $\sigma(\vec{p}_2)$ we find (neglecting errors in $\cos\theta$):

$$M_{inv}^2\ \sigma^2(M_{inv}) = \left(\frac{E_2}{E_1}p_1 - p_2\ cos\theta\right)^2 \sigma^2(p_1) + \left(\frac{E_1}{E_2}p_2 - p_1\ cos\theta\right)^2 \sigma^2(p_2). \tag{2}$$

This method,"B", can be applied to both MC and data events.

Fig. 4 displays the expected mass resolution of pK_S^0 pairs as a function of their reconstructed invariant mass, as obtained using method "A" (MC only), or method "B" (for both MC and data). The results agree well with each other and predict a resolution of about 8.8 MeV/c^2 at the Θ^+ mass (1530 MeV/c^2).

5.3 The statistical analysis

An estimation of the signal significance in the data is performed as follows:

1. A possible difference in the proton $\cos\theta^*$ distribution for the signal and background is exploited to improve the signal sensitivity. We take all K_S^0–proton pairs with $1510 < M < 1550$ MeV/c^2, and we split them into 10 intervals with similar statistics: five mass intervals with $\cos\theta^*$ in the interval $[-1, -0.5)$, and another five mass intervals with $\cos\theta^*$ in the interval $[-0.5, 1]$. The total mass interval ($1510 < M < 1550$ MeV/c^2) covers well the expected Θ^+ mass. The mass bin width, 10 MeV/c^2, is comparable to the expected invariant mass resolution of K_S^0–proton pairs.

2. We compute two likelihoods:

$$\begin{aligned} \ln L_B &= \sum_{i=1,10} \left(-b_i + n_i \cdot \ln b_i\right), \\ \ln L_{B+S} &= \sum_{i=1,10} \left(-b_i - s_i + n_i \cdot \ln\left(b_i + s_i\right)\right) \end{aligned} \tag{3}$$

   where b_i, s_i, n_i are the number of predicted background and signal events, and observed data events in the i-th bin.

3. We compute the signal statistical significance as:

$$S_L = \sqrt{2\left(\ln L_{B+S} - \ln L_B\right)} \tag{4}$$

4. We find the resonance mass position M and Breit-Wigner width Γ and the number of signal events N_s which maximize S_L.

For the background we use the procedure decribed in Sec. 4. The signal is modeled by a Breit-Wigner distorted by a Gaussian resolution with $\sigma = 8.8$ MeV/c^2. This algorithm was checked on several generated distributions containing a Breit-Wigner signal of width Γ distorted by a Gaussian resolution of width σ and superimposed on a fluctuating background. We considered three cases, $\sigma \ll \Gamma$, $\sigma = \Gamma$, $\sigma \gg \Gamma$, and found that in all cases the procedure of maximizing S_L correctly determined the number of signal events and Γ (with Γ around zero for the case $\sigma \gg \Gamma$).

5.4 Opening the box

We split the data into five x_F intervals: $[-1, -0.6)$, $(-0.6, -0.3)$, $(-0.3, 0)$, $(0, 0.4)$, $(0.4, 1]$. In each interval we optimize the proton identification cuts as described in Sec. 3.2, and estimate a possible signal in the region $1510 < M < 1550$ MeV/c^2 as described in Sec. 5.3. All the plots have no significant structure for the Θ^+ state in any x_F interval. In Fig. 5 we display the invariant mass distributions of combinations of a positively charged track (assumed to be a proton) and a K^0_S for the two cases of no proton identification and optimum proton identification, for $-1 < x_F < 1$.

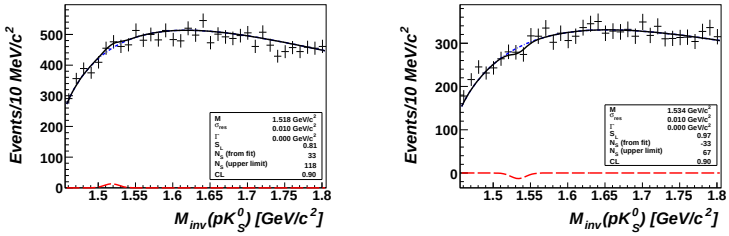

Figure 5: Invariant mass distributions of combinations of positively charged track with the assigned mass of the proton $+K^0_S$ in the data. (Left) Positives without proton identification. (Right) Positives with optimized proton identification. $-1 < x_F < 1$

Table 2 summarizes the results and provides also the upper limits at 90% confidence level (CL) on the number of Θ^+s candidates (N^{up}_s) and on the production rate R^{up} for both cases. The calculation of the upper limits for the production rate include corrections for inefficiencies, including the lack of detection of K^0_L mesons, and take into account the $K^0_S \to \pi^+\pi^-$ branching ratio. The results are presented for each bin of x_F, and also integrated over x_F. Fig. 6 displays the sensitivity and upper limits (90% CL) for the Θ^+

x_F interval	$[-1,-0.6)$	$(-0.6,-0.3)$	$(-0.3,0)$	$(0,0.4)$	$(0.4,1]$	all
no ID						
N_s (fit)	18	26	35	30	65	77
SL	1.96	1.49	1.01	1.18	2.61	1.82
N_s^{up}	41	61	88	81	101	161
R^{up}	*3.84*	*2.18*	*1.74*	*1.37*	*0.83*	*4.36*
optimal ID						
N_s (fit)	12	29	-26	-34	24	-33
SL	1.38	1.72	1.35	1.85	1.25	0.97
N_s^{up}	28	68	39	36	52	67
R^{up}	*2.80*	*2.60*	*0.84*	*0.79*	*1.00*	*2.13*

Table 2: Upper limits (90% CL) on the number of Θ^+ candidates (N_s^{up}) and on the Θ^+ production rate (R^{up}, in units of events per 10^3 interactions) for the case of no proton identification and with optimal proton identification.

production rate as a function of x_F. The upper limits are given as five curves, each corresponding to a fixed Θ^+ mass, obtained by varying both the number of signal events and the Θ^+ width to maximize S_L as outlined in Sec. 5.3.

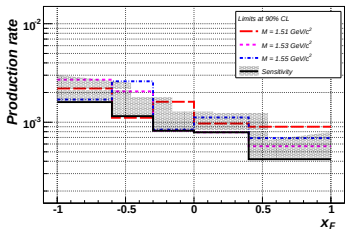

Figure 6: Sensitivity and upper limits at 90% CL for Θ^+ production rates as a function of x_F in the NOMAD data. The Θ^+ is fixed to 1510, 1520, 1530, 1540, 1550 MeV/c^2 as shown in the legend.

We also measure the x_F distribution of a potential Θ^+ state as follows. We build the x_F distributions in two side-bands, $1460 < M < 1500$ MeV/c^2 and $1580 < M < 1600$ MeV/c^2. We then normalize the average of these two distributions to the expected number of background events in the "signal" region ($1510 < M < 1550$ MeV/c^2), and subtract it from the x_F distribution of the data in the "signal" region. The result can be considered as the x_F distribution of the signal, and could shed a light on the Θ^+ production mechanism.

Fig. 7 displays the result with no proton identification and with optimal proton identification. We observe no statistically significant accumulation of events at any x_F value.

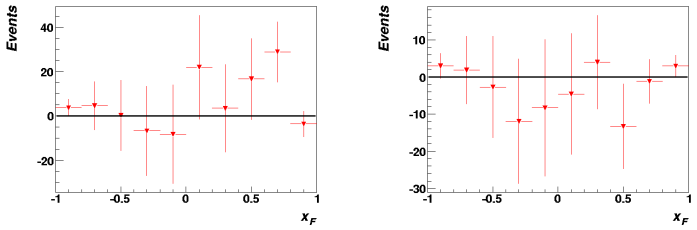

Figure 7: x_F distribution of potential Θ^+ signal in the data. (Left) Positives without proton identification. (Right) Positives with optimized proton identification.

6 Conclusions

We have performed a blind search for the Θ^+ exotic baryon in the $\Theta^+ \to p + K^0_S$ decay mode in the NOMAD $\nu_\mu N$ data. We have built a robust background estimation procedure which has been tested against various known cases like $\Lambda \to \mathrm{p}\pi^-$, $K^0_S \to \pi^+\pi^-$ and $K^\star \to K^0_S\pi$. In all cases good agreement between data and estimated background has been found. Good agreement has also been found between the invariant mass distribution of K^0_S–proton pairs in the data and the estimated background in the whole mass region excluding the Θ^+ signal region. We have developed proton identification tools based on the discrimination power of three sub-detectors, and we have tuned the proton identification criteria by maximizing the sensitivity to the expected signal in five x_F intervals independently. We have checked this approach for $\Lambda \to \mathrm{p}\pi^-$ and found that this procedure indeed maximizes the signal significance in both MC and data. Finally, we have "opened the box", i.e. examined the Θ^+ signal in the data and found good agreement between the data and the background for the whole M region, including the "signal" region, in each x_F interval. We observe no evidence, therefore, for any Θ^+ signal in the $\Theta^+ \to p + K^0_S$ decay channel in the NOMAD $\nu_\mu N$ data. We give an upper limit at 90% CL on Θ^+ production rate of $2.13 \cdot 10^{-3}$ events per neutrino interaction at $M = 1530$ MeV/c^2 after integrating over x_F.

It is interesting to compare this result with the recent analysis of old bubble chamber neutrino experiments which provide an estimation of the Θ^+ production rate as large as $\sim 10^{-3}$ events per neutrino interaction [11]. As shown in Fig.6, for a large fraction of the x_F range, except in the region $x_F \to -1$,

such a value is excluded. Unfortunately, ref. [11] does not provide information on the x_F region in which a Θ^+ signal was observed. Furthermore, in ref. [11] we find no information that the background estimation procedure took into account the effects mentioned in Sec. 4, which can result in an underestimation of the background and thus in an overestimation of both the signal significance and the production rate.

This NOMAD results is already published there [12]. You can turn to it to get more details. It is significant that there is no any interesting news about *pentaquark* on 2007.

Acknowledgement

Samoylov Oleg gratefully acknowledge all him co-authors and colleagues. Special thanks go to all the people arranged the Hadron07 Conference in Frascati.

References

1. D. Diakonov, V. Petrov, M. V. Polyakov. *Z. Phys.*, A359:305–314, 1997. hep-ph/9703373.
2. T. Nakano et al. *Phys. Rev. Lett.*, 91:012002, 2003. hep-ex/0301020.
3. Michael Danilov and Roman Mizuk. Experimental review on pentaquarks. 2007.
4. Takumi Doi. Theoretical status of pentaquarks. 2007.
5. J. Altegoer et al. *Nucl. Instrum. Meth.*, A404:96–128, 1998.
6. P. Astier et al. *Nucl. Phys.*, B621:3–34, 2002. hep-ex/0111057.
7. Ingelman, G., A. Edin and J. Rathsman. *Comp.Phys.Comm*, 101:108–134, 1997.
8. T. Sjostrand. *Comput. Phys. Commun.*, 82:74–90, 1994.
9. R. Brun, F. Carminati. CERN Program Library Long Writeup, W5013, 1992.
10. S.I. Alekhin. *Phys. Rev. D*, 68:014002, 2003.
11. A. E. Asratyan, A. G. Dolgolenko, M. A. Kubantsev. 2003. hep-ex/0309042.
12. O. Samoylov et al. Search for the exotic Θ^+ resonance in the nomad experiment. *Eur. Phys. J.*, C49:499–510, 2007.

Frascati Physics Series Vol. XLVI (2007), pp. 1415–1422
HADRON07: XII Int. Conf. on Hadron Spectroscopy – Frascati, October 8-13, 2007
Baryon Spectroscopy

σ CHANNEL THRESHOLD ENHANCEMENT IN DOUBLE PIONIC FUSION – THE ABC EFFECT AND ITS POSSIBLE ORIGIN IN A DIBARYONIC RESONANCE

M.Bashkanov, H. Clement, E. Doroshkevich,O. Khakimova,
F. Kren, T. Skorodko and G. J.Wagner
for the CELSIUS-WASA Collaboration
Physikalisches Institut der Universität Tübingen,
Auf der Morgenstelle 14, D-72076 Tübingen, Germany

Abstract

The ABC effect – an intriguing low-mass enhancement in the $\pi\pi$ invariant mass spectrum – is known from inclusive measurements of two-pion production in nuclear fusion reactions. First exclusive measurements carried out at CELSIUS-WASA for the fusion reactions leading to d or ^{3}He reveal this effect to be a σ channel phenomenon associated with the formation of a $\Delta\Delta$ system in the intermediate state and combined with a resonance-like behavior in the total cross section. Together with the observation that the differential distributions do not change in shape over the resonance region the features fulfill the criteria of an isoscalar s-channel resonance in pn and $NN\pi\pi$ systems, if the two emitted nucleons are bound. Since the ABC effect is also observed in fusion reactions leading to ^{3}He and ^{4}He with an resonance-like energy dependence, this pn s-channel resonance is obviously robust enough to survive in nuclei as a dibaryonic resonance configuration.

1 Introduction

The ABC effect – first observed by Abashian, Booth and Crowe [1)] in the double pionic fusion of deuterons and protons to ^{3}He – stands for an unexpected enhancement at low masses in the spectrum of the invariant $\pi\pi$-mass $M_{\pi\pi}$. Follow-up experiments [2, 3, 4, 5, 6, 7, 8, 9, 10, 11)] revealed this effect to be of isoscalar nature and to show up in cases, when the two-pion production process leads to a bound nuclear system. With the exception of low-statistics bubble-chamber measurements [4, 8)] all experiments conducted on this issue have been inclusive measurements carried out preferentially with single-arm magnetic spectrographs for the detection of the fused nuclei.

Initially the low-mass enhancement had been interpreted as due to an unusually large $\pi\pi$ scattering length and as evidence for the σ meson, respectively [1)]. Since the effect showed up particularily clearly at beam energies corresponding to the excitation of two Δs in the nuclear system, the ABC effect was interpreted lateron by a $\Delta\Delta$ excitation in the course of the reaction process leading to both a low-mass and a high-mass enhancement in isoscalar $M_{\pi\pi}$ spectra [12, 13, 14, 15, 16)]. In fact, the missing momentum spectra from inclusive measurements have been in support of such predictions. It has been shown [17)] that these structures can be enhanced considerably in theoretical calculations by including ρ exchange and short-range correlations.

2 Experiment

In order to investigate this issue in more detail we have carried out exclusive measurements of the reactions $pd \to pd\pi^0\pi^0$ (T_p = 1.03 and 1.35 GeV) and $pd \to {}^3\mathrm{He}\pi\pi$ (T_p = 0.893 GeV) in the energy region of the ABC effect at CELSIUS using the 4π WASA detector setup with pellet target system [18)], see Fig. 1. The selected energies have been close to the maximum of the ABC effect observed in the respective inclusive measurements. The $pd \to pd\pi^0\pi^0$ reaction proceeds as quasifree $pn \to d\pi^0\pi^0$ reaction with a spectator proton of very small momentum in the lab system. Since all ejectiles with the exception of the spectator have been measured, the spectator momentum has been reconstructed by kinematical fits with three overconstraints. Preliminary results for the reaction can be found in recent conference proceedings [19, 20, 21, 22)]. The experimental results on the $pd \to {}^3\mathrm{He}\pi^0\pi^0$ and $pd \to {}^3\mathrm{He}\pi^+\pi^-$ reactions

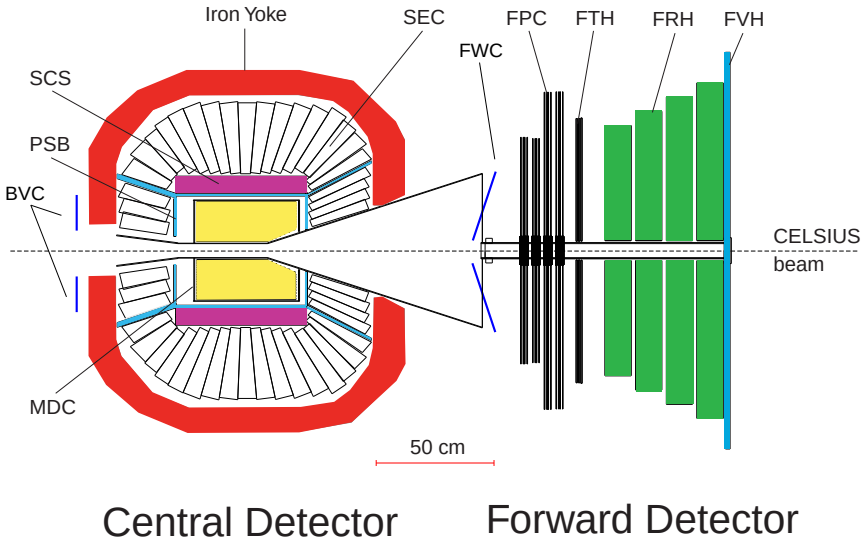

Figure 1: Schematic cross section of the WASA detector: The SuperConducting Solenoid (SCS) and the iron yoke for the return path of magnetic flux is shown shaded. Plastic scintillators are situated in the Plastic Scintillator Barrel (PSB), Forward Window Counters (FWC), Forward Trigger Hodoscope (FTH), Forward Range Hodoscope (FRH), Forward Range Intermediate Hodoscope (FRI), Forward Veto Hodoscope (FVH) and Backward Veto Counters (BVC). Cesium Iodide scintillators are situated in the Scintillator Electromagnetic Calorimeter (SEC). Proportional wire drift tubes, straws, make up the Mini Drift Chamber (MDC) and the Forward Proportional Chambers (FPC).

have been published already in Ref. [23, 24].

3 Results and Discussion

Some specific results of the CELSIUS-WASA measurements are shown in Figs. 2 and 3 for the double-pionic fusion to the deuteron, which is the most basic reaction for studying the ABC-effect. Fig. 2 exhibits the spectra of the invariant masses $M_{\pi^0\pi^0}$ and $M_{d\pi^0}$ for the quasifree $pn \to d\pi^0\pi^0$ reaction at a beam energy of $T_p = 1.03$ GeV .

The $\pi^0\pi^0$ channel, which is free of any isospin I=1 contributions, shows

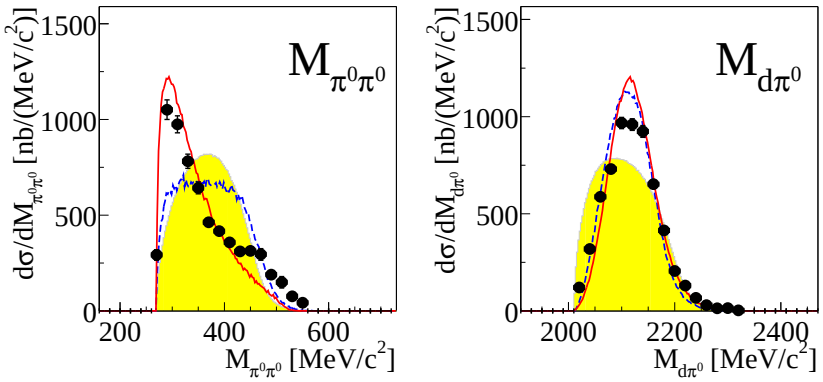

Figure 2: Distributions of the invariant masses $M_{\pi^0\pi^0}$ and $M_{d\pi^0}$ from the exclusive measurement of the quasifree $pn \to d\pi^0\pi^0$ reaction at a beam energy $T_p = 1.03$ GeV. The shaded areas show the pure phase space distributions. Solid and dashed curves give $\Delta\Delta$ calculations with and without the assumption of a quasibound state in the $\Delta\Delta$ system leading to a resonance in the pn and $d\pi^0\pi^0$ systems (from Ref. [20]).

a very large low-mass enhancement (ABC effect) in the $M_{\pi^0\pi^0}$ spectrum both in the fusion process to the deuteron and in the one resulting in ^{3}He [23, 24]. We note that in the $^3\mathrm{He}\pi^+\pi^-$ channel the threshold enhancement is observed [23] too, however, less pronounced. The reason for this is that this channel in addition contains isovector contributions - as may be seen [25] by the small shifts between the Δ peaks in the $M_{^3He\pi^+}$ and $M_{^3He\pi^-}$ spectra – see Fig. 5 of Ref. [23]. However, the main result of these measurements is that indeed two Δs are excited simultaneously in this reaction – in support of the hypothesis that a $\Delta\Delta$ system is excited in the course of the double pionic fusion process.

From the experimental angular distributions [20, 23, 24] we find the following features:

- The pion angular distribution in the $\pi\pi$ subsystem is flat for the low-mass enhancement region in the $M_{\pi\pi}$ spectrum, i.e., the ABC-effect is of scalar-isoscalar nature – in other words it is a σ channel phenomenon.

- The distribution of the opening angle between the two pions shows that

the ABC-effect is associated with two pions leaving the interaction vertex in parallel.

- The angular distribution of the $\pi\pi$ system (which is aquivalent to the angular distribution of the residual nucleus) in the overall center-of-mass system is not flat. It rather corresponds to a double p-wave distribution as expected from the decay of the $\Delta\Delta$ system.

.

From the measurements of the quasifree $pn \to d\pi^0\pi^0$ reaction at various energies we observe that the differential distributions do not change in shape significantly with energy. This points to a dominance of just a single partial wave in the entrance channel – as is the case for the excitation of a s-channel resonance. As a consequence of such an assumption we should find a resonance-like energy dependence in the total cross section. Actually this is what in fact is observed for this reaction. Fig. 3 depicts the energy dependence of the total cross section of the double-pionic fusion to the deuteron. Shown are the results for the $pn \to d\pi^+\pi^-$ reaction from bubble chamber measurements at DESY [4] and JINR [8] together with the preliminary CELSIUS-WASA results [19, 20] for the quasifree $pn \to d\pi^0\pi^0$ reaction at two incident energies, which have been binned into narrow ranges of effective collision energy providing thus four entries below and two entries above the peak energy. Since $\pi^+\pi^-$ and $\pi^0\pi^0$ channels are related by an isospin factor of two, the $\pi^0\pi^0$ results are plotted in Fig. 3 multiplied by this isospin factor. A resonance-like behavior of the total cross section is obvious from these data.

The essential clue to the nature of the ABC effect appears to be in the intriguing energy dependence of the double-pionic fusion in the isoscalar channel. We note that the isovector fusion channel $pp \to d\pi^+\pi^0$, shows **no** ABC effect [26] despite a clear $\Delta\Delta$ excitation signal in its differential spectra. It also exhibits an energy dependence [27] in its total cross section, which is close to the dotted curve in Fig. 3. Contrary to this situation the isoscalar fusion channel exhibits a much steeper energy-dependence in accordance with a resonance having a width of roughly 100 MeV or even less, i.e. much smaller than twice the Δ width, which is expected from usual $\Delta\Delta$ calculations. Also the cross section maximum at $\sqrt{s} \approx 2.4$ GeV means that the resonance mass is below twice the Δ mass, i.e. a quasibound state with regard to the $\Delta\Delta$ system.

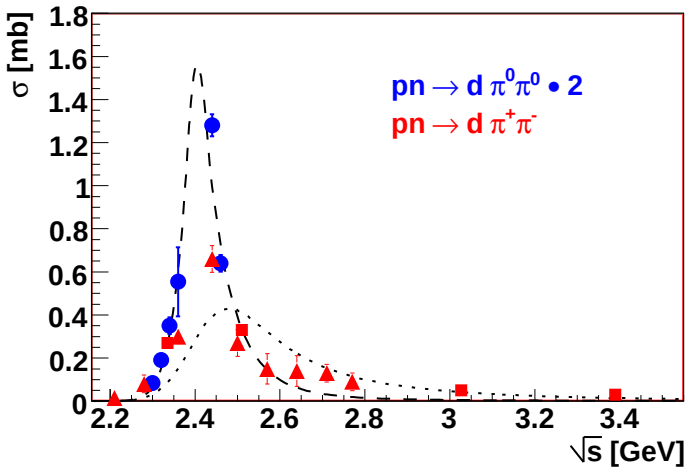

Figure 3: Energy dependence of the $pn \to d\pi\pi$ reaction with preliminary results of this work for the $\pi^0\pi^0$ channel (quasi-free measurements at two incident energies) and results for the $\pi^+\pi^-$ channel from Ref. [8] (squares) and Fig. 2c of Ref. [4] (triangles). Dashed and dotted lines represent calculations with and without the assumption of a quasibound state in the $\Delta\Delta$ system leading to a resonance in the pn and $d\pi^0\pi^0$ systems (from Ref. [20]).

In fact, if we use a Breit-Wigner resonance ansatz with a $q_{\Delta\Delta}$ dependent width and adjust the width parameters not to fit the total cross section data, but to reproduce the ABC-effect in the $M_{\pi^0\pi^0}$ spectra, then we obtain not only a quantitative description of all differential data (see, e. g., solid curves in Fig. 2) but at the same time also a quantitative description of the energy dependence of the total cross section (dashed curve in Fig. 3) thus obtaining automatically the observed width of the total cross section data.

4 Conclusions

The finding of a s-channel resonance in the isoscalar $pn \to d\pi\pi$ channel has the consequence that this resonance should show up also in the elastic pn scattering channel. Unfortunately in the corresponding energy region of T_p = 1.1 - 1.3

GeV there are no data. Moreover, from the analysis of the $pn \to d\pi\pi$ data we expect the s-channel resonance to contribute to total elastic pn cross section only on the percentage level, i.e., only a detailed partial wave analysis of very precise elastic pn scattering data over the energy region T_p = 1.0 - 1.3 GeV would have the potential to sense this resonance in the $^3S_1$, $^3D_1$ or $^3D_3$ partial waves.

Since the ABC-effect shows up in heavier nuclear systems, too, the resonance obviously is a quite stable object, which survives even in the nuclear surroundings. In fact, the energy dependence measured for the ^{3}He and ^{4}He cases in previous inclusive measurements [6] is in support of this conclusion.

Acknowledgments

We acknowledge valuable discussions with R. A. Arndt, I. Strakovski, E. Oset, C. Wilkin, Ch. Hanhart, A. Sibirtsev, L. Alvarez-Ruso, A. Kaidalov, V. I. Kukulin, L. Dakhno and V. Anisovich on this issue. This work has been supported by BMBF (06TU201, 06TU261), COSY-FFE, DFG (Europ. Graduiertenkolleg 683), Landesforschungsschwerpunkt Baden-Württemberg and the Swedish Research Council. We also acknowledge the support from the European Community-Research Infrastructure Activity under FP6 "Structuring the European Research Area" programme (Hadron Physics, contract number RII3-CT-2004-506078).

References

1. N. E. Booth, A. Abashian, K. M. Crowe, *Phys. Rev. Lett.* **7** (1961) 35; **6** (1960) 258; *Phys. Rev.* **C132** (1963) 2296ff
2. R. J. Homer *et al.*, *Phys. Rev. Lett.* **9** (1964) 72
3. J. H.Hall *et al.*, *Nucl. Phys.* **B12** (1969) 573
4. I. Bar-Nir *et al.*, *Nucl. Phys.* **B54** (1973) 17
5. J. Banaigs *et al.*, *Nucl. Phys.* **B67** (1973) 1
6. J. Banaigs *et al.*, *Nucl. Phys.* **B105** (1976) 52
7. F.Plouin *et al.*, *Nucl. Phys.* **A302** (1978) 413

8. A. Abdivaliev *et al.*, *Sov. J. Nucl. Phys.* **29** (1979) 796

9. F. Plouin, P. Fleury, C. Wilkin, *Phys. Rev. Lett.* **65** (1990) 690

10. R. Wurzinger *et al.*, *Phys. Lett.* **B445** (1999) 423

11. for a review see A. Codino and F. Plouin, *LNS/Ph/94-06*

12. T. Risser and M. D. Shuster, *Phys. Lett.* **43B** (1973) 68

13. I. Bar-Nir, T. Risser, M. D. Shuster, *Nucl. Phys.* **B87** (1975) 109

14. J. C. Anjos, D. Levy, A. Santoro, *Nucl. Phys.* **B67** (1973) 73

15. see, e.g., A. Gardestig, G. Fäldt, C. Wilkin, *Phys. Rev.* **C59** (1999) 2608 and *Phys. Lett.* **B421** (1998) 41

16. C. A. Mosbacher, F. Osterfeld, *nucl-th/990364*

17. L. Alvarez-Ruso, *Phys. Lett.* **B452**, 207(1999); PhD thesis, Univ. Valencia 1999

18. J. Zabierowski *et al.*, *Phys. Scripta* **T99** (2002) 159

19. M. Bashkanov *et al.*, *Proc. INPC 2007*, to be published

20. M. Bashkanov *et al.*, *Proc. MENU 2007*, to be published

21. O.Khakimova *et al.*, *Proc. MENU 2007*, to be published

22. H. Clement *et al.*, contribution to Erice School 2007

23. M. Bashkanov *et al.*, *Phys. Lett.* **B637** (2006) 223

24. M. Bashkanov, PhD thesis, Univ. Tübingen 2006, http://tobias-lib.ub.uni-tuebingen.de/volltexte/2006/2636/, urn:nbn:de:bsz:21-opus-26366

25. C. Wilkin, private communication 2007 (2007) 625 (2007) 617

26. F. Kren, PhD thesis Tübingen, in preparation

27. J.Bystricky *et al.*, *J. Physique* **48** (1987) 1901

Frascati Physics Series Vol. XLVI (2007), pp. 1423–1430
HADRON07: XII Int. Conf. on Hadron Spectroscopy – Frascati, October 8-13, 2007
Baryon Spectroscopy

EXCITATION OF THE ROPER RESONANCE IN SINGLE- AND DOUBLE-PION PRODUCTION

T. Skorodko, M.Bashkanov, H. Clement, E. Doroshkevich,
O. Khakimova, F. Kren and G. J.Wagner
for the CELSIUS-WASA Collaboration
Physikalisches Institut der Universität Tübingen,
Auf der Morgenstelle 14, D-72076 Tübingen, Germany

Abstract

In most experimental investigations the $N^*(1440)$ baryon state, commonly known as Roper resonance, can be approached only very indirectly via complex partial wave analyses, since no explicit resonance-like structures are observed. We find indications for its excitation in the invariant $n\pi^+$ mass spectrum of the $pp \to np\pi^+$ reaction at $M \approx 1360$ MeV with a width of 150 MeV. The values fit very favorably to the most recent phase shift results as well as to the observations of J/Ψ decays at BES. In the $pp \to pp\pi^0\pi^0$ reaction near threshold, where the Roper excitation and its subsequent decays via the routes $N^* \to \Delta\pi \to N(\pi\pi)_{I=l=0}$ and $N^* \to NN(\pi\pi)_{I=l=0}$ are the only dominant processes, we find the latter route – which is the direct decay into the $N\sigma$ channel – to be the by far dominating decay process - in favor of a monopole excitation of the Roper resonance.

1 Introduction

The Roper resonance has been a puzzle ever since its discovery in πN phase shifts [1]. Some 40 years ago, when David Roper undertook one of the first energy-dependent phase shift analyses of πN scattering data, he discovered [1] a resonance in the P_{11} partial wave by noting that this particular phase shift proceeds from 0° to 140° in the investigated energy range in much the same way as the P_{33} and D_{13} phaseshifts do. The peculiarity of this resonance, however, has been all the time, that no sign of a resonance-like structure could ever be observed in experimental observables, in particular not in the total cross section, where a resonance should show up by its Breit-Wigner-like energy dependence. However, the Roper resonance obviously is excited in the πN scattering process such weakly, that it is burried underneath a wealth of other processes and can be sensed only via a very detailed partial wave analysis

Even in most investigations up-to-date no apparent resonance signatures could be found in the observables. Not only its nature has been a matter of permanent debate, also its resonance parameters show a large scatter in their values [2].

New phase shift analyses [3, 4] of πN and γN data show nowadays the pole of the Roper resonance to be nearly 100 MeV below its canonical value of 1440 MeV with a width not much different from that of neighboring baryon states. In the pioneering αp scattering experiment at Saclay [5] convincing direct evidence for the Roper resonance has been found for the first time in the missing mass spectrum. And new BES data [6] on $J/\Psi \to \bar{N}N^*$ show for the first time a clear structure in the $M_{p\pi^-}$ invariant mass spectrum at $M \approx 1358$ MeV and a width of $\Gamma \approx 179$ MeV.

Note that with the pole position being now more than 80 MeV below the previously adopted value of the N*(1440), also its decay branchings change dramatically, if evaluated at the physical relevant pole position.

2 Experiment

In order to allow more detailed studies of this issue exclusive measurements of the reactions $pp \to NN\pi$ and $pp \to NN\pi\pi$ have been carried out at several energies from 650 - 1360 MeV at the CELSIUS storage ring using the 4π WASA detector setup (Fig. 1) including the hydrogen pellet target system [9].

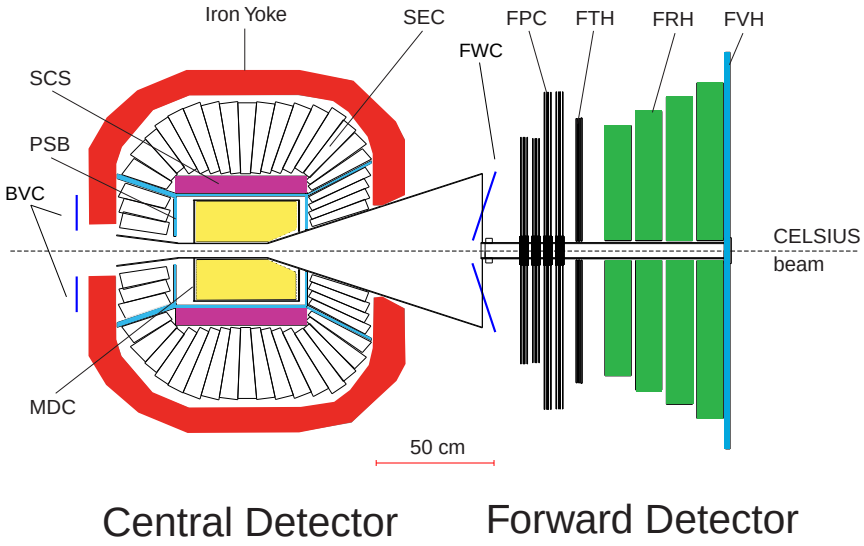

Figure 1: Schematic cross section of the WASA detector: The SuperConducting Solenoid (SCS) and the iron yoke for the return path of magnetic flux is shown shaded. Plastic scintillators are situated in the Plastic Scintillator Barrel (PSB), Forward Window Counters (FWC), Forward Trigger Hodoscope (FTH), Forward Range Hodoscope (FRH), Forward Range Intermediate Hodoscope (FRI), Forward Veto Hodoscope (FVH) and Backward Veto Counters (BVC). Cesium Iodide scintillators are situated in the Scintillator Electromagnetic Calorimeter (SEC). Proportional wire drift tubes, straws, make up the Mini Drift Chamber (MDC) and the Forward Proportional Chambers (FPC).

For the reactions under consideration forward going protons have been detected in the forward detector and identified by the ΔE-E technique using corresponding informations from quirl (FTH) and range hodoscope (FRH), respectively. Charged pions, protons as well as gammas (from π^0 decay) have been detected in the central detector. This way the full four-momenta have been measured for all charged and π^0 particles of an event allowing thus kinematic fits with overconstraints. For the $pp \to pp\pi^0\pi^0$ reaction, which is the main topic of this contribution, the number of overconstraints has been six.

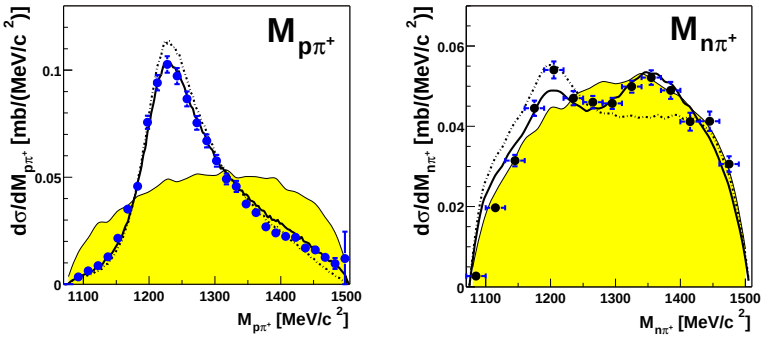

Figure 2: Invariant mass spectra $M_{p\pi^+}$ and $M_{n\pi^+}$ from the measurement of the $pp \to np\pi^+$ reaction at $T_p = 1.3$ GeV. The shaded areas show pure phase space distributions, whereas drawn curves show calculations for Δ^{++} and Δ^+ excitations with (solid) and without(dotted) inclusion of Roper excitation.

3 Results and Discussion

The $pp \to np\pi^+$ measurements carried out at $T_p = 1.1$ and 1.3 GeV exhibit a very strong Δ^{++} excitation in the $M_{p\pi^+}$ spectrum, see Fig. 2. The $M_{n\pi^+}$ spectrum, however, shows only a small structure at the position of the Δ^+ resonance, which is isospin-suppressed by a factor of nine in intensity relative to the Δ^{++} excitation. Towards larger $M_{n\pi^+}$ masses we find another structure around 1360 MeV with a width of about 150 MeV, which we associate with the Roper excitation. At present the details of this structure are still under investigation.

The $pp \to pp\pi^0\pi^0$ reaction separates into a clear Roper excitation region near threshold and a high-energy region governed by $\Delta\Delta$ excitation. Both regions are separated by a dip in the energy dependence of the total cross section [10]. Since in this contribution we deal with the Roper excitation, in the following we will restrict ourselves to the discussion of the near-threshold scenario.

The large sensitivity of the $pp \to pp\pi\pi$ reaction near threshold to the two-pion decay of the Roper resonance has been demonstrated previously for the $\pi^+\pi^-$ channel [7, 8]. According to the theoretical calculations of the

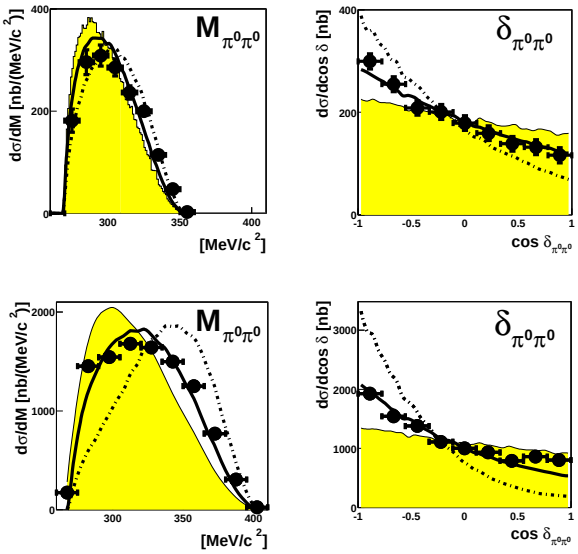

Figure 3: *Differential cross sections of the* $pp \to pp\pi^0\pi^0$ *reaction at* $T_p = 775$ *MeV (top) and 895 MeV (bottom) in dependence of the two-pion invariant mass* $M_{\pi^0\pi^0}$ *(left) and the opening angle* $\delta_{\pi^0\pi^0}$ *(right) between the two pions. Phase-space distributions are shown by the shaded areas, the theoretical prediction* [11] *is presented by the dotted lines, whereas the solid curves give the result, when the amplitude for the Roper decay* $N^* \to \Delta\pi \to N(\pi\pi)_{I=l=0}$ *is reduced by a factor of two (from* [12]*).*

Valencia group [11], which presently constitute the state-of-the-art calculations for two-pion production in NN collisions, the excitation and decay of the Roper resonance is the most dominating process in the $pp \to pp\pi^0\pi^0$ reaction at beam energies close to threshold: on the one hand nonresonant contributions as well as single Δ excitation associated with the production of a second pion via s-wave rescattering are smaller by orders of magnitude. On the other hand the $\Delta\Delta$ process, i.e. the simultaneous excitation of two Δs in the NN system, is still small compared to the Roper process. At higher beam energies $T_p >$ 1.2 GeV the $\Delta\Delta$ excitation gets comparable to the Roper process and finally dominates the high energy region.

The $\pi^0\pi^0$ channel selects specifically the isoscalar part of the Roper decay into the $\pi\pi$ channel. As demonstrated in Refs. [7, 8] the two differential cross sections, which are most sensitive to the branching of the two-pion decay routes of the Roper resonance, are the differential distributions with regard to the two-pion invariant mass $M_{\pi^0\pi^0}$ and the opening angle $\delta_{\pi^0\pi^0}$ between the two pions (in the overall center-of-mass system). Both distributions are shown in Fig. 3 for two incident energies, T_p = 775 and 895 MeV, respectively.

The reaction amplitude for excitation of the Roper resonance and its subsequent decay into the σ channel $(\pi\pi)_{I=l=0}$ is given by the sum of two amplitudes, one for the direct decay into the σ channel and for the decay via the $\Delta\pi$ system:

$$A \sim (a + b\ \vec{k_1} * \vec{k_2}\ D_{\Delta^+})\ D_{N^*}, \qquad (1)$$

where $\vec{k_1}$, $\vec{k_2}$ are the momenta of the emitted pions, D_{Δ^+} and D_{N^*} denote the respective resonance propagators and the coefficients a and b include the coupling constants of the two decay routes. The first amplitude just provides a phase-space like behavior of the differential distributions. The second amplitude, however, provides a very different distribution due to its double-p-wave character expressed by the scalar product of the pion momentum vectors in eq. (1). Since $\vec{k_1} * \vec{k_2} = k_1\ k_2\ cos(\delta_{\pi^0\pi^0})$ the distribution of the opening angle $\delta_{\pi^0\pi^0}$ directly measures the admixture of the second amplitude. If the Roper resonance decays solely via the $\Delta\pi$ system, then $\sigma(\delta_{\pi^0\pi^0}) \sim cos^2(\delta_{\pi^0\pi^0})$. Simultaneously the $M_{\pi^0\pi^0}$ distribution will exhibit a double-hump structure. In reality both amplitudes contribute and interfere.

The data shown in Fig. 3 for the $M_{\pi^0\pi^0}$ distribution are shifted towards higher masses relative to the phase space distribution, whereas the data for the opening angle distribution exhibit a steeper angular dependence than phase space. The predictions of Ref. [11], which are based on the branchings given in PDG [2], are shown in Fig.3 by the dotted lines. As seen there these calculations predict shifts in the invariant mass spectra, which are much too large. At the same time they give much too steep angular distributions in the opening angle spectra in comparison to the data. The solid lines on the other hand, which represent the same kind of calculations, but with an amplitude for the $N^* \to \Delta\pi \to N\sigma$ process decreased by a factor of two, give a very good account for the data. We note in passing that then also all other measured differential distributions are consistently described in the same quantitative

way.

Since the branching ratios crucially depend on the resonance mass used for their evaluation, we quote this branching for both the pole mass of 1358 MeV and the socalled Breit-Wigner mass [2] of 1440 MeV.

From the analysis of the $pp \to pp\pi^0\pi^0$ data at $T_p = 775$ and 895 MeV we obtain a ratio of approximately 5:1 (1:1) for the decay branching into $N\sigma$ and $\Delta\pi$ channels at a pole mass of 1358 MeV (Breit-Wigner mass of 1440 MeV) - in favor of a monopole mode interpretation of the Roper excitation.

Note that though the branching ratios in the PDG convention are quoted at the Breit-Wigner mass, the ones at the pole position reflect the physics of the decay of a resonance. Usually this distinction is not of much importance, since usually pole and Breit-Wigner mass positions are very close. However, the Roper resonance is one of the big exceptions, since its Breit-Wigner mass of 1440 MeV (on the basis of the P_{11} scattering amplitudes in the πN system) is 70 -80 MeV above the pole position. In the PDG convention our branching ratio is 1:1 in very good agreement with the most recent partial-wave analysis [4].

We emphasize that compared to the PDG values our result gives a branching ratio for the Roper decay via the $\Delta\pi$ system relative to its direct decay into the $N\sigma$ channel, which is smaller by a factor of four. This in turn changes profoundly the interpretation of the Roper excitation from a $\Delta\pi$ dominated configuration to a $N\sigma$ dominated one - which in turn means a monopole excitation mode of a the $N(1440)$ Roper resonance.

Acknowledgments

We acknowledge valuable discussions with L. Alvarez-Ruso, E. Oset, A. Kaidalov, L. Dakhno, A. and V. Anisovich and A. Sarantsev on this issue. We are particularily grateful to L. Alvarez-Ruso for using his code. This work has been supported by BMBF (06TU261), COSY-FFE, DFG (Europ. Graduiertenkolleg 683), Landesforschungsschwerpunkt Baden-Württemberg and the Swedish Research Council. We also acknowledge the support from the European Community-Research Infrastructure Activity under FP6 "Structuring the European Research Area" programme (Hadron Physics, contract number RII3-CT-2004-506078).

References

1. L. D. Roper, Phys. Rev. Lett. **12**, 340 (1964)
2. Particle Data Group, J. Phys. **G33**, 1 (2006)
3. R. A. Arndt *et al.*, Phys. Rev.**C69**, 035213 (2004) and Phys. Rev.**C74**, 045205 (2006)
4. A. V. Sarantsev *et al.*, arXiv:0707.3591 [hep-ph]
5. H. P. Morsch *et al.*, Phys. Rev. Lett. **69**, 1336 (1992)
6. M. Ablikim *et al.*, Phys. Rev. Lett. **97**, 062001 (2006)
7. W. Brodowski *et al.*, Phys. Rev. Lett. **88**, 92301 (2002)
8. F. Pätzold *et al.*, Phys. Rev.**C67**, 052202R (2003)
9. J. Zabierowski *et al.*,Phys. Scripta **T99**, 159 (2002)
10. T. Skorodko *et al.*, Proc. MENU 2007, submitted for publication
11. L. Alvarez-Ruso, E. Oset, E. Hernandez, Nucl. Phys. **A633**, 519 (1998)
12. T. Skorodko *et al.*, Proc. NSTAR 2007, submitted for publication

Frascati Physics Series Vol. XLVI (2007), pp. 1431–1438
HADRON07: XII Int. Conf. on Hadron Spectroscopy – Frascati, October 8-13, 2007
Baryon Spectroscopy

MASSES AND MAGNETIC MOMENTS OF CHARMED BARYONS USING HYPER CENTRAL MODEL

Bhavin Patel,
*Department of Physics, Sardar Patel University,
Vallabh Vidyanagar-388 120,Gujarat, India.
Ajay Kumar Rai,
Department of Applied Sciences and Humanities,
SVNIT, Surat-395 007,Gujarat, India.
*P. C. Vinodkumar.

Abstract

Heavy flavour baryons containing one or two charm quarks with light flavour combinations are studied using the hyper central description of the three-body system. The confinement potential is assumed as hyper central coulomb plus power potential with power index ν. The ground state masses and the magnetic moments of charmed, $J^P = \frac{1}{2}^+$ and $\frac{3}{2}^+$ baryons are computed for different power index, ν starting from 0.5 to 2.0.

1 Introduction

The investigation of properties of hadrons containing heavy quarks is of great interest in understanding the dynamics of QCD at the hadronic scale. There is renewed interest both experimentally and theoretically in the static properties of heavy flavour baryons such as mass and magnetic moments [1, 2, 3, 4, 5].

Many of the narrow hadron resonances observed recently, brought up surprises in QCD spectroscopy [6]. Recent years, experimental facilities at Belle, BABAR, DELPHI, CLEO, CDF etc have been successful in discovering heavy baryon states along with other heavy flavour mesonic states [4, 7, 8, 9] and many new states are expected in near future. Baryons are not only the interesting systems to study the quark dynamics and their properties but are also interesting from the point of view of simple systems to study three body problems. All these reasons make the study of heavy flavour spectroscopy extremely important and interesting. Here, we employ the hyper central approach to study the three-body problem, particularly the baryons constituting one or two charm quarks. In the present study, the magnetic moments of heavy flavour baryons are computed based on nonrelativistic quark model.

2 Hyper Central scheme for baryons

Quark model description of baryons is a simple three body system of interest. The Jacobi co-ordinates to describe baryon as a bound state of three constituent quarks are given by [13]

$$\vec{\rho} = \frac{1}{\sqrt{2}}(\vec{r}_1 - \vec{r}_2) \; ; \; \vec{\lambda} = \frac{1}{\sqrt{6}}(\vec{r}_1 + \vec{r}_2 - 2\vec{r}_3) \tag{1}$$

Further, defining the hyper spherical coordinates which are given by the angles $\Omega_\rho = (\theta_\rho, \phi_\rho)$; $\Omega_\lambda = (\theta_\lambda, \phi_\lambda)$ together with the hyper radius, x and hyper angle ξ respectively as, $x = \sqrt{\rho^2 + \lambda^2}$; $\xi = \arctan\left(\frac{\rho}{\lambda}\right)$, the model Hamiltonian for baryons can be written as

$$H = \frac{P_\rho^2}{2\,m_\rho} + \frac{P_\lambda^2}{2\,m_\lambda} + V(\rho, \lambda) = \frac{P_x^2}{2\,m} + V(x) \tag{2}$$

Here the potential $V(x)$ is not purely a two body interaction but it contains three-body effects also. The reduced mass m is defined as $m = \frac{2\,m_\rho\,m_\lambda}{m_\rho + m_\lambda}$, where $m_\rho = \frac{2\,m_1\,m_2}{m_1+m_2}$; $m_\lambda = \frac{3\,m_3\,(m_1+m_2)}{2\,(m_1+m_2+m_3)}$ and m_1, m_2 and m_3 are masses of the three constituent quarks. For the present study, we consider the hyper central potential $V(x)$ as [5]

$$V(x) = -\frac{\tau}{x} + \beta x^\upsilon + \kappa + A\; e^{-\alpha x} \sum_{i \neq j} \sigma_i \cdot \sigma_j \tag{3}$$

In this hyperspherical representation of the potential we consider $\tau = \frac{2}{3}\, b\, \alpha_s$, $\beta \approx m\tau$, $\kappa = (\sqrt{2}-1)\alpha_s N_c N_f m$, where $N_c = 3.0$ while $N_f = 4$ for charmed baryons and other model parameters are given in [5]. The trial wave function is taken [1] as the hyper coulomb radial wave function. We study the baryons having different choice of the light flavour(q)combinations for qqc and ccq systems. The computed spin average mass with respect to the potential index, ν are shown in Fig 1. The computed masses of the spin $\frac{1}{2}$ and $\frac{3}{2}$, single charm and double charm baryons are given in Tables 1 and 2 respectively.

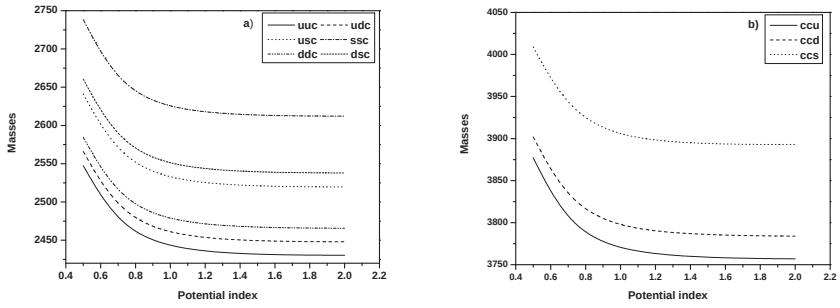

Figure 1: *Variation of spin average masses with potential index υ for single charm baryons [a] and double charm baryons [b].*

3 Effective quark mass and Magnetic moments of heavy baryons

We define an effective mass for the bound quarks within the baryon as

$$m_i^{eff} = m_i \left(1 + \frac{< H >}{\sum\limits_i m_i}\right) \tag{4}$$

and we express the magnetic moment of baryons in terms of its constituent quarks as

$$\mu_B = \sum_i \left\langle \phi_{sf} \mid \frac{e_i}{2m_i^{eff}} \vec{\sigma}_i \mid \phi_{sf} \right\rangle \tag{5}$$

Table 1: *Single charm baryon masses(masses are in MeV)*

Baryon	P.I.(ν)	$\mathbf{J}^P = \frac{1}{2}^+$	Others	$\mathbf{J}^P = \frac{3}{2}^+$	Others
Σ_c^{++}	0.5	2550	2453 [3]	2618	–
(uuc)	0.7	2473	2454±0.18 [15]	2538	2518±0.6 [15]
	1.0	2443	2460±80 [16]	2506	2440±70 [16]
	1.5	2436		2499	
	2.0	2436		2498	
Σ_c^{+}	0.5	2568	2451 [3]	2638	–
(udc)	0.7	2491	2439 [2]	2557	2518 [2]
	1.0	2460	2453 [12]	2525	2520 [12]
	1.5	2454	2452 [10]	2518	2538 [10]
	2.0	2453	2448 [17]	2517	2505 [17]
			2453 ± 0.4 [15]		2518 ± 2.3 [15]
Σ_c^{0}	0.5	2586	2452 [3]	2658	–
(ddc)	0.7	2508	2454±0.18 [15]	2577	2518±0.5 [15]
	1.0	2477		2544	
	1.5	2471		2537	
	2.0	2470		2537	
Ξ_c^{+}	0.5	2642	2466 [3]	2720	–
(usc)	0.7	2561	2481 [2]	2636	2654 [2]
	1.0	2530	2468 [12]	2603	2650 [12]
	1.5	2523	2473 [10]	2596	2680 [10]
	2.0	2523	2496 [17]	2595	2633 [17]
			2468±0.4 [15]		2647±1.4 [15]
			2410±50 [16]		2550±80 [16]
Ξ_c^{0}	0.5	2653	2472 [3]	2734	–
(dsc)	0.7	2579	2471±0.4 [15]	2656	2646±1.2 [15]
	1.0	2548		2623	
	1.5	2541		2616	
	2.0	2541		2615	
Ω_c^{0}	0.5	2720	2698 [3]	2810	–
(ssc)	0.7	2652	2698 [2]	2739	2768 [2]
	1.0	2620	2710 [12]	2704	2770 [12]
	1.5	2613	2678 [10]	2697	2752 [10]
	2.0	2613	2701 [17]	2697	2759 [17]
			2680±70 [16]		2660±80 [16]
			2698±2.6 [15]		

Table 2: *Doubly charm baryon masses (masses are in MeV)*

Baryon	P.I.(ν)	$\mathbf{J}^P = \frac{1}{2}^+$	Others	$\mathbf{J}^P = \frac{3}{2}^+$	Others
Ξ_{cc}^{++}	0.5	3838	3612^{+17} [19]	3915	3706^{+23} [19]
(ccu)	0.7	3760	3620 [2]	3833	3727 [2]
	1.0	3730	3480 [20]	3800	3610 [20]
	1.5	3723	3740 [11]	3792	3860 [11]
	2.0	3723	3478 [21]	3792	3610 [21]
Ξ_{cc}^{+}	0.5	3862	3605 ± 23 [22]	3945	3685 ± 23 [22]
(ccd)	0.7	3786	3620 [2]	3862	3727 [2]
	1.0	3755	3480 [20]	3828	3610 [20]
	1.5	3748	3740 [11]	3821	3860 [11]
	2.0	3748	3478 [21]	3820	3610 [21]
Ω_{cc}^{+}	0.5	3962	3702^{+41} [19]	4056	3783^{+22} [19]
(ccs)	0.7	3889	3778 [2]	3978	3872 [2]
	1.0	3857	3590 [20]	3944	3690 [20]
	1.5	3850	3760 [11]	3936	3900 [11]
	2.0	3850	3590 [21]	3936	3690 [21]
			3733 ± 09 [22]		3801 ± 09 [22]

Here e_i and σ_i represents the charge and the spin of the quark constituting the baryonic state and $\mid \phi_{sf} >$ represents the spin-flavour wave function of the respective baryonic state. Extending the SU(2)$_S \times SU(3)_f$ spin flavour structure of the light flavour sector [18] in SU(2)$_S \times SU(4)_f$ spin flavour structure with charm, we compute the magnetic moments of the spin$\frac{1}{2}$ and spin$\frac{3}{2}$ charmed baryons. Our results are listed in Tables 3 and 4 respectively.

4 Results and Discussion

We have employed the hyper central model with hyperspherical potential of the coulomb plus power potential to study the masses and magnetic moments of baryons containing one or two charm flavour quarks. It is important to see that the baryon mass do not change appreciably for the potential power index $\nu > 1.0$ (See Fig 1). The model parameters are fixed for this saturated value

Table 3: *Magnetic moments of single charm baryons in terms of* μ_N

	Potential index ν						
Baryon	0.5	0.7	1.0	1.5	2.0	RQM	NRQM
Σ_c^{++}	1.8809	1.9394	1.9635	1.9688	1.9692	1.76	1.86
Σ_c^{*++}	3.2806	3.3837	3.4272	3.4373	3.4379	–	–
Σ_c^{+}	0.3959	0.4082	0.4133	0.4144	0.4144	0.36	0.37
Σ_c^{*+}	1.1092	1.1441	1.1588	1.1622	1.1624	–	–
Ξ_c^{+}	0.4542	0.4684	0.4742	0.4755	0.4755	0.41	0.37
Ξ_c^{*+}	1.1893	1.2269	1.2425	1.2460	1.2463	–	–
Ω_c^{0}	-0.9612	-0.9860	-0.9981	-1.0006	-1.0008	-0.85	-0.85
Ω_c^{*0}	-0.8703	-0.8931	-0.9044	-0.9068	-0.9070	–	–
Σ_c^{0}	-1.0854	-1.1193	-1.1332	-1.1362	-1.1364	-1.04	-1.11
Σ_c^{*0}	-1.0540	-1.0873	-1.1012	-1.1044	-1.1046	–	–
Ξ_c^{0}	-1.0231	-1.0526	-1.0655	-1.0683	-1.0685	-0.95	-0.98
Ξ_c^{*0}	-0.9618	-0.9898	-1.0024	-1.0052	-1.0054	–	–

RQM [3], NRQM [3]

to the experimental spin average mass of the $\Sigma_c^*(2518) - \Sigma_c(2454)$(udc) system [15] and the spin hyperfine parameter is fixed to yield their mass difference of 64 MeV [15]. All other baryonic masses are predicted without changing any of these parameters. It is interesting to note that our results are in fair agreement with existing experimental as well as other theoretical model predictions. The result of single charm baryons are in accordance with the lattice results as well as with other model predictions. The mass variations of the single charm baryons with respect to ν from 0.5 to 2.0 are found to be around 100 MeV only.

Our predictions on the doubly charm baryons are compared with other theoretical model predictions in Table 2. Since there are larger disagreement among the different model predictions, only the future experiments on these doubly charm baryons would be able to test the validity of the theoretical model predictions. However, the hyperfine splitting of 76.6 MeV for $\Xi_{cc}^* - \Xi_{cc}$ obtained from Lattice predictions [22] is very close to our calculations of 73 MeV. It is important to note that the predictions of the magnetic moment of all the heavy hadrons studied here are with no free parameters. Our results for the magnetic moment of single charm baryons with spin $\frac{1}{2}$ are in accordance with the predictions of the full treatment of relativistic quark model as well as

Table 4: *Magnetic moments of doubly charm baryons in terms of* μ_N

Baryon	**Potential index** ν 0.5	0.7	1.0	1.5	2.0	NRQM	AL1
Ξ_{cc}^{++}	-0.0151	-0.0154	-0.0156	-0.0156	-0.0156	-0.01	-0.208
Ξ_{cc}^{*++}	2.1934	2.2406	2.2602	2.2646	2.2649	–	2.670
Ω_{cc}^{+}	0.6910	0.7040	0.7098	0.7110	0.7110	0.67	0.635
Ω_{cc}^{*+}	0.0908	0.0926	0.0934	0.0936	0.0936	–	0.139
Ξ_{cc}^{+}	0.7279	0.7426	0.7487	0.7500	0.7501	0.74	0.785
Ξ_{cc}^{*+}	0.0031	0.0031	0.0032	0.0032	0.0032	–	-0.311

NRQM [3], AL1 [19]

with the nonrelativistic approximation reported in [3]. In the case of doubly charm baryons, our predictions for both $J = \frac{1}{2}$ and $\frac{3}{2}$ baryons are found to be in good accordance with the recent predictions based on a potential model, AL1 [19] and NRQM [3] results [See Table 4].

We conclude that the three body interaction assumed in our model plays a significant role in the description of heavy flavour baryonic properties in particular their masses and magnetic moments. The behavior of the masses against the potential index ν as shown Fig. 1 indicates saturation of the basic quark-quark interactions within the heavy baryons as the potential index $\nu > 1.0$. We hope that, the predicted many of the baryonic ground state will be observed in the future high luminosity heavy flavour experiments.

Acknowledgement: Part of this work is done with a financial support from University Grant commission, Government of India under a Major research project **F. 32-31/2006 (SR)**.

References

1. M. M. Giannini et al., Eur. Phys. J. A **12**, 447-452 (2001).
2. D. Ebert et al., Phys. Rev. D **66**, 014008 (2002).
3. Amand Faessler et al., Phys. Rev. D **73**, 094013 (2006).
4. S. B. Athar et al., (CLEO Collaboration), Phys. Rev. D **71**, 051101 (2005).

5. Bhavin Patel et al., arXiv:hep-ph/0710.3828v1.

6. J.L. Rosner, Phys. Rev. D **75**, 013009 (2007).

7. Mizuk R et al. (Belle Collaboration), Phys. Rev. Lett. **94**, 122002 (2005).

8. Aubert B et al. (BABAR Collaboration), Phys. Rev. Lett. **98**, 122011 (2007).

9. I. V. Gorelov (CDF Collaboration), arXiv:hep-ex/0701056.

10. N. Mathur, R. Lewis and R. M. Woloshyn, Phys. Rev. D **66**, 014502 (2002).

11. S. P. Tong et al., Phys. Rev. D **62**, 054024 (2000).

12. R. Roncaglia et al., Phys. Rev. D **52**, 1722 (1995).

13. Yu. A. Simonov , Sov J. Nucl. Phys. **3**, 461 (2001).

14. M. V. N. Murthy, Z. Phys. C-Particles and Fields **31**, 81-86 (1986).

15. W. M. Yao et al. (PDG), J. Phy. G : Nucl Part. Phy. **33**(2006)

16. K.C. Bowler et al., Phys. Rev. D **57**, 6948 (1998).

17. H Garcilazo et al., J. Phys. G:Nucl. Part. Phys., **34**,961-976(2007)

18. Yu. A. Simonov et al., Phys. Rev. D**65**, 094013 (2002).

19. C. Albertus et al., arXiv:hep-ph/0610131v1 , arXiv:hep-ph/0610030v2.

20. V.V.Kiselev and A. K. Likhoded, Phys. Usp. **45**, 455 (2002).

21. S.S.Gershtein et al., Phys. Rev. D **62**, 054021 (2000).

22. R. Lewis et al., Phys. Rev D **64**, 094509 (2001).

Frascati Physics Series Vol. XLVI (2007), pp. 1439–1446
HADRON07: XII Int. Conf. on Hadron Spectroscopy – Frascati, October 8-13, 2007
Baryon Spectroscopy

HEAVY HADRONS IN THE RELATIVISTIC QUARK MODEL

D. Ebert
Institut für Physik, Humboldt–Universität zu Berlin, Germany
R.N. Faustov and V.O. Galkin
Dorodnicyn Computing Centre, Russian Academy of Sciences, Russia

Abstract

Masses of heavy baryons and tetraquarks are calculated in the relativistic quark model using the heavy-quark–light-diquark and diquark-antidiquark approximations, respectively.

1 Introduction

Recently significant experimental progress has been achieved in heavy hadron spectroscopy. Masses of the Ω_c^*, Σ_b, Σ_b^* and Ξ_b baryons as well as masses of several excited charmed baryons have been measured. In the heavy meson sector several new states, such as $X(3872)$, $Y(4260)$, $D_{s0}^*(2317)$, $Z(4430)$ etc., were observed which cannot be simply accommodated in the quark-antiquark ($q\bar{q}$) picture. These states can be considered as indications of the possible existence of exotic multiquark states. In this talk we briefly review our recent

results for the masses of heavy baryons and tetraquarks in the framework of the relativistic quark model based on the quasipotential approach in quantum chromodynamics. We use the heavy-quark–light-diquark and diquark-antidiquark approximations to reduce a very complicated relativistic three- and four-body problem to the subsequent two more simple two-body problems. The first step consists in the calculation of the masses, wave functions and form factors of the diquarks, composed from two light quarks or a light and heavy quark. At the second step, a heavy baryon is treated as a relativistic bound system of a light diquark and heavy quark. The heavy tetraquark is considered to be a bound diquark-antidiquark system. It is important to emphasize that we do not consider a diquark as a point particle but explicitly take into account its structure by calculating the form factor of the diquark-gluon interaction in terms of the diquark wave functions.

2 Relativistic quark model

In the quasipotential approach the two-particle bound state with the mass M and masses of the constituents $m_{1,2}$ in momentum representation is described by the wave function $\Psi(\mathbf{p})$ satisfying the quasipotential equation of the Schrödinger type

$$\left(\frac{b^2(M)}{2\mu_R}-\frac{\mathbf{p}^2}{2\mu_R}\right)\Psi_{d,B,T}(\mathbf{p})=\int\frac{d^3q}{(2\pi)^3}V(\mathbf{p},\mathbf{q};M)\Psi_{d,B,T}(\mathbf{q}), \qquad (1)$$

where

$$\mu_R=\frac{M^4-(m_1^2-m_2^2)^2}{4M^3},\quad b^2(M)=\frac{[M^2-(m_1+m_2)^2][M^2-(m_1-m_2)^2]}{4M^2}.$$

The subscript d refers to the diquark, B refers to the baryon composed of a light diquark and heavy quark, and T refers to the tetraquark composed of a diquark and antidiquark. The explicit expressions for the corresponding quasipotentials $V(\mathbf{p},\mathbf{q};M)$ can be found in Refs. [1, 2].

At the first step, we calculate the masses and form factors of the light and heavy diquark. As it is well known, the light quarks are highly relativistic, which makes the v/c expansion inapplicable and thus, a completely relativistic treatment of the light quark dynamics is required. To achieve this goal we closely follow our recent consideration of the spectra of light mesons and adopt the same procedure to make the relativistic potential local by replacing

Table 1: *Masses of the Λ_Q baryons (in MeV).*

	Qd	$Q=c$		$Q=b$		
$I(J^P)$	state	M	$M^{\rm exp}$ 3)	M	$M^{\rm exp}$ 3)	$M^{\rm exp}$ 4)
$0(\frac{1}{2}^+)$	$1S$	2297	2286.46(14)	5622	5624(9)	5619.7(2.4)
$0(\frac{1}{2}^-)$	$1P$	2598	2595.4(6)	5930		
$0(\frac{3}{2}^-)$	$1P$	2628	2628.1(6)	5947		
$0(\frac{1}{2}^+)$	$2S$	2772	2766.6(2.4)?	6086		
$0(\frac{3}{2}^+)$	$1D$	2874		6189		
$0(\frac{5}{2}^+)$	$1D$	2883	2882.5(2.2)?	6197		
$0(\frac{1}{2}^-)$	$2P$	3017		6328		
$0(\frac{3}{2}^-)$	$2P$	3034		6337		

$\epsilon_{1,2}(p)=\sqrt{m_{1,2}^2+\mathbf{p}^2}\to E_{1,2}=(M^2-m_{2,1}^2+m_{1,2}^2)/2M$. Solving numerically the quasipotential equation (1) with the complete relativistic potential, which depends on the diquark mass in a complicated highly nonlinear way [1)], we get the diquark masses and wave functions. In order to determine the diquark interaction with the gluon field, which takes into account the diquark structure, we calculate the corresponding matrix element of the quark current between diquark states. Such calculation leads to the emergence of the form factor $F(r)$ entering the vertex of the diquark-gluon interaction [1)]. This form factor is expressed through the overlap integral of the diquark wave functions.

3 Mass spectra of heavy baryons

We calculated the masses of heavy baryons as the bound states of a heavy quark and light diquark. For the potential of the heavy-quark–light-diquark interaction we used the expansion in p/m_Q ($Q=c,b$). Since the light diquark is not heavy enough for the applicability of a p/m_d expansion, it has been treated fully relativistically. The obtained values of masses of the ground state and excited baryons are given in Tables 1-4 in comparison with available experimental data.

At present the best experimentally studied quantities are the mass spectra of the Λ_Q and Σ_Q baryons, which contain the light scalar or axial vector diquarks, respectively. They are presented in Tables 1, 2. Masses of the

Table 2: *Masses of the Σ_Q baryons (in MeV).*

	Qd	$Q=c$		$Q=b$		
$I(J^P)$	state	M	$M^{\rm exp}$ [3, 5]	M	$M^{\rm exp}(\Sigma_b^+)$	$M^{\rm exp}(\Sigma_b^-)$ [6]
$1(\frac{1}{2}^+)$	$1S$	2439	2453.76(18)	5805	5807.5(2.5)	5815.2(2.0)
$1(\frac{3}{2}^+)$	$1S$	2518	2518.0(5)	5834	5829.0(2.3)	5836.7(2.5)
$1(\frac{1}{2}^-)$	$1P$	2805		6122		
$1(\frac{1}{2}^-)$	$1P$	2795		6108		
$1(\frac{3}{2}^-)$	$1P$	2799	$2802(\frac{4}{7})$	6106		
$1(\frac{3}{2}^-)$	$1P$	2761	2766.6(2.4)?	6076		
$1(\frac{5}{2}^-)$	$1P$	2790		6083		
$1(\frac{1}{2}^+)$	$2S$	2864		6202		
$1(\frac{3}{2}^+)$	$2S$	2912	2939.8(2.3)?	6222		
$1(\frac{1}{2}^+)$	$1D$	3014		6300		
$1(\frac{3}{2}^+)$	$1D$	3005		6287		
$1(\frac{3}{2}^+)$	$1D$	3010		6291		
$1(\frac{5}{2}^+)$	$1D$	3001		6279		
$1(\frac{5}{2}^+)$	$1D$	2960		6248		
$1(\frac{7}{2}^+)$	$1D$	3015		6262		

ground states are measured both for charmed and bottom Λ_Q, Σ_Q baryons. The masses of the ground state Σ_b and Σ_b^* baryons were first reported very recently by CDF [6]. CDF also significantly improved the accuracy of the Λ_b mass value [4]. For charmed baryons the masses of several excited states are also known. It is important to emphasize that the J^P quantum numbers for most excited heavy baryons have not been determined experimentally, but are assigned by PDG on the basis of quark model predictions. For some excited charm baryons such as the $\Lambda_c(2765)$, $\Lambda_c(2880)$ and $\Lambda_c(2940)$ it is even not known if they are excitations of the Λ_c or Σ_c. [1] Our calculations show that the $\Lambda_c(2765)$ can be either the first radial ($2S$) excitation of the Λ_c with $J^P=\frac{1}{2}^+$ containing the light scalar diquark or the first orbital excitation ($1P$) of the Σ_c with $J^P=\frac{3}{2}^-$ containing the light axial vector diquark. The $\Lambda_c(2880)$ baryon in our model is well described by the second orbital ($1D$) excitation of the Λ_c

[1] In Tables 1, 2 we mark with ? the states which interpretation is ambiguous.

Table 3: *Masses of the Ξ_Q baryons with the scalar diquark (in MeV).*

	Qd	$Q=c$			$Q=b$	
$I(J^P)$	state	M	$M^{\rm exp}$ [3]	$M^{\rm exp}$ [7]	M	$M^{\rm exp}$ [8]
$\frac{1}{2}(\frac{1}{2}^+)$	$1S$	2481	2471.0(4)		5812	5792.9(3.0)
$\frac{1}{2}(\frac{1}{2}^-)$	$1P$	2801	2791.9(3.3)		6119	
$\frac{1}{2}(\frac{3}{2}^-)$	$1P$	2820	2818.2(2.1)		6130	
$\frac{1}{2}(\frac{1}{2}^+)$	$2S$	2923			6264	
$\frac{1}{2}(\frac{3}{2}^+)$	$1D$	3030			6359	
$\frac{1}{2}(\frac{5}{2}^+)$	$1D$	3042		3054.2(1.3)	6365	
$\frac{1}{2}(\frac{1}{2}^-)$	$2P$	3186			6492	
$\frac{1}{2}(\frac{3}{2}^-)$	$2P$	3199			6494	

with $J^P=\frac{5}{2}^+$ in agreement with the recent spin assignment [5] based on the analysis of angular distributions in the decays $\Lambda_c(2880)^+\to\Sigma_c(2455)^{0,++}\pi^{+,-}$. Our model suggests that the charmed baryon $\Lambda_c(2940)$, recently discovered by BaBar and confirmed by Belle [5], could be the first radial ($2S$) excitation of the Σ_c with $J^P=\frac{3}{2}^+$ which mass is predicted slightly below the experimental value. If this state proves to be an excited Λ_c, for which we have no candidates around 2940 MeV, then it will indicate that excitations inside the diquark should be also considered. [2] The $\Sigma_c(2800)$ baryon can be identified in our model with one of the orbital ($1P$) excitations of the Σ_c with $J^P=\frac{1}{2}^-,\frac{3}{2}^-$ or $\frac{5}{2}^-$ which predicted mass differences are less than 15 MeV. Thus masses of all these states are compatible with the experimental value within errors.

Mass spectra of the Ξ_Q baryons with the scalar and axial vector light (qs) diquarks are given in Tables 3, 4. Experimental data here are available mostly for charm-strange baryons. We can identify the $\Xi_c(2790)$ and $\Xi_c(2815)$ with the first orbital ($1P$) excitations of the Ξ_c with $J^P=\frac{1}{2}^-$ and $J^P=\frac{3}{2}^-$, respectively, containing the light scalar diquark, which is in agreement with the PDG [3] assignment. Recently Belle [9] reported the first observation of two baryons $\Xi_{cx}(2980)$ and $\Xi_{cx}(3077)$, which existence was also confirmed by BaBar [7]. The $\Xi_{cx}(2980)$ can be interpreted in our model as the first radial

[2] The Λ_c baryon with the first orbital excitation of the diquark is expected to have a mass in this region.

Table 4: *Masses of the Ξ_Q baryons with the axial vector diquark (in MeV).*

	Qd	$Q=c$				$Q=b$
$I(J^P)$	state	M	$M^{\rm exp}$ 3)	$M^{\rm exp}$ 9)	$M^{\rm exp}$ 7)	M
$\frac{1}{2}(\frac{1}{2}^+)$	$1S$	2578	2578.0(2.9)			5937
$\frac{1}{2}(\frac{3}{2}^+)$	$1S$	2654	2646.1(1.2)			5963
$\frac{1}{2}(\frac{1}{2}^-)$	$1P$	2934				6249
$\frac{1}{2}(\frac{1}{2}^-)$	$1P$	2928				6238
$\frac{1}{2}(\frac{3}{2}^-)$	$1P$	2931				6237
$\frac{1}{2}(\frac{3}{2}^-)$	$1P$	2900				6212
$\frac{1}{2}(\frac{5}{2}^-)$	$1P$	2921				6218
$\frac{1}{2}(\frac{1}{2}^+)$	$2S$	2984		2978.5(4.1)	2967.1(2.9)	6327
$\frac{1}{2}(\frac{3}{2}^+)$	$2S$	3035				6341
$\frac{1}{2}(\frac{1}{2}^+)$	$1D$	3132				6420
$\frac{1}{2}(\frac{3}{2}^+)$	$1D$	3127				6410
$\frac{1}{2}(\frac{3}{2}^+)$	$1D$	3131				6412
$\frac{1}{2}(\frac{5}{2}^+)$	$1D$	3123			3122.9(1.3)	6403
$\frac{1}{2}(\frac{5}{2}^+)$	$1D$	3087		3082.8(3.3)	3076.4(1.0)	6377
$\frac{1}{2}(\frac{7}{2}^+)$	$1D$	3136				6390

$(2S)$ excitation of the Ξ_c with $J^P = \frac{1}{2}^+$ containing the light axial vector diquark. On the other hand the $\Xi_{cx}(3077)$ corresponds to the second orbital $(1D)$ excitation in this system with $J^P = \frac{5}{2}^+$. The new charmed baryons $\Xi_c(3055)$ and $\Xi_c(3123)$, very recently announced by BaBar [10] can be interpreted in our model as the second orbital $(1D)$ excitations of the Ξ_c with $J^P = \frac{5}{2}^+$ containing scalar and axial vector diquarks, respectively. Few months ago the D0 Collaboration reported the discovery of the Ξ_b^- baryon. The CDF Collaboration [8] confirmed this observation and gave the more precise value of its mass. Our model prediction is in a reasonable agreement with these new data.

4 Masses of heavy tetraquarks

To calculate the masses of heavy tetraquarks we considered them as the bound states of a heavy diquark and antidiquark. In Table 5 we compare our results (EFG [2]) for the charm diquark-antidiquark bound states with the predictions

Table 5: *Comparison of theoretical predictions for the masses of charm diquark-antidiquark states $cq\bar{c}\bar{q}$ (in MeV) and possible experimental candidates.*

State	Theory			Experiment	
J^{PC}	EFG	Maiani et al.	Maiani et al.$(cs\bar{c}\bar{s})$	state	mass
$1S$					
0^{++}	3812	3723			
1^{++}	3871	$3872^{\dagger}$		$X(3872)$	3871.9(0.5)
1^{+-}	3871	3754			
0^{++}	3852	3832			
1^{+-}	3890	3882			
2^{++}	3968	3952		$Y(3943)$	3943(11)(13)
$1P$					
1^{--}	4244		4330(70)	$Y(4260)$	$4259(8)(^{2}_{6})$

† input

of Ref. [11]. The differences in some of the mass values can be attributed to the substantial distinctions in the used approaches. We describe the diquarks dynamically as quark-quark bound systems and calculate their masses and form factors, while in Ref. [11] they are treated only phenomenologically. Then we consider the tetraquark as purely the diquark-antidiquark bound system. In distinction Maini et al. consider a hyperfine interaction between all quarks which, e.g., causes the splitting of 1^{++} and 1^{+-} states arising from the SA diquark-antidiquark compositions. From Table 5, where we also give possible experimental candidates for the neutral tetraquarks with hidden charm, we see that our calculation supports the assumption [11] that $X(3872)$ can be the axial vector 1^{++} tetraquark state composed from the scalar and axial vector diquark and antidiquark in the relative S state. On the other hand, in our model the lightest scalar 0^{++} tetraquark is predicted to be above the open charm threshold $D\bar{D}$ and thus to be broad, while in the model [11] it lies few MeV below this threshold, and thus is predicted to be narrow. Our 2^{++} tetraquark also lies higher than the one in Ref. [11]. We find that $Y(4260)$ cannot be interpreted as P state 1^{--} of charm-strange diquark-antidiquark, since its mass is found to be ~ 200 MeV higher. A more natural tetraquark interpretation could be the P state $([cq]_{S=0}[\bar{c}\bar{q}]_{S=0})$ which mass is predicted in our model to be close to the mass of $Y(4260)$ (see Table 5). Then the $Y(4260)$ would decay dominantly into $D\bar{D}$ pairs.

5 Conclusions

We found that presently available experimental data for the masses of the ground and excited states of heavy baryons can be accommodated in the picture treating a heavy baryon as the bound system of the light diquark and heavy quark, experiencing orbital and radial excitations between these constituents. It was argued that the $X(3872)$ and $Y(4260)$ can be the neutral charm tetraquark states. If they are really tetraquarks, one more neutral and two charged tetraquark states should exist with close masses.

This work was supported in part by the *Deutsche Forschungsgemeinschaft* under contract Eb 139/2-4 and by the *Russian Foundation for Basic Research* under Grant No.05-02-16243.

References

1. D. Ebert, R. N. Faustov and V. O. Galkin, Phys. Rev. D **72**, 034026 (2005); arXiv:0705.2957 [hep-ph].
2. D. Ebert *et al*, Phys. Lett. B **634**, 214 (2006); arXiv:0706.3853 [hep-ph].
3. Particle Data Group, , W.-M. Yao *et al.*, J. Phys. G **33**, 1 (2006).
4. D. Acosta *et al.* [CDF Collaboration], Phys. Rev. Lett. **96**, 202001 (2006).
5. B. Aubert *et al.* [BABAR Collaboration], Phys. Rev. Lett. **98**, 012001 (2007); R. Mizuk *et al.* [BELLE Collaboration], arXiv:hep-ex/0608043.
6. T. Aaltonen *et al.* [CDF Collaboration], Phys. Rev. Lett. **99**, 202001 (2007)
7. B. Aubert *et al.* [BABAR Collaboration], arXiv:hep-ex/0607042.
8. V. M. Abazov *et al.* [D0 Collaboration], Phys. Rev. Lett. **99**, 052001 (2007); T. Aaltonen *et al.* [CDF Collaboration], Phys. Rev. Lett. **99**, 052002 (2007).
9. R. Chistov *et al.* [BELLE Collaboration], Phys. Rev. Lett. **97**, 162001 (2006).
10. B. Aubert *et al.*, arXiv:0710.5763 [hep-ex].
11. L. Maiani, F. Piccinini, A. D. Polosa and V. Riquer, Phys. Rev. D **71**, 014028 (2005); Phys. Rev. D **72**, 031502(R) (2005).

Frascati Physics Series Vol. XLVI (2007), pp. 1447 –1454
HADRON07: XII Int. Conf. on Hadron Spectroscopy – Frascati, October 8-13, 2007
Baryon Spectroscopy

HEAVY QUARK SPIN SYMMETRY IN SEMILEPTONIC DECAYS OF DOUBLY HEAVY BARYONS

E. Hernández
Departamento de Física Fundamental e IUFFyM,
Universidad de Salamanca, E-37008 Salamanca, Spain
J.Nieves
Departamento de Física Atómica, Molecular y Nuclear,
Universidad de Granada, E-18071 Granada, Spain
J.M. Verde-Velasco
Departamento de Física Fundamental e IUFFyM,
Universidad de Salamanca, E-37008 Salamanca, Spain

Abstract

The disagreement between different quark model calculations of doubly heavy baryon semileptonic decay widths is explained in terms of heavy quark spin symmetry constraints violation by some of those calculations.

1 Introduction

In the infinite heavy quark mass limit the dynamics of hadrons with two heavy quarks is invariant under independent rotations of the two heavy quark spins. This is known as heavy quark spin symmetry (HQSS). HQSS has a number of consequences that have to be met by any quark model calculation. For instance, HQSS is sufficient to derive relations between form factors for the decay of hadrons containing two heavy quarks [1, 2]. This leads to approximate

relations between decay widths that can be exploited to test the validity of different quark models calculations.

Table 1: Quantum numbers of doubly heavy baryons analyzed in this study. J^P is the spin parity of the baryon, and S_h is the spin of the heavy degrees of freedom. l denotes a light u or d quark. Mass predictions from Ref. [3] obtained using the AL1 interquark potential of Ref. [4] are also given.

Baryon	Quark content	S_h	J^π	Mass [MeV]
Ξ_{cc}	c c l	1	$1/2^+$	3612
Ξ^*_{cc}	c c l	1	$3/2^+$	3706
Ξ_{bb}	b b l	1	$1/2^+$	10197
Ξ^*_{bb}	b b l	1	$3/2^+$	10236
Ξ_{bc}	b c l	1	$1/2^+$	6919
Ξ^*_{bc}	b c l	1	$3/2^+$	6948
Ξ'_{bc}	b c l	0	$1/2^+$	6986
Ω_{cc}	c c s	1	$1/2^+$	3702
Ω^*_{cc}	c c s	1	$3/2^+$	3783
Ω_{bb}	b b s	1	$1/2^+$	10260
Ω^*_{bb}	b b s	1	$3/2^+$	10297
Ω_{bc}	b c s	1	$1/2^+$	6986
Ω^*_{bc}	b c s	1	$3/2^+$	7009
Ω'_{bc}	b c s	0	$1/2^+$	7046

In Ref. [3] we have studied, within a nonrelativistic quark model framework, static properties of doubly heavy baryons and their semileptonic decays driven by a $b \to c$ transition at the quark level. For the semileptonic decays we limited ourselves to spin 1/2 to spin 1/2 baryon transitions. While we showed our wave functions had the correct limit for infinite heavy quark masses, we did not check HQSS constraints on the form factors or decay widths. We now extend our previous study to include also doubly heavy spin 3/2 baryons and test our model and others against HQSS predictions. These type of decays have been studied in different relativistic quark model approaches [5, 6, 7], with the use of heavy quark effective theory [8], using QCD sum rules [9] and three-point nonrelativistic QCD sum rules [10], or in the framework of the operator product expansion using the inverse heavy quark mass technique [11]. Discrepancies between different quark models are sometimes very large. In this presentation we use HQSS relations among decay widths to check the validity

of the different calculations. A more detailed study and further results can be found in Ref. [12].

2 Semileptonic decay

The decay width for a $b \to c$ driven transition is given by

$$\Gamma = \frac{G_F^2}{32\pi^4}|V_{cb}|^2 \frac{m_{B'}}{m_B^2} \int_1^{\omega_{max}} d\omega \ \sqrt{\omega^2-1}\ \mathcal{L}^{\mu\nu}\,\mathcal{H}_{\mu\nu} \tag{1}$$

where $G_F = 1.16637(1)\times 10^{-11}\,\mathrm{MeV}^{-2}$ is the Fermi decay constant, $|V_{cb}|$ is the modulus of the corresponding Cabibbo–Kobayashi–Maskawa matrix element, $m_B(m_{B'})$ is the mass of the initial (final) baryon, $\omega = v\cdot v'$ is the velocity transfer [with $v(v')$ the four velocities of the initial (final) baryon], and $\mathcal{L}^{\mu\nu}$ and $\mathcal{H}^{\mu\nu}$ are the leptonic and hadronic tensors respectively. $\mathcal{L}^{\mu\nu}$ is given by

$$\mathcal{L}^{\mu\nu} = \int \frac{d^3k}{2E}\frac{d^3k'}{2E'}\,\delta^{(4)}(q-k-k')\left(k'^{\mu}k^{\nu} + k'^{\nu}k^{\mu} - g^{\mu\nu}k\cdot k' + \mathrm{i}\epsilon^{\mu\nu\alpha\beta}k'_{\alpha}k_{\beta}\right) \tag{2}$$

where k, k' represent the momenta of the final charged lepton and antineutrino respectively, and q is the momentum transferred to the leptons. We use the convention $\epsilon^{0123} = -1$. Using Lorentz covariance one can write

$$\mathcal{L}^{\mu\nu} = A(q^2)\,g^{\mu\nu} + B(q^2)\,\frac{q^{\mu}q^{\nu}}{q^2} \tag{3}$$

where neglecting neutrino masses

$$A(q^2) = -\frac{I(q^2)}{6}\left(2q^2 - m_l^2 - \frac{m_l^4}{q^2}\right) \quad ; \quad B(q^2) = \frac{I(q^2)}{3}\left(q^2 + m_l^2 - 2\frac{m_l^4}{q^2}\right) \tag{4}$$

with m_l the charged lepton mass and

$$I(q^2) = \frac{\pi}{2q^2}(q^2 - m_l^2) \tag{5}$$

For a light lepton $l = e, \mu$ we can neglect terms in m_l^2/q^2 over most of the q^2 (ω) interval and thus use $B(q^2) \approx -A(q^2)$.

The hadron tensor is given by

$$\mathcal{H}_{\mu\nu}(p,p') = \frac{1}{2S+1}\sum_{r,r'}\left\langle B'(S'), r'\ \vec{p}\,' \,\middle|\, \overline{\Psi}^c(0)\gamma_{\mu}(I-\gamma_5)\Psi^b(0)\right| B(S), r\ \vec{p}\,\Big\rangle$$
$$\times \left\langle B'(S'), r'\ \vec{p}\,' \,\middle|\, \overline{\Psi}^c(0)\gamma_{\nu}(I-\gamma_5)\Psi^b(0)\right| B(S), r\ \vec{p}\,\Big\rangle^{*} \tag{6}$$

where $|B(S), r\ \vec{p}\rangle$ represents a baryon state with total spin S, spin projection r and three-momentum $\vec{p}$. In Ref. [3], we have shown how the $1/2 \to 1/2$ hadronic matrix elements are evaluated within our model. The extension to the $1/2 \longleftrightarrow 3/2$ and $3/2 \to 3/2$ cases is straightforward.

Table 2: Semileptonic decay widths in units of 10^{-14} GeV for doubly heavy Ξ and Ω baryons. Here l stands for a light charged lepton, $l = e,\ \mu$.

	This work	5)	6)	7)	8)	10)
$\Gamma(\Xi_{bb} \to \Xi_{bc}\, l\bar{\nu}_l)$	$3.84^{+0.49}_{-0.10}$	3.26	28.5			8.99
$\Gamma(\Xi_{bb} \to \Xi'_{bc}\, l\bar{\nu}_l)$	$2.12^{+0.26}_{-0.05}$	1.64	4.28			
$\Gamma(\Xi_{bb} \to \Xi^*_{bc}\, l\bar{\nu}_l)$	$1.21^{+0.08}$	1.05	27.2			2.70
$\Gamma(\Xi^*_{bb} \to \Xi'_{bc}\, l\bar{\nu}_l)$	$2.08^{+0.11}$	1.63	8.57			
$\Gamma(\Xi^*_{bb} \to \Xi_{bc}\, l\bar{\nu}_l)$	$0.69^{+0.06}$	0.55	52.0			
$\Gamma(\Xi^*_{bb} \to \Xi^*_{bc}\, l\bar{\nu}_l)$	$4.17^{+0.32}$	3.83	12.9			
$\Gamma(\Xi_{bc} \to \Xi_{cc}\, l\bar{\nu}_l)$	$5.13^{+0.51}_{-0.05}$	4.59	8.93	0.79	4.0	8.87
$\Gamma(\Xi'_{bc} \to \Xi_{cc}\, l\bar{\nu}_l)$	$2.71^{+0.19}_{-0.05}$	1.76	7.76			
$\Gamma(\Xi_{bc} \to \Xi^*_{cc}\, l\bar{\nu}_l)$	$1.49^{+0.11}$	1.43	14.1		1.2	2.66
$\Gamma(\Xi'_{bc} \to \Xi^*_{cc}\, l\bar{\nu}_l)$	$4.66^{+0.31}$	3.40	28.8			
$\Gamma(\Xi^*_{bc} \to \Xi_{cc}\, l\bar{\nu}_l)$	$0.85^{+0.11}$	0.75	27.5			
$\Gamma(\Xi^*_{bc} \to \Xi^*_{cc}\, l\bar{\nu}_l)$	$5.25^{+0.80}$	5.37	17.2			

	This work	5)		This work	5)
$\Gamma(\Omega_{bb} \to \Omega_{bc}\, l\bar{\nu}_l)$	$4.28^{+0.39}_{-0.03}$	3.40	$\Gamma(\Omega_{bc} \to \Omega_{cc}\, l\bar{\nu}_l)$	$5.17^{+0.39}$	4.95
$\Gamma(\Omega_{bb} \to \Omega'_{bc}\, l\bar{\nu}_l)$	$2.32^{+0.26}$	1.66	$\Gamma(\Omega'_{bc} \to \Omega_{cc}\, l\bar{\nu}_l)$	$2.71^{+0.17}$	1.90
$\Gamma(\Omega_{bb} \to \Omega^*_{bc}\, l\bar{\nu}_l)$	$1.33^{+0.15}$	1.1	$\Gamma(\Omega_{bc} \to \Omega^*_{cc}\, l\bar{\nu}_l)$	$1.52^{+0.26}$	1.48
$\Gamma(\Omega^*_{bb} \to \Omega'_{bc}\, l\bar{\nu}_l)$	$2.26^{+0.22}_{-0.15}$	1.70	$\Gamma(\Omega'_{bc} \to \Omega^*_{cc}\, l\bar{\nu}_l)$	$4.72^{+0.65}$	3.66
$\Gamma(\Omega^*_{bb} \to \Omega_{bc}\, l\bar{\nu}_l)$	$0.75^{+0.07}_{-0.04}$	0.57	$\Gamma(\Omega^*_{bc} \to \Omega_{cc}\, l\bar{\nu}_l)$	$0.88^{+0.11}$	0.80
$\Gamma(\Omega^*_{bb} \to \Omega^*_{bc}\, l\bar{\nu}_l)$	$4.58^{+0.62}_{-0.07}$	3.99	$\Gamma(\Omega^*_{bc} \to \Omega^*_{cc}\, l\bar{\nu}_l)$	$5.57^{+1.19}$	5.76

In Table 2 we compare our results for Ξ and Ω decay with the ones calculated in different models. Our central values have been obtained with the AL1 potential of Ref. [4], while the errors shown indicate the spread of the results when using four other interquark potentials, three more taken from Ref. [4] and another one from Ref. [13]. In all cases we have used a value $|V_{cb}| = 0.0413$. Our results are in a global reasonable agreement with the ones obtained by Ebert *et al* in Ref. [5] where they use a relativistic quark

model evaluated in the quark-diquark approximation. In contrast to these two calculations, in Ref. [6] they obtain much larger results for all $\Xi \to \Xi$ transitions. There is also an approximate factor of two discrepancy between the, few, results obtained in the nonrelativistic QCD sum rules calculation of Ref. [10] and our results or the ones by Ebert *et al.*

3 HQSS constraints on semileptonic decay widths

Using HQSS it has been shown [1, 2] that near zero recoil all hadronic matrix elements of the semileptonic $bc \to cc$ baryon decay are given in terms of just one universal function $\eta(\omega)$, known as the Isgur-Wise (IW) function. Indeed, HQSS predicts for those hadronic matrix elements evaluated with the initial baryon at rest [2]

$$B_{bc} \to B_{cc} \qquad \eta\ \bar{u}'_{r'}(-\vec{q})(2\gamma^\mu - \frac{4}{3}\gamma^\mu\gamma_5)u_r(\vec{0}) \tag{7}$$

$$B'_{bc} \to B_{cc} \qquad -\frac{2}{\sqrt{3}}\eta\ \bar{u}'_{r'}(-\vec{q})(-\gamma^\mu\gamma_5)u_r(\vec{0}) \tag{8}$$

$$B_{bc} \to B^*_{cc} \qquad -\frac{2}{\sqrt{3}}\eta\ \bar{u}'^{\mu}_{r'}(-\vec{q})u_r(\vec{0}) \tag{9}$$

$$B'_{bc} \to B^*_{cc} \qquad -2\eta\ \bar{u}'^{\mu}_{r'}(-\vec{q})u_r(\vec{0}) \tag{10}$$

$$B^*_{bc} \to B_{cc} \qquad -\frac{2}{\sqrt{3}}\eta\ \bar{u}'_{r'}(-\vec{q})u^\mu_r(\vec{0}) \tag{11}$$

$$B^*_{bc} \to B^*_{cc} \qquad -2\eta\ \bar{u}'^{\lambda}_{r'}(-\vec{q})(\gamma^\mu - \gamma^\mu\gamma_5)u_{\lambda r}(\vec{0}) \tag{12}$$

where here B stands for a Ξ or Ω baryon. The IW function which controls the Ξ decays is different to that appearing in Ω decays since the IW function depends on the light degrees of freedom. Similar results can be obtained for semileptonic $bb \to bc$ baryon decays, but with different IW functions because of heavy flavor symmetry breaking in hadrons with two heavy quarks. The implications of the above relations on form factors have been studied in Ref. [12].

To the extent that one is close enough to the infinite heavy quark mass limit and near zero recoil we can combine the HQSS results in Eqs.(7-12) with Eq.(3), to get approximate values for the tensor product $\mathcal{LH} = \mathcal{L}^{\mu\nu}\,\mathcal{H}_{\mu\nu}$

$$B_{bc} \to B_{cc} \qquad \mathcal{LH} \approx \eta^2\frac{1}{9}\Big\{A(q^2)\,(-52\,\omega + 40) + B(q^2)\left[52\,\frac{(v'\cdot q)(v\cdot q)}{q^2} + (10 - 26\,\omega)\right]\Big\} \tag{13}$$

$$B'_{bc} \to B_{cc} \quad \mathcal{LH} \approx \eta^2 \frac{1}{9} \Big\{ A(q^2)\,(-12\,\omega - 24) + B(q^2) \left[12\,\frac{(v'\cdot q)(v\cdot q)}{q^2} - 6(1+\,\omega) \right] \Big\} \quad (14)$$

$$B_{bc} \to B^*_{cc} \quad \mathcal{LH} \approx \eta^2 \frac{1+\omega}{9} \left\{ -12A(q^2) + 4B(q^2) \left[\frac{(v'\cdot q)^2}{q^2} - 1 \right] \right\} \quad (15)$$

$$B'_{bc} \to B^*_{cc} \quad \mathcal{LH} \approx \eta^2 \frac{1+\omega}{3} \left\{ -12A(q^2) + 4B(q^2) \left[\frac{(v'\cdot q)^2}{q^2} - 1 \right] \right\} \quad (16)$$

$$B^*_{bc} \to B_{cc} \quad \mathcal{LH} \approx \eta^2 \frac{1+\omega}{9} \left\{ -6A(q^2) + 2B(q^2) \left[\frac{(v\cdot q)^2}{q^2} - 1 \right] \right\} \quad (17)$$

$$B^*_{bc} \to B^*_{cc} \quad \mathcal{LH} \approx \eta^2 \frac{1}{9} \Big\{ -A(q^2)\,\omega\left(8+16\omega^2\right) + B(q^2) \left[-\omega\left(12+8\omega^2\right) + \frac{(v'\cdot q)(v\cdot q)}{q^2}\left(40+16\omega^2\right) \right] \Big\} \quad (18)$$

and similar ones for $bb \to bc$ decays.

Working in the strict near zero recoil approximation, $\omega \approx 1$ or equivalently q^2 quite close to its maximum value $q^2_{\rm max}$, we can approximate $(v\cdot q)^2/q^2 \approx (v'\cdot q)(v\cdot q)/q^2 \approx (v'\cdot q)^2/q^2 \approx 1$ and $A(q^2) \approx -B(q^2)$. In these circumstances, and using $m_{B_{bb}} \approx m_{B^*_{bb}}$; $m_{B_{bc}} \approx m_{B'_{bc}} \approx m_{B^*_{bc}}$; $m_{B_{cc}} \approx m_{B^*_{cc}}$ one can obtain predictions for relative ratios between decay widths. Those predictions and the results in different models are given in Ref. [12]. We can relax the strict near near zero recoil approximation to obtain more accurate predictions based on HQSS in the following way. For the actual doubly heavy baryon masses $\omega_{max} \approx 1.22\,(1.08)$ for $bc \to cc\,(bb \to bc)$ transitions while the different differential decay widths $d\Gamma/d\omega$ show a maximum at around $\omega \approx 1.05\,(1.01)$. We can thus still use $\omega \approx 1$ and $A(q^2) \approx -B(q^2)$. On the other hand the quantities $(v\cdot q)^2/q^2$, $(v'\cdot q)^2/q^2$, $(v\cdot q)(v'\cdot q)/q^2$, that are all equal to 1 near zero recoil, can deviate rapidly from 1 because of the q^2 factor in the denominator. What is true, in and around the maximum of the differential decay width, is that we can reasonable approximate $(v\cdot q)^2/q^2 \approx (v'\cdot q)(v\cdot q)/q^2$ and $(v'\cdot q)^2/q^2 \approx (v'\cdot q)(v\cdot q)/q^2$.

With the above consideration we can still predict approximate ratios between different decay widths that one expects to be satisfied to an accuracy of $20 \sim 30\%$. We have chosen to define those ratios so that they are all equal to

one. In Table 3 we show the above ratios evaluated in different quark model

Table 3: Decay width ratios for semileptonic $bb \to bc$ and $bc \to cc$ decay of doubly heavy Ξ and Ω baryons. In all cases the approximate result obtained using HQSS is 1. l stands for a light charged lepton, $l = e,\ \mu$.

	This work		5)		6)
	Ξ	Ω	Ξ	Ω	Ξ
$\frac{\Gamma(B^*_{bb}\to B'_{bc}\, l\bar{\nu}_l)}{3\,\Gamma(B^*_{bb}\to B_{bc}\, l\bar{\nu}_l)}$	$1.00^{+0.01}_{-0.04}$	$1.00^{+0.03}_{-0.01}$	0.99	0.99	0.05
$\frac{\Gamma(B_{bb}\to B^*_{bc}\, l\bar{\nu}_l)}{\frac{2}{3}\,\Gamma(B_{bb}\to B'_{bc}\, l\bar{\nu}_l)}$	$0.86^{+0.08}_{-0.06}$	$0.86^{+0.05}$	0.96	0.99	9.53
$\frac{\Gamma(B^*_{bb}\to B_{bc}\, l\bar{\nu}_l)}{\frac{1}{3}\,\Gamma(B_{bb}\to B'_{bc}\, l\bar{\nu}_l)}$	$0.98^{+0.09}_{-0.03}$	$0.97^{+0.06}_{-0.14}$	1.01	1.03	36.4
$\frac{\Gamma(B^*_{bb}\to B^*_{bc}\, l\bar{\nu}_l)}{\Gamma(B_{bb}\to B_{bc}\, l\bar{\nu}_l)+\frac{1}{2}\,\Gamma(B_{bb}\to B^*_{bc}\, l\bar{\nu}_l)}$	$0.94^{+0.07}_{-0.06}$	$0.93^{+0.11}_{-0.10}$	1.01	1.01	0.31
$\frac{\Gamma(B'_{bc}\to B^*_{cc}\, l\bar{\nu}_l)}{3\,\Gamma(B_{bc}\to B^*_{cc}\, l\bar{\nu}_l)}$	$1.04^{+0.03}_{-0.01}$	$1.04_{-0.03}$	0.79	0.82	0.68
$\frac{\Gamma(B_{bc}\to B^*_{cc}\, l\bar{\nu}_l)}{\frac{2}{3}\,\Gamma(B'_{bc}\to B_{cc}\, l\bar{\nu}_l)}$	$0.82^{+0.06}_{-0.01}$	$0.84^{+0.13}_{-0.01}$	1.22	1.17	2.72
$\frac{\Gamma(B^*_{bc}\to B_{cc}\, l\bar{\nu}_l)}{\frac{1}{3}\,\Gamma(B'_{bc}\to B_{cc}\, l\bar{\nu}_l)}$	$0.94^{+0.11}$	$0.97^{+0.10}_{-0.01}$	1.28	1.26	10.6
$\frac{\Gamma(B^*_{bc}\to B^*_{cc}\, l\bar{\nu}_l)}{\Gamma(B_{bc}\to B_{cc}\, l\bar{\nu}_l)+\frac{1}{2}\,\Gamma(B_{bc}\to B^*_{cc}\, l\bar{\nu}_l)}$	$0.89^{+0.11}$	$0.94^{+0.13}_{-0.01}$	1.01	1.01	1.08

approaches. Calculations in this work and the ones in Ref. [5] are compatible, within the expected accuracy, with the approximate ratios (all equal to 1) obtained using HQSS results. On the other hand the deviations found in the results by Guo *et al* [6] for Ξ decays are, in most cases, too large.

4 Summary

We have checked the constraints imposed by HQSS on $b \to c$ semileptonic decay widths of doubly heavy baryons. The approximate ratios obtained using HQSS compare well with the results in our model and the one by Ebert *et al* [5], but they are incompatible with the calculation in Ref. [6]. We think that although this is not enough guarantee for the predictions here and in Ref. [5] to be fully

correct (in fact the few results in Ref. [10] are not incompatible with HQSS constraints while they are a factor of two larger than ours), it certainly indicates problems either in the model or in the calculation performed in Ref. [6].

5 Acknowledgements

This research was supported by DGI and FEDER funds, under contracts FIS2005-00810, FPA2004-05616, FIS2006-03438 and FPA2007-65748, by Junta de Andalucía and Junta de Castilla y León under contracts FQM0225 and SA016A07, and it is part of the EU integrated infrastructure initiative Hadron Physics Project under contract number RII3-CT-2004-506078.

References

1. M.J. White *et al* , Phys. Lett. B **271**, 410 (1991).
2. J.M. Flynn *et al*, Phys. Rev. D **76**, 017502 (2007).
3. C. Albertus *et al*, Eur. Phys. J. A **32**, 183 (2007).
4. C. Semay *et al*, Z. Phys. C 61, 271 (1994); B. Silvestre-Brac, Few-Body Systems 20, 1 (1996).
5. D. Ebert *et al*, Phys. Rev. D 70, 014018 (2004).
6. X.-H. Guo *et al*, Phys. Rev. D 58, 114007 (1998).
7. A. Faessler *et al*, Phys. Lett. B 518, 55 (2001).
8. M. A. Sanchis-Lozano, Nucl. Phys. B 440, 251 (1995).
9. V.V. Kiselev *et al*, Phys. Usp. 45, 455 (2002) (Usp. Fiz. Nauk 172, 497 (2002)).
10. A.I. Onishchenko, hep-ph/0006295; hep-ph/0006271.
11. V.V. Kiselev *et al*, Eur. Phys. J. C 16, 461 (2000).
12. E. Hernández *et al*, arXiv:0710.1186.
13. R. K. Bhaduri *et al*, Nuovo Cim. A 65, **376** (1981).

POSTER

Frascati Physics Series Vol. XLVI (2007), pp. 1511
HADRON07: XII Int. Conf. on Hadron Spectroscopy – Frascati, October 8-13, 2007
Poster Session

ANALITICAL DETERMINATION OF THE MAGNETIC MOMENT OF THE Δ-RESONANCE AND SCREENING IN THE BREMSTRAHLUNG REACTIONS

A. Machavariani
JINR Dubna, Russia and TSU Georgia

Written contribution not received

Frascati Physics Series Vol. XLVI (2007), pp. 1515–1518
HADRON07: XII Int. Conf. on Hadron Spectroscopy – Frascati, October 8-13, 2007
Poster Session

CONSTRUCTION OF LORENTZ INVARIANT AMPLITUDES FROM REST FRAME WAVE FUNCTIONS IN HQET – APPLICATION TO ISGUR-WISE FUNCTION

Takayuki Matsuki
Tokyo Kasei University, 1-18-1 Kaga, Itabashi, Tokyo 173-8602, JAPAN
Kohichi Seo
Gifu City Women's College, 7-1 Hitoichiba-Kitamachi, Gifu 501-0192, JAPAN

Abstract

Succeeding in predicting/reproducing the heavy-light mesons by our semi-relativistic quark potential model, we examine a method how to calculate the semileptonic weak form factors out of the rest frame wave functions of heavy mesons and numerically calculate the dynamical $1/m_Q$ corrections to those for the process $\bar{B} \to D^{(*)}\ell\nu$ based on our model for heavy mesons. It is shown that nonvanishing expressions for $\rho_1(\omega) = \rho_2(\omega)$ and $\rho_3(\omega) = \rho_4(\omega) = 0$ are obtained in a special Lorentz frame, where $\rho_i(\omega)$ are the parameters used in the Neubert-Rieckert decomposition of form factors. Various values of form factors are estimated, which are compatible with recent experimental data as well as other theoretical calculations.

1 Introduction

Discovery of narrow meson states $D_{s0}(2317)$ by BaBar and $D_{s1}(2460)$ by CLEO and the following confirmation by Belle has driven many theorists to explain

these states since the former study of these states using quark potential model seems to fail to reproduce these mass values. More recent experiments have found many other heavy-light mesons, broad $D_0^*(2308)$ and $D_1'(2427)$ mesons by Belle collaboration, which have the quantum numbers $j^P = 0^+$ and 1^+; narrow B and B_s states of $\ell = 1$, $B_1(5720)$, $B_2^*(5745)$, and $B_{s2}^*(5839)$ by CDF and D0 whose decay widths are also narrow because of their decay through the D-waves; and seemingly radial excitations ($n = 2$) of 0^+ $D_{s0}(2860)$ state by BaBar and 1^- $Ds^*(2715)$ state by Belle. Furthermore $c\bar{c}$ quarkonium-like states have been discovered one after another, $X(3872)$, $X(3940)$, $Y(3940)$, $Z(3930)$, and $Y(4260)$. These mesons have been successfully predicted and/or reproduced by our formulation [1, 2, 3], except for the quarkonium-like states. What we need to do next is to show that our approach can also give a method to calculate scattering amplitudes and decay widths using the rest frame wave functions.

Recently there appears a paper [5] in which the authors use the "relativistic" formulation to calculate masses of heavy mesons and apply it to calculate the Isgur-Wise functions for semileptonic B decays. Although this paper adopts a different approach from ours, they present how to calculate higher order corrections in $1/m_Q$ to form factors, which is one of the same purposes as we intend to do in this paper. In our former paper [1], we have developed a semi-relativistic formulation how to calculate the meson masses and wave functions for heavy-light $Q\bar{q}$ system introducing phenomenological dynamics. Meson wave functions obtained thereby and expanded in $1/m_Q$ can be used in principle to calculate ordinary form factors or Isgur-Wise functions and their higher order corrections in $1/m_Q$ for semileptonic weak or other decay processes. However what we have obtained are wave functions in the rest frame so that we need to develop a method to obtain Lorentz invariant amplitudes or Lorentz-boosted wave functions.

The problem how to construct a Lorentz-boosted wave function is in that there is ambiguity to determine space-time coordinates of two composite particles from information of one bound state, in this case a heavy meson. We study four cases of reference frames for composite particles and then give a prescription how to calculate matrix elements of currents using the rest frame wave functions. We give form factors in the zeroth order for four reference frames, show that they agree with each other in the HQET limit, and give those in the first order for just one special reference frame. The lowest order calculation in $1/m_Q$ gives the numerical value of the slope for the Isgur-Wise function at the origin and the semi-leptonic weak form factors are calculated up to the first order in $1/m_Q$. It is derived that *there are no dynamical contributions to the form factors*, i.e., the first order corrections to the wave functions do not contribute to the form factors. Studying $\bar{B} \to D\ell\nu$ and $\bar{B} \to D^*\ell\nu$ processes, physical quantities related to the CKM matrix elements are obtained. The

summary and discussions are given for this paper. [1]

2 Results

As an example of this formulation, we have calculated the semi-leptonic weak form factors up to the first order in $1/m_Q$. What we have found in this paper is

1. The Isgur-Wise function has the following form up to the first order in $1/m_Q$ and in $(\omega - 1)$.

$$\xi(\omega) = 1 - \left(\frac{1}{2} + \frac{1}{3}\bar{\Lambda}^2 \left\langle r^2 \right\rangle\right)(\omega - 1), \qquad \bar{\Lambda} = \bar{\Lambda}_u = \lim_{m_Q \to \infty} \tilde{E}_D = \lim_{m_Q \to \infty} \tilde{E}_B,$$

   and hence

$$\xi(1) = 1, \qquad \xi'(1) = -\frac{1}{2} - \frac{1}{3}\bar{\Lambda}^2 \left\langle r^2 \right\rangle.$$

   Here since $\bar{\Lambda}$ depends only on light quark mass and we treat only heavy mesons D, D^*, and B which include only u and d light quarks with $m_u = m_d$, the subscript of $\bar{\Lambda}_u$ expresses this fact.

2. We find that there is no contribution from correction terms in the first order of m_Q for the rest frame wave functions to the six form factors. That is, some terms do not contribute to the physical quantities.

3. The first order corrections are derived from phase factors of the wave functions and also given by kinetic terms and there are no contributions from the first order corrections to the wave functions. That is, in the terminology of Neubert and Rieckert in [7],

$$\rho_1(\omega) \quad = \quad \rho_2(\omega) = -\frac{1}{3} C^1 \bar{\Lambda} \left\langle r^2 \right\rangle (\omega - 1), \quad \rho_3(\omega) = \rho_4(\omega) = 0.$$

4. We have calculated the values for the form factor $\mathcal{F}(\omega)$ at the zero recoil and/or their first derivatives up to the first order in $1/m_Q$ as

$$\begin{aligned}
&\mathcal{F}_D(1) = 1.07, \qquad \mathcal{F}_D{}'(1) = -0.875, \\
&\mathcal{F}_{D^*}(1) = \xi(1) = 1, \qquad \mathcal{F}_{D^*}{}'(1) = -1.09, \\
&R_1(1) = 1.45, \quad R_1(1) = -0.222, \quad R_2(1) = 0.942, \quad R_2'(1) = 0.0286,
\end{aligned}$$

   the first equations are obtained by analyzing $\bar{B} \to D\ell\nu$ process and the second by $\bar{B} \to D^*\ell\nu$. These values are consistent with experimental data as well as other theoretical estimates listed in Tables I and II of [5].

[1] This paper is based on the recent paper [6].

5. The above values can be used to estimate the CKM matrix element $|V_{cb}|$ which we have obtained as

$$|V_{cb}| = 0.0387 \pm 0.0060,$$

for the $\bar{B} \to D\ell\nu$ process and

$$|V_{cb}| = 0.0380 \pm 0.0021,$$

for the $\bar{B} \to D^*\ell\nu$ process. These values are consistent with the value in PDG [8]

$$|V_{cb}| = 0.0409 \pm 0.0018 \quad \text{(exclusive)}.$$

Here to give theoretical predictions for $|V_{cb}|$ we have neglected theoretical undertainties although experimental errors are taken into account.

We have developed a method to obtain the relativistically invariant results using the rest frame wave functions, and to do this the four different Lorentz-boosted frames are adopted to check the validity of our results. The same form is obtained for the Isgur-Wise function in all four cases up to the zeroth order in $1/m_Q$ and the first order in $(\omega - 1)$, however their first order corrections in $1/m_Q$ are not the same for all four cases. Only the case, written as 2-ii) in [6], i.e., in the Breit frame with $t' = x'^0 = y'^0$ both for $\bar{B}$ and $D^{(*)}$, gives consistent results with the relativistic ones given by [7].

References

1. T. Matsuki *et al.*, Phys. Rev. D **56**, 5646 (1997); Phys. Lett. B **606**, 329 (2005).
2. T. Matsuki *et al.*, Eur. Phys. J. C **31**, 701 (2007), hep-ph/0610186.
3. T. Matsuki *et al.*, Prog. Theor. Phys. **117**, 1077 (2007), hep-ph/0605019 (2006).
4. See for review, M. Neubert, Phys. Rep. **245**, 259 (1994).
5. D. Ebert *et al.*, hep-ph/061130.
6. T. Matsuki *et al.*, hep-ph/0703158, to be published in Prog. Theor. Phys. Vol. 118, No. 6.
7. M. E. Luke, Nucl. Phys. B **252**, 447 (1990); C.G. Boyd and D.E. Brahm, Nucl. Phys. B **257**, 393 (1991); M. Neubert and V. Rieckert, Nucl. Phys. B **382**, 97 (1992).
8. Particle Data Group, W.-M. Yao et al., J. Phys. **G 33**, 1 (2006).

Frascati Physics Series Vol. XLVI (2007), pp. 1519–1522
HADRON07: XII Int. Conf. on Hadron Spectroscopy – Frascati, October 8-13, 2007
Poster Session

BOTTONOMIUM MASSES, DECAY RATES AND SCALAR CHARGE RADII

J N Pandya
Department of Physics, Veer Narmad South Gujarat University, Surat 395 007, India
Ajay Kumar Rai
Applied Sciences and Humanities Department, SVNIT, Surat 395 007, India
P C Vinodkumar
Department of Physics, Sardar Patel University, Vallabh Vidyanagar 388 120, India

Abstract

The masses of bottomonium s and p-states, decay constants, leptonic as well as radiative decay widths are computed in the framework of extended harmonic confinement model without any additional parameters.

1 Bottomonia masses from ERHM

The mass of a hadron having p number of quarks in ERHM can be obtained as [1],

$$M_N(q_1q_2.....) = \sum_{i=1}^{p} \epsilon_N(q_i,p)_{conf} + \sum_{i<j=1}^{p} \epsilon_N(q_iq_j)_{coul} + \sum_{i<j=1}^{p} \epsilon_N^J(q_i,q_j)_{SD} \quad (1)$$

where the first sum is the total confined energies of the constituting quarks of the hadron, the second sum corresponds to the residual colour coulomb

Table 1: Masses (in MeV/c^2) of the bottomonium system

State	Present	9)	11)	12)$_p$	12)$_{np}$	13)	14)
$\eta_b(1^1S_0)$	9425	9300 ± 23	9457	9414	9421	9400	9300
$\eta_b(2^1S_0)$	10012	–	10018	9999	10004	9993	9974
$\eta_b(3^1S_0)$	10319	–	10380	10345	10350	10328	10333
$\eta_b(4^1S_0)$	10572	–	10721	10623	10632	–	–
$\eta_b(5^1S_0)$	10752	–	11059	–	–	–	–
$\Upsilon(1^3S_1)$	9461	9460	9460	9461	9460	9460	9460
$\Upsilon(2^3S_1)$	10027	10023	10023	10023	10024	10023	10023
$\Upsilon(3^3S_1)$	10329	10355	10385	10364	10366	10355	10381
$\Upsilon(4^3S_1)$	10574	10579	10727	10643	10643	–	10787
$\Upsilon(5^3S_1)$	10753	10865	11065	–	–	–	11278
$\chi_{b0}(1^3P_0)$	9839	9859	9894	9861	9860	9863	9865
$\chi_{b1}(1^3P_1)$	9873	9893	9941	9891	9892	9892	9895
$\chi_{b2}(1^3P_2)$	9941	9912	9983	9912	9910	9913	9919
$h_{b1}(1^1P_1)$	9907	–	9955	9900	9900	9901	9894
$\chi_{b0}(2^3P_0)$	10197	10232	10234	10231	10231	10234	10238
$\chi_{b1}(2^3P_1)$	10207	10255	10283	10255	10258	10255	10264
$\chi_{b2}(2^3P_2)$	10227	10268	10326	10272	10271	10268	10283
$h_{b2}(2^1P_1)$	10217	–	10296	10262	10263	10261	10260

p = perturbative and np = nonperturbative computations in Tables 1 & 2

Table 2: Leptonic decay widths (in keV) of $\Upsilon(n^3S_1)$

State	Present	9)	11)	12)$_p$	12)$_{np}$	15)	16)
$\Upsilon(1^3S_1)$	1.320	1.340 ± 0.018	–	5.30	1.73	1.45 ± 0.07	1.314
$\Upsilon(2^3S_1)$	0.628	0.612 ± 0.011	0.426	2.95	1.04	0.52 ± 0.02	0.576
$\Upsilon(3^3S_1)$	0.263	0.443 ± 0.008	0.356	2.17	0.81	0.35 ± 0.02	0.476
$\Upsilon(4^3S_1)$	0.104	0.272 ± 0.029	0.335	1.67	0.72	–	0.248
$\Upsilon(5^3S_1)$	0.040	0.310 ± 0.070	0.311	–	–	–	0.310

Table 3: Radiative M1 transitions of bottomonia (eV)

Transition	Present	12)	13)	16)	17)	18)
$1^3S_1 \to 1^1S_0$	2.242 (36)	4.0	5.8 (60)	9.2	7.7 (59)	8.95
$2^3S_1 \to 2^1S_0$	0.145 (15)	0.5	1.40 (33)	0.6	0.53 (25)	1.51
$3^3S_1 \to 3^1S_0$	0.041 (10)	–	0.80 (27)	–	0.13 (16)	0.826

The values in the parentheses are the energy of emitted photons in MeV.

is the ground state mass of the pseudoscalar/vector meson. In the present computations, $f_P = 711$ MeV which is closer to the experimental value of 710 $\pm$ 15 MeV, while the other results are 660 [6], 772 [8] and 812 [10].

The scalar charge radii and M1 transitions of the bottomonia in a given eigenstate are obtained using $\langle r^2_{nS}\rangle^{1/2} = \left[\int_0^\infty |R^h_{nS}(r)|^2\ r^2\ r^2 dr\right]^{1/2}$, $\Gamma(V \to P\gamma) = \frac{16}{3}\alpha e_q^2 \frac{k_\gamma^3}{M_V^2}$ where $k_\gamma = (M_V^2 - M_P^2)/2M_V$ is the energy of the emitted photon. The computed values of M1 transitions are shown in Table 3. The scalar charge radii (in fm) of s-wave bottomonia are 0.1854 (2.2338), 0.3997 (1.6325), 0.7070 (1.0890) and 1.1649 (0.9623) respectively from 1S through 4S states, where the values in the brackets are wave functions (in $\mathrm{GeV}^{3/2}$).

References

1. P C Vinodkumar *et al*; Eur. Phys. Jnl. **A4**, 83 (1999)
2. K Gottfried, V F Weisskopf, Concepts of Particle Physics; 397 (1986)
3. J N Pandya, P C Vinodkumar, Pramana J. Phys **57**, 821 (2001)
4. P C Vinodkumar *et al*; Pramana Jnl. of Phys. **39**, 47 (1992)
5. Close F E, Quarks and Partons (1979)
6. C Quigg, J L Rosner, Phys. Reports **56**, 222 (1979)
7. R Van Royen, V F Weisskopf, *Nuovo Cimento* **A50**, 617 (1967)
8. Cvetic *et al*, Phys. Lett. **B596**, 84 (2004)
9. Y M Yao *et al* [Particle Data Group]; J. Phys. **G33**,1 (2006)
10. Z Wang et al, Phys. Lett. **B 615**, 79 (2005)
11. R A Coimbra, O Oliveira; hep-ph/0610142 (2006)
12. S F Radford, W W Repko; Phys. Rev. **D75**, 074031 (2007)
13. D Ebert, R N Faustov, V O Galkin; Phys. Rev. **D 67**, 014027 (2003)
14. A V Shoulgin, G M Vereshkov, O V Lutchenko; J. Phys. **G29**, 1245 (2003)
15. S M Ikhdair, R Sever; Int. J. Mod. Phys. **A 21**, 3989 (2006)
16. V V Anisovich *et al*; Phys. Atom. Nucl. **70**, 63 (2007)
17. T A Lähde; Nucl.Phys. **A714**, 183 (2003)
18. World average, N Brambilla et al; hep-ph/0412158v2

Frascati Physics Series Vol. XLVI (2007), pp. 1523
HADRON07: XII Int. Conf. on Hadron Spectroscopy – Frascati, October 8-13, 2007
Poster Session

TESTING CP AND TIME REVERSAL SYMMETRIES IN Λ_b DECAYS INTO POLARIZED RESONANCES

O. Leitner
Laboratori Nazionali di Frascati, Frascati, Italy

Written contribution not received

Frascati Physics Series Vol. XLVI (2007), pp. 1525
HADRON07: XII Int. Conf. on Hadron Spectroscopy – Frascati, October 8-13, 2007
Poster Session

MULTIQUARK DESCRIPTION OF OPEN-CHARM MESONS

A. Valcarce
University of Salamanca, Spain

Written contribution not received

Frascati Physics Series Vol. XLVI (2007), pp. 1527
HADRON07: XII Int. Conf. on Hadron Spectroscopy – Frascati, October 8-13, 2007
Poster Session

GLUEBALL OPTION FOR $X(1835)$

M. L. L. Da Silva
Instituto de Fsica, Universidade Federal do Rio Grande do Sul, Brazil
D. Hadjimichef
Departamento de Fsica e Matemtica, Universidade Federal de Pelotas, Brazil

Written contribution not received

Frascati Physics Series Vol. XLVI (2007), pp. 1529
HADRON07: XII Int. Conf. on Hadron Spectroscopy – Frascati, October 8-13, 2007
Poster Session

SPECTROSCOPY OF THE HEAVY QUARKONIA: ENERGY LEVELS SPLITTING AND TETA-SINGULAR POTENTIALS

O. Khetselius
Odessa University, Ukraine

Written contribution not received

Frascati Physics Series Vol. XLVI (2007), pp. 1531
HADRON07: XII Int. Conf. on Hadron Spectroscopy – Frascati, October 8-13, 2007
Poster Session

DISCHARGE OF METASTABLE NUCLEI DURING MUON CAPTURE: ENERGY APPROACH

A. Glushkov
Odessa University, Ukraine

Written contribution not received

Frascati Physics Series Vol. XLVI (2007), pp. 1533
HADRON07: XII Int. Conf. on Hadron Spectroscopy – Frascati, October 8-13, 2007
Poster Session

KAON PHOTOPRODUCTION ON DEUTERIUM USING POLARISED PHOTONS WITH CLAS

R. Johnstone
University of Glasgow and Hall-B with CLAS at Jefferson Lab, Virginia, USA

Written contribution not received

Frascati Physics Series Vol. XLVI (2007), pp. 1535–1538
HADRON07: XII Int. Conf. on Hadron Spectroscopy – Frascati, October 8-13, 2007
Poster Session

RHO-LIKE MESONS FROM ANALYSIS OF THE PION-PION SCATTERING

Yu.S. Surovtsev
Joint Institute for Nuclear Research, 141980 Dubna, Russia
P. Bydžovský
Nuclear Physics Institute, 25068 Řež, Czech Republic

Abstract

In the model-independent and Breit–Wigner (BW) analyses of experimental data on the isovector P-wave of $\pi\pi$ scattering, it is shown that in the 1200-1800-MeV region, there are evidently three states: $\rho(1250)$, $\rho(1450)$ and $\rho(1600)$.

1 The model-independent approach

Let us outline the model-independent approach (MIA) [1] to studying the 2-channel $\pi\pi$ scattering. Let the S-matrix be determined on the 4-sheeted Riemann surface with the right branch-points at $s = 4m_{\pi^0}^2$ and $(m_\omega + m_{\pi^0})^2$ and with the left one at $s = 0$. The surface sheets are numbered according to the signs of analytic continuations of the channel momenta $k_1 = [s - 4m_{\pi^0}^2]^{1/2}/2$ and $k_2 = [s - (m_\omega + m_{\pi^0})^2]^{1/2}/2$ as follows: signs$(\mathrm{Im}k_1, \mathrm{Im}k_2) = ++, -+, --,$ and $+-$ correspond to sheets I, II, III, and IV, respectively. The 2-channel resonances are represented by the three possible types of pole clusters (poles and zeros on the Riemann surface) [1] (**a**), (**b**) and (**c**): (**a**) the state is described by a pair of conjugate poles on sheet II and by a pair of shifted poles on sheet III; (**b**) by a pair of conjugate poles on sheet IV and by a pair of shifted poles on sheet III; (**c**) by a pair of conjugate poles on sheet II and by other on sheet IV, and by two pairs of conjugate poles on sheet III.

The supposed Riemann surface is mapped by the uniformizing variable $v = [(m_\omega + m_{\pi^0})k_1 + 2m_{\pi^0}k_2]/[s(((m_\omega + m_{\pi^0})/2)^2 - m_{\pi^0}^2)]^{1/2}$ onto the v-plane [2]. In the S-matrix, $S = S_{res}S_{bg}$, the resonance part is [2] $S_{res} = d(-v^{-1})/d(v)$, where $d = v^{-M}\prod_{n=1}^{M}(1 - v_n^* v)(1 + v_n v)$ with M the number of pairs of the conjugate resonance zeros. The background part is $S_{bg} = \exp[2i(2k_1/\sqrt{s})^3(\alpha_1 + \alpha_2\theta(s - s_1)(s - s_1)/s + \alpha_3\theta(s - s_2)(s - s_2)/s)]$ where $\alpha_i = a_i + ib_i$, and s_1 and s_2 are the thresholds of the 4π and $\rho 2\pi$ channels, respectively.

In analysis of data [3] for η and δ ($S(\pi\pi \to \pi\pi) = \eta\exp(2i\delta)$), we considered three ($\rho(770)$, $\rho(1250 - 1580)$, and $\rho(1550 - 1780)$), four (the previous three and $\rho(1860 - 1910)$) and five (the previous four and $\rho(1450)$) states. Satisfactory description of data was obtained. The χ^2/NDF and the constant systematic error of δ in data by Estabrooks *et al.* [3] (see [2] for discussion) are, respectively, 1.72 and -1.885° for three, 1.68 and -1.897° for four, 1.65 and -1.876° for five states. The analyses prefer the case in which $\rho(770)$ is described by the type-(**a**) cluster and the others by (**b**). The cluster poles for the 5-resonance description, located on the lower $\sqrt{s}$-half-plane, are (in MeV) $765.8 - i73.3$ (sheet II) and $778.2 - i68.9$ (sheet III) for $\rho(770)$, $1250 - i131.4$ (III) and $1249.4 - i130.7$ (IV) for $\rho(1250)$, $1469.2 - i89.3$ (III) and $1465.4 - i100.4$ (IV) for $\rho(1450)$, $1634.8 - i145.9$ (III) and $1593.4 - i72.9$ (IV) for $\rho(1600)$, and $1883 - i106.5$ (III) and $1893.4 - i87.6$ (IV) for $\rho(1900)$. The background parameters are: $a_1 = b_1 = b_2 = 0$, $a_2 = 0.0248$, $a_3 = 0.0841$, $b_3 = 0.0019$. The pole clusters and background parameters for the 3- and 4-resonance descriptions are given in [2]. Though the description is practically the same in all three cases, careful consideration of the obtained parameters and energy dependence of the fitted quantities suggests that $\rho(1900)$ is strongly desired and that $\rho(1450)$ should be also present improving slightly the description.

Masses and total widths are, respectively (in MeV): 769.3 and 146.6 for $\rho(770)$, 1256.2 and 261.4 for $\rho(1250)$, 1468.8 and 200.8 for $\rho(1450)$, 1595.1 and 145.8 for $\rho(1600)$, and 1895.4 and 175.2 for $\rho(1900)$.

2 The Breit–Wigner analysis

The considered mesons possess also other important decay channels in addition to those considered above [4]. The $\rho(1450)$ and/or a possible $\rho(1250)$ can decay also to $\eta\rho^0$, 4π and $\phi\pi$. The $\rho(1700)$ has a large branching to the 4π, $\rho 2\pi$ and $\eta\rho^0$. To obtain coupling constants with some selected channels from analysis of the $\pi\pi$-scattering data, we used the 5-channel BW forms, constructing the

$d(k_1,\cdots,k_5)=d_{res}d_{bg}$ in the formula [2] $S_{res}=d(-k_1,\cdots,k_5)/d(k_1,\cdots,k_5)$, where k_1, k_2, k_3, k_4 and k_5 are the $\pi\pi$-, $\pi^+\pi^-2\pi^0$-, $2(\pi^+\pi^-)$-, $\eta 2\pi$- and $\omega\pi^0$-channel momenta, respectively. $d_{res}(s)=\prod_r[M_r^2-s-i\sum_{j=1}^5\rho_{rj}^3\ R_{rj}\ f_{rj}^2]$, where $\rho_{rj}=k_i(s)/k_i(M_r^2)$, f_{rj}^2/M_r is the partial width, $R_{rj}(s,s_j,r_{rj},M_r)$ is a Blatt–Weisskopf barrier factor [2] with s_j the j-channel threshold and radii $r_{rj}=0.7035$ fm for all resonances in all channels. We have taken $f_{r2}=f_{r3}/\sqrt{2}$. The background part is $d_{bg}=\exp[-i(2k_1/\sqrt{s})^3(\alpha_1+\alpha_2\theta(s-s_1)(s-s_1)/s)]$, where $\alpha_i=a_i+ib_i$ ($b_1=0$) and s_1 is the $\rho 2\pi$ channel threshold.

The data were analyzed considering three, four and five resonances. A reasonable description of all three cases was obtained: $\chi^2/\mathrm{NDF}=1.87$ for three, 1.92 for four and 1.91 for five resonances. The resonance parameters for the last case are shown in tab.1. The systematic error of data by Estabrooks *et al.* [3] is $-1.987°$. The background parameters are: $a_1=-0.00121\pm0.0018$, $a_2=-0.1005\pm0.011$, and $b_2=0.0012\pm0.006$. We have calculated also the

Table 1: *The ρ-like resonance parameters (in MeV).*

State	$\rho(770)$	$\rho(1250)$	$\rho(1450)$	$\rho(1600)$	$\rho(1900)$
M	777.7±0.3	1249.8±15.6	1449.9±12.2	1587.3±4.5	1897.8±38
f_{r1}	343.8±0.7	87.7±7.4	56.9±5.4	248.2±5.2	47.3±12
f_{r2}	24.6±5.8	186.3±39.9	100.1±18.7	240.2±8.6	73.7
f_{r3}	34.8±8.2	263.5±56.5	141.6±26.5	339.7±12.5	104.3
f_{r4}		231.8±111	141.2±98	141.8±33	9
f_{r5}		231±115	150±95	108.6±40.4	10
Γ_{tot}	≈154.3	>175	>52	>168	>10

isovector P-wave length of $\pi\pi$ scattering: $a_1^1=33.9\pm2.02$ $[10^3m_{\pi^+}^{-3}]$. Compare it with values evaluated by using the NJL model [5], local (34, Bernard *et al.*) and non-local (37, Osipov *et al.*), and Roy's equations [6]: 38.4 ± 0.8 (Peláez *et al.*), 37.9 ± 0.5 (Carpini *et al.*), and 39.6 ± 2.4 (Kamiński *et al.*).

3 Conclusions

The reasonable description of the accessible data on the isovector P-wave of $\pi\pi$ scattering [3] has been obtained up to 1880 MeV in MIA ($\chi^2/\mathrm{NDF}=1.654$) and applying the BW forms ($\chi^2/\mathrm{NDF}=1.906$).

For $\rho(770)$, the mass is smaller in MIA (769.3 MeV) and a little bigger in the BW analysis (777.69 MeV) than the averaged mass (775.5 ± 0.4 MeV) in

the PDG tables [4]. The total width in MIA (146.6 MeV) coincides with the PDG one (146.4 ± 1.1 MeV) but in the BW analysis it is larger (154.3 MeV).

The 2nd ρ-like meson has the mass 1256.2 MeV in MIA and 1249.8±15.6 MeV in the BW analysis. This differs significantly from the PDG value ($1459 \pm$ 11 MeV). The $\rho(1250)$ was discussed some time ago [7] and it was confirmed relatively recently in analyses [8]. An existence of three ρ-like mesons in the 1200-1800-MeV region does not contradict the data, the 3rd meson having the mass about 1450 MeV. In MIA, the description is even slightly improved with this state included. The 4th ρ-like meson has the mass 1590 MeV rather than 1720 MeV cited in the PDG tables. Note that a rather large coupling of these ρ-like mesons with the 4π channels was obtained.

In the case of $\rho(1900)$, there are practically no data in this energy region. Whereas MIA testifies in favor of existence of this state, the BW analysis gives equivalent results with and without the $\rho(1900)$.

The P-wave $\pi\pi$-scattering length, obtained in the BW analysis, mostly matches the result of the local NJL model [5].

4 Acknowledgements

Yu.S. acknowledges support provided by the Votruba-Blokhintsev Program. P.B. thanks the Grant Agency of the Czech Republic, Grant No.202/05/2142.

References

1. D. Krupa *et al.*, Nuovo Cim. **A109**, 281 (1996); Yu.S. Surovtsev *et al.*, Eur. Phys. J. **A15**, 409 (2002).
2. Yu.S. Surovtsev and P. Bydžovský, E-Print Archive: hep-ph/0701274.
3. S.D. Protopopescu *et al.*, Phys. Rev. **D7**, 1279 (1973); B. Hyams *et al.*, Nucl. Phys. **B64**, 134 (1973); P. Estabrooks *et al.*, Nucl. Phys. **B79**, 301 (1974).
4. W.-M. Yao *et al.* [PDG], J.Phys. **G33**, 1 (2006).
5. V. Bernard *et al.*, Phys. Lett. **B285**, 119 (1992); A.A. Osipov *et al.*, E-Print Archive: hep-ph/0603130.
6. J.R. Peláez *et al.*, Phys. Rev. **D71**, 074016 (2005); I. Carpini *et al.*, Int. J. Mod. Phys. **A21**, 954 (2006); R.Kamiński *et al.*, Phys. Lett. **B551**, 241 (2003).
7. N.M. Budnev *et al.*, Phys. Lett. **B70**, 365 (1977); S.B. Gerasimov and A.B. Govorkov, Z. Phys. **C13**, 43 (1982).
8. D. Aston *et al.*, Nucl. Phys. Proc. Suppl. **B21**, 105 (1991); T.S. Belozerova and V.K. Henner, Phys. Elem. Part. Atom. Nucl. **29**, part 1, 148 (1998).

Frascati Physics Series Vol. XLVI (2007), pp. 1539–1542
HADRON07: XII Int. Conf. on Hadron Spectroscopy – Frascati, October 8-13, 2007
Poster Session

STABILITY OF THE SOLUTIONS OF INSTANTANEOUS BETHE–SALPETER EQUATIONS WITH CONFINING INTERACTIONS

Wolfgang Lucha
Institute for High Energy Physics, Austrian Academy of Sciences, Nikolsdorfergasse 18, A-1050 Vienna, Austria
Franz F. Schöberl
Faculty of Physics, University of Vienna, Boltzmanngasse 5, A-1090 Vienna, Austria

Abstract

For two bound-state equations derived as simplified forms of the Bethe–Salpeter equation with confining interaction, stability of all solutions is rigorously shown.

1 Motivation: Instabilities of Klein-Paradox Type

The Salpeter equation is a frequently applied three-dimensional reduction of the Bethe–Salpeter formalism describing bound states within quantum field theory, derived by assuming all interactions to be instantaneous. For given interactions, encoded in its *integral kernel* $K(\boldsymbol{p}, \boldsymbol{q})$ depending on relative three-momenta $\boldsymbol{p}, \boldsymbol{q}$ of the bound-state constituents, it can be regarded as an eigenvalue equation for the Salpeter amplitude $\Phi(\boldsymbol{p})$, with the mass M of the bound state as eigenvalue. For confining interactions, however, its solutions exhibit in *numerical* studies [1)] certain instabilities, possibly related to Klein's paradox, causing states to decay.

In view of this highly unsatisfactory state of the art, we began a systematic rigorous analysis of the conditions for stability of the energy levels predicted, for confining interactions, within this framework. We regard a bound state as *stable* if its mass eigenvalue M belongs to a *real discrete* spectrum *bounded from below*.

On energetic grounds, any instabilities should manifest themselves first for pseudoscalar bound states; accordingly, we focus to fermion–antifermion bound states characterized by spin-parity-charge conjugation assignment $J^{PC} = 0^{-+}$. This allows to take advantage of experience gained in earlier studies [2, 3, 4, 5].

We analyze three-dimensional reductions of the Bethe–Salpeter formalism for increasing complexity of the problem: the *reduced* Salpeter equation [6, 7], a generalization thereof, proposed in Ref. [8] and applied in Ref. [9], towards exact propagators of the bound-state constituents [10], and the *full* Salpeter equation.

With Dirac couplings Γ, assumed to be identical for both constituents, and related potential functions $V_\Gamma(\boldsymbol{p},\boldsymbol{q})$, the action of some kernel $K(\boldsymbol{p},\boldsymbol{q})$ on $\Phi(\boldsymbol{p})$ is

$$[K(\boldsymbol{p},\boldsymbol{q})\,\Phi(\boldsymbol{q})] = \sum_\Gamma V_\Gamma(\boldsymbol{p},\boldsymbol{q})\,\Gamma\,\Phi(\boldsymbol{q})\,\Gamma\ .$$

For all interactions of harmonic-oscillator type in configuration space, the above bound-state equations simplify to ordinary differential equations, which may be cast into the form of "tractable" eigenvalue equations for Schrödinger operators, at least in the case of the *reduced* bound-state equations studied in Secs. 2 and 3.

Our primary tool is a (well-known) *theorem* which states that the *spectrum* of a Schrödinger Hamiltonian operator with a locally bounded positive potential V rising to infinity in all directions, $V(x) \to +\infty$ for $|x| \to \infty$, is purely discrete.

2 Reduced Salpeter Equation

Approximating the propagation of both bound-state constituents by that of free particles of *constant* effective "constituent" mass m yields the Salpeter equation

$$\begin{aligned}\Phi(\boldsymbol{p}) \;=\; \int \frac{\mathrm{d}^3q}{(2\pi)^3}\Bigg(&\frac{\Lambda^+(\boldsymbol{p})\,\gamma_0\,[K(\boldsymbol{p},\boldsymbol{q})\,\Phi(\boldsymbol{q})]\,\Lambda^-(\boldsymbol{p})\,\gamma_0}{M-2\,E(\boldsymbol{p})}\\ &-\frac{\Lambda^-(\boldsymbol{p})\,\gamma_0\,[K(\boldsymbol{p},\boldsymbol{q})\,\Phi(\boldsymbol{q})]\,\Lambda^+(\boldsymbol{p})\,\gamma_0}{M+2\,E(\boldsymbol{p})}\Bigg)\,,\end{aligned}\tag{1}$$

with *one-particle energy* $E(\boldsymbol{p})$ and *energy projection operators* $\Lambda^\pm(\boldsymbol{p})$ defined by

$$E(\boldsymbol{p}) \equiv \sqrt{\boldsymbol{p}^2+m^2}\ , \qquad \Lambda^\pm(\boldsymbol{p}) \equiv \frac{E(\boldsymbol{p}) \pm \gamma_0\,(\boldsymbol{\gamma}\cdot\boldsymbol{p}+m)}{2\,E(\boldsymbol{p})}\ .$$

Dropping of the second term on its RHS yields the *reduced Salpeter equation* [11]

$$[M - 2\,E(\boldsymbol{p})]\,\Phi(\boldsymbol{p}) = \int \frac{\mathrm{d}^3 q}{(2\pi)^3}\,\Lambda^+(\boldsymbol{p})\,\gamma_0\,[K(\boldsymbol{p},\boldsymbol{q})\,\Phi(\boldsymbol{q})]\,\Lambda^-(\boldsymbol{p})\,\gamma_0\ . \qquad (2)$$

Because of its projector structure, a pseudoscalar $\Phi(\boldsymbol{p})$ has just one independent component. For a large class of kernels, all its solutions prove to be stable [6, 7].

3 Instantaneous Bethe–Salpeter Equation with Exact Propagators

By Lorentz covariance, the exact fermion propagator $S(p)$ is fully determined by two real p-dependent (Lorentz-scalar) functions, which may be interpreted, e.g., as this fermion's mass function $m(p^2)$ and wave-function renormalization $Z(p^2)$:

$$S(p) = \frac{\mathrm{i}\,Z(p^2)}{\not{p} - m(p^2) + \mathrm{i}\,\varepsilon}\ , \qquad \not{p} \equiv p^\mu\,\gamma_\mu\ , \qquad \varepsilon \downarrow 0\ .$$

If these propagator functions are assumed to depend *approximately* only on the three-momentum $\boldsymbol{p}$, an *exact-propagator bound-state equation* may be found [8], from which, for free propagators, $m(p^2) \to m$, $Z(p^2) \to 1$, Salpeter's equation is recovered, and which may be reduced to the exact-propagator version of Eq. (2):

$$[M - 2\,E(\boldsymbol{p})]\,\Phi(\boldsymbol{p}) = Z^2(\boldsymbol{p}^2) \int \frac{\mathrm{d}^3 q}{(2\pi)^3}\,\Lambda^+(\boldsymbol{p})\,\gamma_0\,[K(\boldsymbol{p},\boldsymbol{q})\,\Phi(\boldsymbol{q})]\,\Lambda^-(\boldsymbol{p})\,\gamma_0\ ; \quad (3)$$

here, one-particle energy $E(\boldsymbol{p})$ and energy projection operators $\Lambda^\pm(\boldsymbol{p})$ now read

$$E(\boldsymbol{p}) \equiv \sqrt{\boldsymbol{p}^2 + m^2(\boldsymbol{p}^2)}\ , \qquad \Lambda^\pm(\boldsymbol{p}) \equiv \frac{E(\boldsymbol{p}) \pm \gamma_0\,\left[\boldsymbol{\gamma}\cdot\boldsymbol{p} + m(\boldsymbol{p}^2)\right]}{2\,E(\boldsymbol{p})}\ .$$

For reasonably well-behaved $m(\boldsymbol{p}^2) > 0$ and $Z(\boldsymbol{p}^2) > 0$, bound states are stable.

4 (Full) Salpeter Equation

Trivially, similar considerations may be applied to the full Salpeter equation (1). There any analogous analysis is, however, considerably more complicated for, at least, two reasons. On the one hand, full-Salpeter amplitudes involve more than one independent components. Eq. (1) therefore reduces to a *set* of second-order differential equations, equivalent to a single differential equation of higher order. On the other hand, although all mass eigenvalues squared M^2 are guaranteed to be real, the spectrum of mass eigenvalues M is in general not necessarily real: for the phenomenologically perhaps most relevant interaction kernels this spectrum is a union of real opposite-sign pairs $(M, -M)$ and imaginary points $M = -M^*$.

References

1. J. Parramore and J. Piekarewicz, Nucl. Phys. A **585**, 705 (1995) [nucl-th/9402019]; J. Parramore, H.-C. Jean, and J. Piekarewicz, Phys. Rev. C **53**, 2449 (1996) [nucl-th/9510024]; M. G. Olsson, S. Veseli, and K. Williams, Phys. Rev. D **52**, 5141 (1995) [hep-ph/9503477]; M. Uzzo and F. Gross, Phys. Rev. C **59**, 1009 (1999) [nucl-th/9808041].

2. W. Lucha, K. Maung Maung, and F. F. Schöberl, Phys. Rev. D **63**, 056002 (2001) [hep-ph/0009185].

3. W. Lucha, K. Maung Maung, and F. F. Schöberl, in: Proc. Int. Conference on *Quark Confinement and the Hadron Spectrum IV*, eds. W. Lucha and K. Maung Maung (World Scientific, Singapore, 2002), 340 [hep-ph/0010078].

4. W. Lucha, K. Maung Maung, and F. F. Schöberl, Phys. Rev. D **64**, 036007 (2001) [hep-ph/0011235].

5. W. Lucha and F. F. Schöberl, Int. J. Mod. Phys. A **17**, 2233 (2002) [hep-ph/0109165].

6. Z.-F. Li, W. Lucha, and F. F. Schöberl, arXiv:0707.3202 [hep-ph], Phys. Rev. D (in print).

7. W. Lucha and F. F. Schöberl, arXiv:0707.1440 [hep-ph], to appear in Proc. *QCD@Work 2007, International Workshop on Quantum Chromodynamics – Theory and Experiment*, Martina Franca, Italy, June 16–20, 2007.

8. W. Lucha and F. F. Schöberl, J. Phys. G: Nucl. Part. Phys. **31**, 1133 (2005) [hep-th/0507281].

9. Li Z.-F., W. Lucha, and F. F. Schöberl, Mod. Phys. Lett. A **21**, 1657 (2006) [hep-ph/0510372].

10. Z.-F. Li, W. Lucha, and F. F. Schöberl, HEPHY-PUB 855/07 (2007).

11. A. B. Henriques, B. H. Kellett, and R. G. Moorhouse, Phys. Lett. B **64**, 85 (1976).

Frascati Physics Series Vol. XLVI (2007), pp. 1543–1546
HADRON07: XII Int. Conf. on Hadron Spectroscopy – Frascati, October 8-13, 2007
Poster Session

RELATION BETWEEN THE IN-MEDIUM ω MESON MASS AND QUARK CONDENSATE UN THE LIGHT OF THE RECENT EXPERIMENTAL DATA ON THE MESON PROPERTIES IN NUCLEAI

R. Huguet, J.C. Caillon and J. Labarsouque
Université Bordeaux 1 ; CNRS/IN2P3 ;
Centre d'Etudes Nucléaires de Bordeaux-Gradignan, UMR 5797
Chemin du Solarium, BP120, 33175 Gradignan, France

Abstract

We have determined the relation between the in-medium ω meson mass and quark condensate in the framework of a Nambu Jona-Lasinio model constrained by both the in-medium pion decay constant to the value measured in experiments on deeply bound pionic atoms and the in-medium ω meson mass to the experimental value obtained either by the TAPS collaboration or by the E325 experiment at KEK. Our results are compared to several scaling laws and in particular to that of Brown and Rho.

1 Introduction

Recently, the modification in nuclei of the ω meson has been investigated in photoproduction experiments by the TAPS collaboration [1)] and its mass was found to be $m^*_\omega = 722^{+4}_{-4}$ (stat)$^{+35}_{-5}$(syst) MeV at 0.6 times the saturation

density of nuclear matter. The same order of magnitude, a 9% decrease of the in-medium ω mass at saturation, has been observed by Naruki et al. [2] in 12 GeV proton-nucleus reactions (E325/KEK).

On the other hand, experimental indications of the in-medium modification of the quark condensate, $\langle\overline{q}q\rangle$, has been obtained in experiments on deeply bound pionic atoms where the observed enhancement of the isovector πN interaction parameter over the free πN value indicates a reduction of the pion decay constant in the medium which was found [3] to be $f_\pi^{*2}/f_\pi^2 = 0.64$ at saturation density of nuclear matter. The in-medium quark condensate is then connected to f_π^* through the Gell-Mann-Oaks-Renner relation.

These recent experimental data should provide stringent tests for the models and for the relation between the in-medium ω meson mass and quark condensate. An indication on the consequences of these new constraints could be obtained by enforcing them in quark models incorporating the most prominent features of QCD. In this context, the NJL model [4] appears as a good candidate since it allows a dynamical description of both the breaking of chiral symmetry and of the modification of the in-medium ω meson mass.

In this work, we have determined the dependence of the in-medium ω meson mass on the quark condensate in a NJL model constrained by the meson properties in the vacuum as well as in the medium through the pion decay constant and ω meson mass. Our results will be compared to several scaling laws and in particular to that of Brown and Rho [5] : $m_V^*/m_V \sim \left[\langle\overline{q}q\rangle \,/\, \langle\overline{q}q\rangle_0\right]^{1/2}$ (where $\langle\overline{q}q\rangle$ and $\langle\overline{q}q\rangle_0$ are respectively the in-medium and vacuum quark condensates).

2 The NJL model parameters

We consider the chirally invariant two-flavor NJL Lagrangian [4] up to eight-quark interaction terms [6]. The free parameters have been determined using the pion mass $m_\pi = 135$ MeV, the pion decay constant $f_\pi = 92.4$ MeV and the ω meson mass $m_\omega = 782$ MeV in vacuum, but we have also used $f_\pi^{*2}(\rho_B = \rho_0)/f_\pi^2 = 0.64$ (where ρ_0 is the saturation density of nuclear matter) in accordance with what is obtained in experiments on deeply bound pionic atoms [3]. Moreover, the in-medium ω meson mass has been constrained to reproduce the experimental central value obtained either by the TAPS collaboration [1], $m_\omega^*(\rho_B = 0.6\rho_0) = 722$ MeV, or by the E325 experiment at KEK [2],

$m^*_\omega(\rho_B = \rho_0) = 711$ MeV. In addition, we have considered several values of the in-vacuum constituent quark mass, m_{vac}, values ranging between 400 MeV and 500 MeV. Thus, two families of parametrization sets denoted respectively by TAPS and KEK will be considered.

3 Results

The results are shown on Fig.1 where we have plotted m^*_ω/m_ω as a function of $\langle\overline{q}q\rangle$ / $\langle\overline{q}q\rangle_0$ for the two parametrization sets TAPS and KEK. The shaded areas correspond to values of the ω meson mass for a constituent quark mass ranging from 400 MeV to 500 MeV. As we can see, these areas are rather narrow and the results are thus only weakly dependent on the value of m_{vac} used.

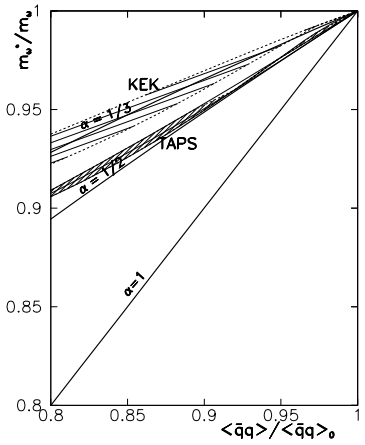

Figure 1: *In-medium ω meson mass as a function of the quark condensate. The shaded areas correspond to values obtained for a constituent quark mass in the range $400 < m_{vac} < 500$ MeV. The full lines represent the scaling laws given by Eq.1 for α =1/3, 1/2 and 1.*

In order to determine an approximate form for the relation between the vector meson mass and the quark condensate, we have considered scaling laws

of the general form :

$$\frac{m^*_\omega}{m_\omega} = \left[\langle\overline{q}q\rangle \,/\, \langle\overline{q}q\rangle_0\right]^\alpha . \tag{1}$$

Any value of α can be considered but we have chosen to show here the results for $\alpha = 1/2$ which corresponds to the Brown and Rho scaling and for neighboring values: $\alpha = 1/3$ and $\alpha = 1$.

The full lines on Fig.1 represent the scaling laws given by Eq.1 for $\alpha = 1/3$, $1/2$ and 1. A rather good agreement with the case $\alpha = 1/2$ corresponding to the Brown and Rho scaling law is obtained for the TAPS parametrization set while the KEK result clearly favours $\alpha = 1/3$.

4 Conclusion

We have determined the in-medium ω meson mass and quark condensate in a NJL model with eight quark interaction terms. The parameters of this model have been determined using the meson properties in the vacuum but also in the medium. When the in-medium ω meson mass is constrained to the experimental data obtained by the TAPS collaboration, the Brown and Rho scaling law is approximately recovered. On the other hand, when the KEK result is used, the in-medium ω meson mass varies rather like the third root of the quark condensate.

References

1. D. Trnka et al., *Phys. Rev. Lett.* **94**, 192303 (2005).
2. M. Naruki et al., *Phys. Rev. Lett.* **96**, 092301 (2006).
3. K. Suzuki et al. *Phys. Rev. Lett.* **92**, 072302 (2004).
4. Y. Nambu and G. Jona-Lasinio, *Phys. Rev.* **122**, 345 (1961); *Phys. Rev.* **124**, 246 (1961).
5. G. E. Brown and M. Rho, *Phys. Rep.* **398**, 301 (2004).
6. R. Huguet, J.C. Caillon and J. Labarsouque, *Phys. Rev.* **C75**, 048201 (2007).

Frascati Physics Series Vol. XLVI (2007), pp. 1549–1565
HADRON07: XII Int. Conf. on Hadron Spectroscopy – Frascati, October 8-13, 2007
Round Table

METHODS AND MODELS FOR HADRON PHYSICS
Round Table

Panelists: C. Davies, S. Faccini, H. Lipkin, L. Maiani (Chair), F. J. Ynduráin
Contributors: C. Bugg, S. Eidelman, P. Faccioli, S. Glazek, Y. Glozman, E. Klempt, H. Koch, J. Lee-Franzini, R. Mussa, E. Pallante, S. Paul, K. Seth, U. Wiedner
Convenors: M. P. Lombardo, S. Miscetti, S. Pacetti

Abstract

A round table held during the Hadron07 Conference focusing on experimental observations of new hadronic states, on theoretical perspectives for their description, and on the role of hadronic spectroscopy in furthering our knowledge of the fundamental theory of strong interactions.

1 Opening Statements

L. Maiani

As I have already given the introductory review this morning, I will just invite Professor Ynduráin to begin, and Professor Davies and Doctor Faccini to continue after him. Which are the problems that you would like to put to the attention of the audience?

F. J. Ynduráin

Since, for obvious reasons of age, I imagined I was going to be the first panelist to talk, I have prepared a list of questions, experimental and theoretical, that I would like to have solved or, at least, understand them better.

1) We are all convinced that the particle η_b exists, but I for one will have nagging doubts until it is actually discovered. Particularly since there are sound theoretical calculations of its mass (some 35 MeV lighter than the upsilon), so one could check ideas in QCD for bound states. I am aware that this is not an easy experiment, but there you are.

2) One of the mysteries of QCD is the extent to which the *constituent* quark model works. I mean, it is OK to say that as quarks move in the soup of gluons and quark-antiquark pairs in a hadron they acquire an effective mass of some 300 MeV; but, except for the Goldstone mesons, this simple model works much better than what it should. For example, the relations of total cross sections

$$\sigma_{\pi\pi} : \sigma_{\pi N} : \sigma_{NN} = 2 \times 2 : 2 \times 3 : 3 \times 3,$$

$\sigma_{\pi N} = \sigma_{KN}$, etc. work at the level of 10%. Yet they are obtained assuming that hadrons consist of only constituent quarks, that behave as if they were free. These relations were obtained in the sixties of last century, and we are nowhere near understanding them; for example, they are contrary to what one finds in deep inelastic scattering, where hadron structure functions have a strong gluonic component.

3) We have a challenge in obtaining the pion-pion scattering amplitudes at low energy. Much improvement has been achieved recently, particularly for the S0 wave thanks to precise measurements of two-pion and three-pion kaon decays here at Frascati, and of K_{e4} decays by the NA48/2 collaboration. In this way, one can start to test predictions of chiral perturbation theory, and contribute to the construction of very precise $\pi\pi$ scattering amplitudes.

4) Of course, the resonances found in charmonium (the X, Y, Z_s) have shown a rich structure that ought to be investigated further.

5) (This in response to a question from the audience). I would like to remark that a much-publicised "discrepancy" between the pion form factor as measured in $e^+e^- \to \pi\pi$ and in $\tau^- \to \nu\pi^-\pi^0$ is not incomprehensible nor does it pose a problem for incorporating $\tau^- \to \nu\pi^-\pi^0$ results into e.g., calculations of the muon $g-2$. All one has to do is to take into account that the rho states

contributing there are different, ρ^0 in the first case and ρ^- in the second. And, because the rho contribution is so large (about a factor 50 at the peak) even a small mass and width difference between the two produces a large difference in the form factors. In fact, one can make the calculation and, once this effect is taken into account, the discrepancy between the pion form factor in $e^+e^- \to \pi\pi$ and in $\tau^- \to \nu\pi^-\pi^0$ is quite compatible with the systematic normalization uncertainties in these processes [see e.g. F. Jegerlehner, Proc. Int. Frascati Conf., 2003, hep-ph/0310234; S. Ghozzi and F. Jegerlehner, Phys. Lett. B **583**, 222 (2004); J. F. de Trocóniz, and F. J., Ynduráin, Phys. Rev. D **71**, 073008 (2005)].

H. Lipkin [1]

We still have a great deal to learn about how QCD makes hadrons out of quarks and gluons. We don't know enough about QCD to believe any hadron model. All the theoretical approaches including the lattice have drastic over-simplifications which leave us still far from our goal.

The following questions may lead to a better understanding of how hadrons are made from quarks and gluons.

1) What is the constituent quark picture? There are several versions.

2) Where does a particular version work very beautifully? Where does it not work so beautifully? Where does it not work at all?

3) Why?

Most theoretical treatments start with well defined models with a number of free parameters and try to use the data to fix the parameters. We look for clues in the data, for puzzles that challenge the conventional wisdom.

Our approach is very different from that of few-body nuclear physics which begins with a system of particles whose masses and interactions are assumed to be known. Our version of the constituent quark model begins with constituent quarks whose nature, masses and structures are not known, have an unknown dynamical origin, may differ between different hadrons and have so far not been explained by QCD. One challenge we face is how to use the new data on heavy quark hadrons to find clues to the nature, masses and structures of these constituent quarks.

Our quark masses are effective masses which contain contributions from

[1] H. Lipkin could not participate and sent his contribution via e-mail.

complicated interactions in ways that are not understood. The fact that the same values for these effective quark masses are found in experimental masses of mesons and baryons is a striking challenge to all attempts to construct a more basic microscopic theory. This may indicate a new yet undiscovered symmetry or supersymmetry. We go far beyond conventional quark model investigations which use either a nonrelativistic or relativistic few-body model with fixed mass parameters. Lattice QCD has been so far unable to get the kinds of predictions between mesons and baryons that have been obtained with this phenomenological constituent quark model.

We start with experimental facts and surprising agreements from models with very simple assumptions. We want to find how maximum agreement with experiment can come from minimum assumptions.

A. Hadron Mass predictions and relations.

1) The simplest assumptions were first proposed by Sakharov and Zeldovich and later independently discovered by me. The hadron mass operator consists of (1) an effective quark mass containing all the spin-independent contributions including potential and kinetic energies. and (2) a two-body hyperfine interaction proportional to $\sigma_i\sigma_j$.

a) The difference between the effective mass contributions for any two flavors is the same for all ground state hadrons, both mesons and baryons.

b) The ratio between the hyperfine energies for any two combinations of flavors is the same for all ground state hadrons, mesons and baryons. The number of experimental regularities that follow from these simple assumptions is striking, and leads to the remarkable results in our paper hep-ph/0611306.

We compare a meson consisting of a valence quark of flavor i and a light quark system having the quantum numbers of a light antiquark with a baryon consisting of a valence quark of the same flavor i and a light quark system having the quantum numbers of a ud diquark of spin S. We make no assumption about the nature and structure of the valence quark or the light quark system. Our results apply not only to simple constituent quark models but also to parton models in which hadrons consist of valence current quarks and a sea of gluons and quark-antiquark pairs. When the hyperfine interaction between the quark and the antiquark or diquark is taken out (a simple procedure with no free parameters), the baryon-meson mass difference is independent of the flavor i of the quark which can be u, s, c or b. This alone is a striking challenge for QCD

treatments which so far have not found anything like this regularity between meson and baryon masses. These results can be seen in hep-ph/0611306.

2) The next version is that of DeRujula, Georgi and Glashow which assumes that the two-body hyperfine interaction is inversely proportional to the product of the two effective quark masses. The magnetic moments of the quarks are inversely proportional to same effective quark masses. This gives the remarkably successful predictions for the magnetic moments of the neutron, proton and Lambda and also some new mass relations.

B. Use of constituent quarks in weak decays.

Most treatment of weak decays assume that the weak transition is only between the valence quarks of the initial and final states. Quark diagrams are classified and assumptions are made like factorisation, etc. which neglect certain diagrams.

Here again I look for simple relations that work based on simple approximations like the following:

1) Charmless strange B decays are assumed to be dominated by the penguin diagram. The discovery of CP violation in these decays indicates that there must be some other amplitude that interferes with the penguin. In the limit where there is only a penguin contribution the four independent branching ratios for $B \to K\pi$ decays are all related and proportional to the penguin amplitude. We define three linear combinations of the four branching ratios which vanish if there is only the penguin contribution. Any linear combination differing from zero provides a clue to an additional contribution which interferes with the penguin. Before recent new more precise experimental data were available all three of these linear combinations were statistically consistent with zero. But new data show two of the three to be appreciably different, while one of them is still consistent with zero. If this is correct it tells us something about which contributions are producing the CP violation. It may imply a cancellation that makes one of these contributions vanish. We now need more and better data to check this out. It is on the Los Alamos Archive at hep-ph/0608284.

In vector-pseudoscalar charmless strange B decays like $K - \rho$ a phenomenological parity selection rule agrees surprisingly well with the data, but does not agree with simple models. But it comes from a simple description using hadron spectroscopy. The dominant penguin diagram produces a strange

antiquark, a u or d spectator quark, and gluons. In flavor SU(3) this state must be in an octet with the isospin and strangeness quantum numbers of a kaon. There are only two possible states with these quantum numbers, a normal kaon which is a quark-antiquark pair and an "exotic kaon" which has the opposite generalised charge conjugation and cannot be constructed from a single quark-antiquark pair. The data are consistent with a model which excludes the exotic kaon. This fits naturally into a picture where the strong interaction scattering producing the final state is dominated by intermediate resonances and these all have normal quantum numbers so the exotic contribution is suppressed. This is discussed in my paper hep-ph/0703191. But this exotic suppression ansatz does not make sense in the standard treatments which only assume states of two quark-antiquark pairs and no multiparticle intermediate states.

C. Davies

Lattice QCD is now able to calculate precise values for gold-plated hadron masses. These are summarised in the "ratio plot" of lattice QCD/experiment in my talk. Gold-plated means stable, well away from decay thresholds and accurately measured experimentally. For the calculations in lattice QCD that have been done so far there is excellent agreement with experiment when realistic sea quark effects are included in the calculation. This is after having fixed the 5 parameters of QCD for these calculations (4 quark masses and a coupling constant) from 5 other hadron masses. For example, D and D_s masses have been calculated, and agree with experiment, to 7 MeV. This level of accuracy would be impossible in any approximate model of QCD and is a very stringent test of the theory. So lattice QCD is now testing QCD. Most of the calculations have been done for mesons so far since they are easier. Gold-plated baryon masses will be calculated in the next few years and these will provide additional tests of QCD.

The masses of excited and unstable states are not nearly so easy to calculate. The precision possible from a lattice QCD calculation will not be as good. There are still interesting results to be had from doing the calculations, but you need to decide what question is being asked i.e. what level of precision is needed to answer it? You also then need to pay attention to the sources of systematic error in lattice calculations of these states.

One interesting lattice calculation underway is that of the baryon spec-

trum by the LHPC collaboration. The ground-state nucleon is gold-plated - the other states are not, and some are very broad and poorly known experimentally. A basic issue here is exactly how many states there are, and it is one that experimentalists are tackling. The LHPC collaboration is beginning preliminary tests on quenched gluon field configurations (i.e. not including the effects of sea quarks) of the kinds of operators, lattice volumes etc that they would need for a complete lattice calculation. They have obtained approximate masses for a lot of states, so it is encouraging news that this calculation is possible. The quenched results may be accurate enough (with, say, 20% systematic errors) to answer some of the interesting issues. On including sea quark effects, multihadron states in the spectrum will be an additional problem and it is not clear how well that can be tackled. It may obscure some of the masses you would like to extract even further and will certainly make quantitative analysis as a function of light quark mass very hard.

Flavor singlet/glueball masses are even harder - see the plenary talk by C. McNeile at LAT07, 0710.0985[hep-lat]. A summary of the lattice results contrasted with some experimental meson masses is reproduced below. The key to calculations in this area will be very high statistics, i.e. fast sea quark formalisms, and a good operator basis, so that all the mixing issues can be handled.

Summary

1) High precision results for gold-plated hadrons will continue to improve. These are the ones that provide the stringent tests of QCD because of the accuracy that is possible. For example, accurate simultaneous (i.e. with only one set of quark masses and coupling constant) calculations of heavy-heavy, heavy-light and light-light meson masses are now possible in lattice QCD and could not be done in any derived model of QCD.

2) This needs to be extended to gold-plated baryons and to 'silver-plated' mesons (particles that are unstable but relatively narrow like the phi, D* etc). Eventually there will also be results for higher-lying and more unstable particles. The same level of accuracy will not be possible, however.

3) The same remarks apply to electroweak decay rates. The gold-plated ones are those having at most one gold-plated hadron in the final state. We now have f_D and f_{D_s} to 2%. Calculations are in progress for $\Gamma_{e^+e^-}$ for J/ψ and ϕ. This is having a strong impact on the flavor physics programme. We also expect accurate form factors for semileptonic decay and structure function

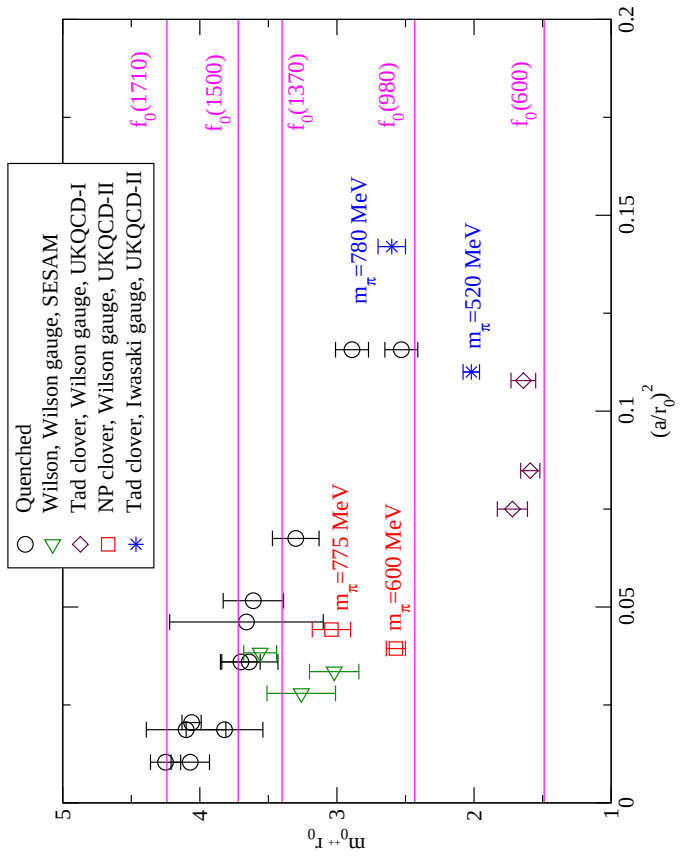

Figure 1: *Summary of unquenched results for lightest flavour singlet* 0^{++} *mesons, from McNeile, Lat07. The unquenched results are from SESAM, and UKQCD.*

moments for baryons to be possible.

4) It is important to test lattice QCD with different quark formalisms and more results from a variety of formalisms will become available over the next few years.

R. Faccini

There are several areas where flavour physics can probe strong interactions and therefore verify or falsify models and lattice calculations:

- fits to the unitarity triangle parameters, $\bar{\rho}$ and $\bar{\eta}$. The current accuracy of the experimental measurements is such that the implications of the measurement of ϵ' in kaon decays is entirely dominated by the theoretical uncertainties and that the other quantities measured on the lattice can be overconstrained by other experimental measurements, if the Standard Model is assumed. This implies, as detailed in the dedicated publication [M. Bona *et al.* [UTfit Collaboration], JHEP **0610** (2006) 081], that before bringing a significant contribution to the unitarity triangle the measurements on lattice of f_{B_d} and f_{B_s} must improve by at least a factor three. On the other side the current measurements are still critical for the interpretations of the current data that include physics beyond the Standard Model.

- Semileptonic B, D and K decays. The best probes of QCD come in these systems where only two quarks interact. Inclusive measurements are particularly dependent on the availability of models that describe the data and can also be used to probe the parton-hadron duality assumed in all predictions. Exclusive measurements rely instead on the availability of the form factors. The statistics is high enough to allow the data to constraint the q^2 dependencies, and can therefore often discriminate among theoretical models that estimate the overall normalization.

- Most of the techniques to measure weak phases exploit the interference between amplitudes that have both weak and strong phases. The best environment to apply such techniques are the multibody decays, and their actual success depends on the possibility of properly modelling the strong phases of multibody decays. Several approaches have been developed in the past decades to take this problem (isobar model, K-Matrix,...) but there is still large arbitrariness in this kind of analyses. The field would profit from a systematic study that gives precise rules on the approach to follow and the resonances/poles to consider. There is an increasing wealth of experimental results of direct production of light mesons [see the contribution from C. Bini at this Conference] that must be used to support such a study.

- Heavy quarkonium spectroscopy. The spectroscopy of the bound states of a pair of heavy quarks can be predicted with relatively good accuracy

with potential models [N. Brambilla *et al.* [Quarkonium working Group], hep-ph/0412158] This makes this field a good ground to observe new forms of aggregation. Indeed there have been recently a large number of experimental evidences that QCD does not only bind quark pairs but also groups of four quarks or of two quarks and gluons [Contribution from R. Mussa at Hadron'07 and from R. Faccini at Lepton Photon '07 (arXiv 0801.2679)].

The path towards the full understanding of the new spectroscopy is still long, both from the theoretical and the experimental point of view. In particular as far as the latter is concerned, only a very small fraction of possible final states and production mechanisms have been studied on the data available from B-Factories. Finally some of the measurements, in particular those implying D-meson reconstruction, will require a significantly larger statistics than what the current generation of experiments will collect.

The diagram below summarizes the current status

2 Discussion

L. Maiani We can now open the general discussion. It might be useful perhaps to divide the rest of the session in two, one devoted to experiments and the other to theory.

K. Seth I am an experimentalist and I have a question for the theorists. When lattice came out we though that experimentalists will soon be out of business. Now I feel our existence is not so much threatened, as I occasionally ask them questions, and they answer: we cannot handle that. I give you an example: Timelike form factors, and they tell me that quarks in Euclidean time cannot be studied. Is this really true that there are things which cannot be measured on the lattice?

C. Davies Yes. Lattice QCD calculations serve a number of useful purposes but they were never intended to put experimentalists out of business, more as

away of providing good tests of QCD against experiment in hadron physics. It is true that there are also only certain things that we can calculate.

K. Seth Thank you for being honest! (smiles).

L. Maiani I have a comment: I think that the purpose of Lattice Gauge Theory is to make explicit what QCD can say, but certainly this does not imply that experimentalists have to go away. What we would like to do is validate QCD by comparing the results of lattice calculations with experiments. Christine Davies was very honest, but even if things such as timelike form factors and multiquark resonances were measured on the lattice, this certainly should not prevent the experimentalists from challenging such predictions. Consider charmonium: this is a case in which potential models in principle should work. We can compute everything, and yet we find different things by doing experiments. This is what is meant for discovery.

K. Seth There are then other cases, such has charmonium decay in two photon. Leading order is a pure QED effects, and QCD comes at the next order. Can we trust anything there, given that QCD is a loop corrections. One loop corrections next to the lowest order is one hundred per cent.

C. Davies There have been exploratory calculations at Jefferson Lab on charmonium two-photon decays and it is certainly on the list of things that we can do better. Potential models can do well for bottomonium and charmonium but when we look in any detail we find discrepancies with experiment for a given potential, especially if we are not allowed to readjust the parameters, and if we look at decay rates as well as the spectrum. Lattice QCD calculations can provide a big improvement in accuracy here, which is important because the experimental results are very accurate. And we can also predict heavy-light physics with no additional parameters (because we are doing real QCD).

L. Glozman First I would like to make a comment on a statement by our chairman and by prof . Ynduráin that quark models work extremely well. It might work well for spectroscopy of the ground state, but we know that it fails for excited states. My second point concerns mass generation, confinement and chiral

symmetry breaking. Heavy quarks do not allow the study of chiral symmetry. To address these issues it is important to consider light quark spectroscopy, which is not well represented in the plenary program at this Conference. Moreover, light quarks have probably an impact on the understanding of the QCD phase diagram.

U. Wiedner I would like to correct a statement that hadron machines are not very useful for spectroscopy. For instance Antiproton proton machines yield the most precise charmonium states.

R. Faccini I haven't said they did not contribute, but, simply, that they importance is limited.

U. Wiedner Panda experiment at Fair will address this problem Theorists should tell us the precise tetraquark spectrum, would be good if lattice and models would come together in order to give some guidance to the experiments.

J. Lee Franzini I think we have lots of light quark presentations, in particular from DAFNE. This is in response to Glozman comment. I also have a question to Christine: can lattice calculate $g-2$?

C. Davies There are lattice calculations addressing the hadronic contribution, still exploratory, led by Tom Blum at BNL. The time scale is hard to estimate since it is a difficult calculation.

F. J. Ynduráin Lattice results for the $g-2$ are not for tomorrow, and it will also be difficult to improve on the naive models for light by light scattering.

L. Maiani I would like to come back to Juliet's concern. This problem is going to be solved in a different way. You want to know $g-2$ to a high precision to understand if there are deviations from the Standard Model. But if such deviations are there, the LHC will see the new particles. So I think LHC will see such effects before we solve the light by light scattering, which is an interesting problem, but after all I agree with what Paco said, it is not for tomorrow.

D. Bugg I would like to follow up to Glozman's remark. We would like much more data. Statistics on charmonium order of hundred events after ten years. Many of these big detectors are now running to the end of present experiments. Big detectors should go in a pion beam. If you do so you can collect an enormous statistics. You need a polarized target, and you can get roughly one million event per day, and all good events. You can cover the entire mass spectrum up to 2.5 GeV in one year. I would like to see JPARC or other machines with a pion beam do such an experiment. Beam intensity is 'trivial'. All of the baryon and meson spectroscopy up to third excitations could be calculated in a couple of years run.

P. Faccioli In this discussion it has been recognized the importance of understanding the interrelation between Quark model and QCD. Other models have been examined in the past few years, and we have learned that dynamical symmetry breaking produces a dynamical mass.

E. Klempt Chiral symmetry breaking is certainly responsible for mass generation, but how about constituent quark mass for the excited states? I also agree with Bugg, that we need new data. But we can also use the available data from B-factories. It is very important that people publish the data in such a way that everybody can use them for further analysis. We (Crystal Barrel) have set up WEB pages from where you can get lots of information.

L. Maiani I this point I feel I would like to make a comment. I think the table shown by Faccini [the table was still displayed on the screen, note of the Editor] is illuminating, and helps answering a previous question about guidance from theory. Guidance from theory is difficult to get, if you do not have data to start with. The question is, how long it is going to take to fill all the 'grey boxes' in the table, i.e. all gap in the spectroscopy, and which machines can do that? Are the present facilities enough or not?

K. Seth The problem is that so far these new states are only populated by B decays, and we would need actobarns before reaching an acceptable statistics. Best data are coming from Tevatron. We have to find other ways tor each these states. Otherwise it will take a lot, unless we will go to a Super$B$-factory.

L. Maiani Can Belle do that?

K. Seth We are trying to look for these states but the cross sections are very very small. New machines like Panda should definitively try.

E. Pallante Another comment on $g-2$, what might be feasible on the lattice is the prediction of the hadronic component. From an experimental point view is more important to reach an agreement between e^+e^- and τ data.

S. Paul This is a comment on Bugg's statement. I would like to comment that Compass is still collecting data and I would like to comment to Eberhardt that LEP has already thought us how to combine data from different collaborations. And this requires people from different collaborations to work together.

R. Faccini Theorists always want more data. The main challenge involves the D's, there we would need at least one hundred times more statistics.

R. Mussa Beauty factories are perfect tools for discovery, but detailed studies ask for dedicated facilities. How high in energy will BES-III go? Will it be possible to scan the $Y(4260, 4350, 4660)$ states recently discovered and discussed at this conference? BES-III has good chances to contribute to these studies. Concerning $p\overline{p}$ experiments like Panda, so far we have no evidence of $X(3872)$ coupling to $p\overline{p}$, or to any other baryon-antibaryon pair. Only the detection of the $X(3872)$ decay to any baryon-antibaryon pair (for instance, η_c preferentially decays in lambda antilambda) would indicate that we have a realistic possibility to study the newly discovered exotic states in a ppbar formation experiment.

S. Glazek One main point of discussion is why quark model works, and if lattice can help with understanding that. The major point is how quarks and gluons lump into constituent quarks. In standard approaches one has nontrivial ground states to explain. This question prompted Wilson and others to develop a light-front approach to QCD. I would say, lattice is not enough: once we have lattice data we need some theory to interpret it.

L. Maiani Concerning constituent quarks, it seems to me that the audience is

divided in two parties, one has very clear idea about them, the other has not. So I suggest that they get together and discuss, and one part explain to the other what to do. Speaking for myself, I am in the middle: there are things we do understand. Concerning lattice, this is a field theoretic approach and when we extract the masses from the propagator, this is a sound procedure which does not need any further interpretation. Would Christine like to comment on this?

C. Davies I do certainly agree.

S. Eidelman This is again on muon $g-2$, and the need of more data to resolve the discrepancy between τ and e^+e^-. There is no real problem, but still there is a puzzle to be resolved, but luckily we also see the outcome of the data analysis from different groups, Kloe and Novosibirsk, from e^+e^- coming together, and also new data from the τ decays in two pions from Belle where we see that our results for the hadronic contributions to $g-2$ are in agreement with previous results from Cleo. Upcoming new machines, one already being commissioned in Novosibirsk, continuing a low energy e^+e^- scan, up to 2 GeV, 10 to 50 times better statistics, and of course I very strongly vote for DAFNE2. At the same time Belle and BaBar will help with τ decays. There is also a theoretical question, as to whether we understand well enough the SU(2) breaking corrections in τ decays.

F. J. Ynduráin You can fit e^+e^- data and τ data together just allowing a slightly different ρ mass and width. So I do not think there is any real disagreement to worry about.

H. Koch This is a comment on the relevance of the proton antiproton physics for the search of new particles. It is true that so far we haven't seen a coupling of $p\overline{p}$ to these new states. In BaBar there might be a good chance to observe thee states.

K. Seth I would like to add one remark on the $p\overline{p}$ possibilities. Of course a new machine should try what it can, but the point is that the coupling to $p\overline{p}$ is going to be small, we have seen it, if we take the pQCD Brodsky type of

prediction, the coupling goes like q to the power minus eight, the cross section will become much smaller with respect to LEAR. So one can try, but it is going to be hard.

L. Maiani One should keep in mind the difference between between the cross section in $p\overline{p}$, the other is the inclusive production in $p\overline{p}$ collisions. $p\overline{p}$ at Tevatron, we know the order of magnitude of the cross section. If we go to FAIR, there is a matter of energy. Any comment from FAIR?

U. Wiedner For Production of J/ψ we have about 120 nb.

L. Maiani As now it is time to conclude, I have basically three points.

- We seem to be worried about applications of QCD to experiments. This is a very interesting message, with all the limitations QCD might have. Feedback from theories to experiments for these kind of states will be very interesting, but do not expect too much, since we do not know how to solve QCD, we can make guesses, but sometimes guesses might be wrong, although of course this does not kill the model.
- Coming to the data, my personal worry is, which are the machines which will produce the data? A Super$B$-factory might take some time. So I hope the issue can be addressed at $p\overline{p}$ colliders, at the Tevatron, or maybe at FAIR.
- Finally, I think that a workshop on quark constituent masses will be a very appropriate outcome of this discussion.

This report was partly based on transcriptions of the recording, necessarily shortened to remain within a reasonable page limit. The Editors thank all the participants, apologize for any mistake and/or incomplete rendering of their contributions, and hope that they nonetheless managed to convey the basic messages and the feeling of a very lively discussion.

The observation matrix

	$J/\psi\pi^+\pi^-$	$D^{(*)}D^{(*)}$	$J/\psi\omega$	$J/\psi\pi^+\pi^0$	$\psi(2S)\pi$	$J/\psi K,\pi$	$\Psi(2S)\pi\pi$	$J/\psi\phi,\eta$	$J/\psi\gamma$
Notes	Mass range for B	Low stat	Only B dec	Mass range! No ISR	No ISR No π^0	No Search	No B-dec	Only B dec	Mass window
X(3872)	Seen	Seen	Not seen	Not seen	Not seen	No search	N/A	Not seen	Seen
Y(3940)	No search	X(3940) ?	Seen	No search	Not seen	No search	No search	No Fit	No fit
Y(4260)	Seen	No fit	No fit	No search	No search	No search	Not seen	No fit	N/A
Y(4350)	Not seen	No fit	No fit	No search	No search	No search	Seen	No fit	N/A
Z(4430)	No search	No search	No fit	No search	Seen	No search	No search	No Fit	No search
Y(4660)	Not seen	No fit	No fit	No search	No search	No search	Seen	No Fit	N/A

PARTICIPANTS

FRASCATI PHYSICS SERIES VOLUMES

Volume I
Heavy Quarks at Fixed Target
Eds.: S. Bianco and F.L. Fabbri
Frascati, May 31–June 2, 1993
ISBN—88–86409–00–1

Volume II – Special Issue
Les Rencontres de Physique de la Vallée d'Aoste – Results and Perspectives in Particle Physics
Ed.: M. Greco
La Thuile, Aosta Valley, March 5 –11, 1995
ISBN—88–86409–03–6

Volume III
Heavy Quarks at Fixed Target
Ed.: B. Cox
University of Virginia, Charlottesville
October 7–10, 1994, 11
ISBN—88–86409–04–4

Volume IV
Workshop on Physics and Detectors for DAΦNE
Eds.: R. Baldini, F. Bossi, G. Capon, G. Pancheri
Frascati, April 4–7, 1995
ISBN—88–86409–05–2

Volume V – Special Issue
Les Rencontres de Physique de la Vallée d'Aoste – Results and Perspectives in Particle Physics
Ed.: M. Greco
La Thuile, Aosta Valley, March 3–9, 1996
ISBN—88–86409–07–9

Volume VI
Calorimetry in High Energy Physics
Eds.: A. Antonelli, S. Bianco, A. Calcaterra, F.L. Fabbri
Frascati, June 8–14, 1996
ISBN—88–86409–10–9

Volume VII
Heavy Quarks at Fixed Target
Ed.: L. Kőpke
Rhinefels Castle, St. Goar, October 3–6, 1996
ISBN—88–86409–11–7

Volume VIII
ADONE a milestone on the particle way
Ed.: V. Valente 1997
ISBN—88–86409–12–5

Volume IX – Special Issue
Les Rencontres de Physique de la Vallée d'Aoste – Results and Perspectives in Particle Physics
Ed.: M. Greco
La Thuile, Aosta Valley, March 2–8, 1997
ISBN–88–86409–13–3

Volume X
Advanced ICFA Beam Dynamics
Workshop on Beam Dynamics Issue for e^+e^- Factories
Eds.: L. Palumbo, G. Vignola
Frascati, October 20–25, 1997
ISBN—88–86409–14–1

Volume XI
Proceedings of the XVIII International Conference on Physics in Collision
Eds.: S. Bianco, A. Calcaterra, P. De Simone, F. L. Fabbri
Frascati, June 17–19, 1998
ISBN—88–86409–15–X

Volume XII – Special Issue
Les Rencontres de Physique de la Vallée d'Aoste – Results and Perspectives in Particle Physics
Ed.: M. Greco
La Thuile, Aosta Valley, March 1–7, 1998
ISBN—88–86409–16–8

Volume XIII
Bruno Touschek and the Birth of thee$^+e^-$
Ed.: G. Isidori
Frascati, 16 November, 1998
ISBN—88–86409–17–6

Volume XIV – Special Issue
Les Rencontres de Physique de la Vallée d'Aoste – Results and Perspectives in Particle Physics
Ed.: M. Greco
La Thuile, Aosta Valley, February 28–March 6, 1999
ISBN—88–86409–18–4

Volume XV
Workshop on Hadron Spectroscopy
Eds.: T. Bressani, A. Feliciello, A. Filippi
Frascati, March 8 2 1999
ISBN—88–86409–19–2

Volume XVI
Physics and Detectors for DAΦNE
Eds.: S. Bianco, F. Bossi, G. Capon, F.L. Fabbri, P. Gianotti, G. Isidori, F. Murtas
Frascati, November 16 –19, 1999
ISBN—88–86409–21–4

Volume XVII – Special Issue
Les Rencontres de Physique de la Vallée d'Aoste – Results and Perspectives in Particle Physics
Ed.: M. Greco
La Thuile, Aosta Valley, February 27 March 4, 2000
ISBN—88–86409–23–0

Volume XVIII
LNF Spring School
Ed.: G. Pancheri
Frascati 15–20 May, 2000
ISBN—88–86409–24–9

Volume XIX
XX Physics in Collision
Ed.: G. Barreira
Lisbon June 29–July1st. 2000
ISBN—88–86409–25–7

Volume XX
Heavy Quarks at Fixed Target
Eds.: I. Bediaga, J. Miranda, A. Reis
Rio de Janeiro, Brasil, October 9–12, 2000
ISBN—88–86409–26–5

Volume XXI
IX International Conference on Calorimetry in High Energy Physics
Eds.: B. Aubert, J. Colas, P. Nédélec, L. Poggioli
Annecy Le Vieux Cedex, France, October 9–14, 2000
ISBN—88–86409–27–3

Volume XXII – Special Issue
Les Rencontres de Physique de la Vallée d'Aoste – Results and Perspectives in Particle Physics
Ed.: M. Greco
La Thuile, Aosta Valley, March 4–10, 2001
ISBN—88–86409–28–1

Volume XXIII
XXI Physics in Collision
Ed.: Soo–Bong Kim
Seoul, Korea, June 28 30, 2001
ISBN—88–86409–30–3

Volume XXIV
International School of Space Science – 2001 Course on: Astroparticle and Gamma–ray Physics in Space
Eds.: A. Morselli, P. Picozza
L'Aquila, Italy, August 30 September 7, 2000
ISBN—88–86409–31–1

Volume XXV
TRDs for the 3rd Millennium Workshop on Advanced Transition Radiation Detectors for Accelerator and Space Applications
Eds. N. Giglietto, P. Spinelli
Bari, Italy, September 20–23, 2001
ISBN—88–86409–32–X

Volume XXVI
KAON 2001 International Conference on CP Violation
Eds.: F. Costantini, G. Isidori, M. Sozzi
Pisa Italy, June 12th 17th, 2001
ISBN—88–86409–33–8

Volume XXVII – Special Issue
Les Rencontres de Physique de la Vallée d'Aoste – Results and Perspectives in Particle Physics
Ed.: M. Greco
La Thuile, Aosta Valley, March 3–9, 2002
ISBN—88–86409–34–6

Volume XXVIII
Heavy Quarks at Leptons 2002
Eds.: G. Cataldi, F. Grancagnolo, R. Perrino, S. Spagnolo
Vietri sul mare (Italy), May 27th June 1st, 2002
ISBN—88–86409–35–4

Volume XXIX
Workshop on Radiation Dosimetry: Basic Technologies, Medical Applications, Environmental Applications
Ed.: A. Zanini
Rome (Italy), February 56, 2002
ISBN—88–86409–36–2

Volume XXIX – Suppl.
Workshop on Radiation Dosimetry: Basic Technologies, Medical Applications, Environmental Applications
Ed.: A. Zanini
Rome (Italy), February 56, 2002
ISBN—88–86409–36–2

Volume XXX – Special Issue
Les Rencontres de Physique de la Vallée d'Aoste –
Results and Perspectives in Particle Physics
Ed.: M. Greco
La Thuile, Aosta Valley, March 9–15, 2003
ISBN—88–86409–39–9

Volume XXXI
Frontier Science 2002 – Charm, Beauty and CP,
First International Workshop on Frontier Science
Eds.: L. Benussi, R. de Sangro, F.L. Fabbri, P. Valente
Frascati, October 6–11, 2002
ISBN—88–86409–37–0

Volume XXXII
19th International Conference on x–ray and Inner–Shell Processes
Eds.: A. Bianconi, A. Marcelli, N.L. Saini
Universitá di Roma La Sapienza June 24–28, 2002
ISBN—88–86409–39–07

Volume XXXIII
Bruno Touschek Memorial Lectures
Ed.: M. Greco, G. Pancheri
Frascati, May 11, 1987
ISBN—88–86409–40–0

Volume XXXIV – Special Issue
Les Rencontres de Physique de la Vallée d'Aoste –
Results and Perspectives in Particle Physics
Ed.: M. Greco
La Thuile, Aosta Valley, February 29 – March 6, 2004
ISBN—88–86409–42–7

Volume XXXV
Heavy Quarks And Leptons 2004
Ed.: A. López
San Juan, Puerto Rico, 1–5 June 2004
ISBN—88–86409–43–5

Volume XXXVI
DAΦNE 2004: Physics At Meson Factories
Eds.: F. Anulli, M. Bertani, G. Capon, C. Curceanu–Petrascu,
F.L. Fabbri, S. Miscetti
Frascati, June 7–11, 2004
ISBN—88–86409–53–2

Volume XXXVII
Frontier Science 2004, Physics and Astrophysics in Space
Eds.: A. Morselli, P. Picozza, M. Ricci
Frascati, 14–19 June, 2004
ISBN—88–86409–52–4

Volume XXXVIII
II Workshop Italiano sulla Fisica di ATLAS e CMS
Eds.: Gianpaolo Carlino and Pierluigi Paolucci
Napoli, October 13 – 15, 2004
ISBN—88–86409–44–3

Volume XXXIX – Special Issue
Les Rencontres de Physique de la Vallée d'Aoste –
Results and Perspectives in Particle Physics
Ed.: M. Greco
La Thuile, Aosta Valley, February 27 – March 5, 2005
ISBN—88–86409–45–1

Volume XL
Frontier Science 2005 – New Frontiers in Subnuclear Physics
Eds.: A. Pullia, M. Paganoni
Milano, September 12 - 17, 2005
ISBN—88–86409–46–X

Volume XLI
Discoveries in Flavour Physics at e^+e^- Colliders
Eds.: L. Benussi, S. Bianco, C. Bloise, R. de Sangro, C. Gatti,
G. Isidori, M. Martini, F. Mescia, S. Miscetti
Frascati, February 28th - March 3rd, 2006
ISBN—88–86409–51–6

Volume XLII – Special Issue
Les Rencontres de Physique de la Vallée d'Aoste –
Results and Perspectives in Particle Physics
Ed.: M. Greco
La Thuile, Aosta Valley, March 5 March 11, 2006
ISBN—88–86409–47–8

Volume XLIII – Special Issue
Neutral Kaon Interferometry at A Phi-Factory: from Quantum Mechanics to Quantum Gravity
Ed.: A. Di Domenico
Frascati, March 24th 2006
ISBN 978—88–86409–50–8

Volume XLIV– Special Issue
Les Rencontres de Physique de la Vallée d'Aoste –
Results and Perspectives in Particle Physics
Ed.: M. Greco
La Thuile, Aosta Valley, February 28, 2 March 5, 2007
ISBN 978—88–86409–49–4

Volume XLV *Frontier Science – Science with the New Generation*
High Energy Gamma-ray Experiments
Eds.: A. Lionetto, A. Morselli
Villa Mondragone, Monteporzio, Italy June 18 -20, 2007
ISBN–978—88–86409–54–0

FRASCATI PHYSICS SERIES VOLUMES – Italian Collection

Collana: Scienza Aperta Vol. I (2006) - ComunicareFisica2005
Atti 1 Convegno "Comunicare Fisica e altre Scienze",
Frascati 24-27 Ottobre 2005
Eds: Franco L. Fabbri, Piero Patteri
ISBN – 88-86-409-48-6